EA02-027

FORD 8/5/03
LETTER TO ODI

APPENDIX A

5 BOXES
BOX 2 OF 5

PART 2 OF 4

2002	6116	S11	1FMYU03162KD66516	3.0L	TAD	6	2002	2G04	12A650	D21	1	2034236	0	STALLS
2002	6122	S11	1FMYU03162KD62760	3.0L	TAD	6	2002	2.00E+03	6B936	D21	1	2287675	0	WHILE DRIVING
2002	6125	S11	1FMYU03162KD62225	3.0L	TAD	6	2002	1H03	6J460	D21	1	1819539	0	WHILE DRIVING
2002	6130	S11	1FMYU03164KD40656	3.0L	TAD	4	2002	2.00E+03	9F715	D21	2	3365018	1000	WHILE DRIVING
2002	6134	S11	1FMYU03165KD24765	3.0L	TAD	4	2002	2.00E+03	9F715	D21	3	2322647	2000	NO TEXT
2002	6135	S11	1FMYU03162KD23661	3.0L	TAD	4	2002	2.00E+04	9C915	D21	1	1943305	0	WHILE DRIVING
2002	6136	S11	1FMYU03162KD23661	3.0L	TAD	4	2002	2.00E+03	9B936	D21	2	2358159	1000	WHILE DRIVING
2002	6137	S11	1FMYU03162KD22822	3.0L	TAD	4	2002	2G04	DIAG	D21	2	1808008	3000	AT IDLE
2002	6153	S11	1FMYU03162KD01789	3.0L	TAD	3	2002	2.00E+03	9F715	D21	3	1911521	4000	WHILE DRIVING
2002	6172	S11	1FMYU03162KC61942	3.0L	TAD	3	2002	2.00E+04	9C915	D21	4	1858648	3000	WHILE DRIVING
2002	6173	S11	1FMYU03165KC61925	3.0L	TAD	3	2002	2002	12B579	D21	3	1799514	3000	WHILE DRIVING
2002	6174	S11	1FMYU03162KC61654	3.0L	TAD	2	2002	2G04	12A650	D21	2	1119653	2000	WHILE DRIVING
2002	6176	S11	1FMYU03165KC61617	3.0L	TAD	2	2002	2.00E+03	9F715	D21	5	2307577	5000	COASTING
2002	6186	S11	1FMYU03165KC57510	3.0L	TAD	2	2002	2.00E+03	9F715	D21	1	2047143	0	NO TEXT
2002	6190	S11	1FMYU03162KC46660	3.0L	TAD	2	2002	2G01	12A650	D21	1	1998092	0	WHILE DRIVING
2002	6191	S11	1FMYU03162KC45650	3.0L	TAD	2	2002	2G05	RECALEM	D21	2	2359023	1000	WHILE DRIVING
2002	6192	S11	1FMYU03162KC45650	3.0L	TAD	2	2002	2G01	12A650	D21	0	1760894	0	WHILE DRIVING
2002	6197	S11	1FMYU03162KC35725	3.0L	TAD	2	2002	2G04	12A650	D21	4	1719253	5000	WHILE DRIVING
2002	6204	S11	1FMYU03162KC30405	3.0L	TAD	2	2002	2.00E+03	9F715	D21	3	1999772	5000	WHILE DRIVING
2002	6205	S11	1FMYU03162KC30239	3.0L	TAD	2	2002	2.00E+03	9F715	D21	2	1859404	2000	WHILE DRIVING
2002	6220	S11	1FMYU03162KC10148	3.0L	TAD	1	2002	7C05	14M089	D21	5	1979183	4000	WHILE DRIVING
2002	6222	S11	1FMYU03165KC09639	3.0L	TAD	1	2002	2.00E+03	9F715	D21	4	1840213	4000	AT STOP
2002	6224	S11	1FMYU03162KC09436	3.0L	TAD	1	2002	7C05	14M089	D21	2	1152389	0	WHILE DRIVING
2002	6239	S11	1FMYU03164KC06436	3.0L	TAD	1	2002	2G05	12A648	D21	3	1344216	5000	AT STOP
2002	6243	S11	1FMYU03162KB66060	3.0L	TAD	1	2002	7C05	14M089	D21	1	586070	0	WHILE DRIVING
2002	6245	S11	1FMYU03162KB66507	3.0L	TAD	1	2002	2G04	12A650	D21	3	1117536	1000	WHILE DRIVING

TSB		TEST DRIVE FOR VEHICLE STALLING. COULD NOT DUPLICATE. FOUND TSB 02 11 04. WDS TEST FOR COD ES. NO CODES. DRIVE CYCLE MONITOR. CHECKED IAC. MONITOR EVM. DISCONNECT VENT LINE TO EVAP EMISSION SYSTEM
TSB		WDS TEST PERFORM TSB 2 11 8 REPL THROTTLE BODY EVAP MGMNT VALVE DIFFE A (AC PER JEFF HAZEL, FIELD ENG.
TSB		INSTALL WDS;CHECK EEC, DCL DISPLAY. PINPOINT TEST.PERFORM TEST PER TSB 2 11 8. NO PROBLEM FOUND. CA LL HOTLINE, CK GROUNDS AND CONNECTORS. CALL HOTLINE. REPLACE PFE SENSOR PER HOTLINE. RETEST. MTIME U
TSB		1500 0F715 42 EEC TESTED PASS CODES KOEO, KOER, KOEC. PINPOINTED WITH DLC DISPLAY, FUEL SYSTEM TESTS, IGNITION SYSTEM TESTS, AND ROAD TEST MONITOR. PERFORMED TSB 02 11 06. FOUND THAT IAC SOLENOID
REFLASH		TEST DROVE WDS TESTED REMOVED AND REPLACED IAC, REFLASHED PROCESSOR, RETEST OK
TSB		VERIFIED CUSTOMER CONCERN. PERFORMED WDS QUICK TEST AND KOER. NO DTCS FOUND, CHECKED FUEL PRESSURE FOUND OK. FOUND TSB 02 11 06 PERF TSB TO SPECS, CHECKED IAC DUTY CYCLE EVAP DUTY CYCLE, CLEANED EVAP
REPLACED		MO 1296 AUTH T4674 VERIFIED CONCERN, PERF EEC TEST PASS. PERFORMED PINPOINT TEST , IGNITION TEST, PASSED PERF MED CHECKED DUTY CYCLE OF IAC FOUND AT 15 PERCENT. REPLACED IAC RECHECKED FOUND STILL LOW.
TSB		WDS HOOK UP, VERIFIED INTERMITTANT HIGH IDLE KOEO AND KOER NO CODES DCL DISPLAY, MONITOR PIDS IAC PID HIGHER THAN NORMAL, 46 PER CENT PCM CALIBRATION IS LATEST EVAP VMV PID OK, BUT POSSIBLY STICKING A
TSB		RAN EEC TEST NO CODE MONITOR PID REPLACE TBODY, VAPOR MANAGEMENT VALVE, IAC VALVE, EEC RELAY PER TSB 2 11 06
TSB		EEC TEST NO CODES CK FUEL PRESSURE NORMAL PERFORM TSB REPLACE IAC AND REPROGRAM PCM
DIAG		DIAG CC 42 149102 EEC TEST PASSED. PIN POINT TEST. PID MONITOR. TEST DRIVE. SIGNAL SIMULATION TEST. FUEL PRESSURE TEST. WIRING WIGGLE
NPF		PERFORMED EEC AND PINPOINT TESTS. USED GENSTAR TO RUN KOEO KOER TESTS NO CODES. TESTED SEM MODULE PASSED ALL SYSTEMS TEST GOOD AT THIS TIME.
TSB		5105 EEC TEST KOEO PASS PASS KOER PASS DCL DISPLAY A ND MONITORED PIDS PER TSB 02 11 6 FOUND IAD DUT Y CYCLE OUT OF SPEC REPLACED IAC WITH NEW UPDAT ED NUMBER 0F715 RETESTED IAC OK STEP 2 VERIFIED C
NO TEXT		
DIAG		PCM EEC (QUICK TEST) DIAGNOSIS
REFLASH		PCM UPDATE EEC (QUICK TEST) DIAGNOSIS
DIAG		. EEC (QUICK TEST) DIAGNOSIS
TSB		Del ROAD TEST VERICLE EED V SELF TEST PASS CODES FUEL PSI 39 LEAK DOWN 0 PSI IN 1 MINUTE PERFORM 02 11 8 TSB PCM UPDATED
REPLACED		RAN EEC TEST, REPROGRAMMED PCM, REPLACED IAC, RETESTED OK
DIAG		EEC (QUICK TEST) DIAGNOSIS
REPLACED		1 EEC TEST,PINPOINT TEST,ENGI MONITOR ROAD TEST,REPLACED PCM RELAY,INOPERATIVE,RE PROGRAMMED PCM,ROADTESTED.
TSB		WDS SELF TEST DCL DISPLAY MONITOR DIAG AND PERFORM TSB02116 REPLACED IAC OUT OF SPEC RETEST
DIAG		CALIBRATION 5505 EEC TEST DIAG PINPOINT IDLE DATA FUEL PRESSURE INJ FLOW POWER BALANCE DCL MONITOR
REFLASH		RECALIBRATE PCM EEC (QUICK TEST) DIAGNOSIS
IMDP		IMDP BODY CHASSIS ELECTRICAL (BCE) TEST
SSM		CHECK OUT AND REPROGRAMED PCM ACCORDING TO SSM 16599 DID NOT REPLACED EEC RELAY BECAUSE IT HAD BLACK LETTERING

. BLEW OUT VENT LINE WITH COMPRE SSOR. REPLACED ENGINE CONTROL RELAY. ROAD TEST AND MONITOR RPMS WHILE DOING CLOSE THROTTLE DEC ELERATION STOPS. NO PROBLEM. WDS REPROGRAM PCM.	CUSTOMER STATES THAT ON 7 8 02 SHE EXPERIENCED THE SAME CONCERN THAT HAPPENED ON 7 1 02. THE DRIVE.
	C S ENGINE QUIT SUDDENLY WHILE DRIVING 35 40 MPH STEADY SPEED
SED TO PERFORM ADDITIONAL TEST.	CUSTOMER STATES VEHICLE DIED WHILE DRIVING
ONLY AT 25% DURING PRESCRIBED CHECKS. REPLACED IAC SOLENOID PER INSTRUCTIONS RETESTED IAC PID READING 32%. CHECKED EVAP SYSTEM PER INSTRUCTIONS. ACCESSED AND CLEARED EVAP VENT HOSE	C S ENGINE STALLED ONE TIME TODAY WHILE DRIVING 35 MPH...NO WARNING LITES PRIOR TO STALL
VENT LINE OF OBSTRUCTION.	CUSTOMER REPORTS VEHICLE DIES WHEN DRIVING DOWN HILL AT 40 MPH,CHECK ENGINE LIGHT COMES ON ENGINE SURGES BEFORE IT
REPLACED THROTTLE BODY, RETESTED	CUSTOMER REPORTS VEHICLE DIES WHEN DRIVING 40 MPH DOWN HILL GRADE,CHECK ENGINE LIGHT COMES ON 4 5 SECONDS BEFORE
T TIMES OK FUEL PRESSURE, NORMAL REFER TO TSB 02 11 05 NO PROBLEM FOUND AT THIS TIME	CHECK FOR ERRATIC IDLE STALL OCCURS WHEN IN A LINE AT DRIVE THROUGH
	CUST STATES ON A PULL ENGINE WILL START RUNNING SLUGGISH OR AROUND STEEP CURVES LOSS OF POWER AND WILL DIE D21
	C S THAT THE CAR STALLED BETWEEN 40 45 MPH A C WAS ON CAR RESTARTED FINE
	CUSTOMER REPORTS WHILE DRIVING ABOUT 40 MPH LOST POWER AND THEN DIED. EMISSION LIGHT CAME ON . PULLED OVER EASY
	VEHICLE STALLED OUT THE OTHER DAY WHILE THE CUSTOMER WAS DRIVING DOWN THE ROAD.
ALIBRATION OK STEP 4 PERFORMED COMPLETE EVAP T ESTING OK STEP 5 CHECKED EEC RELAY OK REPLACED MAF SENSOR WITH NEW UPDATED NUMBER PER THE HOTL INE ROAD TEST PER STEP 6 RAN GOOD	ENGINE DIED WHILE IN FLIGHT COASTING DOWN A INCLINE. 1ST TIME HAPPENED ABOUT 55 MPH, SECOND ABOUT 20 25 MPH CHK
	CUST REPORTS VEH STALLS WHILE DRIVING AND SLOWING DOWN
	CUST REPORTS VEH STALLS WHILE DRIVING ... SEE HISTORY
	NEW OWNER REPORTS VEH STALLS WHILE DRIVING
	CUST STATES INTERMITTENTLY VEHICLE STALLS OUT WHILE DRIVING AND CAN RESTART VEHICLE
	CHECK VEHICLE SHUT OFF WHILE DRIVING WOULD RECRANK
	WHEN DRIVING AROUND 40 MPH AND TAKING A CURVE VEHICLE WILL SHUT OFF AND OIL LIGHT WILL COME ON
	CUSTOMER STATES ENGINE STALLS WHEN DRIVING WILL RESTART AFTER IT STALLS
	CUSTOMER STATES: ENGINE STALLED OUT WHEN SLOWING TO A STOP
	CUST STATES THE TRUCK JUST DIED WHILE DRIVING ABOUT 35 MPH
	ENGINE DIES AT TIMES WHEN COMING TO A STOP
	CUST STATES TRUCK STALLED WHILE DRIVING, WAITED 20 MIN. THEN STARTED
	CHECK OUT WHY WHEN DRIVING TRUCK STALLED CHECK FOR SSM ON THIS

2002	8246	511	1FMYU03162KB67516	3.0L	TAUD	1	2002	7C05	14N099	D21	1	1060365	0	COASTING
2002	8247	511	1FMYU03162KB67516	3.0L	TAUD	1	2002	2.00E+03	9E508	D21	5	2259930	6000	STALLS
2002	8248	511	1FMYU03162KB67406	3.0L	TAUD	1	2002	2G04	DIAG	D21	8	2450878	13000	STALLS
2002	8249	511	1FMYU03162KB67406	3.0L	TAUD	1	2002	2.00E+03	9F715	D21	7	2144945	12000	WHILE DRIVING
2002	8250	511	1FMYU03162KB66787	3.0L	TAUD	1	2002	2G04	DIAG	D21	1	666545	1000	WHILE DRIVING
2002	8251	511	1FMYU03162KB66787	3.0L	TAUD	1	2002	2G02	12B579	D21	1	913675	3000	STALLS
2002	8257	511	1FMYU03162KB66574	3.0L	TAUD	1	2002	7C05	14N099	D21	2	727275	0	WHILE DRIVING
2002	8260	511	1FMYU03162KB77507	3.0L	TAUD	1	2002	2.00E+03	9B598	D21	3	2130876	3000	WHILE DRIVING
2002	8267	511	1FMYU03162KB66992	3.0L	TAUD	12	2001	2B05	RECAL	D21	7	1772610	6000	WHILE DRIVING
2002	8880	511	1FMYU03162KB64972	3.0L	TAUD	12	2001	2G04	DIAG	D21	8	2208987	8000	WHILE DRIVING
2002	8262	511	1FMYU03162KB64957	3.0L	TAUD	12	2001	2.00E+03	9F715	D21	4	1423027	3000	WHILE DRIVING
2002	8263	511	1FMYU03162KB64958	3.0L	TAUD	12	2001	1H05	9J460	D21	5	2151466	5000	WHILE DRIVING
2002	8264	511	1FMYU03162KB64826	3.0L	TAUD	12	2001	2B05	RECAL	D21	5	1886165	5000	WHILE DRIVING
2002	8265	511	1FMYU03162KB63773	3.0L	TAUD	12	2001	2G04	12A650	D21	6	1761278	7000	WHILE DRIVING
2002	8294	511	1FMYU03162KB44992	3.0L	TAUD	12	2001	2G04	DIAG	D21	4	1328987	1000	NO TEXT
2002	8297	511	1FMYU03162KB44589	3.0L	TAUD	12	2001	2G04	12A650	D21	2	676517	1000	COASTING
2002	8304	511	1FMYU03162KB36660	3.0L	TAUD	12	2001	2G01	12A650	D21	4	1286588	3000	AT STOP
2002	8311	511	1FMYU03162KB60896	3.0L	TAUD	11	2001	5B02	9C997	D21	8	2178865	7000	WHILE BRAKING
2002	8315	511	1FMYU03162KB63797	3.0L	TAUD	11	2001	2G02	12B579	D21	7	1762157	7000	STALLS
2002	8316	511	1FMYU03162KB63797	3.0L	TAUD	11	2001	7C05	14N099	D21	1	404866	0	WHILE DRIVING
2002	8318	511	1FMYU03162KB62646	3.0L	TAUD	11	2001	2G04	12A650	D21	8	1660694	7000	STALLS
2002	8320	511	1FMYU03162KB14312	3.0L	TAUD	11	2001	7C05	14N099	D21	2	489281	2000	WHILE DRIVING
2002	8322	511	1FMYU03162KB13885	3.0L	TAUD	11	2001	2.00E+03	9F715	D21	7	1449534	15000	WHILE DRIVING
2002	8323	511	1FMYU03162KB13858	3.0L	TAUD	11	2001	1H09	9J460	D21	9	2253629	14000	WHILE DRIVING
2002	8325	511	1FMYU03162KB13858	3.0L	TAUD	11	2001	7B05	14301	D21	6	2327861	2000	WHILE DRIVING

SSM		RAN CODES NONE FOUND,FOUND SSM 15699 TO REPROGRAM PCM AND REPLACE EEC RELAY,THEN TEST DROVE AGAIN,SEEMS OK
TSB		VERIFIED COMPLAINT,FOUND TSB 02116 MADE REPAIRS,OK NOW
TSB		2 1653 DIAG,NO MIL. EEC TEST PASS,DCL DISPLAY TO REVIEW PID DATA AS OUTLINED IN TSB 02 11 06,ALL W I SPECS,CALLED
TSB		RECAL 42 N36 DIAG,NO MIL. EEC TEST PASS,RAN OASIS ON CONCERN W TSB 02 11 5,PERF DIAG AS OUT LINED IN TSB,DCL MONITOR
SSM		CALIBRATION EEC TEST, DCL MONITOR TEST REPROGRAM PCM PER SSM 15699 RETEST
REPLACED		MAF INOP PER HOTLINE EEC TEST KOEO PASS KOEC PASS KOER P1000 DCL MONITOR TEST IDLE DATA TEST FUEL PRESSURE TEST PINPOINT REPLACED MAF
REPLACED		TESTED COMPUTER SYSTEM AND TESTED FOR MOBY CURRENT PROGRAM,PINPOINT TEST AND REPLACED EEC POWER RELAY PER OASIS MESSAGE 15699
TSB		INSP AND ROAD TEST,UNABLE TO VERIFY CONCERN, PERFORMED QUICK TEST,PASSED. MONITOR PIDS,NO FAULTS DETECTED. PERFORMED TSB 2 11 6 FOUND IAC AT 41.4% WHEN RPM IS AT 750 ECT 197F AND NO PURGE FLOW. IAC
TSB		EEC TEST NO CODES PINPOINT TEST REPROGRAM PCM PER TSB 02 11 6
REFLASH		UNABLE TO VERIFY C O. DID EEC TESTS,N36 DISPLAY,RECORDER MON ITOR ROAD TESTS,FUEL PRESS TEST,IGN TESTS,CYL BAL & FUEL INJ REPROGRAMMED PCM. RETESTED WITH WOS. IAC PERCENTAGE & IDLE R PM CORRECT. ROAD
TSB		3659 TSB 02 06 06 WP W36, EEC TEST, DCL DISPLAY, RUN OASIS AND DID NOT FIND ANY NEW UP DATES OR MESSAGES. READING NEWEST TSB BOOK AND FOUND TSB 02 06 06 PERFORMED TSB. ROAD TEST DCL MONITOR TO VER
REPLACED		EEC TEST, REPLACED PIP SENSOR
REFLASH		EEC TEST, REPROGRAM PCM
TSB		CHECK FOR DYING WHILE DRIVING. TEST EEC KOEO DTC P1111 KOER P1111 PREFORM TEST PER TSB 02 11 06 ARTICLE 02 8 6 TEST IAC PASS REPROGRAM PCM RETEST.
NPP		EEC TEST GNS DCL MONITOR NPP
REPLASH		VERIFIED CONCERN RAN EEC REPROGRAMMED PCM TO CORRECT THE CONCERN.
REPLACED		UNKNWON EEC TEST, PINPOINT TEST, RETEST, DCEL TEST, MONITOR, REPLACE MAF, B/G SWITCH, CHECK VALVE, PFE, RELAY, IAC
ADJUST		ROAD TEST TO VERIFY CUSTOMER CONCERN, N36 START UP, N36 EEC TEST PASS, DCL DISPLAY, PINPOINT TEST Z. READJUST THROTTLE STOP AND BASE IDLE
SSM		7363 CAUSAL PART #12A650 CC (42) TECH 4535 KOEO KOER CODE PASS GM DTC: PASS OASIS CONTACT ID #110 180 661 UNABLE TO VERIFY CONCERNS, PERFORM EEC SELF TESTS, PASS, NO FAULT CODES. PERFORM DCL DISPLAY
SSM		405 CAUSAL PART #14A099 CC (42) TECH 4535 OASIS CONTACT ID# 311 220 046 KOEO KOER CODE: P1111 GM DTC: P1111 ROAD TEST VEHICLE, UNABLE TO VERIFY CONCERNS, CUSTOMER STATES ONLY HAPPENED ONCE. RUN EEC
SSM		7365 W36 EEC PINPOINTS DATA DISPLAY REPROGRAMED PCM PER SSM RETEST NOTE DID NOT DUPLICATE CONCERN
SSM		RAN EEC TEST PASS. RAN MON ROAD TEST REPLACED IAC AND PCM RELAY R AND R BATTERY AND TIGHTENED GROUNDS CHECKED CONN FOR DAMAGE PER SSM 15434 RETEST PASS
STICKING		STICKS EEC (QUICK TEST) DIAGNOSIS
INOP		INOPERATIVE EEC (QUICK TEST) DIAGNOSIS
POOR CONNECTION		ROAD TEST TO VERIFY CUSTOMER CONCERN, N36 EEC TEST PASS, DCL DISPLAY, PINPOINT TEST Z. REPAIR LOOSE POSITIVE BATTERY CABLE. EEC RETEST AND ROAD TEST

	CUSTOMER COMPLAINS ENG STALLS ON DECEL.
	COMPLAINS ENG GOES DEAD AT TIMES
	CUSTOMER STATES KEEPS CUTTING OFF WHEN PUSHES ON GAS WITH OR WITH OUT A C ON
	CAR STALLS WHILE DRIVING & FEELS MISSING
	CUST STATES ENGINE STALLED WHILE DRIVING AT HWY SPEEDS
	CUST STATES ENGINE STALLS WITH FOOT ON THE GAS SEE HISTORY
	CUSTOMER STATES: VEHICLE DIED WHILE DRIVING. IT STARTED BACK UP AND SEEMS TO BE DRIVING OK. D21
AND THROTTLE BODY IN ORDER. REPLACED IAC VALVE AND THROTTLE BODY PER TSB, IAC VALVE CYDLE AT 34.2%. CALLED TECH HOTLINE 07 12 02 2:50PM SPOKE WITH MATT AND ADVISED TO REPLACED	CUSTOMER STATES THE VEHICLE STALL,WHILE DRIVING AT 5 10MPH,CUSTOMER STATES IT TOOK THREE ATTEMPT T
	VEHICLE HAS DIED 2 TIMES WHILE DRIVING ONCE AT APPROX 50MPH AND TODAY AT APPROX 50 60 MPH RESTART IMMEDIATLY D21
TESTED AGAIN, AGAIN DID NOT STALL. CUSTOMER	CK FOR CK ENGINE LIGHT ON AND BATTERY LIGHT AND OIL LIGHT WHEN DRIVING DOWN ROAD AT 40MPH ENGINE DYES
W/V DUTY CYCLE OF IAC. PINPOINT TEST AND DIAGNOSED. REPLACED BAD IAC VALVE. REPLACED PCM RELAY WITH A HELLA SERVICE RELAY. RE PROGRAMMED PCM WITH LATEST UP DATE PER TSB. RE TEST. ROAD	INSPECT FOR WHILE DRIVING AT 45MPH ENGINE TEMP WAS WARM CUST HAD FOOT STEADY ON ACCELRATOR ENGINE STALLED,ALL ACESSORIES STAYED ON ENGINE DID RESTART D21
	CHECK ENGINE STALLS WHILE DRIVING
	CHECK ENGINE DIES WHILE DRIVING
	DIES WHILE DRIVING
	CUST INFORM ME THE CAR CUT OFF WHILE DRIVING AT 25 MPH GOING ON FLAT GROUND STARTED BACK UP CUST INFORM ME LET IT WARM UP THEN TOOK OFF DROVE FOR A MILE THEN THIS HAPPEN SEEMS T
	CUSTOMER STATES WHEN STOPED AT RED LIGHT VEHICLE STALLED THEN ROLLED BACK WOULD NOT RECRANK FOR A FEW MIN ADVISE
	(D21) CUST STATES WHEN COMING TO A STOP VEHICLE STALLED AND CK ENGINE AND OIL LIGHT CAME ON
TESTS AND PINPOINT TESTS, CHECK BASE IDLE SPEEDS, IAC %, RPM AND DPFE. PASSED, PERFORM FUEL PRESSURE TESTS, CHECK PRESSURE AND LEAKDOWN, PASSED, IN SPECS, NO LEAKDOWN DETECTED AFTER 30	D21 INSP AFTER SITTING AWHILE ENGINE LUNGES AND HAS NO POWER TILL WARMED UP AND WILL OSCASSIONALLY DIE
SELF TESTS, PASSED, NO FAULT CODES DETECTED. RUN PINPOINT TESTS, CHECK BASE IDLE SPEED AND RUN DGL DISPLAY TESTS, PASSED. RUN FUEL PRESSURE TESTS, PASSED, PRESSURE IN SPECS AND NO LEAKDOWN	D21 VEHICLE STALLED WHILE DRIVING, CUSTOMER LET VEHICLE SIT 2 OR 3 MINUTES AND VEHICLE STARTED FINE.
	CUST STATES VEH STALLED AND HAD NO BRAKES OR STEERING
	VEHICLES WHILE DRIVING.
	ENGINE STALLS OUT WHILE DRIVING AT TIMES
	STALLS WHEN YOU LET OF GAS WHEN DRIVING AT AROUND 30 MPH ALSO AT STOPS SEE HIST
	(D21) CUSTOMER STATES WHILE DRIVING VEHICLE STALLED AND CK ENGINE AND OIL LIGHT CAME ON PULLED OVER PUT IN GEAR

2002	8337	S11	1FMYU03182KB13696	3.0L	TAD	11	2001	1H03	BJ460	D21	7	1646672	10000	AT IDLE
2002	8338	S11	1FMYU03182KB12978	3.0L	TAD	11	2001	2.00E+03	9F715	D21	3	831436	3000	WHILE BRAKING
2002	8339	S11	1FMYU03182KB12978	3.0L	TAD	11	2001	7C05	14N069	D21	2	602606	2000	TURNING
2002	8348	S11	1FMYU03182KB03469	3.0L	TAD	11	2001	2.00E+03	9F715	D21	1	378461	2000	WHILE DRIVING
2002	8359	S11	1FMYU03182KB00999	3.0L	TAD	11	2001	7C05	14N069	D21	4	790139	6000	WHILE DRIVING
2002	8364	S11	1FMYU03182KB00905	3.0L	TAD	10	2001	2901	12A650	D21	6	1160465	6000	WHILE DRIVING
2002	8359	S11	1FMYU03182KB01897	3.0L	TAD	10	2001	2905	RECALEM	D21	5	919131	0	STALLS
2002	8360	S11	1FMYU03182KB01866	3.0L	TAD	10	2001	2.00E+03	9F715	D21	10	2224466	8000	WHILE DRIVING
2002	8361	S11	1FMYU03182KB01740	3.0L	TAD	10	2001	2904	12A650	D21	4	855480	3000	WHILE DRIVING
2002	8362	S11	1FMYU03182KB01351	3.0L	TAD	10	2001	7C05	14N069	D21	1	200085	0	STALLS
2002	8363	S11	1FMYU03182KB01074	3.0L	TAD	10	2001	2.00E+03	9F629	D21	2	941221	1000	WHILE BRAKING
2002	8364	S11	1FMYU03182KB01074	3.0L	TAD	10	2001	2901	12A650	D21	2	1171400	3000	WHILE DRIVING
2002	8365	S11	1FMYU03182KB01074	3.0L	TAD	10	2001	2902	12B670	D21	1	747342	0	WHILE DRIVING
2002	8366	S11	1FMYU03182KB00149	3.0L	TAD	10	2001	2904	DIAG	D21	7	1284731	6000	WHILE DRIVING
2002	8369	S11	1FMYU03182KA85034	3.0L	TAD	10	2001	2.00E+03	9F715	D21	2	417057	1000	WHILE DRIVING
2002	8372	S11	1FMYU03182KA92506	3.0L	TAD	10	2001	2905	RECAL	D21	8	1631969	7000	WHILE DRIVING
2002	8385	S11	1FMYU03182KA83465	3.0L	TAD	10	2001	2.00E+03	9F715	D21	0	460204	0	WHILE DRIVING
2002	8386	S11	1FMYU03182KA76769	3.0L	TAD	10	2001	2904	12A650	D21	4	799776	6000	TURNING
2002	8387	S11	1FMYU03182KA76769	3.0L	TAD	10	2001	7C05	14N069	D21	3	567576	1000	WHILE DRIVING
2002	8388	S11	1FMYU03182KA76741	3.0L	TAD	10	2001	7C05	14N069	D21	8	1039988	4000	WHILE DRIVING
2002	8392	S11	1FMYU03182KA76845	3.0L	TAD	10	2001	2.00E+03	9F715	D21	9	1479900	16000	WHILE DRIVING
2002	8396	S11	1FMYU03182KA76829	3.0L	TAD	10	2001	2.00E+03	9F715	D21	7	1312227	11000	WHILE DRIVING
2002	8397	S11	1FMYU03182KA76198	3.0L	TAD	10	2001	2F01	DRIVE	D21	6	730776	4000	WHILE DRIVING

REPLACED		RAN WDS TESTS ALL PASS CODES RAN PID DATA DISPLAY DPFE VOLTAGE TOO HIGH AT HOT IDLE REPLACED DPFE SENSOR
REPLACED		ROAD TEST EEC TEST PINPOINT TEST DCL DISPLAY REPLACE SUSPECT IAC VALVE RETEST AND ROAD TEST
DIAG		ROAD TEST AND CONCERN NOT VERIFIED. TEST EECV,PASS 10 PASS,P A88 KOER,PINPOINT TEST PER PC ED. PRECHECK AND PASS. PID DAT
SSM		561 WDS DIAG.PERFORMED EEC TEST,RECEIVED PASS CODES KOEO & KOER.DCL MONITOR & RECORD SHOWS ALL IN PUTS & OUTPUTS WITHIN SPECS.FUEL PRESSURE & LEAK DOWN TEST PASSED.FOUND SSM #15494.REPLACED IAC VA
SSM		WDS HOOK UP, SELF TEST, RUN OASIS, PERFORM SSM 15555, INSPECT GROUNDS, REPROGRAM PCM, REPL PCM RELAY RETEST REPR VERIFIED.
DIAG		EEC (QUICK TEST) DIAGNOSIS
DIAG		OUT OF ADJUSTMENT EEC (QUICK TEST) DIAGNOSIS
REPLACED		SCANNED FOR DTCS NO CODES, MONITOR PIDS. REPLACE IAC MOTOR, AND RETEST.
SSM		EEC TEST AND RECEIVED PASS CODE P1000, PERFORMED FUEL PRESSURE TEST, PASSED. TESTED IGNITION SYSTEM, PASSED. INJECTOR FLOW TEST, PASSED. DLC DISPLAY TEST & MONITORED ON ROAD TEST, ALL PIDS OK. RAN SSM
REPLACED		RAN EEC TEST ON WDS, NO CODES. REPLACE EEC RELAY PER SSM 15434 CK IAC VALVE PTNOK CK GANDS PER SM 15434 CK
DIAG		EEC (QUICK TEST) DIAGNOSIS
DIAG		EEC (QUICK TEST) DIAGNOSIS
DIAG		MAF EEC (QUICK TEST) DIAGNOSIS
TSB		6799 42 12A650 126500 0.2 D45 0.3 D60 0.1 D84 0.2 0.8 PERFORM OBD 2 ENGINE DIAGNOSIS NO CODES SELECT AND MONITOR PARAMETER READINGS UPDATE THE PCM CALIBRATION RETEST AND ROAD TEST OK
SSM		DEFECTIVE IAC AND EEC POWER RELAY. PERFORMED DIAGNOSIS REPLACED IAC AND EEC POWER RELAY PER SSM 15434
REFLASH		EEC, DCL, FUEL PRESSURE TEST, INJECTOR FLOW TEST. PINPOINT TEST, REPROGRAMMED PCM, RETEST.
DIAG		IAC VALVE AND POWER RELAY EEC (QUICK TEST) DIAGNOSIS
REFLASH		5075 12A650 PURGED EVAP SYSTEM, AND REPROGRAMMED PCM PER HOTLINE.5667.WAS NOT ABLE TO DUPLICATE CUSTOM ERS CONCERN.
SSM		1373 OC 42 (14h0B 6F715) SSM15434 EEC TESTED SYSTEM, MIL OFF CONT PASS KOEO PASS KOER PASS, DATALOGGER, PINPOINT TEST, ROADTEST CHECKED OASIS AND FOUND SSM#15434 REMOVED BATTE RY AND CHECKED GROU
SSM		4781 OC 42 EEC TESTED SYSTEM, MIL OFF CONT PASS KOEO PASS KOER PASS, PER SSM 15555, REPLACED EEC RELAY AN D CHECKED PINS IN CONNECTOR FOR PUSH OUT, TIGHT ENED ALL PCM AND EEC GROUNDS, REPROGRAMMED
REPLACED		RUN EEC DIAG MONITOR PIDS ON TST DRIVE REPLACE TBODY, IAC, VAPOR MANAGEMENT VALVE AND EEC RELAY REPROGRAM PROCESSOR
REPLACED		11712 WDS SELF TEST DCL DISPLAY PIN POINT TEST REPLACED ABPV CHECKED EVAP VALVE REPROGRAMMED PCM TO LATEST REVISION AND ROAD TEST RE RUN SELF TEST KOER P1111 KOEO P1111 KOEC P1111 CO42
SSM		THE POWERTRAIN CONTROL MODULE NEEDS TO BE UPDATED WE TESTED THE SYSTEM NO CODES ARE PRESENT WE THEN FOLLOWED THE SSM 15555 WITH WDS TEST EQUIPMENT AND ROADTESTED VEHICLE

	ENGINE WONT TAKE GAS, DIED AT IDLE, SURGES ON ROAD JUMPS WHEN FINALLY TAKES GAS HAS ROUGH IDLE
	CUSTOMER REPORTS THAT 2 TIMES SINCE 1 25 02 WHILE SLOWING DOWN ON A HILL (BRAKING) ENG INSTANTANEOUSLY STALLED
	CUSTOMER REPORTS WHEN GOING AROUND A TURN AND DOWN A HILL, THE VEHICLE STALLED...PULLED OVER TO SIDE OF ROAD AND
LVE,REPLACED EEC POWER RELAY PER SBM. TEST DRIVE,RETEST,PASSED.	CK,ENG.DIED W DRIVING 30 40 MPH
	CUST STATES STALLED WHILE DRIVING AFTER ABOUT 10 MIN OF DRIVING RESTARTED AFTER ABOUT 5 MIN
	CUST REPORTS VEH STALLS WHILE DRIVING
	CK ENGINE OIL LIGHT CAME ON THEN CK ENGINE LIGHT CAME ON THEN CAR CUT OFF CAR HAD ONLY BEEN DRIVEN ABOUT 5 MINUTES
	CS THE TRUCK DIES WHILE DRIVING AND LETTING OFF THE GAS. ADVISE.
AND TSB INFO. PERFORMED SBM 11599 FOR PCM REPROGRAMMING. CHECKED RELAYS AND EVAP SYSTEM, OK. RETESTED AND ROAD TESTED, PASSED	CUSTOMER STATES THAT VEHICLE INTERMITTENLY DIES WHEN DRIVING AT 65 70MPH
	OIL LIGHT CAME ON AND CAR WENT DEAD, CRANKED BACK UP AND HAS BEEN RUNNING FINE SINCE
	CHECK ENGINE, CUST SAYS STALLED OUT AFTER 5 9 MILES OF DRIVING, WAS SLOWING DOWN TO MAKE A TURN, HAS ALSO DIED UP HILL AND WHEN SLOWING, SEE LARRY R
	CUST REPORTS VEH STALLS WHILE DRIVING...SEE HISTORY
	CUST REPORTS VEH HAS STALLED WHILE DRIVING THE LAST 2 DAYS....THE FIRST TIME IT STALLED AT A STEADY SPEED 40 50MPH...THE SECOND TIME 35 AND SLOWING
	CK ENG HAS DIED ONCE WHILE DRIVING FUEL CAP WARNING LIGHT COMES ON
	CUSTOMER STATES ENGINE STALLS ENGINE DIED WHILE DRIVING STARTED BACK UP HAPPEN TWICE
	CS WHILE DRIVING TO WORK VEH ALL OF A SUDDEN STALLED OUT &RAW BATTERY LIGHT AND OIL LIGHT COME ON THEN REALIZED VEH HAD STALLED
	CUST STATES ENGINE DIED WHILE DRIVING 40 MPH OIL LIGHT AND ENGINE LIGHT CAME ON CAR RESTARTED
	CC D21 CUST STATES ENG IS STALLING WHEN MAKING LEFT TURNS (SEE HIST.)
NDS G104,G105. REINSTALLED BATTERY, CHECKED GROUND G101 AND BULKHEAD AND REPLACED EEC RELAY, CHECKED TERMINALS INSIDE FU SE PANEL UNDER HOOD WHERE EEC RELAY IS LOCATED REPLACED IAC AND	D21 OWNER REPORTS ENGINE STALLED WITHOUT ANY WARNING WHEN DRIVING
PCM WITH LATEST CALIBRATION AND ROAD TEST TRUCK..	CC D21 CUST STATES ENG SI CUTTING OFF AT TIMES WHILE DRIVING ADVISE
	CUST STATES WHILE DRIVING DOWN THE ROAD ENGINE WILL DIE CCD21
	VEHICLE STALLED WHILE DRIVING AT 45 MPH, COASTED OVER TO SIDE OF ROAD, VEHICLE WOULD RESTART, COULD SMELL A FAINT FUEL SMELL COMING IN THROUGH VENTS., D21
	CUSTOMER STATES:THE VEHICLE STALLED OUT WHILE DRIVING CHECK AND REPORT

2002	8403	S11	1FMYU03182KA70335	3.0L	TAUD	10	2001	7C05	14N089	D21	5	758175	1000	WHILE DRIVING
2002	8404	S11	1FMYU03182KA69727	3.0L	TAUD	10	2001	2G04	12A650	D21	4	642102	4000	STALLS
2002	8418	S11	1FMYU03182KA69071	3.0L	TAUD	9	2001	1A09	6007	D21	1	507642	0	NO TEXT
2002	8460	S11	1FMYU03182KA69071	3.0L	TAUD	9	2001	1A09	6007	D21	1	376650	0	NO TEXT
2002	8432	S11	1FMYU03182KA61486	3.0L	TAUD	9	2001	2.00E+03	9F715	D21	11	2295063	12000	STALLS
2002	8436	S11	1FMYU03182KA60677	3.0L	TAUD	9	2001	2G04	12A650	D21	6	840441	7000	STALLS
2002	8442	S11	1FMYU03182KA49582	3.0L	TAUD	9	2001	7C05	14N089	D21	1	256221	0	STALLS
2002	8443	S11	1FMYU03182KA48559	3.0L	TAUD	9	2001	2G04	12A650	D21	5	1523094	12000	WHILE DRIVING
2002	8444	S11	1FMYU03182KA48545	3.0L	TAUD	9	2001	2.00E+03	9F715	D21	9	2388985	13000	WHILE DRIVING
2002	8456	S11	1FMYU03182KA44699	3.0L	TAUD	9	2001	1A09	6007	D21	1	391861	0	NO TEXT
2002	8457	S11	1FMYU03182KA44699	3.0L	TAUD	9	2001	1A09	6007	D21	1	276204	0	STALLS
2002	8460	S11	1FMYU03182KA44732	3.0L	TAUD	9	2001	2.00E+03	9E926	D21	7	1998442	7000	WHILE DRIVING
2002	8463	S11	1FMYU03182KA44695	3.0L	TAUD	9	2001	7C05	14N089	D21	3	410291	2000	WHILE DRIVING
2002	8466	S11	1FMYU03182KA43435	3.0L	TAUD	9	2001	2.00E+03	9F715	D21	10	1529417	13000	UPHILL
2002	8467	S11	1FMYU03182KA39078	3.0L	TAUD	9	2001	2G05	RSCAL	D21	6	807980	7000	WHILE DRIVING
2002	8512	S11	1FMYU03182KA35857	3.0L	TAUD	9	2001	1H05	9J480	D21	7	2351971	8000	DOWNHILL
2002	8514	S11	1FMYU03182KA35643	3.0L	TAUD	8	2001	2.00E+03	9E926	D21	10	2169229	11000	WHILE DRIVING
2002	8522	S11	1FMYU03182KA29535	3.0L	TAUD	8	2001	2F09	8C216	D21	0	164091	0	STALLS
2002	8523	S11	1FMYU03182KA27543	3.0L	TAUD	8	2001	2G04	12A650	D21	11	2189729	21000	STALLS
2002	8536	S11	1FMYU03182KA25047	3.0L	TAUD	8	2001	2.00E+03	9E926	D21	9	1392169	8000	WHILE DRIVING
2002	8559	S11	1FMYU03182KA09709	3.0L	TAUD	8	2001	7C05	14N089	D21	9	1688505	6000	WHILE DRIVING
2002	8562	S11	1FMYU03182KA08944	3.0L	TAUD	8	2001	7C05	14N089	D21	1	257325	1000	DOWNHILL
2002	8564	S11	1FMYU03182KA08515	3.0L	TAUD	8	2001	2.00E+03	9F715	D21	11	2302305	22000	WHILE DRIVING
2002	8580	S11	1FMYU03182KA07096	3.0L	TAUD	8	2001	2.00E+03	9F715	D21	0	270149	0	WHILE DRIVING
2002	8585	S11	1FMYU03182KA06855	3.0L	TAUD	8	2001	7W04	15R001	D21	10	2428704	7000	FATS
2002	8586	S11	1FMYU03182KA06479	3.0L	TAUD	8	2001	2G04	12A650	D21	8	1620469	9000	DECEL

INOP		INOP EEC (QUICK TEST) DIAGNOSIS
REFLASH		TEST AND REPROGRAM ENGINE CONTROL MODULE
ENGINE FAILURE		REQUESTING DEALER'S P/A CODE 01634
ENGINE FAILURE		REPL ENGINE FOR VERY LOUD ROD KNOCK & REPL STARTER. ENTERED AT WPI
T3B		TESTED AND PINPOINT TESTED EEC WITH WDS. PERFORMED DCL AND SYSTEMS IGNITION TESTS. REPLACED IAC VALV E AND PCM POWER RELAY. REPROGRAMMED PCM AND RETESTED PER T3B 02.09.06.
S5M		WDS EEC SELF TEST PASS PASS PASS. DCL DISAPLAY VALUES IN RANGE. ROAD TEST MONITOR COULD NOT DUPLICATE CONCERN. PINPOINT TEST CHECK EEC POWR RELAY AND PINS PER S5M OK REPROGRAM PCM TO LATEST LEVEL PWR
REPLACED		213 TESTED EEC SYSTEM ALL PASS CODES MONITERED SYSTEM WHILE RUNNING AND CHECKED FUEL PRESSURE CHECKED CHARGING SYSTEM RAN OASIS R AND I BATTERY AND TRAY ASSY. CHECKED GROUNDS UNDER BATTERY BOX AND
T9B		RAN DIAG TESTS, RECD NO CODES CHECKED OASIS, FOUND T9B 02 11 6 FOLLOWED STEPS BY CHECKING IAC, EVAP, RELAY, VENT HOSE, ALL OK REPROGRAMMED PCM ROADTESTED, OK
T9B		DIAGNOSE AND REPLACED IDLE AIR CONTROL MOTOR AN D EEC RELAY PER T9B 02 11 06
ENGINE FAILURE		REQUESTING DEALER'S P/A CODE 04699
DIAG		EEC (QUICK TEST) DIAGNOSIS
T9B		CK & REPLACED T BODY PER T9B.
REPLACED		OPEN CIRCUIT 141099 CC39 DIAG AND PINPOINT TEST. REPLACE EEC RELAY. RETEST P1111 P1111 P1111
T9B		VERIFIED CONCERN AND PERFORMED EEC TEST AND RAN T9B. FOUND 02 11 6, R&R IAC VALVE AND REPROGRAM PCM, PER T9B, RETEST OK
S5M		7405 PCM 42 W ROAD TEST DID NOT VERIFY CONCERN;TEST EEC KOEO PASS KOER PASS KOEC PASS;TEST FUEL PRESS;RUN OASIS;AS PER S5M#10589 REPROGRAM PCM;BLOW OUT EVAP VENT LINE AND REPLACE PWR RELAY 14N089 R
REPLACED		DPFE EEC (QUICK TEST) DIAGNOSIS
STICKING		STICKING WDS DIAG PID MONITOR TEST PINPOINT TEST FUEL PRESSURE TEST REPLACE IAC VAPOR MANAGEMENT VALVE AND THROTTLE BODY AND
REPAIR		HOOK TO WDS, TEST EEC, PERFORM SEVERAL PINPOINT TEST. R&I INTAKE & ENGINE UPPER MOUNT FOR ACCESS. TRACED AND FOUND SHORT TO CONNECTOR C139. REPAIR CONNECTOR
T9B		21092 CP12A650 CC42 128600,D45,D80,D81,D84,DX1 1.4 FLAG 106 EEC TEST PASSED ROAD TESTED W N3S RECORDER & MONITORED PID DATA PER T9B 02 11 06 NORMAL PID DATA REFLASHED PCM & RETEST P1600 E
REPLACED		RAN PIDS AND EEC TEST ALSO RAN WORLD DIAGNOSTIC TEST NO CODES TEST DROVEREPLACED THE IDLE AIR CONTROL VALVE,THROTTLE BODY AND REPROGRAMED POWER CONTROL MODULE
T9B		T9B 02 11 06 INFO ONLY CC 42 BASIC 12A650 1147 ROAD TEST VECHILE RAN NORMAL RUN EEC TEST PASS CODES PERFORM DCL DISPLAY ALL DATA WITHIN NORMAL LIMITS,RUN OASIS
REPLACED		EEC TEST,PID TEST,FUEL PRESSURE TEST,INJECTOR TEST,R&I PCM, CK PINS & WIRING,R&I BATTERY,BOX & FUSE BOX,CK CONNECTORS, R&I REAR SEAT,CK FUEL PUMP WIRING & GROUNDS,R&I FILTER HOUSING,REPLACED POWER REL
REFLASH		EEC DCL RPL POWER RELAY RPL PFE RPL IAC REPROGRAM PCM RETEST
REPLACED		121 IAC 9F715, KOEO PASS, WDS SELF TEST, DATA LOGGER, PIN POINT TEST, REPLACED IAC, RETEST TEST DROVE CC42
REFLASH		PROGRAM PATS KEY PATS KEY PROGRAM
T9B		ROAD TESTED, UNABLE TO DUPLICATE. SCOPED ON WDS, PERFORMED ALL DIAGNOSTICS. REPROGRAM PCM PER T9B 02 09 06.PERFORMED OBD II DRIVE CYLE ALL PASSED.T26020

	CUST STTAES CHECK VEHICLE WILL STALL OUT WHILE DRIVING AT OR 20 MPH IN TRAFFIC AFTER 25 MIN OF DRIVING WILL RESTART NO PROBLEM ADVISE
	CHECK AND ADV FOR INTERMITTENT ENGINE RUNNING AND ALL WARNING INDICATOR STAYING ON NO POWER STEERING OR BRAKE SYSTEM WORKING (ATTN JOHN LYNCH)
	CUSTOMER STATES THAT THE VEHICLE SOMETIMES STALLS
SSM 15549 42 3.0 QC TECH 226	C IS TRUCK STALL AT TIMES WHEN SCREECHING NOISE IS HEARD D21
CHECKED WIRE CONNECTION REPLACED EEC RELAY ROAD TESTED 12 MILES RAN OK POSSIBLE EEC RELAY INTERMITTENT OPEN	VEH QUIT RUNNING, PULLED OVER AND RESTARTED,SEEMS TO RUN OK NOW
	CS THE VEH SHUT WHILE DRIVING ONE TIME LAST WEEK SHE WAS SLOWING DOWN WHEN IT HAPPENED HAS NOT HAPPENED SINCE
	CHECK ENGINE WILL QUIT RUNNING WHILE DRIVING AT A STEADY SPEED. ENGINE WILL RESART RIGHT AWAY AND RUN FINE. THIS HAS HAPPENED 3 TIMES.
	CS ENGINE IS STALLING
	C S THAT THE VEHICLE IS STALLING WHILE DRIVING TECH#150
	CS ENGINE JUST SHUT OFF WHILE DRIVING DOWN THE HIGHWAY CC D50
	CUSTOMER STATES ENGINE STALLED WHEN STARTING UP A HILL.
EPEAT ROAD TEST	(D21) CK ENGINE DIES WHILE DRIVING
	CUSTOMER STATES WHEN GOING UP A HILL AND DOWN A HILL THE VEHICLE SHUTS OFFBY ITSELF
	CUSTOMER SAYS VEHICLE HAS COMPLETELY SHUT DOWN ON TWO SEPERATE OCCASIONS WHILE DRIVING
	ENGINE QUIT WHILE ON POI TEST DRIVE
	D21 ADVISE ON WHEN ENGINE IS COLD DIES
	CHECK CUSTOMERS CONCERN VEHICLE STALLS WHILE DRIVING
	CUST STATES ENG STALLED WHILE DRIVING
AY,TEST.	ENG DIED ON INCLINE RUNNING 45 50 MPH
	CUSTOMER STATES VEHICLE DIES WHILE DRIVING WHILE GOING DOWN HILL
	D21 ENGINE DIES WHILE DRIVING
	CUST STATES FATS KEYS NOT WORKING
	CHECK INTERMITTANT STALL ON DECEL ON COLD START

2002	8591	S11	1FMYU03182KA05758	3.0L	T/LD	6	2001	2.00E+03	9F715	D21	2	1301788	9000	AT STOP
2002	8594	S11	1FMYU03172KE00239	3.0L	T/LD	6	2002	2.00E+03	9F715	D21	-1	2084400	0	WHILE DRIVING
2002	8595	S11	1FMYU03172KD99116	3.0L	T/LD	6	2002	7D05	14N089	D21	2	2413522	1000	STALLS
2002	8596	S11	1FMYU03172KD99464	3.0L	T/LD	6	2002	2F02	9E926	D21	2	2271694	1000	STALLS
2002	8600	S11	1FMYU03172KD61618	3.0L	T/LD	6	2002	2G04	12A650	D21	1	2038321	1000	WHILE DRIVING
2002	8601	S11	1FMYU03172KD67581	3.0L	T/LD	5	2002	2.00E+03	9F715	D21	2	2133725	1000	WHILE DRIVING
2002	8603	S11	1FMYU03172KD68002	3.0L	T/LD	5	2002	2.00E+03	9F715	D21	1	2071650	0	STALLS
2002	8606	S11	1FMYU03172KD61674	3.0L	T/LD	5	2002	2G04	DIAG	D21	2	1814926	2000	STALLS
2002	8607	S11	1FMYU03172KD34475	3.0L	T/LD	4	2002	2.00E+04	9C915	D21	3	2117680	5000	WHILE DRIVING
2002	8609	S11	1FMYU03172KD33951	3.0L	T/LD	4	2002	2.00E+03	9F715	D21	2	1580393	1000	WHILE DRIVING
2002	8620	S11	1FMYU03172KD02402	3.0L	T/LD	4	2002	2G01	12A650	D21	3	2099185	3000	WHILE DRIVING
2002	8622	S11	1FMYU03172KD02402	3.0L	T/LD	4	2002	2G01	12A650	D21	3	2190888	3000	STALLS
2002	8627	S11	1FMYU03172KD01169	3.0L	T/LD	3	2002	2.00E+03	9F715	D21	4	2330004	2000	WHILE DRIVING
2002	8628	S11	1FMYU03172KD00689	3.0L	T/LD	3	2002	2G02	12B579	D21	1	1753334	1000	WHILE DRIVING
2002	8631	S11	1FMYU03172KC99947	3.0L	T/LD	3	2002	2G05	RECALEM	D21	1	1434699	5000	WHILE DRIVING
2002	8635	S11	1FMYU03172KC99811	3.0L	T/LD	3	2002	2G02	12B579	D21	2	1854695	1000	STALLS
2002	8640	S11	1FMYU03172KC61348	3.0L	T/LD	2	2002	2.00E+03	9F715	D21	0	1870178	0	WHILE DRIVING
2002	8642	S11	1FMYU03172KC60619	3.0L	T/LD	2	2002	2G02	12B579	D21	4	1994791	4000	WHILE DRIVING
2002	8649	S11	1FMYU03172KC48368	3.0L	T/LD	2	2002	2.00E+03	9E926	D21	5	2071078	3000	COASTING
2002	8655	S11	1FMYU03172KC30441	3.0L	T/LD	2	2002	2G05	RECAL	D21	3	2127800	3000	WHILE DRIVING
2002	8675	S11	1FMYU03172KC19911	3.0L	T/LD	2	2002	2.00E+03	9E926	D21	4	2188536	6000	WHILE DRIVING
2002	8682	S11	1FMYU03172KC19432	3.0L	T/LD	1	2002	2.00E+04	9C915	D21	3	2057845	3000	WHILE DRIVING
2002	8690	S11	1FMYU03172KC15101	3.0L	T/LD	1	2002	2.00E+04	9C915	D21	5	1903116	3000	WHILE DRIVING

REFLASH		NIL OFF NO CODES PIN TEST NGS ROAD TEST REGAL PCM RMR IAC VALVE PCM RELAY.
INOP		INOP EEC (QUICK TEST) DIAGNOSIS
REPLACED		REPLACE PCM RELAY WITH UPDATED RELAY
ADJUST		PERFORMED ENGINE DIAGNOSIS. HOOKED UP WDS AND SET THE THROTTLE POSITION SENSOR VOLTAGE. SET BASE IDLE SPEED WITH
TSB		WDS HOOKUP RETRIEVED CODES PASS TSB 02 11 06 DCL DISPLAY CHECK IAC OK STEP 4 EVAP VAPOR MAN OK EVAP VM OK EVAP PURGE PERFORMED EVERYTHING ON TSB 02 11 06
TSB		12/7 HOOK UP WDS TEST EEC ALL PASS DATA LOGGER AND CHECK OUT AL PER TSB 02 11 6 TRACE TO AND REPLACE IAC MOTOR RETEST ALL PASS
REPLACED		REPL IAC VALVE ASY
TSB		2000 RAN KOEO PASS CONT PASS KOER PASS RAN OASS. TSB 2 11 6 PERFORMED STEPS IN TSB NPV CUSTOMER NEEDS TO BRING VEHICLE IN WHEN LIGHT FIRST COME S ON SO WE CAN RETRIEVE CODES.
TSB		EEC TEST NO CODES ROADTEST BY OC AND DISPATCHER 40 MILES PERFORM TSB 02 11 6 IAC 94 % PASS UNABLE TO TEST EVAP
REPLACED		DIAG REPLACE IAC EEC (QUICK TEST) DIAGNOSIS
REFLASH		FAULTY PROCESSOR PCM REPROGRAMMING TEST
HOTLINE		COMPARTMENT, ABOUT 2 FROM CONNECTOR 134. RUBED ON A C LINE. CK V REF 2351. SHORTED TO CKT2359. IGNITION TRANSFORMER COMPASITOR. REPAIRED SHORT, HEAT SHRINKED & REPOSITION WIRING HARNESS. REINSTALLED A
REPLACED		OKED FOR STALLING ON ACCEL. NO CODES IN SYS TEM. PERFORMED PIN POINT TEST AND MONITOR TEST REPLACED IAC VALVE AND RETESTED
NPF		DIAG CC42 9F715, 96886, 90916 EEC TEST PASSED. PIN POINT TEST PASSED. PID MONITOR. TEST DROVE 20 MILES. UNABLE TO DUPLICATE CONCERN. PERFORM
TSB		9807 SELF TEST PASS REPROGRAM PCM PER TSB 020605.
REPAIR		PERFORM NGS EEC SYSTEM TEST, PERFORM PINPOINT TEST. RECORD PIDS WITH NGS ON ROAD TEST. FUEL PRESSURE TEST 40 PSI, FOUND POOR MAF SIGNAL, REPAIR PUSHED OUT PIN. RETEST
TSB		294 ROAD TESTED BY ARTHUR COULDNT VERAFY AT THIS TIME, HOWEVER DID RUN OASS AND FOUND TSB 02 11 6 FOR STALLING CONCERN EEC V ON DEMAND SELF TEST PASSED, MONITOR PIDS, RAN DCL DISPLAY, RAN SCOPE
TSB		4999 IAC 9F715, MAF 128579, WDS SELF TEST, DATA LOGGER, PERFORMED ALL CHECKS IN TSB 02 11 06. CALLED HOTLINE, WAS TOLD TO REPLACE MAF WITH NEW PART NUMBER, TEST DROVE FIVE TIMES FOR TOTAL OF THIRT
DIAG		EEC (QUICK TEST) DIAGNOSIS
TSB		ROAD TEST RAN EEC TEST RAN FUEL PRESSURE TEST 35 PSI RAN PID MONITOR TEST RAN PINPOINT TEST REPROGRAM PCM PER TSB 02 11 06 INSPECT IAC EEC RELAY AND EVAP SYSTEM RETEST VERIFIED REPAIR
TSB		ROADTEST TO CONFIRM HOOK TO WDS RAN NEGC TEST PINPOINT RUN TSB AND OASS PERFORM TSB 02 6 06
TSB		9894 DEL OFF HOOK TO WDS PINPOINT TEST PASS PASS PASS CHECK PIDS CHECK IDLE SPEED CHECK TSB 02 11 6 CHECK IAC % OK 33 % CHECK PCM CALIBRATION CHECK EEC POWER RELAY OK CHECK EVAP REPLACED EVAP VALVE
REPLACED		DOES NOT OPERATE PROPERLY. EEC TEST, PINPOINT TEST, EVAP EMISSION SYSTEM STATIC LEAK TEST, RUNNING LOSS SYSTEM DRIVE CYCLE TEST, SYSTEM LEAK TEST, REPLACED FUEL VAPOR CANISTER PURGE REGULATOR VALVE,

	CHECK INTERMITTENT STALLING PROBLEM WHEN COMING TO A STOP BRAKING (HAPPENS WHEN VEHICLE IS NOT TOTALLY COOLED DOWN)
	ENGINE DIED WHILE DRIVING
	C S THAT VEHICLE IS DIEING INTERMITTENLY, VEHICLE STARTS BACK UP
	CUSTOMER STATES;ENGINE STALLS WHEN SLOWING DOWN TO STOP RE STARTS OK NO WARNING WHEN THIS HAPPENS NO WARNING LAMPS
	CUST STATES WHILE DRIVING DOWN THE ROAD VEH JUST DIES
	VEHICLE STALLS WHILE DRIVING,RESTARTS FINE
	ENGINE STALLS
	E29 CHECK ENGINE LIGHT CAME ON & VEH ACTED AS IF GOING TO STALL, BEEN ABOUT 5 6 DAYS SINCE LIGHT HAS BEEN ON
	TOTAL SHUTDOWN WHEN DRIVING AT 40 MPH
	AT TIMES WHILE DRIVING QUITS RUNNING
	CUSTOMER STATES THAT WHILE DRIVING CAR STALLED AND WILL NOT RESTART, WONT EVEN CRANK.
LL TRIM PANELS. CALLED HOTLINE & ADVISED. RETEST & CLEARED CODES. ROAD TEST OK. P&S DIRECTOR DROVE FOR 2 1 2 HOURS STRAIGHT WITH NO PROBLEMS.	
	DIES AND NO RESTART HAS HAS 3 PCMS REPLACED ADVISE
	D21 C S 2 TIMES WHILE DRIVING WITH THROTTLE APPLIED THE VEH STALLED OUT RETARTED FINE HAD OVER 1 2 TANK OF FUEL NV
	CUST STATES VEH DIES WHILE DRIVING,,CAN PULL OVER AND WILL RESTART,,, DID IT TWICE OVER THE WEEKEND
	DIE WHILE DRIVING
	D21 ENG STALLED CUSTOMER DID NOT TRY TO RESTART CK AND ADVISE TOWED IN BY ROADSIDE ASST
TEST, RAN FUEL PRESS TEST OK, RAN PIN POINT TESTS PER TSB 02 11 06, AND VIEW OK, BUT IAC DUTY CYCLE DROPS BELOW 25% REMOVED AND REPLACED IAC MOTOR, RESET PCM, ROAD TEST AND RETEST PASSED.	
	CORRECT FOR DIED WHILE DRIVING INTERMITLY SEE TSB 02 11 6 ON BACK OF TICKET ALSO SEE ARTHUR WHEN IN
Y FOUR MILES. REPLACED MAF AND IAC, RETEST, TEST DROVE OC42	
	D21 ENGINE DIES WHILE DRIVING, CRANKS RIGHT BACK UP
	CUSTOMER STATES VEH. DIED WHILE COASTING DOWN HILL,ONCE BEFORE WHEN PULLING OFF, WHILE IDLEING ALSO.
	CUST STATES WHILE DRIVING UP A SLIGHT GRADE GOING UP WEST 8TH FOOT ON GAS ENGINE QUIT RUNNING PULLED RESTARTED OK,CONCERN HAPPENED ONE TIME
	CHECK THE ENGINE STALLS WHEN DRIVING 55 MPH RESTARTS RIGHT AWAY
STICKING ROAD TEST RETEST OK	
	CAR HAS STALLED DRIVING VERY INTERMITTENT INSPECT FOR TSB IF APPLICABLE D21
AND RERUN EEC TEST	
	CK ENG STALLS WHILE DRIVING, RESTARTS OK, ANY TYPE DRIVING

2002	8691	S11	1FMYU03172KC15101	3.0L	T/LD	1	2002	2G02	12B570	D21	1	1018782	0	WHILE DRIVING
2002	8694	S11	1FMYU03172KC09184	3.0L	T/LD	1	2002	2.00E+03	9E928	D21	4	1062037	3000	WHILE DRIVING
2002	8697	S11	1FMYU03172KC08928	3.0L	T/LD	1	2002	2G05	REGAL	D21	3	1228328	3000	STALLS
2002	8700	S11	1FMYU03172KC01480	3.0L	T/LD	1	2002	1H03	9J460	D21	3	2287099	3000	WHILE DRIVING
2002	8703	S11	1FMYU03172KB99174	3.0L	T/LD	1	2002	2.00E+03	9F715	D21	4	1464118	6000	AT IDLE
2002	8704	S11	1FMYU03172KB99174	3.0L	T/LD	1	2002	2G04	DIAG	D21	3	1078092	3000	ACCELERATING
2002	8705	S11	1FMYU03172KB98624	3.0L	T/LD	1	2002	7G02	14401	D21	3	2098843	4000	STALLS
2002	8706	S11	1FMYU03172KB98090	3.0L	T/LD	1	2002	7C05	14N069	D21	3	2159359	2000	ACCELERATING
2002	8712	S11	1FMYU03172KB97747	3.0L	T/LD	1	2002	7C05	14N069	D21	1	1077994	1000	WHILE DRIVING
2002	8716	S11	1FMYU03172KB97992	3.0L	T/LD	1	2002	2G03	12B577	D21	1	1112084	0	WHILE DRIVING
2002	8720	S11	1FMYU03172KB97428	3.0L	T/LD	1	2002	2G04	12A660	D21	2	915366	2000	AT STOP
2002	8727	S11	1FMYU03172KB96520	3.0L	T/LD	1	2002	1H03	9J460	D21	3	1024343	2000	WHILE DRIVING
2002	8728	S11	1FMYU03172KB96520	3.0L	T/LD	1	2002	2.00E+03	9F715	D21	5	1590491	4000	STALLS
2002	8729	S11	1FMYU03172KB77613	3.0L	T/LD	1	2002	7G05	14300	D21	3	1556660	2000	WHILE DRIVING
2002	8734	S11	1FMYU03172KB76878	3.0L	T/LD	12	2001	2G04	DIAG	D21	2	1412202	1000	NO TEXT
2002	8736	S11	1FMYU03172KB75201	3.0L	T/LD	12	2001	2.00E+03	9F715	D21	7	1974058	6000	WHILE DRIVING
2002	8738	S11	1FMYU03172KB69892	3.0L	T/LD	12	2001	7C05	14N069	D21	4	1126121	4000	ACCELERATING
2002	8740	S11	1FMYU03172KB67882	3.0L	T/LD	12	2001	7V01	12A661	D21	-1	460826	0	AT STOP
2002	8741	S11	1FMYU03172KB67017	3.0L	T/LD	12	2001	2.00E+03	9F715	D21	2	2133268	2000	WON'T IDLE
2002	8742	S11	1FMYU03172KB66904	3.0L	T/LD	12	2001	2G04	12A660	D21	4	1077744	6000	WHILE DRIVING
2002	8743	S11	1FMYU03172KB66479	3.0L	T/LD	1	2002	2G04	12A660	D21	7	1974302	9000	WHILE DRIVING
2002	8745	S11	1FMYU03172KB66112	3.0L	T/LD	12	2001	2G05	REGAL	D21	4	1117751	2000	WHILE DRIVING
2002	8746	S11	1FMYU03172KB66112	3.0L	T/LD	12	2001	2G04	12A660	D21	4	1161903	3000	STALLS

REPLACED		DOES NOT OPERATE PROPERLY. EEC TEST, PINPOINT TEST, NGS MONITOR TEST, IGNITION SYSTEM DIAGNOSTIC TEST, FUEL SYSTEM PRESSURE TEST, NGS DCL DISPLAY TEST, TEST PCM REPROGRAMMING, REPLACED MASS AIR FLOW S
DIAG		WDS SELF TEST PASS CONT KOER PASS PINPOINT TEST ON CONCERN MANUAL FUEL PRESSURE TEST PASS DATALOGGER MONITOR INSTALL
REFLASH		3674 ERRATIC OPERATION 42 TESTED EEC KOEO, KOER, MONITORED PIDS NO CODES ROAD TESTED MONITORED PIDS CK FUEL PRESSURE, CK FUEL LEAKDOWN, CK INJ FLOW TEST, RAN POWER BALANCE TEST REPROGRAM EEC PROCE
TSB		1 ROAD TEST CNV. EEC TEST MONITORED PIDS CHECKED OASIS FOUND TSB 02116 REMONITORED PIDS REPROGRAMMED PCM REMONITORED
REPLACED		SELFTESTED EEC REVIEWED RECORDINGS FROM PID MONITOR VDR FROM RO189273 INFECTED IAC DUTY CYCLE AND REPLACED IDLE AIR
NPF		SELFTESTED EEC TESTED FUEL PRESSURE 65 KOEO PERFORMED DCL MONITOR ROADTEST UNABLE TO DUPLICATE CONCERN ALL READINGS
REPLACED		TEST DROVE VEHICLE TO DUPLICATE CONCERN. RAN PINPOINT TESTS HOOKED UP VDR TO UNIT. RECORD PROBLEM WITH O2 SENSORS, CHECK FUEL PRESSURE. PRESSURE IS FLUCTUATING OUT OF SPECS. REMOVED AND REPLACED FUEL
DIAG		CUTTING OFF EEC (QUICK TEST) DIAGNOSIS
SSM		1394 PCM RELAY 42 1.8L EEC TESTS KOER KOEO KOEC PASS FUEL PRESSURE NGS DCL RECORDER PERFORMED SSM 15500 PCM REPROGRAM HAS LATEST CALIBRATION EVAP TESTS VENT LINE CLEAR REPLACED PCM RELAY DROVE OK NO
REFLASH		HOOK UP WDS EEC TEST NO LIGHT NO CODES TEST PCM REPROGRAM PCM MONITOR ROAD TEST
REFLASH		1 2001 ROAD TEST CONFIRM VEHICLE STALLS PERFORM WDS DIAG PASS CODES CHECK AND PINPOINT TO PCM NECESSARY TO REPROGRAM PCM MODUEL RECHECK OK
DIAG		TEST DROVE WDS TEST CONT CODE PASS KOEO KOER PASS EEC RELAY &ODD EVAP TEST PASS CHECKED PINS IN PCM CONNECTOR AND PCM
TSB		WDS DIAG NO CODES TSB 02 11 05 PERFORMED ALL STEPS REPLACED IAC (OUT OF RANGE) REPLACED RELAY CHECKED EVAP
REFLASH		PCM NOT UPDATED & LOOSE POSITIVE BATTERY CABLE. ROAD TEST TO VERIFY CONCERN NGS START UP EEC TEST PASS DCL DISPLAY PIN POINT TEST Z WDS START UP REPROGRAM PCM & REPAIR LOOSE CABLE. RETEST AND ROAD TE
NPF		STALLING DIAGED AND FOUND NO PROBLEM
TSB		WDS TEST CODE P1111,RAN TSB 02 11 6,MONITER DATA REPLACED IAC VALVE REPROGRAM PCM,CHECKED EDC RELAY OK,TEST DRIVE OK
REPLACED		CK CODES NO CODES RECORD AND MONITOR PIDS REPLACED EEC RELAY AND REPROGRAMMED PCM CLEARED CODES RETEST RO TST
POOR CONNECTION		EEEC TEST ROAD TEST AND MONITER PIDS WITH NGS . PINPOINT TEST, FOUND R W WIRE PUSHED OUT OF CONNECTOR AT IAC VALVE. REPAIR WIRE AND RETEST
REPLACED		EEC TEST. REPLACE IAC VALVE
DIAG		PCM PERFORMED BEDS DIAGNOSIS,DCL,PIN POINT, POWER BALANCE,FUEL PRESSUR
SSM		1 KOEO KOER,NO CODES PRESENT,REFERED TO SSM/02 11 6,PID DATA MONITOR TEST FTP,IAC,EVAPVM,FOLLOWED PINPOINT TEST,RECAL.
REFLASH		2977 CK FOR STALL WHEN DRIVING WARR RAN WDS TESTING NO CODES REPROGRAMMED PCM REMOVED AND CLEARED PCM GROUNDS CK EDC RELAY TEST DROVE
TSB		3054 WARR CHECKED FOR STALLED WHEN DRIVING. RESTARTED FINE. RAN FOR SSMS OR TSBS. FOUND SSM 15429 CHECKED HISTORY AND FOUND THE SSM TO HAVE ALREADY BEEN PERFORMED. CALLED HOTLINE. OASIS ID SSS 193

ENSOR AND RERUN EEC TEST	CK ENG STALLS WHILE DRIVING DOWN HILL & BRAKING, GIVE NO WARNING, RESTARTSOK, ON NORMAL OPERATING TEMP.
	CHECK ENGINE OWNER STATES STALLS WHILE DRIVING THE ENGINE WILL TURN OFF AFTER WILL NOT CRANK OR WILL START RIGHT UP.
SSOR RESET KEEP ALIVE MEMORY RETESTED ROAD TESTED	VEHICLE HAS DIED ONCE, AT TIMES RUNS ROUGH, JERKS, HESITATES
	CUSTOMER STATES THAT WHEN DRIVING VEH IT WILL JUST SHUT OFF
	D21 CUST STS ENG STALLS AT IDLE AT TIMES
	D21 CUST ST ENG HESITATES AND AT TIMES TRIES TO STALL WHEN ACCELERATED
PUMP. PROBLEM PERSISTING. CALL HOTLINE, CHECK GROUNDON DIFFE WIRE. FOUND BAD GROUND AND REPAIR. PROBLEM STILL PERSIST. CHECK GROUNDS 100,101,104, 105. ALL OK. REPLAC AC CONTROL BRACKET AS INSTRUCTED BY	UNIT DYING AT TIMES
	RECHECK FOR CUTTING OFF ON ACCELERATION, ADVISE
STALL 9991 S20	D21 CK INT STALLS WHILE DRIVING MORESO AROUND CORNERS ADVISE
	ENGINE STALLED WHILE DRIVING,STARTED BACK UP,CK ENGINE LIGHT IS NOW ON
	CUSTOMER STATES CAR STALLS ON DECELERATION OR COMING TO A STOP
	THE ENGINE WILL QUIT WHILE DRIVING STARTS RIGHT BACK UP
	STALLS OUT AT TIMES WILL RESTART OK HAS STALLED ONCE SINCE LAST REPAIR
ST	D21 CUST. STATES ENGINE LOSES POWER WHILE DRIVING AND DIES HAS TO WAIT TO RESTART AFTER COOL DOWN DOWN
	CK CUST STATES VEHICLE STALLS DRIVING DOWN THE ROAD
	CK ENGINE CUTS OFF ON ACCELERATOR
	D21 ENGINE STALLS AT STOPS, AT TIMES.
	ENGINE WILL NOT IDLE
	CUST STATES THE ENGINE STALLED WHILE DRIVING HWY SPEEDS ENGINE RESTARTED
	D02 ENGINE STALLS AT TIMES WHEN DRIVING, WILL RESTART OK, ADVISE
	CUST STATES THAT WHILE DRIVING THE OIL LIGHT AND BATTERY LIGHT CAME ON AND THE VEH BECAME HARD TO STEER AND THE VEH QUIT RUNNING VEH DID RESTART (TOW IN)
759. WAS TOLD TO REFLASH THE PCM TO CAL CODE 3L8A 12A650 AD, DOWN LOADED THE CALIBRATION TO THE WDS VIA SATTALITE. REFLASHED THE PCM PER HOTLINE AND THEN ROADTESTED 19 MILES, OK	CUST STATES THE VEH WAS DRIVEN APPR. 20 MILES TO WORK THEN AFTER WORK APPRX. 2 3 MILES AND THE VEH

2002	8763	S11	1FMYU03172KB65140	3.0L	T/LD	12	2001	2.00E+05	9F715	D21		4	1966666	3000	WHILE DRIVING
2002	8764	S11	1FMYU03172KB63889	3.0L	T/LD	12	2001	2904	12A650	D21		3	2365721	9000	WHILE DRIVING
2002	8765	S11	1FMYU03172KB66697	3.0L	T/LD	12	2001	2.00E+05	9F715	D21		5	1466166	6000	AT STOP
2002	8766	S11	1FMYU03172KB65186	3.0L	T/LD	12	2001	2904	12A650	D21		6	2447227	10000	AT STOP
2002	8784	S11	1FMYU03172KB54887	3.0L	T/LD	12	2001	2904	12A650	D21		2	1276666	3000	STALLS
2002	8767	S11	1FMYU03172KB54171	3.0L	T/LD	12	2001	2905	RECAL	D21		7	2437766	10000	AT STOP
2002	8774	S11	1FMYU03172KB46544	3.0L	T/LD	12	2001	2904	12A650	D21		3	873166	4000	WHILE DRIVING
2002	8782	S11	1FMYU03172KB67645	3.0L	T/LD	11	2001	2905	RECALEM	D21		4	899487	6000	WHILE DRIVING
2002	8768	S11	1FMYU03172KB50666	3.0L	T/LD	11	2001	2.00E+05	9F665	D21		5	1666402	7000	NO START
2002	8788	S11	1FMYU03172KB50534	3.0L	T/LD	11	2001	2905	RECALEM	D21		6	1299999	8000	WHILE DRIVING
2002	8790	S11	1FMYU03172KB20663	3.0L	T/LD	11	2001	2904	12A650	D21		3	754957	1000	WHILE DRIVING
2002	8800	S11	1FMYU03172KB16942	3.0L	T/LD	10	2001	2.00E+05	9F715	D21		10	2114666	11000	STALLS
2002	8805	S11	1FMYU03172KB14678	3.0L	T/LD	10	2001	2.00E+05	9F715	D21		1	410937	1000	DOWNHILL
2002	8812	S11	1FMYU03172KB12809	3.0L	T/LD	10	2001	7C05	14N089	D21		3	631099	3000	WHILE DRIVING
2002	8816	S11	1FMYU03172KB06642	3.0L	T/LD	11	2001	1H09	6J460	D21		6	2075860	9000	WHILE DRIVING
2002	8820	S11	1FMYU03172KB03257	3.0L	T/LD	11	2001	2904	DIAG	D21		10	2269731	13000	WHILE DRIVING
2002	8821	S11	1FMYU03172KB05267	3.0L	T/LD	11	2001	2905	RECALEM	D21		4	820566	5000	COASTING
2002	8826	S11	1FMYU03172KB02066	3.0L	T/LD	10	2001	2905	RECAL	D21		8	1166044	11000	WHILE DRIVING
2002	8830	S11	1FMYU03172KB01177	3.0L	T/LD	10	2001	7C05	14N089	D21		3	559875	6000	WHILE DRIVING
2002	8836	S11	1FMYU03172KB00174	3.0L	T/LD	10	2001	2.00E+05	9660	D21		4	776970	9000	WHILE DRIVING
2002	8836	S11	1FMYU03172KB00174	3.0L	T/LD	10	2001	7902	14401	D21		9	1957670	6000	WHILE DRIVING
2002	8842	S11	1FMYU03172KA92805	3.0L	T/LD	10	2001	2.00E+05	9F715	D21		8	2311170	7000	WHILE DRIVING
2002	8843	S11	1FMYU03172KA92769	3.0L	T/LD	10	2001	2905	RECALEM	D21		5	994205	4000	WHILE DRIVING
2002	8844	S11	1FMYU03172KA92432	3.0L	T/LD	10	2001	2904	12A650	D21		6	1291662	8000	WHILE DRIVING
2002	8857	S11	1FMYU03172KA79160	3.0L	T/LD	10	2001	2.00E+05	9F715	D21		8	1685386	13000	STALLS
2002	8858	S11	1FMYU03172KA79097	3.0L	T/LD	10	2001	2904	12A650	D21		9	1460363	8000	WHILE DRIVING
2002	8864	S11	1FMYU03172KA71453	3.0L	T/LD	10	2001	2905	RECAL	D21		9	1826201	4000	WHILE DRIVING

REPLACED		3031 9F715, ART 02 11 8,42 WF VERIFIED CUST COMPLAINT, CONNECTED NGS RUN EEC TEST, PREFORMED MONITOR ROAD TEST & CKED PIDS PREFORMED ART 02 11 8,CONNECTED NGS & FOLLOWED ARTICLE, REPLACED IAC
REFLASH		9903 REQAL REPROGRAMMED THE P.C.M.,RETEST O.K.
DIAG		EEC & NGS TEST
TSB		EEC TEST MONITOR TEST PERFORM TSB 02 11 06 REPROGRAM PCM CLEANED THROTTLE PLATES RETEST AND ROAD AND INSTALLED MODIFICATION DECAL#1401000000000000015492000000000000015492
DIAG		CUTTING OFF CONCERN EEC (QUICK TEST) DIAGNOSIS
TSB		RUN EEC TEST ALL PASS CODES,MONITOR PIDS AND REPROGRAMMED PCM PER TSB 02.11.8,ROAD TEST
REFLASH		INOP REPROGRAM PCM EEC (QUICK TEST) DIAGNOSIS
SSM		PERFORM EEC TEST SEE8 DIAGNOSIS POWER BALANCE AND SPARK DURATION TEST REPROGRAM PROCESSOR PER SSM 15599
REPLACED		TECH 169 VERIFY CONCERN EEC TEST REPALCE STICKING IAC AND THROTTLE BODY RECHECK OK
INOP		INOP EEC (QUICK TEST) DIAGNOSIS
SSM		ROAD TEST VEHICLE, PERFORM EEC SELF TEST AND PID DATA MONITOR, SYSTEM PASS. RUN OASIS WITH CODE 607000, FOUND SPECIAL SERVICE MESSAGE 15599, PROGRAM PCM, USE SHOP AIR TO BLOW AIR THROUGH VENT LINE
REFLASH		PERFORM EEC TEST, NO CODES PRESENT. MONITOR PID S AND CK OVER. REPLACED IDLE AIR CONTROL VALVE AND REPROGRAM PCM. RETEST AND DRIVE
SSM		1647 9F715 42 12990D, .2 D45, .3 D60, .1 D81, .5 D65, .3 DX1, .1 D9, .1 MT, 14N069, .2 14200A, .4 TEST EEC KOEO PASS KOEC PASS KOER PASS PINPOINT TEST ,MONITOR IMG FOR INTERMITTENT STALL,CK OASIS A
REFLASH		VERIFY CONCERN EEC TEST NO CODES DCL MONITOR ROAD TEST PIN TEST REPL EEC RELAY REPROGRAM PCM AND ROAD TEST
REPLACED		D21 42 2F1Z 8J461 AA W.D.S TEST REPLACE D.P.F.E SENSOR AND REPROGRAM PROCESSOR & RETEST SYSTEM
TSB		WDS HOOK UP, EEC SELF TEST, KOEO, KOER, PASS. DATA LOGGER RECORD MONITOR, TEST FUEL PRESSURE, LET IDLE FOR EXTENTED PERIOD OF TIME. ROADTEST WITH WDS MONITOR PIDS TSB 2 11 06 HAS LATEST CALIBRATION, N
REFLASH		WDS, EEC, PID MONITOR, COMPRESSION TEST, POWER BALANCE SPARK DURATION, FUEL PRESSURE, INJECTOR FLOW, PIN POINT, REPROGRAM PCM, RETEST, ROAD TEST
NO TEXT		
TSB		EEC TEST VEH FOUND NO CODES,CK TSBS FOUND SSM#16434 REPL EEC POWER RELAY,TEST DROVE VEH AND RETESTS SYST ALL OK
NPT		EEC TEST KOEC PASS KOER PASS KOEO PASS TEST DRIVE ROAD MONITOR TEST COULD NOT DUPLICATE PROBLEM AT THIS TIME
TSB		EEC TEST NOT DTC PAN OASIS PERFORMED TSB 02 11 61 DLC DISPLAY NGS RECORDER MONITOR TEST DRIVE PCM REPROGRAM CHECK EEC RELATY REMOVED WEIGHT FROM KEY RING RETEST DRIVE OKAY
REFLASH		CC990 REPROGRAMMED PCM & REPLACED IAC
SSM		4992 RECALEM 42 12990D,D60,D81,D65,DX1 EEC V DIAG;KOEO P1111 KOEC P1111 KOER P1111 DCL DISPLAY,PID MONITOR AND ROAD TEST,REPROGRAM THE PCM TO THE UPDATED CALIBRATION PER SSM#1599 SUCK EEC RELAY O
NO TEXT		
DIAG		IAC VALVE EEC (QUICK TEST) DIAGNOSIS
REFLASH		REPROGRAM PCM
TSB		4995 REPAIR VEHICLE PER TSB 02 8 8L

MOTOR & REPROGRAMED PCM WITH WDS & VERIFIED REPAIR.	D21 CUST STATES ENGINE FALLS DEAD WHEN DRIVING 40 45 MPH CK AND REPORT
	STALLS WHILE DRIVING INT...40 MPH...HAPPENED TWICE
	VEHICLE DIES AT STOPS
	OWNER STATES RUNNING STALLING AT STOPS
	CUST.REPORTS ENG CUTS OFF AT TIMES,ADVISE IF NEEDED
	DIED ONCE AT A STOP
	CUST STATES CUT WHILE DRIVING
	VEHICLE CUTS OFF WHILE DRIVING
	CAR TOWED TO THE SHOP NO START WILL CALL FOR MORE DETAILS
	CUSTOMER STATES ENGINE QUIT WHILE DRIVING HAPPENED ONE TIME EASY RESTARTA C ON QUIT LIKE THE KEY WAS TURNED OFF
FROM CHECK VALVE SIDE. REPROGRAM PCM AS PER SPECIAL SERVICE MESSAGE 16599. ATTACH LABEL TO HOOD AND ROAD TEST VEHICLE TO VERIFY REPAIR.	CHECK ENGINE STALLS WHEN DRIVING
	TOWED IN, QUIT RUNNING BUT WONT RESTART
NO REPLACED IAC MOTOR AND EEC POWER RELAY PER SSM 15434,RECOMMENDS IF NO CODES AND CONCERN NOT VERIFIED TO REPLACE IAC MOTOR ,POWER RELAY AND INSPECT GROUNDS AT G 101,G104,G105,G100 LOOM	D21 ENGINE STALLED GOING DOWN HILL WITH FULL TANK OF GAS
	CUST STATES WHILE DRIVING VEHICLE DIES AND ALL GAUGE LIGHTS COME ON AND HAD TO PULL OFF ROAD AND RESTART VEHICLE..
	WHILE DRIVING THE VEHICLE CUTS OUT ABOUT A 10 MINUTE DRIVE ALL DASH LIGHTS CAME ON RESTARTED WITH NO DIFFICULTY
O PROBLEM FOUND.	CK ENGINE FOR STALLING OUT WHILE DRIVING SLOW SPEEDS D1
	CK FOR ENGINE STALLS AT TIMES WHEN AT SLOW SPEEDS D21
	CK FOR VEH CUT OFF DRIVING,VEH WAS ACCELERATING OUT OF A TURN WHEN ENG CUT OFF @FOOT WAS ON ACCEL PE
	CHECK WHILE DRIVING ENGINE JUST STALLED DID RESTART
	CUST STATES VEHICLE DIED WHILE GETTING ON TO HIGHWAY, HAD TO RESTART, ALSO DIES WHEN DRIVING LESS THAN 20 MPH IN PARK GARAGE, ACCELERATES THEN OK
	CHECK ENGINE FOR STALLING WHEN DRIVING, CUST. HAS TO RESTART ENGINE WITH KEY WHEN THIS HAPPENS
	CUST STATES VEH WILL STALL GOING DOWN HILL AND DRIVING ON FREEWAY VEH NEEDS TO BE WARMED UP
K,RETEST ALL OK AT THIS TIME: NKOEO P1000 KOEC P1000 KOER P1000 R T 6 MILES	QCP D21 VEH STALLED OUT AFTER 20 MINS OF DRIVING AND 2 MINS BEFORE IT STARTED UP AGAIN
	RPR VEHICLE STALLED AT 40 MPH WHEN DRIVING , ALSOWHEN PUTTING IT IN REVERSE THEN STOPPED PUT
	CUSTOMER STATES OK, ENGINE STALLS AT TIMES
	CUSTOMER STATES WHILE DRIVING CAR WILL CUT OFF
	CHECK FOR INTERM. STALL WHILE DRIVING SEE FORD TSB

2002	8868	S11	1FMYU03172KA70418	3.0L	T/LD	10	2001	2G05	RECALEM	D21	5	1067771	6000	WHILE DRIVING
2002	8869	S11	1FMYU03172KA70254	3.0L	T/LD	10	2001	2G05	RECAL	D21	8	1561762	6000	ON HIGHWAY
2002	8874	S11	1FMYU03172KA69492	3.0L	T/LD	10	2001	7C05	14N069	D21	5	727157	7000	WHILE DRIVING
2002	8875	S11	1FMYU03172KA69217	3.0L	T/LD	10	2001	2.00E+03	9F715	D21	8	1434851	11000	TURNING
2002	8881	S11	1FMYU03172KA69777	3.0L	T/LD	10	2001	2G04	12A650	D21	7	1166226	7000	WHILE DRIVING
2002	8882	S11	1FMYU03172KA69459	3.0L	T/LD	10	2001	2G04	DIAG	D21	7	1245446	6000	AT STOP
2002	8884	S11	1FMYU03172KA69097	3.0L	T/LD	9	2001	2G04	12A650	D21	9	1676803	7000	WHILE DRIVING
2002	8885	S11	1FMYU03172KA68918	3.0L	T/LD	10	2001	2B01	6C315	D21	5	1034315	3000	WHILE DRIVING
2002	8886	S11	1FMYU03172KA68918	3.0L	T/LD	10	2001	2B01	6C315	D21	10	2113406	5000	ACCELERATING
2002	8905	S11	1FMYU03172KA52936	3.0L	T/LD	9	2001	2G05	RECAL	D21	9	1563481	6000	WHILE DRIVING
2002	8912	S11	1FMYU03172KA51466	3.0L	T/LD	9	2001	2.00E+03	9F715	D21	10	2148534	13000	ACCELERATING
2002	8915	S11	1FMYU03172KA50566	3.0L	T/LD	9	2001	7C05	14N069	D21	2	383403	2000	WHILE DRIVING
2002	8926	S11	1FMYU03172KA46581	3.0L	T/LD	9	2001	2G02	12B679	D21	10	2098857	7000	WHILE DRIVING
2002	8927	S11	1FMYU03172KA46502	3.0L	T/LD	9	2001	2G05	RECALEM	D21	11	2113435	15000	WHILE DRIVING
2002	8935	S11	1FMYU03172KA44895	3.0L	T/LD	9	2001	2G05	RECALEM	D21	5	670382	5000	WHILE DRIVING
2002	8946	S11	1FMYU03172KA40069	3.0L	T/LD	9	2001	7C05	14N069	D21	4	550284	5000	DOWNHILL
2002	8948	S11	1FMYU03172KA39589	3.0L	T/LD	9	2001	2.00E+04	9C915	D21	11	2412193	12000	WHILE DRIVING
2002	8949	S11	1FMYU03172KA39409	3.0L	T/LD	9	2001	2G05	RECAL	D21	8	1508013	5000	WHILE DRIVING
2002	8955	S11	1FMYU03172KA38071	3.0L	T/LD	9	2001	2C01	11002	D21	1	280607	0	WHILE DRIVING
2002	8960	S11	1FMYU03172KA37092	3.0L	T/LD	9	2001	2.00E+03	9E895	D21	12	2418997	23000	STALLS
2002	8972	S11	1FMYU03172KA36369	3.0L	T/LD	9	2001	2G05	RECALEM	D21	8	1484048	8000	HARD START
2002	8977	S11	1FMYU03172KA29921	3.0L	T/LD	8	2001	2.00E+03	9F715	D21	3	436548	4000	WHILE DRIVING
2002	8988	S11	1FMYU03172KA26173	3.0L	T/LD	8	2001	2G01	12A650	D21	7	1127148	4000	WHILE DRIVING

DIAG		PCM OUT OF RANGE EEC (QUICK TEST) DIAGNOSIS
REFLASH		D21 SELF TESTED EEC SYSTEM NO FAULTS FOUND ROAD TESTED W WCIDS UNABLE TO DUPLICATE CONCERN. REPROGRAMMED PCM WITH LATEST CALIBRATI ON AND RETESTED
SSM		SERVICE MESSAGE 16589. PERFORMED EEC TEST. P1111. CHECKED FUEL PRESSURE. PERFORMED SSM 16589. REPROGRAMMED PCM. REPLACED EEC POWER RELAY.
TSB		EEC TEST NO CODES) MONITOR RD TEST MONITOR PIDS IN BAY REPL IAC VALVE REPROGRAM PCM INSPECT EEC RELAY TIEROAD TEST 1.8 HRS PER FORD TSB 02 06 06 TO REPAIR STALLS AT SLOW SPEEDS & WHEN TURNING
DIAG		W TIME TIME FOR ABNORMAL DIAGNOSIS
TSB		6387 EEC TESTS AND CHECK FUEL PRESSURE AND MONITOR PIDS NO CODES AND PERFORMED TSB 02 9 6 AND CHECKED IAC DUTY CYCLE PERCTAGE (WITHIN SPECIFIED RANGE) AND REPROGRAMMED PCM TEST DRIVE AND RETEST B.
TSB		7912 12660 .2 D45 .3 D55 .9 D80 .1 D84 .2 6360B .9 9000D .4 TOTAL 1.8 NGS DIAG KOEO PASS KOEC PASS KOER PASS. DCL D85 PLAY, IGN DIAG, AND FP ALL OK. PINPOINT TEST PO LLOWED TSB 02 11 6 IAC, VMV,
REPLACED		1 NGS DIAGNOSIS. NO CODES. PINPOINT TEST. FOUND CRANK POSITION SENSOR NOT RESPONDING AT TIMES. PID DATA
REPLACED		1 EEC TESTED, PINPOINT TESTED, PERFORMED DCL MONITOR RECORDER TESTS, TESTED FUEL PRESSURE AND IGNITION SYSTEM, REPLACED
TSB		5580 ENG STALL W TEST DROVE TO TRY TO VERIFY CONCERN. COULD NOT DUPLICATE. LOOKED UP ON OASIS AND FOUND A TSB # 02 11 06. WE DIDNT HAVE IT YET SO HAD TO CALL H OTLINE AND WAIT FOR THEM TO FAX ME O
REFLASH		OUT OF SPEC CK WDS TEST CK EEC PASS CODES CK DATA LOGG PIDS. REPLACE OUT OF SPEC IAC FLASH PCM ROAD TEST SEEMS OK AT THIS TIME
REPLACED		2945 BAD EEC RELAY TEST DRIVE,HOOK UP NGS,EEC TEST NO CODES, PERFORM PINPOINT TESTS,CK OASIS,CK ALL GROUNDS AND G270B,270C,270D,AND G270E,TIGHTEN PINS TO EEC RELAY,REPLACE RELAY,REDRIVE,OKAY
DIAG		EEC TEST NO CODES RECIEVED PASS TEST FUEL PRESS WITH GAUGE 40PSI PASS NGS MONITOR TEST CK VPWR 13.2 PASS PINPOINT
TSB		RECAL PCM PER TSB 2 11 5
REFLASH		FAULTY PCM PROGRAMMING (1950) PASS PERFORMED EEC,NGS AND PINPOINT TESTS AND REPROGRAMMED PCM
SSM		RD TEST AND NGS SYSTEM ALL IN SPECS REPL EEC RELAY INSPECT CONNECTOR C1016 AND PIN AT EEC RELAY R R BATT AND TRAY INSPECT GROUND G101 G100 AND IAC CK CONN C270B C270C C270D C270E ALL ARE OK PER SSM 16
TSB		EEC TEST PASS RUN OASIS TSB 021105 PID DATA MONITOR ROAD TEST DIAG IAC OUT OF SPEC REPLACE MT TO PID DATA RECORD ROAD TEST 2ND TIME REPROGRAMPCM R R TBODY AND VAPOR MGMNT VALVE RETEST
TSB		CK EEC DIAG KOEO KOER CONT MEMORY CK PIDS MONITOR AND RECORD PINPOINT TEST CK OASIS FOR SSM AND TSB PERFORM TSB 2 11 6
REPLACED		224 LOCKED UP 3.2 HRS CK WOULD CLICK AND NOT TURN OVER. CK REPLACE SHORTED OUT STARTER. RETEST ENGINE SPIN OVER BUT MAKING NOISE AND THEN LOCKED UP. CONTACT HOTLINE ADVISE TO R R SPARK PLUGS AND CK C
REFLASH		WDS HOOK UP, SELF TEST, PINPOINT TEST, FUEL PRESSURE TEST, DCL DISPLAY, REPL IAC, REPL THROTTLE BODY, REPL POWER RELAY, REPROGRAM PCM, RETEST REPAIR VERIFIED.
INOP		OUT OF SPECS EEC (QUICK TEST) DIAGNOSIS
REPLACED		TEST DROVE UNABLE TO DUPLICATE PERFORM WDS REPLACEIAC AND EEC RELAY PER SPECIAL SERVICE MESSAGE
REPLACED		WDS TEST NO CODES FUEL PRESS TEST PASS POWER BAL TEST PASS REPROGRAM PCM AND REPLACE EEC POWER RELAY RETEST AND TEST

	CHECK ENGINE HAS DIED 3 TIMES WHEN DRIVING HWY SPEEDS STARTS TO RUN ROUGH THEN STALLS OUT RESTART
	D21 CHECK CUSTOMER STATES THAT VEHICLE DIED OUT WHILE COMING OFF FREEWAY. VEH RESTARTED AND DROVE OK.
	CUSTOMER STATES: VEHICLE DIES WHILE DRIVING, ALL WARNING LIGHTS COME ON AT THIS TIME
	CHECK FOR INTERM. STALL AT SLOW SPEEDS OR TURNING
	CS THE TRUCK DIES WHEN DRIVING, STARTS RIGHT BACK UP. ADVISE
L	CHECK IDLE DIPS AND ENGINE DIES AT STOPS.
AND EEC RELAY TEST OK. RAN EVAP TEST TO TEST CHECK VALVE AND VMV O K. REPROGRAMMED PCM PER TSB.	D21 CUST SAYS THE VEHICLE DIED OUT WHILE DRIVING CUST LET VEHICLE SETT FOR ABOUT 30 SECONDS AND THE VEHICLE STARTED BACK UP.
	ENGINE STALLED ONE TIME WHEN DRIVING. DID RESTART. HAVE HAD TROUBLE STARTING AT TIMES, HAVE TO TRY 2 3 TIMES TO GET
	CUSTOMER STATES ENGINE WILL NOT START AT TIMES HAS TO DEPRESS ACCELL PEDAL TO START
VER A COPY. PERFORMED SELF TEST AND NO CODES AND THEN MONITORED PIDS AS TOLD IN TSB. THE IAC WAS AT 37. 5% WHICH IS O.K. TOLD TO REPROGRAM PCM. SO I DID AND THEN TEST DROVE. RERAN SELF	CUST STATE S ENG STALLS WHILE DRIVING OR AT STOP....WARMED UP....DOES RESTART
	CUST STATES VEHICLE HESITATES WHEN ACCELERATING AFTER SLOWING TO TURN OR YIELD, CAN HAPPEN COLD OR WARM..D21
	THE VEH IS STALLING BETWEEN 0 35 MPH. THE CUST DROVE BETWEEN 6 8 MILES WHEN STALLING HAPPENS.CUST LOST POWER EXCEPT FOR RADIO ON BOTH OCCURANCES.
	ENGINE STALLED WHILE DRIVING,STARTED RIGHT BACK UP
	CUSTOMER STATES VEH CUT OFF WHILE DRIVING 2X
	WHILE DRIVING CUSTOMER STATES THAT THE EMMISIONS AND OIL LIGHT COME ON. AFTER THAT THE ENGINE STALLED. RESTARTED
434	D21 ENG STALLED AT APPX 35 MPH COASTING DOWN HILL RESTART ED O.K.
	ADVISE CUST STATES VEH STALLS WHILE DRIVING VEH WILL START BACK UP
	CK STALLED WHILE DRIVING
OMPRE OR TO INSPECT INSIDE CYCLINDER WITH BORE SCOPE, FOUND #5 CYCLINDER SPARK PLUG COMPLETELY DAMAGE BY PISTON.RECONTACT HOTLINE TALED TO BLAINE H. AND WILL SEND COMPLETED ENGINE	CUSTOMER STATES ENGINE DIED WHILE DRIVING (SMOKE COMES FROM RIGHT FIREWALL WHEN IGNITION KEY IS TURNED
	C S STALLS WHEN MAKING RIGHT TURN. INTERMITTENT
	O R WILL STALL AFTER STARTING , AND HAVE A HARD TIME STARTING
	CHECK OUT WHY WHEN DRIVING TRUCK WILL STALL WILL RESTART BEAMS TO BE WHEN RAINING NOTE WHILE DRIVING
	CUST STATES ENG HAS STALLED OUT SEVERAL TIMES WHILE DRIVING

2002	8998	S11	1FMYU03172KA17588	3.0L	TALD	6	2001	2.00E+03	9F715	D01	9	1454199	10000	DECELL
2002	8999	S11	1FMYU03172KA17588	3.0L	TALD	6	2001	1H03	9J460	D21	11	1883782	12000	WHILE DRIVING
2002	9013	S11	1FMYU03172KA15109	3.0L	TALD	6	2001	2G04	12A650	D21	8	1172544	11000	COASTING
2002	9014	S11	1FMYU03172KA15109	3.0L	TALD	6	2001	2.00E+04	9F845	D21	8	1675119	10000	WHILE DRIVING
2002	9028	S11	1FMYU03172KA06509	3.0L	TALD	6	2001	2G04	12A650	D21	5	624618	10000	ON HIGHWAY
2002	9030	S11	1FMYU03172KA06239	3.0L	TALD	6	2001	7C05	14N069	D21	5	764337	8000	WHILE DRIVING
2002	9049	S11	1FMYU03162KD65571	3.0L	TALD	5	2002	2G04	12A650	D21	2	2397213	0	STALLS
2002	9054	S11	1FMYU03162KD65951	3.0L	TALD	5	2002	2F02	9E926	D21	1	1933882	0	WHILE DRIVING
2002	9055	S11	1FMYU03162KD65951	3.0L	TALD	5	2002	2.00E+03	9F715	D21	2	2340766	1000	WHILE DRIVING
2002	9057	S11	1FMYU03162KD63549	3.0L	TALD	5	2002	2.00E+03	9F715	D21	1	2220842	1000	WHILE DRIVING
2002	9061	S11	1FMYU03162KD41289	3.0L	TALD	4	2002	2G02	12E579	D21	0	1318852	0	STALLS
2002	9069	S11	1FMYU03162KD39317	3.0L	TALD	4	2002	2.00E+03	9F715	D21	1	2436869	1000	NO TEXT
2002	9072	S11	1FMYU03162KC69895	3.0L	TALD	3	2002	2F01	DRIVE	D21	1	1293864	1000	DOWNHILL
2002	9076	S11	1FMYU03162KC69901	3.0L	TALD	3	2002	2.00E+03	9F715	D21	2	2126417	5000	TURNING
2002	9077	S11	1FMYU03162KC69901	3.0L	TALD	3	2002	7C05	14N069	D21	1	2039711	2000	AT STOP
2002	9078	S11	1FMYU03162KC62560	3.0L	TALD	3	2002	3M11	7153	D21	3	1883389	4000	AT STOP
2002	9088	S11	1FMYU03162KC61857	3.0L	TALD	2	2002	2.00E+03	9F715	D21	1	2169449	0	WHILE DRIVING
2002	9091	S11	1FMYU03162KC60462	3.0L	TALD	2	2002	2F02	9E926	D21	1	1150761	2000	WHILE DRIVING
2002	9096	S11	1FMYU03162KC48955	3.0L	TALD	2	2002	2G02	12E579	D21	1	941094	0	DOWNHILL
2002	9098	S11	1FMYU03162KC47269	3.0L	TALD	2	2002	2.00E+03	9F715	D21	3	1418815	1000	AT IDLE
2002	9100	S11	1FMYU03162KC41124	3.0L	TALD	2	2002	2.00E+03	9E926	D21	1	1175770	0	WHILE BRAKING
2002	9104	S11	1FMYU03162KC37478	3.0L	TALD	2	2002	2E01	12A650	D21	0	1435079	0	WHILE DRIVING
2002	9107	S11	1FMYU03162KC30627	3.0L	TALD	2	2002	2G04	DIAG	D21	4	1706315	8000	WHILE DRIVING

TSB		10990 ROAD TEST FOR CAR STALLS ON DIECEL COULD NOT VERIFY PERFORMED EEC TEST NO CODES FOUND CHECK SERVICE MESSAGES FOUND TSB 02 s 6 MONITORED PIDS WITH WDS PERFORMED ALL STEP IN TSB REPLACED IAC RBM
NPT*		12972 ROAD TEST FOR VEH STALLING WHILE DRIVING COULD NOT VERIFY PERFORMED EEC TEST FOR CODES NO CODES FOUND CHECK FUEL PSI NO PROBLEM FOUND CHECK SERVICE MESSAGES PERFORMED TEST FOR PERFORMANCE WHI
SSM		ROADTESTED VEHICLE EXTENSIVELY AND COUND NOT DUPLICATE THE STALLING. TESTED VEHICLE ON THE WDS PASS CODES. CALLED FORD ENGINEERING, PERFORMED TEST SUGGESTED BY FORD, 1) WIGGLE IGNITION KEY 2) DISCONNEC
REPLACED		INSTALLED WDS AND FOUND CODES P0171 AND 174, AND P0455. CAR RUNNING LEAN, PINPOINT TESTED. R&R GAS TANKS SECURED EVAP LINES AND TESTED WITH WDS. RAN PIDS AND VEHICLE WITH SPECS. ROADTESTED OK.
REFLASH		VERIFY CUSTOMER COMPLAINT. PERFORMED EEC DIAG PASSED, PERFORMED MANUAL FUEL PRESSURE PASSED. PERFORMED IGNITION UPDATE THE WDS TO THE CURRENT CALIBRATION CODE AND THAN RE CALIBRATE THE PCM. ROAD TEST
SSM		PERFORMED EEC, PINPOINT TESTS NO CODES PRESENT,(MT)PER SSM 15434 REPLACED PCM POWER RELAY, PER SSM 9474 REPROGRAM PCM TO LATEST CALIBRATION
NPF		DRIVE, UNABLE TO VERIFY CONCERN
ADJUST		EEC TEST WDS MONITER TEST ADJ HARD IDLE
REPLACED		EEC TEST WDS RECORD AND MONITOR TEST PINPOINT TEST REMOVE AN REPLACE IAC VALVE RETEST
STICKING		DIAGNOSED AND FOUND IAC AND VMV NOT CLOSING ALL THE WAY IAC NOT WITHIN SPEC, REPLACED IAC, MOTOR AND TEST OK
TSB		295 129679 42 WDS HOOK UP NO LIGHT KOEO PASS DATALOGGER POWER BAL FUEL PRESSURE TEST AND INJECTOR FLOW TEST. IGNITION TEST PINPOINT TEST PERFORM TSB 02 s 6 DIAGNOSTIC ROUTINE. R&R FUEL TANK TO CK
NO TEXT		
SSM		EEX004 REPORT NUMBER. RELAY ALL SPECS TO ENGINE WAS ADVISED TO RESET BASE IDLE RESET IAC PERFORMED ADAPTIVE STRATEGY ROAD TEST AGSIN ALL ACCEPTABLE AT THIS TIME. IDLE SEEMS TO HOLD.
REFLASH		1 NGS START UP EEC TEST NO DTC PID MONITOR AND RECORD IGN SYST DIAG DCL DISPLAY REPROGRAM PCM PINPOINT TEST REPLACED
REFLASH		NGS START UP EEC TEST NO DTC PID MONITOR AND RECORD IGN SYST DIAG CHECK FUEL PRESSURE DCL DISPLAY REPROGRAM PCM PINPOINT
LEAK		LEAKING ELECTRONIC TRANSMISSION DIAGNOSIS DIAGNOSIS
UNOP		FAILED IAC VALVE EEC (QUICK TEST) DIAGNOSIS
TSB		2350 CODE 42 WP94 NGS TEST FOR CODES NONE RAN TSB AND SSM TSB SAID TO CK NUMBER ON PCM AND REPROGRAM THE PCM TO THE LATEST CAL HOOKED CAR UP TO WDS AND FOUND CAR HAS THE LATEST CAL AND I CK THE ECC
SSM		WDS EEC SELF TEST SYSTEM PASSED DATA LOGGER FUEL PRESSURE TEST ING SYS TEST RAN OASIS PERFORMED SSM 15549 PCM
NO TEXT		
TSB		RAN NGS, DCL TSTS NO FAULTS RAN OASIS DID TSB 02 s 6 REPL IAC, THROTTLAND PLM RELAY PER TST RESULTS IN STEPS RETST OK
DIAG		EEC (QUICK TEST) DIAGNOSIS
TSB		NO PROB FOUND EEC DIAG,DCL MONITOR,PINPT TST,SEE TSB 02 11 6 FOR INTERM ENG CUTS,TSB NOT AVAL YET,CALL HTLN,SPOKE WITH RAY MORRISON,HE FAXED ARTICLE 2 11 6,IN ADDITION BUGG CKING CONNS C270,C110,C139

ONITORED PIDS TO VERIFY REPAIR CC42 10694 ROAD TEST FOR CAR STALLS ON DECEL.	CUST STATES THE CAR STALLS ON DECEL. NO CK ENGINE LIGHT THE CAR DOES IT MORE OFTEN AFTER THE CUST PUTS GAS IN IT
LE DRIVING CHART #1 IN PCED FOUND DPFE NOT WORKING PROPERLY REPLACED DPFE SENSOR REMONITORED PIDS TO VERIFY REPAIR CC42	CUST STATES THE VEH IS STALLING WHILE DRIVING STALLED WHEN GOING UP HILL WITH FOOT ON ACCEL
T PCM AND INSPECT PINS, 3] MORE DETAIL FROM CUSTOMER, 4] TEST IDLE AIR CONTROL VALVE DUTY CONNECTORS, INSPECTED GROUNDS ROAD TESTED, COULD NOT DUPLICATE	CUSTOMER STATES CAR KEEPS CUTTING OFF, ALREADY WARMED UP AND AT A COAST SPEED VEH WOULD START RIGHT
	CHECK ENGINE INTERMITTEMLY SHUTS DOWN WHILE DRIVING
RETEST ALL O.K. A THIS TIME.	D21 ENGINE DIED AT HWY SPEEDS,PULLED OVER AND RESTARTED OK SPUTTERED ON ACCEL
	CHECK CUSTOMER STATED WHILE DRIVING CHECK OIL LITE, ENGINE LITE, CAME ON HARD TO STEP ON BRAKE PEDAL CAR STALLED OUT. COULD NOT RESTART NOW IT DOES
	CUTS OUT AND STALLED
	DIES WHILE DRIVING DOWN THE ROAD
	TRUCK DIED WHILE DRIVING DOWN THE ROAD.
	CUSTOMER STATES JUST BOUGHT, WHILE DRIVING ENGINE HAS JUST SHUT OFF TWICE FOR NO REASON, AS IF IGNIT
ALL EVAP LINES FOR OBSTRUCTION, NONE FOUND, TEST DROVE VEHICLE WITH WDS AND FOUND IAC DUTY CYCLE OUT OF SPEC, REPLACE IAC WITH NEW NUMBER PER TSB. ALSO FOUND MAF VOLTS TO LOW 0.5	D21 CUST STATES STALLS INTERMIT
	AFTER DRIVING 2 MILES WHEN COLD VEHICLE WILL STALL HAS HAPPENED TWICE COASTING DOWN HILL ON VIA VERDE
	REPEAT VISIT WITHIN 6 MONTHS OR 6,000 MILES VEH INTERMIT DIES GOING UP A HILL AND TURNING LEFT D21
	CUST STATES SLOWING AND TURNING LEFT VEH DIED AFTER STOPPED DID RESTART D21
	CUSTOMER STATES WHEN VEHICLE SITS AT A STOP IT STALLS, AND WHEN GAS PEDALIS DEPRESSED IT LAGGS
	CUSTOMER STATES WAS DRIVING DOWN THE ROAD AT ABOUT 45MPH AND THE ENGINE JUST DIED, PULLED OVER AND ENGINE RESTARTED
RELAY AND IT WAS THE NEW ONE! CALLED THE HOT LINE AND THEY SAID TO REMOVE THE THROTTLE BODY AND DRILL A .071 HOLE IN THE BUTTERFLY OF THE THROTTLE BODY AND SET THE TP SENSOR TO 1 VOLT	VEH STALLS while DRIVING DOWN ROAD
	CUST STATES THAT WAS DRIVING DOWN HILL AND ENGINE STALLED PULLED OVER STARTED BACK UP
	CRUDV IDLE IS ERRATIC & TRUCK WILL STALL12/12
	CST STATES HAD 1/2 TANK OF GAS SHE BRAKED HARD & VEH STALLED NO LIGHTS CAME ON VEH RESTARTED
	VEHICLE SHUT DOWN ON ROAD TOWED IN SEE FRANK K
AND CKING GROUND CONNS G150,G107,G104,G105 AND G300 WHICH MENT R I DRIVERS SEAT AND FLR CARPET TO ACCESS,COMPL TSB 2 11 8,INCL BLOWING SHOP AIR THRU VENT TUBE FOR POSS RESTRICTION SPIDERS,STEP #5 HAD	C S VEHICLE TURNED OFF WHILE DRIVING,WAS ABLE TO PULL OVER AND RESTART VEHICLE,NEED TO CHECK IT TURNING OFF

2002	9111	S11	1FMYU03162KC20099	3.0L	TALD	2	2002	2E04	12A650	D21	4	1760999	2000	WHILE DRIVING
2002	9112	S11	1FMYU03162KC20099	3.0L	TALD	2	2002	7V01	12A561	D21	5	2146319	2000	WHILE DRIVING
2002	9128	S11	1FMYU03162KC15722	3.0L	TALD	2	2002	2.90E+03	9F715	D21	4	2036512	5000	WHILE DRIVING
2002	9130	S11	1FMYU03162KC15123	3.0L	TALD	1	2002	2.00E+03	9F715	D21	7	2159494	19000	STALLS
2002	9135	S11	1FMYU03162KC10147	3.0L	TALD	1	2002	2G02	13B579	D21	2	1636865	1000	WHILE DRIVING
2002	9139	S11	1FMYU03162KC10116	3.0L	TALD	1	2002	2E05	RECAL	D21	1	867079	0	WHILE DRIVING
2002	9142	S11	1FMYU03162KC09518	3.0L	TALD	1	2002	7C05	14N669	D21	6	2089092	16000	AT IDLE
2002	9144	S11	1FMYU03162KC00782	3.0L	TALD	1	2002	2E04	12A650	D21	7	2220850	6000	WHILE BRAKING
2002	9148	S11	1FMYU03162KB97897	3.0L	TALD	1	2002	7C02	19A549	D21	3	2077627	2000	WHILE DRIVING
2002	9158	S11	1FMYU03162KB96157	3.0L	TALD	1	2002	2.00E+03	9F715	D21	5	1304638	3000	WHILE DRIVING
2002	9163	S11	1FMYU03162KB95782	3.0L	TALD	1	2002	2E04	12A650	D21	1	867064	0	WHILE DRIVING
2002	9180	S11	1FMYU03162KB95419	3.0L	TALD	1	2002	2E04	DIAG	D21	6	1669448	5000	WHILE DRIVING
2002	9186	S11	1FMYU03162KB75619	3.0L	TALD	12	2001	2E05	RECAL	D21	5	2389411	5000	WHILE DRIVING
2002	9171	S11	1FMYU03162KB67864	3.0L	TALD	12	2001	2E05	RECALEM	D21	2	911490	1000	WHILE DRIVING
2002	9172	S11	1FMYU03162KB66091	3.0L	TALD	12	2001	2.00E+03	9F715	D21	4	3378281	10000	WHILE BRAKING
2002	9176	S11	1FMYU03162KB65456	3.0L	TALD	12	2001	2E04	12A650	D21	4	1660704	4000	WHILE DRIVING
2002	9184	S11	1FMYU03162KB55151	3.0L	TALD	12	2001	2.00E+03	9F715	D21	5	1669274	6000	AT STOP
2002	9194	S11	1FMYU03162KB44117	3.0L	TALD	11	2001	2.00E+03	9F715	D21	5	1636425	3000	STALLS
2002	9195	S11	1FMYU03162KB39371	3.0L	TALD	12	2001	2.00E+03	9F705	D21	5	2275665	11000	WHILE BRAKING
2002	9196	S11	1FMYU03162KB39354	3.0L	TALD	12	2001	2G04	DIAG	D21	3	2417201	3000	WHILE DRIVING
2002	9197	S11	1FMYU03162KB34259	3.0L	TALD	12	2001	2G04	12A650	D21	2	676463	2000	WHILE DRIVING
2002	9200	S11	1FMYU03162KB30650	3.0L	TALD	12	2001	2.00E+04	9C215	D21	9	2139500	5000	WHILE DRIVING
2002	9201	S11	1FMYU03162KB30521	3.0L	TALD	12	2001	2G04	12A650	D21	2	972543	1000	WHILE DRIVING
2002	9202	S11	1FMYU03162KB30021	3.0L	TALD	12	2001	7V01	12A561	D21	4	2276431	2000	WHILE DRIVING
2002	9203	S11	1FMYU03162KB30007	3.0L	TALD	12	2001	2.00E+03	9E705	D21	5	1743555	3000	WHILE DRIVING
2002	9204	S11	1FMYU03162KB30007	3.0L	TALD	12	2001	2F02	9E705	D21	3	1900573	3000	ACCELERATING

REFLASH		2878 12A650 WDS KOEO P1000 MANUAL FUEL TEST 35 PSI ROAD TEST MONITOR IAC AIRFLOW & FUEL TRIM REPROGRAM PCM & RETEST P1000 CC42
DIAG		WRNG EEC (QUICK TEST) DIAGNOSIS
DIAG		EEC TEST TEST IGNITION AND FUEL MONITOR PIDS RESETIAC AND RETEST
TSB		PERFORMED TSB 02 11 6 CONFIRMED PROPER OPERATION INSTALLED IDLE AIR CONTROL VALVE TEST DRIOVE FOUND NO PROBLEMS 1
REPLACED		HOTLINE AT 10:15 AM AND TALKED WITH ADAM DEALLETE HE SAID IF ALL TESTS PASSED TO CHECK DPFE MASS AIRFLOW SENSOR PART NUMBERS BOTH NUMBERS WERE WRONG REMOVED REPLACED DPFE SENSOR AND MASS A
SSM		619 42 12A650 W 2928 KOEO TEST(P1000 P1000), RECORDER MONITOR TEST, PINPOINT TEST, REPROGRAM PCM PER SSM #15599, ROAD TEST. 12990D,D45,D81,D84.
TSB		15060 TSB02 11 06 VERIFIED ENG. STALL FOUND TSB02 11 06 FOLLOWED STEP 1,2,4,5,6REPLACED ECC RELAY STEP 7&8 ROAD TEST VEHICLE RUNS FINE NOW
TSB		CC 42 TSB 02 11 06 NGS DIAG,KOEO KOER AND CONT.PASSED,DCL DISPLAY,PID MONITOR AND RECORDER,SIMULATION TEST,DIAGNOSE AND CHECK OASIS
REFLASH		1 EEC TEST (PASS),ACCESS PIDS TO DIAG,FUEL PRESSURE TEST 35 65 PSI,OK, IGNITION SYSTEM TEST,GOOD PATTERN,OK,REPL FUEL RELAY TO UPDATE REPROGRAMMED PCM TO THE LATEST CALIBRATION UPDATE RDTST
TSB		3879 EEC V ON DEMAND SELF TEST PASSED @NO FAULT CODE SO PRESENT. MONITOR PID DATA, RAN DCL DISPLAY, RAN IGNITION SCOPE TEST, RAN FUEL PRESSURE TEST CHECKED OASIS AND FOUND TSB 02 09 06, FOR ABOVE
SSM		REPROGRAM PCM SSM 15599 CC 42 BASIC 12A650 1147 ROAD TEST VECHILE SEVERAL MILES AND VECHILE RAN NORMAL RUN WDS DIAG.CHECK FOR CODES ALL PASS CODES EVERY MODULE
NPF		EEC TEST NO CODES UNABLE TO VERIFY CUSTOMERS CONCERN
REFLASH		NGS DIAG. REPROGRAMED PCM PER TSB 02 11 6.
REFLASH		EEC TEST CODE PASS P P TEST CKED POWER RELAY AND REPROGRAM P ASPER OASIS BROADCAST MESSAGE 15599 RETEST OD RECAL
TSB		15599 TEST DRIVE VERIFY CONCERN, KOEO,KOER NO CODES PRESENT. REPLACE IAC AND REPROGRAM PER TSB 2 11 6
REFLASH		RAN TESTS. REPROGRAMMED PCM.
REPLACED		A TSB REPLACE AZRBYPASS VALVE
REPLACED		IDLE AIR CONTROL VALVE THROTTLE BODY AND VAPOR MGMT VALVE FAILURE RUN DIAGNOSTIC AND REMOVE AND REPLAE IAC VMV AND T.BODY RECHECK SYSTEM
REFLASH		CALIBRATION THROTTLE BODY VERIFIED CONCERN, TEST & DIAGNOSE, REC TO REPLACE THROTTLE BODY & IDLE AIR CONTROL VALVE, REPROGRAM PCM TO LATEST
DIAG		EEC V TEST KOEO PASS, KOEC PASS, KOER PASS, ROAD TESTED WITH NGS MONTORE PIDS
REFLASH		TECH 299 VERIFY CONCERN REPROGRAM PCM RECHECK OK
SSM		SELFTEST NO CODES TEST FUEL PRESSURE PINPT TEST MONITOR PIDS REFER TO SSM REPLACED EEC RELAY, IDC MOTOR RETEST REPLACED THROTTLE BODY AND RETEST ROADTEST REPLACE EVAPMANAGEMENT VALVE REPROGRAM PROCE
DIAG		KAM EEC (QUICK TEST) DIAGNOSIS
TSB		HOTLINE CONTACT NO. 516 411 472. THIS WAS FOR INSTRUCTIONS SENT TO US D ENGINEERING (ENGINEER SCOTT MOORHOUSE) THIS WAS INSTRUCTIONS ON THE ON GOING STALLING PROBLEM ON ESCAPES BEFORE THE ANNOUNCED TS
HOTLINE		EEC TEST HOTLINE ADVISED TO R&R IAC VALVE & THROTTLE BODY CHECK BATTERY JUNCTION BOX FOR GOOD CONNECTIONS..ALSO G104 G105 C110 C113...REF RO 128035
ADJUST		EECTEST, RESET HARDSTOP, ROADTEST & RETEST PER FORD DSE

	D21 SNSP FOR ENGINE QUIT WHILE DRIVING CONCERN SEE HIST IN PACKAGE & CABS
	CUST STATES ENGINE QUIT WHILE DRIVING
	WHILE DRIVING YESTERDAY,VEH STALLED ON DOWN GRADE RESTARTED OK
	CUSTOMER STATES CHECK ENGINE LIGHT CAME ON THEN DIED HAS DIED 3 TIMES IN 30 MINS
BELOW SENSOR, RESET PCM, TEST DROVE RETEST, OK	OK VEHICLE HAS STALLED A COUPLE OF TIMES WHILE DRIVING WILL RESTART
	D21 CUST STATES VEHICLE STALLED OUT WHILE DRIVING CHECK & ADVISE
	CHECK FOR ROUGH IDLE AND STALL
	CUSTOMER STATES CUT OFF TWICE THIS WEEK NO CHECK ENG LIGHT HAPPENED WHEN SLOWING DOWN COMING TO A STOP
	D21,0524,30 03,CUSTOMER STATES ENGINE STALLED WHILE DRIVING AFTER BATTERY & ENGINE LIGHTS CAME ON, ENGINE RESTARTED
CONCERN. RAN PIN POINT TESTS PER TSB, FOUND IAC TO BEINTERMITTENTLY HIGH AT 48%. REMOVED AND REPLACED IAC MOTOR, REPROGRAMED PCM, ROAD TEST AND RETEST PASSED.	CORR FOR INTERMITTLY CAR WILL JUST DIE WHILE DRIVING, D02. ALWAYS RESTARTS, HOT OR COLD SEE BOS B WHEN IN
	CUST SAID THAT SHE WAS DRIVING AT HWY SPEEDS AND CAR SHUT OFF IT DID RESTART BUT THEN SHUT OFF AGAIN AND RESTARTED
	CUSTOMER STATES ENGINE STALLED WHILE DRIVING THEN RESTARTED
	CUST STATES W DRIVING, VEHICLE STALLS OUT, WILL IMMEDIATELY RESTART, COLD OR HOT
	D21 4 TIMES WHILE DRIVING AND IN A COAST SITUATION ENGINE STALLS RESTARTS FINE.SEE INCH
	WHEN COMING TO A STOP CUTS OFF THEN THE EMMISION SYSTEM LIGHT COMES ON
	VEHICLE CUTS OFF WHEN GOING DOWN ROAD.
	OK CAUSE AT TIMES WHEN COMES TO STOPS,ENGINE WILL CUT OFF,WILL RESTART RIGHT BACK UP
	VEHICAL SHUT OFF ONCE YESTERDAY RESTARTED OK AND SEEMS OK SINCE
	HOT SOMETIMES WILL STALL ON TURNS OR SLOWING TO STOP RESTARTS OK
	REPORTS VEHICLE STALLED OUT WHILE DRIVING
	CUST STATES WHEN DRIVING VEHICLE IT SHUTS OFF HAS HAPPENED A FEW TIMES SPEED HAS VARIED WHEN CONDITION OCCURRED
SSOR PERFORM EVAP LAK TEST WITH SMOKE MACHINE NO LEAK DETECTED RETEST	CUST STATES WHILE DRIVING DOWN THE ROAD ENGINE DIES D21
	C S VEH IS CUTTING OF GOING DOWN ROAD
B. THE PROBLEM WAS NOTIDENTIFIED IN THE MEMO. WE HAD TO REPORT BACK OUR FINDINGS TO OUR FSE. IF YOU WOULD LIKE TO CALL OUR FIELD SERVICE ENGINEER ABOUT THIS CONCERN, I WILL BE HAPPY TO GIVE YOU HIS DI	CUSTOMER STATES VEHICLE STALL WHILE DRIVING
	CAR SHUTS OFF WHILE DRIVING DOWN THE ROAD
	DIES WHEN LET OF ACCELLERATOR D21

2002	9205	S11	1FMYU03162KB89697	3.0L	TAD	12	2001	2G05	RECAL	D21	3	1656469	2000	WHILE DRIVING
2002	9213	S11	1FMYU03162KB89696	3.0L	TAD	11	2001	2.00E+03	9F715	D21	3	696323	1000	STALLS
2002	9222	S11	1FMYU03162KB89696	3.0L	TAD	11	2001	2G04	12A650	D21	3	695943	2000	ON HIGHWAY
2002	9224	S11	1FMYU03162KB94804	3.0L	TAD	11	2001	2G05	RECALEM	D21	6	1435712	4000	WHILE DRIVING
2002	9226	S11	1FMYU03162KB24739	3.0L	TAD	11	2001	1H03	8J460	D21	3	691209	3000	WHILE DRIVING
2002	9226	S11	1FMYU03162KB24739	3.0L	TAD	11	2001	2G01	12A650	D21	4	695094	4000	WHILE DRIVING
2002	9227	S11	1FMYU03162KB94708	3.0L	TAD	11	2001	2.00E+03	9F715	D21	8	2010662	11000	ON HIGHWAY
2002	9231	S11	1FMYU03162KB94808	3.0L	TAD	11	2001	2G04	DIAG	D21	6	2309145	13000	ACCELERATING
2002	9232	S11	1FMYU03162KB23709	3.0L	TAD	11	2001	2G05	RECAL	D21	4	1078061	2000	WHILE DRIVING
2002	9235	S11	1FMYU03162KB22508	3.0L	TAD	11	2001	2.00E+04	9F045	D21	3	695220	3000	WHILE DRIVING
2002	9245	S11	1FMYU03169KB14280	3.0L	TAD	10	2001	2G05	RECAL	D21	5	1641916	5000	WHILE DRIVING
2002	9246	S11	1FMYU03169KB14213	3.0L	TAD	11	2001	2G04	DIAG	D21	7	1561948	7000	TURNING
2002	9252	S11	1FMYU03162KB12708	3.0L	TAD	11	2001	2.00E+03	9F715	D21	4	794774	5000	WHILE DRIVING
2002	9253	S11	1FMYU03162KB12738	3.0L	TAD	11	2001	2.00E+04	9C015	D21	6	1695306	10000	WHILE DRIVING
2002	9264	S11	1FMYU03162KB03010	3.0L	TAD	10	2001	2G04	12A650	D21	9	2147923	4000	WHILE DRIVING
2002	9269	S11	1FMYU03162KB03002	3.0L	TAD	10	2001	2.00E+03	9F715	D21	2	357047	0	AT STOP
2002	9273	S11	1FMYU03162KB02790	3.0L	TAD	11	2001	1D02	9439	D21	8	2391116	29000	STALLS
2002	9274	S11	1FMYU03169KB02711	3.0L	TAD	10	2001	2.00E+03	0H307	D21	4	1029579	6000	STALLS
2002	9281	S11	1FMYU03162KB03970	3.0L	TAD	10	2001	2G04	12A650	D21	1	1499507	1500	WHILE BRAKING
2002	9282	S11	1FMYU03162KB02143	3.0L	TAD	10	2001	2G04	12A650	D21	6	2067145	10000	WHILE DRIVING
2002	9285	S11	1FMYU03162KB01204	3.0L	TAD	10	2001	2G04	DIAG	D21	5	1061291	3000	STALLS
2002	9285	S11	1FMYU03162KB01204	3.0L	TAD	10	2001	2G02	129679	D21	1	359170	0	WHILE DRIVING
2002	9287	S11	1FMYU03169KB00117	3.0L	TAD	10	2001	2G04	12A650	D21	1	332433	0	WHILE DRIVING
2002	9294	S11	1FMYU03162KA93010	3.0L	TAD	10	2001	2G05	RECAL	D21	6	1557826	10000	WHILE DRIVING

TSB		EEC TEST P POINT TEST WDS RECORDER & MONITER TEST REPROGRAM PCM PER TSB 02 11 06
REPLACED		INOPERATIVE VALVE ASSEMBLY (IDLE AIR CONTROL) IAC REPLACE
INOP		DOES NOT OPERATE PROPERLY EEC (QUICK TEST) DIAGNOSIS
SSM		QUICK TEST PASS CK OASIS SSM 18589 REPROGRAMED PCM BLOW AIR THRU EVAP VENT LINE CK EEC POWER RELAY CK POWER DIST BOX
REPLACED		VERIFIED CONCERN PERFORMED EEC TEST CODE PO 401 PERFOMRED PINPOINT TEST NGS DCL PID DATA ROAD MONITOR TEST FOUND DPFE MO 3149
SSM		VERIFIED CONCERN PERFORMED NGS DCL PID DATA ROAD MONITOR TEST PASS PERFORMED IGNITION TEST PASS PERFORMED FUEL PRESS TEST 65 PSI CHECKED OASIS FOUND SSM 18589 CALLED FORD HOTLIN TALKED WITH JOHN OWEN
REPLACED		IAC & EVAP VALVE PASS EEC MONITOR EVAP TEST REPLACED IAC & EVAP VALVE REPROGRAMMED PCM.
DIAG		HOOK UP NGS. PERFORM KOEO, KOER SELF TEST. PIN POINT TEST, DCL DISPLAY, ROAD TEST AND MONITOR, FUEL PRESSURE TEST,
REFLASH		SELFTESTED EEC TESTED FUEL PRESSURE 65 KOED PERFORMED MONITOR ROADTEST ALL READINGS NORMAL RAN OASIS REPROGRAMMED
REFLASH		S RAN NGS AND P P TEST REPROGRAM PCM CLEANED VENT LINE IN EVAP SYS
REFLASH		5548 12/450 WDS KOEO P1000 MANUAL FUEL PRESSURE TEST 55PSI ROAD TEST MONITOR IGNITION,INJECTOR & FUEL TRIM % REPROGRAM PROCESSOR & RETEST P1000 CC4I
DIAG		NGS TEST CODE MONITOR TESTING ROADTESTED COULD NOTDUPLICATE CONCERN OR VERIFY
REPLACED		OPERATE,CK OASIS,#18589,QUICK TEST PASS,REPROGRAM PCM,BLOW AIR THRU EVAP VENT LINES,REPLACE EEC POWER RELAY,TIGHTEN
TSB		NGS TEST NO CODES. ROAD TESTED TO MONITOR PIDS AS PER TSB 02 11 6. REPLACE VAPOR
REFLASH		PCM PERFORMED WDS DIAGNOSIS,DCL,PIN POINT,REPROGRAMMED PCM.PERFORMED F
DIAG		IAC EEC (QUICK TEST) DIAGNOSIS
REPLACED		VEHICLE STALLS NECESSARY TO REPLACE IAC
REPLACED		EEC TEST, CODES O P1111 C P1111 R P1111, DCL TEST WITH THE NGS TESTER FUEL PRESSURE TEST, IGNITION TEST AND ROAD TEST WITH THE NGS TESTER. SEARCH TO FIND THE VEHICLE LOOSES FUEL PRESSURE AT TIMES, VE
REFLASH		PERFORMED EEC TEST FOUND NO CODES PRESENT,REPROGRAMMED PCM
TSB		PERFORMED STEPS 1 THRU 8 ON TSB 2 8 8,RECALPCM
DIAG		CHECK EEC SYSTEM, NO CODES. PERFORMED DCL DISPLAY. EEC SYSTEM NORMAL. CHECK FUEL PRESSURE, FLOW TEST INJECTORS,
REPLACED		894 CO 42 WARR REQUEST A TIME M TIME ABOVE OPERATIONS PER FORD FSE JOHN GENTA FOR EXTENSIVE TESTING AND TROUBLESHOOTING. REPLACE ALL PART PER FSE. MAF SENSOR,DPFe SENSOR,IAC,CRANKSHAFT SENSOR, R R
HOTLINE		488 WDS START UP EEC TEST RETRIEVED NO CODES PINPOINT TEST TEST DRIVE COULD NOT VARIFY COMPLAINT ,FUEL PRESSURE AND LEAK DOWN CK VIEWED DATALOGGER FOUND NO PIDS OUT OF SPEC. CONTACTED HOTLINE AND
DIAG		EEC (QUICK TEST) DIAGNOSIS

	THE TRUCK DIES WHEN DRIVING DOWN THE ROAD SOMETIME AND THEN PICKS BACK UP
	CUSTOMER STATES THAT IT IS STALLING, WHEN STALLS THE CHECK ENGINE LIGHT COMES ON CHECK AND ADV
	CUST STATES ENG CUT OFF WHEN DRIVING AT HWY SPDS, RESTARTED FINE & HAS BEEN OKAY SINCE THEN, SEE ATTACHED
	CUSTOMER STATES VEH CUT OFF WHILE DRIVING 3 TIMES. VEH GAVE NO WARNING AND RESTARTED RIGHT AWAY
	D21 CUSTOMER STATES ENGINE STALLED WHILE DRIVING RESTARTED OK
S SAID TO CHECK GROUNDS 300, 100 BATT	D30 CUSTOMER STATES ENGINE STALLS AFTER DRIVING SEVERAL MILES 35 40 MPH WILL RESTART
	D21 STALLS HWAY SPEED ROUGH IDLE 1ST START COLD
	ENGINE STALLS WHILE ACCELERATING PER CUST.
	D21 CUST STS ENG STALLED WHILE DRIVING. STS CUIT CLEAN LIKE SOMEONE HAD TURNED OFF KEY, DID RESTART
	WHILE DRIVING ENGINE CUT OFF. FEELS AS IF SOMETHING IS HOLDING IT BACK WHEN GOING UP A HILL. FEELS L
	D21 CUST STATES CAR STALLS WHILE DRIVING
	CUSTOMER STATES THAT VEHICLE STALLED WHILE MAKING A TURN ONLY HAPPENED 1 TIME
	CUSTOMER STATES VEH CUIT RUNNING WHILE GOING DOWN THE ROAD
	CUSTOMER STATED THAT VEHICLE SHUT DOWN WHILE DRIVING STARTED BACK UP. ALSO HAD VEHICLE STALL AT IDLE. CK AND ADVISE
	CUST STATES VEH DIED WHILE DRIVING
	CUST STATES YESTERDAY WHILE SLOWING TO A STOP THE ENGINE STALLED...RESTARTED NORMALLY
	CUSTOMER STATES THAT THE CHECK ENGINE LIGHT IS ON AND WHEN THE CAR SITS AT A LIGHT FOR A WHILE IT STALLS
RY ERRATICREPLACE PUMP AND RETEST.	ON THREE OCASIONS MOTOR HAS DIED WHEN TURNED ON A C SLOW TO START ENG TURNS OVER SEVERAL TIMES BEFORE STARTING
	BLOWING DOWN GOING INTO CURVE CUT OFF 25MPH ONE TIME
	CUSTOMER STATES ENG CUIT WHEN DRIVING
	STALL CUITS ACCEL, ALL ENG TEMPS REASON FOR BUY BACK
BATTERY CASE AND CHECK MULTIPLE GROUNDS AND CLEAN AND TIGHTEN CONNECTIONS UNDER HOOD R R CHECK PCM CONNECTOR FOR PIN OUT O K CHECK CONNECTORS INSIDE LEFT KICK PANEL O K EEC	STALLS WHILE DRIVING , GOING DOWN HILL AND BRAKING TO MAKE A TURN
PREPORMED FOLLOWING PER FORD HOTLINE TECH. ADJUSTED BASE IDLE AND BROUGHT IAC DUTY CYCLE DOWN TO 33 35% TAP CHECK EEC POWER RELAY ,UPDATED PCM TO LATTEST UPDATE,CHECKED ALL	VEH WILL STALL WHEN DRIVING AT 45 50 MPH ,CUST PULLS OVER TO RESTART.(WARM) ADV .
	TRUCK CUT OFF TWICE WHILE DRIVING BUT IT RESTARTED AFTER IT CUT OFF

2002	9308	S11	1FMYU03182KA80882	3.0L	T/LD	10	2001	7C05	14N069	D21	7	1130494	4000	WHILE DRIVING
2002	9315	S11	1FMYU03182KA71094	3.0L	T/LD	10	2001	2G04	D5A3	D21	10	2076460	12000	STALLS
2002	9321	S11	1FMYU03182KA85942	3.0L	T/LD	10	2001	2.00E+03	9F715	D21	11	2411429	8000	WHILE DRIVING
2002	9327	S11	1FMYU03182KA85902	3.0L	T/LD	10	2001	7C05	14N069	D21	2	362291	2000	ON HIGHWAY
2002	9335	S11	1FMYU03182KA84039	3.0L	T/LD	10	2001	2.00E+03	9F715	D21	4	616992	4000	AT IDLE
2002	9336	S11	1FMYU03182KA84039	3.0L	T/LD	10	2001	2.00E+03	9F715	D21	8	1808898	12000	WHILE DRIVING
2002	9341	S11	1FMYU03182KA83069	3.0L	T/LD	10	2001	2G02	129579	D21	10	2246200	11000	STALLS
2002	9353	S11	1FMYU03182KA82827	3.0L	T/LD	9	2001	7C05	14N069	D21	7	1917530	7000	WHILE DRIVING
2002	9359	S11	1FMYU03182KA80800	3.0L	T/LD	9	2001	2.00E+03	9F715	D21	8	1805997	12000	AT STOP
2002	9361	S11	1FMYU03182KA80388	3.0L	T/LD	9	2001	2.00E+03	9F715	D21	11	2313437	10000	AT IDLE
2002	9365	S11	1FMYU03182KA46535	3.0L	T/LD	9	2001	2G05	RECAL	D21	5	786795	4000	AT IDLE
2002	9366	S11	1FMYU03182KA46987	3.0L	T/LD	9	2001	2.00E+03	9F715	D21	11	2297115	17000	WHILE DRIVING
2002	9370	S11	1FMYU03182KA46541	3.0L	T/LD	9	2001	2.00E+03	9F715	D21	10	1993533	15000	WHILE DRIVING
2002	9381	S11	1FMYU03182KA43861	3.0L	T/LD	8	2001	7C05	14N069	D21	10	1640483	17000	WHILE DRIVING
2002	9390	S11	1FMYU03182KA39500	3.0L	T/LD	9	2001	2.00E+03	9F715	D21	2	404628	1000	AT STOP
2002	9391	S11	1FMYU03182KA39254	3.0L	T/LD	9	2001	7C05	14N069	D21	3	392194	1000	WHILE DRIVING
2002	9396	S11	1FMYU03182KA39139	3.0L	T/LD	9	2001	2G04	12A660	D21	7	1107745	8000	WHILE DRIVING
2002	9420	S11	1FMYU03182KA34409	3.0L	T/LD	8	2001	2.00E+03	9F715	D21	11	2126853	22000	WON'T IDLE
2002	9422	S11	1FMYU03182KA29882	3.0L	T/LD	9	2001	7C05	14N069	D21	2	382204	3000	WHILE DRIVING
2002	9423	S11	1FMYU03182KA29882	3.0L	T/LD	9	2001	2.00E+04	9C815	D21	5	636795	9000	DOWNHILL
2002	9427	S11	1FMYU03182KA27885	3.0L	T/LD	9	2001	2G02	9G444	D21	6	843910	6000	MIL
2002	9428	S11	1FMYU03182KA27220	3.0L	T/LD	8	2001	1H08	9J480	D21	8	853582	8000	WHILE DRIVING
2002	9429	S11	1FMYU03182KA27220	3.0L	T/LD	8	2001	2G02	129579	D21	6	853168	8000	COASTING
2002	9430	S11	1FMYU03182KA27220	3.0L	T/LD	8	2001	7V01	12A581	D21	6	853581	8000	DOWNHILL

SSM		EEC TEST KOEO PASS KOEC PASS CHECK FUEL PRESSURE CHECK IGN SYSTEM DCL DISPLAY AND MONITOR RECORD PINPOINT TEST RUN OASIS AS PER SSM 15439 REPLACED POWER RELAY PERFORM EVAP SYSTEM PRESSURE TEST RUNNIN
NPF		ROAD TEST, NO STALL. EEC DIAGNOSIS, NO CODES STORED. COULD NOT DUPLICATE CONCERN.
REFLASH		DIAGNOSED AND REPLACED IDLE AIR CONTROL VALVE, WE ALSO NEED TO REPROGRAM THE PCM, PLEASE RETURN FOR THIS, WDS DOWN.
REPLACED		PCM UPDATE AND GROUND CHECK ROADTEST EDS TEST RUN OASIS,CALL HOT LINE REFLASH PCM WITH NEW UPDATE VERSION 16.0.REPLACE FUEL PUMP RELAY
DIAG		ROADTESTED.EEC TEST,PINPOINT TESTS,IGNITION TESTS,FUEL SYSTEM TESTS,NGS DCL DISPLAY TEST,NGS MONITOR ROAD TEST.
REPLACED		1 EEC TEST,PINPOINT TESTS,NGS MONITOR ROAD TEST,REPLACED IAC VALVE,INOPERATIVE,REPLACED PCM RELAY,DOES NOT OPERATE
TSB		RUN EEC TEST NO CODES. PERFORM TSB 02 11 @. CONTACT TEC. HOT LINE SAID REPLACE MAF SENSOR AND DPFE SENSOR.
REPLACED		POWERTRAIN CONTROL MODULE RELAY REPLACE
REPLACED		DIAG AND REPLACED IAC VALVE
TSB		TSB 021100. PERFORMED EEC TEST. PASS. CK FUEL PRESSURE. 44 PSI. REPLACED IAC VALVE AND REPROGRAMMED PCM PER TSB. ROAD TEST.
SSM		4250 CC 42 W VERIFY CONDITION TEST DROVE VEHICLE STALLS AT IDLE TEST EEC V KOEO NO CODES KOER NO CODES RAN OASIS FOUND SSM#15599 RE PROGRAMM PCM PEFORMED SSM TEST DROVE OK
REFLASH		QUICKTEST,RE EEC,PINPOINT,RECAL PCM,REPLACED IAC
REPLACED		INSPECT FOR CUSTOMERS CONCERN WDS TEST CODE P0100 PERFORMED PINPOINT TEST IAC VOLTAGE LOW REPLACED IAC RETEST OK OK
TSB		INTAKE & AIR INDUCTION TESTING ALL PASS. FOLLOWED INTERMIT STALLING DIAGNOSIS, CHECKED TSB 02 11 B AND FOLLOWED TEST
SSM		1400 SSM 15494 1.1 RH PERFORM NGS TEST NO CODES, PASS PERFORM PINPOIN TESTS OK PIDS AND MONIOTR TEST ALL PASS. UNABLE TO VERIFY CONCERN BUT FOUND SSM ON OASIS TO REPLACE IAC VALVE AND TO REPLACE PC
DIAG		1 42 NGS STARTUP TEST SELF TEST KOEO PASS CONT PASS KOER PASS DCL DISPLAY TEST SIGNAL SIMULATION TEST RECORDER MONITOR TEST
SSM		8805 ROAD TEST, COULD NOT VERIFY STALLING CONCERN. SELF TEST WITH WDS, NO DTCS, ALL PASS. RAN OASIS, FOUND SSM #15599. REPROGRAMMED PCM AS PER SSM. ROAD TEST, VEHICLE OPERATES NORMAL.
DIAG		IAC, EEC RELAY MALFUNCTIONS EEC (QUICK TEST) DIAGNOSIS
HOTLINE		3750 CUST CONCERN OF STALLED WHILE DRIVING 45 MPH COASTED TO STOP THEN RESTARTED. ROADTEST, DID NOT CONFIRM, EEC TEST, PASS. CALL TECH HOTLINE,PERFORM LIST OF CHECKS, TEST GROUNDS 100,101. REMOVE BAT
SSM		9728 TEST DRIVE, DID NOT CONFIRM STALL ON DIESEL. HOOK UP WDS & CHK FOR CODES. NONE. USE PIDS AND CHK BARO, IAC, IN RANGE. CHK FUEL PRESSURE, NORMAL. PERFORM CYL BALANCE, ALL EVEN, 0%. CHK BASE ENG
REPLACED		CAT. MONITOR SENSOR C2932 INOP EEC TEST KOEO PASS KOEC P0161 KOER P1000 DCL MONITOR TEST IDLE DATA TEST PINPOINT TEST REPLACED C2932 SENSOR (CAT.
REPLACED		PFE REPLACE PFE SENSOR AND RESET KEEP ALIVE MEMORY AS PER ENGINEERING
HOTLINE		MASS AIR FLOW SENSOR REMOVE MASS AIR FLOW SENSOR AND SET DUTY CYLE TO 30% AS PER FORD ENGINEERING
SSM		WDS TEST IGN AND FUEL TEST PINPOINT TEST CHECK OASIS REPROGRAM PCM BLOW OUT VENT LINES FOR EVAP CHECK EEC POWER RELAY TIGHTEN PINS IN DIST BOX AS PER SSM 15599 CALL HOTLINE AGAIN REFLASH WITH NEW UPDA

G TEST REPROGRAM PCM AND RETEST	VEHICLE DIES WHILE DRIVING 30,40 MPH WILL RESTART AND RUN OK
	CUSTOMER STATES ENGINE STALLED OUT TWO TIMES
	C S TRUCK CUT OUT STALLED WHILE DRIVING, PULLED OVER, PUT IN PARK & RESTARTED, HAPPENED ONCE, 3 WEEKS AGO, NO CK ENG. LTS
	C S VEHICLE WILL JUST CUT RUNNING WHEN AT HWY SPEEDS VEHICLE ACTS LIKE IF YOU WOULD JUST TURN KEY OFF
	CUSTOMER STATES ENGINE WILL ALMOST STALL AT IDLE AND MAKES KNOCKING NOISE AT TIMES BOTH SEEM TO OCCUR AT THE SAME TIME
	CUSTOMER STATES ENGINE SEEMS TO STALL WHILE DRIVING AT TIMES BATTERY LIGHT COMES ON AND PWR STEERIN
	GOING DOWN ROAD, POWER STEERING WENT OUT AND LIGHTS ON DASH ACME ON, ENGINE STALLED.
	C S ENGINE STALLED WHILE DRIVING AND TURNING AT INTERSECTION
	C S CEL CAME AND THE ENG DIED WHEN THEY CAME TO A STOP
	CUSTOMER STATES VEHICLE DIED WHILE IDLING UP TO A STOP SIGN DID NOT APPLY BRAKES, TURN A C ON, ETC....VEHICLE JUST DIED
	CK ENGINE STALLED WHILE SITTING IDLING,RESTARTED EASILY
	CHECK DIED WHILE DRIVING. HAPPENED WHEN ACCEL UP HILL. HAS ONLY DONE IT ONCE.
	C S VEHICLE DIED W DRIVING DID RESTART NO WARNING LIGHTS PRIOR TO ENGINE SHUTTING OFF CK AND ADVISE
	INSPECT & REPORT STALLED W DRIVING 30 35 MPH CUSTOMER STATES RESTARTED OK, CHECK AS NEEDED
M RELAY AND TO CK PINS ON RELAY. RETEST ALL PASS.	CUSTOMER STATES CAR DIES AT STOPS AND RESTARTS
	CUST STATES CHECK ENGINE STALLED WHEN DRIVING AT 40 ALL LIGHTS CAME ON D21
	CUST STATES DIED WHILE DRIVING CHECK ENG OIL AND BATT LIGHTS CAME ON LOST FULL BRAKE POWER
	CK. TRUCK WILL NOT STAY RUNNING CUTS OFF BUT WILL RESTART AND MUST KEEP FOOT ON GAS
TERY TRAY AND CHECK GROUNDS 104 105, ALL GOOD. CHECK CONNECTOR 270, FINE. INSPECT IAC AND SET DUTY CYCLE TO 36 TO 38 % PERFORM TAP TEST ON EEC RELAY, FAILED. REPLACE RELAY RECHECK, OK	CUST STATES THE VEH STALLED OUT WHEN DRIVING AT 45 MPH COASTED VEH TO SIDE OF ROAD AND VEH STARTED RIGHT BACK UP NO LIGHTS ON
INE W COMPRESSION TEST, OK, RUN OASIS & PERFORM RECALIBRATE PCM PER SSM 15569. ALSO CALLED HOTLINE & SPOKE TO KEITH REGARDING SSM 15569 FOR CLARIFICATION, REMOVE VAPOR CANISTER,	CUST STATES THE VEH STALLED OUT WHEN ON A DECEL ON A DOWNHILL SLOPE VEH RESTARTED CHK AND ADVISE
	CUSTOMER STATES CHECK ENGINE LIGHT ON
	SHUTS OFF WHEN DRIVING
	CUTS OFF AT 45 ON DECELL ON HILL CALL ENGINEERING
TE	STALLS OUT AND THEN RESTARTS WILL SHUT DOWN WHEN MOVING 35MPH UASSALLY ON HILLS

2002	9491	S11	1FMYU03162KA27119	3.0L	TAUD	6	2001	2G04	12A650	D21	5	696766	6000	WHILE DRIVING
2002	9449	S11	1FMYU03162KA16766	3.0L	TAUD	6	2001	7C05	14N069	D21	1	410831	0	TURNING
2002	9453	S11	1FMYU03162KA16203	3.0L	TAUD	6	2001	2.00E+03	9F715	D21	9	1750709	12000	NO TEXT
2002	9464	S11	1FMYU03162KA06204	3.0L	TAUD	6	2001	2.00E+03	9F715	D21	6	693777	8000	STALLS
2002	9479	S11	1FMYU03162KA06070	3.0L	TAUD	6	2001	2G05	RECAL	D21	8	1091358	14000	NO TEXT
2002	9496	S11	1FMYU03162KE01983	3.0L	TAUD	6	2002	2G05	RECAL	D21	1	2322843	0	WHILE DRIVING
2002	9498	S11	1FMYU03162KD97886	3.0L	TAUD	6	2002	2.00E+03	9F715	D21	1	2279609	2000	AT IDLE
2002	9504	S11	1FMYU03162KD86700	3.0L	TAUD	5	2002	2.00E+03	9F715	D21	1	1610573	0	WHILE DRIVING
2002	9511	S11	1FMYU03162KD63425	3.0L	TAUD	5	2002	2.00E+03	9E926	D21	3	2322221	2000	AT STOP
2002	9514	S11	1FMYU03162KD40466	3.0L	TAUD	4	2002	7C05	14N069	D21	3	2366812	6000	WHILE DRIVING
2002	9516	S11	1FMYU03162KD32728	3.0L	TAUD	4	2002	2G03	12B577	D21	-1	2466859	0	WHILE DRIVING
2002	9524	S11	1FMYU03162KD12510	3.0L	TAUD	4	2002	2.00E+03	9F715	D21	4	2283706	8000	STALLS
2002	9526	S11	1FMYU03162KD09421	3.0L	TAUD	3	2002	2G05	RECAL	D21	4	2080640	3000	WHILE DRIVING
2002	9528	S11	1FMYU03162KD02996	3.0L	TAUD	3	2002	2.00E+03	9E926	D21	2	1902754	1000	STALLS
2002	9529	S11	1FMYU03162KD02995	3.0L	TAUD	3	2002	2.00E+03	9F715	D21	1	1903983	1000	COASTING
2002	9530	S11	1FMYU03162KD01474	3.0L	TAUD	3	2002	2G05	RECAL	D21	1	1977936	0	WHILE DRIVING
2002	9537	S11	1FMYU03162KC92758	3.0L	TAUD	3	2002	2G04	DIAG	D21	1	2324411	1000	WHILE DRIVING
2002	9538	S11	1FMYU03162KC92758	3.0L	TAUD	3	2002	2.00E+03	9E926	D21	2	2412042	3000	WHILE DRIVING
2002	9551	S11	1FMYU03162KC81705	3.0L	TAUD	2	2002	7C05	14N069	D21	3	1626817	1000	STALLS
2002	9553	S11	1FMYU03162KC81381	3.0L	TAUD	2	2002	2G04	12A650	D21	5	3455314	6000	WHILE DRIVING
2002	9554	S11	1FMYU03162KC80716	3.0L	TAUD	2	2002	2.00E+03	9H307	D21	4	2089466	3000	STALLS
2002	9554	S11	1FMYU03162KC48620	3.0L	TAUD	2	2002	2G04	DIAG	D21	2	1366045	3000	AT STOP
2002	9566	S11	1FMYU03162KC46453	3.0L	TAUD	2	2002	2G04	DIAG	D21	4	1997041	7000	WHILE DRIVING
2002	9572	S11	1FMYU03162KC30006	3.0L	TAUD	2	2002	2.00E+03	9F715	D21	3	1764715	5000	AT STOP
2002	9580	S11	1FMYU03162KC29787	3.0L	TAUD	2	2002	2.00E+03	9F715	D21	8	2161151	8000	WHILE DRIVING
2002	9586	S11	1FMYU03162KC19759	3.0L	TAUD	2	2002	1H03	9J460	D21	5	2457852	2000	WHILE DRIVING

DIAG		1 VERIFY. EEC DIAG, NO CODES. PERFORM MANUAL FUEL PRESSURE TEST AND LEAKDOWN, PERFORM IGN SYSTEM DIAG. PERFORM PID
REPLACED		PERFROM TEST REPLACE EEC RELAY
NO TEXT		
DIAG		VEHICLE DIED TWICE PERFORMED SSD6 DIAGNOSIS,DCL,POWER BALANCE,FUEL PRESSURE,INJECTOR
NO TEXT		
REFLASH		CK EEC DIAG KOEO KOER CONT MEMORY CK PCM MONITOR AND RECORD PINPOINT TEST REPROGRAM PCM TO LATEST CALIBRATION RETEST
TSB		CHECK OUT ENGINE DIES AT IDLE, SOMETIMES, IVDS, ROAD TEST WITH MONITOR, DCL, PINPOINT TEST, PID MONITOR, RUN OASIS, REPLACED IAC PER TSB 02 11 06, RETEST, PASSED
TSB		PERFORMED TSB 02 11 6 ADJ AIR BYPASS,CHECKED PCM FOR LATEST CALIBRATION O.K. CHECKED HARNESS CONNECTORS O.K.
REPLACED		PERFORM EEC TEST KOEO PASS KOER PASS,PERFORM RECORDER MONITOR TEST, PERFORM FUEL SYSTEM TEST,PERFORM IGN.SYSTEM TEST,REPLACE IAC VALVE, & THROTTLE BODY,RETEST PASS
TSB		EEC RELAY NOT OPERATING PROPERLY CHECK FOR ENGINE STALLING RUN TSB 02 11 6 CHECK IAC WITHIN SPEC CHECK EVAP WITHIN SPEC R AND R EEC RELAY
POOR CONNECTION		POOR CONNECTION EEC (QUICK TEST) DIAGNOSIS
TSB		CHECKED AND REPAIRED PER TSB 2 11 6
TSB		WDS EEC TEST NO CODES, MONITOR TEST PER TSB 02 11 06, IGN TEST, FUEL PRESS TEST, REPROGRAMMED PCM, RETESTED OK
REPLACED		THROTTLE BODY FAULTY EEC (QUICK TEST) DIAGNOSIS
REPLACED		IAC FAULTY EEC (QUICK TEST) DIAGNOSIS
REFLASH		FOUND BASE IDLE OUT OF ADJ. 49 12A650 760 M O VERIFIED CONCERN,IVDS DIAG. SYSTEM PASS,FUEL PRESSURE TEST 42 PSI,PID DATA MONITER FOUND BASE IDLE LOW,RESET BASE
TSB		TEST DRIVE VEHICLE COULD NOT VERIFY CHECK OASIS FOR SSM OR TSBINFORMATION TSB 02 11 06 PERFORM TSB OPERATION ALL TESTS OK RETEST VEHICEL NO PROBLEM FOUND
TSB		WDS HOOKUP NO CODES INTERMITTENT PROBLEM CHECKED OASIS DCL DISPLAY MONITOR FUEL PIDS PER TSB 02 11 6 REPLACED IAC VALVE OUT OF SPEC 46% RECHECKED STILL OUT OF RANGE REPLACED THROTTLE BODY IAC OK 32 TO
REPLACED		CHANGE EEC RELAY EEC (QUICK TEST) DIAGNOSIS
HOTLINE		TEST DROVE CHECK FOR CODES NONE FOUND CALLED TECH HOT LINE, WAS TOLD TO CHECK JUNCTION BOX FOR ANY CONTAMINATION, NONE PRESENT AT THIS TIME, ALL SYSTEMS ARE OK AT THIS TIME
REPLACED		EEC TEST. DCL RECORDER MONITOR ROAD TEST. TEST FUEL PRESSURE AND FLOW. TEST IGNITION SYSTEM. REPLACED IN TANK FUEL PUMP. TEST EVAP SYSTEM AFTER REPLACE.
TSB		PERFORMED WDS PINPOINT TEST AND DCL.UNABLE TO VERIFY CONCERN AT THIS TIME.ALSO CHECKED FOR SSM AND TSB
TSB		7047 ROAD TEST,VEHICLE 18 MILES.UNABLE TO VERIFY. EEC TEST,NO CODES. FOUND TSB 02 11 6,DATALOG IAC,EVAPVM AND FTP,MSP. EEC RELAY. ALL OK. AT THIS TIME. NO PROBLEM FOUND.
REPLACED		EEC TEST REPLACE IAC VLAVE,PROGRAM PCM PASS
TSB		6080 CALIBAL PART #XF7Y,12B579,BA60 CC (48) TECH 4656 OASIS CONTACT ID 2209 036 406 REF TSB 02 11 06 INFO ONLY KOEO KOER CODE: PASS CM DTC: PASS UNABLE TO VERIFY CONCERNS, PERFORM EEC SELF TESTS,
TSB		2944 EEC TEST PASS CODES DCL DISPLAY AND DCL ROAD TEST NPF PER TIM REPLACE DIFFE DO TSB 02 11 06 A8 FOLLOWS #1 IDLE AT 760 RPM IAC READING AT37% WITHIN SPECS #2 BUILD DATE OF 02 02 DOESNT APPLY GO T

	D02 ENGINE STALLED WHEN DRIVING, LOST P S AND BRAKES DID RESTART AFTER SITTING FOR A WHILE BUT CUSTOMER HAD TOWED
	CUST STATES WHILE GOING INTO A PARKING LOT CAR STALLED
	CUST STATES VEH DIED TWICE
	OK VEHICLE STALLED DRIVING DOWN THE ROAD ALL LIGHTS CAME ON
	C8 ENGINE DIES AT IDLE, SOMETIMES
	CUSTOMER STATES WHILE DRIVING THE ENG STALLED, WAITED A FEW MINUTES AND RESTARTED.
	C S WHEN AT A STOP AND THE AC IS ON MAX AND THE FAN ON HIGH THE VEHICLE SHUT OFF ON HER TWICE
	CHECK FOR VEHICLE GOING DEAD WHILE DRIVING
	DIAG VEHICLE WILL DIE WHILE DRIVING
	CUSTOMER STATES VEHICLE DIES AT TIMES WITHOUT WARNING RESTARTS FINE
	CUST STATES THAT THE VEHICLE DIES INTERM. WHILE JUST DRIVING DOWN THE ROAD WITH NO WARNING, PUTS IT INTO NUETRAL AND IT
	CUST. STATES ENGINE STALLED ONCE YESTERDAY SEE FILE
	CUST. STATES WHEN COASTING ENGINE DIED TWICE IN SAME DAY WED. OF THIS WEEK AND DIED ONCE LAST WEEK R
	CUSTOMER STATES CAME OVERBRIDGE AND VEH STALL OUT WHILE DRIVING, PULLED OVER & RESTARTED AND DROVE FINE, CHECK & ADV
	DIAGNOSE FOR A ONE TIME STALL OUT CONCERN WHILE DRIVING
40% CHECK PCM CALIBRATION OK CHECK EVAPUM PID DUTY STOPS INCREASING STAYS AT 99% REPLACED EVAPUM VALVE RECHECKED OK CHECKED VALVE AND ECC RELAY OK CLEAR CODES RECHERCK TEST DRIVE OK	DIAGNOSE FOR VEHICLE STLLING WHILE DRIVING INTERMITTENT
	ENGINE STALLED & WOULD NOT RESTART
	AT TIMES WHILE DRIVING VEHICLE WILL STALL AND WILL LOSE ALL ACESSORIES HAS HAPPENED 2 TIMES
	CUSTOMER STATES THAT THE ENGINE DIED ON SUNDAY TOWED IN
	C S DIED WHILE COMING TO A STOP NO DASH LIGHTS ON NOW
	DIED WHILE DRIVING WOULD NOT CRANK OVER AFTER THIS HAPPEND ALL THE DASH LIGHTS WERE LIT UP AND BAT
	CUST STATES CAR STALLS WHEN COMING TO A STOP D21
PASSED, NO DTCS RETRIEVED. PERFORM PINPOINT TESTS AND DCL DISPLAY TESTS, CHECK BASE IDLE SPEEDS AND FUEL TRIM, PASSED. CHECK FUEL SYSTEM PRESSURE, PASSED, IN SPECS, NO LEAKDOWN	D21 VEHICLE INTERMITTENTLY STALLS WHILE DRIVING, RESTARTS RIGHT BACK UP.
O STEP 4 SEE KEITH IN EVAP SELF TEST IDLE IS AUTOMATICALLY INCREASED AS VMV COMES ON FTP DROPS AS IT IS SUPPOSED TO S NO SUDDEN DROP OR OBSTRUCTION #6 RELAY IS STAMPED LETTERING TYPE #7	CUSTOMER STATES THAT THE TRUCK DIES WHILE DRIVING DOWN THE INTERSTATE AND YOU LOOSE ALL POWER THROW IT IN NEUTRAL IT WILL RESTART

2002	9687	511	1FMYU03152KC19758	3.0L	T/LD	2	2002	2G06	RECAL	D21	2	1566990	1000	WHILE DRIVING
2002	9686	511	1FMYU03152KC19177	3.0L	T/LD	2	2002	2G02	122579	D21	6	2460088	8000	WHILE DRIVING
2002	9689	511	1FMYU03152KC19177	3.0L	T/LD	2	2002	2.00E+03	9F715	D21	4	1780747	5000	AT STOP
2002	9690	511	1FMYU03152KD19139	3.0L	T/LD	2	2002	2.00E+03	9F715	D21	9	2079612	9000	WHILE DRIVING
2002	9686	511	1FMYU03152KC17154	3.0L	T/LD	1	2002	7B02	10346	D21	1	1086572	0	STALLS
2002	9609	511	1FMYU03152KC16148	3.0L	T/LD	1	2002	2.00E+03	9F715	D21	2	1961360	0	WHILE DRIVING
2002	9620	511	1FMYU03152KB99095	3.0L	T/LD	1	2002	2G04	12A650	D21	2	1612653	2000	WHILE DRIVING
2002	9622	511	1FMYU03152KB98489	3.0L	T/LD	1	2002	2G04	12A650	D21	3	1666603	6000	WHILE DRIVING
2002	9626	511	1FMYU03152KB98154	3.0L	T/LD	1	2002	2G04	12A650	D21	1	668639	0	WHILE DRIVING
2002	9623	511	1FMYU03152KB95095	3.0L	T/LD	1	2002	2G04	DIAG	D21	3	1162587	9000	NO TEXT
2002	9644	511	1FMYU03152KB77804	3.0L	T/LD	1	2002	2.00E+03	9F715	D21	5	2127493	10000	WHILE DRIVING
2002	9648	511	1FMYU03152KB76777	3.0L	T/LD	12	2001	7C05	14N069	D21	5	1225511	8000	AT STOP
2002	9658	511	1FMYU03152KB64884	3.0L	T/LD	12	2001	2.00E+03	9F715	D21	9	2387794	3000	STALLS
2002	9657	511	1FMYU03152KB64584	3.0L	T/LD	12	2001	7C05	14N069	D21	1	2127783	0	WHILE DRIVING
2002	9673	511	1FMYU03152KB46050	3.0L	T/LD	12	2001	2G04	12A650	D21	7	1807783	7000	WHILE DRIVING
2002	9676	511	1FMYU03152KB43F14	3.0L	T/LD	11	2001	1D02	9439	D21	2	676736	2000	WON'T RUN
2002	9661	511	1FMYU03152KB36907	3.0L	T/LD	12	2001	2.00E+03	9F715	D21	5	1211544	6000	STALLS
2002	9687	511	1FMYU03152KB30699	3.0L	T/LD	11	2001	2.00E+03	9F715	D21	6	2166985	7000	STALLS
2002	9699	511	1FMYU03152KB30547	3.0L	T/LD	11	2001	2.00E+03	9F716	D21	8	1691258	12000	AT IDLE
2002	9700	511	1FMYU03152KB23799	3.0L	T/LD	11	2001	2.00E+03	9E886	D21	5	2086986	4000	WHILE DRIVING
2002	9705	511	1FMYU03152KB23287	3.0L	T/LD	11	2001	2.00E+03	9F715	D21	5	1978900	4000	AT STOP
2002	9704	511	1FMYU03152KB22805	3.0L	T/LD	11	2001	2G04	12A650	D21	2	1466686	1000	STALLS
2002	9705	511	1FMYU03152KB22805	3.0L	T/LD	11	2001	2.00E+03	9F715	D21	2	1439090	1000	STALLS
2002	9706	511	1FMYU03152KB22805	3.0L	T/LD	11	2001	2.00E+03	9E886	D21	2	1532074	2000	STALLS
2002	9707	511	1FMYU03152KB21466	3.0L	T/LD	11	2001	7C05	14N069	D21	1	404243	0	ON HIGHWAY

REFLASH		1/30 ROAD TEST CHECKED THE FUEL PRESSURE 40 PSI AT IDLE. CHECKED FOR FUEL PRESSURE BLEED DOWN. IT HELD. MONITORED THE FUEL PRESSUR E WHILE DRIVING. IT MAINTAINTED PRESSURE. RAN A MONITOR TEST ON THE
REPLACED		ENGINE DIAG TEST AND PION POINT AND MONIOTOR TEST AND REPLACED MASS AIR FLOW SENSOR RETEST
REPLACED		ENGINE DIAG TEST AND PIN POINT TEST AND REPLACED IDLE CONTROL VALVE AND REPALCED VAPOR MANAGEMENT VALVE AND RETEST
NPF		TEST DROVE FOR CONCERN,UNABLE TO VERIFY,RAN EECTEST NO CODES,ALL PASSED CHECK DATA STREAM GOOD.CHECK OASIS
REPLACED		BURNED OUT VERIFY CUSTOMER CONCERN CHECKED STARTER DRAW TEST 155 OK CHECK CHARGING SYSTEM 12.02 VOLTS CHECK ALTERNATOR 12.1 VOLT
TSB		RUN OASIS,PERFORM TSB 2 11 6 EEC TEST WDS TEST PASS DCC CHECK I.A.C. OVER 42 %, R AND R IAC STIL NO R AND R THROTTLE
TSB		TSB 02 11 6 COULD NOT VERIFY CONCERN, RAN VIN THROUGH OASIS AND FOUND TSB 02 11 6 STATING THAT A PCM REPROGRAM
TSB		TECH 105 WP OC 06 TEST EEC SYSTEM. PERFORM TSB 02 11 06. MONITOR PIDS. REPROGR AM PCM. CHECK EEC RELAY, MONITOR EVAP, CHECK IGNITION SWITCH
REFLASH		REPROGRAM PCM EEC (QUICK TEST) DIAGNOSIS
NPF		EEC TEST ROADTEST UNABLE TO VERIFY STALL CONCERN.
REFLASH		EEC SYSTEM TEST & DIAGNOSIS, NGS MONITOR DIAGNOSIS, RE PLACED IDLE AIR CONTROL VALVE AND REPROGRAMMED PCM.
TSB		9535 PERFORM EEC TESTS, KOEO PASS, KOEC PASS, KOER PASS, MONITOR PCM PIDS, TEST FUEL PRESS. PERFORM TSB 02 06 06, TEST IACV OP, TEST EVAP SYSTEM AND VMV FOR PROPER OP. CHECK EEC RELAY. IAC OK AT T
REPLACED		SPN 9F715, CC 42, CCC 021 CONNECTED TO NGS,TESTED EEC SYSTEM CODE KOEO P1111, KOEC P1111,PIN POINT TESTED ,REPLACED IAC VALVE, REPROGRAMMED PCM RETESTED EEC SYSTEM KOER P1000
REPLACED		NEEDS RELAY EEC (QUICK TEST) DIAGNOSIS
REFLASH		DIAG AND REPROGRAM PCM R&R KICK PANEL TO OK PCM POWER CONNECTIONS
REPLACED		REPLACED UPPER AND LOWER INTAKE GASKETS
TSB		EEC 5 TEST, DCL MONITOR, REPROGRAM PCM PER TSB 2 5 6. REPLACE IAC VALVE.
TSB		ROAD TEST AN ECC TEST IDLE WDS TESTING,DATALOGER IAC OUT OF RANGE AS PER TSB02.11.6,REPLACE IAC ASPER TSB,RECAL PCM RETEST IAC WAS 41%,NOW 37%,IN RANGE ROAD TEST OK
TSB		643414 9F715 06596 9C915 14N099_CC42 12489 MILEAGE OUT 3.0L PER TSB 02 11 06 NO TIME ALLOTED IN TSB PEFORM DIAG USING NGS ROAD TEST PID DATA MONITOR R R IAC VALVE R R THROTTLE BODY R R CANISTER VENT
DIAG		TRUCK CUTTING OFF EEC (CLICK TEST) DIAGNOSIS
NO TEXT		
REFLASH		EEC TEST,NOP CODES,DCL DISPLAY,PID MONITOR,RECORDER PINPOINT TEST,REPROGRAM PCM,RETEST,TEST DRIVE
TSB		IMPROPER OPERATION 9F715 9J460 CC42 DIAG AND PINPOINT TEST. CALL HOTLINE. REPLACED DPFE AND IAC VALVE AS PER TSB 02 06 06. VEHICLE DID NOT STALL. RELEASED
REPLACED		IMPROPER OPERATION 9E925 CC42 DIAG AND PINPOINT TEST. REPLACED THROTTLE BODY. RETEST; P1111 P1111 P1111
999M		WDS DIAG PASS CODES. RUN DATALOGGER, POWER BALA NCE, FUEL PRESSURE. GO THROUGH 99M 15494. REPLA CE PCM RELAY AND RETEST

EVAP AND FUEL TANK PRESSURE IT IS NORMAL. ROAD TEST RAN A MONITOR TEST ON THE IAC. THE ENGINE SPEED WAS DROPING BELOW 600 RPM. REPLACED THE IAC DUE TO A FAULTY IAC. ROAD TEST. THE	CUSTOMER STATES VEHICLE DIED WHILE DRIVING
	CHECK TO SEE WHY ENGINE STALLS WHILE DRIVING
	CHECK FOR AN INT STALLING CONCERN THAT SEEMS TO HAPPEN WHEN STOPPED
	CUST STATES THAT WHEN DRIVING DOWN THE ROAD AT ABOUT 30 35 MPH TRUCK WILL JUST STAHLAND AT A STOP LIGHT
	O S ENGINE STALLED WHILE DRIVED HAD TO BE TOWED IN CK AND AD VI?
	VEH STALLS WHEN DRIVING HAPPENS AFTER GOING UP SMALL HILL AND LETTING OFF GAS ON DOWN SIDE RESTARTS OK
	CHECK ENGINE DIED WHEN DRIVING
	CUST SAID THAT CAR SHUT OFF WHILE DRIVING HAS ONLY HAPPENED ONCE PLEASE CHECK.
	ENGINE STALLED WHILE DRIVING
	C S ENGINE STALLS WHILE DRIVING, MUST PULL OVER & RESTART, HAPPENS APPROX. 2 TIMES A WEEK.
HIS TIME. REPROGRAM PCM AND REPLACE EEC RELAY PER TSB. RETEST, OK AFTER REPAIR. JH	CHECK ENGINE DIES AT TIMES AT STOPS.
	CHECK ENGINE OPERATION,ENGINE STALLED 1 TIME AT LOW SPEED RESTARTED OK
	CUST STATES THE ENGINE IS STALLED WHILE DRIVING AT NORMAL SPEEDS
	CHECK ENGINE FOR INTERMITENT STALL WHILE DRIVING AND WHEN STOPPED AT LIGHT
	VEHICLE BARELY STAYS RUNNING
	CUSTOMER STATES THAT THE VEHICLE IS SHUTTING OFF
	VEHICLE STALLS
VALVE R R EEC RELAY REPROGRAM PCM AND RETEST ALL PASS ROAD TEST	OK. FOR REASON ENGINE STALLS AT IDLE AT TIMES, SEE RAY
	CUSTOMER STATES THE TRUCK IS CUTTING OFF WHILE DRIVING,SAYS IT STARTS BACK UP OK,NO LIGHTS ARE COMING ON,SAYS HAS HAPPENED 2 TIMES
	W D21 CUSTOMER STATES ENGINE STALLED ONCE LAST NIGHT WHEN CAME TO STOP WITH A C AND HEADLIGHTS ON
	CS INTERM STALL
	CS VEHICLE IS STILL STALLING D21
	C8 STILL STALLING BUT DOES NOT CUT OFF SOP IN
	VEHICLE STALLED AT A LIGHT...IN THE SAME DAY IT STALLED OUT WHILE CUSTOMER WAS GOING DOWN HIGHWAY AT 65 MPH..VEHICLE SHUT DOWN.

2002	9708	S11	1FMYU03152KB21895	3.0L	T/LD	11	2001	2G01	12A650	D21	1	443576	0	ON HIGHWAY
2002	9710	S11	1FMYU03152KB21847	3.0L	T/LD	11	2001	2G04	DIAG	D21	9	2066613	4000	WHILE DRIVING
2002	9711	S11	1FMYU03152KB20922	3.0L	T/LD	11	2001	2G04	12A650	D21	2	606602	1000	STALLS
2002	9712	S11	1FMYU03152KB20922	3.0L	T/LD	11	2001	2G01	12A650	D21	1	565915	0	WHILE DRIVING
2002	9716	S11	1FMYU03152KB14865	3.0L	T/LD	11	2001	2.00E+03	9F715	D21	2	604882	0	AT STOP
2002	9718	S11	1FMYU03152KB13585	3.0L	T/LD	11	2001	2G04	12A650	D21	3	678340	3000	WHILE DRIVING
2002	9726	S11	1FMYU03152KB03764	3.0L	T/LD	11	2001	7B05	14A060	D21	1	360049	0	WHILE DRIVING
2002	9728	S11	1FMYU03152KB03516	3.0L	T/LD	10	2001	2.00E+03	9F715	D21	5	957091	6000	STALLS
2002	9742	S11	1FMYU03152KA92975	3.0L	T/LD	10	2001	2G04	DIAG	D21	1	341071	1000	WHILE DRIVING
2002	9748	S11	1FMYU03152KA91572	3.0L	T/LD	10	2001	2.00E+03	9F715	D21	10	2322322	13000	WHILE BRAKING
2002	9761	S11	1FMYU03152KA91037	3.0L	T/LD	10	2001	2.00E+03	9F715	D21	2	432666	2000	WHILE DRIVING
2002	9769	S11	1FMYU03152KA70429	3.0L	T/LD	10	2001	7C05	14N060	D21	5	1056214	1000	AT STOP
2002	9781	S11	1FMYU03152KA66981	3.0L	T/LD	10	2001	2G04	12A650	D21	6	1091476	7000	WHILE DRIVING
2002	9784	S11	1FMYU03152KA66153	3.0L	T/LD	10	2001	2G05	REGAL	D21	8	1078259	5000	WHILE DRIVING
2002	9772	S11	1FMYU03152KA64873	3.0L	T/LD	9	2001	2G03	9E455	D21	6	795768	7000	WHILE DRIVING
2002	9773	S11	1FMYU03152KA64856	3.0L	T/LD	9	2001	2.00E+03	9F715	D21	10	2023200	10000	AT STOP
2002	9785	S11	1FMYU03152KA63335	3.0L	T/LD	10	2001	2.00E+03	9F715	D21	11	3947888	6000	WHILE DRIVING
2002	9809	S11	1FMYU03152KA49466	3.0L	T/LD	9	2001	2G04	12A650	D21	7	1118556	6000	WHILE DRIVING
2002	9813	S11	1FMYU03152KA49549	3.0L	T/LD	9	2001	2G04	12A650	D21	6	678439	11000	WHILE DRIVING
2002	9822	S11	1FMYU03152KA44073	3.0L	T/LD	8	2001	1H03	BJ460	D21	4	515002	3000	ME
2002	9837	S11	1FMYU03152KA39575	3.0L	T/LD	9	2001	2G04	DIAG	D21	6	1289669	12000	WHILE DRIVING
2002	9843	S11	1FMYU03152KA37852	3.0L	T/LD	9	2001	1H03	BJ460	D21	3	390346	0	WHILE DRIVING
2002	9845	S11	1FMYU03152KA37852	3.0L	T/LD	9	2001	2G04	DIAG	D21	5	815833	6000	AT STOP
2002	9849	S11	1FMYU03152KA37785	3.0L	T/LD	9	2001	2G04	12A650	D21	7	1118466	7000	STALLS
2002	9864	S11	1FMYU03152KA34694	3.0L	T/LD	9	2001	1.00E+04	6333	D21	12	9412838	21000	STALLS

SSM		WDS DIAG PASS CODES. RUN DATALOGGER AND POWER BALANCE. RUN FUEL PRESSURE, RUN OASIS REPORT. CALLED HOTLINE, SPOKE WITH JON, REF #1LMR007. RECHECK ALL GROUND CONNECTIONS AS PER SSM 15434 TEST DROV
NPF		ROAD TEST; RAN EEC TEST, PASSED; MONITORED PIDS; RAN FUEL PRESS TEST; COULD NOT DUPLICATE OR FIND ANY PROBLEMS
REFLASH		PER FORD TECH ASSIST INSTALLED LATEST CALIBRATION FOR STALLING
REPLACED		RESET IDLE STOP PER FORD, REPLACED IAC VALVE PE R FORD, ROAD TESTED VEHICLE FOR 347 MILES DID N OT STALL AT ANY TIME FOR US
SSM		PERFORMED WDS TEST SYSTEM PASSED, PERFORMED PINPOINT TEST. REPLACED IAC AND POWER RELAY AS PER SSM #15434. RETESTED OK.
REFLASH		IMPROPER OPERATION 12A650 CC42 DIAG AND PINPOINT TEST. IGNITION TEST. REPROGRAMMED PCM. RETEST. TEST DRIVE. P1111 P1111 P1111
SSM		704 TEST DROVE NEVER DIED. PERFORMED NGS DIAG NO CODES. PERFORMED KOEO PASS, KOER PASS, PERFORME D PID MONITOR TEST ON TEST DRIVE EVERYTHING IN NORMAL RANGE. PERFORMED PINPOINT TEST BY SYMPTON. PASS
REPLACED		SNOP WDS EEC TEST DCL TEST POWER BALANCE TEST INJ FLOW TEST RECOR DER ROAD T.PIN POINT REPLACED IAC +MAP AND REP.PCM RETEST
REFLASH		EEC DIAG PINPOINT CK ALL PASS CODES. CK IGN SYSTEM CK CK FUEL PRESS. 55PSI CK TEST DR MONITROR CK PIDS. CK REPROGRAM
REPLACED		NGS TEST, REPLACE IDLE CONTROL VALVE.
SNOP		SNOP EEC (QUICK TEST) DIAGNOSIS
REFLASH		EEC TEST, NO MIL LIGHT ONROAD TEST W MONITOR, OK TEST FUEL PRESSURES, OK; HAD NO STALL DURING TESTING; REPROGRAM PCM
SSM		REF SSM 15569 PCM RECALL
SSM		?????????? TECH 63042 MILES 6976 CK EEC SYSTEM KOEC PASSED KOER PASSED,ROAD YEST CAN NOT VERIFY BUT RAN OASIS,SSM 15569,REPROGRAMED PCM
VACUUM LEAK		VAC LEAK PCM PERFORMED WDS DIAGNOSIS,DATALOGGER,POWER BALANCE,FUEL PRESSURE,INJ
REPLACED		ERRATIC OPERATION WDS TEST, PINPOINT TEST. REPLACE IDLE AIR CONTROL. REPROGRAM PCM. RETEST. ROAD TEST.
TSB		PERFORMED EEC TEST, FOUND NO CODES STORED IN MEMORY. FOUND TSB ON PROBLEM. TSB 02 11 6.....REPLACED IAC, EEC RELAY, AND REPROGRAMMED THE PCM TO THE LATEST CALIBRATION 2L8A 12A650 AD...PER THE T
SSM		PCM UPDATE SSM 15569 12A650...RECALEM REPROGRAM PCM PER SSM 15569,CHECK CANISTER VENT AND CK OPER, OK..CC..DD
REPLASH		VERIFIED STALLING CONDITION, PERFORM EEC TEST PASS CODES REPROGRAM PCM AND RDTEST OK AT THIS TIME
REPLACED		DIAG AND REPAIR
NPF		NONE FOUND EEC (QUICK TEST) DIAGNOSIS
REPLACED		BURNT. EEC TEST, PINPOINT TEST, NGS MONITOR TEST, FUEL SYSTEM PRESSURE TEST, REPLACED PFE SENSOR AND RERUN TEST
NPF		NO PROBLEM FOUND. EEC TEST, NGS MONITOR TEST, NGS DCL DISPLAY TEST, IGNITION SYSTEM DIAGNOSTIC TEST, FUEL SYSTEM PRESSURE TEST, EVAPORATIVE EMISSIONS SYSTEM STATIC LEAK TEST AND ROAD TEST
UNOP		SNOP EEC (QUICK TEST) DIAGNOSIS
DIAG		D OLD MOTOR RECHARGED AC BLED COOLING SYSTEM ROAD TESTED OK

E HOME FOR THE WEEKEND, NO PROBLEMS. CALLED RSE, TOLD TO CHECK PURGE VALVE TO EVAP. ADJUST IAC AND UPDATE PCM MONITOR. RETEST KAM AND DRIVE, FUEL TRIM DID NOT UPDATE. CALL RSE ORDER	VEHICLE IS DYING GOING DOWN THE HIGHWAY
	ENGINE DIED ONCE WHILE DRIVING, BUT SEEMS TO RUN FINE NOW.
	REPROGRAM PCM WITH LATEST CALIBRATION PER TECH SERVICE
	WHILE DRIVING AT 35 40 MPH ENGINE STALLED VEH WAS ON DECLINE WHEN THIS OCCURRED
	CUSTOMER STATES ,AT TIMES ENG.WILL DIE OUT AT STOPS WILL RESTART OK.
	C6 INTERM WHILE DRIVING ENGINE CUTS OFF
. RAN CASS FOUND SSM 15434. PERFORMED SSM REMOVED BATTERY AND BATTERY TRAY. CHECKED GROUNDS ALL GOOD AND TIGHT. REMOVED ALL GROUNDS AND CLEANED AND REINSTALLED. REINSTALLE D ALL BATTERY	CUSTOMER STATES THE ENGINE STALLED ONCE WHILE DRIVING
	CUSTOMER STATES CAR STALLS LOOSES POWER
	CUSTOMER STATES THE TRUCK HAS BEEN STALLING HAPPENED WHEN DRIVING ABOUT 25 30 MPH HAPPENED 1 TIME NO
	WHEN SLOWING DOWN & MAKING TURN, VEHICLE CUTS OFF.
	CUST STATES THE VEH STALLED WHILE DRIVING
	C S ENGINE HAS STALLED SEVERAL TIMES IN LAST 2 DAYS WHEN COMING TO A STOP IN TRAFFIC, RESTART IS NORMAL, NO MIL
	CAR DIED WHILE DRIVING PULLED CAR TO SIDE PUT IN PARK RESTARTED
	021 CUST STATES VEH WILL INTERMITT CUT OFF WHEN DRIVING AROUND SPEEDS OF 35 MPH, VEH WILL RESTART
	CUST STATES THE ENGINE STALLED WHILE DRIVING 30 40 MPH CUST STATES SHE LOST POWER STEERING ASSIST SH
	CUSTOMER STATES ENGINE STALLED COMING TO A STOP
69. TEST DROVE....OK	CUSTOMER STATES THAT VEHICLE DIED WHILE DRIVING, LOSS ALL POWER
	INTERMITTENLY WHEN DRIVING WITH A C ON AND COMING TO A STOP VEH WILL DIE,.CUST HAS NOTICED IT MOST WHEN COMING DOWN
	CUSTOMER STATES CAR SHUT OFF WHILE DRIVING
	CUST STS ENGINE LITE COMES ON
	CUST STATES VEH CUT OFF WHILE DRIVING AND ALL LIGHTS CAME ON
	CUSTOMER STATES ENGINE STALLS WHILE DRIVING
	CUSTOMER STATES ENGINE STALLS WHEN ON DECEL (ANY SPEEDS) AND AT STOPS TOO ALSO NOTICED WITHOUT AC ON
	ENGINE STALLS OUT, RIGHT BEFORE STALLING OUT THE CHK ENGINE LITE, OIL, AND BATTERY LITE COME ON AND CAR LOSSES POWER FOR 2 4 MILES THEN STALLS OUT
	VEHICLE TOWED IN. QUIT RUNNING. ENGINE OIL LIGHT WAS FLASHING. ENGINE IS MAKING A TICKING NOISE.

2002	9875	S11	1FMYU03162KA59217	3.0L	TAD	6	2001	2.00E+03	9F715	D21	9	1737303	9000	WHILE DRIVING
2002	9874	S11	1FMYU03162KA59217	3.0L	TAD	6	2001	7C06	14KD69	D21	2	360575	2000	STALLS
2002	9861	S11	1FMYU03162KA59804	3.0L	TAD	6	2001	2.00E+03	9F715	D21	5	932012	3000	WON'T RUN
2002	9862	S11	1FMYU03162KA59091	3.0L	TAD	6	2001	7C06	14KD69	D21	9	1609307	4000	WHILE DRIVING
2002	9860	S11	1FMYU03162KA17763	3.0L	TAD	6	2001	7W07	15807	D21	11	2010636	3000	WHILE DRIVING
2002	9859	S11	1FMYU03165KA15569	3.0L	TAD	6	2001	2.00E+03	9F715	D21	4	945265	8000	AT STOP
2002	9913	S11	1FMYU03166KA14935	3.0L	TAD	6	2001	2B02	12B570	D21	10	1813604	21000	WON'T RUN
2002	9918	S11	1FMYU03165KA09907	3.0L	TAD	6	2001	2B05	RECAL	D21	9	1380560	8000	TURNING
2002	9926	S11	1FMYU03166KA09056	3.0L	TAD	6	2001	2.00E+03	9H307	D21	10	1977494	9000	WHILE DRIVING
2002	9928	S11	1FMYU03166KA07721	3.0L	TAD	6	2001	1H05	9J460	D21	8	1484195	8000	WHILE DRIVING
2002	9941	S11	1FMYU03166KA09214	3.0L	TAD	6	2001	2B05	RECALEM	D21	8	1226170	11000	WHILE DRIVING
2002	9949	S11	1FMYU03142KD97866	3.0L	TAD	6	2002	7V01	12A561	D21	1	1944514	1000	AT STOP
2002	9955	S11	1FMYU03142KD94594	3.0L	TAD	6	2002	1H05	9J460	D21	3	2079660	8000	STALLS
2002	9957	S11	1FMYU03142KD93690	3.0L	TAD	6	2002	2.00E+03	9F715	D21	2	2136390	1000	WHILE DRIVING
2002	9958	S11	1FMYU03142KD88891	3.0L	TAD	6	2002	2B02	12B570	D21	1	2044363	0	WHILE DRIVING
2002	9961	S11	1FMYU03142KD42949	3.0L	TAD	6	2002	2.00E+03	9F715	D21	2	1797291	0	WHILE DRIVING
2002	9966	S11	1FMYU03142KD41578	3.0L	TAD	4	2002	7W07	15807	D21	2	2008012	1000	WHILE DRIVING
2002	9964	S11	1FMYU03142KD33528	3.0L	TAD	4	2002	2G01	12A650	D21	1	1543096	0	STALLS
2002	9965	S11	1FMYU03142KD23169	3.0L	TAD	4	2002	1H05	9J460	D21	3	2229256	3000	WHILE DRIVING
2002	9970	S11	1FMYU03142KD22283	3.0L	TAD	4	2002	2B04	DIAG	D21	2	2117316	1000	WHILE BRAKING
2002	9975	S11	1FMYU03142KD11445	3.0L	TAD	4	2002	2B05	RECALEM	D21	1	1554460	0	WHILE DRIVING
2002	9979	S11	1FMYU03142KD82485	3.0L	TAD	4	2002	1H05	9J460	D21	0	1098003	0	AT STOP
2002	9981	S11	1FMYU03142KD81081	3.0L	TAD	3	2002	7C05	14KD69	D21	-1	1697177	0	WHILE DRIVING
2002	9985	S11	1FMYU03142KC94406	3.0L	TAD	3	2002	1H05	9E476	D21	0	1092350	0	WHILE DRIVING
2002	9989	S11	1FMYU03142KC76978	3.0L	TAD	3	2002	2.00E+03	9F715	D21	1	2009442	0	WHILE DRIVING

TSB		6619 ROAD TEST VERIFIED CONCERN. SELF TEST PASS TSB 02 11 06 PERFORM DCL DISPLAY MONITOR IAC. SHOULD BE BETWEEN 32 42 PERCENT. DROPS BELOW 32. REPLACE IAC WITH UPDATED PART AND UPDATED PCM. PERFOR
SSM		2580 EEC POWER RELAY TEST DRIVE VEHICLE DID NOT VERIFY COMPLAINT. PERFORM EEC TEST RECIEVED PASS CODES PERFORM FUEL PRESSURE TEST 45 PSI PERFORM IGNITION RECORDER MONITOR TEST PASS. PERFORM PID RE
REPLACED		TEST SYSTEM CALLED TECH ASSIST HOOK UP WDS PERFORM DIAGNOSTICS REPROGRAM PCM AND REPLACE IAC
TSB		5234 149089 42 TEST DROVE, TESTED THE EEC SYSTEM ALL SYSTEM PASSED, RETEST DROVE WHILE MONITORING PIDS AS PER TSB 2 11 6, ENGINE NEVER STALLED, REPLACED THE EEC RELAY AND ADVISED
REPLACED		TRANSCEIVER SHORTED ROAD TEST TO VERIFY CUSTOMER CONCERN, NGS EEC TEST P1354 DCL DISPLAY, PINPOINT TEST. REPLACE PATS TRANSCEIVER, EEC RETEST AND ROAD TEST
REPLACED		RAN A WDS TESTING KOEO,KONT,KOER DCL AND POWER BALANCE FOUND THAT IAC VALVE IS STICKING REPLACED IAC VALVE TO CORRECT PROBLEM
REPLACED		21467 42 TESTDROVE FOR HOT IDLING RAN NGS TEST RAN KOEO AND KOER TEST CODE PASS RAN PID DATA DISPLAY TEST SHORT FUEL TRIM AT 33 PERCENT AND MAFV .40 AND LAMB 43 RAN PINPOINT TEST REPLACED MAF SENS
REFLASH		EEC TEST NO CODES ROAD TEST UNABLE TO VERIFY STALLING RUN OASIS REPROGRAMMED PCM RETEST
REPLACED		EEC TEST P0179 & P0174,PID TEST,FUEL PRESSURE TEST,INJECTOR TEST,ROAD TEST WITH FUEL GAUGE PRESSURE DROPPED,REPLACED FUEL PUMP,ROAD TEST.
REPLACED		WDS TEST, EEC TEST, DCL ROADTEST 4 MILES, PINPOINTTEST DPFE VOLTAGEOUT OF SPECS, AND REPLACED DPFE SENSOR AND RETESTED
REFLASH		EEC TEST PINPOINT TEST REPROGRAM PCM RETEST
TSB		PERFORMED TSB # 02 11 6 FOUND LOOSE GROUND AT C104 REPAIRED GROUND RETESTED OK.
TSB		EEC DCL PERFORM TSB 2 11 6 CK EVAP SYSTEM RPL PFE
TSB		FORD TECH BULLETIN 02 11 06 RAN EEC TEST ALL PCM CODES CHECKED FOR SERVICE MESSAGES FOUND TSB 02 11 06 RAN TESTING PER TSB IAC SHOWS 35% OK,
TSB		DOES NOT OPERATE PROPERLY WDS KOEO PASS KOEC PASS KOER PASS R&R IAC PER TSB 02 11 06 CALLED TECH HOTLINE PERFORM ADD TESTS R&R MAP SENSOR TEST DRIVE OK
TSB		PERFORM STALLING TSB REPLACE IDLE AIR CONTROL VALVE
PATS		TRANSCEIVR SHORTED ROAD TEST TO VERIFY CUSTOMER CONCERN, NGS EEC TEST P1332 DCL DISPLAY, PINPOINT TEST A. REPLACE PATS TRANSCEIVER
TSB		HOOK UP TO WDS EEC TEST PINPOINT MONITOR PIDS, CK FUEL SYSTEM AND IGNITION, CK FOR AIR OR VACUUM LEAKS, REPLACE IDLE AIR CONTROL PER TSB 02 11 06 REPLACE THROTTLE BODY REPLACE MAF PER HOTLINE, CLE
REPLACED		1 ROAD TESTED, PERFORMED EEC TEST, CODE P0401, PINPOINT TESTED AND MONITORED PIDS ON ROAD TEST WITH NGS. REPLACED DPFE
TSB		DCL ROADTEST CK OASIS PERFORM TSB 01 11 16 TEST IAC DUTY CYCLE USE WDS CK PCM CALIBRATION CURRENT TEST EVAP SYSTEM BLOW AIR THROUGH CK EEC RELAY ALL AREAS IN SPECS
REFLASH		EEC TEST, NO CODES, DCL, REPROGRAMMED PCM CC42 9804
REPLACED		DPFE SENSOR CHECKED EEC AND FUEL PRESSURE 34 PSI IGN SYSTEM DIAG AND NGS RECORDING AND PINPOINT TO DPFE REPLACE AND RECHECK EEC OK
TSB		DIAGNOSE USING WDS AND REPLACE EEC POWER RELAY PERTSB 02 11 06
REPLACED		ON 67 MILES ROADTEST EGR FLOW DROPPED TO 0 AT MID RANGE R AND R EGR REROADTEST OK
DIAG		ECC RELAY MALFUNCTION EEC (QUICK TEST) DIAGNOSIS

MED FINAL ROAD TEST	CUST STATES INTERMITTENTLY WHILE DRIVING ENGINE STALLS BUT WILL RESTART. USUALLY STALLS WHILE DECELLERATION. SEE CUST ATTACHED NOTES
CORDER MONITOR TEST PASS FOUND IAC AT 38% DUTY CYCLE IN SPEC. CONTACTED FORD HOTLINE WAS INSTRUCTED TO CHECK GROUNDS IAC AND EEC RELAY. REMOVE BATTERY BOX TIGHTEN GROUNDS 101,104 FOUND	CUST STATES ON WAY TO WORK FROM HOME TODAY BEFORE GETTING TO WORK AFETR TRUCK WAS WARMED UP TRUCKED STALLED AND WOULD NOT RESTART CUST DID NOT NO IF IT CRANKED OR NOT CUST WORKS ABOUT 10
	CUST REPORTS ENG STARTS THEN STALLS WHEN STARTING ENG COLD ENG SPUTTERS ON ACCEL. COLD START CONDITION
	D21 CUS STS HAS STALLED 2 TIMES WHILE DRIVING, STARTS EASILY
	D21 CUST STATES VEH DIES WHILE DRIVING, STARTS RIGHT BACK UP WHEN IT DIES, ACTS LIKE TURN KEY OFF
	CUSTOMER STATES VEH STALLS WHEN COLD AND WHEN HE STOPS AT A STOP SIGN RPMS GO TO 0 PLEASE CHECK AND ADVISE
OR RETEST MAF SENSOR MAFV AT .90 LAMB 80 AND SHORT FUEL TRIM 2	CK LOST POWER WONT STAY RUNNING
	WHEN TURNING THE STEERING WHEEL LEFT OR RIGHT THE VEHICLE DIES OUT DOES NOT HAPPEN ALL THE TIME 2 3 TIMES A DAY
	ENG DIED GOING DOWN THE ROAD
	E29 CUST STATES, ENGINE STALLED WHILE DRIVING, AND CHECK ENGINE LIGHT STAYS ON, ADVISE
	CK DIED TWICE WHILE DRIVING
	CUST STATES WHEN THE TRUCK WAS AT A STOP LIGHT IT STALLED OUT(STARTED BACK UP)
	OWNER STATES ENGINE STALLED AND WOULD NOT RESTART HAD NO CRANKING POWER FOR 40 MIN THEN WOULD RESTART
	VEHICLE TOWED IN, CUSTOMER WAS DRIVING UPHILL THEN SLOWED AND TURNED INTO SUBDIVISIONAT APPROX 10 15 MPH
	VEHICLE DIED 2 TIMES GOING DOWN THE HWAY STARTED BACK UP
	CK ENGINE STALEED WHEN DRIVING ABOUT 35 MPH CK TSB FOR THIS
	D21 CUST. STATES ENGINE STALLS OUT WHILE DRIVING LOSES ALL POWER
AR KAM AND RETEST REPLACE PCM ENTER PAT 8 YSTEN FLASH 2 KEYS, AND ROADTEST, RECHECK NEXT DAU ADDITIONAL TIME TO RECONFIGURE KAM AND DIAGNOSPER HOTLINE, 9065220276 3FLD8001 PER ALEX KNOLL	CUSTOMER STATES VECHILE KEEPS STALLING AND SURGING
	DIAGNOSE VEHICLE STALLS INTERMITTENTLY WHILE DRIVING.
	VEHICLE STALLS WHEN COMING TO A STOP, WILL RESTART AFTER A COUPLE OF MINUTES. (INTERMITTANT, VEHICLE AT OPERATING TEMP)
	D21 CUST STATES ENGINE STALLING AT TIMES WHILE DRIVING.
	STALLS AT STOPS
	STALLS WHILE DRIVING
	VEHICLE DIES WHILE DRIVING
	C S CAR CUT OFF WHILE DRIVING, DID RESTART NO PROBLEM ADVISE

2002	10001	S11	1FMYU03142KC46997	3.0L	TAD	2	2002	2.00E+06	9950	D21	5	2114669	6000	STALLS
2002	10005	S11	1FMYU03142KC47410	3.0L	TAD	2	2002	2.00E+03	9F715	D21	1	1418813	1000	WHILE DRIVING
2002	10006	S11	1FMYU03142KC47309	3.0L	TAD	2	2002	7C05	14N089	D21	1	2307966	1000	WHILE DRIVING
2002	10011	S11	1FMYU03142KC37931	3.0L	TAD	2	2002	2.00E+03	9F715	D21	6	2207765	3000	WHILE DRIVING
2002	10013	S11	1FMYU03142KC37982	3.0L	TAD	2	2002	2905	RECALIBM	D21	1	2237510	0	WHILE DRIVING
2002	10021	S11	1FMYU03142KC30910	3.0L	TAD	2	2002	2904	DIAG	D21	1	945415	0	ON HIGHWAY
2002	10022	S11	1FMYU03142KC29478	3.0L	TAD	2	2002	2904	12A650	D21	1	1100476	0	WHILE DRIVING
2002	10041	S11	1FMYU03142KC16985	3.0L	TAD	1	2002	2.00E+03	9E998	D21	5	2103205	3000	WHILE DRIVING
2002	10044	S11	1FMYU03142KC16724	3.0L	TAD	1	2002	2905	RECAL	D21	6	2008998	6000	COASTING
2002	10052	S11	1FMYU03142KC16315	3.0L	TAD	1	2002	2.00E+03	9F715	D21	4	1904899	3000	STALLS
2002	10059	S11	1FMYU03142KC09092	3.0L	TAD	1	2002	2.00E+03	9F715	D21	3	2190801	1000	AT STOP
2002	10063	S11	1FMYU03142KC00791	3.0L	TAD	1	2002	2905	RECALIBM	D21	3	1160904	5000	WHILE DRIVING
2002	10072	S11	1FMYU03142KB96547	3.0L	TAD	1	2002	2.00E+03	9F715	D21	6	2202494	6000	WHILE DRIVING
2002	10078	S11	1FMYU03142KB97113	3.0L	TAD	1	2002	2904	12A650	D21	7	2135351	6000	ON HIGHWAY
2002	10079	S11	1FMYU03142KB96952	3.0L	TAD	1	2002	2904	12A650	D21	8	1978240	12000	STALLS
2002	10085	S11	1FMYU03142KB95491	3.0L	TAD	1	2002	2.00E+03	9E998	D21	7	2247990	12000	WHILE DRIVING
2002	10090	S11	1FMYU03142KB76936	3.0L	TAD	1	2002	2.00E+03	9F715	D21	4	1752377	9000	AT STOP
2002	10094	S11	1FMYU03142KB66973	3.0L	TAD	12	2001	2904	DIAG	D21	6	1709440	6000	WHILE DRIVING
2002	10095	S11	1FMYU03142KB66715	3.0L	TAD	12	2001	7C05	14N089	D21	2	1270949	0	WHILE DRIVING
2002	10096	S11	1FMYU03142KB66594	3.0L	TAD	12	2001	2904	DIAG	D21	5	1956492	4000	WHILE DRIVING
2002	10097	S11	1FMYU03142KB66455	3.0L	TAD	12	2001	1H03	9J460	D21	8	2397327	15000	STALLS
2002	10102	S11	1FMYU03142KB66242	3.0L	TAD	1	2002	2905	RECALIBM	D21	4	1149295	6000	WHILE DRIVING
2002	10103	S11	1FMYU03142KB66211	3.0L	TAD	12	2001	2.00E+03	9F715	D21	4	1135571	6000	WHILE DRIVING
2002	10112	S11	1FMYU03142KB63592	3.0L	TAD	12	2001	2.00E+03	9F715	D21	8	2376213	12000	WHILE DRIVING
2002	10125	S11	1FMYU03142KB37831	3.0L	TAD	12	2001	2.00E+03	9F715	D21	1	1948099	1000	WHILE DRIVING

DIAG		5013 COULD NOT VERIFIED CRANK NO START CONCERN PERFORMED WDS EEC SELF TSET ALL SYST PASSED MONITOR AND RECORD VARIOUS PID DATA ALLPID DATA OPERATING WITHIN NORMAL RANGES PERFORMED FUELPRESSURE
NO TEXT		
TSB		1205 NO MIL LIGHT , COULD VERIFY STALL , PERFORMED TSB 02 11 6 ,, PETRFORMED EEC TEST KOEO PASS , PID MONITOR & RECORD , REPLACED DPFE SENSOR & EEC & FUEL PUMP RELAYS WITH UPDATED PARTS. RETEST PAS
TSB		6F715,6E666,42 TSB 02 11 6 RAN EEC TEST, NO DTC, PINPOINT TEST, MONITOR ROAD TEST REPLACE IAC, THROTTLE BODY AS PER TSBL ROAD TEST
SSM		0007 SELF TEST,PASS,REPROGRAM PCM PER SSM AND RETEST,PASS. DID NOT DUPLICATE CONCERN AT THIS TIME.
SSM		WDS KOEO P1111 KOEC P1111 KOER P1111. INSPECT FOR REVISED PCM CALIB & EEC POWER RELAY PER OASIS NGS PID DATA
REFLASH		RUN EEC TEST, DCL DISPLAY TEST, AND REPROGRAM PCM.
DIAG		VAN IAC THROTTLE BODY EEC (QUICK TEST) DIAGNOSIS
REFLASH		C CODE 42 RECAL TEST EEC CODE PASS PINPOINT TEST NGS DCL DISPLAY NGS ROAD TEST IGNITION TEST FUEL PRESSURE TEST PERERFORM EVAPORATIVE
REPLACED		RAN DIAGNOSIS TEST REPLACE IDLE CONTROL VALVE REPROGRAM PCM 1 6F715,D21,42
NPF		1107 POSSIBLE CONCERN 126500 D01 RAN EEC TEST NO CODES RAN NGS ROADTEST FOUND NO CONCERNS UNABLE TO DUPLICATE
REFLASH		PERFORM EEC TEST SDDS DIAGNOSIS POWER BALANCE AND SPARK DURATION TEST REPROGRAM PROCESSOR AND RETEST
TSB		TSB2 11 06 EEC (QUICK TEST) DIAGNOSIS
REFLASH		EEC TEST PIN POINT TEST AND REPROGRAM PCM
TSB		RUN SYSTEM TEST, REPROGRAM PCM PER TSB 020606 AND TEST DRIVE.
TSB		12200 POSS TSB UPDATE NO 02 11 06 CK AND INSTALLED NEW AIR BYPASS VALVE AND TROTTLE BODY ASSY AND ECC RELAY AND REPROGRAMED PCM ASSY AND RE RD TEST AND RE CK OK AT THIS TIME MILAGE OUT 12209
TSB		2226 VERIFY CONCERN, NGS TEST SYSTEM PASS. IGNITION AND FUEL SYSTEM TEST PASS. DCL DISPLAY AND MONITOR ROAD TEST ALL PIDS IN SPECS. CHECK OASIS AND SSM. REFER TO TSB 02 11 6. PERFORM SERVICE PROCE
NPF		ROAD TEST TO VERIFY CONCERN NGS START UP EEC TEST PASS DCL DISPLAY PIN POINT YTEST Z NEED CUSTOMER ASST COULD NOT VERIFY OWNER CONCERN THIS REPAIR VISIT
DIAG		EEC RELAY AND CALIBRATION CONT PASS KOEO PASS KOER PASS SDDS EEC TEST DIAG PINPOINT IDLE DATA FUEL PRESSURE INJ FLOW POWER BALANCE DCL MONITOR
NPF		DID NOT VERIFY, CAR STARTED, HOOK UP NGS, EEC TEST, PASS, PERFORM FUEL PRESSURE TEST, 65 PSI, PERFORM IGNITION SYSTEM DIAGNOSIS, PERFORM PINPOINT TEST, ROADTEST AND MONITOR PIDS, CAR OPERATING NORM
REPLACED		NGS SYS TST PASS DCL TST DPFE READING 1.27V PINPNT & REPL DPFE SENSOR RPCM & RETST PASS PID MONITOR & ROADTST OK NOT STALLING
REFLASH		EEC TEST CODE PASS,P P TEST REPROGRAM PCM ASPER OASIS RETEST ROAD TEST CC 06 TECH 9991
REPLACED		EEC TEST NO DTCS NGS ROD TEST DCL TEST CK IGN SYSTEM CK FUEL SYSTEM PERFORM PINPOINTEST REPLACE IAC RETEST ALL OK
INOP		VALVE NOT WORKING PROPERLY PERFORM DIAGNOSTICS AND REPLACE IAC VALVE
TSB		PERFORMED DIAG TEST REPAIRED PER TSB 02 11 06

LEAKDOWN TEST PASSED GEARORED OASIS FOR RELATED CONCERNS NONE FOUND OASIS CONTACT ID#409 886 727 CALLED CUSTOMER FOR MORE INFO ON CONCERN CRANK NO START CONCERN OCCURED	AFTER VEH WARMS UP IT IS CRANKING BUT NOT WANTING TO START
	CK/ADV THE TRUCK STALLED WHILE DRIVING ALL INDICATOR LIGHTS CAME ON & THERE WAS A LOSS OF POWER 12
8.	D21 CUST STATES VEHICLE STALLED WHILE DRIVING,20 40 MPH,TRAFFIC,SEE MS
	C S WHILE DRIVING THE VEH WILL STRT SLOWING DONW AND STALL WILL START BACK UP, HAPPENS ABOUT ONCE A MONTH
	D02 CUST STATES ENGINE DIED WHILE DRIVING ONCE, ENGINE RESTARTED FINE. THIS HAS NOT HAPPENED AGAIN.
MONITOR RECORD ROAD TEST. UNABLE TO DUPLICATE AT THIS TIME. MIL OFF. TECH 117.	CUST STATES VEH SHUT DOWN ON HIGHWAY HAD TOWED IN
	ENGINE STALLS INTERMITTANTLY WHILE DRIVEING,EASY RESTART
	REPAIR ENG IS STALLING WHILE DRIVING WHEN ENG IS HOT OR COLD
	STALLS OCCASSINALY AND DIES WHILE COASTING AROUND 30 MPH
	RUN COMPUTER DIAGNOSTICS FOR PERFORMANCE CONCERNS CAR STALLED AND WOULD NOT START, TOWED IN
	D21 ENG DIED CUST STATES THE ENG DIED WHILE DRIVING LOST POWER STEERING RESTARTED NO PROBLEMS NOT AT STOP OR ACCEL OR DECCEL STEADY SPEED
	VEHICLE STALLED WHILE DRIVING
	CUSTOMER STATES THAT ENGINE STALLS AT TIMES WHILE DRIVING
	VEHICLE DIED TWICE WHILE ON THE HIGHWAY PLEASE CHECK AND ADVISE D21
	CHECK ENGINE; STALLS.
	CUST STATES VEICH DIES WHILE DRIVING ,WILL CRANK BUT WONT START FOR ABOUT A HALVE HOUR SEE HISTORY HAS HAPPENED BEFORE ,,,NPF 7
DURE. CHECK IAC DUTY CYCLE AND REPLACE IAC. RECHECK DUTY CYCLE AND REPLACE THROTTLE BODY. CHECK PCM CALIBRATION LEVEL AND REPROGRAM TO LATEST LEVEL. CHECK EVAP SYSTEM AND	CHECK ENGINE STALLING AND STOPS POOR IDLE ON START UP IN THE MORNING
	D21 REPAIR STALLED A6 IF KEY SHUT OFF WHILE DRIVING AT APPRO X 45 MPH ENGINE WAS WARMED UP
	C S THAT THE VEHICLE STALLED WHILE DRIVING STARTS OKAY
ALLY, CUSTOMER CAME AND TOOK CAR OVER THE WEEKEND, BEFORE I COULD VERIFY DIEING CONCERN	ENG CUIT WHILE DRIVING , VEH WS TOWED IN
	CST STATES AT TIMES RIGHT AFTER STRT VEH & TAKES OFF VEH STALLS WILL RESTRT RIGHT AWAY
	REPAIR ENGINE DIES AT SPEEDS OF 30MPH AT TIMES AND BOX AROUND GEAR INDICATING WHICH GEAR IT IS IN DISSPEARED
	CUST. STATES ENGINE DIED WHILE DRIVING
	OWNER STATES THAT WHILE DRIVING AND SLOWING DOWN TO TURN ON ST THAT THE CAR DIED AND LOST POWER STEERING ETC.. TURNED KEY AND STARTED BACK UP
	CUST. STATES WHEN DRIVEING THE VEHICLE CUTS OFF AND THE CHECK ENGINE LIGHT COMES ON. THIS HAS HAPPENED 3 TIMES.

2002	10127	S11	1FMYU03142KB30827	3.0L	TALD	11	2001	2.00E+03	9F715	D21	1	1785412	0	WHILE DRIVING
2002	10129	S11	1FMYU03142KB25727	3.0L	TALD	11	2001	7C05	14N089	D21	1	693251	0	WHILE DRIVING
2002	10131	S11	1FMYU03142KB34805	3.0L	TALD	11	2001	7V01	12A581	D21	1	351109	0	WHILE DRIVING
2002	10139	S11	1FMYU03142KB34026	3.0L	TALD	11	2001	7C05	14N089	D21	3	747223	3000	WHILE DRIVING
2002	10140	S11	1FMYU03142KB34075	3.0L	TALD	11	2001	2.00E+05	9H537	D21	6	1700602	4000	WHILE DRIVING
2002	10144	S11	1FMYU03142KB23590	3.0L	TALD	11	2001	2.00E+03	9F715	D21	6	2236141	12000	ROUGH IDLE
2002	10157	S11	1FMYU03142KB05736	3.0L	TALD	10	2001	7V01	12A581	D21	2	639041	2000	WHILE DRIVING
2002	10159	S11	1FMYU03142KB03825	3.0L	TALD	10	2001	2.00E+03	9F715	D21	7	2448593	8000	WHILE DRIVING
2002	10162	S11	1FMYU03142KB03880	3.0L	TALD	10	2001	2C05	RECAL	D21	5	994228	3000	WHILE DRIVING
2002	10163	S11	1FMYU03142KB03880	3.0L	TALD	10	2001	1H03	9J460	D21	9	2099521	7000	WHILE DRIVING
2002	10164	S11	1FMYU03142KB03494	3.0L	TALD	10	2001	2C01	12B665	D21	10	2145027	12000	WHILE DRIVING
2002	10169	S11	1FMYU03142KB02691	3.0L	TALD	10	2001	2.00E+04	9C915	D21	1	710668	2000	WON'T RUN
2002	10174	S11	1FMYU03142KB01877	3.0L	TALD	10	2001	2C04	DIAG	D21	3	640049	5000	WHILE DRIVING
2002	10194	S11	1FMYU03142KA80367	3.0L	TALD	10	2001	2C05	RECAL	D21	5	785564	8000	WHILE DRIVING
2002	10195	S11	1FMYU03142KA80967	3.0L	TALD	10	2001	2.00E+03	9F715	D21	7	1484724	14000	STALLS
2002	10196	S11	1FMYU03142KA80272	3.0L	TALD	10	2001	2.00E+03	9F715	D21	5	1505980	7000	WHILE BRAKING
2002	10200	S11	1FMYU03142KA80259	3.0L	TALD	10	2001	2C05	RECAL	D21	9	1852804	8000	WHILE DRIVING
2002	10206	S11	1FMYU03142KA79579	3.0L	TALD	10	2001	2C04	12A650	D21	6	1039909	7000	AT STOP
2002	10209	S11	1FMYU03142KA79462	3.0L	TALD	10	2001	7V01	12A581	D21	4	882899	8000	WHILE DRIVING
2002	10215	S11	1FMYU03142KA71085	3.0L	TALD	10	2001	2C04	12A650	D21	4	836773	4000	STALLS
2002	10216	S11	1FMYU03142KA71085	3.0L	TALD	10	2001	7C05	14N089	D21	2	386402	1000	STALLS
2002	10219	S11	1FMYU03142KA71023	3.0L	TALD	10	2001	2.00E+03	9F715	D21	7	1369645	6000	WHILE DRIVING
2002	10224	S11	1FMYU03142KA70194	3.0L	TALD	10	2001	2C04	12A650	D21	7	1187142	8000	WHILE DRIVING
2002	10227	S11	1FMYU03142KA69648	3.0L	TALD	10	2001	2C05	RECALEM	D21	9	1572613	9000	WHILE DRIVING
2002	10242	S11	1FMYU03142KA64265	3.0L	TALD	9	2001	5C01	3504	D21	4	795368	2000	ENGINE NOISE

REPLACED		1 REPLACED IAC VALVE
DIAG		1 EEC TEST, PINPOINT TEST IGN SYSTEM TEST FUEL SYSTEM TESTS,NGS DCL DISPLAY RESET,NGS MONITOR ROAD TEST
POOR CONNECTION		NGS EEC TEST KOEO P1000 10 P1000 ER P1000 DCL DISPLAY PIDS OK FUEL PRESSURE TEST 60 PSI HOLDS 60 SEC TEST IGNITION SYSTEM OK ROADTEST WITH NGS DCL MONITOR PINPOINT ERRATIC PIP SIGNAL NE
REFLASH		VERIFY CONCERN EEC TEST DCL MONITOR ROAD TEST REPL EEC RELAY AND REPROG PCM ROAD TEST
DIAG		0221 91/307 42 VERIFIED CONCERN EEC TEST NO CODES FOUND FUEL VOLUME LOW AT 1 TIME FOR A COUPLE OF SECONDS WHEN CONCERN DUPLICATED
INOP		PEFORMED WDS TEST HAS NO CODES RAN PPT FOUND IAC OUT OF RANGE REMOVED AND REPLACED IAC VALVE RETESTED
TSB		CK EEC KOEO KOER CONT MEMORY PINPOINT TEST CK PIDS MONITOR AND RECORD ON ROAD TEST ALL PIDS NORMAL CK OASIS FOR TSBS
REFLASH		RAN WDS TEST, PER QUICK TEST SOT PASS CODES, RAN VARIOUS TEST, RAN PINPOINT, REPROGRAMMED PCM, REPL IAC VALVE, RD TEST, RETEST, OK
TSB		TEST DRIVE, EEC TEST, PERFORM P P TEST, CALL OASIS, REPROGRAM PCM PER TSB, RETEST, DRIVE
REPLACED		7974 USE NGS KOEO P0401 KOER P0401 POERFORM PIDS DIAG MONITOR PERFORM PIN POINT TEST REPLACE PFE SENSER RETEST PASS.
TSB		NGS TEST SELF TEST DCL DIS IGN TEST ROAD TEST SIM TEST REPROGRAM PCM PER TSB 02 11 08 RETEST KOEO PASS PASS KOER PASS MILAGE IN 12789 OUT 12789
STUCK OPEN		2047 9F715 42 STICKS PARTIALY OPEN AT TIMES USED WDS TESTER , RAN KOEO TEST PASSED , RAN OASIS FOR HARD START CONSERNS , CALLED HOT LINE , REMOVED FUEL TANK AND INSPECT VAPOR HOSES , REMOVED AND IN
NPF		PERFORM WDS DIAGNOSTIC TEST, FOUND NO PROBLEM
DIAG		PROCESSOR EEC (QUICK TEST) DIAGNOSIS
DIAG		IAC VALVE EEC (QUICK TEST) DIAGNOSIS
REPLACED		KOEO KOER DATALOG FUEL SYSTEM REPLACED IAC VALV E EEC RELAY REPROGRAM PCM ROAD TEST
TSB		EEC SYSTEM DIAG PERFORMED,NO DTC,S ROAD TEST MONITOR AND RECORD DATA. PERFORMED.TSB #02 11 0 REPROGRAMED PCM ROAD TESTED FOR NORMAL OPERTION. MONITOR AND RECORD DATA ALL
NPF		UNABLE TO DUPLICATE CONCERN EEC (QUICK TEST) DIAGNOSIS
TSB		EEC TEST, NO CODES, VERIFIED PCM HAS LATEST CALIBRATION AN AND NEW STYLE EED RELAY IS USED, ACCESS BATTERY TO CLEAN GROUNDS 104 AND 105, ADJUSTED BASE IDLE CO42 9904
REFLASH		4160 REPROGRAM PCM PER HOTLINE
REPLACED		1768 HOOK UP WDS EEC TEST NO CODES. PERFORM PINPOINT TEST CALL HOT LINE, CK GROUNDS UNDER BATTREY AND ON TRNAS. REPLACE BAD EEC RELAY AND TIGHTEN LOOSE TERMINALS. DROVE WITH FLIGHT RECORDER. RETES
REPLACED		ROADTEST AND CK FOR STALLING OUT WHEN DRIVING (REPLACE IDLE AIR CONTROL VALVE AND THROTTLE BOD Y ASSEMBLY,RECALIBRATE PCM AND ROADTEST FOR APP ROX.22 MILES)
REFLASH		6644 42 W,9650 WDS TEST PCM. NO CODES LISTED. PID MONITOR RECORDER, NO ABNORMAL VALUES FOUND. CHECK OASIS CONTACT ID 606 131 400 SSPECIAL SERVICE MESSAGE 16589 STATES TO REPROGRAM PCM AND CHECK PCM
REFLASH		TEST EEC,MONITOR TEST,REPROGRAM PCM
HOTLINE		2206 CODE 42 W IN CHASSIS ENGINE DIAG.CONTACTED HOTLINE CHECK OIL PRESSURE,INDIVIDUAL CYL. CONTRIBUTION TEST NEC. TO RNR SUBFRAME,AND ENGINE TRANS. ASSEMBLY EVAC A C RNR COMPRESSOR,LIQUID,AND SUCTI

	CUST STATES VEICHLE WONT STAY RUNNING STALLS WHILE DRIVING WILL RESTART
	CUST STATES ENGINE STALLED WHILE DRIVING. HAD TO PULL OVER. ENGINE DID RESTART. CHECK AND ADVISE. GCC: D21
CC TO REPAIR LOOSE WIRE TERMINAL CLEAR KAM ROADTEST OK RETREST OK P1000 P1000 P1000	CUSTOMER STATES ENGINE STALLED WHILE DRIVING WOULD NO RESTART (CRANKED) STARTED THIS MORNING IS TAGGED 999
	CUST STATES VEHICLE CUT OFF IN MIDDLE OF TRAFFIC. VEHICLE RESTARTED
	CHECK VEHICLE LOOSES POWER WHEN DRIVING TO A STALL WILL RE START BUT DOES NOT KEEP SPEED CONTINUES TO SLOW
	CUSTOMER STATES ROUGH IDLE ON COLD STARTS ENGINE WILL CUT OFF ON COLD STARTS
	OK STALLED WHILE DRIVING
	CUSTOMER STATES ENGINE STALLS DRIVING DOWN THE ROAD
	OK ENGINE WILL DIE WHILE DRIVING AT TIMES AROUND 45 MPH
	OK STALLS AT TIMES DRIVING 40 45 MPH STALLED YESTERDAY
	E35 ENGINE DIED WHILE DRIVING,WHEN THIS HAPPENED ALL POWER WAS LOST EXCEPT HEAD LAMPS WIPERS STOPPED WORKING
SPECT VAPOR CANISTER , TEST EVAP. SYS PASSED , TOOK VEH. AND FILLED WITH FUEL TO SEE IF I COULD DUPLICATE CONCERN , DUPLICATED CONCERN , BROUGHT BACK TO SHOP AND INSPECT OPPERATION OF EVAP. VENT	RECHECK: (D21) ENGINE DIES AFTER STARTING AFTER REFUELING (DOES NOT IDLE)
	CUS STATES WHILE DRIVING VEHICLE IT WILL CHUG AND GO TO STALL THEN THE BATT LITE COMES, THEN IT WILL SMOOTH OUT IT DOES THIS WARM OR COLD
	CUST STATES TWICE, WHILE DRIVING, ENGINE DIED ONLY TO IMMEDIATELY RESTART.
	ENGINE STALLS INTERMITTENTLY. WILL IMMEDIATELY RESTART. SEE HISTORY,SEE ATTATCHED. SEE SCOTT.
	1203 ENGINE STALLED WHEN SLOWING AND TURNING RIGHT
	D21 DIES WHILE DRIVING ...STARTS RIGHT BACK UP
	CHECK CUT OFF 1 ONCE AT STOP
	D21 ENGINE WENT DEAD WHILE DRIVING RESTARTS FINE
	CUSTOMER CONCERNED WITH ENGINE STALLING
T DRIVE.	THE VEH IS CUTTING OFF,SEE ADVISOR
	CUST STATES THAT THE CAR KEEPS STALLING OUT AT ANY TIME WHEN DRIVING (OK AND ADVISE) REFER TO NEW T.S.B FOR THIS CONCERN
RELAY AND EVAPORATIVE EMISSIONS SYSTEM. REPROGRAM PCM WITH UPDATE SUBA 12A650 AD CHECKED PCM RELAY,OK NEW STYLE INSTALLED. CHECK AND CLEAN EVAP EMISSIONS SYSTEM PER SSM.	OWNER STATES:INTERMITTANT STALLING JUST DRIVING ALONG, RESTARTS OK
	ENGINE STALLED 1 TIME WHILE DRIVING RESTARTED OK ENGINE SEEMS TO LOSE POWER FOR A SECOND WHEN TRANS SHIFTS
ON LINE REPLACE W NEW MOTOR 3.0L V6 VACCUM DOWN A C RE CHARGED SYSTEM REQUEST 4TIME 1.5 STRIPPED SUB FRAME BOLT OK PER DANA	N12_UNUSUAL ENGINE NOISE TOWED IN

2002	10247	S11	1FMYU03142KA63049	3.0L	T/LD		9	2001	2901	139373	D21		8	1079949	28000	WHILE DRIVING
2002	10256	S11	1FMYU03142KA62184	3.0L	T/LD		9	2001	2.00E+03	9F715	D21		6	866224	4000	WHILE DRIVING
2002	10271	S11	1FMYU03142KA62184	3.0L	T/LD		9	2001	2.00E+03	9E928	D21		10	2127004	10000	WHILE DRIVING
2002	10277	S11	1FMYU03142KA61225	3.0L	T/LD		9	2001	1H03	9J460	D21		9	1950529	13000	WHILE DRIVING
2002	10269	S11	1FMYU03142KA51004	3.0L	T/LD		9	2001	2906	RECAL	D21		7	1248103	4000	AT STOP
2002	10257	S11	1FMYU03142KA46556	3.0L	T/LD		9	2001	2.00E+03	9F715	D21		7	1234080	8000	TURNING
2002	10268	S11	1FMYU03142KA46719	3.0L	T/LD		9	2001	2906	RECAL	D21		10	1964027	11000	DOWNHILL
2002	10293	S11	1FMYU03142KA46862	3.0L	T/LD		9	2001	2906	RECAL	D21		10	1999703	28000	WHILE DRIVING
2002	10288	S11	1FMYU03142KA46845	3.0L	T/LD		9	2001	1A03	6007	D21		1	991850	0	NO TEXT
2002	10296	S11	1FMYU03142KA46845	3.0L	T/LD		9	2001	1A03	6007	D21		1	266745	0	WHILE DRIVING
2002	10297	S11	1FMYU03142KA46455	3.0L	T/LD		9	2001	2904	12A650	D21		7	1126892	7000	WHILE DRIVING
2002	10309	S11	1FMYU03142KA39605	3.0L	T/LD		9	2001	2904	DIAG	D21		1	307665	0	WHILE DRIVING
2002	10308	S11	1FMYU03142KA39606	3.0L	T/LD		9	2001	7V01	14289	D21		5	762576	3000	WHILE DRIVING
2002	10314	S11	1FMYU03142KA39975	3.0L	T/LD		9	2001	2.00E+04	9C915	D21		9	1783630	12000	WHILE DRIVING
2002	10317	S11	1FMYU03142KA39519	3.0L	T/LD		9	2001	2.00E+03	9F715	D21		11	2246021	14000	WHILE DRIVING
2002	10325	S11	1FMYU03142KA37597	3.0L	T/LD		9	2001	2904	DIAG	D21		8	1510775	10000	STALLS
2002	10329	S11	1FMYU03142KA37485	3.0L	T/LD		9	2001	2906	RECALEM	D21		12	2350255	14000	TURNING
2002	10335	S11	1FMYU03142KA36953	3.0L	T/LD		9	2001	7602	10348	D21		10	2027640	10000	WHILE DRIVING
2002	10337	S11	1FMYU03142KA35445	3.0L	T/LD		9	2001	7C05	14N099	D21		9	1360606	7000	WHILE DRIVING
2002	10338	S11	1FMYU03142KA35445	3.0L	T/LD		9	2001	2906	RECAL	D21		9	2055518	8000	WHILE DRIVING
2002	10339	S11	1FMYU03142KA35249	3.0L	T/LD		9	2001	2904	12A650	D21		11	2369619	24000	WHILE DRIVING
2002	10357	S11	1FMYU03142KA17298	3.0L	T/LD		9	2001	2.00E+03	9F715	D21		12	2329962	22000	WHILE DRIVING
2002	10375	S11	1FMYU03142KA16801	3.0L	T/LD		9	2001	2.00E+03	9F715	D21		5	1666629	8000	AT STOP
2002	10395	S11	1FMYU03142KA08164	3.0L	T/LD		9	2001	2904	DIAG	D21		4	410762	3000	WHILE DRIVING
2002	10404	S11	1FMYU03132KD84902	3.0L	T/LD		6	2002	1H03	9J460	D21		2	2159145	1000	STALLS
2002	10409	S11	1FMYU03132KD67666	3.0L	T/LD		6	2002	2.00E+03	9E926	D21		1	1779023	0	WHILE DRIVING

POOR CONNECTION		OPEN CIRCUIT EE TEST PINPOINT TEST SECURED LOOSE CONNECTION AT CAM SHAFT SENSOR AND RETEST
REPLACED		PERFORMED DIAGNOSIS REPLACED IDLE AIR CONTROL VALVE AND REPROGRAMMED PROCESSOR
TSB		UNKNOWN PERFORM 02 11 06 TSB. SELF TEST PASS. CHECK FOR LATEST PCM CALIBRATION CURRENT. REPLACE THROTTLE BODY ASSY AND
TSB		13656 PERFORM TSB 02 06 05 AND TSM 02 05 049 PASS PID DATA IAC MAF REPLACE DPFE SENSOR PCM RLY PASS CK GROUNDS AND CONECTORS PER TSM COMPLEYTED
TSB		WDS DIAG NO CODES IAC VALVE OUT OF SPECS REPLACE IAC VALVE RUN OASIS TSB 02 06 05 REPROGRAM PCM RETEST
REPLACED		RAN TESTS. REPLACED IDLE AIR CONTROL VALVE.
REFLASH		RECAL DIAGNOSE EEC SYSTEM PINPOINT TEST RECALIBRATE PCM
REFLASH		29862 12A650 (REPROGRAM PCM) WF 7 NGS TEST EEC V. NO CODES FOUND PINPOINT TEST, NGS DCL DISPLAY, AND CHECK PIDS. NGS DCL ROAD TEST AND RECORD DATA. NO ABNORMAL READINGS. TEST FUEL PRESSURE (42 PSI)
ENGINE FAILURE		REQUESTING DEALERS P/A CODE 05725
REPLACED		CONTROL NO 11699AF REMOVED VALVE COVER FOUND BROKEN VALVE CALLED ENGINE PLANT REPLACED ENGINE WITH DROP IN ENGINE PER ENGINE PLANT
REFLASH		REPROGRAM PROCESSOR NON PCM REPROGRAMMING TEST
TSB		TEST EEC,MONITOR TEST,R & R BATTERY FOR ACCESS,INSPECT WIRE HARNESS OK,INSPECT FUSE PANEL OK,RESET BASE IDLE
REFLASH		TEST EEC,PIN POINT & MONITOR TEST,REPROGRAM PCM REPAIR WIRE CONNECTOR AT EEC POWER RELAY
REFLASH		PERFORM EEC DIAGNOSIS PINPOINT TEST IGNITION TEST PID MONITOR EVAP SYSTEM LEAK TEST REPROGRAM PCM R&R EVAP CANISTER AND CLEAN PASSAGE CHECK FTP SENSOR/ROAD TEST
REFLASH		RDTEST VERIFY CONCERN, WDS IGN SYS TEST FUEL PRESS/PERFORM DIAG BY SYMPTOM PINPOINT TEST IAC REPLACE IAC RETEST REPROGRAM PCM, RETEST ,OK
NPF		RAN NGS TEST , PASSED CODES , RAN ROAD TEST , COULD NOT DUPLICATE CONCERN
TSB		14790 SELF TEST CODES KOEO PASS KOER PASS CONT PASS LIGHT OFF. INSTALLED NGS ROADTEST MONITOR PIDS CK FUEL PRESSURE OK AT 55 PSI. REPROGRAMMED PCM PER TSB 02 11 06. POST ROADTEST OK 12A650 CC42
REPLACED		ALTERNATOR REMOVE AND INSTALL OR REPLACE
REPLACED		NGS TEST SYS PASS PERFORMED FUEL TEST PERFORMED POWER BALANCE TEST AND REPLACE EGC RELAY RETEST AND ROADTEST 12MILES 7792 ;;8004
TSB		EEC TEST FUEL PRESSURE TEST PID MONOTER (TSB 2 11 6) REPROGRAM PCM TEST DRIVE RETEST PASS
DIAG		NA EEC (QUICK TEST) DIAGNOSIS
TSB		792903 WARR S.D. EEC TEST NO CODES, REPLACED EEC RELAY, IAC VALVE, THROTTLE BODY AND VAPOR MANAGEMENT VALVE PER TSB 02 09 05, RETEST 9F7Y9 E9DB-9C915 14N089 CC 42
REPLACED		PERFORMED DIAG TEST, REPLACED IAC AND ROAD TEST, STICKING INTERMITTENT
DIAG		1 EEC V ON DEMAND SELF TEST PASS (NO FAULT CODES) ROAD TEST AN MONITOR PID DATA ALL SYSTEMS OPERATING NORMALLY AT THIS TIME
REPLACED		HOOK UP WDS RETRIEVE CODE P1000 KOEO KOER P1000 KOEO KOER ON DEMAND TEST P1000 INSPECT DPFE SENSOR FOR PART
TSB		405 ROAD TEST ENGINE STALLING CHECK FOR CODES NO CODES RUN PINPOINT TEST CHECK OASIS PERFORM TSB 02 5 6 CHECK PIDS REPLACE OUT OF RANGE IAC THROTTLE BODY AND EVAP/VM VALVE RETEST OK

	CUST STATES VEHICLE CUT OFF WHILE DRIVING AFTER VEHICLE SAT FOR A COUPLE OF HOURS WOULD RESTART BUT CUT RIGHT OFF
	CUSTOMER STATES VEHICLE STALLED WHILE DRIVING, COASTED TO THE SIDE AND RESTARTED OK, DUE TO PREVIOUS TRANS FAILURE
	CUSTOMER STATES ENGINE STALLED WHILE DRIVING
	ENGINE SHUTS OFF WHEN DRIVING CCD50
	ENGINE STALLS IN STOP AND GO TRAFFIC WILL RESTART
	CAR IS STALLING WHEN TURNING.
	CK CAR STALL OUT GOING DOWN HILLS RESTART OK NOT ENGINE LIGH
. TEST IGNITION SYSTEM, OK. CHECK OASIS AND FOUND BULLETIN (02 11 8) GO THROUGH ADDITIONAL TEST ACCORDING TO BULLETIN, THEN REPROGRAM PCM TO CALIBRATION LEVEL (1UYA 12A650 AXB), ROAD TEST	D21 CUST STATES WHILE DRIVING 35 40 MPH VEHICLE STALLS OUT OK AND REPORT
	VEH CUT OFF GOING DOWN RD, WILL NOT RESTART.
	CUSTOMER STATES VEHICLE WILL CUT OFF GOING DOWN ROAD SEE RON
	THE ENGINE STALLED ON THE CUSTOMER WHILE DRIVING THE CUSTOMER WAS DRIVING ON A SIDE STREET THEN THE
	ENGINE STALLED AFTER HYWAY DRIVING,RESTARTS BUT HAS NOISE FROM UNDER HOOD. ADVISE AFTER PROBLEM FOUND, SEE RECORD.
	CORRECT WILL DIE WHILE DRIVING AT SLOWER SPEEDS
	CUST REPORTS ENG STALLS WHEN DRIVING THE VEHICLE NO CHECK ENG LIGHT BEFORE THE VEH CUTS OUT D21
	CUSTOMER FOUR DAYS EARLIER THE CHECK ENGINE LIGHT CAMEON IN ROUTE AND THE ENGINE DIED , HAS NOT HAPPENED SINCE
	DR VECH STALLS WHEN TURNING, CUST SAY THE FUEL TANK SEEMS TO BE AROUND 3 4 OF A TANK WHEN STALLING TEMP DOESNT APPEAR TO BE A FACTOR THIS IS A INTERMITTEN VEH HAS STALLED 3 TIMES IN T
	C S RADIO STOPPED WORKING WHILE DRIVING, 3 4 OF A MILE LATER VEH STOPPED RUNNING WHILE DRIVING (TOWED IN)
	C S THE CAR SHUTS OFF WHILE DRIVING, ENGINE WARM, CRUISING ON INTERSTATE, IDIOT LIGHTS COME ON AND VEHICAL SLOWS
	C S THAT ENGINE SEEMS TO SHUT OFF WHEN DRIVING(2ND TIME)
	C S THAT DRIVING AND VEH WILL DIE (COMPLETE STOP WILL START BACK UP & SOMETIMES IT TAKES A FEW MINS)
	OK. FOR REASON ENGINE IS STALLING WHILE DRIVING 35 40 MPH
	WHEN COMING TO A STOP OR LET OFF ACCEL TO COAST VEH, DIES
	CUST STATES WHILE DRIVING 40 MPH THE ENGINE DIED, STARTED OK AND HAS BEEN OK SINCE. D50
	DIAGNOS INTERMITTENT STALLING ON ACCELERATION
	CAR STALLED WHILE DRIVING

2002	10418	511	1FMYU03138KD48578	3.0L	TAU	6	2002	1A03	6007	D21	2	2123026	3000	STALLS
2002	10428	511	1FMYU03132KD03682	3.0L	TAU	4	2002	2G06	RECALRM	D21	4	2571125	3000	WHILE DRIVING
2002	10429	511	1FMYU03132KD08540	3.0L	TAU	4	2002	2.00E+03	8F715	D21	4	2116934	2000	STALLS
2002	10427	511	1FMYU03139KD03453	3.0L	TAU	4	2002	2G04	12A650	D21	-1	2242066	0	STALLS
2002	10428	511	1FMYU03132KD10286	3.0L	TAU	4	2002	2.80E+03	9E208	D21	2	1664666	0	WHILE DRIVING
2002	10466	511	1FMYU03139KC80947	3.0L	TAU	3	2002	2G04	12A650	D21	0	987666	0	WHILE DRIVING
2002	10460	511	1FMYU03139KC46150	3.0L	TAU	2	2002	2G05	RECAL	D21	1	924526	0	WHILE DRIVING
2002	10467	511	1FMYU03139KC16116	3.0L	TAU	1	2002	2.80E+04	9C915	D21	3	1639629	4000	WHILE DRIVING
2002	10468	511	1FMYU03132KC16116	3.0L	TAU	1	2002	2.00E+03	9B926	D21	5	2026694	6000	WHILE DRIVING
2002	10462	511	1FMYU03134KC16556	3.0L	TAU	1	2002	2.00E+03	9F716	D21	5	2921550	6000	STALLS
2002	10500	511	1FMYU03132KC06382	3.0L	TAU	1	2002	2G04	DIAG	D21	1	1136614	0	WHILE DRIVING
2002	10507	511	1FMYU03132KC08159	3.0L	TAU	1	2002	2G04	DIAG	D21	5	2306654	6000	WHILE DRIVING
2002	10517	511	1FMYU03132KB66099	3.0L	TAU	1	2002	2G06	RECAL	D21	2	1090291	1000	WHILE DRIVING
2002	10515	511	1FMYU03132KB67630	3.0L	TAU	1	2002	1H09	9J460	D21	2	1642766	3000	WHILE DRIVING
2002	10520	511	1FMYU03132KB67601	3.0L	TAU	1	2002	2G04	12A650	D21	2	1506660	1000	WHILE DRIVING
2002	10527	511	1FMYU03139KB77091	3.0L	TAU	1	2002	2G04	12A650	D21	5	2522116	7000	WHILE DRIVING
2002	10535	511	1FMYU03139KB67483	3.0L	TAU	12	2001	2G05	RECAL	D21	5	1747291	7000	STALLS
2002	10539	511	1FMYU03139KB66780	3.0L	TAU	12	2001	2.00E+03	8F715	D21	3	946717	3000	HARD START
2002	10545	511	1FMYU03139KB66194	3.0L	TAU	12	2001	7C05	14N089	D21	7	2449788	8000	TURNING
2002	10547	511	1FMYU03132KB64468	3.0L	TAU	12	2001	2G04	12A650	D21	7	2156450	8000	WHILE DRIVING
2002	10555	511	1FMYU03132KB62844	3.0L	TAU	12	2001	2.00E+03	9F715	D21	5	1460251	4000	WHILE DRIVING
2002	10559	511	1FMYU03139KB62844	3.0L	TAU	12	2001	2F02	9E896	D21	3	2466391	3000	WHILE DRIVING
2002	10559	511	1FMYU03139KB44695	3.0L	TAU	12	2001	7B05	12B037	D21	2	767280	3000	STALLS
2002	10560	511	1FMYU03139KB59954	3.0L	TAU	12	2001	2G04	DIAG	D21	7	1711309	8000	DOWNHILL
2002	10565	511	1FMYU03132KB66987	3.0L	TAU	12	2001	7C05	14N089	D21	3	1267626	4000	WHILE DRIVING
2002	10566	511	1FMYU03139KB66730	3.0L	TAU	12	2001	2G04	12A650	D21	4	1679850	4000	WHILE DRIVING
2002	10572	511	1FMYU03132KB63306	3.0L	TAU	11	2001	2G06	RECAL	D21	4	1941473	3000	STALLS

REFLASH		5521 ROAD TEST FOR STALLING CONCERN RESEARCH OASIS AND FOUND TSB 02 11 8 NECESSARY TO PERFORM ALL TEST STEPS MONITOR IAC PERCENTAGE AND FOUND NORMAL NECESSARY TO REMOVE EVAP SYSTEM AND BLOW OUT VE
REFLASH		EEC TEST, NO CODES, IGNITION SYSTEM TEST, REPROGRAMMED PCM PER 021 106, CC42 9904
REPLACED		KKOEO PASS, KEOC PASS, KOER PASS, PIN POINT TEST, REPLACE IAC MOTOR, RETEST
DIAG		ROADTESTED VEHICLE AND ATTEMPTED TO DUPLICATE CUSTOMERS CONCERN. INSTALLED THE WDS SCAN TOOL AND RAN ELECTRONIC
TSB		THROTTLE BODY PER TSB020806 EEC (QUICK TEST) DIAGNOSIS
SSM		PERFORM CHECK LIST,CALLED RANDY CORLEW IS AS BEST AS POSSIBLE
REFLASH		121 W PERFORMED EXTENDED ROADTEST ATTEMPTING TO DUPLI CATE,UNABLE. NGS 12650D DX1 D84.KOEO KOER CONT PASS,NO EEC CONCERNS FOUND. REPROGRAM PCM.OK QUALITY CK BY SSI.OK
TSB		VAPOR MST VALVE REPLACED PER TSB02 11 06
TSB		PERFORMED TSB #02 11 6; REPLACED IAC AND THROTTLE BODY ASSEM EVAPVM PER TSB; REPROGRAMMED PCM
REPLACED		EEC TEST PINPOINT TEST NO CODES DIAG BY SYMPTOM REPLACE IAC
SSM		TECH 105 TEST EEC SYSTEM. PASS CODES. CHECK PER SSM 16566. ALREADY HA S LATEST CALIBRATION, RELAY AND EVAP LINE IS CLEAR. UNABLE
NPF		5709 NPF WARR CUST STATES STALL 1 TIME EEC TEST KOEO PASS MEMORY PASS KOER PASS FUEL PRESSURE TEST 36 PSI IN SPEC. CHECKED. 6YEL ALL PASS CODES ROAD TEST DCL DISPLAY TO MONITOR RECORD PIDS UNABLE
REFLASH		EEC (QUICK TEST) DIAGNOSIS PCM REPROGRAMMING TEST
TSB		EEC TEST HAS ALL PASS CODES, COMPLETED INTER MIT FALT DIAG. COMPLETED TSB 02 06 06, CALLED HOT LINE REPORT 3FCE9005. REPLACDE MASS AIR FLOW , DPFE SENSOR, AND EEC RELAY WITH NEW STYLE, ROAD TEST AND C
REFLASH		HOOKED UP WDS PREFORMED PCM SELF TEST. NO CODES PREFORMED PATS SYSTEM TESTS, AND PPT. REPROGRAM PCM AND RESTEST
NPF		CUTS OFF ON THE ROAD CHECK CODES AND NO CODES SHOWN AT THIS TIME
REFLASH		CCC D21 EEC TEST PASS CD NGS RETEST MONITOR PIDS ALL WITHIN SPECS IGN TEST PASS/FUEL TEST PASS REPROGRAM PCM RETEST PASS CODES
REPLACED		INOP WDS EEC TEST DCL TEST POWER BALANCE TEST INJ FLOW TEST PIN POINT REPLACED ISC RETEST
TSB		COULD NOT CONFIRM COMPLAINT BUT DID NOTICE SLIGHT HESITATION ESP WITH A C ON. CHECKED FOR CODES AND CHECKED OASIS FOR TSB02 11 8. MONIT ORED PIDS ON THE IAC. FOUND THAT THE IAC WAS STICKING AT TIMES
INOP		DOESNT OPERATE PROP EEC (QUICK TEST) DIAGNOSIS
REPLACED		INSPECTED.HOOK UP WDS,KOEO,KOER,DCL DISPLAY,FUEL PRESSURE & LEAKDOWN,RELATIVE INJ FLOW,IGN TEST,PINPOINT TEST.REPLACED THOTTLE BODY.REPLACED AIR BYPASS VALVE.REPROGRAM PCM.TEST & RETEST.
DIAG		HOOK UP WDS,KOEO,KOER,DCL DISPLAY,IDLE DATA DISPLAY,POWER BALANCE,FUEL PRESSURE & LEAKDOWN,RELAITVE INJ FLOW,PINPOINT TEST.RESET IDLE STRATEGY.TEST & RETEST.
REFLASH		CK EEC FUEL AND IGNITION REPROGRAM PCM REPAIR IDLEAIR CONTROL VALVE SIGNAL SENSOR WIRE AND RETEST
DIAG		CUST STATES TRUCK DIED THREE TIMES EEC (QUICK TEST) DIAGNOSIS
TSB		4329 PERFORM TSB ARTICLE 02 9 6 USE WDS MONITOR PIDS CK & REPLACE PFE SENSER & TWO EEC RELAYS RETEST PASS.
TSB		WDS DIAGNOSIS KOEO P1000 KOER DATALOGGIER CK FUEL PRESSURE INJECTOR FLOW TEST PERFORM TSB 02 11 06 REPROGRAM PCM RETEST
DIAG		PROCESSOR EEC (QUICK TEST) DIAGNOSIS

INT LINE INSTALL VEH. ON WDB AND REPROGRAM PROCEESOR ROAD TEST AND RECHECK FOR STALLING COULD NOT DUPLICATE CONCERN AFTER REPAIRS OASIS #511 325 378 ALSO ON ROAD TEST FOUND VEH. TO BUCK	CUST STS CAR STALL, AND BUCKS
	VEHICLE QUIT WHILE CUSTOMER DRIVING
	CUST STATES ENGINE DIED THIS MORNING WHEN MAKING A TURN, D50
	CHECK AND ADVISE VEHICLE RUNS ROUGH AND STALLS. .
	CUSTOMER STATES ENGINE STALLS WHILE DRIVING ON DE CELL AT TIMES. RE STARTS RIGHT AWAY.
	CHEKC VEHICLE STALLS WHILE DRIVING
	D21 CHECK CUST CONCERN THINKS VEH STALLED OUT WHILE DRIVING AT HIGHWAY SPEED YESTERDAY, PULLED OVER SAW OIL AND ENG LIGHT COME ON TURNED KEY TO OFF POSITION, THEN TOW TRUCK DRIVER START
	ENGINE DIES WHILE DRIVING STUMBS DOWN HILL OR SLOWING DOWN
	ENGINE DIES WHILE DRIVING DOWN HILL INTERMITTENLY ENGINE STARTS WITH NO PROBLEMS NO LIGHTS COME ON
	STALLS IN AM
	CUST STATES VEH IS CUTTING OUT WHILE DRIVING MOST ON ACCEL WITHOUT WARNING BUT WILL START BACK UP
TO DUPLICATE A PROBLEM AT THIS TIME	D21 DIED ONE TIME WHILE DRIVING (JUST STARTED AND WAS EXITING PARKING GARAGE)
	CUSTOMER STATES VEHICLE DIED WHILE DRIVING ABOUT 40 MPH STARTED RT BACK?
OULD NO LONGER DUPLACTE.	CUST STATES VEHICLE DIES WHILE DRIVING
	CS THE TRUCK DIES WHILE DRIVING, HAS HAPPENED TWICE AT THE SAME SPOT. ADVISE.
	CUTS OFF ON THE ROAD
	C S TRUCK DIED IN FLIGHT AFTER GOING OVER SPEED BUMP AND IS SLUGGISH WHEN PASSING OTHER VEH
	CUST STATES AT AM CRANKING HARD TO START
. REPLACED AND MONITORED PIDS FOR THE PROPER DUTY CYCLE ALL OK REPROGRAMED PCM ACCORDING TO TSB. FOUND THAT THE DUTY CYCL E WAS NOT HAPPING WITH THE VMV. REPLACED VALVE AND CLEANED AND	CHECK REASON CAR DIED WHEN TURNING DIDNT RESTART FOR 30 MINUTES
	CUST STATES DIED WHILE DRIVING (RESTARTED OK)
	CK CUTTING OFF WHILE DRIVING
	CK CUTS OFF WHILE DRIVING
	CK EMISSION LIGHT CAME ON AND ENGINE DIED, REFIRED AND RAN O K
	CUSTOMER STATES TRUCK DIED 3X YESTERDAY GOING DOWN HILL WITH ENG WARM
	ENGINE STALLS WHILE DRIVING
	CHECK VEHICLE CUTTING OFF WHILE DRIVING AFTER WARMED UP STARTS BACK UP FINE
	CUST STATES ENGINE IS LOSING ALL POWER STALLS OUT BUT WILL RECRANK WHEN THIS HAPPENS

2002	10580	S11	1FMYU03132KB92001	3.0L	TAUD	11	2001	2G05	RECALEM	D21	5	1226531	5000	WHILE DRIVING
2002	10583	S11	1FMYU03132KB20602	3.0L	TAUD	11	2001	2G05	RECAL	D21	3	787442	3000	WHILE DRIVING
2002	10584	S11	1FMYU03132KB20602	3.0L	TAUD	11	2001	2.00E+03	9F715	D21	9	2276863	9000	WHILE DRIVING
2002	10585	S11	1FMYU03132KB15402	3.0L	TAUD	10	2001	2G05	RECAL	D21	9	1821812	6000	WHILE DRIVING
2002	10586	S11	1FMYU03132KB14749	3.0L	TAUD	10	2001	2G05	RECAL	D21	3	1155378	2000	WHILE DRIVING
2002	10588	S11	1FMYU03132KB13653	3.0L	TAUD	11	2001	2.00E+03	9F715	D21	5	2274770	17000	WHILE DRIVING
2002	10591	S11	1FMYU03132KB12186	3.0L	TAUD	10	2001	7C05	14N069	D21	4	1096710	2000	STALLS
2002	10526	S11	1FMYU03132KB02133	3.0L	TAUD	10	2001	2.00E+03	9F536	D21	8	1624460	7000	WHILE DRIVING
2002	10599	S11	1FMYU03132KB02133	3.0L	TAUD	10	2001	2G05	RECAL	D21	4	1096269	4000	AT STOP
2002	10603	S11	1FMYU03132KB00821	3.0L	TAUD	10	2001	7C05	14N069	D21	2	457887	2000	WHILE DRIVING
2002	10604	S11	1FMYU03132KB00804	3.0L	TAUD	10	2001	2.00E+03	9F715	D21	8	1636150	14000	DOWNHILL
2002	10605	S11	1FMYU03132KB00804	3.0L	TAUD	10	2001	2.00E+03	9F715	D21	9	2289809	17000	WHILE DRIVING
2002	10611	S11	1FMYU03132KB00081	3.0L	TAUD	10	2001	2G04	12A650	D21	6	1150329	7000	WHILE DRIVING
2002	10614	S11	1FMYU03132KA93711	3.0L	TAUD	10	2001	2.00E+03	9F715	D21	9	1767228	14000	STALLS
2002	10615	S11	1FMYU03132KA93711	3.0L	TAUD	10	2001	2.00E+03	9F715	D21	2	426229	3000	AT IDLE
2002	10617	S11	1FMYU03132KA93336	3.0L	TAUD	10	2001	2G05	RECAL	D21	7	1271468	5000	AT STOP
2002	10618	S11	1FMYU03132KA93210	3.0L	TAUD	10	2001	2G04	DIAG	D21	3	590380	0	AT STOP
2002	10644	S11	1FMYU03132KA78438	3.0L	TAUD	10	2001	1H08	9J480	D21	6	1117888	9000	DOWNHILL
2002	10648	S11	1FMYU03132KA70252	3.0L	TAUD	10	2001	2G04	12A650	D21	6	1306715	6000	WHILE DRIVING
2002	10649	S11	1FMYU03132KA70166	3.0L	TAUD	10	2001	2G05	RECALEM	D21	10	2173570	6000	WHILE DRIVING
2002	10654	S11	1FMYU03132KA66873	3.0L	TAUD	9	2001	2.00E+03	9H307	D21	11	2288870	30000	WHILE DRIVING
2002	10662	S11	1FMYU03132KA59110	3.0L	TAUD	9	2001	7C05	14N069	D21	6	824142	6000	WHILE DRIVING
2002	10663	S11	1FMYU03132KA52080	3.0L	TAUD	9	2001	2.00E+03	9F715	D21	1	300879	1000	WHILE DRIVING
2002	10694	S11	1FMYU03132KA51999	3.0L	TAUD	9	2001	2G04	DIAG	D21	7	1096866	7000	STALLS
2002	10695	S11	1FMYU03132KA51999	3.0L	TAUD	9	2001	7C05	14N069	D21	4	609206	6000	WHILE DRIVING
2002	10700	S11	1FMYU03132KA50666	3.0L	TAUD	9	2001	2G04	12A650	D21	5	616827	3000	DOWNHILL

REFLASH		5757 42 NOT WORKING PROPERLY EEC SELF TEST PASS CODE REPROGRAM PCM FINAL RETEST
REFLASH		WDS TEST REPROGRAM PROBLEM AS PER OASIS MESSAGE #16599
T99		PERFORM T99 02 11 6
REFLASH		1 EEC TEST,NO CODES,PID DATA,RECORDER MONITOR,FUEL PRESSURE TEST 59PSI,FUEL TRIMS 0,BARO 199,MAFV 1.2,REPROGRAMMED
REFLASH		DIAG AND REPROGRAMED PCM
T99		HOOKUP N99 CHECK DTC NONE CHECKED T99 01 11 6 REPLACED IAC PER BULLITER READINGS COME TO SPEC
REPLACED		EEC TEST KOEO PASS KOEC PASS REPLACED BOTH PCM AND FUEL PUMP RELAY RETESTS
T99		REPLACE THOTTLE BODY PER T9902 11 6
REFLASH		N99 DIAG. REPROGRAMED PCM WITH UPDATE CARBRATION.
REPLACED		ROCK PANEL, INSPECT AND REPLACE EEC RELAY. ORDERED REVISED INC
REPLACED		EEC TEST CODE REPLACED IAC SOLENOID DONE
T99		EEC TEST NO CODES MONITOR WITH PIDS REPLACED IAC SOLENOID AN D EEC POWER RELAY PER T99 02 11 6
REFLASH		VERIFY CONCERN RESET BASE IDLE AND REPROGRAM PCM
T99		11.6 EEC TEST,PINPOINT TESTS,N99 MONITOR ROAD TEST,EVAP TESTS AS PER T99 02 11 06,REPLACED IAC VALVE,INOPERATIVE.
REPLACED		1 N99 TEST, PINPOINT TEST. NO CODES. CHECKED OASIS. NECESSARY TO REPLACE IAC VALVE AND EEC RELAY. RETEST TO VERIFY REPAIR
REFLASH		5757 09 KOEO PASS KOER PASS W TECH 371,ROIDA TEST UNABLE TO DUPLICATE CONCERN PERFORM WDS DIAG,19550D D84 D91,PERFORM VISUAL INSPECTION OK,REPROGRAM PCM,ROAD TEST TO TRY AND DUPLICATE CONCERN,STILL
FUEL CAP LOOSE		3000 LOOSE FUEL CAP, WDS SELF TEST DATA LOGGER, PIN POINT TEST, HAD LOOSE FUEL CAP IN THE PAST, A LOOSE FUE LOAP WILL CAUSE A STALL AT IDLE CONCERN, INSURED CAP WAS INSTALLED PROPERLY. RETEST, TEST
REPLACED		3991 NO GEL HOOK TO WDS PINPOINT TEST PASS PASS PASS CHECK PIDS CHECK IDLE SPEED SET THROTTLE STOP UP LITTLE REPLACED AIR BYPASS REPLACED EEC POWER RELAY CHECK GROUNDS OK CHECK DPFE SENSOR BUILD D
T99		DIAG STALLS WHILE DRIVING NO CODES EVAP TESTED REPROGRAMMED PCM PER T99 020609 RECHECKED
T99		WDS TEST 1.0 PINPOINT TEST REPLACE IAC MOTOR ROAD TEST OK REFLASH PCM PER T99 02 11 6 NO CODES
REPLACED		30455 EEC TEST,RECEIVED PASS CODES KOEO & KOER,DCL DISPLAY SHOWS ALL INPUTS & OUTPUTS WITHIN SPECS,FUEL PRESSURE & LEAK DOWN TEST FAILS, PRESSURE DROPS 25 PSI WITHIN 60 SEC,PINPOINT TEST,REPLACED F
SSM		WDS SYSTEM AND DATA LOGGER ALL IN SPECS REPROGRAM PCM AND REPL EEC RELAY AND TEST EVAP SYSTEM RETEST ROAD TEST PER SSM 15599
REPLACED		REPLACE IAC VALVE
REFLASH		TEST DROVE 20MILES,UNABLE TO VERIFY STALLING,RAN WDS TEST,PA SSED,CHECK OASIS,REPROGRAMM PCM WITH UPDATED CALIBRATION,CHE
SSM		TEST DROVE,RAN WDS TEST,NO CODES,REPLACED ECC POWER RELAY PER SSM 15494,REMOVED BATTERY,CHECKED GROUNDS,OK,IAC OK
DIAG		07 12A650 EEC TEST PASS; DCL DISPLAY; FUEL PRESSURE TEST 40 PSI; IGNITIO

	C S VEHICLE STALLED OUT WHILE DRIVING DID RESTART
	CUSTOMER STATES CHK FOR ENG STALLS WHILE DRIVING AT HY SPEEDS IDLE SEEMS LOW AT STOPS
	CUST STATES CHK FOR ENG STALLS WHILE DRIVING
	C S VEHICLE STALLS WHILE DRIVING. JUST CUTS OFF. WILL RESTART AND RUN FINE AFTERWARD.
	CUST STATES THE VEHICLE STALLS WHEN DRIVING
	CUSTOMER STATES THE ENGINE DIES WHILE DRIVING, RUNS SLUGGISH
	DIES AFTER RUNNING FOR SHORT PERIOD OF TIME INTERN
	CUST STATES VEHICLE STALLS W DRIVING, WILL IMMEDIATELY RESTART. SEE HIST
	CUST STATES VEHICLE STALLS OUT WHEN COMING TO STOP. WILL IMMEDIATELY RESTART.
	CUST STATES VEH CUT OUT WHILE DRIVING, WAITED ABOUT 5 MIN AND SEEMS TO BE RUNNING FINE
	ENGINE STALLED WHEN GOING DOWN HILL RESTARTED OK
	DIED DRIVING
	WHILE DRIVING OIL LIGHT ALTERNATOR CHECK ENGINE LIGHT COMES ON ACCERATION HAD NO POWER IF SHUT OFF THEN RESTARTED ENGINE WILL OPERATE NORMALLY
	CUSTOMER STATES ENGINE STALLS AT TIMES
	INTERMITTANTLY STALLING AT IDLE. WILL RESTART. CHECK AND ADVISE
UNABLE TO VERIFY QUALITY INSPECTED BY 371 5741	D21 CUST STATES VEH STALLS AT STOPS,SLOW TURNS,AT TIMES. ATLEAST ONCE A WEEK..
DROVE CC36	D21 ENGINE STALLS AT STOPS AT TIMES
ATE REPLACED DPFE SENSOR REPROGRAMMED PCM TO NEWER CALIBRATION ROAD TEST RETEST OK	ENGINE STALLED WHEN GOING DOWN HILL,RESTARTED IMMEDIATLEY,CEL NOT ON CODE D21
	C S THAT VEHICLE STALLS AT TIMES WHILE DRIVING HAS HAPPENED TWICE WHEN HOLDING CONSTANT SPEED HAPPENED LAST TWO WEEKS AGO
	CK HAS BEEN HARD TO START STALLED WHILE DRIVING
UEL PUMP ASSEMBLY,RETEST,PASSES.	C S ENGINE STALLED WHILE DRIVING 40 45MPH, SERV ENG AND BATTERY LIGHTS CAME ON
	D21, PER GUEST ENGINE STALLED WHILE DRIVING AT 10 15 MPH IN TRAFFIC SEE TSB#15699, AND AT TIMES ENGINE WILL CRANK
	GOES DEAD WHEN DRIVING
	CUST STATES VEH STALLS (CAN HAPPEN ANY TIME)
	CUST STATES VEH INTER STALLS WHILE DRIVING,CHECK TSB FOR RELATED CONCERN
	CUST STATES VEH STALLS WHEN COASTING DOWN HILLS HAS TO PULL OVER PUT IN PARK AND THEN WILL RESTART

2002	10709	S11	1FMYU03132KA46002	3.0L	T/LD		6	2001	2905	RECAL	D21	10	1992399	13000	DOWNHILL
2002	10714	S11	1FMYU03132KA46321	3.0L	T/LD		6	2001	2.00E+03	9E606	D21	7	1110709	9000	WHILE DRIVING
2002	10716	S11	1FMYU03132KA46299	3.0L	T/LD		6	2001	1A05	6007	D21	1	507635	0	NO TEXT
2002	10718	S11	1FMYU03132KA45899	3.0L	T/LD		6	2001	1A05	6007	D21	1	400418	0	AT STOP
2002	10719	S11	1FMYU03132KA45306	3.0L	T/LD		6	2001	2905	RECAL	D21	5	837061	8000	WHILE DRIVING
2002	10727	S11	1FMYU03132KA44932	3.0L	T/LD		6	2001	1A03	6012	D21	2	335075	0	HESITATION
2002	10730	S11	1FMYU03132KA43617	3.0L	T/LD		6	2001	2904	12A650	D21	11	1899028	22000	WHILE DRIVING
2002	10738	S11	1FMYU03132KA40149	3.0L	T/LD		6	2001	7C05	14N069	D21	10	2194380	7000	TURNING
2002	10737	S11	1FMYU03132KA39368	3.0L	T/LD		6	2001	2.00E+03	9F715	D21	8	1674081	12000	AT IDLE
2002	10749	S11	1FMYU03132KA37431	3.0L	T/LD		6	2001	2904	DIAG	D21	5	2277873	4000	WHILE DRIVING
2002	10751	S11	1FMYU03132KA36460	3.0L	T/LD		6	2001	2904	12A650	D21	10	2221504	10000	WHILE DRIVING
2002	10752	S11	1FMYU03132KA36406	3.0L	T/LD		6	2001	2.00E+03	9F715	D21	10	1853448	16000	WHILE DRIVING
2002	10763	S11	1FMYU03132KA35288	3.0L	T/LD		6	2001	1H09	9J460	D21	11	2129666	6000	WHILE DRIVING
2002	10776	S11	1FMYU03132KA27109	3.0L	T/LD		6	2001	8.00E+03	9F715	D21	4	569010	5000	COASTING
2002	10780	S11	1FMYU03132KA26431	3.0L	T/LD		6	2001	7C05	14N069	D21	11	1999998	14000	WHILE DRIVING
2002	10806	S11	1FMYU03132KA15059	3.0L	T/LD		6	2001	2904	12A650	D21	10	1795113	16000	WHILE DRIVING
2002	10807	S11	1FMYU03132KA10693	3.0L	T/LD		6	2001	2905	RECAL	D21	0	1166822	9000	AT STOP
2002	10812	S11	1FMYU03132KA15431	3.0L	T/LD		6	2001	1H09	9J460	D21	6	842064	3000	AT STOP
2002	10819	S11	1FMYU03132KA14435	3.0L	T/LD		6	2001	2.00E+03	9F715	D21	10	1894402	17000	HARD START
2002	10822	S11	1FMYU03132KA09188	3.0L	T/LD		6	2001	2.00E+03	9F715	D21	6	707662	15000	AT STOP
2002	10824	S11	1FMYU03132KA07632	3.0L	T/LD		6	2001	2.00E+03	9F715	D21	2	353278	2000	AT STOP
2002	10855	S11	1FMYU03122KE10088	3.0L	T/LD		7	2002	2904	12A650	D21	1	2205060	0	WHILE DRIVING
2002	10858	S11	1FMYU03122KD99007	3.0L	T/LD		6	2002	2904	12A650	D21	1	1990105	1000	WHILE DRIVING
2002	10864	S11	1FMYU03122KD70414	3.0L	T/LD		6	2002	2904	12A650	D21	1	1855029	0	WHILE DRIVING
2002	10866	S11	1FMYU03122KD64791	3.0L	T/LD		5	2002	1A03	6007	D21	3	2125853	2000	STALLS

TSB		TEST EEC SYSTEM PASS KOER0 AND KOER1 MONITOR ROAD TEST AND RECORD EVAP IAC RPM PID DATA PER TSB 02 11 6 CHECK EEC RELAY PER TSB AND REPROGRAM PCM PER TSB RETEST KOER0 P1000
INOP		INOP EEC (QUICK TEST) DIAGNOSIS
ENGINE FAILURE		REQUESTING DEALER'S P/A CODE 04903
REPLACED		STARTED VEHICLE KNOCKING NOISE FROM ENGINE,PERFORMOIL PRESSURE TEST 60 COLD,PERFORM COMPRESSION TEST175 IN ALL CYLINDERS DROVE VEHICLE OUTSIDE ENGINE LOCK UP CONTACT HOT LINE TOLD ME TO REPLACE ENGINE
REPLASH		1 REPROGRAM PCM. EEC TEST NO CODES.
HOTLINE		PERFORM FULL WDS DIAG CALL HOTLINE #4 CYL LOW COMPRESSION REMOVE LT VALVE COVER PER HOTLINE AND CK VALVES AND CAMS O.K. CALL HOTLINE PERFORM WET COMPRESSION 100 DRY 225 WET LEAKING ON LOWER END DURING
REPLASH		WDS EEC SELF TSBEST DATALOGGER FUEL PRESSURE LEAK DOWN REPROGRAM PCM AND RETEST RD TEST
TSB		EEC TEST PASS, TEST IGNITION SYSTEM AND FUEL SYSTEM, RUN WDS DATA LOGGER, FOLLOW TSB 02 11 06, REPLACE
REPLACED		12572 0F715 42 WTY RAN EEC TEST AND NO CODES, RAN PID DATA MONITOR AND INTERMITTENT PINPOINT TEST AND DIAG AS IAC MOTOR STICKING AT TIMES, REPLACED IAC MOTOR AND ROAD TEST AND RETEST AND OK
TSB		4252 CK ENG DIES WDS CHECK FOR ENGINE DIES AT TIMES RUN TEST ON WDS EEC TEST DCL DISPLAY NO CODE IN SYSTEM ROAD TEST CHECK FOR TSB NONE NO PROMBLEM FOUND AT TIME 4252
REPLASH		REPROGRAM PCM EEC (QUICK TEST) DIAGNOSIS
TSB		RAN EEC TESTS. RAN PINPOINT TESTS. MONITORED PIDS,CHECK FUEL PSI. RAN OASIS. TSB 02 11 6 PERTAINS TO THIS CONCERN. WENT THROUGH PINPOINT TESTS ON TSB. REPROGRAMMED PCM. REMOVE AND REPLACE IAC. REMOVE
REPLACED		REPLACED PFE SENSOR
REPLACED		EEC TEST, DCL MONITOR, PINPOINT TEST, REPLACED IAC AND EEC RELAY, RETEST OK/P1401000004944000007916000000060000012990
REPLACED		PERFORMED EEC DIAGNOSTICS, PERFORMED FUEL PRESSURE TEST AND IGNITION SYSTEM TEST, REPLACED EEC POWER RELAY AND REPROGRAMMED PCM AND ROAD TESTED AND RE TESTED OK.
TSB		OBD II DIAGNOSIS, DCL DISPLAY, FUEL PRESSURE TEST AND REPROGRAMMED PCM AS PER TSB 02 11 06
SSM		ENG LIGHT OFF KOER PASS KOEO PASS CONT PASS CHECK EEC CHECK DCL DISPLAY ROAD TEST AND MONITOR PID DATA CHECK OASIS REPROGRAMM PCM PER SSM 15999 AND RETEST
SSM		3995 NGS SETUP NGS SELF TEST KOEO CONT PO401,PO402 NGS DCL DATA DISPLAY NGS EGR SYSTEM TEST PINPOINT TEST R&R DELTA PFE SENSOR TH9 WAS FOR THE CHECK ENGINE LIGHT NOW FOR THE SECOND PROBLEM ON TH9
REPLACED		17305 42,KOEO,PASS,PASS,KOER,PASS. WARR. 461. ATTEMPT TO VERIFY. 12550D,DX1,D45,D64. CODES OA,KE,ACCESS PIDS,IAC PID ERRATIC,REPLACE BY PASS VALVE. REPROGRAM PROCESSOR. RETEST,ROAD TEST 3 MILES. OK
REPLACED		CHECKED FOR STALLING QUICKTESTED CHECKED BASE IDLEAND ADJUSTED AND REPLACED IAC MOTOR AND RETESTED OK
DIAG		IDLE AIR CONTROL VALVE EEC (QUICK TEST) DIAGNOSIS
INOP		DOES NOT OPERATE PROPERLY EEC (QUICK TEST) DIAGNOSIS
TSB		RAN DIAG PINPOINT TEST AND TSB PINPOINT TEST PER TSB 02 11 06 ALL OK, CK CONNECTIONS 104 & 105 UNDER BATTERY TRAY CK EXP HARNESS REAR A C COMPRESSOR FOR BENT OR DAMAGED PINS CK CONNECTING 110 &139 FOR
REPLASH		RAN WDS. NO CODES. REPROGRAMED PROCESSOR. M TIME TO RUN DIAG. NO LABOR OPERATIONS FOR THIS REPAIR.
DIAG		STALLS EEC (QUICK TEST) DIAGNOSIS

	ENGINE DIES AT TIMES WHEN COASTING DOWNHILL AND ALSO AT STEADY SPEEDS, WARM 3 30
	CUST STATES THE VEH WILL STALL OUT WHILE DRIVING
REMOVE ENGINE CRADLE,REMOVE AND REPLACE ENGINE ASSY,TRANSFER COMPONENTS EVACUATE AND RECHARGE AC REFILL COOLANT SYSTEM PRESSURE CHECK COOLANT FOR LEAKS TEST DROVE VEHICLE 5 MILES OK,REPLACED START	CUSTOMER STATES WHILE AT A LIGHT VEHICLE SHUT OFF AND WONT START,ADVICE.
	CUST STATES CHECK FOR STALLING WHILE DRIVING
CYL LEAKDOWN TEST REPL ENGINE SENT BY HOTLINE PER HOTLINE TIME NEEDED FOR DRILLING AND TAPPING SUBFRAME BOLT ROAD TEST O.K. TIME NEEDED FOR ABNORMAL DIAG AND TESTING	CS BUCKS ACTS LIKE WANTS TO CUT OFF MAKES A RATTLE SUND IN EGNINE AT TIMES LIKE A CARD IN BICYCLE
	CUTS OFF AT TIMES WHEN DRIVING WILL START BACK UP NO PATTERN JUST DIES
	ENGINE WILL JUST SHUT OFF LOW SPEEDS HOT COLD CUST WAS TURNING LEFT OTHER TIME LANE CHANGE NO MIL LIGHT
	D21 C 6 VEH. KILLS AT IDLE INTERMITTENTLY
	ENGINE DIED WHILE DRIVING FOR NO APPARANT REASON CRANKED BACK UP AFTER SITTING FOR AWHILE NO LIGHT
	WHILE DRIVING BETWEEN 5 AND 10 MPH VEHICLE SHUT OFF,CUSTOMER HAD TO TURN KEY TO OFF AND RESTART,RESTARTED RIGHT AWAY HAS ACCURED TWICE.
AND REPLACE THROTTLE BODY. TEST DROVE. RETEST OK.	CUST WAS DRIVING 35 MPH,LOST POWWER STEERING ASSIST,ENFG STALLED OUT THEN THE BATTERY,ENGINE,OIL WARNING LIGHT CAME ON,CUST WAS ABLE TO RESTART THE ENG BUT HAD THE VEH TOWED
	D21 PER CUST, WHILE DRIVING THE SES LIGHT CAME ON AND ENG CUT OFF. RESTARTED AND HAS RAN FINE.
	AT SLOWER SPEEDS DIED AND RESTARTED OKAY
	O S CAR SEEMS TO DIE WHILE DRIVING DOWN THE ROAD
	CUST STATES VEH STALLED WHILE DRIVING AND STARTED BACK UP
	THE ENG WILL STALL COMING TO A STOP HOT AND COLD 35 35 ERRATIC
ONE LINE OASIS CALL PERFORME THE SPECIAL MESSAGE FOR STALLING AT STOPS R&R POWER RELAY R&R IAO ROAD TEST,IN 3995,OUT 3997 QUALITY CHECK WF	D21 ENGINE DIES AT STOPS, CHECK ENGINE LIGHT ON, OWNER STATE
AT THIS TIME. QUALITY INSPECTED BY 491. 17995	D05 CUST STATES VEHICLE HARD TO START COLD AND WANTS TO STALL AT TIMES
	STALLS AT STOPS AT TIMES
	AT TIMES DIES WHEN SLOWING FOR STOPS
	HAS DIED WHILE DRIVING
PRIOR WATER PROBLEMS CK PCM HARNESS AND CK PCM REFLASH ALL OK HOTLINE SAYS THEY ARE STILL WORKING ON PROBLEM NO FIX YET, ALL DONE PER HOTLINE	CK STALLED WHILE DRIVING
	CHECK DIED WHILE DRIVING. STARTED BACK UP. RUNNING OK NOW.
	CAR BEGAN TO STUMBLE, RUN ROUGH, STALLED. WILL TURN BUT WILL NOT START

2002	10896	S11	1FMYU03122XD09425	3.0L	TAD	3	2002	7C05	14N099	D21	2	2154639	1000	NO TEXT
2002	10897	S11	1FMYU03122XD09036	3.0L	TAD	3	2002	2.00E+03	9F715	D21	4	1836886	2000	AT STOP
2002	10899	S11	1FMYU03122XC94404	3.0L	TAD	3	2002	2.00E+03	9F715	D21	4	2271693	3000	WHILE DRIVING
2002	10898	S11	1FMYU03122XC79667	3.0L	TAD	3	2002	2.00E+03	9E928	D21	0	1609800	0	WHILE DRIVING
2002	10900	S11	1FMYU03122XC81603	3.0L	TAD	2	2002	2.00E+03	9F715	D21	1	1341442	2000	AT STOP
2002	10899	S11	1FMYU03122XC81404	3.0L	TAD	3	2002	2.00E+03	9F715	D21	3	2386485	1000	WHILE DRIVING
2002	10904	S11	1FMYU03122XC98957	3.0L	TAD	2	2002	2.00E+03	9F715	D21	1	2277032	0	WHILE DRIVING
2002	10906	S11	1FMYU03122XC49453	3.0L	TAD	2	2002	2B04	DIAG	D21	3	1691359	6000	STALLS
2002	10910	S11	1FMYU03122XC47910	3.0L	TAD	2	2002	2.00E+03	9F715	D21	4	1865319	3000	WHILE DRIVING
2002	10913	S11	1FMYU03122XC47486	3.0L	TAD	2	2002	2B04	12A650	D21	4	2357272	2000	WHILE DRIVING
2002	10915	S11	1FMYU03122XD41280	3.0L	TAD	3	2002	2.00E+03	9F715	D21	4	1752329	2000	WHILE DRIVING
2002	10925	S11	1FMYU03122XC30542	3.0L	TAD	2	2002	2B04	DIAG	D21	3	2275261	2000	STALLS
2002	10927	S11	1FMYU03122XC09855	3.0L	TAD	2	2002	2.00E+03	9F715	D21	1	931035	0	WHILE DRIVING
2002	10931	S11	1FMYU03122XC20889	3.0L	TAD	2	2002	1A04	9434	D21	1	915176	0	AT STOP
2002	10933	S11	1FMYU03122XC19704	3.0L	TAD	2	2002	2.00E+03	9F715	D21	3	1730648	3000	WHILE DRIVING
2002	10934	S11	1FMYU03122XD18584	3.0L	TAD	2	2002	2B04	DIAG	D21	1	1109170	0	COASTING
2002	10937	S11	1FMYU03122XC18978	3.0L	TAD	2	2002	2.00E+03	9F715	D21	4	1800230	6000	ACCELERATING
2002	10940	S11	1FMYU03122XC10811	3.0L	TAD	1	2002	2.00E+03	9F715	D21	6	2836760	12000	AT STOP
2002	10936	S11	1FMYU03122XD00857	3.0L	TAD	1	2002	2B05	RECALEM	D21	2	1198634	3000	ACCELERATING
2002	10939	S11	1FMYU03122XD00356	3.0L	TAD	1	2002	2.00E+03	9F715	D21	2	1109660	3000	STALLS
2002	10959	S11	1FMYU03122XD00540	3.0L	TAD	1	2002	7B02	14401	D21	0	888888	1000	AT STOP
2002	10978	S11	1FMYU03122XD77160	3.0L	TAD	1	2002	2B04	12A650	D21	1	977420	0	WHILE DRIVING
2002	10988	S11	1FMYU03122XD78045	3.0L	TAD	15	2001	2B04	12A650	D21	2	1078617	2000	WHILE DRIVING
2002	10989	S11	1FMYU03122XD67988	3.0L	TAD	15	2001	2B04	12A650	D21	4	1625716	4000	WHILE DRIVING

NO TEXT		
TSB		2873 TSB 02 11 6 CC42 TIME INVOLVED VERIFIED STALLING CONDITION. WDS, EEC TEST, NO CODES. SYSTEM PASSED. DCL DISPLAY. RUN OASIS AND FOUND TSB FOR STALLING CONCERNS. PERFORMED TSB. RE PROGRAMMED PC
REPLACED		PERFORMED EEC TEST AND RECIEVED NO FAULT CODES. PERFORMED PID MONITOR ROAD TEST AND FOUND THE IAC VALVE IS OUT OF
TSB		N/A EEC TEST DCL RECORDER MONITOR PINPOINT TEST REPLACED IAC VALVE AND THROTTLE BODY PERFORMED DIAG OUTLINED IN TSB 021105
REPLACED		INSPECT TEST AND PINPOINT AND MONITOR DIAG AND REPLACE IAC VALVE AND RETEST
TSB		PER TSB 02 11 06 PLUS MAF & DPFE PER HOTLINE
TSB		625 BASIC 9F715 CC 42 KOEO 1111 KOEC 1111 KOER 1111 ROAD TEST CUSTOMER CONCERN STALLS NOT FOUND WDS DIAG QUICK TEST AS PER TSB 02 11 06 INFO ONLY FUEL PRESSURE TESTS DCL DISPLAY PINPOINT TESTS REPLA
NPF		021 DIAG 02 EEC TEST SYSTEM AND PCM,NO CODES,PIDMONITOR IGNITION AND FUEL SYSTEM,PASSED,COULD NOT DUPLICATE CONCERN AT THIS TIME
SSM		3458 IAC TEST DRIVE VERIFY COMPLAINT.EEC TEST NO CODES. PERFORMED DIAG BY SYMPTOM,PERFORMED PINPOINT TEST Z,H,PERFORMED FUEL PRESSURE TEST. 52 PSI,PERFORMED ELECTRONIC IGNITION SYSTEM TEST.OK,PERF
REFLASH		HOOK UP TO WDS EC 5 SYSTEM PASS CODES CHECK PIN POINT CK FUEL SYSTEM CHECK IGNITON, MONITOR PID S CK AIR OR VACUUM LEAKS, REPROGRAM PCM AND CLE AR AND RETEST
TSB		2015 ROAD TEST VEHICLE ENGINE DID NOT STALL USING WDS RTERIVE CONT CODES PASS RUN KOEO PASS RUN KOER PASS PERFORM FUEL PRESSURE TEST FUEL IN SPEC RAN OASIS FOR SSM OR TSB FOUND TSB 02 11 6 INFO ONLY
NPF		NO PROBLEM FOUND EEC DIAG, PID MONITOR ON ROAD TEST WITH FUEL GAUGE, COULD NOT DUPLICATE CONCERN AFTER DRIVING 2 MILES, ALL RELEVANT PIDS WITHIN SPECS, ROAD TEST 2 MILES
SSM		039 EEC V TESTED RETRIEVED NO CODES RAN KOEO KOER NO CODES PASSED ALL TEST CHGECKED OASIS FOUND SSM 12599 FOR CONCERN PERFORMED SSM PCM AT LATEST CALIBRATION CHECKED PCM MPC 181 REMOVED AND REPLACED
LOOSE HOSE		VACUUM LINE LOOSE EEC TEST KOEO PASS KOEC P0171 P0174 KOER P0171 P0174 PINPOINT INTAKE VACUUM HOSE LOOSE REINSTALL CLEAR CODES RETEST PASS
TSB		3015 TSB 02 11 06 EEC TEST KOEO PASS PASS KOER PASS. RAN OASIS NO UNID TSB 02 11 06. MONITOR PIDS FOR IAC DUTY CYC LE OUT OF SPECS. REPLACED IAC #9F715 RETESTED G OOD.WENT TO STEP 4. PERFORMED EVAP
NPF		WDS DIAG MONITOR NPF
TSB		6796 PERF TEST PER TSB 01 6 6. REPL IAC VALVE , REP RGM PCM ,
REPLACED		DIAG, REPLACED IAC VALVE REPROGRAMED PCM
SSM		QUICK TEST PASS CK OASIS SSM #15564 CHECKED EEC RELAY RECALIBRATED PCM BLOW AIR IN EVAP LINES MONITOR PIDS
REPLACED		EEC TEST PIN POINT TEST MONITOR TEST CODE B1352 IN MEMORY FOUND LOOSE IGNITION SWITCH BARRELL SPECIAL ORDERED REPLACED IAC (AIR BYPASS VALVE) FOR LOW IDLE AT START UP AND STALLS
DIAG		ROAD TEST WAS ABLE TO DUPLICATE CONCERN I TIME NO RELATION TO TILT TEST FOR FAULT CODES B1352 OUTPUT CLEARED CODES AND RETEST, NO CODES OUTPUT, TEST IN STALL CODE RESET PINPOINT TEST PER B1352 NO FAUL
REFLASH		WDS KOEO DCL POWER BAL FUEL PRESS ROAD TEST REPROGRAM PCM RETEST SYS
REFLASH		REPROGRAMED PCM
REFLASH		RUN WDS, NO CODES, REPROGRAM PCM

M WITH UPDATE TO PART NUMBER 2L8AAD. INSPECT EEC POWER RELAY AND REPLACED WITH HELLA SERVICE RELAY WITH STAMPED PART NUMBER. VERIFIED CUSTOMER NOT HAVING TOO MANY KEYS OR OTHER ITEMS	CHECK ENGINE STALLS AT STOPS WARM,RESTARTS O.K.D21
	THE ENGINE SHUT OFF WHILE DRIVING. THE ENGINE DID RESTART.
	ENGINE SHUT OFF WHILE DRIVING ONLY ONE TIME 628
	CUST STATES WHEN PULL AWAY FROM STOP,VEH WILL SOMTIMES CUT OFF,HAS DONE IT 6 TIMES
	CHECK FOR DIES WHILE DRIVING
CE ISC ACTUATOR IAC SIGNAL HIGH REPROGRAM PCM TO LATEST LEVEL RETEST OK	CUST STATES THAT WHEN THEY ARE DRIVING TO WORK IN THE MORNING IT HAS STALLED TWICE AND THE CEL,OIL AND GAS CAP LIGHT HAS COME ON
	CUSTOMER STATES CAR STALLED ONE TIME
ORMED MONITOR TEST FOR IAC,EVAP. PERFORMED EVAP EMISION SYSTEM TEST.PERFORMED STATIC TEST.CHECKED FOR TSBS AND SSMS.FOUND TSB 2 11 4,REPLACED IAC AND MONITORED EVAP AND	CS WHILE DRIVING VEH IT STALLED CUST PULLED OFF ROAD AND VEH STARTED BACK UP
	CUSTOMER STATES VEHICLE STALLED WHILE DRIVING TWICE, RESTARTED RIGHT AFTER STALLING VEHICLE WAS AT NORMAL OPERATING TEMP.
TSB USING WDS DATALOGGER PERFORMED STEPS REQUIRED IN TSB CHECK AND FOUND IAC VALVE BORDERLINE REPLACED IAC VALVE AND ATTEMPT TO REPROGRAM PRO CESSOR LATEST VERSION ALREADY	OWNER STATES CUTS OUT WHILE DRIVING WILL RESTART
	C/S ENGINE STALLED ONCE AT A STOP WITH A/C ON, STARTED BACK UP
EEC POWER RELAY BVLEW AIR THRU EVAP VENT LINE LINE CLEAR CALLED HOTLINE TOLD TO CHECK GROUNDS 300 104 100 AND 101 CONNECTORS C270 C & D C110 AND C139 CHECKED GROUNDS AND CONNECTORS	TRUCK STARTED TO LOSE SPEED WHILE DRIVING AND THEN STALLED. CHECK ENGINE LIGHT CAME ON
	C S THAT WHEN PULLED UP TO A STOP THE RPMS WENT DOWN AND DIE AND SMOKE CAME OUT OT GRILL
TEST TESTED PER SPECS. STEP 5 TESTED GOOD. STEP 6 INSPECTED EEC RELAY OK. STEP 7 OK. STEP 8 ROAD TESTED WIT H MONITOR GOOD. RETESTED GOOD C C ROAD TEST 6 M ILES BY TECH 467.	THE ENGINE IS STALLING WHEN DRIVING AT SPEEDS OF 40 MPH OR LESS
	CHECK VEHICLE CUT OUT ON DECEL FROM X WAY SPEEDS, RPMS SEEM TO BE TOO LOW??, RESTARTED OK
	CHECK FOR INTERM. STALL UNDER ACCELERATION
	C S STOP AT LIGHT AND IT DIES...DRIVING ACROSS BRIDGE AND IOT JUST DIED...
	CUSTOMER STATES ENGINE STALLED ONE TIME WHEN STUCK IN TRAFFIC WHEN STARTING TO ACCELERATE.
	CUST STATES ENGINE STALLED (COLD) AND THEN RESTARTED WITH NO PROBLEM
TS FOUND INSPECT WIRE HARNESS	CUSTOMER STATES WHILE SITTING AT A STOP LIGHT THEY TRIED TILTING THE STEERING WHEEL UP AND DOWN THE
	C S VEH SOMETIMES STALLS OUT WHILE DRIVING ALSO HAS VIBRATION AND LOUD NOISE ON ACCEL
	D/S THE VEHICLE WILL CUT OFF WHILE DRIVING
	VEHICLE SHUTS OFF WHILE DRIVING

2002	10990	S11	1FMYU03122KB66932	3.0L	TALD	12	2001	2G04	12A650	D21	6	1606864	6000	WHILE DRIVING
2002	10991	S11	1FMYU03122KB64894	3.0L	TALD	12	2001	2.00E+03	9F715	D21	6	1667116	5000	UPHILL
2002	10992	S11	1FMYU03122KB64894	3.0L	TALD	12	2001	2G04	12A650	D21	7	2304864	6000	DOWNHILL
2002	10993	S11	1FMYU03122KB64894	3.0L	TALD	12	2001	2G02	128579	D21	7	2037369	6000	WHILE DRIVING
2002	10997	S11	1FMYU03122KB66935	3.0L	TALD	12	2001	2.00E+03	9F715	D21	7	1957046	10000	WHILE DRIVING
2002	10999	S11	1FMYU03122KB65129	3.0L	TALD	12	2001	2.00E+03	9F715	D21	5	1481018	6000	WHILE DRIVING
2002	11003	S11	1FMYU03122KB54031	3.0L	TALD	12	2001	2G05	RECAL	D21	5	2259792	10000	WHILE DRIVING
2002	11012	S11	1FMYU03122KB30674	3.0L	TALD	11	2001	7C05	14N089	D21	0	616482	0	WHILE DRIVING
2002	11022	S11	1FMYU03122KB25553	3.0L	TALD	11	2001	2.00E+03	9F715	D21	6	1795741	8000	STALLS
2002	11023	S11	1FMYU03122KB24852	3.0L	TALD	11	2001	2.00E+03	9F715	D21	8	2270999	14000	WHILE BRAKING
2002	11026	S11	1FMYU03122KB24012	3.0L	TALD	11	2001	2G05	RECAL	D21	6	1884165	10000	STALLS
2002	11034	S11	1FMYU03122KB20509	3.0L	TALD	11	2001	2.00E+03	9F715	D21	5	1741632	12000	WHILE DRIVING
2002	11035	S11	1FMYU03122KB17125	3.0L	TALD	11	2001	2.00E+03	9F715	D21	5	2246331	7000	WHILE DRIVING
2002	11037	S11	1FMYU03122KB16441	3.0L	TALD	10	2001	2.00E+03	9H307	D21	9	2545091	18000	WHILE DRIVING
2002	11038	S11	1FMYU03122KB16892	3.0L	TALD	10	2001	2G04	12A650	D21	5	1573872	6000	STALLS
2002	11041	S11	1FMYU03122KB14866	3.0L	TALD	10	2001	2.00E+03	9F715	D21	5	1224717	9000	AT STOP
2002	11045	S11	1FMYU03122KB14462	3.0L	TALD	11	2001	2G05	RECAL	D21	5	1600660	5000	WHILE DRIVING
2002	11046	S11	1FMYU03122KB13921	3.0L	TALD	10	2001	2G04	12A650	D21	1	1066666	0	WHILE DRIVING
2002	11046	S11	1FMYU03122KB13921	3.0L	TALD	10	2001	2G04	12A650	D21	1	2143058	0	STALLS
2002	11050	S11	1FMYU03122KB13740	3.0L	TALD	11	2001	2.00E+03	9F715	D21	1	336000	1000	STALLS
2002	11056	S11	1FMYU03122KB12748	3.0L	TALD	11	2001	1H03	9J480	D21	3	646577	1000	STALLS
2002	11070	S11	1FMYU03122KB06673	3.0L	TALD	10	2001	2G04	12A650	D21	5	777172	9000	WHILE DRIVING
2002	11071	S11	1FMYU03122KB02673	3.0L	TALD	10	2001	2.00E+03	9F715	D21	10	2143442	9000	WHILE DRIVING

REFLASH		ROAD TESTED VEHICLE FOR CONCERN, CONNECTED TO DIAGNOSTIC ANALYSER TO TEST FOR FAULT CODES TEST EEC PASS. CHECKED FUEL PRESSURE AND INJECTOR FLOW. CHECKED DCL. PERFORMED PINPOINT TESTS. REPROGRAMMED
REPLACED		EEC TEST (NO CODES) MONITOR TEST AND PIN POINT TEST (BULLETIN 02 5 6) MONITORED IAC VALVE, FTP SENSOR AND EVAP VM. VERIFIED FUNCTIONAL REPLACED IAC VALVE, CHECKED EEC RELAY OK AND RE PROGRAMMED P
TSB		CUSTOMER CONCERN IS PRESENT,DID PROCEDURES FOR TSB 02 11 6 LATEST PCM CALIBRATION PROGRAMMED PREVIOUSLY 2L12A650 AD
REPLACED		DPFE SENSOR CODE C270B C270C C270D WDS DIAG CALL HOTLINE REPLACED MASS AIRFLOW SENSOR REPLACED DPFE SENSOR TEST DROVE CND
REPLACED		CHECKED AND UNABLE TO VERIFIEY CONCERN, CHECKED EEC SYSTEM AND NO CODES STORED IN MEOMORY AND NO UPDATED MASS AIR FLOW AND REPLACED UP DATED DPFE STUCK AT 2.1 VOLTS AND REROAD TESTED AND ALL OK
TSB		6SS 9F715.42 WARR TEST DROVE AND VERIFIED CUST CONCERN PERFORMED WDS STARTUP,PERFORMED EEC SELF TESTS KOEO PASS KOER PASS CONT PASS PERFORMED DCL MONITOR ROAD TESTS MONITORED PIDS AND FOUND ALL SE
REFLASH		10540 NO CHECK ENG LIGHT ON D,D01,D48,D47,D55,D81,D84,85808,15808E24 USE WDS TO RUN EEC TEST PASS PASS, RUN DCL TO CHECK SYSTEM, CHECK POWER BALANCE, CHECK IGN SYSTEM, CHECK COMP, CHECK FUEL PRESSUR
DIAG		AIR BYPASS POWER RELAY INOP EEC (QUICK TEST) DIAGNOSIS
REPLACED		WDS DIAGNOSIS...PINPOINT TEST...REPLACE IAC VALVE/FINAL QUICK TEST...
REPLACED		SCAN TEST NO CODES PINPOINT TEST REPLACED IAC MOTOR RETEST
TSB		10551 C042 PERFORM TSB 2.11.6 REPROGRAM PCM TO UPDATED AND LATEST CALIBRATION 12A650 REPLACE IDLE AIR CONTROL 9F715 REPLACE THROTTLE BODY 9E926 RE
REPLACED		PWR RELAY BAD IAC INOP EEC (QUICK TEST) DIAGNOSIS PINPT TST MONITOR ROAD TST REPLACED IAC, CONTROL MODULE RELAY, REPROGRAM PCM, RETST
REFLASH		7645 CC 42 TECH 52 VERIFIED CONCERN. ROAD TESTED. HOOK UP WDS, 3.0,KOEO SELF TEST (PASS), KOER SELF TEST (PASS). WDS FUEL PRESSURE AND LEAK DOWN TEST. (PASS). WDS DCL MONITOR PIDS. REPLACED IDLE AIR
DIAG		INTERMITTENT EEC (QUICK TEST) DIAGNOSIS
REFLASH		PERFORMED EEC DIAG. TESTS AND REPROGRAM PCM
TSB		IAC PERFORMED EEC TEST NO DTCS PERFORMED TSB 02 5 6 PERFORMED PID MONITOR REPLACED IAC AND REPROGRAMED PCM RETESTED CONCER
TSB		8317 INCORRECT CAL. PROCESSOR 07 12A650 12650D, 12650DX1, 12650D45,12650D60, 12650D64 KOEM PASS 111, KOER PASS, TEST FUEL PRESSURE GOOD LTD DURRING ROAD TEST. CHECKED OASIS RECAL. PROCESSOR PER TSB
REFLASH		VERIFIED CONCERN RAN EEC PINPOINT AND MONITOR FUEL/PRESSURE TEST REPROGRAMMED PCM RETEST TO CORREC T HE CONCERN.
TSB		ECC MONITOR AND PINPOINT TEST NO CODES,CHECKED FUEL PRESSURE OK,CHECKED TSB AND SSM,CONTACTED HOT LINE CHECKED C270B C 270C C270D C110 C135 G100 G8000104 G105 G101 CKP HARNESS OK,REPROGRAM PCM,TEST D
REPLACED		VERIFY CONDERN,ECC TEST,NO CODES PID MONITOR TEST,IAC NOT WORKING STICKING,REPLACED IAC AND RETEST TEST DROVE OK
DIAG		42 EEC (QUICK TEST) DIAGNOSIS
NO TEXT		
NO TEXT		

PCM. RETEST AND ROAD TEST. P60H	DIES OUT AFTER DRIVING FOR 1 2 AN HOUR
CM TO LATEST CALIBRATION	CUST. STATES THE ENGINE CUTTING OFF WHEN GOING UP AN INCLINE
	WHEN GOING UP COOPER RIVER BRIDGE AND GOING DOWN BRIDGE VECHICLE STALL
	CHECK VEHICLE CUTS OFF WHILE DRIVING HAPPENED WHEN GOING OVER BRIDGE HAPPEND 40 45MPH
	CHECK CUSTOMER STATES THAT THE VEHICLE HAS STALLED OUT TWICE WHILE DRIVING AND STARTS RIGHT BACK UP NO CHECK
INJORS WORKING AS DESIGNED PERFORMED FUEL PRESS LEAKDOWN TESTS FUEL PRESS IS WITHIN NORMAL RANGES AND NO LEAKDOWN PRESENT AT THIS TIME PERFORMED TSB# 02 08 06 REPROGRAMMED PCM PER TSB	CUSTOMER STATES ENGINE DIES WHILE DRIVING HOT OR COLD HAPPENED 3 TIMES THE LAST TWO DAYS RESTARTS BACK UP
E AND DROP, CHECK INJ FLOW, CHECK IDLE DATA, CHECK FOR LATEST CALIB, REPROGRAM PCM, USE NGS TO ROAD TEST, RETEST P1000 P1009	C S VEH. DIES OUT WHILE DRIVING OR AT A STOP DOES IT INTERMITTENLY
	CHECK WHILE DRIVING 30 TO 40 MPH DASH LIGHTS BLINKED ON AND OFF THEN ENGINE STALLED OUT COASTED TO A STOP THEN RESTARTED HAD HALF A TANK OF FUEL
	CK ENG CUTS OFF
	DIED WHEN SLOWING DOWN TO TURN (RIGHT)
	ENGINE STALLS INTERMITTENTLY STALLED YESTERDAY AND TODAY ONCE NOT H
	CK ENGINE LIGHT CAME ON AND DIED WHILE DRIVING, DID RESTART
CONTROL VALVE & REPROGRAM PCM AS PER TSB 02 11 6. RETEST SYSTEM. ROAD TESTED OK. RMC.	WF D21 ENGINE DIED WHILE DRIVING AND AT STOPS
	O R MONDAY AM, CAR IDLED ROUGH. MONDAY PM CAR STALLED WHILE DRIVING, WITH NO SHUTTER PRIOR TO STALL
	CHECK ENGINE FOR STALL AT TIMES (SEE JIM)
	INTERMITTEN, DIES AT STOPS OR LOW SPEEDS, COASTING
01 11 6 RETEST AND ROAD TEST.	(D21) CK ENGINE HAS DIED WHILE DRIVING AND 2 TIMES WHEN ACCEL FROM A STOP DIDNT HAVE ANY POWER
	ENGINE STALLED WHILE DRIVING.
ROVE 300 MILES	ENGINE HAS STALLED WHILE AT SPEED.
	CUSTOMER STATES VEHICLE KEEPS STALLING
	STALLS, ETC.
	D21*CUST STATES WHILE DRIVING, VEHICLE STALLED MIDSTREAM...
	D21* ENG INTERM DIES WHILE DRIVING, AFTER A FEW MINUTES VEH RESTART OK* AMBER CHECK ENG LIGHTR COMES ON AND STAYS ON

2002	11075	S11	1FMYU03122KB02625	3.0L	TALD	10	2001	2.00E+03	9F715	D21	8	1672770	12000	WHILE DRIVING
2002	11076	S11	1FMYU03122KB02625	3.0L	TALD	10	2001	2.00E+03	9F715	D21	10	2298954	16000	STALLS
2002	11080	S11	1FMYU03122KB02169	3.0L	TALD	10	2001	2.00E+03	9F715	D21	3	570030	6000	WHILE DRIVING
2002	11087	S11	1FMYU03122KB01474	3.0L	TALD	10	2001	7805	14801	D21	7	1600412	8000	WHILE DRIVING
2002	11096	S11	1FMYU03122KA93460	3.0L	TALD	10	2001	7C05	14N089	D21	2	344695	1000	WHILE DRIVING
2002	11096	S11	1FMYU03122KA93361	3.0L	TALD	10	2001	2G04	12A650	D21	4	740721	2000	STALLS
2002	11096	S11	1FMYU03122KA92923	3.0L	TALD	10	2001	7C05	14N089	D21	2	384031	1000	WHILE DRIVING
2002	11096	S11	1FMYU03122KA92923	3.0L	TALD	10	2001	2.00E+04	9C915	D21	10	2162096	9000	STALLS
2002	11100	S11	1FMYU03122KA92713	3.0L	TALD	10	2001	2.00E+03	9F715	D21	2	430379	2000	AT STOP
2002	11106	S11	1FMYU03122KA80707	3.0L	TALD	10	2001	2.00E+03	9F715	D21	10	2260175	11000	WHILE DRIVING
2002	11114	S11	1FMYU03122KA79217	3.0L	TALD	10	2001	2.00E+03	9F715	D21	8	1696466	10000	WHILE DRIVING
2002	11120	S11	1FMYU03122KA71022	3.0L	TALD	10	2001	2.00E+03	9F715	D21	11	2446662	10000	STALLS
2002	11122	S11	1FMYU03122KA70573	3.0L	TALD	10	2001	2G04	12A650	D21	7	1110951	8000	WHILE DRIVING
2002	11126	S11	1FMYU03122KA69559	3.0L	TALD	10	2001	2G05	RECAL	D21	5	530532	2000	STALLS
2002	11132	S11	1FMYU03122KA68469	3.0L	TALD	9	2001	2G04	12A650	D21	6	911794	1000	WHILE DRIVING
2002	11133	S11	1FMYU03122KA68469	3.0L	TALD	9	2001	7C05	14N089	D21	3	473084	3000	WHILE DRIVING
2002	11138	S11	1FMYU03122KA67973	3.0L	TALD	9	2001	7C05	14N089	D21	9	1711208	30000	STALLS
2002	11140	S11	1FMYU03122KA66696	3.0L	TALD	9	2001	2G04	12A650	D21	11	2127650	14000	ACCELERATING
2002	11141	S11	1FMYU03122KA66695	3.0L	TALD	9	2001	1H03	9J460	D21	7	1048666	6000	WHILE DRIVING
2002	11142	S11	1FMYU03122KA66695	3.0L	TALD	9	2001	2.00E+03	9E928	D21	7	1138427	9000	STALLS
2002	11150	S11	1FMYU03122KA65990	3.0L	TALD	10	2001	2.00E+03	9F715	D21	8	1547436	10000	WHILE DRIVING
2002	11152	S11	1FMYU03122KA65184	3.0L	TALD	10	2001	2G05	RECAL	D21	10	2036889	6000	WHILE DRIVING
2002	11154	S11	1FMYU03122KA62560	3.0L	TALD	9	2001	2.00E+04	9C915	D21	10	2236668	14000	STALLS
2002	11155	S11	1FMYU03122KA62577	3.0L	TALD	9	2001	2.00E+03	9F715	D21	9	2071619	13000	STALLS

REPLACED		12703 9F715 CC 42 EEC TEST DCL DISPLAY RECORDER MONITOR PINPOINT TESTS REPLACE IAC RETEST OK
REPLACED		15565 9F715 CC 42 EEC ETST DCL DISPLAY RECORDER MONITO PINPOINT T ESTS REPLACE IAC RETEST OK
INOP		INOP WDS EEC TEST DCL TEST POWER BALANCE TEST FUEL PRESSURE TEST INJ FLOW TEST RECORDER PIN POINT REPRO. PCM+REP.IAC RET
POOR CONNECTION		RESECURED NEGATIVE BATTERY CABLE
REPLACED		RELAY EEC (QUICK TEST) DIAGNOSIS ,RAN EEC DIAG TESTS,REPLACE STARTER RELAY
REFLASH		2582 PCM RECAL 1.6 HRS WARR VERIFIED CUSTOMER CONCERN OF VEH STALLS WHEN COLD. PERFORMED EEC TEST, KOEO PASS, KOER PASS, CONT MEM PASS. PERFORMED FUEL PRESS TEST, OK AT 48 PSI. USING NGS ROAD TEST
SSM		1533 HOOK UP WDS AND PERFORM KOEO TEST SYSTEM PASS RUN OASIS AS PER SSM 15434 PERFORM DATA LOGGER TEST CHECK IAC AND FUEL TRIM PIDS ALLOK CHECK GROUND AT BATTERY CHECK PART NUMBER ON IAC AOK REPLA
TSB		9784 ROAD TEST TO VERIFY CONCERN PERFORM KOEO PASSED PERFORM PINPOINT TEST DIAG PERFORM NGS MONITOR TEST UNABLE TO PINPOINT CONCERN CHECK OASIS TSB 02 11 8 MONITOR IAC DUTY CYCLE 45% OUT OF RANGE
REPLACED		PERFORMED DIAGS, REMOVED AND REPLACED IAC, RETEST
STICKING		11630 INSPECT INSTALL GEN STAR TESTE,INSTALL FUEL PRESS GAUGE EEC TEST,DCL TEST,IDLE DATA TEST, FUEL PRESS TEST(58 LBS),INJECTOR FLOW TEST,POW ER BAL TEST PINPOINT TEST MAF SENSOR PINS OHMS TEST AIR
REPLACED		TEST WITH NGS HAS CODE P1705 IAC VALVE PIN POINT TEST PER SERVICE MAN,FOUND IAC INOP REPLACED IAC VALVE
REPLACED		OPEN PERFORM EEC TEST AND REPLACE IAC RE EEC OKAY
SSM		9088 NGS EEC SELF TEST DCL DISPLAY DCL RECORDER MONITOR REPROGRAMMED PCM PER SSM 15580 INSP EEC POWER RELAY PER SSM AMD INSPECT EVAP HOSE PER SSM OK RETEST ROAD TEST KOEO PASS KOEC PASS KOER PASS
REFLASH		2561 W ATTEMPT TO VERIFY NG NGS 12650D D61 D64,KOEO KOER CONT PASS,OK REPROGRAM PCM,OK QUALITY CK BY 662. NO EEC CONCERNS AT THIS TIME.
REFLASH		1547 FAULTY PROCESSOR PROGRAMMING 1.7 12650D,2,D55,3,D60,1,D61,4,D64,2,DX1.1,SSSDLS EEC TEST PASSED, IGNITION SYSTEM TEST PASSED, DCL DISPLAY TEST PASSED, NGS MONITOR ROADTEST PASSED, CHECKED OASIS
SSM		20113 SSM 15454 1.9 NGS QUICK TEST P0300,P0000,P0200,P0000,DCL DISP LAY IAC, MAF PIDS NORMAL PARAMETERS MONITER ROAD TEST SMAERESULTS COULD NOT DUPLICTE CONCER N OASIS SSM 15434 CHK IAC PART NUMBER,RE
TSB		RAN ON WDS KOEO KOER, NO CODES, RAN DATA LOGGER, ALL READING NORMAL, FUEL PRESSURE TEST, RAN OASIS, PERFORMED TSB 02 11 8
ADJUST		14000 CHV CK AND TEST EEC SYS COULD NOT VERIFY AND DTCS CK PID DATA SET IDLE HARD STOP CLEAN AIR BYPASS VALVE AND CK FOR ANY VACUUM LEAKS OK ROAD TEST 140MI OK COULD NOT VERIFY STALL NO FURTHER REP
REPLACED		1 WDS SELF TEST DATA LOGGER ROAD TEST FUEL PRESSURE PIN POINT REPLACED DPFE SET HARD STOP RMR BATTERY AND TRAY
SSM		GROUNDS G300 100 104 105 &101 & C110 & 139 INSTALL IAC INSTALL T BODY & REBET HARD STOP
REPLACED		PERFORMED DIAG REPLACED DPFE SENSOR RECHECK OK
DIAG		PCM EEC (QUICK TEST) DIAGNOSIS
REPLACED		FOUND IDLE AIR CONTROL OUT OF LIMITS AND EVAP VM 19 NOT FUNCTIONING REPLACED CAC VALVE
REPLACED		REPL AC VALVE ASY

	CUST STATES CHECK STALLING WHILE DRIVING
	ENGINE STALLS AT SLOW SPEEDS AND AT HWY SPEEDS HAS HPPENED 3 TIMES
	CUST STATES ON TWO OCCASIONS WHILE DRIVING AT APPX. 30 MPH ENGINE LOOSES POWER PULLS OVER AND RESTAR
	STALLED OUT WHILE DRIVING WHEN WARM ALL WARNING LIGHTS WENT ON AT DASH WHEN CAR STALLED D 21
	CK VEH STALLING WHILE DRIVING
VEH AND MONITERED RPM, HO2, DPFE, CMP PIDS. WHEN COMING TO A STOP, RPM WOULD DROP BELOW 300 RPM. PERFORMED PPT PER PCED Z SECTION FOR INTERMITTE STALL. RAN OASIS AND FOUND SSM	CUST STATES UPON START UP COLD IN AM VEHICLE STALLS ADVISE
CE PCM RELAY AS PER FORD SSM ROAD TEST AFTER REPAIR VEHICLE IS OK AT THIS TIME	CUST STS VEHICLE STALLED WHILE DRIVING 40 45 MPH RESTARTED OK
REPLACE IAC VALVE & RERUN TEST DUTY CYCLE STILL OUT OF RANGE 43% REPLACE THROTTLE BODY ASSY RERUN TEST 39% OK NOW REPROGRAM PCM MPC 161 NEW SUBA 12A990 AD MONITOR EVAPVM PID FTP	CUST RPTS TRUCK STALLED AT 40 45 MPH ON BLACK HORSE PIKE CURVE, UNDER AC EXPWY OVERPASS CHECK HISTORY
	VECHILE DIES AT STOPS
BY PASS VALUE REMOVE AND REPLACE AIR BY PASS VALUE RETEST TEST DRIVE NO CODES VALUE STICKS REPLACED	D21 CUST STATES VEH HAS STALLED WHILE DRIVING THEN RESTARTS ADVISE
	CUST STATES VEHICLE STALLED WHILE DRIVING 3 TIMES.
	TOW IN TRUCK STARTS AND DIES
	D21 CUST STATES ENGINE STALLS OUT WHILE DRIVING. THIS HAPPENS ERRATIC AND WILL START BACK UP
	#29 AMBER CHECK ENGINE LIGHT ON, STALLED, HAPPENED 1 TIME, CUST STATES.
. REPROGRAMMED PROCESSOR PER SERVICE MESSAGE #15699, EEC RETEST PASSED	VEHICLE HAS STALLED TWICE WHILE DRIVING
PLACE EEC RELAY ACCESS BATTERY BOX FOR GRND CHK G104 105,G101,G103,CHK CONNECTERS C270B,C270C,C270E NO WATER INTRUSION FOUND,RETEST P0340, 128000,D60,D61,MT 1.0 HR FOR SSM	CUSTOMER STATES: CAR DIED WHILE DRIVING. NO CHECK ENGINE LIGHT ON
	CHECK ENGINE DIES OUT WILL RESTART RIGHT AWAY
AIRS ATTEMPTED	3580 STATES STALL OUTS ACCEL ALL ENG TEMP D21
	STALLED WHILE DRIVING COASTING
	CHECK AND REPORT ON ENGINE STALLS RUN WDS CLEAN & INSPECT CONNECTOR #C 2709 C&D
	CHECK FOR ENGINE CUTS OFF GOING DOWN RD AT TIMES.
	CUSTOMER COMPLAINS THAT CAR STALLED CUT OFF, WHILE DRIVING.
	ENGINE STALLS
	ENGINE STALLS.

2002	11156	S11	1FMYU03122KA69494	3.0L	TALD	10	2001	2.00E+04	8C915	D21	11	2360457	18000	WHILE DRIVING
2002	11162	S11	1FMYU03122KA61666	3.0L	TALD	9	2001	2.00E+03	9F715	D21	7	1574179	8000	COASTING
2002	11164	S11	1FMYU03122KA61691	3.0L	TALD	9	2001	9G05	RECAL	D21	9	1990997	11000	ON HIGHWAY
2002	11169	S11	1FMYU03122KA62275	3.0L	TALD	9	2001	2G02	1285579	D21	10	1954740	10000	WHILE DRIVING
2002	11174	S11	1FMYU03122KA61671	3.0L	TALD	9	2001	1A04	9434	D21	5	731535	7000	WHILE DRIVING
2002	11192	S11	1FMYU03122KA44579	3.0L	TALD	8	2001	2.00E+03	9F715	D21	11	1999470	19000	WHILE DRIVING
2002	11203	S11	1FMYU03122KA40143	3.0L	TALD	9	2001	7905	14900	D21	9	1711899	24000	WHILE BRAKING
2002	11214	S11	1FMYU03122KA39149	3.0L	TALD	9	2001	7V01	12A561	D21	6	902320	6000	WHILE DRIVING
2002	11223	S11	1FMYU03122KA37615	3.0L	TALD	9	2001	2904	12A560	D21	7	1160159	3000	STALLS
2002	11224	S11	1FMYU03122KA39695	3.0L	TALD	8	2001	2904	12A560	D21	5	749661	9000	WHILE DRIVING
2002	11225	S11	1FMYU03122KA39695	3.0L	TALD	8	2001	1H03	9J460	D21	4	671302	9000	WHILE DRIVING
2002	11226	S11	1FMYU03122KA39659	3.0L	TALD	8	2001	2.00E+03	9F715	D21	8	1422607	10000	STALLS
2002	11241	S11	1FMYU03122KA35051	3.0L	TALD	8	2001	2.00E+03	9E926	D21	7	1174668	8000	WHILE DRIVING
2002	11242	S11	1FMYU03122KA35234	3.0L	TALD	8	2001	2.00E+03	9F715	D21	7	1387681	12000	RENTAL
2002	11243	S11	1FMYU03122KA35234	3.0L	TALD	8	2001	2.00E+03	9F715	D21	7	1368649	12000	COASTING
2002	11244	S11	1FMYU03122KA35184	3.0L	TALD	8	2001	2904	12A560	D21	11	2306502	17000	WHILE DRIVING
2002	11264	S11	1FMYU03122KA27619	3.0L	TALD	8	2001	2.00E+03	9F715	D21	11	2339965	28000	STALLS
2002	11272	S11	1FMYU03122KA26125	3.0L	TALD	8	2001	2904	DIAG	D21	2	345198	1000	NO TEXT
2002	11273	S11	1FMYU03122KA20809	3.0L	TALD	8	2001	1H03	9J460	D21	7	1025369	6000	WHILE DRIVING
2002	11274	S11	1FMYU03122KA19812	3.0L	TALD	8	2001	1H03	9J460	D21	5	601269	5000	MIL
2002	11276	S11	1FMYU03122KA19101	3.0L	TALD	8	2001	2905	RECALIBM	D21	5	736045	4000	WHILE DRIVING
2002	11306	S11	1FMYU03122KA28936	3.0L	TALD	8	2001	2.00E+03	9F715	D21	11	1941776	6000	WHILE DRIVING
2002	11311	S11	1FMYU03122KA09691	3.0L	TALD	8	2001	2F01	DRIVE	D21	4	510979	2000	NO TEXT
2002	11314	S11	1FMYU03122KA08944	3.0L	TALD	8	2001	2.00E+03	9F715	D21	12	2236236	35000	WHILE BRAKING
2002	11348	S11	1FMYU03112KD69185	3.0L	TALD	6	2002	2.00E+03	9F715	D21	1	2269960	1000	COASTING
2002	11349	S11	1FMYU03112KD62134	3.0L	TALD	6	2002	2904	DIAG	D21	2	2176867	3000	WHILE DRIVING
2002	11356	S11	1FMYU03112KD69072	3.0L	TALD	5	2002	2.00E+03	9E926	D21	1	2126800	0	LOW SPEEDS
2002	11357	S11	1FMYU03112KD66774	3.0L	TALD	5	2002	2.00E+03	9F715	D21	1	2226514	1000	STALLS

REPLACED		REPLACED VAPOR VALVE
REPLACED		REPROGRAMMED PCM PER SVC MESSAGE 18B99 AND REPLACED VALVE 9F715 PER HOTLINE
TSB		TSB 2 11 6 REPROGRAM PCM AND ROAD TEST
TSB		REPAIRS ARE PER TSB 02 11 6 & ARTICLE #02 05 029 FROM NAV OPERATIONS DATED 5 71 02
TSB		EEC, IGN SYSTEM, FUEL PRESSURE, INJECTOR FLOW, PID MONITOR, PINPOINT, TSB 18B99. REPROGRAMED PCM AND RETESTED. ALL OK AT
SSM		19206 CEL OFF HOOK TO WDS PINPOINT TEST PASS PASS PASS CHECK PIDS CHECK FUEL TRIMS OK RAN OASIS FOUND SSM 15434 REPLACED EEC POWER RELAY. REPLACED AIR BYPASS CHECK GROUNDS OK REPROGRAMMED PCM TO NEW
POOR CONNECTION		TESTED BATTERY AND CHARGING SYSTEM, TESTED EEC SYSTEM, TRACED WIRING FOR STARTER AND BATTERY, REPAIRED LOOSE CONNECTION IN BATTERY WIRING
DIAG		WIRING EEC (QUICK TEST) DIAGNOSIS
REFLASH		3958 WF WDS TESTED EEC DCL MONITORED PIDS NO FAULTS FOUND ROADTESTED WITH RECORDER REPROGRAMMED PCM
REFLASH		EEC TEST DIAGNOSIS NO FAULT CODES FOUND,FOUND A SERVICE MESSAGE FROM FORD,RECOMMENDING TO REPRO GRAM PCM,ROAD TEST MORE THAN 20 MILES,PERFORM R ECOMENDATION AND ROAD TEST AGAIN COULD NOT GET CAR TO
REPLACED		DPFE SENSOR FAILURE EEC TEST PINPOINT TEST DCL DISPLAY MONITOR ROAD TEST REPLACE DPFE
REPLACED		DIAG REPLACE IAC EEC (QUICK TEST) DIAGNOSIS
TSB		702295 WARR EEC TEST NO CODES, REPLACED IAC, THROTTLE BODY, VAPOR MANAGMENT VALVE AND EEC RELAY, REPROGRAMMED PCM, PER TSB 020805 RETEST
REFUND		RENTAL ESP 6 5 RF 65559 THIS CHARGE IS FOR LOANER CHARGES INCURRED FOR REPAIRS ON RO 59999
STICKING		IAC STICKING EEC (QUICK TEST) DIAGNOSIS
REFLASH		EEC TEST, DCL, PINPOINT, FUEL PRESSURE, INJECTOR FLOW, POWER BALANCE, IGNITION TEST, REPROGRAMMED PCM
REPLACED		EEC TEST & REPLACED IAC VALVE
NO TEXT		
SSM		5043 PCM CALIBRATION & DPFE SENSOR WARRANTY TEST DROVE. COULD NOT DUPLICATE CONCERN. PERFORMED EEC TEST'S. ALL PASSED. PERFORMED PID MONITOR. ALL NORMAL. RAN OASIS. FOUND SPECIAL SERVICE MESSAGE #15
REPLACED		INOP EEC TEST KOEO PASS KOEC P0401 KOER P1000 DCL MONITOR TEST IDLE DATA TEST PINOINT REPLACED DPFE SENSOR ROAD TEST RETEST
SSM		4007 WARR VERIFY CONCERN, HOOK UP WDS, REPROGRAM PCM WITH LATEST CUBRATION PER SSM, RETEST OK.
REPLACED		EEC QTEST NO DTCS, ROAD TEST RECORDER/MONITOR AND PINPOINT, REPLACED IAC VALVE,RETEST OK
TEST DRIVE		VEHICLE TEST DRIVE
REFLASH		PERFORM EEC TEST SEE DIAGNOSIS POWER BALANCE AND SPARK DURATION TEST REPLACE IAC AND REPROGRAM PROCESSOR RETEST
TSB		CAUS 9F715 CCC D21 CC 42 PERFORMED EEC TEST,PASS CODES,RAN OASIS AND PERFORMED TSB 2 11 6 HOOKED UP WDS,CHECKED IAC AT 50%,REPLACED IAC SOLENOI
LOOSE GROUND		3931 OK FOR STALLS WARR RAN NGST TESTING NO CODES SYSTEM PASSED RELOCATED GROUND UNDER BATTERY TRAY CK EEC RELAY FOR MADE IN THE U.S. TEST DROVE
TSB		474 TSB 02 11 6 TESTED, UNABLE TO VERIFY STALL, FOUND TSB FOR C ONCERN,TSB 02 11 6 PULLED CODES, RAN EEC TESTS, CONT NONE, KOEO NONE , KOER NONE, MONITORED PIDS, TEST DROVE REPLACED IAC VALVE, THR
DIAG		12A680 EEC (QUICK TEST) DIAGNOSIS

	CUSTOMER STATES CUTS OFF AT 40 MPH
	ENGINE STALLS AT LOW SPEEDS
	CUST STATES VEHICLE STALLED WHILE GETTING OFF FREEWAY
	ENGINE STALLS WHEN DRIVING SEE NOTE
	TOW IN DRIVER STATES THAT WHILE DRIVING ON 696 LAST NIGHT ENGINE TURNED OFF PUSHED TO PARKING LOT RESTARTED 15 MINUTES
ER CALIBRATION ROAD TEST RETEST OK AT THIS TIME	ENGINE STALLS INTERMITTANTLY WHILE DRIVING,OCCURS ACCEEL OR COASTING RANDOMLY CODE D21
	CUST STATES WHEN SLOWING FROM 55 MPH TO 10 MPH, ALL DASH LIGHTS CAME ON AND VEH STALLED, LOST STEERING AND POWER BRAKES.
	CHECK ENGINE, CUST SAYS 3 TIMES WHILEE DRIVING AT 40 45 MPH AND LET OFF GAS THE ENGINE STALLED. BUT RE STARTED RIGHT AWAY.
	ENGINE STALLS AT TIMES
STALL AGAIN.(COULD NOT INSTALL FLYRECOR DER DUE TO SSDS NOT BEING UP TO DATE.)	ENGINE STALLS WHILE DRIVING(CUSTOMER REMOVE ALARM SYSTEM,THEN ENGINE START AND RUN OK)ALSO ENGINE CRANK BUT WONT START SOME TIMES.
	TRUCK STALLS WHEN DRIVING, HAS TURNED OFF A FEW TIMES, CHECK AND ADVISE
	CUSTOMER STATES STALING
	C S HE WAS DRIVING 45 MPH AND VEHICLE CUT OFF, DID RESTART
	LOANER $25.00 A DAY
	DIAG. VEH. STALLD 2X WHEN TAKING FOOT OFF GAS & COASTING AFTERR DRIVING AT FREEWAY SPEEDS
	ENG QUIT WHILE DRIVING,OCCURED ONE TIME AFTER BEING IN PULL UPHILL AND LEVELING OFF
	CHECK VEHICLE STALLS
589. M TIME TO DISCONNECT VENT LINE FROM CHECK VALVE & BLEW AIR THROUGH HOSE. INSPECTED EEC POWER RELAY. O.K. REPROGRAMMED PCM PER S.S.M. CALLED FORD FIELD SERVICE ENGINEER TO DISCUSS	OWNER STATES WHILE DRIVING CAR HOT, HE WAS GOING AROUND CURVE. CAR WANTED TO STALL OUT. STEERING LOCKED.
	CUSTOMER STATES CHECK ENGINE LIGHT ON
	THE VEH IS CUTTING OFF WHILE DRIVING
	ENGINE CUT OFF WHILE DRIVING
	VEHICLE CUTS OFF WHILE SLOWING DOWN
	CUST STATES WAS COASTING DOWN HILL, ONCE AND ENGINE STALLED. STARTED UP AND HASNT HAPPENED AGAIN.D21
	CUST STATES THAT VEH SEEMS TO LOOSE POWER AND YOU COULD NOT GIVE IT GAS, NO RPM AND CUSTOMER WAS ON
OTTLE BODY, EEC RELAY CANNISTER PURGE SOLENOID, CHECKED PCM FOR LATEST CALIBRATION, CALLED HOTLINE, TALKED TO BLAINE CONTACT 234F7020, ADVISED DO ADDITIONAL TESTING, CHECKED	CUST STATES VEH DIES AT AT TIMES AT LOW SPEEDS
	OK. FOR ENG. STALLING AFTER IDLING DOWN REAL LOW

2002	11382	S11	1FMYU03112XD33618	3.0L	TAD	4	2002	2922	129679	D21	-1	1664380	0	WHILE DRIVING
2002	11389	S11	1FMYU03112XD11929	3.0L	TAD	4	2002	2905	RECAL	D21	3	1857135	3000	WHILE DRIVING
2002	11378	S11	1FMYU03112XC78895	3.0L	TAD	3	2002	7C05	14N089	D21	2	1143668	0	WHILE DRIVING
2002	11379	S11	1FMYU03112XC73415	3.0L	TAD	3	2002	2C04	12A650	D21	3	1497643	6000	AT STOP
2002	11382	S11	1FMYU03112XC81619	3.0L	TAD	3	2002	2C04	12A650	D21	1	651574	1000	STALLS
2002	11391	S11	1FMYU03112XC50690	3.0L	TAD	3	2002	2F02	0E089	D21	3	1606304	2000	STALLS
2002	11396	S11	1FMYU03112XC48716	3.0L	TAD	2	2002	2.00E+03	9F715	D21	5	2358028	6000	DECELL
2002	11400	S11	1FMYU03112XC41206	3.0L	TAD	2	2002	7611	14499	D21	5	2118030	3000	AT STOP
2002	11405	S11	1FMYU03112XC37660	3.0L	TAD	2	2002	2G02	129679	D21	4	2290643	4000	WHILE DRIVING
2002	11406	S11	1FMYU03112XC36804	3.0L	TAD	2	2002	2C04	DIAG	D21	6	1903714	4000	WHILE DRIVING
2002	11414	S11	1FMYU03112XC19757	3.0L	TAD	2	2002	2.00E+03	9F715	D21	3	1671645	2000	STALLS
2002	11418	S11	1FMYU03112XC16650	3.0L	TAD	2	2002	2C04	12A650	D21	4	2152335	7000	WHILE BRAKING
2002	11431	S11	1FMYU03112XC17149	3.0L	TAD	2	2002	2.00E+03	9F715	D21	2	1547770	2000	WHILE DRIVING
2002	11432	S11	1FMYU03112XC17149	3.0L	TAD	2	2002	2C04	12A650	D21	3	2347769	4000	WHILE DRIVING
2002	11435	S11	1FMYU03112XC16851	3.0L	TAD	1	2002	2C01	12A650	D21	1	735139	0	WHILE DRIVING
2002	11436	S11	1FMYU03112XC16851	3.0L	TAD	1	2002	2G02	129679	D21	1	947666	0	AT STOP
2002	11470	S11	1FMYU03112XB97578	3.0L	TAD	1	2002	2905	RECAL	D21	6	2134544	7000	WHILE DRIVING
2002	11471	S11	1FMYU03112XB97744	3.0L	TAD	1	2002	2C04	12A650	D21	3	941212	2000	WHILE DRIVING
2002	11498	S11	1FMYU03112XB96727	3.0L	TAD	1	2002	2C04	12A650	D21	1	2006102	0	STALLS
2002	11499	S11	1FMYU03112XB97837	3.0L	TAD	1	2002	2C04	12A650	D21	4	1894560	10000	TURNING
2002	11467	S11	1FMYU03112XB97829	3.0L	TAD	12	2001	2.00E+03	9F715	D21	6	1799884	9000	AT STOP
2002	11466	S11	1FMYU03112XB97322	3.0L	TAD	12	2001	2905	RECALEM	D21	3	852999	3000	WHILE DRIVING
2002	11506	S11	1FMYU03112XB95702	3.0L	TAD	12	2001	2.00E+03	9F715	D21	1	536532	0	AT STOP
2002	11510	S11	1FMYU03112XB94778	3.0L	TAD	12	2001	2905	RECAL	D21	7	2958169	3000	WHILE DRIVING

INOP		INOPERATIVE EEC (QUICK TEST) DIAGNOSIS
TSB		REPROGRAM PCM CHECKED EEC AND FUEL PRESSURE 39 PSI IGN SYSTEM DIAG AND NGS RECORDING AND PINPOINT TO TSB 02 11 6 REPROGRAM PCM AND
SSM		VEHICLE DIES WHILE STOPPING, CONNECTING TO WDS KOEO PASS KOEC PASS KOER PASS. PERFORM DATA LOGGER. REPLACED EEC POWER RELAY PER SSM 15599
DIAG		CUST# 021 CONC# 45 BAS# 12A650 DIAG AND RESET THROTTLE STOP
SSM		STALLED CK OUT NO CODES SSM ON THIS REPROGRAM PCM SSM 15599
HOTLINE		TEST DROVE, SCOPED ON WDS,RAN SELF TESTS, PER TECH HOTLINE, ADJUSTED IDLE SET SCREW. T25099
REPLACED		EEC QUICK TEST NGS ROAD TEST REPLACE IAC RE TEST
POOR CONNECTION		VEHICLE DIES AT STOP SIGNS RUN POORLY RD TEST VERIFY INTERMITTENT DIES WDS DIAG P1504 IN MEMORY & HARD FAULT INSTALL BREAK OUT BOX PINPOINT TEST IAC CIRCUITS (WHITE/RED) WIRE WIRE BROKEN FROM
REFLASH		1 NGSTEST NO CODES REPLACE IAC REPLACE THROTTLE BODY REPLACE EVAP MANGEMENT IN VAVLE &REPROGRAM PCM
NPF		UNKNOWN DIAGNOSE EEC SYSTEM MONITOR PIDS DID NO ACT UP
REPLACED		2001 CHECKED THE IAC DUTY CYCLE. CHECKED THE PURGE FLOW . CHECKED THEFUEL PRESSURE 49 PSI. CHECKED FOR FUEL PRESSURE BLEED DOWN. IT HELD REPROGRAMED THE PCM. REPLACED THE IAC DUE TO OUT OF SPEC PR
NPF		WT TIME FOR WDS DIAG TESTING,CK IAC,NORMAL AT 37 PERCENT DUTY CYCLE,CK VMV,PASS, CK PURGE OPERATION,OK,CK PCM RELAY,OK, CK CALIBRATION OF PCM,LATEST ALREADY IN VEH,PERFORMED 3 CLOSED THROTTLE STOPS FR
REPLACED		TECH 236 ROAD TEST EEC TEST REPLACE STICKING IAC REPROGRAM PCM RECHECK OK
TSB		TECH 236 WDS DIAG CHECK PCM REPROGRAM PERFORM TSB 021105 CHECK EVAP SYSTEM RECHECK OK
REPLACED		REPL PCM RD TEST PIN POINT TEST (SEE06) TEST
HOTLINE		AS PER TECH HOTLINE CK & REPL MAF T BODY & ISC VALVE WRONG PART # CK CONNECTS 300 100 101 104 105 270 BCD 110 173 NUMEROUS ROAD TEST APPROX 60 MILES TOTAL CK BASE IDLE RESET KAM CASE #02C007006
REFLASH		DOES NOT OPERATE PROPERLY. EEC TEST, PINPOINT TEST, IGNITION SYSTEM DIAGNOSTIC TEST, FUEL SYSTEM PRESSURE TEST, NGS MONITOR TEST, NGS DGL DISPLAY TEST, REPROGRAMMED PCM AND RERUN EEC TEST
SSM		RUN EEC TEST SCOPED MOTOR PERFORMED SSM 16599 REPROGRAMMED PCM AND CLEANED VENT LINE
TSB		AS PER INFO TSB 02 11 06 EEC (QUICK TEST) DIAGNOSIS
REFLASH		DIAGNOSE AND TEST, NO CODES,PERFORMED PCM RECALIBRATION RETESTED, ROAD TEST PASSED
TSB		07/15 EEC TEST NO CODES NGS HOOK UP AND RECORDED ROAD TEST FOUND THAT THE IAC WAS AT 45% AT 750 RPMS AS PER FORD TSB 02 11 6
REFLASH		EEC TEST CODE PASS,CHECK OASIS PP TEST POWER RELAY CONNECTION AND NUMBER AND REPROGRAMED PCM PER BROADCAST MESSAGE 15599,ROAD TEST CC RECAL TECH 0001.
REPLACED		EEC RELAY AND IAC SOLENOID 3.0L DOHC WDS DIAG EEC TEST P1111 10 P1000,CK FUEL PRESS PASS,IGNITION TEST PASS,PID DATA MON REC NO ABNORMAL PIDS,REPLACE EEC
REFLASH		3004 REPROGRAMED PCM WARRANTY PERF NGS TEST KOEO,KOER AND NO CODES FOUND IN EEC SYSTEM. PERF FUEL PRESSURE TEST,IGN SYSTEM TEST,CHECKED GROUNDS AND HARNESS CONNECTIONS. MONITORED PID DATA,ALL WITH

	QUITS WHILE DRIVING
	ENGINE SHUTS OFF WHILE DRIVING
	DIES AT STOPD WHILE DRIVING
	CUST STATES VEHICLE DIED SEVERAL TIMES WHEN SLOWING TO A STOP. STARTS RIGHT BACK UP
	ENGINE STALLED LAST NIGHT BUT RESTARTED
	CHECK ENGINE STALLING OUT AFTER ENGINE IS WARME DUP AT TIMES RUNS VERY ROUGH AND HAS NO POWER
	CUSTOMER STATES DIES ON DECELL
MISINSTALLED WIRE LOOM RETAINER REPAIR WIRING & REPLACE CONNECTOR RETEST	VEHICLE DIED AT STOP SIGNS RUN POORLY
	CUST STATES VEH CUT OFF WHILE DRIVING CEL CAME ON VEH DID RESTART
	WHILE DRIVING THE VEHICLE LAST WEEK IT DIED OUT WHILE CUST WAS DRIVING THE CAR
EFORMACE. ROAD TEST. THE ENGINE RPM DID NOT DROP BELOW 650 RPM ON TH EROAD TEST THE. ENGINE IS NOT STALLING AT THIS TIME.	CUSTOMER STATES VEHICLE JUST DIES
OM 40 TO 10 MPH, ALL PASS AT THIS TIME.	CUST STATES VEH STALLING WHEN COMING TO A STOP SEE STB
	CUST. STATES ENGINE IS STALLING WHILE DRIVING, HAS STALLED 3 TIMES. RESTARTS OK. DOES NOT HAPPEN EVERYTIME DRIVING. NOT LONG DISTANCE DRIVING.
	CUST. STATES ENGINE IS STALLING AGAIN, HAPPENS WHILE DRIVING. SEE HISTORY.
	CUSTOMER STATES ENG QUIT RUNNING WHILE DRIVING.STARTED RIGHT BACK UP
	CUSTOMER STATES ENG STALLED COASTING TO STOP
	CUST STATES CAR STALLED DRIVING ON FREEWAY CAR STARTED RIGHT UP AGAIN
	WHILE DRIVING MOTOR CUTS
	CUST STATES VEH STALLS AT TIMES
	C S THAT THE VEHICLE WILL CUT OFF WHEN MAKING TURNS CAN FEEL THE STEERING WHEEL GET VERY STIFF AND THEN
	CUSTOMER STATES VEHICLE ENGINE CUT OFF ON HWY, HEAVY STOP GO TRAFFIC, A C ON, RADIO ON, ENGINE WOULD NOT RESTART
	DID ENGINE SHUT OFF WHILE DRIVING
	DIES AT STOPS OR DECEL COMING TO STOPS HAS DIED 1 TIME WHILE ACCELERATING GETTING ONTO HWY
IN SPECS. CHECKED OASIS AND REPROGRAMED PCM AND CHECKED IAC VALVE PER TSB 02 11 8, RETEST AND ROAD TEST OK AT THIS TIME.	INSP. ENGINE DIED DRIVING OVE BUMPY ROAD CUST SAID RESTARTED RIGHT AWAY ACTED LIKE NO FUEL

2002	11512	S11	1FMYU03112KB84636	3.0L	TALD	12	2001	2G05	RECALEM	D21	6	3409668	6000	WHILE DRIVING
2002	11525	S11	1FMYU03112KB86309	3.0L	TALD	12	2001	2G04	12A650	D21	6	1492733	6000	WHILE DRIVING
2002	11526	S11	1FMYU03112KB89609	3.0L	TALD	12	2001	1H03	9J460	D21	4	1228225	8000	WHILE DRIVING
2002	11534	S11	1FMYU03112KB84007	3.0L	TALD	11	2001	2G05	RECALEM	D21	4	906577	3000	WHILE DRIVING
2002	11541	S11	1FMYU03112KB82268	3.0L	TALD	11	2001	2G05	RECAL	D21	4	1166167	7000	WHILE DRIVING
2002	11542	S11	1FMYU03112KB80775	3.0L	TALD	11	2001	2G04	12A650	D21	3	690439	1000	WHILE DRIVING
2002	11547	S11	1FMYU03112KB15429	3.0L	TALD	10	2001	7V01	12A591	D21	3	808851	3000	WHILE DRIVING
2002	11561	S11	1FMYU03112KB14819	3.0L	TALD	11	2001	2G05	RECAL	D21	6	1788238	5000	WHILE DRIVING
2002	11565	S11	1FMYU03112KB13745	3.0L	TALD	11	2001	2G05	RECAL	D21	10	2327441	12000	WHILE DRIVING
2002	11567	S11	1FMYU03112KB13638	3.0L	TALD	11	2001	2.00E+03	9F715	D21	1	361094	0	WHILE DRIVING
2002	11568	S11	1FMYU03112KB13635	3.0L	TALD	11	2001	2G05	RECAL	D21	3	831065	2000	WHILE DRIVING
2002	11569	S11	1FMYU03112KB13633	3.0L	TALD	11	2001	7C06	14H089	D21	3	823402	2000	WHILE DRIVING
2002	11580	S11	1FMYU03112KB13468	3.0L	TALD	10	2001	2G04	DIAG	D21	6	934841	4000	AT STOP
2002	11571	S11	1FMYU03112KB03378	3.0L	TALD	11	2001	2G04	DIAG	D21	6	1532155	8000	WHILE DRIVING
2002	11576	S11	1FMYU03112KB03408	3.0L	TALD	10	2001	2G05	RECAL	D21	6	1037715	3000	WHILE DRIVING
2002	11577	S11	1FMYU03112KB01845	3.0L	TALD	10	2001	2G05	RECAL	D21	6	1509870	8000	WHILE DRIVING
2002	11578	S11	1FMYU03112KB00829	3.0L	TALD	10	2001	2G04	12A650	D21	4	736169	8000	WHILE DRIVING
2002	11584	S11	1FMYU03112KA93061	3.0L	TALD	10	2001	2G04	12A650	D21	4	672189	8000	STALLS
2002	11585	S11	1FMYU03112KA90179	3.0L	TALD	10	2001	2.00E+03	9F715	D21	11	2436819	23000	WHILE DRIVING
2002	11589	S11	1FMYU03112KA79144	3.0L	TALD	10	2001	2G05	RECAL	D21	9	1738898	11000	WHILE DRIVING
2002	11606	S11	1FMYU03112KA89987	3.0L	TALD	10	2001	1H03	9J460	D21	9	1306914	9000	WHILE DRIVING
2002	11613	S11	1FMYU03112KA86701	3.0L	TALD	10	2001	2G04	12A650	D21	10	2179187	13000	WHILE DRIVING
2002	11620	S11	1FMYU03112KA84485	3.0L	TALD	9	2001	2G04	DIAG	D21	6	1556433	4000	WHILE DRIVING
2002	11635	S11	1FMYU03112KA83894	3.0L	TALD	9	2001	2G04	12A650	D21	7	1217621	14000	STALLS
2002	11657	S11	1FMYU03112KA81790	3.0L	TALD	9	2001	2G04	DIAG	D21	1	255557	0	WHILE DRIVING
2002	11658	S11	1FMYU03112KA81750	3.0L	TALD	9	2001	2G04	DIAG	D21	7	1540541	4000	WHILE DRIVING
2002	11666	S11	1FMYU03112KA48286	3.0L	TALD	9	2001	2.00E+03	9F715	D21	10	1851432	19000	WHILE DRIVING

REFLASH		EEC TEST CODE PASS,REPROGRAM PCM ASPER OASIS AND P P TEST AND ADJUST BASE IDLE RETST CC 06
TSB		TEST AND FLASH PCM PER TSB 02 06 6
REPLACED		6580 PERFORMED EEC DIAG,DCL;,PID MONITOR RECORD ROAD TEST REMOVED AND REPL IAC VALVE AND DPFE SENSOR AND RETEST PO 406
SSM		5070 TECH 677 TEST,SYSTEM PASS,PINPOINT,CHECK EEC RELAY PASS, UPDATE PCM TO LATEST LEVEL CALIBRATION,ROADTEST RETEST OK AT THIS TIME,NOTE VEHICLE NEVER STALLED DURING TESTS 42
REFLASH		REPROGRAM PCM EEC (QUICK TEST) DIAGNOSIS
REFLASH		REPROGRAM PCM
HOTLINE		WIRING HARNESS INSPECT WIRING HARNESS AND ACCESS AS PER HOTLINE
TSB		PERFORMED EEC TEST NO CODES, CHECKED FUEL PRESSURE TST OK, PER TSB 02 06 05 REPROGRAMMED POWERTRAIN CONTROL MODULE, RESET KAM
TSB		EEC TESTED,PER TSB 02 11 06,USED WDS TO CHECK DUTY CYCLE ON IAC OK REPROGRAMMED PCM TO LATEST CALIBRATION
REPLACED		PERFORMED DIAGS, REMOVED AND REPLACED IAC, RETEST
REFLASH		ROAD TEST EEC TEST NO CODES DCL MONITOR ROAD TEST FUEL PRESSURE TEST REPROGRAM PCM AND ROAD TEST
REPLACED		PERFORMED DIAGS, REPLACED POWER RELAY, RETEST
NPF		PERFROM TEST ROAD TEST VEH SEVERAL MILES VEH WITHIN FACTORY SPECIFICATION
NPF		D2,02,DIAG ROAD TEST 21 MILES HOT SOAK 1 HR WDS TEST NO CODES NO CONCEARN AT THIS TIME,QUALITY CHECKED BY R S
REFLASH		WDS TEST REPROGRAM PROBLEM
REFLASH		WDS TEST NO CODES MONITOR PIDS TEST REFLASH PCM RETEST OK
REFLASH		RUN EEC TEST, DCL DISPLAY TEST, PINPOINT TEST AND REPROGRAM PCM, RETEST SYSTEM.
REFLASH		ROAD TEST PERFORM SBDS TESTS 15650E,E1,E2,E4, E5,E10,E11,E16,E69,E84,E20,E72,E73 PERFORM OASIS CHECK PERFORM PCM REPROGRAMMING PERFORM ADAPTIVE STRATEGY PERFORM FINAL SELF TEST 15650E1X1
REPLACED		REPLACED IAC VALVE SELOINID
TSB		EISTED AND MONITORED ALL NORMAL RAN OASIS FOUND TSB REBURNED PCM FOR REPAIR
TSB		WDS EEC SELF TEST PASSED RAN OASIS PER TSB 2 11 6 MONITOR IAC DUTY CYCLE 39% MONITOR EVMV AT 84% DROPPED FTP TO
REFLASH		CC42 CCCD21 ENTERED WDS RAN TEST NO CODES REPROGRAMED PCM
TSB		4744 DIAG, CC 82 DIAG. MIL OFF KOEO PASS KOEO PASS KOER PASS UNABLE TO VERIFY OR DUPLICATE DIES WHILE DRIVING . WDS TEST KOEO PASS PASS TEST PID DATA MONITERING VERIFY NORMAL PID P
TSB		CONFIRM COMPLAINT FOUND NO CODES PERFORM TSB0286 RETEST OK
NPF		EEC TEST, NO CODES. MONITOR PIDS WHILE ON ROAD TEST. COULD NOT DUPLICATE THE CONCERN.
TSB		TECH 105 WP CC 06 TEST EEC SYSTEM. PASS CODES. CHECK PER TSB 02 06 06. ALREADY CLEARED ADD LATEST CALIBRATION TEST DROVE. SHOP FOREMAN DROVE. CONCERN STILL PRESENT. TECH AND SHOP FOREMAN WORKED WITH
TSB		FOUND THAT THERE WAS TSB 02 06 06 FOR IAC MOTOR NOT READING PROPERLY NECESSARY TO PERFORM WDS DIAG AND PERFORMED PIN POINT TEST REPLACED IAC MOTOR AND RETEST ALL OK.

	D11 CUSTOMER STATES WHILE DRIVING ENGINE JUST SHUTS OFF AS IF IGNITION SWITCH IS TURNED OFF
	VEHICLE DIES IN TRAFFIC, BUT WILL RESTART. OIL, ENGINE, BATTERY LIGTHS ALL COME ON. STEERING & BRAKES TIGHTEN WHEN THIS HAPPENS.
	CUST STATES THAT VEH DIED WHILE DRIVING YESTERDAY, STATES THAT VEH RE STARTED IMMEDIATELY
	D21 CUSTOMER STATES ENGINE STALLS WHILE DRIVING ADVISE
	CUST STATES VEHICLE CUT OFF AT 35 MPH AND ALL DSH AND GAUGE LIGHTS CAME O N
	CUST SAYS DIED WHILE DRIVING RESTARTED AFTER 5 MINUTES
	CUST ST'S VEHICLE STALLED WHILE DRIVING TOOK 10 MINUTE BEFORE ABLE TO RESTART VEHICLE WAS DRIVING FOR ABOUT 20 MINUTES
	CHECK CUSTOMER STATES WHILE DRIVING CAR STALLED OUT THREE TIMES
	C S HAS STALLED TWICE WHEN DRIVING...ENGINE HOT..NO CK ENGIN LIGHT....
	F S CUIT GOING DOWN ROAD
	CUST STATES VEHICLE DIED WHILE DRIVING, HAS BEEN INTO ANOTHER DEALER FOR SAME COMPLAINT. RESTARTS AFTER DYING
	CUST SAYS DIED WHILE CRUISING ABOUT 55MPH PULLED OFF RESTARTED OK
	CUSTOMER STATES THAT THE ENGINE WILL STALL OUT WHEN ACCELERATING FROM A STOP.
	CUST. STATES DIES WHEN DRIVING.
	CUST STATES CPK FOR ENGINE STALLS WHILE DRIVEING WILL RESTART
	STALLED WHILE DRIVING
	CUSTOMER STATES ENG STALL OUT WHILE DRIVING PULLED OVER AND STARTED BACK UP OK SEE OASIS 2474 77
	CHECK ENGINE STALLS AT TIMES
	CUSTOMER STATES DRIVING ALONG AND AUTO DIES, SPECIAL ORDER PART ON ROM 247877 69 IN TECH 416
	CUSTOMER STATES WHILE DRIVING AROUND 35 MPH VEHICLE JUST STOPED RUNNING. VEHICLE DID START AGAIN BUT CUSTOMER HAS CONCERN
	CUST STATES THAT IS STALLING OUT WHEN DRIVING STARTS UP
	CUSTOMER STATES ENGINE DIES DRIVING DOWN ROAD SEEMS TO NOTICE WHEN ON A COAST
ARAMETERS, TEST IGNITION POWER BALLANCE OK TEST KOER PASS CALL OASIS CONTACT # 114 243 194 FOUND TSB 02 11 8 VERIFY ALL PID READINGS REPROGRAM PCM PER TSB SIGT. TK #111	D11 INSP ENGINE DIED WHILE DRIVING DID RESTART AND HAS NOT DIED SINCE
	CUSTOMER STATES VEHICEL STALLED AND AT TIMES WOULD NOT START (PLEASE READ NOTE LEFT BY CUSTOMER)
	CUST STATES THAT DIED OUT WHILE DRIVING THEN RESTARTED CHECK AND ADVISE
FORD FIELD ENGINEER DAVID WRIGHTSMAN, RECEIVED MEMO FROM MURIEL SANDERS WITH SUGGESTED FIXES FOR 3.0L ESCAPE ENGINE INTERMITTANT CONDITION , FOLLOWED LENGTHY PROCEDURES, CONCERN STILL PRESENT, CALL M	CUST STATES THAT CAR DIES OUT WHILE DRIVING CUST BRINGING BACK TO HAVE RECALIBRATION
	STALLED WHILE DRIVING 35MPH

2002	11670	811	1FMYU03112KA40265	3.0L	TAD		9	2001	2.00E+03	9F715	D21	10	2303800	21000	WHILE DRIVING
2002	11676	811	1FMYU03112KA46141	3.0L	TAD		9	2001	2605	RECAL	D21	7	1394822	6000	WHILE DRIVING
2002	11679	811	1FMYU03112KA46139	3.0L	TAD		9	2001	2604	12A650	D21	6	902276	9000	WHILE DRIVING
2002	11680	811	1FMYU03112KA44361	3.0L	TAD		8	2001	7C05	14H089	D21	2	262801	1000	STALLS
2002	11687	811	1FMYU03112KA44037	3.0L	TAD		8	2001	2605	RECAL	D21	1	1348182	6000	AT STOP
2002	11694	811	1FMYU03112KA46654	3.0L	TAD		9	2001	2604	12A650	D21	6	1542309	9000	WHILE DRIVING
2002	11696	811	1FMYU03112KA40654	3.0L	TAD		9	2001	2602	12B579	D21	10	2023999	13000	STALLS
2002	11696	811	1FMYU03112KA40368	3.0L	TAD		9	2001	2.00E+03	9F715	D21	9	1569852	12000	WHILE DRIVING
2002	11697	811	1FMYU03112KA40356	3.0L	TAD		9	2001	1A03	6006	D21	6	1800585	12000	WHILE DRIVING
2002	11708	811	1FMYU03112KA39713	3.0L	TAD		9	2001	2604	12A650	D21	6	1314746	6000	COASTING
2002	11711	811	1FMYU03112KA39405	3.0L	TAD		9	2001	2604	DIAG	D21	6	1436277	6000	DOWNHILL
2002	11716	811	1FMYU03112KA39145	3.0L	TAD		9	2001	7C05	14H089	D21	7	1030695	11000	WHILE DRIVING
2002	11720	811	1FMYU03112KA39772	3.0L	TAD		9	2001	2605	RECAL	D21	7	1027478	13000	WHILE DRIVING
2002	11721	811	1FMYU03112KA39772	3.0L	TAD		9	2001	2.00E+04	9C915	D21	11	2044814	21000	STALLS
2002	11734	811	1FMYU03112KA39660	3.0L	TAD		9	2001	2.00E+03	9F715	D21	5	659855	8000	WHILE DRIVING
2002	11733	811	1FMYU03112KA39620	3.0L	TAD		9	2001	1A03	6006	D21	1	391841	0	END TEXT
2002	11734	811	1FMYU03112KA39660	3.0L	TAD		9	2001	1A03	6006	D21	1	388869	0	WHILE DRIVING
2002	11742	811	1FMYU03112KA39462	3.0L	TAD		9	2001	2604	12A650	D21	6	1286632	4000	WHILE DRIVING
2002	11748	811	1FMYU03112KA34604	3.0L	TAD		9	2001	2605	RECALEM	D21	11	2274233	11000	WHILE DRIVING
2002	11757	811	1FMYU03112KA27849	3.0L	TAD		8	2001	7V01	12A691	D21	5	234094	4000	AT STOP
2002	11762	811	1FMYU03112KA28007	3.0L	TAD		8	2001	6B13	9030	D21	2	256656	0	WHILE DRIVING
2002	11787	811	1FMYU03112KA16092	3.0L	TAD		8	2001	7C05	14H089	D21	3	480707	1000	WHILE DRIVING
2002	11808	811	1FMYU03112KA16279	3.0L	TAD		8	2001	7C05	14H089	D21	4	647401	5000	WHILE DRIVING
2002	11818	811	1FMYU03112KA14892	3.0L	TAD		8	2001	2604	12A650	D21	11	1985743	19000	WHILE DRIVING
2002	11825	811	1FMYU03112KA09569	3.0L	TAD		8	2001	2604	12A650	D21	11	2220267	19000	WHILE DRIVING

SSM		SPOKE TO FIELD SERVICE ENGINEER ABOUT FIX FOR STALL WHILE DRIVING WAS DIRECTED TO SET BASE IDLE DISCONNECT IAC AND SET TO 30 33 % ADJUSTED TP VOLTAGE TO 1.00 VOLT ENLOGATED HOLES FOR THROTTLE BODY RECH
TSB		1 RAN OASIS FOUND A TSB ON THIS CONCERN FOLOWED STEPS FOR 02 09 05
DIAG		CUTTING OFF CONCERN EEC (QUICK TEST) DIAGNOSIS
REPLACED		ENGINE DIAG TEST AND REPLACED POWER RELAY AND RETEST
TSB		WDS DIAG. NO CODES RAN OASIS REPROGRAM PCM TSB 02 09 09 RETEST
TSB		TSB 021105 REPROGRAM PCM CHECKED EEC AND FUEL PRESSURE 54 PSI IGN SYSTEM DIAG AND NGS RECORDING AND PINPOINT TO TSB 02 11 05 AND REPROGRAMMED PCM
REPLACED		MASS AIR FLOW CHECKED EEC AND FUEL PRESSURE 58PSI IGN SYSTEM DIAG AND NGS RECORDING AND PINPOINT TO MASS AIR FLOW REPLACE AND RECHECK
REPLACED		EEC TEST, KOEC PASS KOEO PASS KOER PASS, PIN POINT TEST, DCL DIAGNOSIS, NGS RECORDER, IGNITION DIAGNOSIS, REPLACE IAC
REPLACED		ENG EXCHANGE DIAG INSPECT ENG REPLACED ENG SWAP NESSARY PARTS ENG LOCKED UP MTIME FOR TEAR DOWN & INSPECT & AC &
REFLASH		TESTEEC SYSTEM NO CODES RUN PINPOINT ON SYMPTOM REMOVE FLIGHT RECORDERM VIEW PIDS RECORDING NORMAL INSTALL NGS& ROAD TEST CK DCL PERFORM IN JECTOR FLOW AND PRESS OK REPROGRAM PCM WITH VER.17.1 UP DATE
TSB		1 CHECKED OUT, HOOKED UP WDS PERFORM PINPOINT TEST, PERFORM DATA LOGGER MONITOR IAC & RPM PER TSB # 02 9 5, FOUND IAC
REFLASH		11700 VIEWS PCM RECAL 42 12A690 EEC TEST MIL OFF KOEO P1111 KOEC P1111 KOER P1111 DCL DISPLAY ROAD TEST MONITOR IGNITION SYSTEM DIAG SPARK DURATION AND POWER BALANCE TESTS FUEL PRESSURE TEST PASS LE
REPLASH		EEC, PINPOINT, RETEST, RECAL PCM PER 18580
TSB		EEC,PINPOINT,RETEST,FOLLOW TSB 02 11 5,SYSTEM OK,CALL HOTLINE,REPLACE DPFE NEW WITH WHITE DOT, REPLACE MAF WITH REVISED & VAPOR VALVE ALL PER HOTLINE,CHECK GROUNDS 300,109,104,106,101, CHECK CONNECTOR
REPLACED		A PINPOINT TEST REPLACED IDLE AIR CONTROL VALVE
ENGINE FAILURE		REQUESTING DEALER'S P/A CODE 01014
REPLACED		DIANGOSE FULL ENGINE AND DIAGS SEIZED UP WONT TURN REPLACE ENGINE ASSY CONTROL # 1J2E0002
REFLASH		REPROGRAM PCM EEC (QUICK TEST) DIAGNOSIS
REFLASH		11599 PCM RECALIBRATION PERFORM EEC SELF TEST KOEO PASS PASS KOER PASS PINPOINT TEST AND TEST IGN. SYSTEM ALL PASSED. TEST FUEL PUMP HAS NORMAL 66PSI, VIEW NGS DCL DISPLAY, ROAD TEST AND RECORD D
REFLASH		REPAIR WIRING TO DPFE SENSOR PCM REPROGRAMMING TEST
NPF		NGS TEST, NO CODES, MONITOR, PIDS, PID RECORDER MONITOR TEST DRIVE, OK AT THIS TIME
REPLACED		1599 42 14A499 12B580 .2 D80 .1 D81 .5 D45 .3 D7 .1 MT16732 .3 EEC TEST KOEO PASS KOEO PASS KOER PASS DCL DISPLAY ROAD TEST PIN POINT TEST REPLACE EEC POWER RELAY CHECK IAC PART NUMBER R R BATTERY T
REPLACED		RELAY SHORTED EEC TEST CHECK WIRING AT FUSE BOX REPLACE EEC RELAY ROAD TEST
TSB		REPROGRAM AS PER TSB 2 11 5
DIAG		1 42 NGS STARTUP TEST SELF TEST KOEO PASS CONT PASS KOER PASS DCL DISPLAY TEST SIGNAL SIMULATION TEST

ECKED TO SEE IF TSB DONE	CUSTOMER STATES: ENGINE SHUT OFF WHILE DRIVING, APPROX. 30MPH. VEHICLE RESTARTED AND RAN OK.
	TRUCK CUT OFF WHILE DRIVING
	CUST REPORTS ENG CUTS OFF AT TIMES AT ABOUT 40 45 MPH,RESTARTS,ADVISE IF NEEDED
	CUST STATES THAT VEH STALLS INT NO PARTICULAR CIRCUMSTANCES SEEM TO CAUSE THIS
	ENGINE STALLED OUT WHEN COMING TO A STOP
	WHILE DRIVING STALLS THEN STARTS BACK UP
	STALLS IN MORNINGS CHECK AND ADVISE
	D21 CUST STATES CK STALLS WHILE DRIVING INTERMITTENT DRIVING SLOW 40MPH
	D21 CUST STATES ENGINE DIED WHILE DRIVING SEE HISTORY
A RETEST.	CHK FR VECH DIED ONE TIME IN TRAFFICE UNDER 35 MPH
	STALLS INTERM. ON STEEP INCLINE
AK DOWN PASS INJECTOR FLOW PASSEVAP SYSTEM ROAD TEST MONITOR EVAP FLOW AND STATIC TEST PINPOINT REPROGRAM PCM REPLACE EEC RELAY CLEAR EVAP SYSTEM HOSES RETEST 42	D21 CUTS OUT WHILE DRIVING INTERMITTANTLY AFTER YOU TAKE FOOT OFF GAS PEDAL HAPPENS AT LOW OR HIGHWAY SPEEDS HAS HAPPENED APPROX 6X LAST WAS YESTERDAY
	ENGINE DIED WHILE DRIVING ON 3 DIFFERENT OCCASIONS AT HWAY SPEEDS WOULD START RIGHT BACK UP
2700,110,139	CUST STATES THE CAR WILL DIE AND RESTART SEE HISTORY
	CK CAUSE ENGINE WILL CUT OFF DRIVING AT TIMES,WONT IDLE ON START UP AT TIMES
	CUSTOMER STATES VEH QUIT RUNNING IN THE MIDDLE OF THE ROAD AND WONT START UP.
	CUST STATES ENGINE HAS STALLED A FEW TIMES WHILE DRIVING, ALWAYS STARTS BACK UP
CL. ALL DATA NORMAL. RECALIBRATE PCM TO LATEST FILE. RETEST EEC KOEO PASS PASS. TK4110	VEHICLE STALLING WHEN DRIVING
	WANTS TO DIE AT STOPS AND WILL SURGE
	CUT OFF WHILE DRIVING
RAY CHECK AND SECURE ALL EEC GROUNDS PER SERVICE MESSAGE	D21 CUST STATES VEHICLE STALLED QUIT RUNNING WHILE DRIVING VEHICLE WAS ON DIESEL STARTED RIGHT BACK UP SEE ADVISOR
	C S AT 30 MPH THE CAR JUST CUT AND PULLED OVER CRANKED BACK UP DONE IT IN AFTERNOON BEEN DRIVING ABOUT 20MINS
	CK DIES WHILE DRIVING AT TIMES,IT WILL START BACK UP
	STATES HAS STALLED 2 TIMES WHILE DRIVING STARTS BACK FINE

2002	11944	S11	1FMYU03112KA07804	3.0L	T/LD	5	2001	7C05	14N069	D21	4	654146	3000	WHILE DRIVING
2002	11869	S11	1FMYU03102KD68375	3.0L	T/LD	6	2002	2.00E+03	9F715	D21	2	2923506	3000	STALLS
2002	11869	S11	1FMYU03102KD67651	3.0L	T/LD	6	2002	2.00E+03	9F715	D21	1	20131	0	STALLS
2002	11870	S11	1FMYU03102KD67651	3.0L	T/LD	6	2002	1H03	9J460	D21	1	20131	0	STALLS
2002	11880	S11	1FMYU03102KD70430	3.0L	T/LD	6	2002	2904	12A650	D21	1	2246287	0	WHILE DRIVING
2002	11881	S11	1FMYU03102KD67897	3.0L	T/LD	6	2002	2904	12A650	D21	6	1766519	0	WHILE DRIVING
2002	11883	S11	1FMYU03102KD68382	3.0L	T/LD	5	2002	2.00E+04	9C915	D21	2	2010466	3000	STALLS
2002	11888	S11	1FMYU03102KD41469	3.0L	T/LD	4	2002	7C05	14N069	D21	3	2336217	1000	WHILE DRIVING
2002	11890	S11	1FMYU03102KD34477	3.0L	T/LD	4	2002	2.00E+03	9F715	D21	4	2460037	2000	WHILE DRIVING
2002	11893	S11	1FMYU03102KD22218	3.0L	T/LD	4	2002	6J09	11562	D21	0	1163333	0	TILT WHEEL
2002	11914	S11	1FMYU03102KC89091	3.0L	T/LD	3	2002	2901	12A650	D21	5	1990180	7000	STALLS
2002	11921	S11	1FMYU03102KC78881	3.0L	T/LD	3	2002	2.00E+03	9E925	D21	1	1197718	0	WHILE DRIVING
2002	11922	S11	1FMYU03102KC73101	3.0L	T/LD	3	2002	2.00E+03	9F715	D21	5	3571501	6000	WHILE DRIVING
2002	11925	S11	1FMYU03102KC81269	3.0L	T/LD	3	2002	2.00E+03	9F715	D21	4	2296331	3000	STALLS
2002	11942	S11	1FMYU03102KC39199	3.0L	T/LD	2	2002	1A03	6007	D21	0	1120706	0	WHILE DRIVING
2002	11944	S11	1FMYU03102KC31194	3.0L	T/LD	2	2002	2.00E+04	9C915	D21	5	2958142	7000	STALLS
2002	11946	S11	1FMYU03102KC31194	3.0L	T/LD	2	2002	2.00E+03	9F715	D21	2	1357034	1000	WHILE DRIVING
2002	11950	S11	1FMYU03102KC20882	3.0L	T/LD	2	2002	2.00E+03	9F715	D21	5	2165788	2000	WHILE DRIVING
2002	11953	S11	1FMYU03102KC19801	3.0L	T/LD	2	2002	2.00E+03	9E925	D21	6	2068087	7000	STALLS
2002	11954	S11	1FMYU03102KC19801	3.0L	T/LD	2	2002	1H03	9J460	D21	7	2263088	10000	WHILE DRIVING
2002	11956	S11	1FMYU03102KC19801	3.0L	T/LD	2	2002	2.00E+03	9F715	D21	5	1626935	6000	STALLS
2002	11968	S11	1FMYU03102KC16164	3.0L	T/LD	2	2002	7B02	10348	D21	0	2024515	0	STALLS
2002	11975	S11	1FMYU03102KC09575	3.0L	T/LD	1	2002	2.00E+03	9F715	D21	3	2539302	6000	WHILE DRIVING
2002	11978	S11	1FMYU03102KC09155	3.0L	T/LD	1	2002	2.00E+04	9C915	D21	4	1620637	4000	WHILE DRIVING
2002	11980	S11	1FMYU03102KC09809	3.0L	T/LD	1	2002	2.00E+03	9E925	D21	3	1916395	1000	WHILE DRIVING
2002	11981	S11	1FMYU03102KC09779	3.0L	T/LD	1	2002	2904	DMG	D21	4	1627666	6000	WHILE DRIVING

NPF		UNKOWN, LIGHT WAS OFF KOEO PASS,KOEC PASS,KOER PASS #0010 RUN EEC TEST, PINPOINT TEST, EEC MONATOR TEST ROADTEST 10 MILES ALL READINGS WITHIN FACTORY SPECS.
TSB		PERFORMED EEC DIAGNOSTIC TESTS. REPLACED FAULTY IAC, THROTTLE BODY, AND EVAP PER TSB 02 11 06.
TSB		EEC TEST NO CODES PERFORM TSB 02 11 6 REPLACE IAC MOTOR MONITOR IAC WITHIN SPEC
TSB		EEC TEST REPLACE DPFE SENSOR AS PER TSB HOT BAYS TO REPLACE WITH WHITE DOT DPFE
TSB		EEC TEST KOEO P1000 CHECK OASIS PERFORM STEPS 1 7 TSB 02 11 6 ROADTEST 5 MILES WITH WDS PID MONITOR ALL TESTS PASSED COULD NOT VERIFY CONCERN AT THIS TIME CALLED HOTLINE REPROGRAMED PCM OK
TSB		WDS EEC SELFTEST SYSTEM PASSED ROADTEST DATALOGGER PERFORM TSB 2 11 6 MONITOR IAC DUTY CYCLE. CHECK PCM CALIBRATION
TSB		VERIFY CONCERN CHECK TSB AND SSM REPAIR AS PER TSB02 11 06 TEST DRIVE AND VERIFY REPAIR
TSB		1309 TEST KOEO PASS KOER PASS TEST DCL OK PERFORM TSB 02 11 06 REPLACED EEC RELAY TEST EVAP SYSTEM NO BLOCKAGES UP DAET PCM ROAD TEST OK IAC 32% RPM 710 LOWEST RETEST OK PASSES
REPLACED		ENGINE DIAG TEST PIN POINT AND MONITOR TEST EVAP EMISSION TEST AND REPLACED IAC VALVE AND RETEST
POOR CONNECTION		RUN ELECT CHK REMOVE COLUMN COVER & LOCK DOWN IGN SWITCH CONNECTOR LOOM.
REPLACED		VERIFIED CONCERN REMOVED AND REPLACED PCM WHILE WORKING WITH WDS IT ERASED BOTH OATS KEYS REPROGRAMMED BOTH PATS KEY AND TEST DROVE TO CORRECT THE CONCERN.
TSB		RD TEST TSB 02 06 06 CK REPL IBC REPL T BODY CK PCM FOR LATEST CALIB RETEST
TSB		WDS TEST MONITOR PIDS NO CODES ROAD TEST MOMITOR OK PERFORM DCL DISPLAY PER TSB 02 11 06 IAC OUT OF SPEC TEST EVAP VAPOR VALVE OK CK FUEL PUMP RELAY CONN OK REPLACE IAC RECHEOK OK
REPLACED		REPLACED IAC VALVE AND RECHECKED EVERYTHING CHECKED OUT OK AT THIS TIME
NPF		TEST DROVE VEH. FOR 5 6 MILES, CHECKED FOR LOOSE HOSES OR WIRES, RAN DIAG. TEST TO CHECK FOR CODES, NO PROB. FOUND
TSB		ROAD TESTED CHECKED OASIS AND TSB S FOUND TSB #02 11 06 REPLACED VAPOR MANAGEMENT VALVE AND EEC RELAY REPROGRAMMED PCM PER TSB POST REPAIR ROAD TEST VERIFIED REPAIR
TSB		REPLACED PER TSB 02 6 6 IDLE AIR CONTROL VALVE,THROTTLE BODY AND PCM PROGRAM.
STICKING		TECH 314 EEC TEST ROAD TEST WITH DATALOGGER CHECK EVAP SYSTEM REPLACE STICKING IAC RECHECK OK
TSB		7307 REPLACED THE THROTTLE BADY ASSY AS OUTLINED IN TSB 2 11 6
TSB		10084 CHECKED THE IAC IT IS OK CHECKED THE VAPOR MANAGEMENT VALVE IT IS OK. REPLACED THE THROTTLE BODY AND THE DPFE SENSOR AS OUTLINED IN TSB 2 11 6. PCM ALLREADY HAS THE UPDATED CALIBRATION.
STICKING		8380 CHECKED THE FUEL PRESSURE 40 PSI AT IDLE CHECK FOR FUEL PRESSURE BLEED DOWN IT HELD. RAN A PID MONITOR TEST ON THE MAPP SENSOR. THE BARO IS 153. RAN A PID MONITOR TEST ON THE IAC. THE IT WAS
REPLACED		ALT HAS INTERNAL OPEN REPLACE ALT ASM
REPLACED		EEC TESTED REPLACED IDLE AIR CONTROL VALVE, AND PURGE VALVE
REPLACED		INTERNAL FAILURE WDS TEST, EVAPORATIVE SYSTEM TEST. REPLACE IDLE AIR CONTROL REPROGRAM PCM. REPLACE THROTTLE BODY AND EVAPORATIVE VALVE#1401000158790000184800000112800000046539
REPLACED		IAC & THROTTLE BODY STUCK THROTTLE BODY AIR INTAKE REPLACE
NPF		RAN WDS, PINPOINT TEST AND IGNITION TEST; NO CODES FOUND VEHICLE OPERATES AS DESIGNED

	CUSTOMER STATES VEH HAS STALLED TWICE AND RPMS WILL JUMP UP AND DOWN WHILE DRIVING.
	ENGINE STALLED A COUPLE OF TIMES
	CUST STATES VEH JUST QUIT RUNNING AND ALL DASH LIGHTS CUT OUT
	CUST STATES VEH CUTS OUT WITH OUT WARNING
	STALLED OUT WHILE DRIVING 2 TIMES, 35 40MPH
	CUST STATES THAT WAS DRIVING APROX 45 MPH WITH A C ON ENGINE STALLED RESTARTED
	CUST STATES THAT THE VEHICLE JUST CUT OFF ON HER
	INTERMITTENT ENGINE STALL WHILE DRIVING, RESTARTS EASILY WHEN THIS OCCURS
	ONE TIME WHEN VEHICLE WAS WARMED UP IT JUST STALLED OUT WHILE DRIVING AND STARTED RIGHT BACK UP
	DIES OUT WHEN STEERING WHEEL TILT IS MOVED IN CERTAIN POSITIONS
	CUST INFORM ME WHILE DRIVIGN THE CAR IT WILL CUT OFF AT ANY TIME IT WILL START BACK UP THIS HAS HAPPEN BEFORE
	CUSTOMER STATES WHILE DRIVING 25 35 MPH THE ENG SHUTS OFF. WILL RESTART
	CUTTING OFF WHILE DRIVEING DOWN ROAD HAPPEN TWO DIFFERANT TIMES
	ENGINE STALLS OUT AND HARD TO RESTART
	ENGINE DIED ON TEST DRIVE
	DIAGNOSTICS CUSTOMER STATES VEHICLE STALLED WHILE SLOWING TO A STOP..STARTED UP OK..
	CUSTOMER STATES VEHICLE STALLED WHILE DRIVING..OIL LIGHT HAD COME ON..CUSTOMER PUT OIL IN VEHICLE STARTED VEHICLE
	CUST. STATES ENGINE STALLS WHILE DRIVING. HAPPENS AROUND 35 TO 40 MPH WHEN COASTING LIKE COMING DOWN A HILL HAPPENED ABOUT 4 TIMES
	CHECK AND ADVISE VEH DIES WHILE SEE HISTROY
	CUSTOMER STATES VEHICLE CUTS OUT WHILE DRIVING
OUT OF RANGE. REPLACED THE IAC DUE A INTERMINTANT FAULT. ROAD TEST. THE IAC IS WITHIN FANGE AT THIS TIME. THE ENGINE HAS NORMAL ACCELERATION AT THIS TIME.	CUSTOMER STATES VEHICLE JUST DIES AND BOGGS DOWN ON HILLS
	ENGINE DIES RUNNING DOWN THE ROAD STARTS BACK UP BUT WONT STAY RUNNING
	WHILE DRIVING VEHICLE ABOUT 30 MPH THE VEHICLE JUST SHUT OFF. WOULD RESTART RIGHT AWAY. HAS HAPPENED TWICE.
	CUSTOMER STATES ENGINE SHUTS OFF WHILE DRIVING
	VEHICLE STALLS OUT WHILE DRIVING & INTERMITTENT HARD START
	C S DRIVING ON HWY.5 THIS MORNING AND ENGINE DIED, ALL LIGHTS CAME ON,PULLED OVER AND RESTARTED....1ST TIME ITS

2002	11986	S11	1FMYU03102KC01055	3.0L	TALD	1	2002	7C05	14N089	D21	1	603104	0	AT STOP
2002	11991	S11	1FMYU03103KB97606	3.0L	TALD	1	2002	7B02	10946	D21	6	2222927	14000	BATTERY DEAD
2002	12002	S11	1FMYU03103KB75170	3.0L	TALD	12	2001	2B01	8C315	D21	4	1471898	2000	WHILE DRIVING
2002	12006	S11	1FMYU03103KB85756	3.0L	TALD	12	2001	2B02	125679	D21	3	1038914	3000	STALLS
2002	12014	S11	1FMYU03103KB89271	3.0L	TALD	12	2001	2B04	DIAG	D21	6	1520505	4000	WHILE BRAKING
2002	12015	S11	1FMYU03103KB85081	3.0L	TALD	1	2002	2.00E+03	9E825	D21	4	1480309	3000	AT STOP
2002	12021	S11	1FMYU03103KB85575	3.0L	TALD	12	2001	2.00E+03	9F715	D21	8	2431817	8000	DECELL
2002	12023	S11	1FMYU03103KB88274	3.0L	TALD	12	2001	2B04	DIAG	D21	2	808096	1000	WHILE DRIVING
2002	12025	S11	1FMYU03103KB85259	3.0L	TALD	12	2001	2B04	12A850	D21	3	1023813	1000	HESBURGE
2002	12026	S11	1FMYU03103KB85209	3.0L	TALD	12	2001	2.00E+03	9E825	D21	5	1483899	3000	ENGINE NOISE
2002	12031	S11	1FMYU03103KB84139	3.0L	TALD	12	2001	2.00E+03	9F715	D21	2	2555481	3000	WHILE DRIVING
2002	12036	S11	1FMYU03103KB45019	3.0L	TALD	12	2001	7C05	14N089	D21	1	1210858	1000	WHILE DRIVING
2002	12037	S11	1FMYU03103KB45019	3.0L	TALD	12	2001	2.00E+03	9H307	D21	2	1516990	2000	WHILE DRIVING
2002	12039	S11	1FMYU03103KB44585	3.0L	TALD	12	2001	7C05	14N089	D21	5	1270342	4000	WHILE DRIVING
2002	12041	S11	1FMYU03103KB99901	3.0L	TALD	12	2001	2B04	DIAG	D21	6	1807840	12000	DOWNHILL
2002	12048	S11	1FMYU03103KB37493	3.0L	TALD	11	2001	2B04	12A850	D21	5	1130039	2000	WHILE DRIVING
2002	12049	S11	1FMYU03103KB30488	3.0L	TALD	11	2001	2B04	12A850	D21	8	2174394	8000	STALLS
2002	12052	S11	1FMYU03103KB35089	3.0L	TALD	11	2001	9B04	12A850	D21	3	827716	1000	STALLS
2002	12057	S11	1FMYU03103KB29490	3.0L	TALD	11	2001	7B07	14B07	D21	0	2066505	0	WHILE DRIVING
2002	12064	S11	1FMYU03103KB14486	3.0L	TALD	10	2001	7C05	14N089	D21	3	862600	1000	WHILE DRIVING
2002	12065	S11	1FMYU03103KB14486	3.0L	TALD	10	2001	2B06	RECAL	D21	9	2122241	7000	TURNING
2002	12069	S11	1FMYU03103KB14449	3.0L	TALD	11	2001	1H09	9J480	D21	6	1171735	11000	AT STOP
2002	12076	S11	1FMYU03103KB13321	3.0L	TALD	10	2001	9G04	12A850	D21	5	909445	5000	WHILE DRIVING
2002	12083	S11	1FMYU03103KB03999	3.0L	TALD	11	2001	1H09	9J480	D21	2	402940	2000	DOWNHILL
2002	12090	S11	1FMYU03103KB01991	3.0L	TALD	10	2001	2.00E+03	9E825	D21	10	2338827	8000	WHILE DRIVING
2002	12095	S11	1FMYU03103KA93617	3.0L	TALD	10	2001	2G05	RECAL	D21	6	1066914	4000	WHILE DRIVING
2002	12100	S11	1FMYU03103KA92992	3.0L	TALD	10	2001	9G05	RECAL	D21	10	2225084	15000	WHILE DRIVING
2002	12101	S11	1FMYU03103KA92992	3.0L	TALD	10	2001	2.00E+03	9F715	D21	1	356987	0	WHILE DRIVING

REPLACED		SIR BASE IDLE ADJUSTMENT POOR GROUNDS WARRANTY EEC TEST PASS ROADTEST WITH PID DATA MONITOR PINPOINT TEST PULLED CABS R&R BATTERY R&R BATTERY TRAY CLEANED SURFACES AROUND GROUNDS REPLACE
REPLACED		CK ENGINE GUITS ON HWY CK ENGINE LAMP BATTERY AND ABS LAMP CHARGE AND TEST BATTERY CK CHARGIN SYSTEMREPALCE ALTERNATOR CK EEC FUEL AND IGNITION REPLA CE DPFE SENSOR REPROGRAM PCM
REPLACED		SC315 SELF TESTED NO CODES,WIGGLE TESTED,REPLACED CRANK SENSOR, PER DENNIS PETERSON
REPLACED		MAF SENSOR INOP EEC TEST KOEO PASS KOEC PASS KOER P1000 DCL MONITOR TEST IDLE DATA TEST FUEL PRESSURE TEST PINPOINT TEST REPLACED
NPF		WDS STARTUP. EEC TEST PASS. DATALOGGER. FUEL PRESSURE TEST. PINPOINT TEST. ALL TESTS PASS AT THIS TIME.
TSB		PERFORMED EEC TEST, MONITOR PIDS, CHECKED AND REPLACED IDLE AIR BY PASS VALVE AND THROTTLE VALVE TO CORRECT PROBLEM. PER TSB 02 09 09
INOP		INOP EEC (QUICK TEST) DIAGNOSIS
SSM		1191 EEC TEST,PASS,PINPOINT TEST,CK CABS,DO SSM,RECALIBRATE PCM WITH LATEST CAL.,CK FOR LATEST EEC RELAY,CK EVAP SYSTEM FOR
DIAG		D21 42 12A650 EEC (QUICK TEST) DIAGNOSIS PIN POINT TEST DIAGNOSIS
REPLACED		D21 42 NGS TEST,PINPOINT TEST,REPLACED IAC VALVE,REPLACED THROTTLE BODY,RECHECKED OK.
TSB		NEEDED TSB, IAC PCM RELAY REPROGREEC (QUICK TEST) DIAGNOSIS
REFLASH		VERIFY CONCERN EEC TEST P1000 DCL MONITOR ROAD TEST FOR CUTTING OUT PINPOINT TEST AND REPL BOTH EEC AND FUEL RELAYS AND REPROGRAM PCM ROAD TEST AND RETESTR
REPLACED		VERIFY CONCERN EEC TEST NO CODES DCL MONITOR ROAD TEST AS PER FORD ENGINEERING REPLACED CRANK SENSOR , VAPOR MGNT VALVE , CANISTER VENT SOLENOID , CARBON CANISTERS , FLAPPER VALVE , FUEL PUMP AN
DIAG		EEC RELAY AND CALIBRATION CONT PASS KOEO PASS KOER P1000 SIDS EEC TEST DIAG PINPOINT IDLE DATA FUEL PRESSURE INJ FLOW POWER BALANCE DCL MONITOR
TSB		TEST NO DTCS RUN FUEL PRESS OK RUN NGS PID DATA DCL DISPLAY PINPOINT PCM AAS PER TSB 02 111 REPROGRAM AND RETETS P1000
SSM		2044 NGS EEC PASS DCL DISPLAY CABS REPROGRAMMED PCM AS PER SSM 16600 CK RELAY & VALVE RETEST & ROAD TEST OK
TSB		TEST AND PERFORM TSB 02 11 06 STEPS 1 6 REPROGRAM PCM
SSM		FOUND THAT THERE WAS A SSM FOR UPDATE ON PCM NECESSARY TO PERFORM WDS DIAG AND PERFORMED PIN POINT TEST REPLACED PROGRAMMED PCM AND RETETS ALL OK.D21 16600 42
INOP		INOP EEC (QUICK TEST) DIAGNOSIS
SSM		REPLACED POWER RELAY PER SSM 16434
REFLASH		REPROGRAM PCM
REPLACED		11930 DPFE 42 ROAD TEST WITH NGS DCL RECORDER MONITOR FOUND THAT INTERMITTANTLY DPFE VOLTAGE GOES TO .7 VOLTS AT CRUISE WHEN SHOULD BE AT 2 VOLTS CAUSEING EXCESSIVE EGR FLOW PIN POINT TEST REPLACE
REFLASH		REPROGRAMMED THE PCM
INOP		FOUND FAILED DPFE REMOVE AND REPALCED DPFE
TSB		REPAIRS DONE PER TSB 02 11 6
DIAG		1 VERIFY. EEC DIAG. NO CODES. PERFORM MANUAL FUEL PRESSURE TEST AND LEAKDOWN. PERFORM IGN SYSTEM DIAG. PERFORM PID
DIAG		42 EEC (QUICK TEST) DIAGNOSIS
DIAG		42 EEC (QUICK TEST) DIAGNOSIS

D EEC POWER RELAY INSPECTED PART # ON IAC PER SSM #16494 OK ADJUSTED BASE IDLE PER PREVIOUS DISCUSSION WITH HOTLINE TEST DROVE OK	CHECK FOR ENGINE STALLED AT STOP HAD TO WAIT FOR AWHILE TO GET RESTARTED
	CK CHARGING SYSTEM BATTERY DEAD
	D21 ENGINE STALLS CUST STATES VEH STALLED WHILE DRIVING.
	C S ENGINE HAS STALLED TWICE ON HER
	WHEN BRAKING OR SLOWING DOWN, CAR DIES
	CUSTOMER STATES IDLE STALLS AT TIMES WHILE TURNING OR COMING TO A STOP
	INTERMITTENTLY THE CAR WILL STALL ON DECEL. TSB IS ATTACHED
	CUST STATES WHILE DRIVING VEH HAD CUT OFF BUT STARTED BACK UP JUST AFTER
	CUST SAYS VEHICLE SHAKES AND HESITATES FEELS LIKE ITS GOING STALL
	FEELS LIKE ITS GOING TO STALL TAPPING NOISE IN MOTOR ON ACCEL
	C S WHILE DRIVING CAR DIED. PLS ADVISE DID START BACK NO PROBLEM
	CUST STATES VEHICLE DIED WHILE DRIVING. HAPPENED WHILE DECELERATING INTO A TURN INTO A PARKING LOT. VEHICLE RESTARTED OK.
D SENDER ,ROAD TEST	CUST STATES VEHICLE DIES WHILE DRIVING, STARTS BACK. SEE HISTORY
	CUSTOMER STATES ENGINE WONT START STALLED WHILE DRIVING AND WOULD NOT RERSTART SES LIGHT
	CHECK AND ADVISE CUSTOMER STATES CAR SHUT OFF WHEN GOINING A SMOOTH DIP, WILL RE START AFTER 10MIN
	D21 CUST STATES ENGINE STALLED WHILE DRIVING, IT DID START BACK UP INSTANTLY
	CHECK VEHICLE STALLED OUT AT HWY SPEEDS AT TIMES
	STALLED TWICW
	STALLS WHILE DRIVING
	C8 CK ENGINE STALLING OUT WHILE MAKING TURN ALOS WHILE DRIVING SEE AMADOR
	C S ENGINE STALLS AFTER 15 20 MIN. USUALLY IN THE MORNING WHEN BRAKING, DOWN HILL , SOMETIMES TURNING, STALL ACCELL IN AFTER NOON, 4 TIMES IN LAST MONTH
D DPFE SENSOR AND RE TEST CC 42	CHECK FOR ENGINE STALLS AT STOPS , IN GEAR, ENGINE HOT D21
	D21 PER CUST, ENG HAS STALLED 4 TIMES IN 2 DAYS, STALLS WHILE DRIVING.
	CHECK AND ADVISE, CUSTOMER STATES WHEN SLOWING DOWN TO MAKE TURN (DOWNHILL) ENGINE STALLED, HAPENED MONDAY. STOPED WITH PROBLEMS BUT RESTARTED AGAIN
	ENGINE STALLS OUT WHILE DRIVING 55 MPH WILL RESTART O K HAS HAPPENED TWICEIN TWO WEEKS
	CUSTOMER STATES CAR DIED WHEN DRIVING, ONE TIME, THEN RESTARTED WITH NO PROBLEM, ADVISE
	SHUTS OFF WHILE DRIVING WILL RE START AGAIN
	ENGINE CUTS OFF AT TIMES GOING DOWN ROAD WILL RESTART

2002	12102	611	1FMYU03102KA69800	3.0L	TALD	10	2001	2304	12A650	D21	6	885781	6000	ON HIGHWAY
2002	12109	611	1FMYU03102KA82189	3.0L	TALD	10	2001	2.00E+03	9F715	D21	1	2273588	0	WHILE BRAKING
2002	12104	611	1FMYU03102KA82001	3.0L	TALD	10	2001	2.00E+04	9C915	D21	6	1127300	3000	WHILE BRAKING
2002	12127	611	1FMYU03102KA79869	3.0L	TALD	10	2001	2304	12A650	D21	7	1247605	6000	WHILE DRIVING
2002	12131	611	1FMYU03102KA79514	3.0L	TALD	10	2001	2304	12A650	D21	8	2266362	11000	WHILE DRIVING
2002	12143	611	1FMYU03102KA70280	3.0L	TALD	10	2001	2.00E+03	9F715	D21	11	2325178	12000	WHILE DRIVING
2002	12145	611	1FMYU03102KA70063	3.0L	TALD	10	2001	2.00E+03	9F715	D21	10	2103536	16000	WHILE DRIVING
2002	12148	611	1FMYU03102KA69821	3.0L	TALD	10	2001	2304	DIAG	D21	11	2430155	16000	STALLS
2002	12160	611	1FMYU03102KA69821	3.0L	TALD	10	2001	2.00E+03	9E928	D21	9	1942883	13000	STALLS
2002	12151	611	1FMYU03102KA69429	3.0L	TALD	10	2001	7V01	12A581	D21	1	355634	0	WHILE DRIVING
2002	12153	611	1FMYU03102KA68443	3.0L	TALD	10	2001	2305	RECAL	D21	8	1605815	16000	WHILE BRAKING
2002	12184	611	1FMYU03102KA52369	3.0L	TALD	9	2001	2305	RECAL	D21	6	873372	9000	WHILE DRIVING
2002	12180	611	1FMYU03102KA52369	3.0L	TALD	9	2001	2304	12A650	D21	10	1984336	16000	WHILE DRIVING
2002	12187	611	1FMYU03102KA52061	3.0L	TALD	9	2001	2304	DIAG	D21	1	243642	0	STALLS
2002	12189	611	1FMYU03102KA51125	3.0L	TALD	9	2001	2305	RECALEM	D21	4	823705	4000	STALLS
2002	12190	611	1FMYU03102KA50413	3.0L	TALD	9	2001	2302	12B579	D21	6	885895	3000	WHILE DRIVING
2002	12204	611	1FMYU03102KA48548	3.0L	TALD	9	2001	2304	DIAG	D21	7	1245825	17000	WHILE DRIVING
2002	12214	611	1FMYU03102KA44051	3.0L	TALD	9	2001	2.00E+03	9F715	D21	9	1672917	5000	WHILE DRIVING
2002	12217	611	1FMYU03102KA40582	3.0L	TALD	9	2001	2.00E+03	9F715	D21	10	1880957	9000	WHILE DRIVING
2002	12220	611	1FMYU03102KA39881	3.0L	TALD	9	2001	2304	12A650	D21	10	2077697	7000	COASTING
2002	12231	611	1FMYU03102KA38245	3.0L	TALD	9	2001	2.00E+03	9F715	D21	2	286653	1000	WHILE DRIVING
2002	12232	611	1FMYU03102KA38245	3.0L	TALD	9	2001	7C05	14K366	D21	3	355571	9000	WHILE DRIVING
2002	12233	611	1FMYU03102KA38245	3.0L	TALD	9	2001	2.00E+03	9F715	D21	12	2655840	13000	WHILE DRIVING
2002	12235	611	1FMYU03102KA37600	3.0L	TALD	9	2001	2304	12A650	D21	6	746658	5000	COASTING
2002	12238	611	1FMYU03102KA36639	3.0L	TALD	9	2001	2305	RECAL	D21	11	2272436	16000	ON HIGHWAY

REFLASH		PROGRAM PCM EEC TEST KOEO PASS KOEC PASS KOER P1000 DCL MONITOR TEST IDLE DATA TEST FUEL PRESSURE TEST PINPOINT REPROGRAMMED PCM
TSB		REPLACED IAC PER TSB
SSM		5521 DIAGNOSE INSTALL WDS RUN EEC TEST NO CODES. CHECK OASIS SSM CAME UP TO REPROGRAM PCM TO LATEST LEVEL WHICH I DID. BLOW OUT VENT LINE FOR EVAP PER SSM. CHECK RELAY IN BJB HAD NO WHITE LETTERIN
NPF		UNABLE TO DUPLICATE EEC (QUICK TEST) DIAGNOSIS
TSB		OPERATE QUICK TEST, PASS. CK OASIS TSB 2 11 6 RECALIBRATE PCM. TEST DRIVE ALL OK.
REFLASH		VERIFIED CONCERN PERFORMED WDS DIAG TRACED TO AND REPLACED IAC AND REPROGRAMMED PCM RETESTED ALL OK
TSB		PERFORMED TSB 021106
NPF		SSDS,EEC,NO CODES HALLED HOTLINE WAS TOL THERE WAS NO REPAIR AT THIS TIME
TSB		RD TEST SSDS REPL EEC RELAY ACCESS AND REPLACE IAC DIRE THROTTLE BODY REPROGRAM PCM ALL PER JEFF HAZEL FIELD SERV ENG ALSO PERFORMED TSB 02 11 6 PER FSE
DIAG		WIRING EEC (QUICK TEST) DIAGNOSIS
DIAG		PCM EEC (QUICK TEST) DIAGNOSIS
SSM		CK CODES NO CODES PINPOINT TEST RECORD AND MONITOR PIDS REPROGRAMED PCM PER SSM 15589 CLEARED CODES RETEST ROAD TEST
DIAG		EEC (QUICK TEST) DIAGNOSIS
NPF		CHECK EE, COULD NOT DUPLICATE PROBLEM
SSM		ROAD TEST, DIAG FOR STALL, NO CODES, CONCERN DID NOT RE OCCUR, VERIFY OASIS. RE PROGRAM PCM AS PER SSM
DIAG		INTERMITTENT OPERATION EEC TEST KOEO PASS KOEC PASS KOER PASS DCL MONITOR TEST IDLE DATA TEST FUEL PRESSURE TEST CK. GROUNDS & CONNECTORS CK.
NPF		MO 17610,UNABLE TO DUPLICATE PERFORMED EEC 5 DIAG,KOEO PASS,KOER PASS,KOEC PASS,PERFORMED ROAD TEST AND MONITOR DIAG,ALL OK,UNABLE TO DUPLICATE AT
TSB		5308 WARRANTY RUN ON WDS NO CODES SYSTEM RUN FUEL PRESSURE TEST IN SPECS RUN INJECTOR FLOW TEST SYSTEM PASSED RUN IGNITION TEST SYSTEM PASSED RUN OASIS FOUND TSB 02 11 06 TO REPROGRAM PCM REPLA CE I
REFLASH		ENGINE DIA GTEST AND PIN AND MONITOR TEST AND REPALCED IAC VALVE AND REPROGRAMED PCM AND RETEST
REFLASH		WDS DIAG REPROGRAM TEST DROVE COULD NOT VERIFY COMPLAINT
REPLACED		WDS, SELF TEST, PASS CODES, DATALOGGER, IGNITION SYSTEM, POWER BALANCE, RELATIVE COMPRESSION, FUEL PRESSURE, REPLACED IAC VALVE, RETESTED
REPLACED		WDS, SELF TEST, PASS CODE, DATALOGGER, IGNITION SYSTEM, POWER BALANCE, RELATIVE COMPRESSION, FUEL PRESSURE, REPLACED EEC POWER RELAY, CHECKED GROUND CONNECTIONS CHECKED RELAY PINS FOR PUSH OUT, RETEST
TSB		WDS SELF TEST, PASS CODE, DATALOGGER, IGNITION SYSTEM, POWER BALANCE, RELATIVE COMPRESSION, FUEL PRESSURE, PERFORMED TSB 02 1105, MONITOR IAC DUTY CYCLE, REPLACED IAC VALVE, REPROGRAMMED PCM, MONITOR
SSM		5290 INSTALL WDS RUN EEC TEST NO CODES, CHECK FUEL PRESSURE AND INPUTS TO PCM ALL OK. CHECK EGR OPERATION OK AND IAC WAS WORKING CORRECTLY. RUN ON OASIS SSM CAME UP TO REPROGRAM PCM AND CHECK FOR L
REFLASH		PERFORM WDS TEST: PASS CODES ONLY CHECK IGNITION SYSTEM; OK CHECK FUEL PRESSURE; 47 PSI ROAD TEST WITH MONITOR; OK CHECK COMPRESSION; 155 160 PSI ALL CYLINDERS REPROGRAM PCM TO LATEST UPDA

	CUST STATES STALLING WITH FOOT ON GAS AT HWY SPEEDS
	VEHICLE DIED WHEN CAME TO A STOP. HAPPENED ONCE. RESTARTED RIGHT AWAY
G WHICH IS OK PER SSM, ROAD TEST OK	THE VEHICLE WANTS TO STALL WHEN SLOWING DOWN AND WITH THE AIR ON MORE EVIDENT
	ENGINE STALLED WHILE DRIVING YELLOW CHECK ENGINE LIGHT CAME ON IT WAS 6 MINUTES BEFORE IT WOULD RESTART
	C.S VEHICLE JUST STOPS RUNNING WHILE DRIVING.
	CUSTOMER STATES ENGINE SHUT OFF WHILE DRIVING RESTARTED AFTER
	* ALL ELECTRICAL CUSTS OUT WHILE DRIVING HAS DONE 2 TIMES WHILE DRIVING
	STALLING
	CHK ENGINE CAME ON STALLING,LOST POWER,BRAKE PEDAL GOT VERY HARD LOST ALL POWER ELECTRICAL
	CUST STATES THE ENGINE DIED WHILE DRIVING 50MPH...INDICATOR LIGHTS CAME ON STEERING WENT STIFF...RECRANKED AFTER SITTING 5 MINUTES
	CUST STATES ONCE, WHILE SLOWING DOWN, ENGINE DIED. WOULD IMMEDIATRELY RESTART.
	CK, VEH. CUT OFF ON CUST. WHILE DRIVING
	CUSTOMER STATES: CK ENGINE STALLS WHILE DRIVING (WILL RESTART)
	CUSTOMER STATES CHECK ENGINE LIGHT ONIN CC 829
	CUST STATES VEHICLE CUT OFF UNEXPECTEDLY, CK AND ADVISE
	C S ENGINE HAS JUST DIED ABOUT 3 TIMES, DRIVING DOWN THE ROA TOOK ABOUT 15MINUTES TO START BACK UP ONE TIME
	1021...CUSTOMER STATES VEH STALLED NORMAL DRIVING TO WORK STEERING WHEEL GOT STIFF BRAKE PEDAL LOST POWER, OIL & CHECK
AC DID SO VEHICLE DOES NOT STALL NOW	DIES WHILE DRIVING CRANK NO START AT TIMES
	VEHICLE HAS STALLED OUT TWICE ON CUSTOMER WHILE DRIVING AND HAS STARTED RIGHT BACK UP
	WHILE DRIVING THE ENGIN DIED COASTED OVER IT RESTARTED
	CUSTOMER STATES THAT TRUCK WILL CUT OFF WHEN DRIVING...THE OIL AND BATTERY LIGHT WILL COME ON BEFORE IT CUTS OFF.
ED, ROAD TESTED	THE ENGINE WILL STALL AT 45MPH WILL START BACK UP AFTER STALLING
SWAP DUTY CYCLE, OK, ESC	ENGINE IS STALLING WHILE DRIVING AND AT TIMES WILL STALL AFTER DRIVING IN REV.
ATEST UPDATE ON THE PCM RELAY. REPROGRAM PCM TO LATEST CALIBRATION LEVEL. CHECK RELAY WAS THE LATEST AVAILABEL NO WHITE LETTERING ON IT. TIGHTEN THE CONNECTIONS AT THE RELAY PER SSM.	ENGINE STALLS ON DECELL GOING DOWN A GRADE
TE	CUSATOMER STATES AT TIMES WHEN 1ST STARTING OF ENGINE DIES RESTARTS OK, WARM OR COLD ONCE EXITING THE HIGHWAY PLEASE CHECK OUT AND ADVISE

2002	12247	S11	1FMYU03108KA36734	3.0L	T/A,D		8	2001	2G04	DM9	D21		4	2616299	4000 WHILE DRIVING
2002	12248	S11	1FMYU03102KA36703	3.0L	T/A,D		8	2001	1A03	8006	D21		4	1089417	5000 NO TEXT
2002	12249	S11	1FMYU03102KA35705	3.0L	T/A,D		8	2001	1A03	8006	D21		4	941800	9000 WHILE DRIVING
2002	12250	S11	1FMYU03102KA35104	3.0L	T/A,D		8	2001	2G03	12226	D21		0	572851	0 STALLS
2002	12251	S11	1FMYU03102KA34177	3.0L	T/A,D		8	2001	2G04	12A650	D21		6	697369	5800 DOWNHILL
2002	12255	S11	1FMYU03108KA27922	3.0L	T/A,D		8	2001	7C06	14N069	D21		2	384801	1000 STALLS
2002	12274	S11	1FMYU03102KA36791	3.0L	T/A,D		8	2001	7B06	14900	D21		3	522835	1000 WHILE DRIVING
2002	12276	S11	1FMYU03102KA35993	3.0L	T/A,D		8	2001	2.00E+03	6F715	D21		4	1082146	11000 STALLS
2002	12277	S11	1FMYU03102KA35993	3.0L	T/A,D		8	2001	2G04	12A650	D21		5	2299763	13000 STALLS
2002	12311	S11	1FMYU03102KA06307	3.0L	T/A,D		8	2001	3A09	7002	D21		6	1126309	3500 SHIFTS ROUGH
2002	12316	S11	1FMYU03102KA07027	3.0L	T/A,D		8	2001	2.00E+03	6F715	D21		10	1892350	14000 WHILE DRIVING
2002	12782	S11	1FMYU021X2KC01751	3.0L	T/A,D		1	2002	2.00E+03	6F715	D21		4	1408928	11000 STALLS
2002	12808	S11	1FMYU021X2KC09189	3.0L	T/A,D		11	2001	2B05	RECAL	D21		5	1245132	16000 WHILE DRIVING
2002	12812	S11	1FMYU021X2KC21662	3.0L	T/A,D		11	2001	1R09	0J460	D21		1	655401	12900 NO TEXT
2002	12814	S11	1FMYU021X2KC21459	3.0L	T/A,D		11	2001	2G01	12A650	D21		9	2142311	19000 WHILE DRIVING
2002	12878	S11	1FMYU021X2KA76188	3.0L	T/A,D		10	2001	2B05	RECAL	D21		9	2130002	6500 WHILE DRIVING
2002	12882	S11	1FMYU021X2KA66884	3.0L	T/A,D		9	2001	1A03	8006	D21		5	526474	1000 WHILE DRIVING
2002	12885	S11	1FMYU021X2KA16489	3.0L	T/A,D		8	2001	2.00E+03	6F715	D21		12	2258118	17000 STALLS
2002	12870	S11	1FMYU021X2KA07117	3.0L	T/A,D		8	2001	2B05	RECAL	D21		4	677810	2500 STALLS
2002	12888	S11	1FMYU021X2KB64749	3.0L	T/A,D		12	2001	2G01	12A650	D21		3	1706314	4900 WHILE DRIVING
2002	12916	S11	1FMYU021X2KB01280	3.0L	T/A,D		10	2001	7C05	14N069	D21		6	1247345	4000 NO TEXT
2002	12935	S11	1FMYU02102KA36890	3.0L	T/A,D		8	2001	2B05	RECAL	D21		8	1648021	11800 LACKS POWER
2002	12942	S11	1FMYU02102KA36896	3.0L	T/A,D		8	2001	1A09	8007	D21		1	308709	0 NO TEXT
2002	12943	S11	1FMYU02102KA36898	3.0L	T/A,D		8	2001	1A09	8007	D21		1	250287	0 STALLS
2002	12956	S11	1FMYU02102KA15881	3.0L	T/A,D		8	2001	7B11	14486	D21		1	157488	0 WHILE DRIVING
2002	12971	S11	1FMYU02102KA06890	3.0L	T/A,D		8	2001	2.00E+03	6H307	D21		11	2411519	11600 WHILE DRIVING

HOTLINE		CALLED HOTLINE, CONTACT #2R3C5005EEC (QUICK TEST) DIAG,PINPOINT CKS,IGNITION TEST,FUEL PRESSURE,
ENGINE FAILURE		REQUESTING DEALER'S P/A CODE 01311
ENGINE FAILURE		MOTOR LOCKED UP R AND R MOTOR
VACUUM LEAK		KOEO,KOER,KOEOC,P1000 MONITORED PIDS PINPOINT AND REPAIRED VACUUM LEAK AT PVV VACUUM SOURCE CLEANED OIL SATURATION RETEST AND ROAD TEST KOEO,KOER,KOEOC,P1000.
SSM		ROAD TESTED TRUCK PERFORMED WDS DIAG EEC AND DCL PINPOINT TEST PERFORMED SSM # 16599 RECALIBRATED PCM RETESTED OK
REPLACED		EEC TEST,FUEL PRESSURE TEST,PID MONITOR TEST,WIGGLE TEST, INJECTOR TEST,REPLACED POWER RELAY,R&I PCM,CK PINS,CK WIRE LOOM AT BOTH FUSE BOXES & RELAY BOX,CK GROUNDS 101, 104 & 105 ,CK FUEL PUMP WIRING,T
SSM		1994 CK FOR STALLED OUT WARR RAN WDS TESTING NO CODES SYSTEM PASSED REMOVED BATTERY AND RELOCATED BATTERY GROUND FROM THE BATTERY TRAY TO THE FRAME CK IDC RELAY HAS NEW STYLE IN IT ALREADY
REPLACED		CHECK IGNITION SYSTEM AND GOT NO CODES RAN PID DATA AND FOUND IAC STICKING AND REPLACED
TSB		RAN EEC DIAG NO DTC S PERFORMED TSB 02 11 05 REPLACED PCM RELAY AND REPROGRAMMED PCM TO NEWEST UPDATE 1U7A 12A650 AXC TEST DROVE AND RETESTED OK
REPLACED		3351 CONVERTOR W 2002 ESCAPE 2.0L CODE PERFORMED ELECT TRANS DIAG KOEO KOER KOEC P1111 ROD TESTED VERIFIED CUST CONCERN RR TRANS ASY FLUSHED COOLER AND LINES TESTED AND REPLACED CONVERTOR ASY REINS
REPLACED		14074 EEC TESTS ALL CODES PASS***PINPOINT TESTS PER SYMPTON***MONITOR PIDS THRU DCL ON ROAD TEST*** ***REPLACE IAC VALVE***REPROGRAM PCM***DO STATIC AND DYNAMIC EVAP EMISSION TESTS***CHECK EEC RELAY
REPLACED		ROAD TESTED AND PIN POINT TESTED, FOUND IAC MOTOR STICKING. REPLACED IAC MOTOR
TSB		TEST DROVE AND VERIFIED CONCERN, BROUGHT IN AND TESTED EEC SYSTEM AND PERFORMED COMPLETE LIST FOR STALLING RECEIVED CODE P0113 PERFORMED PINPOINT TESTS AND FOUND MASS AIR FLOW SENSOR SHORTED OUT, REPL
REPLACED		EEC TEST, PIN POINT, REPLACE SENSOR
DIAG		PCM EEC (QUICK TEST) DIAGNOSIS
REFLASH		WDS DIAGNOSIS. PERFORM DCL DATALOGGER TEST. REPROGRAM PCM AND RETEST
REPLACED		DIAG & REPLACE ENGINE
DIAG		DIAGNOSTICS PARTS ORDERED
REFLASH		DIAGNOSE WITH NGS, P1000 10 P1000 30 P1000. DIAGNOSE BY SYMPTOM AND INSTALL FUEL PRESSURE GAUGE AND RECORDER PINPOINT TP CIRCUIT AND SENSOR, BOTH WITHIN SPECS. R&R THROTTLE BODY AND INSPECT. THROTTLE
NO TEXT		
NO TEXT		
TSB		VERIFIED CUSTOMER CONCERN. DIAGNOSED PER TSB# 02 11 6 AND REPROGRAMMED PCM PER TSB. MT TIME TO DIAGNOSE PER TSB# 02 11 6, NO OPERATIONS IN 2002 SLT3 MANUAL.
ENGINE FAILURE		REQUESTING DEALER'S P/A CODE 20004
REPLACED		SUPPLIED NEW ENGINE LOOKS LIKE CRANKSHAFT DAMAGE REPLACED ENGINE R&R/PERED ALL NECESSARY PARTS CONTROL 1JEG9001 1
NFF		918 TEST EEC P1000 P1000 P1000 NGS DISPLAY NGS ROADTEST MONITER CH IGNITION SYSTEM. NO PROBLEMS CH FUEL PRESSURE 40 PSI AND STEADY TRANSMISSION STARTS OUT AND STAYS IN SECOND GEA STALLING RELATED
REPLACED		FUEL PUMP FAILURE RT FUEL TANK,TEST & REPLACE FUEL PUMP MODULE ASSY

	CUST REPORTS VEHICLE DIED WHILE DRIVING & WOULD NOT RESTART
	CUSTOMER STATES THE ENGINE STALLED WHILE DRIVING WILL NOT CRANK TO R
	CUSTOMER STATES THE VEHICLE STALLS
	CHECK TRUCK STALLED OUT GOING DOWN HILL
EST.	ENG DIES AND WILL NOT RESTART
	CHECK FOR VEH STALLED WHILE DRIVING,RESTARTED WITH NO PROBLEM
	CUST STATES VEHICLE HAS DIEING AT TIMES
	CUSTOMER STATES CHECK FOR VEH DIEING AT TIMES WHILE
TALLED REFILLED AND ROAD TESTED AFTER REPAIRS CC 42	P95 CUST STS TRANSMISSION JERKS WHEN SHIFTING 40 65 MPH
FOR LATEST ONE***RETEST AND ROAD TEST*** ****ALL PER TSB 02 11 6****	VEH STALLS WHEN DRIVING SOMETIMES,SEE HISTORY
	STALLS INTERMITTENTLY
ACED MASS AIR FLOW SENSOR, AIR BYPASS, THROTTLE BODY AS PER TSB 2 8 8. ALSO STUMBLES ON ACCEL. PINPOINT TEST. FOUND CIRCUIT 138, 139 RUBBED THRU AT EVAPORATOR. REPAIR WIRING, CLEAR CODES	CHECK CUSTOMER STATES THAT VEHICLE KEEPS DIEING OUT WHILE DRIVING, CHECK AND ADVISE
	CUST STATES THE ENGINE HAS DIED 2X SINCE LAST REPAIR WHILE DRIVING COASTING...SEE HISTORY
	INTERMITTENTLY VEH DIES WHILE DRIVING THIS HAS HAPPENED 3 TIMES
	SHUT DOWN ON CUSTOMER WHILE DRIVING, WAITED A COUPLE MINUTES AND STARTED UP AGAIN BUT FELT LIKE IT WAS GOING TO STALL AGAIN
	CUSTOMER STATES VEHICLE STALLED A FEW TIMES
PLATE BINDING IN	WHEN FIRST STARTING VEHICLE, RPMS REV UP TO 2K 3K AND THEN INTERMITTENTLY STALLS
	CHECK FOR DIEING PROBLEMS GOING DOWN ROAD RESTART IS OK FORD TECH HOTLINE SAYS TO RECALIBRATE PCM
	CUST STATES THE ENGINE ACTS AS IF GOING TO STALL AND LACKS POWER WHEN CLIMBING A HILL
	VEHICLE QUIT RUNNING WILL NOT RESTART CALLED ENGINE PLANT AND THEY
TO TRANS PROBLEM NEEDS TO GO TO TRANS. RETEST	ENGINE STALLS TAKES ABOUT 20 SECONDS TO RESTART, ALSO STALLS WHILE DRIVING WHEN COLD
	VEHICLE SHUTS OFF WHILE DRIVING.

2002	12974	S11	1FMYU02102KA07668	3.0L	TAUD	8	2001	2G05	RECALEM	D21	12	2222576	16000	WHILE BRAKING
2002	12979	S11	1FMYU02102KA07264	3.0L	TAUD	8	2001	2B04	DIAG	D21	2	209032	1000	STALLS
2002	13004	S11	1FMYU02102KB67102	3.0L	TAUD	1	2002	2.00E+03	9F715	D21	7	2189061	7000	AT STOP
2002	13027	S11	1FMYU02102K812667	3.0L	TAUD	10	2001	2B01	12A650	D21	10	2458587	13000	NO TEXT
2002	13081	S11	1FMYU02102KA30444	3.0L	TAUD	8	2001	2.00E+03	9F715	D21	5	609885	5000	AT STOP
2002	13104	S11	1FMYU02172KD41345	3.0L	TAUD	6	2002	2.00E+03	9F715	D21	1	2225146	0	STALLS
2002	13122	S11	1FMYU02172KB64820	3.0L	TAUD	12	2001	2B04	DIAG	D21	6	1961411	6000	WHILE DRIVING
2002	13134	S11	1FMYU02172KB21074	3.0L	TAUD	11	2001	1A08	6006	D21	6	1536486	12000	WON'T RUN
2002	13163	S11	1FMYU02172KA69035	3.0L	TAUD	10	2001	7W01	12A581	D21	8	1691892	14000	WHILE DRIVING
2002	13164	S11	1FMYU02172KA69035	3.0L	TAUD	10	2001	2.00E+03	9E926	D21	6	1675545	14000	WHILE DRIVING
2002	13173	S11	1FMYU02172KA39089	3.0L	TAUD	9	2001	2B04	DIAG	D21	6	1057691	4000	STALLS
2002	13174	S11	1FMYU02172KA39691	3.0L	TAUD	9	2001	1B22	9731	D21	1	291058	0	WHILE DRIVING
2002	13176	S11	1FMYU02172KA39874	3.0L	TAUD	9	2001	7C05	14N089	D21	3	480885	3000	WHILE DRIVING
2002	13183	S11	1FMYU02172KA39691	3.0L	TAUD	9	2001	2F02	9E926	D21	6	1208537	13000	WHILE DRIVING
2002	13184	S11	1FMYU02172KA39391	3.0L	TAUD	9	2001	2.00E+04	9C015	D21	10	2134450	18000	STALLS
2002	13195	S11	1FMYU02172KA27291	3.0L	TAUD	8	2001	2.00E+03	9F715	D21	4	389989	3000	WHILE BRAKING
2002	13197	S11	1FMYU02172KA26796	3.0L	TAUD	8	2001	2.00E+03	9F715	D21	10	2161652	8000	WHILE DRIVING
2002	13199	S11	1FMYU02172KA19090	3.0L	TAUD	8	2001	7C05	14N089	D21	8	1171673	3000	WHILE DRIVING
2002	13200	S11	1FMYU02172KA17720	3.0L	TAUD	8	2001	2G05	RECAL	D21	5	636808	5000	COASTING
2002	13216	S11	1FMYU02172KA14770	3.0L	TAUD	8	2001	7B06	12B657	D21	0	240068	0	INOP
2002	13237	S11	1FMYU02162KC39491	3.0L	TAUD	2	2002	2B01	12A650	D21	2	1149845	1000	WON'T RUN
2002	13257	S11	1FMYU02162KB44824	3.0L	TAUD	12	2001	2.00E+03	9F715	D21	7	2070352	18000	STALLS
2002	13279	S11	1FMYU02162KB13279	3.0L	TAUD	11	2001	2B02	12028	D21	1	475482	0	WHILE DRIVING
2002	13309	S11	1FMYU02162KA51437	3.0L	TAUD	9	2001	2G05	RECAL	D21	3	517732	2000	AT STOP
2002	13314	S11	1FMYU02162KA45136	3.0L	TAUD	9	2001	7B02	14A01	D21	9	1982123	10000	ON HIGHWAY

REFLASH		18725 RECALEM CC42 EEC TEST P1000 P1000 P1000 FUEL PRESS TEST 40 PSI, IGNL SYSTEM TEST, NGS ROADTEST PID MONITOR NGS DCL DISPLAY, FLASHED PCM, ROAD AND RETEST P1000.
NPF		1634 ROADTESTED COULD NOT DUPLICATE HOOKED UP WDS CHECKED FOR CODES NONE STORED MONITORE DATA LOGER FOR MAF BARO O2S LOOKS OKEY RAN OASIS NOTHING FOUND UNDER STALLING RAN OKEY NO PROBLEM FOUND
REPLACED		EEC TEST, QUICK TEST, PPT TEST, MONITOR RECORD, DCL DISPLAY, & REPLACED IDLE AIR CONTROL MOTOR
ANS BUILD		WDS TEST EEC REPLACE PCM UNIT HAD PCM IN CAR FOR OVERSEAS
REPLACED		RAN COMPLETE SYSTEM TEST RAN PINPOINT TEST RAN IGN TEST RAN FUEL PRESSURE TEST REPROGRAMED PCM TO LATEST LEVEL REPLACED EEC RELAY AND REPLACE D IDLE AIR CONTROL VALVE RETEST PASS
REPLACED		PERFORM TESTS & REPLACE THROTTLE BODY & VALVE.
DIAG		EEC (QUICK TEST) DIAGNOSIS
ENGINE FAILURE		HOLE IN SIDE OF BLOCK ENGINE ASSEMBLY REMOVE AND INSTALL
NO TEXT		
NO TEXT		
NPF		PERFORMED EEC TEST AND NO CODES WERE FOUND FUEL PRESSURE CHECKED O.K. UNABLE TO DUPLICATE PROBLEM AT THIS TIME
ENGINE FAILURE		021 69 ENGINE ASSEMBLY REMOVE AND INSTALL (6007) TRANSFER PARTS,AC EUPLIMENT
TSB		AS PER TSB16434 REPLACED EEC POWER RELAY, RETESYT, PASSED
SSM		WDS TEST,NO CODES,CHECK ALL GROUNDS AND IGNITION SWITCH CONNECTIONS,MONITOR PIDS IAC AT 49%,ADJUST BASE IDLE TO BRING IAC INTO RANGE AT 35%,ROAD TEST,OK,LABOR TIME TO CHECK GROUNDS AND IGN SWITCH CO
TSB		WDS TEST,NO CODES,REFERR TO TSB #02 11 06,MONITOR PIDS,REPLACE EVAP/VM SENSOR & THROTTLE BODY,RECALIBRATE PCM,INSPECT PCM RELAY,OK,ROADTEST,OK.
REPLACED		VERIFY, RUN WDS TESTING, PASS CODES RECIEVED, PID MONITOR, IAC STICKING, REMOVE & REPLACE IAC SOLENOID
REPLACED		EEC TEST TEST FUEL PRESS 48PSI PASS NGS MONITOR TEST CK IAC 6% FAIL REPLACE IAC VALVE ROAD TEST RE EEC TEST
SSM		EEC TEST VEHICLE PASS IN ALL MODES, PERFORM DATA LOGGER TEST PASS, CALLED HOTLINE, PERFORM SSM 16499 REPROGRAM PCM AND RER EEC POWER RELAY. CHECKE PIDS AGAIN WITH DATALOGGER ROAD TEST OK
REFLASH		CHECK FOR STALLING OUT, WDS TEST NO CODES RAN ON OASIS FOUND SPECIAL SERVICE MESSAGE #16699 REPROGRAM PCM AND CHECK PCM RELAY AND EVAP VENT HOSE, CHECK TO BE OK
REPAIR		WDS HOOK UP AND DCL DISPLAY PINPOINT TEST POWER BALANCE TEST INJECTOR FLOW TEST REPSAIRED WIRE CONNECTOR TO INJECTOR AND RETEST
REPLACED		N TIME ABNORMAL DIAG PERFORMED DIAG, CODE P0606 PERFROMED TESTS, FOUND AND REPLACED SHORTED PCM
TSB		RD TEST,CONFIRMED SIDS PREFORMED NECCESSARY TEST,PINPOINT TEST PREFORMED TSB 02 06 6 RETEST OK
REPLACED		EEC TEST DCL DISPLAY AND PINPOINT TEST REPLACED NUMBER 6 SPARK PLUG AND COIL
REFLASH		TEST EEC V KOEO PASS,KOEC PASS,KOER PASS MONITOR PIDS BARO 154HZ. REFLASH PCM #1U7A AXA ROADTEST 6 MILES UNABLE TO VERIFY CONCERN RUN OASIS #410 264 960
TSB		RD TST WDS DIAG CHECK OASIS FOUND TSB 02 11 6 PER EVAP DRIVE CYCLE RER EVAC CANISTER BLOW OUT LINES REPROGRAM TSB RD TST VEH STALLED.TRACE FOUND WIRE CONNECTION POOR HARNESS 14401 TO POWER DIST BOX, R

EMTIRE

	AT TIMES WHEN COMING TO A STOP REMOVE FOOT FROM BRAKE AND ENGINE STALLS
	CUST STATES WHEN WET OUT VEHICHLES STALLS
	CUSTOMER STATES CUTS OFF AT STOP LIGHTS & WHEN COASTING DOWN HILL
	CUST STATES THAT THE VEH WILL DIE AT STOPS INTERMITTINGLY AND AT LOW SPEEDS SOMETIMES THE VEH IS HARD TO START
	ENGINE STALLS ROAD SIDE TOWED.
	STALLED ONCE WHILE DRIVING
	TOWED IN WILL NOT RUN
	CK/ADV STALLS WHILE DRIVING SEE HIST@0
	CK/ADV VEHICLE STALLING WHILE DRIVING@0.00
	WHAT THE CUSTOMER THOUGHT WAS THE OIL LIGHT AND ONE OTHER LIGHT WENT ON AND THE CAR STALLED OUT ON LAKE WHEN THE
	CUSTOMER STATES CHECKED ENGINE STALLED WHILE DRIVING NO W ENGINE JUST CLUNKS WHEN TRYING TO START
	CUSOTMER REPORTS DRIVING DOWN THE RADD AND TRUCK CUT OFF. ONLY HAPPENED 1 TIME. RESTARTED NORMALLY
NNECTIONS AND SET BASE IDLE NOT LISTED USE M TIME.	CUTS OUT WHILE DRIVING.
	CHECK STALLING CONDITION.
	WHEN SLOWING DOWN AND BRAKING VEHICLE WILL DIE, ALSO WHEN MAKING A TURN IT DIES
	ENGINE STALLS WHILE DRIVING,SECOND TIME ENGINE HAS STALLED
	CUSTOMER STATES LAST NIGHT CUST LEFT WORK,VEHICLE SAT ALL DAY 8 HRS,CUST WAS DRIVING 10 15 MIN ENG STALLED WHILE
	STALLED OUT COUPLE TIMES ON A COAST 02 ESCAPE
	NOT RUNNING PROPERLY.
	VEHICLE WILL NOT STAY RUNNING STARTS AND DIES. REPAIR AS NEEDED.
	ENGINE KEEPS STALLING
	OK FOR CAUSE OF ENGINE MISS AND RUNS ROUGH AND WILL NOT GO OVER 40 MPH , ALSO AMBER LIGHT FLASHING
	C S VEHICLE INTERMITTANTLY DIES, WILL RESTART HAS EXPERIENCED THIS WHEN TURNING INTO A DRIVEWAY WITH FOOT ON THE BRAKE AND WHEN COMING TO A STOP. IS INTERMITTANT NO NOICE OF WHEN IT WILL H
EPAIR WIRING QUICK TST OK.	VEHICLE OUTS ON HIGHWAY WAS TOWED IN

2002	13321	S11	1FMYU02152KA28612	3.0L	TALD	6	2001	2305	RECALEM	D21	11	2271878	17000	ACCELERATING
2002	13338	S11	1FMYU02152KA09823	3.0L	TALD	6	2001	2001	9J460	D21	1	251109	1000	STALLS
2002	13370	S11	1FMYU02152KB31828	3.0L	TALD	12	2001	2.00E+03	9F715	D21	9	2370616	18000	STALLS
2002	13378	S11	1FMYU02152KB25469	3.0L	TALD	11	2001	2304	DIAG	D21	8	2158625	8000	STALLS
2002	13380	S11	1FMYU02152KB22167	3.0L	TALD	11	2001	1H09	9J460	D21	3	660669	3000	STALLS
2002	13389	S11	1FMYU02152KB02555	3.0L	TALD	10	2001	2.00E+03	9F715	D21	9	2099493	10000	STALLS
2002	13397	S11	1FMYU02152KA69578	3.0L	TALD	10	2001	1H03	9J460	D21	10	1943817	16000	WHILE DRIVING
2002	13422	S11	1FMYU02152KA91860	3.0L	TALD	8	2001	2.00E+03	9E935	D21	9	1749518	9000	WHILE DRIVING
2002	13434	S11	1FMYU02152KA25579	3.0L	TALD	8	2001	2304	12A650	D21	8	1125309	3000	WHILE DRIVING
2002	13439	S11	1FMYU02168KA15785	3.0L	TALD	8	2001	2.00E+03	9F715	D21	4	549111	7000	STALLS
2002	13483	S11	1FMYU02142KB44411	3.0L	TALD	11	2001	2304	12A650	D21	6	1333909	7000	STALLS
2002	13496	S11	1FMYU02142KB16604	3.0L	TALD	11	2001	2306	RECAL	D21	9	727002	2000	AT IDLE
2002	13507	S11	1FMYU02142KA91767	3.0L	TALD	10	2001	2.00E+03	9F715	D21	7	1250957	8000	WHILE DRIVING
2002	13508	S11	1FMYU02142KA91767	3.0L	TALD	10	2001	2.00E+03	9E935	D21	7	1473217	8000	AT STOP
2002	13563	S11	1FMYU02142KA35616	3.0L	TALD	8	2001	1H08	9J460	D21	9	1887758		ONO TEXT
2002	13572	S11	1FMYU02132KB01945	3.0L	TALD	6	2002	2304	DIAG	D21	1	1957167	1000	HESBURGE
2002	13576	S11	1FMYU02132KB60349	3.0L	TALD	6	2002	2.00E+03	9F715	D21	2	1766077	1000	STALLS
2002	13580	S11	1FMYU02152KB45054	3.0L	TALD	12	2001	7C05	14N089	D21	2	902309	1000	STALLS
2002	13612	S11	1FMYU02152KB29802	3.0L	TALD	11	2001	2.00E+03	9E935	D21	8	2314809	11000	STALLS
2002	13613	S11	1FMYU02152KB29802	3.0L	TALD	11	2001	2.00E+03	9E935	D21	9	2421455	11000	NO TEXT
2002	13614	S11	1FMYU02152KB29821	3.0L	TALD	11	2001	2.00E+03	9F715	D21	8	2168936	22000	WHILE DRIVING
2002	13663	S11	1FMYU02132KA25717	3.0L	TALD	8	2001	2.00E+03	9F715	D21	12	2246183	19000	STALLS
2002	13664	S11	1FMYU02132KA25329	3.0L	TALD	8	2001	1A09	6007	D21	10	2159851	3000	WHILE DRIVING
2002	13675	S11	1FMYU02132KA07921	3.0L	TALD	8	2001	2305	RECAL	D21	11	2134395	8000	STALLS
2002	13681	S11	1FMYU02122KC09899	3.0L	TALD	4	2002	2.00E+03	9F715	D21	4	1997830	8000	WHILE DRIVING
2002	13764	S11	1FMYU02122KA15725	3.0L	TALD	8	2001	7C05	14N089	D21	5	652697	11000	ON HIGHWAY

TSB		17621 ROAD TEST TO VERIFY ENG. OPERATION. CHECK OASIS.TSB 02 11 6 TEST WITH WDS.MONITOR IAC AND IDLE SPEED. IDLE AND IAC IN SPEC. MONITOR EVAPVM AND FTP WORKING OK. CHECK AND CLEAR EVAP. VENT LINE
REPLACED		CC 42 BASIC 9J459 TEST SYSTEM REPLACE EVR REGULATOR
TSB		EEC TEST NO CODES ROAD TEST CHECK OASIS PERFORM TSB 2 11 06 REPLACE IAC CHECK PIDS REPLACE THROTTLE BODY REPROGRAM PCM
TSB		INTERMITTENT STALLING.REPROGRAM PCM PER TSB02 11 6
REPLACED		FOUND IDLE AIR CONTROL SOLENOID HIGH RESISTANCE REPLACED IDLE AIR CONTROL SOLENOID
TSB		10949 PERFORM WDS START UP RETRIEVE CODES NO CODES PERFORM PINPOINT TESTS FUEL PRESSURE AND LEAKDOWN FUEL INJ. FLOW TEST POWER BALANCE IGNITION SYSTEM DIAG. ALL TESTS PASS AT THIS T TIME MONITOR D
REPLACED		10998 9J460 CC,42 TEST OBD II CODES P1111,KOEO,KOER P0401, P1504,CONT. TEST FUEL PUMP 50 PSI & 0 PSI LEAKDOWN OK. PERFORM NGS DCL DISPLAY & IGN SYSTEM DIAG & MONITOR TEST & PIN POINT TESTS DL & KE
TSB		42 PCM & THROTTLE BODY NOT WORKIG PROPERLY,VERIFY CONCERN,PE RFORM TSB 02 11 6,CHK FOR TROUBLE COLDE WITH WDS TESTER OK,M ONITOR PIDS FOR IAC,RPM,ECT,OK,CK & UPDATE PCM TO LATEST CAL IBRATION,CHK EVAP
DIAG		00 EEC (QUICK TEST) DIAGNOSIS
TSB		7371 IAC VALVE 9F715 42 NGS DIAG,KOEO SELF TEST PASS,PERFORM PINPOINT TEST,CH FOR TSB6,66M6,REPLACE IAC VALVE,RETEST, NORMAL START UP AT THIS TIME
DIAG		00 EEC (QUICK TEST) DIAGNOSIS
SSM		CHECK FOR STALL, EEC TEST PASSED. MONITOR NG S TO CHECK IAC AND THROTTLE POSITION MAF VOLTAG ES IN RANGE. TEST. CHECK IGNITION SYSTEM O.K. CHECK OASIS. REPROGRAMMED PCM PER SSM 15699 FOR STALL C
TSB		IAC ERRATIC, PCM REFLASH EEC DIAG, ALSO SEE LINE 1, CK AND REPAIR AS PER TSB 02 6 6 TEST AND REPL IAC MOTOR, REFLASH PCM, RETEST, IAC IN SPEC,
SSM		IDLE TOO SLOW EEC DIAG, NO DTCS, CK PIDS, ALL IN SPEC, CK OASIS, CK FOR LATEST PCM UPDATE, HAS NEWEST CALIB, CK IAC, CK OK, CK
NO TEXT		
NPF		EEC TESTED ALL PASS
REPLACED		VERIFIED CONCERN CKD CODES NO CODES FOUND FOUN D THAT IAC OUT OF SPECS REPLACED IAC ROADTEST O K AT THIS TIME
SSM		DOES NOT OPERATE PROPERLY WDS DIAG PCM REPROGRAM REPLACE EEC RELAY CK FUEL TANK VENT PER SSM 15699
TSB		X RAN EEC TEST R&R VALVE R&R THROTTLE BODY REPROG PCM PER TSB 02 11 06
STICKING		WPI RAN EEC TESTS, RR STICKING IAC AND STICKING THROTTLE BODY
STICKING		CAR STALLS INTERMITTENTLY EEC TEST PASS. CK CONNECTORS ON PCM, CMP, CRANK SENSOR & FUEL INJECTORS OK. DCL ROAD TEST MONITOR PIDS & INJ POWER, RPMS DROP, CAR STALLS COMING TO A STOP IAC STICK
TSB		INSPECTED AND PERFORMED TSB 02 11 6 IAC AT 49% REPLACED IAC AND REPROGRAMMED PCM
NPF		1 NGS TEST AND FUEL PRESSURE TEST ROAD TEST BY TECH AND SHOP FOREMAN UNABLE TO VERIFY CONCERN AT THIS TIME
REFLASH		EEC TEST PERFORM CHECK LIST CK GROUNDS & TIGHTEN CK EEC RELAY OK CK IAC & DPFE OK BLOW AIR THRU EVAPVAPOR HOSE REPROGRAM PCM CK IGNITION SWITCH ROADT EST 12 MILES OK
REPLACED		DIAGNOSTICS AND ORDERED VAPOR MANAGEMIN VALVE REPLACE FUEL VAPOR MANAGMENT VALVE CLEAR CODES AND RETEST REPLACE IDLE AIR CONTROL VALVE
REPLACED		ECC POWER RELAY POWERTRAIN CONTROL MODULE (PCM) REPLACE

. INSPECT EEC POWER RELAY. OK. ROAD TEST WITH SCAN TOOL TO VERIFY ENG. IDLE.	ENGINE SLUGGISH AND WANTS TO STALL AT LIGHTS, ALSO POOR ACCEL AT 40MPH
	CHECK FOR STALLING CONDERN,POSSIBLE IAC MAY NEED TO BE CLEANED.
	CHECK VEH STALLS AT TIMES
	CK FOR STALLING WHEN GOING INTO DRIVE.
	AT TIMES WILL STALL WHEN STARTING
ATALOGGER ALL FUEL TRIMS TP MAF S ARD DPFE WITHIN RANGE PERFORM MONITOR ROAD TEST ALL FRP MAF DPFE AND FUEL TRIMS NORMAL VEHICLE RUNS GOOD AT THIS TIME CHECK TSBS FOUND AND	VEHICLE HAS STALLED 4 TIMES, VEHICLE CRANKS NO START, AFTER SEVERAL TIMES VEHICLE WILL START, AC WA
& REPLACE DPFE SENSOR & IAC VALVE. RETEST CODES P1111. RD.TEST OK.	ENGINE HAS QUIT TWICE WHILE DRIVING
VM DUTY CYCLES,WITH DATALOGGER OK,PERFORM EVAP TEST OK,CK PCM RELAY OK,CK KEYS OK,ROAD TEST,MONITOR RMP PIDS,FOUND RPM DROPS BELOW 600 WOULD DIP DOWN TO 540 RPM,REPLACE THROTTLE BODY,RECHK STAYS ABOV	D21 CUST STATES VEH STALLED OUT & JUST QUIT WHILE DRIVING,HA S HAPPENED 2 TIMES IN LAST 2 WEEKS
	STALLS WHILE DRIVING
	DIAG AFTER START UP AND PUT IN GEAR ENGINE WILL STALL WILL RESTART HAPPENS WARM OR COLD
	VEHICLE STALLS
ONGERIN. ROAD TESTED O.K.	ENGINE WILL DIE AT IDLE AND ALSO ARROUND CORNERS
	GUEST STATES THAT CAR WILL DIE WHEN DRIVING OR WHEN AT A IDL
	GUEST STATES THAT CAR DIED WHEN SITTING AT STOP LIGHT
	CUST STATES THAT THE VEH. JERKS WHEN REV. ENGINE TO 4000RPMS
	CUSTOMER STATES THAT VEHICAL START THEN STALLS
	CUSTOMER STATES VEHICLE STALLS BOP HERE
	CHECK FOR STALLING. CLOSED BY WPI
IAC. REPLACED SAME & RETEST OK.	CUST STATES OUT OUT AT SPEED CK AND REPORT
	CUST STATES WHEN VEHICLE UPSHIFTS STALLS WILL RESTART HAPPENS WHEN ENGINE HOT OR COLD
	CUSTOMER STATES THAT WHILE DRIVING THE ENGINE STALLED AND WOULD NOT RESTART
	CHECK VEHICLE STALLS WHEN COMMING UP A HILL THEN COMming TO A STOPO
	CUSTOMER STAES VEHICLE HAS STALLED TWICE WHILE DRIVING
	CST THAT THE VEHICLE SHUT OFF AT 60 MPH, RE STARTED AND HAS BEEN OK SINCE PLEASE CHECK

2002	13788	611	1FMYU02122KA14353	3.0L	TAD	6	2001	7C05	14N09	D21	4	506357	4000	WHILE DRIVING
2002	13794	611	1FMYU02112KD40402	3.0L	TAD	5	2002	7C05	14N09	D21	0	1780977	0	ACCELERATING
2002	13811	611	1FMYU02112KB98166	3.0L	TAD	11	2001	2.00E+03	9F715	D21	5	2057099	16000	STALLS
2002	13828	611	1FMYU02112KB14495	3.0L	TAD	11	2001	2.00E+02	9A337	D21	6	827994	3000	WHILE DRIVING
2002	13838	611	1FMYU02112KB02950	3.0L	TAD	10	2001	2.00E+03	9F715	D21	6	1766947	6000	STALLS
2002	13840	611	1FMYU02112KA46894	3.0L	TAD	9	2001	1A05	6007	D21	11	2539695	13000	STALLS
2002	13849	611	1FMYU02112KA39092	3.0L	TAD	9	2001	7C05	14N09	D21	7	1069707	12000	WHILE DRIVING
2002	13879	611	1FMYU02112KA09726	3.0L	TAD	8	2001	7C05	14N09	D21	12	2404699	11000	WHILE DRIVING
2002	13899	611	1FMYU02102KD24815	3.0L	TAD	4	2002	2.00E+04	9C815	D21	3	2130287	1000	AT STOP
2002	13899	611	1FMYU02102KD24697	3.0L	TAD	3	2002	7C05	14N09	D21	2	2131577	2000	WHILE DRIVING
2002	13904	611	1FMYU02102KB55044	3.0L	TAD	12	2001	2304	DIAG	D21	3	1514599	1000	WHILE DRIVING
2002	13930	611	1FMYU02102KB51669	3.0L	TAD	11	2001	1H03	9J460	D21	6	2159961	14000	DECELL
2002	13939	611	1FMYU02102KB21501	3.0L	TAD	11	2001	2.00E+03	9F715	D21	5	1941064	20000	STALLS
2002	13945	611	1FMYU02102KB55414	3.0L	TAD	11	2001	2304	12A650	D21	5	1132741	3000	ON HIGHWAY
2002	13975	611	1FMYU02102KA36795	3.0L	TAD	9	2001	2C01	11002	D21	2	408992	1000	AT STOP
2002	13981	611	1FMYU02102KA36418	3.0L	TAD	9	2001	1A09	6007	D21	3	686366	1000	WHILE DRIVING
2002	13984	611	1FMYU02102KA34842	3.0L	TAD	8	2001	2.00E+03	9F715	D21	3	591270	8000	AT STOP
2002	13999	611	1FMYU02102KA34805	3.0L	TAD	9	2001	2.00E+03	9F715	D21	9	1657309	11000	STALLS
2002	14029	611	1FMYU011X2KD61061	3.0L	TAD	6	2002	2304	DIAG	D21	2	2105804	2000	WHILE DRIVING
2002	14039	611	1FMYU011X2KC30078	3.0L	TAD	2	2002	2302	12B679	D21	6	2376788	15000	WHILE DRIVING
2002	14041	611	1FMYU011X2KC29169	3.0L	TAD	2	2002	2304	DIAG	D21	0	884761	0	WHILE DRIVING
2002	14058	611	1FMYU011X2KB66158	3.0L	TAD	1	2002	2.00E+03	9E928	D21	7	2134242	12000	STALLS
2002	14063	611	1FMYU011X2KB65867	3.0L	TAD	12	2001	2F02	9E928	D21	1	612857	0	WHILE DRIVING
2002	14066	611	1FMYU011X2KB62773	3.0L	TAD	12	2001	2.00E+03	9F715	D21	7	2177262	12000	WHILE DRIVING

SSM		VERIFIED, STAR TESTED VEHICLE, PINPOINT TEST, F OUND SSM # 15634 FOR NORMAL DIAGNOSTICS, DID NOT PINPOINT THE CONCERN, REMOVED BATTERY AND BAT TERY TRAY, CHECKED GROUNDS, ALLOK, REMOVED LEFT KICK
TSB		EEC TEST NO CODES FOUND TSB 02 11 6 MONITOR PIDS ON ROADTEST CHECK FUEL PRESSURE CHECK EVAP IAC ECT RPM REPLACE RELAY AS PER TSB AND UPDATE PCM TOLATEST CALIBRATION ROADTEST AND SET IDLE STRATE
STICKING		IDLE AIR VALVE STICKING EEC (QUICK TEST) DIAGNOSIS
REPLACED		REPLACED FUEL LINE REMOVED GAS TANKS MTIMS DUE TO NO SLTS FOR FUEL LINE
REPLACED		HOOKED UP WDS. NO CODES IN SYSTEM. PERFORMED DIAGNOSIS PER H MANUAL COULD NOT PINPOINT CAUSE. STEP1:REPLACE IAC. STEP2:REPROGRAM PCM.
REFLASH		REPROGRAM PCM (59350) 021,42
SSM		EEC TEST KOEO PASS KOEC PASS DCL DISPLAY RECORD MONITOR PIDS PINPOINT TEST SYSTEM FUEL PRESSURE TEST CHECK OASIS REPLACED PCM RELAY AND REPROGRAM PCM AS PER SSM15589 RETEST
TSB		NO DTCS FOLLOW TSB 02 11 06 REPLACE IAC VALVE AND PCM RELAY REPROGRAM PCM
TSB		VERIFIED CONCERN, PERFORM DIAGNOSTICS PER TSB 02 11 6 CHECKED IDLE AIR CONTROL MOTOR, OUT OF SPEC, REPLACED IAC REPLACED THROTTLE BODY, CHECKED PCM CALIBRATION, OK. CHECKED VAPOR MANAGMENT VALVE, OUT
REPLACED		2411 14/099 42 TESTED THE EEC SYSTEM, ALL IP1000, CHECKED IGNITION SYSTEM OK, REPLACED EEC RELAY, AND ADVISED CUSTOMER
TSB		DIAG OK FOU CUTING OUT RAN SSM AND TSB EEC TEST PP TEST COULD NOT VERIFY
TSB		STAR TST NO CODES PER FIELD ENG VALEBEY CHK & ADJ TP & IDLE. SAME. CHK OASIS PER TSB 2 11 6, REPROGRAMMED PCM. CHK EVAP, ALL CONNECTIONS, GROUNDS, ALL OK. CHECKED EEC RELAY OK. CHECKED & REPLACED
REPLACED		DOES NOT OPERATE PROPERLY DIAGNOSE, REPLACE IAC VALVE, AND REPROGRAM PCM 021 42
SSM		DIAGNOSE CONCERN PINPOINT TEST SSM 15589 REPROGRAM PC M AND RECHECK OKAY
REPLACED		ASSEMBLY REPLACE ENGINE ASSEMBLY TRANSFER PARTS AS NEEDED
REPLACED		ENGINE STALLED WHILE DRIVING REPLACED ENGINE ASSY (LONG BLOCK)
REPLACED		IAC VALVE STICKING VALVE ASSEMBLY (IDLE AIR CONTROL) IAC REPLACE
TSB		EEC TESTED, PASS, ROAD TESTED RPM SPIKE TO 3000RPM. RUN PINPOIN TESTING. PASE_ACCESS PIDS,PER TSB 02 11 06,RUN IAC OKAY, ECT OKAY, EVAPVM & FTP ALL WORKING PROPERLY UPDATE PCM TO NEW CALIBRATION. ROAD
TSB		CHECK OUT AND HOOKED UP NGS,NO CODES,RAN KOEO AND KOER,PASS,MONITORED PIDS,OKAY,WENT THROUGH TSB 02 11 6,TEST DROVE,NO PROBLEM FOUND
REPLACED		15991 42 NGS QUICK TESTS, N KOEO PASS, KOEC PASS. WONT STAY RUNNING TO PERFORM KOER TESTS. PID DATA IS OK, FUEL PRESSURE TESTS PASSED, IGNITION DIAG. OK. NGS RECORDER MONITOR, PINPOINT TESTS, REPLA
DIAG		NGS DIAGNOSIS AND PINPOINT PER SYMPTOM. ROAD TESTED WITH NGS MONITOR RECORDER FOR PID DATA APPROX. 20 MILES. ALL PIDS ARE
TSB		IGN TEST 12.6VOLTS, NGS EEC TEST CODE P1000, PID DISPLAY MONITOR IAC AND RPM, REPLACED IAC MOTOR, REPLACED THROTTLE BODY PER TSB 080806, RESET BASE IDLE TO FORD RECOMMENED SPEED TEST DROVE 13 MILES AL
SSM		EEC TEST P1111 PINPOINT TEST,CHECK FOR VACUUM L EAKS OK,IGNITION SYSTEM OK,ROAD TEST WITH NGS MONITER. FOUND IDLE AIR CONTROL VALVE READING A T 62% FUEL TRIM OK. RESET HARDSTOPS TO 32% IAC ROAD TEST
NO TEXT		

PANEL AND INSPECTED FOUND EEC POWER RELAY FAULTY, R&R RELAY ALL OK	ENG STALLED WHEN DRIVING STEADY SPEED 30 MPH 15 MIN AFTER AM START RESTARTED AFTER SHORT WAIT
BY	CHECK VEHICLE FOR SHUTTING OFF WHEN ACCELERATING UP AN INCLINE
	CUST STATES VEHICLE STALLS ON START UP
	TOWED IN ROADSIDE NO START ADVISE DIED OUT WHILE DRIVING CHECK FOR A GAS LEAK
	CUSTOMER STATES THE MOTOR WONT STAY RUNNING AND THE CHECK ENGINE LIGHT IS ON WAS HARD TO RESTART DIAG AND REPAIR
	CHECK ENGINE STALLED OUT ONCE IDLED ROUGH
	CK FOR ENGINE SURGES WHEN DRIVING AND STALLS AT TIMES ONLY HAPPENS ABOUT ONCE A WEEK ONLY DIES AT STOPS NOT AFFECTED BY ENGINE TEMP
	PLEASE CHECK FOR STALLING AT TIMES SHUTOFF WHILE DRIVING AND WHILE STOPPED
OF SPEC, REPLACED VALVE	CUSTOMER STATES THAT THE VEHICLE STALLS OUT AT STOPS SEEMS TO PULL TO LEFT THEN DIE OUT
	D21 CUSTOMER STATES THAT THE ENGINE STALLS WHILE DRIVING WHEN HITTING BUMPS AT TIMES
	CUST ST WHILE DRIVING VEHICLE CUT OUT ONCE
DPFE SENSOR. ROAD TESTED OK. MT NO LOPS.	REPAIR ENG OP, STALLS ON DECEL AT TIMES
	C S VEHICLE STALLS
	STALLED ON HIGHWAY TOWED IN
	CUST REPORTS THAT THE VEHICLE STALLED WHEN COMING TO A STOP AND WOULD NOT RESTART NO CRANK START
	ENGINE STALLED WHILE DRIVING,WOULDNT RESTART, & ENGINE MAKES VERY LOUD KNOCKING NOISE N11 CODE
	CUSTOMER STATES THAT VEHICLE STALLING AT STOPS
TESTED APPROX 20 MILES	CUST.STATES VEH.STALLS AT TIMES
	DIED WHILE DRIVING WOULD NOT RESTART WAS DRIVING 10 15 MIN
CED MAF SENSOR AND RETEST. ALL PASS CODES.	THEY WERE DRIVEING AND IT CUT OFF
	D21 ENGINE DIES WHILE DRIVING INTERMITTENTLY.
L OK	CUSTOMER STATES ENGINE STALLED IN REVERSE WHILE BACKING UP.RESTARTED AFTER TRYING 2 TIMES.SEE HISTORY.
PASS	CS ON 4 TIMES ENGINE DIED OUT WHILE DRIVING (COASTING)
	CK/ADV VEHICLE STALLING WHILE DRIVING AT STOP/INTERM. 80

2002	14697	S11	1FMYU011X2KB54858	3.0L	TALD	12	2001	2.00E+03	9F715	D21	6	1770885	6000	AT STOP
2002	14679	S11	1FMYU011X2KB20668	3.0L	TALD	11	2001	2G04	12A650	D21	3	782102	6000	STALLS
2002	14694	S11	1FMYU011X2KB13942	3.0L	TALD	10	2001	7C05	14N069	D21	2	499126	6000	WHILE DRIVING
2002	14686	S11	1FMYU011X2KB13942	3.0L	TALD	10	2001	2G04	DIAG	D21	2	511008	1000	AT STOP
2002	14702	S11	1FMYU011X2KA62920	3.0L	TALD	10	2001	2G04	DIAG	D21	4	1430757	16000	WHILE DRIVING
2002	14703	S11	1FMYU011X2KA62920	3.0L	TALD	10	2001	2.00E+03	9F715	D21	6	1949992	27000	STALLS
2002	14704	S11	1FMYU011X2KA62920	3.0L	TALD	10	2001	2G01	12A650	D21	2	800366	5000	WHILE DRIVING
2002	14706	S11	1FMYU011X2KA62920	3.0L	TALD	10	2001	2G02	12B579	D21	2	948104	5000	AT STOP
2002	14717	S11	1FMYU011X2KA78951	3.0L	TALD	10	2001	2G05	RECAL	D21	10	2186965	9000	WHILE DRIVING
2002	14721	S11	1FMYU011X2KA69456	3.0L	TALD	10	2001	2.00E+03	9F715	D21	4	788418	6000	STALLS
2002	14722	S11	1FMYU011X2KA69456	3.0L	TALD	10	2001	2G04	DIAG	D21	4	717480	6000	WHILE DRIVING
2002	14736	S11	1FMYU011X2KA62703	3.0L	TALD	9	2001	2G04	DIAG	D21	6	912841	8000	COASTING
2002	14754	S11	1FMYU011X2KA96804	3.0L	TALD	8	2001	1H03	8J460	D21	10	1837678	10000	STALLS
2002	14765	S11	1FMYU011X2KA94891	3.0L	TALD	8	2001	2.00E+03	9F715	D21	7	1045180	18000	AT IDLE
2002	14776	S11	1FMYU011X2KA19818	3.0L	TALD	8	2001	7V01	12A591	D21	1	232156	0	WHILE DRIVING
2002	14784	S11	1FMYU011X2KA17360	3.0L	TALD	8	2001	2G06	RECAL	D21	6	912915	8000	AT STOP
2002	14672	S11	1FMYU01192KB76039	3.0L	TALD	12	2001	2.00E+03	9F715	D21	6	2084356	12000	AT STOP
2002	14674	S11	1FMYU01192KB66935	3.0L	TALD	12	2001	2.00E+03	9F715	D21	7	2125769	9000	WHILE DRIVING
2002	14675	S11	1FMYU01192KB66871	3.0L	TALD	12	2001	2.00E+03	9F715	D21	6	1869917	5000	WHILE DRIVING
2002	14676	S11	1FMYU01192KB65692	3.0L	TALD	12	2001	2G04	12A650	D21	4	1026528	3000	WHILE DRIVING
2002	14697	S11	1FMYU01192KB21970	3.0L	TALD	11	2001	7C05	14N069	D21	9	2201661	15000	DOWNHILL
2002	14698	S11	1FMYU01192KB21367	3.0L	TALD	11	2001	2G05	RECAL	D21	7	1458632	13000	WHILE DRIVING
2002	14661	S11	1FMYU01192KA44610	3.0L	TALD	8	2001	7C05	14N069	D21	12	2256262	20000	WHILE DRIVING
2002	14660	S11	1FMYU01192KA35608	3.0L	TALD	8	2001	2G02	98869	D21	7	1049783	6000	AT STOP

TSB		IAC DUTY CYCLE INCORRECT. EEC TEST. RET CODES PASS KOEO PASS KOER PASS. PERFORM TSB 02 11 6 PID MONITOR AND RECORD IAC. REPLACE IAC VALVE. REPROGRAM PCM W WDS. PID DATA MONITOR AND RECORD EVAPUM AND F
SSM		SSM TEST DRIVE FOR CONDITION TEST FOR CODES NONE UPDATE PCM CALIBRATION PER SSM15555 RETEST ROAD TEST OK MILES OUT 5552
NPF		OK M TIME D.C.S.
SSM		KOEO,KOER,KOEOC,P1000, MONITORED PIDS 7 MILES PINPOINT NO FAULTS PRESENT ORDERED PCM RELAY PER SSM CUSTOMER TO RETURN FOR PART. KOEO,KOER,KOEOC,P1000.
DIAG		WDS DIAG RAN OASIS ADVISED CUSTOMER ABOUT KEY W EIGHT HAD CODE P1000 BATTERY
REPLACED		WDS DIAG PIN POINT REPLACED IDLE AIR CONTROL VA LVE
SSM		WDS DIAG PIN POINT REPROGRAMMED PCM PER SSM
HOTLINE		WDS DIAG CALLED HOTLINE PASS CODES UNABLE TO DU PLICATE FIRST TIME OR NOW WAS TOLD TO AGAIN REP LACED PCM AND MASS AIR FLOW SENSOR FOR INTERFER RING OF TWO WAY RADIO OR CELL PHONE ROAD TESTED 25 3
TSB		EXTENSIVE ROAD TEST TIME, FOLLOWED TSB 02 11 06 INSTRUCTIONS, CK EEC SYS, PF TEST, OK WITH NGS, CK FUEL PRESSURE, REPROGRAMMED PCM,RECHECKED ALL TEST, ROAD TEST. ADD TIME FOR DIAG AND INSPECTION
REPLACED		1 1 REPLACED ICV N C
NPF		EEC TEST DCL DISPLAY IGNITION DIAGNOSIS. PINPOINT OK NGS MONITORED ROAD TEST 29 MILES NO DUPLICATION OF
SSM		TEST DROVE COULD NOT EXPERIENCE CONCERN 1496 DIAG. NO CODES PID MONITOR TEST EVERYTHING NORMAL SSM 15555
REPLACED		NGS, PINPOINT, REPLACED DPFE AND EGR AND RETESTED
REPLACED		WDS TEST AND REPLACE IAC VALVE
CLEARED		EEC TEST,NO CODES, DCL CLEARED GROUND 229 UNDER BATTERY CCA2 5554
NPF		5171 12A650,05 WARR TEST DROVE AND UNABLE TO DUPLICATE CONCERN PERFORMED WDS STARTUP,PERFORMED EEC SELF TESTS KOEO PASS KOER PASS COMT PASS PERFORMED DCL DISPLAY AND FOUND ALL SENSORS ARE WITHIN NO
TSB		12557 ROAD TEST AND COULD NOT VERIFY CONCERN. EEC V ON DEMAND SELF TEST PASSED, MONITOR PID DATA, RAN DCL DISPLAY, RAN SCOPE TEST, RAN FUEL PRESS TEST, CHECKED OASIS FOUND TSB# 02 06 06, FOR TH6 CO
REFLASH		STALLS EEC (QUICK TEST) DIAGNOSIS BY TIME TO REPEAT FINAL QUICK TEST VALVE ASSEMBLY IDLE AIR CONTROL REPLACE PINPOINT TEST DIAG RECORDER MONITOR ROAD TEST PCM REPROG
INOP		NOT OPERATING PROPERLY EEC (QUICK TEST) DIAGNOSIS
REFLASH		NGS EEC SELF TEST PASS PASS PASS, ROAD TEST MONITOR COULD NOT DUPLICATE STALL. PINPOINT TEST CHECK EEC POWER RELAY AND TERMINAL CONTACT OK REPROGRAM PCM TO LATEST LEVEL 42 9.0 QC TECH 206
TSB		TEST DROVE AND COULD NOT DUP STALLING, RAN OASIS FOUND TSB 02 11 6, PERFORMED TSB AND REPLACED EEC RELAY AAND REPROGRAMED PCM, TEST DROVE DID NOT STALL
TSB		ROADTESTED COULD NOT VERIFY PROBLEM NGS TESTED CLEAR CODES CHECKED OASIS AND FOUND TSB 02 06 06 AND FOLLOWED STEPS
REPLACED		POWERTRAIN CONTROL MODULE RELAY REPLACE (14N089 12A648 5345 12B577)
REPLACED		WDS TEST, PINPOINT TEST, POWER BALANCE TEST, RELATIVE COMPRESSION TEST, FUEL PRESSURE TEST, RELATIVE INJECTOR FLOW TEST, DCL RECORDER TEST, IGNITION TEST, REPLACED THROTTLE POSITION SENSOR AND RETEST.

TP. OK. CK EEC RELAY OK. ROAD TEST. OK.	ENGINE STALLS AT STOPS FROM TIME TO TIME
	229 CHECK ENGINE LIGHT COMES ON AT TIMES AND ENGINE STALS SEE PAT
	CUSTOMER STATES ENGINE STALLS AT TIMES WHILE DRIVING SLOW SPEEDS WORSE WHEN TURNING
	CUSTOMER STATES VEHICLE STALLS WHEN COMING TO A STOP
	D21 CUSTOMER STATES WHEN DRIVING AT SLOW SPEEDS ENGINE WILL INTERMITTANTLY CUT OUT
	D21 CUSTOMER STATES ENGINE STALLS AS SOON AS GAS PEDAL IS RELEASED
	D21 CUSTOMER STATES CAR CUTS OUT WHILE DRIVING WILL RESTART
MILES REPROGRAMMED PATS KEYS	D21 CUSTOMER STATES ENGINE WILL CUT OUT WHILE DRIVING ALSO ENGINE STALLS WHEN COMING TO STOP
	VEHICLE CUT OFF WHILE DRIVING, VEHICLE RESTARTED BUT MADE LOUD NOISE AND WOULD NOT MOVE AND STEERING WAS HARD TO TURN PER CUSTOMER
	RECHECK DRIVABILITY, MANAGEMENT INVOLVEMENT IS NEEDED TO COMPLETE BEFORE CLOSING OF TICKET
	D21 CUST STS VEH STALL WHILE DRIVING OR WHEN COMMING TO A STOP
	CHECK AND REPORT ON ENGINE STALLS ON DECELERATION CHECK TSB OR SSM
	CUST STATES OIL COMES ON AND CAR WANTS TO KEEP STALLING CHECK AND ADVISE
	OK FOR ENG STALLS AND CUTS OFF AT TIMES WHEN IDLING IN PARK
	D21 CUST STATES ENGINE DIED WHILE DRIVING.
RMAL PERIMETERS PERFORMED FUEL PRESS LEAKDOWN TESTS AND FOUND FUEL PRESS IS OK AND NO LEAKDOWN PRESENT AT THIS TIME FOUND ALL COMPONENTS WORKING AS DESIGNED RAN OBDII AND FOUND	ENGINE WAS TRYING TO DIE AND STOPS YESTERDAY BUT NO LIGHTS CAME ON AND SEEMS TO BE RUNNING BETTER TODAY
NCERN, PERFORMED EVAP. TEST, SYSTEM INTE GRITY TEST, RAN PIN POINT TESTS AND FOUND VMV, AND IAC BOTH ERRATIC, REMOVED AND REPLACED VMV, IAC, REPROGRAMED PCM ALL PER TSB# 02 06 06,ROAD TEST	STAALS ERRATIC AT STOPS WARM ENG
RAMMING TEST	CUST STATES THE VEH STALLS WHILE DRIVING DOWN THE ROAD
	CAR DIES WHILE DRIVING AFTER STARTING AND DRIVING WORSE WHEN IN THE AFTER NOON HOT INTERMITTANT CHK TSB
	CUSTOMER STATES THAT THE TRUCK STALLED ON THE HIGHWAY WHILE DRIVING
	C S INTERMITTANT TRUCK WILL STALL OUT WHILE GOING DOWN HILLS ... TSB?
	VEHICLE KEEPS STALLING OUT WHEN DRIVING ABLE TO RESTART RIGHT AWAY. INTERMIT PROBLEM
	CUSTOMER STATES WHILE DRIVING VEHICLE KEEPS DYING, INTERMITTENLY.
	HESITATES ON ACCEL FROM A STOP

2002	14999	S11	1FMYU01192KA26016	3.0L	TALD	6	2001	2G04	12A650	D21	11	1769665	16000	STALLS
2002	15008	S11	1FMYU01192KA08048	3.0L	TALD	6	2001	7C05	14N069	D21	6	1641337	20000	WHILE DRIVING
2002	15019	S11	1FMYU01182KD59092	3.0L	TALD	6	2002	2G04	12A650	D21	0	1990740	0	STALLS
2002	15029	S11	1FMYU01182KC61278	3.0L	TALD	2	2002	7C05	14N069	D21	9	1769897	2000	STALLS
2002	15030	S11	1FMYU01182KC49275	3.0L	TALD	2	2002	2.00E+03	9F715	D21	4	2066748	2000	WHILE DRIVING
2002	15047	S11	1FMYU01182KB99221	3.0L	TALD	1	2002	2.00E+03	9F715	D21	5	1597220	3000	TURNING
2002	15060	S11	1FMYU01182KB94937	3.0L	TALD	12	2001	2G05	RECAL	D21	4	1090363	3000	WHILE DRIVING
2002	15068	S11	1FMYU01182KB94103	3.0L	TALD	12	2001	2.00E+03	9F715	D21	2	669000	1000	COASTING
2002	15100	S11	1FMYU01182KB90674	3.0L	TALD	10	2001	2.00E+03	9F715	D21	8	1772160	16000	NO TEXT
2002	15109	S11	1FMYU01182KA91651	3.0L	TALD	10	2001	2.00E+03	9F715	D21	6	1593657	15000	WHILE DRIVING
2002	15125	S11	1FMYU01189KA84725	3.0L	TALD	10	2001	7B13	14405	D21	4	840120	2000	TURNING
2002	15140	S11	1FMYU01189KA82857	3.0L	TALD	9	2001	1A03	6007	D21	6	1288668	13000	WHILE DRIVING
2002	15153	S11	1FMYU01182KA37525	3.0L	TALD	9	2001	2G04	12A650	D21	9	1659636	18000	AT STOP
2002	15161	S11	1FMYU01182KA35205	3.0L	TALD	9	2001	2.00E+03	9F715	D21	3	461165	6000	HESSBURGE
2002	15198	S11	1FMYU01172KD60520	3.0L	TALD	6	2002	7C05	14N069	D21	1	1857912	0	STALLS
2002	15229	S11	1FMYU01172KB87349	3.0L	TALD	1	2002	7B02	14401	D21	4	1271677	8000	WHILE DRIVING
2002	15240	S11	1FMYU01172KB85659	3.0L	TALD	12	2001	6J09	7B28059	D21	1	556469	0	TP?
2002	15260	S11	1FMYU01172KA85985	3.0L	TALD	10	2001	2G04	12A650	D21	4	902206	20000	COASTING
2002	15288	S11	1FMYU01172KA81042	3.0L	TALD	10	2001	2G04	12A650	D21	8	1663096	21000	AT STOP
2002	15357	S11	1FMYU01169KD59677	3.0L	TALD	4	2002	2.00E+04	9C915	D21	1	1295179	0	AT STOP
2002	15400	S11	1FMYU01169KB64021	3.0L	TALD	12	2001	2G04	12A650	D21	2	1130921	1000	WHILE DRIVING
2002	15409	S11	1FMYU01169KB91810	3.0L	TALD	11	2001	2.00E+03	9F715	D21	8	2083587	12000	WHILE DRIVING
2002	15416	S11	1FMYU01169KB84624	3.0L	TALD	11	2001	1H03	9J450	D21	7	1741418	8000	CUST TEXT

TSB		OBD DIAGNOSIS, FUEL PRESSURE TEST, DCL DISPLAY, IAC ECT AND REPROGRAMMED PCM AS PER TSB 02 11 06
TSB		20515 ROAD TEST DID NOT VERIFY CONCERN RAN OASIS FOUN D TSB FOR THIS CONCERN MONITORED IAC FOUND CLOS E TO SPEC STEP 2 ORDERED THROTTLE BODY FOR TSB TECH 127 TOOK OVER FROM HERE ANOTHER TECH DIAGN
TSB		CHECK TSB 02 11 6,SET UP BASE IDLE AND CHANGE TP VOLTAGE
TSB		RAN EEC TEST, HOOKED UP WDS, MONITORED IAC, EVAPVM, & FTP PIDS. REPLACED EEC RELAY AAND TEST DROVE AS PER TSB
REPLACED		2575 IAC DUTY CYCLE FALLING BELOW SPECS. CC 42 9P715 MIL OFF KOEO PASS KOEC PASS KOER PASS ATTEMPT TO VERIFY COMPLAINT UNABLE TO VERIFY WDS TEST KOEO PASS PASS TEST PID DATA MONITER
DIAG		42 EEC (QUICK TEST) DIAGNOSIS
SSM		EEC TEST PCM CHECK LIST INSP ON PCM OK REPROGRAM PCM PER SSM
REPLACED		1156 STICKING WAR EEC SYSTEM TEST PASS CODES NO DTCS.PINPOINT TEST AS PER SYMTOM FLOW CHARTS,CHECK FUEL PRESSURE 30 PSI OK. TO IGNITION SYSTEM DIAGNOSIS,ALL OK.PERFORM PID MONITOR TEST,REPLACE IDLE
REPLACED		REPLACE THROTTLE VALVE ASY
TSB		15784 CC42 RD TEST VERIFY COND X CK OASIS X REFER TO TSB 0211 6X PERFORM NORMAL DIAG X WDS TEST KOEO PASS CONT PASS KOER PASS X PERFORM FUEL PSI TEST 40 PSI OK X PERFORM PID DATA MONITOR RECORD X M
REPLACED		2713 28 14405 W 2228 RECORDER MONITOR TEST, REPLACE DPFE SENSOR, ROAD TEST, R&R FUEL TANK TO REPAIR INT OPEN CIRCUIT IN HARNESS 14405, CIRCUIT 787 TO FUEL PUMP, ROAD TEST. 1268D9,D61,8002A,14200A.
ENGINE FAILURE		R & I MANIFOLD TO INSP CYLINDERS WITH BORESCOPE REMOVE OIL PAN TO INSP, REPL ENGINE WPI
REFLASH		RAN DIAG REPROGRAMMED PROCESSOR ROADTESTED
REPLACED		6159 VERIFIED HOOKED UP TO WDS EEC TESTED CODE P1504 IAC DUTY CYCLE MALF. REFERRED TO DATALOGGER INSP. SENSORS OPERATION TAPPED ON IAC MOTOR AND ENGINE STARTED RUNNING FINE REPLACED IAC MOT
TSB		21 NSS SETUP NSS SELF TEST KOEO CONT KOER P1000 LET CAR SIT OVERNIGHT AND STARTED IN A.M. WITH NO PROBLEMS OASIS CALL #421 073 261 PERFORMED TSB 02 11 06 ROAD TEST,IN 21,OUT 23 QUALITY CHECK WP
TSB		EEC TEST CODE PASS PERFORM CALL OASIS PERFORM TSB 02 6 6 TO CHECK IAC VALVEAND EVAP AND ALL DUTY CYCLE AND REPROGRAM PCM ROAD TEST 6 MILES RESET PCM AND FOUND ALL SENSORS O.K. ALL DONE WAS TO REPROGR
???		TOWING LEFT OFF OF RO 85462 FOR HADLEY CLAIM
DIAG		C EEC (QUICK TEST) DIAGNOSIS
REFLASH		REPROGRAM PROCESSOR
REPLACED		DIES . EEC TEST DCL DISPLAY MONITOR RECORDER EVAP SYSTEM LEAK TEST HAS VERY SMALL LEAK PINPOINT TEST LEAK REPLACED VAPOR
REFLASH		DOES NOT OPERATE PROPERLY RAN NSS DIAGNOSTICS TEST, PINPOINT. RECALIBRATED PCM
TSB		12247 TECH 677 TEST,SYSTEM PASS,PERFORM TSB 02 11 06,REPLACE IAC VALVE,TEST EVAP SYSTEM,TEST EEC RELAY,UPDAT PCM,ROADTEST MULTIPLE MILE WITH DATA MONITOR OK AT THIS TIME 42
DIAG		EEC (QUICK TEST) DIAGNOSIS

	CUST STATES WHILE STARTING VEHICLE SHUTS OFF.
OBD2 CONCERN. TECH 127 STARTED HERE. REMOVED AND REPLACED EOP THROTTLE BODY PER TSB 02 11 06. REPROGRAMME D PCM PER STEP 2 OF TSB TO LATEST LEVEL CALIBRATION. STEP 4 OF TSB. PERFORMED	CUST STATES THAT WHILE DRIVING THE TRUCK WILL JUST SHUT OFF, IT RE STARTS WITH NO PROBLEM AFTER
	TEST DROVE THIS UNIT TO COMPARE TO A CUSTOMER VEHICLE AND IT SHUT OFF. FSE WAS PRESENT, TOLD TO REPAIR.
	CUSTOMER STATES SLOWED DOWN AND ENGINE DIED, RESTARTED IMMEDIATELY, NO INDICATORS ON
IN NO CONCERNS IDENTIFYED TEST POWER BALLANCE OK KOER PASS CALL CASES FOUND TSB 02 11 06 PREFORM TSB SETP ONE VERIFYED DUTY CYCLE SLOW TO FALL INTO SPECS ,DIPPING INTERM.	D21 INSP ENGINE WILL STALL WHILE DRIVING WILL RE START NO WARNING LIGHTS HAVE BEEN ON
	CUST STATES ENGINE CUST OFF AT 50 MPH, LIKE CUTTING OFF KEY, ABLE TO RESTART, ALSO CUT OFF AT LOW SPEED WHEN TURNING.
	DID IT ONE TIME YESTERDAY WHILE DRIVING 35 MPH THE ENGINE DIED SUDDENLY BUT RESTARTED FINE D21
AIR CONTROL VALVE,LOW PERCENT,ROAD TESTED RETEST EEC SYSTEM.	D21 E KILLS WHEN LETTING OFF THROTTLE
CMNTOR IAC DUTY CYCLEX 45 PERCENT X AS PER PROCEDURE 1 I TSB X RM NEW IAC X REPERFORM PID DATA MONITOR RECORD X IAC AT 38 PERCENT X ECT 180 X OK X GO TO PROCEDURE 2 X REPROGRAM PCM NEW	CUST STS VEHICLE SHUT OFF WHILE DRIVING,RESTARTED AND STALLED
	D21 CUSTOMER STATES ENGINE STALLS WHILE MAKING RIGHT OR LEFT TURNS
	TOW IN DIED OUT WHEN DRIVING, RATTLE NOISE FROM ENGINE
	D21 "CUSTOMER STATES VEHICLE STALLS AT TIMES, NOTICED WHEN COMING TO A STOP, CONDITIONS ARE RANDOM AND HAS NO PATTERN
OR CLEARED CODE AND TEST DROVE TO VERIFY ASM STARTED SEVERAL TIMES AND VERIFIED IDLE IS NOW STABLE	TOW IN IDLE VERY ROUGH, NEAR STALL VEH JERKS WHEN IN GEAR. CUSTOMER STATES HAS HAD DIFFICULTY AT TIMES STARTING.
	D21 CK ENGINE DIES OUT IN COLD START, IDLE SEEM LOW, OWNER STATE
AM PCM TO LATEST CALIBRATION 18.1 ON WDS	AT TIMES W WARM UNDER NORMAL DRIVING CONDITION ENGINE STALL SEE CHARLIE
	COWBOY TOWING, LEFT OFF OF RO#65482.
	STALLS ON DEACCEL
	CUSTOMER STATES VEHICLE STALLS AT STOPS AND WHEN BACKING
	CHECK FOR CAR DIES AT STOPS SOMETIMES
	VEHICLE DIED GOING DOWN THE ROAD, CUSTOMER NOTICED THE TEMP GUAGE HOTTER THAN NORMAL, STARTED BACK RAN ROUGH, DROVE IT IN RUNS BETTER
	D21 CUST STATES WHILE DRIVING THE VEH WILL JUST STALL OUT AND DIE. HAS NO ENGINE LIGHTS OR OTHER WARNINGS, ADVISE
	CUST STS VEHICLE STALLS OUT WHEN STOPPING OR ON ACCEL FROM STOPS

2002	15490	611	1FMYU01162KB13484	3.0L	TAU	10	2001	2304	12A650	D21		9	1068952	12000 AT STOP
2002	15434	611	1FMYU01162KB05515	3.0L	TAU	10	2001	1A03	6007	D21		1	693019	1000 WHILE DRIVING
2002	15442	611	1FMYU01162KA69326	3.0L	TAU	10	2001	1H03	6J460	D21		10	2163101	10000 AT STOP
2002	15446	611	1FMYU01162KA62761	3.0L	TAU	10	2001	2.00E+03	9F715	D21		10	2163180	10000 WHILE DRIVING
2002	15485	611	1FMYU01162KA62662	3.0L	TAU	9	2001	1H03	9A474	D21		9	1788128	25000 AT IDLE .
2002	15478	611	1FMYU01162KA45403	3.0L	TAU	9	2001	2.00E+03	9F715	D21		11	2199145	9000 WHILE DRIVING
2002	15522	611	1FMYU01152KB00411	3.0L	TAU	3	2002	2.00E+03	9F715	D21		2	1578085	3000 WHILE DRIVING
2002	15525	611	1FMYU01162KC72805	3.0L	TAU	3	2002	2.00E+03	9F715	D21		3	1726512	5000 WHILE DRIVING
2002	15569	611	1FMYU01152KB94652	3.0L	TAU	12	2001	2.00E+03	9H307	D21		6	1809922	7000 WHILE DRIVING
2002	15569	611	1FMYU01152KB94734	3.0L	TAU	12	2001	2304	12A650	D21		4	1166451	2000 STALLS
2002	15566	611	1FMYU01152KB43918	3.0L	TAU	11	2001	2.00E+03	9B928	D21		7	1521309	6000 AT STOP
2002	15579	611	1FMYU01152KB34797	3.0L	TAU	11	2001	7C05	14N069	D21		1	680419	0 WHILE DRIVING
2002	15574	611	1FMYU01152KB34234	3.0L	TAU	11	2001	2.00E+03	9B928	D21		7	1811951	19000 WHILE DRIVING
2002	15555	611	1FMYU01152KB03586	3.0L	TAU	11	2001	2.00E+03	9F715	D21		4	1399946	3000 AT IDLE
2002	15556	611	1FMYU01152KA63305	3.0L	TAU	10	2001	1H03	9J460	D21		8	1531817	17000 WHILE DRIVING
2002	15539	611	1FMYU01152KA51771	3.0L	TAU	9	2001	2G05	RECALEM	D21		2	380060	0 STALLS
2002	15550	611	1FMYU01152KA39218	3.0L	TAU	9	2001	2.00E+03	9F715	D21		4	517029	5000 DOWNHILL
2002	15559	611	1FMYU01152KA27678	3.0L	TAU	8	2001	2304	DIAG	D21		6	662712	8000 AT STOP
2002	15560	611	1FMYU01152KA27180	3.0L	TAU	8	2001	2304	12A650	D21		11	2225533	11000 WHILE DRIVING
2002	15562	611	1FMYU01152KA59550	3.0L	TAU	8	2001	1H03	9J460	D21		10	2175182	11000 WHILE DRIVING
2002	15563	611	1FMYU01152KA17089	3.0L	TAU	8	2001	5V08	9A411	D21		2	800135	1600 WHILE DRIVING
2002	15565	611	1FMYU01152KA16700	3.0L	TAU	8	2001	2G02	129679	D21		8	1116525	4000 WHILE DRIVING
2002	15569	611	1FMYU01162KA07267	3.0L	TAU	8	2001	7C05	14N069	D21		8	1460008	10000 NO TEXT
2002	15705	611	1FMYU01142KC77168	3.0L	TAU	3	2002	2.00E+03	9H307	D21		2	1725982	1600 HARD START
2002	15756	611	1FMYU01142KC02553	3.0L	TAU	11	2001	7C05	14N069	D21		1	431410	0 WHILE DRIVING
2002	15769	611	1FMYU01142KA09286	3.0L	TAU	10	2001	2G05	RECALEM	D21		4	899800	7000 WHILE DRIVING

REFLASH		SN 12A650 CODE RECAL..TEST EEC AND RECIEVED PASS KOEOD KOEO KOER..PERFORM EVAP TEST,,PASSED..PERFORM DATALOGGER DISPLAY
ENGINE FAILURE		B DETERMINE ENG COND R AND I ENG ASSEM REPL LONG BLOCK ASSEM EVAC AN THIS IS NOT A NO COST EXCHANGE ENGINE IS BULL OUT PART
REPLACED		STAR TST CODE P0401. PP TST REPL DPFE RETST OK
TSB		545 WARR 42 9F715 9C915 9E526 14N089 PASS CODES P1111 MILES OUT 10696 NGS START UP PID DATA TEST PID MONITOR TEST EVAP TEST NGS ROAD TESTREPLACE THROTTLE BODY AIR VALVE EVAP VALVE PCM RELAY CK ALL GRO
LOOSE HOSE		ROAD TESTED VEH TO VERIFY CUSTOMER CONCERN MIL ON AT TIME KOEO,ER,P0139,P0158 MILEAGE IN 35,863 OUT 35,867 PERFORMED EEC TEST MONITOR ROAD TEST BOTH BANKS LEAN RESEOUR VAQUUM TUBE AND REINFORCED WITH
TSB		PERFORMED DIAGNOSTIC TEST AND REPLACED IAC & THROTTLE BODY AS PER TSB 02 11 06UNO CODES PRESENT
TSB		CK, AND DIAG REPLACE ISC AS PER TSB 02 11 06
REPLACED		PERFORMED EEC TEST, DCL DISPLAY, PINPOINT TEST, AND REPLACED IAC. RETESTED OK
REPLACED		VERIFY NGS TEST MONITOR PIDS TEST FUEL PRESSURE TEST REPLACE FUEL PUMP RETEST OK
SSM		EEC TEST WDS SYS PASS NO CODES PINPOINT TEST INTERMIT DIP FOR STALL CHECK OASS REPROGRAMMED PCM PER SSM 15569
TSB		6520 USE WDS,NO CODES,CK OASS,TSB 02 11006 ORDER PARTS FOR TSB INSTALL THROTTLE BODY AND IAC VALVE,USE WDS UPDATE PCM 2L8A 12A650 AD, ROAD TEST OK
REPLACED		PERFORM EEC TEST KOEO PASS KOER PASS,RUN OASS FOR SYMPTOM,REPLACE PCM RELAY PER SPECIAL SERVICE MESSAGE,CK,PCM GROUNDS
REPLACED		OBD II DIAG PASS,FUEL PRESS TEST 45 LBS,DCL IAC 44%,IAC VALVE REPLACED 44%,T BODY REPLACED,RETEST IAC 39%
STICKING		STICKING EEC (QUICK TEST) DIAGNOSIS
REPLACED		PREFORM EEC TEST WAS NO CODES PREFORM PINPOINT TEST AND NGS ROAD TEST REPLACE PFE SENSOR WAS OUT OF RANGE
REFLASH		REPROGRAM PCM EEC TEST NO CODES CHECK AND REPROGRAM PCM ROAD TEST PREVIOUS MILES RECORDED IN CORRECTLY, SHOULD HAVE BEEN 538 MILES NOT 5388.
REPLACED		5301 ROAD TEST,KOEO TEST,KOER TEST,DCL DISPLAY FUEL PRES,AND LEAKDOWN TEST,INJECTOR FLOW TEST IGNITION SYSTEM DIAG.,PINPOINT TEST,REPLACE EEC RELAY AND REPLACE IAC VALVE PER SERVICE MESSAGE,RETEST
SSM		6235 PCM REPROGRAM WR ROAD TESTED AND VERIFIED CONCERN. PERFORMED WDS DIAG. 15660E,E1,E1X1,E2,E5,E10,E20,E24,E30. ALL TEST'S PASS, OK. PERFORMED PCM REPROGRAM 15660EA. AS PER SSM15569. RETESTED AND
TSB		EEC TEST CK FUEL PRESSURE PERFORM TSB 02 11 06 REPROGRAM PCM
REFLASH		WDS TEST, REPLACED DPFE SENSOR AND REPROGRAMMED PCM
NPF		EEC TEST TEST DROVE NO CODES FOUND VACUUM LINE LOOSE TIGHTENED RETESTED NPF
HOTLINE		1 NGS TEST, NO CODES, CALL HOTLINE, PID DATA TEST, IAC 41%, R&R IGNITION SWX TO INSPECT PINS, CLEAN GROUND G100, G101,
REPLACED		RAN ON WDS NO CODES PASSED KOEO,KOER,DATA LOGGER LOOKS GREAT REPROGRAMED PCM AN REPLACED EEC RELAY PER SERVICE MESSAGE
REPLACED		NKOEO PASS, KEOC PASS, KOER PASS, PIN POINT TEST, DCL REPALCE FULE PUMP
SSM		ROAD TESTED,COULD NOT DUPLICATE THIS CONCERN AT THIS TIME. PERFORMED EEC TEST,SYSTEM PASSED,FORD HAS A BULLETIN FOR A
SSM		7079 PROGRAM NGS TEST AND PIN POINT TEST KOEO,KOER,KOEO PASS FUEL SYSTEMS TEST ALL OK,IGNITION SYSTEMS TEST ALL OK,MONITOR DCL DATA DISPLAY AND FOUND ALL SYSTEMS TO OPERATE NORMALLY AT THIS TIME,

	CUSTOMER SAYS THAT CAR STALLS OUT WHEN COMING TO A STOP INTER HOT ENGINE
NUMBER IS 19752AB	CAR DIED WHILE DRIVING OIL LITE CAME ON
	STALLS OUT AT STOPS (AFTER USING POWERPOINT)
UND CONN PER TSB 021106 V6 ENG	VEHICLE JUST CUT OFF ON CUSTOMER WHILE DRIVING CUSTOMER HAD BEEN DRIVING AWHILE
STRAP TIE TO CORRECT CONCER	CUSTOMER STATES WHEN STARTED UP WILL STUMBLE THEN DIE OUT CUSTOMER HAS NOTICED ENGINE LIGHT ON WILL HAPPEN HOT OR COLD
	CUSTOMER STATES WHILE DRIVING THE TRUCK STALLED AND WOULD NOT START AFTER IT SAT FOR A WHILE IT STARTED OK AND DROVE
	CUST STATES STATES WHILE DRIVING CAR TURNED OFF
	STALLS OUT WHILE DRIVING STARTS RIGHT UP AGAIN
	CUST STATES THAT VEH STALLS WHILE DRIVING
	VEHICLE DIED, WAITED 10 MINS STARTED BACK UP, HAPPENED LAST TUE, HAS NOT HAPPENED SINCE
	CUSTOMER STATES THAT YESTERDAY THE VEHICLE STALLED WHILE AT A LIGHT
	CUSTOMER STATES WHILE DRIVING THE VEHICLE SHUT OFF AND AFTER ROLLING TO A STOP CRANKED BACK UP
	CUST STATES, ENGINE STALLS WHILE DRIVING, ESPECIALLY WHEN MAKING TURNS
	CUST STATES AT IDLE ENGINE RPM DROPS LIKE VEH TO STALL
	VEHICLE CUTS OUT WHILE DRIVING
	NO PS DIED AND ALL LIGHTS CAME ON TOW ON ROAD SIDE
TECH 136--42--9F718 KOED,KOER,DONT PASS Q.C. BY 136	D21 CUSTOMER STATES WHEN GOING OVER A HILL (OVERPASS) AND LETTING FOOT OFF GAS, ENGINE WILL STALL OUT (PROBLEM IS INTERMITTANT)ADVISE MR GUCKLE TO RIDE W CUST
PASS.	(D21)CK. ENGINE DIES OUT WHEN COMES TO A STOP,WILL RESTART RIGHT UP.
	C S THE TRUCK STALLS WHEN DRIVING. STARTS BACK UP OK BESIDES ONE TIME.
	C S ENGINE STALLS AND DIES WHILE DRIVING AT40 AND 60 MPH
	CUT OFF WHILE DRIVING
	CUST STATES VEHICLE SHUT OFF WHILE DRIVING, RESTARTED
	CUSTOMER STATES THAT AT TIMES ENGINE IS HARD TO START HAS TO CYCLE KEY SEVERAL TIMES TO START
	KILLS WHILE DRIVING
CONTACT OASIS AND FOUND SSM TO RE PROGRAM PCM FOR CONCERN,RE PROGRAM AND ROAD TEST AND RETEST OK. ""QUALITY CONTROPL,S.S.""	CHECK ENGINE LIGHT ON STALLS WHILE DRIVING

2002	15786	S11	1FMYU01142KA80228	3.0L	TALD	10	2001	2G05	RECAL	D21	5	692278	4000	STALLS
2002	15787	S11	1FMYU01142KA80228	3.0L	TALD	10	2001	2.00E+03	9F715	D21	6	1088225	6000	STALLS
2002	15814	S11	1FMYU01142KA46122	3.0L	TALD	9	2001	1H03	8D475	D21	2	400467	2000	AT STOP
2002	15828	S11	1FMYU01142KA38199	3.0L	TALD	9	2001	2B02	12D69	D21	2	345818	1000	WHILE BRAKING
2002	15836	S11	1FMYU01142KA55980	3.0L	TALD	8	2001	2.00E+03	9F715	D21	5	1437660	8000	DECELL
2002	15875	S11	1FMYU01142KA06157	3.0L	TALD	7	2001	7C05	14N089	D21	7	1449583	15000	STALLS
2002	15886	S11	1FMYU01132KC61785	3.0L	TALD	3	2002	2.00E+03	9F715	D21	1	1086998	0	STALLS
2002	15887	S11	1FMYU01132KC61785	3.0L	TALD	3	2002	1A04	9424	D21	2	1162907	4000	AT STOP
2002	15935	S11	1FMYU01132KB99606	3.0L	TALD	12	2001	2.00E+03	9F715	D21	6	2056624	7000	STALLS
2002	15938	S11	1FMYU01132KB90894	3.0L	TALD	11	2001	2.00E+03	9F715	D21	7	1573000	9000	WHILE DRIVING
2002	15950	S11	1FMYU01132KB14490	3.0L	TALD	10	2001	1H08	8J460	D21	6	1149491	4000	WHILE DRIVING
2002	15958	S11	1FMYU01132KB09541	3.0L	TALD	10	2001	2G01	12A650	D21	3	859941	5000	WHILE DRIVING
2002	15959	S11	1FMYU01132KB09541	3.0L	TALD	10	2001	2G04	12A650	D21	3	702956	3000	WHILE DRIVING
2002	15962	S11	1FMYU01132KA95414	3.0L	TALD	10	2001	2.00E+03	9F715	D21	10	2418825	21000	WON'T IDLE
2002	15963	S11	1FMYU01132KA95347	3.0L	TALD	10	2001	2G05	RECAL	D21	7	1336574	17000	STALLS
2002	15977	S11	1FMYU01132KA70092	3.0L	TALD	10	2001	2G04	DIAG	D21	1	243137	0	AT STOP
2002	16009	S11	1FMYU01132KA40691	3.0L	TALD	9	2001	2G04	12A650	D21	10	2039140	13000	WHILE DRIVING
2002	16066	S11	1FMYU01122KC84599	3.0L	TALD	3	2002	2.00E+03	9E928	D21	3	1582121	1000	AT STOP
2002	16129	S11	1FMYU01122KB16616	3.0L	TALD	11	2001	7C05	14N089	D21	3	586031	1000	STALLS
2002	16134	S11	1FMYU01122KB11957	3.0L	TALD	10	2001	2G02	9G444	D21	6	1668100	6000	NO TEXT
2002	16145	S11	1FMYU01122KB00599	3.0L	TALD	10	2001	2.00E+03	9F715	D21	9	1953530	15000	WON'T RUN
2002	16160	S11	1FMYU01122KA95398	3.0L	TALD	10	2001	2G04	12A650	D21	10	2295470	12000	WHILE DRIVING
2002	16161	S11	1FMYU01122KA95257	3.0L	TALD	10	2001	2G05	RECALEM	D21	5	839691	16000	WHILE DRIVING
2002	16167	S11	1FMYU01122KA83478	3.0L	TALD	10	2001	2.00E+03	9F715	D21	3	657967	4000	AT IDLE
2002	16177	S11	1FMYU01122KA64046	3.0L	TALD	9	2001	2.00E+04	8C815	D21	4	894734	14000	MIL
2002	16203	S11	1FMYU01122KA39813	3.0L	TALD	8	2001	2G04	12A650	D21	8	1237995	4000	WHILE DRIVING

REFLASH		EEC TEST NO DCTS FUEL PRESSURE TEST OK,NGS RECORDER CHECK PIP OK ROAD TEST OPERATING NORMALLY AT THIS TIME CONTACT HOTLINE REPROGRAM PCM AS PER HOTLINE CONTACT 2A98009 CHECK IAC AND PCM RELAY AS PER
HOTLINE		CCR2. EEC TESTS NO DCTS. FUEL PRESSURE TESTS,WITHIN FORD SPECS. CONTACT HOTLINE # 2A98009. INSPECT CONNECTORS,270,PINS B C AND D.OK.CONNECTORS C110,C133,OK.CHECK GROUNDS 300 160 104 105 AND 101 OK,RE
REPLACED		ROADTEST VEHICLE TO VERIFY CONCERN, NECESSARY TO PERFORM WDS DIAGNOSIS, REPLACED EGR VALVE AND RETEST.
REPLACED		PERFOR WDS TEST CODE P0304. MISFIRE ON NUMBER 4 CYLINDER. REPLACE NUMBER 4 COIL AND RETEST
TSB		REPROGRAM PCM PER TSB 020003
DIAG		C EEC (QUICK TEST) DIAGNOSIS
REPLACED		DIAGNOSE VEH FOR STALLING PROBLEM. SPEND TIME ONLINE WITH TECH LINE. TECH LINE SAID REPLACE PCM RELAY. ORDER IAC VALVE AND GASKET PER TECH LINE
VACUUM LEAK		FOUND LEAK AT THE INTAKE, REPAIR LEAK AND ROAD TESTED VEH. OKAY AT THIS TIME
DIAG		EEC & PIM POINT TEST
TSB		RAN ON WDS KOEO, KOER, NO CODES, RAN OASIS, PERFORMED TSB 02 11 6, RAN DATA LOGGER, IAC AT 46.8 REPL IAC VALVE AND
REPLACED		DPFE INOP EEC DIAGNOSIS,REPLACED DPFE SENSOR,EEC REALY AND PROGRAM PCM
SSM		5430 TEST DRIVE,RUN EEC TEST,BYPASS,CHECK OASIS PERFORM SSM 16599,REPLACE PCM AND REPROGRAM. TEST DRIVE,RERUN TEST,OK
REFLASH		3040 UNABLE TO DUPLICATE CONCERN PERFORMED SS 16599 RAN WDS KOEO KOER PASSED RAN OASIS MESSAGES PERFORMED SPEACIAL SERVICE MESSAGE 16599 HAD TO REPROGRAM PCM EEC RELEAY AND EVAP SYSTEM OK TEST DROV
DIAG		42 EEC (QUICK TEST) DIAGNOSIS
TSB		PROFORMED TSB 02 08 06 REPROGRAM PCM ADJ. CURB IDLE ROAD TEST AFTER REPAIR OK
NPF		120 DIAG. 08 W CHECK PERFORM 16599E,E1,E5,E10,E20,E24,E30,E1X1 ROAD TEST VECH FOR SOME MILES VECH RUNS OK CHECK SERVICE ADVISOR ROAD TESTED VEOH VECH NEVER STALLED UNABLE TO DUPLICATE CONCERN AT THI
SSM		13798 VERIFIED THE CONCERN AND CONNECTED WDS TO CHECK FOR CODES, PASSED TESTS, I CHECKED THE PIDS FOR ANY ABNORMAL READINGS AND ALL WERE OK. DID TRY TO GET ON OASIS, SERVER WAS DOWN, DID KNOW OF AN
DIAG		IAC VALVE AND T BODY EEC (QUICK TEST) DIAGNOSIS
REPLACED		EEC TEST AND N96 DIAG AND REPAIRED WIRING AND REPLACED RELAY AND RETEST
REPLACED		REPLACED HEGO SENSOR
REPLACED		WDS DIAG PINPOINT TESTS REPLACE IAC
TSB		PERFORMED EEC TEST NO CODES PRESENT, ROAD TESTED 7 MILES MONITORED PIDS NORMAL, PER TSB 02 11 06 MONITORED IAC 37.2% OK, VERIFIED PCM MPC# MPC101. REPROGRAMMED PCM & MONITORED EVAPVM & FTP PASS
TSB		16599 VEHICLE INTERM, STALLS. OK EEC FOR CODES. NONE RECEIVED. CALLED OASIS FOR PCMS. SSM OR TSB. FOUND SSM LISTING REVISED PCM CALIBRATION TO CORRECT STALL COND. REPROGRAMMED PCM WITH WDS. RETEST
REPLACED		IAC VALVE STAR TEST REPLACED IAC VALVE CLEAR CODES ROAD TEST & RETEST
REPLACED		CHECK EEC, REPALCE VAPOR MANAGEMENT VALVE
HOTLINE		4570 REFLASH PCM & ADJ. IDLE 08 W CHECK PERFORM EEC TESTS CHECK SYSTEM PASS NO CODES CHECK PERFORM REFLASH & SET IDLE AS PER KNOWN CONCERN ON HOTLINE ASSEMBLE RECHECK O.K. ROAD TEST O.K

SSM 4431 ALL OK	CUST STATES ENGINE STALLED THEN OK OIL LIGHT CAME ON
PLACE MAF SENSOR,IAC VALVE AND THROTTLE BODY AS PER HOTLINE ROAD TEST	D21 CUST STS INTERMIT AT SLOWER SPEEDS VEHICLE WILL STALL OUT WITHOUT WARNING HAPPENED ONCE TODAY
	VEHICLE STALLS OUT AT SLOW STOPS,HARD TO START, AND SERVICE ENGINE LIGHT IS ON,
	VEHICLE STARTS TO STALL WHEN COMMING TO LIGHTS , WHEN ACCELERATING MAKES CLUNKING NOISE, CHECK B49
	STALLS AT IDLE OR WHILE DECELERATING&D21
	CUST STATES VEH IS STALLING
	CUSTOMER STATES ESCAPE KEEPS STALLING
	CUSTOMER STATES WHEN SLOWING DOWN IN VEH TO STOP, MAKE A TURN, ESCAPE STALLS AT ANY GIVEN TIME
	CUST STATES VEH CUTTING OFF
	CUSTOMER STATES VEHICLE DIED WHILE DRIVING PLEASE ADVISE
	VEHICLE STALLED WHILE DRIVING, CUST STATES SHE WAS COASTING AND THE ENGINE CUT OFF AND SHE LOST POWER STEERING BRAKEING POWER BUT RADIO STAYED ON
	CHECK DIES WHEN DRIVING TURN KEY OFF AND RESTART AND IT IS FINE
E AFTER REPROGRAMING PCM OK	CHECK ENGINE DIES CAN BE DRIVING AND ENGINE DIES ALSO RADIO GOES OFF
	CUST STATES ENGINE STALL ON COLD STARTS ADVISE
	CUST STATES CAR STALLS IN AM AND HARD TO START
8 TIME VECH RUNNING OK	(D21)CK. ENGINE WHEN CAME TO A STOP,DIED OUT,RESTARTED RIGHT AWAY.
SSM FOR THIS CONCERN, REMOVED THE BATTERY A ND TRAY, REPOSITIONED THE GROUND WIRE UNDER THE TRAY, CHECKED THE RELAY AND VERIFIED THAT WAS A U.S. PART AND NOT CANADIAN RELAY, REPRO GRAMMED	(TOW IN) CUST STATES THAT THE VEH DIED WHILE DRIVING AND THE VEH WOULD RESTART
	CUSTOMER STATES WHEN COMING TO A STOP THE ENGINE WELL CUT OFF
	ENGINE STALLS
	CUST STAES VEH WILL NOT STAY RUNNING
	CUSTOMER RPTS CAR STALLS AT TIMES WHILE DRIVING HAPPENS HOT OR COLD AND CAR RESTARTS RIGHT AWAY OK AND RPT
, O.K.	CUSTOMER STATES STALLED DRIVING SLOWLY
	ACCELERATOR PEDAL STICKS AT TIMES,TRIES TO STALL WHEN AT IDLE AT TIMES...CHECK AND ADVISE
	CUSTOMER STATES CHECK ENGINE LIGHT STAYS ON CC B29
	D21 CUSTOMER STATES SOMETIMES ENGINE STALLS WHEN DRIVING, ERRATIC, RESTARTS IMMEDIATELLY.

2002	16204	S11	1FMYU01122KA29813	3.0L	TALD	8	2001	2902	128579	D21	3	383871	1000	WHILE DRIVING
2002	16213	S11	1FMYU01122KA09164	3.0L	TALD	8	2001	2B01	8C315	D21	0	255868	0	STALLS
2002	16221	S11	1FMYU01122KA06898	3.0L	TALD	6	2001	2B04	12A660	D21	5	665597	6000	WHILE DRIVING
2002	16222	S11	1FMYU01122KA06898	3.0L	TALD	8	2001	7C05	14A089	D21	4	508898	5000	WHILE DRIVING
2002	16230	S11	1FMYU01112KD99016	3.0L	TALD	8	2002	2.00E+04	8C915	D21	1	2174332	0	WHILE DRIVING
2002	16237	S11	1FMYU01112KD23829	3.0L	TALD	4	2002	1H03	9J460	D21	1	1384134	0	STALLS
2002	16245	S11	1FMYU01112KD01489	3.0L	TALD	3	2002	2.00E+03	9F715	D21	0	1176090	0	WHILE DRIVING
2002	16266	S11	1FMYU01112KC38579	3.0L	TALD	2	2002	2.00E+03	9F715	D21	0	741736	0	WON'T RUN
2002	16279	S11	1FMYU01112KC15467	3.0L	TALD	2	2002	2D03	12236	D21	0	734948	0	STALLS
2002	16303	S11	1FMYU01112KB99034	3.0L	TALD	12	2001	2B05	RECAL	D21	1	691853	0	WHILE DRIVING
2002	16306	S11	1FMYU01112KB95783	3.0L	TALD	12	2001	1A03	8007	D21	2	1118139	4000	WHILE DRIVING
2002	16307	S11	1FMYU01112KB95783	3.0L	TALD	12	2001	2B04	12A660	D21	2	1055241	4000	WHILE DRIVING
2002	16308	S11	1FMYU01112KB95783	3.0L	TALD	12	2001	7V01	12A581	D21	2	1152366	4000	WHILE DRIVING
2002	16320	S11	1FMYU01112KB23699	3.0L	TALD	11	2001	7C05	14A089	D21	1	419570	4000	TURNING
2002	16326	S11	1FMYU01112KB21394	3.0L	TALD	11	2001	2.00E+03	9F715	D21	8	1670624	17000	COASTING
2002	16338	S11	1FMYU01112KB12498	3.0L	TALD	11	2001	7B02	10346	D21	8	1921718	18000	STALLS
2002	16339	S11	1FMYU01112KB08765	3.0L	TALD	10	2001	2B04	13A659	D21	10	2458272	8000	WHILE BRAKING
2002	16340	S11	1FMYU01112KB02909	3.0L	TALD	11	2001	7A01	40	D21	4	1864841	4000	AT IDLE
2002	16342	S11	1FMYU01112KB03937	3.0L	TALD	11	2001	2.00E+03	08928	D21	7	1823471	11000	TURNING
2002	16356	S11	1FMYU01112KB00545	3.0L	TALD	10	2001	2.00E+03	9F715	D21	4	687102	8000	COASTING
2002	16394	S11	1FMYU01112KA45795	3.0L	TALD	9	2001	1A03	8007	D21	1	391622	1000	NO TEXT
2002	16396	S11	1FMYU01112KA45795	3.0L	TALD	9	2001	1A03	8007	D21	1	319747	1000	WHILE DRIVING
2002	16401	S11	1FMYU01112KA40185	3.0L	TALD	9	2001	2.00E+03	9F715	D21	7	1294836	8000	AT STOP
2002	16429	S11	1FMYU01112KA29477	3.0L	TALD	8	2001	2B04	DIAG *	D21	10	2379804	13000	WHILE DRIVING
2002	16451	S11	1FMYU01112KA25958	3.0L	TALD	8	2001	2.00E+03	9F715	D21	6	870585	4000	AT STOP
2002	16456	S11	1FMYU01112KA09660	3.0L	TALD	8	2001	2B01	12A659	D21	9	1589035	9000	AT STOP

REPLACED		1300 MAF SENSOR IDLE ADJUSTMENT 07 WR 1650E,E1,E1X1,E5,E50,E10,E20,E24 VERIFIED CUSTOMER CONCERN AND FOUND VEHICLE TURNING OFF INTERMINTENT. PERFORMED WDS SYS TEB TB . IGNITION, FUEL TESTS, POWER
REPLACED		CRANKSHAFT POSITION SENSOR INOP PERF.WDS TESTING,REPLACE CRANKSHAFT POSITION SENSOR,REPAIR WIRING
TSB		TSB APPLIES EEC (QUICK TEST) DIAGNOSIS
SSM		FAULTY RELAY PER SSM 15434 EEC (QUICK TEST) DIAGNOSIS
TSB		TEST AND REPLACE EVAP VALVE PER TSB 021106
REPLACED		092 SJ480 28 EEC TEST CONT P0401 KOEO PASS KOER PAS PINPOINT TEST REPLACED DPFE SENSOR 0.1V OUT OF RANGE CLEARED CODES & RETEST P1000 AC VACUUM LEAK TO CONTROL HEAD VACUUM TO EVAP CASE TRACE WHITE
REPLACED		REPLACE IAC SOLENOID REPLACED THROTTLE BODY REPLACE VMV REPLACE POWER RELAY
REPLACED		1 VERIFY STALLS AT IDLE EEC NO DTCS MONITOR PIDS TEST FUEL IGNITION DIAG PASS CK IAC PARAMETER IRATTIC
VACUUM LEAK		12 VACCUMM LEAK DIAG FOR STALLING CODE P0171 DCL DISPLAY AND DCL ROAD TEST TO PINPOINT AND FX VACCUMM LEAK
REFLASH		REPROGRAMED PCM,WAS UNABLE TO VERIFY CONCERN
HOTLINE		VERIFIED CONCERN PERF EEC,FUEL PRESSURE TEST PINPOINT TEST PIDMONITOR,INJECTOR FLOW. CONTACTED HOTLINE
REPLACED		VERIFIED CONCERN PERF EEC,PERF FLOW TEST PID MONITOR , PIN POINT COMPRESSOR TEST NEED TO REPLACE PCM AND CLEAN ANS FOUL
LOOSE GROUND		RELEASED AND REPAIRED AND CLEANED ALL VISABLE GRONDS ARCING AT LEFT SIDE OF DASH.
REPLACED		4919 14N089 28 RUN NSE EEC TESTS KOEO KOER NO CODES REPLACED EEC POWER RELAY AND TIGHTENED PCM GROUND AS PER SPECIAL SERVICE MESSAGE 15434 RETEST ROAD TEST
INOP		NOT WORKING PROPERLY FUEL PUMP PRESSURE TEST ON VEHICLE DIAGNOSIS
REPLACED		12271 VEHICLE WOULD NOT START. TEST BATTERY, GOOD BATTERY BUT NEEDS CHARGED. CHARGED BATTERY. VEHICLE STARTS, BUT VOLTAGE DROPS QUICKLY. LOAD TESTED ALTERNATOR. ALTERNATOR NOT PUTTING OUT SUFFICIEN
TSB		1 REPROGRAMMED PCM PER TSB# 2 11 06 ROADTESTED CAR FIXED X
REPLACED		BAD BATTERY,BAD CELL,ROAD TEST ONLY ONLY DUPLICATED,BATTERY CONCERN. 14.27 CHARGING PASS CHARGING TEST. FAILED ACES CODE HC4SM,12.58 VOLTS LOAD TEST DROP TO 6 VOLTZ,FAILED ACESS,REPLACE BATTERY AND RE
REPLACED		NGS DIAG,REPLACED THROTTLE BODY THAT WAS STICKING REPLACED AIR BY PASS VALVE,RETEST OK
REPLACED		TEST EEC SYSTEM...CODES:....PASS...PASS.... KOER....PASS.....PERFORM DCL TEST.....DCL SHOWS IAC SOLENOID AT 82 PERCENT.....TEST AND REPLACE IAC SOLENOID AND REPROGRAM PCM TO LATEST CALIBRATIO
ENGINE FAILURE		REQUESTING DEALER'S P/A CODE 09554
HOTLINE		ENGINE SEIZED, ORDERED ENGINE, CONTROL #1KPH9009 ELEC STARTER BATT DIAG,ATTEMPT TO TURN ENG W BRKR BAR,R&R SPRKPLGS CK FOR COOLANT NONE,REPLC ENG PER HOTLINE,NEC TO REMOVE TRANS TO CUT FLEX PLATE FRO
REPLACED		0031 EEC TEST,NO CODES. PIN POINT TEST,NESSARY TO REPLACE IDLE AIR CONTROAL VALVE,RETEST. ROAD TEST. VERIFIED REPAIR.
NPF		1 EEC DIAG SYS PASS PPT PER PCED MONITER OBDS PASS IGN ANA UPD N RT 8 MILES NPF
REPLACED		CHECKED FOR ENGINE STALLING FOUND IAC VALVE INOP. REMOVED AND REPLACED IAC VLAVE AS NEEDED DONE TO CORRECT
TSB		ENGINE DIAG TEST PIN POINT AND MONITOR TEST AND REPROGRAMED PCM AND REPLACED EEC RELAY AND REPLACED IAC VALVE PER TSB 02 11 06 RETEST

BALANCE TESTS DATALOGGER INFO CHECKS. FOUND MAF SENSOR OUT OF RANGE AND RPM NOT WITHIN SPECS. R R MAF SENSOR AND PERFORMED ADJUSTED RPM. PERFORMED ADJUSTED TP SENSOR. RECHECKED AND FOUND	(D21)CK. ENGINE STALLS OUT WHILE DRIVING.
	CUSTOMER STATES CHECK ENGINE LIGHT ON AND VEHICLE QUITS ON ROAD
	CUST STATES INT TRUCK STALLS OUT WHILE DRIVING
	CUST STATES INT WHILE DRIVING TRUCK STALLS OUT AND C.E.L. COMES ON
	CHECK VEHICLE STALLED OUT DRIVING ADVISE
VACUUM LINE TO AC CONTROL HEAD INSTRUMENT PANEL ACCESS TO REPAIR VACUUM LINE PINCHED	APPT MADE BY MAREK...ENGINE STALLS ALSO AC WILL NOT BLOW OUT OF VENTS
	D21, PER GUEST ENGINE STALLED WHILE DRIVING. SEE ATTACHED.
	DURING PDI THIS VEHICLE STALLS WILL NOT STAY RUNNING
	CUST STATES CAR STALLING
	C S VEH WAS WARM GOING ABOUT 55MPH AND VEH SHUT OFF BUT RESTARTED FINE CHECK AND ADVISE
	CUST STATES THAT VEHICLE DIES WHILE DRIVING INSPECT
	CUST STATES THAT VEHICLE DIES WHILE DRIVING AT TIMES,HAPPENS AFTER IT HAS BEEN PARK OR SOMETIMES AFTER IT HAS BEEN DRIVEN
	CUST STATES VEHICLE DIES WHILE DRIVING,CUST SAYS AT TIMES BEFORE IT DIES,ENG STUTTERS.THIS HAPPENS AT ANY TIME OF DAY
	ENGINE STALLED WHILE MAKING TURN HAD TO LET SIT FOR ABOUT A HALF HOUR BEFORE IT WOULD RESTART D23
	SHUT OFF ON DECEL TO MAKE A TURN
T VOLTAGE. REPLACED ALTERNATOR. RETEST OK.	VEHICLE LOST ALL POWER AND CUT OFF PER CUSTOMER
	STALLS WHEN COMING TO A STOP EVERYTIME.
TEST.	CUST STATES, ENGINE STALLS WHILE AT IDLE, IT RESTART RIGHT AFTER, AT TIMES BATT HAD TO BE JUMPED, ADVISE
	CUSTOMER STATES ENGINE STALLS WHEN TAKING RIGHT TURNS
N....RETEST EEC SYSTEM.... CODES...PASS...PASS...CC....42	D21 ENG DIES ON DECEL/ TURNING IRRATIC OPP HAPPENS ONCE PER DAY
M OLD ENG UNABLE TO GET TORQUE CONVERTER NUTS LOOSE. REMOVE OLD T CONVERTER AND INSTALL ON NEW ENG,EVAC AND RECLAIM FREON,CK COOLANT AND OIL LEVELS,ROAD TEST OK	C S THAT VEH. DIED WHILE DRIVING & WILL NOT TURN OVER TO STA RT CC D60
	CUTTING OFF WHEN COMING TO STOP OR SLOWING TO GO AROUND A CURVE
	DIAGNOSE AND ADVISE CUSTOMER STATES VEHICLE DIED WHILE DRIVING. INTERMITTENT.D21
	CHECK ENGINE STALLING AT STOPS OR SLOW SPEEDS D21
	CHECK WHY THE VEH STALLS AT TIMES AT STOPS OR TURNS SEEMS MORE SO WHEN THE ENG IS WARM WITH THE A C OFF

2002	16478	S11	1FMYU01102KC58960	3.0L	TAU	3	2002	2.00E+03	9F715	D21	4	1788338	3000	WHILE DRIVING
2002	16469	S11	1FMYU01102KC58137	3.0L	TAU	2	2002	2904	DIAG	D21	1	948007	0	WON'T IDLE
2002	16512	S11	1FMYU01102KB91661	3.0L	TAU	12	2001	2905	RECALEM	D21	6	1128005	6000	AT STOP
2002	16513	S11	1FMYU01102KB91661	3.0L	TAU	12	2001	1H03	9J400	D21	8	2416833	12000	WHILE DRIVING
2002	16518	S11	1FMYU01102KB92102	3.0L	TAU	11	2001	2.00E+03	9F715	D21	7	2230925	16000	DIESEL
2002	16575	S11	1FMYU01102KA61323	3.0L	TAU	9	2001	2.00E+03	9F715	D21	3	462007	3000	AT STOP
2002	16579	S11	1FMYU01102KA61323	3.0L	TAU	9	2001	7C09	14N009	D21	3	444445	3000	STALLS
2002	16594	S11	1FMYU01102KA46995	3.0L	TAU	6	2001	2905	RECAL	D21	11	2109329	10000	ACCELERATING
2002	16599	S11	1FMYU01102KA57867	3.0L	TAU	9	2001	1A09	6007	D21	3	475995	3000	STALLS
2002	16612	S11	1FMYU01102KA25585	3.0L	TAU	6	2001	2904	12A650	D21	9	1758014	6000	STALLS
2002	16606	S11	1FMCU041D2KE11849	3.0L	TAU	7	2002	2904	12A650	D21	0	2242605	0	WHILE DRIVING
2002	16550	S11	1FMCU041X2KD69007	3.0L	TAU	6	2002	2904	DIAG	D21	0	3075855	0	WHILE DRIVING
2002	16536	S11	1FMCU041X2KD66399	3.0L	TAU	5	2002	2.00E+03	9E939	D21	1	2230462	0	WHILE DRIVING
2002	16544	S11	1FMCU041X2KD41039	3.0L	TAU	5	2002	2.00E+03	9F715	D21	3	1572634	3000	WHILE DRIVING
2002	16548	S11	1FMCU041X2KD10008	3.0L	TAU	4	2002	2904	12A650	D21	3	2306307	1000	WHILE DRIVING
2002	16551	S11	1FMCU041X2KD09858	3.0L	TAU	4	2002	7902	14401	D21	1	1261189	0	WHILE DRIVING
2002	16554	S11	1FMCU041X2KC99849	3.0L	TAU	4	2002	2.00E+03	9F715	D21	3	2032488	1000	STALLS
2002	16555	S11	1FMCU041X2KC99849	3.0L	TAU	4	2002	2.00E+03	9F715	D21	3	2360772	1000	STALLS
2002	16557	S11	1FMCU041X2KC91940	3.0L	TAU	4	2002	2902	128570	D21	2	1912814	2000	STALLS
2002	16558	S11	1FMCU041X2KC89095	3.0L	TAU	3	2002	7902	10346	D21	2	1688364	1000	WHILE DRIVING
2002	16570	S11	1FMCU041X2KC71601	3.0L	TAU	3	2002	2.00E+03	9F715	D21	5	1979888	3000	WHILE DRIVING
2002	16574	S11	1FMCU041X2KC89599	3.0L	TAU	3	2002	2.00E+04	8C815	D21	4	2343166	4000	STALLS
2002	16576	S11	1FMCU041X2KC89599	3.0L	TAU	3	2002	2905	RECALEM	D21	4	2191947	4000	DOWNHILL
2002	16578	S11	1FMCU041X2KC49807	3.0L	TAU	2	2002	2904	12A650	D21	5	2109539	6000	WHILE DRIVING
2002	16564	S11	1FMCU041X2KC49859	3.0L	TAU	2	2002	2.00E+03	9F715	D21	1	1853887	0	STALLS
2002	16566	S11	1FMCU041X2KC50900	3.0L	TAU	2	2002	2.00E+03	9F715	D21	4	2144348	8000	STALLS

ADJUST		EEC TEST TEST IGNITION MONITOR RESET BASE IDLE ANDRETEST
NPF		MIL NOT ON NOT DTC WDS PASS ROADTEST COULD NOT VERIFY
REFLASH		WDS ST UP TESWT EEC MIL OFFF CROP1111 RACEL PCM TREST DRIVE
REPLACED		PFE VOLTS ERRATIC OPERATION VOLTS FROM .2 TP 4.3 RUN EEC TEST NO DTC RUN MONITOR ROADTEST 3MILES FOUND PFE SE NSOR ERRATIC VOLTS FROM .2 TO 4.3 REPLACE PFE SENSOR RETEST
TSB		CHECK SYSTEM WITH WDS FOR STORED CODES NONE FOUND. CHECK OASIS FOR SSM OR TSB INFORMATION. FOLLOW TSB 02 11 6 FOR
STICKING		SF715,CC 42 LIGHT OFF,P1000 P1000 P1000 NGS TEST,DCL TEST P1000,DRIVE STALLS ON DECELL AT PARKING LOT SPEED,IAC VALVE STICKING,R&R IAC,RETEST PASS NO STALL
SSM		148102,CC 42 LIGHT OFF,P1000 P1000 P1000 WDS TEST,DCL TEST,PINPOINT TEST,MONITOR ROAD TEST,IGN SYS TEST,FUEL SYS TEST PASSPASSPASS,SPECIAL SERVICE MESSAGES
REFLASH		TEST EEC KOEO PASS NO CHECK ENG LIGHT TEST EEC KOEC PASS TEST EEC KOER PASS MONITOR DCL WITH NGS, PINPOINT STS, IGN TEST, FUEL PRESS TEST, REPROGRAM PCM TO IMPROVE DRIVABILITY, RETEST EEC P1000
REPLACED		CHECK ENGINE OIL OK, COOLANT OK. ENGINE FROZEN, LOCKED UP. REPLACED ENGINE, AND INSPECT ENGINE AND DIAG.
TSB		PERFORM DIAGNOSTICS ON WDS. NO CODES. RETRIVE TSB FROM OASIS M TEMP IS FOR PERFORMING DIAGNOSTICS TESTS AS OUTLINED IN TSB 02 11 05. REPROGRAM PCM
TSB		DIAGNOSED AND PERFORMED TSB 02 11 06..REPROGRAMED PCM AND SET BASE AND CURB IDLE PER EMAIL
TSB		EEC DCL PERFORM TSB 2 11 6 NPF
TSB		MIL OFF EEC DIAGNOSIS NO DTC DIAGNOSED FUEL SYSTEM 65 PSI DIAGNOSED IGNITION SYSTEM 2.0 MILLISECONDS ROAD TESTED 8 MILES WITH NGS MONITOR ALL PARAMETERS ARE IN RANGE CONTACTED OASIS AND PERFORMED PAR
REPLACED		EEC TEST, NO CODES. TEST DRIVE, IDLED VERY LOW. TAPPED ON IAC AND IDLED UP. REPLACED IAC. RETEST, OK.
NPF		PERFORMED WDS TEST PINPOINT AND MONITERED PIDS NOPROBLEMS FOUND
POOR CONNECTION		INSTALLED WDS 0351, PERFORMED PINPOINT TEST, ROAD MONITOR TEST, FOUND ENGINE HARNESS CONNECTOR BACK OUT, RESECURED CONNECTOR, ROAD TEST, RETEST
TSB		ROAD TESTED, VERIFY CONCERN AND PERFORM TSB 02 11 06 AND REPLACED THE IAC VALVE. REPROGRAMMED PCM AND CHECKED OTHER VALVES RE ROAD TESTED OK
TSB		ROAD TESTED, VERIFY CONCERN, PERFORM TSB 02 11 06. REPLACED IAC VALVE, REPROGRAMMED PCM AND CHECKED OTHER VALVES. RE ROAD TESTED OK.
TSB		ROADTEST. TEST EEC NO FAULT CODES PRESENT. REDO TSB 02 11 6 NO PROBLEM FOUND. ROADTEST WITH VDR COULD NOT CONFIRM REPLACE MAF WITH UPDATED STYLE NEW STYLE LESS VUNERABLE TO RADIO FREQUENCY INTERFEREN
REPLACED		1029 DIAG NO POWER WARR. FOUND BACK OF TERMINAL ON ALT, MELTED OFF. REPLACE ALT. AND RUN FULL CHARGING SYSTEM DIAG, ALSO FOUND BATTERY TO BE BAD. REPLACE BATTERY.
REPLACED		DIAG. AND REPLACE IAC VALVE AND EEC POWER RELAY
TSB		INTERMITTANT OPERATION. EEC TEST,NO CODES,FUEL TEST PASS,PID MONITOR,REPLACE VAPOR MANAGMENT VALVE PER 02 11 06,DID NOT SHOW BAD LAST TIME, ******* MILEAGE CORRECTION *******
TSB		OUT OF CALIBRATION. EEC TEST,NO CODES,FUEL TEST,PERFORM TSB 02 11 06,PID MONITOR ,REPROGRAM PCM WITH LATEST CAL,CK VAPOR MANAGMENT VALVE OP
REFLASH		6570 PERFORMED EEC TEST KOEO PASS, KOEC PASS, MIL OFF. DCL DISPLAY. FUEL PRESSURE LEAKDOWN. PERFORMED T.S.B. 02 11 06. REPROGRAM PCM. REMOVE AND INSPECT EEC RELAY LOSS MONITOR ROADTEST. DCL RECORDE
TSB		PERFORM TSB. EEC TEST AND REPLACE IAC VALVE AND EEC RELAY COME BACK RETEST AND REPLACE THROTTLE BODY AND EVAP VALVE. RE ROAD TEST UP AND DOWN HILLS.
DIAG		IAC MOTOR EEC (QUICK TEST) DIAGNOSIS

	TOW TO SHOP VEHICLE DIED WHILE DRIVING, WILL RESTART BUT LOSES POWER WHILE DRIVING
	CUSTOMER STATES SES ON, RUNS ONLY IF FOOT ON GAS, STALLING LOW SPEEDS
	CUST STATES STALLS WHEN COMING TO A STOP RESTARTS RIGHT AWAY
	CUSTOMER STATES THAT VEHICLE WOULD STALL AT ANY GIVEN TIME.. VEHICLE TURNS RIGHT BACK ON...NOTICES HAPPENING MORE WHEN
	INTERMITTANT STALL ON DIECEL. PLEASE CHECK OASIS AND SEE SCB M FOR SIMILAR CONCERNS OTHER ESCAPES
	QUALITY CHECK INITIALS: CUST. STATES ENG. STALLING WHEN COMING TO A STOP AND MORE
	QUALITY CHECK INITIALS: CUST. STATES AT TIMES ENG STALLING WHEN GOING OVER SPEED
	CUST STS ENGINE SPITTS AND SPUTTERS ON ACCEL, WHEN COLD.
	CS VEH MADE ALOT OF NOISE AND TURNED OFF TOWED IN NO START
	CHECK FOR VECHILE STALLING OUT
	CUST STATES ENGINE STALLED WHILE DRIVING
	OWNER STATES ENGINE STAULLED WHILE DRIVING 40 MPH STEADY SPEED
AMETER CHECKED DESCRIBED IN TSB 2 11 6 REPLACED IAC AD THROTTLE BODY TO GET IAC DUTY CYCLE AT 39 PERCENT REPLACED EEC POWER RELAY WITH UPDATED UNIT	CUST STS WAS DRIVING THIS MORNING AND ENGINE STALLED WHILE DRIVING THEN RESTARTED OK AND NOW DRIVES OK
	CUSTOMER STATES ENGINE STALLS WHILE DRIVING SLOW AND TURNING
	HAS STALLED A COUPLE OF TIMES WHILE DRIVING
	DIES WHILE DRIVING. STARTED AGAIN BUT KEPT DYING
	CHECKED FOR VEHICLE STALLING
	CHECKED FOR VEHICLE STALLING
CE.	ENGINE STALLED AGAIN IN THE SAME SPOT. IT WAS OK FOR 10 DAYS SINCE LAST REPAIR.
	STALLED AS DRIVEN WOULD NOT RESTART TOWIN
	STALLED WHILE DRIVING
	VEHICLE STALLED
	CK VEHICLE STOPPED RUNNING WHILE SLOWING DOWN,CUSTOMER IS GOING DOWN HILL ,HAS CUIT SEVERAL TIMES, SEE CUSTOMERS
R MONITOR DATA LOGGER ROADTEST. NO STALL OR IDLE DIP EXPERIENCED,EVAP% TO 95% FTP 2.2VOLTS. LOWEST RPM ON DECEL 705 . UNABLE TO DUPLICATE STALL CONCERN. TECH #6905	CUSTOMER STATES THAT THE VEH HAS A STALLING PROBLEM WHILE DRIVING PLEASE CK AND ADVISE
	CUSTOMER STATES ENGINE STALLS
	CUST SAYS CK ENG LIGHT WAS ON ENG DIED BUT RESTARTED

2002	16694	S11	1FMCU041X2KC27316	3.0L	T/LD	2	2002	7C05	14N069	D21	2	1004804	1000	WHILE DRIVING
2002	16702	S11	1FMCU041X2KB98769	3.0L	T/LD	1	2002	2.00E+03	9F715	D21	1	2173857	1000	STALLS
2002	16703	S11	1FMCU041X2KB98545	3.0L	T/LD	1	2002	2B02	129579	D21	2	1239980	1000	WHILE DRIVING
2002	16704	S11	1FMCU041X2KB97847	3.0L	T/LD	1	2002	1H03	9J460	D21	4	1347053	1000	STALLS
2002	16705	S11	1FMCU041X2KB98716	3.0L	T/LD	1	2002	2B02	99999	D21	7	2099773	3000	WHILE DRIVING
2002	16711	S11	1FMCU041X2KB95184	3.0L	T/LD	1	2002	2G04	12A650	D21	2	949096	2000	WHILE DRIVING
2002	16716	S11	1FMCU041X2KB95092	3.0L	T/LD	12	2001	2G04	12A650	D21	3	1535478	2000	WON'T RUN
2002	16717	S11	1FMCU041X2KB95948	3.0L	T/LD	12	2001	2G04	DIAG	D21	3	1371727	3000	WHILE DRIVING
2002	16719	S11	1FMCU041X2KB95874	3.0L	T/LD	12	2001	2G05	RECAL	D21	6	1982186	3000	DOWNHILL
2002	16720	S11	1FMCU041X2KB95295	3.0L	T/LD	12	2001	2G04	DIAG	D21	6	1712659	5000	DOWNHILL
2002	16724	S11	1FMCU041X2KB94068	3.0L	T/LD	12	2001	1H03	9J460	D21	6	2176782	9000	UPHILL
2002	16730	S11	1FMCU041X2KB94582	3.0L	T/LD	12	2001	2G04	12A650	D21	7	1977755	12000	STALLS
2002	16737	S11	1FMCU041X2KB93950	3.0L	T/LD	11	2001	2G04	12A650	D21	4	957736	2000	WHILE DRIVING
2002	16738	S11	1FMCU041X2KB93960	3.0L	T/LD	11	2001	2.00E+04	9C915	D21	8	2181438	5000	DOWNHILL
2002	16739	S11	1FMCU041X2KB93950	3.0L	T/LD	11	2001	2.00E+04	9C915	D21	7	1980138	5000	DOWNHILL
2002	16740	S11	1FMCU041X2KB93950	3.0L	T/LD	11	2001	1H03	9J460	D21	7	1798206	5000	DOWNHILL
2002	16741	S11	1FMCU041X2KB93188	3.0L	T/LD	12	2001	7C05	14N069	D21	1	827746	0	WHILE DRIVING
2002	16747	S11	1FMCU041X2KB93382	3.0L	T/LD	11	2001	2.00E+03	9F715	D21	4	1578382	3000	NO TEXT
2002	16748	S11	1FMCU041X2KB92361	3.0L	T/LD	11	2001	2B01	12A650	D21	4	1111494	3000	WHILE DRIVING
2002	16757	S11	1FMCU041X2KB15485	3.0L	T/LD	11	2001	2G04	12A650	D21	5	1488686	4000	AT STOP
2002	16758	S11	1FMCU041X2KB14515	3.0L	T/LD	11	2001	7C05	14N069	D21	1	597220	1000	WHILE DRIVING
2002	16760	S11	1FMCU041X2KB12179	3.0L	T/LD	10	2001	7C05	14N069	D21	1	380390	0	WHILE DRIVING

SSM		ROAD TEST TO VERIFY COMPLAINT,COULD NOT VERIFY,HOOK UP ON WDS,RUN SELF TEST,PASS KOEO AND KOER,REPROGRAMMED AS PER SSM 15569,REPLACE EEC RELAY AND CHEC TO MAKE SURE PINS ARE TIGHT,RETEST AND REROAD TE
REPLACED		1773 WDS DIAG ALL PASS NO CODES PIN POINT TEST REPLACE IAC VALVE ROAD TEST AFTER REPAIR
HOTLINE		ROADTEST8 DID WDS TEtST SELF DCL CHK CALIBRATION LATEST CAL CALLED HOTLINE NEEDS MAF SENSOR REPL MAF FINAL TEtST ROADTEt8 OK
REPLACED		DOES NOT OPERATE PROPERLY DIAGNOSE AND REPLACE DPFE SENSOR D21 42
REPLACED		VERIFIED CONCERN FOUND TP SENSOR BAD REPLACED TP SENSOR ROAD TEST ALL OK
SSM		DID WDS TEST DCL PINPOINT REPROGRAMMED PCM PER SSM1568 RECHECK FINAL TEST ROADTEST OK
LOOSE HOSE		2175 CHECK FOR RUNNING ROUGH VERIFY CHECK FOR CODES IN MEMORY NONE CHECK OASIS CANY GET IN DOWN INSPECT UNDER HOOD CAR RUNNING LEAN AND STALLING INSPECT AIR CLEAN ER BOX NO LEAKS OK FOUND PCV HOSE
REFLASH		CHECKED FOR CONCERN DID NOT VERIFY CONCERN CHEC KED PCM CAN BE PROGRAMED PROGRAMED PCM CHECKED FOR CODES NONE AT THS TIME NO CODES IN THE PCM BUT DID REPROGRAM RECHECKED OK
REFLASH		WDS TESTING NO CODES PINPOINT OK SPECIAL MESSAGE TO UPDATE PCM FOR INTERM STALL NO LIGHT PASS PASS, PASS REPROGRAMMED PCM
NPF		CAR TOWED IN EEC TEST PASS,CRANKED OVER AND STARTED. ROAD TE STED OK. ROAD TEST WITH NGS TO MONITER ENGINE A ND COMPUTER FUNCTION,ALL PASS AT THS TIME S HOP FOREMAN ROAD TEST APPROX 20 MILES ALL OK
T9S		9547 NO CEL HOOK TO WDS PINPOINT TEST PASS PASS PASS CHECK PIDS CHECK IDLE SPEED F PERFORM T9S 02 11 6 CHECK IDLE OK 37% CHECK RELAY OK INSPECT SENSORS REPLACED DPFE SENSOR OLD STYLE REPROGRAMMED PC
T9S		13974 PERFORMED EEC ST9T KOEO PASS KOEC PASS MIL OFF. DCL DISPLAY,FUEL PRESSURE LEAKDOWN. RELATIVE INJECTOR FLOW.CHECKED OASIS,PERFORMED T.S.S. 02 11 06, DOUNSCORDER MONITOR TEST IAC VALVE AT 38 PE
NPF		ROAD TEST, NO STALLING, EEC TEST, NO CODES.
NPF		EEC SYSTEM DIAG NO633, MONITOR IAC AT CLOSED THROTTLE. CHECK EVAP OPERATION AT TIMES EVAP VLAVE FAILS. REPLACE EVAP VM VALVE AND RECHECK. CHECK EEC POER RELAY, ROAD TEST AGAIN MONITORING RPM FOR EXCESS
T9S		ROAD TEST, EEC TEST, CHECK OASIS AND T9S, CHECK IAC AT 750 RPM AT 190F EOT. CHECK PCM CALIBRAION, REPROGRAM PCM WITH NEWEST LEVEL, CHECK EVAPVM AND FTP, PREMATURE SHUTDOWN DOES OCCUR, BLOW VENT HOSE A
HOTLINE		WHILE ON TEST DRIVE, RPM NEVER FELL BELOW 650, CALL HOTLINE AND TALK WITH ANDREW, CHECK PCM CONNECTOR AND PCM, ALL OK. CHECK MAF SENSOR, DPFE SENSOR, OLD STYLE. CHECK CONNECTOR C270, CHECK ENGINE GONT
REPLACED		EEC TEST AND PINPOINT TEST ALL PASS CODES CHECK AND REPLACE PCM POWER RELAY AND REPROGRAM PCM
REPLACED		FAILED PART 9P715 VERIFY,NGS TEST,NO DTCS,PIN TEST,MONITOR PIDS,REPLACE IAC, RETEST.
STICKING		STICKS EEC (QUICK TEST) DIAGNOSIS
REFLASH		PCM NEEDED REPROGRAMED EEC (QUICK TEST) DIAGNOSIS
SSM		EEC POWER RELAY NOT OPER PROPER PERFOEMED SSM#15494, REPLACED EEC POWER RELAY, CK LOOSE GROUNDS, C
SSM		TEST EEC WITH NGS KOEO,KOER ALL PASS OASIS FOR SSMS FOUND SSM 15494 REPLACED EE POWER RELAY INSPECT GROUND CONNECTORS IAC ROADTEST

ST	SHUT OFF WHILE DRIVING, RESTARTED OK.
	INSTALL SOP "TECH49 ENGINE STALLS
	CUST STATES CAR JUST SHUTS DOWN WHILE DRIVING
	C S VEHICLE STALLS SOP IN
	CUSTOMER STATES VEHICLE STALLS WHEN GOING DOWN ROAD
	CSHK PER CUSTOMER VEH CUTTING OUT WHILE DRIVING
OFF AND OTHER VAC LINES OFF REINSTALL AND RUN CLEAR ANY CODES AND ROAD TEST 7 MILES NO CHECK ENG LAMP COME ON OK RUNNING GOOD AT THIS TIME SERVICE TO DRIVE AND VERIFY FIX	CUST STATES: VEHICLE TOWED IN RUNS ROUGH WONT RUNNING ON START UP VEH MADE LOUD BANG AND THE
	CUST STATES: VEHICLE STALLS WHILE DRIVING CHECK AND ADVISE.
	CUSTOMER STATES: THE VEHICLE STALLED TWICE . NO LIGHTS OR ROUGH RUNNING. HAPPENED 1 MONTH APART, ON THE SAME HILL.
RECHECKED IN AM OK NO PROBLEM FOUND AT THIS TIME CHECKED ALL FLUIDS OK	TOWED IN. CS THE CAR DIED OUT AFTER DRIVING APPROX 3 MILES FROM HOUSE. CS THE CAR WAS COASTING DOWNHILL APPROX 40MPH AT TIME OF DIE OUT
M TO NEWER CALIBRATION ROAD TEST RETEST OK AT THIS TIME	WHEN GOING UP HILL ENGINE TURN OFF BUT WILL RESTART DS1
RCENT 700RPM. REPROGRAMMED PCM. EVAP RUNNING. LOSS MONITOR ROADTEST FTP VOLTAGE OK, NO VENT RESTRICTION,NO IDLE DIP. RETEST REMOVED AND INSPECTED SEC POWER RELAY OK. RETEST P 1000. TECH	CUSTOMER STATES VEH STALLS VEH DIED WHEN BRINGING IN THIS AM CHECK & ADVISE
	CUSTOMER REPORTS TRUCK STALLS WHEN TURNING WHEEL..IT DIED WHILE DRIVING AND TURNING AND CHECK ENGINE LIGHT CAME ON AND WAS HARD TO RESTART
SIVE DROP DURING DECELERATION. ALL OKAY.	WHEN GOING GOING DOWNHILL AT SPEEDS OF 25 35 MPH AND LIGHTLY BRAKING TRUCK CUTS OUT,STARTS BACK UP
SSEMBLY OUT. RECHECK EVAPVM AND FTP AGAIN, CHECKED SEC RELAY, OKAY. ROAD TEST AND MONITOR RPM, OK.	CUSTOMER REPORTS WHEN GOING DOWN HILLS AND APPLING BRAKES AROUND 20&25MPH IT WILL STALL OUT
ROL HARNESS, CHECK GROUND G600 AND G100. REMOVE BATTERY TRAY AND INSPECT GROUND G104 AND G105 TO G101, ALL OK. MONITOR PID AGAIN, ON ROAD TEST ONLY PID OUT OF RANGE. REPLACE DPFE SENSOR, RECHECK. OK	CUSTOMER REPORTS ENGINE DIES WHEN GOING DOWN HILLS AND WHEN GOING TO THE LEFT
	STALLED WHILE DRIVING.
	OK FOR DIED WHILE DRIVING, THEN NO CRANK NO START FOR A FEW MINUTES, THEN ABLE TO RESTART, HAS HAPPE
	C S CAR CUT OFF STOPLIGHT, DID START BACK UP WITH NO PROBLEM. PLS ADVISE
	CUSTOMER STATES WHILE DRIVING DOWN THE ROAD, THE VEHICLE WILL CUT OFF, CUSTOMER STATED THEY HAD TO PULL OVER AND COME TO A STOP, VEHICLE RE STARTED.
	OK ON 2 OCCASSIONS CAR HAS QUIT WHILE DRIVEN,RESTARTED AFTER KEY REMOVED FROM IGNITION AND PUT BACK IN,THE OTHER DAY TRUCK FELT AS IF HAD A MISS WHEN DRIVING.

2002	15783	S11	1FMCU041X2KB12108	3.0L	T/LD	10	2001	2.00E+03	9F715	D21	3	671640	2000	STALLS
2002	15785	S11	1FMCU041X2KB53848	3.0L	T/LD	10	2001	2G05	RECAL	D21	6	1161684	8000	WHILE DRIVING
2002	15774	S11	1FMCU041X2KB01691	3.0L	T/LD	10	2001	7C05	14N069	D21	1	788035	1000	STALLS
2002	15780	S11	1FMCU041X2KA89982	3.0L	T/LD	10	2001	2.00E+03	9E829	D21	8	1926277	12000	STALLS
2002	15781	S11	1FMCU041X2KA89982	3.0L	T/LD	10	2001	2.00E+03	9F715	D21	8	1922199	11000	STALLS
2002	15782	S11	1FMCU041X2KA89982	3.0L	T/LD	10	2001	2G02	129579	D21	10	2449085	14000	STALLS
2002	15786	S11	1FMCU041X2KA90927	3.0L	T/LD	10	2001	2G05	RECAL	D21	6	1119183	7000	WHILE DRIVING
2002	15787	S11	1FMCU041X2KA85570	3.0L	T/LD	10	2001	2G04	12A650	D21	10	2242668	9000	STALLS
2002	15793	S11	1FMCU041X2KA90232	3.0L	T/LD	10	2001	2.00E+03	9F715	D21	0	466200	0	WHILE BRAKING
2002	15794	S11	1FMCU041X2KA78278	3.0L	T/LD	10	2001	2.00E+03	9F715	D21	9	1947685	6000	WHILE DRIVING
2002	15799	S11	1FMCU041X2KA89728	3.0L	T/LD	10	2001	7C05	14N069	D21	2	393204	1000	WHILE DRIVING
2002	15801	S11	1FMCU041X2KA80236	3.0L	T/LD	10	2001	2G05	RECAL	D21	8	1372536	8000	WHILE DRIVING
2002	15802	S11	1FMCU041X2KA89236	3.0L	T/LD	10	2001	1H03	9J460	D21	9	2191945	10000	STALLS
2002	15803	S11	1FMCU041X2KA89236	3.0L	T/LD	10	2001	2.00E+03	9E829	D21	8	1780856	8000	STALLS
2002	15807	S11	1FMCU041X2KA84986	3.0L	T/LD	10	2001	2.00E+03	9F715	D21	1	382362	0	WHILE DRIVING
2002	15812	S11	1FMCU041X2KA89307	3.0L	T/LD	9	2001	2.00E+03	9F715	D21	12	2366577	10000	ON HIGHWAY
2002	15813	S11	1FMCU041X2KA89307	3.0L	T/LD	9	2001	2G05	RECAL	D21	7	991827	6000	WHILE DRIVING
2002	15814	S11	1FMCU041X2KA89307	3.0L	T/LD	9	2001	7C05	14N069	D21	4	682180	3000	WHILE DRIVING
2002	15815	S11	1FMCU041X2KA51645	3.0L	T/LD	9	2001	2G04	DIAG	D21	3	373554	2000	WHILE DRIVING
2002	15816	S11	1FMCU041X2KA90786	3.0L	T/LD	9	2001	2G04	DIAG	D21	3	476745	3000	WHILE DRIVING
2002	15821	S11	1FMCU041X2KA80170	3.0L	T/LD	9	2001	1H03	9J460	D21	6	982860	8000	STALLS
2002	15828	S11	1FMCU041X2KA45471	3.0L	T/LD	9	2001	2G04	DIAG	D21	8	1738744	15000	AT STOP
2002	15830	S11	1FMCU041X2KA89342	3.0L	T/LD	9	2001	2G05	RECAL	D21	7	1557775	6000	WHILE DRIVING
2002	15844	S11	1FMCU041X2KA89014	3.0L	T/LD	9	2001	2G04	12A650	D21	11	2275695	15000	WHILE DRIVING
2002	15848	S11	1FMCU041X2KA39851	3.0L	T/LD	9	2001	2.00E+03	9F715	D21	1	317635	0	WHILE DRIVING

REPLACED		WDS KOEO,DATA LOGGER TEST FUEL PRESSURE LEAK DOWN INJ FLOW SPARK DURATION POWER BALANCE KOER REPLACE AIR BY PASS
REPLASH		PCM RECAL EEC (QUICK TEST) DIAGNOSIS
REFLASH		COMPLETED PCM RE PROGRAMMING PER FORD T.S.B. COMPLETED, ROAD TESTED. OK NOW.
REPLACED		FOUND THROTTLE BODY BINDING DIAGNOSE AND ADJUST THROTTLE BODY STILL STALLING REMOVE AND REPLACE THROTTLE BODY AND RESET BASE IDLE
TSB		IDLE AIR CONTROL VALVE AND REG VALVE STICKING DIAGNOSE ROADTEST STARTEST CHK PIDS CHK FUEL PRESSURE RUN OASIS CHK TSBS 02 11 06 REPLACE IDLE AIR CONTROL VALVE+VMV+
REFLASH		MASS AIR FLOW AND DPFE NOT FUNCTIONING CORRECTLY RUN DIAGNOSTIC CONTACT FORD HOTLINE ADVISED OF UPDATED DPFE REPLACE DPFE AND MASS AIR FLOW REPROGRAM PCM
SSM		ROAD TEST DID NOT VERIFY CONCERN. WDS DIAG NO CODES. MONITORED PIDS ALL NORMAL. REPROGRAM PCM AS PER SSM 15589.
TSB		RAN DIAG REC NO CODES,CHK TSB 02 11 06 R R PCM FOR NUMBERS OK,UPDATE PCM WITH WAS ROAD TEST
REPLACED		WDS TEST, SELF TEST, FUEL PRESS, INJ FLOW, PWR BAL, REL COMP DATA LOG IAC 68 PERCENT. REPLACED IAC AND RETEST
REPLACED		EEC TEST DCL PID MONT FUEL PRESS TEST REPLACE IAC REPROGRAM PCM RETEST
REPLACED		EEC PWR RELAY INOP EEC (QUICK TEST) DIAGNOSIS MONITOR ROAD TST REPLACED EEC PWR RELAY & CK IAC RETST
TSB		1 EEC TEST, PASS. PID DATA MONITOR, ALL PIDS IN SPEC. CHECKED OASIS, PERFORMED TSB 02 6 6. PERFORMED ALL CHECKS AND
HOTLINE		ACTUAL TIME REQUESTED FOR WIGGLE TEST AND PERFORMING TEST AS INSTRUCTED BY HOTLINE. TEST DROVE VEHICLE 150 MILES OVER THE WEEK, VEHICLE DID NOT STALL ONCE. EEC TEST PASS. PID DATA MONITOR AND ROAD TES
TSB		4.0 HOURS WAS ACTUAL TIME FOR 1ST VISIT FOR DIAGNOSIS AND TESTING OF VEHICLE. CALLED HOT LINE, INSPECTED AND TESTED EVAP SYSTEM EEC TEST NO CODES EVAP SYS TEST OK BUT DID NOTICE THAT CANISTER VENT PUR
HOTLINE		NGS DIAGNOSIS. FUEL PRESSURE WITH GAUGE OK. IGNITION DIAGNOSIS. NGS SIGNAL SIMULATION TEST EXTENSIVEROAD TESTS TRACE AND REPAIR LOOSE GROUND. ROAD TEST STILL STALLS OUT. CALLED HOTLINE SPOKE WITH BRAD
SSM		EEC TESTED NO CODES SYSTEM PASSED,CHECK IAC SOLINOID PER SPECIAL SERVICE MESSAGE,NEEDS UPDATED IAC. REPLACE IAC AND ADJUST TP SENSOR TO .56 VOLTS,ROAD TESTED OVER NIGHT AND NEVER STALLED.
SSM		PCM NEEDED UPDATED CALIBRATION PER SSM 15589 REPROGRAM PCM
SSM		RELAY ERRATIC PER SSM MESSAGE 15494 PERFORM ING STALL WHILE DRIVING PROCEDURE
NPF		CUSTOMER PULLED OFF THE ROAD AND VEHICLE STARTED RIGHT UP OK FOR CODESNO CODES FOUND
NPF		UNABLE TO DUPLICATE THE STALLING CONCERN ROAD TEST FOR 10 MILES OK ALL TESTS PASS VISUAL INSPECTION PASS KOEO,KOER,CONT MEM,DCL DISP,REC MON,IGNITION,AND FUEL PRESS TESTS PASS ALL OK AT THE TIME OF DI
REPLACED		1 PERFROM A WDS TEST AND SELF TEST PCMLRON DATA LOGGER AND REP LACE DELTA PPE SENSOR.REPLACE TRANS RANGE SENSOR THAT WAS OU T OF RANGE.
NPF		TEST DROVE EEC TEST NO DTCS PRESENT REROAD TEST CHECKED ENGINE OVER COULD NOT DUPLICATE CONCERN
TSB		PERFORM WDS DIAG. NO CODES, FUEL PRESSURE TEST IGN SYSTEM DIAG, NGS MONITOR DCL SCAN. REPROGRAM PCM PER TSB 02 11 06
INOP		NOT OPERATING PROPERLY EEC (QUICK TEST) DIAGNOSIS
INOP		INOP EEC (QUICK TEST) DIAGNOSIS

	CUST STATES STALL AT TIME WONT START STARTS THEN STALLS
	ENGINE QUIT WHILE DRIVING IN TOWN.
	ENGINE STALLS SEE SSM 5559 FOR CORRECT PROCEDURE PAPERWORK WITH JEFF AT X1057
	CUSTOMER STATES ENGINE KEEPS STALLING
	CUST SAYS CAR STALLED OUT ONCE 50 MPH W AC ON RESTARTED OK
	STILL STALLS SEE HISTORY. PULL SLIGHT GRADES WITH AC ON.
	CUSTOMER STATES ENGINE STALLING WHILE DRIVING
	CAR STALLED OUT ON HWY,THEN LATER STALLED IN DRIVEWAY AFTER START
	STALLS WHEN BRAKING.
	YESTERDAY WHILE DRIVING, VEHICLE JUST CUT OUT, NO WARNING, STARTED BACK UP AND NO PROBLEMS SINCE, THE CHECK ENGINE LIGHT DID COME ON WHEN IT DIED
	DIES INTERMITTENTLY WHILE DRIVING (RED BATT. LITE COMES ON, SEEMS TO BE WHEN VEHICLE WARM, DOES RESTART AFTER HAPPENS)
	CUST STATES VEHICLE STALLS WHILE DRIVEING,AFTER IT GETS HOT
T CALLED HOTLINE PERFORMED ALL CHECKS PER HOTLINE REPLACED MAF SENSOR AND DPFE SENSOR CHECKED C 270 B,C,D C 110,130 @ 100,200,104,105,101 WIGGLE TESTED CKP SENSOR AND WIRING HARNESS PER HOLINE ALL OK.	CUST STATES VEHICLE STALLS WHILE DRIVEING
GS8 VERY FAST PERFORMED NEW TSB 02 22 5 CHECKED PCM UPDATE WAS TO LATEST VERSION AND CHECKED PCM TO VERIFY STALL INSTALL NEW IAC THROTTLE BODY AND VAPOR MANAGEMENT VALVE RETEST	CUST STATES VEHICLE STALLED TWICE YESTERDAY WITHIN 10 MINS
INSTALL WDS RECORDER ROAD TESTED, MONITOR FOUND STICKING ISC MOTOR. REPLACED AND ROAD TESTED OK	WEDENSDAY CAR KEPT STALLING WHILE DRIVING SLOW.
	C 6 VEHICLE STALLED WHILE GOING AT 60 MPH ON HIGHWAY
	C 6 VEHICLE STALLED WHILE DRIVING AT 35 MPH UP A SLIGHT HILL
	ENGINE STALLS OUT WHILE DRIVING
	VEHICLE CUT WHILE DRIVING DOWN THE ROAD
AG 10 MILE ROAD TEST OK	ENGINE STALLED 2X WHILE DRIVING CHECK ENGINE LITE CAME ON HIT KEYS WITH KNEE RELATED?
	CUSTOMER STATES THER CAR HAS STALLED THREE TIMES ON THREE DI FFERENT OCCASIONS.
	CUST STATES AC STOPPED AND ENGINE CUT OFF (HAD BEEN DRIVING FOR 15M ABOUT 50 MPH)RESTARTED IMMED.PULLED OFF ROAD ,WAITED 20M &DROVE HOME
	CUSTOMER STATES ENGINE STALLS WHEN DRIVING,INTERMITTENTLY.RUNS SMOOTH,NO WARNING LIGHTS,LAST TIME 40MPH,RESTARTED OK...
	VEHICLE SHUT OFF WHILE DRIVING, DID RESTART, NO WARNING
	CUSTOMER STATES THAT THE WHILE DRIVING 40MPH THE VEHICLE STALLED CHECK ALL TSBS

2002	16648	S11	1FMCU041X2KA39251	3.0L	TALD	9	2001	2B04	12A650	D21	1	428448	0	WHILE DRIVING
2002	16662	S11	1FMCU041X2KA39170	3.0L	TALD	9	2001	7C05	14ND99	D21	4	557453	4000	WHILE DRIVING
2002	16663	S11	1FMCU041X2KA39089	3.0L	TALD	9	2001	2.00E+03	9F715	D21	11	2207107	15000	WHILE DRIVING
2002	16666	S11	1FMCU041X2KA37788	3.0L	TALD	9	2001	2B04	DIAG	D21	4	499139	1000	HARD START
2002	16667	S11	1FMCU041X2KA37746	3.0L	TALD	9	2001	1A05	6007	D21	1	391769	0	NO TEXT
2002	16668	S11	1FMCU041X2KA37748	3.0L	TALD	9	2001	1A09	6007	D21	1	285746	0	ON HIGHWAY
2002	16669	S11	1FMCU041X2KA34090	3.0L	TALD	9	2001	1H09	6J460	D21	11	2026421	10000	WHILE DRIVING
2002	16672	S11	1FMCU041X2KA30033	3.0L	TALD	9	2001	1A05	6005	D21	8	1232457	4000	NO TEXT
2002	16673	S11	1FMCU041X2KA30039	3.0L	TALD	9	2001	1A09	6006	D21	8	1141245	4000	WHILE DRIVING
2002	16674	S11	1FMCU041X2KA27980	3.0L	TALD	8	2001	2.00E+03	9F715	D21	3	419737	3000	DOWNHILL
2002	16676	S11	1FMCU041X2KA27980	3.0L	TALD	8	2001	7V01	12A581	D21	8	1295139	5000	DOWNHILL
2002	16677	S11	1FMCU041X2KA27980	3.0L	TALD	8	2001	2B02	12B579	D21	11	2255457	11000	DOWNHILL
2002	16678	S11	1FMCU041X2KA28636	3.0L	TALD	8	2001	2.00E+03	9F715	D21	7	1291367	3000	AT STOP
2002	16680	S11	1FMCU041X2KA28681	3.0L	TALD	8	2001	2B06	RECAL	D21	10	2128925	15000	WHILE DRIVING
2002	16681	S11	1FMCU041X2KA28439	3.0L	TALD	8	2001	2B04	12A650	D21	10	1800699	19000	DOWNHILL
2002	16690	S11	1FMCU041X2KA18905	3.0L	TALD	8	2001	2.00E+03	9F715	D21	11	1829200	15000	STALLS
2002	16695	S11	1FMCU041X2KA09883	3.0L	TALD	8	2001	2.00E+03	9F715	D21	10	1858772	12000	DOWNHILL
2002	16696	S11	1FMCU041X2KA09886	3.0L	TALD	8	2001	2.00E+03	9F715	D21	8	1306914	2000	WHILE DRIVING
2002	16905	S11	1FMCU041X2KA09422	3.0L	TALD	8	2001	1H03	6J460	D21	9	1706124	10000	WHILE DRIVING
2002	16914	S11	1FMCU04192KD59925	3.0L	TALD	7	2002	7C05	14ND99	D21	-1	2394504	0	WHILE BRAKING
2002	16918	S11	1FMCU04192KD66114	3.0L	TALD	8	2002	7N09	9.00E+256	D21	-1	2119898	0	STALLS
2002	16922	S11	1FMCU04192KD66353	3.0L	TALD	8	2002	2.00E+04	9C915	D21	1	1999050	0	AT STOP
2002	16923	S11	1FMCU04192KD66660	3.0L	TALD	8	2002	2.00E+03	9F715	D21	1	2115547	0	WHILE DRIVING
2002	16925	S11	1FMCU04192KD63551	3.0L	TALD	8	2002	2.00E+03	9E926	D21	2	2428990	0	DOWNHILL

SHOP		SHOP M TIME TO PERFORM EXTENSIVE ROAD TESTS AND CK IAC AND BATTERY
REPLACED		REPLACED RELAY PER SERVICE MESSAGE 15434 RETESTED GROUND AND PIMs FOR RELAY A OK
TSB		EEC TESTED 111 111 111 PERFORMED PINOPINT TESTS 2 OASIS 02 11 06 WDS MONITORED PIDS PER TSB REPROGRAMMED PCM CHECKED EVAP VALVACRIP IAC #SOES TO 42%WITH NO EVAPVM FLOW REPLACED IAC VALVE RECHECKED EEC
DIAG		CAR SLOW OF STARTING AT TIMES EEC (QUICK TEST) DIAGNOSIS
ENGINE FAILURE		REQUESTING DEALER'S P/A CODE 03009
ENGINE FAILURE		VEHICLE TOWED IN, ENGINE LOCKED UP, POSSIBLE CAMBROKE AND VALVE HIT PISTON, PER ENGINE HOTLINETOLD NOT TO TEARDOWN AND REPLACE ENGINE
TSB		10471 NO DTC TSB 02 11 6 AND ISM 02 05 043 CK PCM RELAY PASS CK DPFE SENSOR REPLACE PID DATA IAC PASS EVAP PASS REPROGRAM PCM 1U7A 12A650 AXB INSPECT PCM CONECTOR OK C2078 C2078,C,D,C110,C113 NO WAT
ENGINE FAILURE		REQUESTING DEALER'S P/A CODE 04971
ENGINE FAILURE		DIED WHILE DRIVING STARTS,DIES ENG KNOCKING,KNEP ENG #4ROD BRG SPUN,INSTALL LONG BLOCK,RECHARGE A C,TOP OFF FLUIDS ROAD TEST VERIFY REPAIR.
NPF		1 PERFORMED WDS DIAGNOSIS FOR TROUBLE CODES NONE KEY ON ENGI NE OFF AND KEY ON ENGINE RUNNING TESTS BOTH PASS. ROAD TESTS D 20 MILES NO DUPLICATION OF CONDITION RAN OASIS SINCE A SN
REFLASH		COULD NOT VERIFY...VISUAL INSPECT WIRING...WRAPPED CRANKSHAFT AND MAF SENSOR WITH FOIL...ATTEMPTED TO RECALIBRATE PCM...CALLED HOTLINE STATED CALIBRATION SHOULD BE 2002...INCORRECT...HAD TO USE 2001 CALIBR
TSB		UNKNOWN CONCERN NEVER VERIFIED PER FORD T.A.R. CASE #280DR0 08 REPLACED MASS AIR FLOW SENSOR AND D.P.F.E. ALSO PER FORD FIELD ENGINEER WE DRILLED OUT AIR BLEED HOLES FOR THE ENDS OF THE THROTTLE BOD
REPLACED		1 VERIFY DIAG AND REPLACE THROTTLE BODY, IAC AND REPROGRAM PCM PER 020606
REFLASH		CC 42 BASIC 12A650 EEC TEST, PINPOINT TEST, DSL DISPLAY, TEST FUEL PRESSURE NGS MONITOR, REPROGRAM POWERTRAIN CONTROL MODULE, RETEST
TSB		EEC TEST PINPOINT TEST NO CODES IN SYSTEM PERFORMED TSB # 02 11 6 AFTER PERFORMING ALL TESTS FOUN LOOSE GROUND AT C104 REPAIRED GROUND RETEST.
TSB		ROAD TEST UNABLE TO STALL IDLES LOW, CHECK FUEL AND EEC RELAY AS PER TSB 02 11 06 RELAYS OK CHECK IAC % OK EVAP VENT OK REPROGRAMMED PCM AS PER TSB RD TESTED AND RECHECKED OK
REPLACED		ROAD TESTED VERIFIED STILL PERFORM EEC SYSTEM DIAG AND PP TEST NO DTC MONITOR PIDS IAC AND PFE OUT OF RANGE REPLACE BOTH REBURN PCM WITH LATES AS PER PP TESTS AND ROAD TEST RETEST SYSTEM OPERATION REMO
TSB		IGN SYSTEM TEST 12.6V, NGS EEC TEST CODE P1000, CHECK TSB 02 6 8, CHECK IAC DUTY CYCLE BELOW SPEC, REPLACED IAC, REPLACED THROTTLE BODY PER TSB, REPROGRAM PCM WITH VERSION 17.1, CHK EVAP WORKING CORRE
REPLACED		NGS TEST, DCL DISPLAY, PID MONITOR ROAD TEST, TESTEVAPORATOR SYSTEM, PINPOINT AND REPLACED DEFECTIVE DPFE SENSOR AND RECALIBRATE PCM RETEST, CHECKS GOOD
TSB		16 WDS KOED P1000 CONT P1000 KOER P1000 OK OASIS PERFORM TSB 02 11 06 REPLACED EEC RELAY
TSB		ROAD TESTED AS LIKE VEH STALLED SET BASE IDLE AS PER TSB 2 11 6
TSB		RUN DIAGNOSTICS, REPLACE VMV, IAC, THROTTLE BODY, AND REPROGRAM PCM AS PER TSB 02 11 06
REFLASH		570 48 EEC TEST NKOED NKOEC CODE P1000 NGS MONITOR PINPOINT TEST DIAG REPLACE IDLE AIR CONTROL VALVE AND REPROGRAM PCM TO LATEST CAL LEVEL RETEST ROADTEST OK P1000
REPLACED		TEST EEC SYSTEM, PIN POINT TEST, IGNITION TEST, CHECKED CASE 6, REPLACED UPDATED IAC VALCE AND THROTTLE BODY, CLEARED COD ES, ROAD TESTED, OK

	CUSTOMER STATES THAT THE ESCAPE STALLS WHEN DRIVING RE CHECK TECH 116
	SOMETIMES CAR WILL STALL WHILE DRIVING
RELAY OK RD TESTED OK	CUSTOMER STATES CAR STALLED WHEN DRIVING TRAVELING AROUND 35 MPH CRUISING CAR JUST STALLED REPORT
	CUSTOMER STATES DURING THE MIDDLE OF THE DAY CAR IS SLOW OF STARTING AT TIMES IT FEELS LIKE LESS OF POWER
	CORRECT TRUCK STALLED ON HIGHWAY WOULD NOT RESTART FULL ELECTRICAL 12 12
ER FOUND RR BATTERY TRAY INSPECT G100,G800,G104,G105,G101 INSPECT CKP HARNESS PASS RETEST PASS QT1 PASS RDTEST	ENGINE DIES, WHILE DRIVING, WILL RESTART WITHOUT PROBLEM, 93 OCTAINE FUEL NO WNG LIGHTS CCDSO
	CK VEHICLE DIED WHILE DRIVING , NOW STARTS AND DIES
	CUSTOMER STATES YELLOW CHECK ENGINE LIGHT COMES ON GOING DOWN LONG HILLS AND BRAKE LIGHT COMES ON ALSO OIL LIGHT COMES ON OCCASIONALLY
ATION TO CALIBRATE PCM..ALSO ADVISED TO CHECK GROUNDS, CONNECTORS, VENTS..GAVE VEHICLE BACK TO OWNER..NO PROBLEMS SINCE..MT ADDITIONAL LABOR..TECHNICIAN HAD 6.3 ACTUAL HRS. ON VEHICLE REQUEST 2.5	CUST STATES VEHICLE STALLED OUT RESTARTED HAPPENED AT MARION HEIGHTS HILL SATELLITE DISHES ARE WRITE UP A JOB AID FORM TO HELP TECHNICIAN PIN POINT PROBLEM
Y TO SET THE BASE IDLE IN GEAR AT 510 & 20 RPMS..REMOVED THROTTLE BODY TO PERFORM PROCEDURE..FOLLOWED TSB 02 11 06 PROCEDURE..MT LABORS ON TSB PROCEDURES..CUSTOMER VERY CONCERNED ABOUT VEHICLE	CUST STATES STALL GOING DOWN LARGE HILLS.
	VEH STALLS INTER WHEN SLOWING TO STOP HAS HAPPENED ABOUT A D OZEN TIMES
	VEH WAS TOWED,CUSTOMER STATES WHILE DRIVING,ENGINE DIED BUT SHE DID NOT TRY TO RESTART.
	C S THAT THE CAR STALLED ONE TIME GOING DOWNHILL AT 40 MPH
	CUSTOMER STATES ENGINE STALLS VERY INTERMITTEN REPORT
NITOR PIDS OK	CS: WHEN GOING DOWNHILL CAR STALLS ALSO HESITATES WHEN GOING UP HILLS
QTLY, INSPECT EEC RELAY, REPLACE EEC RELAY TEST DROVE VERIFY REPAIR OK	CUSTOMER STATES VEHICLE STALLED WHILE DRIVING.VEHICLE WAS COASTING AT THE TIME DIED & HAD TO BE RESTARTED.
	CUSTOMER STATES THE VEHICLE STALLS WHILE DRIVING AT STEADY SPEEDS
	REPAIR VEHICLE DIES WHEN COMING TO A STOP
	CHECK VEH STALLS OUT
	TRAVELING STOP AND GO TRAFFIC VEH. LOST POWER PULLED OVER TO SIDE VEH STALLED 1 2 HR LATER STARTED DROVE TO SHOP
	CK ENGINE WILL DRIVING OUT RUNNING,ADVISE POSSIBLE COOLING FAN RELATED
	CUSTOMER STATES VEHICLE STALLED GOING DOWN A HILL ONLY ONCE

2002	16927	511	1FMCU04182KD40321	3.0L	T/LD	5	2002	2G04	DIAG	D21	0	1826799	0	STALLS
2002	16942	511	1FMCU04182KC85880	3.0L	T/LD	3	2002	2G04	DIAG	D21	1	1177613	1000	WHILE DRIVING
2002	16946	511	1FMCU04182KC73015	3.0L	T/LD	3	2002	2.00E+03	9E888	D21	4	2991044	2000	WHILE DRIVING
2002	16949	511	1FMCU04182KC71713	3.0L	T/LD	3	2002	2.00E+03	9C915	D21	2	1300693	0	DECEL
2002	16958	511	1FMCU04182KC59427	3.0L	T/LD	3	2002	2G02	189579	D21	0	1220540	0	STALLS
2002	16960	511	1FMCU04182KC46552	3.0L	T/LD	3	2002	2.00E+03	9F715	D21	4	2009666	5000	NO TEXT
2002	16969	511	1FMCU04182KC56215	3.0L	T/LD	2	2002	2G04	12A650	D21	1	1149056	1000	WHILE DRIVING
2002	16985	511	1FMCU04182KC37805	3.0L	T/LD	2	2002	2.00E+03	9F715	D21	2	1196466	2000	STALLS
2002	16979	511	1FMCU04182KC00869	3.0L	T/LD	1	2002	1H03	9D475	D21	2	754695	2000	HESITURGE
2002	16984	511	1FMCU04182KB89094	3.0L	T/LD	1	2002	2G04	12A650	D21	5	2357084	10000	WHILE DRIVING
2002	16986	511	1FMCU04182KB89905	3.0L	T/LD	1	2002	2.00E+03	9F715	D21	6	2297002	8000	WHILE DRIVING
2002	16988	511	1FMCU04182KB89905	3.0L	T/LD	1	2002	2G04	12A650	D21	1	699572	0	WHILE DRIVING
2002	16989	511	1FMCU04182KB77170	3.0L	T/LD	1	2002	2G05	RECAL	D21	7	2375351	6000	WHILE DRIVING
2002	16995	511	1FMCU04182KB76206	3.0L	T/LD	12	2001	7B02	10946	D21	0	498398	0	WON'T RUN
2002	16995	511	1FMCU04182KB66752	3.0L	T/LD	12	2001	2G04	12A650	D21	4	1291686	2000	STALLS
2002	17002	511	1FMCU04182KB64547	3.0L	T/LD	12	2001	2.00E+03	9F715	D21	5	1838321	7000	WHILE DRIVING
2002	17016	511	1FMCU04182KB57841	3.0L	T/LD	11	2001	2.00E+03	9E888	D21	2	624316	1000	WHILE DRIVING
2002	17022	511	1FMCU04182KB54923	3.0L	T/LD	11	2001	2.00E+03	9F715	D21	7	1545757	6000	WHILE DRIVING
2002	17028	511	1FMCU04182KB54389	3.0L	T/LD	11	2001	2G04	12A650	D21	7	1554983	9000	WHILE BRAKING
2002	17032	511	1FMCU04182KB16336	3.0L	T/LD	11	2001	2.00E+03	9E888	D21	5	2254787	4000	WHILE DRIVING
2002	17035	511	1FMCU04182KB14668	3.0L	T/LD	11	2001	2G05	RECALEM	D21	7	1422186	6000	AT STOP
2002	17037	511	1FMCU04182KB13811	3.0L	T/LD	10	2001	2.00E+03	9E888	D21	9	2152778	12000	WHILE DRIVING

ER02-627 23983

LOOSE HOSE		AIR INTAKE HOSE INSTALL AIR INTAKE HOSE AT THROTTLEBODY AND NGS EEC TEST KOEO P1000 KOEC P0171 P0172 P0300 P0301 P0302 P0306 CLEAR CUSTOMER WAS DEMOING VEHICLE WHEN ENGINE QUIT. VEHICL
NPF		RAN ENGINE DIAGNOSTIC TEST ALL PASS CODES WE WERE UNABLE TO DUPLICATE YOUR CONCERN TODAY
TSB		ROADTEST. TEST EEC NO FAULT CODES PRESENT AT THIS TIME. PERFORM PINPOINT TESTS IGNITION SYSTEM DIAG MONITOR AND RECORD DCL DISPLAY. AS PER TSB 2 11 6 PERFORM PROCEDURES 1THRUS REPLACE IAC AND TBODY RE
TSB		FOLLOWED TSB 02 08 6 RUN ENG TO SEC AT 750 RPM USING WDS FOLLOW TEST PROCEDURES EVAPVM VALVE OUT OF RANGE REPLACE VALVE CHECKED EEC RELAY FOUND TO BE QUESTIONABLE PER TSB REPLACED RELAY RETEST PURG
REFLASH		DID ALL DIAG NEC TO REPROGRAM PCM AND INSTALLED MASS AIR FLOW SENSOR. .
NO TEXT		
DIAG		00 EEC (QUICK TEST) DIAGNOSIS
STICKING		ROAD TEST CUST STATES VEHICLE STALLS PUT ON SIDS WDS NO CODES FOUND IAC CYCLE LOW SUSPECT IAC STICKING R AND R IAC RETEST OK
REPLACED		VERIFY CONCERN FOUND EGR VALVE STUCK OPEN REPLACE AS NEEDED CLEAR CODES RETEST AND ROAD TEST CHECK OK
TSB		TESTED THE EEC SYSTEM AND TESTED OKY RAN MESSAGES AND FOUND A TECNICAL SERVICE BULLITEN 02 11 06 COMPLETE TSB AND REPROGRAMED THE PCM
TSB		0321 ROAD TEST 20 MILES, RUN WDS TESTS, NO DTCS, CHECK DCL DATA PER TSB 02 11 06, IAC % TOO HIGH REPLACE IAC AND T BOD, % OK NOW, CHECK EVAP SYTEM PER TSB, OK ROAD TEST, OK
SSM		900 ROAD TEST SEVERAL TIMES,WAS UNABLE TO VERIFY CONCERN.PERFORMED WDS TESTS,NO CODES STORED. CHECKED SERVICE MESSAGES,REFER TO #15589 FOR INTERMITENT ENGINE QUIT CONTDITION. REPROGROAM PCM PER SERVI
TSB		NGS EEC TEST KOEO PASS KOEC PASS KOER PASS PERFORM TSB 02 11 06 WHICH INCLUDED NGS MONITOR ROAD TEST AND PCM RECALIBRATION. RE EEC TESTED KOER P1000 ROAD TEST NO STALLING PRESENT NOTE TSB IS INFORM
NO TEXT		
TSB		12A650 RAN WDS CHECKED PIDS PIN TEST RAN OASIS FOUND TSB 02 08 06 REPROGRAMMED PCM WITH WDS REPEAT QUICK TEST
TSB		DIAG PINPOINT TEST ROADTEST AND MONITOR CHECK I.A.C. VALVE REPLACE I.A.C. VALVE AS PER FORD TSB 02 11 06 RETEST
REPLACED		ROADTEST NO STALLING OCCURED PERFORM EEC TEST PASS CODES PERFORM DIAG PER CHECK LIST FROM FORD REPLACE IDLE CONTROL VALVE REPLACE THROTTLE BODY REPLACE DPFE SENSOR RECALIBRATE
TSB		6078 IAC VALVE AND EEC RELAY WARR RETESTED,PREFORM SELFTEST AND PINPOINT TEST FOR PREFORM PID DATA MONITORING WHILE DRIVING AND R I MAF SENSOR AND INSPECT FOR CONTAMINATION FO UND OK,R I PCM AND IN
REFLASH		PERFORM DIAGNOSTIC ROUTINE AND REPROGRAM POWERTRAIN CONTROL MODULE PER TECHNICAL SERVICE BULLETIN 02 11 06
REPLACED		VERIFY CONCERN. RUN NGS DIAG, MONITOR PIDS, PINOINT TEST AND IGNITION SYSTEM DIAG. R & R EEC RELAY,THROTTLE BODY AND IAC. SET BASE IDLE. RESET MEMORY .CK VMV DUTY CYCLE AND LINES FOR RAW FUEL. ALL OK.
DIAG		DIAG.PERFORM WDS TEST REBURN AND UPDATE PROCESSOR
TSB		DIAGNOSTIC AN DPINPOINT TESTING..CODES..PASS AS PER TSB 2 11 6 REPLACE THE THROTTLE BODY, THE IDLE AIR CONTROL VALVE, THE VMV THE DPFE SENSOR AND UPDATE THE PCM RETEST ROAD TEST OKAY AT THIS TIME

E WAS STILL DEALER OWNED AT THAT TIME. DEALER WAS TRYING TO SALAVAGE VEHICLE SALE BY GETTING VEHICLE PULLED IN IMMEDIATLY.	D21,CUSTOMER STATES ENGINE DIED WHILE DRIVEING.
	CUSTOMER STATES VEHICLE DIED WHILE DRIVING
PROGRM PCM AND RETEST OK	CUSTOMER STATES HAS ENGINE HAS STALLED TWICE WHILE DRIVING WHEN CUSTOMER WAS SLOWING DOWN STARTED RIGHT BACK UP
E DTC S ALL FUNCTION NORMAL AT THIS TIME	CUSTOMER REPORTS VEHICLE STALLS ON DECEL. FOR NO APPARANT REASON. SEE TSB 02 S 6...COPY ATTACHED.
	CUST STATES VEHICLE STALLS INTERMEDITALLY
	VEHICLE WAS DRIVING ALONG AND DIED
	CST ENGINE STALLS,D21
	CUSTOMER STATES VEHICLE RUNS POOR BUCKS SHAKES ENGINE LAMP ON
	O S THEY SAW LIGHTS ON ON THE DASH WHEN DRIVING AND THE STEERING WAS HARD THE BRAKE PEDAL WAS HARD A
	VEHICLE QUIT IN FLIGHT 45 MPH SEE HISTORY
CE MESSAGE ALSO VERIFIED UPDATED EEC POWER RELAY IN PLACE ROAD TEST BEFORE AND AFTER APPROX 10 MILES EXTRA TIME NEC FOR EXTENSIVE ROADTESTING AND TEST!	CUT OUT WHILE DRIVING, TOWED IN FROM ROADSIDE
ATION ONLY.	CUSTOMER STATES VEHICLE WILL STALL OUT WHILE DRIVING. WILL RESTART RIGHT AWAY. (D21)
	CHECK VEHICLE STALLS, WON,T KEEP RUNNING
	CUST STATES INTERMITT THE VEH UP AND DIES,DOES START RIGHT BACK UP..TSB 8 SSM IF NOT SURE SEE MARK
	WHILE DRIVING APPROX 40 MPH STALLED TWICE AT STOPS FEELS LIKE IDLES UP LUNGES FORWARD
	CUSTOMER STATES VEHICLE STALLED OUT WHILE DRIVING VEHICLE DID START RIGHT BACK UP
SPECT PINS FOUND OK,LOOK UP TSBS FOUND 02116 PREFORM FOUND IAC NOT TOTAL IN SPEC R R IAC AND RERDTEST AND R R EEC RELAY AND PREFORM PCM REPROGRAMING,RERDTEST AND SELFT TEST..TIME REQ	CUST. STATES THAT SOMETIMES WHILE DRIVING THE ENGINE DIES
	VEHICLE STALLS WHEN BRAKING INTERMITTENTLY
RETEST AND VERIFY OK.	CUSTOMER STATES THAT THE ENGINE DIED STALLED OUT WHILE DRIVING S.O.F
	CUSTOMER COMPLAINS THAT VEHICL STALLS AT STOPS
	CUST. STATES ENGINE DIED WHILE DRIVING 30 40 MPH. NO LIGHTS ON BEFORE ENGINE STOPPED, RE STARTED NORMAL.

2002	17041	511	1FMCU04192KB12235	3.0L	TALD	10	2001	2.00E+03	9950	D21	3	839741	4000	NO TEXT
2002	17042	511	1FMCU04192KB00595	3.0L	TALD	11	2001	2995	RECAL	D21	9	1872700	3000	WHILE DRIVING
2002	17044	511	1FMCU04192KB00697	3.0L	TALD	11	2001	2995	RECAL	D21	7	1553713	19000	STALLS
2002	17045	511	1FMCU04192KB00544	3.0L	TALD	10	2001	2995	RECAL	D21	6	1356891	6000	STALLS
2002	17046	511	1FMCU04192KB00039	3.0L	TALD	10	2001	2.00E+03	9F715	D21	9	2128927	8000	WHILE DRIVING
2002	17049	511	1FMCU04192KB00035	3.0L	TALD	10	2001	2.00E+03	9H307	D21	8	1763378	7000	ON HIGHWAY
2002	17063	511	1FMCU04192KA78601	3.0L	TALD	10	2001	2904	12A650	D21	4	824023	3000	WHILE DRIVING
2002	17064	511	1FMCU04192KA78601	3.0L	TALD	10	2001	2902	12B579	D21	6	1128857	4000	WHILE DRIVING
2002	17065	511	1FMCU04192KA78601	3.0L	TALD	10	2001	7302	14401	D21	1	322302	0	WHILE DRIVING
2002	17067	511	1FMCU04192KA78607	3.0L	TALD	10	2001	2904	12A650	D21	10	3972408	7000	WHILE DRIVING
2002	17068	511	1FMCU04192KAP1276	3.0L	TALD	10	2001	7V01	13A651	D21	6	1028724	7000	STALLS
2002	17074	511	1FMCU04192KA69029	3.0L	TALD	9	2001	2.00E+03	9F715	D21	11	2483360	20000	WHILE DRIVING
2002	17078	511	1FMCU04192KA61864	3.0L	TALD	9	2001	7C05	14N069	D21	2	336005	1000	WHILE DRIVING
2002	17079	511	1FMCU04192KA61404	3.0L	TALD	9	2001	7C05	14N069	D21	3	510517	0	WHILE DRIVING
2002	17080	511	1FMCU04192KA65584	3.0L	TALD	9	2001	2904	12A650	D21	5	743406	5000	STALLS
2002	17081	511	1FMCU04192KA63934	3.0L	TALD	9	2001	2.00E+03	9F715	D21	7	1112581	8000	STALLS
2002	17082	511	1FMCU04192KA63934	3.0L	TALD	9	2001	1N03	0J467	D21	5	1260915	6000	WHILE DRIVING
2002	17083	511	1FMCU04192KA63934	3.0L	TALD	9	2001	2.00E+04	9C915	D21	10	1807788	11000	STALLS
2002	17165	511	1FMCU04192KA46595	3.0L	TALD	9	2001	2904	12A650	D21	7	1097855	10000	WHILE DRIVING
2002	17115	511	1FMCU04192KA39652	3.0L	TALD	9	2001	2904	12A650	D21	6	913971	3000	AT STOP
2002	17128	511	1FMCU04192KA57035	3.0L	TALD	9	2001	2904	12A650	D21	7	1169284	7000	WHILE DRIVING
2002	17131	511	1FMCU04192KA56922	3.0L	TALD	8	2001	7C05	14N069	D21	7	1105761	7000	WHILE DRIVING
2002	17135	511	1FMCU04192KA54391	3.0L	TALD	8	2001	2905	RECAL	D21	10	2136671	8000	WHILE DRIVING
2002	17140	511	1FMCU04192KA53974	3.0L	TALD	9	2001	2905	RECAL	D21	12	2552348	22000	NO TEXT
2002	17155	511	1FMCU04192KA29515	3.0L	TALD	8	2001	2904	12A650	D21	9	1356515	10000	WHILE DRIVING

TSB		RDTEST, DID NOT VERIFY CONCERN, SELF TEST SYSTEM, NO CODES IN SYSTEM CK'D FUEL PRESSURE & OKAY AT THIS TIME. 55 PSI CK'D FOR SSM'S & TSB'S PER SSM15559, REPROGRAMMED PCM CK'D RELAY PER SSM & OKAY CK'D
REFLASH		1 ROAD TESTED, PERFORMED EEC TEST, PASS CODES, PERFORMED DCL DISPLAY TEST, AND REPROGRAMMED PCM TO LATEST CALIBRATION.
REFLASH		CHECK VEHICLE IS STALLING PERFORM EEC TEST PINPOINT TEST MONITOR TEST FINAL QUICK TEST REPROGRAM PCMCHECK OK
REFLASH		OPEN CIRCUIT PERFORMED DIAGNOSIS AND REPROGRAMMED PCM D21 25
DIAG		9F715 CC 69 EEC TEST KOEO PASS KOEC PASS KOER PASS PINPOINT TEST DCL DISPLAY NGS MONITOR RECORDER FUEL PRESSURE TEST
DIAG		9H307 CC 42 EEC TEST KOEO PASS KOEC PASS KOER PASS PINPOINT TEST DCL DISPLAY FUEL PRESSURE TEST NGS MONITOR RECORDER
REFLASH		MISCALIBRATED NGS TEST PASS. CONTACT FORD HOTLINE. ADVISED TO REPROGRAM PCM.
REPLACED		AS PER HOT LINE SSDS TEST MONITOR TEST PIN TEST REPLACE MAF SENSOR ,AIR BYPASS VALVE AND THROTTLE BODY ROAD TEST
SSM		CAUSE UNKNOWN ROAD TEST UNABLE TO DUPLICATE. EEC TEST PASS. INSPECT AND CLEAN G104 AND G105 GROUNDS. ISOLATE CKP CIRCUIT HARNESS.
REFLASH		REPROGRAM PCM PERFORMED WDS SYSTEM DIAGNOSIS AND CHECKED FUEL PUMP PRESSUR E IGNITION SYSTEM AND POWER BALANCE,NECESSARY TIME TO
INOP		INOP EEC (QUICK TEST) DIAGNOSIS
TSB		785339 WARR 42 9F715 95826 SC915 14N099 MILES OUT 29099 CODES PASS P1111 NGS START UP EEC TEST PID DATA TEST PID MOINTOR TEST NGS ROA D TEST FUEL PRESSURE TEST IGN. TEST PERFORM TSB 02 11 6 REPLACE AI
HOTLINE		EEC SYSTEM TEST NO DTC FOLOOW PPTEST8 CONTACTED HOTLIENWAS ADVISED TO TRACE G100 101 104 105 RMOEVE BATTERY TRAY AND AIR CLEANER TO ACCESS AND TRACE AND TEST ALL WIRING FOR POSSIBLE SHORTS CHECK ALL P
SSM		519 WDS DIAG, CONT, KOEO, KOER NO CODES DCL DISPLAY PID DATA MONITOR, FUEL PRESSURE AND LEAK DOWN TEST. PERFORM SSM 15434, REPLACE RELAY, REMOVE BATT. AND BATT BOX. INSPECT G104 G105. CHECK GROUND
REFLASH		VERIFIED REPROGRAMED PCM VERIFIED REPAIRS
REPLACED		TESTED TO CONFERM CONDETIN COULDNT DUPLICATE RAN KOEO AND KOER NO CODES MONITERED BARO AND LONF FUELTRIM REMOVED IAC AND REPLACED TEST OK
REPLACED		1 WDS ALL TESTS PASS DATA LOGGER ROAD TEST R&R BATTERY AND TRAY REWORKED GROUND G 101 G 104 REPLACED DPFE R&R
REPLACED		TESTED PID DATA MONITOR WIRE AND CONNECTOR TEST CALLED HOTLINE REPLACED MAF SENSOR WITH NEW STYLE
SSM		1 PERFORM SSM 15559, RE FLASH PCM CHECK VENT TUBE AND POWER RELAY
DIAG		EEC (QUICK TEST) DIAGNOSIS
SSM		42 DOES NOT OPERATE PROPERLY CHK OASIS FOUND SSM 15559 TO CK FOR LATEST PCM CALIBRATION,R ECALIBRATE PCM TO LATEST LEVEL,DISCONNECT VENT LINE IN EVAP SSY,CK EEC POWER RELAY OK,MT TIME CLAIMED TO DO LA
SSM		WDS DIAG ALL PASS CODES RUN SSM FIND INFO ON UPDATED EEC RELAY REPL RELAY FIND INFO ON UPDATD CALIBRATION ON PCM REPROG/Rel PCM
TSB		CHECKED FOR STALLING HOOK UP WDS KOEO PASS KOER PASS FUEL PRESSURE AND LEAKDOWN INJECTOR FLOW POWER BALANCE TEST DROVE DATA LOGGER CHECKED OASIS TSB 02 11 6 MONITOREDPIDS IAC EGT EVAPM C
NO TEXT		
SSM		WDS ..KOEO...PASS...DCL...MODE 6...EVERYTHING IS IN SPEC RAN PINPOINT INCONCLUSIVE...CHECKED OASIS AND PREFORMED

VET LINE HOSE PER SSM & OK	
	DIAGNOSE VEHICLE STALLED WHILE DRIVING AT ABOUT 35 MPH.
	CUSTOMER STATES VEHICLE IS STALLING
	C S VEHICLE STALLS
	D21 WHEN DRIVEING AT 30 45 MPH THE TRUCK WILL SHUT DOWN. CUSTOMER WILL PULL OVER AND THE TRUCK WILL RESTART FINE.
	CUSTOMER STATES VEH DIED ON HIGHWAY SATURDAY. RESTARTED AFTER A FEW MIN. NO WARNING LIGHTS. THIS HAS HAPPENED ONCE
	CUSTOMER STATES TRUCK STALLED OUT WHEN DRIVING
	CK STALLING OUT WHEN DRIVING 278 6452
	CUSTOMER STATES THAT ENGINE STALLED WHILE DRIVING NO TROUBLE RESTARTING
	CUST STATES THAT THE TRUCK INTERMITT CUTS OUT WHEN DRIVING DOWN A HILL OFF THE GAS ,STARTS RIGHT BACK UP
	CUSTOMER STATES THAT VEHICLE STALLS STARTS RT BACK UP
R BYPASS SALVE THROTTLE BODY EVAP VALVE EEC RELAY REPROGRAM PCM RETEST TIGHTEN GROUND WIRE CONN C1016	CUST STATES VEH STALLS WHILE DRIVING AND THEN STARTS RIGHT BACK UP
CM CONNECTORS REMOVE PCM RELAY FOUND PUSHED OUT PIN REPLACED RELAY AND RETEST SYSTEM	CUST STATES VEHICLE STALLED TWICE AT 40 MPH SEE ATTACHED ENVELOPE
ON TRANS, AND GROUND ON BULK HEAD. REINSTALL BATT RETURN TRUCK. 6450	CUSTOMER STATES THAT THE VEH STALLED WHILE DRIVING THE IDLE DROPED LOW AND VEH DIED PLEASE CK AND ADVISE
	CUSTOMER STATES ENGINE STALLS D21
	CUST REPORTS VEH IS STALLING D21
	STALLS WHILE DRIVING
	STALL OUT AT TIMES ON LET OFF SEE LATEST TSB CALL HOT LINE
	CUST STATES STALLED WHILE DRIVING
	C S STALLS WHEN COMING TO A STOP
TEST LEVEL AND CK EEC POWER RELAY PER INSTRUCTION NO OPS FOUND	D21 CUST STATES WHILE DRIVING THE VEH WILL JUST DIE OUT
	ENGINE STALLS WHILE DRIVING STEADY SPEED. RESTARTS OK.
ANVENT FTP ALL PIDS SEEM TO BE NORMAL	VEHICLE STALLS WHEN COASTING DOWN HILLS STALLS OUT WHEN DRIVING 40MPH
	CUST STATES 2 TIMES IN THE PAST WEEK THE VEH HAS JUST UP AND DIED WHILE DRIVING,DID RESTART RIGHT AWAY,D21

2002	17183	S11	1FMCU04192KA19036	3.0L	TALD	8	2001	7C05	14N089	D21	10	2439887	10000	WHILE DRIVING
2002	17177	S11	1FMCU04192KA08105	3.0L	TALD	8	2001	7B02	10346	D21	1	235480	1000	WHILE DRIVING
2002	17181	S11	1FMCU04192KA07679	3.0L	TALD	8	2001	2.00E+03	9E926	D21	9	1494269	9000	DOWNHILL
2002	17182	S11	1FMCU04192KA07679	3.0L	TALD	8	2001	2A01	9E931	D21	10	1822662	11000	WHILE DRIVING
2002	17180	S11	1FMCU04182KD63013	3.0L	TALD	5	2002	2.00E+03	9F715	D21	1	2160969	0	STALLS
2002	17191	S11	1FMCU04182KD60127	3.0L	TALD	5	2002	6U06	9C480	D21	2	2012112	4000	AT STOP
2002	17194	S11	1FMCU04182KD23810	3.0L	TALD	4	2002	2G02	12B578	D21	2	2163269	2000	WHILE DRIVING
2002	17189	S11	1FMCU04182KD11666	3.0L	TALD	4	2002	1A03	6000	D21	2	2432280	2000	STALLS
2002	17217	S11	1FMCU04182KC71704	3.0L	TALD	3	2002	2.00E+03	9F715	D21	4	1710563	4000	WHILE DRIVING
2002	17219	S11	1FMCU04182KC60196	3.0L	TALD	3	2002	2G02	12B578	D21	4	2462961	5000	COASTING
2002	17228	S11	1FMCU04182KC47001	3.0L	TALD	2	2002	2G04	DIAG	D21	4	1761319	2000	WHILE DRIVING
2002	17234	S11	1FMCU04182KC31008	3.0L	TALD	2	2002	2D02	9C915	D21	5	1462208	3000	WHILE DRIVING
2002	17264	S11	1FMCU04182KB75071	3.0L	TALD	12	2001	2G04	12A650	D21	8	2383694	11000	LOW SPEED
2002	17267	S11	1FMCU04182KB66788	3.0L	TALD	12	2001	1H03	9J480	D21	4	1879797	6000	WHILE DRIVING
2002	17269	S11	1FMCU04182KB64944	3.0L	TALD	12	2001	2G04	12A650	D21	6	1990894	12000	WHILE DRIVING
2002	17270	S11	1FMCU04182KB64946	3.0L	TALD	1	2002	2G02	12B578	D21	6	2269111	6000	WHILE DRIVING
2002	17271	S11	1FMCU04182KB64948	3.0L	TALD	1	2002	2G01	12B586	D21	6	2304809	6000	WHILE DRIVING
2002	17275	S11	1FMCU04182KB54618	3.0L	TALD	12	2001	2G04	DIAG	D21	1	955615	0	WHILE DRIVING
2002	17277	S11	1FMCU04182KB54657	3.0L	TALD	12	2001	2G05	RECAL	D21	3	903969	1000	WHILE DRIVING
2002	17276	S11	1FMCU04182KB54012	3.0L	TALD	12	2001	2.00E+03	9F715	D21	2	1109178	2000	WHILE DRIVING
2002	17282	S11	1FMCU04182KB57660	3.0L	TALD	12	2001	1F06	9A080	D21	2	697767	1000	WHILE DRIVING
2002	17294	S11	1FMCU04182KB50776	3.0L	TALD	11	2001	2.00E+03	9F715	D21	7	2269160	6000	STALLS
2002	17296	S11	1FMCU04182KB50006	3.0L	TALD	11	2001	7C05	14N089	D21	7	2036070	8000	WHILE DRIVING

TSB		COULD NOT CONFIRM COMPLAINT. BUT DID NOTICE A SLIGHT STUMBLE. PERFORMED DIAG. CHECKED OASIS AND PERFORMED TSB 02 11 6. MONITORED PIDS AND RAMPING OF IAC. REPLACED IAC DUE TO DUTY CYCLE NOT IN SPEC.
REPLACED		DIAG AND RR ALTERNATOR EXTRA TIME WAS REQUIRED TO PERFORM AND VERIFY CONCERN
TSB		5001 ROAD TEST VEH UNABLE TO DUPLICATE STALLING CONCERN RAN EEC TEST NO CODES MONITOR AND RECORD PID DATA PERFORMED DCL DISPAY TEST RAN OASIS FOUND TSB 02 6 6 PERFORMED TSB 02 6 6 REPLACED THROTTLE
TSB		11993 INSTALLED WDS CHECKED FOR CODES NO CODES MONITORED AND RECORDED PID DATA CHECKED FUEL PRESSURE OK FLOW TESTED FUEL INJECTORS OK R I SPARK PLUGS CLEAN AND INSPECTED OK PERFORMED ENGINE COMPR
TSB		EEC TEST NO CODES,RAN OASIS,FOUND TSB 02 11 06. INSTALLED NEW IAC SOL AS PER TSB,RETEST DCL OK,RETEST EEC
LOOSE HOSE		ENGINE STALLS VACUUM TUBE HOSE REPAIR
HOTLINE		2499 KOEO P1111 KOEC P1111 KOER P1111 7627 5.0L REPLACED MAF SENSOR PER HOTLINE HOOKED UP WDS EEC TEST DCL DISPLAY TO MONITOR EVAP PIDS DCL MONITOR RECORD WHILE DRIVING CHECKED ALL GROUNDS CHECKED
TSB		CMV EEC TEST NO DTCS WATCHED PIDS ON ROAD TEST LOKED OK RAN OASIS TSB 02 11 06 A OK LIST FOR THIS CONCERN FOLLOWED
REPLACED		IAC & EEC PWR RELAY INOP EEC (QUICK TEST) DIAGNOSIS PINPT TST MONITOR ROAD TT REPLACED IAC PCM & REPROGRAM RETST
TSB		VERIFIED, PERFORMED TSB 02 11 06 AS PER INSTRUCTED, ROAD TESTED AND RECHECKED
NPF		2001 ROAD TESTED VEHICLE PERFORMED EEC TEST NO CODES PERFORMED PIDS MONITOR ROAD TEST PERFORMED FUEL PREASURE TEST PERFORMED IGNITION SYSTEM TEST DID NOT FIND ANY THING WRONG WITH VEHICLE WAS UNABL
VACUUM LEAK		3914 DIS NGS EEC TEST PASS NGS ROAD TEST,FUEL DIAG PINPOINT TEST,REPAIR VAC LEAK TO MAF RETEST 199900,DX1,D45,D81,99B8,19222A, 1.8HRS?
TSB		11987 TEST DROVE VEHICLE, COULDNT GET TO STALL ON TEST DRIVE. CHECKED OASIS FOR ANY TSBS OR SPECIAL SERVICE MESSAGES. FOUND TSB 02 11 6 FOR INTERMITTANT ENGINE CUIT WITH NO DTCS. PERFORMED TSB 02
REFLASH		TECH CHECKED THE EEC POWER RELAY. OK TECH CHECKED THE REPROGRAM OF THE PCM AS PER HOTLINE. TECH REPROGRAMMED THE PROCESSOR. AND ROAD TESTED. OK
REFLASH		POSSIBLY CAUSED BY COMPUTER PROCESSOR OUT OF CALIBRATION RECALIBRATE PROCESSOR PER SERVICE MESSAGE
HOTLINE		MASS AIR FLOW CONTACT HOTLINE TALKED WITH ENGINEER REPLACED MASS AIR FLOW PER HOTLINE AND RETEST DROVE SEVERAL TIMES OK TO RELEASE
REFLASH		REPROGRAM PCM CHECKED EEC AND FUEL PRESSURE 39PSI IGN SYSTEM DIAG AND NGS RECORDING AND PINPOINT TO EC REPROGRAMMED PCM AND REPLACED
NPF		TEST DROVE WDS TEST NO CODES PERFORMED MANUAL FUEL PRESS TEST CHECKED IGNITION SYSTEM CHK WIRING COULD NOT VERIFY
REFLASH		ROAD TEST EEC TEST NO STALL RELAY OK REFLASH PCM AND RECALIBRATE
REPLACED		PERFORM EEC AND PIN POINT TEST CHECK FOR CODES NONE FOUND IAC FAILING REMOVE AND REPLACE IACE REFLASH PCM AND ADJUST IAC TO 35%
TSB		1340 TRUCK STALLS INT WHILE DRIVING CK TSB AND SSM FOUND SSM 15494 RPL EEC POWER RELAY PER SSM RPL IAC PER SSM RR BATTERY AND TRAY FOR ACESS TO CHECK GROUNDS G104 ,G105 AND G101 ALSO CHE
REPLACED		REPLACE IAC AND MAPS SENSOR
TSB		TSB 02 11 6 PREFORMED TSB 02 11 6

REPLACED AND RETESTED ALL OK NEXT STEP TO PERFORMED PCM REPROGRAM TO THE LAT EST LEVEL. REPROGRAMED AND TEST AND MONOTRED RPM WITH THE DPFE, FTP AND VMV. DUTY CYCLE AND PRESSURE	C S VEH SHUT OFF WHEN DRIVING DOWN THE ROAD, STARTED BACK UP
	CUSTOMER STATES ENGINE CUTS RUNNING WHEN DRIVING? SAYS WHEN TURNING KEY TO START ONLY GETS A CLICKING NOISE?AFTER SITS A WHILE WILL START O.K.?
BODY, IAC AND EEC RELAY PER TSB REPROGRAMMED PCM PER TSB REROAD TESTED VEH OK	CUST STATES VEH STALLS WHEN GOING DOWN AN INCLINE AND FOOT IS OFF THE ACCELLERATOR CONCERN IS INT
SSION TEST 145 TALK TO FORD DENNIS GOODHART RECHECKED TSB 2 11 6 TALKED TO MIKE SCAMELLE REF NUMBER 03AC 0012 CHECKED PCM CONNETOR INSPECTED MASS AIR GASKET OK REPLACED	CUST STATES VEH STALLS WHEN DRIVING DOWN A DECLINE; CONCERN IS INTERMITTENT
	CUSTOMER STATES VEHICLE STALLED GOING AROUND THE CORNER DID RE START
	ENGINE STALLS AT STOPS
CKP WIRING CHECKED CONNECTORS 110 133 270 CHECKED DPFE SENSOR REPLACED MAF SENSOR RETEST OC BY 395 ROADTEST	CAR DIED AT 35MPH IN TRAFFIC DID RESTART
	CST STATES THAT THE VEH IS STALLING,HAPPENS WHEN COLD,ADVISE
	DIES AT TIMES WHILE DRIVING, DOES RESTART
	CUSTOMER STATES ENGINE STALLED WHILE COASTING IN TRAFFIC.
E TO VERIFY COMPLAINT NO PROBLEM FOUND AT THIS TIME	CUSTOMER STATES THAT WHILE DRIVING AROUND 30 MPH THE CAR DIED
	DIES WHILE DRIVING , RESTARTS RIGHT AWAY
11 6. RAN SELF TEST WITH WDS, SYSTEM PASS. MONITORED PIDS WITH WDS, REFER TO TSB ATTACHED TO REPAIR ORDER, ALL RESULTS ARE WRITTEN IN LEFT SIDE OF EACH STEP. REPROGRAMMED PCM WITH WDS, NEW	ENGINE DIED WHEN PULLING INTO PARKING SPACE, RESTARTED OK AFTER PUT INTO PARK POSITION. STARTS OK NOW
	CUSTOMER STATES THE VEHICEL STALLS WHEN DRIVING
	CK ENG STALLED WHILE DRIVING RESTART ALL OK
	SHUT DOWN WHILE DRIVING ON COUNTRY ROAD AROUND 35 MPH
	DRIVING DOWN ROAD TAKE FOOT OFF GAS CAR DIES
	C S VEHICLE CUTS OFF WHILE DRIVING
	WHEN DRIVING VEHICLE SHUT OFF AND STALLED OUT,IT STARTED RIGHT BACK UP
	CUST STATES CAR TRUCK DOES NOT PERFORM CORRECT VEHICLE STALLED WHILE DRIVING
CKED G100 EEC TEST NO CODES	CUST STS TRUCK STALL OUT WHILE VEH SPEED AROUND 45MPH
	STALLED TWICE FOR NO REASON
	STALLS WHILE DRIVING HAPPENED 1 TIME 1000 MILE AGO AND AGAIN THURS EACH TIME DRIVING HOME FROM D.C.

2002	17299	S11	1FMCU04182KB29921	3.0L	TALD	11	2001	6J09	11582	D21	1	571859	1000	STALLS
2002	17302	S11	1FMCU04182KB93322	3.0L	TALD	11	2001	2G04	12A650	D21	7	1707719	7000	AT STOP
2002	17303	S11	1FMCU04182KB29269	3.0L	TALD	11	2001	6D09	9E455	D21	6	1395106	6000	STALLS
2002	17304	S11	1FMCU04182KB84469	3.0L	TALD	11	2001	2G04	12A650	D21	6	2022941	6000	WHILE DRIVING
2002	17305	S11	1FMCU04182KB84365	3.0L	TALD	11	2001	2G05	RECAL	D21	2	686167	2000	STALLS
2002	17315	S11	1FMCU04182KB20469	3.0L	TALD	11	2001	2G04	12A650	D21	7	1801306	8000	STALLS
2002	17316	S11	1FMCU04182KB15274	3.0L	TALD	11	2001	2G05	RECAL	D21	1	691575	0	WHILE DRIVING
2002	17322	S11	1FMCU04182KB14464	3.0L	TALD	11	2001	2G04	DIAG	D21	0	297079	0	COASTING
2002	17325	S11	1FMCU04182KB12956	3.0L	TALD	11	2001	2G05	RECALEM	D21	9	2031081	7000	WHILE DRIVING
2002	17329	S11	1FMCU04182KB12945	3.0L	TALD	10	2001	7C05	14K069	D21	3	572430	1000	WHILE DRIVING
2002	17330	S11	1FMCU04182KB12346	3.0L	TALD	10	2001	2.00E+03	0E926	D21	8	1559373	4000	WHILE DRIVING
2002	17337	S11	1FMCU04182KB02262	3.0L	TALD	10	2001	7C05	14K069	D21	1	403240	0	DOWNHILL
2002	17338	S11	1FMCU04182KB02262	3.0L	TALD	10	2001	2.00E+03	0E926	D21	8	1760666	8000	DOWNHILL
2002	17339	S11	1FMCU04182KB02262	3.0L	TALD	10	2001	7B02	14401	D21	1	821086	1000	TURNING
2002	17340	S11	1FMCU04182KB01827	3.0L	TALD	10	2001	7C05	14K069	D21	1	376021	0	STALLS
2002	17350	S11	1FMCU04182KA93132	3.0L	TALD	10	2001	2G04	12A650	D21	6	1058560	6000	STALLS
2002	17361	S11	1FMCU04182KA92742	3.0L	TALD	10	2001	2G04	12A650	D21	9	1918606	15000	WHILE DRIVING
2002	17365	S11	1FMCU04182KA80695	3.0L	TALD	10	2001	2G04	12A650	D21	2	329567	0	WHILE DRIVING
2002	17366	S11	1FMCU04182KA79693	3.0L	TALD	10	2001	2.00E+04	9C815	D21	9	1595648	6000	WHILE DRIVING
2002	17358	S11	1FMCU04182KA79665	3.0L	TALD	10	2001	2G04	12A650	D21	9	1657917	6000	WHILE DRIVING
2002	17360	S11	1FMCU04182KA79663	3.0L	TALD	10	2001	2G04	12A650	D21	7	1358615	4000	WHILE DRIVING
2002	17361	S11	1FMCU04182KA79664	3.0L	TALD	10	2001	2G02	12A648	D21	10	2133098	10000	ACCELERATING

REFLASH		REPROGRAM PATS SYSTEM
SSM		CK ALL CONNECTIONS RELAYS AND FUSES FOR PROPER CONNECTION CK PCM CK CODES CK CODES CK SSM FOUND REPAIR TESTED FOUND FIX REPROGRAMED PCM
SSM		9883 CC42 VERIFY ENGINE RUNS ROUGH AND STALLS BUT DID NOT VERIFY BACKFIRE XX PERFORM EEC TEST CODES PO401 AND P1131 AND P1161 XX ALSO CAN HEAR VACUUM HISSING SOUND XX PINPOINT TEST XX FOUND VACUUM LI
DIAG		PCM EEC (QUICK TEST) DIAGNOSIS
TSB		ROAD TEST ENG DIDNOT STALL OUT STAR TEST CK TSB PIDS TEST REFLASH PCM TO LATEST PER SSM
TSB		TEST DROVE VEHICAL COULD NOT VERIFIE CONCERN WDS TEST NO CODES PREFORM TSB 02 11 6 CHK PIDS AND DATTA LOGER ALL PREFORM REPROGRAM VEHICAL IS WITH IN THE BUILD DATE RETEST DROVE OK NO STALLING.
REFLASH		D21,07 ROADTEST AND CHECK FOR STALLING CONCERN, COULD NOT DUPLICATE CONCERN, PERFOM DCL MONITOR AND RECORD, TEST INJECTOR FLOW, ADJUST BASE IDLE AND REPROGRAM PCM
NPF		12 EEC DIAG. P1111. PID MONITOR ROAD TEST. UNABLE TO DUPLICATE SYMPTOM. 6120
TSB		7546 VEHICLE STARTED NORMALLY. EEC TEST, PASSED. ROAD TESTED, DIED ONCE COMING TO STOP, STARTED OK. DCL DISPLAY, NORMAL READINGS. ROAD TEST W WDS, READINGS SEEM OK. CHECK OASIS, FOUND TSB 02 11 0
INOP		INOP EEC (QUICK TEST) DIAGNOSIS
INOP		INOP EEC (QUICK TEST) DIAGNOSIS
SSM		546 STICKING IAC TEST EEC SYSTEM KOEO P1111 KOEO P1111 KOERP1111 PERFORMED DCL DISPLAY PERFORMED ROADTEST MONITOR R+R BATTERY TRAY CK GROUND TO PCM CK GROUND ON BULK HEAD CK CONNECTIONS AT C270D C
REPLACED		DIAGNOSIS,EEC TESTED,PINPOINT TESTED,IGNITION TESTED, MONITOR SYSTEM,REPLACED RELAY AND THROTTLE BODY,RETEST
POOR CONNECTION		1120 POOR CONNECTION TEST EEC SYSTEM KOEO P1111 KOEC P1111 KOERP1111 PERFORM DCL DISPLAY INSTALLED VDR CUSTOMER THEN TOOK VEHICLE CUSTOMER RETURNED VEHICLE UPLOAD AND ANALYZE RECORDINGS PINPOINT TE
TSB		HOOK UP WDS CK FOR CODES NO CODES. CK OASIS FOR TSBS AND SPEC SERVICE S FOUND SSM 16454 CK RELAY CONNEC TIONS AND FOR LOOSE PCM GROUND G104 AND G105 CK G100 AT BULKHEAD CK IAC VALVE FOR CORRECT PART N
ADJUST		CUST# D21 CONC# 07 BAS# 12A650 DIAG AND RESET THROTTLE STOP
REFLASH		PERFORMED EEC QUICK TEST DIAGNOSIS, PINPOINT TEST, DCL DISPLAY TEST, RECORDER MONITOR ROAD TEST, REPROGRAM PCM, REPEAT FINAL QUICK TEST, RECHECK.
NPF		991 KOEO P1111 KOEC P1111 KOER P1111 7627 3.0L COULD NOT VERIFY PROBLEM AT THIS TIME HOOKED UP WDS EEC TEST DCL DISPLAY FUEL PRESSURE TEST DCL MONITOR TEST UVC NO LOG USED WDS QC BY 385 ROADTEST
TSB		WDS...KOEO...PASS...DCL...PREFORMED TSB 02 11 6 IN IT3 INTIRITY. ROAD TESTED ...OK.
ADJUST		WDS...KOEO...PASS...DCL...SUSPECT BASE IDLE...RESET BASE IDLE AND ROAD TESTED 14 MILES WITH WDS...EVERYTHING WAS IN
SSM		WDS...KOEO...PASS...DCL...WDS ROAD TESTED, UNABLE TO DUPLI CATE...RAN OASIS AND FOUND SSM FOR THIS CONCERN.....
POOR CONNECTION		10185 W TEST EEC SYSTEMP0116,P0123, PINPOINT TEST MONITOR AND RECORD PID DATA. TEST CIRCUIT #464 LG RD FROM PCM PIN#36 TO ECT PIN #1 AND CUIRCUIT #69 FROM PCM PIN #61 OG TO PIN #2 AT ECT SENSOR .TR

	CUST STATES THAT VEHICLE CUT OUT, NO P S OR POWER BRAKES AND ALL DASH WARNING LIGHTS CAME ON
	CK CAR STOPPED RUNNING AND ALL THE LIGHT CAME ON
NE OFF AT REAR OF INTAKE WHICH CAUSED THE 3 CODES XX RAN OASIS AND NO SSM OR TSB APPLY XX CLEAR CODES AND ROAD TEST AND PERFORM DRIVE CYCLE TEST AND RETEST EEC PASS XX EEC CODES WERE IN	CUST STS HEARD ENGINE BACKFIRE,RUNS ROUGH AND STALLS
	CUST REPORTS THAT THE VEHICLE STALLED OUT WHILE DRIVING AT APPROX 35 40 MPH BEGAN TO LOOSE POWER THEN DIED OUT STARTS AND RUNS NOW
	CHECK FOR STALLING
	INTERMITT STALLS SEE TSB 02 11 6
	CUSTOMER STATES VEHICLE STALLS WHILE DRIVING.
	CUSTOMER STATES ON DEACCELERATION THE ENGINE STALLED ONCE (CK ENGINE LIGHT IS NOT ON)
6. PERFORMED TSB, REPROGRAMMED PCM W LATEST CALIBRATION, OTHER STEPS IN TSB OK. ROAD TEST, RUNS NORMALLY.	CUSTOMER STATES WHILE DRIVING ALT LIGHT AND CHECK ENG LIGHT CAME ON AND ENG DIED, WONT START
	CK WHILE DRIVING VEHICLE DIED, DIED WHILE ACCELERATING UP A HILL, FIVE MINUTES LATER VEHICLE STARTED RIGHT UP
	AT 40 MPH THE ENGINE HAS DIED0 TWICE IN 4719 MILES
270E C270D PINPOINT TEST AND REPLACED PCM RELAY AND IDLE AIR CONTROL PER SSM 15434 RETEST EEC SYSTEM KOEO P1111 KOEC P1111 KOER P1111	CUST STATES LAST NIGHT CAR STALLED ON CUSTOMER WHEN COMING OFF THE MOUNTAIN NOTE CAR JUST PURCHASED
	VEHICLE STALLS ON DECELL STARTS RIGHT BACK UP MOSTLY ON DECE POSSIBLE DOWN HILL READ RO ON SEAT HAVE DON I INVOLVED
ST AND TRACE WIRING IN ENGINE COMPARTMENT FOUND POOR CONNECTION IN BULKHEAD CONNECTOR AT FIREWALL REPAIRED POOR CONNECTION TO EEC IGNITION CIRCUIT RETEST EEC SYSTEM KOEO P1111	VEHICLE CUTS OUT IN MID DRIVE LAST CUT OUT ON A TURN
O CK CONNECTIONS C270 C AND D AND E FOR LOOSE CONNECTIONS REPLACED PCM POWER RELAY	VEHICLE TOWED IN STALLS OUT
	CUST STATES WHEN COLD VEHICLE DIES AFTER STARTING
	ENGINE DIED WHILE DRIVING,LOCKED STEERING WHEEEL
	LAST NIGHT WHILE DRIVING THE TRUCK SHUT DOWN THEN STARTED UP AGAIN AND RUNNING FINE CHECK ADVISE
	CUSTOMER STATES THAT THE TRUCK WILL DIE WHILE DRIVING. HAS BEEN IN BEFORE FOR THE SAME THING. TAMMY
	CUST STATES VEH STALLS WHILE DRIVING. THIS WILL BE THE SECOND TIME IN FOR THE SAME ISSUE
	CUST STATES THAT THE VEH STALLS WHILE DRIVING SEEMS TO ONLY DO IT WHEN GOING UP HILL AND
ACE WIRING AND REPAIR CONNECTOR #C139. LOOSE PIN INSIDE CONNECTOR REPAIR WIRING AND RETEST,OK ,CLEAR CODES ROADTEST	*** ENG STALLS OA ACCEL OR IN TRAFFIC ERATTIC ENGINE IDLE *** *DRIVEABILITY CHECK ENGINE LIGHT IS ON ALL THE TIME P20 CHECK ENGINE LIGHT TROUBLES L'

2002	17366	S11	1FMCU04162KA71269	3.0L	TALD	10	2001	2.00E+03	9F715	D21	9	3022945	18000	WHILE DRIVING
2002	17367	S11	1FMCU04162KA71276	3.0L	TALD	10	2001	2G02	129579	D21	9	1288885	9000	STALLS
2002	17368	S11	1FMCU04162KA71275	3.0L	TALD	10	2001	2G04	12A660	D21	9	998005	9000	WHILE DRIVING
2002	17377	S11	1FMCU04162KA69804	3.0L	TALD	10	2001	7C05	14N069	D21	9	1138351	4000	AT STOP
2002	17379	S11	1FMCU04162KA69864	3.0L	TALD	10	2001	2G05	RECALEM	D21	10	2113553	18000	STALLS
2002	17383	S11	1FMCU04162KA64662	3.0L	TALD	9	2001	2G04	DIAG	D21	1	288634	0	UPHILL
2002	17385	S11	1FMCU04162KA63113	3.0L	TALD	9	2001	2G04	DIAG	D21	7	1128795	6000	STALLS
2002	17389	S11	1FMCU04162KA62808	3.0L	TALD	9	2001	1H06	9J460	D21	2	340555	2000	AT STOP
2002	17394	S11	1FMCU04162KA60412	3.0L	TALD	9	2001	2.00E+03	9F715	D21	11	2448274	12000	WHILE DRIVING
2002	17396	S11	1FMCU04162KA48559	3.0L	TALD	9	2001	7G02	14401	D21	7	987609	4000	NO TEXT
2002	17400	S11	1FMCU04162KA48559	3.0L	TALD	9	2001	2.00E+03	9F715	D21	6	880054	3000	WHILE DRIVING
2002	17406	S11	1FMCU04162KA44566	3.0L	TALD	9	2001	7C05	14N069	D21	4	555279	6000	CUST TEXT
2002	17407	S11	1FMCU04162KA44569	3.0L	TALD	9	2001	7C05	14N069	D21	1	249702	0	STALLS
2002	17414	S11	1FMCU04162KA43508	3.0L	TALD	9	2001	2.00E+03	9F715	D21	7	1054366	4000	WHILE DRIVING
2002	17415	S11	1FMCU04162KA43461	3.0L	TALD	9	2001	2.00E+03	9F715	D21	12	2139078	17000	DOWNHILL
2002	17417	S11	1FMCU04162KA40575	3.0L	TALD	9	2001	2G06	RECAL	D21	3	411171	3000	WHILE DRIVING
2002	17443	S11	1FMCU04162KA34561	3.0L	TALD	8	2001	2.00E+03	9F715	D21	7	1142401	7000	WHILE BRAKING
2002	17450	S11	1FMCU04162KA34064	3.0L	TALD	8	2001	2.00E+03	9F715	D21	10	1815773	6000	WHILE DRIVING
2002	17453	S11	1FMCU04162KA27440	3.0L	TALD	8	2001	2.00E+03	9F715	D21	4	550235	7000	AT STOP
2002	17457	S11	1FMCU04162KA25874	3.0L	TALD	8	2001	7C05	14N069	D21	8	1139690	3000	STALLS
2002	17459	S11	1FMCU04162KA25812	3.0L	TALD	8	2001	2.00E+03	9F715	D21	4	798579	3000	STALLS
2002	17466	S11	1FMCU04162KA15907	3.0L	TALD	8	2001	2G06	RECAL	D21	12	2314524	12000	WHILE DRIVING
2002	17469	S11	1FMCU04162KA14185	3.0L	TALD	8	2001	2.00E+03	9F715	D21	4	377777	6000	WHILE DRIVING
2002	17477	S11	1FMCU04162KA09507	3.0L	TALD	8	2001	7C05	14N069	D21	8	2101969	11000	WHILE DRIVING

DIAG		VEHICLE IS EQUIPPED WITH REV LIMITER FEATURE WHICH CAUSES CONCERN EXPERIENCED WHEN REVVING ENGINE OVER 4,000 RPM, RAN
HOTLINE		CALLED HOTLINE DID DIAG WDS SELF DCL ETC PER HOTLINE REPL MAF SENSOR REPL RECHECK ROADTEST RELEASEDVEH PER HOTLINE REPAIR ORDERD
REFLASH		ROADTETS RUN WDS SELF DCL PINPWT CK TP VOLTS .89 OK REPROGRAM PCM FINAL TEST ROADTETS OK
SSM		STARTED AND RAN OK ,EEC TEST NO DTCS RAN OASIS SSM15599 TO REPROGRAM PCM, REPLACE EEC RELAY CHECK PINS AND EVAP REPROGRAMED PCM, TIGHTENED PIN9 AND REPLACE RELAY, BLOW OUT EVAP HOSE
REFLASH		DIAG,PERFORM WDS TEST REPROGRAM
NPF		FUEL PRESSURE TEST 42PSI EEC TEST NGS MONITOR DCL DISPLAY IGN TEST PINPOINT TEST ROAD TEST COULD NOTDUPLICATE CONCERN
NPF		PERFORMED DIAG NO CODES STORED, COULD NOT VERIFY AT TIME
REPLACED		DPFE SENSOR INOP PERFORMED EEC DIAGNOSIS. PID MONITOR. REPLACED DPFE SENSOR. RETESTED. ALL OK.
TSB		RAN EEC NO CODES. FOLLOW TSB 02 11 06, MONITOR IDLE AIR CONTROL PID AT750 RPMS, IAC DUTY CYCLE NOT IN SPECS. R&R IAC VALVE, MONITOR AND REPROGRAM PCM. MONITOR EVAP VM DUTY CYCLE, MONITOR FTP VOLTS
SSM		CHECKED COMPLETE MAIN WIRE HARNESS AND ALL OTHER CHECKS PER RANDALL CORLEW (FBE)
STICKING		EEC TEST PASS ROADTEST MONITOR PIDS REPL STICKING IAC RETEST ROADTest
SSM		WDS...KOEO...PASS...DCL...WDS ROAD TESTED 10 MILES...UNABLE TO DUPLICATE CONCERN...RAN OASIS AND FOUND SSM FOR BAD
REPLACED		TESTED EEC AND FUEL SYSTEMS USING WDS. RAN INJECTOR FLOW TEST. REPLACED FUEL PUMP RELAY, CHECKED AND CLEANED GROUNDS AND POWER CIRCUITS TO PCM.
REPLACED		D21 41 YF1Z 9F715 AA WDS TEST,PINPOINT TEST,FUEL PRESS AND LEAKDOWN TEST,DATA LOGGER,REPLACE IAC,REPROGRAM PCM
TSB		VERIFIED, PERFORMED TSB 02 11 06 AS PER INSTRUCTED, ROAD TESTED
ADJUST		3022 BASE IDLE SPEED WARRANTY EEC TEST PASS ROADTEST WITH MONITORS PIN POINT TEST PID DATA MONITOR IAC PERCENTAGE TOO HIGH ADJUSTED BASE IDLE SPEED BROUGHT IAC % DOWN TO 32% RETEST OK
REPLACED		7136 WARRANTY PERFORMED WDS TESTS SEE SHEET AND PRINTOUT. REPLACED PCM EEC RELAY. REPLACED IAC. REPROGRAMMED PCM. RETEST AND ROAD TEST.
TSB		5569 CALLED OASIS. PERFORMED KOEO, KOER SELF TEST NO CODES. PERFORMED POWER BALANCE OK. PERFORMED FUEL PRESSURE LEAKDOWN TEST BOTH STATIC AND RUNNING, NORMAL PRESSURE. PERFORMED FUEL INJECT BALANCE
REPLACED		CUTTING OF AT IDLE WHEN COMING TO A STOP WILL STRART RIGHT BACK UP VERIFY EEC DIAG. MEMORY CODE 1507 IAC PINPOINT REPLACED IAC
DIAG		ENGINE STALLS EEC (QUICK TEST) DIAGNOSIS
REPLACED		FIRST START/RAN ENG STALL WDS KOEO PASS KOEOC PASS KOER PCS06 KE 1 2 3 4 5 6 7 8 9 10 Hz/sF OK REPL IAC R&R IAC MOTOR RE
REFLASH		TEST DRIVE 7.5 MILES NEVER STALLED OR TRIED TO STALL WDS DIAG KOEO PASS KOER PASS DATA LOGGER OK. FUEL TESTS OK IGN TESTS OK COMPRESION GOOD. CHECK PCM CALIB OUT OF DATE REFLASH PCM. NPF
REPLACED		5750 IAC VALVE STICKING WDS DIAG ,KOEO,KOER,DATALOGGER TEST , REPLACE IAC VALVE & RESET KAM , TEST DRIVE OK
TSB		11410 14N089 42 TEST DROVE, TESTED THE EEC SYSTEM, ALL PASSED, REPROGRAMMED PCM, MONITORED PIDS, REPLACED PCM RELAY, AND TESTED EVAP SYSTEM AS PER TSB 02 11 6, RETEST DROVE OK

	CUSTOMER STATES VEHICLE SHUT OFF WHILE DRIVING, NOW IF YOU REV. ENGINE BEYOND 4,000 RPM ENGINE SHUDDERS
	CHK PER CUSTOMER VEH STALLING (REPR AGAIN AND RESET IDLE)
	CUST STATES CAR CUTS OUT INTERMITENLY 40 50MPH.
	CUSTOMER STATES THAT TRUCK JUST DIED ON THE ROAD SITTING AT AN INTERSECTION.
	CUSTOMER COMPLAINS THAT VEHICAL STALLS CUTS OFF WHEN MAKING TURNS..
	CUSTOMER STATES WHEN GOING UP HILL THIS AM VEHICLE STALLED, CUSTOMER WAITED A FEW MOMENTS THAN RESTARTED
	C S VEHICLE KEEPS STALLING OUT
	CUSTOMER STATES ENGINE STALLED SATURDAY AT A STOP AFTER DRIVING ABOUT 5 MINUTES
PIDS OK. DISCONNECT EVAP VENT LINE AND BLOW OUT AIR, NO OBSTRUCTIONS. CHECK ECC RELAY OK. ROAD TEST FOR 5 CLOSED THROTTLE DECLES FROM 40 10 RPMS OK.	CUSTOMER STATES THAT THE VEHICLE STALLS WHILE DRIVING INTERMITTENTLY
	DIES OUT ABOUT 5 MINS AFT YOU START WHILE DRIVING COLD
	CUST STATES CAR IS STALLING ALOT WHEN STOPPING,EVEN WHILE DRIVING IT WILL STALL OUT, BUT RESTARTS IM
	CUSTOMER STATES THAT THE VEHICLE STALLS AND DIES OUT ON HER IN THE MORNING CRANKS BUT WONT START.
	ON ONE OCCASION THE VEHICLE CUT OUT WHILE DRIVING ON A ATRAIGHTAWAY AT ABOUT 40 MPH RESTARTED EASILY
	CUSTOMER STATES ENGINE SHUT DOWN WHILE COASTING DOWNHILL ON OLD DUTCH LANE
	OWNER STATES THAT CAR DIED WHILE DRIVING.
	VEHICLE STALLED WHEN SLOWING AND MAKEING A TURN
TEST PASS. PERFORMED PID DATA TEST. FOUND IAC OUT OF SPECS, TOO HIGH. ASL PER TSB 02 11 06 REMOVED AND REPLACED IAC VALVE WITH UPDATED PART NUMBER. REPERFORMED IAC DUTY CYCLE TEST STILL OUT	THE VEHICLE HAS STALLED WHILE DRIVING ADVISE, SEE ATTACHED
	C S VEH. CUTTING OFF AT IDLE WHEN COMMING TO A STOP WILL START WRIGHT BACK UP
	CK BRAKE PEDAL GOING TO FLOOR,STIG GOT TIGHT ENGINE STALLED ?
	CHECK REASON ENG STARTS & STALLS
	CUSTOMER STATES WHILE DRIVING THE VEHICLE WILL STALL DOES NOT MATTER THE SPEED, HAS HAD A COUPLE OF TIMES WHEN IT
	CUSTOMER STATES VEH STALLS WHILE DRIVING
	D21 CUSTOMER STATES WHILE DRIVING AT 40MPG VEHICLE JUST DIED

2002	17484	511	1FMCU04172KD05401	3.0L	TALD	6	2002	2.00E+03	9F715	D21	2	2104700	1000	WHILE DRIVING
2002	17485	511	1FMCU04172KD05401	3.0L	TALD	6	2002	2.00E+04	9C915	D21	1	2065179	0	STALLS
2002	17486	511	1FMCU04172KD00499	3.0L	TALD	6	2002	4C03	5.00E+212	D21	0	1839580	0	LACKS POWER
2002	17487	511	1FMCU04172KD05733	3.0L	TALD	6	2002	2.00E+03	9F715	D21	3	2419312	1000	WHILE DRIVING
2002	17497	511	1FMCU04172KD21475	3.0L	TALD	5	2002	2G04	DIAG	D21	3	2223079	4000	WHILE DRIVING
2002	17503	511	1FMCU04172KD02179	3.0L	TALD	4	2002	2.00E+03	9F715	D21	3	1899833	0	TURNING
2002	17504	511	1FMCU04172KD02179	3.0L	TALD	4	2002	2G02	128579	D21	3	2306104	0	WHILE DRIVING
2002	17505	511	1FMCU04172KC99995	3.0L	TALD	4	2002	7C05	14N089	D21	5	2259490	2000	WHILE DRIVING
2002	17506	511	1FMCU04172KC99995	3.0L	TALD	4	2002	1H03	9J480	D21	2	2007223	0	STALLS
2002	17513	511	1FMCU04172KC76511	3.0L	TALD	3	2002	2.00E+03	9F715	D21	1	1284506	0	DSCELL
2002	17514	511	1FMCU04172KC73716	3.0L	TALD	3	2002	2B04	12A650	D21	4	2022262	4000	WHILE DRIVING
2002	17525	511	1FMCU04172KC37525	3.0L	TALD	2	2002	2.00E+03	9F715	D21	5	2447170	6000	WHILE DRIVING
2002	17530	511	1FMCU04172KC29959	3.0L	TALD	2	2002	2B06	RECAL	D21	3	1990508	1000	WHILE DRIVING
2002	17548	511	1FMCU04172KC00820	3.0L	TALD	1	2002	2G04	12A650	D21	3	1118699	5000	WHILE DRIVING
2002	17544	511	1FMCU04172KC00820	3.0L	TALD	1	2002	2.00E+03	9H307	D21	7	2273686	13000	STALLS
2002	17545	511	1FMCU04172KC00820	3.0L	TALD	1	2002	7C06	14N089	D21	6	1675752	9000	DOWNHILL
2002	17546	511	1FMCU04172KB99128	3.0L	TALD	1	2002	2.00E+03	9F715	D21	6	1990883	11000	WHILE DRIVING
2002	17549	511	1FMCU04172KB99990	3.0L	TALD	1	2002	7B02	10349	D21	0	1245307	0	STALLS
2002	17554	511	1FMCU04172KB75512	3.0L	TALD	1	2002	2G02	128579	D21	3	2004615	5000	WHILE DRIVING
2002	17555	511	1FMCU04172KB75982	3.0L	TALD	12	2001	2B04	12A650	D21	6	1760553	3000	AT STOP
2002	17557	511	1FMCU04172KB75982	3.0L	TALD	12	2001	2B06	RECALEM	D21	3	1110039	1000	WHILE DRIVING
2002	17558	511	1FMCU04172KB75982	3.0L	TALD	12	2001	2G02	128579	D21	4	1152807	1000	WHILE DRIVING
2002	17565	511	1FMCU04172KB64982	3.0L	TALD	1	2002	2B05	RECALEM	D21	4	1606936	4000	WHILE DRIVING
2002	17568	511	1FMCU04172KB64989	3.0L	TALD	12	2001	1R03	9J480	D21	6	2230013	9000	STALLS
2002	17575	511	1FMCU04172KB64258	3.0L	TALD	12	2001	2B06	RECAL	D21	2	1904133	2000	NO TEXT
2002	17587	511	1FMCU04172KB99900	3.0L	TALD	11	2001	2.00E+03	9F715	D21	7	1990929	17000	WHILE DRIVING

REFLASH		CHECK OUT DIES AT STOPS EEC TEST PINPOINT TEST.MONITOR NO CODES.R AND R IAC.RETEST EEC RESET KAM.REPROGRAM SSM.MT12A650 NO LABOR OP LISTED IN SLTSTO PERFORM DRIVE CYCLE TEST.
REPLACED		TEST DRIVE TO VERIFY DIES.EEC TEST PINPOINT TEST.MONITOR.REPLACE FUEL VAPOR VALVE.RETEST EEC.MT12A650 NO LABOR OP LISTED IN SLTS TO PERFORM DRIVE CYCLE TEST.REPROGRAM PCM.
REPLACED		FAILED CATALYTIC CONVERTOR AND DPFE SENSOR REPLACED CATALYTIC CONVERTOR AND DPFE SENSOR AND VERIFIED RE PAIR
REPLACED		DIAGNOSTICS AND REPLACE IAC MOTOR
TSB		SHOP FOREMAN DROVE VEH 15 MILES NO STALLING AT THIS TIME CCC D21, CC 42, SPN DIAG CONNECTED WDS AND TESTED EEC SYSTEM KOEO,KOER,KOEOC,P1000 PERFORMED PID DATA LOGGER AND ROAD TESTED ALL PID READINGS N
TSB		PERFORM WDS COMPUTER TEST KOEO ALL PASS CHECK DCL PIDS RUNS SSMS AND TSBS FOUND 02 11 06 PERFROM PINOINT TEST REPLACE IAC THROTTLE BODY EVAP VALVE AND RETEST OK REPROGRAMM PCM AS NEEDED AND TEST DRIVE
DIAG		2 WDS CHECKED OVER, TEST PASSED. DCL, PIDS, O.K. IGNITION TEST, PASSED. FUEL SYTEM TEST, PASSED, CALLED
REPLACED		DIAG EEC TEST FOUND EEC NOT OPERATING PROPERLY, RPL RELAY RECK OK
TSB		NO DTC. PERFORM TSB 02 11 06, ALL WITHIN SPECS. INSPECT PCM PINS TO HARNESS CONNECTIONS, OK. INSPECT CONNECTIONS TO C270 C110 AND C133 FOR WATER INTRUSION. RAN DATA LOGGER FOR PIDS. DPFE AND MAF SENSO
TSB		WDS DIAG AND REPLACED IAC MOTOR,UPDATE PROCESSOR PER TSB020909
REFLASH		PROGRAM PCM EEC (QUICK TEST) DIAGNOSIS
DIAG		00 EEC (QUICK TEST) DIAGNOSIS
REFLASH		EEC TEST AND PINPOINT TEST REPROGRAM PCM
DIAG		RAN EEC TEST OK DCL DISPLAY OK MONITOR TEST OK IGNITION SYSTEM TEST OK FUEL PUMP TEST OK TEST DROVE 8 MILES COULD NOT VERIFY CONCERN OC TEST DROVE COULD NOT VERIFY CONCERN
REPLACED		RAN EEC TEST CODE P1000 NO CODES TO INDICATE CHECK ENGINE LIGHT HAS BEEN ON RAN DCL DISPLAY OK MONITOR TEST OK IGNITION SYSTEM TEST OK FUEL PUMP TEST OK REPLACED FUEL PUMP RETEST OK
SSM		WDS...KOEO...P1000...DCL...WDS ROAD TEST...FUEL PRESS. TEST... ...PINPOINT...CK. OASIS AND FOUND SSM REQUARDING THIS CONCERN
REFLASH		PERFORM EEC TESTS AND MONITOR TESTS AND FUEL PRESSURE TESTS. PERFORM PINPOINT TESTS, REPROGRAM POWERTRAIN CONTROL MODULE AS PER FORD HOT LINE ENGINEERING
REPLACED		BATTERY CHARGE INDICATOR WAS ON ALTERANTOR CHARGING SYSTEM RAN PIN POINT TEST REPLACED ALTERNATOR RECHECKED OK
REPLACED		ROAD TEST CUST STATES VEHICEL STALLS CANNOT VERIFYCONCERN NO CODES IN PCM PER HOTLINE REPLACE MAP S ENSOR DPFE SENSOR WITH REVISED PART NUMBERS RD TEST OK
DIAG		DIAG EEC (QUICK TEST) DIAGNOSIS
SSM		T EEC TEST NGS REPROGRAM PCM AS PER SSM15599
REPLACED		TIME TO ACCESS LS FRT SEAT AND CARPET CHECK CONNECTORS NGS TESTS NO CODES. EXTENDED ROAD TEST NO CONDITION REPLACE MAF SENSOR
TSB		RAN EEC TEST,SYSTEM PASSED,CHECKED SPECIAL SERVICE MESSAGES FOUND TSB 02 11 6 ONSTALLING WHILE DRIVING REPROGRAM PROCESSOR PER TSB D21 42 RECAL
INOP		INOP EEC (QUICK TEST) DIAGNOSIS
REFLASH		SCOPE AND EEC TESTS OK ALL TESTS PASS UPDATED PCM TO LATEST CALIBRATION RETESTED OK
REPLACED		CAUSAL 0F715 CC 41 CCC D21 CONNECTED TO NGS, RAN KOEO, KOER, REPLACED IAC (STICKING) RETESTED, ROADTESTED

	DIES WHILE DRIVING.
	VEHICLE DIES INTERMITTENTLY.
	CUSTOMER STATES: LACK OF POWER
	CUST STATES THAT THE CAR STALLS OUT AT ANY TIME WHEN DRIVING (CK AND ADVISE)
ORMAL COULD NOT CONFIRM CONCERN RAN OASIS FOR MESS AND FOUND TSB 02 11 8 PERFORMED TSB OPER AND NO LATER CALIBRATION FOUND TSB SERVICE PROCE	CUST STATES THE ENGINE STALLS WHILE DRIVING, AT HIGHWAY SPEEDS, CUST NOTICES WHEN SLOWING DOWN THEN TRYING TO
	CHECK FOR STALLING WHEN TURNING RIGHT AND AT 40 AND 45 MPH. THIS HAS HAPPEND TWO TIMES. HAD A C ON AND
	REFERENCE TO RO#[illegible]29 ON 7 11 02 TECH#26 STALLING WHILE DRIVING
	D21 CUSTOMER STATES ENGINE WILL STALL AT TIMES WHILE DRIVING.CUTS OUT AT 4000 RPMS
R RESTRICTED. REPLACE DPFE AND MAF SENSOR. RERUN TEST, PASS.	VEHICLE STALLED
	CUSTOMER STATES VEHICLE DIES ON DECELERATION ABOUT 40MPH DOWN DODGE STREET NO WARNING IT HAS DIED
	CUST STATES CK STALLS WHILE DRIVING
	RECHECK ENGINE STALLED OUT AGAIN WHILE DRIVING PRETTY RED WARNING LIGHT CAME ON (OIL LIGHT)
	ENGINE STALLS WHILE DRIVING
	CUSTOMER STATES THE ENGINE DIED WHILE DRIVING
	CUSTOMER STATES THAT THE CHECK ENGINE COMES ON AND OFF INTERMITTENTLY, WHEN THIS HAPPENS, THE VEHICLE STOPS
	CUST STATES THE VEH INTERMITT JUST UP AND DIES,WILL RESTART,SEEMS TO HAPPEN ON DOWNHILLS...SSM ??
	CUSTOMER STATES VEHICLE WILL SHUT OFF WHILE DRIVING, MORE SO AFTER FIRST STARTED
	CUSTOMER STATES VEHICLE DIES INTERMITTENLY EVERYTHING SHUTS DOWN
	CUSTOMER STATES VEHICLE SHUTS OFF WHILE DRIVING.
	CUSTOMER REPORTS CAR WAS STALLING NOW HAS STOPPED
	STALLS OUT WHILE DRIVING. D21 92
	STALLS WITH FOOT ON GAS 35 OR BELOW NO CK ENGINE LIGHT D21 42
	VEHICLE STALLED WHILE DRIVING ON WAY TO WORK TODAY, AFTER SITTING BRIEFLY, RESTARTED AND DROVE OKAY. CHK AND ADVISE
	CUSTOMER STATES THAT THE VEHICLE STALLS AT TIMES WHEN AT A STOP
	STALLS DRIVING

2002	17598	S11	1FMCU04172KB28648	3.0L	T/A,D	11	2001	2.00E+03	9F715	D21	1	409315	0	WHILE DRIVING
2002	17591	S11	1FMCU04172KB22980	3.0L	T/A,D	11	2001	2.00E+03	9E999	D21	7	2400192	8000	WHILE BRAKING
2002	17592	S11	1FMCU04172KB14716	3.0L	T/A,D	10	2001	2905	RECAL	D21	5	1039561	8000	WHILE DRIVING
2002	17595	S11	1FMCU04172KB13151	3.0L	T/A,D	11	2001	2905	RECAL	D21	1	697576	1500	STALLS
2002	17599	S11	1FMCU04172KB12222	3.0L	T/A,D	10	2001	2905	RECAL	D21	6	1218229	6500	COASTING
2002	17601	S11	1FMCU04172KB03985	3.0L	T/A,D	10	2001	2.00E+03	9F715	D21	9	2061067	10000	LOW IDLE
2002	17602	S11	1FMCU04172KB03606	3.0L	T/A,D	10	2001	2905	RECAL	D21	8	1656212	9000	WHILE DRIVING
2002	17603	S11	1FMCU04172KB03596	3.0L	T/A,D	10	2001	7C05	14N069	D21	3	621138	3000	WHILE DRIVING
2002	17611	S11	1FMCU04172KB01448	3.0L	T/A,D	10	2001	2.00E+03	9F715	D21	2	618021	3000	STALLS
2002	17622	S11	1FMCU04172KA83494	3.0L	T/A,D	10	2001	2905	RECAL	D21	6	1523291	7000	COASTING
2002	17627	S11	1FMCU04172KA82291	3.0L	T/A,D	10	2001	7C05	14N069	D21	6	1099336	2000	WHILE DRIVING
2002	17628	S11	1FMCU04172KA80033	3.0L	T/A,D	10	2001	2.00E+04	9C915	D21	11	2382270	12000	WHILE DRIVING
2002	17632	S11	1FMCU04172KA76122	3.0L	T/A,D	10	2001	2905	RECAL	D21	10	2391339	13000	WHILE DRIVING
2002	17637	S11	1FMCU04172KA70019	3.0L	T/A,D	10	2001	2.00E+03	9F715	D21	8	1015971	5000	DOWNHILL
2002	17640	S11	1FMCU04172KA69095	3.0L	T/A,D	9	2001	9G04	12A960	D21	10	2203628	21000	WHILE DRIVING
2002	17641	S11	1FMCU04172KA69095	3.0L	T/A,D	9	2001	2.00E+03	9F715	D21	11	2391165	21000	STALLS
2002	17642	S11	1FMCU04172KA69803	3.0L	T/A,D	10	2001	2.00E+03	9F715	D21	6	961914	4000	WHILE DRIVING
2002	17646	S11	1FMCU04172KA68015	3.0L	T/A,D	10	2001	2905	RECAL	D21	11	2385447	10000	STALLS
2002	17656	S11	1FMCU04172KA61711	3.0L	T/A,D	9	2001	2.00E+03	9F715	D21	5	714627	9000	WHILE DRIVING
2002	17676	S11	1FMCU04172KA44557	3.0L	T/A,D	9	2001	2.00E+03	9F715	D21	3	399629	2000	WHILE DRIVING
2002	17681	S11	1FMCU04172KA44116	3.0L	T/A,D	9	2001	1A03	8006	D21	4	788170	1000	STALLS
2002	17683	S11	1FMCU04172KA40891	3.0L	T/A,D	9	2001	7V01	14289	D21	12	2391791	11000	WHILE DRIVING
2002	17684	S11	1FMCU04172KA39979	3.0L	T/A,D	8	2001	7C05	14N069	D21	3	440389	1000	WHILE DRIVING
2002	17686	S11	1FMCU04172KA34205	3.0L	T/A,D	9	2001	1H03	9J460	D21	3	376335	6000	WHILE DRIVING

REPLACED		ENGINE DIAG TEST AND REPLACED IAC VALVE FOR STICKING AND REPLACED EEC RELAY OPEN AND RETEST
REFLASH		THROTTLE BODY ELECTRONIC DIAG ALL PASSED,ROAD TEST MONITOR PIDS,REPROGRAMED PROCESSOR REPLACED THROTTLE BODY,ANDIAC VALVE,RETEST OK
TSB		NGS DIAGNOSIS, NO CODES. PERFORM PINPOINT AND PID DATA & MONITOR. CHECK FUEL PRESSURE, OK. CHECK IGNITION, OK. CHECK FOR TSBS & SERVICE MESSAGES, FOUND SSM 15599. REPROGRAMMED PCM TO CORRECT. CHECKED
REFLASH		1295 PCM CALIBRATION I HOOKED UP THE WDS 1.RAN CONT CODE RETRIEVAL PCM NO CODES 2.RAN KOEO AND KOER SELF TEST PASSED. 3.RAN DATALOGGER 4.RAN FUEL SYSTEM TEST S 5.REPROGRAMMED PCM 6.RAN CONT CODE
REFLASH		CK SEV PASS CODES DIAG BY SYMPTOM RUN OASIS REPROGRAM PROCESSOR
REPLACED		EEC TST,CODE P1000. PP TEST PID DATA TST FOUND AIRBYPASS DOWN TO 19 PERCENT THEN STALLS. REPL IAC. RETST OK
TSB		ROAD TESTED AFTER REPAIR FOR 8 MILES. NO STALLING. PERFORM TSB 02 11 6, TEST IAC, PASS, RE PROGRAM PCM, TEST EVAP SYSTEM, PASS, ROAD TEST. NO STALLING.
REPLACED		EEC RELAY FAILS HOT AND TP SENSOR VOLTAGE LOW... TESTED SYSTEM AND REPLACED EEC RELAY AND RESET TP VOLTAGE TO SPECS...CHECKED PROCESSOR GROUNDS AND EEC GROUNDS...ROADTEST
REPLACED		REPLACED THROTTLE BODY,IAC,REPROGRAM COMPUTOR
REFLASH		NGS DIAG NO CODE. DO PID DATA AND ALL SEEMS OK. CHECK FUEL PRESSURE, OK. CALL OASIS. REPROGRAM PCM AS PER MESSAGE ADD ON REPAIR.
SSM		TECH 111 ROADTEST COULD NOT VERIFY RAN OASIS FOUND SSM 15599 PERFORM EEC TEST NO CODES CK FUEL PRESSURE FOUND PRESSURE WITHIN SPECS NO LEAKDOWN ROADTEST WITH NGS FOUND NO PENDING DTCS ALL PID DATA NOR
TSB		VEHICLE STALLING WHEN DRIVING CUST. ASK FOR A FEW MINS. AND IT STARTED THEN CUST. SMELLED BURNING R UBBER SMELL VERIFY WDS TEST CONINUOUS PASS KOEO PASS KOERPASS PERFORM TSB 02 11 6 DIAGNOSE AND REPLA
TSB		MIL OFF EC 1111 EC 1111 ER 1111 1 D21 42 (RECAL) WDS TEST & DATALOGGER ALL OK. ROAD TEST UNABLE TO VERIFY CONCERN. CHECK OASIS FOUND TSB02 11 06. CHECK IAC OK
TSB		REPAIR PER ESCAPE V6 STALLS INVESTIGATION CHECKLIST WITH MARK HAYDUK
TSB		EEC TEST AND PINPOINT TEST REPROGRAM PCM PER TSB 02 11 6
REPLACED		EEC TEST AND PINPOINT TEST NO CODES CHECK AND REPLACE IDLE BYPASS VALVE AND THROTTLE BODY
NPF		CAUSAL 9F715 CC 42 CCC D21 CONNECTED TO NGS, RAN KOEO, KOER, ROAD TESTED, UNABLE TO DUPLICATE CONCERN AT THIS TIME
TSB		NGS DIAG, NO CODES. DO TSB 02 11 6. DO PID DATA AND CHECK IAC. CHECK RELAYS AND EVAP SYSTGEM. REPROGRAM PCM AS PER TSB. RETEST, OK
REPLACED		D21 41 STICKS YF12 9F715 AA W.O.S TEST REPLACE LAC SENSOR AND REPROGRAM PROCESSOR . RETEST SYSTEM .
SSM		SNOP DIAG EEC AND REPAIR PER SSM 15494
REPLACED		REPLACED ENGINE ASSEMBLY WITH NEW ASSEMBLY. DOOME MILES ARE CORRECT.
NPF		11104 5.2 ALTERNATOR CIRCUITS TEST, ALT NOT CHARGING WIGILLED WIRE LOOM TO ALTERNATOR, STARTER TO CHARGE, PULL MAIN ENGINE LOOM UP FROM BOTTOME COULD NOT CHECK CONNECTOR IN VEHICLE. DISCONNECTED LOOM
DIAG		00 EEC (QUICK TEST) DIAGNOSIS
REPLACED		CK FOR STALL CONCERN, PERFORM SEDS TEST ALL PAS S, CK EEC RELAY AS PER FORD AND OK, REPLACE ID LE AIR CONTROL VALVE, REPLACE DPFE SENSOR ROAD TEST AND NO STALL

	CHECK WHY THE VEH STALLED WHILE DRIVING ALONG CUST CAME TO A STOP AND THE VEH RESTARTED EVERYTHING SEEMED FINE EXCEPT THE VEH SMELLED OF SOMETHING BURNING THE VEH WAS WARMED UPG
	CHECK FOR VEHICLE DIES EVERY TIME BRAKES ARE APPLIED BELOW 20MPH
ECU RELAY FOR CORROSION, OK.	SHUTS OFF BY ITSELF WHILE DRIVING. RESTARTS AND GOES FOR AWHILE THEN DIES AGAIN
RETRIEVAL. FOR PATS SYSTEM NO CODES 7.RAN ON DEMAND SELF TEST PASSED 8.RAN DATALOGGER MONITOR PIDS OK. 9.PINPOINT TESTED 10.RAN ENGINE CHECKS 11.ROAD TESTED AND MONITOR PIDS AND HOOKED UP	CUSTOMER STATES VEHICLE STALLS AND IS HARD STARTING
	ENGINE DIES WHEN COAST WITH FOOT OFF THEN PUSH ON GAS TO TAKE OFF
	STALLS LOW IDLES AT TIMES
	CUST STATES CAR IS STALLING OUT AT ABOUT 30 35 MPH. SEE LAST REPAIR
	ENGINE STALLED WHILE DRIVING WARM SPEED WAS 30 35 MPH HAPPENED THREE TIMES
	CUST STATES VEHICLE KEEPS STALLING
	CHECK ENGINE STALLS ON DECELERATION.
MAL AND WITHIN SPECS VERIFY EVAP VENT LINE NOT BLOCKED REPROGRAM PCM ALL AS PER SSM 16589 ROADTEST STILL COULD NOT VERIFY STALLING CONCERN AT THIS TIME	CK FOR VEH JUST SHUT DOWN WHILE DRIVING BUT IT STARTED BACK UP WHILE DRIVING 40 MPH, LIGHTS ON DASH CAME ON, WAS DRIVING DOWN HILL, DECEL
CED IAC VALVE VAPOR MANAGEMENT VALVE THROTTLE BODY AND REPROGRAM PCM	CK FOR VEHICEL STALLING WHILE DRIVING CUST SAT FOR A FEW MINS AND IT STARTED THEN CUST SMELLED BURNING RUBBER SMELL
	HARD START AT TIMES ALSO STATES DIE OUT WHILE DRIVING
	THE VEHICLE WILL STALL WHEN GOING DOWN HILL AND FOOT TAKEN OFF ACCELERATOR INTERMITTANT
	STALLS WHILE DRIVING
	D21 ENGINE STALLS
	C S STALLED OUT WHEN DRIVING IN THE RAIN
	VEHICLE SHUT OFF TWICE.
	C S THAT VEHICLE STALED A COUPLER TIMES WHILE DRIVING
	CUSTOMER STATES THE VEHICLE STALLED WHILE DRIVING AT 60 MPH. IT HAS HAPPENED ABOUT FOUR TIMES.
	C S VEHICLE STALLED AND WILL NOT START
FROM SENSORS, VALVE COVER PCM ETC TO PULL OUT BROUGHT TO CHECK WIRES, WIRE PINPOINT, NO BREAK OR SOFT SPOTS WIRES HAVE CONTINUITY, INSERT TERMINAL END IN CONNECT TO CHECK FOR TIGHT	TOW IN VEHICLE STALLED OUT AFTER DRIVING FOR TWO BLOCKS WIPERS SLOWED DOWN AND LIGHTS CAME ON AND STALLED OUT WILL NOT RESTART
	VEH STALLED WHILE DRIVING WOULD NOT RESTART IMMEDIATLEY PUSHED UNLOCK BUTTON ON KEYLESS ENTRY & THEN WAS ABLE TO START VEH
	CUSTOMER STATES VEHICLE STALL WHILE DRIVING

2002	17697	511	1FMCU04172KA84203	3.0L	TAD	9	2001	2304	DIAG	D21	2	288972	3000	WHILE DRIVING
2002	17702	511	1FMCU04172KA88344	3.0L	TAD	5	2001	2304	12A650	D21	7	881884	10000	WHILE DRIVING
2002	17705	511	1FMCU04172KA15681	3.0L	TAD	8	2001	2304	12A650	D21	11	2046501	14000	WHILE DRIVING
2002	17709	511	1FMCU04172KA16236	3.0L	TAD	8	2001	2.00E+03	9F715	D21	3	425769	2000	WHILE DRIVING
2002	17717	511	1FMCU04172KA15148	3.0L	TAD	8	2001	2304	12A650	D21	7	1121310	8000	WHILE DRIVING
2002	17718	511	1FMCU04172KA15148	3.0L	TAD	8	2001	7K07	10969	D21	5	854700	2000	WHILE DRIVING
2002	17719	511	1FMCU04172KA15148	3.0L	TAD	8	2001	2304	12A650	D21	11	2298297	15000	STALLS
2002	17720	511	1FMCU04172KA15148	3.0L	TAD	8	2001	2F02	9E936	D21	3	609447	3000	DOWNHILL
2002	17721	511	1FMCU04172KA15148	3.0L	TAD	8	2001	7C05	14N069	D21	3	401203	3000	WHILE DRIVING
2002	17725	511	1FMCU04172KA08488	3.0L	TAD	8	2001	2.00E+03	9F715	D21	5	650050	8000	WHILE DRIVING
2002	17727	511	1FMCU04172KA08006	3.0L	TAD	8	2001	7B06	14N069	D21	1	303369	1000	WHILE DRIVING
2002	17728	511	1FMCU04172KA08006	3.0L	TAD	8	2001	7C05	14N069	D21	2	219014	1000	WHILE DRIVING
2002	17740	511	1FMCU04162KD01916	3.0L	TAD	5	2002	2.00E+03	9F715	D21	1	1662745	1000	WHILE DRIVING
2002	17757	511	1FMCU04162KD01904	3.0L	TAD	4	2002	2.00E+03	9F715	D21	2	2522085	0	DOWNHILL
2002	17763	511	1FMCU04162KD04418	3.0L	TAD	3	2002	2.00E+03	9F715	D21	2	1493949	8000	WHILE DRIVING
2002	17767	511	1FMCU04162KC74180	3.0L	TAD	3	2002	2.00E+03	9F529	D21	2	1633595	3000	STALLS
2002	17768	511	1FMCU04162KC79364	3.0L	TAD	3	2002	2304	DIAG	D21	2	1695715	8000	WHILE DRIVING
2002	17776	511	1FMCU04162KC80557	3.0L	TAD	3	2002	2302	12B679	D21	1	1152279	0	WHILE DRIVING
2002	17782	511	1FMCU04162KC39916	3.0L	TAD	2	2002	2.00E+03	9F715	D21	5	1695442	4000	WHILE DRIVING
2002	17784	511	1FMCU04162KC39136	3.0L	TAD	2	2002	2.00E+03	9F715	D21	2	1166527	1000	WHILE DRIVING
2002	17788	511	1FMCU04162KC27667	3.0L	TAD	2	2002	2306	RECAL	D21	6	2843081	6000	WHILE DRIVING

HOTLINE		ROAD TEST FOR STALL COULD NOT VERIFY, CONTACT F ORD, CHECK VEHICLE AS PER FORD TECH LINE OK US T, ALL ITEMS IN FACTORY SPECS, COULD NOT DUPLI CATE WILL CONTACT FORD FOR FURTHER DIRECTION
SSM		EEC TEST NO CODES ROAD TEST NPF CHECK CASE FOUND SSM REPROGRAM PCM ROAD TEST OK
TSB		REPROGRAMMED PCM AS PER TSB 02 11 09
DIAG		2007 CUST CONCERN IS STALLING AND NO START VEH STARTED WHEN I GOT IT PREFORMED WDS DIAG KOEO KOER PASSED TEST PREFORMED A IGNITION SYSTEM TEST COIL ON PLUG PASSED AT 30K VOLTS PREFORMED A FUEL SYSTE
SSM		ROAD TEST TO DUPLICATE CONDITION,WDS TEST,NO CODES,MONITOR PIDS,REFER TO CASE,SSM 15690,INSPECT ID # ON PROCESSOR,181,DOWNLOAD NEW CALIBRATION TO PCM,ROADTEST,OK.
DIAG		WDS TEST PIN POINT CODE B1352,IGNITION KEY FAILURE,TRACE TO INSTRUMENT CLUSTER,DOWNLOAD CLUSTER TO WDS,INSTALL NEW CLUSTER &LOAD MEMERY,CLEAR CODES RETEST,OK,LABOR TIME TO TRANSFERR MEMORY NOT LISTED,
REPLASH		REPAIR VEHICLE AS PER T.S.B.#02 11 06,REPLACE THROTTLE BODY EVAP VALVE AND IAC SENSOR,NOT RECALIBRATED,LABOR TIME NOT LISTED USE M TIME.
SSM		THIRD ATTEMPTO RESOLVE PROBLEM,INVALID HOOTLINE,WAS CONTACTED BY ESCAPE SPECIALIST GIVEN LIST OF THINGS TO CHECK,CONTACTED NUMEROUS DEALERS FOR INPUT ON FIX,CHECKED ALL,EXTENDED ROADTESTS FOR FOUR D
SSM		CLEAN BATTERY GROUND & COAT WITH DIELECTRIC COMPOUND,INSPECT IAC VALVE ,OK,REPLACE EEC POWER RELAY & CHECK ALL CONNECTIONS IN RELAY BOX,AS PER SSM 15494,LABOR TIME NOT LISTED USE M TIME
SSM		6340 DIAG USING NGS FOUND NO CODES FOUND SSM 15494 PERFORM ALL STEPS OUTLINED IN SSM AND RETEST AL OK
SSM		ROADTESTED COULD NOT VERIFY CONCERN AT THIS TIME PERFORMED SERVICE DIAGNOSTICS SYSTEM OPERATING NORMALLY CHECK POWERTAIN CONTROL MODULE CALIBRATION OK ACCESS BATTERY TRAY CHECK AND CLEAN GROUNDS
HOTLINE		PERFORM DIAGNOSIS,ADJUST BASE IDLE AS PER HOTLINE
TSB		1116 ROAD TEST DIDNT STALL RUN CASE HAS TSB REGUAR DIND SYMTOM TSB 02 11 6 MONITOR IAC,BCT,BVAPVM, AND FTP EVAPVM AND FTP IN SPEC,WATCH IAC 46% ID LE 735 755 RPMS REPLACE IAC 3.0 L IDLE BETTER INSP
REPLACED		700 IDLE CONTROL CHECKED EEC SYSTEM KOEO PASS RAN PID MONITOR ROAD TEST REPLACED IAC RETESTED
REPLACED		TEST DROVE & RAN WDS EEC CODE SCAN PASS, CKD FUEL PRESSURE & LEAKDOWN, RAN POWER BALANCE TEST & DCL DISPLAY, RAN DATA LOGGER SCAN: REPLACED IDLE AIR CONTROL VALVE & RETESTED, REPLACED THROTTLE BODY &
TSB		EEC TESTED, NO CODES, REMOVED AND REPLACED IAC AND THROTTLE BODY AS PER TSB 02 11 06.
REPLASH		RUN WDS TEST, NO CODES, REPROGRAM PCM
SSM		COULD NOT DUPLICATE PROBLEM BUT TOOK PRECAUTIONARY STEPS SEE BELOW. ROAD TESTED FOR STALLING AND RAN WDS DIAG (NO CODES) PERFORMED SSM 15690. CHECK FOR LATEST PCM UPDATE (OK)
REPLACED		DEFECTIVE IAC,THROTTLE BODY AND EEC RELAY. EEC TEST NO DTC FOUND REPLACE IAC VALVE AND THROTTLE BODY AND REPLACE EEC RELAY
REPLACED		REPALCE IAC
TSB		NGS QUICK TEST PASS DCL DISPLAY PASS MONITOR PIDS ROAD TEST PERFORM TSB 021106 TEST EVAP SYSTEM TEST IAC SYSTEM PINPOINT & REPROGRAM PCM TO LATEST LEVEL PER HOTLINE RETEST OK

	CUSTOMER STATES AFTER DRIVING FOR A WHILE ENGINE IS WARM, ENGINE SHUTS OFF, RESTARTS OK
	CHECK VEH HAS SHUT OFF TWICE WHILE DRIVING
	CAR COMPLETELY SHUTS DOWN WHEN DRIVING 30 40MPH ENGINE CUTS NO BRAKE STEERING HAPPENED TWICE.
M TEST PREFORMED A FUEL PUMP ON THE CAR TEST PASSED TEST 60 PSI PREFORMED A PCM CALIBRATION TEST PREFORMED A NGS DCL PID DATA MONITOR ROAD TEST CHECKED PIDS FOR INJECTOR PULSE WIDTH MASS	CUST STATES AFTER DRIVING ABOUT 3 MILES VEH STALLED ON ACCELLERATION FROM A LIGHT. VEH STARTED OK AT LUNCH TIME THEN AFTER WORK VEH CRANKED BUT WOULD NOT START
	CUTS OUT WHILE DRIVING COMMING TO A STOP.
USE M TIME.	CUTS OUT WHILE DRIVING.
	CHECK STALLING CONDITION.
AYS BEFORE RETURNING TO CUSTOMER.NO REACCURANCE OF PROBLEM.LABOR TIME NOT LISTED USE M TIME.	STALLS,CUTS ON DECELL DOWN HILLS.
	UNIT CUTS OUT WHILE DRIVING.
	CUSTOMER STATES VEHICLE STALLED WHILE DRIVING, CUSTOMER COASTED TO SIDE AND RESTARTED FINE.
	CUST STATES THAT THE VEH JUST DIES WHILE DRIVING. D60 KEN HULSEY TO DRIVE AND OR ADVISE
	CUSTOMER STATES THAT THE TRUCK IS DYING WHILE DRIVING D60
ECT SEC RELAY OK REPROGRAM PCM RELEASE VEHI CLE	CUST STATES ONCE WHILE DRIVING UP A HILL AT A LOW SPEED VEHICLE CUT OFF DID START RIGHT BACK UP
	DIES AT STOPS AND WHILE GOING DOWNHILL ABOUT 40 MPH 1 TIME
EVAP MANAGEMENT VALVE, DROVE	CUSTOMER STATES WHILE DRIVING ENGINE DIED LAST NITE TODAY SEEM SLUGGISH RUNS ROUGH MIL WAS ON??
	ENGINE HAS STALLED SEVERAL TIMES AND VEHICLE STARTS RIGHT UP AGAIN.
	VEHICLE SUDDENLY DIED WHILE DRIVING
	CUSTOMER WAS DRIVING AT APPROX 60 MPH WHEN TRUCK STALLED OUT
	CUST STATES WHEN ACCELERATING FROM 40 MPH LET OFF AND GO BACK INTO FUEL WANTS TO CUT OUT HAS STALLED
	STALLS WHILE DRIVING AT TIMES WILL START BACK UP AGAIN
	CUST STATES VEH CUTS WHILE DRIVING HAPPENS WHEN USING RESUME ON C CONTROL RESTARTS OK AFTER DRIVING HALF HOUR HAS A REMOTE START SEE SEAN

2002	17800	S11	1FMCU04162KC20468	3.0L	T/LD	2	2002	2G04	DIAG	D21	4	1822161	4000	WHILE DRIVING
2002	17816	S11	1FMCU04162KB [illegible]	3.0L	T/LD	12	2001	2G05	RECALEM	D21	4	1149894	8000	WHILE DRIVING
2002	17818	S11	1FMCU04162KB66296	3.0L	T/LD	12	2001	2B01	9C915	D21	6	1727280	6000	WHILE DRIVING
2002	17820	S11	1FMCU04162KB64845	3.0L	T/LD	1	2002	2G05	RECAL	D21	2	1142280	0	WHILE DRIVING
2002	17825	S11	1FMCU04162KB64282	3.0L	T/LD	12	2001	1H03	9J460	D21	7	1768513	7000	NO TEXT
2002	17828	S11	1FMCU04162KB64232	3.0L	T/LD	12	2001	7C05	14N069	D21	3	894394	3000	NO TEXT
2002	17830	S11	1FMCU04162KB64333	3.0L	T/LD	12	2001	2.00E+03	9F715	D21	6	2105669	9000	WHILE DRIVING
2002	17837	S11	1FMCU04162KB63648	3.0L	T/LD	12	2001	2G05	RECALEM	D21	5	1564265	11000	STALLS
2002	17839	S11	1FMCU04162KB37553	3.0L	T/LD	11	2001	2G04	12A650	D21	5	1120591	1000	WHILE DRIVING
2002	17843	S11	1FMCU04162KB24751	3.0L	T/LD	11	2001	7C05	14N069	D21	2	588600	1000	WHILE DRIVING
2002	17846	S11	1FMCU04162KB64507	3.0L	T/LD	11	2001	2G05	RECALEM	D21	6	1665427	12000	WHILE DRIVING
2002	17847	S11	1FMCU04162KB63643	3.0L	T/LD	11	2001	2.00E+03	9F715	D21	9	2446306	8000	IAC FAILED
2002	17848	S11	1FMCU04162KB23643	3.0L	T/LD	11	2001	2.00E+03	9F715	D21	6	1581460	4000	AT STOP
2002	17849	S11	1FMCU04162KB23643	3.0L	T/LD	11	2001	2.00E+03	8E926	D21	9	3446307	8000	DECELL
2002	17850	S11	1FMCU04162KB23562	3.0L	T/LD	11	2001	2.00E+03	9F715	D21	6	1560126	6000	WHILE DRIVING
2002	17861	S11	1FMCU04162KB23562	3.0L	T/LD	11	2001	7C05	14N069	D21	1	414104	0	AT STOP
2002	17862	S11	1FMCU04162KB23562	3.0L	T/LD	11	2001	2G02	12B579	D21	1	1211898	0	AT STOP
2002	17863	S11	1FMCU04162KB22805	3.0L	T/LD	11	2001	2.00E+03	9F715	D21	5	1613069	3000	WHILE DRIVING
2002	17865	S11	1FMCU04162KB18594	3.0L	T/LD	10	2001	1A04	9424	D21	3	767561	2000	WHILE DRIVING
2002	17871	S11	1FMCU04162KB13601	3.0L	T/LD	11	2001	2.00E+04	9C915	D21	5	1904271	10000	WHILE DRIVING
2002	17882	S11	1FMCU04162KB03286	3.0L	T/LD	10	2001	2G04	12A650	D21	7	1911463	4000	AT STOP
2002	17888	S11	1FMCU04162KA82190	3.0L	T/LD	10	2001	1H03	9J460	D21	2	2066654	0	WHILE DRIVING
2002	17901	S11	1FMCU04162KA80988	3.0L	T/LD	10	2001	2B04	12A650	D21	5	793589	4000	WHILE DRIVING
2002	17902	S11	1FMCU04162KA82436	3.0L	T/LD	10	2001	2G04	12A650	D21	4	759884	5000	WHILE DRIVING
2002	17906	S11	1FMCU04162KA78391	3.0L	T/LD	10	2001	7C05	14N069	D21	3	524835	1000	STALLS
2002	17907	S11	1FMCU04162KA78391	3.0L	T/LD	10	2001	2G04	DIAG	D21	1	305006	0	WHILE DRIVING

TSB		4476 ROAD TEST COULD NOT PRODUCE STALL WDS DIAG KOEO PASS PASS KOER PASS DATA LOGGER POWER BALANCE FUEL PREASURE TEST FUEL LEAKDOWN TEST INJECTOR FLOW TEST PREFORM TSB 01 11 6 CHECK IAC DUTY CYCLE
SSM		PER SSM 15589 EEC (QUICK TEST) DIAGNOSIS
TSB		DIED NO CODES, REPLACED CPS PER INFO FROM TSB THEN RT OVERNITE UNABLE T
SSM		PERFORM EEC TEST,DCL DISPLAY,DCL MONITOR,PROGRAMMED PCM TO HIGHEST LEVEL PER SSM 15589,RETEST AND ROADTEST
REPLACED		RAN DIAG REPLACED DPFE SENSOR PER BUILD DATE AS REFERENCED BY JEFF HAZEL
SSM		RUN CODES, REPROGRAM PCM AND REPLACE EEC RELAY PER SSM 15589 RD TEST OK, USE MTIME FOR NO OPS
TSB		ROADTEST,UNABLE TO VERIFY VEHICL SHUTTING OFF WHILE DRIVING,EEC TEST,NO CODES,RAN OASIS,TSB 2 11 6.DS PER TSB.PID MONITOR IAC & ECT AT IDLE,IAC OUT OFSPECS.REPLACED THROTTLE BODY,IAC & EEC RELAY PER T
REFLASH		D21 42 RECAL NGS TESTING, KOEO, KOER, CMDTC S, ALL PASS CODES. RAN OASIS FOUND REPAIR FOR CONCERN, MONITORED PIDS IAO, DUTY CYCLE
SSM		1213 42 WAR RAN WDS FOR DTCS REPROGRAMMED PCM PERFORMED REPAIRS OUTLINED IN SSM 15589 SS 4486
SSM		1354 ROAD TEST NORMAL OPERATION CHECK FUEL PERSSURE OK 45 PSI CHECK FOR CODES NO CODES CHECK OASIS PERFORM SSM 15434 CHECK IAC FOR REVISED IAC OK INSTALL NEW EEC RELAY REMOVE BATTERY AND CLEAN AND CH
TSB		UNABLE TO VERIFY CUSTOMER CONCERN AT THIS TIME TEST SYSTEM FOR CODES NO PROBLEMS RUN OASIS, FOUND TSB 02116 REPROGRAMED PCM PER TSB AND RETEST...OK NOW 614
REPLACED		REPLACED IAC
REPLACED		PERFORMED EEC TESTS, DCL, PINPOINT TESTS, FUEL AND IGNITION TESTS. REPLACED FAUTLY IAC.
REPLACED		PERFORMED EEC TESTING AND REPLACED THROTTLE BODY AND FUEL MANAGEMENT VALVE
TSB		PERFORMED TSB 2 11 6 REPLACED IAC AND THROTTLE BODY
INOP		INOP EEC (QUICK TEST) DIAGNOSIS
INOP		INOP EEC (QUICK TEST) DIAGNOSIS
TSB		TEST DRIVE TO VERIFY,COULD NOT,CHECKED FOR CODES,NONE FOUND FOUND TSB 02 11 06,REPLACED IDLE AIR CONTROL VALVE,THROTTLE
REFLASH		NGS TEST, SMOKE TEST, RANDR UPPER AND LOWER INTAKE GASKETS RETORQUE REPROGRAM PCM
TSB		TEST DRIVE. WDS SET UP. PULL CODES NO CODES. MONITOR PIDS ON ROAD TEST PIDS INDICATE NORMAL OPERATION. POWER BALANCE REPALCED IAC, THROTTLE BODY, AND EVAPVM VALVE AS PER TSB. RECHECK IAC AT 35%
REFLASH		EEC TEST, PIN POINT TEST, AND REPROGRAMED PCM
DIAG		EEC TEST PASS CODES TEST FUEL PRESS WITH GAUGE NGS MONITOR ROAD TEST OK MAF 1.2V PASS PINPOINT TEST AS PER SYMPTOM
SSM		RAN WDS DIAG & RETRIEVED CODES. CHECK SSM & PER SSM 15589 REPROGRAM PCM & CHECK RELAY, ROAD TEST, OK.
REFLASH		PERFORMED DIAGNOSTIC TESTING FOR SOURCE OF CONCERN. CHECKED OASIS FOR MESSAGES. PERFORMED MONITORED ROAD TEST. REPROGRAM PCM. RETEST AFTER REPROGRAM. ALL OK
SSM		VERIFY, WDS HOOK UP, SELF TEST, ROAD TEST WITH DATA LOGGER RPL EEC POWER RELAY PER SSM#15434, RETEST CLEAR CODES REPR VERIFIED.
SSM		DIAG NO START EEC TEST NO CODES NOTLINE CONTACT #1KIDQ011 CHECKED # ON IAC YREIF715AB O CHECKED EEC RELAY EMBOSSED OK CHECKED CON 270 B C D E NO FAULTS RUN OASIS NO PORBLEM FOUND

OK CHECK PCM CALIBRATION OK CHECK VAPOR MANAGEMENT VALVE OK	CUSTOMER STATES VEHICLE STALLED WHILE DRIVING, VEHICLE WAS WARMED UP WHEN THIS HAPPENED, CUSTOMER WAITED ABOUT 15 MIN & VEHICLE RESTARTED OK D21
	CUST REPORTS VEH HAD STALLED ONE TIME WHILE DRIVING,SAID SPUTTERED JUST A LITTLE BUT WAS ABLE TO RESTART SEE SSN
	C S AFTER DRIVING 20 MILES AT APPROX. 60 MPH, VECHILE DIED,PULLED TO SIDE FOUND OIL LIGHT LITE ONLY, RESTARSTED VECHILE OK
	VEH STALLED OUT FRIDAY WHILE DRIVING
SB,RETEST,STILL UNABLE TO DUPLICATE CONCERN,	C S VEHICLE HAS SHUT OFF TWICE WHILE DRIVING. NO WARNING LIGHTS CAME ON, WAS ABLE TO START RIGHT BACK UP AFTER PUTTING IN PARK
	CHECK STALLED W TOOK OFF FROM COLD START.....WAS A CRANK NO START FOR 20 MIN
	STALLS WHILE DRIVING , BUT WILL RESTART
ECK GROUNDS CHECK PIDS RETEST OK	CUSTOMER STATES THE CAR IS STALLING INTERMITTANTLY WHILE DRIVING AT HIGH WAY SPEEDS
	CUSTOMER STATES WHILE DRIVING CAR STOPPED WHEEL WOULD NOT TURN, COULD NOT BRAKE AND OIL INDICATOR WAS LIT...
	IDPW IAO FAILED
	VEHICLE IS STALLING AT LIGHTS
	VEHICLE WILL STALL AT TIMES WHEN DECELLERATING.
	CUSTOMER STATES STALLS CUTS WHILE DRIVING
	CUSTOMER STATES THAT THE VEHICLE STALLS WHEN SITTING AT A LIGHT INTER.
	CUSTOMER STATES THAT THE VEHICLE STALLS INT. JUST STALL AT THE LIGHT OUT FRONT, AND IT STALLED LAST
	CUSTOMER STATES ENGINE STALLS WHILE DRIVING
	STALLED ONCE WHILE DRIVING
AND EVAPVM CYCLING NORMALLY. TEST DRIVE	CUSTOMER CONCERNED WITH THE VEHICLE DYING WHILE GOING DOWN THE ROAD. NO CHECK ENGINE LIGHT CAME ON
	CAR STALLS INTERMITTENT MOSTLY WHEN WARM AND AT STOPS. IDLE ALSO WILL GO WAY DOWN
	CHECK ENGINE DIED WHILE DRIVING ONCE LAST WEEK LAST FRIDAY OIL LIGHT WAS ON NO OTHER LIGHTS ON
	ENGINE WILL DIE WHEN DRIVING DOWN THE ROAD, WILL RESTART THOUGH
	CUST STATES VEHICLE CUTS OUT WHILE DRIVING
	CUST STS ENGINE STALLS AT TIMES
	DIAGNOSE CAUSE OF VEHICLE CUT OFF WHILE DRIVING

2002	17909	S11	1FMCU04162KA76374	3.0L	TAD	10	2001	3G05	RECAL	D21	7	1261232	3000	STALLS
2002	17911	S11	1FMCU04162KA76571	3.0L	TAD	10	2001	2.00E+03	8F715	D21	1	343217	0	WHILE DRIVING
2002	17914	S11	1FMCU04162KA71288	3.0L	TAD	10	2001	2G04	12A650	D21	10	2340134	7000	IDLE
2002	17922	S11	1FMCU04162KA67619	3.0L	TAD	9	2001	7C05	14B589	D21	3	427699	3000	WHILE DRIVING
2002	17923	S11	1FMCU04162KA67619	3.0L	TAD	9	2001	3G05	RECAL	D21	7	1223691	6000	DOWNHILL
2002	17924	S11	1FMCU04162KA67619	3.0L	TAD	9	2001	1H03	8J480	D21	6	1074529	5000	DECELL
2002	17934	S11	1FMCU04162KA64485	3.0L	TAD	9	2001	3G05	RECALEM	D21	2	364686	1000	WHILE DRIVING
2002	17935	S11	1FMCU04162KA64485	3.0L	TAD	9	2001	2.00E+03	8E508	D21	10	2047617	6000	STALLS
2002	17948	S11	1FMCU04162KA61606	3.0L	TAD	9	2001	2G05	RECAL	D21	8	1666661	6000	WHILE DRIVING
2002	17949	S11	1FMCU04162KA62403	3.0L	TAD	9	2001	2G04	DIAG	D21	3	484574	2000	STALLS
2002	17955	S11	1FMCU04162KA60586	3.0L	TAD	9	2001	7C05	14B589	D21	9	1838398	6000	WHILE DRIVING
2002	17964	S11	1FMCU04162KA44107	3.0L	TAD	8	2001	2G05	RECAL	D21	7	1070016	1000	WHILE DRIVING
2002	17966	S11	1FMCU04162KA39912	3.0L	TAD	8	2001	7V01	12A661	D21	1	347549	0	WHILE DRIVING
2002	17967	S11	1FMCU04162KA39912	3.0L	TAD	8	2001	2.00E+03	8F715	D21	4	642252	4000	STALLS
2002	17970	S11	1FMCU04162KA39540	3.0L	TAD	9	2001	1A09	6007	D21	11	2361351	1000	WHILE DRIVING
2002	17977	S11	1FMCU04162KA35455	3.0L	TAD	8	2001	2G04	12A650	D21	5	803163	5000	WHILE DRIVING
2002	17986	S11	1FMCU04162KA29367	3.0L	TAD	8	2001	2G05	RECAL	D21	8	1143260	7000	WHILE DRIVING
2002	17988	S11	1FMCU04162KA29536	3.0L	TAD	8	2001	2G04	12A650	D21	7	1222665	0	SAME SPOT
2002	18001	S11	1FMCU04162KA07551	3.0L	TAD	6	2001	2G04	DIAG	D21	11	1990179	10000	DOWNHILL
2002	18013	S11	1FMCU04162KD08037	3.0L	TAD	6	2002	2G04	12A650	D21	2	2306960	0	WHILE DRIVING
2002	18019	S11	1FMCU04162KD06697	3.0L	TAD	6	2002	2.00E+03	8F715	D21	0	2306137	0	AT STOP
2002	18035	S11	1FMCU04162KD05259	3.0L	TAD	5	2002	2.00E+03	8E508	D21	1	2306368	1000	WHILE DRIVING
2002	18027	S11	1FMCU04162KD24312	3.0L	TAD	4	2002	2G02	129579	D21	2	1784712	1000	WHILE DRIVING
2002	18028	S11	1FMCU04162KD13694	3.0L	TAD	4	2002	2.00E+03	8F715	D21	4	2306755	4000	WHILE DRIVING
2002	18039	S11	1FMCU04162KC91479	3.0L	TAD	3	2002	2.00E+04	8C915	D21	1	2100131	0	WHILE DRIVING
2002	18051	S11	1FMCU04162KC47313	3.0L	TAD	2	2002	2.00E+03	8F715	D21	3	1857026	4000	WHILE DRIVING

ENTIRE PAGE

TSB		WDS DIAG KOEO PASS KOER PASS DATA LOGGER SHOWS ALL LOOKING OK. FUEL SYSTEM TESTS OK IGN TESTS OK. CHECK PCM CALIB PCM OUT OF DATE. REFLASH PCM WITH NEW CALIB PER TSB 020806
SSM		WDS KOEO DATA LOGGER, KOER, WIGGLE TEST SENSORS,EEC POWER RELAY INSPECTED TERMINAL CONNECTIONS,CHECKED PCM WIRING
DIAG		03/11 EEC (QUICK TEST) DIAGNOSIS
REPLACED		PERFORMED EEC TEST ALL PASS CODES NO MIL LIGHT ON REPLACED EEC
TSB		STAR TESTED CLEAN PERFORMED TSB 02 08 06 RESULTING IN REFLASHING OF P
TSB		STAR TESTED HAD ALL PASS CODES RECHECKED PARAMETERS AS PER TSB 02 11
SSM		PCM CALIBRATION. NGS TEST,PID MONITOR TEST,REPROGRAM PCM, M TIME TO CHECK GROUNDS PER SSM
REPLACED		RAN EEC TEST, NO CODES. PERFORMED FURTHER DIAG. REPLACED EGC RELAY, THROTTLE BODY, AND IAC. REPROGRAM PCM.
MPF		1 PERFORM EEC TEST KOEC PASS. RAN FUEL PRESSURE TEST AND ROAD TEST VEHICLE WITH WDS AND MONITOR ALL PIDS UNABLE TO
DIAG		CCC E29 CC 42 BASIC 12A650 DTC P0301 EEC TEST KOEO PASS KOEC P0301 KOER PASS PINPOINT TEST DCL DISPLAY IGNITION TEST PASSED FUEL PRESSURE TEST
REPLACED		WDS, CK IGNITION, NO CODES, REPLACE PCM RELAY
TSB		1316 DROVE VEHICLE, WAS NOT ABLE TO DUPLICATE STALL. RAN OASIS. REVIEW TSB, SSM, & HISTORY WDS HOOK UP. KOEO, KOER, POWER BALANCE, IGNITIO N SYSTEM TEST, FUEL PRESSURE TEST, INJECTOR FLO W TEST, D
REFLASH		EEC FUEL AND IGN SYSTEM DIAGNOSIS ROAD CHECK WITH MONITOR WIGGLE TEST AND REMOVE LOWER ENGINE COVER AND TIGHTEN LOOSE TERMANIL TO CRANK SHAFT SENSOR RECAL TEST ON PCM ROAD CHECK REPAIR WITH CUSTOME
SSM		4784 WARR PC 42 FP 6F718 N P1111 P1111 P1111 M O.T EEC AND FUEL SYSTEM DIAGNOSIS NO SERVICE CODES DCL MONITOR OASIS CHECK REMOVE BATTREY BOX AND PANNELS TO ADDESS GROUNDS TIGITTEN AND CHECK VOLTAGE
ENGINE FAILURE		18570 E EDCTEST VEH. AND DIAG. INTERNAL ENG FAILURE. EVAC A C AND DRAINED OIL AND COOLANT. REMOVED ENG AND REPLACED. CHANGED OVER HARNESSES AND ENG PARTS. REPLACED THERM AND GASK. AND EXH. GASKETS
REFLASH		EEC TESTED REPROGRAMMED PROCESSOR
REFLASH		ROADTEST DID NOT STALL,CHECK SUSPECT EEC RELAY. REPLACED EEC POWER RELAY,REPROGRAM PCM ROADTEST
SSM		REFER TO SSM 15699 REPROGRAM PCM AND CHECK EEC RELAY AND PURGE VENT
TSB		10936 PULLED CODES W WDS PASS REPROGRAMMED PCM PER TSB
ADJUST		RESET BASE IDLE AND ROAD TEST AND VERIFIED REPAIR OK
TSB		97 ST HOOK UP WDS EEC TEST ALL PASS RUN OASIS AND F FOLLOW TSB 2 11 6 GO THRU ALL TESTS CHECK FOR PCM UPDATE, SCAN DCL DATA LOGGER INFO REPLACE IAC MOTOR AND RETEST
INOP		INOPERTIVE EEC (QUICK TEST) DIAGNOSIS
LOOSE HOSE		TEST DROVE,PERFORMED KOEO AND KOER,CODE P1100 PRESENT. MONITORED PID DATA,INSPECTED AND TESTED MAF SENSOR,FOUND MAF SENSOR LOOSE FROM AIR CLEANER BOX AND AIR INTAKE HOSE LOOSE. TIGHTENED MAF SENSOR AN
REPLACED		4035 EEC TEST PASSED DCL DISPLAY TEST IGNITION SYS TEST NGS RECORDERV MONITER TEST PINPOINT TEST R&R IAC R&R DPFE RETEST
TSB		NSS QUICK TEST PASS DCL DISPLAY PASS ROAD TEST MONITOR PIDS REFER TO TSB 021106 TEST & REPLACE VAPOR MANAGEMENT VALVE,IAC & EEC RELAY CALLED HOTLINE SPOKE WITH TO CONTACT # 2S8FT022 ADVISED REPLAC
REPLACED		WDS DIAGNOSIS. REPLACE IDLE AIR CONTROL VALVE, THROTTLE BODY & GASKET. RETEST. OK.

	CUSTOMER STATES THAT TRUCK STALLED AND NOTHING WORKED AT THE TIME
	CHECK WHILE DRIVING AT STEADY SPEED THE ENG. WILL DIE, YOU PULL OVER AND CAR STARTS BACK UP AND GOES SEE HISTORY
	CUST STATES CK ENG LIGHT IS ON
	OWNER STATES VEHICLE STALLS WHILE DRIVING
	OWNER STATES STALLS INTERMITTENTLY ON DECELERATION ON DOWNHILL SEE
	VEHICLE STILL STALLS INTERMITTENTLY NORMALLY ON DECEL POSSIBLY ONCE
	CUSTOMER WAS JUST DRIVING AND CAR STALLED CUST CAME BACK A FEW MINUTES AND STARTED
	CHECK ENGINE LIGHT COMES AND ENGINE DIES
	CUSTOMER STATES WHEN DRIVING SLOWER SPEEDS 30 MPH,ENGINE LOOSES POWER,STALLS OUT WHEN SLOWING DOWN CHECK AND ADVISE
	CUSTOMER STATES THE CHECK ENGINE LIGHT CAME ON AND TRUCK STARTED TO SPUTTER AND WANT TO STALL
	CK VEH CUT OFF ON ROAD
CL PID DATA RECORDED, CHECK GROUND CONNECTIONS. CHECKED EEC RELAY, OK CHECK & REPROGRAM PCM TO LATEST CALIBRATION. RETEST, PASSING, NO OCCURANCES OF CONCERN.	CUST STATES THE ENGINE STALLED OUT WHILE DRIVING.. OIL AND BATTERY LIGHT CAME ON LOST BRAKES AND STEERING.. RESTARTED OK DROVE HERE PLEASE CHECK
R	D21 ENGINE DIES WHILE DRIVING
DROP,REPLACE EEC POWER RELAY AND IAC SOLENOID TIGHTEN TERMANALS ON CONNECTORS IN LEFT	D21 ENGINE DIES ATTEMPS
. ADDED COOLANT AND RECHARGE A C. RUN VEH. AND RECHECK OPS. O.C. BY 660 CC 42, DIAG CODE 0007E 660	D21 CUSTOMER STATES VEHICLE STALLED WHILE DRIVING...VEHICLE WAS TOWED IN
	CK FOR INTERMITTANT STALL DRIVING
	CK CAR STALLS AT TIMES WHEN DRIVING,CAR RESTARTS OK.
	CUSTOMER REPORTS THE ENGINE JUST SHUTS OFF IN THE SAME SPOT ABOUT 2 MI
	VEHICLE DIES WHILE DECELING DOWN HILL
	CUSTOMER STATES SHUT OFF WHILE DRIVING AND RESTARTED OKM ROAD TEST AND VERIFIED CONDITION DIAGNOSE AND TEST SYSTEM
	VEHICLE STALLS AT STOPS, STARTS UP OK
	CUTS WHILE DRIVING
D TIGHTENED AIR INTAKE HOSE,RESET PCM	CUSTOMER STATES ENGINE STALLED WHILE DRIVING GAVE NO WARNING... HAS DONE THIS ONE TIME
	CHECK VEH DIED OUT WHILE DRIVING, ADVISE
E MAF WITH PARTS & DPFE RETEST OK	CUSTOMER STATES VEHICLE STALLED WHILE DRIVING AT 40MPH. DID RESTART IMMEDIATELY AFTER STOPPING ON SIDE OF ROAD.
	VEHICLE DIES WHEN DRIVING (JUST AFTER ACCEL), A C WAS ON

2002	18069	511	1FMCU04152KC47313	3.0L	T/LD	2	2002	2.00E+04	9C915	D21	4	2278199	7000	WHILE DRIVING
2002	18084	511	1FMCU04158KC27069	3.0L	T/LD	2	2002	2.00E+03	9F715	D21	1	772245	0	STALLS
2002	18087	511	1FMCU04152KB97741	3.0L	T/LD	1	2002	2G04	DIAG	D21	6	1851362	2000	WHILE DRIVING
2002	18088	511	1FMCU04152KB97674	3.0L	T/LD	1	2002	7B02	10348	D21	2	1753698	2000	WHILE DRIVING
2002	18089	511	1FMCU04152KB97678	3.0L	T/LD	1	2002	2.00E+03	9F715	D21	4	2041730	5000	WHILE DRIVING
2002	18074	511	1FMCU04152KB76939	3.0L	T/LD	1	2002	2.00E+03	9E926	D21	4	1610022	4000	DOWNHILL
2002	18079	511	1FMCU04152KB76237	3.0L	T/LD	12	2001	2.00E+03	9F715	D21	5	1899950	2000	WHILE DRIVING
2002	18083	511	1FMCU04152KB66942	3.0L	T/LD	12	2001	7C05	14N089	D21	0	525290	0	AT STOP
2002	18085	511	1FMCU04152KB66503	3.0L	T/LD	1	2002	2G05	RECAL	D21	2	1018486	1000	WHILE DRIVING
2002	18086	511	1FMCU04152KB66503	3.0L	T/LD	1	2002	7C05	14N089	D21	6	2119290	7000	STALLS
2002	18090	511	1FMCU04152KB64822	3.0L	T/LD	1	2002	2.00E+03	9E926	D21	7	2006518	8000	STALLS
2002	18095	511	1FMCU04152KB54503	3.0L	T/LD	12	2001	2G04	12A650	D21	7	1899063	10000	WHILE DRIVING
2002	18098	511	1FMCU04152KB53068	3.0L	T/LD	12	2001	2B02	12B679	D21	5	1852982	6000	AT STOP
2002	18102	511	1FMCU04152KB50063	3.0L	T/LD	12	2001	2G04	12A650	D21	4	1108456	3000	ON HIGHWAY
2002	18105	511	1FMCU04152KB39494	3.0L	T/LD	12	2001	2B02	12029	D21	0	515578	0	NO TEXT
2002	18109	511	1FMCU04152KB32695	3.0L	T/LD	12	2001	1H09	6J460	D21	8	2333577	11000	NO TEXT
2002	18112	511	1FMCU04152KB30748	3.0L	T/LD	11	2001	2.00E+04	9C915	D21	6	1679508	17000	WHILE BRAKING
2002	18117	511	1FMCU04152KB28345	3.0L	T/LD	11	2001	2.00E+05	9360	D21	5	1308991	6000	WHILE DRIVING
2002	18124	511	1FMCU04152KB22283	3.0L	T/LD	11	2001	2G04	12A650	D21	3	1547363	6000	WHILE DRIVING
2002	18125	511	1FMCU04152KB22263	3.0L	T/LD	11	2001	1H09	6J460	D21	5	2280539	9000	WHILE DRIVING
2002	18131	511	1FMCU04152KB20691	3.0L	T/LD	10	2001	2B04	DIAG	D21	7	1312943	7000	NO TEXT
2002	18137	511	1FMCU04152KB19818	3.0L	T/LD	11	2001	7C05	14N089	D21	1	409959	0	WHILE DRIVING
2002	18138	511	1FMCU04152KB19818	3.0L	T/LD	11	2001	2.00E+03	9F715	D21	6	1324993	8000	WHILE DRIVING
2002	18150	511	1FMCU04152KB00134	3.0L	T/LD	10	2001	2.00E+03	9F715	D21	8	1852875	9000	STALLS
2002	18155	511	1FMCU04152KA93899	3.0L	T/LD	10	2001	2G05	RECAL	D21	9	1929997	9000	AT STOP

TSB		CONTACT HOTLINE CHECK WIRING GROUNDS OK PER HOT LINE CENCK AND REPLACE PFE SENSOR REPLACE VAPOR SENSOR MANAGEMENT VALVE AS PER TSB 02 11 06 WDS DAIGNOSES SATA LOGGE TEST ROAD TESTED
REPLACED		REPLACED IDLE AIR CONTROL MODULE PER WARRANTY
DIAG		STALLS EEC (QUICK TEST) DIAGNOSIS PASS QUICK TEST PMPT
REPLACED		CK DIAG, CK IGN SYS, CK CK BATT BAD 2 VOLTS, INST BATT, RUN OK FOR 10 MIN, CK START SYS, CK START DRAW, EEC TST, NO CODES VOLY OUPUT INTERNL WILL CHARGE 16.2 VOLTS AND OVER CHARGED BATT. R R ALT DI PI
TSB		PERFORMED WDS DIAGNOSTICS. CHECKED FOR TSB S. PERFORMED ALL TESTS ON TSB 11 02 6. ORDERED IAC & VAPOR MANAGEMENT VALVE M TIME NEEDED FOR WDS AND TSB 02 11 06 R&R IAC & VAPOR MANAGEMENT VALVE. ROAD TES
REPLACED		THE VALVE BODY IS NOT WORKING CORRECTLY
REPLACED		M TIME NEEDED NO LOP FOR WDS SPECIAL ORDERED AND REPLACED IAC AND REPROGRAMMED PCM
SSM		RD TST UNABLE TO VERIFY DTES CLEANED GROUNDS REPLACED PCM RELAY AS PER SSM 15494 RD TST AND RECHK
SSM		HOTLINE & SSM #15666 REPROGRAMED PCM TEST DROVE CNVC CHECKED OASIS FOUND SSM #15666 CALLED HOT LINE TALKED TO RALPH REPORT #2DSS6019 INSTRUCTED ME TO
TSB		EEC RELAY 14N889 TESTED EEC,PASS CODES,CHECKED OASIS,REVIEWED TSB 02 11 06 CALLED HOT LINE TALKED TO JOSE REPORT #2DSS6019 INSTRUCTED
TSB		DIAGNOSTIC AND PINPOINT TESTING..CODES..PASS VERIFIED CONCERN AS PER TSB 02 11 6 REPLACE HT EVMV VALVE AND THE IDLE AIR CONTROL VALVE AND THE THROTTLE BODY ALSO UPDATE THE PCM RETEST ROAD TEST OKAT AT
TSB		FP#1U7Z12A650 AXA PERFORMED EEC TEST NO CODES P1111. MONITORED IAC FLOW RATE AS PER TSB 02 11 06. CHECKED RELAY OK. REPROGRAMMED PCM
HOTLINE		WARR EEC TEST ROADTEST CHECK OASIS CALL HOTLINE DIAGNOSE AND REPL MASS AIR FLOW SENSOR
REFLASH		HOOK UP NGS CK IAC OPERATION TESTED IGNITION SYSTEMIGNITER PIDE AND REPROGRAM PROCESSOR AND RETESTED
REPLACED		TEST WITH WDS AND REPLACE #8 COIL AND PLUG
REFLASH		PERFORMED WDS DIAGNOSIS FOR ENGINE STALLS, CUTS, NO CODES FOUND, REPLACED DPFE SENSOR AND REPROGRAMMED PCM WITH LATEST UPDATE.
TSB		INSPECT AND PERFORMED DIAGNOSIS NO CODES PERFORM TSB AND RETEST ALL PASS
REPLACED		CK FOR CODES IN PCM. NONE RETRIEVED. R&R FUEL PUMP MODULE AND INSPECT FUEL TANK FOR FOREIGN MATERIAL. ROAD TEST.
REFLASH		CK PIN POINT REPROGRAM PCM TO CORRECT
REFLASH		ROAD TEST PINPOINT AND REPLACE DPFE SENSOR AND REPROGRAM PCM
NO TEXT		
SSM		RUN DIAGNOSTICS NO CODES, FOLLOW SSM 15494 AND REPLACE EEC POWER RELAY
TSB		RUN DIAGNOSTICS AND PINPOINT TESTS, NO CODES FOLLOW TSB 02 06 06 REPLACE IAC MOTOR AND REPROGRAM THE PCM
REPLACED		TEST DRIVE TO VERIFY DIES AND RUNS ROUGH,EEC TEST NO CODES,PINPOINT TEST MONITOR IAC,FOUND CYCLE TOO LOW,REPLACE IAC,RETEST EEC,MT12A650 NO LABOR OP LISTED IN SLTS TO PERFORM DRIVE CYCLE TEST,REPROGRA
REFLASH		9483 W ROAD TEST TO VERIFY, WDS TEST EEC SYSTEM, RAN IDLE DATA DISPLAY, VIEW PIDS FOR IAC WAS AT 39% EVAPVM VOLTAGE AT 2.8, RAN PINPOINT TEST, REPROGRAMMED PROCESSOR, VERIFY REPAIR

	CHECK FOR VEHICLE DIES WHILE DRIVING
	CUSTOMER STATES VEHICLE STALLS INTERMITTENLY AFTER MANY ATTEMPTS ON STARTING VEHICLE
	CHECK ENGINE SHUT OFF AROUND 40MPH, HAPPENED ONCE
NPOINT TST, TST DROVE OK	C S DRIVING & ENGINE JUST CUT WOULD FINALLY STARTED BACK UP
TED. FUNCTIONS AS	CUSTOMER STATES VEHICLE WILL NOT RUN, CONTINUES TO STALL WHILE DRIVING
	THE ENGINE DIES AT TIMES ON A DOWN HILL COAST
	CUST STATES THE VEHICLE QUITS JUST DRIVING DOWN THE ROAD NO WARNING LIGHTS COME ON;THE VEHICLE WILL RESTART;TEST AND REP
	ENGINE DIES AT STOPS.
	D21 CUST STATES THAT VEH IS STALLING WHILE DRIVING CUST STATES THAT VEH STALLED OUT 1 TIME BUT ACTED LIKE
	D21 CUST STATES THAT VEH STALLS SEE HIST AND JOB 1
THIS TIME	CUSTOMER STTATES THE VEHICL STALLS AND HAS A HESITATION PROBLEM
	CUSTOMER STATES CAR HAS STALLED TWICE WHILE DRIVING
	CHECK VEH STALLED ON 1 OCCASION WHILE STOPPED AT A LIGHT RESTARTED WITH NO PROBLEM
	CUST STATES DROVE FROM LAKEWOOD GOT OFF HWY ON CLAGUE AND VEH STALLED, STARTED 2ND TIME TRYING
	OS WHEN SLOWING DOWN THROUGH TOLL BOOTHS WILL STALL
	CUSTOMER WAS DRIVING AT 40MPH AND VEHICLE DIED. CUST STATES VEHICLE WOULD NOT RE START.
	CHECK DIES GOING DOWN ROAD
	CUTTING OFF WHILE DRIVING WHEN SLOWING DOWN
	STALLED WHEN DRIVING
	CUSTOMER REPORTSENGINE STALLS WHILE DRIVING
M PCM.	AT TIMES WILL DIE OR RUN VERY ROUGH,RESTART THEN OK.
	VEH STALLS AFTER COMING TO STOP, THEN GOING TO START

2002	16156	S11	1FMCU04152KA69899	3.0L	TAD	10	2001	1H03	6J460	D21	6	1024239	5000	WHILE DRIVING
2002	16157	S11	1FMCU04152KA69899	3.0L	TAD	10	2001	2G02	12B570	D21	6	1075278	5000	DOWNHILL
2002	16158	S11	1FMCU04152KA69899	3.0L	TAD	10	2001	7C05	14N089	D21	2	359089	1000	WHILE DRIVING
2002	16160	S11	1FMCU04152KA69461	3.0L	TAD	10	2001	2.00E+03	6E838	D21	10	2369496	10000	ON HIGHWAY
2002	16163	S11	1FMCU04152KA62116	3.0L	TAD	10	2001	1H03	6J460	D21	8	1405803	6000	NO TEXT
2002	16166	S11	1FMCU04152KA70899	3.0L	TAD	10	2001	7C05	14N089	D21	3	507402	2000	AT STOP
2002	16169	S11	1FMCU04152KA76121	3.0L	TAD	10	2001	2G04	12A650	D21	6	1327663	2000	WHILE DRIVING
2002	16170	S11	1FMCU04152KA76121	3.0L	TAD	10	2001	2G01	12A650	D21	6	1292525	2000	WHILE DRIVING
2002	16171	S11	1FMCU04152KA78085	3.0L	TAD	10	2001	2G04	DIAG	D21	5	675829	2000	DOWNHILL
2002	16178	S11	1FMCU04152KA69821	3.0L	TAD	10	2001	2.00E+03	6F716	D21	9	1837351	17000	WHILE DRIVING
2002	16186	S11	1FMCU04152KA69702	3.0L	TAD	9	2001	2G05	RECALEM	D21	10	2186514	15000	IN REVERSE
2002	16189	S11	1FMCU04152KA61591	3.0L	TAD	9	2001	2G05	RECAL	D21	9	2398410	12000	WHILE DRIVING
2002	16196	S11	1FMCU04152KA60636	3.0L	TAD	9	2001	2G05	RECALEM	D21	8	1794617	10000	STALLS
2002	16200	S11	1FMCU04152KA60724	3.0L	TAD	9	2001	2G05	RECAL	D21	10	1998004	11000	WHILE DRIVING
2002	16201	S11	1FMCU04152KA60724	3.0L	TAD	9	2001	2.00E+03	9B920	D21	10	2183099	12000	DOWNHILL
2002	16210	S11	1FMCU04152KA40419	3.0L	TAD	9	2001	7C05	14N089	D21	4	544657	4000	WHILE DRIVING
2002	16233	S11	1FMCU04152KA39512	3.0L	TAD	8	2001	2G04	12A650	D21	8	804910	5000	WHILE DRIVING
2002	16237	S11	1FMCU04152KA32929	3.0L	TAD	8	2001	2G04	12A650	D21	8	1494000	8000	STALLS
2002	16251	S11	1FMCU04152KA14586	3.0L	TAD	8	2001	2G04	12A650	D21	7	1150327	13000	DOWNHILL
2002	16266	S11	1FMCU04152KA07366	3.0L	TAD	8	2001	2G04	12A650	D21	12	2257400	10000	NO TEXT
2002	16269	S11	1FMCU04152KA06674	3.0L	TAD	8	2001	1H03	6J460	D21	12	2160552	18000	WHILE DRIVING
2002	16276	S11	1FMCU04152KE10572	3.0L	TAD	7	2002	2G04	DIAG	D21	1	2435369	0	WHILE DRIVING

HOTLINE		5987 W ROAD TEST TO VERIFY, WDS START UP, TEST EEC SYS RAN KOEO AND KOER PULLED NO CODES, RAN IDLE DATA DISPLAY, RAN FUEL PRESSURE TEST, RAN FUEL PRESSURE LEAKDOWN, RAN PINPOINT TEST, CONTACT HOTL
REPLACED		5940 WARR EEC SYSTEM TEST WITH WDS NO MEMORY CODES PERFORM KOEO AND KOER TESTS PASSED PERFORMED WDS DATA LOGGER RECORDER ROADTEST,CALLED FORD TECHNICAL SUPPORT,REPLACED MAF SENSOR,RESET BASE IDLE S
SSM		1090 W TEST DROVE TO VERIFY, WDS TEST EEC SYS PULLED NO CODES, RAN IDLE DATA DISPLAY, RAN FUEL PRESSURE TEST, RAN FUEL PRESSURE LEAKDOWN TEST, RAN RELATIVE INJECTOR FLOW TEST, R&R BATTERY & BATTER
TSB		EEC TEST NO CODES MONITOR PID UPDATE PCM REPLACE ISC, THROTLE BODY AND EEC RELAY PER TSB ALSO REPLACE EVAP VALVE
NO TEXT		
REPLACED		2981 42 NOT WORKING PROPERLY EEC SELF TEST PASS CODE REPLACE EEC RELAY AND TIGHTEN GROUND 104 AND105 UNDERNEATH BATTRY TRAY INPECT IDLE VALVE PART NUMBER PER SPECIAL SERVICE MESSAGE 15494 FINAL RE
SSM		PERF NEC DIAG AS PER SSM 15599 REPROGRAM PCM AND CHECK GROUNDS AND EEC POWER RELAY
REPLACED		PERF NEC DIAG REPLACE IAC VALVE AND PROCESSOR AS PER PSE KUNZE MY TO R R PROCESSOR FROM STOCK UNIT
SSM		IDLE TOO SLOW, STALLS AT TIMES EEC (QUICK TEST) DIAGNOSIS, PASS,CHECKED POWER RELAY, SET IDLE
SSM		TEST DRIVE FOR STALL,NO CRANK. RAISE VEHICLE AND INSPECT WIRING TO STARTER,BATTERY AND GROUNDS. ALL OK. CHECK OASIS
REFLASH		ROAD TEST, MONITOR ALL PIDS WITH NGS. NO DTCS. ENGAGEMENTS AND SHIFTS NORMAL AT THIS TIME. FLUID LEVEL AND CONDITION GOOD. REPROGRAM PCM TO LATEST LEVEL CALIBRATION.
TSB		COULD NOT VERIFY,PREFORMED DIAG AS PER TSB 02,11,06 TO REPROGRAM PCM,ENGINEERING IS AWARE OF THIS CONCERN AND IS STILL WORKING ON A FIX
REFLASH		198500 .2; D48 .5; D60 .1; D61 .5; D84 .2; 3.0L V6 DOHC AUTO 4X4 CHECK ENGINE LIGHT NOT ON;PASS;PASS;PASS;CHECKED EEC;RAN PINPOINT,DCL & RECORDER MONITOR TESTS ALL OK;REPROGRAMMED
NPF		11670 ROAD TEST ON HIGHWAY NO STALLING PERFORM QUICK TEST NO CODES PERFORM RECORDER MONITOR PERFORM DCL DISPLAY ALL PIDS IN SPECS PERFORM FUEL SYSTEM TESTING OK PASS 32 PSI PERFORM IGNITION SYSTEM
TSB		ROAD TEST VEHICLE PERFORM QUICK TEST NO CODES PERFORM RECORDER MONITOR PERFORM DCL DISPLAY OK FUEL PRESSURE OK IN SPECS PERFORM IGNITION SYSTEM TESTING OK OASIS WATCHING IAC% PER TSB REPLACE IAC MO
SSM		TECH TESTED EEC, ALL PASS CODES. CHECK OASIS. FOUND SSM 15494. CHECK CONNECTORS 270 B,C,D,E, ALL OK. CHECK GROUNDS
REFLASH		RAN EEC TEST PASSED DCL DISPLAY PID MONITOR ROAD TEST FUEL PRESSURE TEST INJECTOR FLOW TEST IGNITION SYSTEM TEST RAN PINPOINT TEST REPROGRAMMED PCM RETEST PASSED
REFLASH		EEC TEST NO CODES ROAD TESTED UNABLE TO DUPLICATE CHECKED EEC RELAY REPROGRAM PCM 161 ON PCM BLEW OUTVENT HOOSE
REFLASH		COMPLETE RESET OF BASE IDLE ADJUSTMENT CONFIRM PROPER IDLE CONDITION AFTER REPAIR REPROGRAM PCM
DIAG		TEST DROVE FOR STALLING AND DUPLICATED CONCERN. SCANNED FOR CODES WITH NGS AND NO CODES WERE STORED OR RETRIEVED AND
REFLASH		WDS TEST REPLACED DPFE IN OP REPROGRAM PCM TO CURRENT UPDATE RETEST
HOTLINE		539 NGS EEC SELF TEST DCL DISPLAY DCL RECORDER MONITOR ROAD TEST CALLED HOTLINE UTV WAS ADVISED BY HOTLINE RECORDING THAT A REPAIR IS NOT AVAILABLE YET BUT ONE IS COMING KOEO PASS KOEC PASS KOER P

INE, HOTLINE ASSISTANCE DID NOT HELP, CONTACT FORD FIELD REP., FOUND DPFE TO BE CAUSE OF VEHICLE STALLING, REPLACED DPFE WITH UPDATED DPFE, ROAD TEST TO VERIFY REPAIR	CK ENGINE STALLS WHEN DRIVING TWICE NOW AT THIS SPOT.;ROUTE 125 COMING FROM MONTG.RD.ABOUT A MILE AND THERES A HILL THATS BIG AND WHILE GOING DOWN THIS HILL IT STALLS,AC IS ON
PEED,RESET IDLE STRATEGY AND TP VOLT SETTING,ROADTESTED OK	CHECK FOR STALLING DOWN HILL
Y TRAY, INSP. GROUNDS 104 & 105, INSP G101 & G120, R&R LEFT KICK PANEL AND INSP. CONNECTORS 270C & 270D, REPLACED PCM POWER RELAY, REASSEMBLED AND TEST DROVE TO VERIFY REPAIR	CK ENGINE STALLED WHILE DRIVING AND STARTED BACK UP EASILY,NO CK ENGINE LIGHT
	VEH CUTS OUT COGOING DOWN THE HIGHWAY LAST TIME AT 35 MPH, HAS BEEN LOOKED A T AT FORSYTH FORD AND WORKED ON STILL CUTTING OUT CC D21
TEST MILES OYT 2006 D21 WAR.	C S VEH CUTS OUT WHEN COMING TO A STOP ENGINE DIES, BRAKES GET HARD
	C S WHILE DRIVING 35 40 MPH ENGINE CUT OFF (ENGINE HOT) RESTARED OK
	ENGINE CUTS OFF WHILE DRIVING 60MPH RESTARTS OK
	CHECK OWNER STATES ENGINE SHUTS OFF WHILE GOING DOWN HILLS AT TIMES GEN FOREMAN REROADTESTED AND ALL FOUND OK AFTER REPAIRS
	CUSTOMER STATE STHAT WHEN DRIVING 45 MPH AND SLOWED DOWN CAR STALLED AND WOULD NOT RESTART NO CRANK HESIT ON TURNS
	ENGINE DIES REPEATEDLY WHEN PUT IN REVERSE NO PATTERN AC ON OR OFF
	CUSTOMNER STATES THAT THE CAR STALLS WHILE DRIVING DOWN THE ROAD,CAR STARTS RIGHT BACK UP AFTER STALLING
	CUSTOMER STATES THAT VEHICLE DIED IN FLIGHT 2 WEEKS AGO,HAS NOT HAPPENED SINCE,LOUD POPPING NOISE ON COLD STARTS AT TIME
TESTING OK REROAD TEST OK NO CONDITION PRESENT	C S VEHICLE HAS BEEN STALLING BETWEEN 35 40 MPH WHEN FOOT IS OFF THE GAS PEDAL
TOR AND THROTTLE BODY W UPDATED PARTS RETEST REROAD TEST CK PROCESSOR FOR UPDATED CALLIBRATION REROAD TEST OK	C S VEHICLE HAS STALLED TWICE IN THE PAST THREE DAYS; USUALLY HAPPENS WHEN DRIVING DOWNHILL
	CUSTOMER STATES THE ENGINE DIEDE WHILE DRIVING. CHECK AND ADVISE
	CUST STATES THAT THE VEH STALLED WHILE DRIVING. OCCURED ONCE SINCE THEN, FUEL SMELL IN VEH. CK ADV
	DIAGNOSE WHY THE ENGINE STALLS ONE TIME RANDOMLY RESTARTS FINE
	CUSTOMER STATE VEHICLE STALLS WHEN GOING DOWN HILL BRAKINGESPECIALLY IF BRAKING FOR A TURN
	CK. FOR VEH. STALLS WHILE DRIVING AT TIMES
ASB	D21 CUST STATES ENG DIED TWICE WHILE DRIVING THE 1ST DAY THEY GOT VEH., HASNT HAPPENED SINCE.

2002	18276	S11	1FMCU04148KD08026	3.0L	TAUD	6	2002	2.00E+03	9F715	D21	1	2294019	1000	TURNING
2002	18278	S11	1FMCU04148KD64226	3.0L	TAUD	6	2002	2.00E+03	9F715	D21	2	2116229	1000	WHILE DRIVING
2002	18280	S11	1FMCU04148KD69427	3.0L	TAUD	6	2002	2.00E+03	9F715	D21	1	1757607	0	STALLS
2002	18281	S11	1FMCU04148KD80970	3.0L	TAUD	6	2002	1H03	8J460	D21	1	2046165	0	WHILE DRIVING
2002	18283	S11	1FMCU04148KD86913	3.0L	TAUD	6	2002	2.00E+03	9E905	D21	5	2375758	8000	WHILE DRIVING
2002	18284	S11	1FMCU04148KD64601	3.0L	TAUD	5	2002	2.00E+03	9F715	D21	2	2000013	2000	WHILE BRAKING
2002	18288	S11	1FMCU04142KD02854	3.0L	TAUD	6	2002	2.00E+03	9E909	D21	0	1554408	0	STALLS
2002	18300	S11	1FMCU04148KC73285	3.0L	TAUD	3	2002	2.00E+03	9E909	D21	1	1797027	0	STALLS
2002	18304	S11	1FMCU04148KC73285	3.0L	TAUD	3	2002	2002	12B570	D21	2	2257259	1000	WHILE DRIVING
2002	18309	S11	1FMCU04148KC80747	3.0L	TAUD	3	2002	2G04	12A650	D21	2	1806834	2000	ON FREEWAY
2002	18310	S11	1FMCU04148KC80884	3.0L	TAUD	3	2002	2G02	9E909	D21	2	2023414	1000	WHILE DRIVING
2002	18311	S11	1FMCU04148KC80924	3.0L	TAUD	3	2002	2.00E+03	9F715	D21	1	1757040	0	WHILE DRIVING
2002	18312	S11	1FMCU04142KC80924	3.0L	TAUD	3	2002	2.00E+04	9C915	D21	2	1678620	0	WHILE DRIVING
2002	18315	S11	1FMCU04148KC48496	3.0L	TAUD	3	2002	2.00E+03	9F715	D21	3	1726696	1000	WHILE DRIVING
2002	18316	S11	1FMCU04148KD48026	3.0L	TAUD	2	2002	2G04	DIAG	D21	3	1662503	1000	STALLS
2002	18327	S11	1FMCU04148KC36518	3.0L	TAUD	2	2002	2.00E+03	9E909	D21	4	1749045	6000	STALLS
2002	18329	S11	1FMCU04148KC86896	3.0L	TAUD	2	2002	2G04	12A650	D21	5	2130825	8000	STALLS
2002	18331	S11	1FMCU04148KC39722	3.0L	TAUD	2	2002	7V01	14290	D21	0	2010540	4000	WHILE DRIVING
2002	18336	S11	1FMCU04142KC14818	3.0L	TAUD	1	2002	2.00E+03	9F715	D21	6	2366504	8000	WHILE DRIVING
2002	18342	S11	1FMCU04142KB86896	3.0L	TAUD	1	2002	7C05	14N069	D21	1	886031	0	WHILE DRIVING
2002	18345	S11	1FMCU04142KB80206	3.0L	TAUD	1	2002	2.00E+03	9F715	D21	5	1720861	7000	WHILE DRIVING
2002	18347	S11	1FMCU04148KB86029	3.0L	TAUD	1	2002	2.00E+03	9950	D21	6	1686548	8000	WHILE DRIVING
2002	18352	S11	1FMCU04142KB76114	3.0L	TAUD	1	2002	2G04	12A650	D21	6	1758762	6000	AT STOP
2002	18354	S11	1FMCU04142KB77058	3.0L	TAUD	1	2002	2.00E+03	9F715	D21	1	1290008	1000	WHILE DRIVING
2002	18356	S11	1FMCU04148KB76413	3.0L	TAUD	1	2002	2.00E+03	9F715	D21	6	2336716	9000	WHILE DRIVING
2002	18358	S11	1FMCU04142KB76164	3.0L	TAUD	1	2002	2F02	9C873	D21	3	1202145	4000	WHILE DRIVING

TSB		HOOKED UP WDS, EEC TEST, PER TSB 02 11 06, MONM PIDS, IAC, EVAP TEST, ROAD TEST, IAC 59% INTERM ITTANT, REPLACED IAC VALVE, RETEST OK.
ADJUST		DIAGNOSIS. CHECKED FOR CODES, NO CODES. INSALLED VDR AND RECORD WHILE DRIVING. MONITORED PIDS, CHECKED PCM FOR UPDATED CALIBRATION. NONE AVAILABLE. CHECKED BASE IDLE. ADJUSTED IDLE SCREW TO IDLE AT 75
TSB		COMPUTER TEST NO CODES,CK TSB 02 11 6,CHECK VENTS ARE OK,HAS NEWEST EEC RELAY,PERFORM EVAPORATIVE TEST OK,IAC OUT OF SPEC REPLACE IDLE AIR CONTROL VALVE,PCM CONNECTION CHECKS GOOD,CH ECK GROUNDS,REMOV
REPLACED		EEC TEST PASS DCL PASS, ROAD TEST UNABLE TO DUPLICATE, CONTACT HOTLINE. ADVISED TO REPLACE MAF WITH REVISED PART REMOVE AND REPLACE DPFE AND MAF AS PER HOTLINE INSTRUCTIONS
DIAG		ENGINE STALLING WHILE DRIVING EEC (QUICK TEST) DIAGNOSIS
TSB		WDS DIAG KOEO PASS,DLC DISPLAY,FUEL SYS TEST,IN LFLOW TEST,IGN SYS TEST,PERFORMED TSB 02 11 6,DIAG BAD IAC PER DIAG ROUTINES IN TSB,RETEST.
DIAG		ENGINE STALLS EEC (QUICK TEST) DIAGNOSIS
TSB		PERFORMED DIAG ,KOEO,CHECKED CASSIS,NO CODES FOUND PERFORMED TSB 01 11 6 IAC AND THROTTLE BODY
REPLACED		021 42 EEC (QUICK TEST) DIAGNOSIS EGR PRESSURE FEEDBACK (PFE) EXHAUST BACK PRESSURE
DIAG		60 EEC (QUICK TEST) DIAGNOSIS
TSB		WITH FORD ENGINEER DO NEW PROCESS WITH WDS TO SET UP CURB IDLE,ADJUST TP SENSOR,RECHECK TSB PROCESS,TEST DRIVE
TSB		HOOK UP ON WDS,CHECK OUT AND REPAIR AS PER TSB 02 11 6,ORDER AND REPLACE IAC AND THROTTLE BODY AS PER TSB,TEST DRIVE
HOTLINE		HOOK UP ON WDS,SELF TEST,PASS,ROAD TEST,CALL HOTLINE,SEN,LOOK AT PCM HARNESS,MAF GASKET,DPFE SENSOR ,CONNECTOR 270 S C D,CONNECTOR C1 60,C135,GROUND G300 G100,G104,G105,G101,CHECK AC COMPRESSOR WIRING,
SSM		HOOK UP WDS CHECK NO CODES CHECK BUILD DATE OK CHECK RELAY OK BLOW OUT HOSES OK CHECK HAS LATEST CALIBRATION INSTALL AIR BY PASS VALVE ROADTEST OK
DIAG		CHECK NO STALLING AT THIS TIME HOOK UP EEC TEST NOCODES P1000 SYSTEM PASS ROAD TESTED WITH MONITOR OK COULDNT VERIFY
TSB		FOLLOWED TSB ARTICLE 02 11 6, REPLACED IAC SENSOR AND THROTTLE BODY
REFLASH		CHECKED CODES NONE FOUND REPROGRAM PCM.
DIAG		01 WIRING ASSEMBLY REPAIR
REPLACED		LOW READING DPFE AND IAC CUTS OUTREPLACED DPFE SENSOR AND IAC MOTER RECHECKED GOOD
REPLACED		291 WDS SELF TEST,PASS RUN DCL TEST RUN FUEL PRESSURE TEST RUN DCL RECORDER MONITOR TEST RUN OASIS RUN PIN POINT TEST REPLACE EEC RELAY,BLOW OUT EVAP SYSTEM, REPROGRAM PCM PER SPECIAL MESSAGE 1555
NO TEXT		
TSB		COULD NOT VERIFY CONCERN CAR STARTED UP AFTER TOWED IN WDS TEST NO CODES PIN TESTS CHECK FOR SSM OR TSB NON FOR THIS SPECIFIC CONCERN
UNOP		DOESNT OPERATE PROPERLY EEC (QUICK TEST) DIAGNOSIS
SSM		1774 NO CEL HOOK TO WDS PINPOINT TEST PASS PASS PASS CHECK PIDS CHECK FOR STALLING PERFORM SSM 15424 REPLACED EEC POWER RELAY REPLACED AIR BYPASS CHECK ALL GROUNDS AND CONNECTION REPLACED DPFE SEN
DIAG		ROAD TEST. COULD NOT DUPLICATE VISUAL CHK OK, TEST EEC W WDS KOEO PASS, KOEC PASS, KOER PAS
REFLASH		CUST STATE VEHICLE DIES INTERMITTREFALSHED PCM

	CUST STATES ENG DIED 1 TIME ON RIGHT TURN, RESTARTED OK.
0. ROAD TESTED AND RECORD USING WDS VDR, CONCERN NOW GONE.	DIES WHILE DRIVING DIES AFTER 10 15 MIN ONLY AFTER COLD START A COND NOT ON RESTARTS AFTER ABOUT 1 MINUTE USES 87 OCT
E BATTERY THEY CHECK GOOD,RAR LF SEAT GROUN	CUSTOMER STATES OIL & ENGINE LIGHT CAME ON TWICE & LOST POWE R
	CUSTOMER REPORTS THE VEHICLE STALLED IN A RIGHT HAND CURVE CRUISING APPROX 40 M.P.H. A C OFF. CHECK AND ADVISE.
	ENGINE STALLED WHILE DRIVING...RESTARTS OK...WAS TOWED IN.
	INTERMITTENLY STALLS WORSE WHEN SLOWING DOWN OR STOPPING
	OK STALLING CUSTOMER TEST DROVE VEHICLE. CLAIMS STALLED MARK, ASST. SALES MNGR. TEST DROVE NO PROBLEMS
	CUST SAYS VEHICLE STALLED THEN RESTARTED D21 42
	OK ENG SHUTS OFF W DRIVING AND TURNING AT TIMES PREV SEE JAY
	ENGINE WILL QUIT RUNNING AT HIGHWAY SPEEDS,INTERMITTENT PROBLEM.
	VEH SHUTS OFF WHILE DRIVING
	SHUTS OFF WHILE DRIVING
CHECK BARO,RECALL HOTLINE,REPLACE MMAP AND RECHECK/REHOOK UP WDS,ROAD TEST,DID NOT STALL BUT CLOSE,RECALL HOTLINE,REPLACE VMV AND REHOOK UP WDS AND ROAD TEST,ALL CHECKS OK THIS TIME	SHUTS OFF WHILE DRIVING,DOES RESTART
	CUST STATES WHEN DRIVING CAR AT HIGHWAY SPEEDS IN STALLS OUT
	CUST STATES CHECK AND ADVISE AT TIMES VEHICLE STALLS OUT AND ENGINE BUCKS
	ENGINE STALLS
	STALLED ONCE
	WHEN DRIVING ALONG AT SPEED THE CAR DIES
	VEH DIES WHILE DRIVEING
0 RETEST PASS	CUST STATES WHILE DRIVING THE ENGINE QUIT RUNNING.. FOOT ON GAS AND STEADY DRIVING 55 MPH OR SO..RESTARTED OK.. PLEASE CHECK
	CUSTOMER STATES THAT VEHICLE STALLS ON HER WHILE SHE IS DRIVING AND TH
	TOWED TO SHOP STALLED WHILE DRIVING
	ENGINE STALLED ONCE IN STOP & GO TRAFFIC IN HIGH AMBIENT TEMPS,RESTARTED, BEEN RUNNING FINE SINCE,CHECK FOR CODES BULLETINS.
SOR ROAD TEST ON AND OFF RETEST	CUSTOMER STATES THAT SHE WAS DRIVING 60 MPH AND ENGINE DIE D21
	CUSTOMER STATES VEHICLE CUT OUT WHILE DRIVING ABOUT 40 45 MPH ON HIGHWAY
	CUST STATES THE VEHICLE DIES INTERMITTANTLY, IT WAS ON THE STREET AND WHILE DRIVING IT JUST DIED, CHECK AND ADVISE

2002	18371	S11	1FMCU04142KB84407	3.0L	TAUD	12	2001	2G04	12A650	D21	1	980278	1000	STALLS
2002	18383	S11	1FMCU04142KB53195	3.0L	TAUD	12	2001	2G04	12A650	D21	3	812281	2000	WHILE DRIVING
2002	18385	S11	1FMCU04142KB44883	3.0L	TAUD	12	2001	2.00E+03	9F715	D21	2	1276498	1000	STALLS
2002	18391	S11	1FMCU04142KB50709	3.0L	TAUD	11	2001	2.00E+03	9F715	D21	5	1949158	6000	NO TEXT
2002	18398	S11	1FMCU04142KB23422	3.0L	TAUD	11	2001	2G05	RECALIBM	D21	9	2556998	11000	WHILE DRIVING
2002	18405	S11	1FMCU04142KB13778	3.0L	TAUD	11	2001	1H09	8J460	D21	4	1678823	3000	WHILE DRIVING
2002	18411	S11	1FMCU04142KB03059	3.0L	TAUD	10	2001	2.00E+03	9F715	D21	2	979998	1000	STALLS
2002	18413	S11	1FMCU04142KB01585	3.0L	TAUD	10	2001	2G04	12A650	D21	6	1956328	13000	WHILE DRIVING
2002	18418	S11	1FMCU04142KA89788	3.0L	TAUD	10	2001	2.00E+03	9F715	D21	10	2347733	8000	WHILE DRIVING
2002	18425	S11	1FMCU04142KA91135	3.0L	TAUD	10	2001	1H03	8J460	D21	10	2112987	21000	STALLS
2002	18426	S11	1FMCU04142KA91136	3.0L	TAUD	10	2001	2.00E+03	9F715	D21	7	1269409	16000	ON HIGHWAY
2002	18428	S11	1FMCU04142KA79065	3.0L	TAUD	10	2001	2.00E+03	9F715	D21	5	2056891	4000	WHILE DRIVING
2002	18429	S11	1FMCU04142KA79066	3.0L	TAUD	10	2001	2G01	12A650	D21	5	837371	4000	WHILE DRIVING
2002	18435	S11	1FMCU04142KA78129	3.0L	TAUD	10	2001	7C05	14N069	D21	3	535775	3000	STALLS
2002	18444	S11	1FMCU04142KA69869	3.0L	TAUD	10	2001	2G04	12A650	D21	9	1692382	7000	WHILE DRIVING
2002	18453	S11	1FMCU04142KA67069	3.0L	TAUD	9	2001	7C05	14N069	D21	2	382853	3000	DOWNHILL
2002	18457	S11	1FMCU04142KA67787	3.0L	TAUD	10	2001	2.00E+03	9F715	D21	11	2430520	18000	AT STOP
2002	18466	S11	1FMCU04142KA62923	3.0L	TAUD	9	2001	2F01	DRIVE	D21	7	1294863	6000	AT STOP
2002	18467	S11	1FMCU04142KA62223	3.0L	TAUD	9	2001	2F01	DRIVE	D21	7	1401557	6000	NO TEXT
2002	18473	S11	1FMCU04142KA60911	3.0L	TAUD	9	2001	2G04	12A650	D21	6	1064253	6000	WHILE DRIVING
2002	18475	S11	1FMCU04142KA60911	3.0L	TAUD	9	2001	1B02	6731	D21	1	372363	0	WHILE DRIVING
2002	18477	S11	1FMCU04142KA49628	3.0L	TAUD	9	2001	7C05	14N069	D21	5	828823	3000	WHILE DRIVING
2002	18478	S11	1FMCU04142KA49629	3.0L	TAUD	9	2001	2.00E+03	9F715	D21	11	2166063	8000	STALLS
2002	18486	S11	1FMCU04142KA44817	3.0L	TAUD	9	2001	7V01	12A581	D21	5	831822	6000	WHILE DRIVING
2002	18489	S11	1FMCU04142KA40855	3.0L	TAUD	9	2001	2G04	12A650	D21	11	2274137	13000	DOWNHILL

SSM		REPROGRAM PCM PER SSM 15599. BLOW AIR THROUGH VENT LINE PER MESSAGE. CHECK EEC POWER RELAY OK. RIGHT ONE IN VEHICLE.
SSM		2200 EEC TESTS ALL CODES PASS**PINPOINT TESTS PER SYMPTOM**MONITOR PIDS THRU DCL DISPLAY ON ROAD TEST**REPROGRAM PCM PER SSM**CHECK EVAP VENT HOSE AND PCM RELAY PER SSM ALL OK**RETEST*
REPLACED		WDS, PINPOINT, REPLACE IDLE AIR BY PASS
TSB		M TIME TO ROAD TEST VEHICLE, TEST SYSTEM, ALL PASS, FOUND TSB 021106, RAN PINPOINT TEST, NO PROBLEMS, DRIVEABILITY CHECK LIST, FOUND IAC 29 30% ATIDLE, REPLACE IAC PER TSB, RETEST, OK NOW
REFLASH		WDS HOO UP, SELF TEST, EVAP SYSTEM TEST, REPROGRAMPCM, RETEST ROAD TEST OK
REPLACED		DIAG NEEDS IAO MOTOR NOTE ON BACK ORDER
INOP		EEC DIAG,PNPNT TEST,REPL DPCTVE IAC MTR,RETEST,OK
TSB		ROAD TEST COULD NOT VERIFY CK OASIS FOUND TSB 021106 PERFORM MPC CODE 161 BUILT DATE 102401 REPROGRAM PCM ROAD TEST OK
REPLACED		ROAD TESTED TO VERIFY, WDS STAR TESTED, NO CODES. MONITORED PIDS, CHECK & REPLACE I.A.C. & ROAD TESTED TO VERIFY REPAIR.
REPLACED		STILL STALLS INTERMITTANTLY VERIFY NDS TEST CONTINUES PASS KOEO PASS KOER PASS DATA LOGGER TEST DPFEEENSOR OUT OF SPECS ON HIGH SIDE REPLACE DPFE SEN SOR RESET KEEP ALIVE MEMORY
TSB		CK VEH CUT OFF IN THE MIDDLE OF THE HIGHWAY WOULD NOT ACCELERATE LET SIT FOR A COUPLE OF MINUTES IT RESTARTED WDS TEST PASSED DATA LOGGER PERFORM TSB 02 06 06 REPLACE AIR BYPASS VALVE REPROGRAM PCM RE
REPLACED		OUT OF RANGE VALVE ASSEMBLY IDLE AIR CONTROL (IAC) REPLACE
INOP		INOP EEC (QUICK TEST) DIAGNOSIS
REPLACED		PERFORMED DIAG. TESTS AND INSPECT REPLACED EEC POWER RELAY,CHECK CONNECTORS AND GROUNDS AND REPROGRAM PCM
TSB		RAN EEC CODE SCAN PASS, RAN DCL DISPLAY:OK FOUND TSB 02 11 6 TO INSPECT IDLE AIR CONTROL VALVE & EVAP SYSTEM THEN PROGRAMMED PCM TO LATEST STRATEGY CALIBRATION
SSM		ROAD TEST EEC TEST CHECK OUT SSM 16494 REPLACED EEC POWER RELAY
STICKING		RAN SELF TEST WITH NGS KOEC KOEO KOER ALL PASSED TEST DROVE WITH NGS IN DCL FOUND IAC STICKING REPLACED IAC TEST DROVE DID NOT STALL
NPF		TESTED EEC SYS NO CODES CHECKED OASIS NONE APPLY ALL WITHIN SPECS UNABLE TO DUPLICATE PROBLEM AT THIS TIME.
TSB		UNKNOWN CHECK ENGINE TEST EEC SYSTEMS PASS NO CODES. CHECK DCL DISPLAY SENSOR READINGS WITHIN SPECS. PERFORM TSB 02 06 06 CHECK I AC DUTY CYCLE WITHIN SPECS. REMOVE PCM CHECK MPC #
TSB		1 SCOPE AND EEC TEST NO CODES PERD TSB REPROGRAM PROCESSOR RE OK OK
ENGINE FAILURE		4.0 HRS USED WAS TIME TO PERFORM PINPOINT CONCERN ON ENGINE WITH ONLY 287 MILES. ENGINE WAS LOCKED. RAISED VEHICLE AND MANUALLY TURNED CRANK ONEWAY THEN IT LOCKS. TURNED THE OTHER WAY AND IT LOCKS A
REFLASH		PCM SOFTWARE UPDATE AVAILABLE EEC RELAY CONTACTS BAD REPROGRAMED PCM WITH UPDATED SOFTWARE RPL EEC RELAY M TIME NO SLTS
REPLACED		TESYTED AND REPLACED IAC VALVE.
INOP		INOP BODY CHASSIS ELECTRICAL (BCE) TEST
TSB		MTIME TO PERFORM TSB REPROGRAM PCM 02 11 06

	INTERMITTENT STALLING REPROGRAM PCM
	VEH STALLS SOMETIMES WHILE DRIVING WHEN FOOT IS REMOVED FROM GAS CK TSBS
	CK INTERMITTANT STALLING OCCURED TWICE STARTS AND RUNS NORMALLY AFTER CK TSB TAP ON PCM RELAY W VEH RUNNING
	CUST STS ENGINE STALLS WHILE DRIVING AT TIMES
	CUSTOMER STATES THE VEHICLE SHUT OFF TWO TIMES WHILE DRIVING OVER THE PAST 2 WEEKS.
	ENGINE STALLS INTERMITTENTLY ON ACCEL. S O PART IS HERE
	ENGINE SHUTS OFF WHILE DRIVING
	CK FOR ENGINE STALLED WHEN DRIVING
	STILL STALLS INTERMITTANTLY
PLACE THOTTLE BODY AND REPLACE VAPOR MANAGEMENT VALVE ROAD TEST	CUSTOMER STATES VECHICLE CUT OFF IN MIDDLE OF HIGHWAY WOULD NOT ACCELERATE LET SIT FOR A COUPL MINUTES IT RESTARTED
	CUSTOMER STATES THE VEHICLE INTERMITTENTLY STALLS WHILE DRIVING. SEEMS TO HAPPEN WHEN SLOWING DOWN AND AFTER WARMED UP, AROUND 30 MPH.
	CK VEHICLE CUT OFF DRIVING SEE NOTE
	CHECK ENGINE FOR INTERMITENT STALL RESTARTS OK & RATTLE PING FROM ENGINE ON ACCEL (SEE JIM)
	CUSTOMER STATES THAT THE ESCAPE HAS DIED 3 TIMES WHILE DRIVING, RESTARTS OK
	REPAIR ENGINE STALLS WHEN GOING DOWN A HILL,OIL LIGHT COMES ON AND WILL HAVE TO RESTART
	ENGINE WILL INTERMITTENTLY STALL AT STOPS SOP
	CUST STATES VEH WHEN WARM AND COMMING TO A STOP OR AT IDLE VEH DIES OUT NO CHECK ENGINE LIGHT CHECK AND ADVISE.
	C S CUTS OFF WHILE DRIVING AND ENG OIL LIGHT COMES ON
GAIN, REMOVED OIL PAN AND INSPECTED. WHILE TURNING CRANK FOUND NO 1 PISTON NOT GOING UP ALL THE WAY. REMOVED R VALVE COVER, FOUND VALVE IN #1 CYL DROPPED INSIDE CYL, CALLED HOTLINE INSTR TO RPL ENG.	CUT OFF WHILE DRIVING WILL CRANK NO START
	OWNER REPORTS ENGINE CUTS OFF WHILE DRIVING AT ANY SPEED MUST COAST TO SIDE OF ROAD AND IT WILL RESTART
	CHECK ENGINE LIGHT. VEHICLE WILL STALL OUT.
	CHECK CUSTOMER STATES ENGINE STALLS OUT WHILE DRIVING
	C S THAT THE CAR STALLS WHEN GOING 40 MPH AND DOWN HILL

2002	18494	511	1FMCU04142KA40833	3.0L	T/LD	6	2001	2G01	12A650	D21	5	1706921	6000	WHILE DRIVING
2002	18504	511	1FMCU04142KA39822	3.0L	T/LD	5	2001	2.00E+03	8F715	D21	10	2160712	33000	ON HIGHWAY
2002	18509	511	1FMCU04142KA37469	3.0L	T/LD	6	2001	1A09	6000	D21	1	391799	0	NO TEXT
2002	18510	511	1FMCU04142KA37469	3.0L	T/LD	5	2001	1A09	6000	D21	1	283573	0	WHILE DRIVING
2002	18521	511	1FMCU04142KA34941	3.0L	T/LD	6	2001	2.00E+03	8F715	D21	5	1407694	12000	STALLS
2002	18525	511	1FMCU04142KA33601	3.0L	T/LD	6	2001	2G04	12A650	D21	6	799823	6800	DOWNHILL
2002	18530	511	1FMCU04142KA31695	3.0L	T/LD	5	2001	2.00E+03	8F715	D21	8	2275464	7800	WHILE DRIVING
2002	18533	511	1FMCU04142KA28818	3.0L	T/LD	6	2001	2G04	DIAG	D21	2	317910	1000	WHILE DRIVING
2002	18535	511	1FMCU04142KA26484	3.0L	T/LD	5	2001	7C05	14N069	D21	5	722455	2000	WHILE DRIVING
2002	18545	511	1FMCU04142KA18013	3.0L	T/LD	6	2001	3B05	RECAL	D21	5	1789007	14000	NO TEXT
2002	18545	511	1FMCU04142KA14092	3.0L	T/LD	5	2001	7B05	14300	D21	9	2030092	14000	NO TEXT
2002	18563	511	1FMCU04142KA87170	3.0L	T/LD	8	2001	2.00E+03	9E355	D21	9	1548054	11000	ON HIGHWAY
2002	18566	511	1FMCU04132KD61156	3.0L	T/LD	5	2002	2.00E+03	8F715	D21	2	2447149	1000	WHILE DRIVING
2002	18569	511	1FMCU04132KD94498	3.0L	T/LD	5	2002	2.00E+03	9H307	D21	1	2514218	0	WHILE DRIVING
2002	18583	511	1FMCU04132KD15379	3.0L	T/LD	4	2002	2.00E+03	8F715	D21	3	2197441	1000	WHILE DRIVING
2002	18589	511	1FMCU04132KD80617	3.0L	T/LD	4	2002	2A01	9B659	D21	2	2009716	1000	WHILE DRIVING
2002	18591	511	1FMCU04132KD80428	3.0L	T/LD	4	2002	3G02	12B579	D21	2	2449275	1000	STALLS
2002	18604	511	1FMCU04132KC91630	3.0L	T/LD	5	2002	2.00E+03	8F715	D21	5	2109118	3000	NO TEXT
2002	18614	511	1FMCU04132KC71636	3.0L	T/LD	3	2002	3G04	DIAG	D21	0	957806	0	STALLS
2002	18618	511	1FMCU04132KC69786	3.0L	T/LD	3	2002	2.00E+03	8F715	D21	3	2306850	2000	WHILE DRIVING
2002	18621	511	1FMCU04132KC65102	3.0L	T/LD	3	2002	2G04	12A650	D21	0	957804	0	WHILE DRIVING
2002	18622	511	1FMCU04132KC69102	3.0L	T/LD	3	2002	2G04	DIAG	D21	2	1273287	2000	WHILE DRIVING
2002	18623	511	1FMCU04132KC58102	3.0L	T/LD	3	2002	2G02	12B579	D21	2	1353573	2000	UPHILL

REPLACED		RD TEST EEC TEST OK FUEL PRESSURE AND EVAP TEST RELAY AND EVAP MANAGEMENT VALVE
TSB		CHECK FOR NO START. RUN WDS TEST. COULD NOT COM MUNICATE WITH PCM. CHECKED ALL FUSES. CHECKED EEC POWER RELAY, INOP. SWITCHED WITH ANOTHER RE LAY AND CAR STARTED. RUN FOR CODES, NONE. TSB 02 11 6.
ENGINE FAILURE		REQUESTING DEALER'S P/A CODE 61874
REPLACED		CONFIRM NO START GET ENGINE RUNNING EXCESSIVE NOISE IN REAR OF ENGINE REPLACE ENGINE ASSEMBLY PER HOTLINE FIN# 1JXG1014
DIAG		HARD TO START. EEC (QUICK TEST) DIAGNOSIS
REFLASH		EEC DIAG,REPROGRAM PCM WITH LATEST CALIBRATION,RETEST,OK
INOP		INOP EEC (QUICK TEST) DIAGNOSIS
NPF		1606 EEC TEST WDS KOEO PASS KOER PASS. PERFORM PINPOINT TESTS PER SYMPTOM. ROAD TEST VEHICLE TO MONITOR PIDS WITH WDS. VEHICLE STARTS AND RUNS FINE. UNABLE TO CONFIRM CUST CONCERN
SSM		WARR WDS TEST NO CODES ENTER DATA LOGGER MONITOR PIDS PERFORM SSM 15699 REPROGRAM PCM AND REPLACE EEC POWER RELAY
REFLASH		TEST SYSTEM REPROGRAMED PCM WITH UPDATE
POOR CONNECTION		TIGHTENED GROUND BOLTS, FOUND BATTERY POSITIVE CABLE LOOSE TIGHTENED. CLEANED BOTH BATTERY TERMINALS. COULD NOT DUPLICATE CONCERN
TSB		11736 SELF TEST KOEO KOER KOEOCM ALL PASS DCL OK DCL RECORDER ROAD TEST OK REPLACED IAC VALVE THROTT LE BODY AND VAPOR MANAGEMENT VALVE AFTER FOLLOW ING TSB 02 11 06 TEST DRIVE OK
REPLACED		PERFORM 6505 ENGINE DIAG RECORD MONITOR DCL DISPLAY SIGNAL SIMULATION REPLACE IAC MAF THROTTLE BODY EVAP VMV EEC RELAY RETEST OKAY
REPLACED		ROAD TEST, UNABLE TO VERIFY A STALLING OR ANY OTHER ABNORMAL DRIVEABILITY CONCERN, NO ABNORMAL DTCS STORED IN MEMORY, ROAD TEST MONITORING PIDS, FUEL PUMP PRESSURE WITHIN SPEC, REMOVE FUEL PUMP A
REFLASH		DOES NOT OPERATE PROPERLY EEC (QUICK TEST) DIAGNOSIS DCL DISPLAY TEST RECORDER MONITOR ROAD TEST DIAGNOSIS PINPOINT TEST DIAGNOSIS REPLACE ID
NPF		DRIVE. FOUND MAF SIGNAL RETURNED TO PROPER SPEC 164 HZ. FUEL TRIMS OK AND IAC AT 39%.CONCERN NO LONGER PRESENT AT THIS TIME
NPF		ROAD TESTED AND IS OK
NO TEXT		
SSM		CHECK FOR STALLING ROADTEST COULD NOT VERIFY WDS HOOK UP OK FUEL PRESSURE,PCM HARNESS & CONNECTOR,IAC 33 PER CENT AT IDLE,T.P. VOLTAGE .62 VOLTS,CRANKSENSOR FOR DAMAGE,ALL OK REMOVE BATTERY AND CHECK
REPLACED		EEC TEST, PIN POINT, REPLACE IAC MOTOR
NPF		CHECK COULD NOT VERIFY CONDERN, NO PROBLEM FOUND AT THIS TIME
TSB		CHECK TSB 02 6 6 FOR STALLING CONCERN RAN STEPS 1 THRU 8 ON TSB AND ROADTESTED 10 MILES UNABLE TO DUPLICATE CONDERN NORMAL OPERATION AT THIS TIME PERFORMED SERVICE PROCEDURES 1 THRU 8 TSB 02 6 6
TSB		EEC TEST NO CODES TSB 02 6 6 FOR STALLING RAN STEPS 1 8 NORMAL CONTACTED HOTLINE INSTRUCTED TO INSPECT PCM HARNESS INSPECT DPFE SENSOR INSPECT CONNECTORS 270B,270C,276D,110,113,INSPECT GNDS 300,100, 1

	C S THAT THE CAR LOSES POWER INTERMITTENTLY HAPPENS WHEN GOING AT A CONSTANT SPEED BETWEEN 40 45 MPH OIL, BATTERY, ENGINE LIGHTS COME ON AND NOTHING WORKS EXCEPT BRAKES CAR WILL NO
REPLACED EEC POWER RELAY AND THROTTLE BODY. REPLACED AIR BYPASS AND CANISTER PURGE SO LENOID. ROAD TEST.	QUIT RUNNING ON THE TURNPIKE
	TOW IN CUST STATES VEHICLE WILL NOT START. STALLED WHEN SITTING IN TRAFFIC.
	OK SOMETIMES HARD TO START ACTS LIKE HARD TO START IF RELEASE KEY VEHICLE DIES INTERMITENT
	CUST STATES CAR DIED ONCE GOING DOWNHILL..CHECK AND ADVISE
	STALLS WHILE DRIVING DOWN HILL THEN WILL START BACK UP
	CUSTOMER STATES ENGINE DIED WHILE CRUISING AT 45 MPH, NO SES, RESTARTED OK
	CHECK FOR REASON THE ENGINE IS STALLING WHILE DRIVING WHEN ENGINE IS STILL COLD, RESTARTS OK, HAPPENED TWICE THIS PAST
	CUST STATES VEHICLE WAS DRIVING ON HIGHWAY AND VEHICLE STUTTERED AND THEN STALLED...STARTED VEHICLE BACK UP HAPPENED AGAIN FINALLY GOT IT HOME AND HAD IT TOWED IN
	CUSTOMER STATES VEH STALLS WHILE DRIVING AND AT IDLE
NO INSPECT FOR FUEL CONTAMINATION, REPLACE FUEL PUMP AND FILTER, ROAD TEST, COULD NOT GET ENGINE TO STALL	CUSTOMER STATES ENGINE STALLED WHILE DRIVING, RESTARTED OK HAS NOT STALLED SINCE
LE AIR CONTROL VALVE ASSEMBLY RECHECK OK RE PROGRAM POWERTRAIN CONTROL MODULE PERFORM DRIVE CYCLE TEST RETEST EEC SYSTEM	DIES DOWN ROAD **HAPPENED 1 TIME**
	CK FOR CAR WILL STALL WHEN DRIVING FEELS LIKE KEY IS SHUT OFF CAR WILL START BACK UP WITH OUT A PROBLEM SEEMS LIKE WHEN RUNNING IT IS OK
	CUSTOMER STATES THE VEHICLE STALLS
GROUNDS UNDER BATTERY OK EVAP HOSE AND BLOW THROU GH IT TAP ON DPFE OK CK PCM FOR LATEST CALIBRATIONOK HAS NEWEST UPDATE RETEST OK	CK FOR STALLING
	CUSTOMER STATES THE ENGINE STALLED WHEN DRIVING ON THE PARKWAY GOING AROUND A TURN
	CHECK VEHICLE STALLS WHILE DRIVING
	CHECK WHILE DRIVING CHECK ENGINE LIGHT CAME ON SOLID,VEHICLE LOST POWER THEN STALLED,CUSTOMER JUST MADE A LEFT TURN THE AFTER VEHICLE STRAIGHTENED OUT THEN STALLED
04,105,101 INSPECT CKP HARNESS AT COMPRESSOR ALL OK INSTRUCTED TO INSTALL NEW MAF SENSOR,UPDATED PART HOTLINE ID NO.113449822 JOHN ZEMDS006	CHECK AT TIMES WHEN ACCELLERATING UP A HILL VEHICLE STALLED,CUSTOMER LEFT SIT FOR 5 MINUTES THEN VEHICLE STARTED

2002	18624	S11	1FMCU04132XC68102	3.0L	TAD	3	2002	2.00E+03	9F715	D21	4	2419366	6000	WHILE DRIVING
2002	18625	S11	1FMCU04132XC48010	3.0L	TAD	2	2002	1H03	9J460	D21	3	1541544	3000	STALLS
2002	18626	S11	1FMCU04132XC48010	3.0L	TAD	2	2002	2.00E+03	9F926	D21	6	2410919	6000	WHILE DRIVING
2002	18635	S11	1FMCU04132XC29859	3.0L	TAD	2	2002	2304	12A650	D21	6	2411194	10000	DOWNHILL
2002	18650	S11	1FMCU04132XB99302	3.0L	TAD	1	2002	2304	DIAG	D21	6	2429167	4000	WHILE DRIVING
2002	18651	S11	1FMCU04132XB99302	3.0L	TAD	1	2002	2302	129579	D21	3	1129529	2000	AT STOP
2002	18652	S11	1FMCU04132XB99302	3.0L	TAD	1	2002	1H09	9J460	D21	4	1290369	3000	WHILE DRIVING
2002	18653	S11	1FMCU04132XB99302	3.0L	TAD	1	2002	2305	RECAL	D21	7	2399964	5000	NO TEXT
2002	18671	S11	1FMCU04132XB67377	3.0L	TAD	12	2001	2305	RECAL	D21	6	1369692	3000	WHILE DRIVING
2002	18677	S11	1FMCU04132XB66670	3.0L	TAD	12	2001	2.00E+03	9F715	D21	6	1640366	3000	WHILE DRIVING
2002	18684	S11	1FMCU04132XB64642	3.0L	TAD	1	2002	2.00E+04	9C915	D21	3	1848609	3000	COASTING
2002	18689	S11	1FMCU04132XB66052	3.0L	TAD	12	2001	2.00E+03	9F715	D21	6	1844114	6000	WHILE DRIVING
2002	18691	S11	1FMCU04132XB44097	3.0L	TAD	11	2001	2305	RECAL	D21	7	1628127	7000	WHILE DRIVING
2002	18693	S11	1FMCU04132XB30696	3.0L	TAD	11	2001	2.00E+03	9F715	D21	6	1672606	6000	AT STOP
2002	18706	S11	1FMCU04132XB20737	3.0L	TAD	11	2001	2305	RECALEM	D21	5	888880	7000	WHILE DRIVING
2002	18711	S11	1FMCU04132XB20676	3.0L	TAD	11	2001	2305	RECAL	D21	5	2356976	6000	STALLS
2002	18713	S11	1FMCU04132XB20415	3.0L	TAD	11	2001	2304	DIAG	D21	5	1747869	7000	WHILE DRIVING
2002	18715	S11	1FMCU04132XB18851	3.0L	TAD	11	2001	2304	12A650	D21	2	804215	2000	WHILE DRIVING
2002	18722	S11	1FMCU04132XB13674	3.0L	TAD	11	2001	2304	12A650	D21	5	1111025	7000	WHILE DRIVING
2002	18729	S11	1FMCU04132XB03615	3.0L	TAD	11	2001	2305	RECALEM	D21	4	699955	3000	WHILE BRAKING
2002	18736	S11	1FMCU04132XB01279	3.0L	TAD	10	2001	2304	12A650	D21	5	1116995	3000	STALLS

TSB		RDTEST 10 MILES, DIDNT STALL. TEST EEC, NO CODES. CALL HOTLINE, ROLF, 2E4B0008. REPLACE DPFE, THROTTLE BODY, IAC, VAPOR MGT VALVE. CONTACT FSE FOR OPINION, OK TO REPL. RAN TSB 02 06 06. PERFORMED OH
REPLACED		OUT OF RANGE STAR TEST REPLACE DPFE SENSOR
REPLACED		STALLING STAR TEST MONITOR TEST REPLACE THROTTLE BODY DRILL OUT AIR BLEED CHECK EVAP TEST ROAD TEST
REFLASH		RESET BASE IDLE SPEED SETTING REPROGRAMMED POWERTRAIN CONTROL MODULE
HOTLINE		ROAD TEST COULD NOT PRODUCE STALL SELF TEST WITH NGS KOEO PASS PASS KOER PASS CALL HOTLINE CHECK C135 C110 OK CHECK G104 G105 OK
REPLACED		2982 COULD NOT VERIFY CONCERN. MIL OFF. WDS DIAG. KOEO PASS, KOER PASS, CONT PASS, DATALOGGER PASS, FUEL PRESSURE AND LEAKDOWN PAS INJECTOR FLOW PASS, POWER BALANCE PASS. REPLACED MAF SENSOR AND THRO
TSB		3586 DOWNLOAD & INSTALL VDR PERFORM STEP 4 TSB 02 06 06. INSPECT EVAP LINES FOR BLOCKAGE OK MONITOR ALL PIDS EVAP 54% RMP 742 ECT 180 ALL WITHIN SPECS. REPLACE DPFE SENSOR UPDATED PART ROAD TEST
TSB		PERFORMED WDS DIAGNOSIS FOR ENGINE STALLS, CUTS, NO CODES FOUND, PERFORMED EVAPORATIVE TEST, RELATIVE COMPRESSION, PERFORMED TSB 02 11 06 AND REPROGRAMMED PCM
TSB		EEC TEST NO CODES, CHECK OASIS SYMPTOM CODES PERFORM MOTOR ROAD TEST PER TSB 02 6 06 CHECK IAC DUTY CYCLE AT OPP TEMP NO PURGE FLOW WITHIN SPECIFICATION, PROCEED TO STEP 2 VEH BUILT 12 01 RECALLS
TSB		COULD NOT VERIFY CONCERN, FOLLOW RECOMMENDATIONS FROM TSB FORD MESSAGE. REPLACED IDLE AIR CONTROL VALVE, THROTTLE BODY, EVAP VALVE, EEC RELAY AND REPROGRAMMED PROCESSOR.TSB 02 11 6
TSB		3980 STALLS DIES 129600,D01,D3,D7,D48,D66,D80,D81,D84,90000,D1, D2 WDS TESTING EEC TEST NO CODES PINPOINT TEST REPLACE IAC AS PER TSB EVAP SYSTEM TESTING REPL ACE VMV AS PER TSB REPLACE PCM RELAY A
TSB		ROAD TEST, EEC TEST ALL PASS CODES CHECK OASIS AND FOUND TSB 2 11 6, REMOVED AND REPLACE IDLE AIR CONTROL VALVE AND REPROGRAM PCM PER TSB . ROAD TEST AGAIN TO VERIFY PROPER OPERATION
TSB		EEC TEST PASS CODES FOLLOW TSB 2 11 6 MONITOR PIDS REPROGRAM PCM ROADTEST OK
REPLACED		1 CHECKED OUT, RUN EEC TEST P1607, MONITOR PIDS, PID MONITOR RECORDER ON TEST DRIVE, PINPOINT TEST, REPLACED IAC, RERUN
SSM		ROAD TEST FOR DYING, EEC (QUICK TEST) DIAGNOSIS , HOOK UP WDS,KOEO,KOER,DATALOGGER,FUEL PRESSURE, INJ FLOW,PWR BAL, SPARK DURATION,NOTHING ABNORMAL FOUND,FOUND SSM 15599 FOR REFLAS
REFLASH		NGS TEST NO CODES REPROGRAMMED PCM PER ARTICLE 02 11 6
NPF		CHECK FOR STALLING ROAD TST VEHICLE. NO STALL. WDS TESTED. SELF TEST. DATA LOG GER. NO CODES RECEIVED. RAN OASIS. NO MESSAGES. NORMAL OPERATION AT THIS TIME.
SSM		ROAD TEST, COULD NOT DUPICATE. SUN OASIS, SSM 15599, CHECK RELAY, OK. INSTALL NGS, ROADTEST PID MONITOR. REPROGRAM PCM AS PER SSM, DISCONNECT EVAP VENT LINE, CHECK FOR RESTRICTION AND CLEAN WITH AIR A
REFLASH		CHECK FOR CODES NONE PERFORM PNPT TEST CHECK FUEL PRESSURE PASS CHECK IGNITON PERFORM ROADTEST WITH MONITOR AND MONITOR PID DATA REPROGRAM PROCESSOR AND BLOW OUT EVAP LINE AND CHECK RELAY ALL OK RETES
SSM		RUN EEC TEST NO CODES OR LIGHT RUN ON OASIS REPROGRAMMED PCM PER SSM 15599 RECHECKED PROBLEM FIXED
REFLASH		DOES NOT OPERATE PROPERLY DIAGNOSED AND REPROGRAM PCM D01 48

ECK STOPS, RETEST OK RETEST OK	OK VEHICLE, STALLS WHILE DRIVING
	CHECK FOR STALLING
	CK FOR STALLING OUT WHEN DRIVING DOWN ROAD
	CUSTOMER STATES ENGINE CUT OUT ONCE WHEN GOING DOWN A HILL THEN CHOKED OUT GOING UP A HILL
	CUSTOMER STATES VEHICLE STALLED OUT WHILE DRIVING STARTED RIGHT UP
TTLE BODY ASSEMBLY WITH REVISED PARTS AS PER HOTLINE. RETEST IAC 40%	CUSTOMER STATES VEHICLE STOPPED RUNNING WHILE DRIVING, RESTARTED OK, THIS HAPPENED 1 TIME ONLY, AFTER VEHICLE WARMED UP
	CUST STATES THE VEHICLE DIED WHILE DRIVING VEHICLE HAD BEEN DRIVEN ABOUT 20 25 MINUTES BEFORE THIS HAPPENED AND THE VEHICLE DID START RIGHT BACK UP D21
RATE PCM PER TSB, ROAD TEST PROBLEM RESOLVED OK AT THIS TIME.	CUSTOMER STATES ENGINE DIES WHEN DRIVING LIKE THE KEY IS SHUT OFF AND DOES NOT RESTART. OIL LIGHT DID COME ON JUST BEFORE THE ENGINE DIED.
	TRUCK STALLS OUT WHILE DRIVING. HAS STALLED ON 2 OCCASIONS.
ND REPROGRAM PCM AS PER TSB DCL DISPLAY PID DATA MONITOR RECORD RETEST AFTER REPAIR NO DUPLICATION	CUSTOMER STATES THAT WHILE PULLING INTO PARKING AREA,VEHICLE STALLED AND DIED
	CS WHILE DRIVING 30MPH STEERING WHEEL LOCKEDE AND CAR STALLED (WHILE BRAKING) RESTARTED IT HAS BEEN FINE SINCE
	OWNER STATES ENGINE DIED AT 30 MPH AND RESTARTS ...CK ADVISE
	ENGINE CUTS OFF ON ACCEL FROM STOPS ALSO IDLES ERRATIC
H AND CHECKING FOR REVISED EEC RELAY,REFLASH PCM AND RETEST	CHECK ENG DIED WHILE DRIVING, GOING DOWN HILL, WITH FOG LIGHTS ON.
	CUSTOMER STATES: WHEN STOPPED AT INCLINE AFTER GOING OVER INCLINE VEHICLE STALLS SERVICE ENGINE LGT ON OIL LIGHT ON
	CUSTOMER STATES WHEN DRIVING AT 40 MPH THE VEHICLE STALLED ONCE.
S PER SSM.	CUSTOMER STATES:ENGINE SHUT OFF WHILE DRIVING ON WAY TO SHOP, COASTED TO A STOP RESTARTED OK
T PASS OK	CUSTOMER REPORTS THAT ENGINE QUIT RUNNING THIS MORNING WHILE DRIVING COASTED TO SIDE OF ROAD ENGINE RESTARTED 1ST ATTEMPT DROVE TO WORK AND BACK WITH NO FURTHER PROBLEM
	CUSTOMER STATES VEHICLE STALLS SOMETIMES WHEN SLOWING DOWN GENERALLY BETWEEN 45 25 MPH MILEAGE POOR RUNS ROUGH
	C S VEHICLE STALLS

2002	15741	611	1FMCU04132KA69216	3.0L	T/LD	10	2001	2.00E+03	9F715	D21	7	1486802	16000	WHILE DRIVING
2002	15745	611	1FMCU04132KA69560	3.0L	T/LD	10	2001	2.00E+03	9F715	D21	7	1486894	13000	SAME SPOT
2002	15746	611	1FMCU04132KA69560	3.0L	T/LD	10	2001	2G04	13N650	D21	5	976513	9000	SAME SPOT
2002	15761	611	1FMCU04132KA69915	3.0L	T/LD	10	2001	2G05	FBCAL	D21	9	1551460	15000	AT STOP
2002	15763	611	1FMCU04132KA69549	3.0L	T/LD	10	2001	2.00E+03	9F715	D21	10	2306239	9000	WHILE DRIVING
2002	15767	611	1FMCU04132KA76391	3.0L	T/LD	10	2001	2.00E+04	9C915	D21	9	2039708	5000	STALLS
2002	15767	611	1FMCU04132KA69569	3.0L	T/LD	10	2001	2.00E+03	9F715	D21	5	894778	8000	WHILE DRIVING
2002	15770	611	1FMCU04132KA69451	3.0L	T/LD	9	2001	2.00E+03	9F715	D21	10	2042367	9000	STALLS
2002	15771	611	1FMCU04132KA69451	3.0L	T/LD	9	2001	1H03	9J460	D21	10	2269316	9000	STALLS
2002	15776	611	1FMCU04132KA67716	3.0L	T/LD	10	2001	7511	14467	D21	2	469899	1000	ACCELERATING
2002	15780	611	1FMCU04132KA64572	3.0L	T/LD	10	2001	2G01	13A650	D21	7	1335176	8000	STALLS
2002	15786	611	1FMCU04132KA51290	3.0L	T/LD	9	2001	2.00E+03	9F715	D21	3	403922	4000	DOWNHILL
2002	15787	611	1FMCU04132KA51290	3.0L	T/LD	9	2001	2.00E+03	8E939	D21	10	1903206	12000	WHILE DRIVING
2002	15790	611	1FMCU04132KA50562	3.0L	T/LD	9	2001	2.00E+03	9F715	D21	5	828952	4000	WHILE DRIVING
2002	15804	611	1FMCU04132KA43984	3.0L	T/LD	8	2001	2G04	13A650	D21	11	1999016	14000	WHILE DRIVING
2002	15811	611	1FMCU04132KA40273	3.0L	T/LD	9	2001	7V01	12A691	D21	10	1979995	8000	WHILE DRIVING
2002	15813	611	1FMCU04132KA39511	3.0L	T/LD	9	2001	1A03	6008	D21	1	318772	0	WHILE DRIVING
2002	15819	611	1FMCU04132KA39466	3.0L	T/LD	9	2001	2.00E+03	9F715	D21	3	420947	3000	WHILE DRIVING
2002	15820	611	1FMCU04132KA39466	3.0L	T/LD	9	2001	2.00E+03	8E939	D21	10	2414848	12000	WHILE DRIVING
2002	15821	611	1FMCU04132KA39466	3.0L	T/LD	9	2001	1H03	9J460	D21	9	1564391	11000	WHILE DRIVING
2002	15825	611	1FMCU04132KA39692	3.0L	T/LD	9	2001	2.00E+03	9F715	D21	12	2299480	11000	TSB
2002	15831	611	1FMCU04132KA39697	3.0L	T/LD	8	2001	2.00E+03	9F715	D21	11	1624885	9000	WHILE DRIVING

TSB		UNABLE TO VERIFY CONCERN, NO CODES ALL PASS, CHECK OASIS & FOUND TSB 2 6 6 TO INSTALL UPDATED IAC. REPLACE IAC (IDLE AIR CONTROL) & GASKET WITH UPDATED, PROVED THROUGH TSB 2 6 6, FLASH PCM TO 2L8A AD
REPLACED		RAN EEC TEST OK DCL DISPLAY PID MONITOR TEST OK FUEL PRESSURE TEST OK IGNITION SYSTEM TEST OK PINPOINT TEST REPLACED IAC (IDLE AIR CONTROL VALVE) PER SPECIAL SERVICE MESSAGE RETEST OK TEST DRIVE 6 MI
REFLASH		RAN EEC TEST OK DCL DISPLAY OK PID MONITOR TEST OK IGNITION SYSTEM TEST OK FUEL PUMP TEST OK PINPOINT TEST REPROGRAMMED PCM PER SPECIAL SERVICE MESSAGE 16999 RETEST OK
TSB		15694 ROAD TEST NO MIL NO DRIVABILTY WDS DIAG. KOEO PASS 10 PASS KOER PASS DATALOGGER MONITOR PIDS (TSB 02 11 06) REPROGRAM PROSSESSOR OK. RELAYS INSTALL NGS + MONITOR PIDS WHILE DRIVING
POOR CONNECTION		IN TIME TO CHECK CHARGING SYSTEM, PID DATA RECORD, IAC DUTY CYCLE 48 PERCENT, CHECK WIRING, WIRING FROM IAC TO PCM HIGH RESISTANCE, TRACED HARNESS, FOUND LOOSE SPLICE UNDER INTAKE MANIFOLD, REPAIR AND
INOP		C VALVE ASSEMBLY FUEL VAPOR STORAGE CANISTER PURGE REGULATOR
STICKING		ROAD TEST.VERIFIED STALLING CONCERN EEC TEST. DIAGNOSE IAC IS STICKING. RR IAC VALVE. RECHECK OK
REPLACED		DIAGNOSED AND REPLACED AIR BYPASS VALVE REPROGRAMED PROCESSOR
TSB		DIAGNOSED AND PERFORMED TSB 02 11 6...CHECKED CONNECTOR C270B C110 C158.CHECKED GROUNDS G100 G104 G105 G181..
LOOSE GROUND		LOOSE GROUND DIAG AND LOCATE LOOSE GROUNDS RESECURE GROUNDS AND PERFORM ENG TEST ROAD TESTED OK
INOP		INOP EEC (QUICK TEST) DIAGNOSIS
REPLACED		TEST DROVE THE VEHICLE. NGS HOOK UP. EEC SELF TEST PASSED WITH NO CODES. PID DATA MONITOR READING NORMAL. CHECKED OASIS. CHECKED TNE CONNECTIONS AND GROUNDS AS PER SERVICE MESSAGE 15494. REPLACED
TSB		TEST DROVE THE VEHICLE AND WAS UNABLE TO RECREATE THE CONCERN. PERFORMED THE EEC SELF TESTS. FOUND ONLY A SYSTEM PASS WITH NO DTCS IN THE MEMORY. PERFORMED PID DATA MONITOR. PERFORMED A POWER BALAN
REPLACED		NGS, PINPOINT, REPLACED IAC VALVE AND RETESTED
REFLASH		WDS, CK IGNITION, ROAD TEST WITH WDS, REPROGRAM PCM, RETEST
REFLASH		NGS HOOK UP, SELF TEST, PINPOINT, ROAD TEST WITH MONITOR, MONITOR PIDS CHECK RELAYS AND GROUNDS AND12A581 HARNESS, REPROGRAM PCM ROAD TEST REPAIR VE RIFIED.
REPLACED		PRESSURE CK COOLING SYSTEM; COOLANT LOSS. REMOVE INT MANIFOLD, SPARK PLUGS, INSPCT WBORESCOPE, REMOVE RT VALVE COVER; BROKEN VALVE INTO #2 CYL.REMOVE ENGINE AND TRANS, REPLACE ENGINE. REMOVE TRANS
SSM		DTC 42 UNABLE TO VERIFY CONCERN EEC TEST NO CODES IN SYSTEM CHECK OASIS PERFORM PROCEDURE AS PER SSM 15494 ALL OK
TSB		CHECK ON CONCERN UNABLE TO VERIFY CONDERN RUN OASIS TSB 02 11 06 MONITOR IAC PIDS OVER 46% REPLACE IAC RETEST PIDS 45% REPLACE THROTTLE BODY VERIFY PCM REPROGRAM OK MONITOR AVAP AND BLOW OUT EVAP HOSE
REPLACED		ROAD TESTED VERIFIED CONCERN PERFORM EEC SYSTEM DIAG AND PP TEST NO DTC MONITOR PIDS REBURN PCM WITH LATEST CALIBRATION REPLACE PPE OUT OF RANGE AND REPLACE VM VALVE AS PER EVAP TEST RESULTS CLEAN AND
REFLASH		R AND R IAC AND VAPOR MANAGEMENT VALVE. REPLACE THROTTLE BODY. REPROGRAM PCM AS PER 02 11 6
REPLACED		9904 IAC VALVE N G ROAD TESTED TO TRY TO VERIFY CONCERN CHECKED FOR CODES NONE FOUND CHECKED IAC FOUND LIL BUILD UP IN VALVE REPLACED VALVE AND CHECKED OVER SEEMS TO BE OK REPAIR VERIFYED ROAD TSB

AS PER TSB	CUSTOMER STATES ENGINE STALLED WHILE DRIVING DOWN HILL.
LES OK CONCERN NOT VERIFIED	CUSTOMER STATES THE ENGINE WILL DIE ABOUT 4.5 MILES FROM CUSTOMERS WORK, ALWAYS AT THE SAME CROSSWALK AS SHE IS
	CUSTOMER STATES THE TRUK HAS STALLED IN THE SAME AREA OF TOWN 2 TIMES IN THE LAST 15 DAYS PLEASE SEE ADVISOR
	CUSTOMER STATES VEHICLE STALLED WHEN AT A STOP, VEHICLE WAS IN DRIVE, AC SYSTEM WAS ON D21
SOLDERED WIRING, RETEST OK	CUSTOMER STATES VEHICLE CUT OUT WHILE DRIVING. ENTIRE ELECTRICAL SYSTEM. 2ND TIME. STARTS RIGHT BACK.
	CUST STS THAT THE VEHICLE STALLS (INTERMITTEN)
	VEHICLE STALLS WHILE DRIVING AT 55 MPH.EASY TO RESTART
	CUST STATES VEHICLE STALLING AT TIMES
	CUSTOMER STATES: ENGINE STALLS
	CUSTOMER STATES ON ACCEL ENGINE STALL OUT (SOP)
	CHECK ENGINE CUT OUT TWICE VERY INTERMITTEN
THE EEC RELAY AND IAC VALVE AS PER SERVICE MESSAGE 15434	CHECK FOR ENGINE DIEING WHILE DRIVING AT 25 35 MPH DOWNHILL ON CROOKED ROAD
GE TEST. PERFORMED A FUEL PRESSURE TEST. PERFORMED TESTS STATED ON TSB 02 11 08. PERFORMED STEPS 1 8. THE PCM WAS REPROGRAMMED AND THE THROTTLE BODY ASSEMBLY WAS REPLACED PER DIAGNOSTIC	VEHICLE CUT OFF WHEN DRIVING LOW SPEEDS VEHICLE STARTED RIGHT BACK UP HAPPENED ONCE
	VEHICLE DIED WHILE DRIVING HAS HAPPENED TWICE
	CK CUT OFF ON ROAD ONE TIME AS IF TURNED KEY OFF IMMEDIATELY STARTED AND RAN NORMALLY CK PER TSB 99M REGARDING EEC AND PCM RELAYS
	C S VEHICLE STALLS AT 30 MPH
TORQUE CONVERTOR AND SEAL, ROAD TEST. M TIME LABOR; NO LABOR OPS EXIST. ENGINE SEIZED, COULD NOT ROTATE TO REMOVE COVERTOR/CORE. ACTUAL HRS 19.1. NO ENGINE/TRANSMISSION LABOR OPS OR ENGINE OR TRAN	STALLED WHILE DRIVING, WILL NOT RESTART
	VEHICLE DIES WHILE DRIVING
RD TEST FOR 10 MILES RUNS OK DID NOT STALL ON RD TEST RPMS DID NOT DROP UNDER 700	CUSTOMER STATES CAR STALLS WHILE DRIVING REPORT
REGAP PLUGS AND ROAD TEST RETEST OK	CUSTOMER STATES TRUCK STALLS OUT AT TIMES WHILE DRIVING.(SEE RAY 1ST)
	STALLS ON OFF ACCELERATOR REPLACE PARTS ACCORDING TO TSB 11 6 02
TED VERIFYED CONCERN STALLS CHECKED FOR CODES NONE FOUND DID KOEO TEST OK DID KOER OK CHECKED IAC N G WAITING ON PART REMOVED AND	CUSTOMER STATES OK TRUCK IT STALLED WHILE DRIVING IT DID RESTART BUT IT ONLY STALLED ONCE

2002	18939	S11	1FMCU04132KA25654	3.0L	T/LD	8	2001	2C01	11002	D21	3	592241	4000	NO START
2002	18943	S11	1FMCU04132KA25160	3.0L	T/LD	8	2001	2G05	RECAL	D21	11	1998695	6000	STALLS
2002	18955	S11	1FMCU04136KA14857	3.0L	T/LD	8	2001	2G05	RECAL	D21	6	1036153	3000	WHILE BRAKING
2002	18957	S11	1FMCU04132KA14364	3.0L	T/LD	8	2001	2G04	12A650	D21	11	2007646	10000	STALLS
2002	18972	S11	1FMCU04132KA07161	3.0L	T/LD	8	2001	7C05	14N089	D21	4	560126	5000	WHILE DRIVING
2002	18980	S11	1FMCU04132KA06572	3.0L	T/LD	8	2001	7C05	14N089	D21	11	2006661	7000	WHILE DRIVING
2002	18981	S11	1FMCU04122KE09016	3.0L	T/LD	6	2002	2G04	DIAG	D21	2	2458763	6000	ACCELERATING
2002	18983	S11	1FMCU04122KD80451	3.0L	T/LD	6	2002	2.00E+03	9E926	D21	2	2258978	1000	STALLS
2002	18986	S11	1FMCU04122KD67848	3.0L	T/LD	6	2002	2.00E+03	9F715	D21	-1	2410721	0	STALLS
2002	18989	S11	1FMCU04122KD49428	3.0L	T/LD	6	2002	2.00E+03	9E926	D21	4	2456834	5000	WHILE DRIVING
2002	18990	S11	1FMCU04122KD41466	3.0L	T/LD	5	2002	2G05	12A529	D21	-1	1953415	0	WON'T RUN
2002	18995	S11	1FMCU04122KD22324	3.0L	T/LD	4	2002	2G04	DIAG	D21	1	1951378	3000	STALLS
2002	18996	S11	1FMCU04122KD22114	3.0L	T/LD	4	2002	1H03	9J460	D21	1	1922110	1000	WHILE DRIVING
2002	18999	S11	1FMCU04122KD00588	3.0L	T/LD	4	2002	1H03	9J460	D21	5	2102542	7000	STALLS
2002	19005	S11	1FMCU04122KC85579	3.0L	T/LD	3	2002	6J09	11582	D21	4	1978497	4000	STALLS
2002	19012	S11	1FMCU04122KC83072	3.0L	T/LD	3	2002	2G02	98989	D21	3	2427859	2000	AT STOP
2002	19013	S11	1FMCU04122KC82648	3.0L	T/LD	3	2002	7C05	14N089	D21	3	1566051	2000	AT STOP
2002	19019	S11	1FMCU04122KC68910	3.0L	T/LD	3	2002	7V01	12A581	D21	1	1915739	1000	UPHILL
2002	19023	S11	1FMCU04122KC46927	3.0L	T/LD	2	2002	2G04	12A650	D21	4	2007125	3000	STALLS
2002	19025	S11	1FMCU04122KC37515	3.0L	T/LD	2	2002	2G02	12B579	D21	3	2151057	2000	WHILE DRIVING
2002	19031	S11	1FMCU04122KC30193	3.0L	T/LD	2	2002	2F02	9E926	D21	3	1571641	2000	WHILE DRIVING
2002	19032	S11	1FMCU04122KC30195	3.0L	T/LD	2	2002	2.00E+03	9F715	D21	3	1526468	2000	WHILE DRIVING
2002	19035	S11	1FMCU04122KC29578	3.0L	T/LD	2	2002	2G04	12A650	D21	2	2062010	3000	WHILE DRIVING

REPLACED		TRIED TO START VEHICLE, TRIED TO JUMP START VEHICLE, WOULD NOT JUMP, CHECKED BATTERY BATTERY HAS FULL CHARGE, TESTED SYSTEM FOUND STARTER SOLENOID BAD, REMOVED AND REPLACED STARTER, ALSO TEST CHARGING
REPLACED		9198 WDS TEST ALL PASS CODES TEST FOR SPARK,TEST FUEL PRESSURE ROAD TEST, REPLACE EEC RELAY, REPROGRAM PCM
TSB		9176 CK FOR STALLS AT TIMES WARR RAN WDS TESTING NO CODES RAN SSM AND TSB NO MESSAGES REMOVED GROUND AND CLEANED UNDER BATTERY TRAY REFLASHED PCM TEST DROVE
REFLASH		COMPUTER DIAG SYSTEM RESET BASE IDLE AND REPROGRAM PCM
NPF		EEC TESTED NO CODES PINPOINT TESTS O.K. DCL AND NGS RECORD NO PROBLEMS FUEL AND IGN. SYSTEMS O.K. TEST DROVE CND
TSB		1 NGS TEST EEC TEST AND MONITOR PIDS REPL EEC RELAY AND CHECKED PCM UPDATE AS PER TSB 2 11 6 ROAD TEST OK NOW
TSB		6217 VEHICLE STALLS 42 WARRANTY RAN EEC TEST KOEO KOER NO DTCS RAN FUEL PRESSUR E TEST RAN DATA LOGGER ROAD TEST VEHICLE CAN NOT GET VEHICLE TO STALL . RAN OASIS NO TSBS OR SSM FOR STALL ON ACCELER
TSB		DIAG PER TSB REPLACED IDLE AIR CONTROL MOTOR VMV THROTTLE BODY ASSY
TSB		RUN DIAGNSOTICS, NO CODES RUN PINPOINT TSBTS REPLACE IDLE AIR CONTROL PER TSB 02 11 08 REPLACE BRAKE LIGHT SWITCH
REPLACED		IAC, TB BODY RELAY AND EEC RELAY EEC (QUICK TEST) DIAGNOSIS REPL IAC , THROTTLE BODY RELAY AND EEC RELAY PINPTNETEST DCL MONITOR DISPLAY
REFLASH		9 WATER LEAK INTO PROCESSER CHECK ENG NO START XX PATS WILL NO ACCEPT KEY CODES XX STAR TEST CODE P1342 B1601 XX PINPOINT TEST B1601 XX TEST TRANSPONDER AND WIREING ALL OK REPROGRAM PATS XX WILL NO
NPF		TEST WITH NGS NO CODES MONITOR PIDS COULD NOT DUPLICATE CUSTOMERS CONCERN
INOP		NOT WORKING PROPERLY FUEL PUMP PRESSURE TEST ON VEHICLE DIAGNOSIS
INOP		SHORTED EEC (QUICK TEST) DIAGNOSIS
HEAVY KEYS		AND OTHER PARAPHANALIA FROM KEY CHAIN IN ORDER TO REDUCE WEIGHT EXERTED ON IGNITION LOCK. THIS WILL PREVENT VEHICLE FROM BEING TURNED OFF WHILE DRIVING.
ADJUST		TEST SYSTEM CODE PASS ADJUSTED TP SENSOR & BASE IDLE AS PER FSE
REPLACED		ROADTESTED VEHICLE TO VERIFY. PERFORMED EEC TEST. REMOVED BATTERY AND TRAY, TEST GROUNDS, INSPECT AND TIGHTEN. REPLACE EEC RELAY RUN OASIS WITH SYSTOM CODE CALLED TECH HOTLINE OASE 2FUN6003 INSPECT BU
REPLACED		VERIFIED CONCERN, REPLACED EEC RELAY, RECHECKED OK
HOTLINE		ROADTESTED TRUCK. USED WDS TO MONITOR IAC DUTY CYCLE. CHECKED FOR CODES. ROADTESTED TO MONITOR FUEL PRESSURE ALL OK AT THIS TIME. CHECKED COMPRESSION AND POWER BALANCE TEST. PERFORMED STATIC COMPR
TSB		ROAD TEST SEVERAL MILES, THREE DIFFERENT TIMES. WITH WDS HOOKED UP AND MONITORING PIDS...RAN F INE EVERY TIME, WOULD NOT STALL. RAN OASIS, CAL LED HOTLINE. MIKE 7 16 02. ADVISED CHECKING CIR CUITS
TSB		2921 FORD REP KEVIN R. 126500,D45,D60,D61,M WARRANTY WDS DIAG AND TESTING DATA LOGGER PID DATA DISPLAY RECORD MONITOR AS PER FORD REP CHANGED BASE IDLE SETTING AFTER PERFORMING TSB 02 11 06 AS PER
REPLACED		2618 DIES 126500,DX1,D6,D7,D22,D46,D66,D80,D81,99000,D1, D2,99500,9999A WDS TESTING EECTEST NO CODES PINPOINT TEST DCL DISPLAY DATA RECORD MONITOR IGNITION SYSTEM AND FUEL SYSTEM TESTING REPLACE IAC,
DIAG		EEC TEST PID MONITOR ROAD TEST ADJ HARD START IDLE ROAD TEST

SYSTEM ALL OKAY.	C S TOWED IN NO START
	ENGINE STALLING
	VEH HAS STALLED SEVERAL TIMES ON TURNS SLOW SPEEDS, 2X ON RIGHT TURNS, 1X SLOWING DOWN ALL IN A 1 WEEK TIME PERIOD HOT OR COLD
	VEHICLE STALLED IN MOTION
	CUST STATES VEHICLE DIED ONCE WHEN DRIVING...CHECK AND ADVISE
	CUSTOMER STATES TAT TWICE WHILE DRIVING THE VEHICLE SHUT OFF HAD BEEN DRIVING THE VEHICLE FOR ABOUT TEN MIN
ATION	CUST STATES VEHICLE DIED WHILE ACCELERATING,THEN RESTARTED,AND HAS RUN OK SINCE
	C.S. OIL LIGHT, BATT LIGHT CAME ON, LOST P S SEEMS LIKE IT STALLED, HAPPENED TWICE, SEE PAUL
	VEHICLE STALLED ON TEST DRIVE
	DIED THIS AM WHILE DRIVING BUT DID START RIGHT BACK UP CK OUT
T ACCEPT REPROGRAM XX PINPOINT TEST CODE P1942 XX NO DEFINATION OR PINPOINT TEST IN AMY MANUAL OR CD XX CALL HOTLINE TALKED TO MARTI XX PERFORM PCM DIAG ON ALL WIRING POWER AND GROUNDS	VEHICLE WILL NOT STAY RUNNING BLOWING SMOKE RUNNING ROUGH THEFT LAMP FLASHING BATTERY LAMP FLASHING
	CORRECT CAUSE OF CUSTOMER STATES THAT THE CHECK ENGINE LITE CAME ON AND VEHICLE STALLS
	SHUTS OFF WHILE DRIVING
	STALLS OUT
	VEHICLE STALLED AND ALL LIGHTS CAME ON , RAN OK HERE
	ENGINE STALLS AT STOPS
LINHEAD CONNECTOR FOR WATER INTURSION INSPECTED 12A650 FOR PIN DAMAGE OR LOOSE REASSEMBLE AND ROADTEST ALL OK	VEHICLE BUCKS ON ACCELERATION FROM STOP, THEFT LIGHT WILL STAY ON AT THIS TIME.
	CUSTOMER STATES WHILE GOING UP A STEEP HILL,WITH AC ON AND VEHICLE STALLED,PROBLEM OCCURED ONCE
SSION TEST USING THE WDS. PERFORMED INJECTOR FLOW TEST ALL OK. PERFORMED PIN OUT TEST WITH THE BREAK OUT BOX TO CHECK IAC DUE TO PAST CONCERNS WITH THE HELP WITH FORD HOTLINE.	C S CAR STALLED WITH NO WARNING, RESTARTED. CHECK AND ADVISE
AND GROUNDS AND REPLACING DPFE SENSOR, MA 86 AIR FLOW SENSOR. DID WIGGLE WIRE TEST. CHECK GROUNDS G300 G100 CONNECTORS C271 C&D C11 0 C133. REPLACED MAF AND DPFE SENSORS. ROAD TES T AGAIN,	DIED WHILE DRIVING TWICE, COMING TO STOP (SLOWING DOWN FOR TRAFFIC), RESTARTS OK
FORD REP	CUSTOMER STATES THAT THE CAR DIES STALLS WHILE DRIVING PULLED TO THE SIDE CAR RESTARTED RIGHT AWAY
T BODY ASSY, VMV AND EEC RELAY AS PER TSB 02 11 08	CUSTOMER STATES ON 2 OCCASIONS VEHICLE DIED,ONCE AT A STOP SIGN THE OTHER WHILE DRIVING DOWN HILL
	CUSTOMER STATES SHUT OFF WHILE DRIVING ROAD TEST AND VERIFIED CONDITION DIAGNOSE AND TEST SYSTEM

2002	19048	S11	1FMCU04122KB66981	3.0L	T/LD	1	2002	2.00E+04	9C915	D21	5	2041403	4000	WHILE DRIVING
2002	19057	S11	1FMCU04122KB77107	3.0L	T/LD	1	2002	2G06	RECAL	D21	1	052060	0	UPHILL
2002	19058	S11	1FMCU04122KB77107	3.0L	T/LD	1	2002	2F02	8E926	D21	4	1660666	4000	WHILE DRIVING
2002	19059	S11	1FMCU04122KB77107	3.0L	T/LD	1	2002	1H03	9J460	D21	4	1704150	3000	ON HIGHWAY
2002	19063	S11	1FMCU04122KB78247	3.0L	T/LD	1	2002	2G04	12A650	D21	7	2317224	12000	WHILE DRIVING
2002	19070	S11	1FMCU04122KB83952	3.0L	T/LD	12	2001	2G04	DIAG	D21	7	2119830	8000	WHILE DRIVING
2002	19080	S11	1FMCU04122KB43927	3.0L	T/LD	12	2001	2G04	DIAG	D21	4	904555	4000	LOW IDLE
2002	19081	S11	1FMCU04122KB43913	3.0L	T/LD	12	2001	2G05	RECAL	D21	9	2260666	10000	STALLS
2002	19085	S11	1FMCU04122KB36114	3.0L	T/LD	11	2001	2G05	RECALEM	D21	7	1606361	8000	WHILE DRIVING
2002	19086	S11	1FMCU04122KB37612	3.0L	T/LD	11	2001	2G02	12B078	D21	7	2391351	9000	DOWNHILL
2002	19087	S11	1FMCU04122KB37612	3.0L	T/LD	11	2001	1H03	9J460	D21	7	2323499	3000	WHILE DRIVING
2002	19088	S11	1FMCU04122KB60946	3.0L	T/LD	11	2001	2G05	RECAL	D21	2	699274	1000	STALLS
2002	19089	S11	1FMCU04122KB60695	3.0L	T/LD	11	2001	2.00E+03	9F715	D21	6	2000508	6000	STALLS
2002	19090	S11	1FMCU04122KB60952	3.0L	T/LD	11	2001	2.00E+03	9F715	D21	2	699317	0	WHILE DRIVING
2002	19092	S11	1FMCU04122KB54087	3.0L	T/LD	11	2001	2G04	12A650	D21	6	2116393	14000	STALLS
2002	19093	S11	1FMCU04122KB53690	3.0L	T/LD	11	2001	2.00E+03	9F713	D21	1	411170	0	STALLS
2002	19096	S11	1FMCU04122KB16887	3.0L	T/LD	11	2001	2.00E+03	9F715	D21	7	2309827	5000	WHILE DRIVING
2002	19099	S11	1FMCU04122KB14988	3.0L	T/LD	11	2001	7C05	14N069	D21	6	1401166	7000	WHILE DRIVING
2002	19006	S11	1FMCU04122KB13178	3.0L	T/LD	10	2001	2G05	RECAL	D21	4	780418	4000	STALLS
2002	19007	S11	1FMCU04122KB13178	3.0L	T/LD	10	2001	7C05	14N069	D21	1	411410	1000	STALLS
2002	19014	S11	1FMCU04122KB03136	3.0L	T/LD	10	2001	1A08	8008	D21	4	1065561	7000	NO TEXT
2002	19015	S11	1FMCU04122KB03136	3.0L	T/LD	10	2001	1A08	8008	D21	4	777940	7000	WHILE DRIVING
2002	19017	S11	1FMCU04122KB01712	3.0L	T/LD	10	2001	2G01	12A650	D21	7	1749035	8000	STALLS
2002	19021	S11	1FMCU04122KA88948	3.0L	T/LD	10	2001	2.00E+03	9E995	D21	10	2347709	8000	TBB

REPLACED		4196 VAPOR MANAGMENT VALVE WDS TESTS FOUND VAPOR MANAGMENT VALVE AT FAULT. REPLACED VAPOR MANAGMENT VALVE. DIAGNOSED BY 8474. 8332 INSTALLED PART.
SSM		423 ROAD TEST OK FOR INTERMITANT STALLING. UNABLE TO DUPLICATE CONCERN AT THIS TIME. PERFORM SSM 15160 REFLASH PCM AND INSPECT VAPOR LINE.
HOTLINE		4211 ROAD TEST OK AND VERIFY VEHICLE STUMBLES AND HESITATES WHEN CRESTING HILLS AND LIFTING FOOT FROM ACCELERATOR. PERFORM DIAG AND PID MONITOR TEST. CONTACTED HOTLINE AND AND WAS TOLD TO RESET BARE
TSB		3774 ROAD TEST CK FOR INTERMITANT STALLING ON DECEL. UNABLE TO DUPLICATE CONCERN AT THIS TIME. PERFORM TSB 02 11 5 INSPECT PCM CALIBTRATION. INSPECT AND MONITOR PIDS FOR IAC AND EVAP. INSPECT AND
DIAG		PERFORM EEC SYSTEM DIAG AND PF TEST MONITOR PIDS AND REBURN PCM ROAD TEST RETEST OK
NPF		PERFORM SYSTEM DIAGNOSTICS,CODE TEST,KOER TEST,KOEO TEST, MONITOR PID VALUES AND DCL DISPLAY.TEST FUEL PRESSURE AND VOLUME,NORMAL RANGE.UNABLE TO CONFIRM AT THIS TIME.
NPF		4476 CUST STATES FOR PAST WEEK IDLES TOO LOW W COULD NOT VERIFY CONCERN, RAN OASIS AND NOTHING RELATE TO CUSTOMER CONCERN. USED WDS AND CHECKE D FOR CODES AND NO CODES, TEST DRIVE AND NO PROBLEM FOU
REFLASH		ROAD TEST DID NOT STALL. SELF TEST NO CODES. MONITOR PIDS. REPROGRAM PCM. MONITOR PIDS. CHECK EEC RELAY OK. ROAD TEST. INSPECT IAC VALVE OK.
REFLASH		8414 PCM RECALIBRATION PERFORM EEC SELF TEST KOEO PASS PASS KOER PASS PINPOINT TEST AND TEST FUEL PUMP HAS NORMAL 65PSI, TEST IGN. SYSTEM ALL PASSED. VIEW NGS DCL DISPLAY, ROAD TEST AND RECORD DCL
REPLACED		TECH CALLED HOTLINE AND RECOMMENDED REPLACEING THE MAF SENSOR
TSB		TECH CHECKED THE NGS FOR CODES. NO CODES. TECH USED TSB 2 11 6. TECH CHECKED THE PCM FOR UPDATES. TECH UPDATED THE PCM. TECH CHECKED THE POWER RELAY. OK. TECH REPLACED THE DPFE. ROAD TESTED AND IS O
REFLASH		ROAD TEST CHECK AND DIAGNOSE REPROGRAM PCM
REPLACED		ROAD TEST WDS TEST OK OASIS PINPOINT TEST CK AND REFLASH PCM CK EVAP OK EEC POWER RELAY OK REMOVE AND REPLACE IDLE AIR CONTROL VALVE RETEST OK
REPLACED		NGS REPLACE IAC MOTOR
TSB		TSB 021106 WE USED M TIME TO PERFORM TSB CHECKS AND REPROGRAM THE PCM.
SSM		840 ROAD TEST NORMAL OPERATION CHECK FOR CODES NO CODES RUN PINPOINT TEST CHECK PIDS OK CHECK OASIS PERFORM SSM 15534 INSTALL REVISED IAC AND EEC POWER RELAY REMOVE BATTERY AND BATTERY BOX CLEAN AND
REPLACED		EEC TEST AND PINPOINT TEST CHECK AND REPLACE IDLE AIR CONTROL VALVE
REFLASH		WDS HOOK UP, CHK OASIS, REPL PCM RELAY, REPROGRAM PCM, RETEST REPAIR VERIFIED.
SSM		ROADTESTED 20 MILES,NO STALL,WDS ALL PASS CODES, CKD FUEL PRESSURE AND FLOW,INJECTOR FLOW,INGITION SYSTEM AND POWER BALANCE ALL OK,REFERRED TO SSM 15099,RECHECKED FUEL PUMP AND PINS,REPROGRAMED PCM,RO
SSM		NGS,NO CODES. ROADTESTED, NO STALL,REFERRED TO SSM 15494 REPLACED EEC RELAY AND RELAY PINS,AIC IS CORRECT. CKD G104,105 AND 101. CKD CONNECTORS 220 B,C,D AND E. USED MT TIME.
ENGINE FAILURE		REQUESTING DEALERS P/A CODE 01776
REPLACED		REMOVED OIL PAN FOR INSPECTION #3 ROD AND PISTON BROKEN REPLACED ENGINE
TSB		VEHICLE STALLS INTERMITTENTLY WHILE DRIVING. IAC VALVE & CALIBRATION. PERFORMED TSB 02 11 6 REPROGRAMMED PCM & INSTALLED NEW IAC VALVE. RETESTED.
REFLASH		TECH 183 VERIFY CONCERN EEC TEST REPALCE THROTTLE BODY IAC REPROGRAM PCM RECHECK OK

	CUST STATES THAT ON 2 OCCASSIONS WHILE DRIVING VEH HAS DIED..PULLS OVER AND RESTARTS OK
	CHECK FOR TRUCK STALLED WHEN GOING UP HILL. CHECK OIL AND ENGINE LIGHT CAME ON.
IDLE TO CORRECT FOR IAC BEING OUT OF RANGE. ADJUSTED BASE TO GIVE IAC A BASE READING OF 34% DUTY CYCLE. ROAD TEST TO VERIFY CORRECT IDLE.	TRUCK STALLED AT 40 45MPH. SEEMS TO STALL (RMPS DROP) JUST WHEN YOU GET OVER A HILL.
REPLACE DPFE SENSOR PER HOTLINE REQUEST CONTACK ID 2FDK0003 INSPECT GROUNDS G100 AND G300 AND INSPECT CONNECTORS C270,C110 AND C139 PER HOTLINE. NO ABNORMAL CONDITIONS	TRUCK STALLED OUT AT HIGHWAY SPEEDS.
	CS: CAR STALLED ABOUT A MONTH AGO JUST DRIVING, THEN 2ND TIME STALLED WHEN JUST DRIVIG AGAIN.
	STALLED OUT WHILE DRIVING ABOUT 40 MPH,HAPPENED TWICE IN 8000 MILES
NO AT THIS TIME.	CUST STATES FOR PAST WEEK IDLES TOO LOW AND JUST ABOUT DIES
	STALLS AT TIMES.
ALL DATA NORMAL. RECALIBRATE PCM TO LATEST FILE AND RETEST EEC KOEO PASS PASS PASS. TK4110	VEHICLE CUT OFF WHILE DRIVING
	CUSOTMER STATES THE CAR STALLS WHEN YOUR FOOT IS OFF THE GAS(USUALLY DOWN HILL)
K	CUSTOMER STATES THE VEHICLE STALLS WHILE DRIVING
	CAR STALLS AND SHUTS OFF
	CHECK VEHICLE STALLS
	CUSTOMER STATES ENGINE STALLS WHILE DRIVING
	CUSTOMER STATES THAT THE VEHICLE O 2 SEPERATE OCCASSION THE VEHICLE CUT OUT AND WAS DIFFICULT TO STEER RECOMMEND HOOKING UP TO OSILLISCOPE+DMM
CHECK GROUNDS REASSEMBLY RETEST OK	CUSTOMER STATES THE CAR IS STALLING INTERMITTNATLY T
	CHECK FOR STALLING WHILE DRIVING
	CUST STATES INERMITT STALLS WHILE DRIVING AND NOISE COMING FROM ENGINE COMPARTMENT NO WARNING BEFORE STALLING
ADTEST OK,USED MT TIME.	DROVE APPROX 25 MINUTES STALLED LET SET 15 SECONDS RESTART OK
	AFTER DRIVE 25 MINUTES STALLED CAN RESTART RIGHT AWAY
	CK. FOR VEH. DIED WHILE DRIVING TOWED IN
	VEHICLE STALLS.
	CUST STATES ENGINE HAS STOPPED RUNNING TWICE (CK TSBS)

2002	19027	S11	1FMCU04122KA80736	3.0L	TAD	10	2001	2.00E+03	9E926		D21	9	1956287	10000	WHILE DRIVING
2002	19028	S11	1FMCU04122KA80618	3.0L	TAD	10	2001	2G05	RECAL		D21	8	1467181	18000	WHILE DRIVING
2002	19030	S11	1FMCU04122KA80439	3.0L	TAD	10	2001	2304	DIAG		D21	2	311710	1000	AT STOP
2002	19031	S11	1FMCU04122KA80439	3.0L	TAD	10	2001	2.00E+03	9F715		D21	3	470334	2000	WHILE DRIVING
2002	19032	S11	1FMCU04122KA80439	3.0L	TAD	10	2001	2.00E+03	9E926		D21	9	1680349	7000	WHILE DRIVING
2002	19034	S11	1FMCU04122KA79842	3.0L	TAD	10	2001	2.00E+03	9E926		D21	10	2304645	20000	WHILE DRIVING
2002	19036	S11	1FMCU04122KA79209	3.0L	TAD	10	2001	2G05	RECAL		D21	9	1822160	14000	WHILE DRIVING
2002	19038	S11	1FMCU04122KA71364	3.0L	TAD	10	2001	7C05	14N089		D21	7	1111943	7000	DOWNHILL
2002	19039	S11	1FMCU04122KA71305	3.0L	TAD	10	2001	2606	RECAL		D21	6	1150169	6000	WHILE DRIVING
2002	19040	S11	1FMCU04122KA71305	3.0L	TAD	10	2001	7502		14401	D21	1	288004	0	WHILE DRIVING
2002	19041	S11	1FMCU04122KA70361	3.0L	TAD	10	2001	2604	12A650		D21	6	1099462	6000	WHILE DRIVING
2002	19042	S11	1FMCU04122KA69645	3.0L	TAD	10	2001	2605	RECAL		D21	7	1024145	3000	WHILE DRIVING
2002	19043	S11	1FMCU04122KA69645	3.0L	TAD	10	2001	7C05	14N089		D21	7	1117802	3000	WHILE DRIVING
2002	19063	S11	1FMCU04122KA64189	3.0L	TAD	9	2001	7C05	14N089		D21	3	505869	5000	NO TEXT
2002	19062	S11	1FMCU04122KA59222	3.0L	TAD	9	2001	7V01	12A581		D21	9	1574809	12500	WHILE DRIVING
2002	19066	S11	1FMCU04122KA50994	3.0L	TAD	9	2001	7C05	14N089		D21	10	1369511	7000	WHILE DRIVING
2002	19068	S11	1FMCU04122KA50096	3.0L	TAD	9	2001	2604	12A650		D21	10	2061443	16000	NO TEXT
2002	19071	S11	1FMCU04122KA46422	3.0L	TAD	9	2001	1D05		6015	D21	7	1036760	8000	WHILE DRIVING
2002	19062	S11	1FMCU04122KA39258	3.0L	TAD	9	2001	2.00E+03	9F715		D21	9	1464210	9000	DOWNHILL
2002	19064	S11	1FMCU04122KA35755	3.0L	TAD	8	2001	2604	12A650		D21	6	957904	3000	STALLS
2002	19101	S11	1FMCU04122KA33668	3.0L	TAD	8	2001	2602	12B579		D21	10	1747542	6000	NO TEXT
2002	19124	S11	1FMCU04122KA06390	3.0L	TAD	8	2001	7C05	14N089		D21	8	1598612	2000	WHILE DRIVING
2002	19128	S11	1FMCU04112KE11172	3.0L	TAD	7	2002	2.00E+03	9F715		D21	1	2295268	0	STALLS
2002	19129	S11	1FMCU04112KD99976	3.0L	TAD	6	2002	2604	DIAG		D21	1	1975839	0	WHILE DRIVING

TSB		DIAGNOSTIC AND PINPOINT TESTING..NO CODES..PASS ALL IN SPEC. UPDATE THE PCM AND REPLACE THE IDLE AIR CINTROL VALVE, THE THROTTLE BODY, AND THE VMV VALVE AS PER TSB 02 11 8 RETEST ROAD TEST OAKY AT THI
DIAG		1 ROAD TESTED, PERFORMED EEC TEST, PASS CODES, MONITORED PIDS ON ROAD TEST, AND PERFORMED NGS SIMULATION TEST.
SSM		IGN SYSTEM TEST 12.6 VOLTS, EEC SYSTEM TEST CODE P1000 CHK TSM AND SSM NONE FOUND, TEST DROVE UNABLETO DUPLICATE THE CONCERN
REPLACED		EEC TEST REPLACED EEC POWER RELAY AND IAC VALVE
REPLACED		REPLACED IAC VALVE AND THROTTLE BODY AND REPROGRAMPCM PER BULLETIN 02 11 8 AFTER COMPLETING EEC TEST PINPOINT TEST FOUND IAC DUTY CYCLE OUT OF SPECS INSTALL NEW IAC VALVE AND RECHECK FOUND STILL OUT O
NO TEXT		
TSB		14821 ROAD TEST NO MIL NO DRIVABILTY WDS DIAG. KOEO PASS 19 PASS KOER PASS DATALOGGER REPROGRAM PROSSESSOR MONITOR PIDS ON ROAD TEST WITH NGS PER TSB 02 11 09 RETEST ROAD TEST
INOP		SNOP EEC (QUICK TEST) DIAGNOSIS
SSM		OUT OF CALIBRATION SSDS TEST RUN SSM AND REPROGRAM PCM
HOTLINE		ISOLATE CRANK SENSOR HARNESS PER FORD ENGINEERING.
DIAG		PCM EEC (QUICK TEST) DIAGNOSIS
REFLASH		WDS TEST OK FUEL PRESSURE,REPROGRAM PCM TO CURRENTCALIBRATION RETEST
REPLACED		PER FORD ENGINEER JIM NOTESCOM REPLACED EEC RELAY AND FUEL PUMP RELAY TIGHTENED ALL GROUNDS G101 G103 G 104 TEST DROVE 29 MILES,COULDNT DUPLICATE AT THIS TIME FORD IS CURRENTLY INVESTIGATING STALL PRO
SSM		FOUND SSM 15439 C, SSM SAYS TO REPLACE THE EEC RELAY, REPLACED RELAY, REINSTALLED BATTERY AND TRAY, TEST DRIVE, NO STALL, ALL LOOKS GOOD
POOR CONNECTION		PERFORMED EEC TEST KOEO KOER,CHECK FUEL PSI,CHE CK IGNITION SYSTEM,MONITOR CHECK,WIGGLE TEST.TR ACED CONCERN TO A LOOSE MAF SENSOR CONNECTOR,(L OOSE WIRES).REPAIRED AND RETESTED,PASSED,ROAD T ESTE
REPLACED		SSDS TEST FUEL PRESSURE TEST PASS CODES, ROADTEST OK REPLACE EEC POWER RELAY, PROGRAM PCM PER FORDS SPECIAL
NO TEXT		
REPLACED		5200 BASIC 01 BROKEN #3 AND #8 RODS INSPECTED ENGINE, M TIME TO SEPARATE TRANSFER CASE AND REPLACE, EEC TEST AND REPLACED ENGINE ASSEMBLY
REPLACED		D21 41 YFIZ 9F715 AA WDS TEST PINPOINT TEST REPLACE IAC VALVE REPROGRAM PROCESSOR ROAD TEST & RETEST
TSB		ROAD TEST VEHICLE. STALLS ON DECEL. CHECK FO R SSM OR TSB. FOUND SSM 15569. CHECK EEC POWE R RELAY OK. REPROGRAM PROCESSOR AND BLOW OUT VENT LINE. REASSEMBLE AND ROAD TEST.
DIAG		TEST DROVE FOR STALLING. SCANNED FOR CODES WITH WDS AND NO CODES WERE STORED OR RETRIEVED AND ALL RUNNING TESTS
REPLACED		CK AND REPLACE PCM RELAY AND REPROGRAM PCM
TSB		UPDATED IAC VALVE UNABLE TO VERIFY STALLING CONCERN. PER TSB 02 11 06, MONITOR IAC % PID AT 44% REPLACE IAC AND
HOTLINE		M TIME REQUESTED TO PERFORM CHECKLIST AND PERFORM CHECKS AS DIRECTED BY HOTLINE

S IME	CUSTOMER STATES WHILE SHE S DRIVING THE TRUCK CUT OUT BUT IT DID RE START..NO CHECK ENGINE LIGHT CAME AND
	DIAGNOSE VEHICLE STALLS INTERMITTENTLY AT ANY SPEED.
	CUSTOMER STATES THE VEHICLE STALLED WHILE DRIVING.CUSTOMER WAS ACCELERATING UP HILL AFTER A STOP.VEHICLE DIED.RESTARTED,BUT THE THEFT LIGHT WAS FLASHING.WENT OFF AFTER RESTAR.
	CUSTOMER STATES THE VEHICLE STALLED WHILE DRIVING.RESTARTED.
F SPECS INSTALL NEW THROTTLE BODY AND REPROGRAM PCM TO LATEST CALIBRATION RETEST OK TEST DRIVE & RETEST DCL DISPLAY 39% ALL OK	CUSTOMER STATES THAT THE UNIT STALLS OUT WHY DRIVING THE UNIT IT WILL RESTART LOOSE POWER STEERING AND BRAKE BUT RADIO AND A C WORKS SILL HAPPEN IN TRAFFIC SPEEDS
	CUSTOMER STATES ENGINE STALLS WHILE DRIVING
	CUSTOMER STATES VEHICLE STALLS WHILE DRIVING, WILL RESTART OK D21
	C S STALLS WHILE DRIVING UNDER NORMAL CONDITIONS DOWNHILL 40 45MPH WHEN ENGINE IS WARM
	CUSTOMER STATES ENGINE STALLS AT TIMES WHILE DRIVING
	CUSTOMER STATES ENGINE STALLS WHILE DRIVING
	CUST STATES VEHICLE STALLED WHILE DRIVING HAPPENED ONCE
	CUSTOMER CONCERN IS THAT THE CAR DIED WHILE DRIVING ON SATURDAY WAS ABEL TO RESTART SHORTLY AFTER. CHECK ENGINE LIGHT WAS ON.
BLEM	CHECK VEC DIED WHILE DRIVING LIKE SOMEONE TURNED KEY OF VEC DID START RIGHT BACK UP WITH NO PROBLEMS (NOTE WAS JUST IN AND HAD PCM REPROGRAMED FOR SAME PROBLEM LAST WEEK)
D,OK.	ENGINE STALLS OUTS WHEN DRIVING.
	ENGINE JUST CUT WHILE DRIVING AROUND 30 MPH, WOULD NOT RESTART JUST CRANKED OVER DID RESTART AFTER ABOUT 15 MIUNTES
	DRIVING AT 65MPH THE CUIT AND WOULD NOT RESTART
	C S GOING DOWN HILL FOOT OFF GAS TRUCK CUTS OFF
	CUSTOMER STATES ENGINE STALLS CUSTOMER STATES COLD START STALL
	CHECK DBB ON ROAD
	CUSTOMER STATES STALLED
	VEHICLE STALLE WHILE DRIVING, HIGHWAY SPEEDS, CUSTOMER PUT IN NEUTRAL RESTARTED RIGHT AWAY

2002	19130	S11	1FMCU04112KD84690	3.0L	TALD	6	2002	2G05	RECAL	D21	1	2295171	0	WHILE DRIVING
2002	19131	S11	1FMCU04112KD84121	3.0L	TALD	6	2002	2G04	12A650	D21	2	2009170	3000	WHILE DRIVING
2002	19132	S11	1FMCU04112KD83974	3.0L	TALD	6	2002	7C05	14K060	D21	0	1829527	0	WHILE DRIVING
2002	19133	S11	1FMCU04112KD81302	3.0L	TALD	6	2002	2F02	9B936	D21	1	2192642	2000	WHILE DRIVING
2002	19134	S11	1FMCU04112KD80425	3.0L	TALD	6	2002	2E01	9J450	D21	1	1662108	0	ROUGH IDLE
2002	19135	S11	1FMCU04112KD40653	3.0L	TALD	5	2002	2G02	12B579	D21	2	2120412	1000	STALLS
2002	19145	S11	1FMCU04112KD11245	3.0L	TALD	4	2002	2G04	DIAG	D21	1	1442328	1000	COASTING
2002	19146	S11	1FMCU04112KD01694	3.0L	TALD	4	2002	2.00E+03	9F715	D21	4	2174827	6000	WHILE DRIVING
2002	19148	S11	1FMCU04112KD00490	3.0L	TALD	3	2002	2G04	DIAG	D21	3	2377666	4000	ACCELERATING
2002	19149	S11	1FMCU04112KD00490	3.0L	TALD	3	2002	2G04	DIAG	D21	1	1799539	0	AT STOP
2002	19150	S11	1FMCU04112KD00490	3.0L	TALD	3	2002	2.00E+03	9F715	D21	2	2027229	2000	WHILE DRIVING
2002	19153	S11	1FMCU04112KC99764	3.0L	TALD	4	2002	2G04	12A650	D21	1	1395048	0	WHILE DRIVING
2002	19155	S11	1FMCU04112KC99618	3.0L	TALD	4	2002	2.00E+03	9F715	D21	2	1596310	2000	DOWNHILL
2002	19166	S11	1FMCU04112KC99618	3.0L	TALD	4	2002	1H08	9J450	D21	3	1742859	4000	STALLS
2002	19176	S11	1FMCU04112KC97136	3.0L	TALD	2	2002	7C05	14K060	D21	1	1108668	0	STALLS
2002	19180	S11	1FMCU04112KC00780	3.0L	TALD	1	2002	2G04	12A650	D21	2	1693911	3000	WHILE DRIVING
2002	19804	S11	1FMCU04112KB99099	3.0L	TALD	1	2002	2G02	12B579	D21	6	1736699	10000	WHILE DRIVING
2002	19807	S11	1FMCU04112KB76898	3.0L	TALD	1	2002	2G05	RECAL	D21	1	1034295	0	WHILE DRIVING
2002	19810	S11	1FMCU04112KB99276	3.0L	TALD	12	2001	2.00E+03	9F715	D21	6	2231206	8000	STALLS
2002	19811	S11	1FMCU04112KB99280	3.0L	TALD	12	2001	2G05	RECAL	D21	1	736693	0	DOWNHILL
2002	19813	S11	1FMCU04112KB99030	3.0L	TALD	12	2001	2G05	RECAL	D21	3	1779134	4000	WHILE DRIVING
2002	19816	S11	1FMCU04112KB94820	3.0L	TALD	1	2002	2G04	12A650	D21	3	1154859	4000	WHILE DRIVING
2002	19818	S11	1FMCU04112KB99043	3.0L	TALD	12	2001	2G04	12A650	D21	6	1791579	4000	WHILE DRIVING

TSB		PERFROMED EEC TEST,FOLLOWED PPT,ROADTEST AND MONITORED DPFE AND IAC,FOLLOWED STEPS IN TSB 02 11 06.EVAP SYSTEM WORKING NORMALLY.CALLED JAMES AT HOTLINE.SAID THE NEW PCM UPDATE IS THE LATEST FIX FOR S
NPF		PERFORM TEST NO CODE FOUND IN SYSTEM AT THIS TIME NO PROBLEM FOUND
REPLACED		FUEL PUMP RELAY (FP) REPLACE (E945 12B577)
TSB		PERFORMED SYSTEMS TEST,NO CODES IN SYSTEM,PERFORMED SERVICE TSB 02 11 06. PERFORMED THROTTLE BODY MODIFICATION AND TP SENSOR VOLTAGE ADJUSTMENT PER FORD ENGINEEER JIM C
REPLACED		RD. TEST INSP NGS DIAG. KOEO P1409 DCL DISPLAY EGR OPEN AT IDLE. PPT HE110 (0 OHMS) REPL. EGR VACUUM REGULATOR SOLENOID
TSB		RELATED TO TSB 02 11 06 TEST DROVE TO VERIFY THE COMPLAINT, COULD NOT DUPLICATE CNCRN. HOOK UP NGS, DISPLAY EEC TEST, NO CODES. RAN OASIS
NPF		NPF EEC (QUICK TEST) DIAGNOSIS
TSB		ROADTEST. TEST EEC NO FAULT CODES PRESENT. PERFORM DCL DISPLAY MONITOR AND RECORD PINPOINT TESTS KIN SYSTEM DIAGNOSIS REPLACE IAC SENSOR AND REPROGRAM PCM AS PER TSB 02 11 06 RETEST OK
TSB		4995 SELF TEST W.O.S. PASSES ALL SELF TESTS. MONITOR DATALOGGER. INSPECT EVAP LINES AND FIT. AND CHECK IDLE SPEED PER TSB. ALL INPUTS AND OUTPUTS ARE IN RANGE. NO IMPROVEMENTS CAN BE MADE, COULD N
TSB		9479 WDS DIAG, CONT, KOEO, KOER, PID DATA MONITOR ROAD TEST, WATCH IAC AND RPM AS PER TSB 02.11.06. PERFORM TSB, EVAP SYSTEM TEST, CHECK IAC AND T BODY, CHECK PROGRAM. COULD NOT DUPLICATE AT THIS TI
TSB		2498 WDS DIAG, CONT, KOEO, KOER, NO CODES, PINPOINT TEST TSB 02.11.06 PID DATA MONITOR ROAD TEST, EVAP SYSTEM TEST, TEST DRIVE,CHECK OASIS, CALL HOTLINE, REMOVE AIR INTAKE BOX, INSPECT GROUNDS ON
SSM		UNABLE TO VERIFY STALLING CONCERN.CHECK FOR CODES,NONE.PIDMONITOR TEST,NOTHING ABNORMAL.RAN OASIS,SSM 15599 FOR PCM REPROGRAMMING.ATTEMPTED TO REPROGRAM,LATEST CALIBRATION ALREADY INSTALLED.CHECK EEC
TSB		2499 WARRANTY PERFORMED NGS CODE RETRIEVAL NONE RUN OASIS AND PERFORMED TSB#02 06 05 REPLACED PARTS AS RECD IN TSB INCLUDING THROTTLE BODY,IDLE AIR CONTROL VALVE PCM RELAY.HOOK UP WDS AND RETRIEVE
REPLACED		4200 DPFE WARRANTY CONTACTED FORD HOTLINE REPORT CODE 2F1DU00 REPLACED DPFE SENSOR AS PER HOTLINE.INSPECTED FOR ANY CHAFFED OR MISROUTED WIRES AS PER HOTLINE.ROAD TESTED VEHICLE,NO STALL SYMPTOM P
INOP		PCM RELAY FAILURE EEC (QUICK TEST) DIAGNOSIS
REFLASH		CHECK & REPROGRAMMED PCM
TSB		PERFORM TSB 2 11 6 CHECK IAC PERCENT OUT OF RANGE REPLACE BYPASS VALVE RECHECK OUT OF RANGE REPLACE THROTTLE BODY AND RESET IDLE RECHECK OK REPLACE MASS AIR FLOW WITH REVISED
SSM		OK EEC DIAG KOEO KOER CONT MEMORY OK PIDS MONITOR AND RECORD PINPOINT TEST REPROGRAM PCM PER SSM 15599 RETEST ROAD TEST
TSB		ROAD TESTED, MONITOR VEHICLE. REFER TO TSB 02 11 06 REPLACED IAC VALVE REPROGRAMMED PCM. RE ROAD TESTED OK.
SSM		OK FOR STALLING, ROAD TEST, EEC TEST, NO CODES, OK OASIS, PERFORM SSM 15599, REPROGRAM PCM FOR STALLING CONDITION
REFLASH		CHECK WHILE DRIVING VEHICLE STALLS PERFORM EEC TEST PINPOINT TEST MONITOR TEST FINAL QUICK TEST PERFORM SMOKE MACHINE TESTS CHECK FOR VACUUM LEAKS NONE FOUND REPROGRAM PCM CHECK OK
REFLASH		DIAG AND VERIFIED EEC TEST PP TEST INSTALL FLIGHT RECORDER REPROGRAMMED PCM AND RESC
TSB		WDS DIAG. DATA LOGGER. POWER BALANCE. FUEL PRESSURE AND INJECTOR FLOW. PERFORMED TSB 02 11. RE PROGRAMMED PCM. OPERATION NOW O.K.

TALLING CONCERN,REPROGRAMMED PCM TO LATEST LEVEL,OK AT THIS TIME	CUSTOMER STATES WHILE DRIVING VEHICLE STALLED
	STALLED WHILE DRIVING,BURNING ODOR
	DIES WHEN DRIVING
	CUSTOMER STATES THAT THE VEHICLE STALLS OUT WHILE DRIVING ALWAYS RESTARTS
	CK FOR ROUGH IDLE, BURNING SMELL, D21
	CUST. STATES VEHICLE STALLED OUT LAST NIGHT AT SLOW SPEED, AND STATES FEELS ROUGH SLUGGISH??
	CHECK FOR STALLING WHILE LETTING OFF GAS
	CUSTOMER STATES INTERM CUTS WHILE DRIVING STALLS AT STOPS
OT DUPLICATE DURING ROADTEST.	CUSTOMER STATES VEHICLE STALLS WHEN COMING TO STOPS (WHEN YOU LET OFF ACCEL) CHECK AND ADVISE
ME 8420	CUSTOMER STATES THAT THE VEH STALLED AT STOPS AND THE VEH STALLED WHEN TURNING AND SLOWING PLEASE CK AND ADVISE
TRANS, GROUNDS UNDER BATT TRAY, REMOVE BATT AND TRAY, INSTALL JUMPER FROM TRANS TO G401 AND G401 TO BATT, REPLACE IAC AND DPFE, RETEST 8420	CUSTOMER STATES THAT THE VEH HAS A STALLING PROBLEM STALL WHILE DRIVING AT SPEEDS OVER 40 AND AT A COAST OR A STOP
RELAY FOR WHITE LETTERING,OK,CONTACTED HOTLINE,WDS NOT TO LATEST UPDATE,RECEIVED LATEST WDS UPDATE,WENT BACK IN & REPROGRAMMED PCM TO LATEST CONFIGURATION,CONCERN REPAIRED.	ENGINE KEEPS STALLING WHEN DRIVING DOWN THE ROAD.
D CALIBRATION VERIFIED CALIBRATION IS AT LATEST LEVEL,ROAD TESTED CAR,NO SYMPTOMS,CONCERN PRESENT	CHECK FOR AN INTERMITTENT STALL WHEN LETTING OFF GAS TO COAST HAPPENED ON DOWN HILL
RESENT	CHECK FOR THE ENGINE IS STALLING INTERMITENT
	CUST STATES THE VEHICLE STALLS, STARTS BUT STALLS
	VEH STALLS WHILE DRIVING
	CUSTOMER STATES VEHICLE QUIT WHILE DRIVING 3 TIMES WHEN HOT DOWN HILL WITH FOOT OFF GAS
	CK. VEH. HAS CUT OFF ON CUST. TWICE, RADIO STILL WORKS BUT ENGINE CUTS OUT.
	CHECKED FOR VEHICLE STALLING
	CUSTOMER STATES WAS DRIVING DOWN HILL ALL DASH LIGHTS CAME ON AND VEHICLE STALLED. VEHICLE WAS JUST PURCHASED ONE WEEK
	CUSTOMER STATES CHECK WHILE DRIVING ABOUT 40 MPH WITH AC VEHICLE STALLED OUT OIL LIGHT ENGINE LIGHT WENT ON 4 SECONDS LATER VEHICLE STALLED OUT
	CUST ST VEHICLE STALLS AT TIMES WHEN DRIVING
	CUSTOMER STATES VEHICLE DIED WHILE DRIVING.

2002	19225	S11	1FMCU04112KB52909	3.0L	T/LD	12	2001	2.00E+03	9F715	D21	9	2152469	7000	AT STOP
2002	19233	S11	1FMCU04112KB37410	3.0L	T/LD	12	2001	2.00E+03	9F715	D21	9	2275181	7000	STALLS
2002	19236	S11	1FMCU04112KB53506	3.0L	T/LD	11	2001	2G01	12A650	D21	8	2220700	7000	STALLS
2002	19237	S11	1FMCU04112KB52423	3.0L	T/LD	11	2001	2G05	RECAL	D21	4	992790	3000	STALLS
2002	19238	S11	1FMCU04112KB20784	3.0L	T/LD	10	2001	2G04	12A650	D21	8	1692380	4000	COASTING
2002	19239	S11	1FMCU04112KB16847	3.0L	T/LD	11	2001	2G05	RECALEM	D21	7	1668139	5000	STALLS
2002	19240	S11	1FMCU04112KB14208	3.0L	T/LD	11	2001	2.00E+03	9F715	D21	1	424867	1000	AT STOP
2002	19247	S11	1FMCU04112KB14506	3.0L	T/LD	11	2001	2G05	RECALEM	D21	8	972852	7000	STALLS
2002	19252	S11	1FMCU04112KB06721	3.0L	T/LD	11	2001	2G05	RECALEM	D21	7	1664334	11000	DOWNHILL
2002	19255	S11	1FMCU04112KB03189	3.0L	T/LD	10	2001	2G01	12A650	D21	4	660851	8000	WHILE DRIVING
2002	19256	S11	1FMCU04112KB03189	3.0L	T/LD	10	2001	2.00E+03	9F715	D21	3	578970	7000	AT STOP
2002	19259	S11	1FMCU04112KB02264	3.0L	T/LD	10	2001	2.00E+03	9F715	D21	8	1758080	6000	WHILE DRIVING
2002	19267	S11	1FMCU04112KB00955	3.0L	T/LD	10	2001	2.00E+03	9E926	D21	6	1586353	10000	COASTING
2002	19268	S11	1FMCU04112KB00955	3.0L	T/LD	10	2001	2G05	RECAL	D21	9	1966280	11000	DOWNHILL
2002	19269	S11	1FMCU04112KB00955	3.0L	T/LD	10	2001	2G02	12B679	D21	9	2460801	12000	COASTING
2002	19271	S11	1FMCU04112KA83949	3.0L	T/LD	10	2001	2G01	12A650	D21	8	1119671	3000	COASTING
2002	19272	S11	1FMCU04112KA83569	3.0L	T/LD	10	2001	2G04	12A650	D21	10	2109181	16000	WHILE DRIVING
2002	19275	S11	1FMCU04112KA83513	3.0L	T/LD	10	2001	7C05	14N089	D21	2	707314	0	WHILE DRIVING
2002	19276	S11	1FMCU04112KA82274	3.0L	T/LD	10	2001	2G04	DIAG	D21	7	1231603	9000	WHILE DRIVING
2002	19278	S11	1FMCU04112KA80969	3.0L	T/LD	10	2001	7C05	14N089	D21	8	1099687	8000	STALLS
2002	19285	S11	1FMCU04112KA79234	3.0L	T/LD	10	2001	2.00E+03	9F715	D21	11	2561150	15000	AT STOP
2002	19286	S11	1FMCU04112KA78715	3.0L	T/LD	10	2001	2.00E+03	9E926	D21	7	1438899	9000	WHILE DRIVING
2002	19294	S11	1FMCU04112KA69013	3.0L	T/LD	10	2001	2.00E+03	9F715	D21	11	2440101	21000	WHILE DRIVING
2002	19299	S11	1FMCU04112KA67939	3.0L	T/LD	9	2001	2.00E+03	9F715	D21	7	1066091	8000	STALLS
2002	19304	S11	1FMCU04112KA63731	3.0L	T/LD	9	2001	1A03	9007	D21	6	885139	4000	WHILE DRIVING
2002	19311	S11	1FMCU04112KA61980	3.0L	T/LD	9	2001	2G04	12A650	D21	9	1599999	12000	WHILE DRIVING

DIAG		CHECK STALLING EEC (QUICK TEST) DIAGNOSIS
TSB		CK TRUCK OVER RUN OASIS FOUND ARTICLE 02 11 6 ARTICLE STATES TO CK IAC COUNTS AND OTHERS SPECIFIED FOUND IAC PERCENT TO BE ABNORMAL REPLACED IAC WITH UPDATED UNIT
INOP		INOP EEC (QUICK TEST) DIAGNOSIS
SSM		PCM REPROGRAM TEST EEC STST,PINPOINT TEST,NGS RECORD MON,TEST FUEL PRESS,R +I EEC RELAY,REPROGRAM PCM,SSM 15699,CLEAR EVAP LINE,RETEST
NFF		TEST DROVE RVEHICLE FOR STALLING CONCERN,PERFORMED KOEO AND KOER TEST.CHECKED FOR CODES,NO CODES IN SYSTEM,NO PROBLEM FOUND AT THIS TIME
REFLASH		ROAD TEST WDS DATALOGGER REPROGRAM PCM MODULE CHECK VMV OPERATION OK VENT OK CHECK EEC RELAY
DIAG		NO DTC PERFORMED DIAGNOSIS BY SYMPTOM CHART REPL IAC VALVE
REFLASH		WDS TESTS REPROGRAM PCM RETEST OK
TSB		EEC TEST NO CODES PERFORM TSB 02 11 6 ROADTEST ANDMONITOR PIDS OK RECALIBRATE PCM AS PER TSB RO ACTEST OK
REFLASH		1 WDS PASS CODES RECHECKED GROUNDS OK PCM REPROGRAMMED TIME TO DOWNLOAD WDS SYSTEM UPGRADE CONNECT TO LAND LINE
LOOSE GROUND		1 WDS DIAG PASS KOEO KOER NO CONT CODES DATA LOGGER FUEL PRESURE TEST R&R BATTERY AND BOX REPOSITIONED G 104 AND
REPLACED		CAUSAL 9F715 CC 41 CCC 021 TEST WITH NGS RAN KOEO, REPLACED I A C SOLENOID RETEST AND ROAD TEST
REPLACED		10464 COULD NOT REPROGRAMM PCM BECAUSE WDS IS NOT CONNECTED WITH A LAND LINE. REPLACED EVAPORATIV E VAPOR MANAGEMENT VALVE,REPLACED IDLE SPEED CONTROL MOTOR,REPLACED THROTTLE BODY,ROAD TEST
REPLASH		CP RECAL WDS EEC SYSTEM SELF TEST KOEO PASS, KOEO PASS, PINPOINT TESTS SYMPTOM CHART 1, DATALOGGER DISPLAY, IGNITION
DIAG		AUTHORIZED WARRANTY REPAIR PER JUSTIN HOLTKAMP. ****IT SHOULD BE NOTED THAT PRIOR TO ANY REPAIRS THE VEHICLE WAS ROAD TESTED ON 5 8 02 ABOUT 10 MILES AND THE CONCERN
REPLACED		TEST FUEL PRESSURE, TEST WITH EEC QUICK TESTER, REPROGRAM POWERTRAIN CONTROL MODULE ASSEMBLY, AND REPLACE BAD RELAY ASSEMBLY.
TSB		ATTEMPT TO VERIFY STALLING CONCERN CHECK OASIS EECTEST,DOL DISPLAY PER TSB #02 11 06,REPROGRAM PCM & ROADTEST. PCM UPDATE
SSM		CHECK AND ADVISE ON STALLING DIAGNOSTIC TESTING AND PINPOINT TESTING _KOEO_PASS_KOER_PASS AS PER SSM15494 CHECK GROUNDS AND REPLACE POWER RELAY AND UPDATE PCM TO THE LATEST CALIBRATIONS RETEST ROA
NFF		TEST SYSTEMS, TEST EEC. TEST FOR ANY CODES. NONE FOUND CHECK ALL CONNECTIONS AND MAKE SURE THEY ARE TIGHT ROAD TESTED TWICE FOR OVER 30 MIN EACH
REPLACED		EEC TEST AND PINPOINT TEST CHECK AND REPLACE EEC POWER RELAY AND REPROGRAM PCM
REPLACED		DIES AT IDLE WDS DIAG. PINPOINT TEST. FOUND RPL FAILED IAC VALVE. RETEST OK.
REPLACED		502254 SEE 02 3.0 RUN EEC TEST NO CODES REPLACE THROTTLE BODY , IAC VLAVE , VAPOR MANAGEMENT VALVE AND EEC REPLAY AND REPROGRAM PROCESS
DIAG		CHECK STALLS ROAD TEST UNABLE TO VERIFY RETRIEVE CODES NO CODES KOEO NO CODES KOER NO CODES DATA LOGGER FOUND IAC DUTY
SSM		EEC TESTED, ROAD TESTED. PERFORMED FUEL SYSTEM PRESSURE TEST AND IGNITION SYSTEM TEST OK. CHECKED SPECIAL MESSAGE.
TSB		4573 KOEO P1111 KOEC P1111 KOER P1111 7627 3.0L REPROGRAMMED PROCESSOR PER TSB HOOKED UP WDS EEC TEST DOL DISPLAY TO MONITOR FUEL TRIMS AND IAC PIDS REPROGRAMMED PROCESSOR RETEST NO LOG USED WDS
TSB		PERFORMED TSB 02 11 6. RE PROGRAMMED PCM. ROAD TEST. OPERATION NOW O.K.

ENTIRE PAGE

	CHECK CUSTOMER STATES VEHICLE STALLED AT STOP LIGHT AND STEERING LOCKED UP AND EMISSIONS LIGHT AND OIL LIGHT CAME ON, RESTARTED, O K SINCE
	CHECK VEHICLE STALLING
	CUSTOMER STATES THAT THE VEHICLE STALLED WHILE SITTING AT A LIGHT
	CUSTOMER STATES VEHICLE STALLS - -
	ENGINE DIED WHILE COASTING A C WAS ON DID NOT DIE WITH A C OFF
	ENGINE STALLS, RESTART OKAY D21
	DIAGNOSE WHY THE ENGINE RANDOMLY STALLS WHILE MOVING SLOWLY OR COMING TO A STOP OCCURS AFTER DRIVING A GOOD WHILE
	CST THAT ENGINE STALLS AT LIGHTS,HAPPENED 3 TIMES,D21
	CHECK CUSTOMER STATES VEHICLE STALLS OUT INTERMITTENTLY WHEN COASTING DOWN HILL AT ABOUT 40MPH
	STALLS WHILE DRIVING, CAN RESTART IT AFTER SHE PULLS OVER
	STALLED AT HIGHWAY SPEED RESTARTED OK AFTER PULLED OVER AND STOPPED
	C S CAR DIES WHILE DRIVING, AFTER SITTING FOR A FEW MINUTES IT STARTS
	CUSTOMER STATES ENGINE STALLS INTERMITTENTLY WHILE DECELERATING
	D21 OWNER STATES ENGINE STALLS ON DE ACCEL, USUALLY ON DOWNGRADES, INTERMITANT, HAS BEEN IN ANOTHER FORD
	CONCERN CONTACT SEE RO 67482 7 16 02 11,726 MILES STALLS WHILE PEDAL IS IN NEUTRAL POSITION, COASTING, JUST
	AFTER A 10 MINUTE OF DRIVING COLD VEH STALLED WHILE DECEL...REPORT
	ENGINE CUIT WHILE DRIVING HOT
D TEST OKAY	CUST. STATES ENGINE CUIT RUNNING WHILE DRIVING 40 MPH... CUST. PULLED OVER TO SIDE OF ROAD, ENGINE STARTED NORMAL..
	ENGINE STALL,HAD TO WAIT TO RESTART FINALLY STARTED AND MAKE A CLUNKING NOISE STALLED WHILE DRIVING
	STALLED 2 TIMES
	CK VEHICLE DIES WHILE SLOWING DOWN FOR OR AT STOPS
	CK. FOR REASON ENGINE STALLS WHILE DRIVING
	CUSTOMER STATES KEEPS STALLING WHILE DRIVING SLOW WITHOUT GIVING GAS
	CK ENGINE CUTS OFF INTERMITTENT SEE CUSTTOMERS NOTE
OC BBY 999 ROADTEST	CAR TOWED IN ENGINE DIED AT 30 MPH
	CUSTOMER STATES VEHICLE STALLS WHILE DRIVING.

2002	19312	S11	1FMCU04112KA01560	3.0L	TALD	0	2001	2B04	DIAG	D21	7	1418888	9000	WHILE DRIVING
2002	19313	S11	1FMCU04112KA01560	3.0L	TALD	0	2001	2.00E+03	9F715	D21	4	944488	5000	NO TEXT
2002	19320	S11	1FMCU04112KA02017	3.0L	TALD	0	2001	2.00E+03	9F715	D21	10	1924348	14000	DOWNHILL
2002	19345	S11	1FMCU04112KA49345	3.0L	TALD	0	2001	2B04	12A650	D21	11	2212308	9000	WHILE DRIVING
2002	19346	S11	1FMCU04112KA49219	3.0L	TALD	0	2001	7B08	14401	D21	7	1099294	9000	AT STOP
2002	19360	S11	1FMCU04112KA39888	3.0L	TALD	0	2001	7C05	14N089	D21	4	882380	6000	DOWNHILL
2002	19362	S11	1FMCU04112KA39588	3.0L	TALD	0	2001	1A03	6007	D21	8	1697105	10000	WHILE DRIVING
2002	19375	S11	1FMCU04112KA34102	3.0L	TALD	0	2001	7C05	14N089	D21	3	439889	2000	WHILE BRAKING
2002	19376	S11	1FMCU04112KA34102	3.0L	TALD	0	2001	2B04	12A650	D21	8	1158888	8000	COASTING
2002	19378	S11	1FMCU04112KA34102	3.0L	TALD	0	2001	2B04	12A650	D21	11	2220888	9000	WHILE DRIVING
2002	19383	S11	1FMCU04112KA27835	3.0L	TALD	0	2001	2B05	RECAL	D21	4	368033	3000	WHILE DRIVING
2002	19405	S11	1FMCU04112KA08888	3.0L	TALD	0	2001	2B04	12A650	D21	5	727278	5000	WHILE DRIVING
2002	19409	S11	1FMCU04112KA07904	3.0L	TALD	0	2001	7C06	14N089	D21	3	428733	1000	WHILE DRIVING
2002	19410	S11	1FMCU04112KA07804	3.0L	TALD	0	2001	2B05	RECAL	D21	10	2041214	6000	DOWNHILL
2002	19412	S11	1FMCU04112KA07451	3.0L	TALD	0	2001	7C06	14N089	D21	11	1808743	8000	WHILE DRIVING
2002	19423	S11	1FMCU04112KA05681	3.0L	TALD	0	2001	7C06	14N089	D21	3	378811	1000	WHILE DRIVING
2002	19427	S11	1FMCU04103KE10563	3.0L	TALD	7	2002	2B04	DIAG	D21	1	2188817	0	WHILE DRIVING
2002	19428	S11	1FMCU04103KD84575	3.0L	TALD	6	2002	2B04	DIAG	D21	1	2382106	0	WHILE DRIVING
2002	19430	S11	1FMCU04103KD84403	3.0L	TALD	6	2002	2B04	12A650	D21	2	2388816	2000	WHILE DRIVING
2002	19432	S11	1FMCU04103KD86749	3.0L	TALD	6	2002	2.00E+03	9F715	D21	2	2388884	2000	WHILE DRIVING
2002	19433	S11	1FMCU04103KD86735	3.0L	TALD	6	2002	1H03	9J460	D21	-1	2128304	0	NO TEXT
2002	19435	S11	1FMCU04103KD87704	3.0L	TALD	6	2002	2.00E+03	9F715	D21	2	2290511	2000	STALLS
2002	19438	S11	1FMCU04103KD86639	3.0L	TALD	6	2002	2B05	RECAL	D21	1	2288857	1000	NO TEXT
2002	19441	S11	1FMCU04103KD82521	3.0L	TALD	5	2002	7C01	9C734	D21	1	2438175	0	WHILE DRIVING
2002	19442	S11	1FMCU04103KD84508	3.0L	TALD	5	2002	2B04	DIAG	D21	1	2388088	0	WHILE DRIVING
2002	19446	S11	1FMCU04103KD82584	3.0L	TALD	4	2002	1H03	9J460	D21	4	2457880	2000	COASTING
2002	19448	S11	1FMCU04103KD10186	3.0L	TALD	4	2002	2.00E+03	9F715	D21	3	2180848	1000	AT STOP
2002	19449	S11	1FMCU04103KD81670	3.0L	TALD	4	2002	2B04	12A650	D21	8	2118048	4000	WHILE DRIVING

NPF		WDS DIAG. DATA LOGGER. POWER BALANCE. FUEL PRESSURE AND INJECTOR FLOW. UNABLE TOVERIFY CONCERN AT THIS TIME. MISC. EXPENSE OTHER 6.00 OFR GASOLINE TO ROAD TEST VEHICLE.
SSM		DIAG. R AND R EEC RELAY AND IAC. CLEANED AND TIGHTENED ALL GROUNDS. TECH FOUND FAULTY EEC RELAY AND IAC
REPLACED		REPLACE IAC AND THROTTLE BODY
SSM		VERIFY VERIFY VEHICLE STALLS.RD TEST.EEC TEST SYSTEM PASSED.CK FOR VAC LEAK NONE FOUND SSM FOR CONCERN.REPROGRAM PCM.RERDAD TEST.CONCERN REPAIRED
MIS BUILD		AIR BREATHER INSTALLED INCORRECTLY PERFORMED EEC TEST NO CODES KOEO PASS KOER PASS KOEC PASS CHECKED ALL VALUES OKAY REMOVED AND REINSTALLED AIR BREATHER
SSM		9217 SSM 15434 INTERMITTANT ENGINE QUIT ... 12650D .2 HRS. EEC SELF TEST ... 12650D61 .5 HRS. NGS RECORDER MONITOR DIAG ... 12650D45 .3 HRS. EEC PINPOINT TEST ... 12650D60 .1 HRS. NGS DCL DISPLAY .
REPLACED		INTERNAL FAILURE DIAGNOSIS R R OIL PAN AND FOUND ENGINE CAME APART AND IN EXHAUST REPLACE ENGINE ASSY AND CONVERTOR AND ROAD TEST
REPLACED		COMPUTER DIAG SYSTEM REPLACE EEC RELAY AND IAC
REFLASH		PERFORMED SYSTEM DIAGNOSIS RESET BASE IDLE PROGRAM ENGINE PROCESSOR ROAD TEST OK
HOTLINE		PERFORMED REVISED BASE IDLE SETTING PROCEDURE AS PER FORD TECHNICAL SUPPORT COMPUTER DIAG SYSTEM MT TRACE AND REPAIR
DIAG		EEC TEST PASS, FUEL PRESSURE GOOD. 64 PIN. RESET PROCESSOR , ROAD TEST, OK.
REFLASH		REPROGRAM PCM
DIAG		ENGINE STALLS WHILE DRIVING EEC (QUICK TEST) DIAGNOSIS
REFLASH		ENGINE STALLS AT TIMES REPROGRAM PCM
TSB		9951 WDS HOOK UP PASS CODES RAN OASIS PERFORM CHECKS AND REPAIRS PER TSB 02 05 06, MONITOR PIDS WITH WDS TO CHECK IDLE SPEED AND IAC VALVE REPROGRAM MED PCM TO LATEST CALIBRATION REPLACED EEC RELAY
SSM		PERFORMED EEC PINPOINT AND PID MONITOR TESTS REPLACED EEC RELAY AS PER SSM#15454 REMOVE JUNCTION BOX CHECK WIRING NO FAULTS CHECK WIRING UNDER BATTERY TRAY ALL OK AT THIS TIME
NPF		COMPLETED EEC TEST NO CODES. CHECKED BASE IDLE 750 750. CHECKED CONNECTORS OKAY. CLEANED GROUNDS G200 G100 G104 G015 G101. NO PROBLEM FOUND AT THIS TIME.
TSB		HOOK UP WDS SELF TEST EECV SYSTEM CONT PASS KOEO PASS KOER PASS PERFORM TSB 021106 EVERYTHING PASSED CALLED HOT LINE
TSB		DIAG,PERF TSB 02 11 6 REPROGRAM PROCESSOR,PCM RELAY AND EVAP CHECKS OK
HOTLINE		KOE TEST PINPOINT TEST PERFORM MULTIPLE TESTS PERHOTLINE REPLACE IAC
NO TEXT		
REPLACED		PERFORM SELF TEST AND PINPT MONITOR ROAD TEST AND REPLACE IAC RETEST AND CLEAR
NO TEXT		
TSB		DID NOT VERIFY CONCERN.FOLLOWED PROCEDURES IN TSB 02 11 6. HARDSTOP IDLE FAULTY OUT OF ADJUSTMENT.ADJUSTED HARDSTOP IDLE
TSB		232 1650E .1 E1 .2 M TEST EEC. P100L PERFORM TESTS PER TSB 01 11 09. ATTACHED. ALL STEPS CHECKED NORMAL.
TSB		2/13 TSB 02 11 05 WARRANTY RAN OASIS AND PERFORM TSB 02 11 06. IAC DUTY CYCLE WAS 35.94% AT 750RPM AND 160F. CHECKED BUILD DATE ON VEHICLE 4 22 02, NO PCM REPROGRAM REQUIRED. CHECKED EVAPVM DUTY CY
TSB		PERFORM TSB 2 11 05. REPLACE THE IAC MOTOR. VERIFY DUTY CYCLE AT 35%.
DIAG		CUST# DEI CONO# 35 BAS# 12A650

	IC 6 VEHICLE STALLS WHEN DRIVING AND DOESNT ALWAYS TURN OVER
	VEHICLE STALLS AROUND 40 MPH ON SLIGHT DOWNHILL
	VEHICLE HAS STALLED THREE DIFFERENT TIMES AFTER DRIVING ON HOT DAYS FOR ABOUT 2 MILES. COOLANT LIGHT COMES ON RIGHT BEFORE VEHICLE STALLS
	CUSTOMER STATES CAR IS DYING AT STOP SIGNS AND AFTER IDLING FOR A WHILE
.. 14200A .4 HRS. CHECK AND TIGHTEN PCM AND OTHER GROUNDS ... 12650D5 .1 HRS. REPLACE IDLE AIR CONTROL VALVE ... 12650D7 .1 HRS. REPLACE THE PCM POWER RELAY ... 12650DX1 .1 HRS.	CUSTOMER STATES THAT VEHICLE STALLED WHILE DRIVING 35 40 MPH ON DOWNHILL NOT BRAKING OR TURNING
	CHECK DRIVING DOWN HYW STARTED CLATTERING AND DIED WONT CRANK
	CUSTOMER STATES ENGINE HAS SHUT OFF TWICE WHEN APPLYING BRAKES
	CK STALLS ON DECEL
ECC WIRE	CUSTOMER STATES ENGINE STALLED WHILE DRIVING
	CUSTOMER STATES THE STALLS WHILE DRIVING , RESTARTS OK. HASN T HAPPENED IN PAST WEEK.
	CUST REPORTS CAR STALLED WHILE DRIVING ONE TIME AND RESTARTED OK
	CUSTOMER STATES ENGINE HAS STALLED A COUPLE OF TIMES WHILE DRIVING...RESTARTS FINE.
	ENGINE STALLS AT TIMES WHEN COASTING DOWNHILL, WILL RESTART FINE.
WITH UPDATED ONE MONITOR AND CHECK EVAP. SYSTEM WORKING PROPERLY ROAD TEST WHILE MONITOR ING TO CHECK FOR RPM DIPS ALL O.K. AT THIS TIME	CUST STATES STALLED WHILE DRIVING SERVAL TIMES WAITED SERVAL MIN. RESTARTED ...VERY POOR FUEL MILEAGE
	VEHICLE STALLS WHEN DRIVING
	CUSTOMER STATES WHILE DRIVING AND GOING DOWN A HILL CAR DIED
	CUSTOMER STATES VEHICLE STALLED OUT WHILE DRIVING AT 35 45 MPH NORMAL ACCELERATION
	CUST. STATES VEHICLE CUTS OFF WHILE DRIVING ON NEIGHBORHOOD STREETS (20 25 MPH)
	STALLS WHILE DRIVING WITH AC ON
	VEHICLE STALLED LOSS OF PS BRAKES AND EBRAKE HAD TO BE APPLIED TO STOP VEHICLE GO OVER VEHICLE COMPLETELY
	CUSTOMER STATES VEHICLE STALLED WHILE DRIVING DOWNHILL
	CUST STATES WAS DRIVING, VEHICLE DIED WHILE DRIVING, RESTARTED IMMEDIATLY
CLE AND FTP VOLTAGE. EVAPVM INCREASED TO 100% AND FTP DECREASED TO 2.2 VOLTS THEN RECYCLED TO 0% WITH FTP BACK TO 2.8. THERE IS NOT ANY PREMATURE PURGE SHUT OFF. CHECKED EEC RELAY	CHECK CUSTOMER STATES THAT VEHICLE HAD ROTTEN EGG SMELL VEHICLE DIED WHEN COASTING DOWN HILL SOME WARNING LIGHTS CAME ON WHEN THIS HAPPENED.
	CUSTOMER STATES THE ENGINE WILL STALL ON COAST OR AT STOP
	CUST STATES VEHICLE DIED WHILE DRIVING STARTS RT BACK UP

2002	19450	S11	1FMCU04102KC99707	3.0L	TALD		4	2002	2.00E+03	9F715	D21	2	1683363	1000	WHILE DRIVING
2002	19451	S11	1FMCU04102KC92999	3.0L	TALD		4	2002	2.00E+03	9F715	D21	3	2166181	1000	WHILE DRIVING
2002	19457	S11	1FMCU04102KC83457	3.0L	TALD		3	2002	2.00E+03	9F715	D21	1	2055743	0	DOWNHILL
2002	19458	S11	1FMCU04102KC83458	3.0L	TALD		3	2002	2.00E+03	9E926	D21	3	2236734	3000	TBB
2002	19460	S11	1FMCU04102KC76794	3.0L	TALD		3	2002	2.00E+03	9F715	D21	1	1614830	0	AT IDLE
2002	19466	S11	1FMCU04102KC71748	3.0L	TALD		3	2002	2.00E+03	9F715	D21	4	1741469	5000	WHILE DRIVING
2002	19465	S11	1FMCU04102KC71665	3.0L	TALD		3	2002	2.00E+03	9F715	D21	6	2229113	5000	TURNING
2002	19467	S11	1FMCU04102KC61675	3.0L	TALD		3	2002	2.00E+03	9F715	D21	4	2128936	5000	STALLS
2002	19476	S11	1FMCU04102KC39720	3.0L	TALD		2	2002	2.00E+04	9C915	D21	4	2107694	5000	WHILE DRIVING
2002	19481	S11	1FMCU04102KC29660	3.0L	TALD		2	2002	2G04	DIAG	D21	1	1918679	17000	AT STOP
2002	19482	S11	1FMCU04102KC20817	3.0L	TALD		2	2002	1H03	9J460	D21	3	1971884	1000	WHILE DRIVING
2002	19488	S11	1FMCU04102KC10807	3.0L	TALD		1	2002	2G04	12A650	D21	5	2149301	6000	COASTING
2002	19487	S11	1FMCU04102KC00979	3.0L	TALD		1	2002	2.00E+03	9E926	D21	3	1330271	9000	STALLS
2002	19496	S11	1FMCU04102KB95469	3.0L	TALD		1	2002	2G01	12A650	D21	2	1188117	1000	STALLS
2002	19492	S11	1FMCU04102KB89206	3.0L	TALD		1	2002	2G04	12A650	D21	7	2299905	10000	WHILE DRIVING
2002	19494	S11	1FMCU04102KB89206	3.0L	TALD		1	2002	2.00E+04	9C915	D21	1	725469	1000	WHILE DRIVING
2002	19499	S11	1FMCU04102KB79719	3.0L	TALD		12	2001	7V01	14290	D21	8	2222631	15000	STALLS
2002	19505	S11	1FMCU04102KB67143	3.0L	TALD		12	2001	2G04	12A650	D21	6	1634376	9000	WHILE DRIVING
2002	19512	S11	1FMCU04102KB64145	3.0L	TALD		12	2001	7C05	14NX99	D21	4	1045972	4000	WHILE DRIVING
2002	19514	S11	1FMCU04102KB54411	3.0L	TALD		12	2001	2G05	RECAL	D21	5	2371654	6000	STALLS
2002	19516	S11	1FMCU04102KB50050	3.0L	TALD		12	2001	2G05	RECAL	D21	7	1775120	5000	WHILE DRIVING
2002	19518	S11	1FMCU04102KB44154	3.0L	TALD		11	2001	2.00E+03	9F715	D21	4	886260	4000	STALLS
2002	19521	S11	1FMCU04102KB40088	3.0L	TALD		11	2001	2.00E+03	9F715	D21	7	1705451	6000	DOWNHILL
2002	19526	S11	1FMCU04102KB37660	3.0L	TALD		11	2001	1H03	9J460	D21	5	1486007	4000	WHILE DRIVING
2002	19530	S11	1FMCU04102KB37668	3.0L	TALD		12	2001	2G04	12A650	D21	7	2030429	7000	WHILE DRIVING
2002	19535	S11	1FMCU04102KB29167	3.0L	TALD		11	2001	2G04	12A650	D21	6	1768995	4000	WHILE DRIVING

TSB		EEC TEST NO CODES, CHECK OASIS PERFORM TSB 02 11 05 MONITOR ROAD TEST IAC 27% WARM NO PURGE FLOW, REPLACE IAC VALVE PER TSB. ROAD TEST PASSES 3 CONCED STOPS ABOVE 40MPH OK.
TSB		EEC TEST NO CODES, NGS ROAD TEST, FUEL & IGNITION TESTS, PINPOINT TEST, REPLACED IAC, RETESTED (REF TSB 02 11 05)
TSB		RECKED AND FOUND TSB FOR CONCERN. REPLACED IAC,T BODY,FLASHED PCM,AND REPLACED EVAP VALVE AS PER TSB,OK NOW.
TSB		EEC DIAG. PIN POINT TEST, IGNITION DIAG, CHECKED TSB, REPLACED UPDATED IAC, COMPLTED TSB 2 11 5, MONITORED IAC AGA IN, REPLACED THROTTLE BODY, MONITORED DLT CYCLE, REPROGRAMME D PCM WITH LATEST UPDATE
TSB		DEFECTIVE IDLE AIR CONTROL. PERFORM ALL SIX STEPS OF TSB 02 11 05
INOP		DOES NOT OPERATE PROPERLY EEC (QUICK TEST) DIAGNOSIS
STICKING		IDLE AIR BINDING EEC (QUICK TEST) DIAGNOSIS
DIAG		SP715 CC 42 EEC TEST KOEO PASS KOEC PASS KOER PASS PINPOINT TEST DCL DISPLAY FUEL PRESSURE TEST NGS MONITOR RECORDER
TSB		NGS PASS CODES PID MONITOR ROAD TEST PASS FUEL PSI TEST PASS IGNITION SYSTEM TEST PASS. CONTACT HOT LINE REGAURDING TSB 02 11 05 INSTRU CTED TO INSPECT WIRING HARNESS AND CONNECTORS F OR WATER INT
NPF		CHECK FOR ENGINE STALLS AT STOPS HAPPENED 1X UNABLE TO DUPLICATE NO CODES FOUND .
REPLACED		TESTED EEC,PERFORMED PIN POINT TESTS REPL D DPFE SENSOR,ROADTESTED OK
TSB		INTERNAL PCM PROBLEM MT NO OPERATION LISTED TO PERFORM TSB02116
TSB		TECH RAN TESTS AND FOUND IAC,THROTTLE BODY NEEDS TO BE REPLACED,REPLACED AND RAN TESTS TO CHECK OUT,REPAIR AS PER TSB 02 05 05
REPLACED		CK AND TRY TO REPROGAM REPLACE PCM TO CORRECT
REPLACED		10253 NO MIL NO DTCS (12A650) 126500 .2 DX1 .1 D5 .2 TESTED EEC SYSTEM PASS. REPLACED PCM W EXPERIMENTAL PCM PER ENGINEERING AND C.L.T. RETESTED SYSTEM PASS.
SSM		1252 W.I.P. 505 NO MIL NO DTCS (DIAG) 126500 .2 D55 .3 D50 .1 D61 .5 99508 .3 M TIME .5 (TIME TO CALL HOTLINE AND PERFORM TESTS TO EVAP VENT HOSE PER SSM) EEC TESTS PASS. DCL DISPLAY OK. FUEL S
DIAG		TEST EEC SYSTEM CODE P0151 TEST EEC SYSTEM CODE P0151 PERFORM PINPOINT TEST AND RECIEVE FUEL DELIVERY TEST 43 PSI PERFORM LEAK DOWN TEST PASS
REFLASH		WDS PASS MIL NOT ON CK 02 11 5 REPROGRAM PCM LATEST CALIBRATION LEVEL UPDATE
REPLACED		RUN WDS TESTS KOEO PASS, CONTINUOS PASS, ELECTR ICAL TEST AND FOUDN NECESSARY TO REPLACE THE EE C RELAY.
TSB		TEST EEC 5 PASSES IN ALL ROAD TEST MONITOR PIDS CHK TSBS 021106 REPROGPCM SO IAC MOTOR AND THROTTLE BODY
TSB		6305 RAN EEC TEST KOEO PASS CONT PASS KOER PASS. RAN OASIS AND TESTED PER TSB 021106. REPROGRAMM ED PROCESSOR. RERAN EEC TEST SYSTEM PASS.
REPLACED		4770 BINDING WDS KOEO PASS FUEL PRESSURE TES T60PSI OK DCL MONITOR COLD START PINPOINT AND REPLACE IDLE AIR BYPASS RETEST OPERATION OK
DIAG		1 42 NGS DIAG START UP TEST DCL DISPLAY TEST KOEO PASS KOER PASS CONT PASS PID DATA MONITOR RECORD SIG SIM CHECK IAC AND
REPLACED		EEC TEST NO CODES MONITOR PIDS CHECK FUEL OK CHECK IGNITION OK FOUND VREF SHORTED TO PFE REPLACED PFE ROAD TEST OK
TSB		INSPECTED RAN NGS FOUND TSB 02 11 05 CHECKED OK REPROGRAMMED PCM NO PROBLEM FOUND
TSB		ROAD TEST. NO STALL BUT NOTICED IDLE DIP DOWN BELOW 600 RPM. WDS DIAG. DATA LOG GEN. POWER BALANCE. FUEL PRESSURE AND INJECTOR FLOW. PERFORMED TSB 02 11 5. RE PROGRAMMED PCM. ROAD TEST. IDLE RECOVERY

	VEHICLE WAS IN AN ACCIDENT, WHILE DRIVING VEHICLE DIES
	CUSTOMER STATES THE VEHICLE DIED WHILE DRIVING, HAD ONLY DRIVEN SEVERAL MILES WHEN THIS OCCOURRED. HAPPENED IN EARLY
	CUSTOMER STATES:THAT THE VEHICLE DIED WHILE COMMING DOWN HILL ON HARTNELL.WOULD NOT RE START.CHECK AND ADVISE.
, REROAD TEST, OK	CUSTOMER STATES VEHICLE STALLS INTERMITTENTLY, CHECK FOR TSB
	CUSTOMER STATES ENGINE STALLS WHEN IDLING ENGINE SURGES
	CHECK DIES WHILE DRIVING
	CHECK FOR DIED WHILE GOING AROUND CORNER
	D31 THIS TRUCK HAS STALLED TWO TIMES IN ONE DAY DRIVEING 35 45 MPH.IT DID RESTART JUST FINE BOTH TIMES
FUSION AND GROUNDS R AND I BATTERY BOX TO INSPECT G 104, G105,G101 ALSO INSPECTED C270 SDC AND C110,C133 ALL OK. THEN HOT LINE IN STRUCTED TO REPLACE VAPOR MANAGEMENT VALVE AND IDLE AIR	CUST STATES VEHICLE STALLED WHILE DRIVING
	CHECK FOR ENGINE STALLS AT STOPS
	CUSTOMER STATES STALLED WHILE DRIVING,RESTARTED OK,DEL DID S TAY ON FOR A SHORT TIME
	CUSTOMER STATES CHECK FOR VEHICLE STALLS MOSTLY WHEN COASTING AND MOSTLY WHEN HOT BUT WILL START RIGHT UP
	CUSTOMER STATES HAS STALLED 6 TIMES WITH NO WARNING BUT STARTS BACK UP
	CK ENGINE DIES STALLS
	CK UNIT DIES W DRIVING INTERMITTENTLY ADV
YSTEM TESTS PASS. IGNITION SYSTEM TESTS PASS. ROAD TESTS W NGS FINDS NO APPARENT FAULTS AT THIS TIME. SSM# 16589 INSTRUCTS TO ATTEMPT TO REPROGRAM PCM, PCM IS AT THE LATEST AVAILABLE	INSPECT DIES WHILE DRIVING DOWN THE ROAD.
	CUSTOMER STATES STALLS DOWN LOST IN POWER ON EXELL ADVISE OPERATIONS CONT;WRK NUMBER ANY CONCERNS.
	CUSTOMER STATES CAR WILL LOOSE POWER WHEN DRIVING AT A CONSTANT SPEED 40 50 MPH, HARD TO START SOMETIMES, AND STALLS OUT WHEN DRIVING INTERMIT.
	ENGINE DIES OUT WHILE DRIVING STARTS RIGHT BACK.
	CHECK FOR INTERM STALLS
	CHECK AND REPORT VEH STALLED WHEN CUST WAS DRIVING AT ABOUT 45 MPH . WOULD NOT RESTART FOR APPOX 5
	CK ENGINE AT TIMES ON COLD START WILL STALL OUT AFTER START UP OR PUT INTO GEAR.ADVISE
	CUSTOMER STATES VEHICLE STALLED OUT WHEN COASTING DOWNHILL (AFTER CUSTOMER LET SIT FOR A WHILE VEHICLE RESTARTED)
	VEH SHUT OFF WHILE DRIVING NO CRANK HAD VEH TOWED IN VEH DID START UP AFTER WAS
	CUSTOMER STATES ENGINE DIED WHILE DRIVING RESTARTED OK INSPECT & ADVISE
BETTER. NOW O.K.	CUSTOMER STATES VEHICLE STALLS WHILE DRIVING INTERMITTENTLY.

2002	19541	S11	1FMCU04102KB23840	3.0L	T/LD	11	2001	7V01	12A581	D21	7	1690465	8000	AT STOP
2002	19542	S11	1FMCU04102KB23840	3.0L	T/LD	11	2001	7V01	12A581	D21	8	1781641	8000	COASTING
2002	19544	S11	1FMCU04102KB23742	3.0L	T/LD	11	2001	2.00E+03	9F715	D21	8	1954603	8000	NO TEXT
2002	19545	S11	1FMCU04102KB22140	3.0L	T/LD	11	2001	2F02	9E996	D21	2	2116768	1000	WHILE DRIVING
2002	19551	S11	1FMCU04102KB15401	3.0L	T/LD	11	2001	7C05	14N069	D21	3	607405	0	WHILE DRIVING
2002	19552	S11	1FMCU04102KB15401	3.0L	T/LD	11	2001	2.00E+03	9F715	D21	0	336914	0	WHILE DRIVING
2002	19553	S11	1FMCU04102KB15401	3.0L	T/LD	11	2001	2G02	12B579	D21	5	994348	2000	STALLS
2002	19559	S11	1FMCU04102KB12045	3.0L	T/LD	10	2001	2.00E+03	9F715	D21	10	2247850	5000	WHILE DRIVING
2002	19564	S11	1FMCU04102KB00901	3.0L	T/LD	10	2001	2G04	12A650	D21	7	2081394	5000	INSPECTION
2002	19575	S11	1FMCU04102KA99462	3.0L	T/LD	10	2001	2.00E+03	9F715	D21	7	1229445	3000	WON'T RUN
2002	19576	S11	1FMCU04102KA99153	3.0L	T/LD	10	2001	2G04	12A650	D21	0	1055394	0	WHILE DRIVING
2002	19579	S11	1FMCU04102KA91052	3.0L	T/LD	10	2001	2.00E+03	9F715	D21	2	359164	2000	WHILE DRIVING
2002	19580	S11	1FMCU04102KA79662	3.0L	T/LD	10	2001	2G02	12B579	D21	9	2096074	3000	WHILE DRIVING
2002	19585	S11	1FMCU04102KA70328	3.0L	T/LD	10	2001	2.00E+03	9E926	D21	9	1946977	3000	WHILE DRIVING
2002	19598	S11	1FMCU04102KA69011	3.0L	T/LD	10	2001	2G04	D9A9	D21	11	2349307	11000	STALLS
2002	19601	S11	1FMCU04102KA67777	3.0L	T/LD	10	2001	2G04	12A650	D21	4	761691	5000	WHILE DRIVING
2002	19602	S11	1FMCU04102KA67777	3.0L	T/LD	10	2001	2.00E+03	9F715	D21	9	1996198	11000	DOWNHILL
2002	19603	S11	1FMCU04102KA66424	3.0L	T/LD	10	2001	7V01	12A581	D21	7	1155601	4000	STALLS
2002	19605	S11	1FMCU04102KA66203	3.0L	T/LD	10	2001	7C05	14N069	D21	2	491299	3000	WHILE DRIVING
2002	19606	S11	1FMCU04102KA66262	3.0L	T/LD	9	2001	2G04	12A650	D21	5	784429	4000	DOWNHILL
2002	19607	S11	1FMCU04102KA66547	3.0L	T/LD	10	2001	7C05	14N069	D21	4	579690	3000	DOWNHILL
2002	19608	S11	1FMCU04102KA66502	3.0L	T/LD	9	2001	1H03	9J460	D21	10	1942341	14000	STALLS
2002	19609	S11	1FMCU04102KA67723	3.0L	T/LD	10	2001	2.00E+03	9F715	D21	8	1466812	15000	WHILE DRIVING
2002	19621	S11	1FMCU04102KA50499	3.0L	T/LD	9	2001	2G04	12A650	D21	6	1646769	13000	DECEL

REFLASH		PER CASE #2FTFC001 CK GROUNDS & CONNECTORS REPROG PCM CK DPFE CK FOR BENT AND BURNT PINS
TSB		CALL HOTLINE NEW REVISED TSB 02 11 6 CK ALL CIRCUITS CK PCM IAC TB EVAP VALVE EEC RELAY REPL MAF SE
REPLACED		R AND R IAC AND RETEST EEC SYSTEM
REPLASH		ON MONDAY. PERFORMED SYSTEMS TEST,NO CODES IN SYSTEM ADJUSTED TP VOLTAGE AND IAC %,MODIFIED THROTTLE BODY AND REPROGRAMMED PCM W LATEST CALIBRATION PER FORD ENGINEER JIM C.
DIAG		RELAY EEC (QUICK TEST) DIAGNOSIS
DIAG		IAC EEC (QUICK TEST) DIAGNOSIS
DIAG		MAF EEC (QUICK TEST) DIAGNOSIS
REFLASH		5499 WAR WDS SELF TEST, NO DTC, PINPOINT TEST, DCL DISPLAY, POWER BALANCE TEST, ROAD TEST WITH RECORDER, REPLACED IAC VALVE, REPLACED EEC POWER RELAY, EVAP SYSTEM TEST, REPLACED VAPOR MANAGEMENT VA
REFLASH		HOOD FUNCTIONS NORMALLY UPDATE PCM FOR INTERMITTENT STALL CONCERN
REPLACED		CONFIRMED STALLING CONCERN. RAN EEC TEST PASSED ALL. REPLACED IAC. RETEST OK.
SSM		CHECK OUT AS PER SSM 15699,REPROGRAMMED PCM TO LATEST UPDATE,RECHECK
REPLACED		2783 DIAGNOSE EEC SYS PASS IGNITION TEST FUEL PRESSURE OK MONITOR PIDS RD TEST REPLACE IAC VALVE RETEST OK
INOP		INOP EEC (QUICK TEST) DIAGNOSIS
TSB		TSB EEC (QUICK TEST) DIAGNOSIS
NPF		11609 CHECK STALLED ONE ENG LIGHT CAME ON RAN WDS TEST KOEO KOER NO DTC ROAD TEST OK SHOP ALL OK NPF AT THIS TIME
SSM		TEST SYSTEM UNABLE TO VERIFY, CHECK FORD FOUND SSM 15699 PERFORM SSM, REPROGRAM PCM AND INSPECT EEC RELAY RETEST OK
REPLACED		TECHNICIAN VERIFIED CONCERN. TECHNICIAN PERFORMED EEC TEST AND FOUND IDLE TOO LOW. TECHNICIAN RECOMMENDS TECHNICIAN REPLACED IDLE AIR CONTROL VALVE.
DIAG		EEC DIAG,PWR BLNCE TST,RLTVE CMPRSSN TST,FUEL PRESS TST,PNPNT TST,CK CIRCS AND PWR TO SYSTM,LCTE AN
SSM		D21 42 PP ROAZ 14N699 A ROAD TESTED EEC TESTED PASSED PINOPINT TESTS Z INTERMITTENT OASIS SSM15434 INSPECTED AND REPLACED EEC POWER RELAY CHECK
SSM		4205 SSM 15699 12A650 42 DIAG STALLS INT TEST DROVE CONFIRMED CONCERN PERFORMED NGS DIG 12650D NO DTCS CK FUEL PRESS 93508 35PSI LEAK DOWN PASSED PINPOINT TEST 12650D45 CK ELEC CONN AND HOSES OK C
SSM		EEC TEST. NO CODES. PINPOINT TEST. ROAD TEST DCL DISPLAY. CONCERN INTERMITTENT. REFER TO SSM 15494. NORMAL DIAG REPLACE EEC RELAY AND PERFORM WIRE HARNESS REPAIR BY TIGHTENING RELAY PINS. CHECK GROUND
TSB		TECH CHECKED FOR THE STALLING PROBLEM, TECH CHECKED THE PROCESSOR FOR THE NEWEST UPDATES AS PER TSB. TECH ALSO CHECKED THE POWERE RELAY AND THE RELAY WAS OK BUT THE PROCESSOR NEEDED TO BE UPDATED. TE
SSM		CK CAR WILL STALL WHEN DRIVING, STARTS BACK UP, VERIFIED CONCERN. WDS DIAG, PCM SELF TEST KOEO EC ER PASS, RE CK PID DATA EVAPVM ECT RPM FTP, EVAPMA RISES TO 100%, FT DROPS TO 2.0 VOLTS THEN RECYCLES
TSB		ROAD TEST TO VERIFY..DID NOT STALL ON TEST..CHECK TSB, SSM AND OASIS..REFER TO TSB 02 6 6 ENGINE CUT CONDITION..PERFORM DIAGNOSIS TESTS PER TSB..REPROGRAM PCM PER TSB..NO PARTS REPLACED..RETEST SEVE

	CUSTOMER STATES,INTERMITTENTLY LOSES STEERING & BRAKES HARD TO STOP,& OIL LIGHT COMING ON
	CUST STATES VEH STALLED AGAIN ON DEACCEL
	CUS STS WHILE DRIVING THE CAR STALLED, CUS WAITED 1 MIN. AND CAR STARTED. THIS HAPPNED ONCE FRIDAY AND ONCE ON MONDAY
	CUST REPORTS CHECK ENGINE STALLS WHILE DRIVING IN STOP AND GO TRAFFIC (HOT) (RPMS GET LOW STEERING GETS HARD, CUST TURNS OFF AND RESTARTS)
	CUST STATES WAS DRIVING 55 MPH DOWN THE INTERSTATE AND THE VEH STALLED AND THE OIL LIGHT CAME ON
	GUEST STATES THAT VEHICLE CUTS OFF AT TIMES. INSTALL SOP PARTS PER FORD SEE LARRY
LVE, RERUN TEST, SYSTEM PASSED REPROGRAM PCM TO LATEST UP DATE	CUST STATES ENGINE DIED WHILE DRIVING
	PERFORM QUALITY CARE MULTIPOINT INSPECTION
	ENGINE WONT STAY RUNNING AFTER STARTING, DOES NOT WANT TO GO ON FAST IDLE,DOS
	SHUT OFF WHILE DRIVING
	CUST STATES TRUCK DIED ON ROAD AT APROX 35 MPH BUT WAS ABLE TO RESTART WITHOUT A PROBLEM
	STALLS AT TIMES WHILE DRIVING
	LOST POWER AND STALLED DRIVING RESTARTED A MIN LATER
	CK VEH STALLED ONCE AND RESTARTED OK,SEEMS IT DOESNT HAVE POWER IT SHOULD,NO CK ENG LT COMES ON EXCEPT WHEN IT STALLED
	CUSTOMER STATES WHILE HE WAS DRIVING ON A WINDY ROAD WITH ENGINE FULLY WARMED UP IT DIED FOR NO REASON, RESTARTED
	CUSTOMER STATES WHEN COASTING DOWNHILL AT A REAL SLOW SPEED, ENGINE STALLS.
	CUSTOMER REPORTS ENGINE DIES, SEE EARLY BIRD
	CUSTOMER STATES WHILE DRIVING SOME OF THE DASHBOARD RED LITES CAME ON STEERING LOCKED AND PULLED TO ONE SIDE 2X RPRT
K EGR SYSTE M 12650D80 VACC TEST EGR VALVE PASSED CK OPERATION OF VALVE PASSED CK PIDS 12650D80 81 CK IAC 34 41% CK BARO 156HZ FUEL TRIM AND O2 SENSOR OK CK INGITION SYSTEM 12650D65	CUST SAYS WHEN DRIVING DOWNHILL VEHICLE HAS STALLED 3 TIMES IN THE LAST WEEK
S. OK. CHECK CONNECTIONS.	SOMETIME STALLS WHILE IN GEAR WHEN TAKING FOOT OFF ACCEL. GOING DOWN HILL AND WHILE BACKIN
CH REPROGRAMMED THE PROCESSOR. TECH PERFORMED PIN POINT TESTING AT THE IAC AND MASS AIR FLOW SENSOR. BOTH WERE WITHIN SPECS.	CUSTOEMR STATES THE VEHICLE STALLED AND WOULD NOT START
TO 2.8 V, EVAP DROPS TO	CHECK CAR WILL QUIT RUNNING DRIVING IT WILL START BACK UP
RAL MILES WITHOUT STALLING..	CUSTOMER STATES THAT ENGINE CUTS OUT WHEN DECELERATING STARTS RIGHT AWAY

2002	19822	511	1FMCU04102KA60178	3.0L	TAU	9	2001	2005	RECALEM	D21		8	1396453	11000	AT STOP
2002	19695	511	1FMCU04102KA46242	3.0L	TAU	9	2001	2.00E+03	9F715	D21		11	2436816	20000	ACCELERATING
2002	19691	511	1FMCU04102KA44262	3.0L	TAU	9	2001	7C05	14N069	D21		3	417208	4000	WHILE DRIVING
2002	19694	511	1FMCU04102KA45289	3.0L	TAU	9	2001	2.00E+03	9F715	D21		10	1699567	12000	NO TEXT
2002	19640	511	1FMCU04102KA97611	3.0L	TAU	9	2001	1A05	9007	D21		9	1656069	16000	NO TEXT
2002	19662	511	1FMCU04102KA99911	3.0L	TAU	8	2001	2.00E+04	9C915	D21		11	2151557	3000	WHILE DRIVING
2002	19666	511	1FMCU04103KA94786	3.0L	TAU	8	2001	7C05	14N069	D21		8	1394808	13000	TURNING
2002	19667	511	1FMCU04103KA94786	3.0L	TAU	8	2001	2.00E+03	9F715	D21		8	1449461	13000	AT STOP
2002	19697	511	1FMCU04103KA95178	3.0L	TAU	8	2001	2.00E+03	9F715	D21		10	2127800	20000	WHILE DRIVING
2002	19675	511	1FMCU04103KA96091	3.0L	TAU	8	2001	2.00E+03	9F715	D21		10	1691740	10000	TURNING
2002	19693	511	1FMCU04103KA96993	3.0L	TAU	8	2001	2.00E+04	9C915	D21		9	2156221	14000	WHILE DRIVING
2002	19661	511	1FMCU04103KA96741	3.0L	TAU	8	2001	1H09	9J460	D21		6	700912	2000	NO TEXT
2002	19664	511	1FMCU031D2KC66459	3.0L	TAU	6	2002	2.00E+03	9F715	D21		1	1529932	0	WHILE DRIVING
2002	19665	511	1FMCU031D2KC66970	3.0L	TAU	5	2002	1H03	9J460	D21		2	1787095	2000	WHILE DRIVING
2002	19669	511	1FMCU031D2KC66984	3.0L	TAU	3	2002	2.00E+03	9E926	D21		1	1129615	1000	AT STOP
2002	19699	511	1FMCU031D2KC66945	3.0L	TAU	2	2002	2.00E+03	9F715	D21		4	1934052	3000	WHILE DRIVING
2002	19700	511	1FMCU031D2KC66119	3.0L	TAU	3	2002	7C05	14N069	D21		3	1663508	3000	WHILE DRIVING
2002	19711	511	1FMCU031D2KC17795	3.0L	TAU	1	2002	2.00E+03	9F715	D21		4	2879141	1000	WON'T IDLE
2002	19729	511	1FMCU031D2KC66495	3.0L	TAU	12	2001	2.00E+03	9F715	D21		8	2210172	6000	STALLS
2002	19725	511	1FMCU031D2KC66570	3.0L	TAU	1	2002	2B04	12A690	D21		5	2010510	6000	WHILE DRIVING
2002	19736	511	1FMCU031D2KC64236	3.0L	TAU	11	2001	2.00E+03	9F715	D21		4	1065728	3000	WHILE BRAKING
2002	19741	511	1FMCU031D2KC13064	3.0L	TAU	10	2001	7C05	14N069	D21		8	2166856	11000	NO TEXT
2002	19743	511	1FMCU031D2KC01572	3.0L	TAU	10	2001	2G05	RECAL	D21		5	653007	6000	WHILE DRIVING
2002	19750	511	1FMCU031D2KA76205	3.0L	TAU	10	2001	7C05	14N069	D21		4	730827	5000	WHILE DRIVING
2002	19761	511	1FMCU031D2KA66495	3.0L	TAU	10	2001	1H03	9J460	D21		10	2030416	16000	STALLS
2002	19781	511	1FMCU031D2KA63469	3.0L	TAU	10	2001	7C05	14N069	D21		4	807851	5000	WHILE DRIVING
2002	19782	511	1FMCU031D2KA63469	3.0L	TAU	10	2001	2.00E+03	9E926	D21		8	1804964	11000	WHILE DRIVING

REFLASH		RAN TESTS,REPROGRAMMED PCM,RETESTED,OK.
REPLACED		POWER RELAY FAILED EEC (QUICK TEST) DIAGNOSIS REPL CANISTER PURGE REGULATOR PINPOINT DCL REPL IAC RETST
TSB		4547 RAN OASIS FOR SSM & TSB INFORMATION. WDS HOOK UP. KOEO, KOER, FUEL PRESSURE TEST, DC I, PID DATA RECORDER & MONITOR. HAD NO CODES IN MEMORY. REFERED TO SSM 15494. INSPECTED CONNECTORS LIST SD,
NO TEXT		
ENGINE FAILURE		ENGINE LOCKED UP VERIFY NO START. INSPECT & DETERMINE ENG LOCKED UP. PULL STARTER, REMOVE SPARK PLUGS. FILLED OUT PTS FROM WEB.
REPLACED		REPLACED VMV
SSM		WDS, CK IGNITION, CK OASIS, REPLACE EEC RELAY PER SSM
TSB		ROAD TEST, WDS, NO CODES, CK IGNITION, OPERATING NORMAL, CONTACT CUSTOMER, HAD ANOTHER TECH CHECK, NO CODES, ROAD TEST, CK OASIS, TSB, SSM, PERFORM TSB 02 06 6
REPLACED		REPLACED AIR BY PASS VALVE, AND CLEANED LINE.
REPLACED		PERFORM EEC TEST PINPOINT TEST REPL AIR BYPASS RETEST
TSB		Y278 AND PERFORM TSB 021106 REPLACE EVAP VALVE AND REPROGRAM PCM
NO TEXT		
TSB		1. CHECKED FOR CODES FOUND NO CODES RAN OASIS FOUND A TSB FOR THIS CONCERN 02 11 06 FOLLOWED THRU STEP 4 FOUND THE IAC
REPLACED		VERFIED CONCERN EEC TESTED REPLACED SENSOR INOP
HOTLINE		CK FOR FRESH & VAC LEAKS, CHK FUL PRES, NGS DCL MONITOR CK SENSORS & ACT ALL IN SPECS. CALL FORD ASSISTANCE, WITH NGS DCL BRING PIDS IAC % RPM SET. EVAP SYS CK IAC WITH NO LOAD OR PURGE FLOW (42%) R
INOP		IAC VALVE DOES NOT OPERATE PROPERLY
DIAG		. EEC (QUICK TEST) DIAGNOSIS
REPLACED		TEST DRIVE TO VERIFY. WDS TEST. NO CODES DATA LOGGER TEST AND PINPOINT TEST AND CHECK AND REPLACED IABP AND RETEST AND REDRIVE
TSB		WDS KOEO, DATA LOGGER, PIN POINT, REPL AIR BY PASS VALVE, DUTY CYCLE WAS 49% NOW 34% RETEST EEC CHK TSB 02 11 06 OK
TSB		EEC DATA LOGGER PERFORM TSB FOLLOW INSTRU ON TSB COMPLETED STEPS IN SERVICE PREDEDURE AND ROAD TEST
INOP		INOP REPL IAC VALVE FUEL PUMP PRESSURE TEST ON VEHICLE DIAGNOSIS
INOP		OPEN CIRCUIT 14N089 VERIFY,NGS TEST PIN TEST NO DTCS,MONITOR PIDS,ISOLATE EEC RELAY,TAP ON RELAY,ENG.STALLED,REPLACE RELAY,RE TEST OK.
REFLASH		ECC TEST. WDS MONITORED ROAD TEST 4 MILS. INSPECT PCM NO. REPROGRAM PCM. RETEST PASS.
SSM		SEE SSM 15599 FOR THIS CONCERN,GIVES EXACT DETAILS ON WHAT T O DO. EEC TEST,PinPoint TESTS,IGNITION TESTS,FUEL SYSTEM TESTS: FUEL PRESSURE AND RELATIVE INJECTOR FLOW WITHIN SPECKS.
REPLACED		WDS TEST AND CK OUT NO CODES STORED IN PCM DIAG BY SYMPTOM A AND DCL MONITOR ROAD TEST FOUND PFE SENSOR VOLT OVERRANGE ALSO AIR LEAKS AT TUBE R AND R PFE SENSOR AND REPAIRED TUBE RETESTED
REPLACED		1 RUN ALL NECESSARY TESTS. REPROGRAMMED PCM. REPLACED EEC RELAY.
TSB		WDS TESTED. KOEC PASS. RUN DCL DISPLAY. PERFORMED TSB02 11 06

	ENGINE DIES AT STOPS AT TIMES
	CUST STATES HAS DIED 4 5 TIMES WHEN TRY TO ACCEL FROM A STOP, DOES RESTART FINE. HAS NOTICED 2 3 TIMES WAS W COLD ENGINE.
GROUNDS LISTED, IAC PART NUMBER OK. NO PUSHED PINS, WATER, CORROSION FOUND. IAC PER CENTAGE 39% IDLE SPEED, GOOD. REPLACED EEC RELAY WITH NEW PER 99M. RE EEC TESTED PASS. NO OCCURANCES OF	CUST STATES THE ENGINE DIED WHILE DRIVING AND ALL THE LIGHTS CAME BACK ON, VEH RESTARTED BUT CHECK AND ADVISE. ONLY HAPPENED ONCE
	VEH DIES WHE DRIVING OR STALLS
	CK INTERMITTANT ENGINE SHUT OFF MOST NOTICABLY MAKING TURNS CK FOR TSB REGARDING EEC RELAY SEE TONY
	CK LOST OF POWER AND CUTS OFF AT STOPS
	CUSTOMER STATES: STALLS WHILE DRIVING OR AT A STOP.
	CUSTOMER STATES WHEN TURNING VEHICLE STALLED
	CHECK VEHICLE STALLED WHILE DRIVING ADVISE
	ENGINE CUT OFF WHILE MOVING AT 35MPH POWER DIED FIRST
	CUST STATES THAT THE VEH STALLED OUT WHILE DRIVING AT ABOUT 45MPH IT RESTARTED RIGHT AFTER THIS HAPPENED
REPLACE IAC RETEST SAME. REPLACE THROTTLE BODY 39% (IAC) CK EVAP SYS PURGE SYS WORKING PROPERLY AT THIS TIME, CHK DTF HAD BLOWN OUT EVAP LINE ON EARLIER DATE RELAYS UPDATED.	STALLS AT STOPS SEE LIN FOR INFO
	C S INTERMITT STALL WHILE DRIVING, WILL RESTART RIGHT AWAY MOST THE TIME. INTERMITT LONG CRANK TIM
	CUSTOMER STATES AS SHE WAS DRIVING THE CEL CAME ON THEN THE OIL LIGHT AND THE VEHICLE LOST POWER STEERING AND CUT OFF.
	SOMETIMES STARTS AND DIES, OTHER TIMES CRANKS AND WONT START.
	GOING ABOUT 30 MPH WARM OR COLD, VEH HAS STALLED. SEE HISTORY.
	CUST STATES ENGINE DIED WHILE DRIVING ON THE FREEWAY ONCE
	ENGINE WILL STALL WHILE DRIVING, RESTARTS OK, HAS HAPPENED 4 TIMES, SEEMS TO HAPPEN WHEN SLOWING DOWN
	CUST STATES VEHICLE SHUTTING OFF WHILE DRIVING, WHEN DECELING AROUD 25 30 MPH.
	ENGINE STALLED WHILE DRIVING, ALL WARNING LIGHTS CAME ON. CHECK AND ADVISE. CCC: D21
	C6 VEH STALLS OUT AND MAKES VIBRATING NOISES
	CUSTOMER STATES THAT VEHICLE DIED WHILE DRIVING AND WOULD NOT RESTART
	CUST STATES THAT THE CAR STALLED OUT WHILE DRIVING, BACK ON 1 31 02 WE REPROGRAMED PCM, AND REPLACED EEC RELAY FOR SAME

2002	19772	S11	1FMCU031X2KA34175	3.0L	T/LD	8	2001	2.00E+03	9E928	D21	10	1888308	9000	WHILE DRIVING
2002	19779	S11	1FMCU031X2KA14125	3.0L	T/LD	6	2001	2.00E+03	9F715	D21	12	2227937	17000	AT IDLE
2002	19782	S11	1FMCU03182KD84270	3.0L	T/LD	5	2002	2G04	DIAG	D21	2	2245826	1000	ON HIGHWAY
2002	19795	S11	1FMCU03182KD41695	3.0L	T/LD	4	2002	2.00E+03	9E928	D21	4	2144288	3000	STALLS
2002	19797	S11	1FMCU03182KC92465	3.0L	T/LD	3	2002	2.00E+03	9F715	D21	2	2144954	2000	WHILE DRIVING
2002	19802	S11	1FMCU03182KC72536	3.0L	T/LD	3	2002	2G02	125579	D21	3	2220348	7000	WHILE DRIVING
2002	19807	S11	1FMCU03182KC86462	3.0L	T/LD	2	2002	2G04	12A850	D21	2	1054760	1000	ACCELERATING
2002	19808	S11	1FMCU03182KC29219	3.0L	T/LD	2	2002	2G04	12A850	D21	1	2048892	2000	WHILE DRIVING
2002	19809	S11	1FMCU03182KC17585	3.0L	T/LD	1	2002	2G04	DIAG	D21	5	1328693	1000	STALLS
2002	19812	S11	1FMCU03182KC06760	3.0L	T/LD	1	2002	2.00E+03	9E928	D21	6	1918513	6000	AT STOP
2002	19814	S11	1FMCU03182KB97832	3.0L	T/LD	1	2002	2.00E+03	9H307	D21	7	2122874	5000	WHILE DRIVING
2002	19816	S11	1FMCU03182KB86483	3.0L	T/LD	1	2002	2G04	12A850	D21	3	1181855	2000	AT STOP
2002	19817	S11	1FMCU03182KB76764	3.0L	T/LD	1	2002	2G05	12228	D21	1	1125517	0	STALLS
2002	19821	S11	1FMCU03182KB64486	3.0L	T/LD	12	2001	7G02	14401	D21	0	537345	0	NO CRANK
2002	19825	S11	1FMCU03182KB43856	3.0L	T/LD	11	2001	2.00E+03	9F715	D21	9	1887405	9000	STALLS
2002	19827	S11	1FMCU03182KB22001	3.0L	T/LD	11	2001	7C05	14N069	D21	4	667694	6000	WHILE DRIVING
2002	19828	S11	1FMCU03182KA99500	3.0L	T/LD	10	2001	2.00E+03	9E928	D21	6	1505954	6000	WHILE DRIVING
2002	19830	S11	1FMCU03182KA99500	3.0L	T/LD	10	2001	7C05	14N069	D21	4	730586	3000	STALLS
2002	19831	S11	1FMCU03182KA93500	3.0L	T/LD	10	2001	2G02	125579	D21	9	2075717	7000	WHILE DRIVING
2002	19833	S11	1FMCU03182KA80574	3.0L	T/LD	10	2001	7C05	14N069	D21	4	591800	3000	STALLS
2002	19834	S11	1FMCU03182KA80574	3.0L	T/LD	10	2001	2.00E+03	9F715	D21	10	2078373	10000	WHILE BRAKING
2002	19844	S11	1FMCU03182KA69878	3.0L	T/LD	10	2001	2.00E+03	9E928	D21	11	2449898	19000	WHILE DRIVING
2002	19857	S11	1FMCU03182KA35757	3.0L	T/LD	9	2001	2G05	RECAL	D21	8	1457239	5000	WHILE DRIVING
2002	19858	S11	1FMCU03182KA35757	3.0L	T/LD	9	2001	2G04	DIAG	D21	1	269018	0	DOWNHILL
2002	19864	S11	1FMCU03182KA34074	3.0L	T/LD	8	2001	2G04	DIAG	D21	3	358293	3000	WHILE DRIVING

REPLACED		WDS EEC IDLE TEST DATLOGGER FUEL PRESSURE LEAK DOWN PP EEC AND REPLACE THROTTLE BODY REPROGRAM PCM AND FINAL QUICK TEST
REPLACED		17737 NGS TEST IGNITION TEST DCL DISPLAY NGS RECORDER MONITOR REPL AIRBYPASS VALVE RETEST
TSB		EEC TEST NO CODES, FOLLOWED DIAG PROCEEDURE PER TSB 02 11 6 PERFORMED STEPS 1,2,4,5,6,7, WRITER SPOKE TO CUSTOMER AND SHE HAS A BUNCH OF KEYS THAT SHE WILL PUT ON ANOTHER RING
TSB		5665 C C 43 W VERIFY CONCERN, RAN WDS START UP, EEC SELF TEST PASS, RAN PPT TEST, RAN IDLE DATA DISPLAY, RAN FUEL PRESSURE AND LEAKDOWN, RAN POWER BALANCE AND SPARK DURATION, NO FAULTS INDICATED
TSB		EEC TEST PASSED ROADTEST 15 MILES LET RUN AND RET HOT PRIOR TO ROAD TEST PERF TSB 02 11 06 TWICE WDS DATA LOGGER ROADTEST OK RELAYS PID MONITOR ROADTEST DIES AT STOPS AND TURNS REPLACED IAC SOL RETEST
REPLACED		REPLACED SENSOR
SSM		ROADTESTED AND RAN EEC TEST WITH WDS (NO CODES) PERFORMED SSM #15589. REPROGRAMMED PCM, CHECKED EVAP VENT LINE AND CHECKED FOR PROPER EEC POWER RELAY. RETESTED AND ROAD TESTED.
NPF		UNABLE TO DUPLICATE EEC (QUICK TEST) DIAGNOSIS
SSM		1171 STALLING OIL LITE ON W WDS POWER UP E1 DCL DISPLAY E6 CONTINUOUS DTC P1000 KOER P1000 FUEL PRESSURE E20 DATA LOGGER ROAD TEST E30 ALL PIDS NORMAL TEST DROVE CAR OVER 41 MILES OVER A COUPLE OF D
REPLACED		16586 THROTTLE BODY AND 9F715 PER OASIS MESSAGE OASIS MESSAGE NAMED THERE PART #6 TO BE REPLACE TO CORRECT STALLING ON DECELERATION TO STOPS.
REPLACED		SYSTEM. TEST FUEL PRESSURE AND FLOW. PINPOINT TEST. REPLACED IN TANK FUEL PUMP. NOTE FUEL PRESSURE WAS AT 12PSI. TEST EVAP SYSTEM AFTER REPAIR. RETEST.
TSB		WDS TESTS PINPOINT TESTS REPROGRAM PCM AS PER TSB
NPF		CHECK FOR STALLING CHECK EEC SYSTEM AND FOUND NO FAULT CODES
INOP		23 ENGINE WILL NOT CRANK. COLUMN AND DASH SWITCH DIAGNOSIS. STARTER DRAW TEST. NO SIGNAL TO STARTER. ACCESS INSTRUMENT PANEL. TRACE CIRCUIT 20 FOR OPENS. ACCESS LEFT SIDE KICK PANEL. LOCATED OPEN
ADJUST		EEC TEST MONITOR TEST IGNITION AND FUEL RESET IDLEAND AND CONNECTIONS FOR RELAYS RETEST
SSM		INOP PERFORM SSM 15589
TSB		5784 IAC VALVE, THROTTLE BODY, PCM PROGRAMMING WF40 PERFORM TSB 2 11 6.
REPLACED		ROAD TEST. CK EEC SYS. PP TEST. CK WITH NGS, CK PCM. REPLACED RELAY, RECHECKED AND ROAD TEST
TSB		EXCESSIVE DIAG AND REPAIR PROCEDURES, FOLLOWED TSBAND SSM, CONTACTED HOTLINES AND FOLLOWED ADVISE, THIS IS A FACTORY BUY BACK.
SSM		PERFORM WDS TEST; NO CODES WAS NECESSARY TO RENEW EEC POWER RELAY AS PER SSM 15434 ALSO PER SSM CHECK ALL PCM GROUNDS, CHECK GROUND 101 ON TRANSMISSION AND TIGHTEN, AND CHECK CONNECTORS C270S C
TSB		RUN WDS TEST; PASS CODES ONLY CHECK FUEL PRESSURE; 47 PSI CHECK IGNITION SYSTEM; OK RUN MONITOR TEST; ALL SYSTEMS OK RENEW IDLE AIR CONTROL VALVE WITH UPDATED PART NUMBER FROM TSB REPROGRA
REFLASH		REPROGRAM PCM EEC (QUICK TEST) DIAGNOSIS
TSB		PERFORMED EEC, PINPOINT TESTS NO CODES PRESENT, PERFORMED SERVICE PROCEDURES PER TSB 02 06 06, REPROGRAMMED POWERTRAIN CONTROL MODULE & AFFIXED MODIFICATION STICKER
NPF		UNKNOWN, PERFORMED EEC TEST NO CODES PRESENT, MONITORED PIDS ALL OK, NO PROBLEM FOUND
NPF		4022 CC62 DIAG UNABLE TO VERIFY STALL. WDS TEST EEC SYS, KOEO PASS KOER PASS KOEC PASS. ROADTEST & MONITOR DCL DATALOGGER, ALL PARAMETERS OK. INSTALLED VEHICLE DATA RECORDER. ANALYZED CUSTOMERS RE

	ENGINE CUTS OFF WHILE DRIVING
	IDLES LOW AT TIME LIKE ITS GOING TO CUT OFF HAS CUT OFF ONE TIME CST REQ #32
	AS DRIVING ENGINE CUT OFF, LOST ALL POWER ASSIST AT HIGHWAY SPEEDS. CUSTOMER USES 89 OCTANE AMOCO
DURING TESTS, REFER TO TSB 02 11 6, RECALIBRATE PCM, RAN DCL RECORDER MONITOR WATCH IAC SOLENOID READS 43% AT IDLE, REPLACE IAC SOLENOID STILL READS 42%, REPLACE THROTLE BODY	VEH STALLING
OK	DIED WHILE DRIVING TOWED
	CUST STATES VEH CUTS OFF AT TIMES WHILE DRIVING DOWN THE ROAD
	CUSTOMER STATES THAT VEHICLE STALLED THE OTHER DAY WHEN ACCELERATING
	VEH STALLED WHILE DRIVING NO OTHER INFORMATION
AYS LET RUN IN SHOP FOR A COUPLE OF HOURS NEVER MISSED A LICK CHECK ALL TSB SSM NONE THAT APLY NO PROBLEM FOUND AT THIS TIME	D21 OIL LIGHT CAME ON STALLED OUT WILL START BACK UP 2ND TIME TODAY
	ENGINE STALLS ON DECEL AND STOPS
	CUSTOMER STATES THAT THIS CAR DIED WHILE DRIVING EEC TEST. DCL RECORDER MONITOR ROAD TEST. TEST IGNITION
	ENGINE STALLED AFTER PULLING FROM STOP D21
	STALLING AT TIMES
IN CENTRAL JUNCTION BOX. REPLACED CENTRAL JUNCTION BOX ASSEMBLY IN 14401 HARNESS. CC 29 QUALITY CHECKED BY MJM	D01 ENGINE WONT CRANK
	ROADSIDE TOW: CHECK ENGINE LIGHT ON,VEHICLE STALLED
	CUST STATES TRUCK STALLED WHILE DRIVING
	DIES WHEN DRIVING DOWN ROAD WITH FOOT ON GAS PER CUSTOMER
	THIS IS THE THIRD TIME VEHICLE HAS TOTALLY DIED
	VEHICLE CUTTING OFF AT TIMES WHILE DRIVING PER CUSTOMER
D E FOR WATER INTRUSION; OK	CUSTOMER STATES CAR LOST ALL POWER AND DIED ON THE SIDE OF THE ROAD PLEASE CHECKOUT AND ADVISE
M PCM RENEW SUSPECT EVM AFTER TESTING HOOK UP BREAKOUT BOX AND CHECK EVM CIRCUIT AND IDLE AIR CONTROL CIRCUIT RUN EVAP SYSTEM TEST TO INSURE INTEGRITY	CUSTOMER STATES ENGINE CUIT AND STALLED RESTARTED OK, WAS SLOWING DOWN TO MAKE A TURN AND THE ENGINE WAS WARM PLEASE CHECK HISTORY
	CUST STATES VEH STALLED ONE TIME CUST WAS DRIVING AND COMMING TO A STOP WHEN THE VEH STALLED THE VEH HAS 3 4 OF A TANK AND ITS ONLY OCURRED ONCE
	CHECK FOR PAST 3X TIMES CAR STALLS OUT WHILE DRIVING
	CHECK WHILE COMING DOWN HILLS CAR STALLED OUT
CORDINGS, NO EVIDENCE OF STALLING. CALLED CUSTOMER, WAS ADVISED THAT VEHICLE NEVER STALLED WITH RECORDER IN VEHICLE.	D21 ENGINE STALLS WHEN DRIVING

2002	19669	S11	1FMCU03192KA27349	3.0L	TALD	6	2001	7C05	14N069	D21	11	2087143	12000	WHILE DRIVING
2002	19670	S11	1FMCU03192KA27349	3.0L	TALD	6	2001	2.00E+04	9C915	D21	10	1871983	11000	WHILE DRIVING
2002	19686	S11	1FMCU03192KA05710	3.0L	TALD	6	2001	7C05	14N069	D21	7	625448	6000	WHILE DRIVING
2002	19688	S11	1FMCU03182KD66816	3.0L	TALD	6	2002	2F02	9E926	D21	1	2157569	0	STALLS
2002	19689	S11	1FMCU03182KD64182	3.0L	TALD	6	2002	1H09	9J460	D21	1	2227886	0	STALLS
2002	19690	S11	1FMCU03182KD64182	3.0L	TALD	6	2002	2.00E+03	9F715	D21	1	2133662	0	STALLS
2002	19691	S11	1FMCU03182KD66404	3.0L	TALD	6	2002	2.00E+04	9C915	D21	2	2371401	8000	TSB
2002	19695	S11	1FMCU03182KD40618	3.0L	TALD	4	2002	2G04	12A650	D21	5	2455463	7000	WHILE DRIVING
2002	19698	S11	1FMCU03182KC19249	3.0L	TALD	1	2002	1H09	9J460	D21	2	2128696	1000	STALLS
2002	19699	S11	1FMCU03182KC19249	3.0L	TALD	1	2002	2G04	12A650	D21	1	1912917	0	STALLS
2002	19923	S11	1FMCU03182KB53329	3.0L	TALD	12	2001	2G05	RECAL	D21	7	1825238	3000	WHILE DRIVING
2002	19924	S11	1FMCU03182KB53329	3.0L	TALD	12	2001	7C05	14N069	D21	1	480654	0	WHILE DRIVING
2002	19931	S11	1FMCU03182KB29421	3.0L	TALD	11	2001	2.00E+03	9F715	D21	9	2176874	10000	WHILE DRIVING
2002	19935	S11	1FMCU03182KB25546	3.0L	TALD	11	2001	2.00E+03	9F715	D21	2	1902021	4000	STALLS
2002	19937	S11	1FMCU03182KB22517	3.0L	TALD	11	2001	2G04	12A650	D21	5	1116254	1000	WHILE DRIVING
2002	19940	S11	1FMCU03182KB13679	3.0L	TALD	10	2001	2G04	12A650	D21	4	736084	4000	WHILE DRIVING
2002	19948	S11	1FMCU03182KA62824	3.0L	TALD	10	2001	2G02	12B679	D21	9	1886370	7000	WHILE DRIVING
2002	19952	S11	1FMCU03182KA79480	3.0L	TALD	10	2001	2.00E+03	9F715	D21	10	2259213	5000	WHILE DRIVING
2002	19955	S11	1FMCU03182KA63907	3.0L	TALD	9	2001	2F01	DRIVE	D21	6	614853	3000	DOWNHILL
2002	19969	S11	1FMCU03182KA53257	3.0L	TALD	10	2001	2.00E+04	9C915	D21	11	2311057	11000	WON'T IDLE
2002	19974	S11	1FMCU03182KA45868	3.0L	TALD	9	2001	2G05	RECAL	D21	7	1117748	5000	AT STOP
2002	19976	S11	1FMCU03182KA45809	3.0L	TALD	9	2001	1A05	5007	D21	1	391792	0	NO TEXT

REPLACED		TEST DRIVE SEEMS OK TEST SYSTEM NPF TRY REPLACEING EEC RELAY HAS FIXED IN PASSED TEST SEEMS OK
TSB		ALSO HAD TO REPLACE GAS CAP EEC TEST NO CODES CHECK TSB FOUND TSB 02 11 6 DO STEPS 1 2 3 4 HAD TO REPLACE EVAPVM NOT FUNCTIONING CORRECTLY WENT
REFLASH		WDS TESTED AND TESTED CODE PASS PINPOINT TTESTED, DCL & IDLE DISPLAY. PERFORM POWER BALANCE, RELATIVE COMPRESSION AND FUEL AND LEAKDOWN. PERFORMED INJECTOR FLOW AND ROAD TESTED WITH MONITOR PIDS, FOU
ADJUST		999 CC 07 (B5999) REMOVED THROTTLE BODY AND ADJUSTED THROTTLE STOP PER DAVE DRIPPS..5667..
REPLACED		621 CHECK FOR CODES WITH NGS NO CODES ROAD TEST TO VERIFY CONCERN CONTACTED TECH HOTLINE INSPECTED DPFE AND MASS AIR FLOW PART NUMBERS AND REPLACED DPFE AND MASS AIR FLOW SENSOR PER HOTLINE AND CHE
TSB		645 CHECK FOR CODES WITH WDS NO CODES PERFORMED PINPOINT TEST WITH WDS PER TSB 02 06 06 AND REPLACED IDLE AIR CONTROL VALVE, THROTTLE BODY, AND VAPOR MANAGEMENT VALVE CHECKED PCM CALIBRATION HAD LA
REPLACED		INTERMITTED VALVE ASSEMBLY FUEL VAPOR STORAGE CANISTER PURGE REGULATOR PINPOINT TEST DIAG EX TIMETO REPEAT FINAL QUICK TEST
TSB		7020 NTF. TECH 117 N. KOEO PASS, KOEC PASS, KOER PASS. PERFORMED TSB 02 11 6. ALL CHECKED OK. COULD NOT DUPLICATE SYMPTOM.
REPLACED		RETRIEVE CODE P1000 KOEO KOER ON DEMAND P1000 HOTLINE SPOKE WITH CHRIS REPORT 62HNF0010 INSTRUCTED TO CHECK DPFE SENSOR
TSB		INSPECT HOOK UP WDS RETRIEVE CODE P1000 KOEO KOER P1000 LIGHT OFF VEHICLE NEVER STALLED FOUND SSM AND TSB 02 11 06
TSB		ENG LIGHT OFF KOER PASS KOEC PASS CONT PASS CHECK EEC NO CODES CHECK DCL DISPLAY ROAD TEST AND MONITOR PID DATA CHECK OASIS REPROGRAM PCM PER TSB 2 11 03 ROAD TEST AND RETEST
SSM		ENG LIGHT OFF KOER PASS KOEO PASS CONT PASS CHECK EEC CK DCL ROAD TEST AND MONITOR PID DATA CHECK OASIS PERFORM SSM 15434 INSPECT IAC VALVE REPLACE EEC POWER RELAY REPAIR WIRING AT EEC RELAY PUSHED OU
REFLASH		IAC & PCM CALIBRATION PASS EEC TEST PIN POINT MONITOR REPLACED IAC REPROGRAMMED PCM FUEL PSI TEST.
STICKING		4640 NO LIGHT I EEC TEST NO CODES DLC DISPLAY NGS ROAD MONITOR PPT AND FOUND IAC VALVE STICKING I R AND R IAC VALVE AND RETEST TO FIX
REFLASH		DIOGNOSED CAR STALLING OUT EEC TEST NO CODES ROAD TEST RAN OASIS REPROGRAMED PCM RE ROAD TEST VEHICLE
REFLASH		REPROGRAM PCM TO LATEST CALIBRATEEEC (QUICK TEST) DIAGNOSIS
REPLACED		REPLACE MAF AND REPROGRAM PCM
TSB		785230 WARR 42 6F715 6C915 6E628 14N089 MILES OUT 5659 CODES P1111 PASS CODES PERFORM TSB 02 11 3 6 CK GROUND WIRING CONN AT C1016 REPROG RAM PCM MONITOR EVAP VALVE REPLACE EVAP VALVEREPLACE AIR VALV
SSM		TEST EEC, SYSTEM PASS. ROAD TEST 5 MILES WHILE MONITORING PIDS, UNABLE TO DUPLICATE CONCERN. PINPOINT TEST PER SSM 15599. ATTEMPT TO RECALIBRATE BUT WDS INCAPABLE OF CALIBRATING AT THIS TIME. AFTER RU
TSB		DIAG AND REPLACED VAPOR MANAGEMENT VALVE PER TSB 02 11 6
DIAG		5036 ROAD TEST FOR A STALL AT TIMES WHEN COMING TO A STOP. NO CHECK ENGINE LIGHT ON AT THIS TIME. OASIS CONTACT NO 408 482 072. WDS TEST OF THE EEC FOR POSSIBLE CODES, KOEO ALLL PASS (111), CONT ALL
ENGINE FAILURE		REQUESTING DEALER'S P/A CODE 01709

	CUSTOMER STATES THAT THE ENGINE STALLS WHEN DRIVING. PLEASE INSTALL SOP. SEE DICK CLARK.
	CUSTOMER STATES ENGINE JUST DIES WHILE DRIVING. HAS HAPPENED TWICE
ND ERRATIC EEC POWER RELAYS AND PROGRAM PCM. DROPED FUEL TANK AND CLEAN OUT FUEL TANK VAPOR LINE AND RETESTED CODE P1000 AND ROAD TESTED AFTER REPAIRS OK.	CHECK AND ADVISE CUSTOMER STATES CUSTOMER WAS DRIVING VEHICLE LOST ALL POWER BATTERY LIGHT AND OIL LIGHT CAME ON C PULLED OVER AND RESTARTED
	D21 -CUSTOMER REPORTS VEHICLE STALLED WHEN SLOWING DOWN IN TRAFFIC
CKED G104 AND 105 UNDER BATTERY GROUNDS WHERE TIGHT AND ROAD TEST	CUSTOMER STATES THE ENGINE STALLED AGAIN
TEST CALIBRATION AND ROAD TEST TO VERIFY REPAIR	CUSTOMER STATES THE ENGINE STALLED AND POWER STEERING GOT HARD
	C S INTERMITTED ONE TIME AROUND 40 50 VEH CUT OUT SEE TSB
	DET CUST SAYS THE VEHICLE HAS DIED 3 TIMES NOW WHILE DRIVING AT HWY SPEEDS AND CITY DRIVING IT ALWAYS ABLE TO BE RESTARTED AND WOULD DRIVE FINE FOR THE REST OF THE DAY.CK TSB.
	DIAGNOS INTERMITTENT STALLING CONCERN
	DIAGNOS INTERMITTENT STALLING TSB 02 11 06
	WHEN DRIVING & TURNING CORNERS ENGINE HESITATES & STALLS OUT , ENGINE STARTS RIGHT UP 3 36 SEE HISTORY
T PIN ROAD TEST AND RETEST	WHEN DRIVING VEHICLE STALLED AND CHECK ENGINE LIGHT CAME ON VEHICLE STARTED RIGHT UP AFTER PULLING OVER TO THE SIDE , LIGHTS STILL ON 3 36
	D21 AT TIMES ENG STALLS WHEN DRIVING, WILL NOT MAINTAIN RPMS
	CUST STATES ENGINE STARTS AND DIES AT TIMES
	CAR STALLED OUT WHILE DRIVING ABOUT 45MPH DROP OFF WED AM
	CUST STATES 2 TIMES YESTERDAY WHILE DRIVING THE CAR CUT OFF. THEY ROLLED TO A STOP AND RESTARTED.
	ENGINE STALL WHILE DRIVING WHEN GOING ON AN EXIT RAMP
E REPLACE THROTTLE BODY ALSO REPLACE PPE SENSOR	VEHICLE JUST CUT OFF DRIVING AND CHECK ENGINE LIGHT IS ON
MEROUS ATTEMPTS, PCM WAS CALIBRATED	CUST STATES VEHICLE STALLED ONCE GOING DOWN HILL WHILE BRAKING
	CUSTOMER STATES THE ENGINE WOULDN T STAY RUNNING HAD TOWED IN
PASS (111), KOER ALL PASS (111). USING THE WD SIN DATALOGGER MODE TO PINPOINT TEST THE AIR INTAKE, FUEL DLEVEYR, IGNITION, BASE ENGINE, EGR SYSTEMS. ALL ARE OK AT THIS TIME. CHECK AND	AFTER 5 MINUTES OF DRIVING AND AT A STOP VEH STALLED DID RESTART FINE NO WARNING THAT VEH WAS GOING TO STALL, NO CHECK ENGINE LIGHT CAME ON.

2002	19978	511	1FMCU03168KA49809	3.0L	T/LD	9	2001	1A09	6007	D21	1	285251	0	STALLS
2002	19989	511	1FMCU03162KA39362	3.0L	T/LD	8	2001	7C05	14N069	D21	4	514232	8000	WHILE DRIVING
2002	19987	511	1FMCU03162KA33780	3.0L	T/LD	8	2001	2304	12A650	D21	6	1388744	8000	WHILE DRIVING
2002	19988	511	1FMCU03163KA39790	3.0L	T/LD	9	2001	1H03	9J460	D21	6	1554615	8000	WHILE DRIVING
2002	19985	511	1FMCU03165KA16889	3.0L	T/LD	8	2001	7C05	14N069	D21	4	1291665	11000	WHILE DRIVING
2002	19998	511	1FMCU03163KA09925	3.0L	T/LD	6	2001	2304	DIAG	D21	3	373490	4000	BACKFIRE
2002	20002	511	1FMCU03172KD69364	3.0L	T/LD	6	2002	2305	RECAL	D21	0	2030612	0	DOWNHILL
2002	20006	511	1FMCU03172KD49135	3.0L	T/LD	5	2002	2.00E+03	9F715	D21	3	2253275	3000	NO TEXT
2002	20008	511	1FMCU03172KD42199	3.0L	T/LD	5	2002	2305	RECAL	D21	1	2307379	1000	ACCELERATING
2002	20009	511	1FMCU03172KD00546	3.0L	T/LD	3	2002	2.00E+03	9F715	D21	3	2429730	4000	ON HIGHWAY
2002	20018	511	1FMCU03172KC81586	3.0L	T/LD	3	2002	2304	12A650	D21	2	2061662	1000	WHILE DRIVING
2002	20019	511	1FMCU03172KD01606	3.0L	T/LD	3	2002	2.00E+04	9C915	D21	2	2243635	1000	WHILE DRIVING
2002	20023	511	1FMCU03172KC00345	3.0L	T/LD	2	2002	2.00E+03	9F715	D21	2	1548096	1000	NO TEXT
2002	20024	511	1FMCU03172KC99795	3.0L	T/LD	3	2002	2304	DIAG	D21	1	1948576	0	WHILE DRIVING
2002	20027	511	1FMCU03172KC99906	3.0L	T/LD	2	2002	7V01	12A681	D21	4	1720766	3000	DOWNHILL
2002	20028	511	1FMCU03172KC99806	3.0L	T/LD	2	2002	2.00E+03	9F715	D21	4	2067317	4000	DOWNHILL
2002	20029	511	1FMCU03172KC99496	3.0L	T/LD	2	2002	2.00E+03	9F715	D21	2	2299525	1000	STALLS
2002	20031	511	1FMCU03172KC97896	3.0L	T/LD	2	2002	2.00E+03	9F715	D21	4	2353787	4000	STALLS
2002	20042	511	1FMCU03172KC99469	3.0L	T/LD	1	2002	2304	12A650	D21	2	999000	1000	STALLS
2002	20045	511	1FMCU03172KC97990	3.0L	T/LD	1	2002	7C05	14N069	D21	1	1999511	0	WHILE DRIVING
2002	20049	511	1FMCU03172KB54650	3.0L	T/LD	12	2001	7B13	14406	D21	1	886150	3000	NO START
2002	20052	511	1FMCU03172KB22948	3.0L	T/LD	11	2001	2304	DIAG	D21	2	1597350	2000	WHILE DRIVING
2002	20053	511	1FMCU03172KB02348	3.0L	T/LD	11	2001	2.00E+04	9C915	D21	2	1427730	2000	WHILE DRIVING
2002	20057	511	1FMCU03172KB00999	3.0L	T/LD	11	2001	2.00E+03	9B936	D21	-1	2133891	3000	WHILE DRIVING

REPLACED		CK VEH WONT CRANK; RR UPPER INTAKE FOR ACCESS TO REAR 3 PLUGS; RR ALL PLUGS AND FOUND #2 SMASHED; BORESCOPE #2 CYLINDER; HEAD DESTROYED; REPLACED ENGINE; M TIME TO GET ENGINE TO TURN OVER TO GET FOUR
TSB		EEC TEST NO CODES, P P TEST, REPLACED EEC RELAY PER TSB, RETEST
TSB		0020 NO DTC TSB 02 6 6 INTERMITTENT ENGINE QUIT PASS KOEO KOER PID DATA NORMAL MONOTER ROAD TEST PASS PCM NUMBER MC 161 CK RR MASS AIR CK GASKET CK PCM CALIBRATION TEST VAPOR MGMNT VALVE OPERA PCM
REPLACED		0000 EEC TEST PIN TEST MONITOR TEST REPLACE SENSORRETEST NO FIX UNTIL JULY PER DAVE WRIGHTSMAN PRD ENGINEERMT TIME FOR EXCESS DIAG AND RESEARCH
TSB		11201 ROAD TEST VERIFIED CONCERN CHECKED TSBS AND 00M6 FOUND TSB 02 9 6 PERFORMED TSB NECESSARY TO REPROGRAM PCM TO LATEST CALIBRATION INSP ALL NECESSARY PIDS AND CHECK OPERATIONS OK REPLACED PCM
NPF		WDS TEST, PINPOINT TEST, UNABLE TO SIMULATE OR DUPLICATE CUSTOMERS CONCERN AT THIS TIME
REPLASH		20 12M60 (CODE 42) 12650D 0.2 DX1 0.1 D61 0.5 D84 0.2 1.0 HR PERFORMED EEC TESTS, KOEO P1111, CONT TEST P111 KOER P1111. ROAD TEST VEHICLE AND PERFORMED NGS RECORDER MONITOR TEST. REPROGRAMMED PCM
NO TEXT		
REPLASH		1030 ROAD TEST HOOK UP WDS AND TEST FOR CODES PASS PERFORM DATA LOGGER AND RECORDER ROAD TEST REPROGRAM PCM TO LATEST UPDATE
00M		PERFORM ALL EEC TESTS CHECKED ONLINE FORD FOUND TECHNICAL SERVICE BULLETIN THAT ADDRESSED THIS ISSUE REPLACED IDLE
NPF		TEST DROVE, DIAGNOSED, NO CODES FOUND, PERFORMED PIN POINT TEST, ALL OKAY
TSB		PERFORMED TSBS ON VEHICLE. CHECKED THROTTLE BODY, CHECKED IAC VALVE, REPLACED PURGE VALVE, TEST DROVE, RETESTED, ALL OK
NO TEXT		
TSB		UNKNOWN, PERFORMED EEC TEST NO CODES PRESENT, MONITORED PIDS OK, PER TSB 02 06 00 PERFORMED EVAP SYSTEM TEST OK, CHECKED FOR LATEST PCM CALIBRATION OK, NO PROBLEM FOUND
TSB		AS PER KNOLL AT TECH HOTLINE PERFORM TSB 02 11 6 CK CONNECTORS 970 BCD 110 155 CK GROUNDS 100 104 1
TSB		PERFORM TSB 02 11 6 TRACE AND ACCESS ALL CONNECTS ON CIRCUITS OUTLINED REPL SENSORS REPROGRAM PCM
TSB		EEC TEST (NO CODES) TSB #02 11 6, REPLACED EEC RELAY, IDLE AIR CONTROL VALVE AND RE PROGRAMMED TO LATEST CALIBRATION
REPLACED		KNOW PROBLEM WITH IAC TEST DRIVE DID NOT STALL NGS TEST NO CODES CK PIDS ALL LOOK GOOD FUEL PRE TEST KOEO 30 KOER 35 PSI OK & SMOKE ENG TO CK
REFLASH		PERFORM DIAG REPROGRAM PCM
DIAG		FUEL PUMP RELAY EEC (QUICK TEST) DIAGNOSIS
CHARGE BATTERY		CHARGED BATTERY UP, PERFORMED CHARGING SYSTEM TEST VOLT. DIODE GOOD, PEAK AMPS W/ LOAD TEST BATTERY, BATTERY TEST
REPLACED		PASSENGER COMPARTMENT GROUND INSP REQUIRES REMOVAL OF ALL SEATS CARPET/QUARTER TRIM PANELS THERE ARE LBAOR OPERATION FOR REPLACE BUT NOT R AND R INSP ENG COMPARMENT GROUNDS REQUIRES THE REMOVAL OF BATTER
TSB		2258 9C915 COND. CODE 42 12650D .2 DX1 .1 D45 .3 D65 .3 D80 .1 D81 .5 D84 .2 D22 .4 9000D .4 D1 .4 D2 .1 55300 .3 EEC TEST IN KOEO PASS KOEC PASS, KOER PASS, NGS DCL DISPLAY.
TSB		0040 ROAD TEST FOR CONCERN CHECK FOR CODES WITH WDS NO CODES PERFORM PINPOINT TEST PER TSB AND REPLACED VAPOR MANAGEMENT VALVE, IDLE AIR CONTROL VALVE, AND THROTTLE BODY PER TSB 02 06 00 AND ROAD T

CONVERTOR NUTS OFF; TRANSFERRED PARTS FROM OLD ENGINE TO NEW; RECHECK OK.	VEHICLE STALLED...WILL NOT CRANK
	CUSTOMER STATES THE ENGINE STALLS OUT GOING DOWN ROAD REPLACE EEC RELAY PER TSB
HAS BEEN REPLACED TECH ASST NUMBER 105 32A 453 INSTALL FLIGHT RECORDER RETURN TO CUSTOMER TO DUPLICATE NO ABNORMAL CONDITION NOTED REPROGRAM PCM 1LBU 12A650 AC COMPLETED CUSTOMER HAS 5	ENG DIES DRIVING;LET SET SHORT WHILE;WILL RESTART & RUN SEE HIST
	CF ENGINE DIES WHILE DRIVING CCD60
POWER RELAY WITH UPDATED RELAY PERFORMED ROAD TEST AS OUTLINED IN TSB OK NO OTHER DRIVEABILITY SYMPTOMS NOTED AT THIS TIME	CUSTOMER STATES WHILE DRIVING THE ENGINE WILL SUDDENLY CUT OFF AND ALL ELECTRICAL POWER IS LOST
	SOMETIMES ENGINE BACKFIRES WHEN 1ST STARTED
AS PER SPECIAL SERVICE MESSAGE TO LATEST LEVEL CALIBR, RAN FINAL EEC QUICK TEST KOEO P1111, CONT P1111 KOER P1111.	CK ENG DIES WHEN GOING DOWNHILL 30MPH SEE ALEX MOLINA FOR TSB INFO
	CUST RPTS WHILE ACCELERATING TO GET ON FREEWAY, TRUCK STALLED PULLED OVER AND IT RESTARTED FINE, NO WARNING LIGHTS ON
	C S CHECK ENGINE LITE CAME ON AND THEN VEHICLE CUT OUT AT HIGHWAY SPEED.RESTARTED RIGHT AWAY.
	C S VEHICLE DIES WHILE DRIVING
	C S VEHICLES DIES WHILE DRIVING
	CHECK WHILE DRIVING CAR DIED AND LOST POWER, RESTARTED FINE
	CUST STATES VEH STALLS AT TIMES GOING DOWNHILL AND DEACCELARATING
	CUST STATES VEH STILL STALLS GOING DOWNHILL ON DEACCEL SEE HIST
	CUST. STATES THE ENGINE STALLED WHEN COMING OVER THE COOPER RIVER BRIDGE, ENGINE DID RE START
	C S STALLED TWICE WITHOUT WARNING, THEN STARTS RIGHT AWAY AS IF IT NEVER HAPPENED
	W CUST STATES ENGINE HAS STALLED A FEW TIMES
	ENGINE STALLED WHILE DRIVING, IMMEDIATELY RESTARTED.
	BATTERY GOES DEAD OVERNIGHT. CUSTOMER ASSITANT ADVISED THAT BATTERY HAS BEEN REPLACE 2 TIMES ON OWNE
Y AND BATTERY TRAY	INSPECT DYING CONDITION WHEN DRIVING. DIES MOSTLY IN A.M. & AT LOWER SPEEDS LIKE IN TOWN DRIVING. I
MSB DCL RECORDER MONITOR. ROADTEST. IGNITION SYSTEM TEST. FUEL SYSTEM TEST. PINPOINT TEST PER TSB 02 09 02. PERFORM EVAP SYSTEM LEAK TEST. PERFORM RUNNING LOSS TEST. PERFORM STATIC LEAK	CK UNIT DIED W DRIVING 29 MPH OR SO IT STARTED BACK UP CK ADVISE REPAIRS
EST TO VERIFY COMPLINT	CUSTOMER STATES THE ENGINE STALLS INTERMITANTLY WHILE DRIVING

2002	20091	S11	1FMCU03172KB03277	3.0L	TALD	10	2001	2.00E+03	9F715	D21	5	1894374	3000	WHILE DRIVING
2002	20097	S11	1FMCU03172KA91777	3.0L	TALD	10	2001	2.00E+03	9F715	D21	9	1804096	4000	STALLS
2002	20099	S11	1FMCU03172KA89709	3.0L	TALD	9	2001	2.00E+03	9F715	D21	9	1637104	6000	WHILE DRIVING
2002	20109	S11	1FMCU03169KD02369	3.0L	TALD	4	2002	2B05	RECAL	D21	2	1980548	0	WHILE DRIVING
2002	20110	S11	1FMCU03169KD24606	3.0L	TALD	4	2002	2.00E+03	9F715	D21	3	3064342	4000	WHILE DRIVING
2002	20117	S11	1FMCU03169KC71616	3.0L	TALD	3	2002	2G04	DIAG	D21	2	1199648	1000	WHILE DRIVING
2002	20116	S11	1FMCU03169KC81240	3.0L	TALD	3	2002	2B02	128579	D21	4	1839767	3000	WHILE DRIVING
2002	20116	S11	1FMCU03169KC81240	3.0L	TALD	3	2002	2.00E+03	9E928	D21	3	1599497	3000	ON HIGHWAY
2002	20128	S11	1FMCU03169KC46389	3.0L	TALD	2	2002	2G04	DIAG	D21	1	1579886	3000	WHILE DRIVING
2002	20134	S11	1FMCU03169KB77616	3.0L	TALD	1	2002	2B02	128579	D21	1	691784	0	WHILE DRIVING
2002	20135	S11	1FMCU03169KB75279	3.0L	TALD	12	2001	2G04	12A650	D21	1	857886	1000	WHILE DRIVING
2002	20143	S11	1FMCU03169KB24611	3.0L	TALD	11	2001	2G05	RECAL	D21	4	972518	4000	WHILE DRIVING
2002	20146	S11	1FMCU03169KB24611	3.0L	TALD	11	2001	2.00E+03	9E928	D21	5	2096424	14000	COASTING
2002	20147	S11	1FMCU03169KB14142	3.0L	TALD	10	2001	2G04	DIAG	D21	9	2185559	7000	WHILE DRIVING
2002	20162	S11	1FMCU03169KA61091	3.0L	TALD	9	2001	2.00E+03	9F715	D21	8	1439028	7000	WHILE DRIVING
2002	20166	S11	1FMCU03169KA90572	3.0L	TALD	9	2001	2.00E+03	9F715	D21	11	2377100	20000	WHILE DRIVING
2002	20169	S11	1FMCU03169KA90572	3.0L	TALD	9	2001	7C05	14N069	D21	5	871478	7000	WHILE DRIVING
2002	20172	S11	1FMCU03169KA89691	3.0L	TALD	9	2001	1H03	9J460	D21	11	2374694	14000	WHILE DRIVING
2002	20174	S11	1FMCU03169KA89691	3.0L	TALD	8	2001	9A11	7000	D21	0	309577	0	NO TEXT
2002	20179	S11	1FMCU03169KA89691	3.0L	TALD	8	2001	9A11	7000	D21	0	218132	0	TRANS LEAK
2002	20177	S11	1FMCU03169KA89699	3.0L	TALD	8	2001	2.00E+04	9D669	D21	7	1173992	6000	DOWNHILL
2002	20170	S11	1FMCU03169KA17026	3.0L	TALD	8	2001	2B05	RECALIBM	D21	7	1699928	17000	WHILE DRIVING
2002	20151	S11	1FMCU03169KA09746	3.0L	TALD	8	2001	1H03	9J460	D21	7	1138503	7000	NO TEXT
2002	20182	S11	1FMCU03169KA09605	3.0L	TALD	8	2001	2.00E+03	9F715	D21	4	466617	6000	AT STOP
2002	20152	S11	1FMCU03168KD19408	3.0L	TALD	4	2002	2.00E+03	9E928	D21	1	2377024	1000	WHILE DRIVING
2002	20169	S11	1FMCU03168KD09701	3.0L	TALD	4	2002	2B04	12A650	D21	4	2355274	5000	NO TEXT

DIAG		ROAD TEST WITH WDS NO CODES CHECK OASIS CHECKED FUEL PRESSURE CHECKED FUEL TRIM MONITOR DATA LOGGER WHILE
REPLACED		4867 W CK EEC SYSTEM FOR CODES NO CODES GO TO PINPOINT TEST CK PIDS IAC MOTOR OUT OF SPECS WITH RPMS REPLACE IAC MOTOR ROAD TEST OK AT THIS TIME
REPLACED		HOOKED UP WDS CHECKED EEC FUEL PRESSURE IGNITION TEST DROVE WITH DATALOGGER COMPLETE PINPOINT TEST R&R THROTTLE BODY
REFLASH		DOES NOT OPERATE PROPERLY. EED TEST, PINPOINT TEST, FUEL SYSTEM PRESSURE TEST, NGS MONITOR TEST, NGS DCL DISPLAY TEST, REPROGRAMMED PCM AND RERUN EEC TEST
REPLACED		CHECK EEC, REPLACE IAC MOTOR
NPF		UNKOWN PERFORMED EEC DIAG NO CODES, CHECK IDLE AIR CONTROL VALVE , UNABLE TO DUPLICATE
INOP		INOP EEC (QUICK TEST) DIAGNOSIS
INOP		INOP EEC (QUICK TEST) DIAGNOSIS
DIAG		DIAG NOCDOES EEC (QUICK TEST) DIAGNOSIS
DIAG		514 CPDIAG CC62 129500,D61 0.7 FLAG 106 EEC TEST PASSED ROAD TESTED 6 MILES W NGS RECOR DER NORMAL OPERATION AT THIS TIME
REFLASH		VEHICLE DIES WHILE DRIVING PERFORMED ROAD TEST,BATTERY CHARGE TEST,PROGRAMED TWO FATS KEYS
SSM		WDS DIAG PASS PID DATA MONITOR ROAD TEST PASS FUEL PRESSURE LEAK DOWN TETS PASS REPROM PCM PER SSM 15599
REPLACED		VERIFY CONCERN EEC TEST DCL MONITOR ROAD TSEST PIN TEST KC6 REPL IAC AND THROTTLE BODY EVAP SYSTEM TEST , EVAP VENT TEST , REPL VAPOR MONT VALVE RE TEST AND ROAD TEST AS PER FRED VILLA
NPF		START SEVERAL TIMES & LET RUN COULD NOT DUPLICATE SCAN NO DTC
REPLACED		IMPROPER OPERATION 97715 14N355 CC42 DIAG AND PINPOINT TEST. REPROGRAM PCM, REPLACED IAC SOLENOID REPLACED EEV RELAY.
REPLACED		CC660 REPLACED IAC VALVE
REPLACED		CC651 ENGINE PERFORMANCE DIAGNOSIS REPLACE PROCESSOR AND RELAY AND REPROGRAMMED PASSIVE ANTI THEFT SYSTEM
REPLASH		WDS HOOKUP EEC TESTED P0401. DPFE OUT OF SPECS. REPLACED DPFE SENSOR AND CLEARED CODES.REPROGRAMMED PCM
ENGINE FAILURE		REQUESTING DEALER'S P/A CODE 02999
REPLACED		395 CRACKED TRANS CASE AND BENT TORQUE CONVERTER LEAK TEST R&R U224 TRANS AND DRAINED AND REPLACED UNIT DUE TO TRANS HSG BOLT TOP CAME OUT PUNCHED THRU CASE IN SEVERAL PLACES AND TORQUE CONVERTER DAMAGE
NPF		ROAD TEST WDS DIAG NPF MT TO R AND R VAPOR MANAGEMENT VALVE TO CK AND SEE IF CLEAN
TSB		RUN CODE TEST NO CODE IN SYSTEM, FOUND TSB FROM FORD TO REPROGRAM POWER TRAIN CONTROL MODULE. REPROGRAMED PCM PER TSB AND RETEST....OK NOW. 514
NO TEXT		
REPLACED		QUICK TEST PASS. MONITORED PIDS AND RECORDED IAC DROPS 39%. REPLACED THE IAC MOTOR AND TEST DROVE
REPLACED		IMPROPER OPERATION 98928 CCC42 DIAG AND PINPOINT TEST. REPLACED THROTTLE BODY AND IAC VALVE RETEST. P1111 P1111 P1111
NO TEXT		

	DRIVING ON WINDING ROAD ABOUT 35 MPH THE ENGINE SHUT OFF WITHOUT WARNING RESTARTED BUT NEEDS CHECKED OUT
	D02 C S VEH STALLING WHEN HUMID OR RAINING
	CUSTOMER STATES ENGINE HAS STALLED 5X WHEN DRIVING
	CK ENGINE STALLED WHILE DRIVING
	CUSTOMER STATES TRUCK DIES WHEN DRIVING JUST CUTS OFF HAVE TO RESTART. D21.
	CUSTOMER STATES ENGINE STALLED WHEN DRIVING , HAPPED ONCE CHECK AND ADVISE
	CUST STATES ENG STALLED WHEN IN GEAR & ROLLING, ENG WARM OR HOT, EASY TO RESTART, SEE FILE INFO.
	CUST STATES ENG CUT OFF WHEN DRIVING AT HWY SPDS
	CST STS VECHILE STALLED WHILE DRIVING ONE TIME GOT OFF ROAD CRANKED BACK UP OK
	D21 DRIVING DOWN A STEEP CURVY MOUNTAIN ROAD THE ESCAPE LOST POWER BRAKES AND POWER STEERING I HAD
	CUST STATES VEH DIES OUT WHILE DRIVING
	CUST STATES VEHICLE HAD STALLED TWICE WHILE DRIVING AROUND 40MPH.,
	CUST STATES,CAR STALLS AROUND 40 MPH ON DECELL SEE FRED FOR INFO
	CUST STATESIT ENG DIED ONCE WHILE DRIVING BUT STARTED RIGHT BACK UP.
	CS VEHICLE STALLS WHILE DRIVING DOWN THIS ROAD D21
	D21.....CUST STATES VEHICLE STALLED OUT WHILE DRIVING CITY STREETS, LOST ALL POWER PULLED OVER RESTARTED OK ..WAS DRIVING FOR ABOUT 15 20 MIN IN MORNING
	CUST STATES ENGINE INTERMIT STALLS HAS DONE TWICE WARM BOTH TIMES WHILE MOVING IN SLOW TRAFFIC BOTH TIMES RESTARTS RIGHT BACK UP
	CUS REPRTS ENG STALLS WHILE DRIVING OR AT STOP RESTARTS IMMD SVC ENG SOON LIGHT WAS ON
D FLUSHED COOLER LINES FILLED AND ROAD TEST TRANS IS PLANT SUPPLIED UNIT CONTROL#17041AS 822 COND.CODE#42	TRANSMISSION FLUID LEAK
	VEHICLE STALLS GOING DOWNHILL, WHEN WARM
	CUSTOMER STATES VEHICLE DIED TWICE WHILE DRIVING, CHECK ENGINE LIGHT HAS COME ON EACH TIME IT DIED VEHICLE
	CUSTOMER STATES THAT THE ENGINE CUTS OFF WHEN AT A STOP WHEN THE ENGINE IS COLD
	CS ENG STALLS WHEN GOING DOWN HILL. CS HAS HAPPENED 5X LAST WEEK IN 2 DAYS. CS VEH CUTS OFF WHILE DRIVING

2002	20202	511	1FMCU03152XC72647	3.0L	TAD	3	2002	2G04	DIAG	D21	3	2185393	4000	WHILE BRAKING
2002	20204	511	1FMCU03158XC69810	3.0L	TAD	3	2002	2B04	12A650	D21	3	1942297	0	WHILE DRIVING
2002	20212	511	1FMCU03152XC68928	3.0L	TAD	3	2002	2B04	DIAG	D21	4	2270650	6000	WHILE DRIVING
2002	20215	511	1FMCU03152XC17939	3.0L	TAD	1	2002	2G04	12A650	D21	6	2271742	6000	ACCELERATING
2002	20216	511	1FMCU03152XC17939	3.0L	TAD	1	2002	1H03	9J460	D21	1	1101636	1000	AT STOP
2002	20217	511	1FMCU03152XC17939	3.0L	TAD	1	2002	2.00E+03	9F715	D21	2	1186724	3000	AT STOP
2002	20218	511	1FMCU03152XC17939	3.0L	TAD	1	2002	2.00E+03	9E826	D21	4	1829039	4000	DOWNHILL
2002	20231	511	1FMCU03152XB75869	3.0L	TAD	12	2001	2.00E+03	9F715	D21	1	711354	0	NO TEXT
2002	20238	511	1FMCU03152XB94209	3.0L	TAD	11	2001	2G04	12A650	D21	1	594766	0	WHILE DRIVING
2002	20239	511	1FMCU03152XB93415	3.0L	TAD	11	2001	7C05	14N069	D21	1	416522	0	STALLS
2002	20244	511	1FMCU03152XB91833	3.0L	TAD	10	2001	2G02	12B579	D21	10	2173571	10000	WHILE DRIVING
2002	20245	511	1FMCU03152XB01708	3.0L	TAD	10	2001	2G05	RECAL	D21	1	954491	0	WHILE DRIVING
2002	20250	511	1FMCU03152XA99586	3.0L	TAD	10	2001	2G05	RECAL	D21	4	639200	3000	WHILE DRIVING
2002	20251	511	1FMCU03152XA99586	3.0L	TAD	10	2001	1H03	9J460	D21	6	1139416	6000	WHILE DRIVING
2002	20252	511	1FMCU03152XA99586	3.0L	TAD	10	2001	2.00E+03	9F715	D21	8	1647384	8000	WHILE DRIVING
2002	20259	511	1FMCU03158XA97800	3.0L	TAD	9	2001	2.00E+03	9F715	D21	6	1316170	6000	DOWNHILL
2002	20264	511	1FMCU03152XA49449	3.0L	TAD	8	2001	2G05	RECAL	D21	9	1993997	10000	WHILE BRAKING
2002	20265	511	1FMCU03152XA31662	3.0L	TAD	8	2001	7C05	14N069	D21	2	257066	1000	WHILE DRIVING
2002	20270	511	1FMCU03152XA31662	3.0L	TAD	8	2001	2G02	12B579	D21	6	719643	6000	WHILE DRIVING
2002	20274	511	1FMCU03152XA25061	3.0L	TAD	8	2001	2G02	12B579	D21	7	1117099	4000	AT STOP

NPF		4076 NPF @ 12000, .2 D46, .3 D60, .1 D61, .5 DX1, .1 CORECTION;TEST EEC KOEO PASS KOEC PASS KOER PASS .PINPOINT TEDST CK DCL DATA AND MONITOR FUEL TRIM AND IDLE CONTROL;RD TESTED ON FREEWAY COULD
TSB		PERFORMED REPAIR ACCORDING TSB.
TSB		M TIME TO PERFORM TSB 021106 RELAY GOOD PIPE GOOD MAF SHST OK NO PCM UPDATE UNABLE TO DUPLICATE
REFLASH		6001 HOOK UP N/S PERFORM EEC TEST AND RETRIEVE CODES KOEO PASS KOEC PASS KOER P1000 ROADTEST AND MONITOR PID DATA AND RECORD RECALIBRATE PCM TO LATEST CALIBRATION VEHICLE DID NOT STALL AT THIS TIME
SSM		1342 GROUND WARRANTY PERFORMED EEC TEST NO CODES IN PCM. PERFORMED OASIS FOR BULLITINS,PERFORMED SSMP 15580,PERFORMED WDS SETUP FOR PCM CALIBRATION PCM SET AT LATEST CALIBRATION OF 18.1 VERSION. CO
TSB		9146 IAC WARRANTY PERFORMED EEC TESTED FOR CODES NONE PRESENT CONTACTED OASIS FOUND TSB02 02 5 A6 PER TSB HOOKUP WDS PERFORMED PID MONITOR ON IAC CONTROL VALVE..REPLACED VALVE W PART #YPIZ-9F715 A
TSB		4305 WARRANTY REPLACED THROTTLE BODY IDLE AIR CONTROL VALVE,PCM RELAY AS PRER TSB #02 06 06 ROAD TESTED CAR W PIDS STALL DID NOT REOCCURR,.
DIAG		M TIME TO DIAGNOSE WIRE PROBLEM
REFLASH		720 CALIBAL PART NO. 12A650. COND. CODE 42. N/S6 START UP DIAG. AND PERFORMED EEC.V. DIAG. KOEO P1111 CONT. P1111 AND PERFORMED KOER P1111 AND PERFORMED DCL. DISPLAY AND PERFORMED PID MONITOR AND RE
SSM		643414 14HDBL.26 286 ML 3.0L EEC TEST PASS N/S6 PID DATA DISPLAY MONITOR AND ROAD TEST REPLACE EEC RELAY PER SSMP 15494 RETEST ALL PASS
TSB		10365 EEC TEST PASSED DCL DISPLAY TEST RECORDER MONITER TEST IGNITION SYS TEST PERFRMED TSB 02 5 05 AND SSM 02 05 043 RWR DPFE SENSER RWR MAF SENSER REPROGRAMED PCM RETEST TEST DROVE 10 MILES
REFLASH		CK FUEL PRESSURE AND INJECTOR FLOW OK CK DIAGS RECALIBRATE PCM CK EEC RELAY OK ROAD TEST OK
REFLASH		3559 C C 42 W TEST DROVE, RAN WDS START UP, RAN EEC SELF TEST, RAN PPT TEST, RAN IDLE DATA DISPLAY, RAN DCL RECORDER MONITOR, RAN FUEL PRESSURE AND LEAKDOWN, RAN POWER BALANCE, RECALIBRATE PCM, RE
REPLACED		4387 C C 42 W VERIFY CONCERN, RAN WDS START UP, EEC SELF TEST , RAN IDLLE DATA DISPLAY, RAN DCL RECORDER MONITOR, RAN FUEL PRESSURE AND LEAKDOWN REPLACE DPFE SENSOR EEC POWER RELAY AND RECALIBRAT
TSB		6364 C C 42 W TEST DROVE DID NOT STALL, RAN WDS START UP, RETRIEVEN DIAGTCS NONE, KOEO PASS, KOER PASS, RAN FUEL PRESSURE AND LEAKDOWN PASS, REFER TO TSB 02 11 5, RAN DCL RECORDER MONITOR WITH WDS
TSB		EEC TEST NO CODES PIN POINT TEST Q1 Q10 FUEL PRESSURE TEST 34 PSI IAC MOTOR STICKS AND REFERRED TO TSB 02 06 06 FOR PCM REPLACED IAC MOTOR REFLASHED PCM PER TSB RETEST P1000
TSB		VERIFY STALLS ON DECEL. EEC TEST AND PID MONITER AND RECORD, PINPOINT TEST AND CHECK FUEL PRESSURE TEST AND RECALIBRATE PCM AS OUTLINE IN TSB 021106 AND RETEST
REPLACED		REPLACE EEC POWER RELAY
REPLACED		MASS AIRFLOW SENSOR ASSEMBLY REPLACE (129579) : EXTENDED TIME NEEDED TO ROADTEST TO INTERSECTION WHERE FAILURE OCCURS, CK PCM CALIBRATION, RUN SSTS AND CONTACT AND RCONTACT TECH SERVICE HOTLINE.
REPLACED		PERFORM SELF TEST.CHECK ALL HRANESS GROUNDS AND REPLACE EEC RELAY PER SPECIAL SERVICE MESSAGE 15434,SET IDLE TO HIGH SETTING.REPLACE IAC,PRESSURE FEEDBACK SENSOR,MASS AIRFLOW SENSOR,CANISSTER PURGE VA

NOT DUPLICATE INTERMITTENT CONCERN.CHECK OASIS ,AND TEST COMPUTER FOR PROPER CALIBRATION,PASSED TEST.NO FAULT FOUND AT THIS TIME	D21 ENGINE QUIT RUNNING AT FREEWAY SPEED,ENGINE RESTARTED AFTER COMING TO A STOP
	CUSTOMER STATES CAR CUTS OFF WHILE DRIVING
	C S VEH DIED WHILE DRIVING ON INTERSTATE,ENGINE RESTARTED,HAS NOT DIED AGAIN
AND COULD NOT FIND ANY PROBLEMS ROADTESTED VEHICLE SECOND TIME OK	8529 STATES STALL CUTS ACCEL ALL ENG TEMP CODE D21
NTACTED FORD SERVICE HOTLINE,REPORT CODE 8C8Z9G11,PERFORMED WDS,VEHICLE DATA RECORDER ROAD TESTED CAR TO CAPTURE DATA,NO REACURRANCE OF SYMPTOM,DISCONNECTED PCM HARNESS CONNECTOR	CHECK FOR THE ENGINE IS INTERMITTENTLY STALLING WHEN COASTING TO DECELL OR COMING TO A STOP
A,ORIGINAL IAC FAILED TEST. ROAD TESTED CAR.	CHECK FOR THE ENGINE IS STALLING ON COAST OF WHEN PREPARING TO STOP
	CHECK FOR INTERMITTENT STALLING WHEN COASTING DOWN HILL (SEE HISTORY)
CORD AND PERFORMED IDM, SYSTEM DIAG. AND CHECK AND REPROGRAMED PCM WITH LATEST CALIBRATION AND RETEST KOEO P1000 CONT. P1000, KOER P1000. ROAD TEST. THE CHECK ENG. LIGHT WAS NOT ON.	OCP D21 STALLED ON HILL AFTER DRIVING APPROX 10 15 MINUTES,RESTARTED OK
	CUST STATES QUITS RUNNING AT TIMES SEE EDDIE
	VEH JUST DIED WHILE DRIVING ADVISE
	OWNER STATES VEHICLE STALLED ONCE WHILE DRIVING AT 45MPH LOST PWR STEERING/CAR RESTARTED FINE HAS NOT ACTED UP SINCE ALSO LOW OIL PRES. LIGHT CAME ON
DRIVE, RETEST OK	VEH STALLED WHILE DRIVING
E PCM, REDRIVE, RETEST OK	VEH STOPPED 2 TIMES WHILE DRIVING AT 45 MPH
MONITOR RPM AND IAC %, IN PARK AT 750 RPM THE IAC IS DUTY CYCLING AT 42%, REPLACE IAC SOLENOI STILL AT 42%, REPLACE THROTTLE BODY WITH UPDATED PART IAC DROPS TO 37 35%, MONITOR FUEL TANK	OK FOR STALLING AT 45 MPH
	D21 CUST STATES WHILE DRIVING DOWNHILL AT 40MPH STEADY ENGINE STALLED.
	D 21 CUSTOMER STATES UPON SLOWING DOWN VEHICLE WILL STALL WILL RESTART
	CUSTOMER SAYS MIL LAMP CAME ON AND VEHICLE LOST POWER WHEN DRIVING, CUSTOMER SHUT OFF AND RESTARTED THEN IT WAS OK
SENSOR WAS REPLACED PER HOTLINE INSTRUCTIONS	CUST REPORTS AT TIMES WHILE DRIVING AND DECEL DOWN HILL BATTERY LIGHT, CHECK ENGINE LIGHT AND SYSTEM MALFUNCTION
LVE AND REPROGRAM PCM PER SSM 2474.	CUSTOMER STATES ENGINE STALLS WHEN SLOW DOWN TO STOP

2002	20293	S11	1FMCU03152KA09921	3.0L	TALD	8	2001	2.00E+03	9F715	D21	4	549382	8000	STALLS
2002	20294	S11	1FMCU03152KA00092	3.0L	TALD	8	2001	7V01	12A661	D21	0	849119	0	WONT RUN
2002	20296	S11	1FMCU03142KE00539	3.0L	TALD	7	2002	2.00E+03	9E828	D21	1	2363542	0	WHILE DRIVING
2002	20300	S11	1FMCU03142KD33389	3.0L	TALD	4	2002	9F03	9C315	D21	1	1533089	0	WHILE DRIVING
2002	20301	S11	1FMCU03142KC49085	3.0L	TALD	2	2002	2305	RECAL	D21	2	1699911	1000	AT STOP
2002	20302	S11	1FMCU03142KD49085	3.0L	TALD	2	2002	2302	129579	D21	2	1547980	1000	WHILE DRIVING
2002	20311	S11	1FMCU03142KB67302	3.0L	TALD	1	2002	2305	RECALSM	D21	3	1131429	3000	WHILE DRIVING
2002	20314	S11	1FMCU03142KB45017	3.0L	TALD	12	2001	2305	RECAL	D21	4	952277	4000	WHILE DRIVING
2002	20322	S11	1FMCU03142KB22546	3.0L	TALD	11	2001	2304	DIAG	D21	2	742148	0	DOWNHILL
2002	20327	S11	1FMCU03142KA82943	3.0L	TALD	10	2001	2304	12A650	D21	5	722759	3000	WHILE DRIVING
2002	20336	S11	1FMCU03142KA84408	3.0L	TALD	10	2001	2.00E+03	9H307	D21	2	436165	2000	WHILE BRAKING
2002	20337	S11	1FMCU03142KA84227	3.0L	TALD	10	2001	2304	12A650	D21	9	1749445	18000	WHILE DRIVING
2002	20346	S11	1FMCU03142KA81188	3.0L	TALD	9	2001	2304	12A650	D21	3	616510	4000	STALLS
2002	20347	S11	1FMCU03142KA44026	3.0L	TALD	8	2001	2.00E+03	9F715	D21	11	2337709	13000	STALLS
2002	20348	S11	1FMCU03142KA43443	3.0L	TALD	8	2001	7V01	12A661	D21	2	401361	3000	WHILE DRIVING
2002	20349	S11	1FMCU03142KA43449	3.0L	TALD	8	2001	2305	RECAL	D21	5	988540	8000	ON HIGHWAY
2002	20358	S11	1FMCU03142KA29169	3.0L	TALD	9	2001	2305	RECAL	D21	10	1999001	10000	WHILE DRIVING
2002	20359	S11	1FMCU03142KA29169	3.0L	TALD	9	2001	2.00E+03	9F715	D21	1	317129	1000	WHILE DRIVING
2002	20360	S11	1FMCU03152KD06485	3.0L	TALD	6	2002	2.00E+03	9F715	D21	2	2128469	2000	WHILE BRAKING
2002	20367	S11	1FMCU03152KD24844	3.0L	TALD	4	2002	2304	DIAG	D21	1	1177611	0	WHILE DRIVING
2002	20368	S11	1FMCU03152KD02446	3.0L	TALD	4	2002	7902	14401	D21	0	1319172	0	STALLS
2002	20371	S11	1FMCU03152KD11916	3.0L	TALD	4	2002	2304	12A650	D21	3	1967402	2000	TURNING
2002	20373	S11	1FMCU03152KD11785	3.0L	TALD	4	2002	2302	129579	D21	-1	2175439	0	STALLS
2002	20387	S11	1FMCU03132KC91526	3.0L	TALD	2	2002	2.00E+03	9H307	D21	4	1517183	3000	STALLS
2002	20391	S11	1FMCU03132KC11542	3.0L	TALD	1	2002	2304	DIAG	D21	3	1356567	2000	WHILE DRIVING
2002	20392	S11	1FMCU03132KC09211	3.0L	TALD	1	2002	2.00E+03	9F715	D21	1	1603899	1000	COASTING
2002	20396	S11	1FMCU03132KB99079	3.0L	TALD	1	2002	2.00E+03	9F715	D21	2	2228461	1000	DOWNHILL
2002	20402	S11	1FMCU03132KB63940	3.0L	TALD	12	2001	7822	14A088	D21	1	480992	0	WHILE DRIVING
2002	20403	S11	1FMCU03132KB44103	3.0L	TALD	11	2001	2.00E+03	9E828	D21	6	2517549	9000	WHILE BRAKING

SSM		8928 + TEST DR,NGS HOOK UP,RAN EEC TEST,KOEO PASS. KOEC PASS,KOER PASS,MONITORED DCL PID DATA AND RECORD,FUEL PRESSURE TEST,PASS,RAN OASIS. CKED ALL GROUNDS AND PINS AT POWER DISTRIBUTION BOX,REPL
REPAIR		SELF TEST KOEO KOER KOEC PID DATA DISPLAY PINPO INT TEST TRACE TO #5 INJECTOR,INJECTOR REPAIR,C LEAR CODES RETEST TEST DRIVE WPI
REPLACED		EEC TEST TEST FUEL PRESS WITH GAUGE 60PSI PASS NGS MONITOR TEST CK DIFFE .9 VOLTS PASS PINPOINT TEST PER 2 11 06 PASS
REPAIR		D21 26 157Z 6C315 A6 ROAD TEST,WDS TEST,PINPOINT TEST,DATALOGGER,FUEL PRESS AND ,CODE P1000,INSPEC HARNESS CONNECTIONS,REPAIR HARNESS
REFLASH		DIAG. REPROGRAM PCM
REPLACED		DIAG. REPLACE MASS AIR FLOW SENSOR AND IAC
INOP		INOP EEC (QUICK TEST) DIAGNOSIS
SSM		TEST DROVE VERIFIED CONCERN,EEC TEST NO CODES,PID MONITOR RAN OASIS,FOUND SSM 15599 REPROGRAMED PCM AS PER SSM 15599
NPF		708 120000.2 D46.3 D80.1 D86.3 93508.3 TEST EEC KOEO PASS KOER PASS KOEC PASS. PIN POINT TEST DCL DISPLAY ALL IN SPEC. TEST IGN SYSTEM PASS. PERFORM FUEL PRESSURE AND LEAK DOWN, PASS. CHECK OASIS, V
SSM		REPROGRAM PCM PER SSM 15599 EEC (QUICK TEST) DIAGNOSIS
REPLACED		REPLACED FUEL PUMP
NPF		STALLS WHILE DRIVING ON INTERSTATE AT 75 MPH CHECK CODES AND NO CODES SHOWN AT THIS TIME TESTDROVE VEHICLE 30 MILES ON INTERSTATE AND NO PROBLEM FOUND AT THIS TIME
ADJUST		IDLE SET LOW PIN POINT TEST (SSDS) TEST
INOP		INOP EEC (QUICK TEST) DIAGNOSIS
DIAG		CK CODES EEC (QUICK TEST) DIAGNOSIS
DIAG		EEC (QUICK TEST) DIAGNOSIS PIN POINT TEST DIAGNOSIS
REFLASH		PCM CALIBRATION IS INCORRECYT PERFORM PCM RECALIBRATION AND RETEACH STRATEGY
REPLACED		DIAG WITH NGS AND PP TEST, ROAD ETST AND REPLACE IAC VALVE
REPLACED		WDS TEST AND REPLACED IAC VALVE
NPF		RAN ENGINE DIAGNOSTIC TEST ALL PASS CODES ADVISOR TO TALK W CUSTOMER REGARDING CONCERN
POOR CONNECTION		WIRING CONNECTION CC 32 VERIFY CONCERN LOSS OF BATTERY POWER AND DIES CHARGE BATTERY AND TEST OK TEST CHARGING SYSTEM NOT CHARGING RED
SSM		EEC QUICK TEST DIAGNOSIS USE CAUSAL PART DIAG ONLY WHEN NO REPA IR IS NECESSARY INCLUDES TIME TO BRING THE VEHICLE INTO THE SERVICE BAY HOOK U
REPLACED		EEC TEST A7/RECORD MONITOR PINPOINT REPLACED MAPF SENSOR RETEST AND ROADTEST
REPLACED		RUN EEC TEST SCOPED MOTOR WENT THROUGH PIN POINT TEST REPAIRED OPEN TO FUEL PUMP RELAY IN POWER DISTRIBUTION BOX AND REPLACED FUEL PUMP
NPF		ROAD TEST AND DIAGNOSE STALLING CONCERN. NO PROBLEMS FOUND AT THIS TIME.
TSB		INSTALL WDS TEST EEC SYS PERFORM PIDS TEST DCL TEST CK TSB PERFORM TSB 02 11 6 REPL AIR BYPASS VALVE ASSY RD TEST
STICKING		IAC STICKS CLOSED EEC (QUICK TEST) DIAGNOSIS
REPLACED		NGS TESTED AND FOUND FUSE BOX INTERMITTENLY OPEN CIRCUIT,REPLACE FUSE PANEL AND RETESTD OK.
REPLACED		ENGINE STALLS REPACLED THROTTLE BODY

AC/ID IDLE CONTROL VALVE.REPLACED EEC RELAY PER SSM 15494.TEST DR,RETEST,PASS.	CUT OFF FOR NO REASON SEVERAL TIMES
	DIES WONT STAYN RUNNING
	CUST SAID WHILE DRIVING 45MPH COASTING DOWN HILL ENGINE STALLS. DOES RESTART RIGHT
	CHECK CAR STALLED WHILE DRIVING WAITED 5 MINUTES IT RESTARTED AND DROVE FINE
	VEHICLE STALLS AT STOPS
	CUT OFF 3 TIMES WHILE DRIVING
	C S THE TRUCK STALLED ONCE WHILE DRIVING BUT RESTATRED SMIED. CK ENGINE LIGHT IS ON
	CUSTOMER STATES CUT OFF WHILE DRIVING
EHICLE HAS LATEST CALIBRATION INSTALLED. ROAD TEST VEHICLE DID NOT STALL. POSIBLE FUEL QUALITY ISSUE. DIAG 82	D21 CUST STATES ENGINE HAS STALL TWICE WHEN COASTING DOWN HILL
	CST STS JUST DRIVING DOWN HWY VECHILE CUT OFF WENT TO SIDE OF ROAD CRANKED BACK UP DROVE OK THEN
	CHECK NO START, DIED WHILE SLOWING DOWN
	STALLS WHILE DRIVING ON INTERSTATE AT 75 MPH
	CUST REPORTS AT A TIME VEHICLE STALLED ADVISE
	EMS STALLS AT RED LIGHTS WHEN ENG COLD
	ENGINE QUIT RUNNING WHEN DRIVING 25 30 MPH. RESTARTED OK.
	REPAIR VEH STALLS ON HWY AT TIMES INTERMITTENT PROBLEM
	CUSTOMER STATES THAT SHE WAS DRIVING AND THE VEHICLE SHUT OFF(HAD SAME PROBLEM 6 MTH AGO HAD IAC VALVE REPLACE)
	C S THE TRUCK STALLED 3 TIME TWICE WHILE COMING TO A STOP AND THE 3RD TIME WHILE DRIVING
	CUSTOMER STATES CUT OFF WHEN COMING TO STOP
	C S ENGINE DIED ON ONE OCCASION WHILE DRIVING
	CUST STATES THAT VEH DIED TWICE ON TEST DRIVE AND WOULD NOT START
	CUSTOMER STATES THE VEHICLE STALLED WHEN TURNING A CORNER AND A C WAS ON FULL SPEED
	C S TRUCK KEEPS SHUTTING OFF
	STALLING AND WILL NOT CRANK
	CUSTOMER STATES VEHICLE STALLED WHILE MOVING AND AC WAS ON
	TRUCK JUST CUT OFF AND HAD TO COAST OFF THE ROAD DID GET IT RESTARTED BUT WANTS IT CHECKED OUT
	CUST STATES ENGINE STALLED ONE TIME GOING DOWN HILL AROUND CORNER WITH FOOT OFF THE GAS PEDAL SRS TODD
	CHK VEHICLE STALLED AGAIN IN TRAFFIC WHILE DRIVING JUST SHUT OFF.NO CRANK NO START.WAITED FOR 20 30 MIN.THEN STARTED
	CUST STATES THE ENGINE STALLS WHILE COMING TO A STOP

2002	20405	511	1FMCU03133KB98723	3.0L	TALD	12	2001	7B02		10348	D21	0	548926	0	WHILE DRIVING
2002	20413	511	1FMCU03133KA93797	3.0L	TALD	10	2001	2.00E+03	9F715		D21	4	666054	4000	AT IDLE
2002	20414	511	1FMCU03133KA93836	3.0L	TALD	10	2001	2.00E+03	9F715		D21	2	359510	1000	WHILE DRIVING
2002	20415	511	1FMCU03133KA93836	3.0L	TALD	10	2001	7C05	14N089		D21	2	362786	2000	WHILE DRIVING
2002	20417	511	1FMCU03133KA79844	3.0L	TALD	10	2001	2.00E+03	9E826		D21	9	2375899	7000	WHILE DRIVING
2002	20422	511	1FMCU03132KA93890	3.0L	TALD	10	2001	2.00E+03	9F715		D21	10	1999800	7000	WHILE DRIVING
2002	20433	511	1FMCU03133KA43284	3.0L	TALD	8	2001	2B04	DIAG		D21	11	2013900	4000	STALLS
2002	20434	511	1FMCU03133KA93822	3.0L	TALD	9	2001	1A03		9006	D21	1	309976	0	NO TEXT
2002	20435	511	1FMCU03133KA93822	3.0L	TALD	9	2001	1A03		9006	D21	1	234882	0	STALLS
2002	20439	511	1FMCU03133KA93435	3.0L	TALD	9	2001	2B04	12A650		D21	7	1210785	4000	WHILE BRAKING
2002	20442	511	1FMCU03133KA37407	3.0L	TALD	9	2001	2.00E+03	9F715		D21	1	224464	0	COASTING
2002	20460	511	1FMCU03122KD67135	3.0L	TALD	5	2002	1H03	9J480		D21	1	2447846	1000	STALLS
2002	20461	511	1FMCU03122KD61971	3.0L	TALD	5	2002	2.00E+03	9F715		D21	1	2294473	1000	AT STOP
2002	20463	511	1FMCU03122KD00096	3.0L	TALD	4	2002	9N01		7810178	D21	4	2439096	2000	WHILE BRAKING
2002	20471	511	1FMCU03122KC56139	3.0L	TALD	3	2002	2B04	DIAG		D21	3	1399806	0	WHILE DRIVING
2002	20472	511	1FMCU03122KC18451	3.0L	TALD	2	2002	2.00E+03	9F715		D21	5	1619964	1000	WHILE DRIVING
2002	20474	511	1FMCU03122KC16191	3.0L	TALD	1	2002	2B04	DIAG		D21	1	781336	0	COASTING
2002	20479	511	1FMCU03122KB97881	3.0L	TALD	1	2002	2B05	RECALEM		D21	4	1758876	3000	AT STOP
2002	20481	511	1FMCU03122KB76007	3.0L	TALD	12	2001	7C05	14N089		D21	2	1053958	1000	WHILE DRIVING
2002	20486	511	1FMCU03122KB85416	3.0L	TALD	12	2001	2B05	RECAL		D21	5	1313360	8000	WHILE DRIVING
2002	20491	511	1FMCU03122KB80760	3.0L	TALD	11	2001	2.00E+03	9F715		D21	5	2287023	8000	WHILE DRIVING
2002	20493	511	1FMCU03122KB84120	3.0L	TALD	11	2001	2.00E+03	9F715		D21	7	1894716	13000	WHILE DRIVING
2002	20509	511	1FMCU03122KA79084	3.0L	TALD	10	2001	2B04	12A650		D21	6	1139880	6000	AT STOP
2002	20508	511	1FMCU03122KA66746	3.0L	TALD	9	2001	2B04	DIAG		D21	2	823269	0	WHILE DRIVING
2002	20509	511	1FMCU03122KA66745	3.0L	TALD	9	2001	2.00E+03	9E826		D21	7	1225740	7000	WHILE DRIVING
2002	20510	511	1FMCU03122KA66676	3.0L	TALD	10	2001	7C05	14N089		D21	6	1561318	18000	NO TEXT

REPLACED		VERIFIED CONCERN PERFORMED ALTERNATOR CIRCUITS TEST TRACED TO OPEN IN ALTERNATOR REPLACED ALTERNATOR HAD TO REMOVE EXHAUST MANIFOLD RIGHT SIDE TO GAIN ACCESS TO ALTERNATOR
STICKING		IAC STICKS EEC (QUICK TEST) DIAGNOSIS
REPLACED		IAC MOTOR INOP REPLACED IAC MOTOR
REPLACED		EEC RELAY OPEN CIRCUIT REPLACE EEC RELAY AND INSPECT IAC MOTOR PER FORD HOTLINE
TSB		VERIFY CONCERN..PER TSB 02 11 16..CHECK IAC DUTY CYCLE,REPROGRAM PCM..INSPECT PCM RELAY..PERFORM EVAP MANAGEMENT VERIFICATION..CHECK T BODY AFTER IAC DUTY CYCLE CHECK..NECC TO REPL IAC,REPROGRA
REPLACED		1 RUN EEC SYSTEM TEST. KOEO PASS. KOEC PASS. KOER PASS. RUN DCL DISPLAY OK. REPLACE IAC, REPROGAMME PCM. REPLACE EEC
DIAG		ROAD TEST EEC TEST KOEO PASS NO CONT CODE KOER PASS OK OASIS ID 312 303 699 COULD NOT VERIFY CONCERN AT THIS TIME.(NEED TO MAKE SURE USING RIGHT OCTANE GAS)
ENGINE FAILURE		REQUESTING DEALER'S P/A CODE 20515
ENGINE FAILURE		100 5708 PC 56 DETERMIND ENG COND. FOUND THAT ENG HAD NO COMP ON ONE CYLINDER AND THAT ROD HAD LET GO RR ENG AND TRANSAXLE ASSY TO INSTALL NEW ENG TRANSFER NESS PARTS FROM ONE ENG TO OTHER THAT WER
TSB		PERFORMED PIN POINT TEST. FOUND TSB MODULE REPROGRAMMING. REPROGRAMMED PCM WITH WDS. RETESTED AND ROAD TESTED OK.
REPLACED		RAN EEC TEST, ALL PASS CODES, CHECK DATALOGGER, CHECK FUEL PRESSURE, BLEEDDOWN, CALL HOTLINE, REPLACEIAC VALVE, ADJUST THROTTLE BODY SCREW TO 30%, RET EST EEC
REPLACED		1159 INTERMITANT OPEN IN DPFE & RELAY NGS TEST NO CODES REPLACE DPFE & RELAY PER ISSL ROAD TEST OK.
TSB		1250 WARRANTY PERFORM TSB 02 09 06 CHECK FOR STALLING REPLACE IAC VALVE REP T BODY REPLACE EVAPVM VALVE. HECK FOR CURRENT CALIBRATION
REPLACED		VMV T BODY & IAC EEC (QUICK TEST) DIAGNOSIS
INPF		EEC TESTS KOEO CONT PASS KOER PASS. FUEL PRESSURE TEST PASS 45 60 PSI LEAKDOWN NORMAL. MONITOR PIDS OK IGN SYST DIAG POWER BALANCE PASS CHK PATS SYST OK NO CODES. TEST BATTERY AND CHARGING SYST OK
TSB		RUN GUIDED DIAG. RESET IDLE PER TSB 021106
SSM		ROAD TEST VEHICLE AND COULD NOT DUPLICATE CONCERN. RETRIEVED CODE, SYSTEM PASS. CHECKED OASIS AND FOUND SSM# 15559 THAT
REFLASH		FAULTY PCM PROGRAMMING (12650) PASS PERFORMMED EEC,PINPOINT,NGS TESTS AND REPROGRAMMED PCM
DIAG		08 EEC (QUICK TEST) DIAGNOSIS
REFLASH		0069 WARR CHECKED FOR STALLING OUT AT TIMES. WDS TESTED THE SYSTEM, SYSTEM PASS. REMOVED THE BATTERY AND BATTERY TRAY. REMOVED AND REPOSITIONED THE PCM GROUND. CHECKED THE EEC POWER RELAY, OK. REF
REFLASH		VERIFIED CUSTOMER CONCERN, REPLACED IAC AND REPROGRAMED PCM.
INOP		INOP EEC (QUICK TEST) DIAGNOSIS
REFLASH		EEC AND PIN POINT TESTS, FUEL SYSTEM PRESSURE TEST, REPROGRAMMED PCM. ROADTESTED OK.
TSB		CHECKED ON NGS. NO CODES WIGGLE TESTED WIRING HARNESSES UNDER THE HOOD. SELECT DATA LOGGER. ALL PIDS REACTED OK. OK OASIS NO SSMS OR TSBS
TSB		WDS TST CODES P1000 OK OASIS FOR TSB & SSM FOUND TSB 02 8 6 H LINE CONTACT KEVIN PERFORMED TSB IF NOT CORRECTED CALL BACK. PERFORM TSB 02 8 6 REPROGRAM PCM ROAD TST NOT REPAIRED. WDS OK IAC DUTY CY AT
NO TEXT		

	CUSTOMER STATES THAT VEH. DIED WHILE DRIVING AND WOULD NOT RESTART
	CUST STATES ENG CUT OFF WHEN DRIVING, WAS AT IDLE SPD. HAPPENED TWICE
	CHECK ENGINE STALLED WHILE DRIVING DID RESTART
	ENGINE STALLED WHILE DRIVING AT 35 MPH DASH LIGHT CAME ON ENGINE DID RESTART
M PCM. EVAP SYSTEM OK,REPL T BODY,RETEST ****TECH REQUEST M TIME FOR LENGTH OF DIAG AND MULTIPLE TEST PER TSB**	OK ENGINE QUIT RUNNING WHILE DRIVING
	CUSTOMER STATES THAT VEHICLE DIED WHILE DRIVING AND WOULD NOT RESTART
	STALLED IN MOTION,STARTED BACK UP,ONLY HAPPENED 1 TIME,HAD HALF TANK OF GAS
E NOT SUPPLIED WITH NEW ENG REPAIR ONE MOTOR MOUNT THAT BOLTS STRIPPED OUT WHEN REMOVING ENG MOUNT 3.0 V6 AC PS AUTO TRANS 2+2 ,JV	C S VEHICLE MADE LOUD RATTLING NOISE THEN DIED IN FLIGHT. CUST THEN PULLED OVER AND TRIED TO RESTAR
	CUSTOMER STATES ENGINE CUTS OFF INTERMITTENTLY MOSTLY WHEN SLOWING DOWN OR WHILE TURNING AT SLOW
	CONCERN; COASTING DOWN A HILL, THE OIL LIGHT CAME ON AND CAR QUIT RUNNING
	CHECK VEHICLE DIES OUT INTERMITTENTLY, ADVISE
	CHECK FOR INTERMITTENT STALLING AT STOPS
	REPAIR ENGINE DIES WHEN COMING TO A STOP LIKE KEY SHUT OFF, RESTARTS OK
14.5 VLT ROAD TEST. ALLOW ENG TO IDLE IN PARKING LOT FOR OVER 2 HRS NEVER STALLED, NO PROBLEM FOUND AT THIS TIME. CHK ALL WIRING AND CONNECTORS OK	STALLED OUT WHILE DRIVING NO CRANK NO START THEN RESTARTED AFTER 5 MINS
	CUSTOMER STATES THAT ENGINE STALLS AT TIMES WHILE DRIVING. HAPPENS AT LOWER SPEEDS, MORE SO WITH A C ON.
	CUSTOMER STATES UNDER DECELL GOING DOWN A HILL VEHICLE WILL STALL
	D21 AT TIMES ENG STALLS WHEN UNDER 10 MPH & SLOWING TO STOP
	VEHICLE STALLED OUT WHILE DRIVING AT HWY SPEEDS
LASHED THE PCM TO THE LATEST CALIBRATION AND RECHECKED OPERATION	CK FOR INTERMITTENTLY WHILE DRIVING THE VEH STALLS AND WHEN YOU TURN IT OFF IT RESTARTS FINE NO TIME EXACTLY WHEN IT STALLS HAPPENS ON DEACCELERATION, LAST TIME AT 30MPH
	C S CAR DIED WHILE DRIVING ON HIGHWAY, PULLED OVER AND STARTED BACK UP. 2ND TIME ITS HAPPENED IN 2 MONTHS
	CK VEHICLE DIED WHILE DRIVING
	ENGINE SHUTS OFF WITH NO WARNING, TWICE WHILE IN MOTION ONCE AT STOP LIGHT,
	CUST STATES VEH STALLED WHILE TRAVELING WITHOUT WARNING ATTN RIP
28% REPL IAC. REPAN DIAG DUTY CYL AT 48% REPL THROTTLE BODY. CK EVAPVM DUTYCYL 98% W 2.8 VTS REPL EVAPVM. MON PIDS W WDS OK NECESS TO REPL EEC REL WHT LTER. R TST VER REPAIR	CUTS WHEN DRIVING AFTER ABOUT 30 MIN AND WILL START RIGHT BACK UP

2002	20513	S11	1FMCU03122KA64910	3.0L	TALD	6	2001	2G04	12A650	D21	4	930942	3000	WHILE DRIVING
2002	20514	S11	1FMCU03122KA64266	3.0L	TALD	6	2001	2G04	12A650	D21	6	1734678	12000	WHILE DRIVING
2002	20515	S11	1FMCU03122KA63660	3.0L	TALD	10	2001	2G04	DIAG	D21	11	2347666	15000	STALLS
2002	20516	S11	1FMCU03122KA63159	3.0L	TALD	10	2001	2.00E+03	9F715	D21	7	1367425	15000	CUST TEXT
2002	20528	S11	1FMCU03122KA60825	3.0L	TALD	9	2001	2.00E+03	9H907	D21	11	2348502	12000	STALLS
2002	20532	S11	1FMCU03122KA39949	3.0L	TALD	9	2001	2G04	DIAG	D21	6	1299630	1000	NO TEXT
2002	20533	S11	1FMCU03122KA39649	3.0L	TALD	9	2001	2.00E+03	9F715	D21	1	628939	0	WHILE DRIVING
2002	20534	S11	1FMCU03122KA39343	3.0L	TALD	9	2001	2G05	RECAL	D21	2	666936	1000	WHILE DRIVING
2002	20555	S11	1FMCU03112KC28642	3.0L	TALD	2	2002	2.00E+03	9F715	D21	2	1004509	1000	AT STOP
2002	20556	S11	1FMCU03112KC28644	3.0L	TALD	1	2002	1H03	9J480	D21	1	2127224	1000	WHILE DRIVING
2002	20560	S11	1FMCU03112KC28519	3.0L	TALD	1	2002	2G02	129579	D21	1	1128008	0	WHILE DRIVING
2002	20571	S11	1FMCU03112KB99911	3.0L	TALD	12	2001	2.00E+03	9E928	D21	8	2277053	8000	WHILE DRIVING
2002	20572	S11	1FMCU03112KB95192	3.0L	TALD	12	2001	2.00E+03	9F715	D21	5	1634563	7000	STALLS
2002	20577	S11	1FMCU03112KB92798	3.0L	TALD	12	2001	2G04	12A650	D21	6	1633097	4000	WHILE DRIVING
2002	20579	S11	1FMCU03112KB92088	3.0L	TALD	11	2001	1H09	9J480	D21	5	1296691	6000	WHILE DRIVING
2002	20581	S11	1FMCU03112KB19072	3.0L	TALD	11	2001	2G02	9F479	D21	6	1204399	6000	WHILE DRIVING
2002	20585	S11	1FMCU03112KA91092	3.0L	TALD	10	2001	2G04	12A650	D21	1	280543	0	WHILE DRIVING
2002	20587	S11	1FMCU03112KA89806	3.0L	TALD	10	2001	2.00E+03	9F715	D21	10	2060067	11000	STALLS
2002	20607	S11	1FMCU03112KA36736	3.0L	TALD	6	2001	7G02	14401	D21	4	739287	10000	NO CRANK
2002	20609	S11	1FMCU03112KA36468	3.0L	TALD	6	2001	2G05	RECALEM	D21	5	831080	6000	WHILE DRIVING
2002	20610	S11	1FMCU03112KA36466	3.0L	TALD	5	2001	2.00E+03	9F715	D21	3	579017	3000	WHILE DRIVING
2002	20621	S11	1FMCU03112KA15496	3.0L	TALD	8	2001	2.00E+03	9F715	D21	5	799178	9000	WHILE DRIVING
2002	20627	S11	1FMCU03112KA08200	3.0L	TALD	8	2001	2G01	12A650	D21	10	1604104	15000	DOWNHILL
2002	20655	S11	1FMCU03102KD03443	3.0L	TALD	6	2002	2.00E+04	9C915	D21	2	2160244	1000	WHILE DRIVING
2002	20657	S11	1FMCU03102KD03072	3.0L	TALD	5	2002	2.00E+03	9F715	D21	2	1955012	5000	WHILE DRIVING

SSM		EEC TEST NO CODES PERFORMED SSM 18589 REPROGRAMMED PCM INSPECTED PCM POWER RELAY TEST DRIVE OK
REFLASH		DIAG END STALLS EEC TEST RUN CHASS PIN POINT TEST REPROGRAM PCM
TSB		STAR TEST PASS VISUAL O K ROAD TEST PID MONITOR O K. CK CHASS PERFORMED TSB 021106. INSP PCM TO INSPECT
DIAG		EEC (QUICK TEST) DIAGNOSIS
REPLACED		1 DEFECTIVE FUEL PUMP PERFORMED EEC PINPOINT AND FUEL PRESSURE TESTS AND REPLACED THE FUEL PUMP RETESTED.
DIAG		ECC NGS DCL RESODE TEST
REPLACED		CC860 REPLACED EEC RELAY AND IAC VALVE
REFLASH		CC860 REPROGRAMMED PCM
REPLACED		RUN ALL NECESSARY TESTS. REPLACED IAC MOTOR. RESET IDLE STRATEBY. CHECKED INTAKE. ALL VACUUM HOSES OK. ROAD TESTED.
REPLACED		MDS TEST, REPLACED DPFE SENSOR
REPLACED		882254 128579 42 9.0 724 RUN EEC TEST NO CODES CHECK FOR LATEST PROGRAM CALL TECH HOTLINE REMOVE BATTERY ADN CHECK GROUNDS REPLACE MASS AIR SENSOR AND RETEST COULD NOT DUPLICATE CONCERN BEFORE OR AFTE
REPLACED		DPFE VMV T BODY EEC (QUICK TEST) DIAGNOSIS
DIAG		IAC AND POM ERRATIC EEC (QUICK TEST) DIAGNOSIS
REFLASH		EEC TESTED NO CODES CHECKED EEC REALY REPORGRAMMED PCM 161
REPLACED		PERFROM EEDV TESTS. DTC SET FOR REV LIMITER REACHED. PERFORM PIN POINT TESTS. FOUND DPFE SENSOR GIVING PCM FAULTY
DIAG		1 TESTED FOR TROUBLE CODES, NO CODES, PID TESTED AND NOTED WHEN HITTING BUMPS ENGINE ACTED UP _ VISUAL
NPF		ROAD TESTED COULD NOT VERIFY CONCERN MDS TESTED FOUND NO CODES PERFORMED SYMPTOM TESTS FOR STALLING NPF AT THIS TIME
INOP		11795 BAD IDLE AIR CONTROL VALVE PERFORM SYSTEMS TESTS ON 3.0 ESCAPE. NO CODES IN SYSTEM UNDER ANY TEST MODES, ALL SYSTEMS WERE P1111, SYSTEM PASS, NO DTCS AVAILABLE. CHECKED OVER ENGINE, ROAD TES
REPLACED		VERIFIED. CIRCUIT TEST. R&R AIRBOX,BATTERY,PINESTREPAIR OPEN CIRCUIT 32 PINPOINT TEST NO. A5 PIN P USHED OUT AT JUNCTION BOX
REFLASH		PCM REPROGRAM EEC (QUICK TEST) DIAGNOSIS
REPLACED		BYPASS VALVE REPLACE EEC (QUICK TEST) DIAGNOSIS
INOP		FAULTY IAC EEC (QUICK TEST) DIAGNOSIS
DIAG		EEC (QUICK TEST) DIAGNOSIS
REFLASH		1804 VAPOR MGN VALVE ADJ BASE THROTTLE REFLASH PCM W TEST DRIVE VERIFY STALLS ON DECEL EEC TEST CODE PASS CHECK FUEL PRESSURE PASS RUN EVAPORITIVE EMISSIONS TEST PASS HOOK UP VEHICLE DATA RECORD ER
REPLACED		TESTED EEC SYSTEM, MONITOR AND DCL TESTED SYSTEM, REPLACED POWER RELAY, PIN POINT TESTED AND REPLACED I.A.C VALVE...

	VEHICLE CUT OFF WHILE DRIVING DID RESTART
	DIAGNOSE WHY THE VEHICLE STALLED WHILE DRIVING
	CUSTOMER STATES CUT WITH NO WARNING ,PULLED OVER,RESTARTED OK,HAPPENED ONE TIME LAST FRIDAY
	CUST STATES IDLE DROPS STALLS OUT STOPPING
	CHECK LIGHT ON,ALSO WONT STAY RUNNING,TOWED IN
	D21 CUSTOMER STATES SHE WAS DRIVING DOWN DEEP CANYON WHEN THE VEHICLE STALLED SO SHE PULLED OVER AND WAS TOO SCARED TO DRIVE THE REST OF THE WAY DOWN THE CANYON THIS MAY HAVE TO BE DRIVEN
	D21 RECHECK CUSTOMER STATES WHEN DRIVING DOWN DEEP CANYON OR AND TYPE CANYON THE VEHICLE STALLS RES
	CUSTOMER STATES THAT WHEN SHE WAS GOING ABOUT 35MPH AND UP A HILL AND TURNING TO THE RT IT CUT OFF.STOPED AND PUT IT
	C S DIES WHILE DRIVING AT STEADY SPEEDS OR WHEN SLOWING DOWN TO TURN
R REPLACEMENT	CUST STATES VEHICLE WAS DRIVING DOWN THE ROAD AND VEHICLE SHUT DOWN AND THEN WAS ABLE TO START BACK UP
	ENGINE STALLS WHEN DRIVING STOP N GO RESTARTED OK HAS DONE THIS A COUPLE OF TIMES
	THE ENGINE STALLED FOR NO REASON BUT IT RESTARTED RIGHT AWAY?? CHECK AND ADVISE FOR SAFTY REASONS...
	DIAGNOSE CAUSE OF VEHICLE HAS STALLED TWICE WITHIN A MONTH & 1 2, WHILE DRIVING AT ABOUT 35 45MPH, VEHICLE RESTARTS FINE. (CHECK T.S.B.S)
	CAR DIED WHILE DRIVING DOWN THE ROAD
	CUSTOMER STATE ENGINE DIED WHILE DRIVING, ALSO DIED WHILE BACKING UP... WE JUST REPLACED TRANS AND RACK&PINION
	CAR STALLED AFTER 3 MINUTES OF DRIVING AT 40 MPH, GOING AROUND CURVE IN ROAD
T VEHICLE. REPLACED IAC MOT OR ASSY. ROADTEST VEHICLE AGAIN. COULD NOT GET VEHICLE TO STALL AT ANY TIME DURING ROADTEST. R RUN SYSTEMS TESTS, STILL NO CODES IN SYSTEM.	CUST STATES VEHICLE STILL STALLS ? THEY ORDERED PART ON THERE OWN
	TRUCK WILL NOT CRANK
	CUSTOMER STATES VEHICLE STALLS AT 40 MPH, TWICE HAS DONE THIS CUST STATES CUT DRIVING AT 40 MPH AND HAS TO RESTART ONE TIME MORE SINCE LAST VISIT
	CUST STATES WAS DRIVING AT 40 MPH AND WENT TO ACCL VEH STALLED ONE TIME HAS NOT HAPPENED SINCE CK ADVISE ON ANY CODES
	CUSTOMER STATES WHEN DRIVING AT 30 35 MPH AND SLOWING TO MAKE A STOP OR TURN ENG WILL DIE WHEN FOOT TAKEN OFF GAS, WITH FOOT ON GAS ENG WONT DIE
	CHECK ENGINE, CUST SAYS WHEN COASTING DOWNHILL THE ENGINE STALLS AT TIMES.
TEST DRIVE AND MAKE COUPLE OF RECORDINGS DOW NLOAD AND RECHECK FOUND FUEL TRIMS GO UP THEN S TALLS OUT RUN PID DATA DISPLAY FOUND IAC AT HIG H LEVEL 45 PERCENT ADJ BASE IDLE TO 35 PERCENT IAC	ENGINE STALLED WHILE DRIVING AND DECELERATING WITH NO BRAKING THEN RESTARTED AND WAS FINE
	CUST SAYS ENGINE CUT WHILE DRIVING AND WILL NOT RESTART.

2002	20639	S11	1FMCU03102KD52690	3.0L	T/LD	5	2002	2G04	12A650	D21	3	2173870	1000	WHILE DRIVING
2002	20644	S11	1FMCU03102KD01652	3.0L	T/LD	3	2002	2B04	12A650	D21	2	2258185	1000	WHILE DRIVING
2002	20649	S11	1FMCU03102KC80407	3.0L	T/LD	2	2002	7W07	15607	D21	2	1511557	1000	NO TEXT
2002	20666	S11	1FMCU03102KB64169	3.0L	T/LD	12	2001	2G01	12A650	D21	7	1948695	10000	WHILE DRIVING
2002	20668	S11	1FMCU03102KB64428	3.0L	T/LD	12	2001	1H03	9J460	D21	6	2096420	2000	WHILE DRIVING
2002	20673	S11	1FMCU03102KB50821	3.0L	T/LD	11	2001	2B05	RECAL	D21	2	777020	4000	WHILE DRIVING
2002	20674	S11	1FMCU03102KB24567	3.0L	T/LD	11	2001	2.00E+03	9F715	D21	8	2013257	8000	AT STOP
2002	20675	S11	1FMCU03102KB21605	3.0L	T/LD	11	2001	2G05	RECAL	D21	2	665696	8000	WHILE DRIVING
2002	20676	S11	1FMCU03102KB21696	3.0L	T/LD	11	2001	2B04	12A650	D21	2	1866851	0	WHILE DRIVING
2002	20682	S11	1FMCU03102KA91991	3.0L	T/LD	10	2001	2.00E+03	9B825	D21	9	1678251	9000	STALLS
2002	20684	S11	1FMCU03102KA80835	3.0L	T/LD	10	2001	2.00E+03	9F715	D21	3	467309	3000	CUST TEXT
2002	20685	S11	1FMCU03102KA79744	3.0L	T/LD	10	2001	7C05	14N069	D21	4	663166	1000	WHILE DRIVING
2002	20686	S11	1FMCU03102KA79422	3.0L	T/LD	10	2001	2.00E+03	9F715	D21	8	1146286	4000	WHILE DRIVING
2002	20690	S11	1FMCU03102KA69019	3.0L	T/LD	10	2001	2.00E+03	9F715	D21	1	286680	0	AT STOP
2002	20691	S11	1FMCU03102KA69019	3.0L	T/LD	10	2001	2G05	RECALEM	D21	5	858590	4000	DOWNHILL
2002	20694	S11	1FMCU03102KA68929	3.0L	T/LD	10	2001	2.00E+03	9F715	D21	4	1326686	8000	WHILE DRIVING
2002	20705	S11	1FMCU03102KA60062	3.0L	T/LD	9	2001	2.00E+03	9F715	D21	11	3417674	10000	STALLS
2002	20714	S11	1FMCU03102KA17471	3.0L	T/LD	8	2001	7B02	10800	D21	5	694728	4000	NO START
2002	20720	S11	1FMCU03102KA15394	3.0L	T/LD	8	2001	2G04	DIAG	D21	8	1224519	10000	STALLS
2002	20721	S11	1FMCU03102KA15394	3.0L	T/LD	8	2001	1H03	9J460	D21	7	1065874	9000	COASTING
2002	20722	S11	1FMCU03102KA14540	3.0L	T/LD	8	2001	2.00E+03	9F715	D21	9	1470512	8000	WHILE DRIVING
2002	20785	S11	1FMCU021X2KA61970	3.0L	T/LD	10	2001	2.00E+06	9H907	D21	5	706205	7000	NO TEXT
2002	20797	S11	1FMCU02102KB06460	3.0L	T/LD	10	2001	2G04	12A650	D21	6	1236044	6000	WHILE DRIVING
2002	20811	S11	1FMCU02162KD09921	3.0L	T/LD	4	2002	7B22	14535	D21	2	1548720	0	WHILE DRIVING
2002	20827	S11	1FMCU02152KA07176	3.0L	T/LD	8	2001	2.00E+03	9F715	D21	8	1430569	2000	STALLS
2002	20829	S11	1FMCU02142KB64660	3.0L	T/LD	12	2001	2G05	RECALEM	D21	5	2438295	7000	WHILE DRIVING

TSB		1998 NO DTC PERFORM TSB 02 11 06 ISM 02 05 043 COMPLETED TSB HAS NEW PCM RLY LATEST CALIBRATIO AND DPFE SEN TECH ASST 213 581 035 MARTY NEW PCM CALIBRATION IN 2 WKS UNDER INVESTIGATION RETEST PASS
TSB		TEST AND CK OASIS REPROGRAMED PCM PER TSB 02116
TSB		KEY HALO INTERMITTENT NO CRANK WITH ALL KEYS, THEFT LIGHT FLASHES, RAN OASIS NO TSB S FOUND. REPLACED PATS TRANSCIEVER &
REPLACED		POWERTRAIN CONTROL MODULE RELAY REPLACE (12A648 9345 128877 14N060)
TSB		2251 NO DTC TSB 2 11 6 ISM 2 5 043 PID DATA IAC 32% PASS PCM MPC 181 REPROGRAM PCM 2L8A 12A650 AS PASS EVAP TEST HAS BLACK PCM RLY CK PCM HARNESS OK INSPECT C3078,C,D,C110,C113 PASS,INSPECT G300,G1
SSM		QUICK TEST,PASS,PID DATA DISPLAY,REPROM PCM PER SSM,RETEST,NGS MONITOR ROADTEST CC 42
REPLACED		ENGINE STALLS AT STOPS TURNING A CORNER QUICK TEST KOEO CODE P1111 KOEO P1111 PINPOINT TEST REPLACE AIR BYPASS VALVE. RETEST P1111
REFLASH		5805 WARR R T AND VERIFY CONCERN,WDS START UP AND PERFORM SELF TEST,NO DTC AVA,CHECK VEH POWERS AND GROUNDS,REMOVE BATTERY,AND BATTERY TRAY, AND CLEAN AND TIGHTEN EEC GROUND,REMOVE EEC POWER RELAY A
DIAG		CKOUT FOR STALL CONCERN HOT 35 40 WILL RESTART ROADTEST 3.0L AUTO TRANS PERFORM VISUAL INSP FOR VACUME LEAKS OK INSTALL
REPLACED		VALVE ASSEMBLY IDLE AIR CONTROL (IAC) REPLACE
DIAG		IAC EEC (QUICK TEST) DIAGNOSIS
SSM		EEC TESTS REPLACE PCM RELAY,CLEAN EVP LINE PER SSM 15599 PASS
SSM		SYSTEM CHECK OUT EEC TEST NO CODE PERFORM ROAD TEST PIDATA RECORD MONITOR PERFORM SSM 15599 REPLACE EEC RELAY AND REPROGRAM PCM RETEST AND PERFORM PID DATA RE CORD ROAD TEST HAVE TO REPLACE IAC MOTOR
DIAG		IAC EEC (QUICK TEST) DIAGNOSIS
DIAG		PCM UPDATE EEC (QUICK TEST) DIAGNOSIS
REPLACED		REPLACED IAC VALVE
REPLACED		REPLACE IDLE AIR CONTROL VALVE.
DIAG		CHECK FOR NO START CHECK CHARGING SYSTEM
DIAG		CK W FK TO SEE WHAT HAS OCCURED. CK AND MONITOR FUEL PRESSUR E. PERFORM EEC TESTS ON SYSTEM TO CK FOR ANY CODES. PERFORM
REFLASH		CK VEHICLE RUNNING. CK FUEL PRESSURE. PROGRAM AND HOOK UP WDS CK FOR ANY CODES. PERFORM PID DATA CK S ON VOLTAGES AS
TSB		EEC TEST RAN CODES CK PIDS ON TEST DRIVE RAN OASIS FOUND TSB 020606 PINPOINT TO IAC VALVE OUT OF SPECS AT IDLE 42PERCENT RPM 880 REPL IAC RETEST TEST DR OK
REPLACED		WDS TEST FUEL PRESSURE TEST CK IGNITION SWITCH REPLACE FUEL PUMP WPI
TSB		ROAD TEST WDS SELF TEST FUEL PRESSURE TEST INJECTOR FLOW POWER BALANCE DATA LOGGER PERFORMED TSB 020606
REPAIR		REPAIRED SHORT CKT361 WIRED CHAFFED AT AC SUCTION LINE CKT 361
TSB		PERFORM DIAG AND VERIFY COMPLAINT PERFORM TSB 02 6 6 AIR BYPASS VALVE INOP REPLACE VALVE AND EEC RELAY AND REPROGRAM PCM ROADTEST ALL OK AT THIS TIME
REFLASH		100KM3 PREV RO 430716 CAUS PART 92092 EEC TEST,MONITOR RECORD ROAD TEST,NO DTCS,REPAIR TO 02 11 6 REPROGRAM PCM ,ROAD TEST

QT1 PCM CALIB 2L8A 12A650 AD	CHECK VEH DIED OUT WHILE DRIVING BUT RESTARTED, ADVISE
	CHECK VEHICLE STALLED WHILE DRIVING AND RESTARTED ADVISE
	CUST REPORTS ENGINE DIED WHILE DRIVING DID RESTART OK BUT CUSTOMER WOULD LIKE CHECKED OUT.
00 RR BATTERY TRAY INSPECT G104,G105,G101 CK ROUTE CRANK SENSOR AROUND AT A C COMPRESSOR RETEST PID DATA NORMAL PASS QT1	CHECK VEHICLE INTERMITTENTLY DIES OUT WHILE DRIVING, ADVISE
	CUST STATES ENGINE STALL WHILE DRIVING 60P PART HERE
	CUSTOMER STATES ENGINE STALLS AT STOPS TURNING A CORNER
ND CHECK PINS FOR TIGHTNESS.REMOVE EVAP SYSTEM VENT TUBE AND CHECK WITH SHOP AIR FOR RESTRICTIONS OK,RE PROGRAM PCM TO LATEST CALABRATION AND R T NO STALLING HAPPENED AFTER	CK VEHICLE STALLS OUT WHEN DRIVING STRAIGHT.STARTED BACK UP EASILY
	CK CUST STATES VEHICLE STALLED OUT DRIVING DOWN EXPRESSWAY VEHICLE DID RESTART
	C S OIL LITE AND CHECK ENGINE LITE CAME ON AND HAD NO POWER ASSIST TO BRAKES THEN ENGINE STALLED TOOK ABOUT 15 MINS TO RESTART
	CUST STATES ENGINE STALLING WHEN STOPPING WILL RESTART
	C S THAT THE ENGINE JUST DIED OUT WHILE DRIVING D21
IT IS STUCK INTERMITEN RETEST OK ROAD TEST OK	CUST STATES VEH STALLS AT TIMES WHEN DRIVING AT SPEEDS BETWEEN 35 AND 40MPH
	CHECK ENGINE, CUST SAYS WAS SLOWING FROM 40MPH DOWN HILL, SAYS ENGINE STALLED, MIL CAME ON AND STEERING GOT STIFF. STOPPED, TURNED KEY OFF. RESTARTD
	CHECK ENGINE, CUST SAYS ENGINE DIED ON TIME AT 40MPH DOWN HILL AFTER DRIVING ABOUT 15 MIN 7 MILES. RESTARTED IMMEDIATELY.
	C S 3 TIMES THE ENGINE HAS DIED WHILE DRIVING, STARTS RIGHT BACK UP
	ENGINE STALLS WHEN PUT INTO REVERSE INTERMITTENTLY (D21)
	CHECK VEHICLE WILL NOT START AT TIMES HAVE TO KEEP MESSING AND THEN IT WILL START
	CHECK ON STALLING TWO TIMES TSB ON DASH
	CHECK STALLING ON DECELL 20 TO 40MPH HOT SEE TSB ON DASH OF CAR OR SEE FRANK
	CUST STATES THAT THE VEHICLE HAS SHUT OFF WHEN DRIVING AND YOU LOOSE EVERYTHING...THE BRAKES THE STEERING
	STALLS AT TIMES GOING 40 MPH
	OWNER REPORTS VEHICLE DIED WHILE DRIVING, CHECK AND ADVISE.
	CUST STATES VEH STALLS
	CUSTOMER STATES ENGINE CUT OUT TWO TIMES WHILE DRIVING. INSPECT AND REPORT.

2002	20903	S11	1FMCU01139XD10099	3.0L	TALD	1	2002	2.00E+03	9F715	D21	0	1256199	0	WHILE DRIVING
2002	20929	S11	1FMCU01139XD13331	3.0L	TALD	4	2002	1H03	9J460	D21	3	2211911	2000	AT STOP
2002	20932	S11	1FMCU01139XD01985	3.0L	TALD	10	2001	2.00E+03	9F715	D21	6	2325018	3000	WHILE BRAKING
2002	20954	S11	1FMCU01139XD12549	3.0L	TALD	10	2001	1H03	9J460	D21	6	2428791	22000	AT IDLE

TSB		1SB WARRANTY REQUEST TIME SPENT VERIFY CONCERN RUN OR WDS NO CODES P1000 NO PROBLEM DETECTED RUN OASIS FOUND TSB 2 & 6 FOLLED INSTRUCTIONS TO MONITOR PIDS IAC AND VERIFY BUILD DATE IN STEP 1 DID SO
REPAIR		2009 VERIFIED CONCERN WDS SELF TEST P0171, P0174, P0401 PINPOINT TEST, FOUND A VACCUM LEAKS REPAIRED VACUUM LEAK AT INTAKE MANIFOLD REPLACED A PFE SENSOR. RESE PCM QUALITY CHECK AND ROAD TEST MILES
REPLACED		REPLACE IAC VALVE, ROAD TESTED AND RETESTED OK
REPLACED		PFE SENSOR OUT OF RANGE, SEC DIAG; REPLACE DPFE

FOUND IAC DUTY CYCLE AT 48% OUT OF SPECS REPLACED IAC NOW AT 37% INS SPECS AND RPM AT 750 WENT TO STEP 2 SAID TO GO TO STEP 4 TO CHECK VAPOR MANAGMENT VALVE DUTY CYCLE AND CHECK VOLTS	DIES WHILE DRIVING See ME
2808 2821	D21 CK ENG. DIES AT STOP, SURGES AT IDLE, CHECK ENGINE LIGHT ON, OWNER STATE
	CUSTOEMR STATES THE CAR DIES WHEN COMMING TO A STOP OR AT REAL SLOW SPEEDS. S.C.P. IAC, ORDERED RO 351698, TECH 122
	CUSTOMER STATES ENGINE STALLS AT IDLE AND ENGINE HESITATES ACCELERATING

From: Waud, Sachiko (S.)
Sent: Monday, February 04, 2002 2:34 AM
To: McGee, Brett (B.L.); Miyamoto, Noriaki (N.); O'Callaghan, John (J.T.); Stassen, Tamara (T.M.)
Cc: Kawasaki, Shunsuke (S.); Perkins, Gary (G.R.); Takubo, Hiroichi (H.); Williamson, David (D.E.); Kwon, Soon (S.K.); Shiraishi, Masaru (M.); Ichikawa, Jiyunichiro (J.); 'yamada-san'; Yamamoto, Nobuhiro (N.); Sullivan, Jamie (J.P.)
Subject: RE: DPFE: Mazda input to Duratec and Zetec Timing Charts

This concern has been UOed by hofu.
Please make this concern for kcap only and not resource hofu parts.

John, Tamara,

I have left the PGMA * I * incase for need to change the concern screen.
Please handle it.

Thank you

HOFU AND KD CONCUR THIS CONCERN ONLY BECAUSE IT IS ASSUMED THAT THIS IS MADE
INTO KCAP ONLY CHANGE PER N.MIYAMOTO PMT SD. A CONCERN FOR HOFU TO RESOURCE THE
DPFE WILL BE RAISED NEXT WEEK. PLEASE REMOVE HOFU FROM THIS CONCERN.
WAUD, SACHIKO (81-82-287-1093 N MZDA204 SWAUD ML00
02/02/04

Sachiko Waud
FORD Program and Pre-Production
Management (PPM)
swaud@ford.com
Phone:81-82-287-1093 (820-440)
Fax:81-82-287-5399 (20399)

> -----Original Message-----
> From: McGee, Brett (B.L.)
> Sent: Monday, February 04, 2002 1:37 PM
> To: Waud, Sachiko (S.); Miyamoto, Noriaki (N.)
> Cc: Kawasaki, Shunsuke (S.); Perkins, Gary (G.R.); Takubo, Hiroichi (H.); Williamson, David (D.E.); Kwon, Soon (S.K.); Shiraishi, Masaru (M.); Ichikawa, Jiyunichiro (J.); 'yamada-san'; Yamamoto, Nobuhiro (N.); Sullivan, Jamie (J.P.)
> Subject: RE: DPFE: Mazda input to Duratec and Zetec Timing Charts
>
> Sachiko-san/Gary, thank you for your help. If Miyamoto-san doesn't respond this afternoon, we need to remove the Hofu/RHD rejection anyway, as the Concern is explicitly a KCAP ONLY change (no Hofu parts affected with the Concern properly rewritten) and I do not want to hold up this important change an additional day for paperwork that is not contentious.
>
> If a Mazda person is necessary to remove the Hofu/RHD rejection then I believe that Ichikawa-san's or Kawasaki-san's concurrence should be

sufficient.
>
> Brett McGee
> Ford Resident Engineer - Hofu Assembly Plant
> e-mail: bmcgee@ford.com
> Telephone: 011-81-82-287-1095
> Fax: 011-81-82-287-5399
>
> -----Original Message-----
> From: Waud, Sachiko (S.)
> Sent: Monday, February 04, 2002 11:59 AM
> To: Miyamoto, Noriaki (N.)
> Cc: Kawasaki, Shunsuke (S.); Perkins, Gary (G.R.); Takubo, Hiroichi (H.); Williamson, David (D.E.); Kwon, Soon (S.K.); Shiraishi, Masaru (M.); Ichikawa, Jiyunichiro (J.); McGee, Brett (B.L.); yamada-san; Yamamoto, Nobuhiro (N.)
> Subject: RE: DPFE: Mazda input to Duratec and Zetec Timing Charts
>
> Miyamoto-san
>
> Please respond to this concern today if possible or let me know the status so I will be able to add the status
> in the WERS description.
>
> Thank you.
>
>
> Sachiko Waud
> FORD Program and Pre-Production
> Management (PPM)
> swaud@ford.com
> Phone:81-82-287-1093 (820-440)
> Fax:81-82-287-5399 (20399)
>
>
> -----Original Message-----
> From: McGee, Brett (B.L.)
> Sent: Monday, February 04, 2002 11:10 AM
> To: Ichikawa, Jiyunichiro (J.); Waud, Sachiko (S.)
> Cc: Perkins, Gary (G.R.); Takubo, Hiroichi (H.); Miyamoto, Noriaki (N.); Williamson, David (D.E.); Kwon, Soon (S.K.); Shiraishi, Masaru (M.)
> Subject: FW: DPFE: Mazda input to Duratec and Zetec Timing Charts
> Importance: High
>
> Ichikawa-san for C11262413, the DPFE resourcing Concern has been made into a KCAP ONLY Concern. Please have the rejection status changed (I believe adding a comment to the Description screen is also appropriate), ASAP -- today if possible. The approval of C11262413 is necessary to kick-off the suppliers to support the planned KCAP timing.
>
> A different Concern for changing the DPFE sourcing at Hofu will be raised next week.
>
> Please contact me if you have any questions.
>
> As standard process -- this means that until a Hofu WERS Concern -> WERS notice -> purchase order/MRD is received at the suppliers they are to continue to support Hofu with old level parts.

>
> Sachiko-san, can you ensure that the Hofu plant code N051 gets removed from the plants affected section (there is a comment in the Product Affected field that it should be a KCAP only change, but the Plant Affected field still needs updating).>
>
> Thanks,
> Brett McGee
> Ford Resident Engineer - Hofu Assembly Plant
> e-mail: bmcgee@ford.com
> Telephone: 011-81-82-287-1095
> Fax: 011-81-82-287-5399
>
> -----Original Message-----
> From: Williamson, David (D.E.)
> Sent: Saturday, February 02, 2002 1:52 AM
> To: McGee, Brett (B.L.); Shiraishi, Masaru (M.)
> Cc: Kwon, Soon (S.K.); Sullivan, Jamie (J.P.); Plattenberger, Karl (K.J.); Jordan, Donald (D.E.); Grandas, Joseph (J.M.)
> Subject: RE: DPFE: Mazda input to Duratec and Zetec Timing Charts
> Importance: High
>
> Brett, for C11262413, Shiraishi-san, Kwon-san & me would like to make this concern KCAP ONLY. We will open new concern for Hofu only (I will forward number to you next week.) Purpose is to not jeopardize KCAP Lear timing. Please have Mazda remove X from authority so we can close to kick off Lear.
>
> Also will provide the below requested Duratec information when it becomes available (Shaker test, calibration data) as requested. Zetec testing & negotiation is still ongoing so project is lagging Duratec. New info will be provided when available.
>
> Thanks Brett.
>
>
>
> -----Original Message-----
> From: McGee, Brett (B.L.)
> Sent: Friday, February 01, 2002 3:26 AM
> To: Williamson, David (D.E.)
> Cc: Kwon, Soon (S.K.); Ichikawa, Jiyunichiro (J.); Taketomo, Noriko (N.)
> Subject: DPFE: Mazda input to Duratec and Zetec Timing Charts
>
> David, I met with Ichikawa-san this afternoon to get the wiring information for Duratec and discuss other questions/issue with the DPFE resourcing.
>
> Hofu Duratec wiring harness timing Please add the following timing milestones/tasks
> A) Feb 4 -- need shaker test results
> B) Feb 7 -- Mazda agree/disagree with shaker test results
> C) Feb 7-21 -- Mazda prepares drawings and releases WERS and MIDAS(ECN) for the change (note: there may be some opportunity to compress this if necessary)
> D) Feb 21 -- release drawing
> E) Feb 21-May 21 (3 months) -- Lear creates/PSW production wiring harness and ships to Hofu

> F) April 25-May 21 -- ship EGR tubes to Hofu (approx. 4 week shipping time assumed)
> G) May 21 -- Hofu MRD
> H) May 23 -- Implementation date at Hofu
>
> Hofu Zetec timing Please add the following timing milestones/tasks
> I) March 29-April 5 ship EGR tubes to Hiroshima
> J) April 5-April 17 Evaluate EGR tubes: assembility and packaging
>
> QUESTIONS/REQUESTS
> 1) Please provide the test procedure and pass/fail criteria for the shaker test (e.g., ES number is fine Mazda can look it up via the Intranet)
> 2) Can prototype Zetec EGR tubes be supplied sooner than March 28th (item #17 on 1/22/02 Zetec timing chart)
> 3) Is Zetec timing correct? As many items will not be completed until just before the listed MRD, for example, shaker test is completed 5/13/02 and EGR tube is PSWed on 5/22/02. Is the plan to kick off Emsa before testing is complete?
> 4) Provide calibration results as soon as possible after testing is completed on 2/8/02 (Whitepaper -- including data)
>
> Brett McGee
> Ford Resident Engineer - Hofu Assembly Plant
> e-mail: bmcgee@ford.com
> Telephone: 011-81-82-287-1095
> Fax: 011-81-82-287-5399
>

From:	Waud, Sachiko (S.)
Sent:	Monday, February 04, 2002 2:34 AM
To:	McGee, Brett (B.L.); Miyamoto, Noriaki (N.); O'Callaghan, John (J.T.); Stassen, Tamara (T.M.)
Cc:	Kawasaki, Shunsuke (S.); Perkins, Gary (G.R.); Takubo, Hiroichi (H.); Williamson, David (D.E.); Kwon, Soon (S.K.); Shiraishi, Masaru (M.); Ichikawa, Jiyunichiro (J.); 'yamada-san'; Yamamoto, Nobuhiro (N.); Sullivan, Jamie (J.P.)
Subject:	RE: DPFE: Mazda input to Duratec and Zetec Timing Charts

This concern has been UOed by hofu.
Please make this concern for kcap only and not resource hofu parts.

John, Tamara,

I have left the PGMA ' I ' incase for need to change the concern screen.
Please handle it.

Thank you

HOFU AND KD CONCUR THIS CONCERN ONLY BECAUSE IT IS ASSUMED THAT THIS IS MADE
INTO KCAP ONLY CHANGE PER N.MIYAMOTO PMT 8D. A CONCERN FOR HOFU TO RESOURCE THE
DPFE WILL BE RAISED NEXT WEEK. PLEASE REMOVE HOFU FROM THIS CONCERN.
WAUD, SACHIKO (81-82-267-1093 N MZDA204 SNAUD ML00
02/02/04

Sachiko Waud
FORD Program and Pre-Production
Management (PPM)
swaud@ford.com
Phone:81-82-287-1093 (820-440)
Fax:81-82-287-5399 (20399)

> -----Original Message-----
> From: McGee, Brett (B.L.)
> Sent: Monday, February 04, 2002 1:37 PM
> To: Waud, Sachiko (S.); Miyamoto, Noriaki (N.)
> Cc: Kawasaki, Shunsuke (S.); Perkins, Gary (G.R.); Takubo, Hiroichi (H.); Williamson, David (D.E.); Kwon, Soon (S.K.); Shiraishi, Masaru (M.); Ichikawa, Jiyunichiro (J.); 'yamada-san'; Yamamoto, Nobuhiro (N.); Sullivan, Jamie (J.P.)
> Subject: RE: DPFE: Mazda input to Duratec and Zetec Timing Charts
>
> Sachiko-san/Gary, thank you for your help. If Miyamoto-san doesn't respond this afternoon, we need to remove the Hofu/RHD rejection anyway, as the Concern is explicitly a KCAP ONLY change (no Hofu parts affected with the Concern properly rewritten) and I do not want to hold up this important change an additional day for paperwork that is not contentious.
>
> If a Mazda person is necessary to remove the Hofu/RHD rejection then I believe that Ichikawa-san's or Kawasaki-san's concurrence should be

sufficient.
>
> Brett McGee
> Ford Resident Engineer - Hofu Assembly Plant
> e-mail: bmcgee@ford.com
> Telephone: 011-81-82-287-1095
> Fax: 011-81-82-287-5399
>
> -----Original Message-----
> From: Waud, Sachiko (S.)
> Sent: Monday, February 04, 2002 11:59 AM
> To: Miyamoto, Noriaki (N.)
> Cc: Kawasaki, Shunsuke (S.); Perkins, Gary (G.R.); Takubo, Hiroichi (H.); Williamson, David (D.E.); Kwon, Soon (S.K.); Shiraishi, Masaru (M.); Ichikawa, Jiyunichiro (J.); McGee, Brett (B.L.); yamada-san; Yamamoto, Nobuhiro (N.)
> Subject: RE: DPFE: Mazda input to Duratec and Zetec Timing Charts
>
> Miyamoto-san
>
> Please respond to this concern today if possible or let me know the status so I will be able to add the status
> in the WERS description.
>
> Thank you.
>
>
> Sachiko Waud
> FORD Program and Pre-Production
> Management (PPM)
> swaud@ford.com
> Phone:81-82-287-1093 (820-440)
> Fax:81-82-287-5399 (20399)
>
>
> -----Original Message-----
> From: McGee, Brett (B.L.)
> Sent: Monday, February 04, 2002 11:10 AM
> To: Ichikawa, Jiyunichiro (J.); Waud, Sachiko (S.)
> Cc: Perkins, Gary (G.R.); Takubo, Hiroichi (H.); Miyamoto, Noriaki (N.); Williamson, David (D.E.); Kwon, Soon (S.K.); Shiraishi, Masaru (M.)
> Subject: FW: DPFE: Mazda input to Duratec and Zetec Timing Charts
> Importance: High
>
> Ichikawa-san for C11262413, the DPFE resourcing Concern has been made into a KCAP ONLY Concern. Please have the rejection status changed (I believe adding a comment to the Description screen is also appropriate), ASAP -- today if possible. The approval of C11262413 is necessary to kick-off the suppliers to support the planned KCAP timing.
>
> A different Concern for changing the DPFE sourcing at Hofu will be raised next week.
>
> Please contact me if you have any questions.
>
> As standard process -- this means that until a Hofu WERS Concern -> WERS notice -> purchase order/MRD is received at the suppliers they are to continue to support Hofu with old level parts.

>
> Sachiko-san, can you ensure that the Hofu plant code N051 gets removed from the plants affected section (there is a comment in the Product Affected field that it should be a KCAP only change, but the Plant Affected field still needs updating).>
>
> Thanks,
> Brett McGee
> Ford Resident Engineer - Hofu Assembly Plant
> e-mail: bmcgee@ford.com
> Telephone: 011-81-82-287-1095
> Fax: 011-81-82-287-5399
>
> -----Original Message-----
> From: Williamson, David (D.E.)
> Sent: Saturday, February 02, 2002 1:52 AM
> To: McGee, Brett (B.L.); Shiraishi, Masaru (M.)
> Cc: Kwon, Soon (S.K.); Sullivan, Jamie (J.P.); Plattenberger, Karl (K.J.); Jordan, Donald (D.E.); Grandas, Joseph (J.M.)
> Subject: RE: DPFE: Mazda input to Duratec and Zetec Timing Charts
> Importance: High
>
> Brett, for C11262413, Shiraishi-san, Kwon-san & me would like to make this concern KCAP ONLY. We will open new concern for Hofu only (I will forward number to you next week.) Purpose is to not jeopardize KCAP Lear timing. Please have Mazda remove X from authority so we can close to kick off Lear.
>
> Also will provide the below requested Duratec information when it becomes available (Shaker test, calibration data) as requested. Zetec testing & negotiation is still ongoing so project is lagging Duratec. New info will be provided when available.
>
> Thanks Brett.
>
>
>
> -----Original Message-----
> From: McGee, Brett (B.L.)
> Sent: Friday, February 01, 2002 3:26 AM
> To: Williamson, David (D.E.)
> Cc: Kwon, Soon (S.K.); Ichikawa, Jiyunichiro (J.); Taketomo, Noriko (N.)
> Subject: DPFE: Mazda input to Duratec and Zetec Timing Charts
>
> David, I met with Ichikawa-san this afternoon to get the wiring information for Duratec and discuss other questions/issue with the DPFE resourcing.
>
> Hofu Duratec wiring harness timing Please add the following timing milestones/tasks
> A) Feb 4 -- need shaker test results
> B) Feb 7 -- Mazda agree/disagree with shaker test results
> C) Feb 7-21 -- Mazda prepares drawings and releases WERS and MIDAS(ECN) for the change (note: there may be some opportunity to compress this if necessary)
> D) Feb 21 -- release drawing
> E) Feb 21-May 21 (3 months) -- Lear creates/PSW production wiring harness and ships to Hofu

> F) April 25-May 21 -- ship ERG tubes to Hofu (approx. 4 week shipping time assumed)
> G) May 21 -- Hofu MRD
> H) May 23 -- Implementation date at Hofu
>
> Hofu Zetec timing Please add the following timing milestones/tasks
> I) March 29-April 5 ship EGR tubes to Hiroshima
> J) April 5-April 17 Evaluate EGR tubes: assembility and packaging
>
> QUESTIONS/REQUESTS
> 1) Please provide the test procedure and pass/fail criteria for the shaker test (e.g., ES number is fine Mazda can look it up via the Intranet)
> 2) Can prototype Zetec EGR tubes be supplied sooner then March 28th (item #17 on 1/22/02 Zetec timing chart)
> 3) Is Zetec timing correct? As many items will not be completed until just before the listed MRD, for example, shaker test is completed 5/13/02 and EGR tube is PSNed on 5/22/02. Is the plan to kick off Ensa before testing is complete?
> 4) Provide calibration results as soon as possible after testing is completed on 2/8/02 (Whitepaper -- including data)
>
> Brett McGee
> Ford Resident Engineer - Hofu Assembly Plant
> e-mail: bmcgee@ford.com
> Telephone: 011-81-82-287-1095
> Fax: 011-81-82-287-5399
>

From:	Powers, Ken (K.W.)
Sent:	Monday, June 24, 2002 11:48 AM
To:	Fascetti, Bob (R.J.); Hofman, Michael (M.V.)
Cc:	Takasawa, Keith (K.D.)
Subject:	FW: Stalls update

Here's the latest ICCD data for your reference.

Ken Powers
Escape/Tribute PVT Manager, KCAP
Ph: 816-459-1729; Fax: -1726

-----Original Message-----
From: Walker, Carrie (C.J.)
Sent: Monday, June 24, 2002 10:22 AM
To: Powers, Ken (K.W.)
Subject: RE: Stalls update

Ken,

Here's the F/1000 chart for engine stalls.

[redacted]

;ine Stalls Trend.]

Carrie J. Walker
ICCD - Customer Relations Specialist
Ford Motor Company
Kansas City Assembly Plant
Ph# 816-414-5557
Fax# 816-459-1970
Pager# 913-567-1747

-----Original Message-----
From: Powers, Ken (K.W.)
Sent: Friday, June 21, 2002 4:56 PM
To: Walker, Carrie (C.J.)
Subject: Stalls update

Can you check on the F/1000 Stalls data again? We want to see if the rate has changed for the Thursday VQR. (Can you also send me the overall vehicle F/1000 chart? I want to see what happened when we went to Toronto to see if it correlates to some of the increases we're seeing).

Thanks.

Ken Powers
Escape/Tribute PVT Manager, KCAP
Ph: 816-459-1729; Fax: -1726

From:	Peplone, Gil (J.)
Sent:	Thursday, June 27, 2002 2:11 AM
To:	Johnson, Jim (J.S.); Billoki, John (J.R.); Corbett, Sandra (S.M.); Ahoonian, Don (D.J.); Ayvazzian, Kem (K.); Bauer, Scott (S.C.); Bholwani, Kamal (K.); Blackburn, Thomas (T.J.); Bogema, John (P.); Chick, John (J.); Chih, Ming-Niu (M.N.); Chin, Darrel (D.); Corbett, Sandra (S.M.); Dalbo, Bob (R.J.); Rothweiler, Daniel (D.); De Pena, Juan (J.E.); Diez, Timothy (T.P.); Fascetti, Bob (R.J.); Fourmala, Gilbert (G.); Freeland, Mark (M.); Giles, Stuart (S.); Gokhale, Renuka (R.V.); Grimes, Jeff (J.R.); Hansen, George (G.C.); Herr, George (G.J.); Hofman, Michael (M.V.); Holmes, Jeffrey (J.R.); Ichikawa, Jiyunichiro (J.); Jensen, Ted (T.E.); Mcdonald II, John (J.M.); Jordan, Donald (D.E.); King, Robert (R.F.); Kosko, Jeff (J.R.); Kwon, Soon (S.K.); Limtaco, Steven (S.); Linde, Peter (P.A.); Liu, Jane (J.); Mandziuk, Roger (R.S.); Marok, Edmond (E.C.); Matsas, John (J.); Maurer, James (J.B.); Mazzella, Gary (G.R.); Mooney, Larry (L.); Moorhouse, Scott (S.R.); Morgan, Tomiko (T.T.); Morishima, Shigeki (S.); Nematollahi, Sonya (S.); Noteboom, Jim (J.E.); Ortman, James (J.W.); Powers, Ken (K.W.); Price, Martin (M.); Raquepau, Alden (A.P.); Sanders, Muriel (M.S.); Shah, Kiran (K.C.); Shiraishi, Masaru (M.); Stilpenbauer, Jeffrey (J.R.); Suarez, Rhae (R.); Takasawa, Keith (K.D.); Takubo, Hiroichi (H.); Veenstra, Tim (T.W.); Wakenell, Ray (R.A.); Wettach, Bill (B.); Williams, Les (LHW.); Yeung, Lam (.); Benintende, Robert (R.F.); Goering, Kimberly (K.L.); Suarez, Rhae (R.); Terzea, Laura (L.D.); Martin, Mike (M.S.); Wexler, Mark (M.A.); Amely, Felix (F.A.); Bradley, Joe (J.C.); Linde, Peter (P.A.); Goering, Kimberly (K.L.); Terzea, Laura (L.D.); Benintende, Robert (R.F.); Wexler, Mark (M.A.); Amely, Felix (F.A.)
Cc:	Peplone, Gil (J.); DiAngelo, Renaldo (R.); Berenter, Joel (J.R.); Surti, P. J. (P.J.); Noteboom, Jim (J.E.)
Subject:	PFQS's Investigation Results of Virgin Islands Escape Driveability Concerns
Importance:	High

Good evening everyone:

Here's my report on my trip.

[redacted]

lts of Virgin Isl
Escap...

I will be calling in on the Conference all at 2pm today.

Call-in Info: 1-877-670-3529 or Ford net 9-1-954-1144
International Participants: 1-630-893-1704
Passcode: 7673538, then hit #

I thank the Team for all their assistance.

Gil Peplone
Powertrain Field Quality Specialist-"PFQS" in
South Florida
Office/Answering Machine: 954-753-9969
Cell Phone 954-242-2066
"With Warranty you are Paying for the Sins of the Past"

ER62-627 24839

Results of St. Croix/St. Thomas Virgin Island Investigation of 3.0L Escape

Executive Summary

A total of 22 Concern Units were inspected by Powertrain Field Quality (PFQS) Gil Pepitone from 6/15-6/25/02.

18% of inspected vehicles with certain key Service Actions applied and containing uncontaminated fuel were fully resolved for the "Stalling during Deceleration" Concern, as reported by Owners.

The vehicle population which had prior repair attempts, (55%) did not have TSB/Oasis SSM Service repairs fully applied for various reasons, including test data mis-interpretation, component ordering wait time, WDS test equipment procedures/hardware issues, and "Repair Holds" for pending Engineering visitation.

However, 67% Units had **contaminated fuel and restricted fuel filters**, which may have been a **contributor** to the unverified **Deceleration Stalling** issue.

A second Driveability Concern (which included Units that contained the latest calibration level) of **Hesitation during moderate engine temp** was listed as a Concern for 32% of the Units. The Hesitation Concern was then verified and data /reviewed or recorded by PFQS. However, resolution was not determined. Local fuel volatility and/or PCM calibration may root cause, but this is speculation. Further investigation is in progress.

An omission of a Diagnostic procedure in TSB 02-8-6 was found, involving the requirement for a drive cycle in order to prompt the start of the Purge Cycle for proper EVAP System evaluation.

The surface blistering of multiple MAF sensor's plastic case was reported, with a sample captured.
A second MAF related issue of tight MAF retaining nuts resulted in airbox lid breakage.

A third MAF sensor related issue of missing Part Number imprint was found on two Units.

Idle Air Control {IAC} Duty Cycles were found in 27% Units to be on the high end of the spec. In some cases, IAC replacements did not reduce DC. Also, there is a need for multiple improved IAC diagnostic procedures for TSB
02-8-6.

PFQS recommendations are listed at the end of this report.

Background

PFQS was contacted in early June to inspect and resolve the reported Decell Stalling Concern on a minimum of 10 3.0L 2001/02 Escapes on the Islands of St. Croix and St. Thomas, U.S. Virgin Islands. Both dealerships use the same name of Metro Motors.

Figure 1 Metro Motors, St. Croix, VI

Figure 2 Burnete Matto, Service Manager

Figure 3 Isaac, Drivability Technician

Figure 4 Service area at Metro Motors

Figure 5 Service area, alternate view

A review of Service records and Oasis repair histories as compared to the actual PFQS inspection of the 22 Units, indicated that corrective Service procedures were only partially performed on 55% of Units.
However, 18% of Units had been fully serviced per the existing Service Communications.
The remaining percentile involved Units which had not been to the Dealership for the Decell Stalls Concern prior to the Inspection period.

Both Islands are small (St. Croix, the larger, is 28x7 miles). The terrain is very hilly, with some considerable grade angles. The

Concern of Decell Stall for 3.0L Escape is reported as most common in uneven topography as evidenced from a prior PFQS review of North American CQIS data.

Of the 22 Units inspected, 20 were at the St. Croix location, while two were done in St. Thomas. A total of four Units were originally scheduled for St. Thomas, but two were no-shows. The majority of this report's data stems from the St. Croix Dealership.

Investigation of Decell Stall

PFQS arrived on Saturday, 6/15. Basic inspection and VDR recorder Drive Testing began that day and throughout the weekend for the three high priority Units as designated by the Dealership.

PFQS's original plan was to first verify the Drive Concern, but soon realized that Concern replication was difficult.
None of the Units ever exhibited a Stall in any drive mode during PFQS use.

On 6/17, the Inspection worksheet,

, was started to be used.

Over the course of the investigation, some Units (18%) had arrived to the Dealership that had been "Owner Determined" as resolved because of prior service actions performed by the St. Croix Metro Motors.
Being a small island, word of the "Ford Rep" presence prompted some Owners to return to the Dealership for a "Health Check" on their prior resolved Units.

Only one Unit was found by PFQS with the known Concern of "spider web" EVAP line restriction.

As cited, some Units had only part of the necessary Service actions completed. Also, interpretation of some data was either misunderstood, or the existing TSB diagnostics required additional

description. On this last point, details are provided throughout Sections below.

Fuel Quality Issues

The first priority Unit investigated was described as having a different Drive Concern of **"Hesitation after Cold Start"**.
Note that this Unit did **NOT** have the Concern of **Decell Stall** as part of the original listed complaint.

The heavy hesitation {lasting about 3 seconds} from a dead stop on a 30 degree upgrade acceleration, during a moderate engine temp range {approx 100F-160F} was replicated by PFQS. A fuel gauge had been installed along with a WDS VDR recorder. All parameters, including both fuel pressure and volume were confirmed as acceptable.
However, because this was a Returnless Fuel application, PFQS felt that his old method to check volume {filling 12oz bottle in 15 sec at idle} may not be valid.

As a result, the fuel filter was removed and blew backwards into a glass bottle:

Figure 6 Contaminated fuel, after sitting overnight

Figure 7 Bottom view of the fuel sample-Nasty Stuff

Figure 8 This is the fuel sample after the bottle is shaken, not stirred. This is what it looks like after you blow out the fuel filter.

PFQE then realized that perhaps local fuel is a negative influence in the generation of Decell Stalls, as well as possibly contributing to the Hesitation Concern.

From that point on, every Unit was inspected for restricted fuel filter/dirty fuel. 67% of inspected Units had restricted fuel filters and dirty fuel.

However, **32%** of the Units which had "Complete Service Actions" (see below), **PLUS** a new fuel filter, were **STILL** verified by PFQS **for the Hesitation Concern.**
Note that the latest PCM flash is included, and this includes some Units of which had the latest PCM Flash prior to PFQS visitation: the need for Adaptive Learning Strategy was NOT a factor for some of the repeatable **Hesitation** Concern Units.

It appears that the **replacement** of the restricted **fuel filter** did **not** resolve the **Hesitation** Concern.
However, **filter replacement** may be a **positive factor** in resolving the **Decell Stalls** Concern.

In defining "Complete Service Actions", PFQS includes a PCM Reflash to the latest available calibration level, the latest level EEC Relay, the latest level DPFE, a complete check of ALL grounds and connectors, proper evaluation of the EVAP Purge D.C. vs. FTP sensor voltage data and conformation of acceptable IAC D.C. values when observed during the PROPER conditions. Note that MAF replacement is not included unless the Owner cited a specific,

repetitive location during the Decell Stall event, implying local electrical "noise" generation (i.e. radio towers, etc).

New Concern of Moderate Engine Temp Hesitation discovered

PFQS then concluded: this repeatable Hesitation Concern could possibly be caused by one of two items, or perhaps both.

a. Local Fuel Quality (suspect volatility, not just the "dirt factor")
b. PCM Calibration

Please note that PFQS has no proof to indict either suspected root cause. PFQS is in communications with the St. Croix Service Manager for feedback of alternate fuel brand usage as recommended in an attempt to resolve those Units with the unresolved Hesitation Concern.
PFQS welcomes Engineering feedback on possible calibration issues and is willing to assist further.

In addition, a VDR recording was captured in this Hesitation drive mode on 6/25 on one Unit, which had all "Complete Service Actions" and a clean fuel filter. This data will be shared with Engineering in the very near future.

Procedural Omission in TSB 02-6-6
The Repairing Tech described the following prior repair effort.

The Tech stated that while following Step #4 of the above TSB, the EVAPVM (VMV Duty Cycle) percentage was not seen to change from Zero % at Idle (as specified by the TSB) after a one hour idle.
PFQS was able to replicate this scenario on the same Unit and also for a second Unit. The fuel tanks were above ¼ full.
During discussions with Engineering during his visitation, it was suggested that the vehicle be driven to prompt the Purge Process. As a result, the purge cycle started to increase.

While Step #4 described Purge Cycle function over 84%, it's diagnostic do not describe what must be done if the value does not change from Zero% while at prolonged Idle.

The Tech's interpretation of the lack of VMV Duty Cycle change from Zero % at Idle resulted in the ordering of a VMV. The Tech mentioned that if VMV replacement did not prompt a purge cycle DC increase from Zero%, a PCM would have been considered for order. Potential TNI Warranty for both the VMV (9C915) and the PCM (12A650) exists.

MAF and Related Hardware Issues

Three different issues were experienced during this inspection. Pls note that none involved the actual FUNCTION of the MAF. DTCs were NOT set, nor were inappropriate MAF voltage values witnessed.

However, Warranty, TNI and Real, have been generated as a result.

Item #1: The Tech described prior MAF replacements based upon the observation of the blistering of the MAF's Sensor's Surface:

Figure 9 Blister on the MAF' sensor's Case

Figure 10 Close up of the Blister

The Tech cited two replacements. The Parts Dept search only produced the one item photographed here. The Tech said the other one was "worst" with multiple blisters present.

Item #2: During PFQS inspection, one of the 3.0L Escapes MAF was found to be missing the imprinted part number on the sensor's plastic body:

Figure 11 MAF without a imprinted part number

A second Unit, a lone 2.0L Zetec Escape was presented for inspection. This Unit (which was not supposed to be part of the Study) was reviewed as a courtesy. It too did not have a PN imprinted on it. It was not replaced. However, the Tech felt it should be, because of the uncertainly of the level of the MAF component. This indicates that TNI Warranty may result for MAF due to the missing PN.

Item #3: During the removal of the MAF for one Unit for updates per the TSB (Owner reported Stalls in one particular location), the retaining nuts were found very tight. Hand tools, not power tools were used.
During the attempted removal, the studs started to unscrew from the airbox lid. One of the plastic bosses of the airbox stud broke as a result:

Figure 12 Airbox lid that contains MAF retaining studs

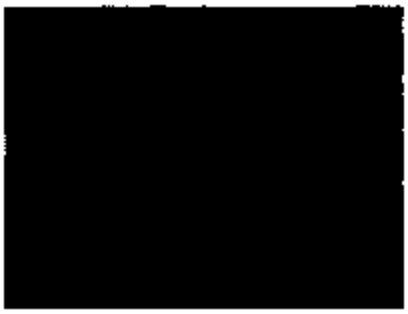

Figure 13 As stud walked out, it broke the case's boss

Figure 14 This is the rear view of the case's boss

Figure 15 A second stud walked out, but the case did not break. The witness marks are pliers on the threads.

At first PFQS suspected the nuts as over torque. A subsequent inspection found "Lock Tite" substance on the fine thread end of the studs. It is possible the adhesive is too strong.

As these MAFs are being replaced per the TSB, it is possible Warranty will be generated for the YL8U-9643-BC Airbox Lid.

Intake Airflow Control (IAC) Solenoid Duty Cycle Value Results

As part of requested Engineering data, IAC Duty Cycle values were monitored per Step #1 of TSB 02-8-6. Note that awareness of proper

conditions to determine acceptable IAC D.C. were not understood by all repair Techs interviewed. While IACs had been replaced on some Units, those were probably changed mainly as part of a general repair attempt, and not necessarily due to data acquisition.

As a result, some repeat Concern Units (46%) required IAC and in some instances, Throttle Body (TB) replacement.
Pls note, however, TBs were not available at the Dealership, and Engineering shipment did not arrive during PFQS visitation. The Engineering shipment of IACs did arrive and most were used.

Idle Air Control (IAC) Duty Cycles were found in 27% Units to be on the high end (greater than 40%) of the allowable spec.

30% of Units with IAC replacement did NOT realize a substantial change (less than 1%) for IAC D.C. value.
Other Units (8%) realized a desired small decrease in D.C., but their final value was still above acceptable range of 40% per the TSB, which would then require a TB replacement.

The high airflow D.C. after IAC replacement indicts either initial throttle body airflow set and/or plate sludge build-up.
Mileage range for unchanging D.C. values after IAC replacement were 2K-18K.

If the pending shipment of TBs arrive at Metro Motors St. Croix, PFQS is to be contacted. Concern Units will be requested for return and their TB will be replaced and then sent to PFQS, who in turn will return same to Engineering.

Additional IAC Diagnostic Improvements are provided below in the Recommendations Section.

<u>Recommendations</u>

1. A Market directed "Info Only" Oasis Broadcast Message should be generated to emphasize fuel filter/fuel quality as part of routine inspection when diagnosing all Driveability Concerns. Locations could include the Caribbean Islands and other

Markets were local Service Facilities practices come into question.

2. A review of TSV 02-8-6, Step #4 should be conducted for consideration of the inclusion of a drive cycle prior to inspection of EVAP Purge VMV Duty Cycle values. This drive cycle would only be used for those Units which do not show an increase from 0% at idle. A time factor should be provided to aid the Tech on when he should perform the drive cycle.
   Also, if fuel tank level is an influencing factor for valid EVAP evaluation, an acceptable fill range should be included in any TSB revision.

3. The three issues cited which involve MAF should be investigated by Ford Engineering and Visteon. MAF Sensor blistering, missing MAF PNs, and tight MAF retaining nut on airbox studs are subject.

4. A review of TSB 02-8-6, step #1 should be conducted to clarify and emphasize the definition of "no purge flow". This subtle reference was overlooked by all Techs interviewed. Specific reference, similar to Step #4 wording, which involves a PID definition and values (i.e.: observe IAC D.C. while EVAPVM is Zero%) is necessary to enable ALL Techs to properly diagnose the true need for IAC replacement.
   If there is confusion, the part will be replaced on an assumption, and not the result of data acquisition.

   Also, the converse is true: some Units will quickly START the purge cycle, before IAC D.C. could be read under proper conditions. A work around can be done by shutting off ignition and immediately restarting, and then waiting for all other conditions (RPM to return to 750) to be proper before reading IAC D.C. This additional procedure should be considered for inclusion to any TSB revision.

   A reference to the Catalyst Protection of a 50 RPM increase for a base idle of 800RPM should be included. Also, instructions to apply throttle briefly to reduce this RPM value to return to 750

RPM is necessary to allow the Techs to determine true IAC D.C. and is recommended for TSB revision inclusion.

5. A review for the need to spray insect/spider removal agent should be conducted. It is conceivable that the above TSB's Step #5 will temporarily remove a spider from the EVAP fresh air line, but there is nothing to prevent the return of another spider. Should we use something to stop the potential cycle of web build up?

I will be calling into the "Escape Stalls Team" 2PM conference call on 6/27/02 to discuss my inspection.

Gil Peplone
Powertrain Field Quality Engineer in South Florida

gpeplon@ford.com
Office 954-753-9989
Cell 954-242-2066

From:	Pepitone, Gil (J.)
Sent:	Thursday, June 27, 2002 9:38 AM
To:	Johnson, Jim (J.S.); Bilicki, John (J.R.); Corbett, Sandra (S.M.); Altoonian, Don (D.J.); Aynessazian, Kam (K.); Bauer, Scott (S.C.); Bhotwani, Kamal (K.); Blackburn, Thomas (T.J.); Bogema, John (P.); Chick, John (J.); Chih, Ming-Niu (M.N.); Chin, Darrel (D.); Corbett, Sandra (S.M.); Dalbo, Bob (R.J.); Rothweiler, Daniel (D.); De Pena, Juan (J.E.); Diaz, Timothy (T.P.); Fascetti, Bob (R.J.); Fournelle, Gilbert (G.); Freeland, Mark (M.); Giles, Stuart (S.); Goldsale, Renuka (R.V.); Grimes, Jeff (J.R.); Hansen, George (G.C.); Herr, George (G.J.); Hofman, Michael (M.V.); Holmes, Jeffrey (J.R.); Ishikawa, Jiyunichiro (J.); Jensen, Ted (T.E.); Mcdonald II, John (J.M.); Jordan, Donald (D.E.); King, Robert (R.F.); Kosko, Jeff (J.R.); Kwon, Soon (S.K.); Limtiaco, Steven (S.); Linde, Peter (P.A.); Liu, Jane (J.); Mandziuk, Roger (R.S.); Marok, Edmond (E.C.); Matese, John (J.); Maurer, James (J.B.); Mazzella, Gary (G.R.); Mooney, Larry (L.); Moorhouse, Scott (S.R.); Morgan, Tomiko (T.T.); Morishima, Shigeki (S.); Namatelahi, Sonya (S.); Noteboom, Jim (J.E.); Ortman, James (J.W.); Powers, Ken (K.W.); Price, Martin (M.); Raquepau, Alden (A.P.); Sanders, Muriel (M.S.); Shah, Kiran (K.C.); Shiraishi, Masaru (M.); Stilpenbauer, Jeffrey (J.R.); Suarez, Rhea (R.); Takasawa, Keith (K.D.); Takubo, Hiroichi (H.); Veenstra, Tim (T.W.); Wakenell, Ray (R.A.); Wettach, Bill (B.); Williams, Les (LHW.); Young, Lem (J.); Benintende, Robert (R.F.); Goering, Kimberly (K.L.); Suarez, Rhea (R.); Terzes, Laura (L.D.); Martin, Mike (M.S.); Wexler, Mark (M.A.); Amely, Felix (F.A.); Bradley, Joe (J.C.); Linde, Peter (P.A.); Goering, Kimberly (K.L.); Terzes, Laura (L.D.); Benintende, Robert (R.F.); Wexler, Mark (M.A.); Amely, Felix (F.A.)
Cc:	Pepitone, Gil (J.)
Subject:	RE: Inspection Sheet for St. Croix Vehicle Inspection

Good Morning: Mr. Jim Johnson informed me that he was unable to review the Inspection Sheet listed within my Summary Report on Escape Drive Concerns in the Virgin Islands. It appears my use of a "shortcut" prevented the Icon's data transfer.

I am providing it here as an aid. Pls review as you see fit.

[redacted]

St. Croix Escape
Vehicle Inspe...

Gil Pepitone
Powertrain Field Quality Specialist-"PFQS" in
South Florida
Office/Answering Machine: 954-753-9989
Cell Phone 954-242-2068
"With Warranty you are Paying for the Sins of the Past"

-----Original Message-----

From:	Pepitone, Gil (J.)
Sent:	Friday, June 14, 2002 6:50 PM
To:	Dalbo, Bob (R.J.)
Cc:	Sanders, Muriel (M.S.); Altoonian, Don (D.J.); Moorhouse, Scott (S.R.); DiAngelo, Renaldo (R.); Pepitone, Gil (J.)
Subject:	RE: Inspection Sheet for St. Croix Vehicle Inspection
Importance:	High

Hi Bob: ok, I will not.

Question: If I have high IAC DC, what should I do?
Clean the TB?
Turn the Throttle stop in to get o the desired 32% IAC DC?
If you want me to change the TB, I'm not prepared, since I d not have any, and I expect a long delay in getting TB from the States.

From: Fournelle, Gilbert (G.)
Sent: Thursday, January 16, 2003 8:05 AM
To: Hofman, Michael (M.V.); Nakano, Hideki (H.); Lawler, Dave (D.A.); Grimes, Jeff (J.R.); Price, Martin (M.); Moorhouse, Scott (S.R.); Hoshino, Jun (J.); Hofman, Michael (M.V.); Blackburn, Thomas (T.J.); Marlance, Tom (T.E.); Altoonian, Don (D.J.); Andy Jones (E-mail); Bauer, Scott (S.C.); Bernie Nikolai (E-mail); Bhotwani, Kamal (K.); Bogema, John (P.); Cary Powell (E-mail); Chick, John (J.); Chih, Ming-Niu (M.N.); Chin, Darrel (D.); Corbett, Sandra (S.M.); Dalbo, Bob (R.J.); De Pena, Juan (J.E.); Diez, Timothy (T.P.); Duvall, Allen (A.W.); Fasoldt, Bob (R.J.); Fournelle, Gilbert (G.); Freeland, Mark (M.); Giles, Stuart (S.); Gokhale, Renuka (R.V.); Goodwin, William (W.R.); Grewal, Bill (B.S.); Hansen, George (G.C.); Herr, George (G.J.); Holmes, Jeffrey (J.R.); Ishikawa, Jiyunichiro (J.); Jensen, Ted (T.E.); John McDonald (E-mail); Jordan, Donald (D.E.); Kanai, Shinji (S.); Koeko, Jeff (J.R.); Le, Dzung (D.H.); Limtiaco, Steven (S.); Linde, Peter (P.A.); Liu, Jane (J.); Marok, Edmond (E.C.); Matese, John (J.); Maurer, James (J.B.); Mazzella, Gary (G.R.); McCarthy, Fran (F.); McGee, Brett (B.L.); Mooney, Larry (L.); Morishima, Shigeki (S.); Naveed Khan (E-mail); Nematollahi, Sonya (S.); Noteboom, Jim (J.E.); Ortman, James (J.W.); Ott, David (D.J.); Powers, Ken (K.W.); Raquepau, Alden (A.P.); Rothweiler, Daniel (D.); Shah, Kiran (K.C.); Shiraishi, Masaru (M.); Stilpenbauer, Jeffrey (J.R.); Suarez, Rhea (R.); Takasawa, Keith (K.D.); Takubo, Hiroichi (H.); Veenstra, Tim (T.W.); Wakanell, Ray (R.A.); Wettach, Bill (B.); Williams, Les (L.H.W.); Yeung, Lam (.)
Subject: 3.0L U204 phantom stall meeting agenda 1/16/03

1/16/03 2:00pm MEETING AGENDA

- **Reports from Field** *2:00-2:10*
  - **Don Altoonian**
  - **Dan Rothweiler**
  - **Scott Moorhouse**
  - **Steve Limtiaco**
  - **Marti Price**
  - **Jim Noteboom**
- Issue of reprogramming a new (MPC-161) PCM with the old (MPC-160) calibration *2:15-2:25*
  - Update from Tom Marlance on possible software fix
  - Discuss SSM if necessary
- Walk-in *2:25-2:45*

KCAP Implementation Timing

KCAP Actions	Concern #	Revised Part #	Implementation Timing
1. Omron to Hella Relays	C11293441	No Change	07/27/01
2. Updated production calibration	C11299149	See concern	1/16/02 (3 out of 7)
3. Inverted delta status- G101 ground		N/A	01/15/02
4. Inverted delta status- G100 ground	C11294758	N/A	
5. Inverted delta status- G104/G105	C11294758	N/A	
6. Implementation of robust MAF	C11299286	1L2F-12B579-BA	05/30/02
7. IAC change from Guide A to Pinned Pintle (CRP2 action)	C11252737	1L8E-9F715-AA	5/30/02 Cleveland
			9/16/02 KCAP

8. 3.0L dPFE change from Kavlico to Motorola	C11262413	2F1Z-9J460-AA	07/22/02	
9. 2.0L dPFE change from Kavlico to Motorola	C11274132	2F1Z-9J460-AA	07/22/02	
10. Revised vent line location	C11326381		09/09/02	
11. Technical Service Bulletin (TSB 02-08-06)	N/A	N/A	4/24/02	
12. Special Service Message (SSM 13589)	N/A	N/A	1/29/02	
13. Internal Service Message (ISM 02-01-070) - pre-TSB	N/A	N/A	2/5/02	
14. ISM 02-05-017 - post-TSB	N/A	N/A	5/6/02	
15. ISM 02-05-043 - Add MAF Gain to ISM 02-05-017	N/A	N/A	5/20/02	
16. TSB 02-11-06 - Modify Calibration Wording	N/A	N/A	6/5/02	
17. ISM 02-06-025 - Update TSB Reference	N/A	N/A	6/14/02	
18. TSB 02-23-1 - Incorporate some of ISM & improve wording		N/A	N/A	11/14/02
19. IAC changed to Pinned Pintle for service (released)	C11390555	1L8Z-9F715-AA	9/13/02	
Estimated availability is 11/08/02				
20. Calibration Enhancements	C11390580	See concern	9/11/02 for N.A.	
21. EEC w/modified capacitor - production	C11371349	See concern	8/12/02 Est.	
22. EEC w/modified capacitor - service	C11350478	See concern	8/12/02 Est.	
23. Inverted delta status - G102/103	C11394835	N/A	TBD	

dial in info:

toll free: 1-866-227-7015
Ford net: 954-1206
International: 1-630-893-6145
pass code: 8402370#
moderator code: 3457370

Thursday, January 16th
TEE building CR#1

Regards,

Gilbert Faunelle
V6 U204 Calibration Engineering
1AE27 Truck Engine Engineering (TEE)
Phone:(313)3904968 Fax:(313)3231786

From: Marlanos, Tom (T.E.)
Sent: Thursday, January 16, 2003 8:12 AM
To: Fournelle, Gilbert (G.); Hofman, Michael (M.V.); Nakano, Hideki (H.); Lawler, Dave (D.A.); Grimes, Jeff (J.R.); Price, Martin (M.); Moorhouse, Scott (S.R.); Hoshino, Jun (J.); Hofman, Michael (M.V.); Blackburn, Thomas (T.J.); Altoonian, Don (D.J.); Andy Jones (E-mail); Bauer, Scott (S.C.); Bernie Nikolai (E-mail); Bhojwani, Kamal (K.); Bogema, John (P.); Cary Powell (E-mail); Chick, John (J.); Chih, Ming-Niu (M.N.); Chin, Darrel (D.); Corbett, Sandra (S.M.); Dalbo, Bob (R.J.); De Pena, Juan (J.E.); Diaz, Timothy (T.P.); Duvall, Allen (A.W.); Fascett, Bob (R.J.); Freeland, Mark (M.); Giles, Stuart (S.); Gokhale, Renuka (R.V.); Goodwin, William (W.R.); Grewal, Bill (B.S.); Hansen, George (G.C.); Herr, George (G.J.); Holmes, Jeffrey (J.R.); Ichikawa, Jyunichiro (J.); Jensen, Ted (T.E.); John McDonald (E-mail); Jordan, Donald (D.E.); Kanai, Shinji (S.); Koeko, Jeff (J.R.); La, Dzung (D.H.); Limtiaco, Steven (S.); Linde, Peter (P.A.); Liu, Jane (J.); Marck, Edmond (E.C.); Mateos, John (J.); Maurer, James (J.B.); Mazzella, Gary (G.R.); McCarthy, Fran (F.); McGee, Brett (B.L.); Mooney, Larry (L.); Morishima, Shigeki (S.); Naveed Khan (E-mail); Nematollahi, Sonya (S.); Noteboom, Jim (J.E.); Ortman, James (J.W.); Ott, David (D.J.); Powers, Ken (K.W.); Raquepau, Alden (A.P.); Rothweiler, Daniel (D.); Shah, Kiran (K.C.); Shiraishi, Masaru (M.); Stilgenbauer, Jeffrey (J.R.); Suarez, Rhae (R.); Takasawa, Keith (K.D.); Takubo, Hiroichi (H.); Veenstra, Tim (T.W.); Wakenell, Ray (R.A.); Wettach, Bill (B.); Williams, Les (L.H.W.); Young, Lem (.)
Subject: RE: 3.0L U204 phantom stall meeting agenda 1/16/03

I will be unable to attend this meeting. However, we may have found a problem with our tool that has resulted in the reflashing of the old module's calibration. We are conducting a test that will be concluded tomorrow (1/17). Based on the results of that test, I will make recommendations for the current released WDS version for the U204 group to decide upon.

If the results come back as expected, I would assume that an SSM covering the existing WDS release would be in order and that the next release B24 which should be available in late February, should fix the issue completely. And not update would be required for the existing TSB.

Again, I won't have a definite answer until tomorrow.

Tom

-----Original Message-----
From: Fournelle, Gilbert (G.)
Sent: Thursday, January 16, 2003 6:05 AM
To: Hofman, Michael (M.V.); Nakano, Hideki (H.); Lawler, Dave (D.A.); Grimes, Jeff (J.R.); Price, Martin (M.); Moorhouse, Scott (S.R.); Hoshino, Jun (J.); Hofman, Michael (M.V.); Blackburn, Thomas (T.J.); Marlanos, Tom (T.E.); Altoonian, Don (D.J.); Andy Jones (E-mail); Bauer, Scott (S.C.); Bernie Nikolai (E-mail); Bhojwani, Kamal (K.); Bogema, John (P.); Cary Powell (E-mail); Chick, John (J.); Chih, Ming-Niu (M.N.); Chin, Darrel (D.); Corbett, Sandra (S.M.); Dalbo, Bob (R.J.); De Pena, Juan (J.E.); Diaz, Timothy (T.P.); Duvall, Allen (A.W.); Fascett, Bob (R.J.); Fournelle, Gilbert (G.); Freeland, Mark (M.); Giles, Stuart (S.); Gokhale, Renuka (R.V.); Goodwin, William (W.R.); Grewal, Bill (B.S.); Hansen, George (G.C.); Herr, George (G.J.); Holmes, Jeffrey (J.R.); Ichikawa, Jyunichiro (J.); Jensen, Ted (T.E.); John McDonald (E-mail); Jordan, Donald (D.E.); Kanai, Shinji (S.); Koeko, Jeff (J.R.); La, Dzung (D.H.); Limtiaco, Steven (S.); Linde, Peter (P.A.); Liu, Jane (J.); Marck, Edmond (E.C.); Mateos, John (J.); Maurer, James (J.B.); Mazzella, Gary (G.R.); McCarthy, Fran (F.); McGee, Brett (B.L.); Mooney, Larry (L.); Morishima, Shigeki (S.); Naveed Khan (E-mail); Nematollahi, Sonya (S.); Noteboom, Jim (J.E.); Ortman, James (J.W.); Ott, David (D.J.); Powers, Ken (K.W.); Raquepau, Alden (A.P.); Rothweiler, Daniel (D.); Shah, Kiran (K.C.); Shiraishi, Masaru (M.); Stilgenbauer, Jeffrey (J.R.); Suarez, Rhae (R.); Takasawa, Keith (K.D.); Takubo, Hiroichi (H.); Veenstra, Tim (T.W.); Wakenell, Ray (R.A.); Wettach, Bill (B.); Williams, Les (L.H.W.); Young, Lem (.)
Subject: 3.0L U204 phantom stall meeting agenda 1/16/03

1/16/03 2:00pm MEETING AGENDA

- **Reports from Field** *2:00-2:10*
  - **Don Altoonian**
  - **Dan Rothweiler**
  - **Scott Moorhouse**

- Steve Linstiaco
- Marti Price
- Jim Notaboom

- Issue of reprogramming a new (MPC-161) PCM with the old (MPC-160) calibration — 2:15-2:25
  - Update from Tom Marianos on possible software fix
  - Discuss SSM if necessary

- Walk-in — *2:25-2:45*

KCAP Implementation Timing

KCAP Actions	Concern #	Revised Part #	Implementation Timing
1. Omron to Hella Relays	C11293441	No Change	07/27/01
2. Updated production calibration	C11299149	See concern	1/16/02 (3 out of 7)
3. Inverted delta status- G101 ground		N/A	01/15/02
4. Inverted delta status- G100 ground	C11294758	N/A	
5. Inverted delta status- G104/G105	C11294758	N/A	
6. Implementation of robust MAF	C11299286	1L2F-12B579-BA	05/30/02
7. IAC change from Guide A to Pinned Pintle (CEP2 action)	C11252737	1L8E-9F715-AA	8/30/02 Cleveland
			9/16/02 KCAP
8. 3.0L dPFE change from Kavlico to Motorola	C11262413	2F1Z-9J460-AA	07/22/02
9. 2.0L dPFE change from Kavlico to Motorola	C11274132	2F1Z-9J460-AA	07/22/02
10. Revised vent line location	C11326381		09/09/02
11. Technical Service Bulletin (TSB 02-08-06)	N/A	N/A	4/24/02
12. Special Service Message (SSM 15589)	N/A	N/A	1/29/02
13. Internal Service Message (ISM 02-01-070) - pre-TSB	N/A	N/A	2/5/02
14. ISM 02-05-017 - post-TSB	N/A	N/A	5/6/02
15. ISM 02-05-043 - Add MAF Gait to ISM 02-05-017	N/A	N/A	5/20/02
16. TSB 02-11-06 - Modify Calibration Wording	N/A	N/A	6/5/02
17. ISM 02-06-025 - Update TSB Reference	N/A	N/A	6/14/02
18. TSB 02-23-1 - Incorporate some of ISM & improve wording		N/A	N/A 11/14/02
19. IAC changed to Pinned Pintle for service (released)	C11390555	1L8Z-9F715-AA	9/13/02
Estimated availability is 11/06/02			
20. Calibration Enhancements	C11390580	See concern	9/11/02 for N.A.
21. EEC w/modified capacitor - production	C11371349	See concern	8/12/02 Est.
22. EEC w/modified capacitor - service	C11350478	See concern	8/12/02 Est.
23. Inverted delta status - G102/103	C11394835	N/A	TBD

dial in info:

toll free: 1-866-227-7015 — 8662-627 2976

Ford net: 954-1208
International: 1-630-693-6145
pass code: 84023704
moderator code: 3457370

Thursday, January 16th
TEE building CR#1

Regards,

Gilbert Fournelle
V6 U204 Calibration Engineering
1AE27 Truck Engine Engineering (TEE)
Phone:(313)3904966 Fax:(313)3231766

EP82-627 23677

From: Fournelle, Gilbert (G.)
Sent: Tuesday, January 21, 2003 9:17 AM
To: Altoonian, Don (D.J.); Andy Jones (E-mail); Bauer, Scott (S.C.); Bernie Nikolai (E-mail); Bholwani, Kamal (K.); Blackburn, Thomas (T.J.); Bopema, John (P.); Cary Powell (E-mail); Chick, John (J.); Chih, Ming-Niu (M.N.); Chin, Darrel (D.); Corbett, Sandra (S.M.); Delbo, Bob (R.J.); De Pena, Juan (J.E.); Diez, Timothy (T.P.); Duvall, Allen (A.W.); Fedeteli, Bob (R.J.); Fournelle, Gilbert (G.); Freeland, Mark (M.); Giles, Stuart (S.); Gokhale, Renuka (R.V.); Goodwin, William (W.R.); Grewal, Bill (B.S.); Grimes, Jeff (J.R.); Hansen, George (G.C.); Herr, George (G.J.); Holman, Michael (M.V.); Holmes, Jeffrey (J.R.); Hoshino, Jun (J.); Ishikawa, Jiyunichiro (J.); Jensen, Ted (T.E.); John McDonald (E-mail); Jordan, Donald (D.E.); Kanal, Shinji (S.); Koeko, Jeff (J.R.); Lawler, Dave (D.A.); Le, Dzung (D.H.); Limtiaco, Steven (S.); Linde, Peter (P.A.); Liu, Jane (J.); Marek, Edmond (E.C.); Marianos, Tom (T.E.); Matesa, John (J.); Maurer, James (J.B.); Mazzella, Gary (G.R.); McGee, Brett (B.L.); Mooney, Larry (L.); Moorhouse, Scott (S.R.); Morishima, Shigeki (S.); Nakano, Hideki (H.); Naveed Khan (E-mail); Nematollahi, Sonya (S.); Noteboom, Jim (J.E.); Ortman, James (J.W.); Ott, David (D.J.); Powers, Ken (K.W.); Price, Martin (M.); Raquepeu, Alden (A.P.); Rothweiler, Daniel (D.); Shah, Kiran (K.C.); Shiraishi, Masaru (M.); Stiipenbauer, Jeffrey (J.R.); Suarez, Rhae (R.); Takasawa, Keith (K.D.); Takubo, Hiroichi (H.); Veenstra, Tim (T.W.); Wakanell, Ray (R.A.); Wettach, Bill (B.); Williams, Lee (LHW.); Yeung, Lam (.)
Subject: 3.0L U203 phantom stall meeting minutes

1/16/02 2:00pm MEETING AGENDA

Attendees:

Don Altoonian
Marti Price
Rhae Suarez
Steve Limtiaco
John McDonald
Scott Baner

- **Reports from Field**
  - No new stall complaints from any field engineer or hotline
  - Marti price reported that WDS asks for an M number when a reflashing procedure is performed. The M number refers to a Mazda bulletin which explains which problem the reflash is addressing. This has been occurring since release B22. For Ford vehicles, there should be a refrence to the TSB (2-23-1) instead of a Mazda bulleting

- **Issue of reprogramming a new (MPC-161) PCM with the old (MPC-160) calibration**

  - Tom Marianos tried out new data fix for the latest WDS Releases (B22NM.9 and B22N.5). It appears to work fine now and no revision of the TSBs will be required for the updates. Pending further confirmation, an SSM will be needed to notify technicians to update WDS to this latest version before conducting the PCM replacement/reflash.

KCAP Implementation Timing

KCAP Actions	Concern #	Revised Part #	Implementation Timing
1. Omron to Hella Relays	C11293441	No Change	07/27/01
2. Updated production calibration	C11299149	See concern	1/16/02 (3 out of 7)

3. Inverted delta status- G101 ground		N/A	01/15/02
4. Inverted delta status- G100 ground	C11294758	N/A	
5. Inverted delta status- G104/G105	C11294758	N/A	
6. Implementation of robust MAF	C11299286	1L2F-12B579-BA	05/30/02
7. IAC change from Guide A to Finned Pintle (CEP2 action)	C11252737	1L8E-9F715-AA	8/30/02 Cleveland
			9/16/02 KCAP
8. 3.0L dPFE change from Kavlico to Motorola	C11262413	2F1Z-9J460-AA	07/22/02
9. 2.0L dPFE change from Kavlico to Motorola	C11274132	2F1Z-9J460-AA	07/22/02
10. Revised vent line location	C11326381		09/09/02
11. Technical Service Bulletin (TSB 02-08-06)	N/A	N/A	4/24/02
12. Special Service Message (SSM 15589)	N/A	N/A	1/29/02
13. Internal Service Message (ISM 02-01-070) - pre-TSB	N/A	N/A	2/5/02
14. ISM 02-05-017 - post-TSB	N/A	N/A	5/6/02
15. ISM 02-05-043 - Add MAF Gskt to ISM 02-05-017	N/A	N/A	5/20/02
16. TSB 02-11-06 - Modify Calibration Wording	N/A	N/A	6/5/02
17. ISM 02-06-025 - Update TSB Reference	N/A	N/A	6/14/02
18. TSB 02-23-1 - Incorporate some of ISM & improve wording		N/A	N/A 11/14/02
19. IAC changed to Finned Pintle for service (released)	C11390555	1L8Z-9F715-AA	9/13/02
Estimated availability is 11/08/02			
20. Calibration Enhancements	C11390580	See concern	9/11/02 for N.A.
21. EEC w/modified capacitor - production	C11371349	See concern	8/12/02 Est.
22. EEC w/modified capacitor - service	C11350478	See concern	8/12/02 Est.
23. Inverted delta status - G102/103	C11394835	N/A	TBD

Regards,

Gilbert Fournelle
V6 U204 Calibration Engineering
1AE27 Truck Engine Engineering (TEE)
Phone:(313)3904968 Fax:(313)3231786

From:	Williams, Lee (LHW.)
Sent:	Monday, February 04, 2002 8:31 PM
To:	Altoonian, Don (D.J.); Amanda, Harry (H.F.); Badgley, Joel (J.K.); Bauer, Scott (S.C.); Bhojwani, Kamal (K.); Blackburn, Thomas (T.J.); Bogema, John (P.); Cary Powell; Chick, John (J.); Chih, Ming-Niu (M.N.); Chin, Darrel (D.); Corbett, Sandra (S.M.); Dalbo, Bob (R.J.); De Pena, Juan (J.E.); Diaz, Timothy (T.P.); Fascetti, Bob (R.J.); Fournelle, Gilbert (G.); Giles, Stuart (S.); Gokhale, Renuka (R.V.); Hansen, George (G.C.); Herr, George (G.J.); Holman, Michael (M.V.); Holmes, Jeffrey (J.R.); Hurley, Robert (R.E.); Ishikawa, Jiyunichiro (J.); Jensen, Ted (T.E.); John McDonald (E-mail); Jones, Andy; Jordan, Donald (D.E.); Kanai, Shinji (S.); King, Robert (R.F.); Klostermann, Eric (E.); Kwon, Soon (S.K.); Limtiaco, Steven (S.); Linde, Peter (P.A.); Liu, Jane (J.); Lushnen, Eric (E.A.); Marok, Edmond (E.C.); Mebes, John (J.); Mazzella, Gary (G.R.); Mooney, Larry (L.); Moorhouse, Scott (S.R.); Morgan, Tom; Morishima, Shigeki (S.); Naveed Khan; Nematollahi, Sonya (S.); Nikolai, Bernie; Noteboom, Jim (J.E.); Ortman, James (J.W.); Owens, Karen (K.E.); Powell, Cary; Powers, Ken (K.W.); Price, Martin (M.); Raquepau, Alden (A.P.); Rothweiler, Daniel (D.); Shah, Kiran (K.C.); Shiraishi, Masaru (M.); Stilgenbauer, Jeffrey (J.R.); Suarez, Rhea (R.); Sullivan, Jamie (J.P.); Takesawa, Keith (K.D.); Takubo, Hiroichi (H.); Vecchio, Anne Marie (A.); Wakenell, Ray (R.A.); Williams, Lee (LHW.); Williamson, David (D.E.); Young, Lem (.)
Subject:	Location for stalls meeting 2/5/02

If you are attending the Stalls meeting tomorrow at the TEE bldg, we will be using Conference Room #1.

Regards,
Lee Williams
For More, Count on Lee
U204 3.0L Powertrain Calibration
Truck Engine Engineering, Suite 1AE20
Phone: (313)33-72503
Fax: (313) 32-31786

From:	Williams, Lee (LHW.)
Sent:	Monday, February 18, 2002 10:50 AM
To:	Altoonian, Don (D.J.); Amenda, Harry (H.F.); Beddley, Joel (J.K.); Bauer, Scott (S.C.); Bhojwani, Kamal (K.); Blackburn, Thomas (T.J.); Bogema, John (P.); Cary Powell; Chick, John (J.); Chih, Ming-Niu (M.N.); Chin, Darrel (D.); Corbett, Sandra (S.M.); Dalbo, Bob (R.J.); De Pena, Juan (J.E.); Diaz, Timothy (T.P.); Fascetti, Bob (R.J.); Fourmelle, Gilbert (G.); Giles, Stuart (S.); Gokhale, Renuka (R.V.); Hansen, George (G.C.); Herr, George (G.J.); Holman, Michael (M.V.); Holmes, Jeffrey (J.R.); Hurley, Robert (R.E.); Ichikawa, Jiyunichiro (J.); Jensen, Ted (T.E.); John McDonald (E-mail); Jones, Andy; Jordan, Donald (D.E.); Kanal, Shinji (S.); King, Robert (R.F.); Klostermann, Eric (E.); Kwon, Soon (S.K.); Limtiaco, Steven (S.); Linde, Peter (P.A.); Liu, Jane (J.); Luehrsen, Eric (E.A.); Marok, Edmond (E.C.); Matesa, John (J.); Maurer, James (J.B.); Mazzella, Gary (G.R.); Mooney, Larry (L.); Moorhouse, Scott (S.R.); Morgan, Tom; Morishima, Shigeki (S.); Naveed Khan; Nematollahi, Sonya (S.); Nikolai, Bernie; Notsboom, Jim (J.E.); Orman, James (J.W.); Powell, Cary; Powers, Ken (K.W.); Price, Martin (M.); Raquepau, Alden (A.P.); Rothweiler, Daniel (D.); Shah, Kiran (K.C.); Shiraishi, Masaru (M.); Silljenbauer, Jeffrey (J.R.); Suarez, Rhea (R.); Sullivan, Jamie (J.P.); Takasawa, Keith (K.D.); Takubo, Hiroichi (H.); Vecchio, Anne Marie (A.); Wajcenell, Ray (R.A.); Williams, Lee (LHW.); Williamson, David (D.E.); Yeung, Lam (.)
Subject:	Tuesday Staff Meetings Cancelled
Importance:	High

Hello Everyone:

The Tuesday Staff meetings will be cancelled. We will go to 1 meeting every week now (just meet on Thursdays at 10 AM). This is effective immediately.

Thank you,
Lee Williams

Regards,
Lee Williams
For More, Count on Lee
U204 3.0L Powertrain Calibration
Truck Engine Engineering, Suite 1AE20
Phone: (313)33-72503
Fax: (313) 32-31786

From: Hermann, Thomas (T.J.)
Sent: Wednesday, February 20, 2002 1:03 PM
To: Williams, Les (LHW.); Altoonian, Don (D.J.); Amanda, Harry (H.F.); Badgley, Joel (J.K.); Bauer, Scott (S.C.); Bhojwani, Kamal (K.); Blackburn, Thomas (T.J.); Bogema, John (P.); 'Cary Powell'; Chick, John (J.); Chih, Ming-Niu (M.N.); Chin, Darrel (D.); Corbett, Sandra (S.M.); Dalbo, Bob (R.J.); De Pena, Juan (J.E.); Diez, Timothy (T.P.); Fascetti, Bob (R.J.); Fournelle, Gilbert (G.); Giles, Stuart (S.); Goldvale, Renuka (R.V.); Hansen, George (G.C.); Herr, George (G.J.); Hofman, Michael (M.V.); Holmes, Jeffrey (J.R.); Hurley, Robert (R.E.); Ichikawa, Jiyunichiro (J.); Jensen, Ted (T.E.); John McDonald (E-mail); 'Jones, Andy'; Jordan, Donald (D.E.); Kanal, Shinji (S.); King, Robert (R.F.); Klostermann, Eric (E.); Kwon, Soon (S.K.); Limtiaco, Steven (S.); Linde, Peter (P.A.); Liu, Jane (J.); Lushnaen, Eric (E.A.); Marek, Edmond (E.C.); Matesa, John (J.); Maurer, James (J.B.); Mazzella, Gary (G.R.); Mooney, Larry (L.); Moorhouse, Scott (S.R.); 'Morgan, Tom'; Morishima, Shigeki (S.); 'Nevaad Khan'; Nematollahi, Sonya (S.); 'Nikolai, Bernie'; Noteboom, Jim (J.E.); Ortman, James (J.W.); 'Powell, Cary'; Powers, Ken (K.W.); Price, Martin (M.); Raquepau, Aiden (A.P.); Rothweiler, Daniel (D.); Shah, Kiran (K.C.); Shiraishi, Masaru (M.); Stigenbauer, Jeffrey (J.R.); Suarez, Rhae (R.); Sullivan, Jamie (J.P.); Takasawa, Keith (K.D.); Takubo, Hiroichi (H.); Vecchio, Anne Marie (A.); Wakenell, Ray (R.A.); Williamson, David (D.E.); Yeung, Lam (.)
Cc: Diez, Timothy (T.P.)
Subject: RE: Meeting Minutes: EMC PSW Results for current production Kavlico DPFE

Les, to further clarify what I said.

Current production Kavlico DPFE sensor should not contribute to U204 stalling in the field due to RFI.

On the issue of coupled noise from the wiring harness, the component EMC PSW data does not indicate any issues that would contribute to stalls (it passes the tests) however that does not mean a conducted issue could not exist from an unusual circumstance (such as ignition secondary breakdown or static build up on ungrounded parts).

----Original Message----
From: Williams, Les (LHW.)
Sent: Wednesday, February 20, 2002 12:06 PM
To: Altoonian, Don (D.J.); Amanda, Harry (H.F.); Badgley, Joel (J.K.); Bauer, Scott (S.C.); Bhojwani, Kamal (K.); Blackburn, Thomas (T.J.); Bogema, John (P.); Cary Powell; Chick, John (J.); Chih, Ming-Niu (M.N.); Chin, Darrel (D.); Corbett, Sandra (S.M.); Dalbo, Bob (R.J.); De Pena, Juan (J.E.); Diez, Timothy (T.P.); Fascetti, Bob (R.J.); Fournelle, Gilbert (G.); Giles, Stuart (S.); Goldvale, Renuka (R.V.); Hansen, George (G.C.); Herr, George (G.J.); Hofman, Michael (M.V.); Holmes, Jeffrey (J.R.); Hurley, Robert (R.E.); Ichikawa, Jiyunichiro (J.); Jensen, Ted (T.E.); John McDonald (E-mail); Jones, Andy; Jordan, Donald (D.E.); Kanal, Shinji (S.); King, Robert (R.F.); Klostermann, Eric (E.); Kwon, Soon (S.K.); Limtiaco, Steven (S.); Linde, Peter (P.A.); Liu, Jane (J.); Lushnaen, Eric (E.A.); Marek, Edmond (E.C.); Matesa, John (J.); Maurer, James (J.B.); Mazzella, Gary (G.R.); Mooney, Larry (L.); Moorhouse, Scott (S.R.); Morgan, Tom; Morishima, Shigeki (S.); Nevaad Khan; Nematollahi, Sonya (S.); Nikolai, Bernie; Noteboom, Jim (J.E.); Ortman, James (J.W.); Powell, Cary; Powers, Ken (K.W.); Price, Martin (M.); Raquepau, Aiden (A.P.); Rothweiler, Daniel (D.); Shah, Kiran (K.C.); Shiraishi, Masaru (M.); Stigenbauer, Jeffrey (J.R.); Suarez, Rhae (R.); Sullivan, Jamie (J.P.); Takasawa, Keith (K.D.); Takubo, Hiroichi (H.); Vecchio, Anne Marie (A.); Wakenell, Ray (R.A.); Williams, Les (LHW.); Williamson, David (D.E.); Yeung, Lam (.)
Cc: Hermann, Thomas (T.J.); Diez, Timothy (T.P.)
Subject: Meeting Minutes: EMC PSW Results for current production Kavlico DPFE

Meeting Minutes

Attendees:
Bob Dalbo (U204 V6 Calibration Supervisor)
Gilbert Fournelle (U204 V6 Calibration)
Les Williams (U204 Calibration)
Tom Hermann (EMC Supervisor)
Tim Diez (EMC)

On Friday February 15, 2002 EMC PSW test data for current production Kavlico DPFE sensor was reviewed.

Thomas Hennann has independently investigated the behavior of this sensor. Based on his investigations and this data, he concluded that the current production Kavlico DPFE sensor should not contribute to U204 stalling in the field due to RFI and coupled noise from the wiring harness.

Regards,
Les Williams
For More, Count on Les
U204 3.0L Powertrain Calibration
Truck Engine Engineering, Suite 1AE20
Phone: (313)33-72503
Fax: (313) 32-31786

From:	Hofman, Michael (M.V.)
Sent:	Monday, February 25, 2002 8:34 PM
To:	Takasawa, Keith (K.D.)
Cc:	Corbett, Sandra (S.M.); Fascetti, Bob (R.J.); Alashe, Waheed (W.O.); Dalbo, Bob (R.J.)
Subject:	FW: Escape Email

[redacted] - On this one, it sounds like it could be the slow start / no start syndrome where the Fuel Pressure regulator in the PCM becomes contaminated (I'd ask if it is always on the first start in the morning / after a long soak - if so fuel line bleeds down and fuel system takes a few seconds of cranking to prime - no more than 5-6 seconds however).

If its random, I'd suggest that the customer have the dealer check for any codes stored in the PCM and have the dealer check the fuel system for pressure decay on shutdown.

Beyond that I'd start to look at electrical - probably the best thing there is to have the dealer work with us to get a flight recorder installed and we can possible capture the cranks / no start event! Let me know if /when you'd like us involved and we'll take it from there!!
Thx - Mike

cc's - any other ideas?

-----Original Message-----
From: Takasawa, [redacted]
Sent: Monday, February 25, 2002 12:24 PM
To: Hofman, Michael (M.V.)
Subject: FW: Escape Email

Any advice you can give me to pass on?

Regards,

Keith Takasawa

Escape/Tribute Chief Engineer
PDC 2HD70
MD401
PH: (313) 322-5675
FAX: (313) 248-8599
E-MAIL: KTAKASAW@FORD.COM
TEXT PAGE: [redacted]

-----Original Message-----
From: Escape Email From Website [mailto:escapecc@ford.com]
Sent: Sunday, February 24, 2002 8:42 PM
To: escapecc@ford.com
Subject: Escape Email

name: [redacted]
address:
city:
state:
zipcode:

phonenumber:
email: [redacted]
vehiclemodel: Escape
vehicleyear: 2002

comments

Hello,
I recently bought a new Escape, and I have most definately enjoyed the first 500 miles - this is a great vehicle. Although, there is one thing that is of concern. On two occasions, I have had a hard time starting the escape - both times the vehicle has been on a slight decline. On both occasions, I turn the ignition and it just cranks. I stop, wait ten seconds, and try again....nothing happens it just once again cranks. So, on the third try I depress the accelerator and the vehicle starts. Can you tell me what is going on?
Best Regards,

[redacted]

From:	Williams, Lee (LHW.)
Sent:	Tuesday, February 26, 2002 9:51 AM
To:	Alloonian, Don (D.J.); Amenda, Harry (H.F.); Badgley, Joel (J.K.); Bauer, Scott (S.C.); Bhojwani, Kamal (K.); Blackburn, Thomas (T.J.); Bozema, John (P.); Cary Powell; Chick, John (J.); Chih, Ming-Niu (M.N.); Chin, Darrel (D.); Corbett, Sandra (S.M.); Dalbo, Bob (R.J.); De Pena, Juan (J.E.); Diez, Timothy (T.P.); Fascetti, Bob (R.J.); Fourmello, Gilbert (G.); Giles, Stuart (S.); Gokhale, Renuka (R.V.); Hansen, George (G.C.); Herr, George (G.J.); Hofman, Michael (M.V.); Holmes, Jeffrey (J.R.); Hurley, Robert (R.E.); Ishikawa, Jiyunichiro (J.); Jensen, Ted (T.E.); John McDonald (E-mail); Jones, Andy; Jordan, Donald (D.E.); Kanal, Shinji (S.); King, Robert (R.F.); Klostermann, Eric (E.); Kwon, Soon (S.K.); Limtiaco, Steven (S.); Lincle, Peter (P.A.); Liu, Jane (J.); Lushreen, Eric (E.A.); Marok, Edmond (E.C.); Matesa, John (J.); Maurer, James (J.S.); Mazzella, Gary (G.R.); Mooney, Larry (L.); Moorhouse, Scott (S.R.); Morgan, Tom; Morishima, Shigeki (S.); Naveed Khan; Nemetollahi, Sonya (S.); Nikolai, Bernie; Noteboom, Jim (J.E.); Ortman, James (J.W.); Powell, Cary; Powers, Ken (K.W.); Price, Martin (M.); Raquepau, Alden (A.P.); Rothwaller, Daniel (D.); Sanders, Muriel (M.S.); Shah, Kiran (K.C.); Shiraishi, Masaru (M.); Stilgenbauer, Jeffrey (J.R.); Suarez, Rhae (R.); Sullivan, Jamie (J.P.); Takasawa, Keith (K.D.); Takubo, Hiroichi (H.); Vecchio, Anne Marie (A.); Wakenell, Ray (R.A.); Williams, Lee (LHW.); Williamson, David (D.E.); Yeung, Lem (.)
Cc:	'cpowell3@visteon.com'
Subject:	Stall meeting 2/28/02 moved to 2 PM EST

I will be out of the office this Thursday morning 2/28/02 , therefore the stalls meeting is moved to 2 PM EST. Thank you, this message was sent in addition to a calendar update as a precaution.

Regards,
Lee Williams
For More, Count on Lee
U204 3.0L Powertrain Calibration
Truck Engine Engineering, Suite 1AE20
Phone: (313)33-72503
Fax: (313) 32-31786

From: Williams, Lee (LHW.)
Sent: Tuesday, March 05, 2002 9:25 AM
To: Altoonian, Don (D.J.); Amanda, Harry (H.F.); Badgley, Joel (J.K.); Bauer, Scott (S.C.); Bhojwani, Kamal (K.); Blackburn, Thomas (T.J.); Bogema, John (P.); Cary Powell; Chiok, John (J.); Chih, Ming-Niu (M.N.); Chin, Darrel (D.); Corbett, Sandra (S.M.); Dalbo, Bob (R.J.); De Pena, Juan (J.E.); Diaz, Timothy (T.P.); Fascetti, Bob (R.J.); Fournelle, Gilbert (G.); Freeland, Mark (M.); Giles, Stuart (S.); Gokhale, Renuka (R.V.); Hansen, George (G.C.); Herr, George (G.J.); Hofman, Michael (M.V.); Holmes, Jeffrey (J.R.); Ishikawa, Jiyunichiro (J.); Jensen, Ted (T.E.); John McDonald (E-mail); Jones, Andy; Jordan, Donald (D.E.); Kanal, Shinji (S.); King, Robert (R.F.); Klostermann, Eric (E.); Kosko, Jeff (J.R.); Kwon, Soon (S.K.); Limtiaco, Steven (S.); Linde, Peter (P.A.); Liu, Jane (J.); Lushreen, Eric (E.A.); Marok, Edmond (E.C.); Matsea, John (J.); Maurer, James (J.B.); Mazzella, Gary (G.R.); Mooney, Larry (L.); Moorhouse, Scott (S.R.); Morgan, Tom; Morishima, Shigeki (S.); Naveed Khan; Nematollahi, Sonya (S.); Nikolai, Bernie; Noteboom, Jim (J.E.); Orlman, James (J.W.); Powell, Cary; Powers, Ken (K.W.); Price, Martin (M.); Raquepau, Alden (A.P.); Rothweiler, Daniel (D.); Sanders, Muriel (M.S.); Shah, Kiran (K.C.); Shiraishi, Masaru (M.); Stilgenbauer, Jeffrey (J.R.); Suarez, Rhae (R.); Sullivan, Jamie (J.P.); Takasawa, Keith (K.D.); Takubo, Hiroichi (H.); Vecchio, Anne Marie (A.); Wakenell, Ray (R.A.); Wetzach, Bill (B.); Williams, Lee (LHW.); Williamson, David (D.E.); Yeung, Lem (.)
Subject: U204 Stall Meeting moved to 2-3 PM on Thursdays

Hello Team:

My last day on this assignment is 3/15/02. The Stalls meetings have been moved to 2-3 PM EST on Thursdays. Muriel Sanders will be taking over the stalls issue after I am departed. Thanks!

Regards,
Lee Williams
For More, Count on Lee
U204 3.0L Powertrain Calibration
Truck Engine Engineering, Suite 1AE20
Phone: (313)33-72503
Fax: (313) 32-31786

From: Sventickas, Ed (E.)
Sent: Monday, March 04, 2002 6:00 AM
To: Hofman, Michael (M.V.); Takasawa, Keith (K.D.)
Cc: Bisking, Kevin (K.L.)
Subject: FW: REDCRS - 02-MAR-2002

Pls help .... these pumps, upon return will be found to not be defective (we have even installed pumps into LHD Escape at plant) ... when can we expect to move the needle on this issue with Mazda

-----Original Message-----
From: zeis@pt9570.pose.ford.com [mailto:zeis@pt9570.pose.ford.com]
Sent: Saturday, March 02, 2002 11:58 PM
To: ESVENTIC@ford.com
Subject: REDCRS - 02-MAR-2002

REDCRS REPORT PRODUCED ON 02-MAR-2002 FOR ESVENTIC
ITEMS DATED 01-MAR-2002

****
****

ASM PLT: T525A HOFU (Mazda) DATE: 01-MAR-2002 RESIDENT:
MSOTOMA
BLD PLT: EF02A Cleveland Engine #2 RES TAG: 77515 TYPE:
REPAIR

PART NUMBER	MODEL/TYPE	BUILD DATE	SERIAL NBR	QTY
1G-754-AB	3.0L(4V) ENGINE	05-OCT-2001	111908087	1

VEH TYPE: TRUCK MODEL YEAR: 2002 VIN: U109956 BUILD DATE:
28-FEB-2002

DCL CODES:

CONCERN: (#57026)
PS pump excessive level of operating noise.

****
****

ASM PLT: T525A HOFU (Mazda) DATE: 01-MAR-2002 RESIDENT:
MSOTOMA
BLD PLT: EF02A Cleveland Engine #2 RES TAG: 77516 TYPE:
REPAIR

PART NUMBER	MODEL/TYPE	BUILD DATE	SERIAL NBR	QTY
1G-752-AB	3.0L(4V) ENGINE	18-DEC-2001	216430087	1

VEH TYPE: TRUCK MODEL YEAR: 2002 VIN: F-102144 BUILD DATE:

28-FEB-2002

DCL CODES:

CONCERN: (#57027)
PS pump noise at no load condition.

****
****
NOTE: Please do not reply to or forward this note to DEHailer.
For issues pertaining to the REDCRS "reporting system",
please contact Caroline Day (CDAY).
For issues pertaining to the "concerns" listed in this report,
please contact the PTO Resident Engineer at the appropriate
Assembly Plant. Thank you.

From:	Dalbo, Bob (R.J.)
Sent:	Thursday, March 14, 2002 12:58 PM
To:	Takubo, Hiroichi (H.); Kawasaki, Shunsuke (S.)
Cc:	Inoue, Hiroshi (H.); Takasawa, Keith (K.D.); Williamson, David (D.E.); Soon Kwon
Subject:	FW: U204 V8 MaFS Change

Kawasaki-san, Takubo-san:

This concern for the Improved RFI Immunity MAFS was raised 15-November-2001 to help resolve the stalling issue. However, the drawings are still not approved. We would deeply appreciate any assistance you could provide to expedite this approval.

Bob Dalbo

3.0L Calibration Supervisor
Outfitters Calibration, NAT
Phone: (313) 24-84947 Fax: (313) 32-31786
Pager: (313) 795-2858 Email: *rdalbo@ford.com*

—Original Message—

From:	Boals, Sandra (S.L.)
Sent:	Wednesday, March 13, 2002 1:26 PM
To:	Matsutani, Kazuyuki (K.)
Cc:	Rostck, Kenneth (K.); Boals, Sandra (S.L.); Dalbo, Bob (R.J.); Shiraishi, Masaru (M.); Oda, Tamaki (T.); Williamson, David (D.E.); Williams, Les (LHW.)
Subject:	U204 V8 MaFS Change

Matsutani-San,

RE: 2002MY U204 V8 MAFS Change (Concern C11299286)

The drawings for this change have been updated and sent to you electronically for your approval. The drawings need to be approved by you to continue the release process. Are you the correct person? Or should we have directed this to someone else? Please advise.

The drawings can be viewed at http://tmc.dunton.ford.com/help/?

- Go to the pink box titled "Engineering"
- Select "Show My View List"
- From there select drawing 2L84-9600-BA
- Then approve

Sandy Boals
U204 PTSSE, Air Induction System D&R
Product Development Center (PDC), Cube 2F-E08
Phone: (313) 845-4661 / FAX: (313) 621-8920
Text Pager: (313) 684-2194

From:	HTakubo [takubo.h@dev.mazda.co.jp]
Sent:	Thursday, March 14, 2002 8:23 PM
To:	'Dalbo, Bob (R.J.)'; Kawasaki, Shunsuke (S.)
Cc:	Inoue, Hiroshi (H.); Takasawa, Keith (K.D.); Williamson, David (D.E.); Soon Kwon
Subject:	RE: U204 V6 MaFS Change

Matsutani san has already done the proces of approval,but the process

may

have been mistaken.

I requested the team to double-check again.

Regards,

Hiroichi Takubo

PT Promotion division

E-mail;takubo.h@dev.mazda.co.jp

Tel No.(082)665-1242(Ext.51242)

Fax No.;(082)287-5115(Ext.20015)

---Original Message---

From: Dalbo, Bob (R.J.) [SMTP:rdalbo@ford.com]

Sent: Friday, March 15, 2002 2:58 AM

To: Takubo, Hiroichi (H.); Kawasaki, Shunsuke (S.)

Cc: Inoue, Hiroshi (H.); Takasawa, Keith (K.D.); Williamson, David

(D.E.);

Soon Kwon

Subject: FW: U204 V6 MaFS Change

Kawasaki-san, Takubo-san:

This concern for the improved RFI immunity MAFS was raised

15-November-2001

to help resolve the stalling issue. However, the drawings are still not

approved. We would deeply appreciate any assistance you could provide

to

expedite this approval.

Bob Dalbo
3.0L Calibration Supervisor
Outfitters Calibration, NAT
Phone: (313) 24-84947 Fax: (313) 32-31788
Pager: (313) 795-2869 Email: rdalbo@ford.com

> ----Original Message----
> From: Boals, Sandra (S.L.)
> Sent:Wednesday, March 13, 2002 1:26 PM
> To: Matsutani, Kazuyuki (K.)
> Cc: Roelck, Kenneth (K.); Boals, Sandra (S.L.); Dalbo, Bob (R.J.); Shiraishi, Masaru (M.); Oda, Tamaki (T.); Williamson, David (D.E.); Williams, Lee (LHW.)
> Subject: U204 V6 MaFS Change
>
> Matsutani-San,
>
> RE: 2002MY U204 V6 MAFS Change (Concern C11299288)
>
> The drawings for this change have been updated and sent to you electronically for your approval. The drawings need to be approved by you
to continue the release process. Are you the correct person? Or should we
have directed this to someone else? Please advise.
>
> The drawings can be viewed at http://tmc.dunton.ford.com/help/?
>
> - Go to the pink box titled "Engineering"
> - Select "Show My View List"
> - From there select drawing 2L84-9600-BA
> - Then approve
>
>
>
> Sandy Boals
> U204 PTSSE, Air Induction System D&R

> Product Development Center (PDC), Cube 2F-E08
> Phone: (313) 845-4861 / FAX: (313) 621-8320
> Text Pager: (313) 684-2194
>

From:	Sanders, Muriel (M.S.)
Sent:	Monday, March 18, 2002 10:14 AM
To:	Altoonian, Don (D.J.); Amanda, Harry (H.F.); Badgley, Joel (J.K.); Bauer, Scott (S.C.); Bhojwani, Kamal (K.); Blackburn, Thomas (T.J.); Bogema, John (P.); Cary Powell; Chick, John (J.); Chih, Ming-Niu (M.N.); Chin, Darrel (D.); Corbett, Sandra (S.M.); Dalbo, Bob (R.J.); Dan Rothweiler; De Pena, Juan (J.E.); Diez, Timothy (T.P.); Fascetti, Bob (R.J.); Fournelle, Gilbert (G.); Freeland, Mark (M.); Giles, Stuart (S.); Goldsale, Renuka (R.V.); Hansen, George (G.C.); Herr, George (G.J.); Hofman, Michael (M.V.); Holmes, Jeffrey (J.R.); Ichikawa, Jiyunichiro (J.); Jansen, Ted (T.E.); John McDonald; Jones, Andy; Jordan, Donald (D.E.); Kanai, Shinji (S.); King, Robert (R.F.); Klostermann, Eric (E.); Kosko, Jeff (J.R.); Kwon, Soon (S.K.); Limtiaco, Steven (S.); Linde, Peter (P.A.); Liu, Jane (J.); Lushreen, Eric (E.A.); Marek, Edmond (E.C.); Mateos, John (J.); Maurer, James (J.B.); Mazzella, Gary (G.R.); Mooney, Larry (L.); Moorhouse, Scott (S.R.); Morgan, Tom; Morishima, Shigeki (S.); Naveed Khan; Nematollahi, Sonya (S.); Nikolai, Bernie; Noteboom, Jim (J.E.); Ortman, James (J.W.); Powers, Ken (K.W.); Price, Martin (M.); Raquepau, Alden (A.P.); Sanders, Muriel (M.S.); Shah, Kiran (K.C.); Shiraishi, Masaru (M.); Stiljenbauer, Jeffrey (J.R.); Suarez, Rhea (R.); Sullivan, Jamie (J.P.); Takasawa, Keith (K.D.); Takubo, Hiroshi (H.); Vecchio, Anna Marie (A.); Wakenell, Ray (R.A.); Wettach, Bill (B.); Williams, Les (LHW.); Williamson, David (D.E.); Yeung, Lam (.)
Subject:	U204 Phantom Stall Meeting 3/21/02

Here is the updated meeting information for this week. A meeting notice will follow.

New dial-in information.
Dial in: 1-877-870-3431 or Fortinet: 9-1-954-1143
International Participants # 1 (630) 693-1703
Passcode: 7865386#

For 3/21/2002 Only:
Location is TEE Conference Rm 1

Meeting time remains the same as Thursdays, 2-3pm.

Have a good day.

Muriel Sanders
U204 3.0L Calibration
Ford Motor Company
Phone: 313-32-27307
Fax: 313-32-31786
E-mail: msander6@ford.com

From:	Linde, Peter (P.A.)
Sent:	Tuesday, April 16, 2002 2:16 PM
To:	Takasawa, Keith (K.D.); Powers, Ken (K.W.)
Cc:	Shah, Kiran (K.C.); Chih, Ming-Niu (M.N.)
Subject:	Vent Line Change--Not ready for production

Not exactly...
The final design was not trialed, only the latest attempt.
The detailed changes Ming outlines below are all a result of the last trial.

Additionally, we will require a second 2-way clip that Ming has never seen or acknowledged. It is required to ensure the line doesn't get crushed while decking the fuel tank. It will not be PIA for 1PP since he doesn't acknowledge it is needed.

The export canister (mentioned below as a Visteon drawing issue) has never been addressed at KCAP--even in cobbled form. I don't think we can have Visteon complete drawings without validating the proposed revisions on vehicles first.

The proper sized christmas tree locator has not been found in the searches through standard parts to-date; it may be available but no-one has found it yet. I would anticipate a new design and tool would take 6-8 weeks; this timing might PSW in time for 4P but it will be tight.

Will the spider trap be PSW for 4P? Ready for production is not good enough.

The change can not be a running change due to labor implications based on the current process assessment. We will look again during 1PP if the trial parts are representative. We will need a "blackout" waiver if we determine we can implement without labor impact and want this as a R/C.

The parts are not on any of the 2003 J#1 tracking documents, are not released, and are not recognized by the '03 launch team.

Kiran has assured me that Ming will be on-site for all of the 1PP builds to support. He also indicated he would talk to Tim Veenstra & Joe Redding to inform them about the desire to build the 1PP's with these parts.

Too many open issues to call ready for production. Hopefully, after 1PP we will be able to lock in a final design concept and PSW in time for 4P.

Pete Linde
ENGINEERING SUPERVISOR
ESCAPE/TRIBUTE PVT
8121 US HIGHWAY 69
CLAYCOMO, MO 64119
816-459-1865
816-459-1726 (FAX)

----Original Message----

From:	Takasawa, Keith (K.D.)
Sent:	Tuesday, April 16, 2002 11:59 AM
To:	Linde, Peter (P.A.); Powers, Ken (K.W.)
Subject:	FW: Vent Line Change

Would like your views on this change being ready for production.

Regards,
Keith Takasawa

Bob Dalbo
3.0L Calibration Supervisor
Outfitters Calibration, NAT
Phone: (313) 24-84947 Fax: (313) 32-31786
Pager: (313) 795-2859 Email: *rdalbo@ford.com <mailto:rdalbo@ford.com> <<mailto:rdalbo@ford.com>>*

----Original Message----
From: Moorhouse, Scott (S.R.)
Sent: Monday, April 15, 2002 12:31 PM
To: Dalbo, Bob (R.J.)
Subject:

Bob, if time permits, pls drop a line to Pete Linde explaining why we need to Ming's changes to the canister assy now rather than later. There have been some discussion about delaying these changes.

Scott Moorhouse
U204 PTSE Resident Engineer
Kansas City Assembly Plant
(ph) 816-459-1965 (fax) 816-459-1728
smoorhou@ford.com <mailto:smoorhou@ford.com> <<mailto:smoorhou@ford.com>>

From:	Shah, Kiran (K.C.)
Sent:	Tuesday, April 16, 2002 5:15 PM
To:	Takasawa, Keith (K.D.)
Cc:	Jammoul, Ali (A.); Hofman, Michael (M.V.); Moorhouse, Scott (S.R.); Fasolti, Bob (R.J.); Hopcian, Gordon (G.L.); Redding, Joe (J.M.); Rockel, Royce (R.R.); Syed, Shaheen (Q.); Linde, Peter (P.A.); Chih, Ming-Niu (M.N.); De Pena, Juan (J.E.); Veenstra, Tim (T.W.); Shah, Kiran (K.C.)
Subject:	RE: Vent Line Change

Keith:

This change (to route canister fresh air vent line from engine compartment to the fill pipe area and eliminate the check valve from carbon canister assembly) requested to bring in at **JOB#1** by Powertrain was pushed to **POST JOB#1** by program management. Building 4P vehicles with **non-PSW** parts was seen as a **big risk for our high visibility vehicle.**

While we were aware of the Powertrain desire, it was impossible to bring in PSW parts at 4P when allowed for evaluation of various cost-effective designs, alternate supplier for sourcing, trials at KCAP for successful build process, testing, production tooling and fixturing for mass production, etc.

In spite of the challenges, we thought we had a design that was acceptable to KCAP based on trials last week (Pete Linde thinks we need an extra clip to prevent vent line from getting crushed during fuel tank decking and we want to address this concern).

To answer your question, this is the work plan we have developed to address the issue and expedite the change:

- Examine the part against the preliminary drawing and run a trial in Dearborn -- Thursday (4/18)
- Make arrangements to deliver production representative (non-PSW) parts (25 pieces) to KCAP -- Friday (4/19)
- Ming Chih to support 4P build at KCAP and travel with 2 pieces (and extra clips if required) for early design confirmation -- Monday (4/22)
- Drawings from Shelby for Vent Tube will be available early next week upon confirmation of final design -- Tuesday (4/23)
- Work with Visteon to get revised Canister Drawings (without the check valve) next week -- Tuesday (4/23)
- Release parts as soon as drawings available -- Friday (4/25)
- Work with Program Management to bring in as pull-ahead job#1 change (satisfy all affected parties and get their concurrence)

Also, based on the timing provided by supplier, PSW parts will be available within 8 weeks after the release of an acceptable robust design.

In short, we are making every effort to expedite the change while making sure the design as well as the process are robust.

Let me know if you have any further questions. Thanks.

Regards,

Kiran C. Shah

Supervisor - U204/295 Fuel Systems Engineering
North American Truck - Outfitters
Telephone: (313) 32-31594 Fax: (313) 62-16025
Address: Room: 2DG45, PDC/Mail Drop: 113

Email: kshah1@ford.com

—Original Message—
From: Takasawa, Keith (K.D.)
Sent: Tuesday, April 16, 2002 6:46 AM
To: Shah, Kiran (K.C.); Chih, Ming-Niu (M.N.); De Pena, Juan (J.E.)
Cc: Jamaoui, Ali (A.); Hofman, Michael (M.V.); Moorhouse, Scott (S.R.); Fascetti, Bob (R.J.); Hopcian, Gordon (G.L.); Redding, Joe (J.M.); Rocket, Royce (R.R.); Syed, Shaheen (Q.); Linde, Peter (P.A.); Powers, Ken (K.W.)
Subject: FW: Vent Line Change

I would like very much to get this change into production ASAP. I trust that the issues discovered during the KCAP plant trials will be resolved quickly and another trial scheduled ASAP. Thanks for your support.

Regards,
Keith Takasawa

Escape/Tribute Chief Engineer
RDC 2-U64
MD401
PH: (313) 322-5675
FAX: (313) 248-8588
E-MAIL: KTAKASAW@FORD.COM
TEXT PAGE: 7348045034@mobile.att.net

—Original Message—
From: Dalbo, Bob (R.J.)
Sent: Monday, April 15, 2002 5:15 PM
To: Shah, Kiran (K.C.)
Cc: Hofman, Michael (M.V.); Takasawa, Keith (K.D.); Moorhouse, Scott (S.R.); Fascetti, Bob (R.J.); Hopcian, Gordon (G.L.); Redding, Joe (J.M.); Rocket, Royce (R.R.); Syed, Shaheen (Q.); Linde, Peter (P.A.)
Subject: RE: Vent Line Change

Kiran,
This is the background behind the phone message Pete Linde and I left for you. We appreciate your help in resolving these issues.

Bob Dalbo
3.0L Calibration Supervisor
Outfitters Calibration, NAT
Phone: (313) 24-84947 Fax: (313) 32-31786
Pager: (313) 795-2859 Email: rdalbo@ford.com <mailto:rdalbo@ford.com>

—Original Message—
From: Linde, Peter (P.A.)
Sent: Monday, April 15, 2002 4:27 PM
To: Dalbo, Bob (R.J.); Syed, Shaheen (Q.); Rocket, Royce (R.R.)
Cc: Hofman, Michael (M.V.); Takasawa, Keith (K.D.); Moorhouse, Scott (S.R.); Fascetti, Bob (R.J.); Hopcian, Gordon (G.L.); Redding, Joe (J.M.)
Subject: RE: Vent Line Change

Bob,
I understand the drivers behind implementing these changes ASAP, the only problems are that the parts to-date have not been good enough for customer vehicles. I've pasted below a de-brief of the open issues (minus the photos) identified during the trial last week at KCAP:

Ref: New Vent Line Trial Up-date (4/12/02)

Engineering Supervisor
Escape/Tribute PVT
8121 US Highway 69
Claycomo, MO 64119
816-459-1865
816-459-1726 (fax)

----Original Message----
From: Dalbo, Bob (R.J.)
Sent: Monday, April 15, 2002 1:54 PM
To: Linde, Peter (P.A.)
Cc: Hofman, Michael (M.V.); Takamura, Kaleb (K.D.); Moorhouse, Scott (S.R.); Fucetti, Bob (R.J.)
Subject: RE: Vent Line Change

Pete,
Implementing the vent line change as soon as possible will have three positive outcomes for Ford:

- A significant reduction in "phantom" stalls.
- A demonstration to the National Highway Traffic Safety Administration that Ford is aggressively attempting to resolve the stalling issue.
- A minor reduction in cost.

We appreciate your help in expediting the implementation of this change.

Bob Dalbo
3.0L Calibration Supervisor
Outfitters Calibration, NAT
Phone: (313) 24-84947 Fax: (313) 32-31786
Pager: (313) 795-2859 Email: *rdalbo@ford.com <mailto:rdalbo@ford.com>*

----Original Message----
From: Moorhouse, Scott (S.R.)
Sent: Monday, April 15, 2002 12:31 PM
To: Dalbo, Bob (R.J.)
Subject:

Bob, if time permits, pls drop a line to Pete Linde explaining why we need to Ming's changes to the canister assy now rather than later. There have been some discussion about delaying these changes.

Scott Moorhouse
U204 PTSE Resident Engineer
Kansas City Assembly Plant
(ph) 816-459-1965 (fax) 816-459-1728
smoorhou@ford.com <mailto:smoorhou@ford.com>

From: Fascetti, Bob (R.J.)
Sent: Thursday, May 16, 2002 2:05 PM
To: Takasawa, Keith (K.D.)
Subject: RE: stalls warranty graph

Keith,
My interpretation is that it's too early to tell. My hope is that the change we made in January will bring the numbers down, and the TSB will help the previous issues. We have hard evidence that the calibration change makes us more robust. We are continuing to look for new answers as well.

Until we get the evap line re-routed and the ISC valve in, we will still have some issues in the field.

—Original Message—
From: Takasawa, Keith (K.D.)
Sent: Thursday, May 16, 2002 1:49 PM
To: Fascetti, Bob (R.J.)
Subject: FW: stalls warranty graph

Bob:

What's your view of what's going on (or not)?

Regards,
Keith Takasawa

Escape/Tribute Chief Engineer
PDC 2HJ64
MD401
PH: (313) 322-5675
FAX: (313) 248-6599
E-MAIL: KTAKASAW@FORD.COM
TEXT PAGE: 7348045054@mobile.att.net

—Original Message—

From: Sanders, Muriel (M.S.)

Sent: Thursday, May 16, 2002 12:45 PM

To: Altoonian, Don (D.J.); Badgley, Joel (J.K.); Bauer, Scott (S.C.); Bhojwani, Kamal (K.); Blackburn, Thomas (T.J.); Bogema, John (P.); Cary Powell; Chlok, John (J.); Chih, Ming-Niu (M.N.); Chin, Darrel (D.); Corbett, Sandra (S.M.); Dalbo, Bob (R.J.); Dan Rothweiler; De Pena, Juan (J.E.); Diaz, Timothy (T.P.); Fascetti, Bob (R.J.); Fournelle, Gilbert (G.); Freeland, Mark (M.); Giles, Stuart (S.); Gokhale, Renuka (R.V.); Grimes, Jeff (J.R.); Hansen, George (G.C.); Herr, George (G.J.); Holman, Michael (M.V.); Holmes, Jeffrey (J.R.); Ishikawa, Jiyunichiro (J.); Jensen, Ted (T.E.); John McDonald; Jones, Andy; Jordan, Donald (D.E.); Kanal, Shinji (S.); King, Robert (R.F.); Kloetermann, Eric (E.); Kosko, Jeff (J.R.); Kwon, Soon (S.K.); Limtaco, Steven (S.); Linde, Peter (P.A.); Liu, Jane (J.); Merck, Edmond (E.C.); Meiess, John (J.); Maurer, James (J.B.); Mazzella, Gary (G.R.); Mooney, Larry (L.); Moorhouse, Scott (S.R.); Morgan, Tom; Morishima, Shigeki (S.); Naveed Khan; Nematollahi, Sonya (S.); Nikolai, Bernie; Noteboom, Jim (J.E.); Ortman, James (J.W.); Powers, Ken (K.W.); Price, Martin (M.); Raquepau, Alden (A.P.); Sanders, Muriel (M.S.); Shah, Kiran (K.C.); Shiraishi, Masaru (M.); Stilgenbauer, Jeffrey (J.R.); Suarez, Rhae (R.); Sullivan, Jamie (J.P.); Takasawa, Keith (K.D.); Takubo, Hiroichi (H.); Vecchio, Anne Marie (A.); Wakenell, Ray (R.A.); Wettach, Bill (B.); Williams, Les (LHW.); Yeung,

Lem (.)

Subject:FW: stella warranty graph

See Scott's note below.

Muriel Sanders
U204 3.0L Calibration
Ford Motor Company
Phone: 313-32-27307
Fax: 313-32-31786
E-mail: msander6@ford.com <mailto:msander6@ford.com>

-----Original Message-----
From: Moorhouse, Scott (S.R.)
Sent: Thursday, May 16, 2002 11:21 AM
To: Sanders, Muriel (M.S.)
Subject: stella warranty graph

Please provide to team. I have forwarded to Corbett, Altocumm.

<< File: Stella Graph.doc >>

Scott Moorhouse
U204 PTSE Resident Engineer
Kansas City Assembly Plant
(ph) 816-459-1965 (fax) 816-459-1728
smoorhou@ford.com <mailto:smoorhou@ford.com>

From: Davis, Tim (T.P.)
Sent: Tuesday, June 11, 2002 3:18 AM
To: Takasawa, Keith (K.D.)
Subject: RE: ACT REQ - U204 Stall Meeting Minutes - 6/06/02

I will be back in Dearborn on Monday - my calendar next week is fairly accurate.

In the meantime, I notice that at least one Master Black Belt is on the circulation - are you getting full service from the Black Belt resource?

Tim Davis (cds=tdavis5)
Ford Technical Fellow - Quality Engineering
Room 2517, Scientific Research Laboratory.
Tel: **32-21822** (+1 313 322 1822)
Fax: **24-82206** (+1 313 248 2206) Pager 3138516403@myairmail.com
Admin: TBD (- 32-23364)
For Insights into Quality → http://www.quality.ford.com/quality/rpj_speech/

----Original Message----
From: Takasawa, Keith (K.D.)
Sent: Monday, June 10, 2002 6:17 PM
To: Davis, Tim (T.P.)
Subject: ACT REQ - U204 Stall Meeting Minutes - 6/06/02

Tim:

We just finished our NAOPAM with the VPs, and it's obvious to most (including myself) that we need some fresh eyes to look at the Escape engine stalls issue. We have found a number or root causes, but the rate doesn't seem to be reacting favorably to the fixes. A number of us think there's probably something else going on.

Any chance we can enlist your services? The VPs have made this a top priority, and rightly so.

Thanks.

Regards,
Keith Takasawa

Escape/Tribute Chief Engineer
PDC 2EJ54
MD401
PH: (313) 322-5675
FAX: (313) 248-8599
E-MAIL: KTAKASAW@FORD.COM
TEXT PAGE: 7346045034@mobile.att.net

----Original Message----

From: Sanders, Muriel (M.S.)

Sent: Monday, June 10, 2002 4:09 PM

To: Altoonian, Don (D.J.); Ayvazzadeh, Kam (K.); Badgley, Joel (J.K.); Bauer, Scott (S.C.); Bhojwani, Kamal (K.); Blackburn, Thomas (T.J.); Bogema, John (P.); Cary Powell; Chick, John (J.); Chih, Ming-Niu (M.N.); Chin, Darrel (D.); Corbett, Sandra (S.M.); Dalbo, Bob (R.J.); Dan Rothweiler; De Pena, Juan (J.E.); Diez, Timothy (T.P.); Fascetti, Bob (R.J.); Fournelle, Gilbert (G.); Freeland, Mark (M.); Gries, Stuart (S.); Gokhale, Renuka (R.V.); Grimes, Jeff (J.R.); Hansen, George (G.C.); Herr, George (G.J.); Hofman, Michael (M.V.); Holmes,

From: Klarr, Jerry (G.T.)
Sent: Friday, June 14, 2002 4:00 PM
To: Judge, Surinder (S.S.); Tokarski, Michael (M.J.); Le, Dzung (D.H.); Fascetti, Bob (R.J.); Dalbo, Bob (R.J.)
Cc: Grewal, Bill (B.S.); Garrett, Bruce (B.); Takasawa, Keith (K.D.)
Subject: RE: HOT Quality Analysis HOT

Thanks. Bob/Bob - pls get them engaged right away.

G. T. Klarr (Jerry)
P/T Chief Engineer: PH: 32-26669/Cube: 1BA45
PDC/MD #205/FAX: 62-18083/gklarr@ford.com

----Original Message----
From: Judge, Surinder (S.S.)
Sent: Friday, June 14, 2002 11:00 AM
To: Klarr, Jerry (G.T.); Tokarski, Michael (M.J.); Le, Dzung (D.H.)
Cc: Grewal, Bill (B.S.); Garrett, Bruce (B.); Takasawa, Keith (K.D.)
Subject: FW: HOT Quality Analysis HOT
Importance: High

Jerry:
I and Bill Grewal talked.
I am assigning Allen Duval (Analyst) and Dzung Lee (Tech Spec) to work with Bill Grewal.
B. Grewal will coordinate.
These folks will be availible semi-part time as needed for the next 4-6 weeks for this assignment.
>>> I do not understand why we need another analyst when Sandra already has someone ?
I am very swamped with all other B. Folwer's requests with all the available analysts - but will support you Gerry.
Thx.

Surinder Judge
Manager - Engineering Reliability - Outfitters, NA Trucks
ASQ Certified Reliability Engineer
Tel: (313) 248-5741. Fax: (313) 317-7296
Txt Pager - sjudge

----Original Message----
From: Tracy, Lynn (L.J.) On Behalf Of Klarr, Jerry (G.T.)
Sent: Friday, June 14, 2002 8:04 AM
To: Judge, Surinder (S.S.); Grewal, Bill (B.S.)
Subject: HOT Quality Analysis HOT
Importance: High

Need a quality anaylsis to help work on the Escape Stalls issues ASAP. Please check in Tim Davis' shop and let me know sometime today (6/14) who it is.

G. T. Klarr (Jerry)
Chief P/T Engineer - Outfitters
PH: 32-26669/Fax: 62-18083
PDC/MD #205/Cube 1BA45/Internet: gklarr@ford.com
(Admin. L. Tracy x35205)

However, it would be good for my tan as I wait for them.....heh, hsh.....

If you do want low air flow throttle bodies, maybe a batch (5-8??) could be sent directly to the Dealership Metro Motors in St. Croix??

Please advise via voice mail since I will be disconnecting my laptop soon for packing. But send a note away since I HOPE to be able to use my laptop there. Help desk promised, but you know how that goes.....

You can leave voice mail on both my cell and office phone. I can check the office # from afar.

I will do whatever you wish: I want to get the data we need, and not just fix these Units.
Gil Peplone
Powertrain Field Quality Specialist-"PFQS" in
South Florida
Office/Answering Machine: 954-753-9989
Cell Phone 954-242-2066
"With Warranty you are Paying for the Sins of the Past"

---Original Message---
From: Dalbo, Bob (R.J.)
Sent: Friday, June 14, 2002 5:29 PM
To: Peplone, Gil (J.)
Cc: Sanders, Muriel (M.S.)
Subject: RE: Inspection Sheet for St. Croix Vehicle Inspection

Gil,
Please don't drill out any throttle plates. For one thing, it's not approved practice, and for another, we'd like to get back any you have problems with.

Bob Dalbo

3.0L Calibration Supervisor
Outfitters Calibration, NAT
Phone: (313) 24-84947 Fax: (313) 32-31786
Pager: (313) 796-2859 Email: *rdalbo@ford.com*

---Original Message---
From: Peplone, Gil (J.)
Sent: Friday, June 14, 2002 3:23 PM
To: Johnson, Jim (J.S.); Bilicki, John (J.R.); Corbett, Sandra (S.M.); DiAngelo, Renaldo (R.); Altoonian, Don (D.J.); Ayvazoolan, Kam (K.); Bauer, Scott (S.C.); Bhojwani, Kamal (K.); Blackburn, Thomas (T.J.); Bogema, John (P.); Chick, John (J.); Chih, Ming-Hsu (M.H.); Chin, Darrel (D.); Corbett, Sandra (S.M.); Dalbo, Bob (R.J.); Rothweiler, Daniel (D.); De Pena, Juan (J.E.); Diez, Timothy (T.P.); Fascetti, Bob (R.J.); Fosmalle, Gilbert (G.); Freeland, Mark (M.); Giles, Stuart (S.); Golinski, Ramuka (R.V.); Grimes, Jeff (J.R.); Hansen, George (G.C.); Herr, George (G.J.); Hofman, Michael (M.V.); Holmes, Jeffrey (J.R.); Ichikawa, Syunichiro (J.); Jensen, Ted (T.E.); Mcdonald II, John (J.M.); Jordan, Donald (D.E.); King, Robert (R.P.); Koske, Jeff (J.R.); Kwon, Soon (S.K.); Livdaco, Steven (S.); Linde, Peter (P.A.); Liu, Jane (J.); Mandziuk, Roger (R.S.); Marck, Edmond (E.C.); Matsuo, John (J.); Maurer, James (J.B.); Mazzella, Gary (G.A.); Mooney, Larry (L.); Moorhouse, Scott (S.R.); Morgan, Tomiko (T.T.); Morishima, Shigeki (S.); Namatollahi, Sonya (S.); Notaboone, Jim (J.E.); Ortman, James (J.W.); Powers, Ken (K.W.); Price, Martin (M.); Raquepau, Aidan (A.P.); Sanders, Muriel (M.S.); Shah, Kiran (K.C.); Shiraishi, Masaru (M.); Stilgenbauer, Jeffrey (J.R.); Suarez, Rhea (R.); Takasawa, Keith (K.D.); Takubo, Hiroichi (H.); Veenstra, Tim (T.W.); Watanati, Ray (R.A.); Weltsch, Bill (B.); Williams, Lee (L.H.W.); Young, Lora (.); Benintende, Robert (R.F.); Fernandez, Ruben (R.); Bradley, Joe (J.C.); Goering, Kimberly (K.L.); Suarez, Rhea (R.); Torres, Laura (L.D.); Martin, Mike (M.S.); Weber, Mark (M.A.); Amely, Felix (F.A.)
Cc: Peplone, Gil (J.)
Subject: Inspection Sheet for St. Croix Vehicle Inspection

Good afternoon everyone: I have included all those that I have been in continuous communication, plus all who are part of the "Escape Stalls Team" Conference Call which I have attended.

The file below contains the form I will use. This information is a result of the feedback I have received from Mr. Altoonian, plus all existing Service Communications, both external and internal.

Please note that the items are ordered in such a way to allow me to leave the vehicle in it's original state until I

can replicate the Stalls Concern, if ever.
I intend on extensively driving these Units until I deem it impossible for Concern replication.
At that point, I will perform any modifications to at least leave the Units at the latest repair level possible.

<< File: St. Croix Escape Vehicle Inspection Sheet.doc >>

FYI...
Gil Pepitone
Powertrain Field Quality Specialist-"PFQS" in
South Florida
Office/Answering Machine: 954-753-9989
Cell Phone 954-242-2066
"With Warranty you are Paying for the Sins of the Past"

Escape Stalls Concern Vehicle Inspection Data
In St. Croix by Gil Pepitone 6/15/-6/24/2002

Date:

Owner:

VIN:

M.Y.:

Mileage:

Conditions during Owner's experience, including heavy keys/radio towers?

Calibration level:

DTCs? If P1000, check OBD monitor status/measure KAM Pin 55 if OBD is dumb:

DPFE level {2A07 or later}

MAF level {BA?}

Relay PN level OK? {White letters NG) /Terminals go/no go?

PCM Hardware level/AXB &ATF1 Catch word is latest/ "160" or "161"?

Connectors/Grounds in order of inspection flow
C270b
G300
G104
G105
G101
C110
C133
G100
C270c
C270d
CPS pigtail contacting A/C pulley?

Rattle ignition key/engine cuts out?

Stabilized RPM Value in Park, Fan off, A/C off, no Purge flow, not prolonged idle time:

Stabilized IAC Duty Cycle Percentage in P/N, A/C off:

Does Engine stay running w/ IAC disconnected?

If so, what is base RPM?

TPS voltage {Bogie .9 +-.05}:

Relationship of EVAP % value vs. FTP Voltage ok?

If no OK, what were values?

If relation not ok, did tapping on VMV make FTP voltage jump/engine's reaction?

Position of Flapper Valve ok?

PFQS drive results/Verified?

If verified, what were conditions?

Repairs/adjustments to vehicle:
H2O witness marks/Rust in Left Kickpanel?
Restricted EVAP line?/Blew out??
Replaced Flapper Vlv if web found?
New IAC D.C.?
Replaced TB?
Tightened any Ground/stalled connectors?
Changed DPFE?
Remove IAC/Inspect for sludge/Oil in rear hole?
Changed IAC?
Changed MAF?
Cleaned DTCs?

Additional Comments:

From: Terzea, Laura (L.D.)
Sent: Monday, July 08, 2002 3:34 PM
To: Savoheiz, David (D.W.); Takasawa, Keith (K.D.)
Cc: Fascetti, Bob (R.J.); Klarr, Jerry (G.T.)
Subject: FW: stall customer

Dave/Keith: Ordinarily, I wouldn't send you this stuff, but we need to keep the pressure on to fix this concern for J1 '03 if possible.

----Original Message----
From: Suarez, Rhea (R.)
Sent: Monday, July 08, 2002 3:00 PM
To: Altoonian, Don (D.J.); Delbo, Bob (R.T.); Sanders, Muriel (M.S.); Fournelle, Gilbert (G.)
Cc: Terzea, Laura (L.D.)
Subject: stall customer

FYI - we need to fix this concern.....

read the comments that started the thread.
http://www.escape-central.com/1forum/showthread.php?threadid=3081&referrerid=1436

Cc: Hamatani, Teruo (T.); 'kodama.ma@dev.mazda.co.jp'; Powers, Ken (K.W.)

Subject: RE: IQS improvement task

Powers-san will provide the names to you.

Regards,

Keith Takasawa

Escape/Tribute Chief Engineer
PDC 2HJ54
MD401
PH: (313) 322-8675
FAX: (313) 248-8569
E-MAIL: KTAKASAW@FORD.COM
TEXT PAGE: 7348045034@mobile.att.net

----Original Message----

From: Inoue, Hiroshi (H.)

Sent: Monday, July 15, 2002 6:58 PM

To: Takasawa, Keith (K.D.)

Cc: Hamatani, Teruo (T.); kodama.ma@dev.mazda.co.jp

Subject: IQS improvement task

Takasawa-san,
Would you advise me the counterpart of the following Mazda's champions?
- Hiasa, Wind Noise engineer
- Fujii, Molding engineer
- Okamoto, Body engineer
- Hasegawa, Audio engineer
- Ito, Electric features engineer

Hiroshi Inoue
Mazda Tribute Chief Engineer
Phone: 313-845-8179
Fax: 313-248-7059
Cellular: 248-320-7670

From: Fascetti, Bob (R.J.)
Sent: Wednesday, July 24, 2002 2:16 PM
To: Inoue, Hiroshi (H.); Takasawa, Keith (K.D.)
Cc: Veenstra, Tim (T.W.); Moorhouse, Scott (S.R.); Shiraishi, Masaru (M.); Dalbo, Bob (R.J.); Hofman, Michael (M.V.); Ichikawa, Jiyunichiro (J.); Waud, Sachiko (S.); Fujioka, Kenji (K.); Linde, Peter (P.A.); Rusu, Jessica (J.L.); Klarr, Jerry (G.T.); Corbett, Sandra (S.M.)
Subject: RE: (2) stalls robustness CR's

We need these concerns approved at this Thursday morning meeting. Mazda has had the white papers for these concerns for over a week (sent to Ichikawa-san). All of these concerns have been discussed at our weekly stall meeting, that Kanai-san, and MNAO (Steve Limtiaco) attend.

Takasawa-san has already directed that these concerns be approved. I understand that Mazda gets some time to approve concerns, and that's why we sent the white paper early.

Please come prepared to approve this concern at this meeting. We have now lost two full days of progress due to waiting.

Please address this matter urgently.
Thank you,
Bob Fascetti
Outfitters Calibration Manager

-----Original Message-----
From: Inoue, Hiroshi (H.)
Sent: Tuesday, July 23, 2002 12:06 PM
To: Takasawa, Keith (K.D.)
Cc: Veenstra, Tim (T.W.); Moorhouse, Scott (S.R.); Shiraishi, Masaru (M.); Dalbo, Bob (R.J.); Fascetti, Bob (R.J.); Hofman, Michael (M.V.); Ichikawa, Jiyunichiro (J.); Waud, Sachiko (S.); Fujioka, Kenji (K.); Linde, Peter (P.A.); Rusu, Jessica (J.L.); Klarr, Jerry (G.T.); Corbett, Sandra (S.M.)
Subject: RE: (2) stalls robustness CR's

Takasawa-san,
Per your approval for KCAP, now Hofu change control process starts officially for these CRs.
At this moment, both of C11390580 and C11371349 are "Black Box" for Mazda engineers.

In order to get Hofu approval quickly, please have relating Ford folks give information to
Mazda engineers ASAP. Shiraishi-san will set up a engineering meeting in this week.

The major point to be confirmed is any impact on Certification/Homologation in countries out side US.
I sincerely don't want make you get problems of regulatory recall.

Hiroshi Inoue
Mazda Tribute Chief Engineer
Phone: 313-845-8179
Fax: 313-248-7059

EXS2-027 24882

Cellular: 248-320-7670

-----Original Message-----
From: Takasawa, Keith (K.D.)
Sent: 2002??22? 16:28
To: Corbett, Sandra (S.M.)
Cc: Veenstra, Tim (T.W.); Moorhouse, Scott (S.R.); Shiraishi, Masaru (M.); Dalbo, Bob (R.J.); Fascetti, Bob (R.J.); Hofman, Michael (M.V.); Ichikawa, Jiyunichiro (J.); Waud, Sachiko (S.); Fujioka, Kenji (K.); Linde, Peter (P.A.); Rusu, Jessica (J.L.); Inoue, Hiroshi (H.); Klarr, Jerry (G.T.)
Subject: RE: (2) stalls robustness CR's

Due to the critical nature of these changes and the need to proceed immediately with next steps, I have directed Tim Veenstra to approve the 2 referent CRs. We will follow-up with further information as required.

Regards,
Keith Takasawa
Escape/Tribute Chief Engineer
PDC 2HJ64
MD401
PH: (313) 322-5675
FAX: (313) 248-8599
E-MAIL: KTAKASAW@FORD.COM
TEXT PAGE: 7346045034@mobile.att.net

-----Original Message-----
From: Corbett, Sandra (S.M.)
Sent: Monday, July 22, 2002 3:59 PM
To: Shiraishi, Masaru (M.); Dalbo, Bob (R.J.); Fascetti, Bob (R.J.); Hofman, Michael (M.V.); Ichikawa, Jiyunichiro (J.); Waud, Sachiko (S.); Fujioka, Kenji (K.)
Cc: Takasawa, Keith (K.D.); Veenstra, Tim (T.W.); Moorhouse, Scott (S.R.)
Subject: (2) stalls robustness CR's

I am struggling to get these items ready for release. Here is status for the emergency release for stalls robustness actions:

C11390580- calibration change
-Mazda (Shiraishi-san) indicates they need final white paper, Dalbo will forward
-KCAP (John O'Callaghan) indicates that a plant trial is required...we cannot provide parts until the concern is authorized by Prog. Mgmt....Prog Mgmt (Jessica Rusu) indicates that cr cannot be authorized until trial is complete...HELP/NEXT STEPS???

C11371349- capacitor change
-Mazda (Shiraishi-san) is also requesting white paper--THERE IS NO FUNCTIONAL CHANGE, THEREFORE NO WHITE PAPER WILL BE PROVIDED
-Need Mazda (Fujioka-san and Waud-san) to approve (currently rejected by Mazda)

Tim,
Will there be change control Tuesday at 8am or will these covered at

PST?

Sandy Corbett
Escape Powertrain QRT
Phone/Fax: (313)59-44351
Product Development Center 2H-E66

-----Original Message-----
From: Bob Dalbo (1-313-2484947)
(mailto:viwrk0148drbn004.dearborn.ford.com)
Sent: Monday, July 22, 2002 3:01 PM
To: SCORBETT
Subject: Backup note to the PAGE

Robin Peters postponed the stall fix emergency release meeting until
concerns
(C11390580 & C11371349) are approved.

From:	Corbett, Sandra (S.M.)
Sent:	Wednesday, July 24, 2002 3:48 PM
To:	Inoue, Hiroshi (H.); Fascetti, Bob (R.J.)
Cc:	Veenstra, Tim (T.W.); Moorhouse, Scott (S.R.); Shiraishi, Masaru (M.); Dalbo, Bob (R.J.); Hofman, Michael (M.V.); Ichikawa, Jiyunichiro (J.); Waud, Sachiko (S.); Fujioka, Kenji (K.); Linde, Peter (P.A.); Rusu, Jessica (J.L.); Klarr, Jerry (G.T.); Takasawa, Keith (K.D.)
Subject:	RE: (2) stalls robustness CR's

Both Ichikawa-san and Shiraishi-san are on the invite list for the weekly stalls meeting which occurs on Thursday's at 2pm at TEE and with audio numbers.

Sandy Corbett
Escape Powertrain PMT & QRT
Phone/Fax: (313)59-44351
Product Development Center 2H-E66

-----Original Message-----
From: Inoue, Hiroshi (H.)
Sent: Wednesday, July 24, 2002 3:46 PM
To: Fascetti, Bob (R.J.)
Cc: Veenstra, Tim (T.W.); Moorhouse, Scott (S.R.); Shiraishi, Masaru (M.); Dalbo, Bob (R.J.); Hofman, Michael (M.V.); Ichikawa, Jiyunichiro (J.); Waud, Sachiko (S.); Fujioka, Kenji (K.); Linde, Peter (P.A.); Rusu, Jessica (J.L.); Klarr, Jerry (G.T.); Corbett, Sandra (S.M.); Takasawa, Keith (K.D.)
Subject: RE: (2) stalls robustness CR's

Bob,
I expect your information will get understanding of Mazda engineers shortly.

Just for clarification: Kanai-san and Steve Limtiaco are Quality folks and NOT powertrain engineer for this CR. In US, the right contacts is Shiraishi-san in this case.

-----Original Message-----
From: Fascetti, Bob (R.J.)
To: Inoue, Hiroshi (H.); Takasawa, Keith (K.D.)
Cc: Veenstra, Tim (T.W.); Moorhouse, Scott (S.R.); Shiraishi, Masaru (M.); Dalbo, Bob (R.J.); Hofman, Michael (M.V.); Ichikawa, Jiyunichiro (J.); Waud, Sachiko (S.); Fujioka, Kenji (K.); Linde, Peter (P.A.); Rusu, Jessica (J.L.); Klarr, Jerry (G.T.); Corbett, Sandra (S.M.)
Sent: 02/07/24 14:17
Subject: RE: (2) stalls robustness CR's

We need these concerns approved at this Thursday morning meeting. Mazda has had the white papers for these concerns for over a week (sent to Ichikawa-san). All of these concerns have been discussed at our weekly stall meeting, that Kanai-san, and MNAO (Steve Limtiaco) attend.

Takasawa-san has already directed that these concerns be approved. I

understand that Mazda gets some time to approve concerns, and that's why we sent the white paper early.

Please come prepared to approve this concern at this meeting. We have now lost two full days of progress due to waiting.

Please address this matter urgently.
Thank you,
Bob Fascetti
Outfitters Calibration Manager

-----Original Message-----
From: Inoue, Hiroshi (H.)
Sent: Tuesday, July 23, 2002 12:06 PM
To: Takasawa, Keith (K.D.)
Cc: Veenstra, Tim (T.W.); Moorhouse, Scott (S.R.); Shiraishi, Masaru (M.); Dalbo, Bob (R.J.); Fascetti, Bob (R.J.); Hofman, Michael (M.V.); Ichikawa, Jiyunichiro (J.); Waud, Sachiko (S.); Fujioka, Kenji (K.); Linde, Peter (P.A.); Rusu, Jessica (J.L.); Klarr, Jerry (G.T.); Corbett, Sandra (S.M.)
Subject: RE: (2) stalls robustness CR's

Takasawa-san,
Per your approval for KCAP, now Hofu change control process starts officially for these CRs.
At this moment, both of C11390580 and C11371349 are "Black Box" for Mazda engineers.

In order to get Hofu approval quickly, please have relating Ford folks give information to
Mazda engineers ASAP. Shiraishi-san will set up a engineering meeting in this week.

The major point to be confirmed is any impact on Certification/Homologation in countries out side US.
I sincerely don't want make you get problems of regulatory recall.

Hiroshi Inoue
Mazda Tribute Chief Engineer
Phone: 313-845-8179
Fax: 313-248-7059
Cellular: 248-320-7670

-----Original Message-----
From: Takasawa, Keith (K.D.)
Sent: 2002??22? 16:28
To: Corbett, Sandra (S.M.)
Cc: Veenstra, Tim (T.W.); Moorhouse, Scott (S.R.); Shiraishi, Masaru (M.); Dalbo, Bob (R.J.); Fascetti, Bob (R.J.); Hofman, Michael (M.V.); Ichikawa, Jiyunichiro (J.); Waud, Sachiko (S.); Fujioka, Kenji (K.); Linde, Peter (P.A.); Rusu, Jessica (J.L.); Inoue, Hiroshi (H.); Klarr, Jerry (G.T.)
Subject: RE: (2) stalls robustness CR's

Due to the critical nature of these changes and the need to proceed immediately with next steps, I have directed Tim Veenstra to approve the

2 referent CRs. We will follow-up with further information as required.

Regards,
Keith Takasawa
Escape/Tribute Chief Engineer
PDC 2HJ64
MD401
PH: (313) 322-5675
FAX: (313) 248-8599
E-MAIL: KTAKASAW@FORD.COM
TEXT PAGE: 7346045034@mobile.att.net

-----Original Message-----
From: Corbett, Sandra (S.M.)
Sent: Monday, July 22, 2002 3:59 PM
To: Shiraishi, Masaru (M.); Dalbo, Bob (R.J.); Fascetti, Bob (R.J.); Hofman, Michael (M.V.); Ichikawa, Jiyunichiro (J.); Waud, Sachiko (S.); Fujioka, Kenji (K.)
Cc: Takasawa, Keith (K.D.); Veenstra, Tim (T.W.); Moorhouse, Scott (S.R.)
Subject: (2) stalls robustness CR's

I am struggling to get these items ready for release. Here is status for the emergency release for stalls robustness actions:

C11390580- calibration change
-Mazda (Shiraishi-san) indicates they need final white paper, Dalbo will forward
-KCAP (John O'Callaghan) indicates that a plant trial is required...we cannot provide parts until the concern is authorized by Prog. Mgmt....Prog Mgmt (Jessica Rusu) indicates that cr cannot be authorized until trial is complete...HELP/NEXT STEPS???

C11371349- capacitor change
-Mazda (Shiraishi-san) is also requesting white paper--THERE IS NO FUNCTIONAL CHANGE, THEREFORE NO WHITE PAPER WILL BE PROVIDED
-Need Mazda (Fujioka-san and Waud-san) to approve (currently rejected by Mazda)

Tim,
Will there be change control Tuesday at 8am or will these covered at PST?

Sandy Corbett
Escape Powertrain QRT
Phone/Fax: (313)59-44351
Product Development Center 2H-E66

-----Original Message-----
From: Bob Dalbo (1-313-2484947)
[mailto:viwrk014@drkm004.dearborn.ford.com]
Sent: Monday, July 22, 2002 3:01 PM
To: SCORBETT
Subject: Backup note to the PAGE

Robin Peters postponed the stall fix emergency release meeting until concerns
(C11390580 & C11371349) are approved.

From:	Dalbo, Bob (R.J.)
Sent:	Wednesday, July 31, 2002 3:28 PM
To:	Waud, Sachiko (S.); Shiraishi, Masaru (M.); Ichikawa, Jiyunichiro (J.); Takubo, Hirotshi (H.); Kawasaki, Shunsuke (S.); Hamano, Naoumi (N.)
Cc:	Takasawa, Keith (K.D.); Inoue, Hiroshi (H.); Veenstra, Tim (T.W.); Corbett, Sandra (S.M.); Altoonian, Don (D.J.); Peters, Robin (R.S.); Sanders, Muriel (M.S.); Bob Fescetti; Gilbert Fournelle; John Bogema
Subject:	Need Mazda Part Numbers for Service Calibration Release for Escape/Tribute Stalling
Importance:	High

Waud-san,
Concern C11360580, which releases 2001MY and 2002MY service calibrations and PCMs to address stalling on Escapes and Tributes, needs to have Mazda part numbers inserted in order to proceed. Since the concern has been approved by program management, please input the Mazda part numbers as soon as possible.

Bob Dalbo

3.0L Calibration Supervisor
Outfitters Calibration, NAT
Phone: (313) 24-84947 Fax: (313) 32-31786
Pager: (313) 795-2859 Email: *rdalbo@ford.com*

From: Takasawa, Keith (K.D.)
Sent: Wednesday, January 15, 2003 6:39 AM
To: Powers, Ken (K.W.)
Subject: STALLS

Would like to review all the latest indicators on stalls this afternoon if possible. Thanks.

Regards,
Keith Takasawa

Escape/Tribute Chief Engineer
PDC 2H064
MD401
PH: (313) 322-5675
FAX: (313) 248-8599
E-MAIL: KTAKASAW@FORD.COM
TEXT PAGE: 7346045034@mobile.att.net

Agenda : 1/23/2002 – 1/25/2002

1/23 Arrive at 8:00am

8:00 - 8:30 Introductions/Review Agenda/review Q1 process

8:30 - 9:30 Quality Procedures/QS-9000/QOS

9:30 - 10:30 Sub-Supplier Quality Management

10:30 - 12:00 Manage Change

12:00-1:00 Lunch

1:00 - 3:30 FMEAs/Control Plans(DPFE & other Plastic Sensor)

3:30 - 4:30 Problem Solving/Corrective Actions

4:30 - 5:30 Employee Readiness/Training Review

1/24 8:00 - 9:00 Control of Incoming Quality

9:00 - 10:00 Part Identification/Non-Conforming Parts/Packaging/Shipping

10:00 - 11:30 Process Variability Monitoring

11:30 - 12:30 Lunch

12:30 - 1:30 Gage Calibration and Use

1:30 - 2:30 PM/Housekeeping

2:30 - 3:00 Manufacturing Flow/Lean Manufacturing Metrics

3:00 - 3:30 Operator Instructions

3:30 - 5:30 Run at Rate - DPFE Tube Mount (Please have workers breaks before or after run)

For the run at rates:

- All rework/reject bins emptied prior to start.
- Kavlico personnel needs to record fallout from each station per line on a hourly basis
- Parts produced needs to be documented for each hour
- No rework is allowed during run at rates
- Any downtime needs to be noted

1/25 7:30 - 9:30 Run at Rate for Other Plastic Sensor Line

9:30- 10:30 Any other items

10:30 - 11:30 Wrap up

11:30 Depart

10/22/01

[redacted]

Powertrain Operations
V-Engine CAD Design

Ken,

This timing is unacceptable.
We can not wait 2 wks. for a P.O.
We need it TODAY!!!
Please advise. Thanks!
ASAP.

P.S. a req. # will not suffice

[redacted]

P.O. # current rings, minutes, gyros, and apparent from Jim Swipes #38,095

Maurer, James (J.B.)

From: Gates, Freeman (F.C.)
Sent: Monday, May 06, 2002 12:49 PM
To: Freeland, Mark (M.); Maurer, James (J.B.); 'kperk@kavlico.com'; Plante, Paul (P.G.); 'dayers@kavlico.com'
Cc: Johnson, Joe (J.H.); King II, Lamar (L.L.); O'Neall, Jim (J.D.)
Subject: Zarlink's(Datsa) CMOS Latch-up paper

Team,

I found a very interesting technical bulletin that Zarlink published on CMOS latch-up in 1993 that you may want to reference.

Please refer to http://assets.zarlink.com/products/data/appnotes/maan107.pdf

Freeman Gates
Senior EGR Systems Technical Specialist
Tel (313)02-24807 Fax (313)39-04004
PO&E Rm D-139 CM-173

SL - Norfolk - dle, was O.K.

Service Pick

Jeff Dudne x 89567

Unpublished Cases -

Maurer, James (J.B.)

From:	Freeland, Mark (M.)
Sent:	Friday, July 06, 2001 4:06 PM
To:	Johnson, Joseph (J.H.); Gates, Freeman (F.C.); Maurer, James (J.B.)
Cc:	Akins, Mary (M.)
Subject:	FW: Testing of Production MOV Component

AVX MOVs TDevice.pdf

Joe, Jim & Freeman,

The attached .pdf file is the specification for the MOV (Protection diode Z1) used in the DPFE. I thought you should have this for you're records. The part number we are using is [redacted] 5.6V Zoster P.S

Regards

Mark Freeland

> 6-Sigma Black Belt Candidate
> Physics Department
> Ford Research Laboratory
> P.O. Box 2053
> MD 3028 - SRL - Room 1517
> Dearborn, MI 48121-2053 USA
email: mfreela1@ford.com
Tel.: (313) 594-7645

-----Original Message-----
From: Naushad Hossain [mailto:NHossain@kavlico.com]
Sent: Wednesday, June 27, 2001 10:27 PM
To: mfreela1@ford.com
Cc: Kyong Park; Brady Davies; Don Ayers; Bob Weikal; Grant Heliker; Roger Houston; Rick Palermo; Minh Nguyen; Mark Clifford
Subject: Testing of Production MOV Component

Mark:

Kyong, Roger and I tested the MOV component from the production line after you were gone today. The VI curve of the tested MOV component appeared to be within the specification. So, the production parts are okay. Please see page 9 of the attached MOV specification. The blue line (5.6V, 0.1J) of the first plot is the specification of our component. Should you have any questions, please let me know.

Regards,
Naushad

> -----Original Message-----
> From: Roger Houston
> Sent: Wednesday, June 27, 2001 6:53 PM
> To: Naushad Hossain
> Subject: MOV
>

O'Neall, Jim (J.D.)

From:	O'Neall, Jim (J.D.)
Sent:	Thursday, December 05, 2002 11:59 AM
To:	'kpark@kavlico.com'
Cc:	Maurer, James (J.B.)
Subject:	FW: Kavlico Layouts for the Filter Rev 2.0

[redacted]. He needs some parts and some specific drawings.

J. D. O'Neall
Manager, Fuel Metering, Emissions, and Ignition Dept
V-Engine Engineering, Ford Motor Company
joneall@ford.com, 313-322-6839

-----Original Message-----

From:	Freeland, Mark (M.)
Sent:	Thursday, December 05, 2002 11:01 AM
To:	O'Neall, Jim (J.D.); Tracz, Jarek (J.A.)
Cc:	Gates, Freeman (F.C.); Maurer, James (J.B.); Alles, Sheron (S.A.); Kotwicki, Allan (A.J.)
Subject:	Kavlico Layouts for the Filter Rev 2.0

Jarek,

Thank you for taking the time yesterday to discuss the layout and circuit design with me. Attached are the bitmap files showing the Vref (5 volt) and the Vout (Signal to the PCM) tracks. I am still working on trying to decipher the ground paths.

The first concern that I have and wish to document is that the Kavlico's version of the schematic shows the locations of the C5 and Z1 swapped, and the locations of C2 and D1 swapped, when compared to the schematic that I provided. Although, as far a Net List is concerned the circuits are equivalent, they will behave differently at high frequency. Kavlico's proposed layout is implemented like their schematic (not our schematic) as far as C5 and Z1 are concerned. Kavlico's proposed layout is not implemented like their nor our schematic as far as C2 and D1 are concerned. I am sure that you will cover these two points in greater detail in you're review of the layout.

Jim O'Neall,

As Freeman is out of town, could you please pass on the following request to Dr. Park:

1) When can we set up a meeting to discuss the details of the layout with Kavlico? I would like to do this soon.

2) Please provide two additional [redacted] (B&W .bmp or .tif would be best). One to show ONLY the first conductor layer and the outline of the substrate. The second to show ONLY the second conductor and the outline of the substrate. This is needed as the layout drawings received are difficult to follow because there are multiple layers shown on the same drawings (i.e. conductor and insulator).

Also, I am still waiting for connectors to build additional prototype bread boards for Freeman (for the corner testing). Could you ask Kavlico if they could supply me with 6 or more loom side connectors with short pig tails (I only need them to be 2 or 3 inches long, but will cut if they supply longer).

Thank you.

PS The drawings will follow separately in two emails as they are too big for this one email.

Regards

Mark Freeland

6-Sigma Black Belt
Engine Research Department
Ford Research Laboratory
P.O. Box 2053
MD 2629 - SRL - Room 1517
Dearborn, MI 48121-2053 USA
email: mfreela1@ford.com
Tel.: (313) 594-7645

King II, Lamar (L.L.)

From: Kaercher, Don (D.F.)
Sent: Thursday, August 01, 2002 5:46 PM
To: King II, Lamar (L.L.)
Subject: Demand

MONTH	YEAR	Quantity
08	2002	0
07	2002	18598
06	2002	18238
05	2002	18316
04	2002	18538
03	2002	15701
02	2002	15795
01	2002	13272
12	2001	10180
11	2001	12083
10	2001	13463
09	2001	11177
08	2001	17298
07	2001	16018
06	2001	17735
05	2001	20162
04	2001	18551
03	2001	17799
02	2001	14425
01	2001	12579
12	2000	9546

Don Kaercher
Ford Motor Company
FCSD PS&L QSF/Recall/Top 100 Dept. Mgr.
NPDC 1310C Text Pager: (734) 797-5993
e-mail: dkaercher@ford.com
Phone: (734) 266-9793 Fax: (734) 266-1165

King II, Lamar (L.L.)

From: O'Neall, Jim (J.D.)
Sent: Wednesday, July 31, 2002 5:58 PM
To: King II, Lamar (L.L.)
Subject: FW: Top 25 Selling Powertrain Service Parts

Make sure we understand and can explain lines 4 and 5 and then forward a note to John and Frank for info, cc to me. Is there any other service actions that we should be taking based upon this info?

J. D. O'Neall
Manager, Fuel Metering, Emissions, and Ignition Dept
V-Engine Engineering
joneall@ford.com, 313-322-6839

-----Original Message-----
From: O'Neall, Jim (J.D.)
Sent: Monday, July 29, 2002 1:24 PM
To: King II, Lamar (L.L.)
Subject: FW: Top 25 Selling Powertrain Service Parts

This should have come to you!

J. D. O'Neall
Manager, Fuel Metering, Emissions, and Ignition Dept
V-Engine Engineering
joneall@ford.com, 313-322-6839

-----Original Message-----
From: O'Neall, Jim (J.D.)
Sent: Monday, July 29, 2002 1:23 PM
To: King, Lindon (L.)
Cc: Johnson, Joe (J.H.); Gatas, Freeman (F.C.)
Subject: FW: Top 25 Selling Powertrain Service Parts

Please find out what are lines 4 and 5 in this chart. Is Motorola a replacement for a Kavlico dash mounted DPFE sensor for line item 4? What is being replaced by line item 5?

J. D. O'Neall
Manager, Fuel Metering, Emissions, and Ignition Dept
V-Engine Engineering
joneall@ford.com, 313-322-6839

-----Original Message-----
From: O'Neall, Jim (J.D.)
Sent: Monday, July 29, 2002 7:48 AM

To: Foster Jr., Elmer (E.S.); Jesiolek, Walt (W.J.); Johnson, Joe (J.H.); King II, Lamar (L.L.); Krzyske, Dennis (D.C.); Limatta, Gary (G.D.); Platta, Shari Finn (S.F.); Zamora, Melissa Iafret (M.I.)
Subject: FW: Top 25 Selling Powertrain Service Parts

Info. Please note that our dept has several line items here.

- EGR has lines 1, 4, and 5
- Fuel Metering has lines 15 and 17
- Air Metering has line 22

J. D. O'Neall
Manager, Fuel Metering, Emissions, and Ignition Dept
V-Engine Engineering
joneall@ford.com, 313-322-6839

-----Original Message-----
From: Koszewnik, John (J.J.)
Sent: Sunday, July 28, 2002 3:37 PM
To: Shah, Vastupal (V.B.); Sears, Renee (R.T.); O'Neall, Jim (J.D.); Mazuchowski, Jim (J.A.); Wullaert, Michael (M.G.); Beamer, Jerry (J.D.); Dowding, Peter (P.J.); Svantickas, Ed (E.); McCarthy, Thomas (T.A.); Wagner, Terrance (T.C.); Gray, Chuck (C.E.); Sudjianto, Agus (A.); Kvasnicka, Chuck (C.R.); Liou, Shuh-Yuan (S.); Aversa, Piero (P.)
Cc: Fsadni, Frank (F.); Rusek, Ron (R.J.); DiCicco, Tamara (T.K.); McClimont, Greg (G.A.); Plante, Paul (P.G.); McRoy, Gitanjli (G.)
Subject: FW: Top 25 Selling Powertrain Service Parts

For your info. I've asked that we also receive this info monthly.

We'll be posting it on the Wall of Quality to help assist in focusing our efforts.

John Koszewnik
Chief Engineer
V-Engine Engineering
Ph. 32-28973
Fx. 24-86067
jkoszewn@ford.com

-----Original Message-----
From: Kaercher, Don (D.F.)
Sent: Thursday, July 25, 2002 7:24 AM
To: Krygier, Roman (R.J.); Szczupak, Dave (D.T.); Koszewnik, John (J.J.)
Cc: Histand, Tamara (T.L.); Padilla, Jim (James J.); Kaercher, Don (D.F.)
Subject: Top 25 Selling Powertrain Service Parts

During a management review with Jim Padilla following the Town Hall meeting with Parts Supply & Logistics (FCSD), he requested we send a monthly report that shows the 25 highest selling Powertrain parts. The attached report captures our top 25 Powertrain parts for the month of June. We will send the next report within a few

days of July close of business.

Maintenance items (i.e. spark plugs, filters, fluids, etc) have been filtered out of the report. Please contact me with any questions or suggestions.

Don Kaercher
Ford Motor Company
FCSD PS&L QSF/Recall/Top 100 Dept. Mgr.
NPDC 1310C Text Pager: (734) 797-5993
e-mail: dkaerche@ford.com
☎Phone: (734) 266-9793 Fax: (734) 266-1166

Maurer, James (J.B.)

From:	Johnson, Joe (J.H.)
Sent:	Wednesday, July 24, 2002 10:53 AM
To:	Nielsen, Christian (C.A.)
Cc:	Johnson, Joe (J.H.); O'Neall, Jim (J.D.); Maurer, James (J.B.)
Subject:	DPFE Service

Chris, are we currently servicing product with the Motorola plastic housing sensor (F77Z-9J460-AB) in place of the Kavlico aluminum part (F7UZ-9J460-AA)? According to the 60 day project, the expected implementation was to be about 6/1/01.

Thanks for a quick response.

Joe Johnson
Supervisor, EGR Systems, FMEI Dept
V-Engine Engineering, Powertrain Operations
POEE Bldg, Mail Drop 69
21500 Oakwood Blvd
Dearborn, Mich 48124-4091

Ph: (313) 845-8292
Fax: (313) 390-4084
e-mail: jjohnson@ford.com

Sandia - Tunicaid
Larry Ward - EGR 05112
Process pro.
[redacted] Consolidation
82589 New job with EPD
- Jerry Beamer

Noise measurements
- Website of Doug Smith
- High frequency measurement
- $2,000 / day

www.dsmith.org

after John's meeting

Dave Flach Leakage on Vault

gravity hold

Rich Bezenko
afternoon tomorrow or Thurs morning 10:00 AM
Test cell
steam portion
(313) 410-3127

Get sample of die with bubbles around the

Paul,

Darlene looked at a 10K mile part, had lot of bubbles

Panaretos, Christine (C.M.)

From:	Gates, Freeman (F.C.)
Sent:	Thursday, April 04, 2002 11:55 AM
To:	'kpark@kavlico.com'; Maurer, James (J.B.); Plante, Paul (P.G.); O'Neal, Jim (J.D.)
Cc:	Panaretos, Christine (C.M.); Gates, Freeman (F.C.); 'dayres@kavlico.com'; White-Johnson, Patrice (P.); Johnson, Joe (J.H.); Ogozaly, Jim (J.C.)
Subject:	Analytical Solutions Objective/Work-Plan

Objective:

The objective of the failure analysis from Analytical Solutions is to provide a "Fresh Eyes" review of all failure modes of the TmDPFE sensor. This will be accomplished by the following:

- Provide rapid analysis of difficult to analyze failures i.e. failures which occur within the die that may not be readily visible.
- Pinpoint the exact location of low resistance paths that generate excessive current flow
- Determine if "unprotected area damaged" parts are the actual cause of component failure.
- Determine if "unprotected area damaged" parts are characteristic of corrosion caused by external contaminants or internal processing.

Workplan:

1. Kavlico will provide a Non-Disclosure Agreement that will allow Analytical Solutions and Ford personnel to mutually discuss all aspects of the circuitry and/or process that are pertinent accomplishing the aforementioned objectives.

2. Kavlico Technical personnel will accompany Ford engineering to Analytical Solutions to discuss objective details.

3. A total of 5 baseline "good" parts will be provided to Analytical Solutions by Kavlico to establish reference data.

4. The following failed parts will be taken for analysis:

- At least 2 parts that exhibits high current flow
- 4 confirmed failed parts manufactured between May - August of 2001
- 4 confirmed failures of parts manufactured between June - September of 2000
- 2 random higher mileage failures (greater than 15,000 miles)

Thanks

Freeman Gates
Senior EGR Systems Technical Specialist
Tel (313)32-94807 Fax (313)69-04064
FOME Rm C-135 CM-173

313 755-5698

Maurer, James (J.B.)

From:	Plante, Paul (P.G.)
Sent:	Monday, March 25, 2002 12:34 PM
To:	Maurer, James (J.B.)
Cc:	Plante, Paul (P.G.)
Subject:	Outside Help Contacts-DPFE Sensor

CPARS order help contacts are:
1) Jim Simpson, V Finance
2) Maggie Duke, Ford Procurement, will assist in rapid writing of CPARS order
3) John Blake, MSX, will answer strategic questions on the orders

24267
JSM7887

advise Me if you need more help in getting oders for the below people out this week Loey Sallieh (WSU), Ed Sickafus (FRL), U. of Maryland, and Analytical Solutions, NM.

Paul Plante
V Engine Campaign Prevention Specialist
POEE Building, Drop 20, Cube BG049, Pillar D5
Tele. 313-84-54138; Fax 39-02513
Text Pager: 734-296-1505
E Mail: pplante@ford.cm (CDS ID PPLANTE)

[redacted]

WHO TO ADDRESS ORDERS TO;

RPS, CPARS?

PROFESSIONAL MISCELLANEOUS

[redacted]

INCLUDE A SOLE SOURCE JUSTIFICATION

GET PROPOSALS →

[redacted]

Southfield, MI [redacted]

6982-827 28/05

[redacted]

ED S

GROSSE ILE, MI. [redacted]

[redacted]

1 DAY $3,000

Akolkar, Shrikant (S.V.)

From: Akolkar, Shrikant (S.V.)
Sent: Thursday, September 19, 2002 7:01 PM
To: Maurer, James (J.B.); O'Neall, Jim (J.D.)
Cc: Gates, Freeman (F.C.); Freeland, Mark (M.); Hangas, Jon (.)
Subject: FW: Windstar Sensor #99

Jim & Jim;

Thanks to Mark & John for prompt help they provided today for ele testing & gel removal.

- Sensor is electrically dead/out of spec. Vout is low & impendence are completely beyond limits
- Gel surface & tubes had layer of carbon over 1mm thick implying poorly performing engine. Mark has photos. Ultrasonic alcohol cleaning did not removal the carbon. It had to be mechanically removed which probably damaged bond pad wires
- I am leaving die photos & ele report on Jim Maurer's desk. There is no obvious visible damage. Some bubble anomalies are visible on REF die.

----Original Message----
From: Freeland, Mark (M.)
Sent: Thursday, September 19, 2002 3:07 PM
To: O'Neall, Jim (J.D.)
Cc: Akolkar, Shrikant (S.V.)
Subject: Windstar Sensor #99

Jim,

Please forward me all info you have regarding the sensor Shri brought me to test this afternoon. I would like to make sure the document I send you is clear and concise.

Can you provide the following:

VIN #
Mileage accumulated on the sensor.
Date the sensor was removed.
Were there any stored codes in the PCM, all codes are of interest, not just the dPFE codes?
What is the full repair history for this vehicle from the date the sensor was installed until the date it was removed? I suspect that the engine has a misfire history, of some sort.
Do we have Kavlico's parametric test data for the part.

Thanks

Regards

Mark Freeland

6-Sigma Black Belt
Engine Research Department
Ford Research Laboratory
P.O. Box 2053
MD 2629 - SRL - Room 1517
Dearborn, MI 48121-2053 USA
email: mfreela1@ford.com

Tel.: (313) 594-7645

2.0L Zetec Focus /4.6L/4.2L F150 EGR Calibration-Mapping Data Observations:

Assumptions:

- Sensor gel temp exposure is proportional to the EGR mass flow & exhaust gas temp.
- The observations are based on EGR calibration table & dyno stationary EGR mapping data. The identical transient drive cycle/test procedures data like on MPG/APG tracks for 3 vehicles under considerations is not available.

Observations:

When EGR is Flowing-

1. 2.0L Zetec engine exhibits higher exhaust back pressure spikes range of 0 to 4" Hg. This may be due to the fact that the max EGR calibrated to higher speeds than other engines. The 4.6, 4.2, & 3.0L engines have spike range of 1 to 2"Hg. However, when ~ max EGR is flowing, the exhaust back pressures are very low (1 to 2 in Hg).

2. 2.0L Zetec engine encounters many more back pressure fluctuations/spikes (higher frequency) than 4.6L & 4.2L engines due to speed & load changes at same EGR setting.

3. 2.0L Zetec engine encounters wide exhaust flange temp fluctuations/spikes (ranging from ~ 600 to 1600 deg F) than 4.6L 3.0L & 4.2L engines due to speed & load changes at same EGR setting.

Zero EGR mapping data-

4. At any speeds, 2.0L Zetec engine exhibits higher back pressures than 4.6L & 4.2L engines. The gap further widens at higher speeds. E.g. At 4000 RPM, 2.0L Zetec back pressure is ~10.5"Hg where as 4.6L is ~5.5 & 4.2L is ~9" Hg. The max back pressures also exhibit same trend showing values of ~ 16, 6.5 & 9" Hg respectively.

5. No EGR flow situation is more severe for the sensor pressure pulsations than EGR flow situation.

Akolkar, Shrikant (S.V.)

From: Reichenbach, Ronald (R.W.)
Sent: Wednesday, July 10, 2002 4:27 PM
To: Akolkar, Shrikant (S.V.)
Subject: RE: 2001MY 4.6,4.2L EN/FN, 2.0L Zetec Focus EGR Mapping & Calibration data Analysis

Here is the table that denotes Desired EGR % Rate for a given RPM and Load at sea level:

	0.8	0	0	0	0	0	0	0	0	0	1
	0.7	0	0	2	2	2	2	2	2	2	1
	0.6	0	4	5	6	6	6	6	4	4	1
LOAD	0.5	0	10	11	12	10	8	8	7	4	0
	0.4	0	10	12	12	12	12	7	7	5	0
	0.3	0	10	10	10	10	10	7	6	4	0
	0.25	0	8	8	8	8	8	7	6	3	0
	0.2	0	2	2	2	2	6	6	6	2	0
	0.1	0	0	0	0	0	0	0	0	0	0
		750	1000	1500	2000	2500	3000	3500	4000	4500	5,000
						RPM					

-----Original Message-----
From: Akolkar, Shrikant (S.V.)
Sent: Wednesday, July 10, 2002 3:53 PM
To: Reichenbach, Ronald (R.W.)
Subject: RE: 2001MY 4.6,4.2L EN/FN, 2.0L Zetec Focus EGR Mapping & Calibration data Analysis

Ron,

Can you pl. send me full EGR calibration table with info as noted below. Thanks.

-----Original Message-----
From: Akolkar, Shrikant (S.V.)
Sent: Tuesday, July 09, 2002 6:51 PM
To: Maurer, James (J.B.); Janda, Jon (J.M.); Stump, Steven (S.M.)
Cc: Gates, Freeman (F.C.); Freeland, Mark (M.); Zulczyk, Steve (S.S.); Planta, Paul (P.G.)
Subject: 2001MY 4.6,4.2L EN/FN, 2.0L Zetec Focus EGR Mapping & Calibration data Analysis

Steve Zulczyk was very helpful in pulling mapping data from the Ford intranet. I sorted that data & plotted various ways. After a few meetings with Steve & Freeman Gates with the processed data, it was decided that the mapping data will not help much to determine the differences in environment for Kavlico DPFE sensor. We need to compare actual EGR calibration data points.

I was suggested to approach Steve Stump for 2001MY 2.0L zetec EGR calibration table. Steve, can you help us by providing this data & also suggest 4.6L & 4.2L contacts or request them to provide similar data. We intend to compare exhaust temp, pressure (at flange), % EGR, speed, load(torque, EEC) calibration data points. I need to use the same data for forthcoming MPG & dyno tests. The same sensor is used in all vehicles but warranty numbers are different.

I am one of the members of a large team headed by Jim Maurer to resolve this concern & develop good sensor keylife test so that we can detect customer concern during DV/PV stages.

With Regards,

SHRIkant Akolkar
sakolkar@ford.com Ph:(313) 594-1908 Fax::(313) 390-1229

2001MY Escape-3.0L DOHC - RH

LOAD — %EGR at sea level

EEC %	500	750	1000	1250	1500	2000	2500	3000	4000	6000
0.8	0	0	0	0	0	0	0	0	0	0
0.6	0	0	9.5	10	9.5	6	6	5	0	0
0.5	0	0	11.5	12	11.25	8.5	6	7.5	0	0
0.4	0	0	9.25	11	11	11	8	9	2	0
0.3	0	0	4	8.625	8.25	7	5	3	2	0
0.25	0	0	1.5	5.25	4.25	2.5	0	0	0	0
0.2	0	0	0	0	0	0	0	0	0	0
0.15	0	0	0	0	0	0	0	0	0	0

RPM

RPM

EMS-627 2003A

2001MY F150 with 4.2L Engine EGR Calibration Table

FM05G EGR %

EEC %	500	750	1000	1500	2000	2500	3000	3500	4000
0.8	0	0	0	0	0	0	0	0	0
0.7	0	0	0	0	0	0	0	0	0
0.6	0	0	4	3	2	0	0	0	0
0.5	0	0	7.5	4	2.5	2	0	0	0
0.4	0	0	8	6.5	5	3	0	0	0
0.3	0	0	8	9.5	6	4	0	0	0
0.2	0	0	0	7.5	0	0	0	0	0
0.1	0	0	0	0	0	0	0	0	0

Engine RPM

Mike Glenger
7/1

TABLE: PEV08G OWNER: Engine Parameter ADDRESS: 15954 X-BIN-POINT: 3 STRATEGY: HWAI2
EDITOR: LEVEL5 X-RANGE: 0 TO 31.975 X-ACCURACY: .125 PATLEVEL: [0T]
SYMBOLS: --none-- X-BIN-RANGE: 0 TO 255 OWNER: CEARLY SUBACCOUNT: 1r516068

.8	7	0	0	0	0	0	0	0	0	0	0
		1599A	1599B	1599C	15990	1599E	1599F	159A0	159A1	159A2	159A3
.7	6	0	0	0	4	4	4	4	0	0	0
		15990	15991	15992	15993	15994	15995	15996	15997	15998	15999
.6	5	0	2	7	8	6	4	4	4	0	0
		15986	15987	15988	15989	1598A	1598B	1598C	1598D	1598E	1598F
.5	4	0	0	0	4	8	6	6	5	0	0
		1597C	1597D	1597E	1597F	15980	15981	15982	15983	15984	15985
.35	3	0	9	12	12	12	9	9	6	0	0
		15972	15973	15974	15975	15976	15977	15978	15979	1597A	1597B
.25	2	0	9	7	7	7	7	9	6	0	0
		15968	15969	1596A	1596B	1596C	1596D	1596E	1596F	15970	15971
.15	1	0	0	0	5	5	2	2	0	0	0
		1595E	1595F	15960	15961	15962	15963	15964	15965	15966	15967
.05	0	0	0	0	0	0	0	0	0	0	0
		15954	15955	15956	15957	15958	15959	1595A	1595B	1595C	1595D
		500	750	1000	1250	2000	2500	3000	3500	4000	5000
		0	1	2	3	4	5	6	7	8	9

2001 MY
PN96 4.6L A/T

NAME: SPA LEVEL RPM TABLE
PURPOSE:
X INPUT: NORMALIZED ENGINE SPEED IN RPM - P0870
Y INPUT: NORMALIZED LOAD - P0871
OUTPUT: PERCENT RPM

TO: SHRIKANT AKOLKAR
1 PAGE

FROM: CURT EARLY
X-8687|

Alcolicar, Shrikant (S.V.)

Subject:	Kevlico DPFE Noise Factor/Kaylife Tests on Eng.dyno & Veh. Chassis Rolls
Location:	POEE-BO93 (15); POEE-AO65 (16); CR "B"
Start:	Fri 6/7/02 1:00 PM
End:	Fri 6/7/02 2:30 PM
Recurrence:	Weekly
Recurrence Pattern:	every Friday from 1:00 PM to 2:30 PM
Meeting Status:	Meeting organizer
Required Attendees:	Alcolicar, Shrikant (S.V.); Maurer, James (J.B.); Freeland, Mark (M.); Gaiss, Freeman (F.C.); Fabian, Phil (P.A.); Duncan, Jack (J.L.); POEE-BO93 (15); Herr, Mike (M.S.); POEE-AO65 (16); Petty, Neal (N.E.)

Gentlemen,

Thanks Jack bringing to my attention that CR-B093 is not showing for this meeting. I have now booked CR "B" (not on computer) which is next Henry Ford's glass enclosed office at POEE. Our office assistance checked my meeting & she confirmed that it's a computer screw up. I am booking some other available rooms here for next 2 meetings if required. Let's see if it works. If future 6/14 & 6/21 meetings are required & CRs still conflict, I will sent another meeting notice. Also, pl. note revision in agenda.

Agenda: Determine the details of the following items so that the engine & vehicle tests can be started before July 1st 2002. No standard test exists. Determine the parameters for starting the test quickly & modify test as we learn more.

- EGR-Sensor accelerated test enviornment-Shri, Freeman
- Accelerated test cycles with heating, cooling, condensation, electrical impulses etc-Shri
- Any existing dyno/chassis roll/proving ground tests can be used?-Neal, Jack, Mike
- Discussion on bench or engine/vehicle test- Neal Petty, Mike
- Discussion on testing at Ford or outside
- Mechanical Instrumentation-Shri
- Electrical Instrumentation & monitoring-Mark
- Intermittent inspection
- Test duration/Anticipated failure period/Testing to failure
- Multiple sensor mounting & testing on one engine/vehicle, start with single sensor
- Any other items missed.

Considering the gravity of the Kevlico sensor failure situation on all vehicle lines, your attendance is necessary. The engine & vehicle have been identified & are being prepared. Only key people have been invited to speed up the process. A rough draft for the purpose of start of discussion is attached.

[redacted]

Akolkar, Shrikant (S.V.)

From:	Herr, Mike (M.S.)
Sent:	Wednesday, May 29, 2002 1:45 PM
To:	Akolkar, Shrikant (S.V.)
Cc:	Maurer, James (J.E.); Fabien, Phil (P.A.)
Subject:	RE: DPFE sensor/EGR During DCDC Tests

Shrikant,
Answers to your questions:
EGR is functional and DPFE is electrically connected during all DCDC testing, but the lowest RPM for that test is pk tq RPM - 500. That's pretty high for most engines (>3000 rpm) and we typically don't run EGR there. I'm looking at the cycle right now. At most 15% of the test time is spent with EGR functioning. And that's the only durability test we currently have where the EGR will be functioning.

All engine controls are driven by PCM but we can bring in an RCON or ATI and run the engine from that if needed.

It would be possible to get DPFE sensors that have finished testing. All engines are sent to EMDO for teardown. You can try to grab them before leaving Dyno, or get them at EMDO after teardown. If you are intested only in 3.0L U204, we'll have to get with Phil Fabien.

Some info for you on DPFE failures at Dyno. If they occur during durability testing (doubtful since we don't exercise them) we would never know about it because we have no way of monitoring DPFE function in durability rooms. We have had a history of DPFE failures in development rooms. On past programs I can remember not being able to control EGR and changing DPFE to re-gain control. The failures were blamed on moisture accumulation in the DPFE. We were told this would not occur in vehicles since they would spend more time not running than a Dyno motor and would have time for the water to drain. So we need to check with the 3.0L U204 development engineer(s) to find out if they had any DPFE failures during development. There is no other way because part failures in development rooms are not tracked.

We understand that we don't catch EGR-related failures on Dyno so we are developing new tests that will prevent things like the Kavlico DPFE from slipping through in the future.
1. Dynamic Cycling Test - designed to cycle the VCT mechanism, it will also cycle the EGR system
2. Intake Sludging Test - based on a real customer drive cycle that sludges the intake manifold and throttle. EGR will function at the speeds/loads run here.
3. WRT test - a wear test but it includes simulated city driving and frigid temperatures
4. New Engine Systems Test - there is a BlackBelt project to get rid of the DCDC and replace it with a test that will actually cycle the EGR and other components.

It would be great if one of these test cycles would fail the DPFE. I will support your efforts as best I can. Maybe we need to set-up a meeting, including someone from Phil Fabien's group (I don't recall who develops U204 over there).

Mike Herr
Engine Durability Technical Specialist
mherr@ford.com
(313) 33-71900 (voice and fax)
V-Engine Engineering - Ford Motor Company

—Original Message—
From: Akolkar, Shrikant (S.V.)
Sent: Tuesday, May 28, 2002 5:15 PM

Akolkar, Shrikant (S.V.)

From:	Herr, Mike (M.S.)
Sent:	Wednesday, May 29, 2002 1:46 PM
To:	Akolkar, Shrikant (S.V.)
Cc:	Maurer, James (J.S.); Fabien, Phil (P.A.)
Subject:	RE: DPFE sensor/EGR During DCDC Tests

Shrikant,
Answers to your questions:
EGR is functional and DPFE is electrically connected during all DCDC testing, but the lowest RPM for that test is pk tq RPM - 500. That's pretty high for most engines (>3000 rpm) and we typically don't run EGR there. I'm looking at the cycle right now. At most 15% of the test time is spent with EGR functioning. And that's the only durability test we currently have where the EGR will be functioning.

All engine controls are driven by PCM but we can bring in an RCON or ATI and run the engine from that if needed.

It would be possible to get DPFE sensors that have finished testing. All engines are sent to EMDO for teardown. You can try to grab them before leaving Dyno, or get them at EMDO after teardown. If you are intested only in 3.0L U204, we'll have to get with Phil Fabien.

Some info for you on DPFE failures at Dyno. If they occur during durability testing (doubtful since we don't exercise them) we would never know about it because we have no way of monitoring DPFE function in durability rooms. We have had a history of DPFE failures in development rooms. On past programs I can remember not being able to control EGR and changing DPFE to re-gain control. The failures were blamed on moisture accumulation in the DPFE. We were told this would not occur in vehicles since they would spend more time not running than a Dyno motor and would have time for the water to drain. So we need to check with the 3.0L U204 development engineer(s) to find out if they had any DPFE failures during development. There is no other way because part failures in development rooms are not tracked.

We understand that we don't catch EGR-related failures on Dyno so we are developing new tests that will prevent things like the Kavlico DPFE from slipping through in the future.
1. **Dynamic Cycling Test** - designed to cycle the VCT mechanism, it will also cycle the EGR system
2. **Intake Sludging Test** - based on a real customer drive cycle that sludges the intake manifold and throttle. EGR will function at the speeds/loads run here.
3. **WET test** - a wear test but it includes simulated city driving and frigid temperatures
4. **New Engine Systems Test** - there is a BlackBelt project to get rid of the DCDC and replace it with a test that will actually cycle the EGR and other components.

It would be great if one of these test cycles would fail the DPFE. I will support your efforts as best I can. Maybe we need to set-up a meeting, including someone from Phil Fabien's group (I don't recall who develops U204 over there).

Mike Herr
Engine Durability Technical Specialist
mherr@ford.com
(313) 33-71909 (voice and fax)
V-Engine Engineering - Ford Motor Company

----Original Message----
From: Akolkar, Shrikant (S.V.)
Sent: Tuesday, May 28, 2002 5:15 PM

Jack L. Duncan
Test Development Engineer
Vehicle Durability Systems Engineering
Michigan Proving Ground
Global Test Operations
Research and Vehicle Technology

74240 Fisher Road
Romeo, MI 48065 USA

Tel: [redacted] 752-6993
Fax: [redacted] 752-6993

jduncan1@ford.com

Freedom Rings or Life Member O.K.

Maurer, James (J.B.)

From: Verner, Carol (C.J.)
Sent: Thursday, September 05, 2002 4:26 AM
To: Maurer, James (J.B.)
Subject: RE: dPFE Fleet Measurements: Second note

If possible take off, replace in veh. with new, get veh. back, replace with old

Jim,

Thinking about this some more, it may not be possible for these vehicles to be sitting around to allow the sensors to cool down to atm. conditions. Kyong may realize this as well. In the earlier conversations he mentioned that it was important for the parts to be as close to atm. conditions as possible when measuring. Question, It is more important that data be gathered from these sensors in the lab vs gathering mileage? If so I'll throw this out to you. What would you and the team think about pulling 9 sensors off the fleet titled Freedom Rings (see attached) and leaving the two on LifeMembers. Reason, Freedom Rings will probably have approximately 20K miles by now and it also has the least amount of miles on the vehicle and there is the opportunity to get approximately 90K - 100K miles on some of them. Life Members is getting up there in vehicle mileage and we can keep going on the sensor miles. Mike Chaulk works with this fleet often and if we switch sensors on Freedom Rings they would remain on for the life of the sensor or getting as many miles as possible. The fleet will work with us (unless we want to take 11 vehicles out of commission for an hour). This could also give us the opportunity to see how 9 different sensors from the population sent here will perform. If we get an paralyene coated failure early, ???????.

If not, take off

I am also proposing that the group of paralyene parts on NCH Healthcare in Naples, Florida do not be removed at all. We will need all the miles they are gathering.

I could get to the point where a decision will need to be made in Vegas because I suspect we are not going to be able to hold them for an hour. Mike has them pulled in every day for an oil analysis but I'm sure it does not take that long. If the sensors are warm when the Kavlico person makes the measurements, do we leave ourselves open for, "how reliable is the measurements since the parts were probably not at atm conditions".

Need resp of Vel. temp.

I'll try and call you during the day to get your thoughts.

Carol

Las Vegas Visit Fo
Final.xls

-----Original Message-----
From: Verner, Carol (C.J.)
Sent: Wednesday, September 04, 2002 5:09 PM
To: Maurer, James (J.B.); Gates, Freeman (F.C.)
Subject: dPFE Fleet Measurements

I just spoke with Kyong and he is proposing the following for measurement:

If we can get all 11 vehicles in the garage at the same time then he wants to have all sensors pull off and put in an A/C room to cool down to atmospheric conditions (temperature and pressure).

The Kavlico rep (Simon M.) will take three measurements (he will bring power supply and digital meter) and get in average.

From this we will make a decision regarding which two to pull. If all good, take two random. If all bad (outside of 0.75 v and 1.25V) then they will be pulled and replaced with good ones Kavlico will bring.

I will get the latest mileage off the ODO.

If we cannot pull all in at the same time and let cool then we will get this info the best we can.

If you need to contact me, leave a message on my phone. I will be checking messages.

Carol
x07180

Maurer, James (J.B.)

From: Akins, Mary (M.)
Sent: Tuesday, April 03, 2001 9:19 AM
To: Freeland, Mark (M.); Johnson, Joseph (J.H.)
Cc: Gates, Freeman (F.C.); Maurer, James (J.B.)
Subject: RE: Part numbers

Mark,
YF1E-9J460-AD is the correct part number and level for North America.
YM2A-9J460-AB is the European part number. Only difference with North American part is the part number, otherwise the parts are identical.

YS4Z-9J460-AA is the service part number for the European part.

You can concentrate on YF1E-9J460-AD and it will cover the European part also.

Hope this helps.

Regards,
Mary Akins

-----Original Message-----

From: Freeland, Mark (M.)
Sent: Monday, April 02, 2001 5:19 PM
To: Johnson, Joseph (J.H.)
Cc: Akins, Mary (M.); Gates, Freeman (F.C.); Maurer, James (J.B.)
Subject: Part numbers

Joe, Mary, Freeman or James

Do you have any document which clearly lists all the part numbers associated with the problem Kavlico sensor, and describes the differences.
Specifically, I have several parts on my desk, some of which I got over at the Quality Center this morning, and I am suitably confused. The three part numbers I am aware of are YF1E-9J460-AC, YM2A-9J460-AB and YS4Z-9J460-AA. What are each of them?

Regards

Mark Freeland

6-Sigma Black Belt Candidate
Physics Department
Ford Research Laboratory
P.O. Box 2053
MD 3028 - SRL - Room 1517
Dearborn, MI 48121-2053 USA
email: mfreela1@ford.com
Tel.: (313) 594-7645

IEEE Circuits & Devices
The Magazine of Electronic and Photonic Systems
Vol. 10, No.6
November 1994

Balanced Probe Extends High-Frequency Measurements

Douglas C. Smith
D. C. Smith Consultants
P. O. Box 1457
Los Gatos, CA 95031
Phone: (408) 356-4186
Fax: (408) 358-3799
Email: doug@dsmith.org
Web: http://www.dsmith.org

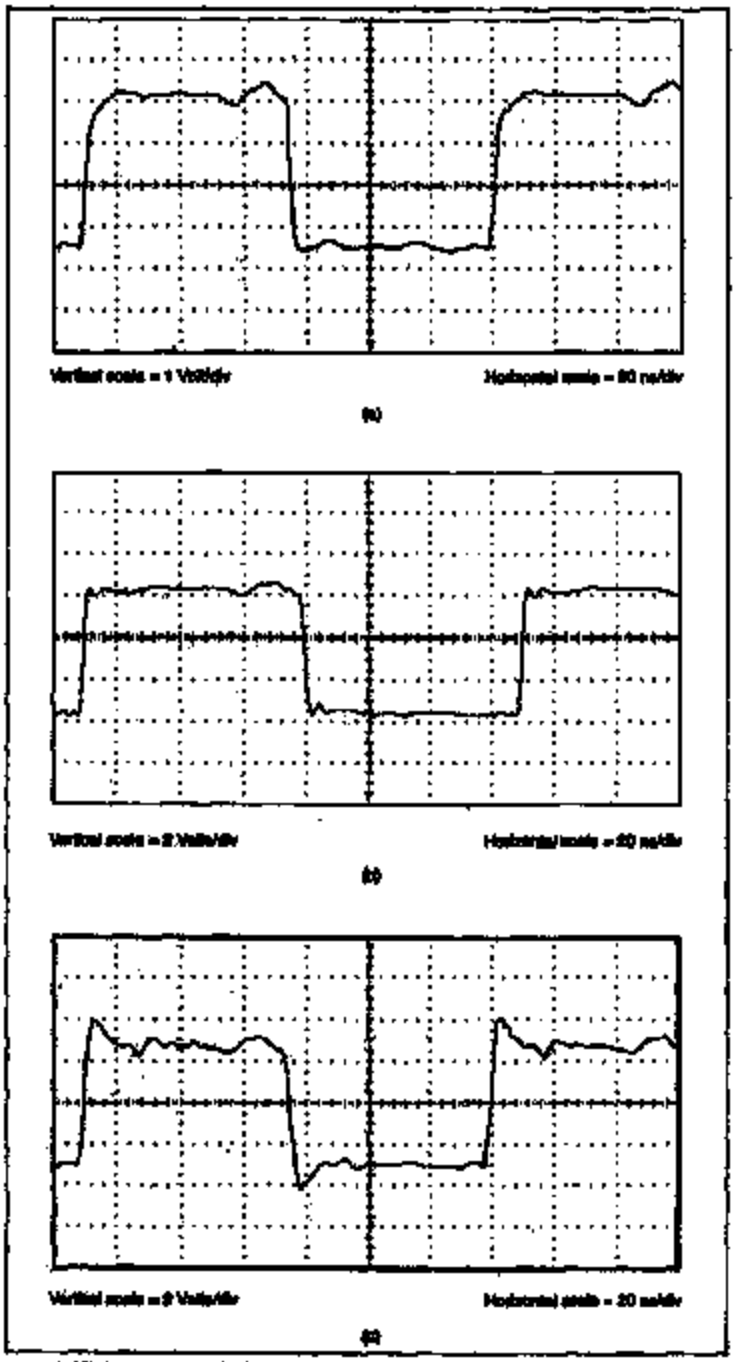

2. (a) HC240 output into 50 ohms; (b) HC240 output into 1800 ohms; (c) HC240 output as viewed by 10X high Z passive probe.

form is not known beforehand. In this case, the peak-to-peak voltage monitored is about 45 percent too high (compare Figs. 2b and 2c). This overshoot, caused by a capacitive input impedance and lead inductance, underscores the problem of probes with a capacitive input impedance. That is, they cannot be used to measure the high frequency potential between two points much more than an inch apart because of the equivalent lead length to make such a measurement.

Figure 3 shows the results of an even more serious problem. The measurement configuration consisted of shorting the inputs of two 10X high-impedance passive probes with their own 15 cm ground leads and connecting them to the output of an HC240 buffer. The output of the buffer is a slightly rounded 40 MHz squarewave. I call this a "null experiment." Such an experiment is one whose outcome is expected (usually zero), and the extent to which the outcome deviates from the expected value indicates the error in a measurement. Experience has shown that all measurements should be checked by an appropriate null experiment, especially if the result indicates additional cost must be invested into a product.

Now that the channels are displaying a waveform of a few volts, even though the probes are shorted! This display is due to ground lead currents generating an L-di/dt drop across the ground leads. This ground lead voltage appears as an input signal to the probe. An interesting point to notice is that the two waveforms bear little resemblance to each other even though the probes and scope amplifiers are essentially identical. This is because the impedance looking into the shields of the two cables are different. Thus, the shield currents are different and, accordingly, so are the ground lead induced voltages. These voltages can be minimized by twisting the cables together. However, the variability rarely exhibits more than 10 dB of common mode rejection above a few tens of MHz if the two probes are used in an A minus B mode for differential measurements.

The Balanced Coupled Probe

The balanced coupled probe eliminates many of the high frequency problems described above by making a balanced measurement with a resistive probe input impedance. Commercially available active balanced

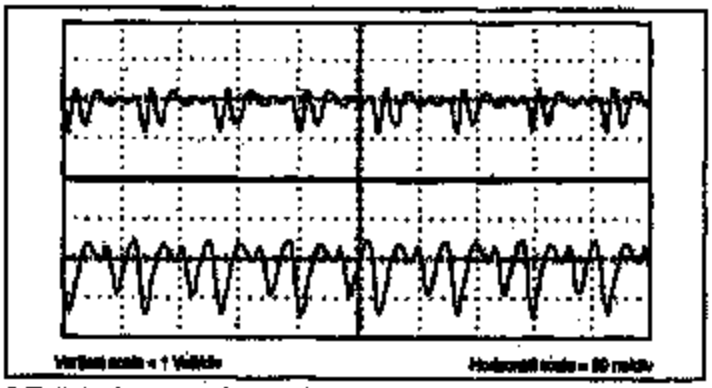

3. Shorted probe response for two probes.

probes are available, but these are limited in frequency response to about 100 MHz. They also tend to be capacitive, have capacitive input impedances, and are sometimes fragile. The balanced coaxial probe is a passive "low" impedance probe that uses a pair of coaxial cables fastened together. It has a typical input impedance of 1000 to 2000 ohms. As mentioned earlier, a standard "high" impedance 10X passive probe has a much lower input impedance than 1000 ohms at frequencies above a few tens of MHz. So, an input impedance of 1000-2000 ohms is not as low as it sounds.

Figure 4 shows the simplified construction of a balanced coaxial probe. Its main features consist of a 180 degree combiner to subtract the signals on the two coaxial cables, a pair of coaxial cables with shields unbonded in contact or with an overshield, resistances to match the cable impedances at the probe tip and at the cables, and the probe tip series resistor. This probe can be built with reasonable effort by someone experienced in VHF/UHF rf design techniques. The configuration of the 50 ohm terminations and control of parasitic capacitances at the probe tip are the most critical portions of the circuit.

The combiner requires 50 ohm terminations on all its ports. This condition is met by providing 50 ohm terminations at the ends of the coaxial cables. Using a single 50 ohm resistor would not work well, as the inductance of the resistor might become comparable to 50 ohms at a few hundred megahertz. In general, a network of resistors or a disc resistor must be used. If a network of resistors is used, the type of resistors and the geometry of the network are important to meeting the goal of achieving a 50 ohm resistive termination that works to hundreds of megahertz. The impedance of the termination should be measured on a network analyzer to assess its performance.

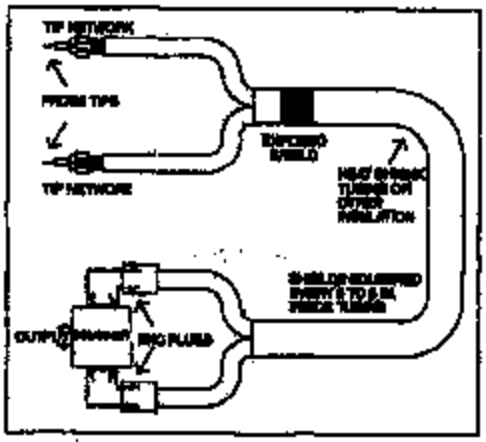

4. Simplified diagram of a balanced coaxial probe.

From the center conductor of the coax cable ends, where the terminations connect from center conductor to shield, we connect a series-probe tip resistor. The free end of this resistor is the probe tip. The value of this resistor determines the input impedance and attenuation factor of the probe. The calculation of this resistor and its effects on the probe performance will be discussed in the next section.

The aforementioned description covers the basics of the probe. In addition, one may find that performance can be improved by further attention to parasitics. For instance, the termination and probe tip resistor could be shielded to prevent proximity of the operator's fingers from affecting probe performance. In any event, the probe must be carefully checked out and calibrated for gain and frequency response. Very small differences between the two halves of the probe will effectively destroy its common mode rejection.

Balanced Probe Performance

In comparison to commercially active balanced probes, the balanced coaxial probe has a relative input impedance (no resonances to well beyond 500 MHz) can be built or purchased relatively inexpensively, and has a bandwidth to 500 MHz with an appropriate 180 degree combiner. The frequency range of 1 to 500 MHz can be covered with a single commercially available combiner. Common mode rejection ratios between 30 and 35 dB are typically achieved over the range of 1-500 MHz.

The probe's input impedance is a function of the attenuation factor. If a 475 ohm probe tip resistor is used, the input impedance will be 1000 ohms, uninterrupted to the probe shield ground (475 + 50 ohm cable in parallel with the 50 ohm terminating resistor). The probe factor will be about 20 dB (32X). Of this, 26 dB (20X) comes from the dividers formed by the tip resistors, terminations, and cable characteristic impedances. About 4 dB of the probe factor is due to the loss of a typical combiner. If 764 ohms of tip resistance is used, a 50X probe will result if the combiner lost is 4 dB.

An input impedance of 1000 ohms uninterrupted to ground may seem low. However, the impedance is much higher at 200 MHz than that of any probe with 5 or 10 picofarads of input capacitance. In addition, with the exception of resonant circuits, most high frequency circuits (above a few tens of MHz) are of lower impedance. If the power-to-ground impedance of a circuit board is comparable to a probe input impedance of 500 ohms, the circuit board design is probably to say troubled. For instance, this probe

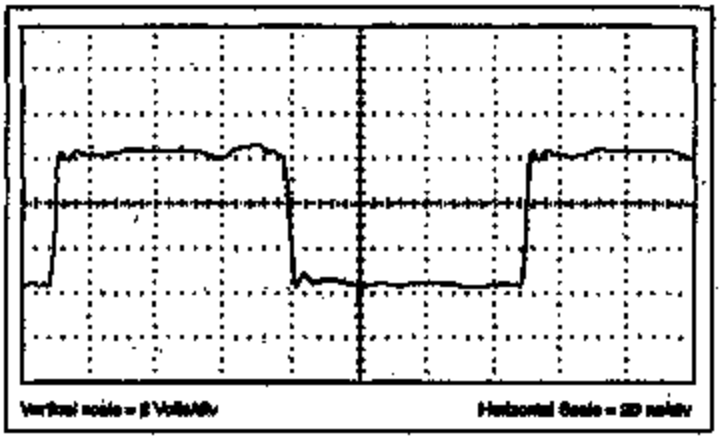

5. HC240 output as viewed with a balanced coaxial probe.

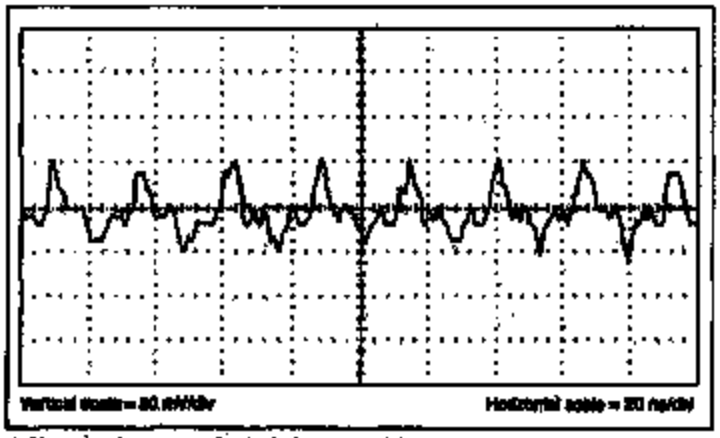

6. Shorted probe response for the balanced coaxial probe.

would not be visible with usual, microvolt circuits and logic gates with low output current. For the vast majority of high-frequency voltage measurements, however, the balanced coaxial probe is preferred.

Although a ground lead can be attached to the probe for safety reasons it is not necessary. If it is used, any voltage induced across it will be common mode to both channels and will be rejected in the measurement by the common mode rejection of the probe. The only reason to use a ground lead is to reduce a large common mode signal or a value where the differential signal can be measured. For most logic circuits, common mode voltage will not be a problem for this probe. The expected shield shown in Fig. 4 is used to connect to the chassis of the EUT (typically

the waveform corresponding to Fig. 2a (standard probe with 15 cm ground lead), but measured with the balanced coaxial probe. This probe also used about 15 cm of lead length for the measurement. Notice how clean the waveform is with no overshoot and a fast risetime (about 2 ns limited by the HC240 buffer). In fact the waveform looks faster than with the coaxial cable, Figure 2a, because the 50 ohm load imposed on the HC240 output tends to almost beyond its drive capability. The HC240 easily drives the 1000 ohm input impedance of the balanced coaxial probe used. Figure 2b is, in fact, Figure 5.

In Figure 6, the probe tips are shorted together and connected to the output of the HC240 which is producing a slightly rounded square wave at about 40 MHz, corresponding to Fig. 3 using the standard probe. The response to this null experiment is only about a hundred millivolts peak-to-peak, instead of the few volts observed before! This illustrates the excellent common mode rejection of this probe and indicates a measurable measurement in Figure 5.

Conclusions

The balanced coaxial probe is a valuable high frequency measurement tool that avoids the limitations of conventional probes, active and passive. Its resistive input impedance and balanced design are the keys to making clean measurements. In fact, this probe represents an extremely effective method to accurately measure a high frequency voltage between nodes a few inches apart, as the required lead lengths for such measurements cause severe overshoots for "normal" probes with capacitive input impedances.

Douglas C. Smith is a Distinguished Member of Technical Staff at AT&T Bell Laboratories, Middletown, NJ.

References

1. *High Frequency Measurements and Noise in Electronic Circuits*, Douglas C. Smith, 1993, VanNostrand Reinhold, p. 62.

2. *High Frequency Measurements and Noise in Electronic Circuits*, Douglas C. Smith, 1993, VanNostrand Reinhold, p. 72.

3. "Techniques and Methodologies for Making System Level ESD Response Measurements for Troubleshooting or Design Verification," D. C. Smith, *1992 EOS/ESD Symposium Proceedings*, EOS-14.

Risetime	Induced Voltage
1 ns	1200 mv
2 ns	600 mv
3 ns	400 mv
4 ns	300 mv
5 ns	240 mv
6 ns	200 mv
10 ns	120 mv

transients is inexpensive, rugged, readily available, and works well in many measurement setups. However, today's high speed electronic circuits have stressed the capabilities of the traditional setup. Above 50 MHz, the 10X probe can seriously distort the waveform. It can also significantly affect the response of the measuring equipment. Thus, when the signal contains frequency components above 50 MHz, an alternative measurement technique is required to ensure accurate results.

Measurement Pitfalls

The main causes of high frequency measurement errors with a 10X passive probe are related to its input impedance and the typical use of a ground lead. Such probes typically have an input impedance of 10 megohms in parallel with 10 pF. [illegible] capacitance has a reactance of only 160 ohms! This presents significant loading on most circuits. If the input impedance (of a "high" impedance probe) is relatively low, and the ground lead has significant reactance, there will be various measurement problems.

Figure 1 shows the calculated input impedance of a 10X high impedance passive probe with a 13 cm ground lead, a typical length supplied with such probes (1). This arrangement exhibits a classic series resonance consisting of the probe's input capacitance and the inductance of its ground lead. Such a configuration acts like a notch filter, and connecting the probe to a malfunctioning circuit will oftentimes bring it into normal operation. This result is the inverse of what might be expected. One explanation is that the "notch filter effect" of the probe filters out any offending noise.

Other signal effects involve the ground lead of the probe, which can be a source of error from induced voltages. Any voltage that appears across the ground lead from the L-di/dt drop is in series with the desired signal and is often indistinguishable from it, especially if the expected waveshape is not known beforehand. Such an induced voltage is generated by current flowing between the equipment under test and the scope, through the ground lead and probe cable shield. There are many sources of such currents at high frequency, including ground noise from logic circuits, and field induced currents from usually unnoticed electrostatic discharge (ESD) events in the same room.

It does not take much ground-lead current to develop a significant induced voltage. Table 1 shows the voltage developed across 13 cm of 24 gauge wire in free space, for a 10 mA change in current at a function of three [2]. Various logic-gate families can source/sink 10 mA in less than 1 ns, so the numbers shown in the table are conservative. Even the output of an IRC gate can cause 2 or 3 volts of inductive drop across a 15 cm ground lead! ESD events in the same room can induce tens of volts or more on a probe ground lead from several feet away.

10X Probe Measurements

Figures 2a-c show oscilloscope traces for the output of an HC240 gate (octal inverting buffer) measured in three ways. First, the waveform in Fig. 2a was obtained by connecting a coaxial cable to the 50 ohm input of a scope. 50 ohms is a heavy load for the HC240 buffer, and this causes the signal to have an output amplitude of about 4 volts peak-to-peak. A one volt per division scale is used in Fig. 2a to make the waveform large enough to see the detail near the rising and falling edges.

The bumps in the waveform are generated by parasitics in the HC240 and its circuit board, such as ground bounce. Since the 50 ohm cable is terminated with its characteristic impedance, it does not contribute to the bumps in the waveshape of Fig. 2a. Due to heavy loading by the 50-ohm termination, this is not a practical method of measuring most signals.

Figure 2b shows the output of the buffer when loaded with 1500 ohms by a method which will be described shortly. A 2 volt per division scale is used to scale the size of the waveform similar to that in Fig. 2a for comparing the features of the waveform. In this figure, the amplitude is slightly more than 5.5 volts because the buffer is being powered from 4 AA cells through a series diode. The rise time is sharper because the load is more reasonable, and there is no overshoot. The bumps in the waveform, as with the 50 ohm measurement, are due to parasitics in the HC240 and its circuit.

Figure 2c shows the output of the HC240 as measured with a common 10X high impedance passive probe with a 13 cm ground lead. Note the significant overshoot on the waveform, which is not present in Figs. 2a or 2b. Not a naive examination waveform, one would not readily be aware of such a significant error in the peak-to-peak measured voltage since the shape of the wave-

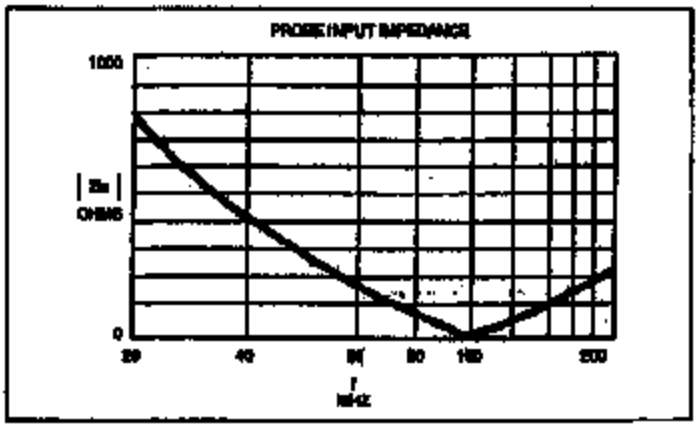

1. 10X high-Z passive probe input impedance.

Balanced Probe Extends High-Frequency Measurements

Coaxial type for 1-500 MHz overcomes the limitations of conventional probes, active and passive

Douglas C. Smith

Making accurate signal and noise measurements at ever higher frequencies becomes more critical for today's complex devices and systems. Many of the standard approaches to making high frequency measurements in design verification, debugging, and the manufacturing of integrated circuits can yield surprisingly large errors that lead to incorrect decisions about the design. This article addresses some of the errors associated with traditional oscilloscope measurements using conventional probes, and offers an improved method of making measurements on electronic circuits of all kinds.

Overview

The conventional 10X high-impedance passive probe and oscilloscope arrangement for performing signal and noise voltage mea-

0733-3996/94/$4.00©1994IEEE

Vehicle Buy Back Process

- Identify a vehicle from buy back list. Once a vehicle is placed on the list it generally will remain there for 3 weeks because it takes this long to process the check.
- If we decide to buy a vehicle back, we must work with our vehicle representative and submit a PSR (procurement) form to start the process.
- We would be responsible for all transportation expenses involved with shipping the vehicle.
- When we are done with all test, the Buy Back organization expect the vehicle to be returned to them "REPAIRED". Their philosophy is when they make a vehicle available to Engineering for evaluation, they will get it back with all repairs made.
- Once the vehicle is repaired, we are responsible for getting it over to an area called Receiving Y here in Metro Detroit. This is a holding area for buy back vehicles. Once there a company called DST Industries will inspect the vehicle and prepare it to go to Auction. DST Industries is a vendor of the Buy Back organization.

Maurer, James (J.B.)

From:	Schiedig, Kurt (K.J.)
Sent:	Wednesday, March 20, 2002 1:23 PM
To:	Maurer, James (J.B.)
Subject:	FW: Billing Address

Jim, they're starting to say "show me the money" at Wayne State. I have some free time today, can I work with someone in your shop to get the order going for Losy?

Kurt.

-----Original Message-----
From: Marty Kusnia [mailto:mkusnia@wayne.edu]
Sent: Wednesday, March 20, 2002 3:18 PM
To: kschiedi@ford.com
Cc: Rita Coyne
Subject: Billing Address

Dear Mr. Schiedi :

RE: Reliability and Analytical Work on the Engine DPFE Issue

To what address should the above referenced project be billed?

Thank you,

Marty Kusnia
Manager, Funded Research Administration
Wayne State University College of Engineering
(313)577-3819

Letter —

[redacted]

Detroit, MI [redacted]

R 020252
Proposal Number

EN02-027 28838

Maurer, James (J.B.)

From: Freeland, Mark (M.)
Sent: Wednesday, October 30, 2002 9:59 AM
To: McCoy, James (J.D.); Maurer, James (J.B.); Gates, Freeman (F.C.)
Cc: Duncan, Jack (J.L.); Verner, Carol (C.J.)
Subject: RE: MPG Focus Testing

Carol Verner and I examined the M6 sensor which failed on this vehicle yesterday.

The observed symptoms were:

The output was saturated low.
The power to ground impedence was unstable.
The ref. die has a dark discoloration of the gold on the Vro, the Hpos and the Hneg bond pads.
The HI die had a large bubble (about 90% of the die area) at the interface between the surface of the die and the potting gel, this is consistent with the die having passed a large current for a short period of time.

I understand that the oscilloscope never triggered, but I have to report that I believe that this part experienced a short duration, high current event.

The unstable iref data form the data logger may be a significant clue and should be looked at again.

Jack,

Can you give me the VIN number, the ODO and date at which the M6 part was installed and the ODO and date at the time it was removed, for my records.

Thanks

Regards

Mark Freeland

6-Sigma Black Belt
Engine Research Department
Ford Research Laboratory
P.O. Box 2053
MD 2629 - SRL - Room 1517
Dearborn, MI 48121-2053 USA
email: mfreela1@ford.com
Tel.: (313) 594-7645

—Original Message—
From: McCoy, James (J.D.)
Sent: Thursday, October 24, 2002 1:53 PM
To: Maurer, James (J.B.); Freeland, Mark (M.); Gates, Freeman (F.C.)
Cc: Duncan, Jack (J.L.)
Subject: MPG Focus Testing

<< File: m6oyc4551.xls >>
Data sent by Jack Duncan on the Focus from MPG.

Chart shows VREF, DPFE out, and VREF current with reference to the DPFE failure.

Regards,
Jim McCoy
Fuel Metering, Emissions & Ignition Systems Engineering
Hardware Control Interface Group

V-Engine Engineering
POEE - MD#69 - Rm. D142 - Cube DF1B6
Phone (313) 33-79690 / Fax (313) 39-04084
E-Mail: jmccoy1@ford.com

Maurer, James (J.B.)

From:	Awad, Mahmoud (M.I.)
Sent:	Monday, December 09, 2002 4:52 PM
To:	O'Neall, Jim (J.D.)
Cc:	Maurer, James (J.B.); Freeland, Mark (M.); Gates, Freeman (F.C.); McCliment, Greg (G.A.)
Subject:	Mark's Repeat repair analysis on the Focus

Jim,

I reviewed the massive work that Mark did as far as the repeat repair for the Zetec Focus and I think both of us agree on the following points:

- The repeat repair percentages are high (especially for August-Oct 00 and June-July 01) Vehicle month of productions. His analysis confirms my old analysis on that.
- The average time/mileage to failure for the 1st repair is pretty much the same for the second and third time/mileage to fail.
- Assuming that every repair after Feb. 02 is done using the new "V transient" sensor, there had been almost 1500 failures for that sensor so far. I think this number is high and the question is did this design is substantially different than the old one? In addition to that, the average time/mileage to failure is similar to the old "non-protected" sensor.

Best Regards
Mahmoud Awad
Reliability Implementation Engineer
FMEI Department Support
Phone: (313) 24-83160
e-mail: mawad@ford.com

① Update 1 pagers for Frank

② Send workplan + documents to team

Freeland, Mark (M.)

From:	Plante, Paul (P.G.)
Sent:	Thursday, June 13, 2002 9:31 AM
To:	Poma, Amy (A.); Janda, Jon (J.M.); Rossi, Roberto (R.A.); Plante, Paul (P.G.)
Cc:	Maurer, James (J.B.); Gates, Freeman (F.C.); Freeland, Mark (M.)
Subject:	Minutes and Agenda for PDFE Vehicle Team Meeting

Monday 6/10 Meeting Overview for 14D Team:
1) J. McCoy/A. Poma to hand out vehicle test plan including vehicle consensed instrumentation and w/ settings.
2) John Johshan Focus vehicle (Vin#0555): Issue was discussed and it was noted that the current spike documented on the V Ref line was not obtained with the correct instrumentation or settings to ensure that it was real to the vehicle and not just improper instramenting technique. Team agreed to stop investigation of this spike, instrament the car properly and continue testing. Is-Is Not to be filled out by John, and discussed Monday.
3) Hussein Bina Focus Car: Vehicle had (2) failed sensors from 9/00 MOP. Discussion lead to agreement that these sensors had high probability of both failing due to MOP, the car is a private owner, and we are already testing Focus vehicles, but need other product lines as well. Conclusion was to not test this car.
4) Alan Ford Focus buy back is complete and now owned by V Engine. It is waiting for instrumentation.

Monday 6/17/02 Agenda:
A) Vehicle Test Plan Overview-J. McCoy/A. Poma
B) Is-Is Not Sheet Overview-Jon Janda
C) EESE Comments on Wiring Issues-Keith Frazier
D) Dyno and Labeco testing overview-Sro Akolkar
E) Cigarette lighter wire bundle affect on DPFE Is-Is Not, R. Rossi
F) Escape brake light switch wiring 12V short to 5V Is-Is Not, R. Rossi
G) John Johshan Focus current spike issue Is Not, J. Johshan
H) J1 connector Is Not, R. Rossi
I) C90 connector Is Not, R. Rossi
J) Walk Ins
K) 14D team update issues
L) Next Monday meeting agenda

Amy/Jon, suggestion: Use flip chart in meeting room to write down conclusions, assignments and next agenda items to get team concensus. There are many issues here with high technical content to track.

Robert Rossi: Please note that you and Keith have considerable issues on Monday 6/17 agenda, please come prepared.

Paul Plante
V Engine Campaign Prevention Specialist
POEE Building, Drop 20, Cube BG049, Pillar D5
Tele. 313-84-84136; Fax 39-02513
Text Pager: 734-296-1905
E Mail: pplante@ford.cm (CDS ID PPLANTE)

Results of St. Croix/St. Thomas Virgin Island Investigation of 3.0L Escape

Executive Summary

A total of **22** Concern Units were inspected by Powertrain Field Quality (PFQS) Gil Pepitone from 6/15-6/25/02.

18% of inspected vehicles with certain key Service Actions applied and containing uncontaminated fuel were fully resolved for the "Stalling during Deceleration" Concern, as reported by Owners.

The vehicle population which had prior repair attempts, (55%) did not have TSB/Oasis SSM Service repairs fully applied for various reasons, including test data mis-interpretation, component ordering wait time, WDS test equipment procedures/hardware issues, and "Repair Holds" for pending Engineering visitation.

However, 67% Units had **contaminated fuel and restricted fuel filters**, which may have been a **contributor** to the unverified **Deceleration Stalling** issue.

A second Driveability Concern (which included Units that contained the latest calibration level) of **Hesitation during moderate engine temp** was listed as a Concern for 32% of the Units. The Hesitation Concern was then verified and data /reviewed or recorded by PFQS. However, resolution was not determined. Local fuel volatility and/or PCM calibration may root cause, but this is speculation. Further investigation is in progress.

An omission of a Diagnostic procedure in TSB 02-8-6 was found, involving the requirement for a drive cycle in order to prompt the start of the Purge Cycle for proper EVAP System evaluation.

The surface blistering of multiple MAF sensor's plastic case was reported, with a sample captured.
A second MAF related issue of tight MAF retaining nuts resulted in airbox lid breakage.

A third MAF sensor related issue of missing Part Number imprint was found on two Units.

Idle Air Control (IAC) Duty Cycles were found in 27% Units to be on the high end of the spec. In some cases, IAC replacements did not reduce DC. Also, there is a need for multiple improved IAC diagnostic procedures for TSB
02-8-6.

PFQS recommendations are listed at the end of this report.

Background

PFQS was contacted in early June to inspect and resolve the reported Decell Stalling Concern on a minimum of 10 3.0L 2001/02 Escapes on the Islands of St. Croix and St. Thomas, U.S. Virgin Islands. Both dealerships use the same name of Metro Motors.

Figure 1 Metro Motors, St. Croix, VI

Figure 2 Burnete Matto, Service Manager

Figure 3 Isaac, Driveability Technician

Figure 4 Service area at Metro Motors

Figure 5 Service area, alternate view

A review of Service records and Oasis repair histories as compared to the actual PFQS inspection of the 22 Units, indicated that corrective Service procedures were only partially performed on 55% of Units.
However, 18% of Units had been fully serviced per the existing Service Communications.
The remaining percentile involved Units which had not been to the Dealership for the Decell Stalls Concern prior to the Inspection period.

Both Islands are small (St. Croix, the larger, is 28x7 miles). The terrain is very hilly, with some considerable grade angles. The

Concern of Decell Stall for 3.0L Escape is reported as most common in uneven topography as evidenced from a prior PFQS review of North American CQIS data.

Of the 22 Units Inspected, 20 were at the St. Croix location, while two were done in St. Thomas. A total of four Units were originally scheduled for St. Thomas, but two were no-shows. The majority of this report's data stems from the St. Croix Dealership.

Investigation of Decell Stall

PFQS arrived on Saturday, 6/15. Basic Inspection and VDR recorder Drive Testing began that day and throughout the weekend for the three high priority Units as designated by the Dealership.

PFQS's original plan was to first verify the Drive Concern, but soon realized that Concern replication was difficult.
None of the Units ever exhibited a Stall in any drive mode during PFQS use.

On 6/17, the Inspection worksheet,

[redacted] , was started to be used.

Over the course of the Investigation, some Units (18%) had arrived to the Dealership that had been "Owner Determined" as resolved because of prior service actions performed by the St. Croix Metro Motors.
Being a small island, word of the "Ford Rep" presence prompted some Owners to return to the Dealership for a "Health Check" on their prior resolved Units.

Only one Unit was found by PFQS with the known Concern of "spider web" EVAP line restriction.

As cited, some Units had only part of the necessary Service actions completed. Also, interpretation of some data was either misunderstood, or the existing TSB diagnostics required additional

description. On this last point, details are provided throughout Sections below.

Fuel Quality Issues

The first priority Unit investigated was described as having a different Drive Concern of **"Hesitation** after Cold Start".
Note that this Unit did **NOT** have the Concern of **Decell Stall** as part of the original listed complaint.

The heavy hesitation (lasting about 3 seconds) from a dead stop on a 30 degree upgrade acceleration, during a moderate engine temp range (approx 100F-160F) was replicated by PFQS. A fuel gauge had been installed along with a WDS VDR recorder. All parameters, including both fuel pressure and volume were confirmed as acceptable.
However, because this was a Returnless Fuel application, PFQS felt that his old method to check volume (filling 12oz bottle in 15 sec at Idle) may not be valid.

As a result, the fuel filter was removed and blew backwards into a glass bottle:

Figure 6 Contaminated fuel, after sitting overnight

Figure 7 Bottom view of the fuel sample-Nasty Stuff

Figure 6 This is the fuel sample after the bottle is shaken, not stirred. This is what it looks like after you blow out the fuel filter.

PFQE then realized that perhaps local fuel is a negative influence in the generation of Decell Stalls, as well as possibly contributing to the Hesitation Concern.

From that point on, every Unit was inspected for restricted fuel filter/dirty fuel. 67% of inspected Units had restricted fuel filters and dirty fuel.

However, **32%** of the Units which had "Complete Service Actions" (see below), **PLUS** a new fuel filter, were **STILL** verified by PFQS **for the Hesitation Concern.**
Note that the latest PCM flash is included, and this includes some Units of which had the latest PCM Flash prior to PFQS visitation: the need for Adaptive Learning Strategy was NOT a factor for some of the repeatable **Hesitation** Concern Units.

It appears that the **replacement** of the restricted **fuel filter** did **not** resolve the **Hesitation** Concern.
However, **filter replacement** may be a **positive factor** in resolving the **Decell Stalls** Concern.

In defining "Complete Service Actions", PFQS includes a PCM Reflash to the latest available calibration level, the latest level EEC Relay, the latest level DPFE, a complete check of ALL grounds and connectors, proper evaluation of the EVAP Purge D.C. vs. FTP sensor voltage data and conformation of acceptable IAC D.C. values when observed during the PROPER conditions. Note that MAF replacement is not included unless the Owner cited a specific,

repetitive location during the Decell Stall event, implying local electrical "noise" generation (i.e. radio towers, etc).

New Concern of Moderate Engine Temp Hesitation discovered

PFQS then concluded: this repeatable Hesitation Concern could possibly be caused by one of two items, or perhaps both.

a. Local Fuel Quality (suspect volatility, not just the "dirt factor")
b. PCM Calibration

Please note that PFQS has no proof to indict either suspected root cause. PFQS is in communications with the St. Croix Service Manager for feedback of alternate fuel brand usage as recommended in an attempt to resolve those Units with the unresolved Hesitation Concern.
PFQS welcomes Engineering feedback on possible calibration issues and is willing to assist further.

In addition, a VDR recording was captured in this Hesitation drive mode on 6/25 on one Unit, which had all "Complete Service Actions" and a clean fuel filter. This data will be shared with Engineering in the very near future.

Procedural Omission in TSB 02-8-6
The Repairing Tech described the following prior repair effort.

The Tech stated that while following Step #4 of the above TSB, the EVAPVM (VMV Duty Cycle) percentage was not seen to change from Zero % at idle (as specified by the TSB) after a one hour idle.
PFQS was able to replicate this scenario on the same Unit and also for a second Unit. The fuel tanks were above ¼ full.
During discussions with Engineering during his visitation, it was suggested that the vehicle be driven to prompt the Purge Process. As a result, the purge cycle started to increase.

While Step #4 described Purge Cycle function over 84%, it's diagnostic do not describe what must be done if the value does not change from Zero% while at prolonged idle.

The Tech's interpretation of the lack of VMV Duty Cycle change from Zero % at idle resulted in the ordering of a VMV. The Tech mentioned that if VMV replacement did not prompt a purge cycle DC increase from Zero%, a PCM would have been considered for order. Potential TNI Warranty for both the VMV (9C915) and the PCM (12A650) exists.

MAF and Related Hardware Issues

Three different issues were experienced during this inspection. Pls note that none involved the actual FUNCTION of the MAF. DTCs were NOT set, nor were inappropriate MAF voltage values witnessed.

However, Warranty, TNI and Real, have been generated as a result.

Item #1: The Tech described prior MAF replacements based upon the observation of the blistering of the MAF's Sensor's Surface:

Figure 9 Blister on the MAF sensor's Case

Figure 10 Close up of the Blister

The Tech cited two replacements. The Parts Dept search only produced the one item photographed here. The Tech said the other one was "worst" with multiple blisters present.

Item #2: During PFQS inspection, one of the 3.0L Escapes MAF was found to be missing the imprinted part number on the sensor's plastic body:

Figure 11 MAF without a imprinted part number

A second Unit, a lone 2.0L Zetec Escape was presented for inspection. This Unit {which was not supposed to be part of the Study} was reviewed as a courtesy. It too did not have a PN imprinted on it. It was not replaced. However, the Tech felt it should be, because of the uncertainly of the level of the MAF component. This indicates that TNI Warranty may result for MAF due to the missing PN.

Item #3; During the removal of the MAF for one Unit for updates per the TSB {Owner reported Stalls in one particular location}, the retaining nuts were found very tight. Hand tools, not power tools were used.
During the attempted removal, the studs started to unscrew from the airbox lid. One of the plastic bosses of the airbox stud broke as a result:

Figure 12 Airbox lid that contains MAF retaining studs

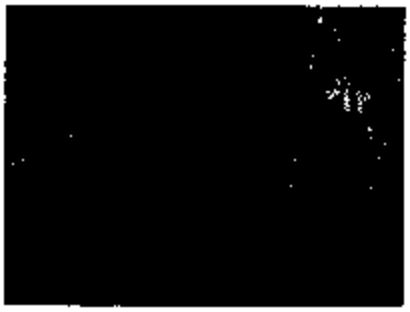

Figure 13 As stud walked out, it broke the case's boss

Figure 14 This is the rear view of the case's boss

Figure 15 A second stud walked out, but the case did not break. The witness marks are pliers on the threads.

At first PFQS suspected the nuts as over torque. A subsequent inspection found "Lock Tite" substance on the fine thread end of the studs. It is possible the adhesive is too strong.

As these MAFs are being replaced per the TSB, it is possible Warranty will be generated for the YL8U-9643-BC Airbox Lid.

Intake Airflow Control (IAC) Solenoid Duty Cycle Value Results

As part of requested Engineering data, IAC Duty Cycle values were monitored per Step #1 of TSB 02-8-6. Note that awareness of proper

conditions to determine acceptable IAC D.C. were not understood by all repair Techs interviewed. While IACs had been replaced on some Units, those were probably changed mainly as part of a general repair attempt, and not necessarily due to data acquisition.

As a result, some repeat Concern Units {46%} required IAC and in some instances, Throttle Body {TB} replacement.
Pls note, however, TBs were not available at the Dealership, and Engineering shipment did not arrive during PFQS visitation. The Engineering shipment of IACs did arrive and most were used.

Idle Air Control {IAC} Duty Cycles were found in 27% Units to be on the high end {greater than 40%} of the allowable spec.

30% of Units with IAC replacement did NOT realize a substantial change {less than 1%} for IAC D.C. value.
Other Units {8%} realized a desired small decrease in D.C., but their final value was still above acceptable range of 40% per the TSB, which would then require a TB replacement.

The high airflow D.C. after IAC replacement indicts either initial throttle body airflow set and/or plate sludge build-up.
Mileage range for unchanging D.C. values after IAC replacement were 2K-18K.

If the pending shipment of TBs arrive at Metro Motors St. Croix, PFQS is to be contacted. Concern Units will be requested for return and their TB will be replaced and then sent to PFQS, who in turn will return same to Engineering.

Additional IAC Diagnostic improvements are provided below in the Recommendations Section.

<u>Recommendations</u>

1. A Market directed "Info Only" Oasis Broadcast Message should be generated to emphasize fuel filter/fuel quality as part of routine inspection when diagnosing all Driveability Concerns. Locations could include the Caribbean Islands and other

Markets were local Service Facilities practices come into question.

2. A review of TSV 02-8-6, Step #4 should be conducted for consideration of the inclusion of a drive cycle prior to inspection of EVAP Purge VMV Duty Cycle values. This drive cycle would only be used for those Units which do not show an increase from 0% at idle. A time factor should be provided to aid the Tech on when he should perform the drive cycle.
   Also, if fuel tank level is an influencing factor for valid EVAP evaluation, an acceptable fill range should be included in any TSB revision.

3. The three issues cited which involve MAF should be investigated by Ford Engineering and Visteon. MAF Sensor blistering, missing MAF PNs, and tight MAF retaining nut on airbox studs are subject.

4. A review of TSB 02-8-6, step #1 should be conducted to clarify and emphasize the definition of "no purge flow". This subtle reference was overlooked by all Techs interviewed. Specific reference, similar to Step #4 wording, which involves a PID definition and values (i.e.: observe IAC D.C. while EVAPVM is Zero%) is necessary to enable ALL Techs to properly diagnose the true need for IAC replacement.
   If there is confusion, the part will be replaced on an assumption, and not the result of data acquisition.

   Also, the converse is true: some Units will quickly START the purge cycle, before IAC D.C. could be read under proper conditions. A work around can be done by shutting off ignition and immediately restarting, and then waiting for all other conditions (RPM to return to 750) to be proper before reading IAC D.C. This additional procedure should be considered for inclusion to any TSB revision.

   A reference to the Catalyst Protection of a 50 RPM increase for a base idle of 800RPM should be included. Also, instructions to apply throttle briefly to reduce this RPM value to return to 750

RPM is necessary to allow the Techs to determine true IAC D.C. and is recommended for TSB revision inclusion.

5. A review for the need to spray insect/spider removal agent should be conducted. It is conceivable that the above TSB's Step #5 will temporarily remove a spider from the EVAP fresh air line, but there is nothing to prevent the return of another spider. Should we use something to stop the potential cycle of web build up?

I will be calling into the "Escape Stalls Team" 2PM conference call on 6/27/02 to discuss my inspection.

Gil Pepitone
Powertrain Field Quality Engineer In South Florida

gpepitan@ford.com
Office 954-753-9989
Cell 954-242-2066

CSQI002 CQIS Indicator Summary 06/19/02 23:25:03

=> 1 of 1

Rpt#: 2FSG8001 CQD Rpt: 06/19/2002 Odom: 3,355 M
Rvwd: File: _ Folder: _____ Images: 0 Print Smy/Dtep Detail(P/D): _
Vehicle: 2002 WINDSTAR,4X2 ,WAGON 2FMZA52432BB55561 Bld: 04/26/2002
Engine: 3.8L EFI F Calb: 2A31ZC0A Trans: 4F50N Axle: FWD 3.56 A/C: YES
Dealer Id: 45262 HERTZ RAC - DETROIT Ph#:
State: Michigan City: Romulus Orig/Caller: JOHN DOMKA
Symptom: 6 96 2 96 DRVABL,INDICATOR,CHECK ENGINE,NOT LISTED
Addl Sym: St: CCRG/EPRC: _ Rvwd: Dt:
Fix: Caus. Comp: SENSOR ASY EGR PR VL -- RPL Condition Code: H5

Region Code: CC Region Name: Rental - CC

CONCER CHECK ENGINE LIGHT ON
REPAIR CODE P0401 - EGR INSUFFICIENT FLOW - REPLACE SUSPECT DPFE SENSOR.
ISSUE CORRECTED. SUSPECT DPFE WILL BE GIVEN TO MARK FREELAND
DPFE BUILD DATE 2D09B
MICHIGAN FQE - JOHN DOMKA
313-433-7910

F1 Help F3 Exit F4 Last Cmts F5 Add Cmts F6 Add Fldr
F7 Bkwd F8 Fwd F9 Ind Corr F10 Next Rpt F11 Prev Rpt F12 Return
I0018-BOTTOM OF DATA LPENJBD

Thanks,

John J. Domka

Field Quality Engineer
Enhanced Concern Identification
Ford Customer Service Division

jdomka@ford.com
Phone 313-433-7910
FAX 734-475-9110

ER02-627 27232

MEETING ANNOUNCEMENT / WORKING TEAM MEETING

Objective:	**Establish and implement corrective and containment actions for Kavlico TM dPFE Sensor**

Meeting Location

Subject:	Kavlico TM dPFE Sensor Core Team
Dates:	June 27, 2002
Time:	1-3:00 p.m.
Location:	POEB, DI-196 (FMEI War Room)
Called By:	Jim Maurer, Team Leader: (313) 39-03672
Next Meeting (s):	June 2, 2002, Core Team Meeting July 9, 2002, Core Team Meeting
Conference Call-in Number(s):	9-1-954-1149 (inside Ford); 847-619-6158 (outside) Passcode: 688 1436# Kavlico Fax: 805-523-7125

Core Team Participants

Black Belts	Kavlico	V-Hasing	Quality Office	BBSE	Purchasing
Mark Freeland	Mary Akins	Jim O'Neail	Mahmoud Awad	Sheran Alles	Chris Nielsen
Shri Akolkar	Don Ayers	Freeman Gates		Robert Rossi	Bill McCarty
Jon Jaeda	Kyong Park	Amy Penna			Shri Reddy
		Paul Plante		PCSE	
Team Leader	Visteon	Carol Verner		Ken Arnold	
Jim Maurer	John Jahshan			Brian Perry	

Meeting Agenda –6/27/02

Order of Agenda Items	Corr. Issue #	Person(s) Responsible	Time Allocated
1. Continued discussions of 6/15 Analytical Sol. Ltr. M. Freeland's feedback from 6/26 Sci Lab mtg.		Mark Freeland/All	20 minutes
2. Parser Data update		Mary Akins	5 minutes
3. Vehicle instrumentation/test status		Jim McCoy	5 minutes
4. Test plan for Norfolk DP field return part.		Brady Davies	5 minutes
5. Walk Ins		All	30 minutes

Proposed Next Meeting Agenda 6/27/02	Person(s) Responsible	Time Estimated

Notes

Bring handouts (paper copies) for all presentations
Provide electronic copies of presentations to sponsor (no later than 1 hour prior to the meeting)
Please be on time as we have a full agenda

Jim Maurer/cp: 6/27/02
Kavlico dPFE Sensor Core Team

Freeland, Mark (M.)

"rom: Freeland, Mark (M.)
ent: Wednesday, June 19, 2002 11:40 AM
To: Dalbo, Bob (R.J.)
Subject: RE: One example of Engine quit

Bob,

I don't want to get in the middle to mess things up, but if they suspect the dPFE is causal part, then could you please get it back for me to test. Thanks

Regards

Mark Freeland

> 6-Sigma Black Belt
> Engine Research Department
> Ford Research Laboratory
> P.O. Box 2053
> MD 2629 - SRL - Room 1517
> Dearborn, MI 48121-2053 USA
email: mfreela1@ford.com
Tel.: (313) 594-7645

-----Original Message-----
From: Dalbo, Bob (R.J.)
ent: Wednesday, June 19, 2002 10:58 AM
To: Kanai, Shinji (S.); Sanders, Muriel (M.S.); Altoonian, Don (D.J.); Aynessazian, Kam (K.); 'Badgley, Joel (J.K.)'; Bauer, Scott (S.C.); Bhojwani, Kamal (K.); Blackburn, Thomas (T.J.); Bogema, John (P.); 'Cary Powell'; Chick, John (J.); Chih, Ming-Niu (M.N.); Chin, Darrel (D.); Corbett, Sandra (S.M.); Dalbo, Bob (R.J.); Rothweiler, Daniel (D.); De Pena, Juan (J.E.); Diez, Timothy (T.P.); Fascetti, Bob (R.J.); Fournelle, Gilbert (G.); Freeland, Mark (M.); Giles, Stuart (S.); Gokhale, Renuka (R.V.); Grewal, Bill (B.S.); Grimes, Jeff (J.R.); Hansen, George (G.C.); Herr, George (G.J.); Hofman, Michael (M.V.); Holmes, Jeffrey (J.R.); Ichikawa, Jiyunichiro (J.); Jensen, Ted (T.E.); 'John McDonald'; 'Jones, Andy'; Jordan, Donald (D.E.); Kanai, Shinji (S.); King, Robert (R.F.); Kosko, Jeff (J.R.); Kwon, Soon (S.K.); Limtiaco, Steven (S.); Linde, Peter (P.A.); Liu, Jane (J.); Mandziuk, Roger (R.S.); Marck, Edmond (E.C.); Matesa, John (J.); Maurer, James (J.B.); Mazzella, Gary (G.R.); Mooney, Larry (L.); Moorhouse, Scott (S.R.); 'Morgan, Tom'; Morishima, Shigeki (S.); 'Naveed Khan'; Nematollahi, Sonya (S.); 'Nikolai, Barnie'; Noteboom, Jim (J.E.); Ortman, James (J.W.); Powers, Ken (K.W.); Price, Martin (M.); Raquepau, Alden (A.P.); Shah, Kiran (K.C.); Shiraishi, Masaru (M.); Stilgenbauer, Jeffrey (J.R.); Suarez, Rhae (R.); Takasawa, Keith (K.D.); Takubo, Hiroichi (H.); Veenstra, Tim (T.W.); Wakenell, Ray (R.A.); Wettach, Bill (B.); Williams, Les (LHN.); Yeung, Lem (.)
Subject: RE: One example of Engine quit

anai-san,
This is the exact problem we have been working on. If your dealer services your vehicle per the TSB and ISM we have released, we believe your issue should be

resolved.

Mr. Limtiaco,
Can you please help ensure Kanai-san's vehicle is properly serviced?

Bob Dalbo
3.0L Calibration Supervisor
Outfitters Calibration, NAT
Phone: (313) 24-84947 Fax: (313) 32-31786
Pager: (313) 795-2859 Email: rdalbo@ford.com

-----Original Message-----
From: Shinji Kanai [mailto:kanai.sh@sv.mazda.co.jp]
Sent: Wednesday, June 19, 2002 10:05 AM
To: 'Sanders, Muriel (M.S.)'; 'Altoonian, Don (D.J.)'; 'Aynessazian, Kam (K.)'; 'Badgley, Joel (J.K.)'; 'Bauer, Scott (S.C.)'; 'Bhojwani, Kamal (K.)'; 'Blackburn, Thomas (T.J.)'; 'Bogema, John (P.)'; 'Cary Powell'; 'Chick, John (J.)'; 'Chih, Ming-Niu (M.N.)'; 'Chin, Darrel (D.)'; 'Corbett, Sandra (S.M.)'; 'Dalbo, Bob (R.J.)'; 'Dan Rothweiler'; 'De Pena, Juan (J.E.)'; 'Diez, Timothy (T.P.)'; 'Fascetti, Bob (R.J.)'; 'Fournelle, Gilbert (G.)'; 'Freeland, Mark (M.)'; 'Giles, Stuart (S.)'; 'Gokhale, Renuka (R.V.)'; 'Grewal, Bill (B.S.)'; 'Grimes, Jeff (J.R.)'; 'Hansen, George (G.C.)'; 'Herr, George (G.J.)'; 'Hofman, Michael (M.V.)'; 'Holmes, Jeffrey (J.R.)'; 'Ichikawa, Jiyunichiro (J.)'; 'Jansen, Ted (T.E.)'; 'John McDonald'; 'Jones, Andy'; 'Jordan, Donald (D.E.)'; 'Kanai, Shinji (S.)'; 'King, Robert (R.F.)'; 'Kosko, Jeff (J.R.)'; 'Kwon, Soon (S.K.)'; 'Limtiaco, Steven (S.)'; 'Linde, Peter (P.A.)'; 'Liu, Jane (J.)'; 'Mandziuk, Roger (R.S.)'; 'Marck, Edmond (E.C.)'; 'Matese, John (J.)'; 'Maurer, James (J.B.)'; 'Mazzella, Gary (G.R.)'; 'Mooney, Larry (L.)'; 'Moorhouse, Scott (S.R.)'; 'Morgan, Tom'; 'Morishima, Shigeki (S.)'; 'Naveed Khan'; 'Nematollahi, Sonya (S.)'; 'Nikolai, Barnie'; 'Noteboom, Jim (J.E.)'; 'Ortman, James (J.W.)'; 'Powers, Ken (K.W.)'; 'Price, Martin (M.)'; 'Raquepau, Aldan (A.P.)'; 'Shah, Kiran (K.C.)'; 'Shiraishi, Masaru (M.)'; 'Stilgenbauer, Jeffrey (J.R.)'; 'Suarez, Rhae (R.)'; 'Takasawa, Keith (K.D.)'; 'Takubo, Hiroichi (H.)'; 'Veenstra, Tim (T.W.)'; 'Wakenell, Ray (R.A.)'; 'Wattach, Bill (B.)'; 'Williams, Les (LHN.)'; 'Yeung, Lem (.)'
Subject: One example of Engine quit

My lease vehicle 2002MY Tribute experienced engine quit last night.

4F2YU08172KM28336 Build 12/11/2001, Retail 1/11/2002
Mileage: 7360 miles Event: 6/18/2002

After 25 minutes Freeway driving, I exited and stopped traffic signal.
About 30 sec. later I started moving to left turn and stopped at traffic signal again about 50m later.
About 30 sec. later I started moving 20m and right turn.
Then I gave throttle accelerating vehicle up to 35 MPH - 40MPH at slight up hill about 200m.
Then road switched down hill, I released throttle. Usually vehicle slight increase speed up to 45MPH about 200m.
I applied throttle gently after changing road up hill. Few seconds later I realized that vehicle kept down speed and three warning lamp illuminated about 40MPH.
I did not calm enough.
I turned key to start position, but engine did not start because shifter was

stayed D range.
I cycled key OFF and ON again, all warning lamp illuminated about 25MPH.
I applied brake to reduce speed and turned vehicle to left.
I shifted N range and cranked. Small gear noise (starter engagement ?) was heard at Engine started normally about 10 MPH.

I remember engine rpm dropped twice on this vehicle during last 6 month.
Possibly engine rpm drop might happen more than two, but I recognized twice.
One is same location same direction, another one was opposite direction almost same location.
No ECM like building or equipment near there, as far as I know.
This is my first V6-4WD model. Previous Tribute was I4-4WD.
I will bring this vehicle to dealer for usual scheduled (7,500 miles) maintenance this week.
I will ask dealer to reflash PCM calibration and continue to monitor.

If you have any question or comment, please feel free to contact to me.

Shinji Kanai
Manager, Tribute Plant QA
Mazda North American Operations

Ford Kansas City Assembly Plant
Plant Vehicle Team
8121 N.E. Hwy. 69, Claycomo, MO 64119 USA
Tel: 816-459-1623/ Fax: -1726/ e-mail: kanai.sh@sv.mazda.co.jp
Local Text Pager: 9135677156@alphapage.airtouch.com

Freeland, Mark (ML)

From: Freeland, Mark (M.)
Sent: Tuesday, June 18, 2002 6:22 PM
To: Dionisi, Anthony (A.J.)
Subject: RE: Parts for Assignment # 02-58 Being Returned

Tony,
The sensors have arrived, Thanks. We will start looking at them tomorrow.

Regards

Mark Freeland

6-Sigma Black Belt
Engine Research Department
Ford Research Laboratory
P.O. Box 2053
MD 2629 - SRL - Room 1517
Dearborn, MI 48121-2053 USA
email: mfreela1@ford.com
Tel.: (313) 594-7645

-----Original Message-----
From: Dionisi, Anthony (A.J.)
Sent: Tuesday, June 18, 2002 8:30 AM
To: Freeland, Mark (M.)
Cc: Dionisi, Anthony (A.J.)
Subject: RE: Parts for Assignment # 02-58 Being Returned

Mark, attached are copies of CQIS reports (I tried to include any AWS history that was related in report). Also, parts are tagged and include VIN # on tag and CQIS report #.

<< File: CQIS # 2FMIO001.doc >> << File: CQIS # 2FMIO002.doc >> << File: CQIS # 2FMIO003.doc >>

-----Original Message-----
From: Freeland, Mark (M.)
Sent: Monday, June 17, 2002 6:11 PM
To: Dionisi, Anthony (A.J.)
Cc: Lovelace, Maria (M.E.)
Subject: RE: Parts for Assignment # 02-58 Being Returned

Thank you Tony,
Could you please let me have the VIN numbers for the three vehicles, so that I can look up the vehicle service histories in AWS. Also, where/how do I look up the CQIS reports on line. Thanks

Regards

Mark Freeland

6-Sigma Black Belt
Engine Research Department

Ford Research Laboratory
P.O. Box 2053
MD 2629 - SRL - Room 1517
Dearborn, MI 48121-2053 USA
Mail: mfreela1@ford.com
Tel.: (313) 594-7645

----Original Message----

From:	Dionisi, Anthony (A.J.)
Sent:	Monday, June 17, 2002 9:47 AM
To:	Freeland, Mark (M.)
Cc:	Lovelace, Maria (M.E.); Dionisi, Anthony (A.J.)
Subject:	Parts for Assignment # 02-58 Being Returned

Mark, you should be receiving three DPFE sensors today - shipped Airborne Express - airbill # 4358965063.
Related to ECI Assignment # 02-58.
CQIS reports involved for these three sensors are: 2FMIO001, 2FMIO002, 2FMIO003.

Tony Dionisi
Ford Motor Company
Enhanced Concern Identification
Denver Field Quality Engineer
Office: 303-346-4788
Cell: 303-921-2517
Fax: 303-346-4798
adionisi@ford.com

Freeland, Mark (M.)

From: Freeland, Mark (M.)
Sent: Monday, June 17, 2002 6:11 PM
To: Dionisi, Anthony (A.J.)
Cc: Lovelace, Maria (M.E.)
Subject: RE: Parts for Assignment # 02-58 Being Returned

Thank you Tony,
Could you please let me have the VIN numbers for the three vehicles, so that I can look up the vehicle service histories in AWS. Also, where/how do I look up the CQIS reports on line. Thanks

Regards

Mark Freeland

6-Sigma Black Belt
Engine Research Department
Ford Research Laboratory
P.O. Box 2053
MD 2629 - SRL - Room 1517
Dearborn, MI 48121-2053 USA
email: mfreelal@ford.com
Tel.: (313) 594-7645

—Original Message—
From: Dionisi, Anthony (A.J.)
Sent: Monday, June 17, 2002 9:47 AM
To: Freeland, Mark (M.)
Cc: Lovelace, Maria (M.E.); Dionisi, Anthony (A.J.)
Subject: Parts for Assignment # 02-58 Being Returned

Mark, you should be receiving three DPFE sensors today - shipped Airborne Express - airbill # 4358965063.
Related to ECI Assignment # 02-58.
CQIS reports involved for these three sensors are: 2FMIO001, 2FMIO002, 2FMIO003.

Tony Dionisi
Ford Motor Company
Enhanced Concern Identification
Denver Field Quality Engineer
Office: 303-346-4788
Cell: 303-921-2517
Fax: 303-346-4798
adionisi@ford.com

Freeland, Mark (M.)

From: Freeland, Mark (M.)
Sent: Friday, June 07, 2002 9:48 AM
To: Awad, Mahmoud (M.I.)
Subject: RE: Assign. 02-58 2001 DPFE's

Thanks Mahmoud

Regards

Mark Freeland

6-Sigma Black Belt
Engine Research Department
Ford Research Laboratory
P.O. Box 2053
MD 2629 - SRL - Room 1517
Dearborn, MI 48121-2053 USA
email: mfreela1@ford.com
Tel.: (313) 594-7645

----Original Message----
From: Awad, Mahmoud (M.I.)
Sent: Friday, June 07, 2002 9:34 AM
To: Freeland, Mark (M.)
Subject: RE: Assign. 02-58 2001 DPFE's

Mark,
AWS server is down for updates for today, I'll do it next week.
Thanks
Mahmoud

----Original Message----
From: Freeland, Mark (M.)
Sent: Friday, June 07, 2002 8:18 AM
To: Maurer, James (J.B.); Gates, Freeman (F.C.); Awad, Mahmoud (M.I.)
Cc: Planta, Paul (P.G.); Janda, Jon (J.M.); McCoy, James (J.D.)
Subject: FW: Assign. 02-58 2001 DPFE's

Mahmoud,
Please check out the vehicle history for the F-150 Stalker below and circulate to the team.
I will report on the dPFE sensor when it arrives.
Thanks

Regards

Mark Freeland

6-Sigma Black Belt
Engine Research Department
Ford Research Laboratory
P.O. Box 2053
MD 2629 - SRL - Room 1517
Dearborn, MI 48121-2053 USA
email: mfreela1@ford.com
Tel.: (313) 594-7645

-----Original Message-----
From: Lovelace, Maria (M.E.)
Sent: Friday, June 07, 2002 7:43 AM
To: Freeland, Mark (M.)
Subject: FW: Assign. 02-58 2001 DPFE's

-----Original Message-----
From: Hayduk, Mark (M.S.)
Sent: Thursday, June 06, 2002 10:49 PM
To: Lovelace, Maria (M.E.)
Cc: Hayduk, Mark (M.S.)
Subject: Assign. 02-58 2001 DPFE's

Maria, below are two CQIS reports I wrote for this assignment which was issued today. 0 days to first find!!!

I found one DPFE with a date code after the date code on the assign. and one DPFE which caused a vehicle stall (which also had a date code after the date on the assign.).

The parts are being shipped to Mark Freeland per the assign.

Thanks.

CSQI002 CQIS Indicator Summary 06/06/02 22:43:13
===> _____ 1 of 2
Rpt#: 2FPG2001 CQD Rpt: 06/06/2002 Odom: 14,642 M
Rvwd: File: _ Folder: _____ Images: 0 Print Smy/Disp Detail(P/D): _
Vehicle: 2001 F150 4X2,REGCAB ,STYSD 1FTRF17W81KC64157 Bld: 07/25/2001
Engine: 4.6L ROM 8 Calb: 1F516M0N Trans: 4R70W Axle: 3800F3.55L A/C:
Dealer Id: 07467 WOLTZ & WIND FORD INC Ph#: (412) 279-4551
State: Pennsylvania City: Heidelberg Orig/Caller: MARK HAYDUK
Symptom: 6 07 5 93 DRVABL,STALL/QUITS,ACCELERATION,ALL ENGINE TEMP
Addl Sym: St: CCRG/EPRC: _ Rvwd: Dt:
Fix: Caus. Comp: SENSOR ASY EGR PR VL -- RPL Condition Code: 08

Region Code: 44 Region Name: Pittsburgh - 44

CONCER CUST. STATES: FROM A DEAD STOP THE ENGINE IS STALLING. ENGINE MISSING BADLY.
REPAIR * TECH. FOUND CODES P0401 AND P1408 (DPFE CODES).
TECH. REPLACED THE DPFE TO CORRECT THE CONCERN. DPFE DATE CODE ON PART IS: 2D03B.
PART SHIPPED TO MARK FREELAND PER ECI ASSIGN. 02-58.
VEHICLE WAS PREVIOUSLY IN FOR A DPFE CONCERN ON 4-19-02 @ 13,997 MI. AT WHICH TIME A NEW DPFE WAS INSTALLED TO CORRECT THAT CONCERN.
* MARK HAYDUK - PITTSBURGH PQE - 724-822-4342

CSQI002 CQIS Indicator Summary 06/06/02 22:43:53
===> _____ 2 of 2
Rpt#: 2FPG2002 CQD Rpt: 06/06/2002 Odom: 4,336 M
Rvwd: File: _ Folder: _____ Images: 0 Print Smy/Disp Detail(P/D): _
Vehicle: 2002 WINDSTAR,4X2 ,WAGON 2FMZA514X2BB02602 Bld: 02/11/2002
Engine: 3.8L EFI F Calb: 2A312C0A Trans: 4F50N Axle: FWD 3.56 A/C: YES
Dealer Id: 07467 WOLTZ & WIND FORD INC Ph#: (412) 279-4551
State: Pennsylvania City: Heidelberg Orig/Caller: MARK HAYDUK
Symptom: 6 98 2 00 DRVABL,INDICATOR,CHECK ENGINE,OTHER-CODE NA
Addl Sym: St: CCRG/EPRC: _ Rvwd: Dt:

Fix: Caus. Comp: SENSOR ASY EGR PR VL -- RPL Condition Code: 08

Region Code: 44 Region Name: Pittsburgh - 44

CONCER CUST. STATES: CHECK ENGINE LIGHT IS ON ALL THE TIME.
REPAIR * TECH FOUND CODE P0401 PRESENT (INSUFFICIENT EGR FLOW).
* TECH REPLACED THE DPFE WHICH CORRECTED THE CONCERN.
* DPFE REMOVED HAS DATE CODE OF 2A25B.
* DPFE SENT TO MARK FREELAND PER ECI ASSIGN. 02-58.
* MARK HAYDUK - PITTSBURGH FQE - 724-822-4342

Mark Hayduk
Field Quality Engineer
Global Concern Definition
Ph: 724-941-6670
Cell: 724-822-4342
Fax: 724-941-5154

Freeland, Mark (M.)

From: Freeland, Mark (M.)
Sent: Friday, June 07, 2002 8:19 AM
To: Lovelace, Maria (M.E.)
Subject: RE: Assign. 02-58 2001 DPFE's

Great,
Thanks for the day 0 report, I await the parts for testing.

Regards

Mark Freeland

6-Sigma Black Belt
Engine Research Department
Ford Research Laboratory
P.O. Box 2053
MD 2629 - SRL - Room 1517
Dearborn, MI 48121-2053 USA
email: mfreela1@ford.com
Tel.: (313) 594-7645

-----Original Message-----
From: Lovelace, Maria (M.E.)
Sent: Friday, June 07, 2002 7:43 AM
To: Freeland, Mark (M.)
Subject: FW: Assign. 02-58 2001 DPFE's

-----Original Message-----
From: Hayduk, Mark (M.S.)
Sent: Thursday, June 06, 2002 10:49 PM
To: Lovelace, Maria (M.E.)
Cc: Hayduk, Mark (M.S.)
Subject: Assign. 02-58 2001 DPFE's

Maria, below are two CQIS reports I wrote for this assignment which was issued today. 0 days to first find!!!

I found one DPFE with a date code after the date code on the assign. and one DPFE which caused a vehicle stall (which also had a date code after the date on the assign.).

The parts are being shipped to Mark Freeland per the assign.

Thanks.

CSQI002 CQIS Indicator Summary 06/06/02 22:43:13
==> _____ 1 of 2
Rpt#: 2PPG2001 CQD Rpt: 06/06/2002 Odom: 14,642 M
Rvwd: File: _ Folder: _____ Images: 0 Print Smy/Disp Detail(P/D): _
Vehicle: 2001 F150 4X2,REGCAB ,STYSD 1FTRF17W81KC64157 Bld: 07/25/2001
Engine: 4.6L ROM B Calb: IF516M0N Trans: 4R70W Axle: 3800F3.55L A/C:
Dealer Id: 07467 WOLTZ & WIND FORD INC Ph#: (412) 279-4551
State: Pennsylvania City: Heidelberg Orig/Caller: MARK HAYDUK

Symptom: 6 07 5 93 DRVABL,STALL/QUITS,ACCELERATION,ALL ENGINE TEMP
Addl Sym: St: CCRG/EPRC: _ Rvwd: Dt:
Fix: Caus. Comp: SENSOR ASY EGR PR VL -- RPL Condition Code: 08

Region Code: 44 Region Name: Pittsburgh - 44

CONCER CUST. STATES: FROM A DEAD STOP THE ENGINE IS STALLING. ENGINE MISSING BADLY.
REPAIR * TECH. FOUND CODES P0401 AND P1408 (DPFE CODES).
TECH. REPLACED THE DPFE TO CORRECT THE CONCERN. DPFE DATE CODE ON PART IS: 2D03B.
PART SHIPPED TO MARK FREELAND PER ECI ASSIGN. 02-58.
VEHICLE WAS PREVIOUSLY IN FOR A DPFE CONCERN ON 4-19-02 @ 13,997 MI. AT WHICH TIME A NEW DPFE WAS INSTALLED TO CORRECT THAT CONCERN.
* MARK HAYDUK - PITTSBURGH FQE - 724-822-4342

CSQI002 CQIS Indicator Summary 06/06/02 22:43:53
2 of 2

Rpt#: 2FF02002 CQD Rpt: 06/06/2002 Odom: 4,336 M
Rvwd: File: _ Folder: _____ Images: 0 Print Stay/Disp Detail(P/D): _
Vehicle: 2002 WINDSTAR,4X2 ,WAGON 2FMZA514X2BB02602 Bld: 02/11/2002
Engine: 3.8L EFI F Calb: 2A31ZCOA Trans: 4F50N Axle: FWD 3.56 A/C: YES
Dealer Id: 07467 WOLTZ & WIND FORD INC Ph#: (412) 279-4551
State: Pennsylvania City: Heidelberg Orig/Caller: MARK HAYDUK
Symptom: 6 98 2 00 DRVABL,INDICATOR,CHECK ENGINE,OTHER-CODE NA
Addl Sym: St: CCRG/EPRC: _ Rvwd: Dt:
Fix: Caus. Comp: SENSOR ASY EGR PR VL -- RPL Condition Code: 08

Region Code: 44 Region Name: Pittsburgh - 44

CONCER CUST. STATES: CHECK ENGINE LIGHT IS ON ALL THE TIME.
REPAIR * TECH FOUND CODE P0401 PRESENT (INSUFFICIENT EGR FLOW).
* TECH REPLACED THE DPFE WHICH CORRECTED THE CONCERN.
* DPFE REMOVED HAS DATE CODE OF 2A25B.
* DPFE SENT TO MARK FREELAND PER ECI ASSIGN. 02-58.
* MARK HAYDUK - PITTSBURGH FQE - 724-822-4342

Mark Hayduk
Field Quality Engineer
Global Concern Definition
Ph: 724-941-6670
Cell: 724-822-4342
Fax: 724-941-5154

Freeland, Mark (M.)

From:	Freeland, Mark (M.)
Sent:	Friday, June 07, 2002 8:16 AM
To:	Maurer, James (J.B.); Gates, Freeman (F.C.); Awad, Mahmoud (M.I.)
Cc:	Plants, Paul (P.G.); Janda, Jon (J.M.); McCoy, James (J.D.)
Subject:	FW: Assign. 02-58 2001 DPFE's

Mahmoud,
Please check out the vehicle history for the F-150 Staller below and circulate to the team.
I will report on the dPFE sensor when it arrives.
Thanks

Regards

Mark Freeland

6-Sigma Black Belt
Engine Research Department
Ford Research Laboratory
P.O. Box 2053
MD 2629 - SRL - Room 1517
Dearborn, MI 48121-2053 USA
email: mfreela1@ford.com
Tel.: (313) 594-7645

—Original Message—
From: Lovelace, Maria (M.E.)
Sent: Friday, June 07, 2002 7:43 AM
To: Freeland, Mark (M.)
Subject: FW: Assign. 02-58 2001 DPFE's

—Original Message—
From: Hayduk, Mark (M.S.)
Sent: Thursday, June 06, 2002 10:49 PM
To: Lovelace, Maria (M.E.)
Cc: Hayduk, Mark (M.S.)
Subject: Assign. 02-58 2001 DPFE's

Maria, below are two CQIS reports I wrote for this assignment which was issued today. 0 days to first find!!!

I found one DPFE with a date code after the date code on the assign. and one DPFE which caused a vehicle stall (which also had a date code after the date on the assign.).

The parts are being shipped to Mark Freeland per the assign.

Thanks.

CSQI002 CQIS Indicator Summary 06/06/02 22:43:13
==> _____ 1 of 2
Rpt#: 2FPG2001 CQD Rpt: 06/06/2002 Odom: 14,642 M
Rvwd: File: _ Folder: _____ Images: 0 Print Smy/Disp Detail(P/D): _
Vehicle: 2001 F150 4X2,REGCAB ,STYSD 1FTRF17W81KC64157 Bld: 07/25/2001
Engine: 4.6L ROM B Calb: 1P516M0N Trans: 4R70W Axle: 3800F3.55L A/C:

Dealer Id: 07467 WOLTZ & WIND FORD INC Ph#: (412) 279-4551
State: Pennsylvania City: Heidelberg Orig/Caller: MARK HAYDUK
Symptom: 6 07 5 93 DRVABL,STALL/QUITS,ACCELERATION,ALL ENGINE TEMP
Addl Sym: St: CCRG/EPRC: _ Rvwd: Dt:
Fix: Caus. Comp: SENSOR ASY EGR PR VL – RPL Condition Code: 08

Region Code: 44 Region Name: Pittsburgh - 44

CONCER CUST. STATES: FROM A DEAD STOP THE ENGINE IS STALLING. ENGINE MISSING BADLY.
REPAIR * TECH. FOUND CODES P0401 AND P1408 (DPFE CODES).
TECH. REPLACED THE DPFE TO CORRECT THE CONCERN. DPFE DATE CODE ON PART IS; 2D03B.
PART SHIPPED TO MARK FREHLAND PER BCI ASSIGN. 02-58.
VEHICLE WAS PREVIOUSLY IN FOR A DPFE CONCERN ON 4-19-02 @ 13,997 MI. AT WHICH TIME A NEW DPFE WAS INSTALLED TO CORRECT THAT CONCERN.
* MARK HAYDUK - PITTSBURGH FQE - 724-822-4342

CSQI002 CQIS Indicator Summary 06/06/02 22:43:53
==> 2 of 2
Rpt#: 2FPG2002 CQD Rpt: 06/06/2002 Odom: 4,336 M
Rvwd: File: _ Folder: _____ Images: 0 Print Smy/Disp Detail(P/D): _
Vehicle: 2002 WINDSTAR,4X2 ,WAGON 2FMZA514X2BB02602 Bld: 02/11/2002
Engine: 3.8L EFI F Calb: 2A31ZC0A Trans: 4F50N Axle: FWD 3.56 A/C: YES
Dealer Id: 07467 WOLTZ & WIND FORD INC Ph#: (412) 279-4551
State: Pennsylvania City: Heidelberg Orig/Caller: MARK HAYDUK
Symptom: 6 98 2 00 DRVABL,INDICATOR,CHECK ENGINE,OTHER-CODE NA
Addl Sym: St: CCRG/EPRC: _ Rvwd: Dt:
Fix: Caus. Comp: SENSOR ASY EGR PR VL -- RPL Condition Code: 08

Region Code: 44 Region Name: Pittsburgh - 44

CONCER CUST. STATES: CHECK ENGINE LIGHT IS ON ALL THE TIME.
REPAIR * TECH FOUND CODE P0401 PRESENT (INSUFFICIENT EGR FLOW).
* TECH REPLACED THE DPFE WHICH CORRECTED THE CONCERN.
* DPFE REMOVED HAS DATE CODE OF 2A25B.
* DPFE SENT TO MARK FREELAND PER BCI ASSIGN. 02-58.
* MARK HAYDUK - PITTSBURGH FQE - 724-822-4342

Mark Hayduk
Field Quality Engineer
Global Concern Definition
Ph: 724-941-6670
Cell: 724-822-4342
Fax: 724-941-5154

Freeland, Mark (M.)

From: Freeland, Mark (M.)
Sent: Tuesday, June 04, 2002 12:31 PM
To: Planta, Paul (P.G.)
Cc: Maurer, James (J.B.); Awad, Mahmoud (M.I.); Bryant, Bruce (B.D.)
Subject: RE: Need some warranty data in presentation form

Good,

I've invited Master BB Bruce Bryant to join us this afternoon.

Regards

Mark Freeland

6-Sigma Black Belt
Engine Research Department
Ford Research Laboratory
P.O. Box 2053
MD 2629 - SRL - Room 1517
Dearborn, MI 48121-2053 USA
email: mfreela1@ford.com
Tel.: (313) 594-7645

-----Original Message-----
From: Planta, Paul (P.G.)
Sent: Tuesday, June 04, 2002 11:29 AM
To: Freeland, Mark (M.)
Cc: Maurer, James (J.B.); Awad, Mahmoud (M.I.); Planta, Paul (P.G.)
Subject: RE: Need some warranty data in presentation form

Sounds good, maybe we can extend this and use for 5 platforms for overall discussions.

Jim/Mahmoud lets discuss after you complete Mark's request.

Mark, I discussed your FRL review w/ John Koszewnik today. He is OK with it. He expressed that V Engine wants to keep your management aligned and invited to generic management presentations also. Your efforts on the sensor are appreciated. Lets review your presentation at 2:30 today w/ Jim M. and I.

-----Original Message-----
From: Freeland, Mark (M.)
Sent: Tuesday, June 04, 2002 11:23 AM
To: Awad, Jute (J.A.)
Cc: Planta, Paul (P.G.); Maurer, James (J.B.); Gates, Freeman (F.C.)
Subject: Need some warranty data in presentation form

Mahmoud,

Could you please make me the following graphs in a format suitable for presentation to a director, I will need the graphs by close of business tomorrow.

For 2.0L Zetec Focus only:

1) (Second repair count/First repair count) v's Month of vehicle production (for 9/2000 through 1/2002)

2) Pareto of top 10 components (i.e. Causal Part) for D21 symptom for vehicles manufactured 9/2000

3) Perado of top 10 components (i.e. Causal Part) for D02 symptom for vehicles manufactured 9/2000

Please include the raw data as well as the charts.

If this request needs clarification let's talk at the 1:00 today.

Thanks

Regards

Mark Freeland

6-Sigma Black Belt
Engine Research Department
Ford Research Laboratory
P.O. Box 2053
MD 2629 - SRL - Room 1517
Dearborn, MI 48121-2053 USA
email: mfreela1@ford.com
Tel.: (313) 594-7645

Freeland, Mark (M.)

From: Freeland, Mark (M.)
Sent: Tuesday, June 04, 2002 4:41 PM
To: Awad, Mahmoud (M.I.)
Subject: FW: Need some warranty data in presentation form

Mahmoud,

I don't know how you knew what I wanted, as I sent it to the incorrect email address!,, But I'm glad someone else spotted my error.

Sorry.

Regards

Mark Freeland

6-Sigma Black Belt
Engine Research Department
Ford Research Laboratory
P.O. Box 2053
MD 2629 - SRL - Room 1517
Dearborn, MI 48121-2053 USA
email: mfreela1@ford.com
Tel.: (313) 594-7645

-----Original Message-----
From: Awad, June (J.A.)
Sent: Tuesday, June 04, 2002 3:51 PM
To: Freeland, Mark (M.)
Subject: RE: Need some warranty data in presentation form

I believe this was sent to me in error – I am the Ford Credit Regional Manager in Boston

<W:\Z22IDRV\pictures\waving flag.gif>

Regards,

June A. Awad
Boston Regional Manager
508 357-6606 fax 508 357-6610 cell 508 612-8554

-----Original Message-----
From: Freeland, Mark (M.)
Sent: Tuesday, June 04, 2002 11:23 AM
To: Awad, June (J.A.)
Cc: Plante, Paul (P.G.); Maurer, James (J.B.); Gates, Freeman (F.C.)
Subject: Need some warranty data in presentation form

Mahmoud,

Could you please make me the following graphs in a format suitable for presentation to a director, I will need the graphs by close of business tomorrow.

For 2.0L Zetec Focus only:

1) (Second repair count/First repair count) v's Month of vehicle production (for 9/2000 through 1/2002)

2) Perado of top 10 components (i.e. Causal Part) for D21 symptom for vehicles manufactured 9/2000

3) Perado of top 10 components (i.e. Causal Part) for D02 symptom for vehicles manufactured 9/2000

Please include the raw data as well as the charts.

If this request needs clarification let's talk at the 1:00 today.

Thanks

Regards

Mark Freeland

6-Sigma Black Belt
Engine Research Department
Ford Research Laboratory
P.O. Box 2053
MD 2629 - SRL - Room 1517
Dearborn, MI 48121-2053 USA
email: mfreela1@ford.com
Tel.: (313) 594-7645

Freeland, Mark (M.)

From: Freeland, Mark (M.)
Sent: Tuesday, June 04, 2002 4:42 PM
To: Awad, June (J.A.)
Subject: RE: Need some warranty data in presentation form

Thanks June, my mistake.

Regards

Mark Freeland

6-Sigma Black Belt
Engine Research Department
Ford Research Laboratory
P.O. Box 2053
MD 2629 - SRL - Room 1517
Dearborn, MI 48121-2053 USA
email: mfreela1@ford.com
Tel.: (313) 594-7645

Freeland, Mark (M.)

From: Freeland, Mark (M.)
Sent: Tuesday, June 04, 2002 4:48 PM
To: Gonzalez, Lebzy (L.)
Subject: RE: Kevlico samples

I will start it as soon as I get in on Thursday morning, probably about 9:15, unless traffic is bad. I have to take my three girls to school at 8:15 in Walled Lake, so I can't get here any earlier. I should be able to have the part in you're hands at 9:30 - 9:45, will that work for you? If that is OK, I will see you in Jon's annex to the lab on Thursday morning.

Regards

Mark Freeland

6-Sigma Black Belt
Engine Research Department
Ford Research Laboratory
P.O. Box 2053
MD 2629 - SRL - Room 1517
Dearborn, MI 48121-2053 USA
email: mfreelal@ford.com
Tel.: (313) 594-7645

----Original Message----
From: Gonzalez, Lebzy (L.)
Sent: Tuesday, June 04, 2002 1:54 PM
To: Freeland, Mark (M.)
Subject: FW: Kevlico samples

Mark,

Dolrene said she can look at the samples whenever we're ready on Thursday--how's 9am for getting the sample prep started?

Regards,

Lebzy Gonzalez
Materials Science Department 20-64167
Scientific Research Laboratory lgonza25@ford.com

Freeland, Mark (M.)

From: Freeland, Mark (M.)
Sent: Tuesday, June 04, 2002 4:56 PM
To: Hermann, Thomas (T.J.)
Cc: McCoy, James (J.D.); Maurer, James (J.B.); Plante, Paul (P.G.); Jande, Jon (J.M.); 'John Jahahan (E-mail)'
Subject: Escape Stalls

Tom,

I came across this from the Escape Stalls Team,

Status of Concern C11371349 (Tim Veenstra) *2:30-2:35*

- Concern Desc: 3.0L Escape experiences engine stalls between 6-12MHZ and 20-25MHZ as low as 73 V/M. The root cause was determined to be the EEC interface to the IAC. By fixing the EEC the anomaly went away completely.
- Concern is for implementing the "EEC w/a capacitor change".

What do you know about the capacitor change, is this a filter cap or what, could there be any link to dPFE going into an SCR latch?

Regards

Mark Freeland

6-Sigma Black Belt
Engine Research Department
Ford Research Laboratory
P.O. Box 2053
MD 2629 - SRL - Room 1517
Dearborn, MI 48121-2053 USA
email: mfreela1@ford.com
Tel.: (313) 594-7645

Freeland, Mark (M.)

From: Freeland, Mark (M.)
Sent: Wednesday, June 05, 2002 10:05 AM
To: Williamson, Richard (E.)
Subject: RE: dPFE sensor Requests

Thanks Rick,

Just one comment, it needs to cover 2002 MY for all applications as well as 2001 MY, 2003 MY for Explorer, and 2000 MY for 3.0L DOHC Taurus/Sable.

Sorry, I know that complicates things a bit, but there are 21 applications out there.

Regards

Mark Freeland

6-Sigma Black Belt
Engine Research Department
Ford Research Laboratory
P.O. Box 2053
MD 2629 - SRL - Room 1517
Dearborn, MI 48121-2053 USA
email: mfreela1@ford.com
Tel.: (313) 594-7645

-----Original Message-----
From: Williamson, Richard (E.)
Sent: Wednesday, June 05, 2002 9:59 AM
To: Lovelace, Maria (M.E.)
Cc: Freeland, Mark (M.)
Subject: dPFE sensor Requests
Importance: High

Hi Maria,
Enclosed please find an FQE request form.
Thanks for all your help, << File: mark freeland request.xls >>

RICK WILLIAMSON
Product Concern Analyst-Powertrain
Enhanced Concern Identification
313-248-6348
rwill110@ford.com

Freeland, Mark (M.)

From: Freeland, Mark (M.)
Sent: Wednesday, June 05, 2002 12:23 PM
To: Awad, Mahmoud (M.I.)
Subject: RE: Focus RR

Mahmoud,

I think this is exactly what I was after. Just to confirm one point, is the D02 and D21 causal part data only for vehicles manufactured in September 2000? If the answer is yes, then I am happy.

Thank you very much for doing the work.

Regards

Mark Freeland

6-Sigma Black Belt
Engine Research Department
Ford Research Laboratory
P.O. Box 2053
MD 2629 - SRL - Room 1517
Dearborn, MI 48121-2053 USA
email: mfreela1@ford.com
Tel.: (313) 594-7645

----Original Message----
From: Awad, Mahmoud (M.I.)
Sent: Wednesday, June 05, 2002 11:13 AM
To: Freeland, Mark (M.); Planta, Paul (P.G.); Maurer, James (J.B.)
Subject: Focus RR

Mark,
Thanks for the info. Enclosed is the data that you asked for. Please let me know if you have any questions. I'll be out tomorrow for the whole day (department meeting), so if you need anything please let me know today.
Paul and Jim,
If you don't have any comments or recommendations, I'm going to carry out the same analysis on the 4 platforms selected next week after the new cutoff date.

Best Regards
Mahmoud Awad
Reliability Implementation Engineer << File: Mark_06_03_02.zip >>
FMEI Department Support
Phone: (313) 24-63669
e-mail: mawad@ford.com

Freeland, Mark (M.)

From: Freeland, Mark (M.)
Sent: Wednesday, June 05, 2002 3:31 PM
To: Awad, Mahmoud (M.I.)
Subject: RE: Focus RR

Great, just what I was looking for.

Thanks for you're help

Regards

Mark Freeland

6-Sigma Black Belt
Engine Research Department
Ford Research Laboratory
P.O. Box 2053
MD 2629 - SRL - Room 1517
Dearborn, MI 48121-2053 USA
email: mfreelal@ford.com
Tel.: (313) 594-7645

-----Original Message-----
From: Awad, Mahmoud (M.I.)
Sent: Wednesday, June 05, 2002 1:11 PM
To: Freeland, Mark (M.)
Subject: RE: Focus RR

Mark,
Yes, it's only for 9/00 only. Keep in mind that the ranking was based on number of claims reported so far,i.e. regardless of Time in service.
Mahmoud

-----Original Message-----
From: Freeland, Mark (M.)
Sent: Wednesday, June 05, 2002 12:23 PM
To: Awad, Mahmoud (M.I.)
Subject: RE: Focus RR

Mahmoud,

I think this is exactly what I was after. Just to confirm one point, is the D02 and D21 causal part data only for vehicles manufactured in September 2000? If the answer is yes, then I am happy.

Thank you very much for doing the work.

Regards

Mark Freeland

6-Sigma Black Belt
Engine Research Department
Ford Research Laboratory
P.O. Box 2053

MD 2625 - SRL - Room 1517
Dearborn, MI 48121-2053 USA
email: mfreela1@ford.com
TEL: (313) 594-7645

-----Original Message-----
From: Awad, Mahmoud (M.I.)
Sent: Wednesday, June 05, 2002 11:13 AM
To: Freeland, Mark (M.); Pierce, Paul (P.G.); Maurer, James (J.B.)
Subject: Focus RR

Mark,
Thanks for the info. Enclosed is the data that you asked for. Please let me know if you have any questions. I'll be out tomorrow for the whole day (department meeting), so if you need anything please let me know today.
Paul and Jim,
If you don't have any comments or recommendations, I'm going to carry out the same analysis on the 4 platforms selected next week after the new cutoff date.

Best Regards
Mahmoud Awad
Reliability Implementation Engineer << File: Mark_06_03_02.zip >>
FMEI Department Support
Phone: (313) 24-63869
e-mail: mawad@ford.com

Freeland, Mark (M.)

From: Freeland, Mark (M.)
Sent: Thursday, June 06, 2002 10:15 AM
To: Bryant, Bruce (B.D.)
Subject: FW: Updated: EESE support of FRL 6S projects

Bruce,

Should Dante be invited to this afternoon's meeting?

Regards

Mark Freeland

6-Sigma Black Belt
Engine Research Department
Ford Research Laboratory
P.O. Box 2053
MD 2629 - SRL - Room 1517
Dearborn, MI 48121-2053 USA
email: mfreela1@ford.com
Tel.: (313) 594-7645

-----Original Message-----
From: Crockett, Dante (D.K.)
Sent: Thursday, June 06, 2002 6:21 AM
To: Freeland, Mark (M.)
Subject: RE: Updated: EESE support of FRL 6S projects

I would prefer to meet with you and Bruce Bryant to start to gauge how my activity, EESE 6-sigma, can assist you. Keith Frazier and Tom Hermann sit close to me so if we need their input, we can still get it.

-----Original Appointment-----
From: Freeland, Mark (M.)
Sent: Wednesday, June 05, 2002 4:54 PM
To: Crockett, Dante (D.K.)
Subject: Accepted: Updated: EESE support of FRL 6S projects
When: Friday, June 14, 2002 2:30 PM-3:30 PM (GMT-05:00) Eastern Time (US & Canada).
Where: Crockett's desk - #5, 2A106

Thanks,

Should we also invite the EESE people who are currently involved?

A new name has just been added to the EESE participants, Keith Frazier, who I first met on Monday this week. Also Tom Hermann, Sheran Alles and Roberto Rosel have been involved.

Freeland, Mark (M.)

From: Freeland, Mark (M.)
Sent: Thursday, June 06, 2002 11:23 AM
To: Bryant, Bruce (B.D.)
Subject: RE: Updated: EESE support of FRL BB projects

I have forwarded the meeting notice with explanation, and tried to call and text page him. Best I can do.

Regards

Mark Freeland

6-Sigma Black Belt
Engine Research Department
Ford Research Laboratory
P.O. Box 2053
MD 2629 - SRL - Room 1517
Dearborn, MI 48121-2053 USA
email: mfreela1@ford.com
Tel.: (313) 594-7645

-----Original Message-----
From: Bryant, Bruce (B.D.)
Sent: Thursday, June 06, 2002 10:19 AM
To: Freeland, Mark (M.)
Subject: RE: Updated: EESE support of FRL BB projects

Couldn't hurt. why don't you invite him?

Cordially,
Bruce Bryant, bbryant2@ford.com, 001-313-39-[illegible]
Six Sigma Master Blackbelt, Ford Research Laboratory

-----Original Message-----
From: Freeland, Mark (M.)
Sent: Thursday, June 06, 2002 10:15 AM
To: Bryant, Bruce (B.D.)
Subject: FW: Updated: EESE support of FRL BB projects

Bruce,

Should Dante be invited to this afternoon's meeting?

Regards

Mark Freeland

6-Sigma Black Belt
Engine Research Department
Ford Research Laboratory
P.O. Box 2053
MD 2629 - SRL - Room 1517
Dearborn, MI 48121-2053 USA
email: mfreela1@ford.com
Tel.: (313) 594-7645

-----Original Message-----
From: Crockett, Dante (D.K.)
Sent: Thursday, June 06, 2002 6:21 AM
To: Freeland, Mark (M.)
Subject: RE: Updated: EESE support of FRL BB projects

I would prefer to meet with you and Bruce Bryant to start to gauge how my activity, EESE 6-sigma, can assist you. Keith Frazier and Tom Hermann sit close to me so if we need their input, we can still get it.

-----Original Appointment-----
From: Freeland, Mark (M.)
Sent: Wednesday, June 05, 2002 4:54 PM
To: Crockett, Dante (D.K.)
Subject: Accepted: Updated: EESE support of FRL BB projects
When: Friday, June 14, 2002 2:30 PM-3:30 PM (GMT-05:00) Eastern Time (US & Canada).
Where: Crockett's desk - #5, ZA106

Thanks,

Should we also invite the EESE people who are currently involved?

A new name has just been added to the EESE participants, Keith Frazier, who I first met on Monday this week. Also Tom Hermann, Sheran Alles and Roberto Rosal have been involved.

Freeland, Mark (M.)

From:	Park, Kyong [KPark@kavlico.com]
Sent:	Saturday, June 15, 2002 10:15 AM
To:	mfreela1@ford.com
Cc:	bdavies@kavlico.com; emcdaniel@kavlico.com; arcsales@kavlico.com
Subject:	FW: Mazda ILDP for Evaluation



Mark,
As I mentioned over the telephone, we replaced the TMDP sensor of a 2001 Mazda Tribute owned by one of our engineer with a new TMDP. The vehicle has been driven 24,707 miles to date and the vehicle was serviced twice. Once for the replacement of one of the headlights and the other for the leaky rear window gasket.

The VIN is 4F2YU08131KM42376, and the sensor date code is 1J21B.
The sensor was passed for its functionality tests, and the sensor is very stable.
The gel and die surfaces are very clean, however, the reference die has two small bubbles. One is near one of the bond pads, and the other is at the center of the sensing diaphragm. The photos are attached below.
Kyong

-----Original Message-----
> From: Caffee, Jay
> Sent: Friday, June 14, 2002 2:40 PM
> To: Park, Kyong
> Subject: FW: Mazda ILDP for Evaluation
>
>
> Definitely a bubble forming from under the ball bond, very likely a bubble
> forming from the diaphragm pedestal. (ref. die)
> sensing die looks good.
> -----Original Message-----
> From: Grzywacz, Kyra
> Sent: Friday, June 14, 2002 2:12 PM
> To: Caffee, Jay
> Subject:
>
>
> <<diaphpost.jpg>> <<diaphpostoverall.jpg>> <<bp4bubble.jpg>>
> Kyra Grzywacz
> Analysis Lab
>

WSAP Powertrain PQR Agenda Schedule

Agenda for 6/19/02

FACTS Overview	R. Wepler
TF -C90 Connection	A. D'Agostino/S. Holloway
Wiring Concerns – Powertrain Warranty	L. Djuric/J. Palmer
Fix Powertrain Actions	M. Bednarek
VPG Leader Report Outs	VPG Leaders

Agenda for 6/26/02

FACTS Overview	R. Wepler
TF – Coolant Return Hose	B. Ajdufoh
Alternator Warranty	D. Paliani/Visteon
Alternator – Six Sigma	Susan Feust-Smith
Coolant Leak Detection Sys – Six Sigma	J. Florasca/C. Trombetta
Gas Caps Update – Six Sigma	D. Tedone/C. Whitsley
Roadmaps Review	D. Obora

Agenda for 7/3/02

No PQR Due to Plant Shutdown

Agenda for 7/10/02

No PQR Due to Plant Shutdown

Agenda for 7/17/02

FACTS Overview	R. Wepler
TF - MTX Cable Adjust	K. Arzulowicz
ATX Shifter Quality – Six Sigma	B. Tobis
Brake Switch Quality – Six Sigma	J. Rezaee
Battery Degradation – Six Sigma	M. Morton(Move to end of August per Mike Morton Request)
Ignition Coil Warranty	D. Paliani/Visteon
New Warranty Data	D. Obora

Freeland, Mark (M.)

From:	Aselage, Jane (J.M.)
Sent:	Tuesday, June 04, 2002 2:55 PM
To:	Bryant, Bruce (B.D.)
Cc:	Bell, Donna (D.L.); Crockett, Dante (D.K.); Freeland, Mark (M.); Amos, David (D.E.); Gearhart, Chris (C.)
Subject:	RE: 6 Sigma support from EESE

Bruce,
Please contact Donna Bell (my EESE Dedicated Project Champion) and Dante Crockett (my EESE Certified BB Project Scoper). You need to discuss the project opportunities with them and they will be able to determine most appropriate support plan. If you need my input along the way, let me know.

Jane M. Aselage
6-Sigma Deployment Director
Global Core Engineering
Bldg #4, 1AK14, MD4007
(313) 594-1974 (Phone)
(313) 32-29862 (Fax)
(313) 851-4980 (Pager)

-----Original Message-----

From:	Bryant, Bruce (B.D.)
Sent:	Tuesday, June 04, 2002 2:02 PM
To:	Aselage, Jane (J.M.)
Cc:	Freeland, Mark (M.); Amos, David (D.E.); Gearhart, Chris (C.)
Subject:	6 Sigma support from EESE

Jane:

I am a Master Blackbelt in the Ford Research Laboratory. We met briefly last year when you came to speak as a 6 Sigma Executive at a greenbelt class that Chris Gearhart and I were teaching for NAC at the Huron Training Center. I have a request that I would normally make to another master blackbelt, but I'm not sure which MBBs service the EESE department, so I'm contacting you.

I would like to request blackbelt support from EESE with some projects that one of our FRL blackbelts, Mark Freeland, is working on, related to the Kavlico dPFE sensor failure problems that many of our vehicles are experiencing. Currently, Mark is working on project #5228, "EGR DPFE Sensor Shorts Out PCM Vref" and # 7163, "EGR TM dPFE Sensor Unprotected Area Damage."

For background information, these projects are operating in support of a 14D team being run from PTO by Jim Maurer's group, which is responsible for the Kavlico dPFE sensor. Team members from EESE include Roberto Rossi, Sheran Alles, and Tom Hermann. They can provide more information on the problem.

Mark's efforts started as a project whose scope initially appeared to be reasonable in size, but ballooned to 4 projects in Mark's area (the two mentioned above, plus #5120 which was closed, and #3618 which was cancelled), plus other blackbelt projects in Jim Maurer's group. The two projects on which Mark is working would benefit from assistance from additional blackbelts, as the scope and associated workload remains enormous, and we would like to resolve these issues in a timely fashion.

We are looking in various areas, including FRL, for more blackbelts and greenbelts to add to the project, and since there appears to be a "systems" component to the problem, i.e., all vehicles lines which use the sensor are affected but at vastly different rates, we thought some of the blackbelts in the EESE area would like to contribute. If you would like to support these projects, please identify one or more blackbelts from EESE, with whom Mark and I could meet to discuss the details of the project.

Thanks for your consideration.

[redacted]

Freeland, Mark (M.)

From: Bryant, Bruce (B.D.)
Sent: Tuesday, June 04, 2002 2:02 PM
To: Asslage, Jane (J.M.)
Cc: Freeland, Mark (M.); Amos, David (D.E.); Gearhart, Chris (C.)
Subject: 6 Sigma support from EESE

Jane:

I am a Master Blackbelt in the Ford Research Laboratory. We met briefly last year when you came to speak as a 6 Sigma Executive at a greenbelt class that Chris Gearhart and I were teaching for NAC at the Huron Training Center. I have a request that I would normally make to another master blackbelt, but I'm not sure which MBBs service the EESE department, so I'm contacting you.

I would like to request blackbelt support from EESE with some projects that one of our FRL blackbelts, Mark Freeland, is working on, related to the Kavlico dPFE sensor failure problems that many of our vehicles are experiencing. Currently, Mark is working on project #5229, "EGR DPFE Sensor Shorts Out PCM Vref" and # 7163, "EGR TM dPFE Sensor Unprotected Area Damage."

For background information, these projects are operating in support of a 14D team being run from PTO by Jim Maurer's group, which is responsible for the Kavlico dPFE sensor. Team members from EESE include Roberto Rossi, Sheran Alles, and Tom Hermann. They can provide more information on the problem.

Mark's efforts started as a project whose scope initially appeared to be reasonable in size, but ballooned to 4 projects in Mark's area (the two mentioned above, plus #5120 which was closed, and #3618 which was cancelled), plus other blackbelt projects in Jim Maurer's group. The two projects on which Mark is working would benefit from assistance from additional blackbelts, as the scope and associated workload remains enormous, and we would like to resolve these issues in a timely fashion.

We are looking in various areas, including FRL, for more blackbelts and greenbelts to add to the project, and since there appears to be a "systems" component to the problem, i.e., all vehicles lines which use the sensor are affected but at vastly different rates, we thought some of the blackbelts in the EESE area would like to contribute. If you would like to support these projects, please identify one or more blackbelts from EESE, with whom Mark and I could meet to discuss the details of the project.

Thanks for your consideration.

Cordially,
Bruce Bryant, bbryant2@ford.com, 601-[illegible]
Six Sigma Master Blackbelt, Ford Research Laboratory

Freeland, Mark (M.)

From: Akolkar, Shrikant (S.V.)
Sent: Monday, June 10, 2002 1:09 PM
To: Duncan, Jack (J.L.)
Cc: Maurer, James (J.B.); Gates, Freeman (F.C.); Freeland, Mark (M.)
Subject: RE: DPFE failure at MPG

Jim,

I requested Jack during our phone conversation this morning to save the failed DPFE sensor. In future, if we begin monitoring all failed/completed parts from current tests at MPG, APG, Dyno etc we may learn about DPFE quality much earlier than in customer's hands. I am trying to get parts from dyno tests. This failure implies that we may not need any special test for DPFE except for acceleration tests.

I think it would be a good idea to monitor the electrical input-output of the sensor in this vehicle for remaining test period. Do you want Jim McCoy to undertake it? Pl. let me or Jack know about it. Thanks.

-----Original Message-----
From: Duncan, Jack (J.L.)
Sent: Monday, June 10, 2002 8:07 AM
To: Akolkar, Shrikant (S.V.)
Subject: DPFE failure at MPG

Shri, just this morning a 2002 Focus running the R312 Structural Trailer Tow procedure came in with the Check Engine light on. Codes P1401 (DPFE circuit high) and P1408 (EGR out of self-test range). Vehicle odometer 16659 miles. Apparently the DPFE code occurred three times during the night.

Would you and/or anyone associated with the DPFE team want to see this vehicle prior to repair? Please let me know ASAP. Thanks!

Jack Duncan | jduncan1@ford.com
MI Proving Ground
74240 Fisher Rd | (586) 75-28563 (w)
Romeo, MI 48065 | (586) 75-28683 (f)

Freeland, Mark (M.)

From:	Freeland, Mark (M.)
Sent:	Thursday, June 13, 2002 12:34 PM
To:	Lovelace, Maria (M.E.); Domka, John (J.J.)
Cc:	Maurer, James (J.B.); Plante, Paul (P.G.); Janda, Jon (J.M.); Frazier, Keith (R.K.); Rossi, Roberto (R.A.)
Subject:	RE: Assignment #58 - Failed DPFE- Tow In

John & Maria,

I suspect this one was due to the dPFE having been previously removed and then reinstalled without pushing the tubes on properly, or using a lubricant on the tubes. We have seen this before coming from B & A, when they used soap to lubricate the tubes, to aid assembly.
I checked the vehicle history and found that the dPFE was replaced in February, and the vehicle had been back several times for intermittent and steady Check Engine lights, which were eventually blamed on a faulty ignition coil at the end of May.

Keith & Roberto,

Could a faulty ignition coil cause excessive V Transients on Vref that could impact the dPFE?

Regards

Mark Freeland

6-Sigma Black Belt
Engine Research Department
Ford Research Laboratory
P.O. Box 2053
MD 2629 - SRL - Room 1517
Dearborn, MI 48121-2053 USA
email: mfreela1@ford.com
Tel.: (313) 594-7645

-----Original Message-----
From: Lovelace, Maria (M.E.)
Sent: Thursday, June 13, 2002 11:24 AM
To: Freeland, Mark (M.)
Subject: FW: Assignment #58 - Failed DPFE- Tow In

-----Original Message-----
From: Domka, John (J.J.)
Sent: Wednesday, June 12, 2002 11:22 AM
To: Lovelace, Maria (M.E.)
Subject: Assignment #58 - Failed DPFE- Tow In

CSQI002 CQI9 Indicator Summary 06/12/02 11:18:53
==> 1 of 1
Rpt#: 2FEA5001 CQD Rpt: 06/05/2002 Odom: 14,483 M
Rvwd: File: _ Folder: _____ Images: 2 Print Smy/Dtap Detail(P/D): _
Vehicle: 2001 TAURUS,SE COMF,SEDAN 1FAFP56S91G272542 Bld: 07/25/2001
Engine: 3.0L EFI M Calb: 1DD14N0A Trans: AX4N Axle: FWD 3.08 A/C: YES
Dealer Id: 02750 Avis Ford Inc Ph#: (800) 358-2778
State: Michigan City: Southfield Orig/Caller: JOHN DOMKA

Symptom: 6 03 0 00 DRVABL,CRANKS/NO STAR,OTHER-CODE NA,OTHER-CODE NA
Addl Sym: St: CCRG/EPRC: S Rvwd: A Dt: 06/06/2002
Fix: Caus. Comp: SENSOR ASY EGR PR VL -- RPL Condition Code: H5

Region Code: 48 Region Name: Detroit - 48

CONCER NO START
REPAIR NO CODES. ANALYSIS DETERMINED THERE WAS NO VOLTAGE REFERENCE.
PINPOINT DETERMINED OPEN CIRCUIT IN DPFE CIRCUIT. DPFE MELTED.
DEALER DID WORK ON VEHICLE PREVIOUS WEEK FOR A MISS COMPLAINT
REPLACED FAILED DPFE - ISSUE CORRECTED
SUSPECT DPFE WILL BE GIVEN TO M. LOVELACE WITHIN 7 DAYS UNLESS OTHER WISE NOTIFIED.
PICTURE ATTACHED
MICHIGAN FQE - JOHN DOMKA 313-433-7910
ADD-ON 06/12/2002 11:17AM JOHN DOMKA CQ - CD&A - CQD - FQE
UNABLE TO READ DPFE BUILD DATE INFO DUE TO DPFE DAMAGE/MELTING CONDITION

F1 Help F3 Exit F4 Last Cmts F5 Add Cmts F6 Add Fldr
F7 Bkwd F8 Fwd F9 Ind Corr F10 Next Rpt F11 Prev Rpt F12 Return
I0018-BOTTOM OF DATA LPENJBD

<< File: 2FEA5001.a.JPG >> << File: 2FEA5001.b.JPG >>
Thanks,

John J. Domka

Field Quality Engineer
Enhanced Concern Identification
Ford Customer Service Division

jdomka@ford.com
Phone 313-433-7910
FAX 734-475-9110

Freeland, Mark (M.)

From: Akolkar, Shrikant (S.V.)
Sent: Tuesday, June 11, 2002 4:59 PM
To: Duncan, Jack (J.L.)
Cc: Gates, Freeman (F.C.); Maurer, James (J.B.); Freeland, Mark (M.)
Subject: RE: DPFE failure at MPG

Jack,

Freeman wants to discuss this failure at weekly Thurs. meeting with Kevlico. Can you pl. email the date code which is punched between the tubes & the any additional test(hours/miles etc)/vehicle info including the veh VIN#. Also, Can you pl. send the sensor either to Freeman Gates or myself or the responsible test/system's engineer from whom we get the sensor. We may want to monitor the ele. input-output of the sensor but it may take some time before we finalize on it. How many miles/hours are remaining for the completion of this test. Thanks.

-----Original Message-----
From: Duncan, Jack (J.L.)
Sent: Monday, June 10, 2002 8:07 AM
To: Akolkar, Shrikant (S.V.)
Subject: DPFE failure at MPG

Shri, just this morning a 2002 Focus running the R312 Structural Trailer Tow procedure came in with the Check Engine light on. Codes P1401 (DPFE circuit high) and P1408 (EGR out of self-test range). Vehicle odometer 16659 miles. Apparently the DPFE code occurred three times during the night.

Would you and/or anyone associated with the DPFE team want to see this vehicle prior to repair? Please let me know ASAP. Thanks!

Jack Duncan | jduncan1@ford.com
MI Proving Ground
74240 Fisher Rd | (586) 75-28563 (w)
Romeo, MI 48065 | (586) 75-28683 (f)

Freeland, Mark (M.)

From:	Bryant, Bruce (B.D.)
Sent:	Thursday, June 13, 2002 3:46 PM
To:	Thakur, Arunima (A.)
Cc:	Freeland, Mark (M.); Crockett, Dante (D.K.)
Subject:	RE: BB help from EESE

For some background on the project, I recommend that you look at Mark Freeland's dPFE sensor-related projects on the PTS. He's MFREELA1. In particular, you may wish to examine the attachment "Warranty data for all applications at 3 MIS" on project 5228 to get a feel for the "systems" aspect of the issue, and the attachment "Initial Report on UPAD inspection" on project 7169 to help understand some of what's happening on the more microscopic level.

Mark's projects have mainly focused on understanding the problem and protecting the sensor from damage, and the direction that we're now going is to look at possible issues with the electrical environment which may be contributing to the problem.

Cordially,
Bruce Bryant, bbryant2@ford.com, 001-313-09-00750
Six Sigma Master Blackbelt, Ford Research Laboratory

—Original Message—

From:	Thakur, Arunima (A.)
Sent:	Thursday, June 13, 2002 12:27 PM
To:	Bryant, Bruce (B.D.)
Subject:	BB help from EESE

Dear Bruce,

I have invited myself to the meeting tomorrow from 2:30 to 3:30 at Dante's desk. I look forward to meeting you there. Is there any background research I could read up on tonight, that may help me? I have secure ID, so feel free to send any attachments via e-mail, even if it is later in the day.

Arunima Thakur

Consumer Driven Six Sigma Black Belt (Candidate)

Building: AVT-5/2G103, athakur@ford.com, Ph:313-317-7244
EESE, Global Core Engineering.

Freeland, Mark (M.)

From: Akolkar, Shrikant (S.V.)
Sent: Thursday, June 13, 2002 12:46 PM
To: Maurer, James (J.B.); Gates, Freeman (F.C.); Freeland, Mark (M.)
Cc: Verner, Carol (C.J.)
Subject: FW: DPFE failure at MPG

Jim,

Do you want me or Carol Verner to follow-up this failure?

-----Original Message-----
From: Duncan, Jack (J.L.)
Sent: Wednesday, June 12, 2002 8:10 AM
To: Akolkar, Shrikant (S.V.)
Subject: FW: DPFE failure at MPG

Shri,

John Rossit will send the part to Freeman today.

The vehicle, 578W635, has been sent to Dearborn. Contact Michelle Lu x85839 if you want to see the vehicle. This vehicle went through R357, R316, and R312-Structural tests, with the DPFE failure occurring during R312.

Jack Duncan | jduncan1@ford.com
MI Proving Ground |
4240 Fisher Rd | (586) 75-28563 (w)
Romeo, MI 48065 | (586) 75-28683 (f)

-----Original Message-----
From: Barnett, Ross (R.)
Sent: Wednesday, June 12, 2002 7:32 AM
To: Duncan, Jack (J.L.)
Subject: RE: DPFE failure at MPG

Contact John Rossit (JROSSIT) at 6-5963. The DPFE sensor in question was sent to Dearborn for evaluation.

-----Original Message-----
From: Duncan, Jack (J.L.)
Sent: Wednesday, June 12, 2002 6:24 AM
To: Barnett, Ross (R.)
Subject: FW: DPFE failure at MPG

Can you provide this info? Thanks!

Jack Duncan | jduncan1@ford.com
MI Proving Ground |
74240 Fisher Rd | (586) 75-28563 (w)
Romeo, MI 48065 | (586) 75-28683 (f)

-----Original Message-----
From: Akolkar, Shrikant (S.V.)
Sent: Tuesday, June 11, 2002 4:59 PM
To: Duncan, Jack (J.L.)

Cc: Gates, Freeman (F.C.); Maurer, James (J.B.); Freeland, Mark (M.)
Subject: RE: DPFE failure at MPG

Jack,

Freeman wants to discuss this failure at weekly Thurs. meeting with Kevlico. Can you pl. email the date code which is punched between the tubes & the any additional test(hours/miles etc)/vehicle info including the veh VIN#. Also, Can you pl. send the sensor either to Freeman Gates or myself or the responsible test/system's engineer from whom we get the sensor. We may want to monitor the ele. input-output of the sensor but it may take some time before we finalize on it. How many miles/hours are remaining for the completion of this test. Thanks.

-----Original Message-----
From: Duncan, Jack (J.L.)
Sent: Monday, June 10, 2002 8:07 AM
To: Akolkar, Shrikant (S.V.)
Subject: DPFE failure at MPG

Shri, just this morning a 2002 Focus running the R312 Structural Trailer Tow procedure came in with the Check Engine light on. Codes P1401 (DPFE circuit high) and P1406 (EGR out of self-test range). Vehicle odometer 18659 miles. Apparently the DPFE code occurred three times during the night.

Would you and/or anyone associated with the DPFE team want to see this vehicle prior to repair? Please let me know ASAP. Thanks!

Jack Duncan | jduncan1@ford.com
MI Proving Ground
74240 Fisher Rd | (586) 75-28563 (w)
Romeo, MI 48065 | (586) 75-28683 (f)

Freeland, Mark (M.)

From: Domka, John (J.J.)
Sent: Thursday, June 13, 2002 7:06 PM
To: Freeland, Mark (M.)
Cc: Lovelace, Maria (M.E.)
Subject: RE: Assignment #58 - Failed DPFE- Tow In

So I take it you dont want the DPFE??????

----Original Message----
From: Freeland, Mark (M.)
Sent: Thursday, June 13, 2002 12:34 PM
To: Lovelace, Maria (M.E.); Domka, John (J.J.)
Cc: Maurer, James (J.B.); Plante, Paul (P.G.); Janda, Jon (J.M.); Frazier, Keith (R.K.); Rossi, Roberto (R.A.)
Subject: RE: Assignment #58 - Failed DPFE- Tow In

John & Maria,

I suspect this one was due to the dPFE having been previously removed and then reinstalled without pushing the tubes on properly, or using a lubricant on the tubes. We have seen this before coming from B & A, when they used soap to lubricate the tubes, to aid assembly.
I checked the vehicle history and found that the dPFE was replaced in February, and the vehicle had been back several times for intermittent and steady Check Engine lights, which were eventually blamed on a faulty ignition coil at the end of May.

Keith & Roberto,

Could a faulty ignition coil cause excessive V Transients on Vref that could impact the dPFE?

Regards

Mark Freeland

6-Sigma Black Belt
Engine Research Department
Ford Research Laboratory
P.O. Box 2053
MD 2629 - SRL - Room 1517
Dearborn, MI 48121-2053 USA
email: mfreela1@ford.com
Tel.: (313) 594-7645

----Original Message----
From: Lovelace, Maria (M.E.)
Sent: Thursday, June 13, 2002 11:24 AM
To: Freeland, Mark (M.)
Subject: FW: Assignment #58 - Failed DPFE- Tow In

----Original Message----
From: Domka, John (J.J.)
Sent: Wednesday, June 12, 2002 11:22 AM
To: Lovelace, Maria (M.E.)
Subject: Assignment #58 - Failed DPFE- Tow In

CSQI002 CQIS Indicator Summary 06/12/02 11:18:53

Rpt#: 2FEA5001 CQD Rpt: 06/06/2002 Odom: 14,433 M
Rvwd: File: _ Folder: _____ Images: 2 Print Smy/Disp Detail(P/D): _
Vehicle: 2001 TAURUS,SE COMF,SEDAN 1FAFP56S91G272542 Bld: 07/25/2001
Engine: 3.0L EFI M Calb: 1DD14N0A Trans: AX4N Axle: FWD 3.98 A/C: YES
Dealer Id: 02750 Avis Ford Inc Ph#: (800) 358-2778
State: Michigan City: Southfield Orig/Caller: JOHN DOMKA
Symptom: 6 03 0 00 DRVABL,CRANKS/NO START,OTHER-CODE NA,OTHER-CODE NA
Addl Sym: St: CCRG/EPRC: S Rvwd: A Dt: 06/06/2002
Fbc: Caus. Comp: SENSOR ASY EGR PR VL -- RPL Condition Code: H5

Region Code: 48 Region Name: Detroit - 48

CONCER NO START
REPAIR NO CODES. ANALYSIS DETERMINED THERE WAS NO VOLTAGE REFERENCE.
PINPOINT DETERMINED OPEN CIRCUIT IN DPFE CIRCUIT. DPFE MELTED.
DEALER DID WORK ON VEHICLE PREVIOUS WEEK FOR A MISS COMPLAINT
REPLACED FAILED DPFE - ISSUE CORRECTED
SUSPECT DPFE WILL BE GIVEN TO M. LOVELACE WITHIN 7 DAYS UNLESS OTHER WISE NOTIFIED.
PICTURE ATTACHED
MICHIGAN FQE - JOHN DOMKA 313-433-7910
ADD-ON 06/12/2002 11:17AM JOHN DOMKA CQ - CD&A - CQD - FQE
UNABLE TO READ DPFE BUILD DATE INFO DUE TO DPFE DAMAGE/MELTING CONDITION.

F1 Help F3 Exit F4 Last Cmts F5 Add Cmts F6 Add Fldr
F7 Bkwd F8 Fwd F9 Ind Corr F10 Next Rpt F11 Prev Rpt F12 Return
!0016-BOTTOM OF DATA LPENJBD

<< File: 2FEA5001.a.JPG >> << File: 2FEA5001.b.JPG >>
Thanks,

John J. Domka

Field Quality Engineer
Enhanced Concern Identification
Ford Customer Service Division

jdomka@ford.com
Phone 313-433-7910
FAX 734-475-9110

Freeland, Mark (M.)

From: Plante, Paul (P.G.)
Sent: Friday, June 21, 2002 1:16 PM
To: Freeland, Mark (M.)
Subject: RE: R. Rossi's IS/IS NOT statements

Good comments, thanks.

-----Original Message-----
From: Freeland, Mark (M.)
Sent: Friday, June 21, 2002 12:10 PM
To: Poma, Amy (A.); Akins, Mary (M.); Allen, Sharon (S.A.); Awad, Mahmoud (M.I.); Gates, Freeman (F.C.); Jarda, Jon (J.M.); John Johnston (E-mail); Maurer, James (J.B.); McCoy, James (J.D.); Plante, Paul (P.G.); Reddy, Srikanth (S.C.); Rossi, Roberto (R.A.); Verner, Carol (C.J.)
Subject: RE: R. Rossi's IS/IS NOT statements

The following are my comments regarding the Is/IS NOT statements proposed:

The cigar lighter/power point fuse opens in the field IS NOT a contributor to DPFE failures. This is based on the fact that on the Focus and Escape they do not share the same harnesses.

This is a poor assumption that if there is an electrical issue which causes a problem for the dPFE, that it will be the same issue on all vehicles, if it were the same issue, then one would expect a similar failure rate on each vehicle line. It would be more realistic to assume that there are some generic (common between vehicle lines) issues and some special (unique to a vehicle line) issues. Therefore this is not a valid way to eliminate the cigar lighter issue as a contributing cause.

The Escape water entry concerns with connector C263 where battery voltage can short to the VREF IS NOT a contributor to DPFE failures. This is based on the fact that this failure rate is known to be low because the PCM will fail with this condition.

What is the failure rate? This needs to be supported with data. Has anyone verified with testing that a intermittent short of this nature can not damage the dPFE, or will as proposed damage the PCM. OR is this a hypothesis that has not been verified?

Please discuss at the next meeting.

Regards

Mark Freeland

6-Sigma Black Belt
Engine Research Department
Ford Research Laboratory
P.O. Box 2053
MD 2629 - SRL - Room 1517
Dearborn, MI 48121-2053 USA
email: mfreela1@ford.com
Tel.: (313) 594-7645

-----Original Message-----
From: Poma, Amy (A.)
Sent: Friday, June 21, 2002 11:00 AM
To: Akins, Mary (M.); Allen, Sharon (S.A.); Awad, Mahmoud (M.I.); Freeland, Mark (M.); Gates, Freeman (F.C.); Jarda, Jon (J.M.); John

Jahshan (E-mail); Maurer, James (J.B.); McCoy, James (J.D.); Plante, Paul (P.G.); Poma, Amy (A.); Reddy, Srikanth; Rossi, Roberto (R.A.); Verner, Carol (C.L.)
Subject: R. Rossi's IS/IS NOT statements

Team-

Below is Robert Rossi's statements for the teams review for Monday's June 24th meeting.

The following are my drafts of the Is/Is Not statements from the open assignments for the Monday meetings.

The cigar lighter/power point fuse opens in the field IS NOT a contributor to DPFE failures. This is based on the fact that on the Focus and Escape they do not share the same harnesses.

The Escape water entry concerns with connector C283 where battery voltage can short to the VREF IS NOT a contributor to DPFE failures. This is based on the fact that this failure rate is known to be low because the PCM will fail with this condition.

Amy Poma
V-Engine Engineering-Project Mgmt.
POEE Building, FMEI Cube CO162
phone-313-390-8849, fax: 313-390-4084
apoma2@ford.com

Freeland, Mark (M.)

From:	Freeland, Mark (M.)
Sent:	Tuesday, June 25, 2002 8:50 PM
To:	Kyong Park (E-mail); Maurer, James (J.B.); Gates, Freeman (F.C.); Rossi, Roberto (R.A.); Frazier, Keith (R.K.); Alles, Sheran (S.A.); McCoy, James (J.D.)
Cc:	Plante, Paul (P.G.); Hangas, Jon (.); Duffy, Paul (P.E.)
Subject:	Post 1/7/2002 Dpfe with evidence of a high current

Attached are the pictures from the Post 1/7/2002 dPFE Warranty return I received this morning.
The part came from a Crown Victoria, VIN 2FAFP71W02X144606. It was changed at 2,973 miles.
Electrically it has one die open circuit (Vref - Signal Return) as received, a large bubble over the HI die, an open wire on the Vdd to the HI die, and a visual anomaly (presumed by the rigiter to be signs of electrical overstress) on the upper surface of the MOV. See attached photographs.
I believe the failure to have occurred quite rapidly, as the die attach adhesive to gel interface for the hi die has not turned dark brown. This indicates that the part probably heated up quickly to form the large bubble in the gel and then cooled rapidly.

If the anomaly on the MOV is in indication of an electrical overstress, then one must conclude that either the vehicle's electrical system caused it, or the technician diagnosing the vehicle did something to cause it, as the die could not have been the electrical source to cause it.

[redacted]

I have given the part to Sheran Alles, he intends to send it to AVX to have the MOV analyzed.

[redacted] [redacted]

Regards

Mark Freeland

6-Sigma Black Belt
Engine Research Department
Ford Research Laboratory
P.O. Box 2053
MD 2629 - SRL - Room 1517
Dearborn, MI 48121-2053 USA
email: mfreela1@ford.com
Tel.: (313) 594-7645

Freeland, Mark (M.)

From: Freeland, Mark (M.)
Sent: Tuesday, June 04, 2002 6:39 PM
To: Janda, Jon (J.M.)
Subject: FW: FREELAND, MARK

Jon,

Here are my flights for the Mavlico trip. Still working on a hotel, will let you know.

Are you planning to come, Jim was unsure this afternoon?

Regards

Mark Freeland

> 6-Sigma Black Belt
> Engine Research Department
> Ford Research Laboratory
> P.O. Box 2053
> MD 2629 - SRL - Room 1517
> Dearborn, MI 48121-2053 USA
email: mfreela1@ford.com
Tel.: (313) 594-7645

-----Original Message-----
From: PNR-american express [mailto:pnr-notification@itn.net]
Sent: Tuesday, June 04, 2002 6:25 PM
Subject: FREELAND, MARK

****

TRAVEL BOOKING CONFIRMATION
****
Your company's Travel Department has requested this Message be sent each time you book travel for company business. If you wish to change that arrangement please contact your Travel Department.
****
****
****
CRS Record Locator # 2LRAG5
Airline Record Locator #1 UA-XJTHDQ
Car Rental Confirmation #1 ZE-B8432744615 (Hertz)

****
Name(s) of people traveling:
Passenger #1: MARK FREELAND
Meal: standard

Fare Details: DTT UA X/DENUA BUR 254.66UA X/DENUA DTT 254.65USD509.31 END UA ZPDTWDENBURDEN XT10.00AY16.50XF DTW4.5DEN4.5BUR 3DEN4.5

Baggage Allowance: 2 pieces

****

ITINERARY
Flight/Equip.: United Airlines 1905 Boeing 737-300
Depart: Detroit(DTW)/Sunday June 9 6:05 pm
Arrive: Denver(DEN)/Sunday June 9 7:09 pm
Stops: non-stop Miles:1123
Class: Coach

Flight/Equip.: United Airlines 1285 Boeing 737-500
Depart: Denver(DEN)/Sunday June 9 8:00 pm
Arrive: Burbank(BUR)/Sunday June 9 9:19 pm
Stops: non-stop Miles:850
Class: Coach

Car: Hertz (airport)
Pick-up: Jun 09 Burbank
Drop-Off: Jun 12 Burbank
Car size: Intermediate Conf: B8432744615
Rate: EUR 57.53/day Extra Hour: 29.59
/day
USD 52.50/day Extra Hour: 27.00

Flight/Equip.: United Airlines 574 Boeing 737-500
Depart: Burbank(BUR)/Wednesday June 12 6:16 am
Arrive: Denver(DEN)/Wednesday June 12 9:25 am
Stops: non-stop Miles:850
Class: Coach

Flight/Equip.: United Airlines 1406 Boeing 757-200
Depart: Denver(DEN)/Wednesday June 12 10:05 am
Arrive: Detroit(DTW)/Wednesday June 12 2:40 pm
Stops: non-stop Miles:1123
Class: Coach

Total Airfare (including taxes) 586.00 586.00
Flight segments must be ticketed by close of business on June 9.

****

AGENCY INFORMATION
Agency: American Express
Dearborn, MI

****

BILLING INFORMATION
Name: Mark Freeland
Address: 2101 Village Road
Mail Stop: SRL Rm 1517 MD 2629
Dearborn, MI 48124
Country: USA
Day Phone: 1-313-5947645
Email: MFREELA1@ford.com

****

PAYMENT INFORMATION
Visa Number: ON FILE
Expires: ON FILE

****

SPECIAL REQUESTS

****

HAVE A GREAT TRIP!

Pergamon

Acta mater. Vol. 47, No. 1, pp. 89–96, 1999
© 1998 Acta Metallurgica Inc.
Published by Elsevier Science Ltd. All rights reserved
Printed in Great Britain
1359-6454/99 $19.00 + 0.00

PII: S1359-6454(98)00346-1

INTERCONNECT DAMAGE BY ELECTROMIGRATION: EXPERIMENT AND NUMERICAL SIMULATION

J.-M. HUANG, W. YANG† and Z.-J. ZHAO

Department of Engineering Mechanics, Tsinghua University, Beijing 100084, P.R. China

(Received 3 August 1998; accepted 23 September 1998)

Abstract—Electromigration is a severe reliability issue for polycrystalline aluminum-based interconnects. The phenomenon is amplified by taking exposed interconnects at an elevated temperature. The intense electric currents they carry would drive atoms to diffuse, and leave hillocks or sinks along the interconnects. Experimental observations revealed that the hillocks grow against the surrounding grains in four stages: the incubation, the jump start, the deceleration, and the final stabilization. An analytical model is proposed to address features such as fluctuating mass flows into grains, partition of mass flows through the surface and the defect layers, stresses induced by the mass flow, and resistance against the grain boundary sliding. The incubation time and the protruding height are determined. The incubation time is proportional, while the protruding height is roughly inversely proportional, to the square of the grain size. Numerical algorithms are exploited to quantify the experimental phenomena. To design against the electromigration, one needs to raise the incubation time of an interconnect beyond its service life. To comply with this criterion, a polycrystal line with large and uniform grains (if not a bamboo line or even a single crystal line) with small variation in grain boundary diffusivities should be pursued. © *1998 Acta Metallurgica Inc. Published by Elsevier Science Ltd. All rights reserved.*

1. INTRODUCTION

Aluminum-based interconnects consist of more than 90% of the metal lines used in integrated circuits. The low resistance and good processing capability give aluminum an advantage with respect to RC delay and allow for higher performance circuit design. In the integrated circuits, the interconnects have small cross-sections (less than 1 μm wide and about 0.5 μm thick), carry intense electric currents (above 10^{10} A/m^2), and may operate at a temperature of nearly half of the melting point (933 K) of aluminum. The flowing electrons exert a force (the electron wind force) on aluminum atoms, which drives aluminum atoms to diffuse. Mass diffusion under electric current, known as electromigration, raises the reliability concerns. The situation is further accentuated by the continuing trend toward miniaturization in integrated circuits, especially in the VLSI and power semiconductor devices.

Experimental observations revealed that single crystal interconnects can sustain a very long life [1, 2], for they have perfect microstructures and homogeneous material properties. The damage by voiding can nucleate only along the interfaces between the interconnect and its passivation [3]. The migration of a void is controlled by the mass flow along the void surface [4]. Subjected to electromigration, a void basically moves by surface diffusion, and may break away from a grain boundary [3–5]. For a bamboo line, electromigration may cause damage nucleation and failure by the unbalanced atomic flux into the triple junctions, creating either a void [5] or a transgranular slit [10–14]. These studies indicated that the failure by electromigration is manifested by the growth, shape change, and migration of voids or hillocks, and an interconnect evolves like a dynamical system that has multiple thermodynamic forces and undergoes dissipative processes.

Electromigration becomes a severe reliability issue for polycrystalline lines [8, 15], especially for the exposed lines. The mass flows along the side surfaces, the top surface, the grain boundaries, the surface grooves, and the defects like dislocations. They provide fast diffusion paths under electromigration, and the mass flow through them might be non-uniform [16, 17]. Surface damage is nucleated by the mass flow instability and intensified by the subsequent morphological evolution [18].

We begin with the electromigration experiment on polycrystalline aluminum lines. At ambient and elevated temperatures, hillocks and sinks are observed along the exposed surfaces of the interconnects, as reported in Section 2. The experiments revealed that hillocks and sinks grow against the surrounding grains in four stages: the incubation, the jump start, the deceleration, and the final stabilization. Section 3 presents an analytical model featuring the mass flow fluctuation and the grain boundary resistance. A scheme for the morphological evolution under electromigration is exploited in

†To whom all correspondence should be addressed.

Table I. Failure times in various tests

Specimen number	Testing temperature (K)	Current density (10^{10} A/m^2)	Line width (μm)	Lifetime (h)
108-08	300	3.56	7.5	1171
108-09	300	3.67	1.5	2.75
109-10	300	3.14	3.5	501
209-01	300	6.16	1.5	6.5
209-02	300	2.64	3.5	2452
210-04	300	2.50	11.5	3098
410-08	300	3.67	1.5	420
610-09	300	3.67	1.5	805

Section 4, where numerical simulations are carried out to quantify the experimental phenomena.

2. ELECTROMIGRATION EXPERIMENT

2.1. Damage of aluminum-based interconnects

The authors conducted a series of electromigration tests of unpassivated polycrystalline interconnects. Only room temperature testing is described here. The metallizations consisted of films of Al/Si (mass fraction 99% Al and 1% Si) alloy of 1 μm thickness, which were sputter deposited at a rate of 0.03 μm/min on silicon substrates covered by a SiO_2 film of 0.4 μm. The film/substrate assembly was then annealed at 723 K for about 30 min. The processing followed the conventional techniques in China to manufacture micron-width interconnects, and was carried out in the Institute of Microelectronics, Tsinghua University. The thin films were then etched to testing lines of 100 μm length and various widths (from 1.5 to 11.5 μm). The failure times of various tests are listed in Table I. They are substantially lower than the testing data reported in the literature. The specimens were observed under a field-emission scanning electron microscope (Hitachi S-4200) at the Institute of Physics, Chinese Academy of Science. The interconnect

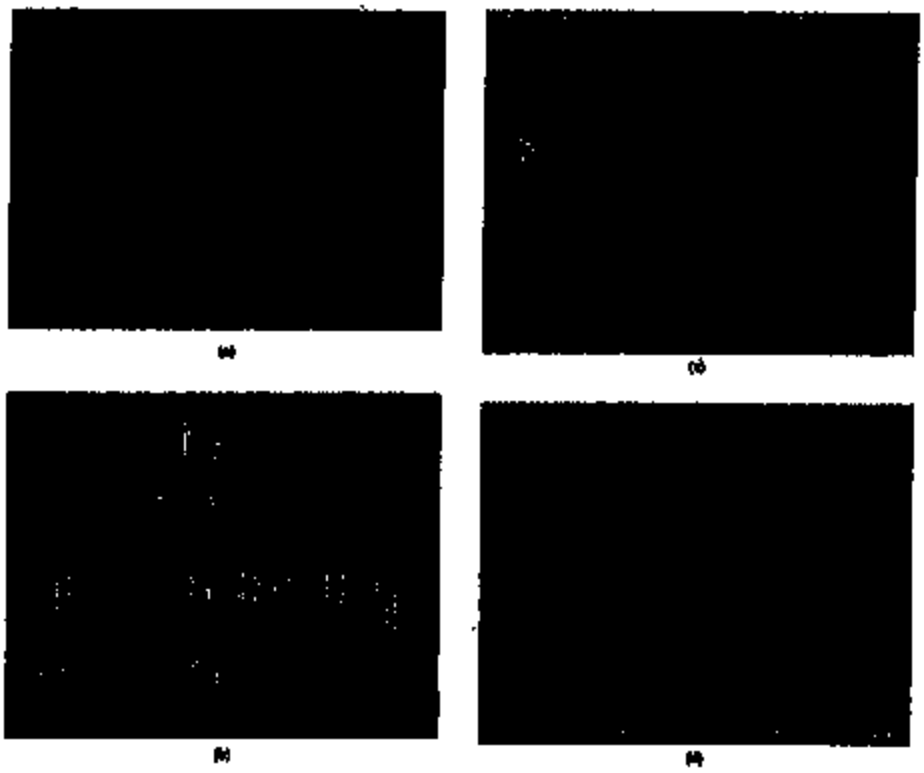

Fig. 1(a, b, c and d).

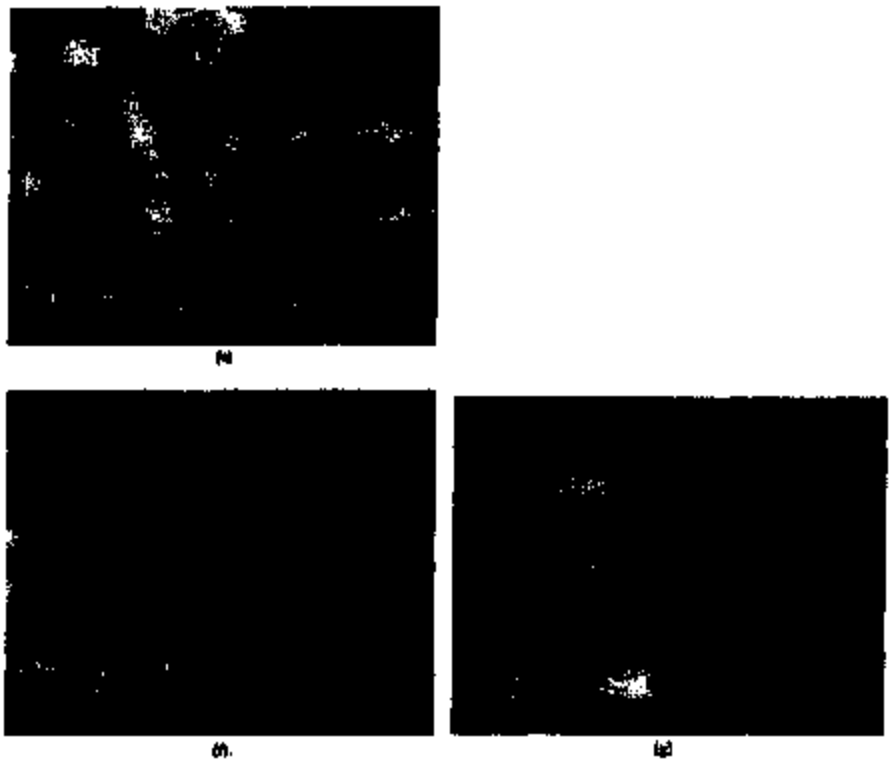

Fig. 1. SEM micrographs following a time sequence showing the damage of an interconnect under electromigration: (a) initial configuration; (b)–(d) 528 h; (e) 904 h; (f), (g) 1171 h.

nects are featured by the tiny columnar grain microstructures. The grains are about 0.115 μm in diameter and 1 μm in height, with possible lateral defects.

2.2. Four stages of protrusion

Figures 1(a)–(g) show a typical sequence of the morphological evolution of an interconnect tested at room temperature (300 K) under a current density of 3.56×10^{10} A/m^2 and a line width of 7.5 μm. These microscopic photographs were taken by interrupting the test after 0, 528, 904, and 1171 h of testing. In all graphs, the direction of the electron flow is from right to left. The exposed surfaces are initially flat, and surface damage is not detected, as shown in Fig. 1(a). The surface damage sets in when the electric current is switched on, but needs an incubation period for the hillocks to appear. As the time increases, the unbalanced mass flux accumulated in local areas becomes unstable. Suddenly many tiny hillocks and sinks burst from the interconnect, as shown in Fig. 1(b) at 528 h. An amplified view for a hillock protruding from the surrounding grains is shown in the lower-left corner of Fig. 1(c). The hillock is about 1.5 μm long and 2 μm in diameter. The detailed structure of a connected sink is shown in Fig. 1(d). The protruding motion of hillocks continues after their formation, see Fig. 1(e) at 904 h. The aspect ratio of the hillock becomes slender. The protruding motion dominates. Gradually the matured hillocks become stabilized, but the new ones are still growing rapidly. The growing kinetics renders the picture shown in Fig. 1(f) at 1171 h. The longest protrusion in the figure has a length of about 4 μm, which imposes a severe threat of short-circuit failure. On the other hand, the local sinking becomes deeper and deeper, and finally cuts the line at 1171 h, see Fig. 1(g). Many sinks can be observed in the broken-down motion. These results agree quantitatively with those of other experiments [6–9].

Grain boundaries play an important role in the electromigration of polycrystalline interconnects. They not only provide a fast path for electromigration, but also shape the evolution of the hillocks and sinks. We attribute the above-mentioned experimental phenomena to the fluctuation in the grain boundary configurations and the variation of the grain boundary diffusivities. These diversities provoke the unbalance of mass flows in the intercon-

Table 2. Evolution of hillocks during the test #100-08

Testing hours	Number of hillocks	Ave. height (μm)	Max. height (μm)
0	0	0	0
89	6	0.4	0.7
112	12	0.5	0.6
362	18	0.6	0.8
536	23	0.7	1.1
598	40	0.75	1.5
744	80	0.8	1.9
904	108	0.85	2.2
1191	150	0.87	4.0

sect. In the area of mass flux surplus, the mass injection into a defect causes compressive stress which pushes the upper grain to protrude, against the sliding resistance by the surrounding grains. In the area of mass flux loss, the mass leakage leads to the formation of sinks which eventually sever the interconnect.

Quantitative counts on the micrographs provide the results listed in Table 2. The number of hillocks assumes an upturn curve with respect to the testing hours. The growth of the average hillock height is much slower than the growth of the maximum hillock height. Several nearby hillocks also have the tendency to merge into a wider hillock, thus the growth of its height decelerates.

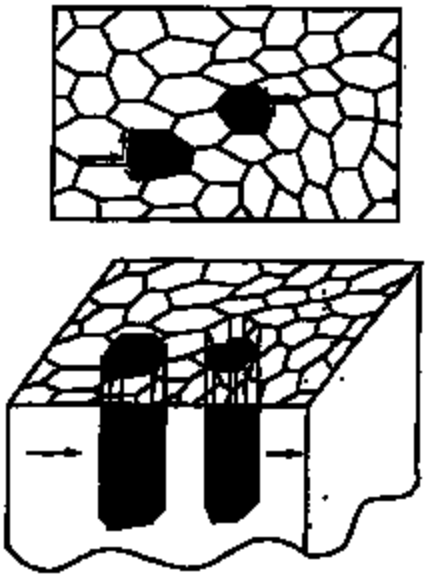

Fig. 2. Sketch on the emergence of a hillock or a sink along the grain boundaries under electromigration.

3. ANALYTICAL MODEL

The experimental observations indicate that the interconnects are composed of tiny columnar grains, whose cross-section can be simplified as the hexagon assembly shown in Fig. 2.

3.1. Mass flow under electromigration

Consider the configuration of a thin film interconnect shown in Fig. 2. Attention is focused on the mass flowing along the grain boundaries. Let J be the atomic flux, namely the number of atoms per unit length per unit time, due to the action of electromigration and the influence of back stress. It is given by [3]

$$J = -\frac{D\delta}{K_B T}\left(\frac{Z^* eE_t}{\Omega} + \frac{\partial \sigma_n}{\partial l}\right) \qquad (1)$$

where D and δ denote the diffusivity and the thickness of the grain boundary, K_B the Boltzmann constant, T the absolute temperature, Ω the atomic volume of the migrating species, Z^* the effective valence of the migrating ions, e the electron charge, E_t the tangential electric field along the grain boundary, σ_n the back stress normal to the grain boundary, and l the tangential coordinate measured along the grain boundary. Equation (1) is rigorous only if the grain boundary is flat.

Since our tests were carried out for unpassivated and exposed lines, the constraining stress is small, and most of the mass flow will be absorbed by the stress-free morphological evolution. A substantial stress gradient like that analyzed by Thouless *et al.* [3] cannot be built up. Thus, the back stress term is neglected in the subsequent analysis, and equation (1) is reduced to

$$J = -\frac{D\delta}{\Omega K_B T} Z^* eE_t. \qquad (2)$$

The rate of accumulation of material at a point in the grain boundary, α_a, relates to the atomic flux, J, by mass conservation

$$\alpha_a = -\Omega \frac{\partial J}{\partial l}. \qquad (3)$$

3.2. Mass flux into a grain

Under electromigration, the mass flows into (or out of) a particular grain by the six grain boundaries it connects, as shown in Fig. 3. Let us introduce a global coordinate system OXY for the grain, with the X-axis aligned with the electric field vector $\mathbf{E}$. The angle between the ith connected grain boundary and the X-axis is denoted by θ_i ($i = 1,2,\ldots,6$). Without loss of generality, we regard that each grain boundary has the same thickness δ but different diffusion constants D_i

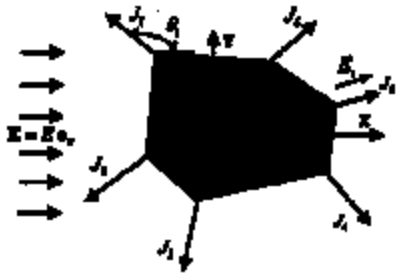

Fig. 3. Calculation of mass fluxes into a grain by electromigration.

($i = 1,2,\ldots,6$). From equation (2), the atomic flux into the grain (termed the grain flux J_g) is given by

$$J_g = -\frac{Z^* e \delta \bar{\delta}}{\Omega K_B T} \sum_{i=1}^{6} D_i \cos\theta_i. \tag{4}$$

First consider the case of regular hexagon grains, as shown in Fig. 7(a). The diffusivities of various grain boundaries are assumed to obey a normal distribution, $N(D,\sigma_D^2)$, with the expected diffusivity D and the standard deviation σ_D. It can be shown that the grain flux, J_g, also obeys a normal distribution. The expectation of the grain flux is zero, and the standard deviation of the grain flux is $\sqrt{3}(Z^* e\delta\bar{\delta}/\Omega K_B T)\sigma_D$.

Next consider the case of general hexagon grains, as shown in Fig. 8(a), where the grain size and the grain shape only have mild fluctuations. The diffusivities of the grain boundaries obey a normal distribution $N(D,\sigma_D^2)$. Through considerable algebra, the expectation of the grain flux is obtained by

$$\begin{aligned} J_g = \frac{Z^* e \delta \bar{\delta}}{\Omega K_B T} D \Big[&\cos\Big(\frac{\pi}{3} - \theta + \varphi_1\Big) + \cos\Big(\frac{\pi}{3} + \varphi_2\Big) \\ &+ \cos\Big(\frac{\pi}{3} + \theta + \varphi_3\Big) - \cos\Big(\frac{\pi}{3} - \theta + \varphi_4\Big) \\ &- \cos(\theta + \varphi_5) - \cos\Big(\frac{\pi}{3} + \theta + \varphi_6\Big) \Big] \end{aligned} \tag{5}$$

Fig. 4. Configuration of a general hexagon grain assembly.

where θ denotes the angle between the X-axis and the ith grain boundary of a hypothetical regular hexagon, and φ_i the angle deviations from the regular hexagon, as depicted in Fig. 4. To fix the value of θ, we require that the sum of φ_i ($i = 1,2,\ldots,6$) vanishes. The standard deviation of the grain flux is given by

$$\begin{aligned} \sigma(J_g) = \frac{Z^* e \delta \bar{\delta}}{\Omega K_B T} \sigma_D \Big[&3 + \cos^2\Big(\frac{\pi}{3} - \theta + \varphi_1\Big) \\ &+ \cos^2\Big(\frac{\pi}{3} + \varphi_2\Big) + \cos^2\Big(\frac{\pi}{3} + \theta + \varphi_3\Big) \\ &+ \cos^2\Big(\frac{\pi}{3} - \theta + \varphi_4\Big) + \cos^2(\theta + \varphi_5) \\ &+ \cos^2\Big(\frac{\pi}{3} + \theta + \varphi_6\Big) \Big]^{1/2}. \end{aligned} \tag{6}$$

We further assume that the deviation angles, φ_i ($i = 1,2,\ldots,6$), obey a normal distribution of $N(0,\sigma_\varphi^2)$. Then the grain flux, J_g, also obeys a normal distribution. The expectation of the grain flux is zero, and its standard deviation is calculated by

$$\sigma(J_g) = \sqrt{3}\frac{Z^* e \delta \bar{\delta}}{\Omega K_B T} \sigma_D \sqrt{2 - \exp(-\sigma_\varphi^2)}. \tag{7}$$

3.3. Partition of mass flow

The lateral defects which might cut through the tiny columnar grains provide channels to accommodate the fluctuation of the mass flow. As shown in Fig. 5, let h represent the distance of the initial defect from the original top surface, W the protruding height of the grain, and H the thickness of the injected mass smeared over the cross-section. The volumetric mass flow is accommodated through two layers: the surface layer and the defect layer. The surface layer covers the region from the top surface to a depth of H_0, where the mass flow is predominantly through surface migration, regardless of the location of the defect. The defect layer covers a range of characteristic sizes H_D^* above and below the current defect height. Accordingly, the evolution law for the height of the injected mass, H, can be phrased by

$$H(t) = \begin{cases} \dfrac{2\Omega J_g}{wR^2} \displaystyle\int_0^t H_D^*(t)\,dt & t < t_0 \\ H_0 + \dfrac{2\Omega J_g}{wR^2} \displaystyle\int_{t_0}^t H_D^*(t)\,dt & t \geq t_0 \end{cases} \tag{8}$$

where t is the time and t_0 the incubation time for a hillock or a slit to appear, and H_0 denotes the critical thickness of mass injection or the value of H at t_0. The size of the influence region of the defect layer, H_D^*, relies on the defect location, $h + (H/2) - W$, from the original top surface. We adopt the following piece-wise linear relation of H_D^* with respect to the defect location

$$H_D^* = \begin{cases} 0, & h+\frac{1}{2}H-W<H_S \\ h+\frac{1}{2}H-W-H_S, & H_S\le h+\frac{1}{2}H-W<H_S+H_D \\ \frac{H_D}{H_S+H_D}\left(h+\frac{1}{2}H-W\right), & h+\frac{1}{2}H-W\ge H_S+H_D \end{cases} \quad (9)$$

where H_D is a characteristic size of the defect layer. The mass injection into the defect will terminate if

$$h+\frac{1}{2}H(t)-W(t)=H_S. \quad (10)$$

The two length parameters H_S and H_D dictate the partition of mass flow.

3.4. Stress due to mass flow

The injection (or leakage) of masses into (or from) these defects would induce local confining stresses normal to the film plane. Though they have little effect on the mass transport along the grain boundaries that are normal to the film plane, they do cause the protruding motion of hillocks. Take the example of mass injection into a defect. The confining stress is compressive and should be balanced by the shear resistance along the grain boundaries around the upper half grain which intends to protrude. If the compressive stress multiplied by the cross-section of the columnar grain reaches the maximum value of the slip resistance offered by the surrounding grains, the hillock will sweep from the grain.

A simple model is adopted to calculate the compressive stress of the grain. We approximate a columnar hexagon grain by a cylindrical grain of the same height and the same cross-section. This approximation enables an axi-symmetric modeling of a prismatic dislocation loop, as shown in Fig. 6. In the figure, C is a planar circular loop of the prismatic dislocation with radius R in the XOY plane, whose normal directs along the Z-axis. The vector r marks the projection of a generic point P on the dislocation plane, while a point on the loop is marked by r'. The vector l forms an angle β with the positive X-direction. By the Peach–Koehler formula [18], the stress field, σ, due to the dislocation loop is given by

$$\sigma = \frac{\mu}{4\pi}\left\{\oint_C (\mathbf{b}\times\nabla')\frac{1}{|\mathbf{r}-\mathbf{r}'|}\otimes d\mathbf{r}' + \oint_C d\mathbf{r}'\otimes(\mathbf{b}\times\nabla')\frac{1}{|\mathbf{r}-\mathbf{r}'|} - \frac{1}{1-\nu}\oint_C [(\nabla\otimes\nabla-1\nabla^2)\mathbf{r}' - \mathbf{r}'[\nabla'\cdot(\mathbf{b}\times d\mathbf{r}')]\right\} \quad (11)$$

where μ denotes the shear modulus, ν the Poisson ratio, and $\mathbf{b}$ the Burgers vector (which relates to the mass injection thickness H). The gradient symbols ∇ and ∇' are operated on the field and on the planar dislocation loop, respectively. Through lengthy algebra, the compressive stress normal to the plane of the dislocation loop can be calculated as

$$\sigma_z = -\frac{\mu H}{4\pi(1-\nu)}\int_0^{2\pi}\frac{4\phi}{\sqrt{R^2+|\mathbf{r}|^2-2rR\cos(\beta-\phi)}} \quad (12)$$

where ϕ is the integration angle around the dislocation loop. The overall compressive force on the upper columnar grain is

$$F_z = -2\pi\int_0^R \sigma_z\, dr = \frac{2\mu}{1-\nu}RH \quad (13)$$

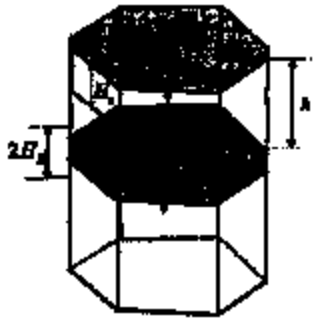

Fig. 5. Geometry and various characteristic lengths for the protruding motion of a grain.

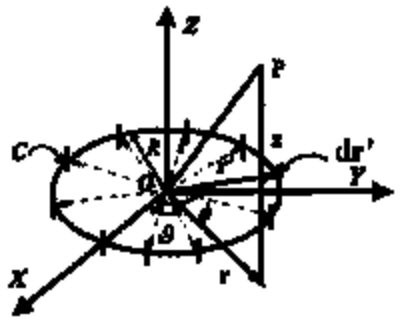

Fig. 6. Compressive stress field by a prismatic dislocation loop induced by the injected mass.

where F_e provides the driving force for a grain to protrude.

3.3. Sliding condition and incubation time

The slip resistance against the grain with mass injection, prior to any movement of the defect, is composed of shear stresses along the vertical surfaces surrounding the grain

$$F_r = 2\pi R h \tau_c \tag{14}$$

where τ_c denotes the shear strength of the grain boundary.

The onset of protrusion instability is dictated by the condition of $F_r = F_e$. Combining equations (13) and (14), one obtains the critical thickness of the mass injection

$$H_c = \pi(1-\nu)\frac{\tau_c}{\mu}R. \tag{15}$$

Substituting equation (15) into equations (8) and (9), one arrives at the incubation time for the appearance of a hillock

$$t_i = \frac{\pi R^2}{\Omega D_b^*}\frac{H_0 + H_D}{H_D}\ln\left(1 + \frac{\pi(1-\nu)\tau_c}{2\mu}\right) \tag{16}$$

provided that $h + \frac{1}{2}H_0 \geq H_0 + H_D$. The incubation time is proportional to the square of the grain size. The hillocks will not form in an interconnect during its service life if the grain size is sufficiently large.

We next introduce the concept of the minimum incubation time. For a normal distribution, the unbalanced material fluxes mostly lie in a region of $\pm 3\sigma(J_a)$. Therefore, the minimum incubation time for a protrusion can be derived by

$$t_{i,\min} = \frac{\pi R^2}{3\Omega|Z|\sigma(J_a)}\frac{H_0 + H_D}{H_D}\ln\left(1 + \frac{\pi(1-\nu)\tau_c}{2\mu}\right) \tag{17}$$

where $\sigma(J_a)$ is equal to $\sqrt{5}(Z^* e\delta\beta/\Omega k_B T)\sigma_a$ for the case of regular hexagon grains, and is given by equation (7) for the case of general hexagon grains.

3.5. Protruding height and sinking depth

Consider the subsequent evolution of a hillock or a sink. As shown in Fig. 5, the slip resistance caused by the surrounding grains against the subsequent evolution is

$$F_r = 2\pi R\left(h + \frac{H}{2} - W\right)\tau_c \tag{18}$$

where it is tacitly assumed that the injected masses are evenly distributed to the top and the bottom grain matrices. The compressive force due to the mass flux into the defect is

$$F_c = \frac{2\mu}{1-\nu}R(H - W). \tag{19}$$

The balance of two forces provides an expression for the amount of grain slide. When a hillock is caused by the mass injection, or a sink caused by the mass leakage, the amount of grain slide, W, is obtained by

$$W(t) = -\frac{\pi(1-\nu)\tau_c}{\mu - \pi(1-\nu)\tau_c}h + \frac{2\mu - \pi(1-\nu)\tau_c}{2\mu - 2\pi(1-\nu)\tau_c}H(t), \quad t \geq t_i. \tag{20}$$

Accordingly, the protruding height is roughly proportional to R^{-2}.

4. NUMERICAL SCHEME AND DAMAGE SIMULATION

We now devise a numerical scheme to simulate the protruding and sinking motions. Two simplified polycrystalline configurations are generated by computer for the aluminum interconnect shown in Fig. 2. The first one is an array of regular hexagon grains. As mentioned before, the ith grain boundary connected to the grain forms an angle θ with the X-axis. The connection angles of other grain boundaries, denoted by $\tilde{\theta}_i$ $(i = 1,2,3,4,6)$, differ from $\tilde{\theta}_0 = \theta$ by multiples of $\pi/3$. The second configuration deviates from the first by fluctuating the connection angles according to $\tilde{\theta}_j = \tilde{\theta}_j + \varphi_j$ $(j = 1,\ldots,6)$, with φ_j being described by a normal distribution of $N(0,\sigma_\varphi^2)$. The diffusivities of different grain boundary segments are assigned by a normal distribution of $N(\bar{D}_b\delta,\sigma_D^2)$. Prior to the switching on of the electric current, the interconnect assumes a perfectly flat top surface and no mass injects in any grain defects. After the switching on of the electric current at $t = 0$, the material fluxes into each grain can be calculated through equation (4). For a particular grain, a protruding or sinking process commences at the critical time determined by equation (16). The subsequent evolution is governed by equations (8), (9) and (20). It consists of a set of integral equations, and can be solved by the explicit Euler iteration. During the simulation, the interconnect is composed of 3445 grains, with 6992 triple junctions and 10 336 grain boundary segments.

The physical constants for aluminum-based interconnects are listed in Table 3. The electric field is calculated from the measured current density and the conductivity of aluminum (3.35×10^7 A/V m). The average grain size $\bar{R} = 0.115$ μm is obtained by counting the grain number in a fixed observation area. The assignments of the mass diffusivity $\bar{D}\delta$, and the effective valence Z^* are worth of explanation. A wide range of the diffusivity data for aluminum exist. For example, Wang *et al.* [14] quoted the surface diffusion data from Wohlfahrt [19] which gives $Z^* = 20$, $D = 10^{-4} \times \exp[-0.7(\text{eV})/k_B T]$ m^2/s, and $\delta = 0.286$ nm. They lead to a small value of $\bar{D}\delta = 5.1 \times 10^{-20}$ m^3/s at 500 K. On the other hand, Bergman *et al.* [20] adopted the value of $Z^* = 10$ and quoted the grain boundary diffusion data by Kaur *et al.* [21], which gives a

Table 1. Physical constants for aluminum interconnects

μ (GPa)	κ_t (GPa)	ν	Ω_0 (J/K)	T (K)	ϵ (C)	E (V/m)	R (μm)	$D\delta$ (m^3/s)	Z^*
24.3	1.34	0.345	1.38×10^{-23}	300	1.6×10^{-19}	1000	0.115	1.03×10^{-25}	20

much larger $D\delta$ value of 6.4×10^{-23} m^3/s. In the present simulation, we adopt the value of $Z^* = 20$ and take an intermediate value of $D\delta = 1.03\times10^{-25}$ m^3/s.

We assume that the location of defect, Λ, obeys a normal distribution $N(\bar{\Lambda},\sigma_\Lambda^2)$. Since the defects appear mostly in the lower-bottom of the film, we take the expected location as $\bar{\Lambda} = 6\bar{R}$, and the standard deviation as $\sigma_\Lambda = 0.5\bar{R}$. The other standard deviations are taken as $\sigma_D = 0.1\bar{D}$ and $\sigma_\psi = \pi/4$ in the calculation. Under this σ_ψ value, the polycrystal configuration, as shown in Fig. 8(a), resembles the statistical feature of the actual microstructure. The thickness for the surface layer H_S and that for the defect layer H_D are taken as $\bar{R}$ and $0.5\bar{R}$, respectively. The latter is less than the former since the attraction for the incoming masses is stronger near the surface layer than that near the defect layer. The evolution is measured by the normalized time

$$\tau = \frac{D\delta}{K_B T\bar{R}^2} Z^* eE t.$$

The simulation indicates that the mass flows in the interconnect indeed have four stages: the incubation stage, the rapid growing stage, the

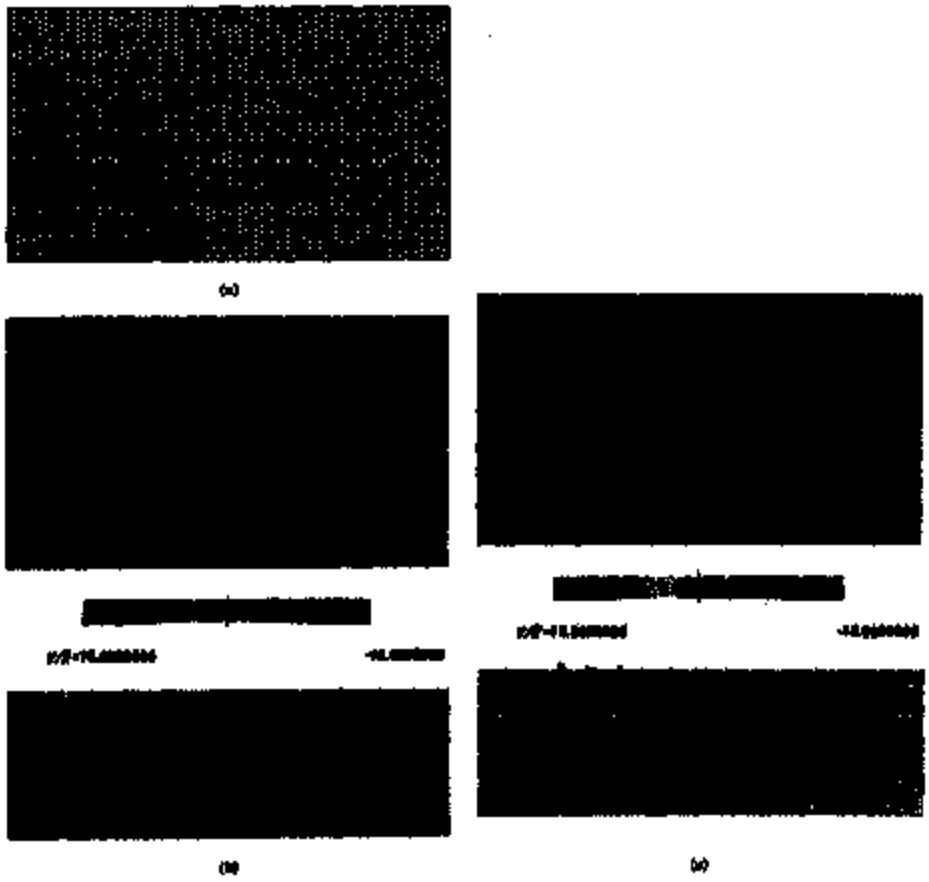

Fig. 7. Morphological evolution for regular hexagonal grains: (a) the initial configuration; (b) at $\tau = 5$; (c) at $\tau = 10$. [h' denotes the protruding height (>0) or the sink depth (<0) and $\bar{R}$ the average grain radius].

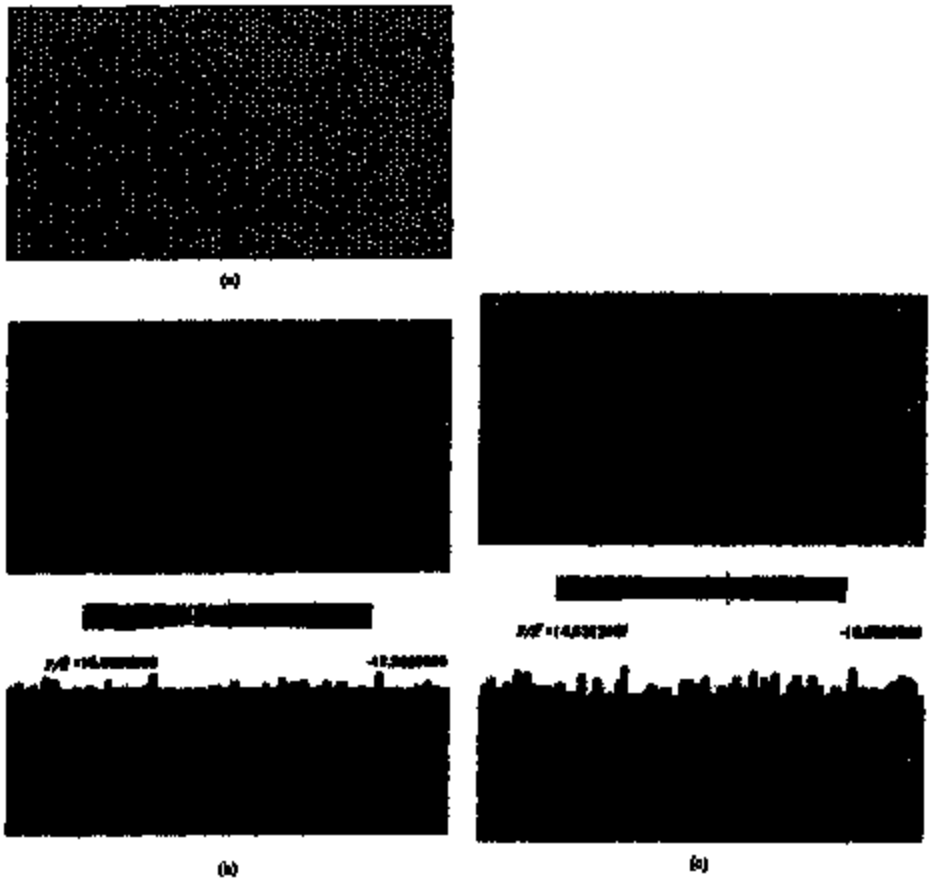

Fig. 8. Morphological evolution for general hexagonal grains: (a) the initial configuration; (b) at $\bar{t} = 5$; (c) at $\bar{t} = 10$.

deceleration stage, and the final stabilization. We now describe the two cases of calculation in detail.

The initial configuration for the case of regular hexagon grains is shown in Fig. 7(a). Figures 7(b) and (c) show two snapshots of the interconnect at $\bar{t} = 5$ and 10, which depict the damage evolution of the grains. The regularity of the configuration suppresses the fluctuation in the grain fluxes. The interconnect will have a relatively long life. The case of general hexagon grains in Fig. 8(a) bears more resemblance to the actual configuration. Figures 8(b) and (c) illustrate two snapshots of the damage evolutions in the interconnect at the instant $\bar{t} = 5$ and 10. In the same time intervals, the hillocks and sinks are more severe, and the number and the average height of the hillocks are greater than the interconnect of regular hexagons. The variations of the protruding height and the sinking depth are shown in Fig. 9 vs the normalized time. The grain flux J_g is taken to be $2.34\kappa(J_g)$ in the calculation. The protruding motion jumps to a fast growing stage after an incubation time, then gradually slows down to approach a stabilized height, in good agreement with our experiments.

The predictions on the morphological fluctuations due to the regular grain assembly and the general grain assembly are very different. Figure 10 plots the curves of $s_W/\bar{R}$ vs $\bar{t}$, where s_W represents the standard deviation of the surface morphology W. The general grain assembly can cause a more severe morphological instability than the regular one. The effect due to the angular deviation s_φ is two-fold. First, the angular deviation leads to larger standard deviation in mass flow, as quantified by equation (7). Second, it also results in the fluctuation of the grain sizes from their average value $\bar{R}$, and that causes further morphological fluctuation

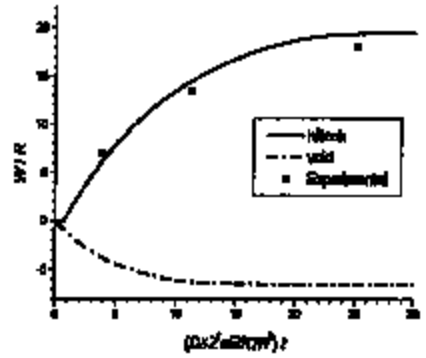

Fig. 9. Protruding height and the sinking depth vs the normalized time, $J_0 = 2.34e(J_0)$.

of the microstructure since the inverse square dependence of the hillock height with respect to R.

To address the importance of grain size on morphological evolution under electromigration, we include a further example of general hexagon array in Fig. 11(a), featuring a much larger average grain size of $3\bar{R}$. The interconnect is composed of 481 grains, with 964 triple junctions and 1444 grain boundary segments. Other parameters are the same as the previous case. Since the incubation time for the case in Fig. 8 is about $\bar{t} = 1$, its square dependence on the grain size would lead to an average incubation time of $\bar{t} = 9$ for the present case (for the sake of comparison, the previous $\bar{R}$ value is used to get the normalized time). The simulation confirms this prediction. At $\bar{t} = 5$, there are hardly any morphological changes. At $\bar{t} = 10$, the damage evolution just starts, as shown in Fig. 11(b). It is much subdued when compared with Fig. 8(c).

To design against the electromigration, one needs to raise the incubation time of an interconnect beyond its service life. To comply with this criterion, a polycrystal line with large and uniform grains (if not a bamboo line or even a single crystal line) with small variation in grain boundary diffusivities is desirable.

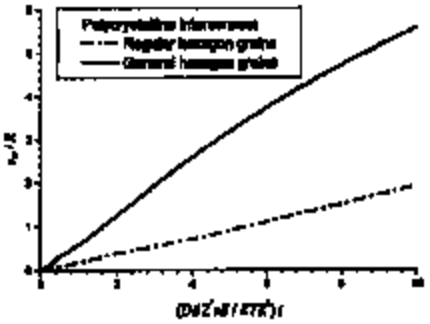

Fig. 10. Development of morphological fluctuation (in terms of the standard deviation of W) with respect to the normalized time.

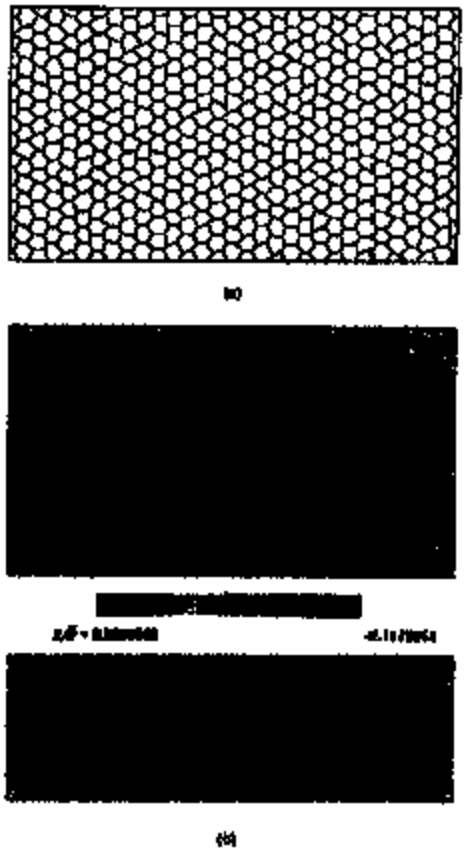

(a)

(b)

Fig. 11. Morphological evolution for a general hexagonal array of much larger grain size of 0.345 μm: (a) the initial configuration; (b) at $\bar{t} = 10$.

To conclude this paper, we mention that the failures of the polycrystalline interconnects often result from a combination of different mechanisms, such as stress migration, grain boundary diffusion, and thermal migration. A coupled analysis is worthwhile in the future.

Acknowledgment—The authors appreciate the support by the National Natural Science Foundation of China.

REFERENCES

1. D'Heurle, F. M. and Ames, I., *Appl. Phys. Lett.*, 1970, 16, 80.
2. D'Heurle, F. M., *Proc. IEEE*, 1971, 59, 1409.
3. Thurdson, M. D., Yu, H., Zhao, Z. and Yang, W., *J. Mech. Phys. Solids*, 1996, 44, 171.
4. Yang, W., Wang, W. and Suo, Z., *J. Mech. Phys. Solids*, 1994, 42, 897.

5. Li, C-Y., Borgesen, P. and Korhonen, M. A., *Appl. Phys. Lett.*, 1992, 61, 411.
6. Besser, P. R., Madden, M. C. and Filter, P. A., *J. appl. Phys.*, 1992, 72, 3792.
7. Kraft, O., Bader, E., Bonzel, J. E. and Arzt, E., *Mater. Res. Symp. Proc.*, 1993, 309, 199.
8. Maniwa, T., Flinn, P., Brennan, J. C., Gardner, D. and Madden, M., *J. appl. Phys.*, 1993, 74, 1026.
9. Arzt, E., Kraft, O., Nix, W. D. and Sanchez, J. E., *J. appl. Phys.*, 1994, 76, 1563.
10. Sanchez, J. E. and Arzt, E., *Scripta metall. mater.*, 1992, 27, 285.
11. Sanchez, J. E., McKnelly, L. T. and Morris, J. W., *J. appl. Phys.*, 1992, 72, 3201.
12. Kuan, J. H., *Appl. Phys. Lett.*, 1992, 61, 2170.
13. Gao, Z., Wang, W. and Yang, M., *Appl. Phys. Lett.*, 1994, 64, 1944.
14. Wang, W., Bao, Z. and Hsu, T.-H., *J. appl. Phys.*, 1994, 75, 2394.
15. Zhao, Z. and Yang, W., *Tsinghua Sci. Technol.*, 1997, 2, 374.
16. Thompson, C. V. and Kahn, H., *J. Electron. Mater.*, 1993, 22, 581.
17. Ren, Z., *Appl metall. mater.*, 1994, 42, 1981.
18. Peach, M. O. and Koehler, J. S., *Phys. Rev.*, 1950, 80, 436.
19. Wuttiker, F. H., *Diffusion and Defect Data—Solid State Data*, Vol. 47. Trans. Tech. Publications, Switzerland, 1986, p. 4.
20. Borgesen, P., Korhonen, M. A., Sullivan, T. D., Brown, D. D. and Li, C-Y., in *Thin Films: Stress and Mechanical Properties III, MRS Symposium Proceedings*, Vol. 239, ed. W. D. Nix, J. C. Bravman, E. Arzt and L. B. Freund, 1992, p. 613.
21. Kaur, I., Gust, W. and Bertram, L., *Handbook of Grain and Interphase Boundary Diffusion Data*. Ziegler Press, Stuttgart, 1989.

SCIENCE DIRECT

[redacted]

Home | Publications | Search | My Alerts | My Profile | Help

Brought to you by: [redacted]

[redacted] results 1 - 29

29 Articles Found

TITLE-ABSTR-KEY(hillocks AND aluminum)
(All Sciences (- All Sciences -))

Quick Search searches the abstracts, titles, keywords within the selected content. To run a more precise search use one of the full featured search forms.

[redacted] | display standard view | display citations only

1. ☐ **Mo-capped Al-Nd alloy for both gate and data bus lines of liquid crystal displays,** *Thin Solid Films, Volume 383, Issues 1-2, 15 February 2001, Pages 287-291*
Toshiaki Arai, Atsuya Makita, Yasunobu Hiromasa and Hiroshi Takatsuji
Summary/Plus | Article | Journal Format-PDF (796 K)

2. ☐ **Microstructure of thermal hillocks on blanket Al thin films,** *Thin Solid Films, Volume 371, Issues 1-2, 1 August 2000, Pages 278-282*
Deok-koo Kim, Birgit Holland, William D. Nix, Eduard Arzt, Michael D. Deal and James D. Plummer
Summary/Plus | Article | Journal Format-PDF (1073 K)

3. ☐ **High performance n-Si:H thin film transistors based on aluminum gate metallization,** *Microelectronics Reliability, Volume 40, Issue 6, 1 June 2000, Pages 947-953*
A. Nathan, R. V. R. Murthy, B. Park and S. G. Chamberlain
Summary/Plus | Article | Journal Format-PDF (1446 K)

4. ☐ **Analysis of local strain in aluminium interconnects by energy filtered CBED,** *Ultramicroscopy, Volume 81, Issue 3-4, April 2000, Pages 245-262*
S. Kramer, J. Mayer, C. Witt, A. Weickenmeier and M. Rühle
Summary/Plus | Article | Journal Format-PDF (1137 K)

5. ☐ **Pure Al thin film protective layer to prevent stress migration in Al wiring for thin-film transistors,** *Surface and Coatings Technology, Volume 125, Issues 1-3, March 2000, Pages 167-172*
H. Takatsuji, K. Haruta, S. Tsuji, K. Kuroda and H. Saka
Summary/Plus | Article | Journal Format-PDF (1070 K)

6. ☐ **Kinetics of hillock growth in Al and Al-alloys,** *Microelectronic Engineering, Volume 50, Issues 1-4, January 2000, Pages 301-309*
Michał Zaborowski and Piotr Dumania
Summary/Plus | Article | Journal Format-PDF (1886 K)

7. ☐ **Electromigration induced aluminum atom migration retarding by grain boundary structure stabilization and copper doping,** *Microelectronics Reliability, Volume 39, Issue 11, November 1999, Pages 1631-1645*
M. Hasunuma, H. Toyoda and H. Kaneko
Summary/Plus | Article | Journal Format-PDF (363 K)

8. ☐ **Reaction of Aluminum-on-Titanium Bilayer with GaN: Influence of the Al/Ti Atomic Ratio,** *Journal of Electronic Materials, Volume 28, Issue 8, August 1999, Pages 949-954*
S. M. Gasser, E. Kolawa and M. A. Nicolet
Abstract

9. ☐ **Effect of aluminum oxide caps on hillock formation in aluminum alloy films,** *Thin Solid Films, Volume 349, Issues 1-2, 30 July 1999, Pages 191-198*
Eiji Iwamura, Katsutoshi Takagi and Takashi Ohsaki
Abstract | Journal Format-PDF (576 K)

10. ☐ **Enhanced optical performance of aluminum films by copper inclusion,** *Thin Solid Films, Volume 348, Issues 1-2, 6 July 1999, Pages 222-226*
C. Kylner and L. Mattsson
SummaryPlus | Article | Journal Format-PDF (201 K)

11. ☐ **The influence of cooling water flowing in the sputtering target on aluminum based thin film nanostructure deposited on glass substrates,** *Thin Solid Films, Volumes 343-344, April 1999, Pages 465-468*
H. Takatsuji, S. Tsuji, K. Kuroda and H. Saka
Abstract | Journal Format-PDF (345 K)

12. ☐ **Novel prevention method of stiction using silicon anodization for SOI structure,** *Sensors and Actuators A: Physical, Volume 72, Issue 2, 19 January 1999, Pages 153-159*
Y. Matsumoto, T. Shimada and M. Ishida
SummaryPlus | Article | Journal Format-PDF (847 K)

13. ☐ **Nitrogen-added Al rare-earth alloys for thin film transistors,** *Thin Solid Films, Volume 337, Issues 1-2, 11 January 1999, Pages 113-117*
Toshiaki Arai, Hiroshi Takatsuji and Hideo Hyori
SummaryPlus | Article | Journal Format-PDF (456 K)

14. ☐ **The growth of epitaxial aluminium on As containing compound semiconductors,** *Journal of Crystal Growth, Volume 196, Issue 1, 1 January 1999, Pages 1-12*
S. J. Pilkington and M. Missous
SummaryPlus | Article | Journal Format-PDF (952 K)

15. ☐ **Interconnect damage by electromigration: experiment and numerical simulation,** *Acta Materialia, Volume 47, Issue 1, 11 December 1998, Pages 89-99*
J.-M. Huang, W. Yang and Z. -J. Zhao
SummaryPlus | Article | Journal Format-PDF (1388 K)

16. ☐ **Application of high temperature deposited aluminum gate electrode to the fabrication of a-Si:H TFT,** *Surface and Coatings Technology, Volumes 108-109, Issues 1-3, 10 October 1998, Pages 588-593*
P. S. Shih, T. C. Chang, S. M. Chen, M. S. Feng, D. Z. Peng and C. Y. Chang
SummaryPlus | Article | Journal Format-PDF (179 K)

17. ☐ **Scanning electron microscope studies of algan films grown by organometallic vapor phase epitaxy,** *Solid-State Electronics, Volume 42, Issue 4, April 1998, Pages 637-641*
A. Y. Polyakov, A. V. Govorkov, N. B. Smirnov, M. G. Mil'vidskii, J. M. Redwing, M. Shin, M. Skowronski and D. W. Greve
Abstract | Journal Format-PDF (791 K)

18. ☐ **Influence of thermal heating effect on pulsed DC electromigration,** *Microelectronics and Reliability, Volume 37, Issues 10-11, 11 October 1997, Pages 1533-1536*
P. Waltz, L. Arnaud, G. Tartavel and G. Lormand
Abstract | Journal Format-PDF (234 K)

19. ☐ **Initial development of the lateral hillock distribution in optical quality Al thin films studied in real time,** *Thin Solid Films, Volume 307, Issues 1-2, 10 October 1997, Pages 169-177*
C. Kylner and L. Mattsson
Abstract | Journal Format-PDF (696 K)

20. ☐ **Electromigration in layered Al lines studied by in-situ ultra-high voltage electron microscopy,** *Thin Solid Films, Volume 300, Issues 1-2, 28 May 1997, Pages 25-29*
H. Mori, M. Komatsu and H. Okabayashi
Abstract | Journal Format-PDF (525 K)

21. ☐ **Transmission electron microscopy of Al-Cu interconnects during in-situ electromigration testing,** *Thin Solid Films, Volume 292, Issues 1-2, 5 January 1997, Pages 103-117*
W. C. Shih and A. L. Greer
Abstract | Journal Format-PDF (1908 K)

22. ☐ **Residual stress and in-situ thermal stress measurement of aluminum film deposited on silicon wafer,** *Thin Solid Films, Volumes 290-291, 15 December 1996, Pages 248-253*
K. Kusaka, T. Hanabusa, F. Inoko and M. Nishida
Abstract | Journal Format-PDF (514 K)

23. ☐ **Al-Sn and Al-Dy alloy thin films with low resistivity and high thermal stability for microelectronic conductor lines,** *Thin Solid Films, Volume 289, Issues 1-2, 30 November 1996, Pages 289-294*
S. Takayama and N. Tsutsui
Abstract | Journal Format-PDF (778 K)

24. ☐ **A comparative study of hillock formation in aluminum films,** *Thin Solid Films, Volume 271, Issues 1-2, 15 December 1995, Pages 64-68*
B. C. Martin, C. J. Tracy, J. W. Mayer and L. R. Hendrickson
Abstract | Journal Format-PDF (745 K)

25. ☐ **A study of hillock formation on Al-Ta alloy films for interconnections of TFT-LCDs,** *Thin Solid Films, Volume 270, Issues 1-2, 1 December 1995, Pages 430-435*
R. Iwamura, T. Ohnishi and K. Yoshikawa
Abstract | Journal Format-PDF (940 K)

26. ☐ **The effect of ion implantation on the properties of Al films,** *Applied Surface Science, Volume 91, October 1995, Pages 239-245*
M. Zaborowski, A. Barcz, G. Gawlik and L. W. Rangelow
Abstract | Journal Format-PDF (748 K)

27. ☐ **Correlation between special grain boundaries and electromigration behavior of aluminum thin films,** *Canadian Metallurgical Quarterly, Volume 34, Issue 3, July-September 1995, Pages 287-292*
K. T. Lee, J. A. Szpunar, A. Morawiec, D. B. Knorr and K. P. Rodbell
Abstract | Journal Format-PDF (337 K)

28. ☐ **Use of fractals and kinetic equations to model thermally induced hillock formation and growth in thin metal films,** *Thin Solid Films, Volume 260, Issue 2, 15 May 1995, Pages 245-251*
J. Chelikowsky and I. Goodenough
Abstract | Journal Format-PDF (741 K)

29. ☐ **Anisotropic etching of silicon in TMAH solutions,** *Sensors and Actuators A: Physical, Volume 34, Issue 1, July 1992, Pages 51-57*
Osamu Tabata, Ryouji Asahi, Hirofumi Funabashi, Kaiichi Shimaoka and Susumu Sugiyama
Abstract | Abstract + References | Journal Format-PDF (636 K)

29 Articles Found

TITLE-ABSTR-KEY(hillocks AND aluminum)
[All Sources (- All Sciences -)]

Quick Search searches the abstracts, titles, keywords within the selected content. To run a more precise search use one of the full featured search forms.

[illegible] results 1 - 29 [illegible]

ELSEVIER

Microelectronic Engineering 50 (2000) 301–309

www.elsevier.nl/locate/mee

Kinetics of hillock growth in Al and Al-alloys

Michał Zaborowski*, Piotr Dumania

Institute of Electron Technology, Al. Lotników 32/46, 02 668 Warsaw, Poland

Abstract

Hillock growth kinetics and size distribution were investigated in Al, Al:Si 1% and Al:Si1%:Cu 0.5% layers. Metallization surface was examined by optical, SEM and TEM microscopy, stylus profiling and an automatic method of hillock recognition from a microscope image. The method allowed for counting hillocks in a desired range of their diameter d. Surface density of hillocks was measured as a function of time of furnace annealing at 400°C and as a function of temperature of RTP annealing. A maximum hillock size was found to increase linearly with metallization layer thickness and with logarithm of annealing time. A total area occupied by hillocks was evaluated. Hillock density decreased versus $1/T$ with an activation energy of 0.28 eV for Al and 0.31 eV for Al:Si. It was found, that a normalized hillock density N may be expressed by a formula $N = N_0 \exp(-cd)$. Values for N_0 and c are given together with a short discussion. © 2000 Elsevier Science B.V. All rights reserved.

Keywords: Metallization; Aluminum thin film; Polycrystalline layer morphology; Hillock growth

1. Introduction

Aluminum-based metallization still remains the most commonly used material for interconnecting lines in silicon ICs and electro-mechanical microsystems. Polycrystalline Al layers alter their surface morphology as a consequence of heat treatment and other processes performed at elevated temperature (250–500°C). Large crystallites, so-called hillocks, can outgrow above the initial metal surface [1,2]. The driving force of hillock growth is a compressive stress caused by large mismatch of thermal expansion coefficients between Al and Si or SiO_2 substrate [3,4]. Hillocks are particularly undesirable in multilevel metal systems.

The aim of this work was to investigate both the growth kinetics and the size distribution of the hillocks.

2. Experimental

Samples were prepared by thermal oxidation of (100) oriented Si wafers to an oxide thickness of

*Corresponding author. Fax: +48-22-716-5951.
E-mail address: mzab@ite.waw.pl (M. Zaborowski)

0167-9317/00/$ – see front matter
PII: S0167-9317(99)00296-8

0.4 μm followed by magnetron sputter deposition of the metallization. The vacuum was better than 1×10^{-4} Pa and Ar pressure was equal to 0.5 Pa. We used pure Al 5 N, Al:Si 1% alloy or Al: Si 1%:Cu 0.5% alloy as a target material. Metal layer thickness ranged from 0.5 to 2.5 μm. Substrates were heated up to approximately 180°C before sputtering. The Al reference layers were produced by means of e-gun evaporation under the same temperature conditions. All samples were annealed in a furnace or RTP reactor. Nitrogen, hydrogen or argon were used as an annealing ambient. Metallization surface was examined by a number of methods: optical, SEM and TEM microscopy, stylus profiling and an automatic method of hillock recognition from a microscope image. The last method consists of the processing of surface images acquired by a monochromatic TV camera and allows hillock-like objects to be visualized separately and measured [5].

3. Results and discussion

All manufactured metallization layers were polycrystalline, with grain dimensions dependent on the layer thickness and annealing conditions. A ⟨111⟩ preferred orientation was found from XRD measurements. SEM micrographs revealed numerous hillocks protruded into the metal layer surface (Fig. 1). Shapes and sizes of hillocks involved in Al:Si:Cu alloy by a 30 min annealing at a temperature of 450°C differ significantly from those in Al and Al:Si metallization. No influence of annealing atmosphere (nitrogen, hydrogen or argon) on the surface morphology was noted. The stylus

a b

Fig. 1. Metallization surface examined by SEM after annealing (450°C, 30 min): (a) magnetron sputtered Al layer 1 μm thick; (b) similar layer of Al:Si:Cu alloy.

profiling method was useless in the case of Al:Si:Cu because of the relatively large radius of the tip (2.5 μm). This technique applied for Al and Al:Si metallization gave results comparable to the results of hillock recognition method. Nevertheless, this last method was extensively used in present investigations for reason of better hillock surface area estimation.

Hillocks start to grow up almost immediately at the beginning of annealing. Two-minute annealing of a 0.7 μm thick Al layer at the relatively low temperature of 400°C is sufficient for creation of small hillocks. Fig. 2 presents surface density of these objects as a function of the time of furnace annealing in flowing nitrogen. Hillocks are collected in 0.4 μm groups with regard to their average diameter, lower measurement limit is equal to 0.33 μm. Longer annealing does not change the population of hillocks inside each group noticeably, but induces greater hillocks. Smaller hillocks seem to be a source of larger ones, therefore it is evident that the hillock number is here in a kind of dynamic equilibrium. A maximum hillock size, defined as a diameter of 1% of the whole hillock population exhibiting largest dimensions in the examined surface, is presented in Fig. 3. The maximum hillock size depends nearly linearly on the logarithm of annealing time. Each curve represents a different wafer and a different metal deposition process. Generally, the values for an Al:Si alloy are close to those for pure aluminum. Maximum hillocks in Al:Si:Cu are several times smaller than in Al, after the same time of annealing.

Samples were divided into four parts and covered with an Al of different thickness in order to estimate the dependence of the maximum hillock size on the layer thickness. Fig. 4 shows the results of furnace annealing at a temperature of 400°C for 8 min in N_2. Maximum hillock size increases linearly with metallization layer thickness ranging from 0.5 to 2 μm, with some scatter from one sample to another. Changing the annealing conditions to 450°C and 5 min (wafer no. 4) does not influence the maximum hillock sizes.

The method of hillock recognition allows for summing the areas of all detected hillocks. A fraction of the sample surface occupied by hillocks increases during annealing (Fig. 5). The total hillock area

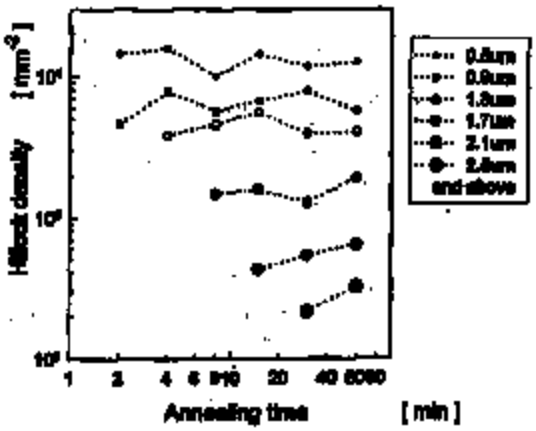

Fig. 2. Surface density of hillocks as a function of annealing time at a temperature of 400°C in N_2 for sputter-deposited Al layer of 0.7 μm thickness.

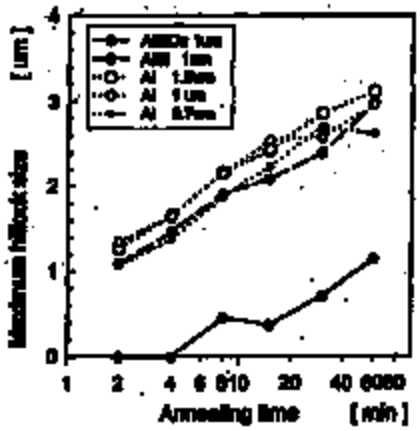

Fig. 3. Maximum hillock size as a function of annealing time at the temperature of 400°C in N_2, for Al:Si:Cu layer, Al:Si layer and three Al layers of different thickness.

does not exceed 3.5% in the aluminum layer. There is roughly two times less hillocks in the Al:Si layer than in pure Al after these rather low-temperature (400°C) annealings. Analogous ratio for the Al:Si:Cu metallization reaches 100.

The total hillock area varies with a metal layer thickness and annealing conditions. Fig. 6 presents results of hillock measurements after a 'moderate' annealing, performed at 400°C for 8 min, and a 'standard' annealing, at 450°C for 30 min. An influence of time and temperature product is predominant; however, both curves demonstrate similar features. The total hillock area decreases to zero for thin Al layers and saturates for the layers thicker than approximately 1.5 μm. Linear dependence of the area on the layer thickness can be easily explained because an average hillock size

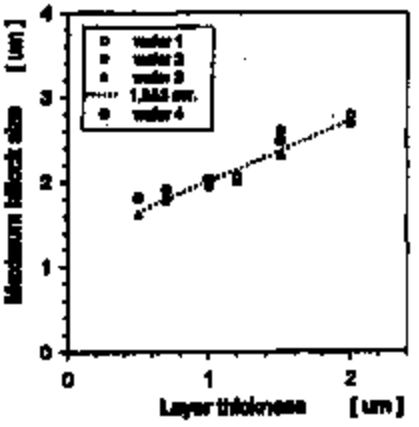

Fig. 4. Maximum hillock size versus Al layer thickness after furnace annealing at a temperature of 400°C for 8 min in N_2 (samples 1, 2 and 3). Sample no. 4 was annealed at 450°C for 5 min.

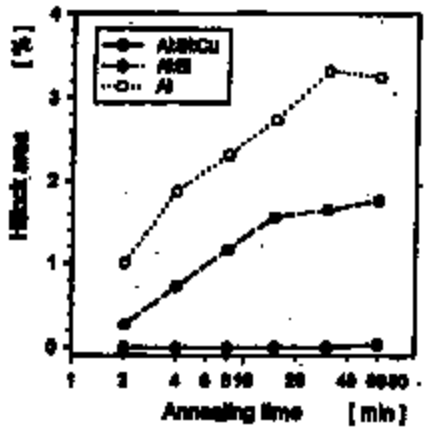

Fig. 5. Total area of hillocks normalized to the sample area as a function of annealing time at a temperature of 400°C in N_2 atmosphere for 1 μm thick Al and Al-based metallization layers.

is also proportional to the thickness of the Al layer in that range. Saturation of the plot, on the contrary, is less obvious. We may suppose that the reason for this phenomenon is a change of mechanism of hillock growth. Grains of the investigated 1 μm thick Al films were found to be columnar from TEM measurements, and the mean grain area was equal to 1.2 μm^2. The authors suppose that the shape of grains may be different in thicker films, but the problem was not studied in detail.

Surface density of hillocks rises with increase of the temperature of annealing. A series of isochronal annealings was performed using an RTP method and an argon atmosphere. A typical Arrhenius dependence was found versus $1/T$. Activation energies of total hillock density were

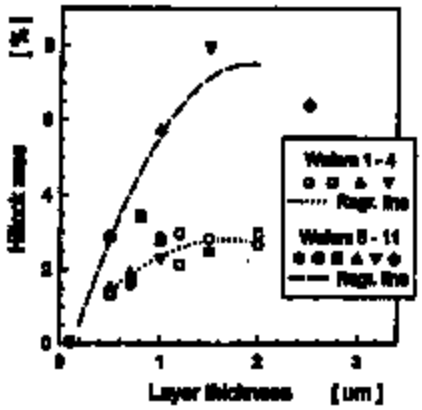

Fig. 6. Total area of hillocks normalized to the sample area versus Al layer thickness. Samples 1–4 were annealed at a temperature of 400°C for 8 min; samples 5–11 at 'standard' conditions (450°C, 30 min).

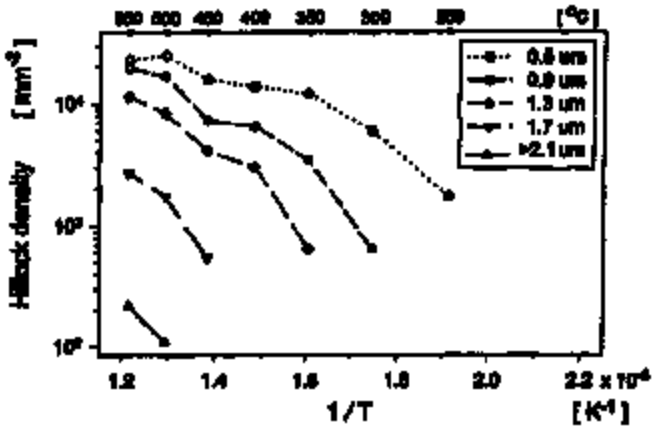

Fig. 7. Distribution of density of aluminum hillocks grouped with regard to their average diameter, as a function of reciprocal of temperature of 5 min isochronal annealings in an RTP reactor in an argon atmosphere.

calculated for the temperature range of 350–550°C, annealing time of 5 min, as 0.28 and 0.31 *eV*, for 1-μm thick Al and Al:Si layers, respectively.

Hillock size statistics depends also on the temperature of annealing. Fig. 7 displays the density of hillocks in an Al layer with a thickness of 1 μm as a function of $1/T$, with the average hillock diameter as a parameter. One can see that the slope of the density curves becomes higher for larger hillocks. An Arrhenius plot of the maximum hillock size represents a near straight line with an activation energy equal to 0.15 *eV* for Al and 0.17 *eV* for Al:Si.

A conclusion can be drawn from the above-presented plots that the surface hillock density, in general, decreases with the hillock diameter. A comparison of the hillock population was done for Al layers of different thickness, subjected to furnace heat treatment at a temperature of 400°C for 8 min in flowing N_2. Fig. 8 shows results for the layers of 0.7 and 1 μm. The hillock density versus hillock size curves do not fall monotonously after such moderate annealing, but its derivative with respect to hillock diameter shows a maximum for 1–1.5 μm hillock size values. This is close to a mean grain size which was established as 1.23 μm for a 1-μm thick Al layer. This suggests that the most probable mechanism of hillock growth during first few minutes of annealing is pushing out a whole grain of the film.

The above-mentioned phenomena have been investigated employing a short time and relatively low temperature of annealing. Such an approach allows for precise analysis of hillock growth kinetics. Nevertheless, the longer annealings have a more practical meaning. In order to effectively compare the morphology of the layers we have introduced a normalized hillock density N, defined as hillock number divided by the examined area of the sample and by the width of the range of diameters of hillocks taken into account. A unit of the normalized hillock density is $mm^{-2}\ mm^{-1}$ ($= mm^{-3}$). Normalized hillock density versus hillock size data for Al and Al-based metallization annealed at a temperature of 450°C for 30 min are gathered in Fig. 9. Data represent mean values from several samples, each layer thickness is equal to 1 μm. The previously mentioned increase of the density of hillocks with dimensions above 1 μm (in the case of a short annealing) is hardly visible here. The

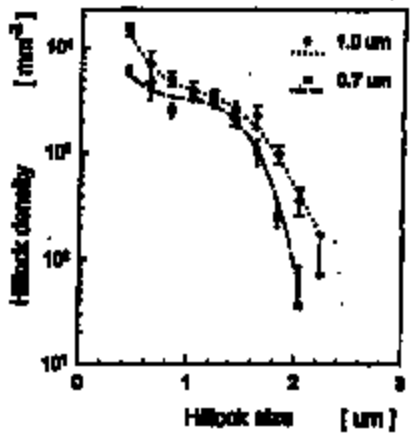

Fig. 8. Distribution of the hillock density versus hillock diameter for aluminum layers of different thickness. Vertical bars represent standard deviations of the measured values.

points for each kind of metallization are scattered near by a straight line in a logarithmic scale given by the formula:

$$N = N_0 \exp(-cd)$$

where d is hillock diameter, N_0 is the density of hillocks of diameter close to zero, and c is the curve slope. Layers made of e-gun-evaporated Al, sputter-deposited Al and Al:Si produce hillocks of similar density (dashed line in Fig. 9). An Al:Si:Cu alloy gives smaller density of hillocks, particularly those of larger size. Values of N_0 and c together with a standard deviation σ_c are gathered in Table 1. Some remarks related to presented parameters can be made. The grain density can be calculated from mean

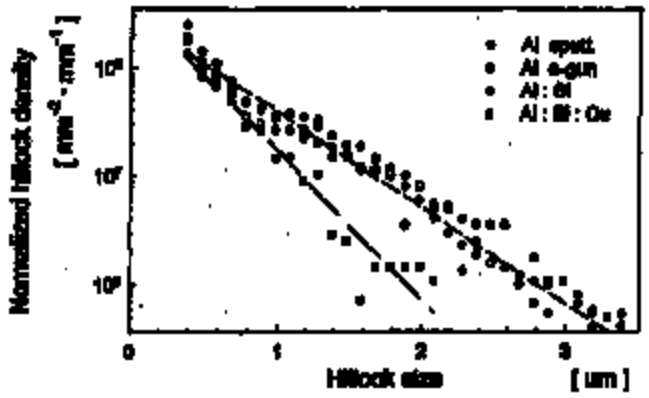

Fig. 9. Normalized density of hillocks versus hillock average diameter for often used metallization materials. Each point represent a mean value, calculated from a number of samples, annealed at a temperature of 450°C for 30 min. Dashed lines, approximate values for both Al together with Al:Si, and for Al:Si:Cu, respectively.

Table 1
Values of N_0, σ and σ_r

Layer	σ (μm^{-1})	N_0 (mm^{-1})	σ_r
Al, sputtering	1.85	2.07×10^{3}	0.25
Al, e-gun	2.03	3.33×10^{3}	0.33
Al:Si alloy	2.14	3.29×10^{6}	0.60
Al:Si:Cu alloy	3.18	4.05×10^{6}	0.45

grain size (1.23 μm) for aluminum layer. The value of N_0 does not exceed the mean grain density in the sputter-deposited Al layer, which is physically reasonable. It means that there are less potential hillocks than grains in Al metallization. A similar consideration for the Al:Si alloy (mean grain size of 1.95 μm) provides a conclusion, that each grain of the layer is accompanied by roughly two nuclei of hillocks. This gives evidence of the importance of Si-precipitations for hillock growth in this alloy.

4. Conclusion

In this paper new details of hillock behavior are described. The size distribution of the hillocks confirms that phenomena responsible for their growth have a statistical character. The increased population of the hillocks of diameter close to the mean grain size of the metal layer was reported for the first time, to our knowledge. A decrease of the density of the smallest hillocks reported by other authors [3,4] may be explained by a sensitivity limitation of the measuring technique (e.g., stylus profiling). We believe that the automatic optical hillock recognition method is more accurate, enabling a minimum hillock size limit of 0.33 μm (laterally). The high sensitivity of the used method calls for definition of the small hillocks. In our measurements we defined hillocks as protruded objects, surrounded by sharp edges. Therefore, an absence of these edges is particularly important in any approach for hillock suppression in metallization technology.

Acknowledgements

Authors wish to acknowledge Professor A. Barcz for productive discussion. The work was partially supported by the State Committee for Scientific Research in Poland under Grant No. 8T 1100114.

References

[1] K.N. Tu, J.W. Mayer, L.C. Feldman, in: Electronic Thin Film Science, Macmillan, New York, 1992.
[2] F.M. d'Heurle, Metallurgical topics in silicon device interconnections: thin film stresses, Int. Mater. Rev. 34 (2) (1989) 53.
[3] B. Baccumalar et al., A study of heating rate and texture influences on annealing hillocks by a statistical characterization of Al thin-film topography, J. Appl. Phys. 64 (11) (1988) 6433.

[4] S. Aoshi, C.Y. Chang, R.W. Vook, Hillock growth on aluminum and aluminum alloy films, Thin Solids Films 219 (1992) 88.
[5] M. Zaborowski, M. Adamiec, A. Barcz, Hillock recognition by digital image processing, Appl. Surf. Sci. 91 (1995) 246.

THE MICROSTRUCTURE AND ELECTROMIGRATION BEHAVIOUR OF Al-0.35%Pd INTERCONNECTS

L.J. ELLIOTT*, D.C. PAINE** AND J.H. ROSE***
*Digital Equipment Corporation, 77 Reed Rd., Hudson, MA 01749
**Brown University, Division of Engineering, Providence, RI 02912
***Digital Equipment Corporation, 50 Forbes Rd., Northboro, MA 01532

ABSTRACT

Al-Pd alloys have shown promise for improved IC interconnect manufacturability and reliability. However, there has been little detailed evaluation of microstructure and conductor failure reported for this material. Microstructure and electromigration behaviour of Al-0.35%Pd unpassivated interconnect was studied on films deposited at 250°C or 450°C and patterned into test structures of varying width. Samples were electrically stressed to failure at $1x10^6$A/cm^2 or $2x10^6$A/cm^2. At 450°C, AlPdx precipitates form while at 250°C, palladium remains in solution and a larger grain size is obtained. Slit voids were found in 1μm and 3μm wide lines, though only in the finer lines were the failures transgranular. A very large increase in lifetime of 1μm wide lines with a decrease in current density from $2x10^6$A/cm^2 to $1x10^6$A/cm^2 suggests a critical current effect due to grain boundary clusters in the finer lines.

INTRODUCTION

Good electromigration resistance has been achieved in submicron VLSI interconnect by addition of the palladium solute.[1] The search for alternatives to Al-Cu based interconnect is driven by two major processing problems. The difficulty of patterning submicron lines containing copper is due to lateral smear during dry etching and the serious corrosion problems during water cleaning. These problems do not arise when copper is replaced with palladium.[2] Ornstil, et al. have reported that because of its high creep strength, Al-Pd alloys have better resistance to stress voids and may be more effective in decreasing hillock growth [1] [3]. This work investigates the microstructure, lifetime statistics, and void morphology of Al-0.35%Pd films subjected to different processing and electrical stress conditions.

EXPERIMENTAL PROCEDURES

Al-0.35wt%Pd films, nominally 610nm thick, were deposited on substrates of silicon with 750nm of thermally grown oxide. For the first 250nm of Al/Pd deposition, the substrate temperature was nominally 150°C. For the remaining 360nm, a backside gas of Argon was used to rapidly heat the wafer to a final deposition temperature of 250°C or 450°C. (This two step procedure was the standard process at the time). The two deposition conditions are referred to as T250 and T450 in the following. All films were unpassivated.

Two accelerated electromigration tests were conducted at 195°C and current densities of $1x10^6$A/cm^2 and $2x10^6$A/cm^2. Three parallel line array (PLA) structures were used for electromigration testing. These test structures contain 16 1μm wide lines 750μm in length, 16 3μm wide lines 750μm in length, or 10 lines 6μm wide 475μm in length. Each structure had in-

Mat. Res. Soc. Symp. Proc. Vol. 309. ©1994 Materials Research Society

terlaced comb lines that remained unstressed.

The PLA structures both as-deposited and after accelerated testing were characterized by transmission electron microscopy (TEM), scanning electron microscopy (SEM) and focused ion beam (FIB) channeling contrast imaging. TEM was used to characterize grain and precipitate size and distribution. SEM and FIB techniques were employed to characterize void sizes. TEM samples were prepared by mechanically backgrinding until approximately 100μm thick. The remaining silicon substrate was removed by a chemical etch HF/HNO3 (1:5). Ion milling at 12 degrees and 4keV was used to remove most of the remaining oxide.

RESULTS

As-Deposited Microstructure

The TEM micrograph of Fig. 1 shows a blanket area of as-deposited wafer T450. It shows aluminum grains of 3μm to 0.3μm across with an average size of 1.19μm. T250 has a similar range of sizes (0.7μm to 3μm), though a somewhat large average grain size of 1.89μm. While T250 is free of precipitates, there is a fine distribution of palladium rich precipitates in T450, as identified by EDS. The precipitates have a diameter of about 0.09μm, and these are evenly distributed throughout the film, both inside grains and on grain boundaries. Dislocations are observed but were not quantified in this study.

Figure 1: As-deposited Wafer T450

Post Electromigration Testing Microstructure

The accelerated test at 195°C and $2x10^6 A/cm^2$ was stopped at 87 hours. All lines, other than a few 1μm in width failed. At $1x10^6 A/cm^2$, all 3μm and 6μm samples were removed from ovens after full failure at 72 hours (1μm lines remained on test since they were slow to fail at this current - see lifetime results in following section).

T450 comb lines showed little evidence of grain or precipitate coarsening. Precipitates remained dispersed throughout the film, both on grain boundaries and in the interiors of grains. T250 comb lines showed some grain coarsening though still no precipitates, though a few very small precipitates were noted in the contact pad.

ig were characterized by
y (SEM) and focused ion
rise grain and precipitate
racterize void sites. TEM
nly 100μm thick. The re-
) (1:5). Ion milling at 12

ted wafer T450. It shows
.9μm. T250 has a similar
in size of 1.89μm. While
h precipitates in T450, as
and these are evenly dis-
ries. Dislocations are ob-

ours. All lines, other than
were removed from ovens
re slow to fail at this cur-

owning. Precipitates re-
in the interiors of grains.
pitates, though a few very

TEM micrograph of T450 in Fig 2 shows a typical void on a 4μm line; there are also large clusters of precipitates decorating grain boundaries and hillock areas. Similar observations were noted for T250 (Fig 3), although away from voids and hillocks, the lines remained free of precipitates. It appears that there may be an area of line being swept clear of precipitates only to be deposited in the grain boundaries either close to a voided area or a hillock.

Figure 2: Wafer T450, Large Clusters of Precipitates Decorating Grain Boundaries

Figure 3: Wafer T250, Large Void and Hillock with Accompanying Precipitates

The samples tested at $1x10^6 A/cm^2$ showed the most striking examples of large precipitate growth and coarsening at the grain boundaries close to both voids and hillocks. TEM micrograph Fig 4 (electron flow is from right to left) shows a tested T450 6μm line with large areas of voiding and accompanying large precipitates decorating grain boundaries 'before' the voids.

Figure 4: Wafer T450, Large Precipitates Decorating Grain Boundaries 'Before' Void

The 1μm lines were stressed for over 1600 hours, but even after this annealing time there appeared to be little grain growth. The grain boundary precipitates did coarsen, although some precipitates did remain in grain interiors.

Electromigration Void Morphology

On 6μm wide lines, the density of voids after testing at $2x10^6 A/cm^2$ is approximately 1 void per 30μm whereas the void density of lines tested at $1x10^6 A/cm^2$ is approximately 1 void per 90μm. The many large, irregular voids usually extended from line edges and propagated along the grain boundaries. In contrast to these large voids and their associated hillocks, fatal voids tended to be almost perpendicular to the line, narrower and in some cases almost slit-like.

The decoration of grain boundaries by very large accumulations of precipitates is most obvious in the 6μm lines tested at $1x10^6 A/cm^2$ as shown Fig 4. Large precipitates can be seen in grain boundaries 'before' the voids and also at accompanying hillocks.

For the 3μm lines, both tests at $2x10^6 A/cm^2$ and $1x10^6 A/cm^2$ showed a similar pattern of void morphology. Almost all fatal voids were narrow and perpendicular to the line, most other voids being small and on the line edge, often wedge shaped.

In contrast to the 3μm wide lines, slit-like voids in the 1μm lines were true transgranular slit voids. Figure 5 shows a void which follows a series of bamboo grains and precedes a grain cluster (electron flow from right to left). FIB micrograph Fig 6 shows a fatal transgranular slit void perpendicular to the width of the line at the end of a long bamboo grain. Downstream a grain appears to have collapsed possibly due to local stress relaxation.

amples of large precipitate
and hillocks. TEM micro-
0 6μm line with large areas
ndaries 'before' the voids.

ndaries 'Before' Void

is annealing time there ap-
coarsen, although some pre-

cm^2 is approximately 1 void
a approximately 1 void per
dges and propagated along
ciated hillocks, fatal voids
ness almost slit-like.
f precipitates is most obvi-
precipitates can be seen in
.
showed a similar pattern of
ular to the line, most other

were true transgranular slit
and precedes a grain clus-
fatal transgranular slit void
grain. Downstream a grain

Figure 5: Slit Void

Figure 6: Transgranular Slit Void

Electromigration Failure Statistics

Figure 7 shows the results of the accelerated life tests at the two current densities of $2x10^6 A/cm^2$ and $1x10^6 A/cm^2$. The median time to fail (MTF) was much longer for the 1μm lines in both tests, consistent with the near-bamboo structure of these lines. However, the standard deviation of fail times was extremely large ~1.6. The most salient result was the slow failure of the 1μm lines tested at $1x10^6 A/cm^2$. After more than 1600 hours, only two failures occurred. This far exceeded the J^2 dependency normally associated with a ...erated electromigration tests. The distribution of fail times for each of the three line ... demonstrated no statistical difference for the two deposition temperatures. The 3μm wid... ...ed to be less reliable than the 6μm lines, this being consistent with the grain size-to-line width dependency of grain boundary diffusion paths.

	Wafer T480		Wafer T489	
2 MA/cm²	Sigma	MTF	Sigma	MTF
6μm	0.59	8.4	0.48	8.79
3μm	0.84	1.48	0.88	1.91
1μm	1.76	16.8	1.5	19.69
1 MA/cm²				
6μm	0.15	88.87	0.3	84.19
3μm	0.88	168	0.39	18.87
1μm	2 fails in 1600 hrs. 868.7, 1679.4 MTF = 7188		2 fails in 1600 hrs. 181, 881 Assumed sigma = 1.4 MTF = 6882	

Figure 7: Results of Accelerated Life Tests

DISCUSSION

There is minimal solid solubility of palladium in aluminum, less than 0.1 wt% in bulk samples. The low diffusivity of palladium at 250°C accounts for the lack of palladium precipitates in wafer T250. At 450°C, palladium precipitates are found throughout the interiors of grains and in grain boundaries. The precipitates at the grain boundaries have apparently retarded grain growth, in light of the unusual observation of smaller grains at a higher deposition temperature.

The results of the electromigration tests at $1x10^6$ A/cm^2 and $2x10^6$ A/cm^2 for the 6μm and 3μm lines of wafer T450 and T250 are not statistically distinguishable. The larger grain size of wafer T250 and the precipitate content of wafer T450 may both provide comparable small increases in reliability. As often found in electromigration failure analysis, the inability to restrict the number of microstructural variables at play, limits understanding of a system's effect. The surprisingly large increase in lifetime of 1μm lines with testing at $1x10^6$ A/cm^2 hints at a critical current effect. Work on cluster length distributions in these lines is required to further investigate this possibility.

The highly visible precipitation occurring in the 6μm lines of wafer T450 tested at $1x10^6$ A/cm^2 is evidence of the supersaturated palladium atoms leaving solution via the grain boundaries and being transported to the growing precipitates. There appears to be a stripe length of ~12μm where the grain boundaries are swept clear of precipitates which begin to accumulate again in the "downwind" direction. This is also evident in the T450 6μm lines tested at $2x10^6$ A/cm^2 although the length of line swept clear is ~6μm. Palladium diffusion enhancement is also seen in tested lines of wafer T250. There are no precipitates in the as-deposited wafer but they are observed close to voids and hillocks on the tested lines. Grain boundary induced mass flux divergences apparently account for both line damage and precipitate occurring here. Clearly, electromigration significantly accelerates palladium diffusion in aluminum. Void morphology and distribution was similar for both wafers. The morphology of voids on the 6μm and 3μm lines were of the typical grain boundary type although fatal voids tended to be narrower and more perpendicular to the line. "Downwind" hillocks were very evident in both 6μm and 3μm lines. Voids on the 1μm lines, detected by FIB, were slit-like, both on grain boundaries and transgranular. Voids appeared to be at the end of bamboo type sections and not in the cluster regions but there was insufficient line length to determine the influence of the cluster regions. The close proximity of an extruded grain and a collapsed grain indicates the presence of considerable stress within the 1μm lines.

CONCLUSIONS

Though a possible alternative to Al-Cu ULSI interconnects, much work remains to determine the optimum processing conditions and manufacturability of Al-Pd interconnects. It appears that the deposition temperature is extremely important in Al-Pd alloys, for once palladium precipitates, it will not dissolve and re-precipitate as copper does during device processing. This precipitation of palladium will apparently tend to pin grain boundaries and prevent secondary grain growth in the film, which will lead to smaller grained lines.

ACKNOWLEDGEMENTS

We would like to thank Rich Sherman of Digital Equipment Corporation and Randy Lee of Micrion Corporation for their FIB expertise. One author , (LE) would like to thank Digital for support during graduate studies at Brown University. Another author, (DCP) gratefully acknowledges the support of the National Science Foundation under grant No. DMR-9002594 and the Office of Naval Research under grant No. N00014-90-J-4051.

[1] J. Onuki, Y. Koubuchi, S. Fukuda, M. Sawa, Y. Misawa, and T. Itagaki, IEEE IRDM Tech. Dig. 88, 454, (1988)
[2] Y. Koubuchi and J. Onuki, IEEE Trans. Electron Devices, vol.37, 5, (1990)
[3] Y. Koubuchi, J. Onuki, M. Sawa, S. Fukuda, S. Moribe and Y. Tanigaki, J. Vac. Sci. Technol. B, 8(6), (1990)
[4] K.P. Rodbell, D.B. Knorr, and J.D. Mis, J. Elec. Mat., 22,597 (1993)

AN-600

Fairchild Semiconductor
Application Note
January 1988
Revised April 1999

Understanding Latch-Up in Advanced CMOS Logic

Latch-up has long been a bane to CMOS IC applications. Its occurrence and theory have been the subjects of numerous studies and articles. The applications engineer and systems designer, however, are not as much concerned with the theory and modeling of latch-up as they are with the consequences of latch-up and what has been done by the device designer and process engineer to render ICs resistant to latch-up.

Of equal interest are those precautions, if any, which need be observed to limit the liability of designs to latch-up.

WHAT IS LATCH-UP?

Latch-up is a failure mechanism of CMOS integrated circuits characterized by excessive current drain coupled with functional failure, parametric failure and/or device destruction. It may be a temporary condition that terminates upon removal of the exciting stimulus, a catastrophic condition that requires the shutdown of the system to clear or a fatal condition that requires replacement of damaged parts. Regardless of the severity of the condition, latch-up is an undesirable but controllable phenomenon. In many cases, latch-up is avoidable.

The cause of the latch-up exists in all junction-isolated or bulk CMOS processes parasitic PNPN paths. Figure 1, a basic N-substrate CMOS cross section, shows the parasitic NPN and PNP bipolar transistors which most frequently participate in latch-up. The P+ sources and drains of the P-channel MOS devices act as the emitters (and sometimes collectors) of lateral PNP devices; the N-substrate is the base of this device and collector of a vertical NPN device. The P-well acts as the collector of the PNP and the base of the NPN. Finally, the N+ sources and drains of the N-channel MOS devices serve as the emitter of the NPN. The substrate is normally connected to V_{CC}, the most positive circuit voltage, via an N+ diffusion tap while the P-well is terminated at GND, the most negative circuit voltage, through a P+ diffusion. These power supply connections involve bulk or spreading resistance to all points of the substrate and P-well.

Similarly, Figure 2, a basic P-substrate CMOS cross section, shows the parasitic PNP and NPN bipolar transistors which most frequently participate in latch-up. The N+ sources and drains of the N-channel MOS devices act as the emitters (and sometimes collectors) of lateral NPN devices; the P-substrate is the base of this device and collector of a vertical PNP device. The N-well acts as the collector of the NPN and the base of the PNP. Finally, the N+ sources and drains of the P-channel MOS devices serve as the emitter of the PNP. The N-well is normally connected to V_{CC}, the most positive circuit voltage, via an N+ diffusion tap while the substrate is terminated at GND, the most negative circuit voltage, through a P+ diffusion. These power supply connections involve bulk or spreading resistance to all points of the substrate and N-well.

Although the rest of this application note will refer to the N-substrate model, the same discussion is true for the P-substrate model, as illustrated by Figure 1, Figure 2.

Normally, only a small leakage current flows between the substrate and P-well causing only a minute bias to be built up across the bulk due to the resistivity of the material. In this case the depletion layer formed around the reverse-biased PN junction between P-well and the substrate supports the majority of the V_{CC}-GND voltage drop. As long as the MOS source and drain junctions remain reverse-biased, CMOS is self-isolated. In the presence of sufficient leakage collection, thermal or over-voltage stress, however, current can be injected into the PNP emitter-base junction, forward-biasing it and causing current to flow through the substrate and into the P-well. At this point, the NPN device turns on, increasing the base drive to the PNP. The circuit now enters a regenerative phase and begins to draw significant current from the external network. Due causing most of the undesirable consequences of latch-up. Once established, a latch-up site, through the fields generated by the currents being conducted, may trigger similar action in both elements of the IC.

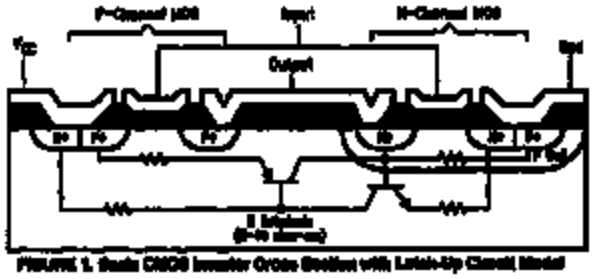

FIGURE 1. Basic CMOS Inverter Cross Section with Latch-Up Circuit Model

FACT™ is a trademark of Fairchild Semiconductor Corporation.

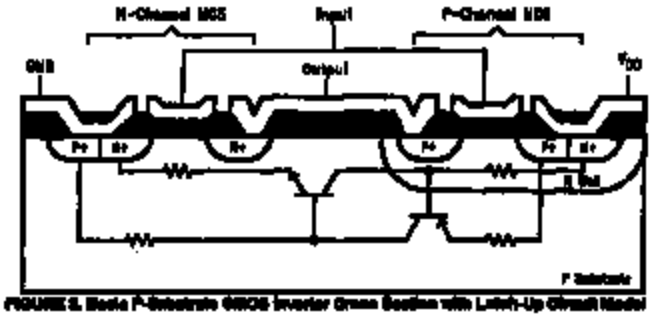

FIGURE 5. Basic P-Substrate CMOS Inverter Cross Section with Latch-Up Circuit Model

WHAT TO DO

As might be expected, latch-up is highly dependent on the characteristics of the bipolar devices involved in the latch-up loop. Device current gains, emitter efficiencies, minority carrier life times and the degree of NPN-PNP circuit coupling are all important factors relating to both the sensitivity of the particular latch-up device and to the severity of the failure once it has been exited. Layout geometry and process both contribute significantly to these parameters; CMOS, like other technologies, has been shrunk to provide more function per unit area, increasing susceptibility to latch-up. All major CMOS vendors have upgraded their processes and/or design rules to compensate for this increased susceptibility some with more success than others. The lateral PNP is typically the weak link in the latch-up loop. As such, various devices can be exploited toward reducing the effectiveness of the PNP to participate in latch-up. Guard banding, device placement, the limitation of pseudo-collectors between the P-channel devices and the P-well, and the use of a low resistivity substrate under an epitaxial layer are a few of the IC design tactics now being practiced to reduce the current gain or to control the action of the lateral PNP structures in state-of-the-art CMOS devices.

Vendors of CMOS ICs have always been aware of the latch-up phenomenon and have consistently improved their designs and processes to reduce the danger of latch-up occurring under normal usage. Abnormal applications and misuse of CMOS ICs may still pose problems that the CMOS vendor has little control over. Hence, CMOS users must be aware of what they are doing and these measures which must be taken to reduce the susceptibility to latch-up. The use of CMOS at or beyond its rated maximum voltage range and the presence of inductive loads(s) are application-related situations which can trigger latch-up. Environment, including thermal stress, poorly regulated or noisy supplies and radiation hardness can also contribute to or cause latch-up. The system engineer must consider these situations when using CMOS in designs.

While latch-up is generally recognized as resulting from regenerative switching along a PNPN path, many designers incorrectly assume that the regenerative action places the device in a state that can only be recovered from if the system is powered down. The fact is that there is probably an equal, if not greater, chance that the regenerative switching, when encountered, will be non-sustaining (the condition, more accurately referred to as current amplification, will disappear when the triggering stimulus is removed); overvoltage applied to properly designed input protection networks is one example of controlled current amplification. For sustained latch-up to occur, the regenerative loop must have sufficient gain and the power source must be able to supply a minimum current. From this we can see that current-limited power supplies might be used to recover from or reduce the effects of latch-up. Another method uses current-limiting series resistors in the power connections of offending ICs in conjunction with storage capacitors shunting the devices. Normal switching current will be drawn from the capacitors while DC current will be limited by the resistors.

In the loop of positive current feedback formed by the parasitic PNP and NPN transistors of the latch-up structures, regenerative switching may result if sufficient loop gain is available. One must remember, though, that three conditions are necessary for latch-up to occur.

1. both parasitic bipolars must be biased into the active state;
2. the product of the parasitic bipolar transistor current gains (beta=ß/(ß+1)) must be sufficient to allow regeneration, i.e., greater than or equal to one;
3. the terminal network must be capable of supplying a current greater than the holding current required by the PNPN path. In processes utilizing an epitaxial silicon, this current is usually in excess of 1A.

If any of these conditions is not met both during the initiation and in the steady state, then the latch-up condition is either non-sustaining or cannot be initiated. If the current in the bipolar structure is not limited, permanent damage may result. Again, any means to prevent any of these conditions from being satisfied will protect the circuit from exhibiting sustained latch-up.

The prevention of biasing the bipolars into the active region and the limiting of the current which may be supplied by the network are the two factors which system designers have under their control. Many of the protective measures long exercised in discrete and TTL designs may also be applied to CMOS designs to reduce susceptibility and prevent damage in these systems. Diode clamping of inductive loads, signal and supply level regulation, and shorting of large DC loads by several devices with suitable series limiting resistors to distribute thermal stress over a larger area or multiple ICs are all positive preventive measures to exhibit.

While we have been considering the CMOS device in a general manner, there are two primary structures used in all CMOS ICs which have latch-up paths associated with them; these are the inverter or gate and the transmission

switch. Both structures may be susceptible under the right conditions. While the CMOS inverter can exhibit latch-up independent of circuit configuration, the transmission switch usually has lower holding current, and thus, a lower threshold for latch-up, but is dependent on its external connections for latch-up to occur. Figure 3 shows the lumped equivalent circuit of the N-substrate inverter. Figure 4 shows the same lumped equivalent circuit of the P-substrate inverter. Notice the shunting resistors across the base-emitter junctions of the bipolar transistors these resistors divert base drive from the bipolars and as a result increase both the trigger current and holding current levels required for the structures to participate in latch-up. A further increase in these current levels can be achieved by further decreasing the shunt resistance. Diffusing all active components into an epitaxial silicon, under which would lie a substrate of substantially less resistivity, will have a dramatic effect on decreasing the shunt resistance, therefore increasing the trigger current and holding current levels required for latch-up.

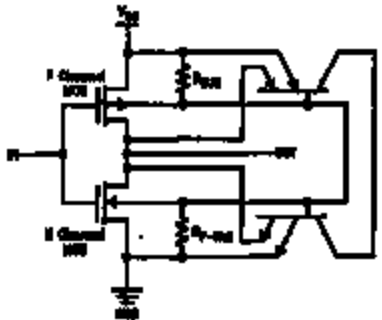

FIGURE 3. N-Substrate CMOS Inverter with Parasitic Bipolars

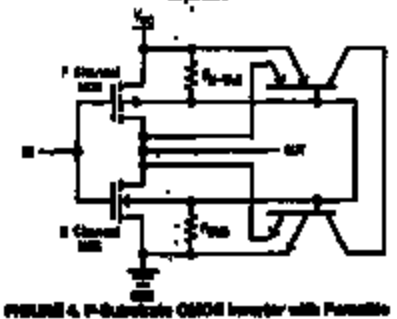

FIGURE 4. P-Substrate CMOS Inverter with Parasitic Bipolars

THE CIRCUIT CONNECTION

As we have seen above, the external circuit connections are regular participants in the latch-up process. The current for latch-up comes from these connections and often the triggering mechanism is external to the latching device. All three classes of external connections (power, input and output) are important in latch-up. We will now look at how these connections relate to this process.

Current injection through the power terminals when the power supply voltage is beyond the maximum rated for the CMOS device can easily cause latch-up through base-collector leakage or breakdown mechanisms. One aspect of high power supply voltages that is not often recognized is the effect of field-aiding lateral currents under the emitter of the PNP devices. This can effect a significant increase in the beta of these devices, making internally bigger latch-up much more prevalent. Again, the warning to the system designer is to avoid using CMOS at maximum rated supply voltages unless precautions are taken to insure latch-up is unlikely or is at least acceptable and recoverable. Switching transients coupled onto power lines has become a problem now that CMOS has become a high-speed logic technology. Attention to power supply decoupling is now a necessity when designing with high-speed CMOS. Of course, CMOS processes incorporating an epitaxial effect over a substrate of very low resistivity is less prone to latch-up under these conditions. These recommended precautions should be taken just the same.

Latch-up involving input terminals, next to gate oxide rupture, used to be one of the most common failure mechanisms of CMOS. Transients exceeding the power supply routinely caused either or both of these effects to occur. Fortunately, CMOS vendors have learned to make better input protection networks and have learned that proper placement of these components with respect to the rest of the chip circuitry is necessary to reduce susceptibility to latch-up. The system designer should review foreign input signals to CMOS systems and take precautions necessary to limit the severity of overshoot/undershoot from these sources. Measures which could be used to reduce the possibility of latch-up induced by input signals are proper termination of transmission lines driving CMOS, series current limiting resistors, AC coupling with DC restoration to the CMOS supplies, and the addition of Schottky diode clamps to the CMOS power rails. As an additional measure there are several CMOS circuits which have input protection networks that can handle over voltage in one direction or the other and which are specifically designed to act as interface circuits between other logic families and CMOS. Judicious application of these will also aid in suppressing any tendencies of CMOS systems to latch-up.

Finally, attention to CMOS outputs, their loading and the stresses applied to them will also enable the designer to generate latch-up free systems. Historically, output terminals of CMOS have been least likely to cause latch-up though they can participate in latch-up once it is initiated. The actual cause of failure in this aspect is, again, the application of voltages beyond the CMOS supplies or the maximum limit for the devices though excessive current has also been linked to latch-up failure at elevated temperatures. Inductive surges and transmission line reflections are the most likely sources of output latch-up in CMOS and should be attended to in the most applicable method, i.e., by clamping, termination or through dissipative resistance.

WHAT WE HAVE DONE

Fairchild Semiconductor, as an important supplier of advanced CMOS to all segments of the industry, has made a commitment to provide IC designs which make use of state-of-the-art latch-up suppression techniques in an effort to support its customers before they need support. The three most important actions which we have taken to guard our customers from latch-up are in the areas of layout, power distribution and process design. These techniques,

along with recognized good design practice, yield a product line that lives up to the label of an advanced CMOS family. In brief review, Fairchild Semiconductor's attack on latch-up is summarized in the following.

Latch-Up Protection Geometries

Every FACT™, VHC, and LCX IO employs special geometries to isolate every input protection device and every output from active areas on the chip. In this way, structures which would normally participate in latch-up loops are decoupled and are thus less troublesome. All devices are scrutinized for potential latch-up sites and are protected by similar geometries where any risk is significant.

Power Distribution

Careful attention to on-chip power distribution and enhanced termination of P-wells or N-wells and substrate is used by Fairchild Semiconductor to improve latch-up resistance. Our metal process affords the advantage in maintaining low impedance distribution of power and ground potentials over the entire chip; the potential ground-current flows which often induce or enhance latch-up are thus minimized while functional performance is enhanced by cleaner on-chip power supplies.

Process Design

By design, the FACT, VHC, and LCX processes are better both in low latch-up susceptibility and in enhanced device performance. The most significant advancement of these processes has been the incorporation of an epitaxial silicon layer. Figure 6 illustrates a modified version of Figure 1, utilizing an epitaxial layer of silicon to contain all of the active components of the CMOS circuit. This epitaxial layer allows the use of a separate layer of substrate silicon, of a resistivity across three orders of magnitude lower than the epitaxial layer. The effect is also modeled in Figure 6.

As illustrated, the resistivity of the epitaxial silicon, R_{11}, is on the order of 5 ohm-cm to 10 ohm-cm. The underlying substrate resistivity, R_{S}, is as low as 0.005 ohm-cm to 0.020 ohm-cm. The result is a parallel combination of resistances, R_1 and R_S, that is equivalent to R_S. What has now happened is that the gain of the parasitic PNP-NPN circuit has been dramatically slashed. Under the same latch-up conditions described earlier, the introduction of the low resistivity substrate now means that at least 10 times more current is needed to trigger the parasitic PNP-NPN combination.

The active components within the epitaxial layer maintain the same performance characteristics as those of the active area. Illustrated in the non-epitaxial CMOS circuit of Figure 1. Therefore the introduction of the epitaxial layer in the FACT,VHC, and LCX processes does not reduce any AC, DC, functional or ESD performance. However, what we have are advanced CMOS logic families that are now virtually latch-up immune.

Thus, through innovative and careful layout, attention to eliminating circuit situations which could be latch-up prone and by careful selection and maintenance of our advanced CMOS process, FACT, VHC, and LCX set the standard for latch-up resistance.

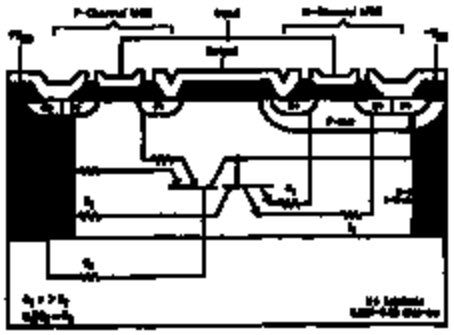

FIGURE 6.

Reliability Services

Check out the RAL's Technical Expertise and Analysis Equipment

The RAL offers a full range of analysis services that bring value to any phase in the product life c initial design through production to field maintenance. The RAL can help assess the reliability of y compare the performance of your products with others, even reverse engineer other products. Pu depth knowledge to work for you.

- Failure Analysis:
  The RAL helps you get to the root cause explanation of a component or material deficiency including processing that may contribute to the problem. This may include recommendations for corrective action and/or follow up with the manufacturer.
- Surface Analysis:
  The RAL's EMSA Laboratory supports analysis of electronic components, especially semiconductor devices and assembled printed circuit boards. The EMSA Laboratory also helps solve problems involving process development and engineering for a wide range of thin film and bulk materials: alloys, semiconductors, ceramics, composites, glasses, and polymers.
- Non-Destructive Evaluation and Test (NDE/NDT):
  Have you ever wished you could look inside a computer or assembly without cutting it ope apart? The RAL's advanced NDE/NDT capabilities range from visual inspection using speci polarization to ultrasonic and radiographic techniques. Our experienced engineers can ass interpretation of NDE/NDT results, select appropriate methods, and develop procedures th the results obtained provide the maximum possible benefit for you.
- Process Improvement:
  For your product to meet the needs of your customers, you must integrate the right desig and processes. Although anyone can buy from your sources, or reverse engineer your pro hits the streets, processing is an area where you can develop a real edge over the compet RAL, our staff is well versed in the relationships among process parameters, micro- and m structure, and the properties of materials. This knowledge can provide meaningful input fo selection and enhancements, giving you the edge you need to thrive in today's tough com environment.
- Design Consultations:
  Your designers are experts in the proper function of your products. At the RAL we know h your products can fail to function. These are fundamentally different and complementary v expert staff can help your design team understand the impact its design choices will have This is important to ensure the final product is optimized for the needs of your customers.
- Construction Analysis/DPA:
  Destructive analysis of a part can be used to identify its construction and constituents, as well as to determine variations in the manufacturing process which may effect quality and reliability. After an initial construction analysis, DPA can be implemented as an on-going program to assess samples of incoming part lots prior to release in manufacturing. Supplier follow-up may be recommended.

Microelectronics

Experts at the RAL possess wide-ranging expertise in all areas of microelectronic processes. Our have many years of experience in this field, and keep up to date with the latest advances. Areas include:

- Die-level analysis and fault isolation
- Die attach materials and processes, including flip-chip and chip-on-board
- Interconnections, including wire-bond, f chip, and TAB
- Chip-on-board and chip-scale-packaging
- Plastic encapsulation
- Hermetic packaging
- MCMs
- ASICs

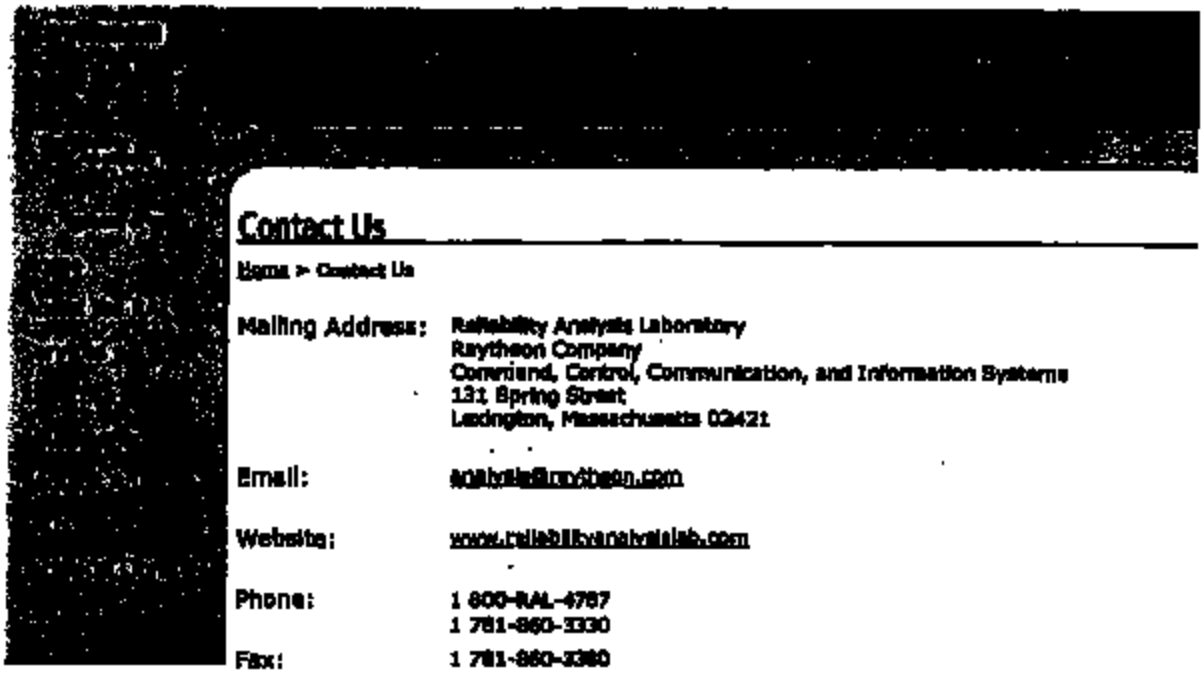

Contact Us

Mailing Address:	Reliability Analysis Laboratory Raytheon Company Command, Control, Communication, and Information Systems 131 Spring Street Lexington, Massachusetts 02421
Email:	[redacted]
Website:	www.reliabilityanalysislab.com
Phone:	1 800-RAL-4787 1 781-860-3330
Fax:	1 781-860-3380

Search

Failure Analysis

Pin-point the Failure. Analyze your failures with an EBEAM prober, Acoustic Imaging, CSAM SEM and /or X-RAY machine. Then repair it by rerouting traces with the FIB. No other test laboratory provides the complete set of IC failure analysis tools.

Ultra High Resolution X-Ray Inspection Service

Our lab uses an X-Tek microfocus X-Ray instrument. The VTX system from X-Tek has outstanding resolution, range of magnification, and automation capabilities. X-Tek's unique microfocus X-Ray transmission technology allows features just 2 microns across to be resolved, at magnifications up to 1800X. Images are viewed in real time, and the superbly accurate 5 axis manipulator will handle anything from small components to large circuit boards.

Microfocus X-Ray System From X-Tek Reveals All

- 2 micron resolution
- magnification to 1800X
- 30 - 160kV x-ray energy
- precision 5 axis manipulator
- advanced image processing
- instant real time results
- output photo prints or TIFF files

Use our X-Ray service to qualify or analyze your components and circuit boards. Everything from Flip Chips to large board assemblies may be rapidly and comprehensively inspected. We offer competitive pricing, fast turn around times, and free expert consultation.

Call ISE Labs now to schedule an appointment for a demonstration of this powerful inspection tool: 408-984-TEST or send an e-mail

Contact Us

ISE Labs, Inc. - Fremont Test
46900 Bayside Parkway
Fremont, CA 94538
Tel: 510-687-2400
Fax: 510-687-2513

ISE Labs, Inc. - Fremont IQL - Reliability
46723 Lakeview Blvd.
Fremont, CA 94538
Tel: 510-687-2500
Fax: 510-687-2513

ISE Labs, Inc. - Santa Clara / DTS
3600 Peterson Way
Santa Clara, CA 95054
Tel: 408-727-9208
Fax: 408-727-9136

ISE Labs, Inc. - Hong Kong
22/D Southeast Ind. Bldg.
611-619 Castle Peak Road
Tsuen Wan, Hong Kong
Tel: 852-24128791
Fax: 852-24111028

ISE Labs, Inc. - Singapore
750-D Chai Chee Road
#03-06 Technopark
@ Chai Chee
Singapore 469004
Tel: 65-441-7977
Fax: 65-441-4755

ISE Labs, Inc. - Austin
The Domain
Building 5, Suite 5160
11400 Burnet Road
Austin, Texas 78758
Tel: 512-835-2500
Fax: 512-247-7204

Email: info@iselabs.com

Home | ISE Profile | Services | IQL | Situations | DTS | Contact Us

About Our [redacted]

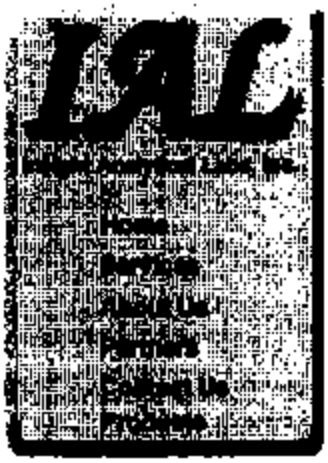

Join our mailing list! Enter your email address below, then click the 'Subscribe Now' button:

[redacted]

Click here to unsubscribe from our announcement list.

Located in Colorado Springs (map to our location) at the f Pikes Peak, Insight Analytical Labs (IAL) was created in 1 address the failure analysis and reliability needs of the semiconductor industry in this locale. As its reputation for quality work at competitive prices spread, IAL's customer expanded to include companies from all over the United S Canada, and Europe. We are a one-stop failure analysis lal

Staff:

Although IAL was started by Tom Paquette, it has been th addition of its key people, their talents and dedication, wh have made it so successful in so few years. Your business benefit from the extensive knowledge and experience of o staff. We have experts in wafer processing, failure analysi experience, acoustic microscopy, wafer fabrication, quick- package decapsulation, X-ray fluorescence, and other serv As our customer, you have direct access to the technical p performing the analysis for you.

Click here for detailed profiles of our key staff membe

Services:

- PC-board defect failure analyses
- X-ray Fluorescence PCB thin film measurements)
- Acoustic microscopy
- Competitor analyse
- Failure analyses
- Destructive Physics Analyses (DPA)
- Electrical failure analyses
- Parametric testing
- Electromigration lifetime studies
- Training (general o house)
- TDDB lifetime studies
- Reliability consultir testing

- Hot carrier lifetime studies

Customer List:

- Aetrium
- AMCC
- Atmel Corporation
- Cypress Semiconductor
- Hewlett Packard
- Keithley Instruments
- Level One Communications
- Ramtron
- Rockwell
- Simtek
- TAELIS
- Texas Instruments
- United Memories

What our Customers Say:

"One of the most important services IAL provides for us is consultation on the best techniques and approach to a problem. Often we are not sure of the right question to ask. Our own lack of expertise can result in asking the wrong question and getting data that does not help us resolve the root cause."

- A. Y., Hewlett Packard

"IAL has provided not only the services to resolve manufacturing and reliability problems, but also the expertise and advice to direct the problems solving efforts, as well as define the quickest path to determining the root cause."

- A. M., Hewlett Packard

Insight Analytical Labs, Inc.
Colorado Springs, CO - 719-570-9549
Email: info@ial-fa.com

Home | Services | About Us | Reference Rooms | Partne
Contact Us

Map to Our Location

Failure Analysis

Pin-point the Failure. Analyze your failures with an EBEAM prober, Acoustic Imaging, CSAM SEM and /or X-RAY machine. Then repair it by rerouting traces with the FIB. No other test laboratory provides the complete set of IC failure analysis tools.

Ultra High Resolution X-Ray Inspection Service

Our lab uses an X-Tek microfocus X-Ray instrument. The VTX system from X-Tek has outstanding resolution, range of magnification, and automation capabilities. X-Tek's unique microfocus X-Ray transmission technology allows features just 2 microns across to be resolved, at magnifications up to 1800X. Images are viewed in real time, and the superbly accurate 5 axis manipulator will handle anything from small components to large circuit boards.

Microfocus X-Ray System From X-Tek Reveals All

- **2 micron resolution**
- **magnification to 1800X**
- **30 - 160kV x-ray energy**
- **precision 5 axis manipulator**
- **advanced image processing**
- **instant real time results**
- **output photo prints or TIFF files**

Use our X-Ray service to qualify or analyze your components and circuit boards. Everything from Flip Chips to large board assemblies may be rapidly and comprehensively inspected. We offer competitive pricing, fast turn around times, and free expert consultation.

Call XBS Labs now to schedule an appointment for a demonstration of this powerful inspection tool: 408-954-TEST or send an e-mail

Home | XBS Profile | Services | XDL | Missions | NTIF | Contact Us

Contact Us

ISE Labs, Inc. - Fremont Test
46800 Bayside Parkway
Fremont, CA 94538
Tel: 510-687-2400
Fax: 510-687-2513

ISE Labs, Inc. - Fremont IQL - Reliability
46723 Lakeview Blvd.
Fremont, CA 94538
Tel: 510-687-2500
Fax: 510-687-2513

ISE Labs, Inc. - Santa Clara / DTS
3600 Peterson Way
Santa Clara, CA 95054
Tel: 408-727-9208
Fax: 408-727-3136

ISE Labs, Inc. - Hong Kong
22/D Southeast Ind. Bldg.
611-619 Castle Peak Road
Tsuen Wan, Hong Kong
Tel: 852-24128791
Fax: 852-24111025

ISE Labs, Inc. - Singapore
750-D Chai Chee Road
#03-06 Technopark
@ Chai Chee
Singapore 469004
Tel: 65-441-7877
Fax: 65-441-4755

ISE Labs, Inc. - Austin
The Domain
Building E, Suite 5160
11400 Burnet Road
Austin, Texas 78758
Tel: 512-835-2500
Fax: 512-347-7204

Email: info@iselabs.com

Home | ISE Profile | Services | IQL | Locations | DTS | Contact Us

TANDEX

[redacted]

[redacted]

The Following links require Acrobat Reader to view.

- **Destructive Physical Analysis (DPA)** **Is the process of disassembling, testing, and inspecting a component for the purpose of determining conformance with applicable design and process requirements. This process of sample testing is used to ensure that a high reliability component or device is fabricated to the required standards. Destructive Physical Analysis is also used effectively to discover process defects for troublesome production lot problems.**

  DPA Processes include:

  - Bond Pull
  - Delidding
  - Internal Photos
  - External Photos
  - Scanning Electron Microscope
  - Energy Dispersive X-ray Analysis (EDXA)

- **Failure Analysis** **Capabilities of Tandex Test Labs are extremely important to support our in-house manufacturing efforts and are also available to analyze customer component and equipment problems. Techniques and equipment utilized in providing our Destructive Physical Analysis capability are also used effectively to analyze failures, determine failure causes, and recommend corrective actions. These failure analysis capabilities are exceptionally important in finding early solutions to troublesome production problems that show up as device or component failures.**

Request for Quotations with immediate responses

[redacted]

TANDEX

TEST LABS, INC.
15849 Business Ctr Dr.
Irwindale, Ca. 91706-2053 U.S.A.
TOLL FREE 800.729.8378
Phone: 626.962.7166 Fax: 626.960.8696

Back to Top

Home

Services - Products - Links/Specs - Quality - Tour - Newsletter - Map - E-Mail

Arch Chemicals, Inc.

FOR ANY EMERGENCY, CALL 24 HOURS/7 DAYS:	1-800-654-6911
FOR ALL TRANSPORTATION ACCIDENTS, CALL CHEMTREC®:	1-800-424-9300
FOR ALL MSDS QUESTIONS & REQUESTS, CALL MSDS CONTROL:	1-800-511-MSDS

PRODUCT NAME: GOLD ETCH

SECTION 1 PRODUCT AND COMPANY IDENTIFICATION

REVISION DATE: 05-22-1998 SUPERSEDES: None
MSDS NO: 00830-0004-882377

MANUFACTURER: Arch Chemicals, Inc. 501 Merritt 7 PO Box 5204 Norwalk, CT 06856-5204

STRENGTH: None
CHEMICAL FAMILY: Not Applicable/Mixture
FORMULA: Not Applicable/Mixture
USE DESCRIPTION: Gold etch
OSHA HAZARD CLASSIFICATION: Skin, eye, respiratory tract irritant

SECTION 2 COMPONENT DATA

PRODUCT COMPOSITION
CAS or CHEMICAL NAME: Sodium Iodide
CAS NUMBER: 7681-82-5
PERCENTAGE RANGE: 15-17%
HAZARDOUS PER 29 CFR 1910.1200: Yes
EXPOSURE STANDARDS: None E stablished

CAS or CHEMICAL NAME: Iodine
CAS NUMBER: 7553-56-2
PERCENTAGE RANGE: 1-2%
HAZARDOUS PER 29 CFR 1910.1200: Yes
EXPOSURE STANDARDS:

	OSHA(PEL)		ACGIH(TLV)	
	ppm	mg/cubic-meter	ppm	mg/cubic-meter
TWA:		None		None
CEILING:	0.1		0.1	
STEL:		None		None

CAS or CHEMICAL NAME: Water
CAS NUMBER: 7732-18-5
PERCENTAGE RANGE: 80-85%
HAZARDOUS PER 29 CFR 1910.1200: No
EXPOSURE STANDARDS: None Established

SECTION 3 PRECAUTIONS FOR SAFE HANDLING AND STORAGE

DO NOT TAKE INTERNALLY. AVOID CONTACT WITH SKIN, EYES AND CLOTHING. UPON CONTACT WITH SKIN OR EYES, WASH OFF WITH WATER.

EM02-627 29259

STORAGE CONDITIONS:
STORE IN A COOL, DRY, WELL VENTILATED PLACE.
DO NOT STORE AT TEMPERATURES ABOVE: 54 Deg.C (130 Deg.F)
PRODUCT STABILITY AND COMPATIBILITY
SHELF LIFE LIMITATIONS: 2 Years
INCOMPATIBLE MATERIALS FOR PACKAGING: None known
INCOMPATIBLE MATERIALS FOR STORAGE OR TRANSPORT: None known

SECTION 4 PHYSICAL DATA

APPEARANCE: Deep, red liquid
FREEZING POINT: No Data
BOILING POINT: 104 Deg.C (220 Deg.F)
DECOMPOSITION TEMPERATURE: No Data
SPECIFIC GRAVITY: 1.151
BULK DENSITY: 1.151 (g/cc)
pH @ 25 DEG.C: 6
VAPOR PRESSURE @ 25 DEG.C: No Data
SOLUBILITY IN WATER: Complete
VOLATILES, PERCENT BY VOLUME: 85%
EVAPORATION RATE: < 1 (Water = 1)
VAPOR DENSITY: No Data
MOLECULAR WEIGHT: Not Applicable/Mixture
ODOR: Odorless
COEFFICIENT OF OIL/WATER DISTRIBUTION: No Data

SECTION 5 PERSONAL PROTECTIVE EQUIPMENT REQUIREMENTS

PERSONAL PROTECTION FOR ROUTINE USE OF PRODUCT:
RESPIRATORY PROTECTION: If air concentrations above the TLV are possible, wear a NIOSH approved respirator.
VENTILATION: Use local exhaust ventilation to maintain levels to below the TLV.
SKIN AND EYE PROTECTIVE EQUIPMENT: Wear gloves, boots, apron and a face shield with safety glasses. A full impermeable suit is recommended if exposure is possible to large portion of body.

EQUIPMENT SPECIFICATIONS (WHEN APPLICABLE):
RESPIRATOR TYPE: NIOSH approved positive pressure supplied air respirator
PROTECTIVE CLOTHING TYPE (This includes: gloves, boots, apron, protective suit): Impervious

SECTION 6 FIRE AND EXPLOSION HAZARD INFORMATION

FLAMMABILITY DATA:
EXPLOSIVE: No
FLAMMABLE: No
COMBUSTIBLE: No
PYROPHORIC: No
FLASH POINT: Not Flammable
AUTOIGNITION TEMPERATURE: Not Applicable
FLAMMABLE LIMITS AT NORMAL ATMOSPHERIC TEMPERATURE AND PRESSURE (PERCENT VOLUME IN AIR): LEL - Not Applicable UEL - Not Applicable

NFPA RATINGS: Not Established
HMIS RATINGS:
Health: 2
Flammability: 0
Reactivity: 0

EXTINGUISHING MEDIA:
Not Applicable-Choose extinguishing media suitable for surrounding materials.
FIRE FIGHTING TECHNIQUES AND COMMENTS:
This product would not be expected to burn.
Use water to cool containers exposed to fire.
See Section 11 for protective equipment for fire fighting.

SECTION 7 REACTIVITY INFORMATION

CONDITIONS UNDER WHICH THIS PRODUCT MAY BE UNSTABLE:
TEMPERATURES ABOVE: No Data
MECHANICAL SHOCK OR IMPACT: No
ELECTRICAL (STATIC) DISCHARGE: No
HAZARDOUS POLYMERIZATION: Will not occur
INCOMPATIBLE MATERIALS: None known
HAZARDOUS DECOMPOSITION PRODUCTS: None known
OTHER CONDITIONS TO AVOID: Extreme heat
SUMMARY OF REACTIVITY:

EXPLOSIVE:	No
OXIDIZER:	No
PYROPHORIC:	No
ORGANIC PEROXIDE:	No

SECTION 8 FIRST AID

EYES:
Immediately flush with large amounts of water for at least 15 minutes, occasionally lifting the upper and lower eyelids. If eye irritation develops, call a physician.
SKIN:
Immediately flush with water for 15 minutes. Wash the contaminated skin with soap and water. If irritation develops, call a physician. If clothing comes in contact with the product, the clothing should be laundered before re-use.
INGESTION:
Immediately drink large quantities of water. Induce vomiting. Call a physician at once. DO NOT give anything by mouth if the person is unconscious or if having convulsions.
INHALATION:
Remove person to fresh air. If respiratory irritation develops, call a physician.

SECTION 9 TOXICOLOGY AND HEALTH INFORMATION

ROUTES OF ABSORPTION
Inhalation, ingestion, skin and eye contact

WARNING STATEMENTS AND WARNING PROPERTIES
HARMFUL IF SWALLOWED. CAUSES SKIN, EYE AND MUCOUS MEMBRANE IRRITATION. MAY CAUSE RESPIRATORY IRRITATION. REPEATED CONTACT MAY RESULT IN DERMATITIS.

HUMAN THRESHOLD RESPONSE DATA
ODOR THRESHOLD: No Data
IRRITATION THRESHOLD: No Data
IMMEDIATELY DANGEROUS TO LIFE OR HEALTH: The IDLH concentration has not been established for this product, for iodine it is 10 ppm.

SIGNS, SYMPTOMS, AND EFFECTS OF EXPOSURE

MATERIAL SAFETY DATA SHEET

Ashland Chemical Co.

Date Prepared: 01/26/98
Date Printed: 08/21/99
MSDS No: 999.0025191-005.004

HYDROGEN PEROXIDE 30% CR

1. CHEMICAL PRODUCT AND COMPANY IDENTIFICATION

Material Identity
Product Name: HYDROGEN PEROXIDE 30% CR
Product Code: 3473099
General or Generic ID: PEROXIDE

Company
Ashland Chemical Co.
P.O. Box 2219
Columbus, OH 43216
614-790-3333

Emergency Telephone Number:
1-800-ASHLAND (1-800-274-5263)
24 hours everyday

Regulatory Information Number:
1-800-325-3751

2. COMPOSITION/INFORMATION ON INGREDIENTS

Ingredient(s)	CAS Number	% (by weight)
WATER	7732-18-5	68.0- 72.0
HYDROGEN PEROXIDE	7722-84-1	28.0- 32.0

3. HAZARDS IDENTIFICATION

Potential Health Effects

Eye
Can cause permanent eye injury. Symptoms include stinging, tearing, redness, and swelling of eyes. Can injure the cornea and cause blindness. Eye effects may be delayed.

Skin
Can cause skin irritation. Symptoms may include redness and burning of skin, and other skin damage. Additional symptoms of skin contact may include: skin blistering abnormal coloring of the skin

Swallowing
Swallowing this material may be harmful or fatal. Ingestion of high concentrations causes rapid release of oxygen which may expand the esophagus or stomach resulting in severe damage (bleeding, ulceration or perforation).

Inhalation
Breathing of vapor or mist is possible.

Symptoms of Exposure
Signs and symptoms of exposure to this material through breathing, swallowing, and/or passage of the material through the skin may include: stomach or intestinal upset (nausea, vomiting, diarrhea), irritation (nose, throat, airways).

Target Organ Effects
No data

Continued on next page

Developmental Information
Based on the available information, risk to the fetus from maternal exposure to this material cannot be assessed.

Cancer Information
Based on the available information, this material cannot be classified with regard to carcinogenicity.

Other Health Effects
No data

Primary Route(s) of Entry
No data

4. FIRST AID MEASURES

Eyes
If material gets into the eyes, immediately flush eyes gently with water for at least 15 minutes while holding eyelids apart. If symptoms develop as a result of vapor exposure, immediately move individual away from exposure and into fresh air before flushing as recommended above. Seek immediate medical attention.

Skin
Immediately flush skin with water for at least 15 minutes while removing contaminated clothing and shoes. Seek immediate medical attention. Wash clothing before reuse and discard contaminated shoes.

Swallowing
Seek medical attention. If individual is drowsy or unconscious, do not give anything by mouth; place individual on the left side with the head down. Contact a physician, medical facility, or poison control center for advice about whether to induce vomiting. If possible, do not leave individual unattended.

Inhalation
If symptoms develop, move individual away from exposure and into fresh air. If symptoms persist, seek medical attention. If breathing is difficult, administer oxygen. Keep person warm and quiet; seek immediate medical attention.

Note to Physicians
Preexisting disorders of the following organs (or organ systems) may be aggravated by exposure to this material: skin, lung (for example, asthma-like conditions).

5. FIRE FIGHTING MEASURES

Flash Point
Not applicable

Continued on next page

Explosive Limit
No data

Autoignition Temperature
No data

Hazardous Products of Combustion
May form: acetic acid.

Fire and Explosion Hazards
Substance is an oxidizer. Will increase fire hazard if in contact with combustibles.

Extinguishing Media
water fog, carbon dioxide, dry chemical.

Fire Fighting Instructions
Wear a self-contained breathing apparatus with a full facepiece operated in the positive pressure demand mode with appropriate turn-out gear and chemical resistant personal protective equipment. Refer to the personal protective equipment section of this MSDS.

NFPA Rating
Health - 2, Flammability - 0, Reactivity - 1

6. ACCIDENTAL RELEASE MEASURES

Small Spill
Absorb liquid on vermiculite, floor absorbent, or other absorbent material and transfer to hood.

Large Spill
Eliminate all ignition sources (flares, flames including pilot lights, electrical sparks). Persons not wearing protective equipment should be excluded from area of spill until clean-up has been completed. Stop spill at source. Prevent from entering drains, sewers, streams or other bodies of water. Prevent from spreading. If runoff occurs, notify authorities as required. Pump or vacuum transfer spilled product to clean containers for recovery. Absorb unrecoverable product. Transfer contaminated absorbent, soil and other materials to containers for disposal. Prevent run-off to sewers, streams or other bodies of water. If run-off occurs, notify proper authorities as required, that a spill has occurred. Persons not wearing protective equipment should be excluded from area of spill until clean-up has been completed. Stop spill at source, dike area of spill to prevent spreading, pump liquid to salvage tank. Remaining liquid may be taken up on sand, clay, earth, floor absorbent, or other absorbent material and shoveled into containers.

7. HANDLING AND STORAGE

Handling
Containers of this material may be hazardous when emptied. Since emptied containers retain product residues (vapor, liquid, and/or solid), all hazard precautions given in the data sheet must be observed.

Continued on next page

8. EXPOSURE CONTROLS/PERSONAL PROTECTION

Eye Protection
Chemical splash goggles and face shield (8" min.) in compliance with OSHA regulations are advised; however, OSHA regulations also permit other type safety glasses. (Consult your industrial hygienist.)

Skin Protection
Wear impervious gloves (consult your safety equipment supplier). To prevent skin contact, wear impervious clothing and boots..

Respiratory Protections
If workplace exposure limit(s) of product or any component is exceeded (see exposure guidelines), a NIOSH/MSHA approved air supplied respirator is advised in absence of proper environmental control. OSHA regulations also permit other NIOSH/MSHA respirators (negative pressure type) under specified conditions (see your industrial hygienist). Engineering or administrative controls should be implemented to reduce exposure.

Engineering Controls
Provide sufficient mechanical (general and/or local exhaust) ventilation to maintain exposure below TLV(s).

Exposure Guidelines
Component

WATER (7732-18-5)
No exposure limits established

HYDROGEN PEROXIDE (7722-84-1)
OSHA VPEL 1.000 ppm - TWA
ACGIH TLV 1.000 ppm - TWA

9. PHYSICAL AND CHEMICAL PROPERTIES

Boiling Point
(for component) 212.0 F (100.0 C) @ 760 mmHg

Vapor Pressure
(for component) 17.500 mmHg @ 68.00 F

Specific Vapor Density
No data

Specific Gravity
1.114 @ 68.00 F

Liquid Density
9.280 lbs/gal @ 68.00 F
1.114 kg/l @ 20.00 C

Percent Volatiles
65.0 - 70.0 %

Continued on next page

Evaporation Rate
SLOWER THAN ETHYL ETHER

Appearance
No data

State
LIQUID

Physical Form
HOMOGENEOUS SOLUTION

Color
CLEAR, APHA COLOR 10 MAX

Odor
No data

pH
3.3

10. STABILITY AND REACTIVITY

Hazardous Polymerization
Product will not undergo hazardous polymerization.

Hazardous Decomposition
No data

Chemical Stability
Stable. Avoid heat, open flame, and prolonged storage at elevated temperatures.

Incompatibility
Avoid contact with: combustible materials, copper, cyanides, ferrous metals, heavy metals, organic materials, reducing agents, strong oxidizing agents.

11. TOXICOLOGICAL INFORMATION

No data

12. ECOLOGICAL INFORMATION

No data

13. DISPOSAL CONSIDERATION

Waste Management Information
Dispose of in accordance with all applicable local, state and federal regulations.

Continued on next page

14. TRANSPORT INFORMATION

DOT Information - 49 CFR 172.101

DOT Description:
HYDROGEN PEROXIDE, AQUEOUS SOLUTIONS,5.1,UN2014,II

Container/Mode:
55 GAL DRUM/TRUCK PACKAGE

NOS Component:
None

RQ (Reportable Quantity) - 49 CFR 172.101

Product Quantity (lbs)	Component
3333	HYDROGEN PEROXIDE

15. REGULATORY INFORMATION

US Federal Regulations

TSCA (Toxic Substances Control Act) Status
TSCA (UNITED STATES) The intentional ingredients of this product are listed.

CERCLA RQ - 40 CFR 302.4(a)
None listed

SARA 302 Components - 40 CFR 355 Appendix A

Section 302 Component(s)	TPQ (lbs)	RQ (lbs)
HYDROGEN PEROXIDE	1000	1000

Section 311/312 Hazard Class - 40 CFR 370.2
Immediate(X) Delayed( ) Fire( ) Reactive( ) Sudden Release of Pressure( )

SARA 313 Components - 40 CFR 372.65
None

OSHA Process Safety Management 29 CFR 1910

PSM Component (s)	Condition	TQ (lbs)
HYDROGEN PEROXIDE	>= 52%	7500

EPA Accidental Release Prevention 40 CFR 68
None listed

International Regulations

Inventory Status
Not determined

State and Local Regulations

California Proposition 65
The following statement is made in order to comply with the California Safe Drinking Water and Toxic Enforcement Act of 1986: This product contains the following substance(s) known to the state of California to cause reproductive harm.
ARSENIC

Continued on next page

New Jersey RTK Label Information
HYDROGEN PEROXIDE 7722-84-1

Pennsylvania RTK Label Information
HYDROGEN PEROXIDE (CONC >52%) 7722-84-1

16. OTHER INFORMATION

The information accumulated herein is believed to be accurate but is not warranted to be whether originating with the company or not. Recipients are advised to confirm in advance of need that the information is current, applicable, and suitable to their circumstances.

Last page

4-12-1999
3:30 pm

Ashland Chemical, Inc.

Dallas, Texas

CUSTOMER CERTIFICATE OF ANALYSIS

Lot Number: 90400270
Customer Product Name: Hydrogen Peroxide, 30%
Customer Part/Spec Number: GB
Revision:

Analysis Description	Specification Minimum	Specification Maximum	U.M.	Result
Assay (H2O2)	30.0	32.0	%	31.7
Color		5	APHA	3
Free Acid		0.6	ueq/g	0.2
Total Organic Carbon		20000.	ppb	9000
Chloride (Cl)		30	ppb	<30
Phosphate (PO4)		100	ppb	<40
Sulfate (SO4)		200	ppb	<40
Aluminum (Al)		1.0	ppb	0.1
Antimony (Sb)		1.0	ppb	<0.1
Arsenic (As)		1.0	ppb	<0.1
Barium (Ba)		1.0	ppb	<0.1
Boron (B)		1.0	ppb	<0.1
Cadmium (Cd)		1.0	ppb	<0.1
Calcium (Ca)		1.0	ppb	0.2
Chromium (Cr)		1.0	ppb	<0.1
Cobalt (Co)		1.0	ppb	<0.1
Copper (Cu)		1.0	ppb	<0.1
Gallium (Ga)		1.0	ppb	<0.1
Germanium (Ge)		1.0	ppb	<0.1
Gold (Au)		2.0	ppb	<0.1
Iron (Fe)		1.0	ppb	<0.1
Lead (Pb)		1.0	ppb	<0.1
Lithium (Li)		1.0	ppb	<0.1
Magnesium (Mg)		2.0	ppb	<0.1
Manganese (Mn)		1.0	ppb	<0.1
Molybdenum (Mo)		1.0	ppb	<0.1
Niobium (Nb)		1.0	ppb	<0.1
Nickel (Ni)		1.0	ppb	<0.1
Potassium (K)		2.0	ppb	<0.1
Silver (Ag)		1.0	ppb	<0.1
Sodium (Na)		1.0	ppb	0.2
Strontium (Sr)		1.0	ppb	<0.1
Tin (Sn)		1.0	ppb	<0.1
Titanium (Ti)		1.0	ppb	<0.1
Vanadium (V)		1.0	ppb	<0.1

MATERIAL SAFETY DATA SHEET

Ashland Chemical Co.

Date Prepared: 01/26/98
Date Printed: 08/21/99
MSDS No: 999.0025191-005.004

HYDROGEN PEROXIDE 30% CR

1. CHEMICAL PRODUCT AND COMPANY IDENTIFICATION

Material Identity
Product Name: HYDROGEN PEROXIDE 30% CR
Product Code: 3473099
General or Generic ID: PEROXIDE

Company
Ashland Chemical Co.
P.O. Box 2219
Columbus, OH 43216
614-790-3333

Emergency Telephone Number:
1-800-ASHLAND (1-800-274-5263)
24 hours everyday

Regulatory Information Number:
1-800-325-3751

2. COMPOSITION/INFORMATION ON INGREDIENTS

Ingredient(s)	CAS Number	% (by weight)
WATER	7732-18-5	68.0- 72.0
HYDROGEN PEROXIDE	7722-84-1	28.0- 32.0

3. HAZARDS IDENTIFICATION

Potential Health Effects

Eye
Can cause permanent eye injury. Symptoms include stinging, tearing, redness, and swelling of eyes. Can injure the cornea and cause blindness. Eye effects may be delayed.

Skin
Can cause skin irritation. Symptoms may include redness and burning of skin, and other skin damage. Additional symptoms of skin contact may include: skin blistering abnormal coloring of the skin

Swallowing
Swallowing this material may be harmful or fatal. Ingestion of high concentrations causes rapid release of oxygen which may expand the esophagus or stomach resulting in severe damage (bleeding, ulceration or perforation).

Inhalation
Breathing of vapor or mist is possible.

Symptoms of Exposure
Signs and symptoms of exposure to this material through breathing, swallowing, and/or passage of the material through the skin may include: stomach or intestinal upset (nausea, vomiting, diarrhea), irritation (nose, throat, airways).

Target Organ Effects
No data

Continued on next page

Developmental Information
Based on the available information, risk to the fetus from maternal exposure to this material cannot be assessed.

Cancer Information
Based on the available information, this material cannot be classified with regard to carcinogenicity.

Other Health Effects
No data

Primary Route(s) of Entry
No data

4. FIRST AID MEASURES

Eyes
If material gets into the eyes, immediately flush eyes gently with water for at least 15 minutes while holding eyelids apart. If symptoms develop as a result of vapor exposure, immediately move individual away from exposure and into fresh air before flushing as recommended above. Seek immediate medical attention.

Skin
Immediately flush skin with water for at least 15 minutes while removing contaminated clothing and shoes. Seek immediate medical attention. Wash clothing before reuse and discard contaminated shoes.

Swallowing
Seek medical attention. If individual is drowsy or unconscious, do not give anything by mouth; place individual on the left side with the head down. Contact a physician, medical facility, or poison control center for advice about whether to induce vomiting. If possible, do not leave individual unattended.

Inhalation
If symptoms develop, move individual away from exposure and into fresh air. If symptoms persist, seek medical attention. If breathing is difficult, administer oxygen. Keep person warm and quiet; seek immediate medical attention.

Note to Physicians
Preexisting disorders of the following organs (or organ systems) may be aggravated by exposure to this material: skin, lung (for example, asthma-like conditions).

5. FIRE FIGHTING MEASURES

Flash Point
Not applicable

Continued on next page

Explosive Limit
No data

Autoignition Temperature
No data

Hazardous Products of Combustion
May form: acetic acid.

Fire and Explosion Hazards
Substance is an oxidizer. Will increase fire hazard if in contact with combustibles.

Extinguishing Media
water fog, carbon dioxide, dry chemical.

Fire Fighting Instructions
Wear a self-contained breathing apparatus with a full facepiece operated in the positive pressure demand mode with appropriate turn-out gear and chemical resistant personal protective equipment. Refer to the personal protective equipment section of this MSDS.

NFPA Rating
Health - 2, Flammability - 0, Reactivity - 1

6. ACCIDENTAL RELEASE MEASURES

Small Spill
Absorb liquid on vermiculite, floor absorbent, or other absorbent material and transfer to hood.

Large Spill
Eliminate all ignition sources (flares, flames including pilot lights, electrical sparks). Persons not wearing protective equipment should be excluded from area of spill until clean-up has been completed. Stop spill at source. Prevent from entering drains, sewers, streams or other bodies of water. Prevent from spreading. If runoff occurs, notify authorities as required. Pump or vacuum transfer spilled product to clean containers for recovery. Absorb unrecoverable product. Transfer contaminated absorbent, soil and other materials to containers for disposal. Prevent run-off to sewers, streams or other bodies of water. If run-off occurs, notify proper authorities as required, that a spill has occurred. Persons not wearing protective equipment should be excluded from area of spill until clean-up has been completed. Stop spill at source, dike area of spill to prevent spreading, pump liquid to salvage tank. Remaining liquid may be taken up on sand, clay, earth, floor absorbent, or other absorbent material and shoveled into containers.

7. HANDLING AND STORAGE

Handling
Containers of this material may be hazardous when emptied. Since emptied containers retain product residues (vapor, liquid, and/or solid), all hazard precautions given in the data sheet must be observed.

Continued on next page

8. EXPOSURE CONTROLS/PERSONAL PROTECTION

Eye Protection
Chemical splash goggles and face shield (8" min.) in compliance with OSHA regulations are advised; however, OSHA regulations also permit other type safety glasses. (Consult your industrial hygienist.)

Skin Protection
Wear impervious gloves (consult your safety equipment supplier). To prevent skin contact, wear impervious clothing and boots..

Respiratory Protections
If workplace exposure limit(s) of product or any component is exceeded (see exposure guidelines), a NIOSH/MSHA approved air supplied respirator is advised in absence of proper environmental control. OSHA regulations also permit other NIOSH/MSHA respirators (negative pressure type) under specified conditions (see your industrial hygienist). Engineering or administrative controls should be implemented to reduce exposure.

Engineering Controls
Provide sufficient mechanical (general and/or local exhaust) ventilation to maintain exposure below TLV(s).

Exposure Guidelines
Component

WATER (7732-18-5)
No exposure limits established

HYDROGEN PEROXIDE (7722-84-1)
OSHA VPEL 1.000 ppm - TWA
ACGIH TLV 1.000 ppm - TWA

9. PHYSICAL AND CHEMICAL PROPERTIES

Boiling Point
(for component) 212.0 F (100.0 C) @ 760 mmHg

Vapor Pressure
(for component) 17.500 mmHg @ 68.00 F

Specific Vapor Density
No data

Specific Gravity
1.114 @ 68.00 F

Liquid Density
9.280 lbs/gal @ 68.00 F
1.114 kg/l @ 20.00 C

Percent Volatiles
65.0 - 70.0 %

Continued on next page

Evaporation Rate
SLOWER THAN ETHYL ETHER

Appearance
No data

State
LIQUID

Physical Form
HOMOGENEOUS SOLUTION

Color
CLEAR, APHA COLOR 10 MAX

Odor
No data

pH
3.3

10. STABILITY AND REACTIVITY

Hazardous Polymerization
Product will not undergo hazardous polymerization.

Hazardous Decomposition
No data

Chemical Stability
Stable. Avoid heat, open flame, and prolonged storage at elevated temperatures.

Incompatibility
Avoid contact with: combustible materials, copper, cyanides, ferrous metals, heavy metals, organic materials, reducing agents, strong oxidizing agents.

11. TOXICOLOGICAL INFORMATION

No data

12. ECOLOGICAL INFORMATION

No data

13. DISPOSAL CONSIDERATION

Waste Management Information
Dispose of in accordance with all applicable local, state and federal regulations.

Continued on next page

14. TRANSPORT INFORMATION

DOT Information - 49 CFR 172.101

DOT Description:
HYDROGEN PEROXIDE, AQUEOUS SOLUTIONS,5.1,UN2014,II

Container/Mode:
55 GAL DRUM/TRUCK PACKAGE

NOS Component:
None

RQ (Reportable Quantity) - 49 CFR 172.101

Product Quantity (lbs)	Component
3333	HYDROGEN PEROXIDE

15. REGULATORY INFORMATION

US Federal Regulations

TSCA (Toxic Substances Control Act) Status
TSCA (UNITED STATES) The intentional ingredients of this product are listed.

CERCLA RQ - 40 CFR 302.4(a)
None listed

SARA 302 Components - 40 CFR 355 Appendix A

Section 302 Component(s)	TPQ (lbs)	RQ (lbs)
HYDROGEN PEROXIDE	1000	1000

Section 311/312 Hazard Class - 40 CFR 370.2
Immediate(X) Delayed( ) Fire( ) Reactive( ) Sudden Release of Pressure( )

SARA 313 Components - 40 CFR 372.65
None

OSHA Process Safety Management 29 CFR 1910

PSM Component (a)	Condition	TQ (lbs)
HYDROGEN PEROXIDE	>= 52%	7500

EPA Accidental Release Prevention 40 CFR 68
None listed

International Regulations

Inventory Status
Not determined

State and Local Regulations

California Proposition 65
The following statement is made in order to comply with the California Safe Drinking Water and Toxic Enforcement Act of 1986: This product contains the following substance(s) known to the state of California to cause reproductive harm.
ARSENIC

Continued on next page

New Jersey RTK Label Information
HYDROGEN PEROXIDE 7722-84-1

Pennsylvania RTK Label Information
HYDROGEN PEROXIDE (CONC >52%) 7722-84-1

16. OTHER INFORMATION

The information accumulated herein is believed to be accurate but is not warranted to be whether originating with the company or not. Recipients are advised to confirm in advance of need that the information is current, applicable, and suitable to their circumstances.

4-12-1999
1:30 pm

Ashland Chemical, Inc.

Dallas, Texas

CUSTOMER CERTIFICATE OF ANALYSIS

Lot Number: 90400270
Customer Product Name: Hydrogen Peroxide, 30%
Customer Part/Spec Number: GS
Revision:

Analysis Description	Specification Minimum	Specification Maximum	U.M.	Result
Assay (H_2O_2)	30.0	32.0	%	31.7
Color		5	APHA	3
Free Acid		0.6	meq/g	0.2
Total Organic Carbon		20000.	ppb	9000
Chloride (Cl)		30	ppb	<30
Phosphate (PO_4)		100	ppb	<40
Sulfate (SO_4)		100	ppb	<40
Aluminum (Al)		1.0	ppb	0.1
Antimony (Sb)		1.0	ppb	<0.1
Arsenic (As)		1.0	ppb	<0.1
Barium (Ba)		1.0	ppb	<0.1
Boron (B)		1.0	ppb	<0.1
Cadmium (Cd)		1.0	ppb	0.2
Calcium (Ca)		1.0	ppb	<0.1
Chromium (Cr)		1.0	ppb	<0.1
Cobalt (Co)		1.0	ppb	<0.1
Copper (Cu)		1.0	ppb	<0.1
Gallium (Ga)		1.0	ppb	<0.1
Germanium (Ge)		1.0	ppb	<0.1
Gold (Au)		1.0	ppb	<0.1
Iron (Fe)		1.0	ppb	<0.1
Lead (Pb)		1.0	ppb	<0.1
Lithium (Li)		1.0	ppb	<0.1
Magnesium (Mg)		1.0	ppb	<0.1
Manganese (Mn)		1.0	ppb	<0.1
Molybdenum (Mo)		1.0	ppb	<0.1
Niobium (Nb)		1.0	ppb	<0.1
Nickel (Ni)		1.0	ppb	<0.1
Potassium (K)		1.0	ppb	<0.1
Silver (Ag)		1.0	ppb	0.2
Sodium (Na)		1.0	ppb	<0.1
Strontium (Sr)		1.0	ppb	<0.1
Tin (Sn)		1.0	ppb	<0.1
Titanium (Ti)		2.0	ppb	<0.1
Vanadium (V)				

Arch Chemicals, Inc.

MATERIAL SAFETY DATA

FOR ANY EMERGENCY, CALL 24 HOURS/7 DAYS:	1-800-654-8911
FOR ALL TRANSPORTATION ACCIDENTS, CALL CHEMTREC®:	1-800-424-9300
FOR ALL MSDS QUESTIONS & REQUESTS, CALL MSDS CONTROL:	1-800-511-MSDS

PRODUCT NAME: GOLD ETCH

SECTION 1 PRODUCT AND COMPANY IDENTIFICATION

REVISION DATE: 05-22-1998 SUPERCEDES: None
MSDS NO: 00830-0004-882377

MANUFACTURER: Arch Chemicals, Inc. 501 Merritt 7 PO Box 5204 Norwalk, CT 06856-5204

SYNONYMS: None
CHEMICAL FAMILY: Not Applicable/Mixture
FORMULA: Not Applicable/Mixture
USE DESCRIPTION: Gold etch
OSHA HAZARD CLASSIFICATION: Skin, eye, respiratory tract irritant

SECTION 2 COMPONENT DATA

PRODUCT COMPOSITION
CAS or CHEMICAL NAME: Sodium Iodide
CAS NUMBER: 7681-82-5
PERCENTAGE RANGE: 15-17%
HAZARDOUS PER 29 CFR 1910.1200: Yes
EXPOSURE STANDARDS: None E stablished

CAS or CHEMICAL NAME: Iodine
CAS NUMBER: 7553-56-2
PERCENTAGE RANGE: 1-2%
HAZARDOUS PER 29 CFR 1910.1200: Yes
EXPOSURE STANDARDS:

	OSHA (PEL)		ACGIH (TLV)	
	ppm	mg/cubic-meter	ppm	mg/cubic-meter
TWA:		None		None
CEILING:	0.1		0.1	
STEL:		None		None

CAS or CHEMICAL NAME: Water
CAS NUMBER: 7732-18-5
PERCENTAGE RANGE: 80-85%
HAZARDOUS PER 29 CFR 1910.1200: No
EXPOSURE STANDARDS: None Established

SECTION 3 PRECAUTIONS FOR SAFE HANDLING AND STORAGE

DO NOT TAKE INTERNALLY. AVOID CONTACT WITH SKIN, EYES AND CLOTHING. UPON CONTACT WITH SKIN OR EYES, WASH OFF WITH WATER.

ER02-027 28278

STORAGE CONDITIONS:
STORE IN A COOL, DRY, WELL VENTILATED PLACE.
DO NOT STORE AT TEMPERATURES ABOVE: 54 Deg.C (130 Deg.F)
PRODUCT STABILITY AND COMPATIBILITY
SHELF LIFE LIMITATIONS: 2 Years
INCOMPATIBLE MATERIALS FOR PACKAGING: None known
INCOMPATIBLE MATERIALS FOR STORAGE OR TRANSPORT: None known

SECTION 4 PHYSICAL DATA

APPEARANCE: Deep, red liquid
FREEZING POINT: No Data
BOILING POINT: 104 Deg.C (220 Deg.F)
DECOMPOSITION TEMPERATURE: No Data
SPECIFIC GRAVITY: 1.151
BULK DENSITY: 1.151 (g/cc)
pH @ 25 DEG.C: 6
VAPOR PRESSURE @ 25 DEG.C: No Data
SOLUBILITY IN WATER: Complete
VOLATILES, PERCENT BY VOLUME: 85%
EVAPORATION RATE: < 1 (Water = 1)
VAPOR DENSITY: No Data
MOLECULAR WEIGHT: Not Applicable/Mixture
ODOR: Odorless
COEFFICIENT OF OIL/WATER DISTRIBUTION: No Data

SECTION 5 PERSONAL PROTECTIVE EQUIPMENT REQUIREMENTS

PERSONAL PROTECTION FOR ROUTINE USE OF PRODUCT:
RESPIRATORY PROTECTION: If air concentrations above the TLV are possible, wear a NIOSH approved respirator.
VENTILATION: Use local exhaust ventilation to maintain levels to below the TLV.
SKIN AND EYE PROTECTIVE EQUIPMENT: Wear gloves, boots, apron and a face shield with safety glasses. A full impermeable suit is recommended if exposure is possible to large portion of body.

EQUIPMENT SPECIFICATIONS (WHEN APPLICABLE):
RESPIRATOR TYPE: NIOSH approved positive pressure supplied air respirator
PROTECTIVE CLOTHING TYPE (This includes: gloves, boots, apron, protective suit): Impervious

SECTION 6 FIRE AND EXPLOSION HAZARD INFORMATION

FLAMMABILITY DATA:
EXPLOSIVE: No
FLAMMABLE: No
COMBUSTIBLE: No
PYROPHORIC: No
FLASH POINT: Not Flammable
AUTOIGNITION TEMPERATURE: Not Applicable
FLAMMABLE LIMITS AT NORMAL ATMOSPHERIC TEMPERATURE AND PRESSURE (PERCENT VOLUME IN AIR): LEL - Not Applicable UEL - Not Applicable

NFPA RATINGS: Not Established
HMIS RATINGS:
Health: 2
Flammability: 0
Reactivity: 0

EXTINGUISHING MEDIA:
Not Applicable-Choose extinguishing media suitable for surrounding materials.
FIRE FIGHTING TECHNIQUES AND COMMENTS:
This product would not be expected to burn.
Use water to cool containers exposed to fire.
See Section 11 for protective equipment for fire fighting.

SECTION 7 REACTIVITY INFORMATION

CONDITIONS UNDER WHICH THIS PRODUCT MAY BE UNSTABLE:
TEMPERATURES ABOVE: No Data
MECHANICAL SHOCK OR IMPACT: No
ELECTRICAL (STATIC) DISCHARGE: No
HAZARDOUS POLYMERIZATION: Will not occur
INCOMPATIBLE MATERIALS: None known
HAZARDOUS DECOMPOSITION PRODUCTS: None known
OTHER CONDITIONS TO AVOID: Extreme heat
SUMMARY OF REACTIVITY:

EXPLOSIVE:	No
OXIDIZER:	No
PYROPHORIC:	No
ORGANIC PEROXIDE:	No

SECTION 8 FIRST AID

EYES:
Immediately flush with large amounts of water for at least 15 minutes, occasionally lifting the upper and lower eyelids. If eye irritation develops, call a physician.
SKIN:
Immediately flush with water for 15 minutes. Wash the contaminated skin with soap and water. If irritation develops, call a physician. If clothing comes in contact with the product, the clothing should be laundered before re-use.
INGESTION:
Immediately drink large quantities of water. Induce vomiting. Call a physician at once. DO NOT give anything by mouth if the person is unconscious or if having convulsions.
INHALATION:
Remove person to fresh air. If respiratory irritation develops, call a physician.

SECTION 9 TOXICOLOGY AND HEALTH INFORMATION

ROUTES OF ABSORPTION
Inhalation, ingestion, skin and eye contact

WARNING STATEMENTS AND WARNING PROPERTIES
HARMFUL IF SWALLOWED. CAUSES SKIN, EYE AND MUCOUS MEMBRANE IRRITATION. MAY CAUSE RESPIRATORY IRRITATION. REPEATED CONTACT MAY RESULT IN DERMATITIS.

HUMAN THRESHOLD RESPONSE DATA
ODOR THRESHOLD: No Data
IRRITATION THRESHOLD: No Data
IMMEDIATELY DANGEROUS TO LIFE OR HEALTH: The IDLH concentration has not been established for this product, for iodine it is 10 ppm.

SIGNS, SYMPTOMS, AND EFFECTS OF EXPOSURE

Application Note MSAN-107
Understanding and Eliminating Latch-Up in CMOS Applications

Contents

- Semiconductor Device Considerations
- Background on SCR's
- Parasitic Bipolar Structures in the ISO-CMOS Topology
- Output SCR Structures
- Input SCR Structures
- System and Circuit Considerations
- A "Worst Case" System
- Insertion/Removal of System PCB's "Live"
- Problems Associated with Multi-Power Supply Voltages and Associated Decoupling Circuitry
- Devices Driving Others on Separate PCB's
- Devices Driving Long Address or Data Busses
- Ribbon Cables - A Special Case
- Systems with End User Accessible Inputs
- Digital and Analog Devices in Same System

Introduction

The purpose of this Application Note is to assist both those designers who are familiar with the use of CMOS devices as well as those considering CMOS designs for the first time.

Attracted by the many advantages offered by CMOS devices, designers using them for the first time are often unaware of, or are overly sensitive to the phenomenom of latch-up. Understanding a few facts will resolve both of these situations. Basically speaking, any analog or digital device fabricated in one of the many CMOS processes available, can be made to latch-up if stressed severely enough. However, when properly applied, CMOS devices are quite insensitive to actual conditions that exist in most systems. Further, if a few simple precautions are taken at the design stage, then latch-up can be completely avoided.

Latch-up is defined as the creation of a low impedance path between the power supply rails by the triggering of parasitic, four-layer bipolar structures (SCR's) inherent in CMOS input and output circuitry. In this note, details of these SCR structures are examined in the context of Mitel's ISO-CMOS technology. By developing an understanding of the aspects of circuit and system design related to the triggering of these SCR's, design methods and guidelines can be acquired to greatly reduce the probability of latch-up occurrence. By implementing the suggested techniques and circuitry, the designer can gain the advantages of CMOS circuitry without major concern about latch-up related problems.

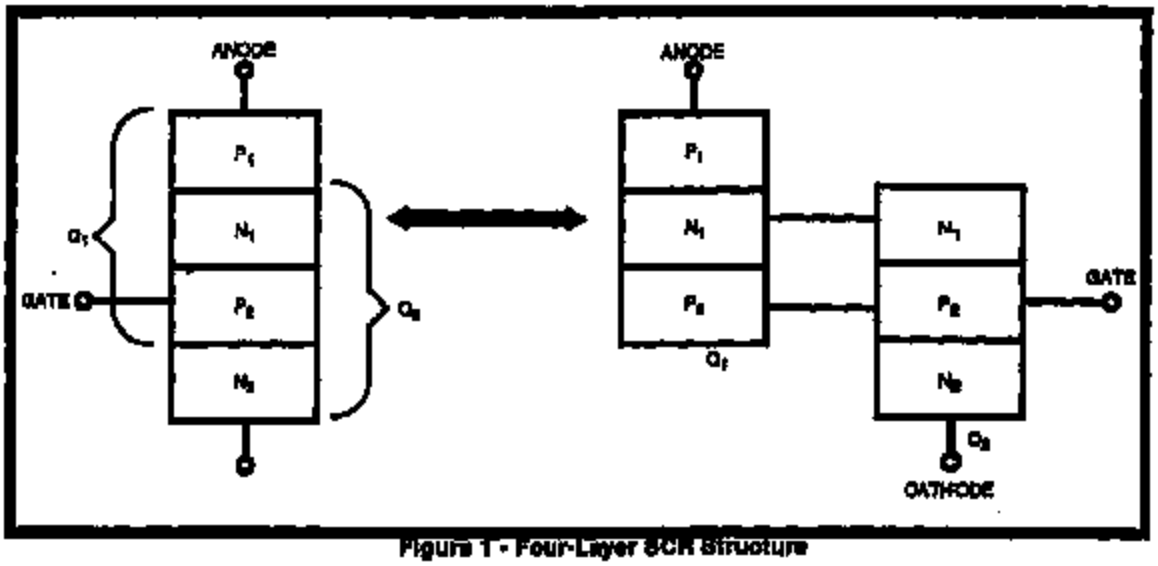

Figure 1 - Four-Layer SCR Structure

Semiconductor Device Considerations

Background on SCR's

Prior to discussing latch-up in CMOS devices, it is advantageous to briefly review the basic theory of SCR operation. This will be helpful in developing an understanding of the relationships between external circuit and system conditions and the resultant triggering of latch-up in CMOS devices. The basic SCR structure is that of a four-layer device as shown in Fig. 1. The device has three terminals: Anode, Cathode and Gate. Fig. 2 shows how the SCR can be modelled with two bipolar transistors, one NPN and one PNP. In the normal mode of operation, the SCR is turned on by injecting sufficient current into the base of Q_2 to turn this transistor on. When this is done, Q_2 begins to draw collector current via the base-emitter junction of Q_1. As a result Q_1 also turns on, injecting additional current into Q_2's base. This in turn causes Q_2 to turn on harder, supplying more base current to Q_1. This positive feedback arrangement sustains conduction, and ensures that the SCR continues to conduct even if the gate current is interrupted.

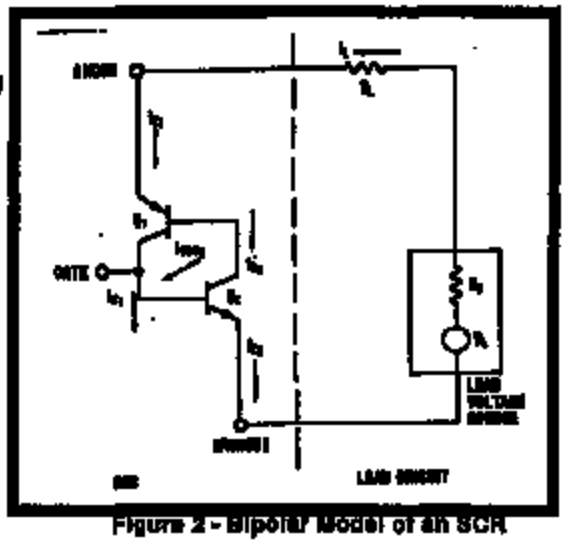

Figure 2 - Bipolar Model of an SCR

The device will remain in this latched state indefinitely. To turn the SCR off, one of two things can be done. If the voltage applied across the SCR is reduced to the point where Q_1's base-emitter junction turns off (V_{BE1}), then Q_2 will be starved of base current and the SCR will turn off. Alternatively, if the current through the SCR is reduced below its holding current then it will also turn off. The holding current is the minimum current required to sustain conduction and is a function of the physical dimensions of the device and the transistor gains (Fig. 3). As mentioned, this is the way that the SCR is controlled in normal applications. There are various other ways that an SCR may be triggered. These must be examined as they are directly related to latch-up problems.

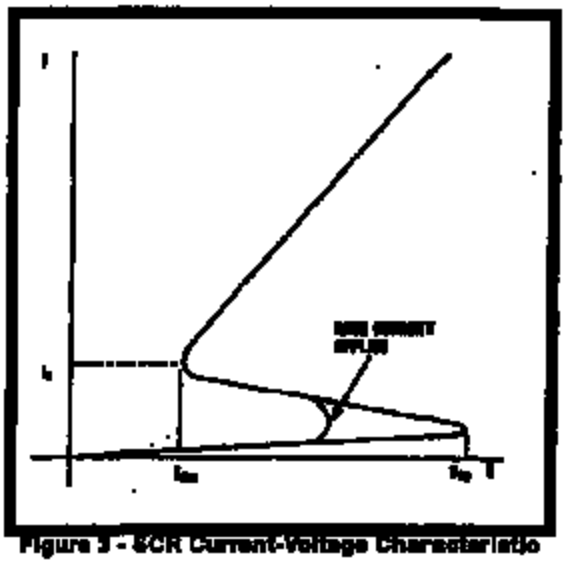

Figure 3 - SCR Current-Voltage Characteristic

Looking at Fig. 2, it can be seen that the load current and the two emitter currents of Q_1 and Q_2 are all equal. Also the load current is equal to the sums of the two collector currents and a leakage current from Q_2's collector to its base (I_{CBO2}). It can be shown (refer to Appendix) that:

$$I_L = I_{CBO_2}\left[\frac{(1+B_1)(1+B_2)}{(1-B_1B_2)}\right] \quad (1)$$

Where B_1 and B_2 are the current gains of Q_1 and Q_2 respectively.

Normally, with no base current supplied to Q_2, the load current will be small since the leakage I_{CBO2} is small, as are the current gains (B_1, B_2) at this low value of collector current. If however, the current gains increase to the point where the product, B_1 B_2, approaches unity, then the load current will become very large, limited only by the load impedance, the series impedance of the SCR, and source impedance of the power supply.There are various applied conditions that will cause this to happen. Increasing the load voltage beyond the breakover voltage, V_{BO}, will have this effect. As the anode-cathode voltage across the SCR increases, the collector-emitter voltages of Q_1 and Q_2 also increase. This corresponds to increases in the collector-base reverse biases. The collector-base junctions of the two transistors are physically the same area, the N_1-P_2 junction (Fig. 1). As the

reverse bias increases, the energy of the minority carriers increases causing more carriers to be dislodged, which in turn pick up energy. This continues until the junction undergoes an avalanche breakdown resulting in an increase in the collector currents of Q_1 and Q_2. The resulting increase in B_1 and B_2 cause the SCR to latch on.

A very rapid change in the anode to cathode voltage of an SCR can also cause it to trigger. This is known as the "dV/dt" effect. The N_1-P_2 junction, being reversed biased, exhibits a capacitance. This capacitance varies with the reverse bias voltage applied across the junction. Hence the current through the capacitor is described by:

$$\frac{d(C_j V_{AK})}{dt} \quad (2)$$

$$= \frac{C_j dV_{AK}}{dt} + \frac{V_{AK} dC_j}{dt} \quad (3)$$

The junction capacitance, C_j decreases with increasing reverse bias and hence the second term of equation (3) is negative. If, however, the rate of change of applied voltage is large enough, the first term of equation (3) will dominate and the current through the SCR will increase. If the current increases sufficiently to cause the B_1B_2 product to approach unity, then the SCR will latch on.

The effects of temperature must also be noted at this point. Increasing temperature will cause an increase in both the leakage current through the SCR and in the current gains B_1 B_2 of the two bipolar transistors. As such, the magnitude of the driving force required to turn the SCR on will decrease with increasing temperature. In other words, the SCR will be more easily triggered as temperature increases for any of the triggering mechanisms described.

Corollaries exist between each of the three methods of turning an SCR on as described, and the ways in which the parasitic SCR structures of CMOS devices are triggered. The normal mode of triggering an SCR is by injecting current into its gate terminal. This corresponds to forcing current into the inputs or outputs of a CMOS device by applying voltages that go outside of the power supply rails. This is by far the most common form of latch-up triggering. The avalanche breakdown mechanism described also applies directly to CMOS devices, although its occurrence is far less prevalent. Excessive voltage on the power supply pins, whether continuous or transient, may result in latch-up occurrence. It is also theoretically possible to trigger parasitic SCR devices by the dV/dt method as a result of high speed transients on the supply rails. However, this will rarely happen in a real application. Each of these triggering methods will be examined in the next section in the context of the ISO-CMOS topology for both the output and input structures.

Parasitic Bipolar Structures in the ISO-CMOS Topology

As with any CMOS technology, ISO-CMOS contains certain parasitic bipolar structures associated with its output devices and input protection circuitry. These parasitic transistors are interconnected in such a way as to form four-layer devices. As such, SCR devices are present at both the inputs and outputs of ISO-CMOS circuits. These devices are normally in their off state and will remain off as long as the absolute maximum ratings of the devices are not exceeded.

Output SCR Structures

A typical ISO-CMOS output driver contains one N-channel MOSFET with its source tied to V_{SS} and one P-channel MOSFET with its source tied to V_{DD}. The drains of the two transistors are connected together to form the output and the gates are connected to form the input (Fig. 4). The fabrication of these transistors in close proximity results in the formation of a parasitic SCR connected directly across the power supply rails. When triggered, this SCR presents a low impedance to the power supply causing excessive current to flow. This situation is potentially destructive, resulting in damage to bond wires or metal supply tracks on the die due to localized overheating. The SCR is formed as follows. A vertical NPN transistor results from the fabrication of the N-channel device. The N- substrate serves as the collector and is biased at V_{DD}. The P- well acts as the base and the source and drain N+ diffusions are the emitters of the transistor. One emitter is tied to V_{SS} and the other to the output. A wide base lateral PNP transistor is formed when a P-channel device is located close to a N-channel transistor. The P-channel source and

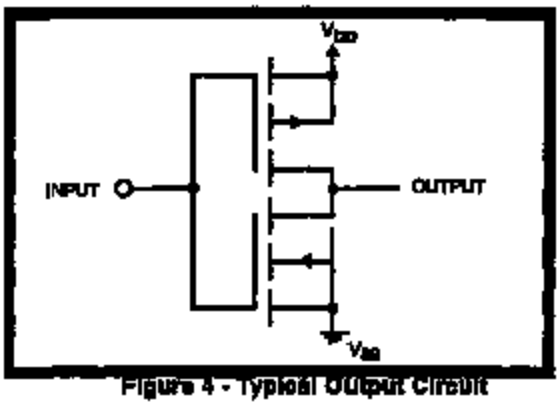

Figure 4 - Typical Output Circuit

drain diffusions are two emitters of the transistor: one tied to V_{DD} and the other to the output. The N- substrate acts as the base and hence, is in common with the collector of the vertical NPN. The P- well is the collector of the PNP which is also base of the NPN. Due to the shared diffusions, the vertical NPN and lateral PNP transistors are effectively connected as an SCR (Fig. 5). This parasitic SCR is connected directly across the supply rails. Hence, when triggered, it can cause excessive current to flow. The SCR is normally turned off for nominal operating supply voltages and with all output voltages within the power supply limits. This SCR may be externally triggered causing the output structure to latch-up. The triggering mechanism can be any one of those mentioned in the previous section.

Output voltages being forced outside of the power supply limits is the most common cause of output latch-up. Two parameters are defined at this point for use in subsequent discussions. These are I_{LU} and V_{LU}. I_{LU} is the current which must flow through the output structure to cause latch-up to occur. V_{LU} is the voltage excursion outside of the power supply rails at the output pin that results in I_{LU} flowing through the output structure. In other words I_{LU} and V_{LU} are the conditions at the output pin that will result in latch-up triggering. These same parameters also apply to input latch-up (see next section). Consider first an output voltage which goes below V_{SS} by more than V_{LU}. This causes the P- well to output base-emitter junction of the vertical NPN transistor to become forward biased. Since this acts as the SCR gate, triggering occurs. Current is pulled from V_{DD} through the lateral PNP and is injected into the P- well, causing a localized drop across this diffusion. This voltage drop will forward bias the base-emitter junction of the NPN which is referenced to V_{SS}. Once this occurs, latch-up will be sustained and a low impedance path is created from V_{DD} to V_{SS}.

A note must be taken here in regard to the amount of over-voltage required to trigger latch-up. In the above paragraph, it was mentioned that voltages exceeding the supply rails by more than V_{LU} will cause a current I_{LU} to flow and hence trigger latch-up. The guaranteed values quoted in the data sheet are 0.3V and 10mA respectively for these parameters. These limits are used in production testing and hence, appear in the Absolute Maximum Ratings for MITEL devices. In practice, it is more likely to require from 0.6V to 2V of over-voltage and from 50 to several hundred milliamps of current to cause output latch-up to occur. For input latch-up to occur, it can take several volts of over-voltage and similar currents to induce latch-up due to the series resistance of the input protection circuitry (Fig. 6).

When the V_{DD} supply rail is exceeded by a voltage greater than V_{LU}, a similar set of events occurs. In this case, the output to substrate base-emitter junction of the lateral PNP becomes forward biased. Collector current from this transistors injected into the P- well, again causing a lateral voltage drop. This voltage drop causes the P- well to V_{SS} referenced base-emitter junction of the NPN to become forward biased. This transistor's collector current, pulled from the substrate, causes a lateral voltage drop across the substrate. This voltage drop, in turn, will forward bias the V_{DD} to substrate base-emitter junction of the PNP. Thus, latch-up will be sustained even if the output over-voltage condition is removed and a low impedance path again exists between V_{DD} and V_{SS}.

There are two other causes of output latch-up that are less likely to occur, but nonetheless must be noted. The first of these is the result of over-voltages on the power supply pins. Excessive voltage between V_{DD} and V_{SS} (i.e., greater than the absolute maximum rating) can cause an avalanche breakdown of the reverse biased substrate to P- well collector base junction of the bipolar transistors.

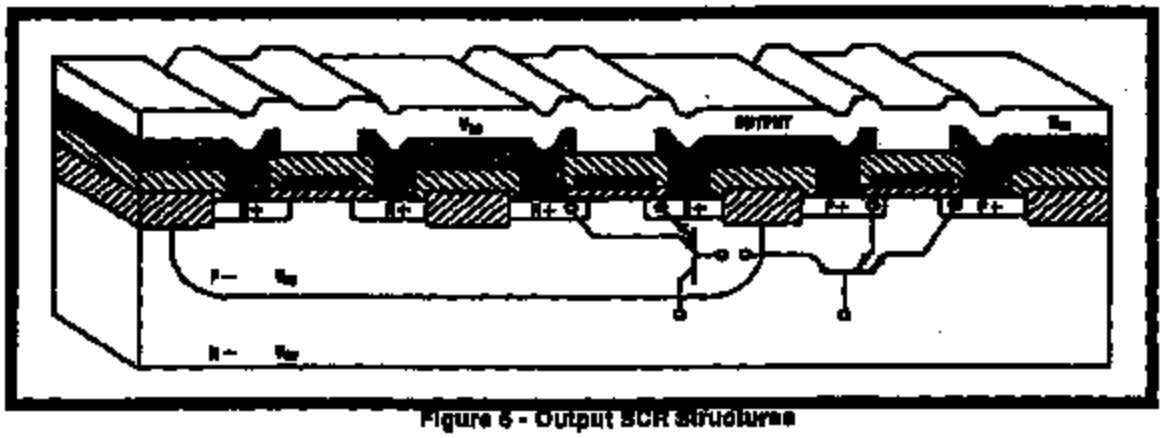

Figure 6 - Output SCR structures

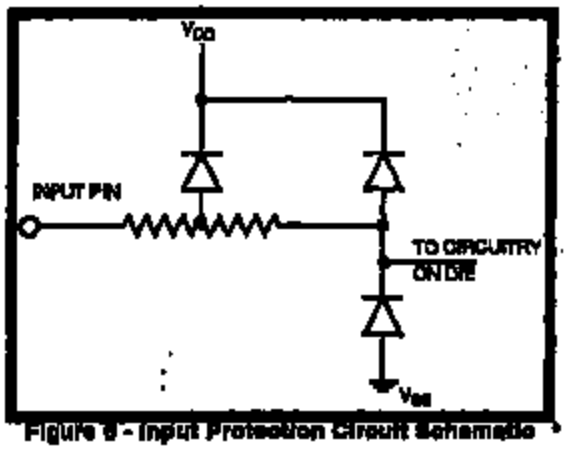

Figure 6 - Input Protection Circuit Schematic

This will cause the SCR to trigger as outlined in the previous section. The second triggering mechanism will be apparent in very few systems. Very fast voltage spikes on the power supply rails can induce a "dV/dt" triggering of the SCR, also as outlined earlier. This can potentially result in circuit damage by transients which in themselves would not have sufficient energy to cause damage due to localized power dissipation. Once triggered, the SCR may remain latched on until the supply voltage is reduced below its sustaining voltage or if the current is reduced below its holding current.

Input SCR Structures

Parasitic SCR structures can also result due to the fabrication of CMOS input protection circuitry. The ISO-CMOS input protection circuit schematic is shown in Fig. 6. As shown, there is a distributed diode connected to V_{DD} and another diode to V_{SS}. The series resistor is primarily intended for static protection, but also provides latch-up protection. The diodes are connected together at the input node. An SCR structure results when the V_{DD} referenced diode is fabricated in close proximity to an N-channel transistor (Fig. 7) or when the V_{SS} referenced diode is located close to a P-channel device. (Fig. 8).

It is important to note here the difference between input and output SCR structures. The output SCR was connected directly between V_{DD} and V_{SS}, and hence, is more likely to be destructive once triggered. The input SCR structure is connected from the input node to one of the supply rails. Thus, for an input to remain latched, the circuitry driving the input must be capable of supplying the sustaining current of the SCR. For this latch-up to be destructive, the input driver must be capable of supplying large amounts of current. A potentially more dangerous situation occurs when a complimentary transistor, to the one forming the SCR, is located nearby. A secondary SCR structure results from this and it is connected across the supply rails (Figs. 7 and 8).

Consider the V_{SS} referenced diode situation first. The source and drain diffusions of the P-channel transistor form the emitters of a lateral PNP transistor. The substrate acts as the base and the P-diffusion of the diode is the collector. This diode, with the substrate, forms a vertical NPN transistor. The two transistors are interconnected as an SCR due to common diffusion areas. If an applied input voltage is below V_{SS} by more than V_{BE}, then the gate-cathode junction of the SCR will become forward biased and turn the SCR on. This latch-up condition will continue as long as this input condition persists or if the input circuitry can supply the minimum holding current. As mentioned, a potentially more hazardous situation can develop if an N-channel transistor is also located nearby. The P-well of this transistor serves as a second collector of the lateral PNP transistor. When the input voltage goes negative, the gate of the SCR is turned on as mentioned. However, this second collector now injects current into the P- well causing a second SCR

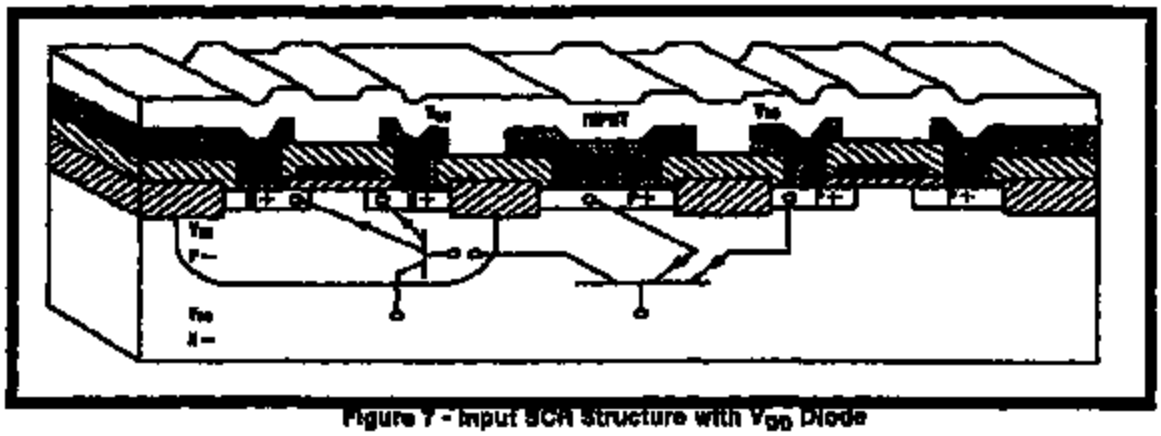

Figure 7 - Input SCR Structure with V_{DD} Diode

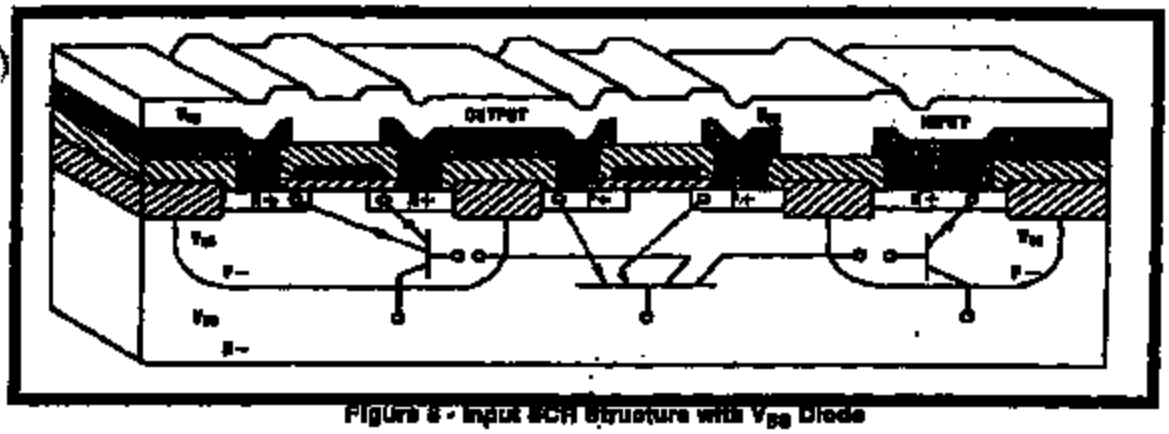

Figure 8 - Input SCR Structure with V_{SS} Diode

Forced I/O Condition	Latch-Up Inducing Conditions	
	V_{LU} (Volts)	I_{LU} (mA)
Outputs above V_{DD}	1.9	200
Outputs below V_{SS}	1.0	90
Inputs above V_{DD}	1.9	80
Inputs below V_{SS}	25.0	25

Table 1. MD74SC640AC Latch-up Inducing Voltages and Currents

structure to latch on. This device is connected across the power supply rails and hence, can be destructive. This same situation can result with the V_{DD} referenced protection diode. In this case, SCR structures will be triggered by voltages which exceed V_{DD} by more than V_{LU}.

As was mentioned earlier, the actual values of V_{LU} and I_{LU} are typically much greater than the 0.3V and 10mA limits on the data sheets. Table 1 shows some of the numbers pertaining to the current production version of the MD74SC640AC, one of MITEL's Octal Interface devices. As can be seen it requires voltages from 1.0V to 1.9V and currents from 90 to 200mA to trigger output latch-up. On the input side, it requires 1.9V for V_{LU} and 80mA for I_{LU} in the V_{DD} case. For the V_{SS} case, I_{LU} is only 25mA, but V_{LU} is 25V and hence this situation would virtually never exist in a system. It has been empirically determined that if a device exhibits values of I_{LU} exceeding a few volts, then this device will be extremely insensitive to latch-up in the majority of circuits and systems. A severe system fault would be required to induce latch-up in such devices.

System and Circuit Considerations

In the majority of systems and circuits using CMOS devices, latch-up should not be a major cause for concern. Being aware of the sources of latch-up problems will aid the designer in even further reducing the probability of latch-up damage to his circuits. Implementing some of the precautionary measures suggested in the following sections will ensure a trouble-free system.

The aspects of system and circuit design that can result in latch-up occurrence will be examined in the context of a "worst case" system example. In other words, systems containing combinations of the attributes of the example system will be more likely to experience latch-up problems. The relationships between these systems aspects and the resultant latch-up triggering mechanisms will be described. Suggestions will be made intent upon reducing the risk of triggering the parasitic SCR's through careful design techniques. The protection circuits, which will be illustrated, should help in preventing circuit damage in case latch-up occurs. It should be noted at this point, that in systems where the input and output pins of the CMOS devices never go outside of the power supply rails either during power-up or in continuous operation, latch-up is not likely to ever occur. The first step, then, is to define a system which contains various components that qualify it for a "worst case" rating in a latch-up sense.

A "Worst Case" System

A circuit or system which has all of the following attributes and/or capabilities is more likely to experience latch-up problems. This is not to say that latch-up is inevitable in systems containing many of these attributes, only that the designer must be aware of potential problems and take steps at the design stage to avoid them. The following list summarizes the system aspects most likely to be associated with latch-up problems:

1) System operation/maintenance procedures allow insertion or removal of printed circuit cards with system power applied.

2) The system is powered by multiple supply voltages (e.g. ± 12V, + 5V, and Gnd) or has a multi-supply at same voltage (e.g. +5V regulated, +5V unregulated).

3) Circuits utilize complex capacitive decoupling techniques particularly associated with multiple power supply voltages.

4) Integrated circuits on one system PCB drive other devices on different PCB's via a backplane, ribbon cable, etc.

5) Devices drive high capacitive loads such as long data or address busses.

6) System contains high speed address and/or data buses of sufficient length to cause their inductive properties to become significant at the frequencies in question (ribbon cables are a prime example).

7) System has electronic inputs that are directly accessible by the end user of the system.

8) Digital devices are driven from analog devices powered from higher supply voltages, utilizing input diodes for clamping.

Each of the above entries will now be examined in terms of its potential for triggering latch-up. The first four items are very interdependent. While each of these will be given consideration in separate sections, cross referencing will be extensive. The remaining items are relatively independent and thus, will be looked at in relative isolation.

Insertion/Removal of System PBC's "Live"

Inserting or removing printed circuit cards from a powered-up system can trigger latch-up in several different ways if certain precautions are not taken. One potential hazard that can occur is for an input or output edge terminal to make contact before the power supply pins are connected. If driven by a device on another circuit card, this input/output pin could have a voltage applied to it with no supply voltage to the device. Even if this situation exists for only a short period of time, then latch-up may be triggered when the power supply pin is connected. It is important to note that three-state outputs are also vulnerable in this situation. Such output drivers only present a high impedance to voltages within the device supply rails. Voltages on these outputs exceeding the supply can indeed trigger latch-up.

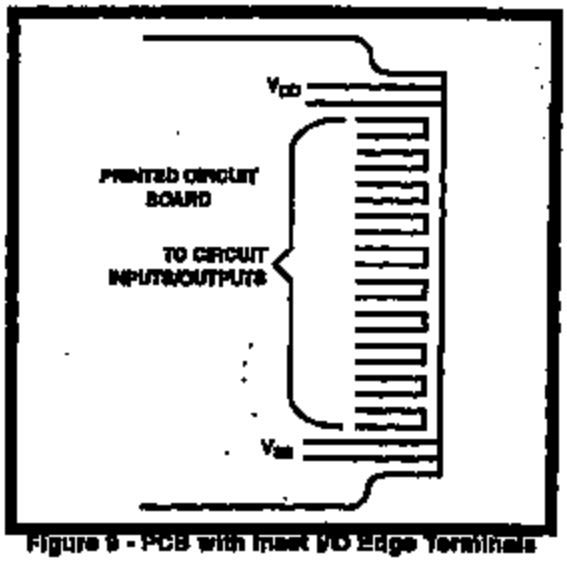

Figure 9 - PCB with Inset I/O Edge Terminals

One solution to this problem is to slightly extend the power supply terminals with respect to the remaining edge terminals on the PCB (Fig. 9). This will ensure that power supply connections are the first made and last broken on insertion and removal of the PCB respectively.

Plugging a circuit card live into a system with multi-power supply voltages can result in the application of power supply over-voltages to certain devices. Consider the local decoupling scheme shown in Fig. 10. If a PCB containing such decoupling was plugged into a system live, then the following situation could result. Assume that all capacitors are discharged and that C_1 is much greater than C_2. It is possible that when the PCB is inserted, the +12V terminal makes connection first, then the ground, and lastly the +5V connection is made. In this situation, C_1 and C_2 are momentarily connected in series. The +12 volts applied to C_1 causes the voltage at the ground point to increase in

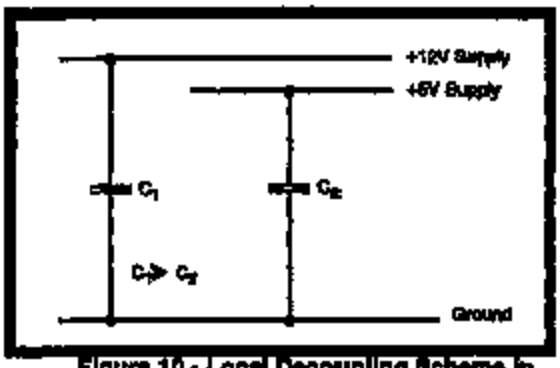

Figure 10 - Local Decoupling Scheme in Multi-Supply System

accordance with the charge sharing between C_1 and C_2. This voltage could approach 12 volts since $C_1 \gg C_2$. When the ground terminal makes connection, the voltage at the nominal 5V rail will jump up by the amount of voltage initially present at the ground point (i.e. almost 12V). This results in an over-voltage condition being applied to the devices supplied by the 5V rail. If the applied voltage exceeds the absolute maximum rating for these devices then latch-up may be triggered by the avalanche breakdown mechanism described in an earlier section. This problem is more likely to be evident in systems with power supplies differing greatly in magnitude since potential over-voltages can become quite large. A prime example is a telephone switching system which would typically contain a -48V supply as well as +5V and other supply voltages.

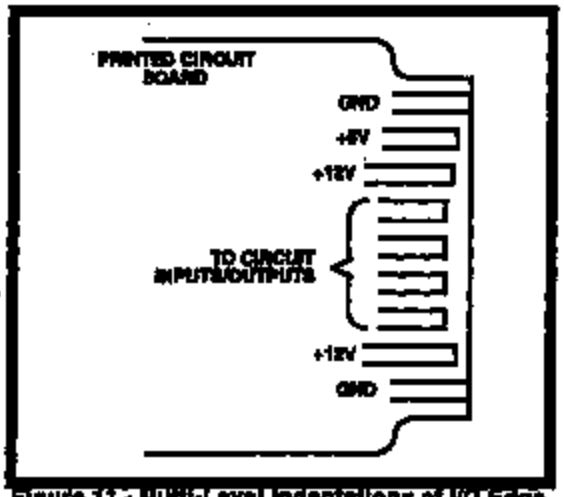

Figure 11 - Multi-Level Indentations of I/O Edge Terminals

This problem can also be overcome by indenting the edge terminals on PCB's. In this case, there must be more than one level of indentation to ensure that the power supply connections are made in a sequence that will alleviate this problem. The safest way to accomplish this is to have power supply connections made in the order of ascending voltage magnitude (Fig. 11). For example, in a system with a +5V supply and±12V supplies, the ground line should make connection first, the +5V supply next and finally, the +12V and -12V supplies at the same time. This ascending order of magnitudes ensures that no over-voltages occur even if one of the power supplies pulls the other through the decoupling capacitors. The ground line should always make connection first to ensure that a positive supply does not pull a negative one or vice versa. Connecting opposing power supplies (e.g. ±12V) at the same time will ensure cancellation of the effects of their connection.

In systems which have large number of power supplies to contend with, it may not be feasible to provide the required number of indentations on the PCB. In this case, a careful analysis of the decoupling used must be done to establish potential problem areas. Where possible, decoupling capacitors on different supplies should be of equal magnitude. This will tend to minimize over-voltages dues to equal charge sharing between the capacitors. If after all possible precautions have been taken, there is still a possibility of power supply over-voltages occurring, then it may be necessary to provide some form of current limiting or local regulation to prevent circuit damage.

The simplest form of protection is to connect a resistor in series with the power supply (V_{DD} or V_{SS}) pin of the devices in question (Fig. 12a). The size of this resistor can be chosen to either prevent latch-up from occurring or to prevent circuit damage when latch-up does occur. If latch-up is to be prevented then the minimum resistor value is chosen as follows:

$$R = \frac{V_{Supply} - V_{DD\,Max}}{I_{DD_{Max}}}$$

where V_{Supply} = Maximum Supply Voltage Generated

V_{DDMax} = Absolute Maximum Rating for V_{DD}

I_{DDMax} = Supply Current at V_{DDMax}

This will ensure that V_{DDMax} is never exceeded at the device.

To simply prevent damage due to latch-up, the resistor is chosen to limit the supply current to a few hundred milliamps at the maximum applied voltage. There are a few factors which must be taken into consideration when the maximum value for this resistor is selected. The source impedance of the power supply will be increased by the amount of the added resistance. This will result in a decrease in the current sourcing or sinking capacity of the device, depending on whether the resistor is in the V_{DD} or V_{SS} line respectively. There is also a corresponding increase in the output propagation delay, proportional to product of the protection resistor and the load capacitance. Finally there is a decrease in the noise immunity of the device proportional to the product of this resistor and the total instantaneous supply current (including the output currents). For devices such as the MD74SCXXX, it is recommended that this resistor be placed in the V_{DD} line as there is more available noise immunity for high level outputs (when driving TTL or other MD74SCXXX devices).

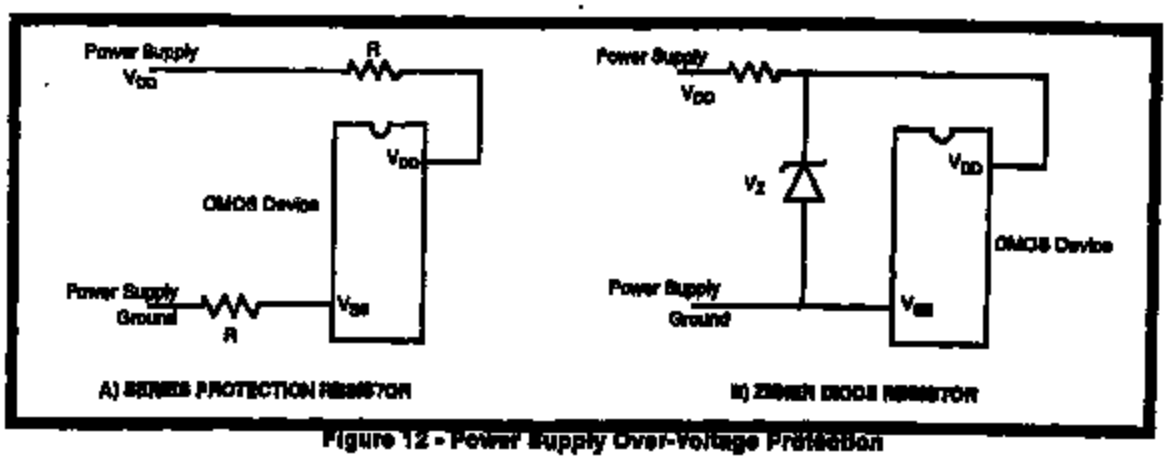

Figure 12 - Power Supply Over-Voltage Protection

If a current-limiting resistor cannot be used due to constraints on output drive, speed or noise immunity, then the alternative is to connect a zener diode between V_{DD} and V_{SS} to prevent over-voltages across the device (Fig. 12b). A current-limiting resistor may still be necessary, but its value can be very small, limited only by the power handling capacity of the zener diode.

There is one last potential hazard that can develop due to "live" insertion of PCB's. On boards with little local decoupling, plugging the card in can result in an extremely fast transient on the power supply leads of devices on the board. These transients could theoretically result in triggering latch-up due to the dV/dt effect described earlier. This problem can be avoided by decoupling the power supply on the board with sufficiently large capacitors to slow down the power supply ramp up when the board is plugged in. These capacitors must be chosen to be compatible with the overall decoupling scheme to prevent the over-voltage problem just described.

Similar transients on the power supply can be generated due to switching of high speed, high current devices such as ECL and Schottky TTL circuits driving heavy DC current loads. Also, back EMF generated by opening of inductive loads such as relays can induce nasty voltage spikes. Adequate high frequency decoupling will usually remedy the problem. A 0.01 to 0.1µF ceramic capacitor connected as close to the device as possible across the power supply pins will shunt most of this high frequency energy to ground (Fig. 13). Connection of flyback diodes around inductive loads is also recommended to limit back EMF surges.

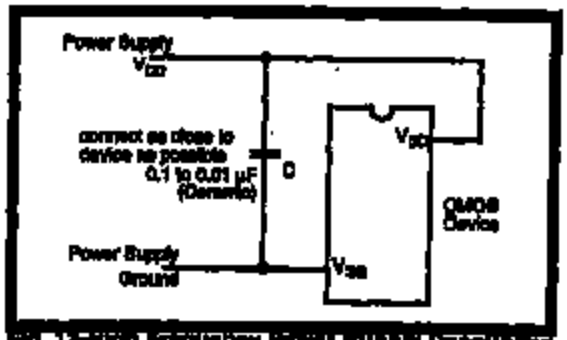

Fig. 13-High Frequency Power Supply Decoupling

Problems Associated with Multi-Power Supply Voltages and Associated Decoupling Circuitry

In systems that have more than one independent power supply, care must be taken to ensure correct sequencing during power-up and power-down cycles. This is required to prevent input and output over-voltage conditions from developing. Consider, for example, a device powered from a +5V supply that has its outputs connected to a device powered from a +7V supply. Under steady state conditions, the output levels from the 5V devices would lie well within the supply voltage of the 7V device. However, if during power-up the 5V supply was to exceed the 7V supply, then the output voltage of the 5V device could exceed the instantaneous supply voltage of the 7V device (Fig. 14). This over-voltage could cause the 7V device to latch-up. A similar situation can occur between two devices powered by separate supplies of equal magnitude such as 5V regulated and 5V unregulated supplies. In this case there is the added concern when three-state outputs are tied together. These outputs are also subject to over-voltage triggering of latch-up. Such outputs present a high impedance only to signals lying within the power supply voltages. It must be stressed that

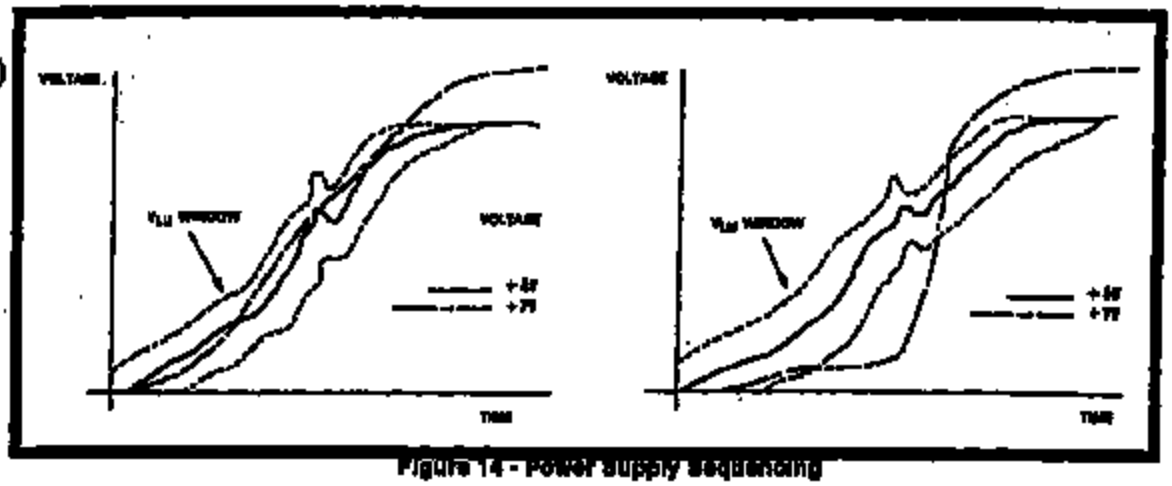

Figure 14 - Power supply sequencing

these over-voltage conditions need only exist for a very brief period of time to trigger latch-up. Thus, even transient over-voltages during power-up may pose a problem.

To ensure proper power supply sequencing, careful attention must be paid to the selection of decoupling components both at the initial design stage and when design revisions are done. This applies to both main power supply decoupling as well as local board decoupling. While proper sequencing may be evident at main distribution points, local sequencing can be altered by large capacitors on individual boards. Boards which have a large DC power requirement are likely to have such decoupling and hence, must be looked at carefully.

One way of ensuring that power supplies track when turning on or off is to connect a diode from the lower supply voltage to the higher one in the case of unequal supplies (Fig. 15). This will cause the supplies to track within one diode drop until they attain proper levels. In the case of two equal supplies, two diodes can be connected back to back, forcing supplies to track, independent of which supply comes up first.

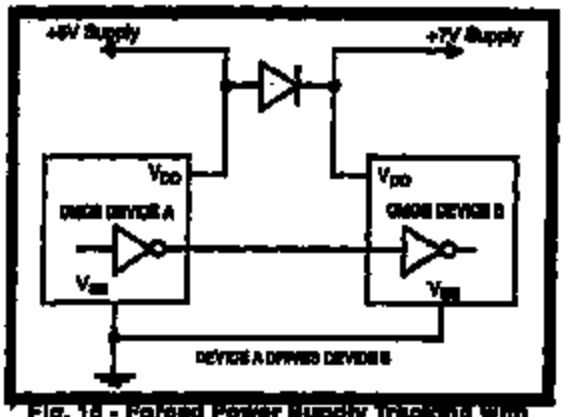

Fig. 15 - Forced Power Supply Tracking With Clamping Diode

Devices Driving Others on Separate PCBs

When integrated circuits in a system drive other devices on separate PCB's (via a backplane for example), then the considerations given in the previous two sections must be applied globally to the system. This was already mentioned in the section on plugging in PCB's "live". That is, when a PCB is plugged into a backplane with the system power applied, there is the danger that an input or output pin will contact an active line on the backplane before the power supply connection is made. The solution to this problem, as mentioned, lies in indenting the I/O edge terminations with respect to power supply terminals on the PCB.

Power supply sequencing should be given special attention in systems with devices that drive off-board. The same criteria applies here as was described for multi-supply systems. However, care must also be taken in single supply systems. In this case, large amounts of local decoupling can cause the supply voltages on some boards in the system to ramp up slower than on others. Devices on boards whose power supply ramps up quickly, can impress an over-voltage on devices on other boards. If this over-voltage is large enough, then latch-up may be triggered.

Whenever possible, local decoupling should be equalized on all boards within the system to minimize these effects. In systems where all off-board drivers are three-state devices, a simple

solution exists. All outputs should be kept in a high impedance state during power-up and power-down. Thus, no current will be available to trigger latch-up even if differential supply voltages develop from board to board. Alternatively, current limiting resistors can be connected in series with any inputs or outputs that may be subjected to over-voltages. These resistors are sized to limit current to less than 10mA:

$$R = \frac{(V_{Diff} - 0.3V)}{10mA}$$

where V_{Diff} = maximum instantaneous voltage differential between power supplies

The side effects of connecting these resistors are the same as mentioned previously for power supply over-voltage protection. There will be reductions in current drive from outputs, in speed, and in noise immunity on outputs driving DC loads through these resistors.

Devices Driving Long Address or Data Buses

Long address and data buses can exhibit quite large capacitances. Devices which drive such buses or have their inputs tied to one, can be subjected to over-voltage conditions. This is especially true if large DC current loads are switched on the same PCB (e.g. a group of LED's during a lamp test). Over-voltages can develop as follows. The change in the power supply current causes a localized voltage drop on the supply pins of the devices near to the device drawing the load current. This is a result of the finite resistance of the power supply tracks and contact resistance of any connectors. At the same time, the bus capacitance tends to hold the voltage on the inputs and outputs connected to the bus at the full supply voltage. If a sufficient voltage differential develops between the bus and the local power supply, then the bus capacitance will discharge via the input and output structures. This current can attain a magnitude of tens of milliamps and hence trigger latch-up (Fig. 16).

Various precautions can be taken to reduce the chances of this problem occurring. Reducing the power supply resistance and bus capacitances can be done at the time of initial design. Wide power supply tracks and low contact resistance connectors should be used whenever possible. Buses should be kept as short as possible and have the largest possible spacings between the lines. If this problem still results due to system restraints on PCB layout, then the connection of a decoupling capacitor across the power supply pins of the devices latching-up should help (Fig. 17). The size of the capacitor depends upon the magnitude of the local current and the local resistance of the power supply. Normally a 10µF capacitor will clear up such problems and should not interfere with the local power supply sequencing on most PCB's.

There is one other way in which an input/output over-voltage can occur on long buses. There exists, on such buses, intertrack capacitance as well as capacitance to ground. When two adjacent tracks are at opposite logic levels (one at 5V, the other at ground), this capacitance charges to the full supply voltage. When the track initially at ground potential suddenly goes high, the signal is coupled through the capacitor to the other track. The voltage on this track increases from its initial value of 5V, impressing over-voltages on any devices connected to this track.

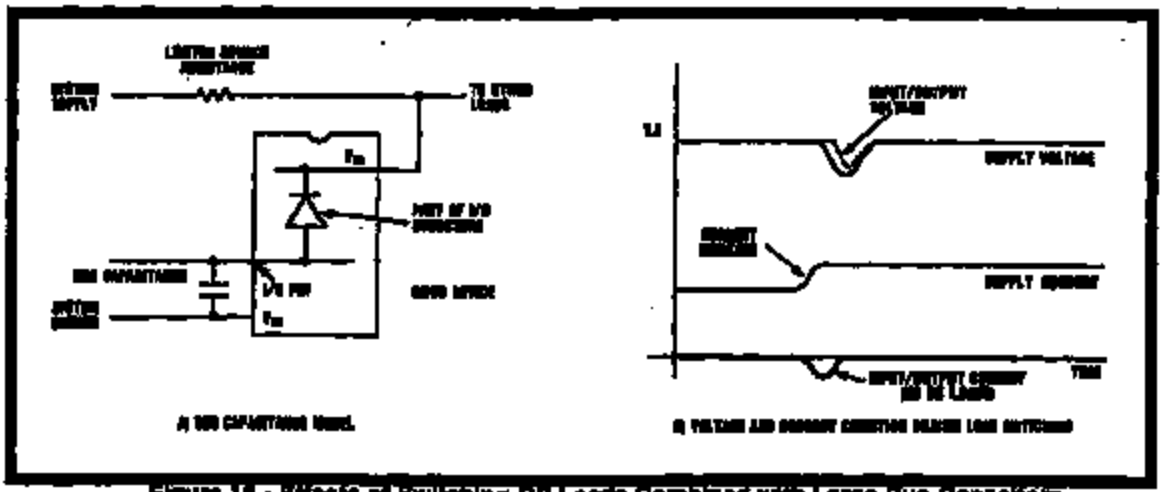

Figure 16 - Effects of Switching DC Loads Combined with Large Bus Capacitors

Minimizing intertrack capacitance by interleaving signal and ground tracks should be done wherever board space permits. Alternatively, external clamping diodes can be connected on tracks exhibiting these voltage excursions. The diodes may need be Schottky diodes if regular ones do not clamp soon enough toprevent current flow through

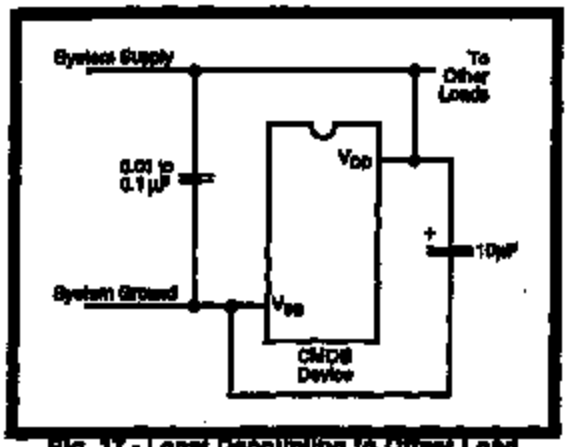

Fig. 17 - Local Decoupling to Offset Load Switching Effects

I/O structures. Regular silicon diodes may still be used if they are referenced to voltages inset by 0.7V from the supply rails. The clamping circuit shown in Fig. 18 should be quite effective, but as can be seen, this circuit will dissipate power. This may or may not be a problem depending on the overall system requirements. The decoupling capacitors help to absorb the high frequency energy. The resistor values shown are selected for a 5V supply and should be scaled for other supply voltages.

Ribbon Cables - A Special Case

A ribbon cable is a special case of long bus structure. The problems mentioned in the previous section also apply here. However, if the ribbon cable is of sufficient length, then its inductive properties become significant. The distributed inductance and capacitance form a second order circuit which can "ring" when driven by fast, digital signals. The result is the generation of damped oscillations centered about the positive and negative supply rails (Fig. 19). The positive and negative excursions outside of the supply rails impress over-voltages on inputs and outputs connected to the ribbon cable. If of sufficient amplitude, these over-voltages may trigger latch-up.

Solving the problem can be as simple as terminating each end of such cables with resistors to reduce the ringing voltages. However, these resistors will dissipate extra power. An alternative is to connect external protection diodes as shown in Fig. 20.

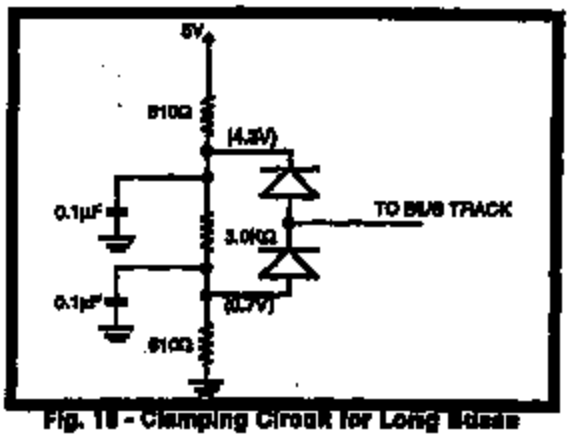

Fig. 18 - Clamping Circuit for Long Buses

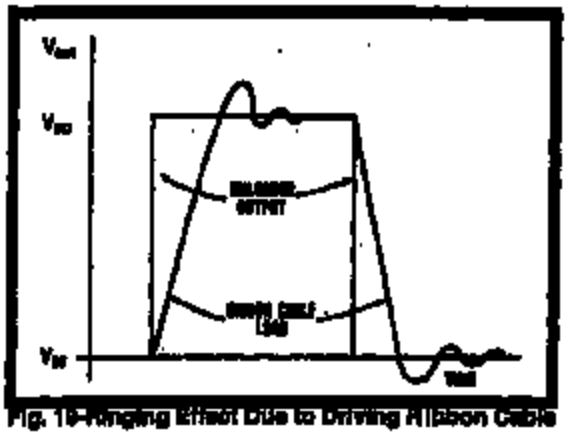

Fig. 19-Ringing Effect Due to Driving Ribbon Cable

These diodes will clamp any generated over-voltages. If the problem persists, it may be necessary to use Schottky diodes to ensure that the external diodes conduct before the input/output structures do.

Systems with End-User Accessible Inputs/ Outputs

An extreme condition of input/output over-voltage can develop in systems which have end user accessible I/O ports. The user may apply signals to these ports when the system power supply is not turned on. Devices in the system connected to these ports are likely to latch-up when the power is turned on due to the current flowing through the I/O structures. Resistors can be connected in series with these I/O's to limit the current during these periods. As mentioned, these resistors will have direct effect on the speed and noise performance of these ports. Latch-up may also be triggered if the end user applies voltages to the I/O ports which exceed the system power supply voltages. The protection resistors suggested above may provide adequate protection against this hazard as well.

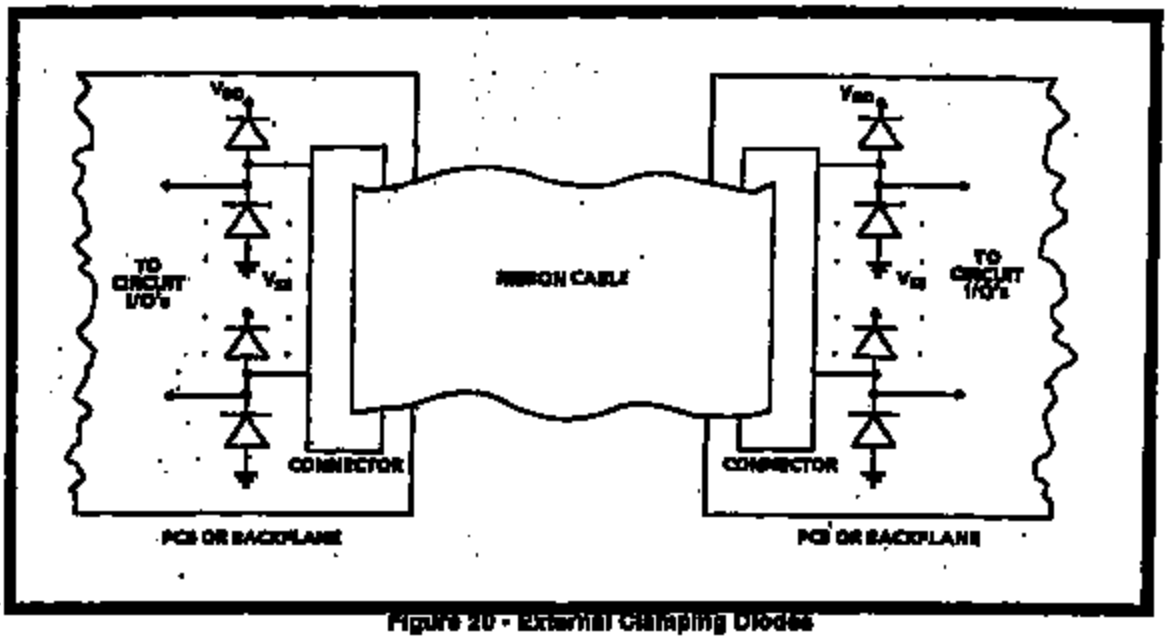

Figure 20 - External Clamping Diodes

However, performance constraints on the port may be such that the current-limiting resistors chosen are too small to protect against severe faults such as accidental connection of the AC mains supply. Protection against such faults can be provided by connection of external clamping diodes in the manner outlined for ribbon cables. Again, Schottky diodes may be required.

If fault conditions are likely to be very severe, it may be necessary to reference external clamping diodes to voltages inset by 0.7V from the power supply (Fig. 21). These diodes will conduct before the input/output structures of the device on the port whenever an over-voltage condition exists. Thus, no current will flow to trigger latch-up. The reference voltages are inset by 0.7V to allow the use of regular, low-cost diodes. Due to the potentially large currents flowing through the protection diodes, a clamping circuit similar to the one in Fig. 18 is not feasible. The output resistance in this case needs to be substantially lower.

Digital and Analog Devices in Same System

In systems which have digital and analog devices powered by different supply voltages, there is the

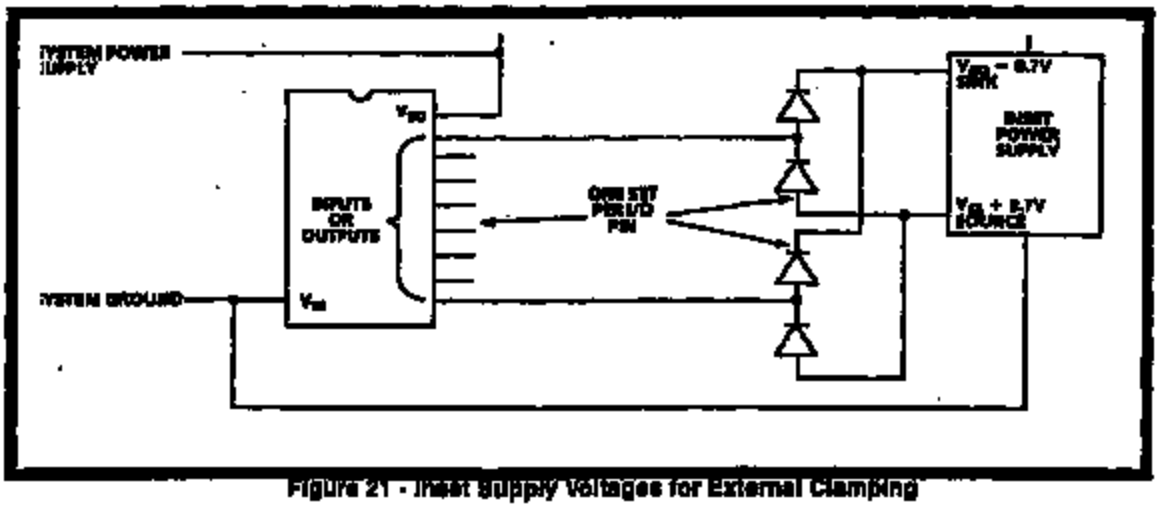

Figure 21 - Inset Supply Voltages for External Clamping

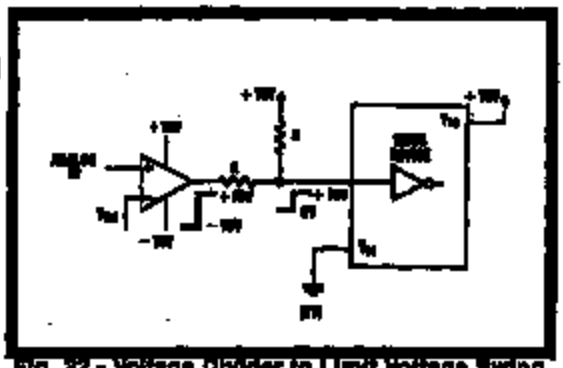

Fig. 22 - Voltage Divider to Limit Voltage Swing on CMOS Input

potential hazard of over-voltage conditions developing. Consider, for example, the case of an analog comparator powered from ±10V driving a digital device powered from a +10V supply. When the comparator output goes low, it will approach -10V and pull the digital input below V_{SS} (0V). If the comparator can pull enough current, then latch-up may be triggered. Putting a resistor in series with the input will limit the current and prevent latch-up. However, it is not a recommended procedure to use the input diodes as clamping circuits. A more advisable solution is to use a resistive divider as shown in Fig. 22. When the comparator output goes low, the divider will have 20V across R. Half of this voltage will be dropped across each resistor so that the digital input sits at 0V. When the comparator output goes high, no current flows through the divider so that the digital input sits at V_{DD}. Since the CMOS input has an extremely high input impedance, the value of these resistors can be very large (>100K) to minimize power consumption.

Conclusion

In the vast majority of circuits and systems employing CMOS devices, latch-up will not be a major concern. When simply applied according to manufacturers' recommendations, CMOS devices are not overly sensitive to the normal circuit conditions that exist within a system. What has been attempted in this application note is to develop an understanding of the latch-up phenomenon and its causes to assist designers in avoiding potential pitfalls caused by a simple lack of knowledge.

Having briefly reviewed the basic theory of SCR operation in general, and as it applies to CMOS input and output structures, an understanding of the mechanism of latch-up was developed. Taking a close look at various aspects of system and circuit design has revealed that various precautionary measures taken at the design stage can greatly reduce the risk of latch-up occurrences. In cases where system performance or features create potentially hazardous situations beyond the designer's control, the implementation of simple protection circuitry will again minimize problems.

Through the use of careful design practices, augmented by protection circuitry when needed, the designer can use CMOS analog and digital integrated circuits extensively. System and circuit reliability will no longer be a function of latch-up related problems.

Reference

1. S.S. Dewan and A. Straughen, "Power Semiconductor Circuits", pp. 77-84, John Wiley and Sons, 1975.

Appendix

The following is a derivation of equation (1) of the main text. Fig. 2 is referenced for this purpose.

The collector and emitter currents of Q_1 and Q_2 are related by:

$$I_{C_1} = \alpha_1 I_{E_1} \qquad I_{C_2} = \alpha_2 I_{E_2}$$

Looking at Fig. 2, it can be seen that the load current and the emitter currents of Q1 and Q2 are all equal. Also the load current is equal to the sums of the two collector currents and a leakage current from Q_2's collector to its base (I_{CBO_2}). Therefore:

$$\begin{aligned} I_L &= I_{C_1} + I_{C_2} + I_{CBO_2} \\ &= \alpha_1 I_{E_1} + \alpha_2 I_{E_2} + I_{CBO_2} \\ &= (\alpha_1 + \alpha_2) I_L + I_{CBO_2} \\ &= \frac{I_{CBO_2}}{1 - (\alpha_1 + \alpha_2)} \end{aligned}$$

The collector-emitter current gains (α_1, α_2) can be expressed in terms of the collector-base current gains (β_1, β_2) as:

$$\alpha_1 = \frac{\beta_1}{1+\beta_1} \qquad \alpha_2 = \frac{\beta_2}{1+\beta_2}$$

Substituting these into the equation above yields:

$$I_L = \frac{I_{CBO_2}}{1 - \left(\frac{\beta_1}{1+\beta_1} + \frac{\beta_2}{1+\beta_2} \right)}$$

$$I_L = I_{CBO_2} \left[\frac{(1+\beta_1)(1+\beta_2)}{1-\beta_1\beta_2} \right]$$

ELSEVIER

Thin Solid Films 383 (2001) 287–291

www.elsevier.com/locate/tsf

Mo-capped Al–Nd alloy for both gate and data bus lines of liquid crystal displays

Toshiaki Arai*, Atsuya Makita, Yasunobu Hiromasu, Hiroshi Takatsuji

IBM Display Business Unit, 1623-14 Shimo-tsuruma, Yamato-shi, Kanagawa 242-8502, Japan

Abstract

Aluminum–neodymium (Al–Nd) alloy and molybdenum (Mo)-capped structures were applied to both gate and data bus lines of liquid crystal displays (LCD). We investigated the hillock resistance and electrical properties of Al–Nd alloys. Their structures were studied by cross-sectional transmission electron microscopy (TEM) and SEM. Adding 2 at.% Nd to Al effectively prevented the Al film from forming hillock and whisker. The electrical resistivity varied with the annealing temperature after deposition: the resistivity was 4.3 μΩ cm with annealing at 350°C and 10.0 μΩ cm with annealing at 250°C. Mo is used not only to suppress hillocks, but also for taper etching of lines and as a contact layer with other materials. We investigated the effects of adding Nd to Al, and found that the Nd addition improved the step coverage, thermal resistance, patternability, and mechanical strength of the lines. By applying a common structure and metals for both gate and data bus lines, we could increase the productivity of TFT-LCDs. © 2001 Elsevier Science B.V. All rights reserved.

Keywords: Aluminum; Neodymium; Capped structure; Hillock

1. Introduction

Bottom-gate thin-film transistors (TFT) have been widely investigated for use in active-matrix liquid crystal displays (AMLCD). In recent years, the panel size and resolution of AMLCDs have increased dramatically, and much effort has been devoted to developing low-resistivity gate bus lines, to meet the need for large, high-resolution LCDs [1,2]. Aluminum (Al) is a nearly ideal material for gate bus lines, because of its low resistivity, low material cost, high adhesion, and superior patternability. However, during high temperature processes such as the deposition of insulator films by chemical vapor deposition (CVD), aluminum is susceptible to stress-migration phenomena, which can cause defects as a result of short-circuits.

The thermal expansion mismatch between Al and the glass substrate produces large compressive stress in the Al film upon heating, and results in the stress-migration to relax the stress [3–5]. Al-based alloys have been studied to minimize hillock formation, and it is known that Al rare earth alloys have high hillock resistance [6–9]. On the other hand, several structures have also been studied to increase the hillock resistance such as anodizing and metal-capped structure [1,2,9,10]. These alloys and structures were studied for gate bus lines. However, if we can use the same metals and structure for both gate and data bus lines, we can use the same equipment and increase productivity.

In our study, aluminum–neodymium (Al–Nd) alloy and molybdenum (Mo)-capped structures were applied to both gate and data bus lines. Capped Mo works as not only a hillock suppressing layer but also aids in taper etching of lines and acts as a contact layer with other materials. In the case of a data bus line, Mo was also added as the bottom layer to prevent the Al from reacting with the n^+ a-Si layer. We fabricated AMLCDs using the same sputtering and etching tools and the same etchant for both gate and data bus lines, which can increase productivity dramatically.

* Corresponding author. Tel.: +81-46-215-2147; fax: +81-46-274-6894.

E-mail address: araitoshi@jp.ibm.com (T. Arai).

PII: S0040-6090(00)01794-6

2. Experiment

The hillock densities of Al and Al–Nd alloys were studied after annealing at 300, 350, and 400°C. Al and Al–Nd alloys were deposited on 5-inch^2 LCD grade glass substrates. Alloys with a range of compositions (0–2 at.% Nd) were deposited in a DC magnetron sputtering tool with an argon gas pressure at 0.4 Pa and a substrate temperature at 120°C from alloy targets. The films were 250–300 nm thick. Hillocks in an area of 0.003–1 mm^2 were counted using a polarized optical microscope.

The sheet resistance of the films was measured with a four-point-probe resistance testing system (Napson RT-8S), and resistivity was calculated from the sheet resistance and the film thickness, which was measured by a surface profiling system (Tencor P-1). An Al–Nd alloy with a nominal Nd composition of 2 at.% was deposited from an alloy target. The samples had a film thickness of 220 nm, and were annealed at 250, 300, 350, and 400°C in a nitrogen atmosphere for 20 min.

Step coverage of Al and Al–Nd (2 at.%) alloys were examined by TEM after samples had been prepared by focused ion-beam (FIB) etching. The steps were fabricated by the wet etching of two layered CVD films, which had different etching rates. For the process test, 360 × 465 mm glass substrates were used.

Voids, hillocks, and mouse bites were observed by SEM (Hitachi S-800). For the observation of whiskers, MoW was used as the gate metal.

Film hardness of Al and Al–Nd alloys were measured by a nano-indentation tester (ELIONIX ENT-110a) at loads of 50 mgf using a triangular diamond pyramid stylus with the angle of 115°. Al–Nd (2 at.%) alloy was sputter-deposited at a substrate temperature of 150°C. The samples had a film thickness of 350 nm, and were annealed at 250, 300, 350, and 400°C in a nitrogen atmosphere for 20 min.

3. Results and discussion

The use of Al–Nd alloys with a Mo-cap was studied as the gate metal for bottom-gate TFTs. For a gate insulator that has a low pin-hole density and a high breakdown voltage, a CVD deposition of 350°C (approx.) is required. Fig. 1 shows the hillock densities of Al–Nd films after 300, 350, and 400°C annealing.

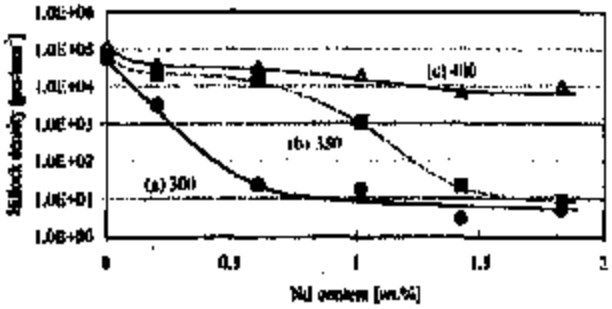

Fig. 1. Hillock density vs. Nd content: (a) 300°C annealed, (b) 350°C annealed, and (c) 400°C annealed.

Higher annealing temperatures resulted in higher hillock densities, and a higher Nd content suppressed hillock formation. The suppression of hillock growth is believed to be caused by the segregation of Nd as a second-phase precipitate at the Al grain boundaries, with the segregated Nd suppressing the migration of Al at the grain boundary, which leads to hillocks or whiskers. More than 1.4 at.% of Nd was found to effectively suppress hillock formation at annealing at 350°C. Therefore, we decided to apply 2 at.% Al–Nd alloy for the gate metal, to allow a margin for various process variations such as process temperature fluctuation and Nd content variation in the sputtering targets.

However, considering the total area of the storage capacitor and crossover between gate lines and data lines this hillock density (1.0E + 01 pcs/mm^2 at 2 at.%-Nd) is not sufficient to allow the fabrication of high resolution, large area TFT-LCDs. Therefore, we also used a Mo-capped structure for the gate line shown in Fig. 2. Top Mo layer suppressed hillock formation on the top of gate lines. The Mo does not cover the tapered edges of Al–Nd, but the Nd suppresses the formation of hillocks there.

We applied this Mo/Al–Nd structure for both gate and data bus lines. Mo is not only used as a hillock suppressing layer but also aids in taper etching of lines and acts as a contact layer with other materials. In the case of data lines, a bottom Mo layer was also used for the contact with the n + a-Si-layer and to prevent the aluminum from reacting with the n + a-Si-layer. Both

Fig. 2. Schematic cross-sectional views of TFT, storage capacitor, and TAB-pad.

Mo/Al–Nd layers and Mo/Al–Nd/Mo layers were patterned by wet etching [10], and taper angles of 20–40° were obtained by this etching method. To get such low taper angles, dip etching is generally applied. Of late, dry etching of the Al with a high-density plasma source has been extensively studied [11]as the etchant cost with dry etching is much lower than that with wet etching. If we apply dry etching, other contact metals such as titanium (Ti) or tungsten (W) can be used in this structure.

In a typical TFT process flow, the highest process temperature for the gate line is the gate insulator deposition — approximately 350°C. For the data line, the highest process temperature is the passivation insulator deposition, at approximately 250°C.

Fig. 3 shows the resistivity of the Al–Nd (2 at.%) alloy and pure Al after annealing at 250, 300, 350, and 400°C. The resistivity dramatically decreased between 250 and 300°C. This phenomenon is believed to be caused by the segregation of Nd and the grain growth of the Al, which mainly happened between 250 and 300°C. Resistivities of 4.3 μΩ cm and 10.0 μΩ cm were obtained for gate line and data line, respectively. The resistivity of the data line is much higher than that of gate line, but the resistivity of gate lines is a more serious design consideration for high-resolution panels,

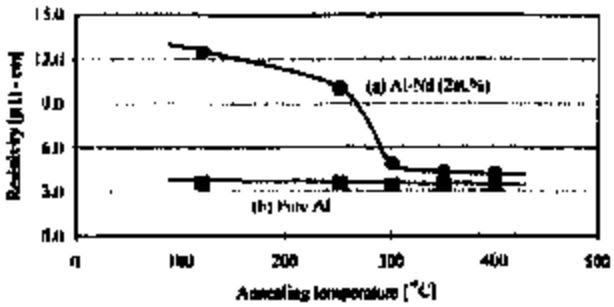

Fig. 3. Resistivity vs. annealing temperature: (a) Al-Nd (2 at.%) alloy, and (b) pure Al.

because the charging time for each line becomes shorter as the resolution increases [12,13].

With Al–Nd alloy for data lines, the step coverage was improved. Fig. 4 shows the difference of step coverage between Al–Nd alloy and pure Al after overcoating with an insulator. These steps were fabricated by the wet etching of two-layered CVD films, which had different etching rates. In the case of pure Al, the step coverage was poor, Al was almost discontinuous over the step and a void was formed in the passivation layer. The Al–Nd data line had adequate step coverage and is suitable for connecting metal layers with via-

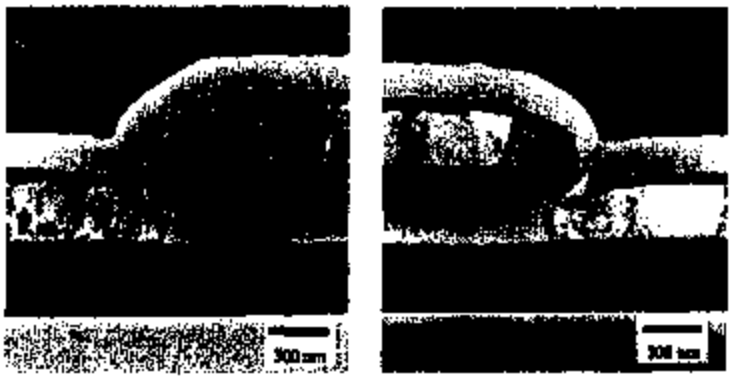

Fig. 4. Cross-sectional TEM views: (a) Al-Nd (2 at.%) alloy, and (b) pure Al.

Fig. 5. SEM views of patterned lines: (a) Mo/Al-Nd (2 at.%)/Mo, and (b) Mo/pure Al/Mo.

Fig. 6. SEM view of whisker on TFT.

holes. The grain size of the Al–Nd is finer than Al (see Fig. 4). We suppose that the improved step coverage with the Al–Nd is due to the finer grain size and reduced grain growth, which may tend to open-up grain boundary and reduce the step coverage.

Fig. 5 shows a top view of a Mo/Al–Nd/Mo line and a Mo/pure Al/Mo line. The grain size of pure Al is much larger than that of Al–Nd, and there were voids and small hillocks at the grain boundary triple points. The Mo/pure Al/Mo data bus lines occassionally showed whisker formation during passivation CVD deposition, resulting in shorting defects between the source and drain electrodes (see Fig. 6). The Al–Nd alloy never formed whiskers. Moreover, pure Al also had 'mouse bite' defects on the edges of data lines. We believe that a reaction between Al and Mo caused this 'mouse bite' defect. With Al–Nd, no 'mouse bite' defects were observed and smooth edges resulted after etching. The Al–Nd data line had a smooth surface without voids, hillocks, whiskers and mouse bites, and can reduce the within-layer and layer–layer shorts problem.

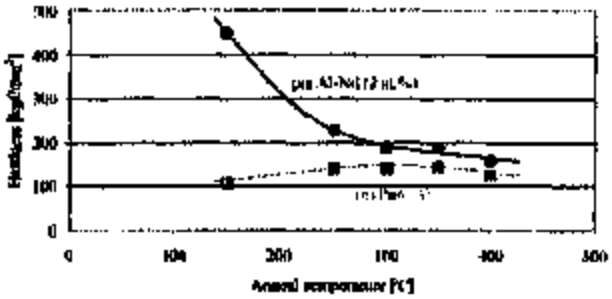

Fig. 7. Hardness vs. annealing temperature: (a) Al-Nd (2 at.%) alloy, and (b) pure Al.

Fig. 7 shows the hardness measured by nano-indentation of Al–Nd and pure Al after 250, 300, 350, and 400°C annealing. The hardness of the Al–Nd alloy decreased as the annealing temperature increased. This decrease in hardness is believed to be caused by the segregation of Nd and the grain growth of the Al. After annealing at 250°C, the hardness of Al–Nd (2 at.%) alloy was 60% higher than that of pure Al. On an AMLCD panel, the bus metals on the tape-automated-bonding (TAB) area are exposed to air or contacted with a TAB. In the TAB process, some defective TABs are removed and repaired. After removing a TAB, the surface is cleaned with a wipe. After cleaning the surface of a pure Al pad after removing a TAB shows many scratches (see Fig. 8). Many hillocks were also observed due to thermal cycling during passivation deposition. These scratches can result in open or corrosion problems. With an Al–Nd alloy pad after TAB removal, no hillocks and only slight scratches were observed. The Al–Nd line is mechanically strong and resists scratches from TAB repair.

In the conventional process, MoW is used for the gate line and Mo/Al/Mo for the data line. Separate deposition and etching tools were used here because the etching method (dry and wet), photo-resist stripping method (chemical, ashing and wholly chemical),

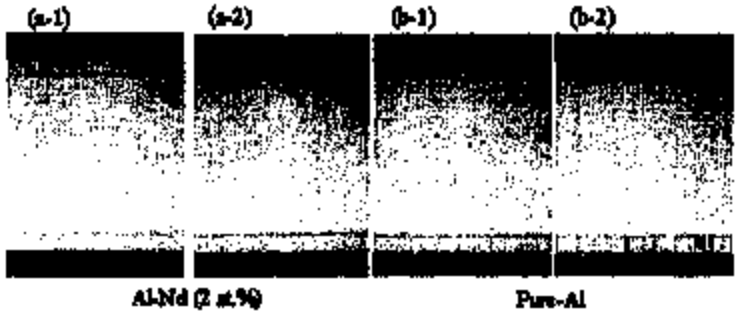

Fig. 8. Photographs of TAB-pads: (a-1) Al-Nd (2 at.%) alloy before scratch test; (a-2) Al-Nd (2 at.%) after scratch test and surface cleaning; (b-1) pure Al before scratch test; and (b-2) pure Al after scratch test and surface cleaning.

and sputtering targets were different. We applied 2 at.% Al–Nd alloy for both gate and data bus lines. By using a common Mo-capped structure and Al–Nd alloy, common tooling (etcher, photo-resist stripper, and sputter) and chemicals (etchant, stripper, and sputtering targets) could be used This increased the productivity.

4. Conclusion

We investigated the hillock densities and resistivity of Al and Al-Nd alloy, and applied 2 at.% Al–Nd alloy for both gate and data bus lines.

The resistivity of 4.3 μΩ cm and 10.0 μΩ cm were obtained for gate line and data line, respectively. Al–Nd alloy had adequate step coverage and resulted in smooth surface without voids, hillocks, whiskers and mouse bites after patterning and insulator deposition. Al–Nd alloy was 60% harder than pure Al after 250°C annealing, and mechanically strong so that it resists scratches during TAB rework. Applying common structure and metals for both gate and data bus lines, we could increase the manufacturing productivity for TFT-LCDs, improve the step coverage, suppress hillock, improve patternability, and increase mechanical strength of the lines.

Acknowledgements

We are grateful to T. Ueki, H. Ueda and N. Tsujimura of IBM Display Business Unit and E. Colgan of IBM Research Division for their support on the publication of this paper, and the engineers at DTI (Display Technologies Inc.) for their devoted contributions to the development of these technologies. We would also like to thank K. Tsujimoto of IBM Display Business Unit for his TEM observations, and T. Uematsu of ELIONIX for his nano-indentation test measurements.

References

[1] T. Tsukada, MRS Symp. Proc. 284 (1993) 371–382.
[2] C.W. Kim, J.H. Lee, H.R. Nam, S.Y. Kim, C.O. Jeong, J.H. Choi, M.F. Hong, H.S. Byun, H.G. Yang, J.H. Souk, in: Proceedings of Euro Display '96 SID, 1996, pp. 591–594.
[3] G. Smith, N. Kristensen, F. Ericson, J.-A. Schweitz, J. Vac. Sci. Technol. A9 (4) (1991) 2527–2535.
[4] E. Iwamura, T. Ohshiki, K. Yoshikawa, K. Inpama, J. Vac. Sci. Technol. A12 A12 (5) (1994) 2922.
[5] T. Onishi, E. Iwamura, K. Takagi, K. Yoshikawa, J. Vac. Sci. Technol. A14 (5) (1996) 2728.
[6] S. Takayama, N. Tsujsei, J. Vac. Sci. Technol. A14 (4) (1996) 2499–2504.
[7] T. Onishi, E. Iwamura, K. Takagi, T. Watanabe, J. Vac. Sci. Technol. A15 (4) (1997) 2339–2348.
[8] H. Takatsuji, H. Iyori, S. Tsuji, K. Tsujimoto, K. Kuroda, H. Saka, Mat. Res. Soc. Symp. Proc. 471 (1997) 99–104.
[9] T. Arai, H. Iyori, Y. Hiromasa, M. Atsumi, S. Ioku, K. Furuta, IBM J. Res. Dev. 42 (3/4) (1998) 491–499.
[10] T. Tsujimura, H. Kitahara, A. Makita, P. Fryer, J. Batey, Conference Record, International Display Research Conference, 1994, pp. 424–427.
[11] R. Christie, S. Johnston, D. Kuriakose, J. Barlow, Proceedings of IEEE/SEMI Advanced Semiconductor Manufacturing Conference and Workshop, 1994, pp. 34–36.
[12] W.E. Howard, Conference Record of the 1994 SID International Display Research Conference, 1994, pp. 6–10.
[13] E.G. Colgan, P.M. Fryer, E. Galligan, W. Graham, R. Horton, D. Hunt, L. Jenkins, R. John, P. Kohn, Y. Kuo, K. Lipske, F. Libsch, A. Lien, J. Lovas, R. Nywening, R. Polastre, M.B. Rothwell, J. Wilson, R. Winkeff, S. Wright, International Display Workshop, 1996, p. 29.

ELSEVIER

Thin Solid Films 300 (1997) 25–29

Thin Solid Films

Electromigration in layered Al lines studied by in-situ ultra-high voltage electron microscopy

H. Mori [a,*], H. Okabayashi [b], M. Komatsu [a]

[a] Research Center for Ultra-High Voltage Electron Microscopy, Osaka University, Yamadaoka, Suita, Osaka 565 Japan
[b] Research and Development Group, NEC Corporation, 34 Miyukigaoka, Tsukuba 305 Japan

Received 3 May 1996; accepted 7 November 1996

Abstract

In-situ side-view transmission electron microscopy (TEM) observations of electromigration in Al-on-TiN lines with a drift velocity measurement structure have been carried out using an ultrahigh voltage (2 MV) electron microscope. Thick chips as-diced from silicon substrates served as TEM samples. The observations revealed the dynamic behavior of electromigration-induced voids and hillocks during forward and reverse current feeding through the Al lines. The results include vertical growth of voids bounded by-faceted Al, refilling of voids, void growth in a hillock upon current reversal, and whisker growth. © 1997 Elsevier Science S.A.

Keywords: Aluminium; Electromigration; Electron diffraction; Electron microscopy

1. Introduction

In-situ observations of electromigration (EM) in Al lines for integrated circuits have employed various microscopy techniques, such as scanning electron microscopy (SEM) [1] and transmission electron microscopy (TEM) (see, for example, Refs. [2–5] and references cited therein). So far, TEM observations have been conducted solely in the plan-view mode, and such aspects as the preferential void evolution at the three-fold node of grain boundaries have been revealed [2]. However, in plan-view observations, it is difficult to obtain the vertically-resolved (in the depth direction) information on the microstructure in Al lines. Such depth-resolved information is indispensable for analyzing electromigration in the layered lines which are currently used in advanced LSIs, because the interlayer interfaces may play an essential role in these lines. Furthermore, in plan-view TEM samples, the Si substrate has to be locally thinned to a thickness of electron transparency. In such samples a non-uniform stress distribution due to both the local thinning and the local joule heating along Al lines is often induced, which eventually leads to bending of the samples.

To overcome these drawbacks, we have developed a side-view TEM technique, in which an Al line on a thick substrate is observed with a high voltage electron microscope (HVEM) with the incident beam parallel to the substrate surface and perpendicular to the Al line [6,7]. This technique utilizes the ability of HVEM to observe relatively thick samples. Additionally, since the substrate does not need to be thinned, difficulties encountered in the preparation and observation of conventional plan-view TEM samples can be avoided. With the use of this technique, the detailed behavior of EM-induced gaps which are formed between the cathode and the anode in Al-on-TiN lines has been studied [6]. Also, the growth process of voids at the cathode in Al–0.5 wt.% Cu-on-TiN lines has been examined [7].

In the present work, successive stages of EM-induced void formation at the cathode and of EM-induced hillock formation at the anode in Al-on-TiN lines have been investigated by the side-view TEM technique.

2. Experimental procedures

An Al-on-Ti/TiN line with a drift-velocity measurement structure, which provides information on electromigration in a line without reservoirs, was fabricated on an oxidized Si wafer [6]. This structure consisted of an Al overlayer lying on the central part of a Ti/TiN underlayer

* Corresponding author. Tel: +81 6 875 0828; fax: +81 6 875 0449; e-mail: s62217s@center.osaka-u.ac.jp

PII S0040-6090(96)09517-X

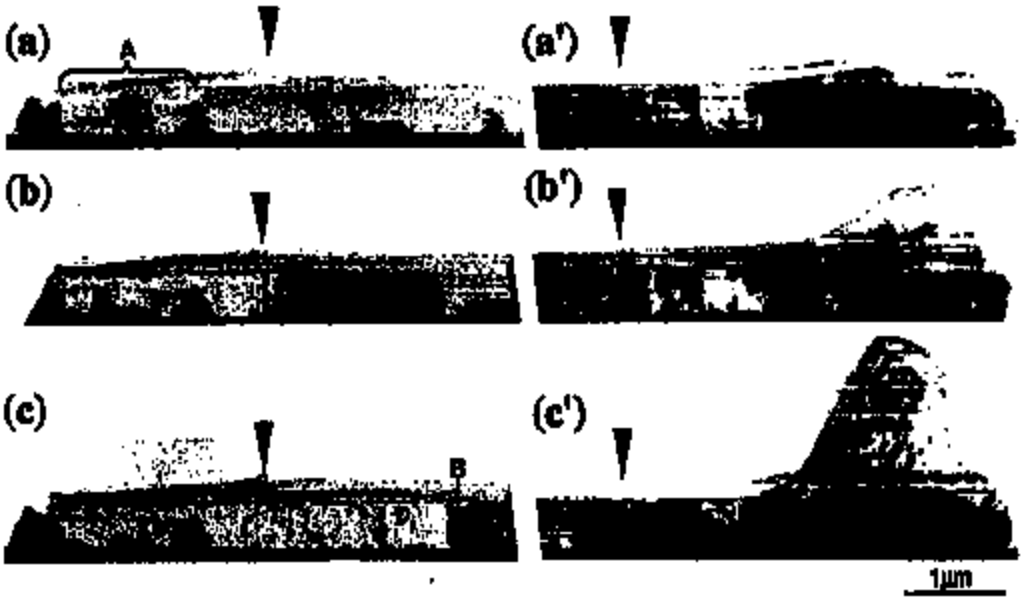

Fig. 1. Successive stages of electromigration in an Al-on-TiN line observed by side-view TEM. Damage evolution at the cathode and the anode of the line during current feeding in the forward direction are depicted in (a)–(c) and (a')–(c'), respectively. Current feeding time t for each figure is as follows: (a) t = 720 s, (b) t = 2.8 ks, (c) t = 7.4 ks, (a') t = 1.6 ks, (b') t = 2.9 ks, and (c') t = 7.6 ks.

conductor [6]. Both the Ti and TiN layers were 0.2 μm thick. The length of the Ti/TiN portion between the bonding pad and the Al was 120 μm. The Al was 0.7 μm wide, 0.5 μm thick, and 100 μm long. The samples used in these experiments varied in width of Ti/TiN underlayer. Sample 1 had a pure Al line on top of a 2 μm wide Ti/TiN underlayer and Sample 2 also had a pure Al line, but the Ti/TiN underlayer was 0.7 μm wide.

The Al lines were not passivated, but a thin photoresist layer remained on the surface after washing in an oxygen

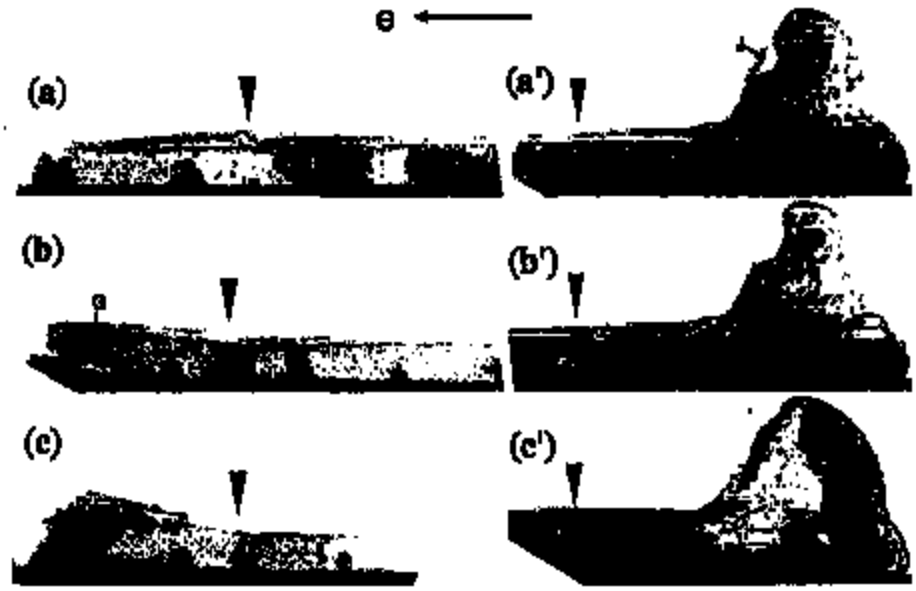

Fig. 2. Electromigration-induced damage at the (new) anode and the (new) cathode of the line during current feeding in the reverse direction are depicted in (a)–(c) and (a')–(c'), respectively. Current feeding time t_r (after the reversal) is as follows. (a) t_r = 1.1 ks, (b) t_r = 11.9 ks, (c) t_r = 15.9 ks, (a') t_r = 2.5 ks, (b') t_r = 2.8 ks, and (c') t_r = 15.7 ks. The black triangle-shaped arrows in Fig. 1(a)–1(c)Fig. 2(a)–2(c) indicate a fixed position of the sample, and those in Fig. 1(a')–1(c')Fig. 2(a')–2(c') another fixed position. The width of the Ti/TiN layer in this sample was 2 μm.

atmosphere. The fabricated wafers were annealed in nitrogen gas at 723 K for 1.8 ks. The Al line exhibited a near-bamboo structure. A chip, ~0.5 mm × ~6 mm in size and 0.45 mm thickness, was then diced from the wafer and served as the side-view HVEM sample. Neither the Al lines nor the silicon substrates were thinned prior to observation.

The Al lines were directly observed from the side with an HVEM operating at an accelerating voltage of 2 MV. The sample was heated during observation by the Joule heating predominantly at the Ti/TiN portions without overlayer Al. The temperature of the Al was not measured, but a comparison of the drift velocities obtained by in-situ HVEM experiments with those from standard accelerated measurements suggested that the average temperature of the Al may have been between 573 and ~623 K.

The results of the experiment using Sample 1 are shown in Fig. 1. A current of 50 mA (current density $j = \sim 13$ MA cm^{-2}) was first fed for ~14 s. This stressing time was limited by the melting of the solder which bonded the current feeding wires to the electrodes of the HVEM sample holder. After the solder bonds were repaired, the in-situ observation was resumed at a current of ~26 mA ($j = \sim 6.5$ MA cm^{-2}). After feeding for 7.8 ks, the current direction was reversed and the observations were continued for 16.2 ks; these results are shown in Fig. 2. (In the text and the caption referring to Figs. 1 and 2, the feeding times of a 26 mA current before and after the current reversal are designated as t and t_r, respectively).

The results of the experiment using Sample 2 are shown in Figs. 3 and 4. Current was fed only in one direction in this case.

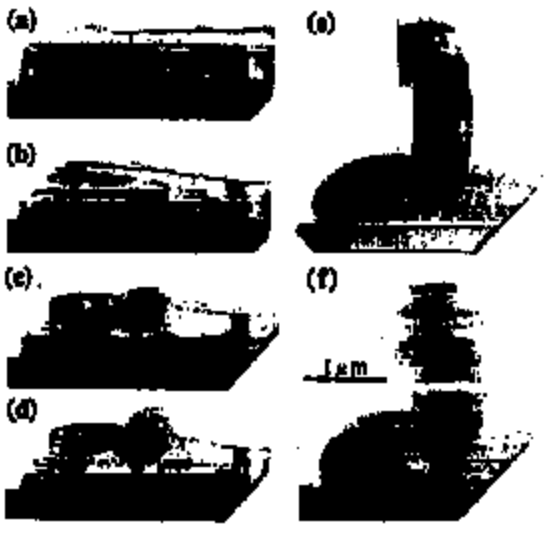

Fig. 3. Successive stages of whisker growth at the anode of an Al-on-TiN line. In this experiment, a 19 mA current was first fed for 5.5 ks and then the current was increased to 25 mA. Current feeding time t is as follows: (a) $t = 0$ s, (b) $t = 4.08$ ks, (c) $t = 5.70$ ks, (d) $t = 6.16$ ks, (e) $t = 9.70$ ks, and (f) $t = 12.48$ ks. Electrons flowed from right to left. The width of the Ti/TiN layer in this sample was 0.7 μm.

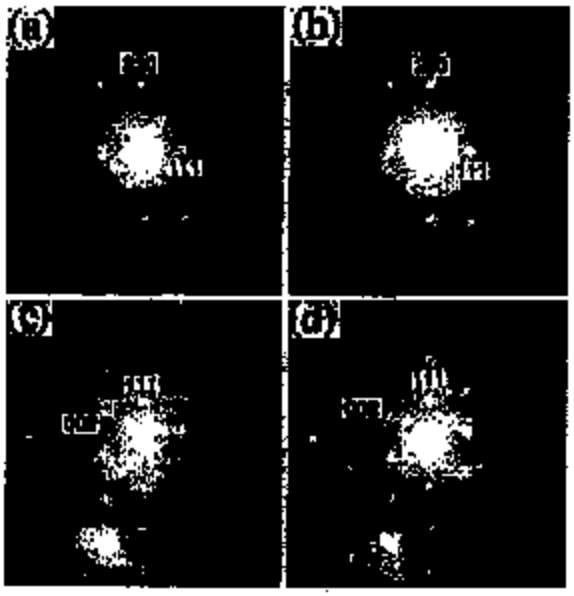

Fig. 4. Selected area electron diffraction (SAED) patterns taken from the whisker and the Al line shown in Fig. 3(e). (a) and (b) are taken from positions A and B in Fig. 3(e) respectively, while (c) and (d) are from positions C and D respectively.

3. Results and discussion

3.1. EM-induced damage at the cathode and the anode in forward current feeding

Fig. 1(a) is a bright-field (BF) image of the cathode of an Al-on-TiN line after feeding of the 26 mA current for 720 s (i.e. $t = 720$ s). A locally depleted region (A) was formed adjacent to the cathode edge. The same area after feeding for 2.8 ks (i.e. $t = 2.8$ ks) is presented in Fig. 1(b), where it is shown that the depleted region extended ~2.5 μm towards the anode from the cathode edge. Fig. 1(c) shows the same area at $t = 7.4$ ks. At this stage, the depleted region extended over ~4.4 μm from the cathode edge.

Two points are noteworthy in Fig. 1(c). (1) One of the characteristic depletion modes verified by side-view TEM appears at B in front of the large depleted region in the figure. Void growth proceeds towards the substrate within a single grain; the top surface of the remaining material at B is (111) faceted. In some cases, this type of voiding proceeded grain by grain sequentially from the cathode end [7]. (2) Small Al islands are formed on the inner surface of the natural oxide film covering the depleted region. Similar islands on the inner surface of the top and bottom natural oxide films were observed in Ref. [4].

Islands close to the front of the growing depleted region were smaller than those further away. For example, the diameter of island D, located near the front, was about 10 nm, whereas that of island C, further from the front, was about 100 nm. This suggests that islands grow by the diffusion and coalescence of Al atoms left on the inner surface of the oxide film [4]. Larger islands further from the front simply reflect the extra time for diffusion and coalescence. The presence of well-defined facets associated with voids in front of the large depleted region, such as a facet seen at B in Fig. 1(c), shows that Al does not melt there and that melting of Al is not a cause of the island formation.

Fig. 1(a′) is a BF image of the anode of the same line after feeding of the 26 mA current for 1.6 ks ($t = 1.6$ ks), where a small hillock is noticed to be formed at the anode. In Fig. 1(b′), which was taken from the same area at $t = 2.9$ ks, it is shown that the hillock grew to a height of approximately 0.9 μm. As seen in this figure, some grains within this hillock exhibited brightness completely different from those of the grains composing the original line, while other grains showed diffraction contrast reminiscent of the epitaxy of the corresponding grains in the line. This fact suggests that hillocking took place not only via an epitaxial growth process but via a nucleation and growth process and differently oriented grains were formed on the top surface of the anode. The microstructure at the interface between the original bamboo grains and the hillock, which might shed light on the mechanism behind the hillocking, is unfortunately not well resolved in this micrograph. The same area after feeding current for 7.6 ks is shown in Fig. 1(c′). At this stage, the height of the hillock reached approximately 1.7 μm. In one of grains composing the hillock, there appears a series of equal thickness fringes, as seen at E in Fig. 1(c′). From the intervals between the neighboring fringes, it is possible to obtain information on the three-dimensional shape of the hillock. In the present case, a hillock in the shape of a dome was deduced from such an analysis, and the shape was in agreement with the result by an independent SEM observation.

3.2. EM-induced damage at the cathode and the anode in reverse current feeding

The cathode before the current-direction reversal served as the anode after the reversal; thus, healing of the depletion damage was expected to occur there. Fig. 2(a) is a BF image of the anode after the current-direction reversal, which was taken at $t_r = 1.1$ ks. This area is the same as that shown in Fig. 1(a)–(c). It is evident from a comparison of Fig. 1(c) with Fig. 2(a) that the preferentially-voided portion B in Fig. 1(c) had already been annihilated at this stage, and aluminum began to fill the depleted region (grain F in Fig. 2(a)). Fig. 2(b) shows the same area at $t_r = 11.9$ ks. The depleted region was now completely filled with aluminum and even a small hillock was formed at the anode (G in Fig. 2(b)). In the grain associated with the hillock, a high density of dislocations was observed (H in Fig. 2(b)). This fact suggests that hillocking of this type took place under somewhat stressed conditions. Possible origins of the stress field are: (1) bending of the grain due to a bulge of underlying grain(s) (I in Fig. 2(b)); and (2) compression due to the mass accumulation. More experiments are necessary to clarify the nature of the stress field. In Fig. 2(c), which shows the same area at $t_r = 15.9$ ks, it is seen that the hillock grew to a height of approximately 0.5 μm in this final stage.

The anode before the current-direction reversal served as the cathode after the reversal; thus, depletion was expected to occur there. Fig. 2(a′) is a BF image of the cathode after the current-direction reversal that was taken at $t_r = 2.5$ ks. This area is the same as that shown in Fig. 1(a′)–1(c′). Voiding did not occur at the Al/TiN interface at the cathode where a high current density is expected, rather it took place halfway up the hillock (J in Fig. 2(a′)). The current density at site J is supposed to be quite low. In high magnification images of the hillock before current reversal (not shown here), a thin line appeared which intersected the surface at a position almost identical with site J in Fig. 2(a′). The thin line might correspond to a grain boundary, a dislocation line, or a slip trace of dislocations. This observation suggests that the void might have nucleated preferentially at a surface defect site. With continued current feeding, this void grew (Fig. 2(b′) at $t_r = 2.8$ ks), and eventually the interior of the hillock was almost completely depleted, leaving only the natural oxide film and the photoresist residue which had covered the hillock (Fig. 2(c′) at $t_r = 15.7$ ks).

3.3. Whisker growth at the anode

Fig. 3 shows an example of whisker growth at the anode, which was observed in another pure Al sample. In this experiment, a 19 mA current ($j = \sim 5$ MA cm^{-2}) was first fed for 5.5 ks and then the current was increased to 25 mA ($j = \sim 6.5$ MA cm^{-2}). Fig. 3(a) is a BF image of the anode before current feeding. Fig. 3(b) shows the same area after feeding 19 mA for 4.08 ks, where it is seen that a small hillock formed on the anode. The same area after feeding 19 mA for 5.46 ks and 25 mA for 240 s is shown in Fig. 3(c). At this stage, a small, faceted whisker appeared on the hillock. With continued current feeding, the whisker grew (Fig. 3(d) and 3(e)), and eventually the height of the whisker reached to approximately 1.6 μm (Fig. 3(f)). Fig. 4 shows a series of selected area electron diffraction (SAED) patterns taken from the whisker and the Al line: the SAED patterns in Fig. 4(a) and 4(b) were taken respectively from positions A and B of the whisker in Fig. 3(e), while those in Fig. 4(c) and 4(d) were taken respectively from positions C and D of the line in Fig. 3(a). The former two patterns are identical to each other

and they can be indexed as the ~[112] aluminum diffraction pattern. The long axis of the whisker is almost parallel to the [110] direction. The latter two patterns can be indexed as the ~[110] aluminum pattern. The normal to the original top surface of the Al line (i.e. the normal to the Si substrate) is nearly parallel to the [111] direction. It is concluded from Fig. 4 that the whisker had a different orientation from the grain on which it nucleated and grew.

4. Summary and conclusions

We have observed the dynamic behavior of electromigration voids and hillocks in Al-on-TiN lines by in-situ side-view TEM using an HVEM. Such side-view observations reveal information not obtainable by conventional plan-view TEM.

It was revealed that, frequently, voids were bounded by faceted Al planes and grew preferentially in the vertical direction on the anode side of grain boundaries. After reversing the current direction, voiding occurred in the hillock at the former anode, not at the Al-underlayer interface, where current crowding was expected.

Polycrystalline hillocks grew partly in epitaxy to the grains in the line. A whisker, however, was found to have a crystallographic orientation different from the grains in the line.

Acknowledgements

We would like to thank Professor H. Nishihara and Dr H. Watanabe for their encouragement. We would also like to thank Dr D. Grosjean for reading the manuscript.

References

[1] See for example, the following papers and references cited therein: R.W. Thomas and D.W. Calabrese, *Proc. 1983 IEEE Int. Reliability Phys. Symp.*, The Institute of Electrical and Electronics Engineer, Inc., New York, 1983, p. 1; T.N. Marieb, E. Ahmetowski, J. Bowman, M. Madden and P. Flinn, in P.S. Ho, C-Y. Li and P. Totta (eds.), *Stress-Induced Phenomena in Metallization*, AIP Conference Proc. 305, AIP, New York, 1994, p. 1.
[2] L. Berenboom, *J. Appl. Phys.*, 42 (1971) 880.
[3] A. Takeuchi, N. Okuyo and K. Ura, *Microsc. Microanal. Microstruct.* 4 (1993) 229.
[4] C.Y. Chang and R.W. Vook, *Thin Solid Films*, 225 (1993)23.
[5] E.P. Riege, A.W. Hunt and J.A. Prybyla, in A.S. Gates, W.F. Filter, R. Rosenberg, A.L. Greer and K. Gadepally (eds.), Materials Reliability in Microelectronics V, *Mater. Res. Soc. Symp. Proc.*, Vol. 391, Mater. Res. Soc., Pittsburgh, PA, 1995, p. 249.
[6] H. Okabayashi, H. Kitamura, M. Komatsu and H. Mori, *Appl. Phys. Lett.*, 68 (1996)1066.
[7] H. Okabayashi, M. Komatsu and H. Mori, *Jpn. J. Appl. Phys., Part 1*, 35 (2B) (1996)1102.

ELSEVIER

Thin Solid Films 290–291 (1996) 248–253

Thin Solid Films

Residual stress and in-situ thermal stress measurement of aluminum film deposited on silicon wafer

K. Kusaka [a], T. Hanabusa [a], M. Nishida [b], F. Inoko [a]

[a] *Department of Mechanical Engineering, Tokushima University, Minamijosanjima, 2-1, Tokushima 770, Japan*

[b] *Polytechnic College, Kagawa, Gunge-cho, Marugame 763, Japan*

Abstract

Residual stresses in aluminum film deposited on a silicon wafer were measured after annealing and quenching. In all cases, residual stresses were tensile, but slow cooling produced larger stresses than quenching. Residual stresses of slow-cooled samples became relaxed after annealing above 300 °C. Film passivation by carbon deposition retarded the relaxation of residual stress. In-situ X-ray stress measurement revealed that compressive stresses developed in a heating stage and tensile stresses in a cooling stage. From a scanning electron microscopy observation, it becomes clear that the former contributes to nucleation of hillocks and the latter to void formation and growth.

Keywords: Aluminum; Internal stress; Stress migration; X-ray stress measurement

1. Introduction

Residual stresses in thin films deposited on substrates [1–5] are an important yardstick on the reliability of film/substrate systems. Large residual stresses cause cracks in the film or delamination of the film from the substrate. If the temperature changes in these systems, thermal stresses develop in the film because of a mismatch in the coefficient of thermal expansion between film and substrate [6–10]. A large temperature change produces large stresses which may induce plastic deformation as well as creep deformation in the film. With large scale integration (LSI) technologies, on the other hand, aluminum film is used in the electronic circuits and the width of interconnect line structures becomes progressively smaller, e.g. less than half a micrometer. Breaking of the fine line as well as short circuits between the adjacent lines have been observed under the application. Voids and hillocks that have developed by applied stress and electronic current are the reason of these phenomena [11–14]. The phenomena of these faults based on the stresses in film or lines are called stress migration [15,16]. Knowledge on the internal stresses in thin structures is important to understand the mechanism of formation of such faults.

The purpose of this study is to investigate a basic mechanism of stress migration. A two-tilt X-ray method is proposed for the measurement of stress in aluminum film with {111} orientation. Residual stresses in the aluminum film deposited on a silicon wafer were measured after annealing and quenching at various temperatures. The effect of passivation by carbon film was also investigated. In-situ X-ray stress measurement was made to investigate a change in thermal stresses during heating and cooling processes. Voids and hillocks that had developed in the aluminum film were observed in the process of heat treatment by scanning electron microscopy.

2. X-ray stress measuring method for aluminum film

In general, the so-called $\sin^2\psi$ method is used in X-ray stress measurement. In this method, it is assumed that the material is composed of fine crystals with random orientation and that the stress state is biaxial and homogeneous through the X-ray penetrating region. Under these assumptions, the lattice strains at any angle ψ, which is defined by the angle between the normal of the specimen surface and the normal of the *hkl* plane, relate linearly against $\sin^2\psi$. The stress is calculated from the gradient of ε_ψ–$\sin^2\psi$ relation with the help of X-ray stress constants. However, as we will see precisely in the following, the Al films deposited on a thermally oxidized Si substrate has a strong preferred orientation; {111} of Al crystal becomes parallel to the macroscopic surface. The $\sin^2\psi$ method cannot be adopted in such a case.

For an Al film with a {111} preferred orientation, we make the following assumptions:

1. the stress state is equiaxial plane stress;
2. the <111> plane of aluminum crystal is perpendicular to the film surface; and

PII S0040-6090(96)09056-6

3. the film is composed of small crystals with 2π rotational freedom about the <111> axis.

On the basis of these conditions, the lattice strain ε_{hkl} is represented by the following equation:

$$\varepsilon_{hkl}=\left(s_{12}+\frac{1}{3}s_0\right)\sigma+\frac{1}{2}s_{44}\sigma\sin^2\psi \quad (1)$$

where $s_0=s_{11}-s_{12}-s_{44}/2$, s_{ij} are the elastic compliances of a single crystal. From the differentiation of Eq. (1) by $\sin^2\psi$, stress σ is represented by

$$\sigma=\frac{1}{s_{44}/2}\frac{\partial\varepsilon_{hkl}}{\partial\sin^2\psi} \quad (2)$$

However, ε_{hkl} values cannot be measured at an arbitrary ψ angle but at particular angles defined by crystal orientation and crystal structure. When [111] lies parallel to the surface, we obtain a strong 111 diffraction at $\psi_1=0°$. Another 111 diffraction can be obtained at $\psi_2=70.5°$ because two crystallographic planes of (111) intercept each other at 70.5° in the cubic lattice. In this case we use the following equation instead of the $\sin^2\psi$ method for the evaluation of residual stress σ:

$$\sigma=\frac{1}{s_{44}/2}\frac{\varepsilon_{\psi_1}-\varepsilon_{\psi_2}}{\sin^2\psi_1-\sin^2\psi_2} \quad (3)$$

where we use $s_{44}=3.5336\times10^{11}\ \mathrm{Pa}^{-1}$ [17].

3. Experimental procedure

3.1. Specimen and heat treatment

The Al film was deposited in vacuum on a thermally oxidized silicon (111) wafer. The conditions of Al film preparation are summarized in Table 1. Carbon-passivated films 0.02 μm in thickness were deposited on the aluminum film on some pieces. This deposition was performed in a vacuum chamber (1×10^{-2} Pa) at room temperature.

For X-ray stress measurement, small pieces each measuring $10\times10\ \mathrm{mm}^2$ were cut out from the wafer. These pieces were then heat-treated in a vacuum furnace. Five levels of temperature were selected in order to investigate the effects of heating temperature on the alteration of residual stresses in the aluminum film. After heating to the desired temperature, the specimen was kept at this temperature for 1 h and then cooled down to room temperature with slowly in the furnace or quickly in water (quenching). The conditions are summarized in Table 2.

Table 1
Conditions of depositing Al films

Purity of aluminum	99.999%
Thickness of aluminum film	1.6 μm
Substrate	SiO_2/Si (111)
Thickness of SiO_2 film	0.1 μm
Thickness of Si wafer	450 μm
Substrate temperature	200 °C
Evaporating temperature of Al films	35 nm s^{-1}
Vacuum condition during evaporation	1.3×10^{-4} Pa

Table 2
Conditions of heat treatments

Annealing temperature	200, 300, 400, 500 °C
Vacuum level	1×10^{-2} Pa
Heating rate	about 0.07 °C s^{-1}
Cooling rate:	
slow cooling in furnace	about 8×10^{-3} °C s^{-1}
quenching into water	about 200 °C s^{-1}

3.2. X-ray lattice strain measurement and its conditions

The X-ray equipment for residual stress measurement is based on parafocusing optics. A ψ diffractometer was used for the measurement of diffraction that appeared at $\psi=0°$ and 70.5°. For the measurement of in-situ thermal stress in a high-temperature vacuum furnace, parallel beam optics were used in order to avoid an experimental error occurring because of a small change in the position of the specimen surface by heating. Table 3 shows the conditions of stress measurement. Cr Kα characteristic X-rays were used for measuring 222 diffraction that appeared at $2\theta=157°$. Diffraction intensities were measured by fixed time counting and corrected by Lorentz polarization and absorption factors. From the corrected intensity distribution, $K\alpha_1$ component was separated by Rachinger's method and then the Gaussian function was fitted to the measured data by the least-squares method to determine the peak position of diffraction.

In order to measure in-situ thermal stresses during heat cycles, a small vacuum furnace was set on the diffractometer. After reaching the desired temperature, we waited for 15 min to stabilize the sample temperature before starting the measurement. The temperature deviation was within ±10 °C at 200 °C, ±5 °C at 300 °C and ±2 °C at 400 and 500 °C throughout the measurement. Temperature cycles were controlled by the computer programming, repeating heat–cool cycles with a successive increase in the maximum heating temperature. The measurement was made in both heating and cooling stages.

Table 3
Condition of X-ray stress measurement

Diffractometer	ψ diffractometer
X-ray optics	Parafocusing for residual stresses Parallel beam for in-situ thermal stresses
Characteristic X-rays	Cr Kα
Tube voltage and current	35 kV and 20 mA
Divergent angle	1°
Receiving slit	0.5 mm
Scattering angle	1°
Irradiation area	$4\times3\ \mathrm{mm}^2$
Diffraction and Bragg's angle	Al 222, 157° (in 2θ)

4. Experimental results

4.1. Structural evaluation of the deposited Al film

In order to make a quick search for the structure of Al film, a diffraction pattern was taken from the sample. Fig. 1 shows an example measured by Cr Kα characteristic radiation at an angle of $\psi = 0°$. It shows that only two diffraction peaks, i.e. 111 at $2\theta = 38.6°$ and 222 at $2\theta = 156.7°$, appear in the whole 2θ range. This means the (111) plane of the aluminum crystal arranges parallel to the surface of the Al film. An additional observation at any orientation of the film surface revealed that the Al film is composed of small crystals and that each crystal has 2π rotational freedom about the <111> orientation which is the same to the normal of the film surface as has been assumed previously.

4.2. Measurement of lattice spacing

Fig. 2 shows the experimental results of d_ψ against $\sin^2\psi$. Measurement at each of the five ψ angles shows that the scatter among the data points is very small. The standard deviation of stress value calculated from a set of five measurements is estimated to be ±4 MPa. The data from the as-received specimen show a very small gradient but those from the heat-treated specimens have a large positive gradient from which large tensile residual stress is expected.

4.3. Residual stress alteration by heat treatment

Initial residual stresses measured from the as-received samples were small tensile stresses within 30 MPa.

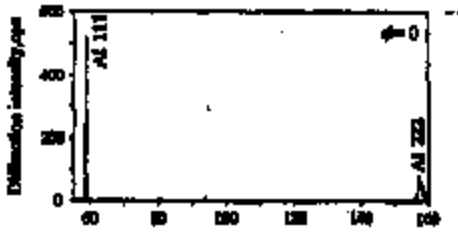

Fig. 1. Diffraction pattern of Al film deposited on a thermally oxidized (111) Si substrate.

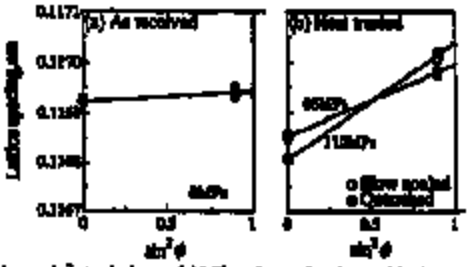

Fig. 2. d_ψ vs. $\sin^2\psi$ relations of Al films for evaluating residual stresses: (a) as-received and (b) heat-treated samples.

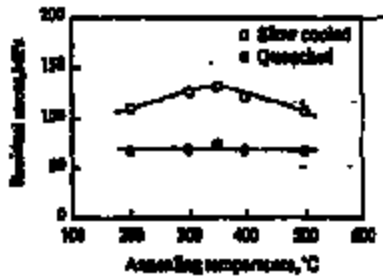

Fig. 3. Alteration of residual stresses in experimental Al films by heat treatments.

Fig. 3 shows a residual stress alteration by heat treatment: one is slow cooling in a furnace and the other is quenching in water from a desired temperature. Heating and furnace cooling treatments were made in a vacuum chamber but quenching was performed by unsealing the chamber and picking out the specimen from it.

Residual stresses in the Al film after each treatment were tensile; those in the slow-cooled samples are larger than those in the quenched samples. It is not yet clear why residual stresses in slow-cooled Al film are larger than those in quenched Al film. Tensile residual stresses are anyway produced by the treatment of heat and cool cycles. As the coefficient of thermal expansion (CTE) for aluminum is much greater than that for silicon, the heating process creates compressive stress in aluminum film. However, most of this compressive stress may relax at high temperature due to decreasing yield strength and creep effects. In the cooling stage, tensile stress develops in aluminum film due to the difference in CTEs between the film and the substrate and, finally, tensile residual stresses will be observed in the film. This behavior in thermal stresses will be precisely investigated by in-situ stress measurement in the Section 4.5.

Residual stresses in Al film for the slow-cooled specimens increased with increasing annealing temperature and then decreased as annealing temperature further increased. The maximum residual stress was attained at about 350 °C. On the other hand, residual stresses in Al film for the quenched specimens were independent of the annealing temperature.

The main reason for internal stresses that have developed in a film/substrate system is thermal potential, i.e. the product of the difference in CTEs between the film and the substrate, $\Delta\alpha$, and temperature change, ΔT. Therefore, tensile residual stress grows large with increasing the annealing temperature, which is kept for 1 h before cooling, because of large thermal potential. This may be the reason why residual stresses in Al film gradually increase with increasing the annealing temperature up to 350 °C.

As will be shown in the later section, when temperature increases beyond 400 °C, small voids begin to develop in the film, growing in number as well as in size. The void growth may affect the relaxation of thermal stresses developing in Al film.

4.4. Effect of carbon passivation on residual stress formation

Carbon-passivated film 0.02 μm in thickness was deposited on the surface of Al/Si sample pieces. These specimens were heated to the same temperatures as those investigated in the previous section, kept at those temperatures for 1 h before cooling down to room temperature in the vacuum furnace. The results of residual stress measurement are shown in Fig. 4. The behavior of residual stress alteration with heating temperature is almost the same as that for the slow-cooled specimens without passivation. However, there is a clear difference between the two; the maximum tensile residual stress develops in the passivated films at 400 °C instead of at 350 °C for the unpassivated films. Carbon passivation of 0.05 μm may not be sufficient to completely prevent void formation, but the effective prevention of void formation is observed by such thin passivation (see Section 4.6), demonstrating the retardation of residual stress relaxation.

4.5. In-situ thermal stress measurement of Al film

To investigate the development of thermal stress in Al film, an in-situ X-ray measurement was made with specimens set in a vacuum furnace attached on a diffractometer with parallel beam optics. Fig. 5 shows typical d_ψ vs. $\sin^2\psi$ diagrams during heating and cooling cycles between room temperature and 300 °C. In the heating stage, a positive gradient measured at room temperature changes to a slight negative gradient at 100 °C followed by successive parallel transitions leading to the maximum temperature of 300 °C. In the cooling stage, a slight negative gradient observed at 300 °C changes to a positive one at 200 °C; the gradient increases until the end of the thermal cycle to a level almost the same as that in the initial state.

Figs. 6–8 show the results of the thermal stress measurement of aluminum film during a series of heating and cooling cycles. Fig. 6 shows thermal stress alterations between room temperature and 200 °C. The initial residual stress is almost zero. As temperature increases, a small compressive stress develops from 100 °C to 200 °C. In the cooling stage, stresses due to a thermal mismatch increase almost linearly with decreasing temperatures. The specimen was then again heated to 300 °C (Fig. 7). The initial high tensile stress of 160 MPa rapidly drops to zero at 100 °C (the first stage) and then the rate of decrease becomes small (the second stage).

The stress originating from the temperature change ΔT of the Al film/Si substrate system is calculated by the following equation:

$$\Delta\sigma = \frac{E_{Al}}{1-\nu_{Al}}\Delta\alpha\Delta T \qquad (4)$$

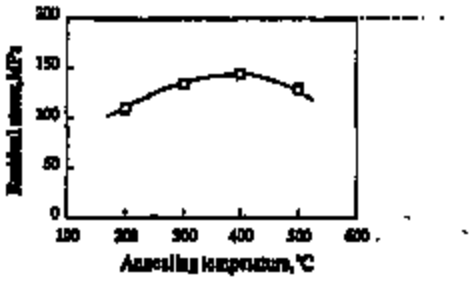

Fig. 4. Alteration of residual stresses in passivated Al films by heat treatments.

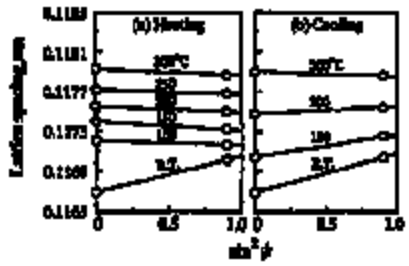

Fig. 5. d_ψ vs. $\sin^2\psi$ relations during heat and cool cycle between room temperature and 300 °C: (a) heating stage; (b) cooling stage.

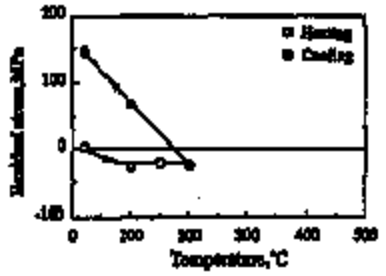

Fig. 6. In-situ thermal stress measurement of Al film during heat cycle from room temperature to 200 °C.

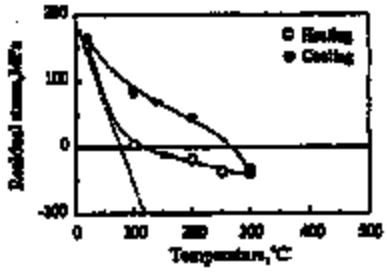

Fig. 7. In-situ thermal stress measurement of Al film during heat cycle from room temperature to 300 °C.

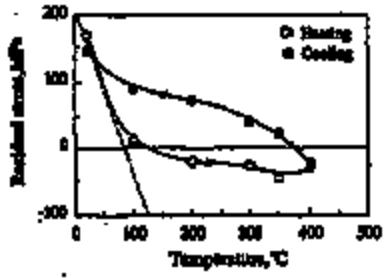

Fig. 8. In-situ thermal stress measurement of Al film during heat cycle from room temperature to 400 °C.

Table 4
Coefficients of thermal expansion and elastic constants of aluminum and silicon

Properties	Aluminum	Silicon
Coefficient of thermal expansion (10^{-6} °C^{-1})	23.9 [18]	2.6 [18]
Young's modulus (GPa)	70 [19]	112.7 [20]
Poisson's ratio	0.33 [20]	

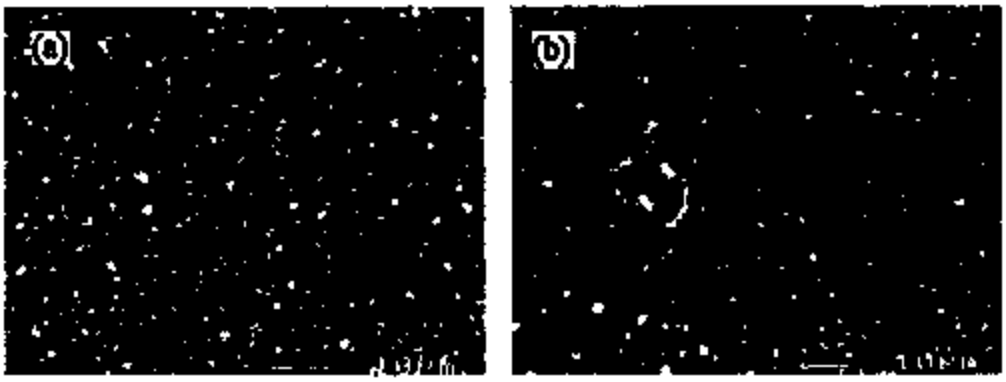

Fig. 9. SEM observation showing surface morphologies of the samples: (a) quenched and (b) slow cooled from 500 °C.

where $\Delta\alpha$ is the difference in CTEs between silicon (α_{Si}) and aluminum (α_{Al}), E_{Al} is Young's modulus and ν_{Al} is Poisson's ratio of aluminum. The values are summarized in Table 4.

The broken line drawn through the data points of initial stress has the gradient $\Delta\sigma/\Delta T$ ($=2.50$ MPa °C^{-1}) calculated by the above equation. Although the measurement involves only two data points, i.e. room temperature and 100 °C, the real stress reducing behavior seems to be along this line. Above 100 °C, the data points deviate from this line due to decreased yield strength as well as creep phenomenon of aluminum crystal in a high temperature range.

The cooling stage can be divided into three stages. In the first stage, stresses rapidly increase to about 50 MPa, then the rate of increase slow down in the second stage. The last stage is from 100 °C to room temperature, during which the increase rate again picks up.

These changes in behavior in the heating and the cooling stages are qualitatively the same in the next heat cycle between room temperature and 400 °C as shown in Fig. 8.

4.6. SEM observation of Al film surface after heat treatments

An SEM observation was made to investigate the surface configuration of Al film after heat treatments. Fig. 9(a) and 9(b) show the surfaces of quenched and furnace-cooled samples which have been kept at 500 °C for 1 h. From a surface analysis of silicon and aluminum components, it has been cleared that a bright part means a silicon-rich region and a dark part an aluminum-rich region, the former with hillocks and the latter with voids.

We have observed from a series of these photographs that the formation of hillocks begins in an early stage of the heating cycle. However, void formation is delayed until temperature is sufficiently high. The detailed observation of hillock and void formations and their development will be reported in the near future.

Fig. 10 shows the area fraction of hillocks counted in the photographs as a function of annealing temperature. Area fraction gradually increases with annealing temperature. Further, it is larger in the quenched samples than in the slow-cooled samples, meaning that the hillocks once formed at high temperature partly disappear during a furnace cooling stage.

Fig. 11 shows void formation and development as a function of annealing temperature. There is a clear difference between quenched and slow-cooled samples. Void formation is very scarce in the quenched samples even during quenching from 500 °C, the maximum temperature in this experiment. However, the area fraction in the slow-cooled samples increases as the annealing temperature increases, meaning that the voids are formed and have developed in size mainly in the furnace cooling stage.

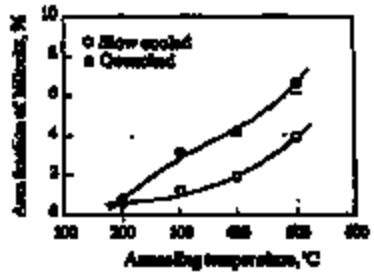

Fig. 10. Development of hillocks by increasing the annealing temperature.

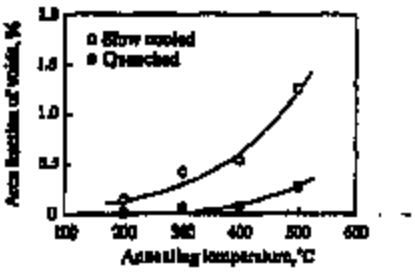

Fig. 11. Development of voids by increasing the annealing temperature.

From the in-situ thermal stress observation, we have seen that tensile stresses are formed in the cooling stage. Voids are formed and have developed when the Al film is subjected to tensile stresses. In the second stage of cooling, void formation relaxes thermal stresses and keeps them almost at a constant level. However, in the third stage (from 100 °C to room temperature), there may be no further void formation or development so that tensile stresses rapidly increase due to a thermal contraction mismatch between Al film and Si substrate.

Hillock formation develops in the second heating stage probably because the stress in the Al film is compressive. In the cooling stage, tensile stresses in the film tend to cause the aluminum atoms to flow out from the hillocks which have been formed as small eruptions or prominences on the surface, resulting in a decrease in the area fraction of hillocks.

The reason why the residual stress in the sample, which was slowly cooled from 500 °C, decreases may be due to relaxation by the increasing area fraction of voids as shown in Fig. 11.

5. Conclusion

Residual stresses and in-situ thermal stresses in Al film deposited on a thermally oxidized silicon substrate were observed by X-ray diffraction. Further, microscopic surface morphology of Al film was inspected by SEM observation. The results obtained are as follows.

1. Residual stresses are tensile after annealing at high temperatures. Residual stresses are larger in slow-cooled samples than in quenched samples, reaching the maximum value at 350 °C.
2. Passivation by carbon film prevents void formation which delays of residual stress relaxation at higher temperatures.
3. In-situ observation reveals that compressive stresses are formed in the heating stage and tensile stresses in the cooling stage due mainly to a thermal expansion and contraction mismatch between aluminum film and silicon substrate.
4. From an SEM observation it is found that hillocks are formed in a heating cycle due to compressive stresses in the film while voids develop in a cooling cycle due to tensile stresses in the film.

Acknowledgements

The authors would like to thank Mr. E. Hanaki for taking the experimental data.

References

[1] W.G. Sloof, R. Delhez, Th.H. de Keijser and E.J. Mittemeijer, *J. Mater. Sci.* 22 (1987) 1701.
[2] B.J. Kooi, W.G. Sloof, M.A.J. Somers, A.C. Vermeulen, R. Delhez, Th.H. de Keijser and E.J. Mittemeijer, in H. Fujiwara, T. Abe and K. Tanaka (Eds.), *Residual Stresses III*, Vol. 1, Elsevier Science Publishers, Amsterdam, 1992, p. 11.
[3] T. Hanabusa, K. Tominaga and H. Fujiwara, in H. Fujiwara, T. Abe and K. Tanaka (Eds.), *Residual Stresses III*, Vol. 1, Elsevier Science Publishers, Amsterdam, 1992, p. 728.
[4] T. Hanabusa, K. Kusaka, K. Tominaga and H. Fujiwara, *Proc. Fourth Int. Conf. on Residual Stresses*, Soc. for Experimental Mechanics, Connecticut, 1994, p. 631.
[5] I.C. Noyan, C.C. Goldsmith, *Adv. X-Ray Anal.*, *35* (1992) 461.
[6] C.J. Shute and J.B. Cohen, *J. Mater. Res.*, *6* (1991) 950.
[7] P.S. Ho, L.-S. Yeo and S.O.H. Anderson, in P.S. Ho, C.-Y. Li and P. Totta (Eds.), *AIP Conf. Proc.*, *205* (1984) 62.
[8] I.C. Noyan and C.C. Goldsmith, *Adv. X-Ray Anal.*, *34* (1991) 387.
[9] M. Sebastiano and G.M. Zorn, in P.S. Ho, C.-Y. Li and P. Totta (Eds.), *AIP Conf. Proc.*, *205* (1994) 111.
[10] C.C. Goldsmith and C.V. Beshkin, *Adv. X-Ray Anal.*, *36* (1993) 203.
[11] T.J. Faith and C.P. Wu, *Appl. Phys. Lett.*, *116* (1984) 470.
[12] A.K. Sinha, and T.T. Sheng, *Thin Solid Films*, *48* (1978) 117.
[13] H. Okabayashi, A. Takimiya, H. Mori and H. Fujita, *Ultramicroscopy*, *9* (1991) 305.
[14] A. Tenaki, T. Misota, H. Egawa and T. Nogashi, *Proc. 1990 IEEE International Reliability Physics Symposium*, *IEEE, New York, NY*, 1990, p. 221.
[15] J. Curry, G. Fitzgibbon, Y. Quan, R. Musilo and A. Thomas, *Proc. 1984 IEEE International Reliability Physics Symposium*, *IEEE, New York, NY*, 1984, 8.
[16] T. Turner and K. Wendel, *Proc. 1984 IEEE International Reliability Physics Symposium*, *IEEE, New York, NY*, 1984, 142.
[17] G. Simmons and H. Wang, *Single Crystal elastic Constants and Calculated Aggregate Properties*, M.I.T. Press, Cambridge, Massachusetts and London, 1971, p. 4.
[18] T. Takayama and T.Hashimoto, *Fabrication Technology of VLSI*, Nikkei BP Co., Tokyo, 1989, p. 191 (in Japanese).
[19] J.M. Gere and S.P. Timoshenko, *Mechanics of Materials*, Chapman and Hall, New York, 1991, p. 778.
[20] American Society for Metals, *Metals Handbook*, Vol. 2, Ohio, 1979, p. 796.

ELSEVIER

Thin Solid Films 271 (1995) 64–68

Thin Solid Films

A comparative study of hillock formation in aluminum films

B. Cao Martin [a], C.J. Tracy [a], J.W. Mayer [b], L.E. Hendrickson [b]

[a] Materials Technology Center, Materials Research and Strategic Technologies, Motorola, Inc., 2200 W. Broadway Rd., Mesa, AZ 85202, USA
[b] Department of Chemical, Bio, and Materials Engineering, Arizona State University, Box 876006, Tempe, AZ 85287, USA

Received 2 December 1994; accepted 12 July 1995

Abstract

Studies were conducted to evaluate the performance of a variety of aluminum alloys with respect to hillock formation. Specifically, the effects of film composition, deposition temperature, and underlayer on hillock formation were investigated. The film compositions included pure Al, Al with 1.5 wt.% Cu (or AlCu), AlCu with 0.2 wt.% W, and AlCu with 0.4 wt.% W. These films were sputter deposited at 300 °C and 450 °C on either oxide- or Ti–W-coated Si substrates. Following deposition, the films were annealed in air for 20 min at 450 °C. For all film compositions, the deposition temperature had the most significant effect on the hillock density. For a given deposition temperature, the addition of Cu to pure Al drastically reduced the hillock density, but the addition of W to AlCu increased the hillock density. The effect of the underlayer on the hillock density was negligible. Cross-sections of the hillocks showed that they were solid from the bottom interface to the top surface, and no voids were found near the hillocks. The grain size did not have a significant effect on the hillock density. However, a correlation between increasing (111) film texture and decreasing hillock density was observed.

Keywords: Alloys; Aluminium; Stress

1. Introduction

In recent years, attempts to improve the performance and reliability of aluminum interconnect materials have motivated studies of a variety of alloying elements [1–7]. The performance of a new alloy material is often measured in terms of its resistance to stress-induced void formation and electromigration failure. Another commonly encountered problem in metallization is hillock formation. Hillocks can lead to excessive surface roughness and interfere with photolithography steps. They can also crack the dielectric film isolating the metal lines and result in interlevel electrical short circuits [8]. Additionally, hillocks can protrude from the sides of metal lines and cause intralevel short circuits among adjacent metal lines [9].

Hillocks form because of large thermal stresses in the metal films, arising from the large difference in the coefficients of thermal expansion (CTEs) of the metal and the underlayer. The CTE of Al is approximately 10 times larger than the CTE of Si; and consequently, when an Al film is deposited on Si and heated, a compressive stress is produced in the Al film. Hillock formation is one mechanism whereby this thermally-induced compressive stress is relieved.

A number of mechanisms have been proposed for the formation of hillocks in thin metal films, including grain boundary diffusion, diffusional creep, and interfacial diffusion [10–25]. Because hillock formation is a stress relaxation mechanism which occurs in localized regions in a polycrystalline metal film, one might expect inhomogeneities in the metal microstructure, such as the mean grain size and grain size distribution, and the grain orientations and their distribution about a reference direction, to play dominant roles. Experimental data will be presented to show the effects of the film composition, deposition temperature, and underlayer on the metal film microstructure, and the effects of the microstructure on hillock formation.

2. Experimental details

Two full 2^3 factorial experiments were run to determine the contributions due to each of the three independent variables (film composition, deposition temperature, and underlayer). Two-variable interactions were also examined. Control sets comprising pure Al films and commonly used Al with 1.5 wt.% Cu (AlCu) films were included for comparison. The two levels of film compositions in the factorial experiments were AlCu with 0.2 wt.% W, and AlCu with 0.4 wt.% W (or 0.2 W and 0.4 W films, respectively). Metal deposition was carried out at 300 °C and 450 °C. The two types of underlayers were Si (100) wafers coated with Ti–

SSDI 0040-6090(95)06941-0

W or plasma-enhanced silicon oxide prepared from a tetraethylorthosilicate (TEOS) precursor.

Four-inch Si (100) wafers were first coated with either TEOS or Ti–W. The TEOS films were approximately 300 nm thick, and the Ti–W, 150 nm. Following underlayer deposition, metal films of varying compositions were sputter deposited to a nominal thickness of 750 nm. The AlCuW and pure Al films were deposited in the Varian 3180 sputter deposition system in the Materials Technology Center (Motorola, Mesa) at a rate of 18.5 nm s^{-1}. The AlCuW films were prepared from homogeneous targets. Argon was the sputtering gas in all depositions. The chamber base pressure was typically 10^{-5} Pa, and during deposition, the chamber was backfilled with Ar to approximately 0.9 Pa. Substrate heating during sputter deposition was accomplished by Ar-gas-coupled backside heating. The AlCu films were sputter deposited in an MRC Eclipse sputter deposition system in the Advanced Technologies Center (Motorola, Mesa).

Following blanket metal film deposition, the wafers were annealed in air in a Flexus PZ300 thin film stress measuring apparatus. All isothermal anneals were performed at 450 °C for 20 min. Wafers were brought from room temperature to 450 °C in 35 min, held at 450 °C for 20 min, then cooled to room temperature.

Following anneal, the wafers were characterized by seven different methods to determine the hillock density, hillock size distribution, hillock morphology, mean grain size and grain size distribution, grain and hillock orientations, and compositional variations. Results will be presented from scanning electron microscopy, transmission electron microscopy, profilometry, Auger electron spectroscopy, focused ion beam cross-sectioning, reflection high-energy electron diffraction, and X-ray/pole figure analysis.

3. Results

3.1. Compositional analysis

A 0.2 W film was analyzed using Auger electron spectroscopy (AES) to compare the elemental compositions of the matrix and hillocking regions. The film was deposited at 300 °C on TEOS then annealed at 450 °C for 20 min prior to analysis by AES. Spectra were acquired on regions inside grains, on grain boundaries, and on hillocks. The Auger beam diameter was approximately < 25 nm (much smaller than the typical hillock diameter of 1 000–2 000 nm), and the detection limit for W and Cu were approximately 1 at.%.

Tungsten was not detected in any of the areas analyzed either before or after a slight sputtering to remove approximately 30 nm of the surface material. Copper was detected in some grain boundaries, suggesting the presence of Cu-rich Al_2Cu precipitates in the grain boundaries. A Cu distribution map using the most intense Cu LMM Auger signal confirmed the presence of Al_2Cu precipitates in many grain boundaries.

The small concentration of W in the analyzed sample, 0.2 wt.%, is below the detection limit of AES (0.1–1 at.%, depending on the element). Segregation of W to the grain boundaries or hillocks may increase the local concentration of W enough to be detected by AES. However, additional analysis on the hillocks using long acquisition times did not detect W (nor Cu), and it was concluded that there was no significant compositional difference between the matrix and the hillocking regions in the 0.2 W film.

3.2. Microstructural analysis

Plan-view transmission electron microscopy (PTEM) was used to determine the mean grain sizes and size distributions of as-deposited and annealed metal films. Several trends were noted. The addition of W to AlCu alloy films decreased the mean grain size. Films deposited on Ti–W had smaller mean grain sizes than compared with films deposited on TEOS, for a given composition and deposition temperature. The grain sizes follow a log–normal distribution, and the plots of log of grain size versus cumulative probability fall along straight lines.

The morphologies of hillocks in annealed samples of different compositions were examined in a Cambridge scanning electron microscope without any sample preparation. The various hillock morphologies found on annealed samples of different compositions can be seen in the SEM micrographs in Figs. 1–3. In some cases, a moat can be seen around the outer edges of the hillocks. These moats probably formed during the cooling cycle, when the films were stressed in tension above their yield strengths. Terraces can also be seen on a number of hillocks, suggesting slip and/or that the hillocks formed in incremental steps.

Cross-sections of hillocks were obtained by using a focused beam of Ga^+ ions to gradually sputter away the material. The analysis was performed in a Micrion 906 focused ion beam (FIB) system in the Materials Characterization Laboratory (Motorola, Mesa). Fig. 4 and Fig. 5 are

Fig. 1. SEM micrograph of a hillock with a relatively smooth, rounded appearance.

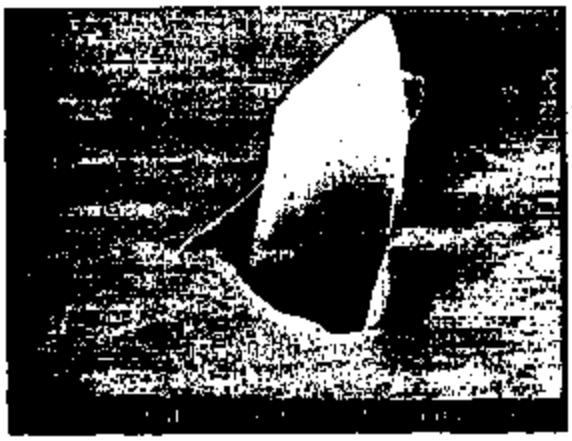

Fig. 2. SEM micrograph of a spike-like hillock with significant protrusion out of the film surface.

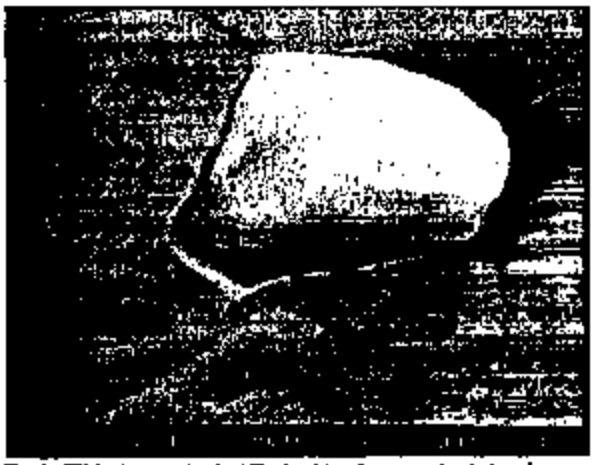

Fig. 3. SEM micrograph of a hillock with a flat top and striations/terraces on the left side.

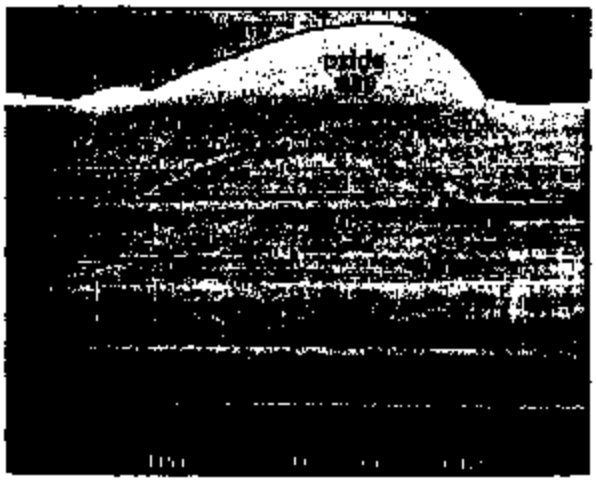

Fig. 4. FIB cross-section of a hillock formed in an annealed 0.4 W film which was deposited at 300 °C on TEOS.

secondary electron micrographs of two different hillocks from the same annealed 0.4 W, 300 °C film. A low-temperature PECVD oxide cap was deposited on the metal surface

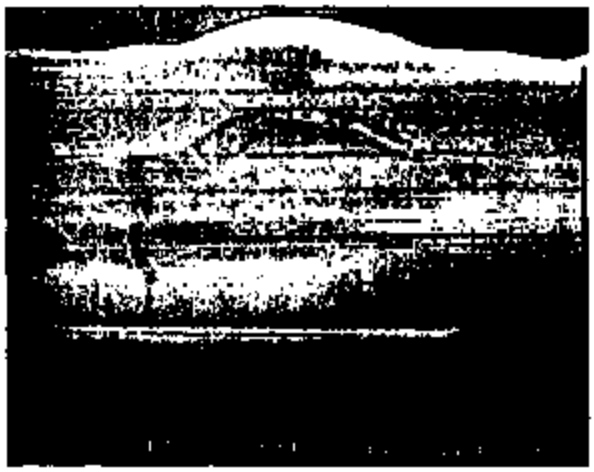

Fig. 5. FIB cross-section of a second hillock formed in an annealed 0.4 W film which was deposited at 300 °C on TEOS.

to prevent erosion of surface features during sputtering. After cross-sectioning in the FIB system, the hillocks were delineated in a mixture of 4:1 NH_4F:HF for 5 s prior to SEM inspection. In all cases, the hillocks were solid from the bottom interface to the top surface, and no voids were seen near the hillocks. Grain boundaries can be seen, sometimes near or at the center of a hillock, but more often 1 000–2 000 nm from the center of the hillock. Because grain growth occurred during the 20 min anneal at 450 °C it is not possible to determine the original positions of the hillocks with respect to the grain boundaries. However, it cannot be excluded that a hillock has formed inside a grain.

Reflection high energy electron diffraction (RHEED) was used to determine the orientations of 8 hillocks in a 0.4 W film which was deposited at 300 °C on TEOS then annealed at 450 °C for 20 min in air. The diffraction patterns were generated using a 200 kV incident beam. The RHEED beam diameter was approximately 10 nm, much less than the mean hillock distance and the mean hillock diameter. Analysis of the diffraction patterns (not shown) generated from the reflection of the beam from the hillocks' surfaces showed that all the hillocks were randomly oriented and deviated from all major crystal axes, such as ⟨100⟩, ⟨110⟩, and ⟨111⟩. Additionally, the orientations of 9 matrix grains surrounding one hillock were analyzed in the standard electron diffraction mode (transmission through a thinned specimen). It was found that the orientations of the matrix grains were very similar to each other, but they deviated significantly from the orientation of the hillock.

The (111) film texture was characterized as a function of deposition temperature, film composition, and anneal treatment by means of X-ray/pole figure analysis. Because the (111) peak intensities were a function of both the degree of texture and the film thickness, corrections were made to account for differences in the film thickness. Several important trends were noted.

1. For a given film composition and deposition temperature, annealing increased the amount of (111) texture. How-

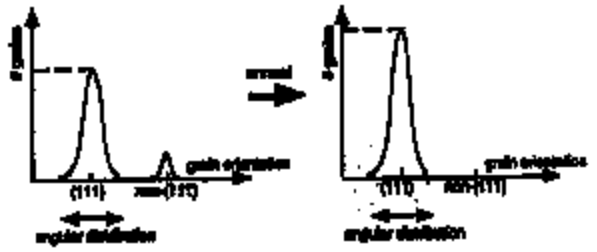

Fig. 6. Schematic representation of changes in the grains' orientations as a result of annealing and increased deposition temperature.

ever, the (111) angular distributions (the diameter of the pole diagram) remained unchanged.

2. Increasing the deposition temperature increased the (111) texture but exerted no significant effect on the (111) distribution.
3. Pure Al films were more textured in (111) than the 0.4 W films deposited at the same temperature.
4. There was no evidence of secondary texturing (no film texture other than (111)).

The physical interpretation of the observed change in (111) intensity and lack of change in (111) distribution as a result of annealing and increased deposition temperature is believed to be as follows. The distribution of grain orientations in these as-deposited metal films is believed to be mainly (111) grains with a small population of non-(111) grains. However, not all of the (111) grains were oriented perfectly parallel to the (111) pole, and there existed a finite distribution about the (111) pole. Upon annealing at 450 °C for 20 min, grain growth occurred, and the (111) grains grew at the expense of the non-(111) grains. The driving force for this process is the minimization of surface energy. However, the grains which deviated only slightly from the (111) pole remained unaffected, perhaps because the energy difference was not great enough to drive the grain growth process described above (see the schematic representation in Fig. 6).

3.3. Hillock density

All annealed metal films were characterized by profilometry to obtain the hillock densities and size distributions. To account for film surface roughness, only protrusions larger than 20 nm were counted as hillocks. For a given film composition, the deposition temperature had the most significant effect on the hillock density (Fig. 7). In AlCuW films, increasing the W concentration increased the hillock density, but the effect due to W was much smaller than that due to deposition temperature. Differences in the hillock densities due to the substrate material (TEOS vs. Ti–W) were statistically insignificant. Two-variable interactions (for instance, the interaction between film composition and deposition temperature) were also insignificant.

The hillock size distribution was a function of the deposition temperature only and was similar across all film compositions and substrate materials. For the 300 °C deposition, approximately 30 to 50% of the total hillock population were

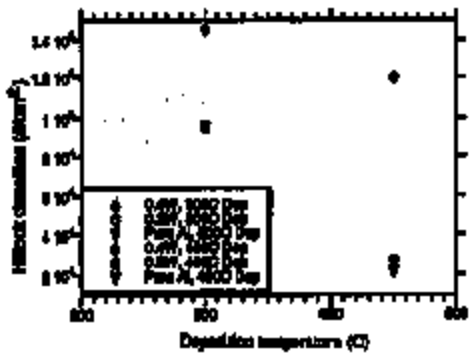

Fig. 7. Hillock densities as a function of deposition temperature for pure Al, 0.2 W, and 0.4 W films. Increasing the deposition temperature resulted in significantly lower hillock densities.

at least 100 nm in height; approximately 10% were at least 200 nm; and less than 1% were equal to or greater than 500 nm. For the 450 °C deposition, virtually all hillocks were less than 100 nm in height.

The addition of Cu to pure Al significantly decreased the hillock density, but the addition of W to AlCu films increased the hillock density. Indeed, no hillocks were observed in AlCu films. However, there was an abundance of Al_2Cu precipitates on the annealed AlCu wafers. For this reason, the hillock densities of AlCu films are not reported.

4. Discussion

Film texture appeared to have the most significant effect on the hillock density, under the conditions studied in this work. Review of the pole figure and hillock density data revealed a correlation between increasing (111) film texture and decreasing hillock density (see Fig. 8). AlCu films had virtually no hillocks and the highest (111) texture. Additionally, for all film compositions, increasing the deposition temperature resulted in an increase in (111) texture and a decrease in hillock density (Fig. 7 and Fig. 8). Pure Al films were more strongly textured in (111) than 0.4 W films deposited at the same temperature, and the hillock densities in the

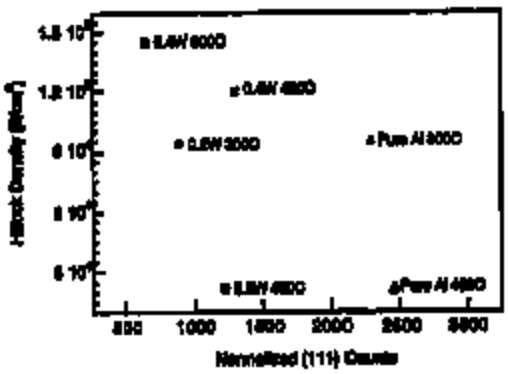

Fig. 8. Hillock density plotted as a function of (111) texture for pure Al, 0.2 W, and 0.4 W films. Films with greater (111) texture formed fewer hillocks.

pure Al films were lower (they were comparable with the 0.2 W densities).

Surprisingly, the film grain size did not have a significant effect on the hillock density. Unannealed films deposited on Ti–W consistently had smaller mean grain sizes than compared with those deposited on TEOS, but the difference in hillock densities was negligible.

Of the three process variables studied, the deposition temperature had the most significant effect on the hillock density and size distribution. From a processing standpoint, a few but very large hillocks can potentially cause more problems than a large number of hillocks of size ~20 nm steps. For the compositions studied, increasing the deposition temperature from 300 °C to 450 °C eliminated all hillocks in the 500 nm range in height. This difference in size distribution may be due to different stress relaxation mechanisms which are operative in the 300 °C and the 450 °C films.

Schwarzer, Gerth and coworkers [14,16–18] have studied the effect of grain orientation on hillock formation. They used electron diffraction to determine the orientations of over 1 100 matrix grains and 80 hillocks in Al–1% Si films and found that while the matrix grains were strongly textured in (111), the orientations of the hillocks were quite different from that of the matrix grains.

Although the RHEED analysis in our study was much less extensive, we found results similar to those reported above. We were able to determine that the orientations of nine grains surrounding a hillock were very similar, but they differed significantly from that of the hillock's. We also analyzed the orientations of eight hillocks and found them to be random.

5. Conclusions

In conclusion, for Al-based alloys, process conditions which enhance (111) texture formation, such as higher deposition temperature, are expected to suppress hillock formation. In addition, a temperature excursion is necessary to produce the compressive thermal strain/stress leading to hillock formation. Therefore, minimizing the temperature difference between the metal deposition step and subsequent high-temperature processing steps is also expected to be advantageous. Finally, characterization of the film texture by X-ray/pole figure has been shown to be a useful analytical method for predicting the susceptibility of a material to hillock formation.

Acknowledgements

The authors are grateful to the Materials Characterization Laboratory (Motorola, Mesa) for performing the various materials analyses and to Dan Sullivan, Materials Technology Center (Motorola, Mesa), for depositing the films. The X-ray/pole figure data were acquired by Dr. Anna Yates, Department of Chemistry (Arizona State University, Tempe).

References

[1] S. Ogawa and H. Nishihara, *IEEE Electron. Dev. Meter.*, (1991) 277.
[2] H. Onoda, E. Takahashi, S. Mukadoro, H. Fukuyo and S. Sawada, *IEEE Symp. VLSI Technology*, IEEE, New York, 1990, p. 57.
[3] F.M. d' Heurle and A. Gangulee, in H. Ha (ed.), *Nature and Behavior of Grain Boundaries*, Plenum Press, 1972, p. 339.
[4] F. Fisher and F. Neppl, *IEEE/IRPS*, (1984) 190.
[5] D.K. Sadana, J.M. Towner, M.H. Norcott and R.C. Ellwanger, *IEEE/IRPS*, (1986) 38.
[6] H.J. Stein, *Appl. Phys. Lett.*, *19* (1971) 30.
[7] F.M. d' Heurle and R. Rosenberg, in G. Hass and R. Hoffman (eds.), *Physics of Thin Films*, Vol. 7, Academic Press, New York, 1975, p. 257.
[8] S. Wolf, *Silicon Processing for the VLSI Era*, Vol. 2, Lattice Press, Sunset Beach, CA, 1990, p. 270.
[9] S. Wolf, *Silicon Processing for the VLSI Era*, Vol. 2, Lattice Press, Sunset Beach, CA, 1990, p. 270.
[10] P. Chaudhari, *J. Appl. Phys.*, *45* (1974) 4339.
[11] M.S. Jackson and C. Li, *Acta Metall.*, *30* (1982) 1993.
[12] M. Murakami, *Thin Solid Films*, *35* (1976) 101.
[13] P.H. Townsend and H.A. Vander Plas, *Mater. Res. Soc. Symp. Proc.*, *47* (1985) 121.
[14] R.A. Schwarzer and D. Gerth, *J. Electron. Mater.*, *22* (1993) 607.
[15] F.M. D' Heurle, *Int. Mater. Rev.*, *34* (1989) 53.
[16] D. Gerth and R.A. Schwarzer, *Mater. Sci. Forum*, *115–117* (1993) 629.
[17] D. Gerth, D. Kaiser and R. Schwarzer, *Mater. Sci. Forum*, *94–96* (1992) 537.
[18] D. Gerth, D. Kaiser and M. Krejca, *Thin Solid Films*, *208* (1992) 67.
[19] F. Brisson, N. Kristensen and J.A. Schweitz, *J. Vac. Sci. Technol.*, *B9* (1991) 58.
[20] S. Asano, C.Y. Chang and R.W. Vook, *Thin Solid Films*, *219* (1992) 80.
[21] C.A. Pico and T.D. Bonifield, *J. Mater. Res.*, *8* (1993) 1010.
[22] I.R. Sanchez, Jr. and E. Arzt, *Scripta Metall. Mater.*, *27* (1992) 285.
[23] S. Baker, P.A. Flinn, B. Arzt and W.D. Nix, *J. Mater. Res.*, *9* (1994) 218.
[24] A.K. Sinha and T.T. Sheng, *Thin Solid Films*, *48* (1978) 117.
[25] D.S. Herman, M.A. Schuster and R.M. Gerber, *J. Vac. Sci. Technol.*, *9* (1972) 515.

ELSEVIER

Surface and Coatings Technology 106–109 (1998) 388–393

Application of high temperature deposited aluminum gate electrode to the fabrication of a-SI:H TFT

P.S. Shih[a,*], T.C. Chang[b], S.M. Chen[c], M.S. Feng[c], D.Z. Peng[a], C.Y. Chang[a]

[a]Department of Electronics Engineering and Institute of Electronics, National Chiao Tung University, 1001 Ta-Hsueh Rd, HsinChu 300, Taiwan, ROC

[b]National Nano Device Laboratory, 1001 Ta-Hsueh Rd, Hsin-Chu 300, Taiwan, ROC

[c]Institute of Materials Science and Engineering, National Chiao-Tung University, Taiwan, ROC

Abstract

Aluminum is a good candidate for low resistivity metal used on TFT-LCD panels as the gate electrode of a-SI:H TFTs. The characteristics of a-Si:H TFTs device are strongly dependent on the morphology of the aluminum film. However, the thermal and mechanical stability of aluminum are inferior. In this work, hot aluminum was firstly used as the gate electrode of a-SI:H TFTs. Effects of aluminum deposition temperature on the surface roughness were investigated. The fraction of Al(111) texture increases with increasing deposition temperature. The surface roughness due to hillock formation decreases with increasing deposition temperature of aluminum films. Therefore, increasing the deposition temperature of aluminum films can suppress hillock formation. The field effect mobility of a-SI:H TFTs increases with the deposition temperature of aluminum gate. The subthreshold swing of a-SI:H TFTs decreases with the deposition temperature of aluminum gate. © 1998 Elsevier Science S.A. All rights reserved.

Keywords: Al; A-Si:H TFT; Hillock; Gate electrode

1. Introduction

Active-matrix liquid crystal displays, especially thin film transistor liquid-crystal displays (TFT-LCDs), are in great demand recently because of their high resolution and contrast. As TFT-LCDs are developed to larger sizes with higher resolution, lower electrical resistivity and higher resistance to hillock formation are required for the interconnections of TFT-LCDs.

So far, refractory metals, such as Ti, Cr, Mo, Ta, etc., have been used as the interconnections of TFT-LCDs because of their high thermal stability and hence a high resistance to hillock formation. However, a disadvantage of these interconnection materials is their high electrical resistivity that causes a delay of address pulses. Al alloy films deposited by sputtering have properties of high hillock suppression and lower electrical resistivity [1,2]. However, it will still be difficult to employ them for advanced TFT-LCDs because of their significantly high electrical resistivity of about 10 μΩ-cm. Adding group VIII transition elements [3] or rare-earth metal elements [4] can further reduce resistivity. However, the resistivity is still large compared with that of pure Al.

On the other hand, Al films have a lower electrical resistivity of 2.7 μΩ-cm, but their thermal and mechanical stability are inferior. Hillocks sometimes form on the Al film surface, which lead to excessive surface roughness and can cause problems, such as short circuits [5,6]. In addition, hillock formation on the Al gate electrode of a-SI:H TFT will degrade SiN_x/a-Si interface and thus deteriorate the a-Si:H TFT performances.

In the VLSI technologies, Al deposited at high temperature is widely used as interconnections. It has higher surface migration and larger grain size than Al deposited at room temperature. The microstructure of hot Al differs from that of room temperature-deposited Al. The formation of hillocks is strongly dependent on the microstructure of the Al film. Therefore, we expect that the deposition temperature of Al will play a dominant role in hillock formation.

In this work, effects of Al deposition temperature on hillock formation were investigated. Atomic force microscopy (AFM) was utilized to determine the roughness of as-deposited and annealed films. In addition, a hot Al gate electrode has been successively applied to the fabrication

*Corresponding author. Tel.: +886-35-712121, ext. 52981; fax: +886-35-715506; e-mail: sd831503@cc.nctu.edu.tw

0257-8972/98/$ – see front matter
PII: S0257-8972(98)00640-9

of a-Si:H TFTs to study the correlation between Al surface morphology and electrical characteristics of a-Si:H TFTs.

2. Experimental

The Al films were sputter deposited at room temperature (RT), 200 and 300°C for this study. All the as-deposited films were annealed at 400°C for 30 min.

The a-Si:H TFTs configuration used in this study has an inverted staggered structure, as shown in Fig. 1. A 150-mm silicon wafer coated with a 500-nm thick thermal oxide was used as the starting substrate. The TFT fabrication process is as follows. First, the 500-nm thick Al layers were sputter deposited at RT, 200 and 300°C, respectively. For comparison, 70-nm thick Al_2O_3 layers were grown on some of the samples by anodic oxidation method [7]. Then the Al (Al/Al_2O_3) layers were defined by photolithography and chemical etching to form gate electrodes. After that, a 250-nm thick and 150-nm thick SiN_x were deposited with a standard parallel plate-type plasma CVD reactor to form the insulating layer on Al and Al/Al_2O_3 layers, respectively. These, along with a 200-nm thick undoped a-Si:H film and 50-nm thick n^+ a-Si:H film were deposited successively without breaking vacuum. The gas mixtures for SiN_x, undoped a-Si:H and n^+ a-Si:H were ($SiH_4+NH_3+N_2$), SiH_4 and ($SiH_4+PH_3+H_2$), respectively. The SiN_x film was deposited under conditions of 300°C, 50 W and 500 mTorr. The a-Si:H film was deposited under conditions of 250°C, 15 W and 300 mTorr. The n^+ a-Si:H was deposited under conditions of 250°C, 70 W and 650 mTorr. Then active region was defined by dry chemical etching. Finally the Al metal was evaporated by thermal coater and patterned to form the source and drain electrodes. The unwanted n^+ layer between two electrodes was removed by dry chemical etching.

AFM was utilized to determine the roughness of as-deposited and annealed films. The texture of Al electrodes was measured by X-ray diffraction (XRD). The electrical characteristics of the a-Si:H TFTs were measured by an HP4145B semiconductor parameter analyzer.

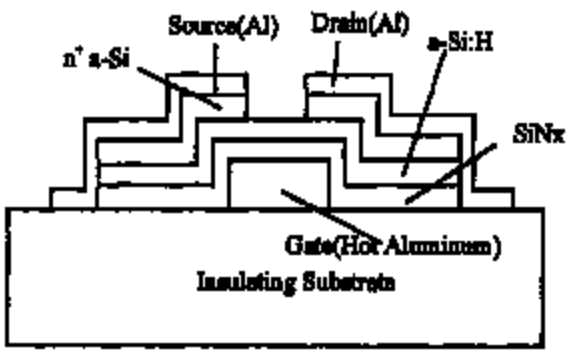

Fig. 1. A-Si:H TFT configuration.

3. Results and discussion

Fig. 2a shows the RMS surface roughness of as-deposited and annealed Al films as a function of deposition temperature. The Al films were deposited at RT, 200 and 300°C. All the as-deposited films were annealed at 400°C for 30 min. The surface roughness of as-deposited Al films decreases with increasing deposition temperature. The surface roughness of as-deposited films dramatically reduces from 5.8 to 4.2 nm as the deposition temperature of Al films increases from RT to 300°C. In addition, the surface roughness of annealed Al films also decreases with increasing deposition temperature. The surface roughnesses of annealed Al films are 9.1 and 6.3 nm for Al films deposited at RT and 300°C, respectively.

The reduction of surface roughness of Al films deposited at high temperature is due to the increase of surface migration. The adsorbed Al atoms can quickly move along

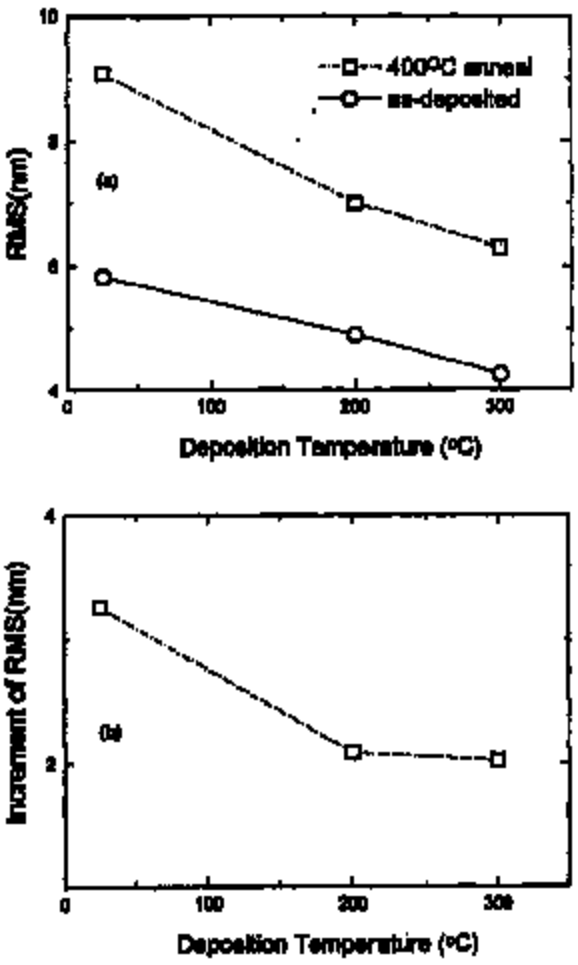

Fig. 2. (a) Surface roughness of as-deposited and annealed Al film as a function of deposition temperature, (b) increment of surface roughness of Al film before and after thermal annealing.

the wafer surface at 300°C. Therefore, a smoother Al film can be deposited at high temperature. On the other hand, the adsorbed Al atoms move slowly at room temperature and may pile up locally on the surface, resulting in a rougher surface.

Fig. 2b shows the increment of surface roughness of an Al film before and after thermal annealing. The roughness increments are 3.3 and 2.1 nm for the sample deposited at RT and 300°C, respectively. The roughness increment of Al films rapidly decreases with increasing deposition temperature. Hillock formation can lead to excessive surface roughness. A smaller increment of surface roughness after thermal annealing indicates higher resistance against hillock formation. Therefore, high-temperature deposition of Al films tends to increase hillock resistance. The experimental results can be interpreted as follows. A temperature excursion is necessary to produce the compressive thermal stress to cause hillock formation. Therefore, minimizing the temperature difference between the Al deposition step and subsequent high-temperature processing steps is expected to reduce hillock formation. In our experiment, the SiN_x film is deposited at 300°C which is the highest process temperature for fabricating a-Si:H TFT devices. Therefore, the temperature difference between the Al deposition step and subsequent high-temperature processing steps is the smallest for Al film deposited at 300°C. On the other hand, the Al film deposited at RT encounters the largest temperature difference during process. It is thus reasonable that an Al film deposited at 300°C has higher hillock resistance than that deposited at room temperature. Furthermore, it is believed that grain orientation of Al can affect hillock formation [8–10]. An earlier study reported that a correlation between increasing (111) film texture and decreasing hillock density was observed [11]. Process conditions which enhance (111) texture formation are expected to suppress hillock formation. Fig. 3 shows the X-ray diffraction spectra of Al films deposited at various temperatures. From the X-ray diffraction analysis, the intensity of the (111) peak increases with increasing deposition temperature of the Al film. This result indicates that Al films with a higher deposition temperature have a better capability to suppress hillock formation. Therefore, the result of X-ray diffraction well agrees with AFM measurement.

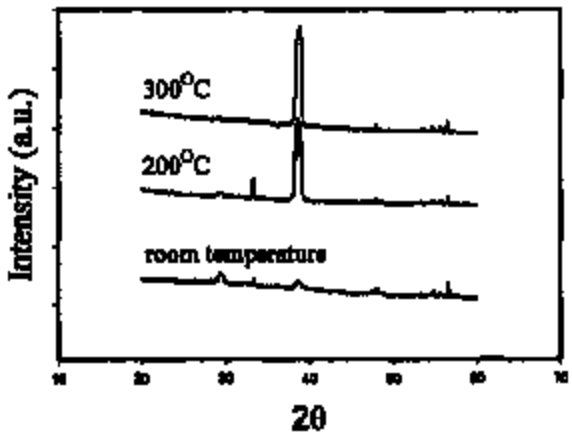

Fig. 3. X-ray diffraction spectra of Al films deposited at various temperatures.

Fig. 4a shows the transfer characteristics of a-Si:H TFTs with single-layered insulator (SiN_x) and Al gate electrodes deposited at various temperatures. The applied drain voltage is 10 V for this measurement. The ON current increases with increasing deposition temperature of the Al gate. Fig. 4b shows the field effect mobility of a-Si:H TFTs as a function of the deposition temperature of the Al gate. The field effect mobility is determined from the characteristics in the saturation region by plotting (drain current)$^{1/2}$ versus gate voltage. The field effect mobility increases almost linearly with the deposition temperature of the Al gate. TFTs with the Al electrode gate deposited at 300°C have the highest ON current and highest field effect mobility. This phenomenon can be interpreted in terms of surface roughness scattering effect. The SiN_x morphology is directly affected by the morphology of the Al electrode gate. The a-Si:H/SiN_x interface roughness is affected by the morphology of the SiN_x. Therefore, a rougher Al gate results in a rougher a-Si:H/SiN_x interface which will cause the reduction of both ON current and mobility. In the case of the Si–SiO_2 interface, the mobility due to surface roughness scattering has been observed [12]. Similar mobility and stability reduction due to roughness scattering was also observed in the case of SiN_x/a-Si interface [13].

Fig. 4c shows the subthreshold swing of a-Si:H TFTs as a function of the deposition temperature of the Al gate. The subthreshold swing reduces linearly with increasing deposition temperature of the Al gate. The subthreshold swing of a-Si:H TFTs with the Al gate deposited at RT and 300°C are 0.83 V/decade and 0.32 cm^2/V-s, respectively. The improvement of the subthreshold swing is also very significant. The result can be interpreted as follows. Rougher SiN_x surface prevents surface diffusion of SiH_3 precursor during a-Si:H deposition. As a result, the rougher SiN_x will degrade the a-Si:H quality at the a-Si:H/SiN_x interface layer. The a-Si:H film grown on rough SiN_x substrate forms many defects near the SiN_x/a-Si:H interface, which will dominate midgap defect states in material. The subthreshold swing relates to gap states as following equation:

$$S_{sub} = \frac{kT}{q} \cdot \ln 10 \cdot \left(1 + \frac{C_d + C_s}{C_i}\right)$$

where C_d is the depletion layer capacitance, C_s is the interfacial layer capacitance and C_i is the insulator capacitance. Gap states due to a rough SiN_x/a-Si:H interface lead to the increase of interfacial layer capacitance and thus increase subthreshold swing.

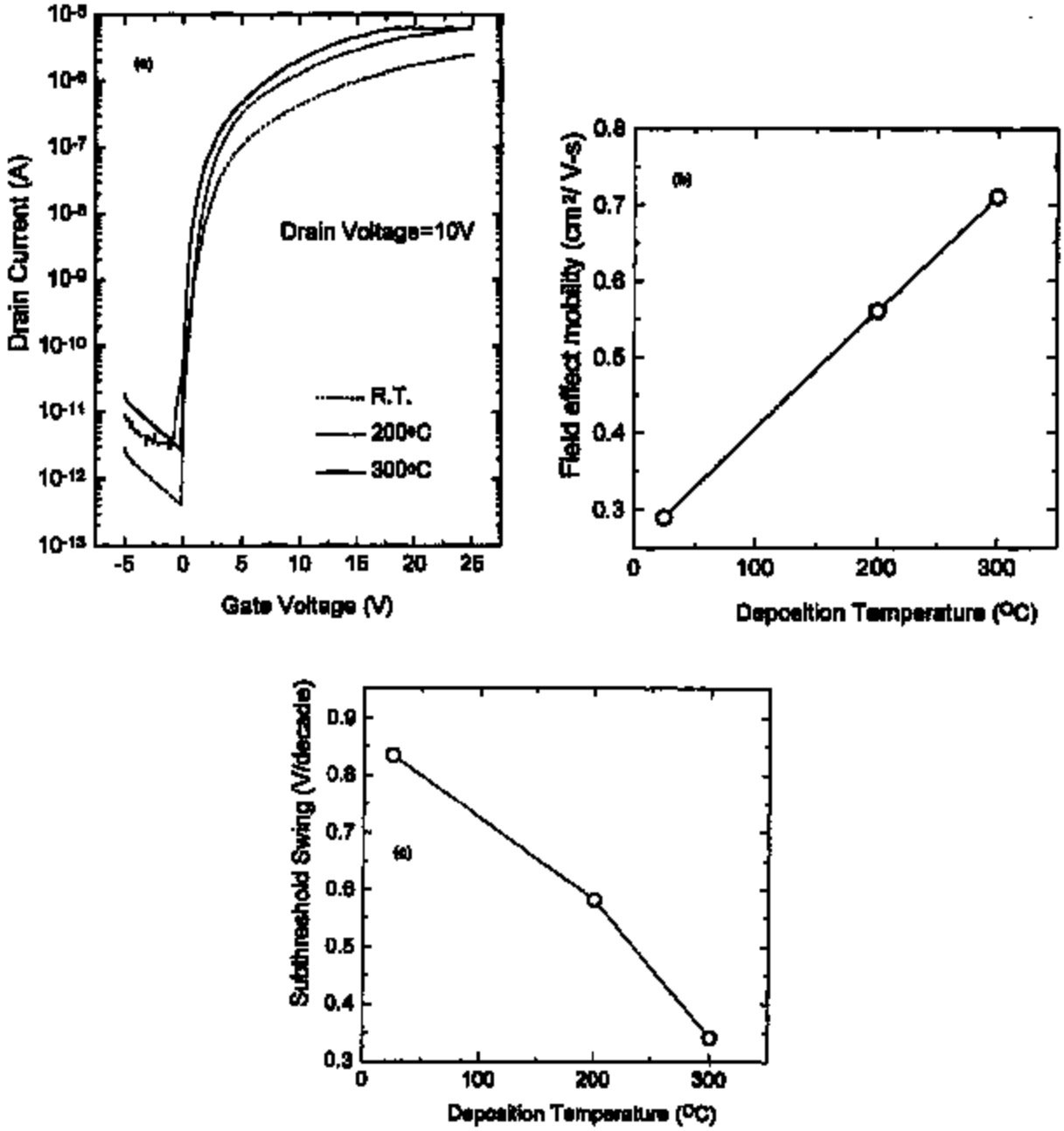

Fig. 4. Device characteristics of single-layered insulator a-Si:H TFTs with the Al gate deposited at various temperatures: (a) transfer characteristics measured at a drain voltage of 10 V, (b) field effect mobility, (c) subthreshold swing.

In addition, we also investigated the a-Si:H TFT with a double-layered insulator (SiN_x/Al_2O_3). Fig. 5a–c shows the transfer characteristics, field effect mobility and subthreshold swing of a-Si:H TFT with a double-layered insulator (SiN_x/Al_2O_3), respectively. The dependence of transfer characteristics, field effect mobility and subthreshold swing on Al gate deposition temperature is similar to that of a-Si:H TFTs with a single-layered insulator. Both the ON current and field effect mobility increase with increasing deposition temperature of the Al gate. The subthreshold swing decreases with increasing deposition temperature of the Al gate. The field effect mobility

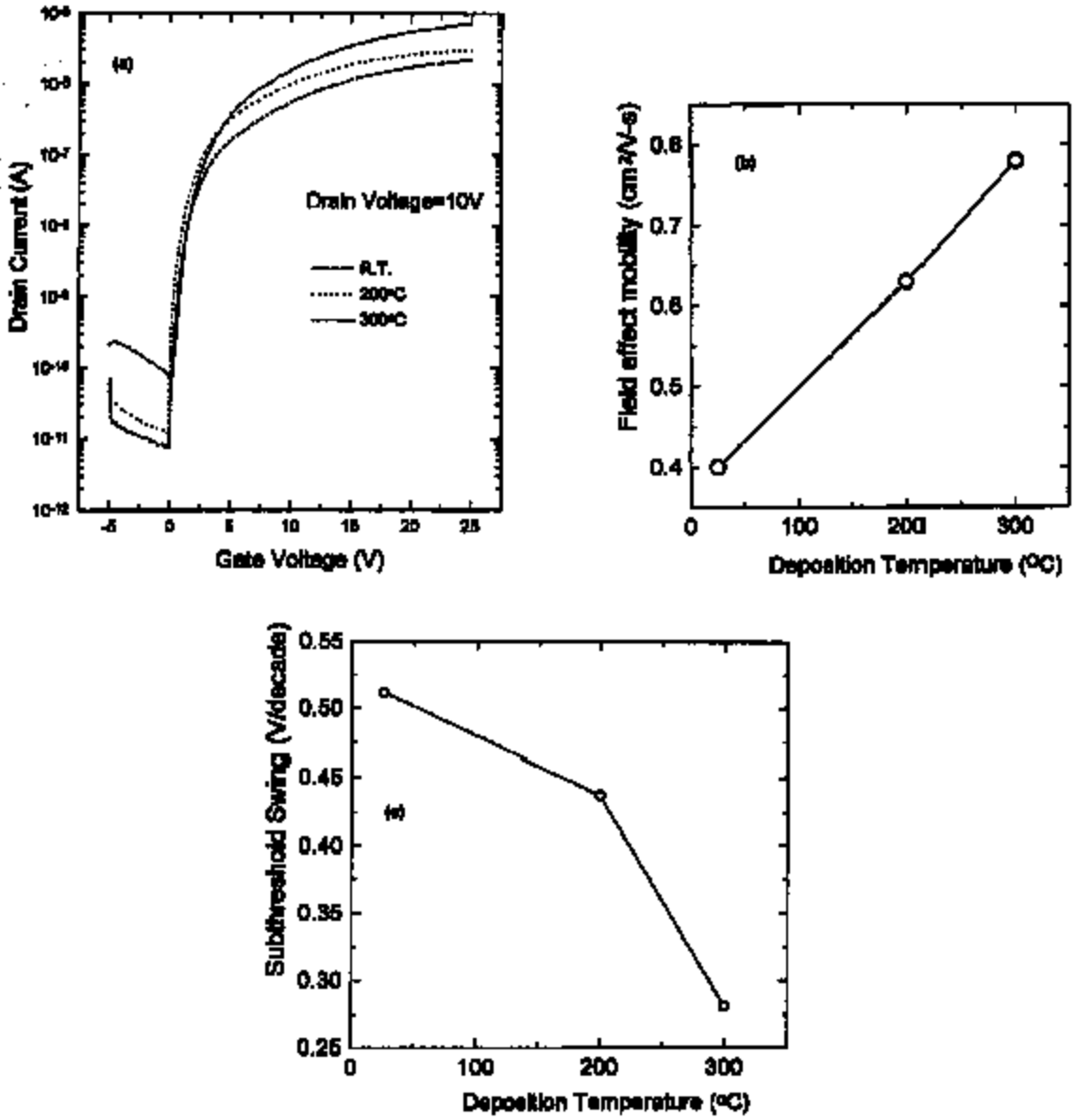

Fig. 3. Device characteristics of double-layered insulator a-Si:H TFTs with the Al gate deposited at various temperatures: (a) transfer characteristics measured at a drain voltage of 10 V, (b) field effect mobility, (c) subthreshold swing.

increases from 0.4 to 0.78 $cm^2/V\text{-}s$ as the deposition temperature of Al gate increases from RT to 300°C. In addition, the subthreshold swing reduces from 0.51 to 0.28 V/decade. It should be noted that the double-layered insulator (Al_2O_3/SiN_x) a-Si:H TFTs show better electrical performances than their counterparts with single-layered insulators (SiN_x) a-Si:H TFTs. This result is reasonable because Al_2O_3 can further suppress hillock formation on the Al gate of a-Si:H TFTs [7].

4. Conclusions

Hot Al is very effective in suppressing hillock formation and has been successfully applied to the fabrication of a-Si:H TFTs. The intensity of the Al(111) texture increases with increasing deposition temperature. The surface roughness decreases with increasing deposition temperature of the Al gate. An Al layer deposited at 300°C has the smoothest surface. Therefore, a-Si:H TFTs with the Al

gate deposited at 300°C have the best electrical performances. In addition, we also investigated a-Si:H TFTs with double-layered insulators (SiN_x/Al_2O_3). The dependence of transfer characteristics, field effect mobility and subthreshold swing on the Al gate deposition temperature is similar to that of a-Si:H TFTs with a single-layered insulator.

Acknowledgements

The authors would like to express their appreciation to all the staff of the Semiconductor Research Center, National Chiao Tung University for their technical support. This work is supported by the National Science Council of the Republic of China (NSC87-2215-E317-002 and NSC-87-2721-2317-200).

References

[1] E. Iwamura, T. Ouishi, K. Yoshikawa, J. Jpn. Inst. Met. 59 (1995) 673.
[2] T. Ouishi, K. Yoshikawa, Y. Koga, R&D Kobe Steel Eng. Rep. 43 (1993) 31.
[3] T. Ouishi, E. Iwamura, K. Takagi, K. Yoshikawa, J. Vac. Sci. Technol. A 14(5) (1996) 2728.
[4] S. Takayama, N. Tsutsui, J. Vac. Sci. Technol. B. 14(5) (1996) 3257.
[5] S.R. Wilson, C.J. Tracy, J.L. Freeman Jr., Handbook of Multilevel Metallization for Integrated Circuits, Noyes Publications, Park Ridge, 1993.
[6] S. Wolf, Silicon Processing for the VLSI Era, vol. 2, Lattice Press, Sunset Beach, CA, 1990.
[7] C.F. Yeh, J.Y. Cheng, J.H. Lu, Appl. Jpn. J. Appl. Phys. 32 (1993) 2803.
[8] R.A. Schwarzer, D. Gerth, J. Electron. Mater. 22 (1993) 607.
[9] D. Gerth, R.A. Schwarzer, Mater. Sci. Forum 94–96 (1992) 557.
[10] D. Gerth, D. Kaiser, M. Kohn, Thin Solid Films 288 (1992) 67.
[11] R. Cao Martin, C.J. Tracy, J.W. Mayer, L.E. Hendrickson, Thin Solid Films 271 (1995) 64.
[12] Y.C. Cheng, E.A. Sullivan, Surf. Sci. 34 (1973) 717.
[13] H. Uchida, K. Takeuchi, S. Nishida, S. Kaneko, Jpn. J. Appl. Phys. 30 (1991) 3691.

ELSEVIER

Thin Solid Films 349 (1999) 191–198

Thin Solid Films

Effect of aluminium oxide caps on hillock formation in aluminium alloy films

Eiji Iwamura*, Katsutoshi Takagi, Takashi Ohniahi

Materials Research Laboratory, Kobe Steel Ltd., 1-5-5 Takatsukadai, Nishi-ku, Kobe 651-22, Japan

Received 19 November 1998; received in revised form 26 February 1999; accepted 26 February 1999

Abstract

The effect of surface oxide layers on thermally induced hillock formation was examined in AlTa and AlCu alloy films. An anodic oxide or a sputter-deposited oxide layer was intentionally formed on the top of the Al alloy films, and subsequently annealed in a vacuum of less than 1×10^{-4} Pa. Hillock formation on the encapsulated films, the dependence of hillock density on types and thickness of the oxides, and film stresses were investigated. It was observed that hillocks preferentially formed under the oxides and extruded out of the films, breaking through them. SEM and cross-sectional TEM micrographs revealed hillock growth along with the oxide/metal interface and deformation of the surface oxides following the change of surface topography by hillock formation. More than 100 nm in thickness of anodic oxide caps or a 230-nm thick sputter oxide were necessary to suppress hillock formation. An identical hillock density was obtained in each Al alloy film with encapsulation up to 62 nm in thickness, independent of the thickness and type of the oxide cap. The results indicate that surface conditions are unlikely to determine hillock density, and hillock suppression in the encapsulated films was presumably achieved by lower film stresses at elevated temperature resulting from higher initial tensile stresses induced by anodization and a smaller gradient of the stress–temperature curve of the metal/oxide multilayered films. © 1999 Elsevier Science S.A. All rights reserved.

Keywords: Anodic oxidation; metallization; Stress; Surface and interface states

1. Introduction

In recent developments of high quality liquid-crystal-displays (LCDs), aluminium and Al-alloy films have begun to be employed as address lines instead of conventional refractory metal films [1,2]. Although Al has the advantage of sufficiently low electrical resistivity to accomplish larger diagonal size and higher resolution of the displays, poor thermal stability has been a serious problem for a long time. Particularly, hillock resistance which will cause electrical short and adhesion problems is the most crucial matter related to the deteriorating reliability of thin film devices in LCDs.

Hillocking in Al thin films during the thermal process is well known in LSI interconnections, and its mechanism and phenomenon have been investigated by a number of researchers. The most accepted model is that hillock formation at elevated temperature is one of diffusional creep. The atoms which compose hillocks are considered to be diffused out of the film due to compressive stress thermally induced in the films, and it is suggested that mass transport is controlled by grain boundary and/or surface diffusion [3,4].

Several techniques have been suggested to prevent hillock formation. Encapsulation by a stiff overlayer and alloying are considered to be the most effective means to practically suppress hillock formation.

Several materials, for example Ti and W [5], Al_2O_3 [6–10], TiN [11], SiO_2 [12,13] and TiW [13,14], were proposed as the cap layer to suppress hillocking with minimal modification of the process flow. Such stiff overlayers are supposed to hinder atomic transportation to the free surface leading to hillocking, whereas a thin surface oxide layer, such as a native or thermal oxide, is generally considered to be essential for hillock formation. Experimentally, an absence of hillocking was observed in the films deposited and subsequently annealed in an ultra high vacuum system [15]. This result was interpreted as showing that the diffused out atoms from inside the films spread out on the surface without hillocking because there was no oxide on the surface. In films with the surface oxides, it is considered that the lower surface energy of Al_2O_3 compared with Al encourages consolidation of the Al atoms to form hillocks [16], and that holes and cracks in the surface oxides are

* Corresponding author. Tel.: +81-78-992-5507; fax: +81-78-992-5512.

E-mail address: e-iwamura@rd.kcr.kobelco.co.jp (E. Iwamura)

0040-6090/99/$ - see front matter
PII: S0040-6090(99)00220-5

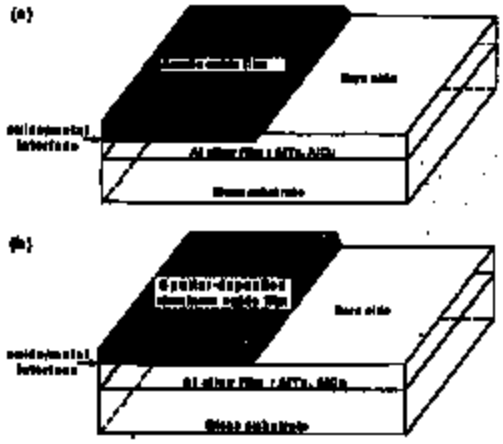

Fig. 1. Schematic drawings of test samples. One side of the film surface was encapsulated by aluminium oxide formed through anodization or sputter deposition.

associated with nucleation and growth sites of hillocks [15–17].

On the other hand, addition of a small amount of appropriate elements into Al significantly affects hillock formation behavior. In a previous report, the addition of Ta into Al distinctly reduced hillock density compared with pure Al and AlCu films [18]. The reduction of hillock density can be related to possible differences of the defects and non-uniformity of the surface oxide in each films. However, the relationship between the number of defects on a film surface and the resultant hillock density is unclear. Moreover, it is difficult to directly identify possible or exact defects on film surface as the origin of hillock nucleation.

In this study, two different types of aluminium oxides, which were intentionally formed on top of Al alloy films by anodization or sputter deposition, were employed to examine the effect of surface oxide layers on hillock formation. The major objectives were to determine how hillocks form in the encapsulated films and how the oxide caps affect hillock density and suppression.

2. Experimental

Aluminium-2 at.% Ta, Al-0.5 at.% Ta and Al-2 at.% Cu alloy films with 1 μm thickness were deposited by dc magnetron sputtering onto BaO-B_2O_3-SiO_2-Al_2O_3 glass substrates (Corning No. 7059, 10 × 20 × 0.5 mm). The substrates were water cooled during deposition. The base chamber pressure was below 1.0×10^{-4} Pa. The Ar gas pressure during deposition was 2.0×10^{-1} Pa. The sputtering power density was 0.033 W mm^{-2}, and the resultant deposition rate was 2.5 nm s^{-1}.

Subsequently, surface oxide caps with various thicknesses from 5 to 230 nm were formed by anodic oxidation or sputter deposition onto half of the film surface. The test structures are illustrated in Fig. 1. The bare sides without oxide caps served as a control to preclude artifacts induced by the oxide formation in hillock formation behavior. As the formation of the cap layers and the deposition of the Al alloy films were not sequential, a native oxide layer was expected to form on the surface of the Al alloy films.

The anodic oxide was grown in a system previously described [10]. The electrolyte was an ethylene glycol solution mixed with 3% tartaric acid with the pH adjusted to 7.0 using 2.9% NH_4OH. The oxidation initially proceeded on a constant current density mode with 0.002 mA mm^{-2} at room temperature. After the designated voltage ranging from 4.5 to 140 V was obtained, the process was switched to a constant voltage mode which yielded a dense and uniform oxide. Oxide thickness was determined by an applied voltage in the procedure. The anodic oxide formed in this way is generally called barrier-type, and is amorphous and dense.

Sputter oxides were formed by rf sputtering using Al_2O_3 sintering type targets with 99.99% purity. No substrate heating was applied during the deposition. The base chamber pressure was below 1.0×10^{-4} Pa. The Ar gas pressure during deposition was 5.0×10^{-1} Pa. The sputtering power density was 0.032 W mm^{-2}, and resultant deposition rate was 0.5 nm s^{-1}.

The test samples were annealed at 473, 573 and 673 K for 1 h in a vacuum less than 1×10^{-4} Pa. There were no specific structures observed on the film surface prior to the annealing.

Optical microscopy and high resolution scanning electron microscopy (HRSEM) was performed to examine surface topography and hillock density. Cross-sectional microstructure was observed with transmission electron microscopy (XTEM). Very careful thinning procedures for preparation of XTEM samples were performed using focused ion beam (FIB) methods in order to obtain cross-sectional microstructures at the center of hillocks. The sample surface was protected by C and/or W layers deposited by evaporation prior to FIB thinning.

The thicknesses of the artificial oxide caps were optically measured by a spectrometric film thickness measurement system, Lambda Ace, and confirmed through high resolution XTEM micrographs. For native and thermal oxide on the film surface, Auger electron spectrometer (AES) was performed to measure their thickness and confirmed through high resolution XTEM micrographs as well. It is estimated that the AES data contains ± 20% of experimental errors. The scale of TEM micrographs was calibrated by a lattice image of Al in the photographs.

Film stresses as a function of temperature were obtained in-situ through the wafer curvature technique [19]. The 400-nm thick test films with artificial oxide caps were prepared through the same sputtering and oxidization conditions as mentioned above onto 2-in-diameter glass substrates. The test samples were heated at a rate of 0.0083 K s^{-1} up to 773 K in a N_2 ambient.

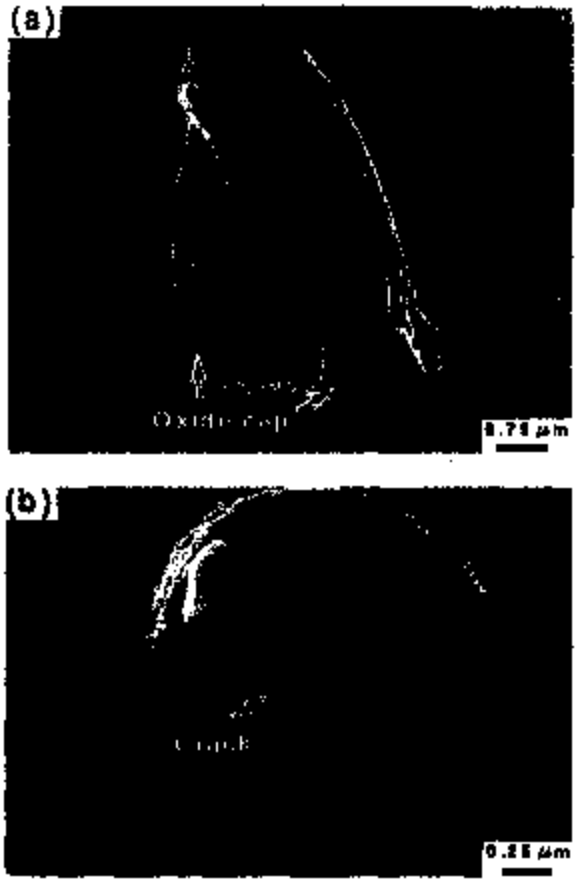

Fig. 2. Hillocks formed in Al alloy films with an anodic oxide cap having a thickness of 20 nm: (a) an Al-2 at% Ta alloy film, (b) an Al-2 at.% Cu alloy film. The samples were annealed at 573 K for 1 h.

3. Experimental results

3.1. Hillocks in encapsulated films

Fig. 2a,b show hillocks formed in an Al-2 at.% Ta film and an Al-2 at.% Cu film with a 20 nm thick anodic oxide cap after annealing at 573 K for 1 h. The size and shape of the hillocks on the encapsulated side of the films were very similar to those on the bare side. Surface roughness apart from hillocks after annealing was the same as that before annealing. The hillock in the Al-2 at.% Ta alloy film had a horn-like shape about 5 μm high and 4.5 μm in diameter. The hillock surface was smooth in comparison with the oxide cap surface with small scale roughness. Streak-like patterns were observed on the hillock surface. A shell of the oxide cap was observed to be stuck on the foot of the hillock. The hillock appeared to extrude, breaking and piling up the oxide cap.

Hillocks formed in Al-2 at.% Cu films were usually much smaller in size than those in AlTa films. The hillock exhibited a mound shape almost covered by the oxide cap. There was an extrusion out of the oxide cap at the top of the hillock. Cracks in the oxide cap were observed at the vicinity of the extrusion as indicated by the arrow.

The hillock shown in Fig. 3a is one of the typical hillocks formed in Al-2 at.% Ta films with a 50-nm thick anodic oxide cap after annealing at 573 K for 1 h. The hillock consisted of two parts, one grew under the oxide cap in the shape of a mound, and the other was extrusions out of the film. The extrusions appeared to break through the oxide cap, and the curled extrusions resembled a soft paste squeezed out of the film.

Fig. 3b shows a cross-sectional microstructure of the same kind of hillocks shown in Fig. 3a. It was clearly seen that the oxide cap clung to the hillock surface at the mound-shaped area, and it was broken at the area of extrusion. The anodic oxide cap appeared to be well deformed to follow the change of the surface topography caused by the hillock growth. The microstructure of the hillock was composed of larger grains in comparison with grains in the film that maintained their original microstructure consisting of a fine semi-columnar structure, i.e. granular at the bottom and columnar on the top. The grains of the hillock appeared to be incorporated into the film microstructures.

Hillocks in films with thin sputter oxide caps up to 20 nm thick formed in a similar way to those in films with the equivalent thick anodic oxide caps. As the thickness of the sputter oxide cap increased, hillocks tended to grow preferentially under the oxide to form a large bulge on the film surface. Fig. 4 shows a cross-sectional microstructure of a hillock formed in the Al-2 at.% Ta film with a 62-nm thick sputter-deposited oxide cap after annealing at 573 K for 1 h. The hillock displayed a mound-like shape about 10 μm in diameter and 1 μm in height. The hillock expanded laterally along the interface between the oxide and the metal layer. The oxide cap was found to be lifted up, deformed and completely covered the hillock.

3.2. Change of hillock density

Fig. 5a,b show hillock density in AlTa and AlCu alloy films after annealing at 573 K for 1 h as a function of thickness of the oxide caps. In the encapsulated films with both anodic and sputter oxides, the Al-2 at.% Cu, Al-0.5 at.% Ta, and Al-2 at.% Ta alloy films exhibited approximately 5×10^4 mm^{-2}, 1×10^3 mm^{-2}, and 1×10^2 mm^{-2} of hillock density, respectively. The addition of 0.5 at.% Ta and 2 at.% Ta into Al reduced the hillock density by factors of 50 and 500 respectively, compared with Al-2 at.% Cu alloy films. The thickness and type of the oxide caps did not affect the relative order of hillock density in these films. In the thickness range up to 62 nm, only the Al-2 at.% Ta alloy films with an anodic oxide cap exhibited a slight tendency of density reduction with a increase of the oxide thickness.

To suppress hillocking when annealing at 573 K for 1 h, more than 100 nm in thickness of anodic oxide cap or a 230 nm thick sputter oxide was needed in each Al alloy film. In

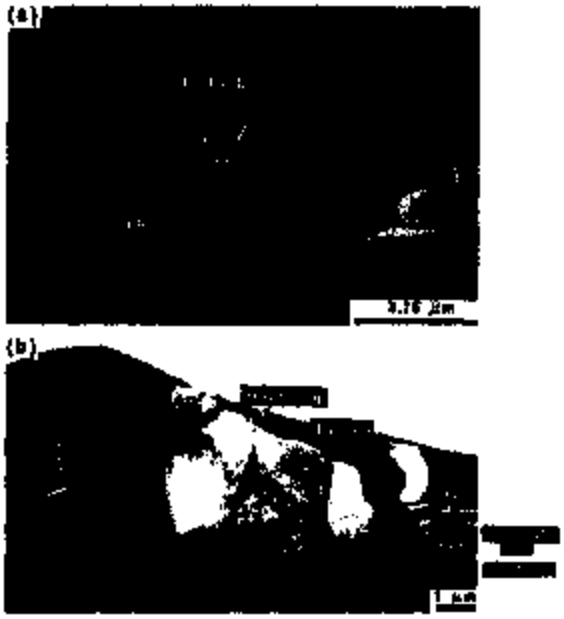

Fig. 3. Hillocks formed in an Al-2 at.% Ta alloy film with an anodic oxide cap having a thickness of 50 nm: (a) SEM appearance, (b) TEM cross-sectional microstructure. The samples were annealed at 573 K for 1 h.

the films encapsulated by such a thick oxide cap, the film surface after the annealing was as smooth as that before annealing.

3.3. Stress-temperature curve of encapsulated films

Fig. 6 shows stress-temperature curves upon heating which were measured for Al-2 at.% Ta alloy films with and without the oxide caps. The stress of the film without encapsulation was about 60 MPa tensile before heating, and decreased as temperature increased. The film was seen to deform elastically in the low temperature range. Film stresses switched from tensile to compressive at about 370 K, and the stress-temperature relation began to deviate from the elastic behavior at about 440 K. On further heating, the stress maintained a constant value about −120 MPa up to 520 K, and thereafter started to decrease gradually towards zero. In the temperature range between 610 and 773 K, film stresses were in a range from 0 to about 20 MPa compressive. In the film with a 114 nm anodic oxide cap, initial stress before heating reached about 440 MPa tensile. Film stresses decreased linearly without showing

Fig. 4. TEM cross-sectional microstructure of a hillock formed in an Al-2 at.% Ta alloy film with a sputter-deposited oxide cap having a thickness of 62 nm.

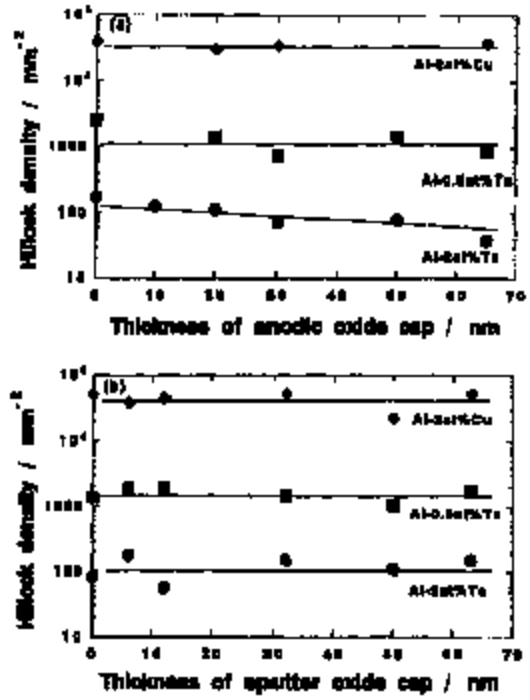

Fig. 5. Hillock density in Al alloy films after annealing at 573 K for 1 h as a function of oxide cap thickness: (a) with anodic oxide, (b) with sputter oxide.

evident stress relaxation and reached about 100 MPa in tensile mode even at 773 K. In the film with 125 nm sputter oxide cap, initial stress was equivalent to that of the bare film, and stress also decreased as temperature increased. However, the slope of the elastic deformation line is more gradual than that of the bare film, and the elastic behavior remained up to 550 K. The stress curve showed a plateau between 550 and 590 K with a compressive value of about 140 MPa. There was significant change in stress toward zero at about 590 K. In the temperature range between 620 and 773 K, film stresses remained in the range from zero to several tens of MPa compressive.

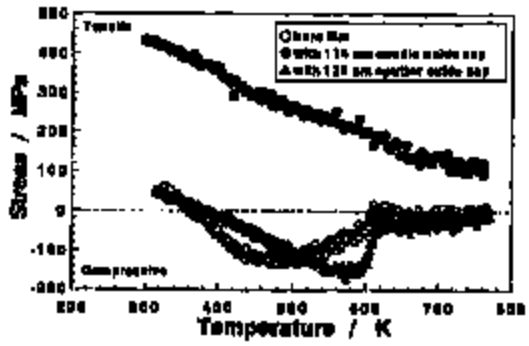

Fig. 6. Film stresses during heating plotted as a function of temperature for Al-2 at.% Ta alloy films: (○) a bare film, (●) an encapsulated film with 100 nm anodic oxide, (▲) an encapsulated film with 200 nm sputter oxide.

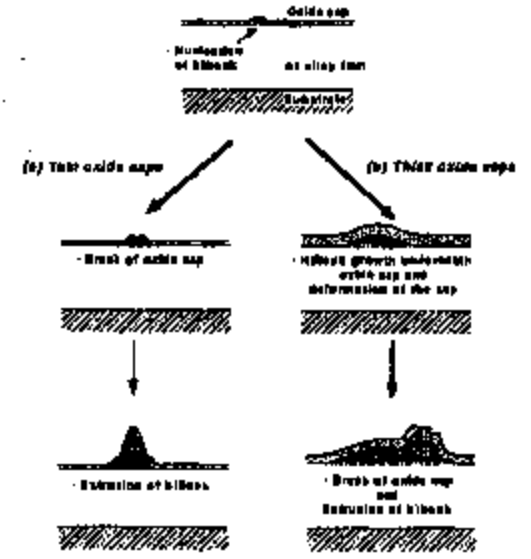

Fig. 7. Schematic drawings illustrating sequence of hillock growth in Al alloy films: (a) with a thin oxide cap, (b) with a thick oxide cap.

4. Discussion

4.1. Hillock growth in encapsulated films

SEM and TEM micrographs observed in this study showed clear images of how hillocks form on the Al alloy films. Considering the difference in hillock size, the hillock in the AlCu film shown in Fig. 2a represents an early growth stage of the hillocks in the AlTa films. The extrusion of hillocks breaking and piling up oxide caps provides support for the model that hillocks are formed through material transfer occurring out of the interior of a film to the free surface. Once the hillocks start to grow, the material transfer of hillocking seems to be concentrated in the selected place, resulting in constant macroscopic hillock density during annealing [18], and leading to the formation of huge hillocks observed in the Al-2 at.% Ta alloy films. The shape of the hillock which appears to have been pushed out of the film like a soft paste implies that the mass was squeezed out with fairly high pressure.

The sequence of hillock growth in the encapsulated films is illustrated in Fig. 7. The hillock formation is characterized by nucleation and growth at the interface between the oxide cap and the Al metal layer, and extrusion breaking through the oxide caps. In films with a thin oxide cap (Fig. 7a), as the volume of the hillock increases after nucleation, it breaks the oxide cap in an early stage of the growth. As a result of the cracking of the oxide cap, the hillock comes out to the free surface. The base of the hillock is not confined to the selected pin point, and the foot expands laterally. In films with a comparatively thick oxide cap (Fig. 7b), hillocks cannot break the oxide caps at the early stage, and hillock growth proceeds along the interface between the oxide layer and the film. When the volume of the hillock increases sufficiently to crack the oxide cap, the hillock extrudes outside.

Both anodic and sputter oxide can be well deformed to follow the change of the surface topography. Sputter oxide caps are more likely to allow the hillock to grow along the oxide/metal interface. This is presumably attributed to an abrupt discontinuity of the oxide/metal interface in the case of sputter oxide caps, compared with anodic oxide caps.

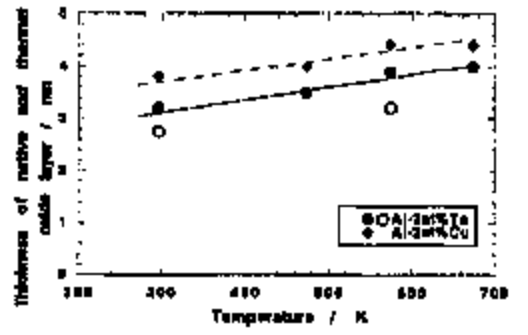

Fig. 8. Thickness of native and thermal oxide in Al alloy films: (●, ◆) measured by Auger electron spectrometer, (○) measured by TEM micrographs.

4.2. Dependence of hillock density on surface conditions

As far as looking at the hillock growth beneath or breaking through the oxide caps and flexibility of the oxides, it is unlikely that the stiffness of the surface oxides affects hillock formation behavior to decrease hillock density.

Differences in hillock density among the Al alloy films were observed even in the bare films. Considering a bare film, it is natural that there is a native oxide on top of the film. The thicknesses of the native and thermal oxides on the Al alloy film surface are expected to be much thinner than those of the artificial oxides examined in this study. Fig. 8 shows thicknesses of native and thermal oxides formed in Al-2 at.% Ta and Al-2 at.% Cu alloy films annealed at 473, 573 and 673 K for 1 h. In both films, the thicknesses of the native oxides were 3–4 nm before annealing. Although the thicknesses increased with increasing annealing temperature, thermal oxides grew to reach about 5 nm in thickness at most even after annealing at 673 K. As shown in Fig. 2, the hillocks in those alloy films broke through the artificial oxides with even 20 nm in thickness. Therefore, it is very likely that the hillocks easily break through the native and thermal oxides to extrude outside.

Since the hillocks are expected to form anywhere without any restriction by the thin surface oxide, identical hillock density in each encapsulated film indicates that there might be differences among them in site selection for hillock nucleation. According to the surface defects model, surface condition is a potential factor in determining the hillock formation sites. Surface oxide layers hinder planar surface

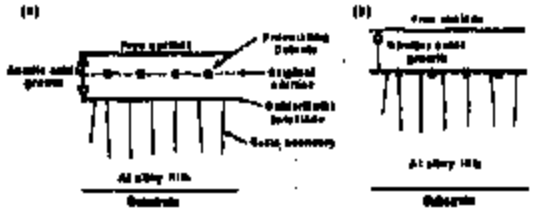

Fig. 9. Schematic drawings illustrating cross-sectional structure of encapsulated films in association with original surface and preexisting surface defects: (a) with an anodic oxide cap, (b) with a sputter-deposited oxide cap.

diffusion and obstruct the diffusion path leading to a free space outside the stressed film system. If the atom flow is interrupted by the oxides, the place where the hillocks nucleate and grow can be related to small defects on the surface, such as grain boundary triple points, misoriented grains and precipitates, and they are supposed to be a site for consolidation of the roaming atoms. This model implies that the number of defects on the film surface or at the interface between the surface oxide layer and an Al alloy film can be correlated with hillock number density.

The encapsulation by the artificial oxides gives the test samples not only restriction of surface diffusion but also a difference in surface condition. Fig. 9 illustrates cross-sectional structure of encapsulated films in association with original surface and preexisting surface defects. In encapsulated films, defects in the original film surface are not on the top layer of the film anymore. Considering the anodization process relating to the level of the original surface, anodic oxides grew on both sides of the original surface (Fig. 9a). Once oxidation is started at the interface between an Al film and electrolyte, the Al cation is transferred up to the top surface passing through the original surface while the O anion is transferred into the film. Since O anion migrates more rapidly than Al cation, the ratio of the oxide thickness outside and inside of the original film is estimated at about 4:6 [20]. Therefore, anodization removes tiny defects preexisting in the original surface from the top surface and involves them in the anodic oxide layer. Large defects, such as pin holes and cracks which possibly remain in the anodic oxide, were not observed in this study and neither did hillocks originate from such defects. On the other hand, sputter deposition forms equivalent oxide layers on top of the original surface in each of the different kinds of Al alloy film. This means that surface defects and defects in the oxide caps are in the same condition in each Al alloy film. The metal/oxide interface is expected to be abrupt and the preexisting defects are trapped at the interface (Fig. 9b).

The facts that each AlTa and AlCu film showed identical hillock density and preferential hillock formation at the oxide/metal interface indicates that hillock formation was not influenced by such surface conditions. The hillock density, which is independent of encapsulation or the type and thickness of the oxide caps, means that it is dominated by neither preexisting defects in the original surface nor defects in the artificial oxides.

As a consequence, the deference in hillock density between AlTa and AlCu alloy films is not explained by the relationship with surface conditions of the film. The place or area where hillocks nucleate and grow seems to be selected before the atoms reach the film/oxide interface, so it is presumably important to consider a driving force which disperses hillocks with specific density in each Al alloy film.

4.3. Hillock suppression by thick artificial oxide caps

In some cases, it is reported that a stiff overlayer results in effective hillock suppression, however, even if the overlayer is strong enough, there may remain problems of hillock and delamination, due to hillock formation at the interface between the Al alloy film and the overlayer as shown in Fig. 7b. Other factors should be considered to explain hillock suppression in encapsulated films with more than 100 nm in thickness of anodic oxides and a 230 nm sputter oxide.

Thermally induced hillocks are believed to form and relieve compressive stresses that develop in a film at elevated temperatures. As temperature increases compressive stresses are induced in the films due to the thermal expansion coefficient mismatch between the metal film and glass substrate. In the elastic deformation region, the stress-temperature curve shows a reversible linear relation and the film stress changes from tensile to compressive, and with further heating compressive stress relaxation takes place.

Fig. 10 depicts stress-temperature relations as temperature increases, in the region where elastic deformation takes place. Lines A, B, and C correspond to the stress curves of an Al alloy film without encapsulation, with a thin oxide cap, and with a thick oxide cap, respectively. The stress

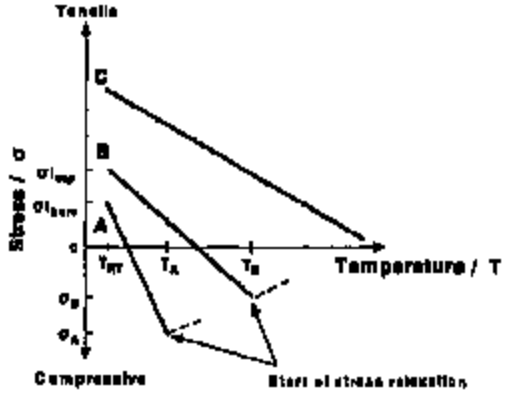

Fig. 10. Schematic representation of stress-temperature relation in Al alloy films with and without encapsulation. Lines A, B and C display elastic deformation for a bare film, for a film with a thin oxide cap, for a film with a thick oxide cap, respectively.

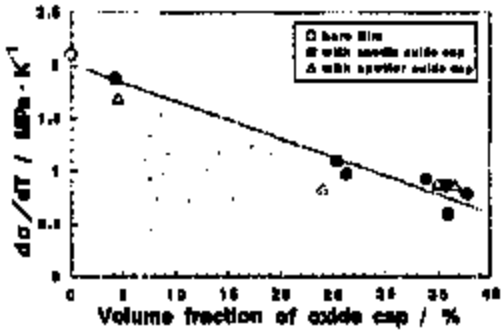

Fig. 11. Measured slopes of stress-temperature curve in elastic deformation region plotted as a function of volume fraction of an oxide cap in Al-2 at.% Ta alloy films: (○) a bare film, (●) encapsulated films with an anodic oxide, (△) encapsulated films with a sputter oxide.

shown in Fig. 10 is the average value of the film with metal and oxide layer. Two specific changes resulting from the encapsulation can be pointed out in the stress-temperature relation. One is the change of initial stresses expressed by $\Delta\sigma i = \Delta\sigma i_{cap} - \Delta\sigma i_{bare}$, and the other is the slope of the stress-temperature curve $\Delta\sigma/\Delta T$ in the elastic deformation region.

The initial stresses of bare Al-2 at.% Cu, Al-0.5 at.% Ta and Al-2 at.% Ta alloy films deposited by dc magnetron sputtering are usually tensile in a range of 0 to 50 MPa. The sputter deposited oxide caps had less effect on the initial stresses, whereas a significant increase in tensile stress was introduced by the formation of the anodic oxide caps, and the σi_{cap} had a strong dependence on thickness. Thermal stress is unlikely to be induced in the films during anodization because it is a chemical process at room temperature. The increase in film stress can be attributed to an increase in volume. The anodization proceeds on both sides of the original surface to form oxides. The volume ratio of the oxide produced to the metal consumed, known as the Pilling–Bedworth ratio, is calculated to be 1.36 [21]. Even though the films can expand freely normal to the film surface, the increase of volume inside the original film creates large tensile stresses in the film, resulting in an increase of the $\Delta\sigma i_{cap}$.

The slope of elastic behavior in the stress-temperature curve was strongly influenced by the encapsulation. According to elasticity theory, the stress changes as a function of temperature, the slope is expressed by

$$\frac{d\sigma}{dT} = E_f(\alpha_f - \alpha_{sub}) \tag{1}$$

where T is the temperature, α_f and α_{sub} are the thermal expansion coefficients of an Al alloy film and a substrate and E_f is the biaxial elastic modulus of the film. The addition of a small amount of element into Al is supposed to have little effect on the values of E_f and α_f. Using the values of 1.143×10^5 MPa and $\alpha_f = 23.1 \times 10^{-6}$ K^{-1} for the Al film and $\alpha_{sub} = 4.6 \times 10^{-6}$ K^{-1} for the Corning glass substrate, it can be calculated that a theoretical value of $d\sigma/dT = 2.11$ MPa K^{-1} for the Al alloy films without encapsulation.

An aluminium film with an oxide cap is a multilayered film, therefore, Eq. (1) is modified by

$$\begin{aligned}\frac{d\sigma}{dT} &= (1 - V_{ox})E_{Al}(\alpha_{Al} - \alpha_{sub}) + V_{ox}E_{ox}(\alpha_{ox} - \alpha_{sub}) \\ &= E_{Al}(\alpha_{Al} - \alpha_{sub}) \\ &\quad - V_{ox}\{E_{Al}(\alpha_{Al} - \alpha_{sub}) - E_{ox}(\alpha_{ox} - \alpha_{sub})\} \\ &= 2.11 - V_{ox}\{2.11 - E_{ox}(\alpha_{ox} - \alpha_{sub})\}\end{aligned} \tag{2}$$

where V_{ox} is the volume fraction of the oxide cap, E_{Al}, E_{ox}, α_{Al} and α_{ox} are the biaxial elastic modules and the thermal expansion coefficient of an Al film and the oxide cap, respectively. There is little information about the values of E_{ox} and α_{ox} of anodic oxides or sputter oxides. However, it is expected that the values are close to those of the glass substrate. Therefore, from the Eq. (2), the slope of the encapsulated films becomes smaller than that of the films without encapsulation and decreases as the volume fraction of oxide caps increases.

Fig. 11 shows the experimental values of $d\sigma/dT$, which were obtained from stress-temperature curves for Al-2 at.% Ta alloy films with various thickness of anodic oxide and sputter oxide cap, as a function of volume fraction of the oxide caps. The gradient of the plots is approximately -3.37, and $d\sigma/dT$ is zero when V_{ox} is 62.6%. In the case of films with 60 MPa tensile at 313 K as shown in Fig. 6, more than 60% of V_{ox} is required to be in tensile stress at 773 K.

Those changes in the initial stress and slope in elastic behavior result in a change in the stress and temperature at which stress relaxation occurs. As can be seen in Fig. 10, increasing initial stress and reduction of the slope leads to an increase in the temperature at which the film stress turns into compressive and a decrease in the value of compressive stress σ_B at the temperature T_B at which stress relaxation starts in comparison with σ_A at T_A in a bare film. Particularly, as shown in Fig. 6, in the film with a 114 nm thick anodic oxide cap, the film stress was still tensile at 773 K, and there was no symptom of stress relaxation. As the result of the tensile film stresses at elevated temperature, the driving force to form hillocks is absent from the film, and therefore hillock formation is completely suppressed. Since the films encapsulated with sputter oxides have similar initial stresses to equivalent bare films, it is a required smaller value of the slope to remain in tensile stress at elevated temperature. This result means a thicker sputter oxide cap should be deposited to suppress hillocking in comparison with an anodic oxide cap.

In conclusion, hillock suppression by thick oxide caps is attributed to the change of mechanical properties of the films rather than the strength or defects of the oxide caps. In addition, it is presumed that the origin of hillock suppression and reduction of hillock density might be different.

Complete hillock suppression is not accomplished via the goal of the method of reduction of hillock density.

5. Summary

Morphology, cross-sectional microstructures and density of hillocks and film stresses were studied in Al-2 at.% Ta, Al-0.5 at.% Ta and Al-2 at.% Cu alloy films encapsulated by an anodic or a sputter-deposited aluminium oxide.

In films having oxide caps of up to 20 nm in thickness, hillocks appeared to form easily and broke through the oxide caps. In films with a comparatively thick oxide cap, having a thickness of more than 20 nm, hillocks preferentially grew along the metal/oxide interface. Both anodic and sputter-deposited oxide caps were flexible and easily deformed, following the change of surface topography by hillock formation. As a result of the increase of hillock volume under the oxide and cracking the oxide caps, hillocks appeared to extrude to the free surface.

The original surface and preexisting surface defects are supposed to be removed from the top surface to the inside or bottom of oxide after encapsulation. Identical hillock density obtained in each Al alloy film with encapsulation, independent of thickness and type of oxide cap, indicates that surface defects are unlikely to be dominant in determining hillock density.

After annealing at 573 K, no hillocks were observed in films encapsulated by an anodic oxide with a thickness in excess of 100 nm or a sputter oxide with 230 nm thickness. The elimination of hillocks is probably achieved by lower film stresses at elevated temperatures resulting from higher tensile initial stresses induced by anodization and a smaller gradient of stress-temperature curve of a metal/oxide multilayered film.

Acknowledgements

The authors wish to thank Kiyoshi Yamamoto of Kobelco Research Institute, Inc. for SEM and TEM works, and Takeshi Kurihara for film preparation.

References

[1] S. Yamamoto, T. Ohnishi, K. Yoshikawa, Y. Koga, Proc.12th Int. Display Research Conf. 1992 p. 217.
[2] K. Takagi, E. Iwamura, T. Ohnishi, K. Yoshikawa, Proc. 15th Int. Display Research Conf. 1995 p. 461.
[3] P. Chaudhari, J. Appl. Phys. 45 (1974) 4339.
[4] M. Murakami, T.S. Kuan, Thin Solid Films 66 (1980) 301.
[5] D.S. Gardner, T.L. Michalka, P.A. Flinn, T.W. Barbee Jr, C. Saraswat, J.D. Meindl, Proc. 2nd Int. IEEE VLSI Multilevel Interconnection Conf. 1985 p. 102.
[6] C.J. Dell'Oca, A.J. Learn, Thin Solid Films 8 (1971) R47.
[7] D.S. Herman, M.A. Schuster, R.M. Gerber, J. Vac. Sci. Technol. 9 (1972) 515.
[8] T.J. Faith, J. Appl. Phys. 52 (1981) 4630.
[9] C.-F. Yeh, J.-Y. Cheng, J.-H Lu, Jpn. J. Appl. Phys. 32 (1993) 2803.
[10] T. Tanluda, Mater. Res. Soc. Symp. Proc. 284 (1993) 371.
[11] M. Rucke, M. Schneegans, J. Vac. Sci. Technol. B6 (1988) 1213.
[12] C.J. Sambuo, J. Electrochem. Soc. 116 (1969) 361.
[13] P.H. Townsend, H.A. Vander Plas, Proc. of V-MIC conference, 1985 p. 76.
[14] C.D. Gruss, Mater. Res. Soc. Symp. Proc. 265 (1992) 211.
[15] C.Y. Chang, R.W. Vook, Thin Solid Films 228 (1993) 205.
[16] R.W. Vook, Mater. Chem. Phys. 36 (1994) 199.
[17] P. Choudhuri, IBM J. Res. Dev. 13 (1969) 197.
[18] E. Iwamura, T. Ohnishi, K. Yoshikawa, Thin Solid Films 270 (1995) 450.
[19] P.A. Flinn, D.S. Gardner, W.D. Nix, IEEE Trans. Electron Devices ED-34 (1987) 689.
[20] H. Nahezaki, K. Shimizu, P. Skeldon, G.E. Thompson, G.C. Wood, Phil. Mag. B 73 (1996) 445.
[21] M. Ohring, The Materials Science of Thin Films, Academic Press, 1992 p. 583.

ELSEVIER

Thin Solid Films 289 (1996) 289–294

Thin Solid Films

Al–Sm and Al–Dy alloy thin films with low resistivity and high thermal stability for microelectronic conductor lines

Shinji Takayama [a,*], Naganori Tsutsui [b]

[a] Hosei University, Department of Electrical Engineering, 3-7-2 Kajino-cho, Koganei, Tokyo 184, Japan
[b] ITEC Co. Ltd, 800 Ichiriyoke, Yasu-cho, Yasu-gun, Shiga 520-23, Japan

Received 14 November 1995; accepted 9 April 1996

Abstract

The addition of either Sm or Dy rare earth metal elements to Al thin films decreases markedly the grain size of the Al matrix and largely suppresses the growth of hillock and whisker thermal defects at high temperatures (350–450 °C). A large number of particles of fine metallic compounds of Al_3RE (RE = Sm or Dy) were segregated in an Al matrix, mostly at grain boundaries, after annealing at 350 °C. The resistivities of the films after annealing at the above temperatures show very low values of less than about 50 nΩ m, without salient formation of hillocks or whiskers on the film surfaces.

Keywords: Aluminium; Conductivity; Heat treatment; Resistivity

1. Introduction

There has recently been a strong need for the development of lower cost, larger size, and higher resolution TFT-LCDs (thin film transistor liquid-crystal displays), to increase the range of their applications. However, the larger the TFT-LCD panel is, the more serious the gate-line pulse delay problem becomes. Moreover, to achieve higher resolution, the gate-line width is being made narrower; thus, the microstructure of thin film conductors is of vital importance as regards their reliability. For these reasons, Al alloy thin films with low resistivity have recently received much attention [1–7]. It was reported by the present authors that Al–rare-earth alloy systems in particular showed very low resistivities without the formation of hillocks and whiskers, even after annealing at high temperatures (350–450 °C) [4–6].

In this report, we study in more detail the effects of adding Sm or Dy to Al thin films on the structure and conductivity after isochronal or isothermal annealing.

2. Experimental details

Al–rare-earth alloy films about 400–600 nm thick were deposited onto 7059 glass substrate using a d.c. magnetron sputtering apparatus at an Ar pressure of 0.7 Pa. The composition of the films was varied by using a composite target consisting of 100 mm Al disks (99.99% purity) and $5 \times 5 \times 1$ mm^3 rare earth metal element chips (99.9% purity). The film composition was determined by inductively coupled plasma (ICP) spectroscopy. The electrical resistance of the film was measured using a conventional four-point probe at room temperature. The film structures were examined using an X-ray diffractometer operated at 50 kV and 200 mA, and a transmission electron microscope (TEM) operated at 400 kV.

3. Results

Fig. 1 shows the change in resistivity in as-made Al–RE (RE = Sm or Dy) alloy thin film samples as a function of the content of the elements added to Al. The resistivities after annealing at 450 °C are also included in the figure for reference. The resistivity increases almost linearly within the composition range of the present study. The slope of the curve for as-made Al–Sm alloy films is steeper than that for as-made Al–Dy alloy films. Note that the resistivities of the samples decrease markedly and lie almost on the same straight line after annealing at 450 °C, regardless of the type of element added, as is discussed later. X-ray diffraction measurements showed that in all the alloy systems studied here, the growth of a highly oriented Al(111) plane was strongly suppressed by adding only a small amount of the

* Corresponding author. IBM Research, Tokyo Research Laboratory, Shimotsuruma, Yamato-shi, Kanagawa 242, Japan.

0040-6090/96/$15.00 © 1996 Published by Elsevier Science S.A.
PII S0040-6090(96)08982-7

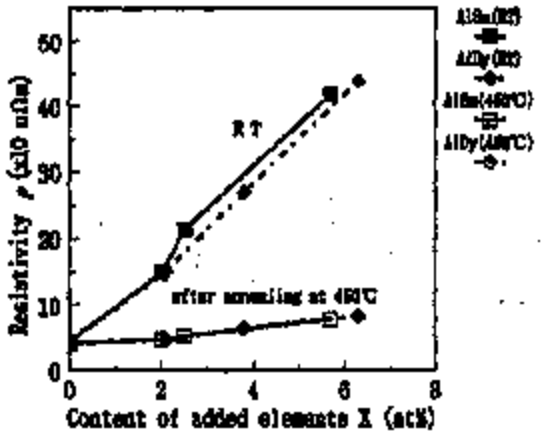

Fig. 1. Change in resistivity ρ with composition in as-made and annealed (at 450 °C) $Al_{100-x}RE_x$ alloy thin films (RE = Sm and Dy).

rare earth metal elements to pure Al, but that the diffraction intensity and width of the peaks continued to increase with a further addition of elements. This is shown representatively in Fig. 2. In the figure, the values shown on the right in atomic per cent indicate the amounts of elements added to Al. The above findings indicate that the thin films tend to lose their initial highly oriented crystal structure and to acquire a more randomly oriented polycrystalline structure with the addition of small amounts of foreign atoms to Al. The increase in the diffraction intensity with further addition of foreign rare earth elements is due most probably to some segregation of metallic compounds, though this is not clear from the X-ray results shown in Fig. 2. Although the solid solubility of the rare earth metal elements is very low (less than 0.01 at.%), the noticeable diffraction peaks associated with Al alloy metallic compounds are barely observable, as the figures show. TEM observation revealed that these as-made Al–light-rare-earth alloy films (containing about 3 at.% added element) have very fine grains less than 100 nm in diameter (see Fig. 3(a) and (b)). Note that these alloy films, like other Al–rare-earth alloy thin films (Al–RE, RE = Y or Gd) reported in [4,5], do not show a clear grain boundary image. Judging from the appearance of the bright field images in Fig. 3, the structure of the alloys may be considered as a metastable phase. Selective area diffraction analysis of the samples in Fig. 3 shows that there is a shift in the position of the diffraction rings with respect to the rings for pure Al, without showing the clear diffraction rings associated with a segregated metallic compound. This indicates that the film structures consist mainly of highly supersaturated solid solutions of the Al phase. The corresponding energy-dispersive X-ray analysis (EDX) of TEM samples in Fig. 3 reveals that the added Sm and Dy elements are distributed almost homogeneously in the Al matrix compared with those in the annealed samples. This is shown representatively in Fig. 4 for the as-made $Al_{97.5}Sm_{2.5}$ thin film sample shown in Fig. 3(a). The left (a) and right (b) images in Fig. 4 show a scanning transmission electron micrograph (STEM) image and the distribution of Sm in the Al matrix, observed by EDX analysis, respectively. Note that the added Sm seems to be distributed not only inside grains,

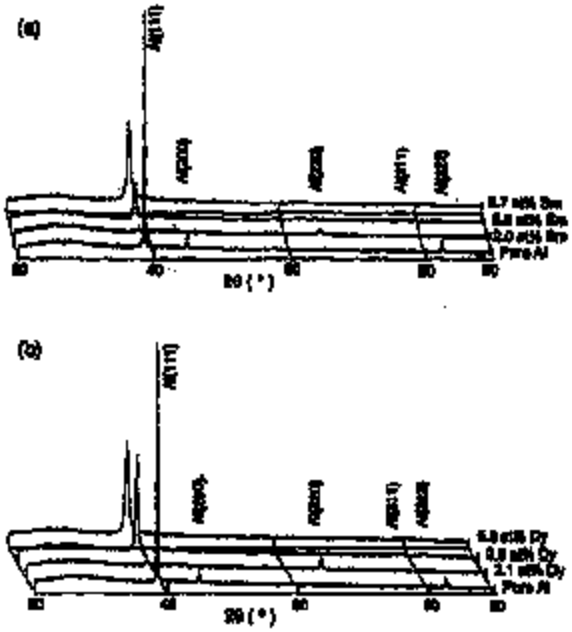

Fig. 2. X-ray diffraction profiles of (a) Al–Sm and (b) Al–Dy alloy thin films as a function of the content of the element added to Al.

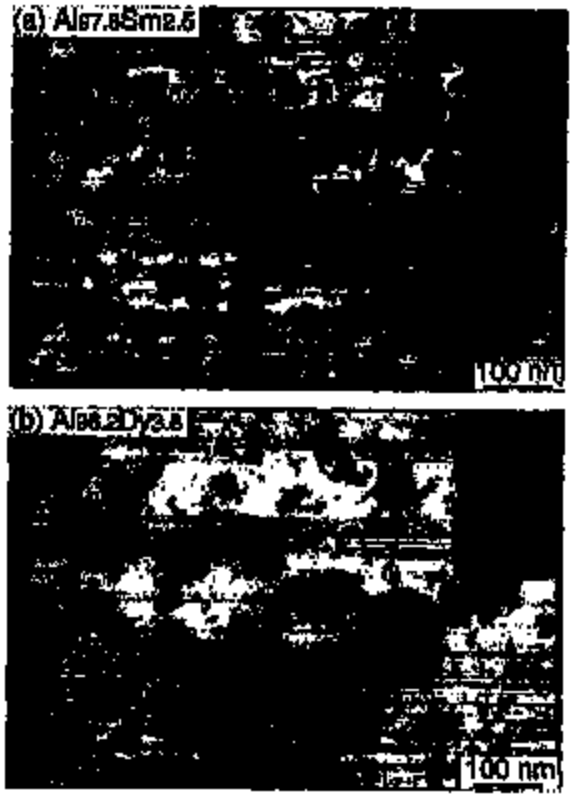

Fig. 3. Bright field images and diffraction patterns of as-deposited (a) $Al_{97.5}Sm_{2.5}$ and (b) $Al_{96.2}Dy_{3.8}$ alloy thin films.

Fig. 4. (a) STEM image of the as-deposited $Al_{97.5}Sm_{2.5}$ alloy film sample in Fig. 3(a), and (b) the distribution of Sm measured by EDX in the same area as (a).

but also along grain boundaries. However, the Sm is distributed relatively homogeneously in the as-made Al matrix compared with the annealed samples, as described below (see Fig. 11).

All the as-made Al–rare-earth alloy film samples in Fig. 1 were annealed isochronally in a vacuum (less than 10^{-4} Pa) at various temperatures for 30 min. The changes in their resistivities are shown in Fig. 5 as functions of both the annealing temperature and the composition of each added element. The results for pure Al films are also included in the figure, for comparison. The solid lines and dotted lines represent the curves obtained for the Al–Dy and Al–Sm alloy systems respectively. The values in atomic per cent shown on the right of the figure indicate the amounts of the elements added to Al. Note that the general features of the change in resistivity in each alloy system are similar, regardless of the composition of added elements. The resistivity starts to decrease sharply at 250 °C and 300 °C for the Al–Dy and Al–Sm alloy systems respectively, and then saturates when it approaches the value for pure Al above 350 °C. Note here that the change in resistivity in pure Al thin films on isochronal annealing is negligibly small (see the bottom part of Fig. 5). This fact probably implies that the changes in resistivity due to grain growth, internal stress relief, and annihilation of point or line defects are small in the present sputtered Al films within the accuracy of the present measurement.

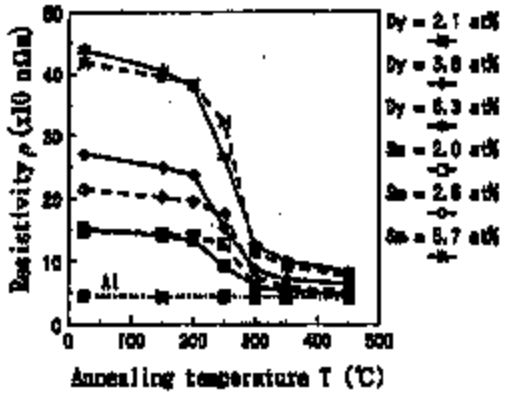

Fig. 5. Change in resistivity ρ of Al–RE alloy films (RE = Sm and Dy) as a function of the isochronal annealing temperature (for 30 min) and composition.

Representative X-ray diffraction profiles of the annealed $Al_{97.5}Sm_{2.5}$ and $Al_{96.2}Dy_{3.8}$ samples in Fig. 5 are shown in Fig. 6(a) and (b) respectively. Visible diffraction peaks associated with the segregation of metallic compounds started to appear after annealing above 250 °C and 300 °C for the Al–Dy and Al–Sm samples respectively. Most of the diffraction peaks that appeared after annealing were indexed, using available data, as belonging to an Al_3RE metallic compound (RE = Sm or Dy), as shown in the figure. It should be noticed here that the appearance of diffraction peaks associated with the segregation of metallic compounds coincides closely with the large drop in resistivity shown in Fig. 5.

Fig. 7 shows the changes in the resistivities of the $Al_{97.5}Sm_{2.5}$ and $Al_{96.2}Dy_{3.8}$ samples when they were annealed

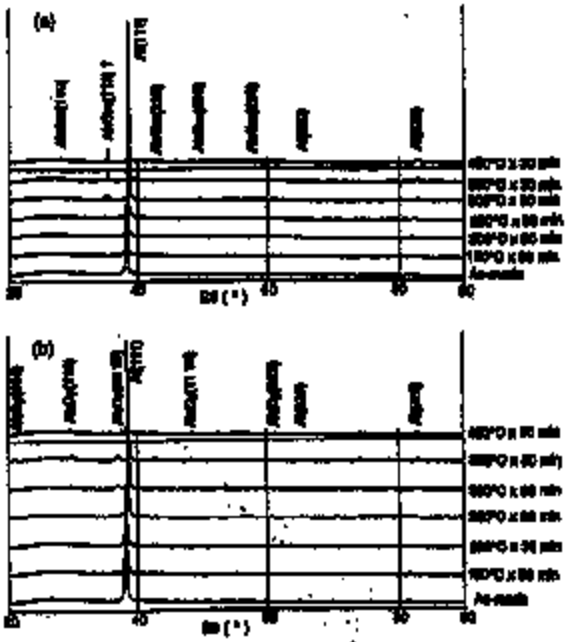

Fig. 6. X-ray diffraction profiles of (a) $Al_{97.5}Sm_{2.5}$ and (b) $Al_{96.2}Dy_{3.8}$ alloy thin films of Fig. 4, annealed isochronally up to 450 °C.

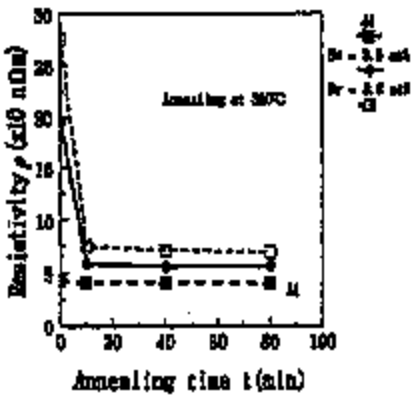

Fig. 7. Change in resistivity ρ of $Al_{97.5}Sm_{2.5}$ and $Al_{94.2}Dy_{5.8}$ alloy thin films after isothermal annealing at 350 °C.

isothermally in a vacuum at 350 °C. In the figure, the results for pure Al films are also included for comparison. The resistivities decreased steeply to low values of less than 80 nΩ m within a very short annealing time, and almost saturated on further annealing. X-ray diffraction profiles corresponding to the annealed $Al_{97.5}Sm_{2.5}$ and $Al_{94.2}Dy_{5.8}$ samples in Fig. 6 are shown in Fig. 8(a) and (b) respectively. These measured profiles, again, clearly demonstrate that segregation of the metallic compounds Al_3RE (RE = Sm and Dy), corresponding to the large drop in resistivity shown in Fig. 7, takes place within 10 min of annealing at 350 °C. The diffraction peaks at $2\theta \approx 35°$ are not clear, but are most probably related to Al_4Sm metallic compounds for the Al–Sm sample and Al_3Dy compounds for the Al–Dy sample, as shown in the figures. It is worth noticing that the growth of hillocks was barely observed on the surface of the above Al–Sm and Al–Dy alloy samples in Figs. 5 and 7. Fig. 9 shows optical micrographs of (a) $Al_{97.5}Sm_{2.5}$ and (b) $Al_{94.2}Dy_{5.8}$ film surfaces annealed at 350 °C for 80 min. The observed features of an $Al_{95}Zr_5$ alloy film annealed under the same heat treatment conditions are also included for comparison, where dark spots (needles) in the photographs indicate hillocks (or whiskers). The figure clearly reveals that hillocks or whiskers are barely observable in the present Al–rare-earth alloy films, whereas relatively

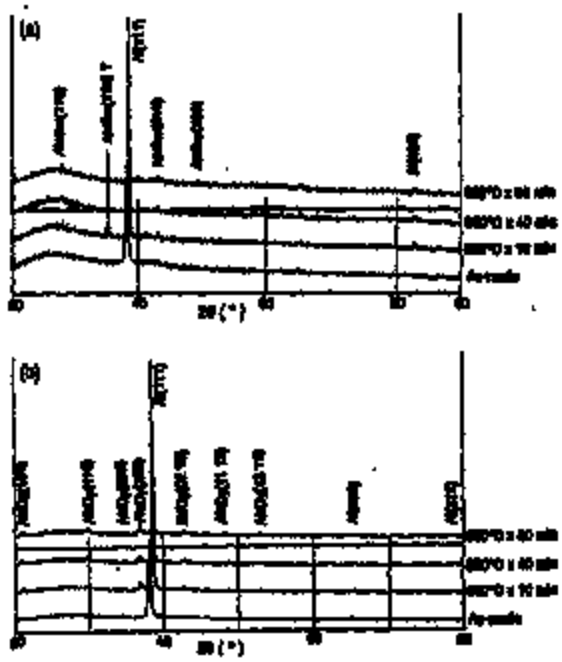

Fig. 8. X-ray diffraction profiles of (a) $Al_{97.5}Sm_{2.5}$ and (b) $Al_{94.2}Dy_{5.8}$ alloy thin films annealed isothermally at 350 °C.

large thermal defects are formed on the annealed Al–Zr film surfaces. This tendency for the growth of thermal defects to be largely suppressed is similar to that reported previously for other Al–rare-earth alloy films [4,5].

TEM observations of samples annealed at 350 °C for 80 min are shown in Fig. 10(a) and (b) for $Al_{97.5}Sm_{2.5}$ and $Al_{94.2}Dy_{5.8}$ alloy thin films respectively. Both selective area diffraction and EDX analyses indicated that most of the relatively small and dark image grains in these photos can be considered to be Al_3RE (RE = Sm or Dy) metallic compounds, while large and bright gray image grains correspond to the pure Al matrix. The photographs clearly reveal that small particles (less than 100 nm in diameter) of metallic compounds are segregated in the Al matrix, mostly at the grain boundaries of the Al matrix. Furthermore, the mean

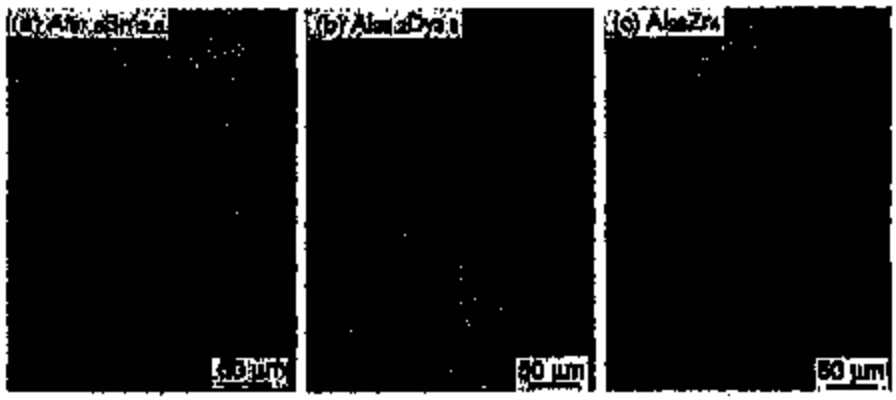

Fig. 9. Polarized optical micrographs of Al alloy thin film surfaces annealed at 350 °C for 80 min: (a) $Al_{97.5}Sm_{2.5}$, (b) $Al_{94.2}Dy_{5.8}$ and (c) $Al_{95}Zr_5$.

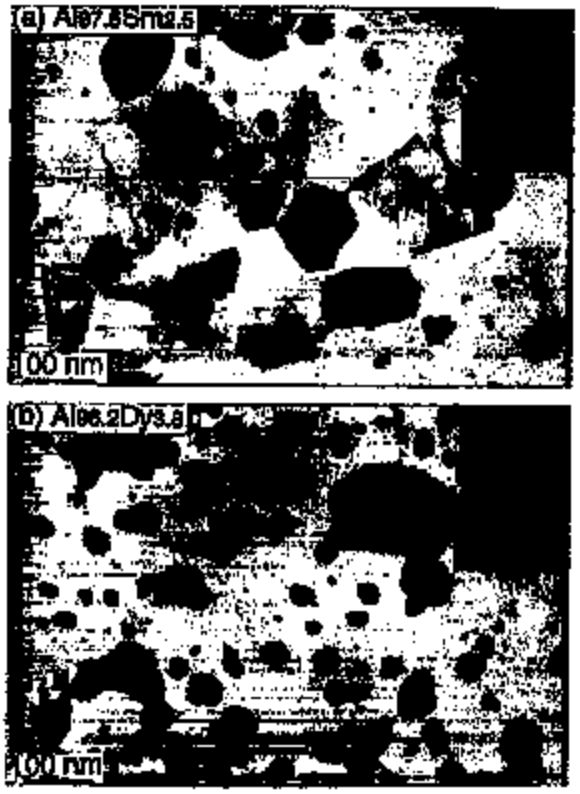

Fig. 10. Bright field images and diffraction patterns of (a) $Al_{97.5}Sm_{2.5}$ and (b) $Al_{96.2}Dy_{3.8}$ alloy thin films annealed at 350 °C for 60 min.

grain size of the Al matrix is relatively small (less than 200 nm) in comparison with that of pure Al thin films (more than 500 nm) annealed under the same heat treatment conditions. Fig. 11 shows the STEM image and the corresponding distribution of Sm in the Al matrix for the annealed $Al_{97.5}Sm_{2.5}$ thin film sample shown in Fig. 10(a). It is worth noting that the added Sm is clearly segregated in the Al matrix after annealing at 350 °C.

4. Discussion

In view of the lack of a salient change in resistivity on isochronal annealing of the sputtered Al films shown in Fig. 5, we can conclude that the large resistivity change in the Al alloy films studied here results mainly from (1) removal of impurities from the Al matrix and (2) segregation of metallic compounds. A detailed discussion of these subjects can be found in Ref. [5]. Thus, since the structure of as-made samples in Fig. 1 consists mainly of a supersaturated solid solution of the Al phase, as previously described, the main cause of the electron scattering resistance of the present as-made samples is most probably the presence of added impurities in the Al matrix. Accordingly, the resistivity is expected to increase in proportion to the amount of impurities, as shown in Fig. 1 (see also Refs. [5] and [6]).

The resistivities started to decrease markedly at 250 °C and 300 °C for Al–Dy and Al–Sm alloy films respectively, as shown in Fig. 5. It is interesting that, on the whole, the annealing temperature at the beginning of the large drop in resistivity was also independent of the amount of added element within the composition range studied. Taking account of the results of both TEM observation and X-ray diffraction analysis of the annealed samples in Figs. 6–8 and Fig. 10, it can be concluded that the sharp drops in resistivity at 250 °C in Fig. 5 result mainly from the segregation of metallic compounds, together with the removal of impurities from the Al matrix, as explained above. Note that metallic compounds Al_3RE (RE = Sm and Dy) appear at Al-rich compositions in the phase diagrams of Al–Sm and Al–Dy alloy systems respectively [7].

The removal of added elements from the Al matrix was confirmed by EDX chemical element mapping analysis, as demonstrated in Fig. 11. Furthermore, the measured mean distance between segregated metallic compounds in Fig. 10 was more than 100 nm, which is much larger than the estimated electron mean free path in pure Al (about 10 nm) [5]. This implies qualitatively that segregated metallic compounds do not significantly obstruct conduction electrons in

Fig. 11. (a) STEM image of the $Al_{97.5}Sm_{2.5}$ alloy film sample annealed at 350 °C for 60 min in Fig. 10(a), and (b) the distribution of Sm measured by EDX in the same area as (a).

the annealed structure of Al–light-rare-earth alloy films, even though they become scattering centers for conduction electrons. In addition, the resistivities of metallic compounds formed in the present alloy systems are expected to be low, as in the well known AuCu alloy systems [5]. This may be one reason why the change in resistivity with composition after annealing at 450 °C follows nearly the same curve, regardless of the type of light rare earth element, as shown in the bottom part of Fig. 1. The increase in resistivity with composition after annealing at 450 °C occurs most probably mainly as a result of the increase in the number of segregated metallic compounds, though we need further study to verify this.

Most segregation of metallic compounds in the present alloy thin films takes place at the grain boundaries of the Al matrix, as can be clearly seen in the TEM results shown in Fig. 10. This segregation at grain boundaries at relatively low annealing temperatures may play a large role in preventing grain boundary diffusion, resulting in strong suppression of the growth of hillocks and whiskers on the film surfaces.

5. Summary

The changes in the resistivity and structure of Al–RE alloy films (RE = Sm and Dy) on annealing were studied as functions of the composition of added elements, in order to assess the potential use of the films as microelectronic gate electrode line materials. The results may be summarized as follows.

1. Al–RE alloy films (RE = Sm and Dy) showed very low resistivities of less than 50 nΩ m (depending on the content of added elements) after annealing above 350 °C. They also showed, on the whole, high thermal stabilities without the growth of hillocks or whiskers on the film surfaces at high temperatures.
2. It was concluded from TEM observation and X-ray diffraction analysis that the large resistivity change on annealing resulted from the segregation of metallic compounds, such as Al_3RE (RE = Sm and Dy), together with the removal of added elements from the Al matrix.

Acknowledgements

The authors are grateful to Mr Michael McDonald for kindly reviewing this paper. Most of this work was performed at IBM Research, Tokyo Research Laboratory, IBM Japan, Ltd. (Shimotsuruma, Yamato-shi, Kanagawa, Japan).

References

[1] K. Yoshikawa, S. Nishi, H. Matsuzaki, T. Onishi and Y. Koga, *Materia Japan, 32* (9) (1993) 732 (in Japanese).
[2] M. Yamamoto, I. Kobayashi, T. Hirose, S.M. Bruck, N. Tsuboi, Y. Mino, M. Onishi and T. Tsutsui, *1994 SID International Display Research Conference, Monterey, CA, USA, Digest, 1994*, p. 142.
[3] Y.K. Lee, N. Fujiwara and T. Ito, *J. Vac. Sci. Technol. B, 9* (1991) 2542.
[4] S. Takayama and N. Tsutsui, *Extended Abstracts of the 1995 Int. Conf. on Solid State Devices and Materials (SSDM '95), Osaka, 1995*, pp. 918–920.
[5] S. Takayama and N. Tsutsui, *J. Vac. Sci. Soc., Technol. A 14(4)* (1996) 2499.
[6] S. Takayama and N. Tsutsui, *J. Vac. Sci. Technol. B*, in press 1996.
[7] W.G. Moffatt, *The Handbook of Binary Phase Diagrams*, Genium, New York, 1987.
[8] N.F. Mott and H. Jones, *The Theory of the Properties of Metals and Alloys*, Dover, New York, 1958, pp. 240–302.

Pergamon

Microelectron. Reliab., Vol. 37, No. 10/11, pp. 1553–1556, 1997

0026-2714/97 $17.00 + 0.00

PII: S0026-2714(97)00187-8

INFLUENCE OF THERMAL HEATING EFFECT ON PULSED DC ELECTROMIGRATION

P. WALTZ[1], L. ARNAUD[1], G. TARTAVEL[1], G. LORMAND[2]

[1] CEA LETI - 17 Av. des Martyrs - 38054 GRENOBLE Cedex 09- France

[2] GEMPPM - INSA - UMR CNRS 5510, Bt 303 - 69621 VILLEURBANNE Cedex - France

Abstract : Pulsed DC Electromigration (EM) tests up to 1MHz have been performed on single level Al-0.5%Cu metallization. The results are in good agreement with an Average Current Model when the thermal heating effect has been corrected with an original thermal model. Thus, Median Time to Failure (MTF) increase in the MHz region also reported by some authors, appears as a thermal effect. Furthermore, SEM observations showed very large metal accumulations and hillocks which were not seen in DC experiments.

INTRODUCTION

Electromigration failure in aluminum interconnects is an issue of continuing interest due to current efforts to increase the integration of circuits. In order to approach the real stress conditions in the circuits and to relax the design rules, many people have investigated pulsed (PDC) EM tests [2-6]. In this perspective, we performed series of tests at frequencies up to 1MHz and for different duty cycles, r, in order to validate the Average Current Model (ACM) [2].This model predicts that the sample is stressed by an efficient current density averaged over the period $J_{av}=rJ$, where J is the peak current density. The use of the generalized Black's equation $MTF = AJ^{-n}r^{-m}\exp(E_a/kT)$ [1-4] allowed us to extract the current density and duty cycle accelerating factors, n and m, using a global exploitation, and to display the difference between experiment and ACM model. Hereafter, on one hand, we demonstrate (in our case) that the MTF increase in the MHz region already reported [5], results from a pure thermal effect [6], and, on the other hand, we show that very large hillocks can be obtained with these stress conditions before failure of the line.

EXPERIMENTAL

The tests were performed on single level AlCu NIST structures [7]. Figure 1 shows a cross-section of the metallization. The thickness of the layers is as follows :

Si/SiO_2(600)nm/Ti(40nm)/TiN(60nm)/AlCu(440nm)/Ti(10nm)/TiN(40nm)/SiO_2(700nm)

The 800µm long and 3µm wide lines are connected to the pads via a 6µm wide current access line.

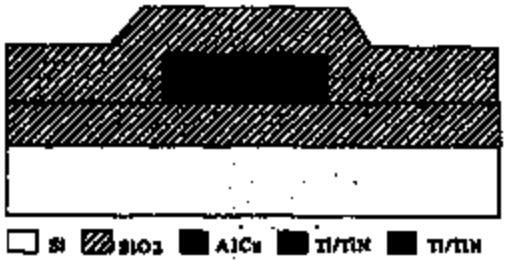

Figure 1 Cross-section of the test structure

For each stress condition, we have tested a batch of 16 samples which were connected to their own current source. All the tests have been performed at an oven temperature of 200°C for all frequencies and 250°C for DC and 10kHz. The other test conditions are summarized in Table 1. We considered the failure of the line after a 40% resistance increase. The DC temperature (T_{dc}) is calculated from resistance measurements.

The PDC temperature (T_{pdc}) is the mean temperature during the on-time of the cycle and is calculated with a thermal model [8] using the measurement of thermal time constant (τ_{th} close to 1µs) and T_{dc}.

THERMAL MODEL

A purely resistive line, described as a first order system, is submitted to a periodic Joule heating. The power P(t) dissipated during the time interval dt is equal to the accumulated heat added to thermal losses (Equation 1).

$$P(t)dt = C_{th}dT + \frac{T - T_s}{R_{th}}dt \qquad (1)$$

T_s, C_{th}, R_{th} : respectively substrate temperature, thermal capacitance and thermal resistance.

From Equation 1 and by using the Laplace transformation, we can calculate T_1 and T_2 corresponding respectively to the steady state minimum and maximum values of the sample temperature during the pulsed EM test. We can then extract the temperature T_{pdc}, which is the average temperature of the sample during the application of an unidirectional power pulse (Equation 2). This value will be used for the exploitation of pulsed EM results.

$$\frac{T_{pdc} - T_s}{\Delta T} = 1 - \frac{f \times \tau_{th}}{r} \cdot \frac{T_2 - T_1}{\Delta T} \qquad (2)$$

ΔT, f, r, τ_{th} : respectively DC Joule heating, frequency, duty cycle and thermal time constant.

RESULTS

From DC tests at two different oven temperatures (200°C and 250°C), we extracted the usual Black's equation parameters. The results are as follows : Ea_{dc}=0.66eV and n_{dc}=2.6. The tests achieved at a frequency of 10kHz allowed us to extract the activation energy in the PDC case. We found Ea_{pdc}=0.67eV. The MTFs for DC and PDC tests as well as the temperatures are summarized in Table 1.

Table 1 Test conditions - Calculated temperatures - MTFs

freq.	DC			100 Hz				10 kHz				1 MHz			
r (%)	-			50		80		20	50		80	50		80	
J (MA/cm2)	2	4	6	4	6	4	6	6	4	6	6	4	6	4	6
Tdc (°C)	205	282	283	225	253	224	255	250	226	262	261	224	253	225	250
Tpdc (°C)	-	-	-	225	253	224	255	254	226	261	260	212	227	220	246
MTF (h)	677	76,7	6,1	480	59,6	158	5,2	606	476	47,7	10	637	190	307	40,7

We studied the ratio MTF_{pdc}/MTF_{dc} by using the PDC activation energy to correct some temperature differences. By fitting the plot $Ln(MTF_{pdc}/MTF_{dc})$ vs Ln(r), we could extract the slope which represents the parameter m (See Figure 2).

Table 2 n and m : linear regression - T_{pdc}
m' : slope of the fit - T_{pdc}
m'' : slope of the fit - T_{dc}

	Lin. Regres.		Tpdc	Tdc
	n	m	m'	m''
100 Hz	3,2	3,1	2,8	2,8
CI 95%	[2,7 - 3,8]	[2,5 - 3,8]		
10 kHz	3,0	2,9	2,9	2,8
CI 95%	[2,6 - 3,4]	[2,6 - 3,3]		
1 MHz	2,5	2,8	2,7	3,5
CI 95%	[2,0 - 3,0]	[2,1 - 3,4]		

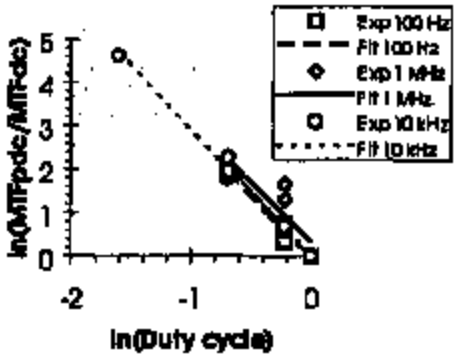

Figure 2 Normalized MTF vs Duty cycle

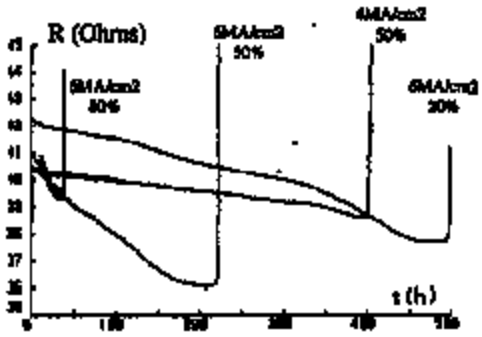

Figure 3 Resistance vs Time - f=10kHz

Depending on the temperature used, T_{pdc} or T_{dc}, we obtain different results, respectively m' and m''. These results are summarized in Table 2. Furthermore, a multilinear regression over J and r after temperature correction (T_{pdc}) allowed us to extract simultaneously n and m for the different frequencies (See Table 2).

All of the plots Resistance vs Time present a linear decrease until failure and the slopes are directly correlated to the stress conditions (See Figure 3).

Figure 4 SEM view of a slit-void

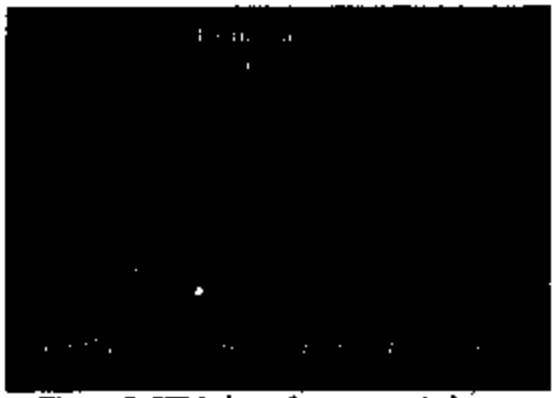

Figure 5 SEM view of an accumulation

Furthermore, many SEM observations have been performed after test and removal of the passivation layer. All the failures are slit-void failures (See Figure 4) and are randomly located in the half part of the line near the cathode in both DC and PDC cases. We found also a lot of metal accumulations and large hillocks all along the line (See Figure 5). Some hillocks are single crystals grown out of the line by cracking the ARC layer and the passivation and, can be up to 10µm long. We did not find any large depletion on the line and AFM measurements showed that the whole accumulated matter comes from the current access line.

ANALYSIS

We found the same activation energy in both DC and PDC cases. So we can suppose the diffusion mechanisms to be the same in both cases. As shown in Table 2, m'' displays a large increase for high frequencies, whereas m' is quite constant. This increase of m'' is due to a pure thermal effect : the actual operating temperature of the sample doesn't reach T_m during the on-time for these frequencies.

Seeing that the 95% confidence intervals are quite large, it appears that the multilinear regression calculated parameters n and m are almost equal (See Table 2) and close to the DC value. This result validates the ACM Model, for which the sample is subject to an efficient current density $J_{eff}=\tau J$ averaged over the period. The obtained value of n appears as a result of the competition between structural induced (n=1) and thermal induced (n=3) failures [9].

The main difference between DC and PDC results concerns the SEM observations. Indeed, the number and size of the accumulations and hillocks are strongly correlated to the test time and the pulsed stress conditions because this phenomenon was much less pronounced on DC-tested samples. A measurement of the accumulation dimensions allowed us to correlate perfectly the local line section increase to the resistance decrease shown in Figure 2, which is not only due to the usual Al_2Cu precipitation. In some cases, this decrease can reach up to 20% of the initial value R_0.

On one hand, we suspect the thermal Joule cycling, due to current pulse stresses, to reduce the mechanical resistance of the passivation. On the other hand, the Ti/AlCu interface seems to be a very easy diffusion path. Then, the metal coming from the pad and travelling along the interface is blocked by a perpendicular grain boundary crossing the line and cracks the weakened passivation layer. So, a very large amount of matter can be accumulated without failure in the PDC-tested single level samples. In structures without large reservoir of matter (eg lines with via access), interfacial diffusion would probably lead to earlier failure. Investigations of PDC EM in such structures are under progress.

CONCLUSION

The PDC test results on single level AlCu metallization are in agreement with the ACM model because we found n, m and m' almost equal. In opposition to some authors, the MTF values are quite high and reflect probably the interface diffusion depleting the 6µm wide current access line. We also showed that for frequencies close to $1/\tau_{th}$, the calculation of the real sample temperature, provided by the thermal model, is needed. Microstructural characterisation of the samples has shown extremely large hillocks without electrical failure of the line.

REFERENCES

1. J.R. Black, *IEEE Trans. Electron Devices*, ED-16, 1969, p. 338.
2. L. Brooks, *IEEE/IRPS*, 1987, p 136-139.
3. K. Hatanaka, T.Noguchi, K.Maeguchi, *Symposium on VLSI Technology*, 1989,p 19-20.
4. X. Gui, S.K. Dew, M.J. Brett, *J. Appl. Phys.*, 80 (9), 1996, p 4948-4951.
5. KK. Hirooka, K. Yasuda, *IEICE Trans. Fundamentals*, E77-A (1), 1994, p 195-203.
6. T. Furusawa, K. Hinode, Y. Homma, *Conference on Solid State Devices and Materials*, 1990, p 255-258.
7. ASTM Standard Guide of Design of Flat, Straight-Line Test Structures for detecting Metallization Open-circuit or Resistance increase Failure Due to Electromigration.
8. P. Waltz, G. Lormand, L. Arnaud, *to be presented at ESSDERC'97 Conference.*
9. D.S. Chhabra, N.G. Ainslie, *IBM Technical Report 22 419*, July 1967.

ELSEVIER

Thin Solid Films 337 (1999) 113–117

Thin Solid Films

Nitrogen-added Al rare-earth alloys for thin film transistors

Toshiaki Arai*, Hiroshi Takatsuji, Hideo Iiyori

IBM Yamato Laboratory, 1623-14 Shimo-tsuruma, Yamato-shi, Kanagawa 242-8502, Japan

Abstract

The effects of nitrogen addition to aluminum-rare-earth alloys were investigated. Yttrium and gadolinium were employed as respective alloy components. The electrical properties and hillock densities of alloy films were investigated, and their nanostructures were studied by cross-sectional transmission electron microscopy. Nitrogen effectively decreases the grain size, and causes the columnar structure, that is generally present in aluminum-based alloys, to disappear. Nitric aluminum-rare-earth alloys have a strong resistance to hillock formation, and formed no micro-voids even after annealing at 450°C. An N_2 flow rate of 1.3–10% in the sputtering gas gives a low hillock density of $2.0E+1$–$7.7E-1$ pcs/mm^2 after annealing at 350°C in both nitric Al-rare-earth alloys. In the case of patterned nitric aluminum-yttrium alloys, an N_2 flow rate of less than 1.3% causes large side-hillocks after annealing at over 350°C. As an optimum value, an N_2 flow rate of 2.5% results in a low hillock density of $1.9E+1$ pcs/mm^2 and a low resistivity of 8.6 μΩ cm after annealing at 350°C. © 1999 Published by Elsevier Science S.A. All rights reserved.

Keywords: Aluminum-rare-earth alloy; Nitrogen; Void; Hillock

1. Introduction

Bottom-gate thin-film transistors (TFTs) have been widely investigated for use in active-matrix liquid crystal displays (AMLCDs). In recent years, the panel size and resolution of AMLCDs have increased dramatically, and much effort has been devoted to developing low-resistivity gate bus lines [1,2]. Aluminum (Al) and its alloys are remarkably good materials for gate bus lines, due to their low resistivity, low cost, high adhesion and superior patternability. However, under thermal processes such as the formation of films by chemical vapor deposition (CVD), aluminum is susceptible to stress migration phenomena such as hillocks and whiskers, which cause defects as a result of short-circuits and current leakage between the gate and the upper electrodes. Voids also occur as stress migration phenomena, and result in open defects of the lines or on-current (I_{on}) defects of TFTs. The thermal expansion mismatch between Al and the glass substrate produces large compressive stress in the Al film upon heating, and results in the stress migration, relaxing the stress [3–5]. The alloying of Al has been studied with the aim of increasing its hillock resistance, and it is known that Al-rare-earth alloys have high hillock resistance [6–9]. The hillock density of 1–2 at.% Al-Y, Al-Gd, or Al-Nd alloy after annealing at 350°C has been measured at $1E+1$–$1E+2$ pcs/mm^2 [9]. This value is not low enough for the fabrication of AMLCDs, but may be suitable if a thermal protective structure such as an anodized or metal-capped structure is used [9]. In a previous paper on the anodic oxidation of nitric Al-rare-earth alloys, we reported that the addition of nitrogen reduces the surface roughness [10]. Kuto et al. have also reported that the nitric Al-boron (B) alloy or nitric Al-nickel (Ni) alloy reduces hillock formation [11]. In the work described in this paper, we employed yttrium (Y) or gadolinium (Gd) as a rare-earth alloy element, and investigated the electrical properties and the resistance of nitric Al-rare-earth alloys to void and hillock formation; such alloys were found to have superior properties for our purpose. We also investigated the nanostructure of the films by transmission electron microscopy (TEM).

2. Experiment

Aluminum alloys were deposited on 5-inch-square LCD grade glass substrates by means of a DC magnetron sputtering apparatus (Tokuda System-512) at a pressure of 0.4 Pa and a substrate temperature of 100°C. The base pressure was lower than $1.0E-4$ Pa at a temperature of 100°C. Argon (Ar) gas or a mixture of Ar and nitrogen (N_2) was used as the sputtering gas, and the total flow rate was kept constant (the N_2 flow rates in the sputtering gas were 0, 0.6, 1.3, 2.5, 5.0, 10 and 15%). Yttrium (Y) and gadolinium (Gd) were

* Corresponding author. Tel.: +81-462-73-2147; fax: +81-462-74-6894; e-mail: arukuab@jp.ibm.com.

0040-6090/99/$ - see front matter
PII S0040-6090(98)01194-8

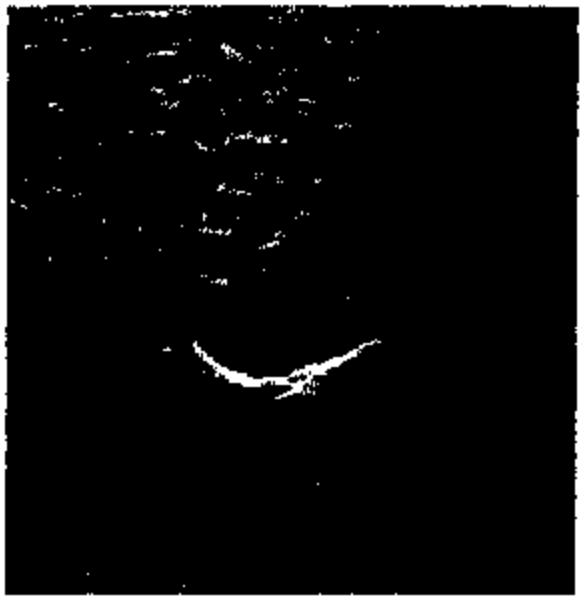

Fig. 1. SEM view of a void formed by annealing of an Al-Y (1 at.%) alloy at 350°C.

employed as respective alloy components, and each alloy with a composition of 1 at.% was sputtered from an alloy target. As a reference, pure Al was also sputtered from a pure Al (5N) target. The film thicknesses of the sputtered samples were determined by the step height measuring system (Tencor P-1), and ranged from 190 to 320 nm. The compositions of the films were determined by electron spectroscopy for chemical analysis (ESCA; SSI M-probe ESCA) after a few periods of surface etching with Ar plasma.

The samples were annealed at 250, 350 and 450°C in a nitrogen atmosphere for 1.0 h, and cooled in air at room temperature. This annealing temperature was determined according to the maximum temperature of the AMLCD fabrication. The sheet resistance of the films was measured with a four-point-probe resistance-testing system (Napson RT-8S), and the resistivity was calculated from the sheet resistance and the film thickness. The numbers of hillocks in areas ranging from 0.003 to 8 mm^2 were counted by polarized optical microscopic examination.

Voids and hillocks in Al-Y and nitric Al-Y alloys were observed by SEM (Hitachi S-800), and cross-sectional views of Al-Y and nitric Al-Y alloys were observed by TEM after a sample had been prepared by focused ion beam (FIB) etching.

Lines of Al-Y and nitric Al-Y alloys 5–100 μm wide were patterned by a photolithographic method. All these alloys were etched with a mixture of phosphoric acid, nitric acid, and acetic acid. The samples were also annealed in the conditions mentioned above. Hillocks in the area of 0.003–5 mm^2 were counted by polarized optical microscopic examination.

3. Results and discussion

The resistance of Al-rare-earth alloys to hillock formation is superior to that of pure Al. For example, the hillock density of Al-Y (1 at.%) or Al-Nd (2 at.%) alloy after 350°C annealing was $1E+1$–$1E+2$ pcs/mm^2 [9]. This value is suitable for TFT-LCD manufacturing if a thermal protective structure such as an anodized or metal-capped structure is used [9].

However, we found that conventional Al-rare-earth alloys such as Al-Y (1 at.%) or Al-Gd (1 at.%) alloys form micro-voids after annealing at temperatures higher than 350°C. The voids formed several days after annealing. Fig. 1 shows an SEM micrograph of a void formed in an Al-Y (1 at.%) alloy after annealing at 350°C. The voids were mostly smaller than 0.5 μm in diameter, and only rarely larger than 1 μm in diameter. The void densities of Al-Y (1 at.%) after annealing at 350 and 450°C were about $3E+4$ and $5E+4$ pcs/mm^2, respectively. The micro-voids look

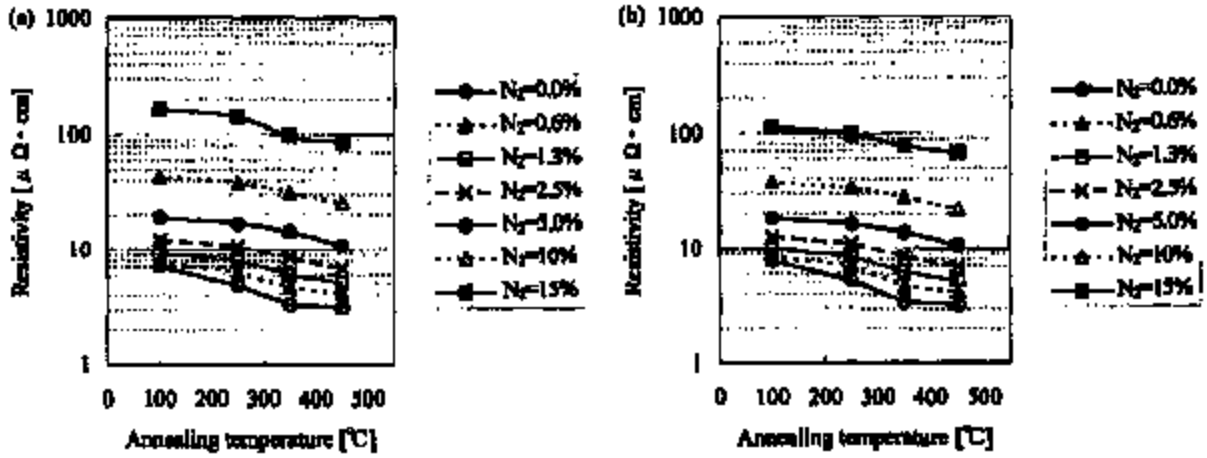

Fig. 2. Resistivity versus annealing temperature: (a) nitric Al-Y (1 at.% Y) alloy, (b) nitric Al-Gd (1 at.% Gd) alloy.

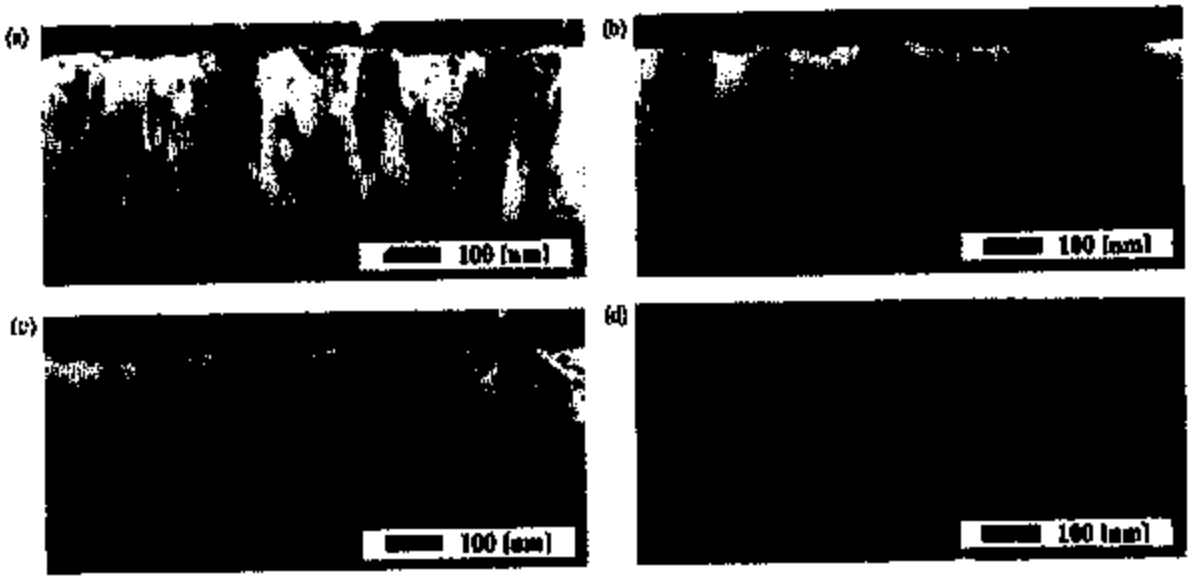

Fig. 3. Cross-sectional TEM views: (a) as-deposited Al-Y (1 at.%) alloy, (b) 350°C-annealed Al-Y (1 at.%) alloy, (c) as-deposited nitric Al-Y (1 at.% Y, 4.6 at.% N) alloy, (d) 350°C-annealed nitric Al-Y (1 at.% Y, 4.6 at.% N) alloy.

as if some grains are missing. It is known that high-temperature annealing of Al alloys leaves high tensile stress in the film after annealing [5,7]. We think that the tensile stress causes vacancy migration to the grain boundaries or grain triple points and creates voids. The formation of voids may be related to the base pressure of the sputtering or the environmental conditions of the clean room in which the sputtered substrates were deposited. Since it is necessary to manufacture fine TFT-LCDs even in difficult conditions, we decided to investigate the effects of nitrogen to Al, predicting that it would reduce the grain size, change the structure from columnar to granular, and make it resistant to the formation of voids.

We formed nitric Al-based alloys by the reactive sputtering method. When pure Al was used as a sputtering target, nitrogen roughened the film surface and colored it to brown. However, when an alloy target was used, a smooth film surface was obtained [10]. Fig. 2 shows the resistivities of the Al-based alloys before and after annealing. As can be seen, the resistivities of the films were decreased by annealing. This phenomenon is considered to be caused by the segregation of the alloying elements as a second-phase precipitate at the Al grain boundaries [5]. Low resistivity of the gate metal is required for AMLCDs, because the gate pulse transmitted to the gate line is distorted as it travels down the line [12]. Our target for the resistivity of large, high-resolution displays is less than 10 μΩ cm. In the fabrication of AMLCDs, high temperature in the deposition of gate insulator, which is usually performed by chemical vapor deposition (CVD), decreases the resistivity of Al-based alloys. The temperature of the CVD is about 350°C in plasma-enhanced CVD (PE-CVD), and about 450°C in

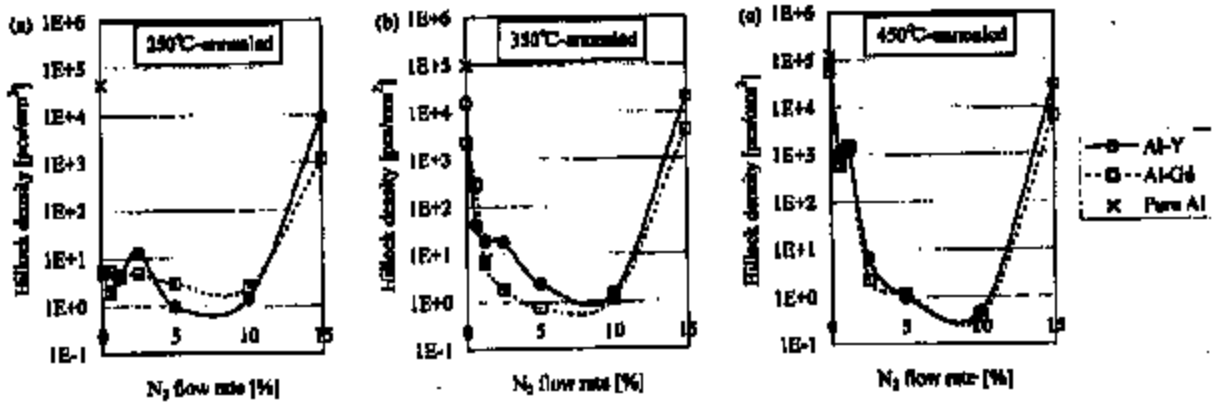

Fig. 4. Hillock density versus N_2 flow rate: (a) 250°C-annealed, (b) 350°C-annealed, (c) 450°C-annealed.

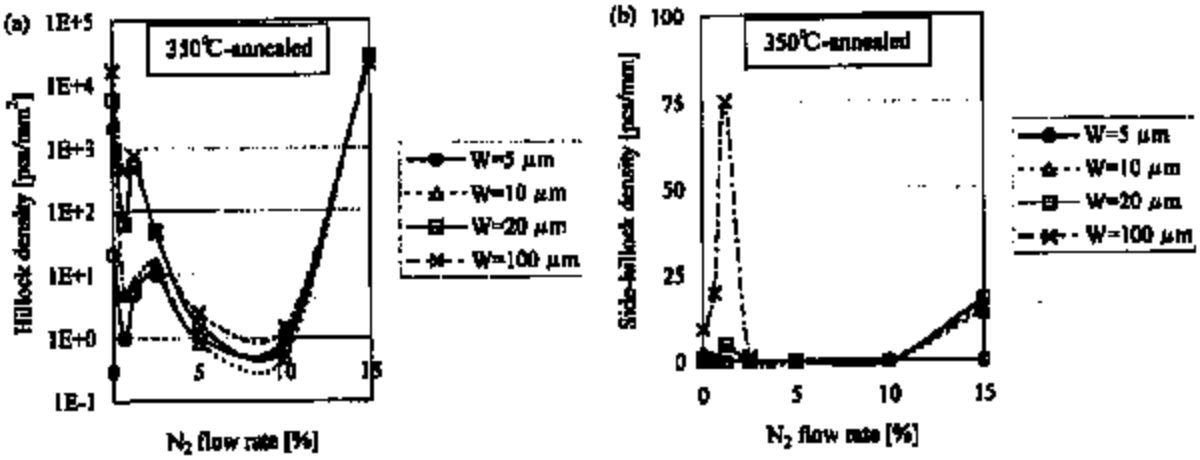

Fig. 5. Hillock density of nitric Al-Y alloy versus line width.

atmospheric pressure CVD (AP-CVD). Therefore, an N_2 flow rate of less than 2.5% will be suitable for the fabrication of AMLCDs as regards the resistivity.

Fig. 3 shows cross-sectional TEM views of Al-Y (1 at.%) and nitric Al-Y (1 at.% Y, 4.6 at.% N) alloys. The nitrogen content of 4.6 at.% was determined by ESCA examination. In the case of Al-Y (1 at.%) alloy, both films (Fig. 3a,b) have columnar structures, and the grain size was increased by the annealing. In the case of nitric Al-Y (1 at.% Y, 4.6 at.% N) alloy, the grain boundary was difficult to distinguish in comparison with that in the Al-Y (1 at.%) alloy, but became well defined with annealing, and a grain-like structure smaller than 50 nm in diameter was observed. This indicates that segregation and growth of the matrix Al by means of high-temperature annealing decreases the resistivity. Moreover, the nitric Al-based alloy did not form any voids even after annealing at 450°C. We consider that this granular (not columnar) structure may prevent nitric Al-based alloys from forming voids.

Fig. 4 shows the hillock density of the annealed films. Nitric Al-Y alloys and nitric Al-Gd alloys showed almost the same tendency with regard to the formation of hillocks in relation to the nitrogen content and annealing temperature. The hillock densities after annealing at 250°C were low enough when the N_2 flow rate was less than 10%. However, the hillock density increased abruptly as a result of annealing at over 350°C, indicating that the structural change shown in TEM views occurs mainly at temperatures between 250 and 350°C. The hillock densities after annealing at 450°C were lower than after annealing at 350°C. This may mean that it is possible to decrease the hillock density by quickly passing the yield point (i.e. the temperature at which hillocks are formed), which would be between 250 and 350°C in these nitric Al-based alloys. The target for the hillock density after annealing at 350°C is lower than $1E+2$ pcs/mm^2. This value is satisfied by the hillock density of Al-rare-earth (1–2 at.%) alloys [9]. In AMLCD fabrication at a maximum temperature of over 350°C, an N_2 flow rate of 0.6–10% for nitric Al-Y alloys or 1.3–10% for nitric Al-Gd alloys seemed suitable for the fabrication of AMLCDs.

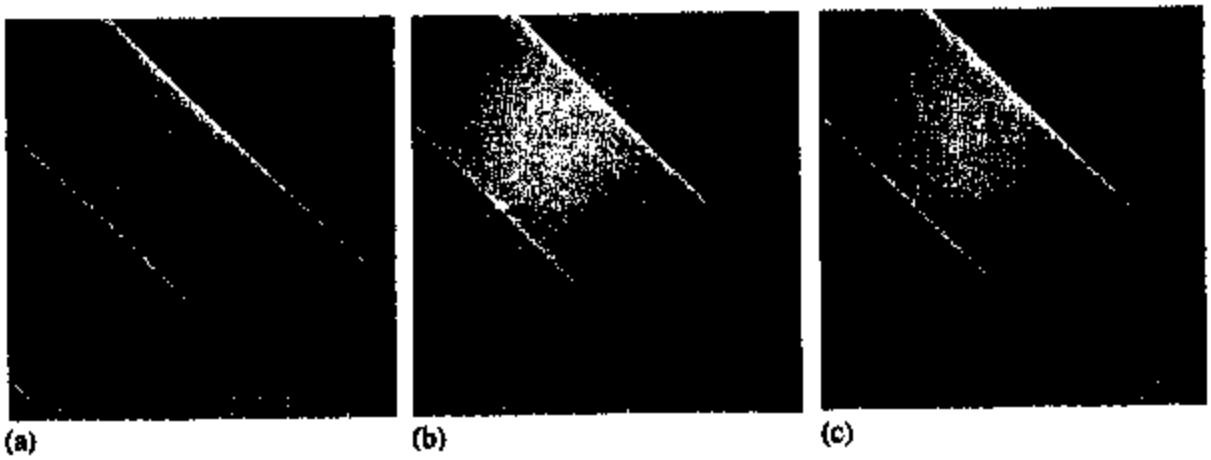

Fig. 6. SEM views of 350°C-annealed lines: (a) Al-Y (1 at.%) alloy, (b) nitric Al-Y (1 at.% Y, 2.3 at.% N) alloy, (c) nitric Al-Y (1 at.% Y, 4.6 at.% N) alloy.

Next, we patterned 5- to 100-μm wide lines, and investigated the relationship between the hillock density and line width. Fig. 5a shows the total hillock density of 5- to 100-μm-wide Al-Y and nitric Al-Y alloys after annealing at 350°C. Narrow lines of, say, 5–10 μm coincided with very low hillock density, whereas lines wider than 20 μm coincided with higher hillock densities, as shown in Fig. 4b, especially at a low N_2 flow rate. The higher density results from the formation of side-hillocks. Fig. 5b shows the side-hillock density of the lines, and Fig. 6 shows SEM micrographs of the 20 μm-wide Al-Y and nitric Al-Y (2.3 and 4.6 at.% N) alloys. The nitrogen contents of 2.3 at.% and 4.6 at.% were determined by ESCA examination. Side-hillocks occur mainly at an N_2 flow rate of 0.0–1.3%. The side-hillocks (see Fig. 6b) are larger than the surface-hillocks (see Fig. 6a), and it is predicted that the incidence of cross-short defects of gate lines to upper electrodes drastically increases. Therefore, an N_2 flow rate of 2.5% is the most suitable value for nitric Al-Y alloy, and the resistivity in this condition is 8.6 μΩ cm in 350°C manufacturing, and 6.9 μΩ cm in 450°C manufacturing.

4. Conclusion

We investigated the electrical properties and hillock densities of plane surfaces and patterned lines, and the nanostructures of Al-Y and Al-Gd alloys and their nitric alloys. Nitrogen effectively decreased the grain size, and caused the columnar structure to disappear. Nitric Al-rare-earth alloys, which were formed at an N_2 flow rate of 1.3–10%, had a strong resistance to hillock formation, and formed no micro-voids even after annealing at 450°C. However, in the case of patterned nitric Al-Y alloys, a N_2 flow rate of less than 1.3% caused large side-hillocks after annealing at over 350°C. Therefore, an N_2 flow rate of 2.5% is the most suitable value for nitric Al-Y alloy, and the resistivity in this condition is 8.6 μΩ cm after annealing at 350°C, and 6.9 μΩ cm after annealing at 450°C.

Acknowledgements

We are grateful to S. Tsuji, K. Furuta and G. Tanaka of IBM Display Technology for their valuable advice. We would also like to thank K. Tsujimoto of IBM Display Technology for his TEM observations, M. Sakauchi of IBM Materials Laboratory for his ESCA measurement, and M. McDonald of IBM Yamato Laboratory for his contributions to this paper.

References

[1] T. Tsukada, MRS Symp. Proc. 284 (1993) 371.
[2] C.W. Kim, J.H. Lee, H.B. Nam, et al., Proceedings of Euro Display '96 SID, 1996, pp. 591–594.
[3] U. Smith, N. Kristensen, F. Ericson, J.-A. Schweitz, J. Vac. Sci. Technol. A 9 (4) (1991) 2527.
[4] E. Iwamura, T. Onishi, K. Yoshikawa, K. Itayama, J. Vac. Sci. Technol. A 12 (5) (1994) 2922.
[5] T. Onishi, E. Iwamura, K. Takagi, K. Yoshikawa, J. Vac. Sci. Technol. A 14 (5) (1996) 2728.
[6] S. Takayama, N. Tsutsui, J. Vac. Sci. Technol. A 14 (4) (1996) 3499.
[7] T. Onishi, E. Iwamura, K. Takagi, T. Watanabe, J. Vac. Sci. Technol. A 15 (4) (1997) 2330.
[8] H. Takasaji, H. Iiyori, S. Tsuji, K. Tsujimoto, K. Kuroda, H. Saka, Mater. Res. Soc. Symp. Proc. 471 (1997) 99.
[9] T. Arai, H. Iiyori, Y. Hiromatu, M. Atsumi, S. Ieku, K. Furuta, IBM J. Res. Dev. 42 (3/4) (1998) 491.
[10] T. Arai, H. Iiyori, Materials Research Society 1997 Fall Meeting, Electrically Based Microstructural Characterization II, 1998, in press.
[11] K. Kato, T. Wada, N. Kakuda, T. Kawada, IEICE Trans. Electron. E80-C(2) (1997) 320.
[12] W.E. Howard, Conference Record of the '94 SID International Display Research Conference, 1994, pp. 6–10.

Pergamon

Acta mater. Vol. 47, No. 1, pp. 89–99, 1999

Printed in Great Britain
PII: S1359-6454(98)00346-2
1359-6454/99 $19.00 + 0.00

INTERCONNECT DAMAGE BY ELECTROMIGRATION: EXPERIMENT AND NUMERICAL SIMULATION

J.-M. HUANG, W. YANG† and Z.-J. ZHAO

Department of Engineering Mechanics, Tsinghua University, Beijing 100084, P.R. China

(Received 5 August 1998; accepted 22 September 1998)

Abstract—Electromigration is a severe reliability issue for polycrystalline aluminum-based interconnects. The phenomenon is amplified by aiding exposed interconnects at an elevated temperature. The intense electric currents they carry would drive atoms to diffuse, and leave hillocks or sinks along the interconnects. Experimental observations revealed that the hillocks grow against the surrounding grains in four stages: the incubation, the jump start, the deceleration, and the final stabilization. An analytical model is proposed to address features such as fluctuating mass flows into grains, partition of mass flows through the surface and the defect layers, stresses induced by the mass flow, and resistance against the grain boundary sliding. The incubation time and the protruding height are determined. The incubation time is proportional, while the protruding height is roughly inversely proportional, to the square of the grain size. Numerical simulations are exploited to quantify the experimental phenomena. To design against the electromigration, one needs to raise the incubation time of an interconnect beyond its service life. To comply with this criterion, a polycrystal line with large and uniform grains (if not a bamboo line or even a single crystal line) with small variation in grain boundary diffusivities should be pursued. © *1998 Acta Metallurgica Inc. Published by Elsevier Science Ltd. All rights reserved.*

1. INTRODUCTION

Aluminum-based interconnects consist of more than 90% of the metal lines used in integrated circuits. The low resistance and good processing capability give aluminum an advantage with respect to RC delay and allow for higher performance circuit design. In the integrated circuits, the interconnects have small cross-sections (less than 1 μm wide and about 0.5 μm thick), carry intense electric current (above 10^{10} A/m^2), and may operate at a temperature of nearly half of the melting point (933 K) of aluminum. The flowing electrons exert a force (the electron wind force) on aluminum atoms, which drives aluminum atoms to diffuse. Mass diffusion under electric current, known as electromigration, raises the reliability concerns. The situation is further accentuated by the continuing trend toward miniaturization in integrated circuits, especially in the VLSI and power semiconductor devices.

Experimental observations revealed that single crystal interconnects can sustain a very long life [1, 2], for they have perfect microstructures and homogeneous material properties. The damage by voiding can nucleate only along the interfaces between the interconnect and its passivation [3]. The migration of a void is controlled by the mass flow along the void surface [4]. Subjected to electromigration, a void basically moves by surface diffusion, and may break away from a grain boundary [5–8]. For a bamboo line, electromigration may cause damage nucleation and failure by the unbalanced atomic flux into the triple junctions, creating either a void [9] or a transgranular slit [10–14]. These studies indicated that the failure by electromigration is manifested by the growth, shape change, and migration of voids or hillocks, and an interconnect evolves like a dynamical system that has multiple thermodynamic forces and undergoes dissipative processes.

Electromigration becomes a severe reliability issue for polycrystalline lines [8, 15], especially for the exposed lines. The mass flows along the side surfaces, the top surface, the grain boundaries, the surface grooves, and the defects like dislocations. They provide fast diffusion paths under electromigration, and the mass flow through them might be non-uniform [16, 17]. Surface damage is nucleated by the mass flow instability and intensified by the subsequent morphological evolution [15].

We begin with the electromigration experiment on polycrystalline aluminum lines. At ambient and elevated temperatures, hillocks and sinks are observed along the exposed surfaces of the interconnects, as reported in Section 2. The experiments revealed that hillocks and sinks grow against the surrounding grains in four stages: the incubation, the jump start, the deceleration, and the final stabilization. Section 3 presents an analytical model featuring the mass flow fluctuation and the grain boundary resistance. A scheme for the morphological evolution under electromigration is exploited in

†To whom all correspondence should be addressed.

Table 1. Failure times in various tests

Specimen number	Testing temperature (K)	Current density (10^{10} A/m^2)	Line width (μm)	Lifetime (h)
100-08	300	3.56	7.5	1171
100-09	300	3.67	1.5	2.75
100-10	300	3.14	3.6	506
200-01	300	6.16	1.5	6.5
200-02	300	2.64	3.5	3408
300-04	300	2.50	11.5	3040
400-09	300	3.67	1.5	409
600-09	300	3.67	1.5	893

Section 4, where numerical simulations are carried out to quantify the experimental phenomena.

2. ELECTROMIGRATION EXPERIMENT

2.1. Damage of aluminum-based interconnects

The authors conducted a series of electromigration tests of unpassivated polycrystalline interconnects. Only room temperature testing is described here. The metallizations consisted of films of Al/Si (mass fraction 99% Al and 1% Si) alloy of 1 μm thickness, which were sputter deposited at a rate of 0.03 μm/min on silicon substrates covered by a SiO_2 film of 0.4 μm. The film/substrate assembly was then annealed at 723 K for about 30 min. The processing followed the conventional technique in China to manufacture micron-width interconnects, and was carried out in the Institute of Microelectronics, Tsinghua University. The thin films were then etched to testing lines of 100 μm length and various widths (from 1.5 to 11.5 μm). The failure times of various tests are listed in Table 1. They are substantially lower than the testing data reported in the literature. The specimens were observed under a field-emission scanning electron microscope (Hitachi S-4200) at the Institute of Physics, Chinese Academy of Science. The interconn-

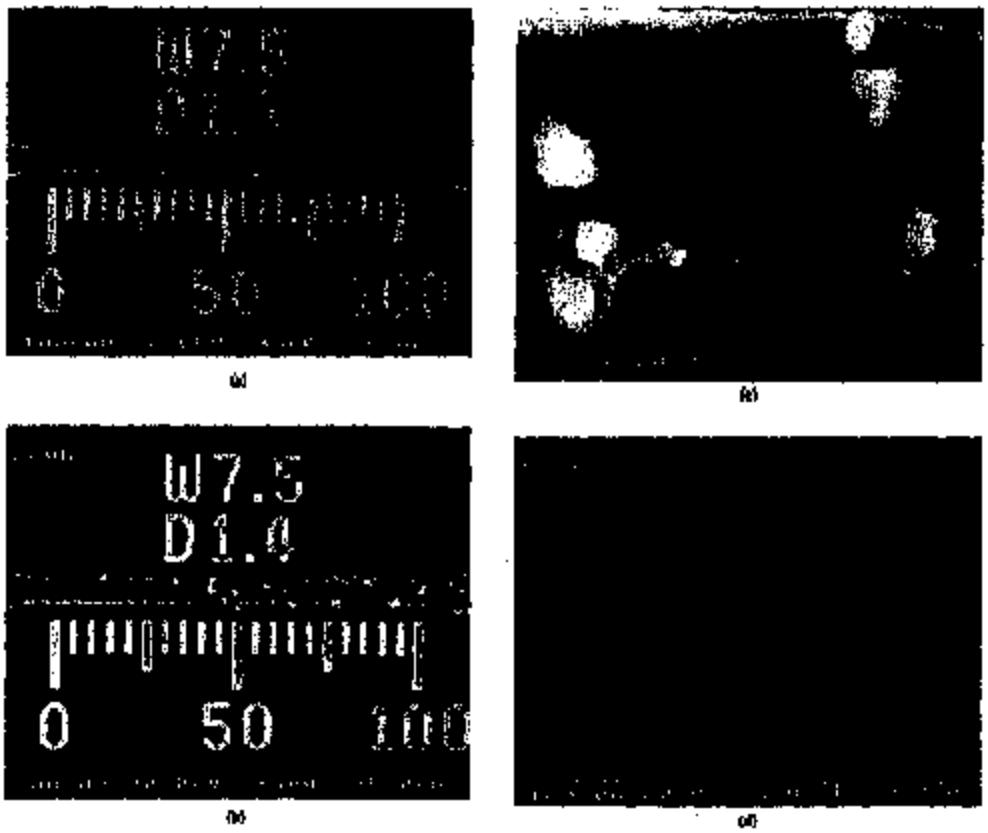

(a) (b)

(c) (d)

Fig. 1(a, b, c and d).

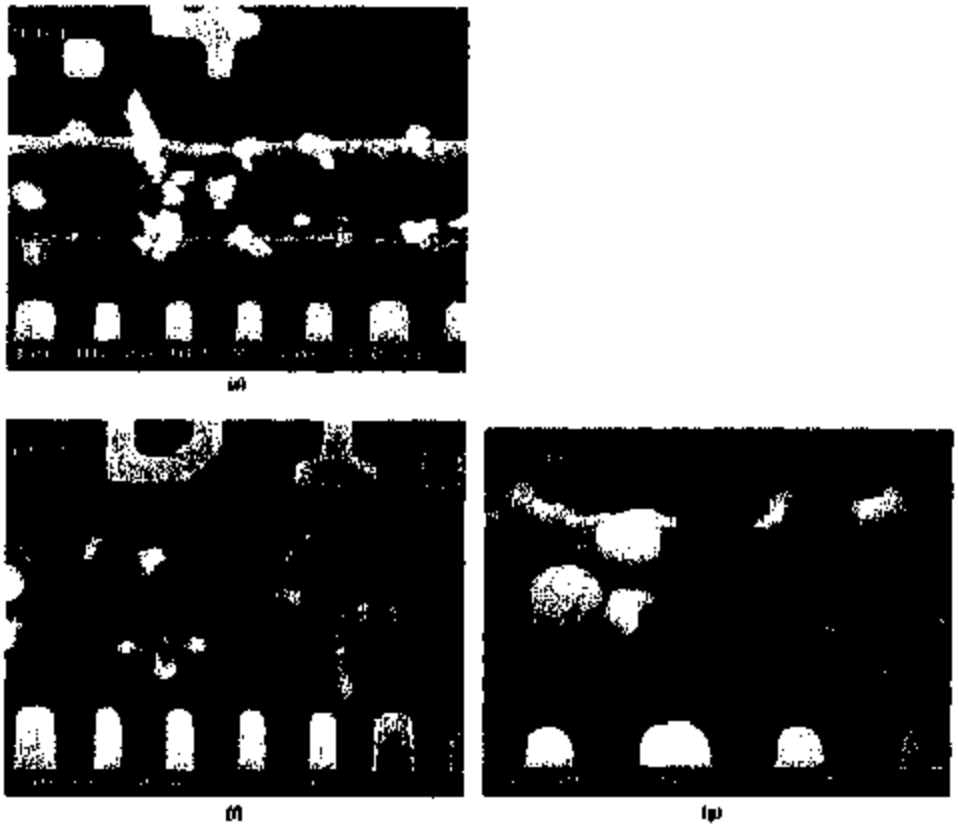

Fig. 1. SEM micrographs following a time sequence showing the damage of an interconnect under electromigration: (a) initial configuration; (b)–(d) 520 h; (e) 904 h; (f), (g) 1171 h.

nects are featured by the tiny columnar grain microstructures. The grains are about 0.115 μm in diameter and 1 μm in height, with possible lateral defects.

2.2. *Four stages of protrusion*

Figures 1(a)–(g) show a typical sequence of the morphological evolution of an interconnect tested at room temperature (300 K) under a current density of 3.56×10^{10} A/m^2 and a line width of 7.5 μm. These microscopic photographs were taken by interrupting the test after 0, 520, 904, and 1171 h of testing. In all graphs, the direction of the electron flow is from right to left. The exposed surfaces are initially flat, and surface damage is not detected, as shown in Fig. 1(a). The surface damage sets in when the electric current is switched on, but needs an incubation period for the hillocks to appear. As the time increases, the unbalanced mass flux accumulated in local areas becomes unstable. Suddenly many tiny hillocks and sinks burst from the interconnect, as shown in Fig. 1(b) at 520 h. An amplified view for a hillock protruding from the surrounding grains is shown in the lower-left corner of Fig. 1(c). The hillock is about 1.5 μm long and 2 μm in diameter. The detailed structure of a connected sink is shown in Fig. 1(d). The protruding motion of hillocks continues after their formation, see Fig. 1(e) at 904 h. The aspect ratio of the hillock becomes slender. The protruding motion decelerates. Gradually the matured hillocks become stabilized, but the new ones are still growing rapidly. The growing kinetics renders the picture shown in Fig. 1(f) at 1171 h. The longest protrusion in the figure has a length of about 4 μm, which imposes a severe threat of short-circuit failure. On the other hand, the local sinking becomes deeper and deeper, and finally cuts the line at 1171 h, see Fig. 1(g). Many sinks can be observed in the broken-down section. These results agree quantitatively with those of other experiments [6–9].

Grain boundaries play an important role in the electromigration of polycrystalline interconnects. They not only provide a fast path for electromigration, but also shape the evolution of the hillocks and sinks. We attribute the above-mentioned experimental phenomena to the fluctuation in the grain boundary configurations and the variation of the grain boundary diffusivities. These diversities provoke the unbalance of mass flows in the intercon-

Table 2. Evolution of hillocks during the test #199-06

Testing hours	Number of hillocks	Ave. height (μm)	Max. height (μm)
0	0	0	0
40	6	0.4	0.5
112	12	0.5	0.6
242	18	0.6	0.8
356	23	0.7	1.1
528	40	0.75	1.5
746	80	0.8	1.9
864	160	0.85	2.8
1171	190	0.87	4.0

nect. In the area of mass flux surplus, the mass injection into a defect causes compressive stress which pushes the upper grain to protrude, against the sliding resistance by the surrounding grains. In the area of mass flux loss, the mass leakage leads to the formation of sinks which eventually sever the interconnect.

Quantitative counts on the micrographs provide the results listed in Table 2. The number of hillocks assumes an upturn curve with respect to the testing hours. The growth of the average hillock height is much slower than the growth of the maximum hillock height. Several nearby hillocks also have the tendency to merge into a wider hillock, then the growth of its height decelerates.

3. ANALYTICAL MODEL

The experimental observations indicate that the interconnects are composed of tiny columnar grains, whose cross-section can be simplified as the hexagon assembly shown in Fig. 2.

3.1. Mass flux under electromigration

Consider the configuration of a thin film interconnect shown in Fig. 2. Attention is focused on the mass flowing along the grain boundaries. Let J be the atomic flux, namely the number of atoms per unit length per unit time, due to the action of electromigration and the influence of back stress. It is given by [3]

$$J = -\frac{D\delta}{K_B T}\left(\frac{Z^* e E_t}{\Omega} + \frac{\partial \sigma_n}{\partial l}\right) \tag{1}$$

where D and δ denote the diffusivity and the thickness of the grain boundary, K_B the Boltzmann constant, T the absolute temperature, Ω the atomic volume of the migrating species, Z^* the effective valence of the migrating ions, e the electron charge, E_t the tangential electric field along the grain boundary, σ_n the back stress normal to the grain boundary, and l the tangential coordinate measured along the grain boundary. Equation (1) is rigorous only if the grain boundary is flat.

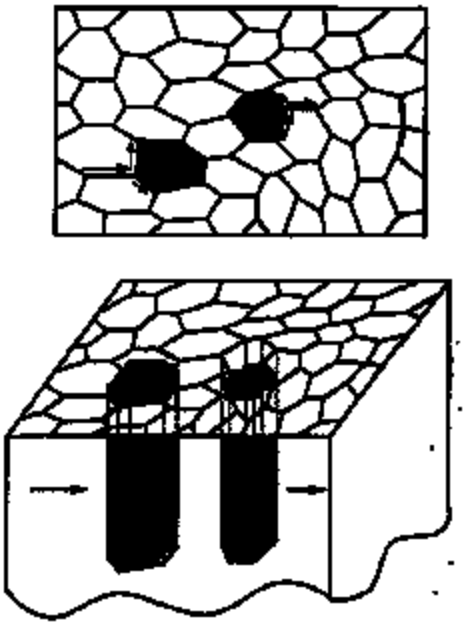

Fig. 2. Sketch on the emergence of a hillock or a sink along the grain boundaries under electromigration.

Since our tests were carried out for unpassivated and exposed lines, the constraining stress is small, and most of the mass flow will be absorbed by the stress-free morphological evolution. A substantial stress gradient like that analyzed by Thouless *et al.* [3] cannot be built up. Thus, the back stress term is neglected in the subsequent analysis, and equation (1) is reduced to

$$J = -\frac{D\delta}{\Omega K_B T} Z^* e E_t. \tag{2}$$

The rate of accumulation of material at a point in the grain boundary, $\dot{\sigma}_n$, relates to the atomic flux, J, by mass conservation

$$\dot{\sigma}_n = -\Omega \frac{\partial J}{\partial l}. \tag{3}$$

3.2. Mass flux into a grain

Under electromigration, the mass flows into (or out of) a particular grain by the six grain boundaries it connects, as shown in Fig. 3. Let us introduce a global coordinate system OXY for the grain, with the X-axis aligned with the electric field vector $\mathbf{E}$. The angle between the ith connected grain boundary and the X-axis is denoted by θ_i ($i = 1, 2, \ldots, 6$). Without loss of generality, we regard that each grain boundary has the same thickness δ but different diffusion constants D_i

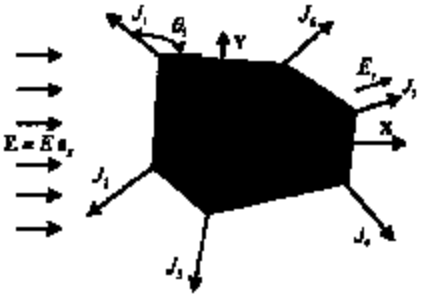

Fig. 3. Calculation of mass fluxes into a grain by electromigration.

$(i = 1,2,\ldots,6)$. From equation (2), the atomic flux into the grain (termed the grain flux J_g) is given by

$$J_g = -\frac{Z^* eE\delta}{\Omega K_B T}\sum_{i=1}^{6} D_i \cos\theta_i. \tag{4}$$

First consider the case of regular hexagon grains, as shown in Fig. 7(a). The diffusivities of various grain boundaries are assumed to obey a normal distribution, $N(\bar{D},s_D^2)$, with the expected diffusivity $\bar{D}$ and the standard deviation s_D. It can be shown that the grain flux, J_g, also obeys a normal distribution. The expectation of the grain flux is zero, and the standard deviation of the grain flux is $\sqrt{3}(Z^* eE\delta/\Omega K_B T)s_D$.

Next consider the case of general hexagon grains, as shown in Fig. 8(a), where the grain size and the grain shape only have mild fluctuations. The diffusivities of the grain boundaries obey a normal distribution $N(\bar{D},s_D^2)$. Through considerable algebra, the expectation of the grain flux is obtained by

$$\begin{aligned} J_g = \frac{Z^* eE\delta}{\Omega K_B T}\bar{D}\Big\{&\cos\left(\frac{\pi}{3}-\theta+\varphi_1\right)+\cos\left(\frac{\pi}{3}+\varphi_2\right)\\ &+\cos\left(\frac{\pi}{3}+\theta+\varphi_3\right)-\cos\left(\frac{\pi}{3}-\theta+\varphi_4\right)\\ &-\cos(\theta+\varphi_5)-\cos\left(\frac{\pi}{3}+\theta+\varphi_6\right)\Big\} \end{aligned} \tag{5}$$

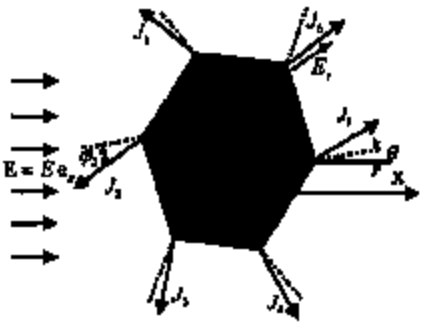

Fig. 4. Configuration of a general hexagon grain assembly.

where θ denotes the angle between the X-axis and the 3th grain boundary of a hypothetical regular hexagon, and φ_i the angle deviations from the regular hexagon, as depicted in Fig. 4. To fix the value of θ, we require that the sum of φ_i $(i = 1,2,\ldots,6)$ vanishes. The standard deviation of the grain flux is given by

$$\begin{aligned} s(J_g) = \frac{Z^* eE\delta}{\Omega K_B T}s_D\Big\{&3+\cos^2\left(\frac{\pi}{3}-\theta+\varphi_1\right)\\ &+\cos^2\left(\frac{\pi}{3}+\varphi_2\right)+\cos^2\left(\frac{\pi}{3}+\theta+\varphi_3\right)\\ &+\cos^2\left(\frac{\pi}{3}-\theta+\varphi_4\right)+\cos^2(\theta+\varphi_5)\\ &+\cos^2\left(\frac{\pi}{3}+\theta+\varphi_6\right)\Big\}^{1/2}. \end{aligned} \tag{6}$$

We further assume that the deviation angles, φ_i $(i = 1,2,\ldots,6)$, obey a normal distribution of $N(0,s_\varphi^2)$. Then the grain flux, J_g, also obeys a normal distribution. The expectation of the grain flux is zero, and its standard deviation is calculated by

$$s(J_g) = \sqrt{3}\frac{Z^* eE\delta}{\Omega K_B T}s_D\sqrt{2-\exp(-s_\varphi^2)}. \tag{7}$$

3.3. Partition of mass flow

The lateral defects which might cut through the tiny columnar grains provide channels to accommodate the fluctuation of the mass flow. As shown in Fig. 5, let h represent the distance of the initial defect from the original top surface, W the protruding height of the grain, and H the thickness of the injected mass smeared over the cross-section. The unbalanced mass flow is accommodated through two layers; the surface layer and the defect layer. The surface layer covers the region from the top surface to a depth of H_s, where the mass flow is predominantly through surface migration, regardless of the location of the defect. The defect layer covers a range of characteristic sizes H_D^* above and below the current defect height. Accordingly, the evolution law for the height of the injected mass, H, can be phrased by

$$H(t) = \begin{cases} \dfrac{2\Omega J_g}{\pi R^2}\displaystyle\int_0^t H_D^*(t)\,dt & t < t_c \\ H_c + \dfrac{2\Omega J_g}{\pi R^2}\displaystyle\int_{t_c}^t H_D^*(t)\,dt & t \geq t_c \end{cases} \tag{8}$$

where t is the time and t_c the incubation time for a hillock or a sink to appear, and H_c denotes the critical thickness of mass injection or the value of H at t_c. The size of the influence region of the defect layer, H_D^*, relies on the defect location, $h + (H/2) - W$, from the original top surface. We adopt the following piece-wise linear relation of H_D^* with respect to the defect location

$$H_D^* = \begin{cases} 0, & h+\frac{1}{2}H-W<H_S \\ h+\frac{1}{2}H-W-H_S, & H_S\le h+\frac{1}{2}H-W<H_S+H_D \\ \frac{H_D}{H_S+H_D}\left(h+\frac{1}{2}H-W\right), & h+\frac{1}{2}H-W\ge H_S+H_D \end{cases} \quad (9)$$

where H_D is a characteristic size of the defect layer. The mass injection into the defect will terminate if

$$h+\frac{1}{2}H(t)-W(t)=H_S. \quad (10)$$

The two length parameters H_S and H_D dictate the partition of mass flow.

3.4. Stress due to mass flow

The injection (or leakage) of masses into (or from) those defects would induce local confining stresses normal to the film plane. Though they have little effect on the mass transport along the grain boundaries that are normal to the film plane, they do cause the protruding motion of hillocks. Take the example of mass injection into a defect. The confining stress is compressive and should be balanced by the shear resistance along the grain boundaries around the upper half grain which intends to protrude. If the compressive stress multiplied by the cross-section of the columnar grain reaches the maximum value of the slip resistance offered by the surrounding grains, the hillock will emerge from the grain.

A simple model is adopted to calculate the compressive stress of the grain. We approximate a columnar hexagon grain by a cylindrical grain of the same height and the same cross-section. This approximation enables an axi-symmetric modeling of a prismatic dislocation loop, as shown in Fig. 6. In the figure, C is a planar circular loop of the prismatic dislocation with radius R in the XOY plane, whose normal directs along the Z-axis. The vector $\mathbf{r}$ marks the projection of a generic point P on the dislocation plane, while a point on the loop is marked by $\mathbf{r}'$. The vector $\mathbf{r}$ forms an angle θ with the positive X-direction. By the Peach–Koehler formula [18], the stress field, σ, due to the dislocation loop is given by

$$\sigma = \frac{\mu}{4\pi}\left\{\oint_C (\mathbf{b}\times\nabla')\frac{1}{|\mathbf{r}-\mathbf{r}'|}\otimes d\mathbf{r}' + \oint_C d\mathbf{r}'\otimes(\mathbf{b}\times\nabla')\frac{1}{|\mathbf{r}-\mathbf{r}'|} - \frac{1}{1-\nu}\oint_C [(\nabla\otimes\nabla - \mathbf{I}\nabla^2)\mathbf{I}\cdot\mathbf{r}' - \mathbf{r}'\mathbf{I}\nabla^2]\cdot(\mathbf{b}\times d\mathbf{r}')\right\} \quad (11)$$

where μ denotes the shear modulus, ν the Poisson ratio, and $\mathbf{b}$ the Burgers vector (which relates to the mass injection thickness H). The gradient symbols ∇ and ∇' are operated on the field and on the planar dislocation loop, respectively. Through lengthy algebra, the compressive stress normal to the plane of the dislocation loop can be calculated as

$$\sigma_z = -\frac{\mu H}{4\pi(1-\nu)}\int_0^{2\pi}\frac{d\phi}{\sqrt{r^2+R^2-2rR\cos(\theta-\phi)}} \quad (12)$$

where ϕ is the integration angle around the dislocation loop. The overall compressive force on the upper columnar grain is

$$P_z = -2\pi\int_0^R r\sigma_z\,dr = \frac{2\mu}{1-\nu}RH \quad (13)$$

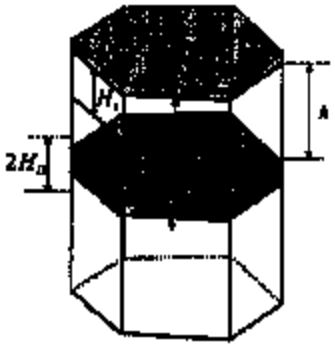

Fig. 5. Geometry and various characteristic lengths for the protruding motion of a grain.

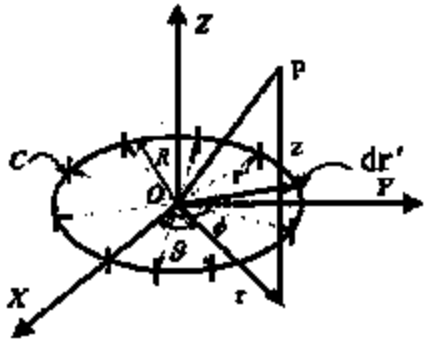

Fig. 6. Compressive stress field by a prismatic dislocation loop induced by the injected mass.

where P_a provides the driving force for a grain to protrude.

3.5. Sliding condition and incubation time

The slip resistance against the grain with mass injection, prior to any movement of the defect, is composed of shear stresses along the vertical surfaces surrounding the grain

$$P_r = 2\pi R h \tau_s \tag{14}$$

where τ_s denotes the shear strength of the grain boundary.

The onset of protrusion instability is dictated by the condition of $P_a = P_r$. Combining equations (13) and (14), one obtains the critical thickness of the mass injection

$$H_c = \kappa(1-\nu)\frac{\tau_s}{\mu}h. \tag{15}$$

Substituting equation (15) into equations (8) and (9), one arrives at the incubation time for the appearance of a hillock

$$t_c = \frac{\pi R^2}{\Omega J_g}\frac{H_S + H_D}{H_D}\ln\left(1 + \frac{\kappa(1-\nu)\tau_s}{2\mu}\right) \tag{16}$$

provided that $h + \frac{1}{2}H_c \geq H_S + H_D$. The incubation time is proportional to the square of the grain size. The hillocks will not form in an interconnect during its service life if the grain size is sufficiently large.

We next introduce the concept of the minimum incubation time. For a normal distribution, the unbalanced material fluxes mostly lie in a region of $\pm 3\sigma(J_g)$. Therefore, the minimum incubation time for a protrusion can be derived by

$$t_{c,\min} = \frac{\pi R^2}{3\Omega\sigma(J_g)}\frac{H_S + H_D}{H_D}\ln\left(1 + \frac{\kappa(1-\nu)\tau_s}{2\mu}\right) \tag{17}$$

where $\sigma(J_g)$ is equal to $\sqrt{3}(Z^* e E\delta/\Omega K_B T)s_D$ for the case of regular hexagon grains, and is given by equation (7) for the case of general hexagon grains.

3.6. Protruding height and sinking depth

Consider the subsequent evolution of a hillock or a sink. As shown in Fig. 5, the slip resistance caused by the surrounding grains against the subsequent evolution is

$$P_r = 2\pi R\left(h + \frac{H}{2} - W\right)\tau_s \tag{18}$$

where it is tacitly assumed that the injected masses are evenly distributed to the top and the bottom grain matrices. The compressive force due to the mass flux into the defect is

$$P_a = \frac{2\mu}{1-\nu}R(H - W). \tag{19}$$

The balance of two forces provides an expression for the amount of grain slide. When a hillock is caused by the mass injection, or a sink caused by the mass leakage, the amount of grain slide, W, is obtained by

$$W(t) = -\frac{\kappa(1-\nu)\tau_s}{\mu - \kappa(1-\nu)\tau_s}h + \frac{2\mu - \kappa(1-\nu)\tau_s}{2\mu - 2\kappa(1-\nu)\tau_s}H(t), \quad t \geq t_0. \tag{20}$$

Accordingly, the protruding height is roughly proportional to R^{-2}.

4. NUMERICAL SCHEME AND DAMAGE SIMULATION

We now devise a numerical scheme to simulate the protruding and sinking motions. Two simplified polycrystalline configurations are generated by computer for the aluminum interconnect shown in Fig. 2. The first one is an array of regular hexagon grains. As mentioned before, the ith grain boundary connected to the grain forms an angle θ with the X-axis. The connection angles of other grain boundaries, denoted by θ_i ($i = 1,2,3,4,6$), differs from $\theta_3 = \theta$ by multiples of $\pi/3$. The second configuration deviates from the first by fluctuating the connection angles according to $\theta_i = \bar{\theta}_i + \varphi_i$ ($i = 1,\ldots,6$), with φ_i being described by a normal distribution of $N(0,\sigma_\varphi^2)$. The diffusivities of different grain boundary segments are assigned by a normal distribution of $N(\bar{D},\sigma_D^2)$. Prior to the switching on of the electric current, the interconnect assumes a perfectly flat top surface and no mass injects in any grain defects. After the switching on of the electric current at $t = 0$, the material fluxes into each grain can be calculated through equation (4). For a particular grain, a protruding or sinking process commences at the critical time determined by equation (16). The subsequent evolution is governed by equations (8), (9) and (20). It consists of a set of integral equations, and can be solved by the explicit Euler iteration. During the simulation, the interconnect is composed of 3445 grains, with 6892 triple junctions and 10336 grain boundary segments.

The physical constants for aluminum-based interconnects are listed in Table 3. The electric field is calculated from the measured current density and the conductivity of aluminum (3.55×10^7 A/V m). The average grain size $\bar{R} = 0.115$ μm is obtained by counting the grain number in a fixed observation area. The assignments of the mean diffusivity $\bar{D}\delta$, and the effective valence Z^* are worth of explanation. A wide range of the diffusivity data for aluminum exist. For example, Wang *et al.* [14] quoted the surface diffusion data from Wohlbier [19] which gives $Z^* = 20$, $\bar{D} = 10^{-5} \times \exp[-0.7(\text{eV})/K_B T]$ m^2/s, and $\delta = 0.286$ nm. They lead to a small value of $\bar{D}\delta = 5.1 \times 10^{-27}$ m^3/s at 300 K. On the other hand, Borgesen *et al.* [20] adopted the value of $Z^* = 10$ and quoted the grain boundary diffusion data by Kaur *et al.* [21], which gives a

Table 3. Physical constants for aluminum interconnects

γ (OPM)	ϵ_0 (GPa)	ν	K_B (J/K)	T (K)	ρ (Ω)	E (V/m)	R (μm)	$D\delta$ (m^3/s)	Z^*
34.5	1.34	0.348	1.38×10^{-23}	300	1.6×10^{-14}	1000	0.115	1.02×10^{-23}	20

much larger $D\delta$ value of 6.4×10^{-23} m^3/s. In the present simulation, we adopt the value of $Z^* = 20$ and take an intermediate value of $D\delta = 1.02 \times 10^{-23}$ m^3/s.

We assume that the location of defect, h, obeys a normal distribution $N(\bar{h}, s_h^2)$. Since the defects appear mostly in the lower-bottom of the film, we take the expected location as $\bar{h} = 6\bar{R}$, and the standard deviation as $s_h = 0.5\bar{R}$. The other standard deviations are taken as $s_D = 0.1\bar{D}$ and $s_\theta = \pi/4$ in the calculation. Under this s_θ value, the polycrystal configuration, as shown in Fig. 8(a), resembles the statistical feature of the actual microstructure. The thickness for the surface layer H_S and that for the defect layer H_D are taken as $\bar{R}$ and $0.5\bar{R}$, respectively. The latter is less than the former since the attraction for the incoming masses is stronger near the surface layer than that near the defect layer. The evolution is measured by the normalized time

$$\bar{t} = \frac{D\delta}{K_B T \bar{R}^3} Z^* \nu E t.$$

The simulation indicates that the mass flows in the interconnect indeed have four stages: the incubation stage, the rapid growing stage, the

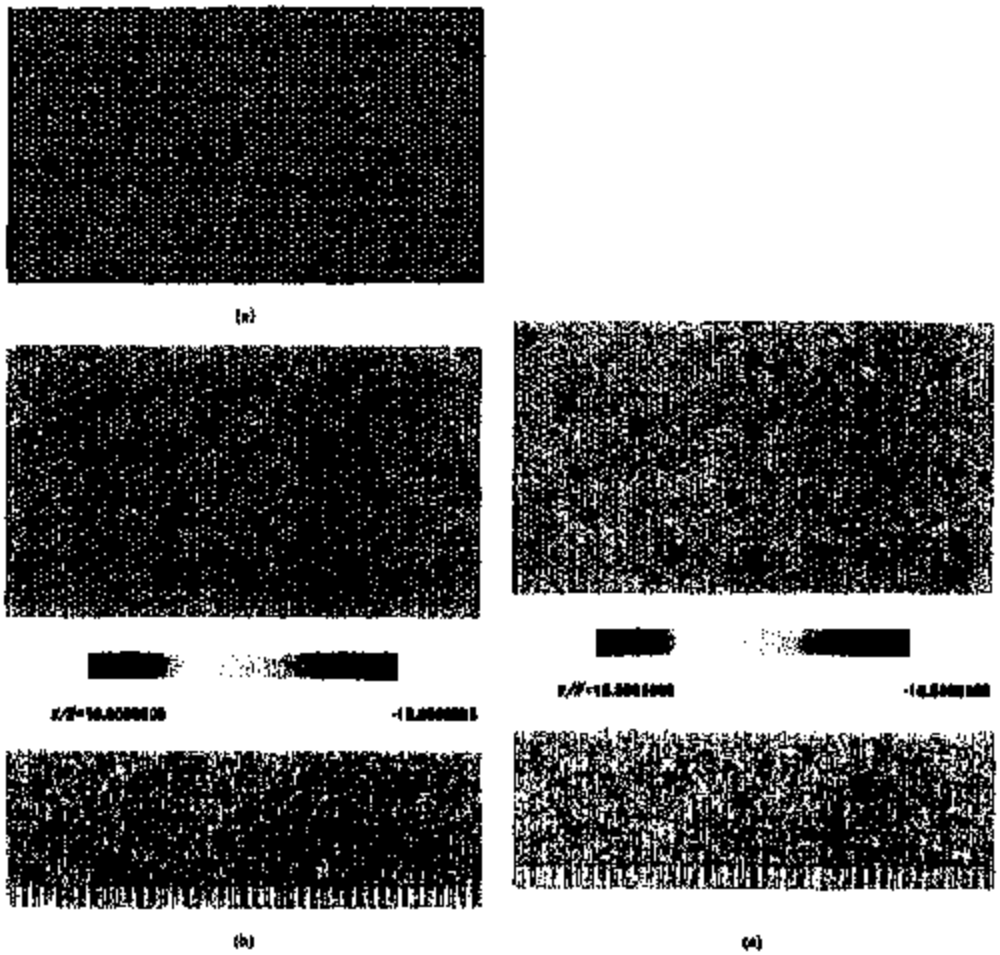

Fig. 7. Morphological evolution for regular hexagonal grains: (a) the initial configuration; (b) at $\bar{t} = 5$; (c) at $\bar{t} = 10$. (W denotes the protruding height (>0) or the sink depth (<0) and $\bar{R}$ the average grain radius).

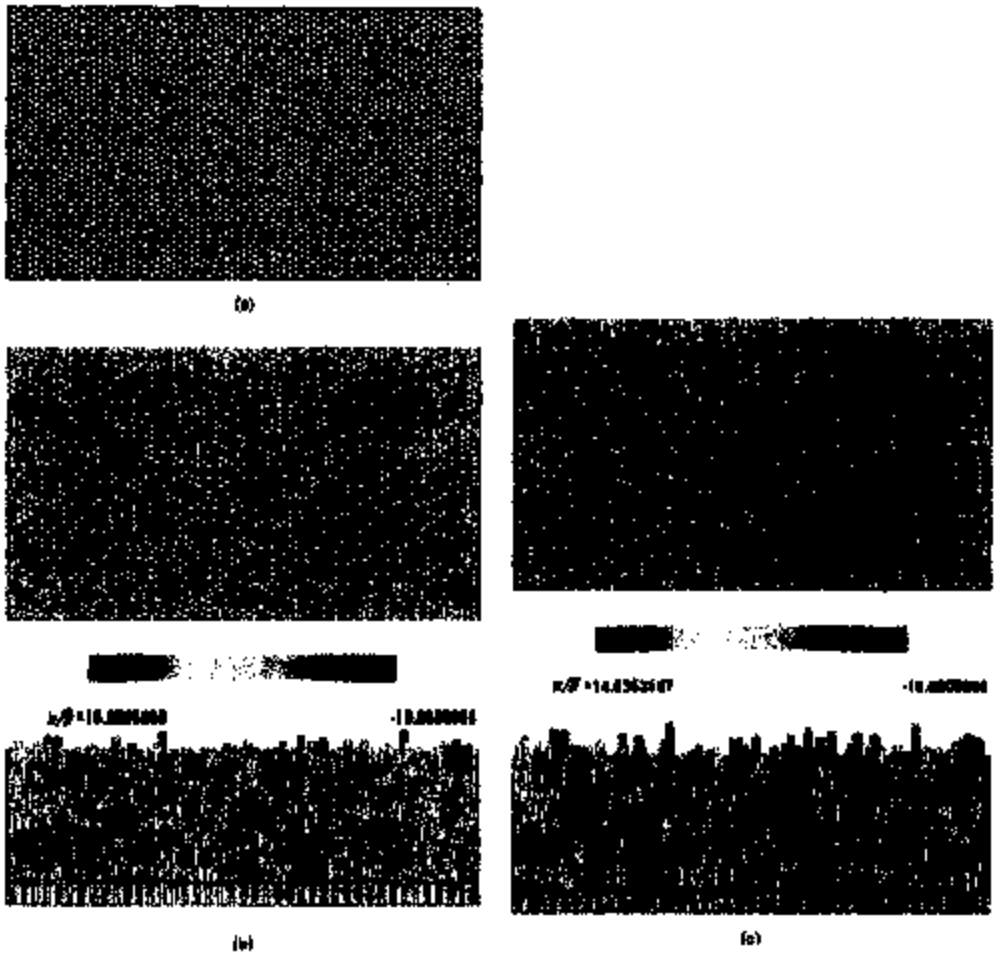

Fig. 8. Morphological evolution for general hexagonal grains: (a) the initial configuration; (b) at $\bar{t} = 5$; (c) at $\bar{t} = 10$.

deceleration stage, and the final stabilization. We now describe the two cases of calculation in detail.

The initial configuration for the case of regular hexagon grains is shown in Fig. 7(a). Figures 7(b) and (c) show two snapshots of the interconnect at $\bar{t} = 5$ and 10, which depict the damage evolution of the grains. The regularity of the configuration suppresses the fluctuation in the grain fluxes. The interconnect will have a relatively long life. The case of general hexagon grains in Fig. 8(a) bears more resemblance to the actual configuration. Figures 8(b) and (c) illustrate two snapshots of the damage evolutions in the interconnect at the instant $\bar{t} = 5$ and 10. In the same time intervals, the hillocks and sinks are more severe, and the number and the average height of the hillocks are greater than the interconnect of regular hexagons. The variations of the protruding height and the sinking depth are shown in Fig. 9 vs the normalized time. The grain flux J_g is taken to be $2.34\sigma(J_g)$ in the calculation. The protruding motion jumps to a fast growing stage after an incubation time, then gradually slows down to approach a stabilized height, in good agreement with our experiments.

The predictions on the morphological fluctuations due to the regular grain assembly and the general grain assembly are very different. Figure 10 plots the curves of $s_W/\bar{R}$ vs $\bar{t}$, where s_W represents the standard deviation of the surface morphology W. The general grain assembly can cause a more severe morphological instability than the regular one. The effect due to the angular deviation s_ϕ is two-fold. First, the angular deviation leads to larger standard deviation in mass flow, as quantified by equation (7). Second, it also results in the fluctuation of the grain sizes from their average value $\bar{R}$, and that causes further morphological fluctuation

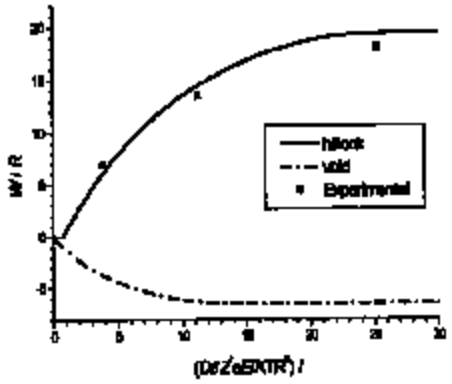

Fig. 9. Protruding height and the sinking depth vs the normalized time, $J_g = 2.34\kappa(J_g)$.

of the microstructure since the inverse square dependence of the hillock height with respect to R.

To address the importance of grain size on morphological evolution under electromigration, we include a further example of general hexagon array in Fig. 11(a), featuring a much larger average grain size of $3\bar{R}$. The interconnect is composed of 481 grains with 964 triple junctions and 1444 grain boundary segments. Other parameters are the same as the previous case. Since the incubation time for the case in Fig. 8 is about $\bar{t} = 1$, its square dependence on the grain size would lead to an average incubation time of $\bar{t} = 9$ for the present case (for the sake of comparison, the previous $\bar{R}$ value is used to get the normalized time). The simulation confirms this prediction. At $\bar{t} = 5$, there are hardly any morphological changes. At $\bar{t} = 10$, the damage evolution just starts, as shown in Fig. 11(b). It is much subdued when compared with Fig. 8(c).

To design against the electromigration, one needs to raise the incubation time of an interconnect beyond its service life. To comply with this criterion, a polycrystal line with large and uniform grains (if not a bamboo line or even a single crystal line) with small variation in grain boundary diffusivities is desirable.

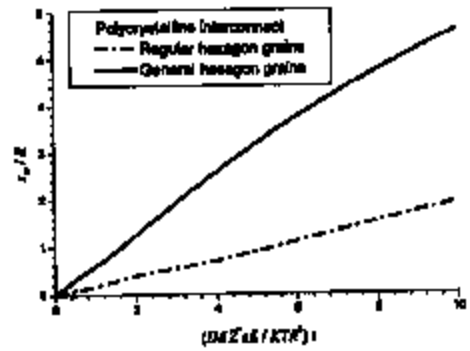

Fig. 10. Development of morphological fluctuation (in terms of the standard deviation of W) with respect to the normalized time.

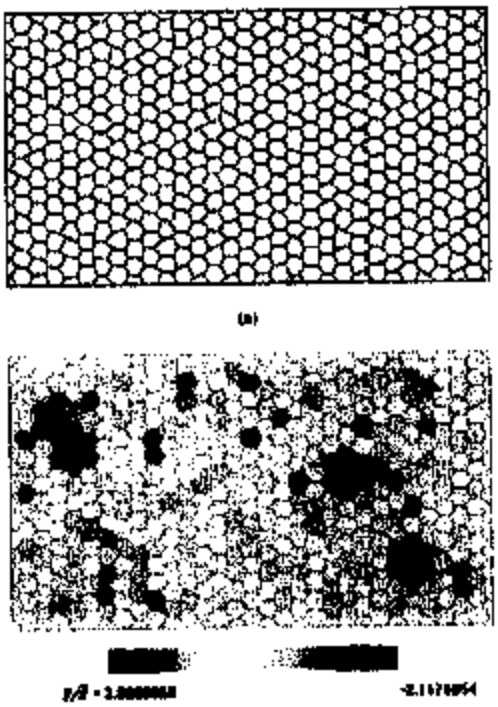

(a)

(b)

Fig. 11. Morphological evolution for a general hexagonal array of much larger grain size of 0.345 μm: (a) the initial configuration; (b) at $\bar{t} = 10$.

To conclude this paper, we mention that the failures of the polycrystalline interconnects often result from a combination of different mechanisms, such as stress migration, grain boundary diffusion, and thermal migration. A coupled analysis is worthwhile in the future.

Acknowledgements - The authors appreciate the support by the National Natural Science Foundation of China.

REFERENCES

1. D'Heurle, F. M. and Ames, I., *Appl. Phys. Lett.*, 1970, 16, 80.
2. D'Heurle, F. M., *Proc. IEEE*, 1971, 59, 1409.
3. Thouless, M. D., Yu, H., Zhao, Z. and Yang, W., *J. Mech. Phys. Solids*, 1996, 44, 371.
4. Yang, W., Wang, W. and Suo, Z., *J. Mech. Phys. Solids*, 1994, 42, 897.

5. Li, C.-Y., Borgesen, P. and Korhonen, M. A., *Appl. Phys. Lett.*, 1992, 61, 411.
6. Besser, P. R., Madden, M. C. and Flinn, P. A., *J. appl. Phys.*, 1992, 72, 3792.
7. Kraft, O., Bader, S., Sanchez, J. E. and Arzt, E., *Mater. Res. Symp. Proc.*, 1993, 309, 199.
8. Marieb, T., Flinn, P., Bravman, J. C., Gardner, D. and Madden, M., *J. appl. Phys.*, 1995, 78, 1026.
9. Arzt, E., Kraft, O., Nix, W. D. and Sanchez, J. E., *J. appl. Phys.*, 1994, 76, 1563.
10. Sanchez, J. E. and Arzt, E., *Scripta metall. mater.*, 1992, 27, 285.
11. Sanchez, J. E., McKelly, L. T. and Morris, J. W., *J. appl. Phys.*, 1992, 72, 3201.
12. Rose, J. H., *Appl. Phys. Lett.*, 1992, 61, 2170.
13. Sun, Z., Wang, W. and Yang, M., *Appl. Phys. Lett.*, 1994, 64, 1944.
14. Wang, W., Sun, Z. and Hao, T.-H., *J. appl. Phys.*, 1996, 79, 2394.
15. Zhao, Z. and Yang, W., *Tsinghua Sci. Technol.*, 1997, 2, 574.
16. Thompson, C. V. and Kuhn, H., *J. Electron. Mater.*, 1993, 22, 581.
17. Sun, Z., *Acta metall. mater.*, 1994, 42, 3581.
18. Peach, M. O. and Koehler, J. S., *Phys. Rev.*, 1950, 80, 436.
19. Wohlfarter, F. H., *Diffusion and Defect Data Solid State Data*, Vol. 47. Trans. Tech. Publications, Switzerland, 1986, p. 4.
20. Borgesen, P., Korhonen, M. A., Sullivan, T. D., Brown, D. D. and Li, C.-Y., in *Thin Films: Stress and Mechanical Properties III. MRS Symposium Proceedings*, Vol. 239, ed. W. D. Nix, J. C. Bravman, E. Arzt and L. B. Freund, 1992, p. 583.
21. Kaur, I., Gust, W. and Bravman, L., *Handbook of Grain and Interphase Boundary Diffusion Data*. Ziegler Press, Stuttgart, 1989.

ELSEVIER

Thin Solid Films 292 (1997) 103–117

Thin Solid Films

Transmission electron microscopy of Al–Cu interconnects during in-situ electromigration testing

W.C. Shih, A.L. Greer

Department of Materials Science and Metallurgy, University of Cambridge, Pembroke Street, Cambridge CB2 3QZ, UK

Received 15 February 1996; accepted 16 May 1996

Abstract

Transmission electron microscopy of 2.1 μm wide Al–4 wt.% Cu interconnects during in-situ electromigration stressing shows microstructural evolution and the development of damage, including failure. Voids which develop early stop growing and are not fatal. Hillocking is associated with Al–Cu precipitates; voiding which leads to failure is associated with copper depletion. Void initiation is at the upstream end of inclined grain boundaries crossing the lines, which have a near-bamboo microstructure. Healing events occur as damage develops, arising from further voiding or from stress build-up. Open-circuit failure can occur when the proximity of grain boundaries impairs the stress-driven healing. A schematic model for open-circuit failure in bamboo lines is proposed. The relative advantages of in-situ and conventional testing are discussed.

Keywords: Transmission electron microscopy; Aluminium; Copper; Electromigration

1. Introduction

As interconnect line-widths decrease, the study of how electromigration damage limits the metallization reliability remains important. New atomic transport paths and damage mechanisms can become dominant, rendering earlier studies invalid. In particular, the damage mechanisms and failure modes can be strongly related to the alloy microstructure in the lines [1]; earlier work concentrated on polycrystalline lines, whereas interest is now in bamboo lines (where all grain boundaries are approximately normal to the line length and there are no grain-boundary junctions), or near-bamboo lines (consisting of bamboo segments with some polygranular segments) [1]. It is possible to derive some links between microstructure and electromigration damage and failure using surface-sensitive techniques such as scanning electron microscopy (SEM) (see, for example, Ref. [2]), and focused ion-beam microscopy (FIB) [3]. Clearly, however, transmission electron microscopy (TEM) is more powerful for characterizing microstructure, and has the greatest potential for elucidating the related mechanisms of damage and failure. This is particularly so if electromigration testing can be performed in-situ in the microscope. TEM has the disadvantage that specimen preparation is much more difficult, the semiconductor substrate needing to be thinned or removed locally to permit electron transparency. A more fundamental concern is that since heat conduction into the substrate is so important in testing, the removal of this heat sink from the area being examined greatly changes the testing conditions, notably leading to high temperature gradients (discussed further in Section 2.2). With limitations on instrument time, in-situ testing in the TEM is also often much accelerated in comparison with conventional accelerated testing. Together with the necessary lack of passivation, these factors lead to uncertainty about whether the mechanisms observed in in-situ testing can apply in the interpretation of conventional testing or of failures in service (discussed in Section 4.1).

Pioneering work on in-situ testing in TEM was carried out by Blech and Meieran [4]. They observed thinning and formation of voids and hillocks in polycrystalline lines (i.e. with grain size < line-width) of nominally pure aluminium. Void formation was associated with grain boundaries. Further work by these authors and others [5–7] on similar specimens related the stages in damage development in-situ to resistance changes and to failure, and showed that the orientation of grain boundaries could be important. Addition of copper to aluminium greatly improves interconnect lifetime [8], and alloys of this kind (with 6 wt.% Cu [9] and 7 wt.% Cu [10], greater than in the present work and much greater than what is now common) have been studied by in-situ testing in TEM. The early work confirmed the slower damage rate [9]. The

PII S0040-6090(96)08944-4

later work found Al_2Cu precipitates, and showed that under electromigration stressing the copper is transported (in the same direction as the electrons) faster than the aluminium, thereby becoming depleted. The depletion was seen in the dissolution of precipitates and, in confirmation of earlier suggestions (see, for example, Ref. [8]), it was in depleted areas that voids formed [10].

The in-situ testing of Al–Cu was again on wide polycrystalline lines. There has been little or no such work on near-bamboo lines. Vavra and Lobotka [11] studied near-bamboo, wide lines of pure aluminium (average grain size 15 μm, in 10 μm line-width). To obtain the large grain size, the metallization was relatively thick (6 μm) and then thinned for TEM observation. Both voids and hillocks were formed in the in-situ testing. In these samples, voids formed inside grains and migrated in an elongated shape along the lines.

In the present study, the lines are 2.1 μm wide, Al–4 wt.% Cu, with near-bamboo microstructure. In contrast to earlier in-situ work, the lines have been the subject of a wider study and have not been patterned specially for the in-situ work. The wider study has included damage morphology and precipitate distribution [2], life-testing [12,13], quantitative monitoring of damage development (by SEM) [12–16], the structure of the Al–Cu precipitates [17] and electrical measurements [15,18]. The SEM shows that there are precipitates in the lines and that these precipitates evolve during electromigration stressing. As is generally known, and confirmed by the electrical resistance measurements in the present project [15], there are in the later stages of line lifetime not only sharp increases but also sharp decreases in resistance. That is, there are healing events, and these form an important part of the overall behaviour under electromigration stressing.

In a number of the above cases of in-situ testing, the current was reversed after some damage had developed. It was found that damage could be at least partially reversed, voids refilling [4,6,10] and precipitates reappearing [10]. There has been study of a.c. stressing [19]. However there appears to have been no study of healing while current stressing in the same direction was continuing. Nor has there been a detailed study of how damage leads to failure. Healing and failure processes are the focus of the present study.

2. Experimental details

2.1. Methods

Samples were supplied by GEC–Plessey Semiconductors Ltd. The metallization was Al–4 wt.% Cu, 1 μm thick, with a nominal sheet resistance of 32.5 mΩ/□. Deposition was by sputtering; the silicon substrate, with 0.5 μm SiO_2 on top was held at 150 °C. The metallization was patterned by standard techniques and then annealed under nitrogen gas for 30 min at 435 °C. The lines are 1.4 mm long, with nominal widths of 1.4, 1.8 and 2.4 μm; only the widest are used in this work. After an etching undercut of 0.3 μm was estimated from the variation of resistance with width, the actual width of the lines in this study was found to be 2.1 μm. Each line has two 4.5 μm wide parallel guard rails of the same metallization, designed for detecting short-circuiting due to hillocking. These guard rails are not subjected to any current. In the present study the unchanging microstructure of the guard rails provides useful reference points for changes in the central, stressed line. No passivation was applied.

To prepare the samples for TEM examination, dice were cut ultrasonically, ground from the back side, and jet-polished from that side to produce a dimple. The polishing solution was $HF–HNO_3–CH_3COOH$ (3:5:3) [20]. The specimens were further etched from the back side using a solution of $HF–HNO_3$ (1:4) until an area transparent to light appeared. The etching solution removed Si substrate and reached the SiO_2 separating the etching solution from the Al–Cu test lines. The degree of etching was then controlled with care until the transparent area grew to include a substantial area of the desired test line. Each die was fixed to a carrier using silver dag. The lines to be tested were Al-wire bonded to the carrier contacts. The carrier contacts were then electrically connected to the holder contacts by soldering a Cu wire. An example of a specimen which has gone through these processing steps is shown in Fig. 1.

TEM examination was performed in a JEOL 2000FX microscope operating at 200 kV. A cold-stage specimen holder was used, with an Oxford Instruments ITC4 temperature controller. After loading the carrier into the holder, electrical connections were made to the holder by soldering

Fig. 1. SEM image of a processed specimen showing the region over which the silicon has been removed and its oxide thinned to leave electron-transparent segments of line. In this case the test line is 10 μm wide, with a length of 3 × 1.4 mm. This sample was used for estimating Joule heating effects. (Montage of two micrographs)

copper wires to the bonding pads. Apart from initial tests, the base temperature of the holder during electromigration stressing was held at 123 K.

For each line tested, the electromigration experiment was completed within one specimen loading, and the line was tested to failure. Initial stressing was at a current density of 0.5×10^{10} A m^{-2} (abbreviated here as 0.5 j) for 30 min. This did not induce damage but did allow the die temperature to increase, reducing thermal transients during the main stressing. The main stressing was at 0.7 and 0.8 j at which damage proceeded rapidly, but from time to time the current density was reduced to 0.5 j to slow down the damage development for the convenience of imaging.

2.2. Temperature profile

In in-situ testing, the central, electron-transparent segment of the line heats up markedly because of the lack of heat-sinking into a massive silicon substrate. In the present work it was not feasible to measure the temperature profiles along the lines under test. However, the heating effects were estimated from the onset of melting in 10 μm lines and the parameters thus determined were used in the calculation of temperature profiles in the 2.1 μm lines used for in-situ testing. The temperature profile in the electron-transparent segment of line was calculated according to the analysis thoroughly discussed in earlier work [6,10]. It is assumed that the only significant heat flow out of this segment of line is conduction along the line itself and the temperature profile $T(x)$ for the segment is then given by

$$T = T_0 + \frac{1}{\alpha}\left(\frac{\cos b\,(d-x)}{\cos b\,d} - 1\right) \quad 0 < x < 2d \qquad (1)$$

where T_0 is the temperature of the ends of the segment and d is the half-length of the segment. The parameter b is given by

$$b^2 = \frac{\alpha \rho_0}{\kappa} j^2 \qquad (2)$$

where α and ρ_0 are the temperature coefficient of resistivity and the resistivity of the metallization at T_0, κ is its thermal conductivity and j is the current density in the line. Tabulated data [21] were used to estimate the resistivity ρ of Al–4 wt.% Cu to be $(53 + 1.27) \times 10^{-10}\ \Omega$ m, where T is the absolute temperature, and this expression was used to derive ρ_0 and α. The thermal conductivity was taken to be 160 W m^{-1} K^{-1} [10]. Lines of 10 μm width (of the kind in Fig. 1) were stressed at current densities in the range $(0.2–0.4) \times 10^{10}$ A m^{-2} (0.2–0.4 j), and it was found that the melting behaviour could not be fitted if it was assumed that T_0 remained equal to the sample holder temperature T_h in the TEM (203 K in these tests). The Joule heating was assumed to give a temperature rise in the die such that

$$T_0 = T_h + c\,w\,j^2 \qquad (3)$$

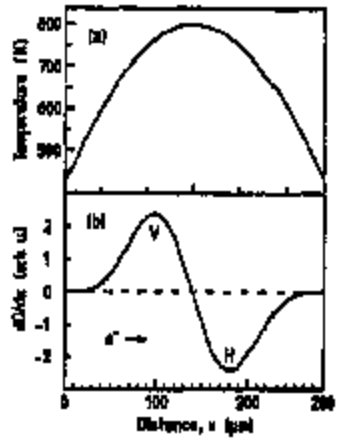

Fig. 2. (a) Calculated temperature profile for an electron-transparent segment of Al–4 wt.% Cu line during electromigration testing in the TEM. The segment is 280 μm long, 2.1 μm wide and 1 μm thick, stressed at 0.8×10^{10} A m^{-2}. In this most severe stressing used in the present study, the maximum temperature approaches the Al–Cu eutectic at 821 K. (b) The spatial derivative of diffusivity (activation energy 0.86 eV atom^{-1}) corresponding to the temperature profile in (a). For electron flow in the positive direction, the maximum in $\partial D/\partial x$ gives fastest voiding (V) and the minimum fastest hillocking (H). The distance between these regions matches that observed (Fig. 3(b)).

where w is the total width of lines under test (i.e. 30 μm in Fig. 1). The constant c was treated as adjustable, and by matching whether lines melted or not, a value of 2.3×10^{-12} K m^3 A^{-2} was estimated.

Calculations based on these parameters were performed for the 2.1 μm lines under current densities of $(0.5–0.8) \times 10^{10}$ A m^{-2}. An example of a calculated temperature profile is shown in Fig. 2(a); this is for a line with an electron-transparent segment 280 μm long ($d = 140$ μm), tested under the most extreme condition, 0.8 j. It can be seen that there is a marked temperature variation in the observable segment of the line and that the maximum temperature approaches the eutectic (821 K) of Al–Cu. In view of the uncertainties in the analysis and in the estimation of the relevant parameters, calculated profiles of this kind can be taken only as rough guides to the temperature; even so, they are useful in interpreting the damage pattern in the tested lines.

Electromigration damage in general arises from a divergence in the atomic flux. If it is assumed that the divergence is caused only by the spatial variation of atomic diffusivity D (i.e. local microstructural effects are ignored), then initial damage would be concentrated at the places of maximum $\partial D/\partial x$. The spatial derivative of diffusivity, $\partial D/\partial x$ corresponding to the temperature profile in Fig. 2(a) is shown in Fig. 2(b). In the calculation of $\partial D/\partial x$ it is assumed that the diffusivity has the same activation energy as the mean time to failure of the same lines; this has been determined to be 0.86 eV atom^{-1} [12,13]. For the case in Fig. 2, it is therefore predicted that the initial voiding and hillocking should occur 40 μm on either side of the centre of the line. This conclusion is not dependent on the specific diffusion being considered (whether of the aluminium or of the copper).

3. Results

3.1. Overall damage development

The effects of temperature profiles such as that in Fig. 2(a) are evident when the overall distribution of damage is examined. Fig. 3(a) is a low magnification SEM image of a 2.1 μm wide line (and associated guard rails) before electromigration stressing, showing an overview of the electron-transparent area. The segment of line in the electron-transparent area shows no difference in microstructure from the rest of the line. After electromigration stressing to failure, the overall pattern of damage can be seen in Fig. 3(b) which is a low-resolution backscattered electron image of the electron-transparent line segment. In the figure, electron flow is from left to right. Almost all of the voids are just to the left of the centre, and the hillocks to the right of the centre. Also, between the voiding and hillocking regions there is an essentially total depletion of the copper-rich precipitates (which appear bright in the backscattered electron image). These features can be seen in greater detail in the enlarged image in Fig. 3(c); this clearly shows that the copper from the central zone has migrated to the hillocking region. All of these phenomena are consistent with the temperature profile suggested in Section 2.2 and with aluminium and copper migration in the direction of the electron flow, the copper being faster. In the left-hand segment of the line the temperature is increasing in the direction of electron and atom flow; at the point of maximum atomic flux divergence (near the point of maximum temperature gradient), voids form. In the right-hand side, with temperature decreasing, correspondingly hillocks form. In the hottest, central area of the line dissolution of the copper-rich precipitates is favoured and the copper migration is fastest, resulting in depletion. The hillocks form in the region where copper is accumulating and mostly consist of copper-rich precipitates. It appears that almost all of the voids (except the early developed voids) do not develop until there is local depletion of copper, reflected in the disappearance of the precipitates. The regions of maximum voiding and hillocking are 30–40 μm on either side of the line centre, in excellent agreement with the positions suggested in Fig. 2(b). Open-circuit failure occurs at the position of maximum voiding in a total test time which is roughly one order of magnitude less than the failure time predicted by extrapolating mean times to failure in conventional testing [12,13] to the temperature at the place of the voiding.

The distribution of damage along the line illustrates the importance of the temperature profile in testing of electron-transparent, poorly heat-sunk, lines. The temperature profile and damage distribution are markedly different from those found in conventional accelerated testing or in service. However, the advantage for in-situ studies is that the damage is concentrated in the electron-transparent portion, and that different types of damage are available for study. Despite the steep temperature gradients, it is assumed that the damage processes reflect electromigration without any significant contribution from thermomigration, which is a small effect in aluminium [22]. That failure is more rapid than expected from extrapolation of conventional test data presumably reflects the influence of temperature gradients on the electromigration flux. The following sections describe more detailed work on particular phenomena within the overall development of damage and failure.

3.2. Microstructural development and hillocking

Fig. 4 shows a short length of a 2.1 μm wide line with its two 4.5 μm wide guard rails. As can be seen, the 200 kV

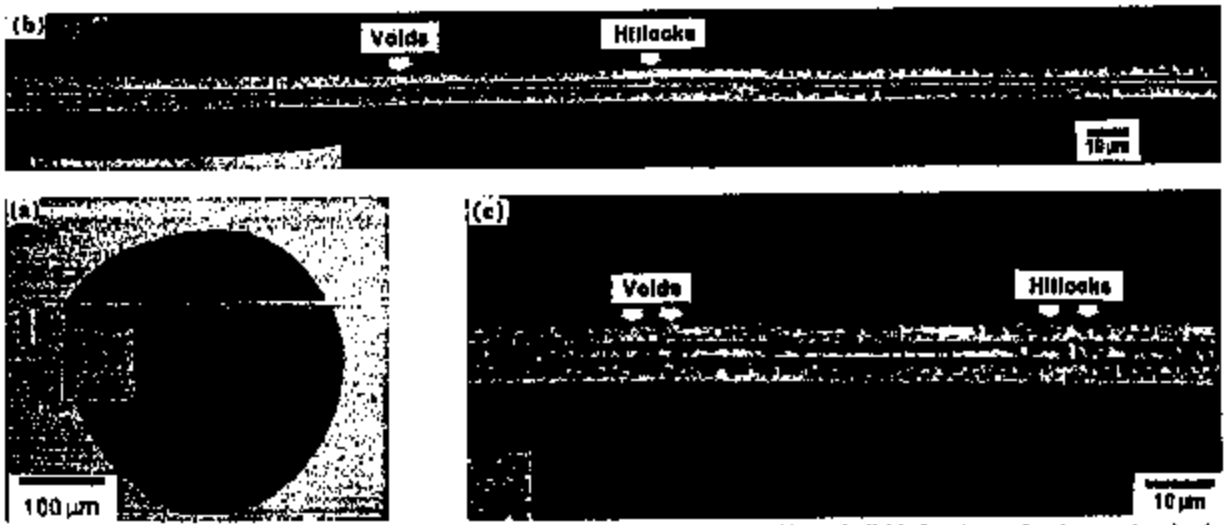

Fig. 3. (a) Low magnification SEM image (montage of two micrographs) for a 2.1 μm wide line (with guard rails) before electromigration stressing, showing the electron-transparent area. (b) and (c) Backscattered electron images in SEM for the electron-transparent segment after failure, showing voids and hillocks in distinct regions on either side of the centre of the transparent segment, with the depletion of the Al–Cu precipitates between these regions. (c) A close-up of (b).

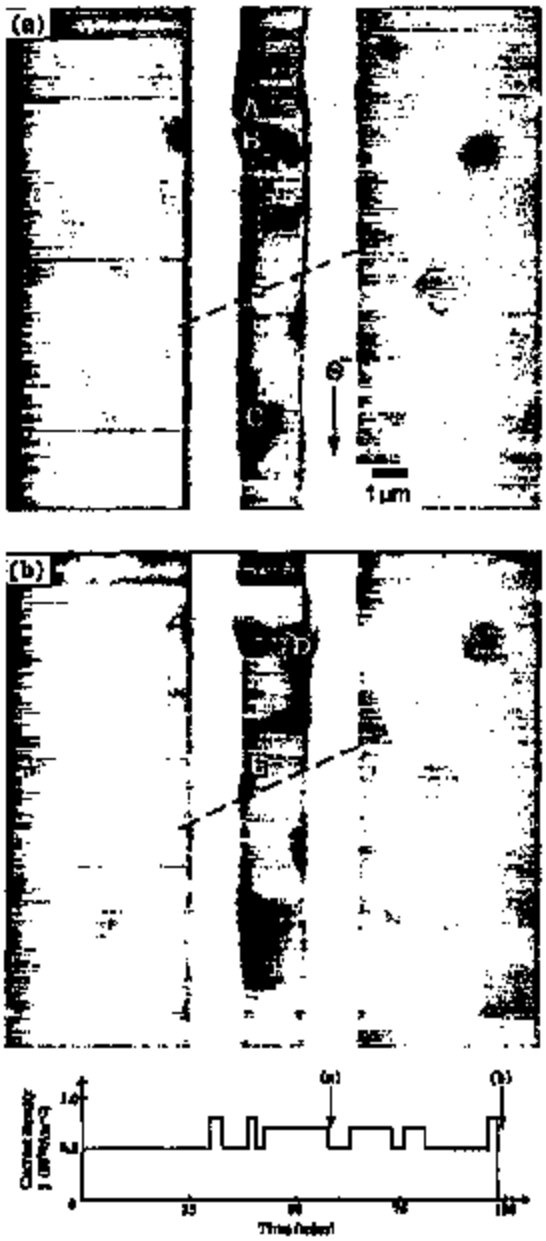

Fig. 4. TEM images for a segment of test line, (a) after 58 min and (b) after a further 40 min of in-situ electromigration testing (profile shown at bottom of figure). Comparison of (a) and (b) shows the formation of an Al–Cu hillock at D, the dissolution of an Al–Cu precipitate at C, and the migration of a precipitate at E—all consistent with the migration of copper parallel to the electron flow (top to bottom).

accelerating voltage used provides sufficient transparency for imaging of the metallization microstructure although the lines are 1 μm thick on a 0.5 μm oxide. There is, however, some degradation of image quality due to charging effects on the non-conducting SiO_2 film. In the microstructure the distribution of Al–Cu precipitates (dark particles) can readily be seen. In some areas individual aluminium grains can also be distinguished. In the narrow test lines generally, and there is evidence for this in Fig. 4, there is a clear tendency for the precipitates to be at the line edges at the end of grain boundaries crossing the line in the "bamboo" configuration.

Fig. 4(a) shows the specimen after current ramping from 0.5 j to 0.8 j over 58 min. As observed during this period, an aluminium hillock has developed at A and two precipitate hillocks at B and C. (The precipitate hillocks can be distinguished because of their darker appearance due to greater absorption.) Given that the electron flow is from top to bottom in Fig. 4, the aluminium hillock can be attributed to the blocking of the line cross-section by precipitates. Evidence for this has been seen also in SEM studies [2]. Fig. 4(b) shows the same line after a further 40 min of stressing. In comparing Fig. 4(a) and 4(b), precipitates in the unstressed guard rails are useful as reference points; the dashed lines linking these points do not always appear in the same orientation because of changing specimen tilt. During the further stressing, an Al–Cu hillock has formed at D and it appears to be a single grain. Also, the precipitates in the centre line have evolved. The changes clearly confirm that the copper migration is parallel to the electron flow; for example, the precipitate C is spreading along the direction of the electron flow (compare in Fig. 4(a) and Fig. 4(b)). The precipitate E has, in effect, migrated 0.7 μm in the direction of electron flow. This appears to occur by erosion of the upstream surface and deposition at the downstream surface, giving a somewhat changing shape. These observations of precipitate evolution provide confirmation of the behaviour in the same type of tracks inferred from intermittent SEM observations [15].

3.3. Early voids and void initiation

Electromigration failure is predominantly associated with voiding, and consequently much electromigration work has focused on the mechanisms of void initiation and growth. In the present work, it is found that voids always initiate at the edge of the lines beneath the aluminium oxide skin, as is shown in Figs. 5 and 6(a) as well as in Figs. 7(a), 8(a) and

Fig. 5. TEM image showing the initiation of voids at the end of the electron-transparent segment of line. The voids developed early, at the edge of the line and beneath the oxide skin. Electron flow: top to bottom.

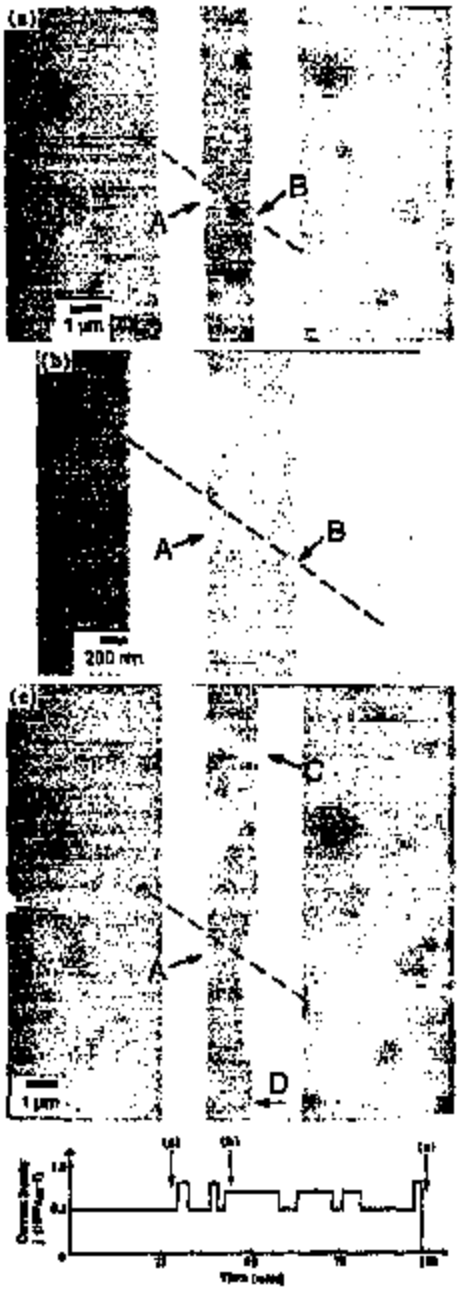

Fig. 6. TEM images of a line segment, showing that voids which develop early stop growing even in the region of maximum atomic flux divergence giving the maximum voiding under electromigration testing. In (a) there are two early voids at A and B with precipitates nearby. After another 13 min of electromigration testing, the slightly higher magnification image (b) shows the depletion of Al–Cu precipitates but unaltered voids at A and B. In (c), the line has failed at C, but despite the heavy damage site in this region of high $\partial\sigma/\partial x$ (Fig. 2(b)), the early void at A has still not grown further. The timing and current density at which each micrograph was taken are presented in the diagram at the bottom of the figure. Electron flow: top to bottom.

9(a). Subsequent growth of the voids can take different forms. In particular, the voids which develop early, such as in Figs. 5 and 6, behave differently from those shown in Figs. 7–9. Whether these early voids would lead to failure has been an issue for discussion [15,23]. Here more direct evidence provides further insight. Figs. 5 and 6(a) were obtained at the end of the first 30 min stressing at 0.5 j. The small voids shown in these two figures have three features which make them significantly different from the others. Firstly, these voids appear before the local depletion of Cu atoms, in contrast to those discussed in Section 3.1; as can be seen in Fig. 5, there are precipitates very close to the voids. Secondly, the position of these voids seems to be not affected by the long-range temperature profile discussed in Section 2.2 and Section 3.1; at about the same time, voids of this type develop at the end of the transparent line segment which experiences a relatively low temperature increase (Fig. 5), and in the hot region with the maximum divergence in atomic flux (Fig. 6). The third feature is that these voids do not grow much during further electromigration stressing, as is shown in Fig. 6 (where, as in Fig. 4, a dashed line based on precipitates in the guard rails is used as a reference to identify the same position in the test line). After Fig. 6(a), Fig. 6(b) was taken after another two cycles of electromigration stressing between 0.5 and 0.8 j (another 13 min). In this slightly higher magnification image, it can be seen that both voids A and B did not grow much while the precipitates nearby are disappearing. After the test line failed with a lifetime of 98 min, Fig. 6(c) was obtained. In the lifetime of this line, these two voids did not grow further, although they are in the most heavily voided region in the vicinity of failure site (labelled C). In Fig. 6(c), void A still retains its initial morphology as in Fig. 6(a); void B also retained its morphology until in this case it was incorporated into another void growing from position D after the local depletion of Al–Cu precipitates (see Fig. 7). These three features of the early voids suggest that they have different mechanism for void development and they are unlikely to be fatal. All the voids discussed in the following sections appeared after the local depletion of copper (Al–Cu precipitates).

3.4. Void development

The most attractive feature of the in-situ work is the ability to follow the development of voids. Fig. 7(a)–7(j) show the evolution of a void under stressing between 0.5 j and 0.8 J. Initial stressing at 0.5 j for 30 min did not produce any detectable damage. In stressing for 3 min at 0.8 j a void appeared at the edge of the line and grew fast. The current density was reduced to 0.5 j to obtain the image in Fig. 7(a). After a further 2 min stressing at 0.8 j and reduction again to 0.5 J, the void evolved into the shape in Fig. 7(b). Subsequent stressing was at 0.7 j, again with periodic interruptions at 0.5 j. Over 30 min, the evolution followed the pattern seen in Fig. 7(c)–7(g). After initial growth across the line the void grew rapidly upstream along the edge. When it encountered

a boundary across the line (Fig. 7(e)–7(g)), sharp growth occurred along the boundary. (Presumably this is a grain boundary, though this was not verified using electron diffraction.) After Fig. 7(g), the current density was reduced to 0.5 J to avert failure. Almost immediately, the new slit-like growth front of the void was filled. After 3 min at 0.5 j, the current density was again raised to 0.7 J for 5 min and the development of the void now followed a different course; as shown in Fig. 7(h) and 7(i), its growth direction changed and it broke through the boundary, continuing its growth along the edge of the line. After a further 15 min at 0.5 J, the void had evolved into the shape shown in Fig. 7(j).

When the void at D (Fig. 7(a)) grew along the edge of the line, the growth front encountered other grain boundaries (judging from the varying contrast level) before it reached the similarly inclined grain boundary at E (Fig. 7(e)). Thus it seems that void growth along the edge of the line does not change into void growth along a grain boundary unless the growth front reaches the upstream end of an inclined grain boundary.

The sequence of images in Fig. 7, when compared using the reference line, shows that the growth of the void is predominantly upstream, with the earlier parts being filled in with aluminium migrating downstream. Such filling in, and the change between Fig. 7(g) and 7(h), can be regarded as healing events. Similar events were then subjected to further study.

3.5. Healing

Fig. 8 shows a sequence of micrographs from a different segment of line. For the specimen tilt used, the predominant contrast is from thickness variations. Again, no damage was evident after 30 min at the initial electromigration stress of 0.5×10^{10} A m^{-2} (0.5 j). After a further 33 min in which

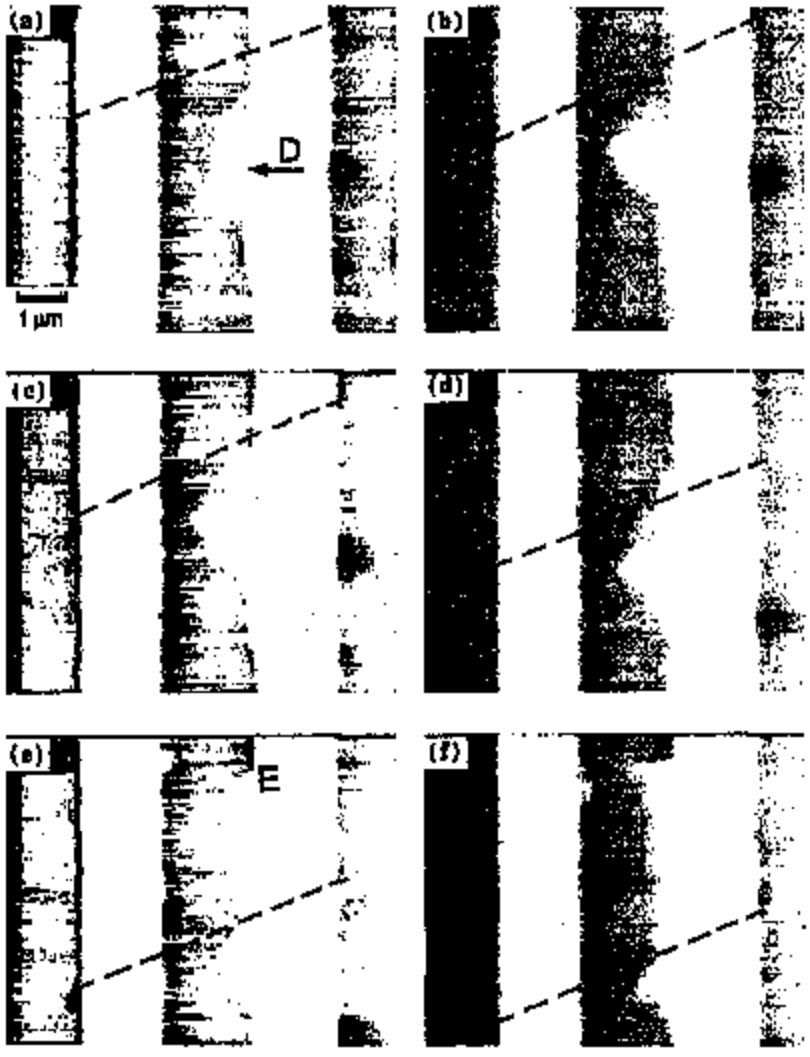

Fig. 7. (continued)

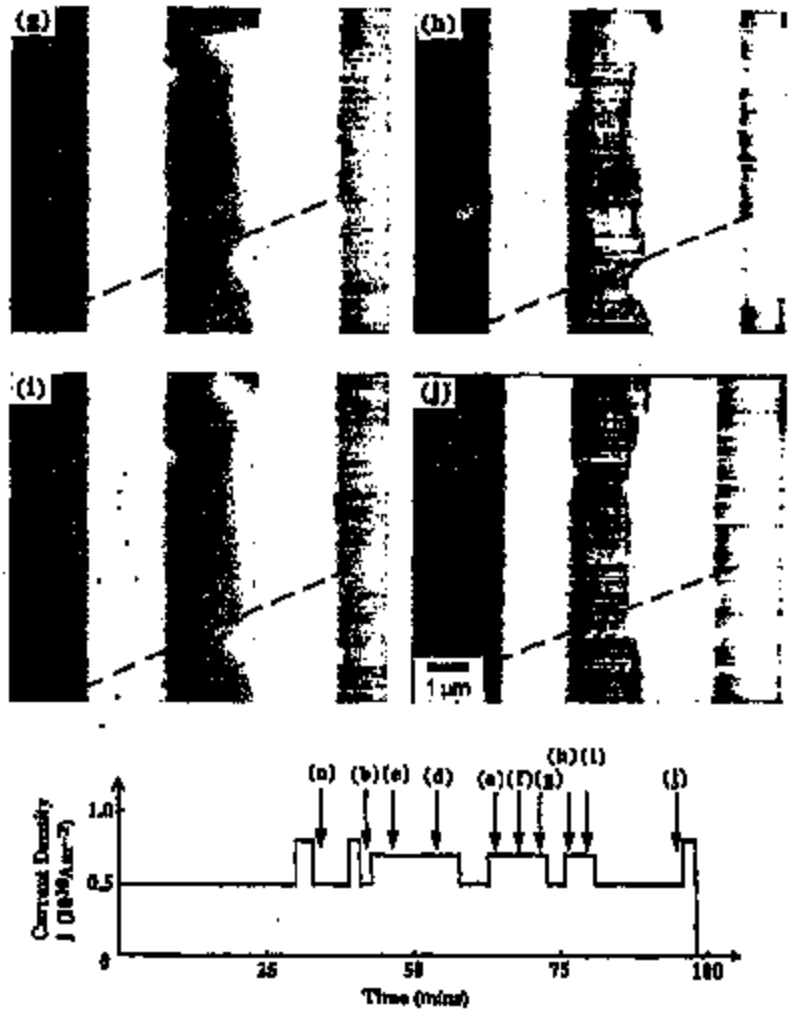

Fig. 7. Sequential TEM images (a)–(j) for a segment of line under in-situ electromigration testing, showing the evolution (initiation, growth along the line, partial refilling, growth across grain boundaries and growth along a grain boundary) of a void stressed with a current density ranging between 0.5×10^{10} A m^{-2} and 0.8×10^{10} A m^{-2}. The timing and current density at which each micrograph was taken are presented in the diagram at the bottom of the figure. Electron flow: top to bottom.

there were three cycles of current density between 0.5 j and 0.8 j, still no damage was evident. A void formed at the edge of the line after further stressing at 0.7 j. Fig. 8(a) shows it after 10 min, and Fig. 8(b) after a further 5 min in which it has crossed the entire width of the line, though not the entire thickness. Observations of line thinning of this kind have often been reported (see, for example, Ref. [24]) and taken as evidence for surface or interface transport. As in Fig. 7, the effective void migration can be seen to be against the electron flow (which is again from top to bottom in the micrographs). Comparing the images, the small void just above the reference line in Fig. 8(a) becomes part of the main void in Fig. 8(b), while the partly thinned lower part of the void in Fig. 8(a) becomes separated from the main body of the void by refilling of aluminium at A. As a result the void appears to migrate about 0.5 μm against the electron flow.

For imaging in Fig. 8(a) and 8(b) the current density was reduced to 0.5 j. After Fig. 8(b), when the current density was held at 0.5 j, it was found that the line structure continued to evolve. The changes in the following 15 min are shown in Fig. 8(c)–8(e). The effect is that the line is healed, apparently by aluminium migrating against the electron flow. When the current density was then increased to 0.8 j, damage recommenced but in a different form, as is shown in Fig. 8(f). In comparison with other observations, the evolution of line structure at 0.5 j was unusual. This observed large-scale healing was close to the centre of the transparent line segment, where higher temperature may contribute to the healing event, as discussed further in Section 4.3.

3.6. Open-circuit failure

Fig. 9 illustrates the development of a void to failure. Initial stressing for 30 min at 0.5 j again produced no detectable

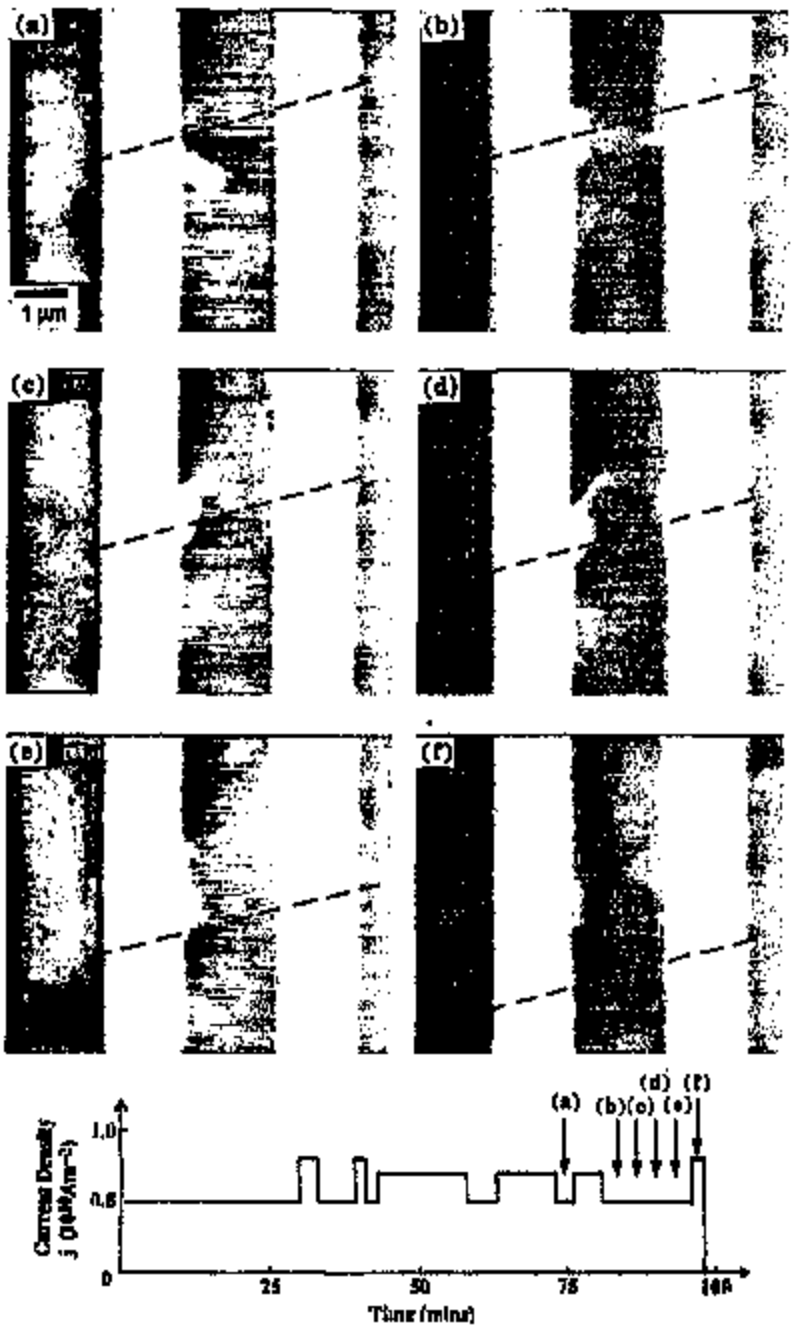

Fig. 8. Sequential TEM images (a)–(f) for a segment of line under in-situ electromigration testing, showing the growing and healing of a void. The timing and current density at which each micrograph was taken are presented in the diagram at the bottom of the figure. Electron flow: top to bottom.

damage. After 3 min at 0.8 j a void had developed as shown in Fig. 9(a), and at higher magnification in Fig. 9(b). Consistent with the observations in Fig. 7 (particularly Fig. 7(g)), it appears that sharp growth across the line occurs when the void meets an inclined plane acting as a barrier.

There is evidence that line failure can be strongly associated with slit-like voids, and that such slits are transgranular [3]. It was therefore of interest to assess whether the sharp void seen in Fig. 9(b), for example, was of this kind. In particular it is important to know whether the plane along which the void is developing has a particular crystallographic orientation within one grain, or whether it is a grain boundary. During a further 6 min at 0.5 j (in which there was no significant damage development), the test line in Fig. 9 was

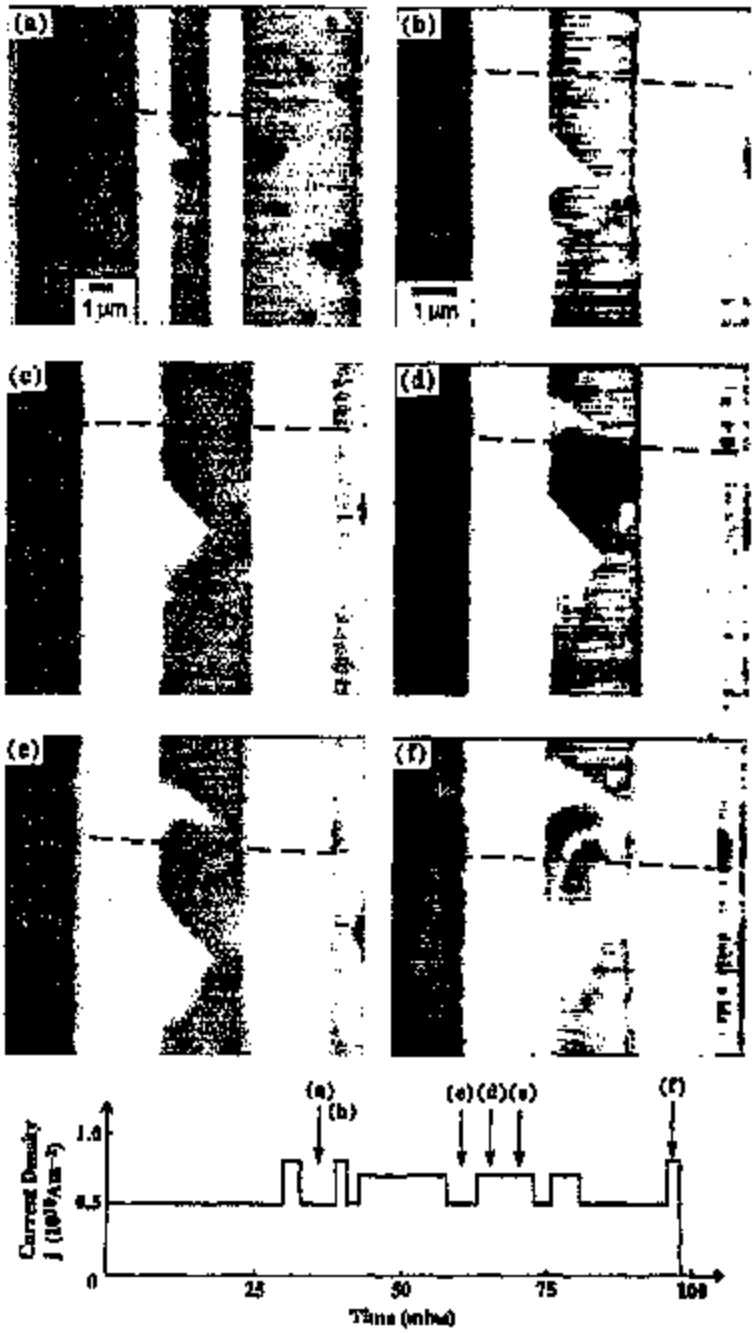

Fig. 9. Sequential TEM images (a)–(f) for a segment of line under in-situ electromigration testing, showing the development of voids to failure. The development suggests that for nucleated voids, the compressive stress built up at the downstream end of the grain boundaries can be relaxed by plastic flow towards large voids nearby and that there can then be failure. The timing and current density at which each micrograph was taken are presented in the diagram at the bottom of the figure. Electron flow: top to bottom.

tilted to a near diffracting condition, imaged and tilted back to the original orientation. As shown in Fig. 10, the plane in this case is confirmed to be a grain boundary across the line; the diffraction pattern in Fig. 10(b) for the grain above the boundary is clearly different from that in Fig. 10(c) for the grain below the boundary.

Resuming the main study of the line, stressing at 0.8 j for 2 min and 0.5 j for 2 min did not give any noticeable change in the void. After a further 15 min at 0.7 j (and return to 0.5 j) Fig. 9(c) was obtained; the void growth has broken through the boundary shown in Fig. 10 and started growing downstream along the left-hand edge of the line. In a further

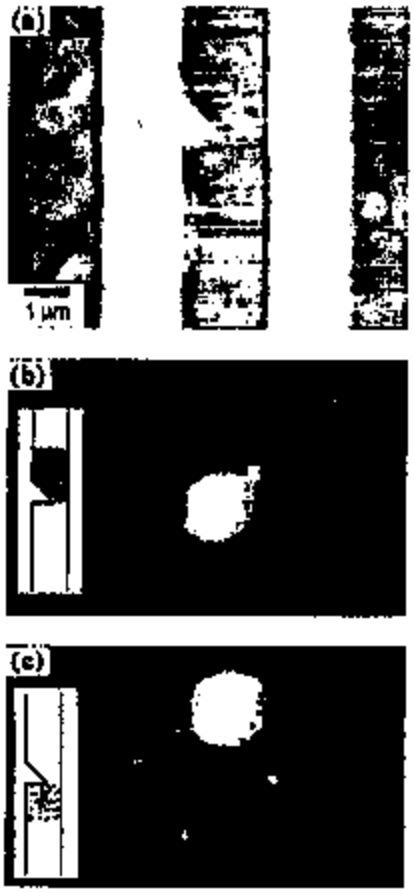

Fig. 10. TEM image for the line segment shown in Fig. 9(b) but in diffraction conditions, confirming that the planar feature is a grain boundary across the width of the test line. The diffraction patterns in (b) and (c) for the grains above and below the boundary demonstrate that they are two different grains.

10 min at 0.7 j, Fig. 9(d) and 9(e) were obtained. A second void develops upstream from the first and grows sharply across the line. The line was subjected to further stressing of 3 min at 0.5 j, 5 min at 0.7 j and 15 min at 0.5 j without much apparent change. The line finally failed in 2 min after increase of the current density to 0.8 j. The failure site is shown in Fig. 9(f).

After 15 min the failure site showed no significant change. However, TEM examination of the failed line four days later (Fig. 11) showed a much wider open-circuit gap. As the thermal expansion coefficient of aluminium is greater than that of silicon (or SiO_2), it can be expected that the differential contraction on cooling would put the aluminium lines into tension (even when relatively unsupported as in the electron transparent regions). Creep to relieve this tension could explain the widening gap. The diffraction patterns in Fig. 11(b) and 11(c), from above and below the failure site respectively, are consistent with different grains with no particular crystallographic orientation relationship. An examination was also made of the other damage sites on this line; four days of ageing at room temperature did not produce any change in their morphology.

4. Discussion

4.1. Relevance of in-situ testing

Given the distinctive temperature profile and distribution of damage in lines which are subjected to in-situ electromigration stressing, it is important to consider whether the mechanisms of damage and failure can be the same as in conventional accelerated testing or in service. For the lines in this study it is fortunately possible to make a direct comparison with the observations of microstructural change and damage development in conventional testing of the same lines (also unpassivated). The phenomena observed in the two cases appear to be the same. In particular, conventional testing also shows the migration of copper and Al–Cu precipitates in the direction of the electron flow [15], the occurrence of hillocks associated with precipitates [2,14], and the initiation of voids at line edges [15]. Electrical measurements in con-

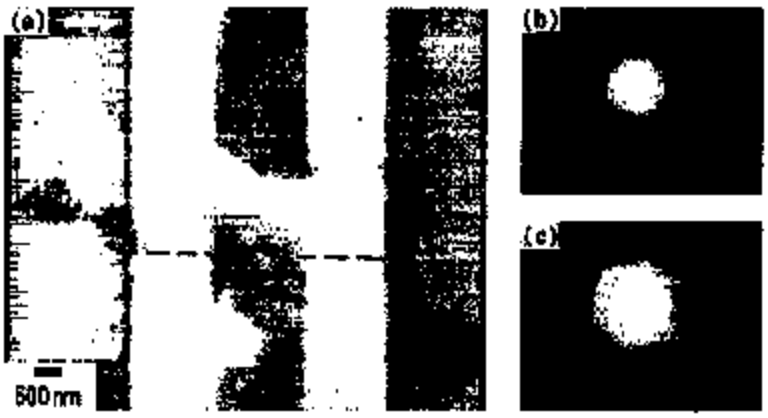

Fig. 11. TEM image of the failure site shown in Fig. 9(f) but taken 4 days after it failed, showing a wider open-circuit gap than in Fig. 9(f). The diffraction patterns in (b) and (c) for the Al line above and below the failure site respectively, do not show any particular relationship in crystallographic orientation.

ventional testing of the same lines show healing events such as could be associated with the changes seen in the in-situ testing [15]. Higher temperatures are likely to be encountered in the in-situ testing, and it has been suggested that at higher temperatures, transport paths other than grain boundaries could become relatively more important [13,25]. However, as the discussion in Section 4.2 will show, grain boundary transport remains of first importance in the development of damage in in-situ testing.

The electromigration phenomena observed here also appear qualitatively the same as those in passivated lines which can be observed through the passivation using high-voltage SEM [23,26,27]. In the passivated lines it is observed that: voids always initiate at the edge of the line; there are voids which do not move during testing; migrating voids do so in the direction opposite to the electron flow; the migrating voids can move across grain boundaries; early voids which grow little do not lead to failure; coalescence of electromigration voids happens in the later stages of the lifetime; final failure is dominated by fast growing and moving voids appearing late in the test; there is healing (refilling) of voids; healing at one place can sometimes be correlated with voiding nearby. Since all these are observed in the unpassivated lines in the present study and/or in earlier studies [2,6,15,28,29], we conclude that the native oxide on our lines can act as a weak passivation. Under applied passivation there will be a higher hydrostatic tensile stress component (e.g. an increase of 0.2% in interplanar spacings of (422) planes of Al–0.5% Cu metallization [30]), suppressing hillocking and promoting voiding, but the basic mechanisms controlling electromigration behaviour are unaltered.

Overall then, it seems that the phenomena observed in the present in-situ testing are similar to those in conventional accelerated lifetesting of the same lines. Undoubtedly the processes are greatly accelerated in in-situ testing, both by increased temperature and by increased atomic flux divergence arising from temperature gradients. In different regions of the lines tested in-situ, the divergences lead to void or hillock formation. Though these divergences are larger than may be usual in conventional testing, divergences of both kinds can still arise in conventional testing through microstructural variations. Since voids are the damage type mostly associated with failure, their formation and development will be considered most closely.

4.2. Void formation and growth

In the present work there is no evidence for the elongated voids apparently within grains reported by Vavra and Lobotka [11] in their near-bamboo lines. This may be because the line-width is less in the present work, because of the different preparation of the metallization (in Ref. [11] the lines were electrochemically thinned), or because of the lack of copper in the metallization in Ref. [11].

In previous work [15] it was observed that, in interrupted testing, voids which developed early did not grow. Since it is known that interruptions or reductions in stressing current can change the pattern of damage development, the behaviour of the early voids could be attributed to the interruptions. However, the present work shows (Fig. 6) that even in periods with a steady current the early voids do not grow. There has been discussion of the distinction between stress-induced and electromigration-induced voids, the former developing early and not growing much during current stressing [27]. In the present work the early voids presumably correspond to the "stress-induced" category. It is found that they appear during electromigration testing, but in the very early stages and at lower values of current than for the development of full electromigration damage. Thus it appears that they may indeed be associated mainly with mechanical stresses present in the lines before electromigration testing.

A classification of voids has recently been proposed [31,32], as shown in Fig. 12. Voids with a basic triangular shape in single crystals are classified as "critical" or "uncritical" on the basis of their orientation relative to the electron flow in the test line. For critical voids the migration along the inclined surface leads to sharp growth of the void across the line, while for uncritical voids the migration along the inclined surface leads to the growth along the edge of the line. It is found in the present work that even for a line with grain boundaries across its width, this classification of void behaviour is still generally valid. For voids with the critical shape, grain boundaries facilitate growth across the line; for voids with the uncritical shape, the electromigration flux along grain boundaries is somewhat balanced by the stress built up at the downstream end of the grain boundaries. This stress-driven back flux would prevent the void from growing further along the grain boundaries. Fig. 7(e)–7(g) show two linked voids associated with grain boundaries across the width of the line. The downstream void is uncritical in orientation, the upstream one critical, and their subsequent development matches the simple model. Also, in Fig. 8(a) and 8(b) the void is critical and does grow to cross the line. For uncritical voids, the compressive stress built up at the

Fig. 12. Schematic diagram of critical and uncritical void geometries as proposed by Arzt et al. [32]. The predominant atomic transport is along the internal free surface of the metallization as shown by the small arrows.

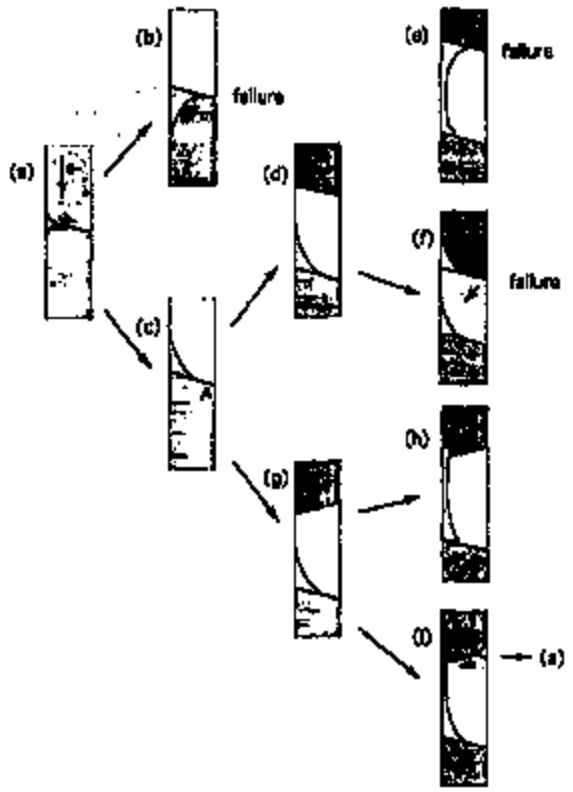

Fig. 13. A schematic model for electromigration-induced open-circuit failure in bamboo lines with inclined grain boundaries, showing possible alternative sequences of events. The shading indicates distinct grains. The unshaded areas are voids forming under the original oxide skin of the line. Damage is concentrated at boundaries which are inclined to the current. Precipitates are not considered in the model as copper depletion (and consequent precipitate dissolution) usually precedes damage.

downstream end of the grain boundaries could be relaxed by plastic flow towards large voids nearby, and there could then be failure. An example of this is shown in Fig. 9(d)–9(f) (no interruption of current), where two uncritical voids at the ends of inclined grain boundaries across the line combine to produce a open-circuit failure site along one of the grain boundaries.

From Figs. 7–9 it is striking that void initiation and development is strongly associated with the upstream end of inclined grain boundaries crossing the lines (shown schematically in Fig. 13(a)). This is exactly as would be expected if grain boundary transport is significant, as this (in the direction shown by the arrow in Fig. 13(a)) would transport atoms away from the void initiation site. The effect of such boundaries on mean time to failure has been studied in detail for controlled boundaries [33]. In a bamboo line, such as illustrated schematically in Fig. 13, the linked development of damage along the line requires atomic transport by paths other than just grain boundaries. Transport at the interface between the metallization and its oxide, or the underlying oxide, seems more likely than bulk diffusion. It appears from the rapid void growth which can occur upstream along line edges (e.g. in Fig. 7(d)–7(g)), that especially significant transport can occur on free surfaces, when these are created under the oxide skin by voiding.

4.3. Healing

In Figs. 7 and 9 there is evidence for successive void formation, later voids forming upstream of earlier ones. As the later voids grow, the material from them is transported downstream to give partial refilling of the earlier voids. In Section 4.4, a model for damage development and failure is developed from these observations. The void refilling can be regarded as a healing event. Subsequent void regrowth at the original site is initially prevented by the supply of atoms from growing upstream voids. Later, when the upstream voids are further away, damage may recur at the original site, but may be in a different form because of changed grain boundary configurations.

A less expected form of healing is shown in Fig. 8. The void refilling may be aided by atomic transport from upstream voids. However, the observation that it occurs at a lowered current density strongly suggests a significant contribution from stresses in the line. It is evident that electromigration can lead to the build-up of stresses through atomic flux divergence [34]. The stress gradients give mechanodiffusion fluxes which act in opposition to the electromigration fluxes. Such effects are responsible for the observation that electromigration damage and failure rates are proportional to the square of the current density used in testing [35]. Stresses can also give rise to plastic flow, such as is associated with hillocking. When the current density is reduced, as is the case before the sequence Fig. 8(c)–8(e), the electromigration force on the atoms is reduced but the stress gradient remains and can now dominate to drive the atoms against the electron flow. If there is local heating due to the reduced line cross-section, this may also act to promote healing by facilitating plastic flow (also in the direction against the electron flow) under the stress. When the current density is returned to a higher value, the damage may not resume in the same way as before, because the stress distribution is now different (partially relaxed) and the grain boundary configurations may have changed. If plastic flow has occurred, the material in the healed zone may also be work-hardened.

The healing event in Fig. 8 seems clearly to be promoted by the reduction in current density, and this effect can be understood. It seems from other observations in the present work that the pattern of damage development can often be altered after a brief reduction in current density, presumably because of small-scale healing processes. On the one hand, this suggests that the nature of the current density (constant, varied or intermittent) applied in a lifetest could have significant consequences. On the other hand, it raises the question of whether the present results are valid in interpreting non-stop conventional lifetests at constant applied current density, and whether the results from non-stop conventional lifetests at constant current density are valid in interpreting the device

performance in service (experiencing switching on and off). It should be noted, however, that even in the non-stop conventional test, the line microstructure and its evolution and the development of damage will lead to local fluctuations in both current density and temperature. These fluctuations could equally promote healing events.

Bernbaum [7] showed that the reversal of damage (in particular, refilling of voids) by reversal of current could not be obtained if the sample was oxidized (by exposure to air for several days) before the reversed current was applied. Oxidation effects are not believed to operate in the present work in which the lines were tested over short periods in the TEM vacuum and with the original oxide skin of the lines still in place.

4.4. A model for failure of bamboo lines

The observations in Figs. 7 and 9 suggest a pattern for void initiation, growth, and healing or failure. This pattern is the basis for a simple model proposed in Fig. 13 for the failure of bamboo and near-bamboo lines. The overall atomic transport down the line (i.e. in the direction of electron flow, from top to bottom in Fig. 13) will be deflected sideways at inclined grain boundaries, resulting in the void initiation at the upstream end of the boundary as shown in Fig. 13(a). Voids can develop into the critical shape (Fig. 13(b)), or the uncritical shape (Fig. 13(c)). In Fig. 13(b), the main growth direction of the critical void (across the line-width) coincides with the grain boundary and growth is thus facilitated leading to open-circuit failure. For uncritical voids (Fig. 13(c)) where the main growth direction would be along the line edge, the grain boundary transport will lead to a compressive stress build up at A (the downstream end of the inclined grain boundary). The resulting stress gradient along the grain boundary path will lead to a mechanodiffusion back-flux, eventually halting the grain boundary transport. The reduced line cross-section near A can lead to local heating which promotes plastic flow. This plastic flow is against the electromigration flux and thus provides some local healing. In this way, there are "restoring forces" to inhibit open circuit failure arising at a single boundary. The restoring forces can also be thought of in terms of a vacancy concentration gradient; the links between the stress and vacancy concentration descriptions are discussed in Ref. [35].

However, these uncritical voids can still lead to failure in two ways. An uncritical void can grow along the edge of the line until it reaches another grain boundary inclined similarly to the first (Fig. 13(d)); then rapid transport along the free surface between the two grain boundaries could give rapid void growth at the upstream boundary leading to failure, accompanied by some refilling (healing) of the original void (Fig. 13(e)). A direct example of this can be seen in Fig. 7(g). If the first void stabilizes and the second boundary which follows the pattern seen in Fig. 13(a) and 13(c) is nearby (Fig. 13(f)), the stress at the downstream end of the second boundary can be relieved by plastic flow in a direction (shown by the arrow) not otherwise available—into the original void. In this case the restoring forces inhibiting continued void growth along the boundary are greatly reduced, and catastrophic failure ensues. A direct example of this is shown in Fig. 9(f).

When an uncritical void growing along the line edge encounters an oppositely inclined boundary (i.e. the downstream end of an inclined grain boundary as is shown in Fig. 13(g)), it may cross the grain boundary (Fig. 13(h)), as seen in Fig. 7; it may also induce the growth of a void at the upstream end of the second grain boundary (Fig. 13(i)). The new void in Fig. 13(i), is similar to that Fig. 13(a) (giving a possible repetition of events), but the possible restoring forces inhibiting void growth along the boundary are greatly reduced.

According to this simple model, damage development and failure in bamboo lines are promoted by similarly inclined boundaries such as are shown in Fig. 13(d).

4.5. Post-mortem observations

The evolution of microstructure and the development of damage which occur during electromigration stressing can be examined either in-situ or by interrupted testing; in the latter, the specimen is periodically removed from stressing for examination, usually at room temperature. Each technique has its advantages and disadvantages. The present observations suggest some advantages of the in-situ technique. Firstly, it seems possible that the interruptions themselves would affect the progress of the test; both the change in current density, and the thermal mismatch stresses arising from the thermal cycling may affect the development of damage. Secondly, as the observations in Fig. 11 show, the mismatch stresses on cooling the sample for observation may change the line structure so that the observations do not accurately reflect the configuration at the test temperature.

5. Conclusions

It is demonstrated that lines patterned for conventional lifetesting can be prepared for in-situ stressing in TEM. The microstructural evolution and damage development in the in-situ testing show the same phenomena as in conventional testing of analogous lines. Despite the very different thermal conditions in the two types of test, the in-situ observations can be relevant for the analysis of failure in conventional lifetesting, or in service. The phenomena also appear to be the same as those observed in passivated lines, suggesting that the different stresses with and without passivation do not change the basic electromigration mechanisms.

The present work confirms a number of earlier observations. Copper migrates faster than aluminium and voiding in the lines occurs mainly in regions of copper depletion. The lines contain precipitates and these are often associated with hillocking. Dissolution of copper at the upstream side of the

precipitates and reprecipitation on the downstream side can lead to their effective downstream (i.e. in the same direction as the electron flow) migration. Conversely, voids migrate upstream.

Voids can develop early, before the depletion of copper. Such voids show very limited growth, and are unlikely to lead to failure.

The lines in this study have a near-bamboo microstructure. In this microstructure, void initiation is at the upstream end of inclined grain boundaries, indicating the importance of grain boundary transport. Rapid atomic transport on free surfaces leads to the upstream spreading of voiding. When boundaries are sufficiently far apart, this leads to a succession of voiding and healing events. When the boundaries are close, open-circuit failure can result, particularly for similarly inclined boundaries.

Healing (void refilling) is a natural process in lines under continuous test and leads to changes in the pattern of damage development. It can occur by surface transport of material from a growing upstream void or by the action of stresses. In the latter case it is promoted by reductions in current density or increases in temperature.

It is concluded that line reliability will be improved if the grain boundaries are more normal to the current flow, if they are further apart and if the copper content of the metallization is higher.

Acknowledgements

This work forms part of projects supported by the Engineering and Physical Sciences Research Council (formerly the SERC) and the Department of Trade and Industry. Interactions with partners and others associated with the project are gratefully acknowledged: GEC Plessey Semiconductors Ltd, who provided the samples for this work; BNR (Europe) Ltd; GEC Marconi Materials Research Ltd; and the Universities of Lancaster, Kent, Newcastle and York. Thanks are due to Dr P. Augustus for advice on specimen preparation.

References

[1] J. Cho and C.V. Thompson, *Appl. Phys. Lett., 54* (1989) 2577.
[2] A.L. Greer and W.C. Shih, *Mater. Res. Soc. Symp. Proc., 265* (1992) 83.
[3] J. Sanchez and E. Arzt, *Mater. Res. Soc. Symp. Proc., 265* (1992) 1311.
[4] I.A. Blech and E.S. Meieran, *Appl. Phys. Lett., 11* (1967) 263.
[5] R. Rosenberg and L. Berenbaum, *Appl. Phys. Lett., 12* (1968) 201.
[6] I.A. Blech and E.S. Meieran, *J. Appl. Phys., 40* (1969) 485.
[7] L. Berenbaum, *J. Appl. Phys., 42* (1971) 880.
[8] F.M. D'Heurle, *Metall. Trans., 2* (1971) 683.
[9] S.J. Horowitz and I.A. Blech, *Mater. Sci. Eng., 10* (1972) 169.
[10] I. Vavra, P. Lobotka, F. Zachar and J. Osvald, *Phys. Status Solidi (a), 63* (1981) 363.
[11] I. Vavra and P. Lobotka, *Phys. Status Solidi (a), 65* (1981) K107.
[12] W.C. Shih, T.C. Deaton and A.L. Greer, *Mater. Res. Soc. Symp. Proc., 265* (1992) 101.
[13] W.C. Shih, T.C. Deaton and A.L. Greer, to be published.
[14] W.C. Shih and A.L. Greer, *ESREF92 Proc.*, (1992) 347.
[15] W.C. Shih, A.L. Greer, Z. Xu and B.K. Ioans, *Mater. Res. Soc. Symp. Proc., 309* (1993) 369.
[16] W.C. Shih and A.L. Greer, *Mater. Res. Soc. Symp. Proc., 391* (1995) 391.
[17] W.C. Shih and A.L. Greer, *J. Electron. Mater., 23* (1994) 1315.
[18] B.K. Jones and Y.Z. Xu, *Microelectron. Reliab., 33* (1993) 1629.
[19] P. Lobotka and I. Vavra, *Phys. Status Solidi (a), 65* (1981) 655.
[20] C.Y. Chang and R.W. Vook, *J. Mater. Res., 4* (1989) 1172.
[21] *Landolt-Börnstein Tables*, New Series, Springer, Berlin, 1993.
[22] R.A. McKee and J.P. Stark, *Acta Metall., 23* (1975) 1145.
[23] P.R. Besser, M.C. Madden and P.A. Flinn, *J. Appl. Phys., 72* (1992) 3792.
[24] J.R. Black, *IEEE Trans. Elec. Dev., ED-16* (1969) 338.
[25] C.Y. Chang and R.W. Vook, *Mater. Res. Soc. Symp. Proc., 225* (1991) 125.
[26] M.C. Madden, E.V. Abramowski, T. Marieb and P.A. Flinn, *Mater. Res. Soc. Proc., 265* (1992) 33.
[27] T. Marieb, J.C. Bravman, P. Flinn, D.S. Gardner and M. Madden, *Appl. Phys. Lett., 64* (1994) 2424.
[28] R.W. Thomas and D.W. Caledwell, *21st Proc. of IEEE IRPS*, IEEE, New York, 1983, p. 1.
[29] B. Castello, I. Mahi, P. Flinn and M. Madden, *Appl. Phys. Lett., 59* (1991) 125.
[30] B. Greenebaum, A.J. Santer, P.A. Flinn and W.D. Nix, *Appl. Phys. Lett., 58* (1991) 1845.
[31] O. Kraft, S. Bader, J.E. Sanchez, Jr., and E. Arzt, *Mater. Res. Soc. Proc., 309* (1991) 199.
[32] E. Arzt, O. Kraft, W.D. Nix, and J.E. Sanchez, Jr., *J. Appl. Phys., 76* (1994) 1563.
[33] H.P. Longworth and C.V. Thompson, *Appl. Phys. Lett., 60* (1992) 2219.
[34] C.A. Ross and J.E. Evetts, *Scr. Metall., 21* (1987) 1077.
[35] M.A. Korhonen, P. Borgesen, K.N. Tu and C.Y. Li, *J. Appl. Phys., 73* (1993) 3790.

ELSEVIER

Thin Solid Films 343-344 (1999) 465-468

Thin Solid Films

The influence of cooling water flowing in the sputtering target on aluminum based thin film nanostructure deposited on glass substrates

Hiroshi Takatsuji[a,*], Satoshi Tsuji[a], K. Kuroda[b], H. Saka[b]

[a]Display Technologies IBM Japan, Ltd., Shimotsuruma, Yamato-shi, Kanagawa 242, Japan
[b]Department of Quantum Engineering, Nagoya University, Nagoya 464-01, Japan

Abstract

The influence of the cooling efficiency of the sputtering cathode on the nanostructure of an aluminum based (Al-based) thin film sputter-deposited on a large glass substrate (550 × 650 mm) was investigated. With high cooling efficiency, a highly (111)-textured pure-Al film was formed. On the other hand, low cooling efficiency contributes to the formation of a three-layer structure Al-Cu thin film that showed strong resistance to hillock and whisker generation. © 1999 Elsevier Science S.A. All rights reserved.

Keywords: Large glass substrate; Hillock; Whisker; Sputtering; Aluminum thin film

1. Introduction

Over the past several years, there has been strong pressure to achieve high productivity in the manufacturing process of thin-film-transistor (TFT) arrays [1,2]. One approach to meeting this requirement has been to use large glass substrates with a consequent reduction in the process time of each array. Accordingly, a high deposition rate is required in the sputtering process for the large glass substrates (550 × 650 mm). Cooling of the sputtering target material is a major concern in high power sputtering processes for TFT arrays, because of the problem of peeling between the target material and the backing plate. However, there has been few reports on the nanostructure of the sputtered film and target cooling. This paper investigates the relation between the nanostructure of Al-based alloy thin films deposited on glass substrate by means of a dc magnet-scan-type sputtering apparatus and the rate of which the cooling water flows in the sputtering target. We find that the flow rate of the cooling water in the sputtering target has a strong influence on nanostructure of the aluminum (Al) film. In the case of a pure-Al thin film, the degradation of the flow rate has an undesirable influence on the film's crystallographic texture. However, an Al-0.2 wt.% Cu alloy thin film deposited at a low cooling water flow rate contained a layered nanostructure that showed strong resistance to hillock and whisker generation. The nanostructure of the thin film was analyzed by atomic force microscopy (AFM), X-ray diffraction (XRD), and cross-sectional transmission electron microscopy (TEM), while the resistance to hillock and whisker generation was investigated by means of our nano-indentation techniques [3]. We demonstrated the mechanism of the layered thin film growth by these nanostructure analysis methods for sputter-deposited thin film and by thermal conductivity analysis for the cooling of the sputtering cathode.

2. Experiment

Fig. 1 shows a cross-sectional schematic diagram of a sputtering chamber for 550 × 650 mm glass substrate, which was used with a dc magnetron multi-chamber sputtering apparatus in this study. A bar magnet behind a target controlled the plasma density by moving the magnet. Cooling water flowed within a backing plate. To investigate the effect of the cooling water flow rate on the nanostructure of a sputter-deposited thin film, two flow rates (20 and 60 l/min) were used in this study.

Pure-aluminum and Al-0.2 wt.% Cu thin films were deposited on large LCD-grade glass substrates (550 × 650 mm) with pure-Al (5N purity) and Al-alloy (0.2 wt.% Cu content) targets. The films were deposited at a power of 44 kW with 10 two-way magnet scans, an argon pressure of 0.7 Pa, and a substrate temperature of 120°C.

The film's crystallographic textures were measured by θ–2θ XRD using Cu K_α radiation at 50 kV/150 mA, with a scan speed of 1°/min, and a scan range of 30–80°. Their

* Corresponding author. Tel.: +81-462-73-2427; fax: +81-462-73-4537.
E-mail address: takatsuj@jp.ibm.com (H. Takatsuji)

PII: S0040-6090(98)01677-0

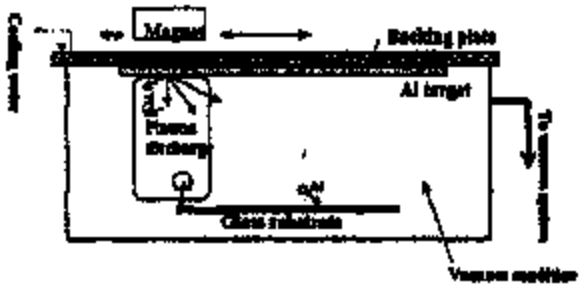

Fig. 1. Cross-sectional schematic diagram of the sputtering chamber.

nanostructures were observed by using an AFM and TEM operated at 400 kV. The resistance to stress migration was investigated by means of our nano-indentation techniques.

3. Results and discussion

3.1. Thermal conductivity analysis for cooling of the sputtering cathode

The cooling efficiency of the sputtering cathode C_ϕ was calculated from the equation

$$C_w = F \times 60 \times \Delta T_w / Q \quad (1)$$

where F is the cooling water flow, ΔT_w is the difference in temperature of the cooling water at input and output, and Q is the sputtering power.

C_w in both conditions was estimated at 33.3% (20 l/min.) and 47.6% (60 l/min.), respectively. It was found that the sputtering chamber heated up more at a low cooling water flow (20 l/min.) than at a high flow rate (60 l/min.) during sputtering. We consider that low cooling efficiency causes transformation of parts in the sputtering chamber and out-gassing from the chamber wall because of heat accumulation. We also confirmed by quadrupole mass spectrometer (Q-mass) analysis that out-gassing of nitrogen and oxygen elements arises toward the end of the sputtering time.

To investigate the effect of the cooling efficiency on the sputtering target, because no direct temperature measurement is possible during sputtering, we calculated the temperature of the target surface during sputtering T_t by using the following equation based on Fourier's law

$$T_t = \bar{T} + \frac{C_w Q}{A_w h} + \frac{C_w Q x_1}{A_w \lambda_{Cu}} + \frac{C_w Q x_2}{A_w \lambda_{Al}} \quad (2)$$

where $\bar{T}$ is the average temperature of the cooling water, C_w is the cooling efficiency of the sputtering cathode, Q is the sputtering power, x_1 is the distance between the bonding surface and the cooling water tube, x_2 is the thickness of the target, A_w is the surface area of the magnet, λ_{Cu} is the thermal transmittance coefficient of copper, λ_{Al} is the thermal transmittance coefficient of aluminum, and h is the thermal conductivity of cooling water given by Colburn's equation [4]

$$h = 0.023 \frac{\lambda}{D} (Re)^{0.8} (Pr)^{1/3} \quad (3)$$

where λ is the thermal transmittance coefficient, Re is the Reynolds number, Pr is the Prandtl number, and D is the diameter of the cooling water tube. The estimated temperature of the target surface was at 61.1°C at a flow rate of 20 l/min. And 43.1°C at a flow rate of 60 l/min. We conclude that the properties of the sputtering target do not change within this temperature range.

3.2. Effect on sputter-deposited thin films

The crystallographic texture of pure-Al films obtained at a low cooling water flow rate (20 l/min.) and a high flow rate (60 l/min.), were investigated, with the results shown in Table 1. The results indicate that deposition at a high flow rate (sample B) produced a highly (111)-textured film, whereas deposition at a low flow rate (sample A) produced a low (111)-textured (i.e., nearly random) film. In the case of a pure-Al thin film, we conclude that the degradation of the flow rate has an undesirable influence on the film's crystallographic texture. On the other hand, there was no significant difference between Al-0.2 wt.% Cu thin films sputter-deposited at a low cooling water flow rate (sample C) and a high flow rate (sample D), as shown in Table 1. However, there is a significant difference between sample C and sample D in the anti-stress migration property obtained by using nano-indentation techniques, as shown in Table 1. No whisker or hillock generation was observed in sample C. The AFM images in Fig. 2a,b show that the grain size of sample C is finer and more uniform than that of sample D. Cross-sectional TEM observation of samples C and D revealed a three-layer structure in the sample C, but no

Table 1
Sample configuration, film texture, and the results of nano-indentation techniques*

Sample ID	(111)	(200)	(220)	(311)	Number of hillocks	Number of whiskers
A	419 (63.4)	86 (13.1)	106 (16.2)	47 (7.2)	39	3
B	1764 (6.1)	125 (4.3)	92 (4.5)	52 (2.6)	27	2
C	723 (14.8)	164 (14.9)	161 (14.5)	62 (5.6)	0	0
D	666 (61.0)	116 (22.3)	244 (22.3)	66 (6.8)	15	0

* A: Pure-Al (20 l/min), B: Pure-Al (60 l/min), C: Al-0.2 wt.% Cu (20 l/min), D: Al-0.2 wt.% Cu (60 l/min). The unit of intensity is in counts per second (cps). Numbers in parenthesis denote the intensity fraction of each texture.

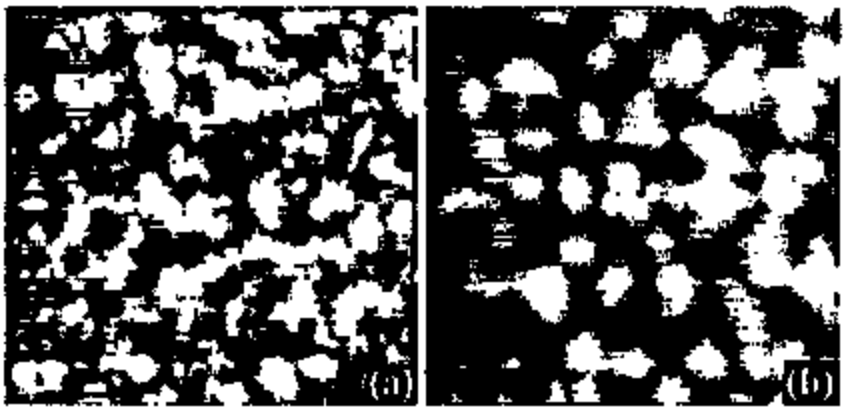

Fig. 2. Two-dimensional AFM images of Al-0.2 wt.% Cu films corresponding to the samples in Table 1: (a) Sample C (20 l/min.), (b) Sample D (60 l/min.). Scale: 2000 × 2000 nm.

significant structure was revealed in sample D, as shown in Fig. 3a,b. In the case of pure-Al, as in samples A and B, no three-layer structure of the Al-Cu thin film like that in sample C was observed. Sample C showed particularly unusual properties, since the structure of the top layer looked like an amorphous film and appeared to be dense, and the wet etching rate was one-eighth that of sample D. To investigate these characteristics of sample C, we performed depth profile electron spectroscopy for chemical analysis (ESCA), as shown in Fig. 4. The results indicated that aluminum oxide (Al-O) constitutes about 50% of the material in the top layer from the film surface to a depth of about 30 nm. They also indicate that the quantity of the aluminum element increases as the Al-O, oxygen, and nitrogen elements are decreased at around 32 nm. These data suggest that the top layers contain very large amounts of oxygen and nitrogen, while the middle layer contains none, and that the thickness of the top layer of sample C is about 30 nm. The

Fig. 3. Cross-sectional TEM micrographs of Al-0.2 wt.% Cu film corresponding to the samples in Fig. 2: (a) Sample C, (b) Sample D.

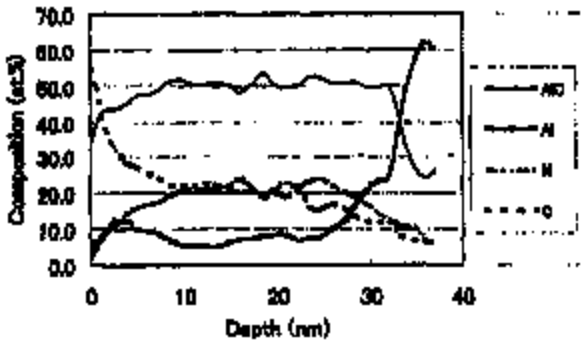

Fig. 4. Depth profile of ESCA spectra of the top amorphous layer of sample C.

thickness can also be estimated at about 30 nm from Fig. 3a. On the basis of TEM, ESCA, Q-mass, and thermal conductivity analysis for cooling of the sputtering cathode, we conclude that the oxygen and nitrogen in the top layer originate in the sputtering chamber wall and the top layer formed during the last magnet scan. We consider this to be the reason that the layered structure formed only with Al-Cu material, which reacts more readily with oxygen and nitrogen during sputter-deposition than pure-Al [5,6].

4. Conclusions

The cooling efficiency of the sputtering cathode influences the nanostructure of the sputter-deposited film. High cooling efficiency contributes to the formation of highly (111)-textured film in pure-Al, while low cooling efficiency causes out-gassing from the sputtering chamber wall during sputtering. However, a three-layer structure Al-Cu thin film that showed strong resistance to the formation of hillocks (including whiskers) when the cooling efficiency was low. We conclude that the mechanism for the formation of the three layer-structure of the Al-Cu thin film was as follows: the top amorphous layer was formed by reaction with the materials (i.e., nitrogen and oxygen) outgassed from the chamber wall, which had been heated up by sputtering energy, and the bottom layer was formed by reaction with small quantities of residual out-gassed materials (i.e. N_2 and O_2) in the sputtering chamber.

Acknowledgements

We wish to thank K. Tsujimoto of IBM Display Technology for TEM observation, M. Sakauchi of IBM Fujisawa plant for ESCA analysis, and M. McDonald of IBM Yamato for his comments on this article.

References

[1] W.E. Howard, J. SID 3/3 (1995) 127.
[2] W.C. O'Mara, Solid State Technol. (July) (1996) 76.
[3] H. Takasaji, S. Tsuji, H. Kitahara, K. Tsujimoto, K. Kuroda, H. Sakai, M.R.S. Symp. Proc. 441 (1997) 415.
[4] T.r. Colbert, AIChE 39 (1933) 174.
[5] W.W.Y. Lee, D. Oblas, J. Appl. Phys. 46 (1975) 1728.
[6] H.P. Wheers, E. Kay, J. Appl. Phys. 43 (1972) 794.

ELSEVIER

Sensors and Actuators A72 (1999) 153–159

A PHYSICAL

Novel prevention method of stiction using silicon anodization for SOI structure

Y. Matsumoto *, T. Shimada, M. Ishida

Department of Electrical and Electronic Engineering, Toyohashi University of Technology, Tempaku-cho, Toyohashi 441-8580, Japan

Received 25 June 1998; revised 27 August 1998; accepted 4 September 1998

Abstract

Silicon anodization process has been applied to prevent both 'after-rinse stiction' and 'in-use stiction' for the sensors with SOI structure. The anodization process roughened the silicon surface causing hillocks of a few tens of nanometer in height and a few hundreds of nanometer in diameter, resulting in increment of water contact angle above 100° as expected from a theory of fractal structure. Prevention effect for 'after-rinse stiction' was evaluated with silicon cantilever beam array fabricated by SOI structure. The maximum detachment length became three times longer than that of the beam on usual silicon surface. The roughening of silicon surface reduces the actual contact area, and hence, it is effective in preventing 'in-use stiction'. The anodization process was also performed using 73% HF solution without causing attack for aluminum metallization.

Keywords: Silicon anodization; Stiction; Fractal; Water contact angle; SOI; 73% HF

1. Introduction

Surface micromachining devices using SiO_2 sacrificial etching have advantages of integration with different type sensors, actuators and IC circuits with batch fabrication process [1]. Recently, micromachining sensors using SOI structure have been reported because the silicon structures above 10 μm thickness can be used with SDB-SOI structure [2–4]. The thick silicon structure results higher sensor capacitance, and the beams with single crystal silicon raises reliability because it does not have hysteresis and creep.

However, stiction is one of the most serious problem for the fabrication of surface micromachining devices and their long-term reliability [5]. The stiction is well known as 'after-rinse stiction' occurring in rinse/dry process after sacrificial wet etching process, and 'in-use stiction' caused by over-range shock or electrostatic force of static electricity etc. Many research groups made an effort to prevent stiction and carried out an analysis of the phenomenon [6]. For 'after-rinse stiction', techniques such as sublimation drying [7], supercritical carbon dioxide [8], photoresist-assisted release [9], SAM (Self-Assembled Mono layer) [10] and Vapor HF etching [11] have been reported, whereas for preventing 'in-use stiction', methods namely, using dimple [7], fluorocarbon film [12,17], SAM [10], roughening silicon surface [14] have been reported.

The present paper shows the systematic study made on the application of silicon anodization process to prevent both 'after-rinse stiction' and 'in-use stiction' for SOI sensors. The anodized process roughened the silicon surface so that its water contact angle was increased to 100° from a theory of fractal structure. The prevention effect for 'after-rinse stiction' was evaluated, and the method was applied to the fabrication process of sensors.

2. Prevention of stiction

2.1. Theory of stiction

The 'after-rinse stiction' occurred in rinse/dry process after the sacrificial SiO_2 wet etching process is shown in Fig. 1. The phenomenon is divided into two processes, namely attracting process and adhesion process.

The attracting process is caused by capillary force of rinse liquid. Surface energy of liquid on solid can be divided to three components as illustrated in Fig. 2, where α_{13}, α_{12} and α_{23} denotes the interfacial tensions of the

* Corresponding author

0924-4247/99/$ - see front matter
PII: S0924-4247(98)00229-3

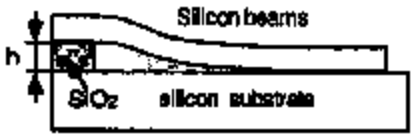

Fig. 1. Schematic diagram of stiction.

solid to liquid, the solid to air, and air to liquid interface, respectively [15].

The water contact angle θ is derived from Young's equation as:

$$\cos\theta = \frac{\alpha_{13} - \alpha_{12}}{\alpha_{23}} \quad (1)$$

The capillary force F_p is derived from the stiction theory [5,6].

$$F_p = \frac{2\alpha_{23}\cos\theta}{h} \quad (2)$$

where h is gap of silicon structure and substrate. Eq. (2) implies that the capillary force becomes zero at $\theta = 90°$ and turns out to be negative for $\theta > 90°$. Therefore, the attracting process does not occur on hydrophobic surface. In other words, if solid to air interfacial tension α_{13} is smaller than solid to liquid interfacial tension α_{12}, the structure is not attracted to the substrate.

The adhesion process is considered as the following process [5]. At first, hydrogen terminals are formed on silicon surface after HF etching process. However, these terminals are broken during rinse process by de-ionized water or upon exposure to atmospheric air. Then, hydroxyl groups are adhered by Van der Waals forces on silicon surface. If the structure get contacted to substrate by capillary force or over-range shock, etc., the structure get stuck to substrate by hydrogen bonding. The strength of hydrogen bonding is 2–5 kg/cm^2 at room temperature, which is enough to make permanent adhesion to substrate.

2.2. Roughening surface and its water contact angle

As mentioned above, the capillary force becomes zero at $\theta = 90°$, and for values of θ greater than 90°, it turns out to be negative for values of θ greater than 90° in accordance with Eq. (2). Although complete hydrogen terminated silicon surface is thought to be hydrophobic with a contact angle of around 90° [5], silicon surface after rinse and exposure to atmospheric air is slightly hydrophillic with water contact angle of around 60° because of the attachment of hydroxyl groups. Hence, formation of hydrophobic surface such as SAM or fluorocarbon film is one of the effective methods to prevent stiction although these methods require additional fabrication process or specific equipment.

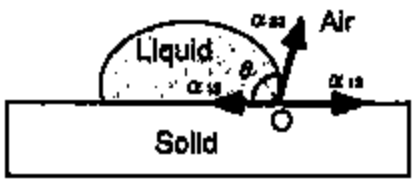

Fig. 2. Diagram of contact angle of liquid on solid.

Fig. 3. Illustration of water contact angle for mirror surface and roughening surface. (a) For mirror surface, (b) for roughening surface.

The water contact angle also can be increased with roughening surface from the theory of fractal structure (roughening surface) as illustrated in Fig. 3 [16]. The water contact angle on roughening surface is given by the following equation [15,17]:

$$\cos\theta_r = r\cos\theta \quad (3)$$

where θ_r is the water contact angle on roughening surface and r is a coefficient giving the ratio of the actual area of a roughening surface to the projected area. Usually, the coefficient r is very large on roughening surface, so that hydrophobic surface becomes ultrahydrophobic (super-water repellent) on roughening surface [16]. Therefore, if contact angle of roughening silicon surface after rinse/dry process becomes greater than 90°, the capillary force becomes negligible. This situation will be effective to prevent 'after-rinse stiction'.

2.3. Silicon anodization and its water contact angle

There are many methods to roughen silicon surface such as etch-back [11], making dimple [4] or chemical etching by NH_4F [2], etc. In the present study, silicon anodization process has been applied to roughen the silicon surface, because the process is simple and can be carried out in HF solution as shown in Fig. 4. HF solution is used in SiO_2 sacrificial etching process, and the HF solution enters under SOI structure during the etching process, therefore, silicon anodization process can be continuously performed after sacrificial etching. The method

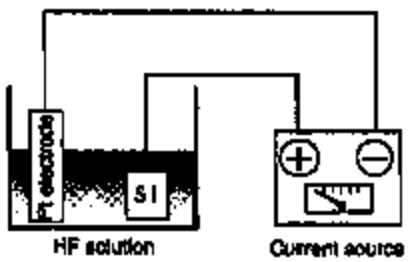

Fig. 4. Principle of silicon anodization.

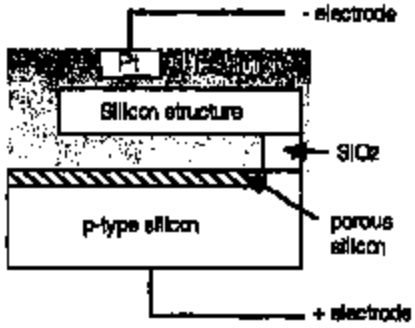

Fig. 5. Electrode contact to SOI structure for anodization process.

is also considered to be effective especially for high trench SOI sensors because entire liquid substitution in chemical treatment is usually difficult for the high aspect ratio SOI structures [19].

It is important to note that an electrode is connected to silicon p-type substrate as illustrated in Fig. 5. Therefore, current does not flow to silicon structure since it is isolated by SiO_2 layer. As a result, the silicon structure is not getting anodized during the process of anodization.

The anodization process is dependent on the doping level of silicon wafer, concentration of HF solution and current density, etc. [20]. In our case, the p-type ($10^{19}/cm^3$) silicon was anodized in 16% HF ($HF:H_2O = 1:5$) solution with a current density 20 mA/cm^2 for 60 min. Fig. 6 shows the SEM photograph of the anodized silicon surface. Small holes of size around a few tens of nanometer to a few hundreds of nanometer were formed on silicon surface. The surface profile was evaluated using AFM measurement. Fig. 7 shows the profile of anodized silicon surface. Many holes (hillocks) in the range of around a few hundreds of nanometer in diameter and a few tens of nanometer in height were formed on silicon surface.

The hydrophobicity of anodized silicon surface was evaluated with contact angle of water droplet. The variation of the measured water contact angle in the relation of anodization time is shown in Fig. 8. As can been seen, the water contact angle increased with anodization time, and about 100° was attained over a 30-min duration. Fig. 9 shows the photograph of the water contact angle on silicon surface as well as on anodized silicon surface, where in the water contact angle of about 100° was clearly observed. The observed value satisfies the condition at which the capillary force can be negligible.

Fig. 6. SEM photograph of anodized silicon surface.

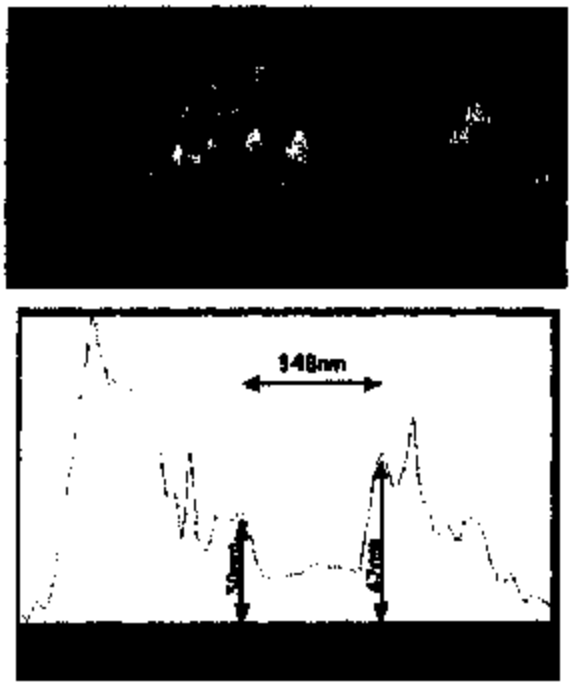

Fig. 7. Surface profile of anodized silicon surface by AFM measurement.

2.4. Evaluation with cantilever beams

The effect of anti-stiction was evaluated using cantilever beam array fabricated by SOI structure. Figs. 10 and 11 show the structure and SEM photograph of silicon

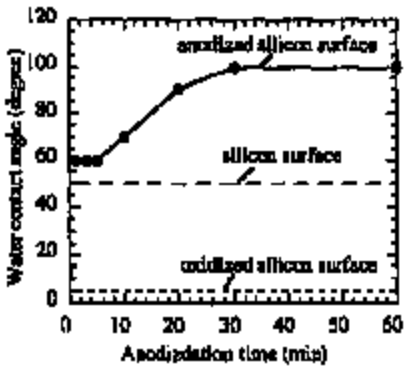

Fig. 8. Relation between water contact angle and anodization time.

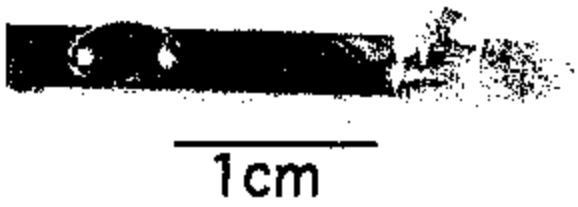

Fig. 9. Photograph of water contact angle on silicon surface (left) and on anodized silicon surface (right).

cantilever beams. The thickness of top silicon layer was 6 μm, and thickness of SiO_2 intermediate layer was 1 μm. The width of beams was 20 μm, and length was in range of 100 μm to 2000 μm. The substrate was high doped p-type ($10^{19}/cm^3$) silicon and beams was low doped p-type ($10^{15}/cm^3$) silicon. First, the silicon dioxide was sacrificial etched in 16% HF solution. Then, the sample was anodized with current density 20 mA/cm^2 in the same 16% HF solution. Further, the sample was rinsed in DI water, and dried in atmospheric air. The sticking probability was measured by SEM as shown in Fig. 12, or laser displacement measurement equipment. Fig. 13 shows the typical example of laser displacement measurement. The displacement between the substrate and beam's surface was measured by the equipment, so that gap between silicon beams and substrate can be calculated by subtracting the silicon thickness from the measured displacement.

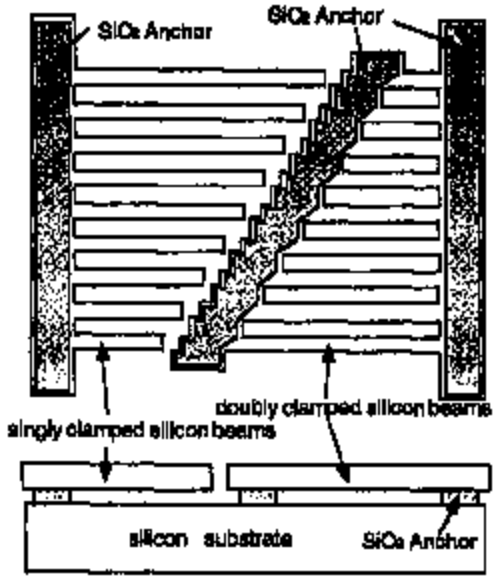

Fig. 10. Structure of SOI singly clamped cantilever beams and doubly clamped cantilever beams.

Fig. 11. SEM photograph of SOI cantilever beams.

Fig. 14 shows the relation between gap and beam's length for doubly clamped cantilever beams. From the results, it is evident that the maximum detachment length increases on anodized silicon surface.

The maximum detachment length of beams is calculated by the equations derived by Mastrangelo [6] as follows:

For singly clamped cantilever beams:

$$N_p = \frac{3}{8}\frac{Eh^2t^3}{\gamma_s L^4} \tag{4}$$

where N_p is peeling number, E is the Young modules of silicon, h is gap between beams and substrate, t and L are thickness and length of beams, and γ_s is adhesion energy of silicon surface.

For doubly clamped cantilever beams:

$$N_p = \frac{128}{5}\frac{Eh^2t^3}{\gamma_s L^4}\left[1 + \frac{4\sigma_R L^2}{21t^3} + \frac{256}{2205}\left(\frac{h}{t}\right)^2\right] \tag{5}$$

where σ_R is the strain of beams.

By substituting $N_p = 1$ in above the equation, maximum detachment length is calculated. The theoretical maximum detachment length on the usual silicon surface and measured maximum detachment length on anodized surface are summarized in Table 1. The maximum detachment length for each cantilever beams was increased with anodized time. For singly clamped beams, it increases 2 times compared to the beams on normal silicon surface with 30 min anodization treatment, and increases 3 times with 60 min anodization treatment.

From Fig. 8, the water contact angle of silicon wafer was maintained at the same value of 100° over 30 min, but

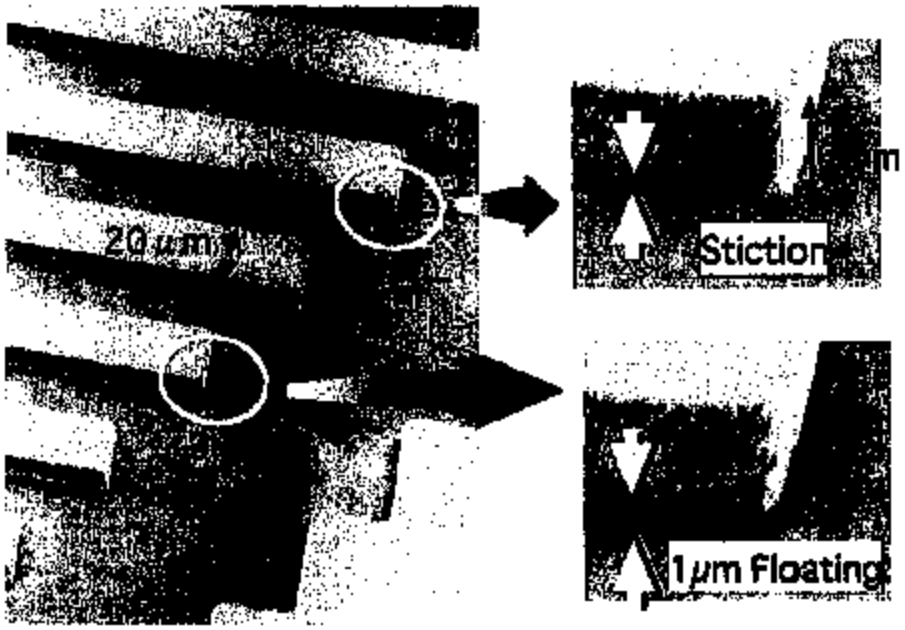

Fig. 12. Evaluation of stiction for SOI cantilever beams using SEM measurement method.

maximum detachment length of cantilever beams was increased with time over 30 min. Its difference was explained that the anodization speed was probably slow under cantilever beams structure because the substitution of HF solution was slow in the narrow gap between beams and substrate. However, it is evident that the maximum detachment length for each cantilever beams increases to about 3 times compared to the beams on normal silicon surface. From Eqs. (4) and (5), adhesion energy γ_s was calculated and found to be about a factor of 2 smaller than on normal silicon surface.

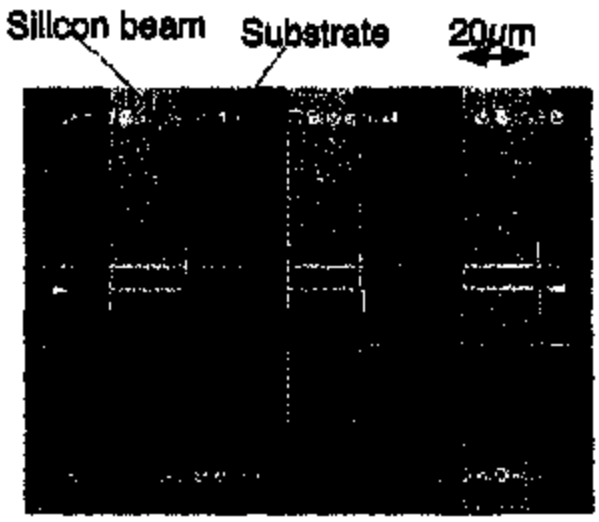

Fig. 13. Photograph of SOI cantilever beams under Laser displacement measurement equipment.

2.5. Long-term stability and thermal stability

The long-term stability of anodized silicon surface was evaluated. The anodized sample was exposed to atmosphere at room temperature for 3 months, and its water contact angle was evaluated. It was found that the water contact angle decreased from 100° to 90°. The slight decrease was probably caused by incomplete thin natural silicon di-oxide formation on anodized silicon surface.

The thermal stability of anodized silicon surface was also evaluated. The sample was placed on hot plate maintained at 300°C in atmosphere for 30 min duration, and its water contact angle was evaluated. The water contact angle decreased from 100° to 5° because of the formation of thick silicon di-oxide on anodized silicon surface. However, after dipping the sample in HF solution in a few

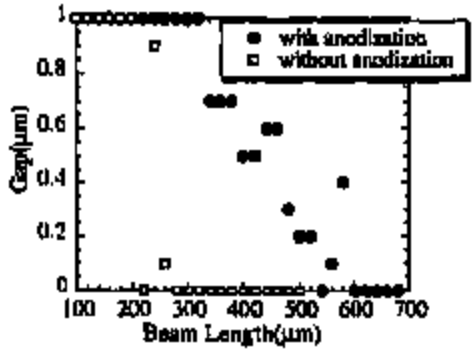

Fig. 14. Relation between gap and beam's length after rinse and drying process for doubly clamped cantilever beams.

Table 1
Maximum detachment length for the different treatments

Maximum detachment length	For singly clamped cantilever beams	For doubly clamped cantilever beams
Theoretical length	94 μm	270 μm
Normal surface	less than 100 μm	less than 200 μm
Anodized (30 min)	180 μm	260 μm
Anodized (60 min)	380 μm	480 μm

seconds, the water contact angle was recovered to 100° because silicon dioxide was removed by HF solution and anodized fractal structure was not broken at 300°C. Further, the sample was annealed in ambient of nitrogen gas at 450° for 30 min duration. The annealing process results in the decrease of water contact angle to 5° due to formation of silicon di-oxide on anodized silicon surface with the remained oxygen gas or water in the anodized structure. However, the water contact angle also recovered to 100° with a dipping in HF solution. It indicates that the anodized fractal structure was not broken at high temperature 450°C. It is in contrast with SAM or fluorocarbon film which were broken at high temperature of over 300° [5,13].

3. Application for sensor

3.1. Compatibility of anodization process with 73% HF solution

Recently, sacrificial etching methods without causing attack to aluminum metallization using 73% HF was reported by Gennissen and French [18]. If the anodized process can be performed with 73% HF without causing attack to aluminum, it is useful in view of the process compatibility for IC factory. Therefore, silicon anodization process with 73% HF (FLUKA Product #47610) was examined.

As mentioned before, the anodization process has to be carried out after SiO_2 sacrificial etching process of over 30 min. However, the etching rate of silicon di-oxide in conc. 73% HF solution was too fast (1.5 μm/min), it causes the attack to 'anchor' structure in SOI sensors. Therefore, 73% HF solution was diluted with IPA to 16% in order to reduce etching rate of silicon dioxide in which aluminum was not attacked [18]. The anodized process was performed for p-type (10^{19}/cm^3) silicon with current density 20 mA/cm^2 for 60 min duration. As the results, holes with sizes of around a few tens of nanometer were observed, and also, an increase in the water contact angle was noticed.

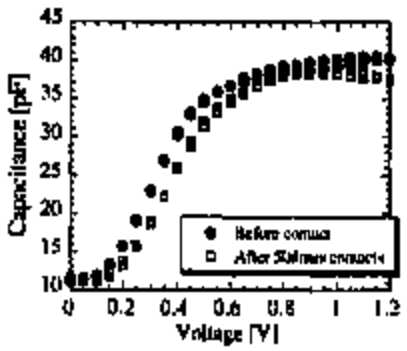

Fig. 15. C–V characteristics of SOI accelerometer using anodization method.

3.2. Sensor fabrication and durability for in-use stiction

The capacitive SOI accelerometers using SOI structure have been fabricated by adopting anodization process to prevent stiction. The thickness of top single-crystal silicon is 6 μm with a sacrificial silicon di-oxide layer of 1 μm. The substrate was p-type (10^{19}/cm^3), and aluminum was used for metallization [21]. After removing silicon dioxide in 73% HF solution, the sample was anodized with current density 20 mA/cm^2 in the same 73% HF solution. It was possible to prevent 'after-rinse stiction', and yield of sensor can be increased using anodization method.

The anodized methods is considered to be effective in preventing 'in-use stiction' because the contact area is drastically decreased on roughened surface. Therefore, durability for in-use stiction was evaluated. Fig. 15 shows the relation between sensor capacitance of anodized sample and DC bias voltage applied to sensor. It was observed that the sensor capacitance was square proportional to bias voltage because of electro static force. The capacitance was saturated above 0.6 V because sensor structure come in contact with the substrate. The bias voltage of 5 V which was equivalent about 800 G was applied to sensor 50 times. After that, the initial capacitance was measured and found to be as of the same value. Further, it was changed by DC bias voltage almost in the same relation before contact test as shown in Fig. 15. The above observation conforms that the sensor structure was not stuck to substrate because of the decrement of contact area.

4. Conclusion

Silicon anodization process has been successfully applied to prevent both of 'after-rinse stiction' and 'in-use

stiction' for SOI structure. The anodization process roughen silicon surface around a few tens of nanometer in height, so that water contact angle was increased over 100° after rinse process from fractal theory. The anodized process was also performed using 73% HF solution and IPA without causing attack to aluminum metallization. Prevention effect for 'after-rinse stiction' was evaluated with silicon cantilever beam array fabricated by SOI structure. The maximum detachment length becomes 3 times longer than that of on normal silicon surface. The reduction of actual contact area on roughening silicon surface made it effective in preventing 'in-use stiction'. Although it is difficult to prevent the formation of silicon di-oxide at high temperature, the anodized fractal structure was not broken at high temperature 450°C in ambient of nitrogen gas. The water contact angle was easily recovered to 100° with a few seconds dipping in HF solution.

Acknowledgements

This work has been partly supported by Japanese Ministry of Education, Science, Sports and Culture under a Grant-in-Aid for Encouragement of Young Scientists No. 10750065, and also partly supported by the Micromachine Technology Research Grant of Micromachine Center, Japan.

References

[1] R.T. Howe, B.E. Boser, A.P. Pisano, Polysilicon integrated microsystems: technologies and applications, Sensors and Actuators A 56 (1996) 167–177.

[2] V.M. Mensil, M.J. Novack, M.A. Schmidt, Design and Fabrication of Thin-film Microaccelerometers using Wafer Bonding, Proc. 7th Int. Conf. Solid State Sensors and Actuators (Transducers'93), 1993, pp. 822–825.

[3] Y. Matsumoto, M. Iwakiri, H. Tanaka, M. Ishida, T. Nakamura, A capacitive accelerometer using SDB-SOI structure, Sensors and Actuators A 51 (1996) 267–272.

[4] T.J. Brosnihan, J.M. Bustillo, A.P. Pisano, R.T. How, Embedded Interconnect and Electrical Isolation for High-aspect-ratio, SOI Inertial Instruments, Proc. 1997 Int. Conf. Solid State Sensors and Actuators (Transducers'97), 1997, pp. 637–640.

[5] R. Maboudian, R.T. Howe, Critical review: adhesion in surface micromechanical structures, J. Vac. Sci. Technol. B 15 (1) (1997) 1–20.

[6] C.H. Mastrangelo, Mechanical stability and adhesion of micro structure under capillary forces: Part 1, Basic theory, Journal of Microelectromechanical Systems 2 (1) (1993) 33–43.

[7] C.-J. Kim, J.Y. Kim, B. Sridharan, Comparative evaluation of drying techniques for surface micromachining, Sensors and Actuators A 64 (1998) 17–26.

[8] G.T. Mulhern, D.S. Soane, R.T. Howe, Supercritical Carbon Dioxide Drying of Microstructures, The 7th Int. Conf. Solid-State Sensors and Actuators, 1993, pp. 296–299.

[9] D. Kobayashi, C.-J. Kim, H. Fujita, Photoresist-assisted release of movable microstructures, Jpn. J. Appl. Phys. 32 (1993) 1642–1644.

[10] M.R. Houston, R. Maboudian, R.T. Howe, Self-assembled Monolayer Films as Durable Anti-stiction Coating for Polysilicon Microstructures, Solid-State Sensor and Actuator Workshop Hilton Head, SC, June 2–6, 1996, pp. 42–47.

[11] J.H. Lee, W.I. Jang, C.S. Lee, Y.I. Lee, C.A. Choi, J.T. Baek, H.J. Yoo, Characterization of anhydrous HF gas-phase etching with CH_3OH for sacrificial oxide removal, Sensors and Actuators A 64 (1998) 27–32.

[12] P.F. Man, B.P. Gogoi, C.H. Mastrangelo, Elimination of Post-release Adhesion in Microstructures Using Thin Conformal Fluorocarbon Films, Proc. IEEE Workshop on MEMS'96, 1996, pp. 55–60.

[13] Y. Matsumoto, K. Yoshida, M. Ishida, Fluorocarbon Film for Protection from Alkaline Etchant and Elimination of In-use Stiction, Proc. 1997 Int. Conf. Solid State Sensors and Actuators (Transducers'97), 1997, pp. 695–698.

[14] R.L. Alley, P. Mai, K. Komvopoulos, R.T. How, Surface Roughness Modification of Interfacial Contacts in Polysilicon Microstructure, Proc. 7th Int. Conf. Solid State Sensors and Actuators (Transducers'93), 1993, pp. 288–291.

[15] T. Onda et al., Super-water repellent fractal surfaces, Langmuir 12 (1996) 2115.

[16] B.D. Hazlett, Fractal applications: wettability and contact angle, J. Colloid Interface Sci. 137 (1990) 527.

[17] A.W. Adamson, Physical Chemistry of Surfaces, 5th edn., Chap. X, Section 4, Wiley, New York, 1990.

[18] P.T.J. Gennissen, P.J. French, Sacrificial Oxide Etching Compatible with Aluminum Metallization, Proc. 1997 Int. Conf. Solid State Sensors and Actuators (Transducers'97), 1997, pp. 225–228.

[19] M. Nishimura, Y. Matsumoto, M. Ishida, The method to prevent stiction in a capacitive accelerometer using SDB-SOI structure, Tech. Dig. of the 15th Sensor Symposium, 1997, pp. 205–208.

[20] Z.C. Feng, R. Tsu, Porous Silicon, Chap. 15, World Scientific, 1994.

[21] Y. Matsumoto, M. Nishimura, M. Matsuura, M. Ishida, Three-axis capacitive accelerometer using SDB-SOI structure, Tech. Dig. of the 16th Sensor Symposium, 1998, pp. 29–32.

Yoshinori Matsumoto was born in Shizuoka, Japan, in 1965. He received his BE and PhD degree in electronic engineering from Tohoku University, Sendai, Japan in 1988 and 1993, respectively. He worked on integrated capacitive pressure sensors and accelerometers. Since 1993 he has been a research associate at the Department of Electric and Electronic Engineering of Toyohashi University of Technology. His current research interest are sensors with SOI technology and smart sensors.

Taiji Shimada was born in Aichi, Japan, in 1975. He received his BE degree in Electronic Engineering from Toyohashi University of Technology, Toyohashi, Japan, in 1998. He is currently working towards an ME degree in Electronic Engineering at the same university.

Makoto Ishida was born in Hyogo, Japan, in 1950. He received his PhD degree in Electronics Engineering from Kyoto University, Kyoto, Japan, in 1979. Since 1979 he has been at Toyohashi University of Technology, and he is a professor of Electrical and Electronic Engineering. He is working on heteroepitaxial growth and processes of SOI material including SiGe, and their device applications including sensor and IC in electron device research center in Toyohashi University of Technology.

ELSEVIER

Surface and Coatings Technology 125 (2000) 167–172

www.elsevier.nl/locate/surfcoat

Pure Al thin film protective layer to prevent stress migration in Al wiring for thin-film transistors

H. Takatsuji [a,*], K. Haruta [b], S. Tsuji [a], K. Kuroda [b], H. Saka [b]

[a] *Display Technology, IBM Japan, Ltd., Shimotsuruma, Yamato-shi, Kanagawa 242, Japan*
[b] *Department of Quantum Engineering, Nagoya University, Nagoya 464-01, Japan*

Accepted 28 June 1999

Abstract

The anti-stress migration property of layered structure aluminum (Al) thin films overcoated with pure Al was investigated for application of such films as interconnect materials in large arrays of high-resolution thin-film transistor liquid crystal displays (TFT-LCDs). It was found that no hillock or whisker generation occurred in a pure Al thin film with a sputter-deposited fine-grained polycrystalline pure Al layer after exposure to mechanical and 300°C thermal stresses. Atomic force microscopy (AFM) and cross-sectional transmission electron microscopy (TEM) analyses revealed the morphology of the layered structure thin film and the mechanism for the prevention of stress migration in the film. © 2000 Elsevier Science S.A. All rights reserved.

Keywords: Nanoindentation techniques; Overcoated pure aluminum thin film; Sputtering; Stress migration; Thin-film transistor liquid crystal displays

1. Introduction

The performance of thin-film transistor liquid crystal displays (TFT-LCDs) has improved over the past several years with a change in standard display size from 10.4 to 12.1 or 13.3 inches, and the resolution has also improved with the transition from VGA to SVGA, XGA, and SXGA. Consequently, pure aluminum (Al) and Al alloys have attracted much attention for their potential use as interconnect materials in high-performance TFT-LCD arrays formed on glass substrates, because of their low resistivity and good patterning ability [1]. However, stress migration due to the thermal expansion mismatch between Al films and the glass substrate, which leads to phenomena such as the growth of hillocks (including whiskers), is a major concern, because it affects the yield loss during TFT device fabrication. There are several ways to protect against stress migration, of which one using Al alloys with rare earth or transition metals has been the subject of many reports [2–5]. However, two shortcomings of such alloys for TFT-LCD applications are their higher electrical resistivity and the higher cost of the sputtering target than in the case of pure Al. Other methods coat clad or capped thin-film layers with transition metals (Ti, Mo, etc.) on Al interconnects, or form anodized Al_2O_3 layers on Al interconnects [6,7]. The shortcoming of these techniques is that they need an additional photolithographic or special anodizing process step, which increases the manufacturing cost. Accordingly, to reduce the thermal expansion stress, we focus on Al interconnects with a layered structure using only pure Al.

In this work, we demonstrate the anti-stress migration property of overcoated pure Al thin film (thickness = 40–200 nm) sputter-deposited on several kinds of pure Al thin film (thickness = 350 nm) and Al–indium (Al–In) thin film (thickness = 270 nm) with a weak anti-stress migration property, formed on LCD grade large glass substrates [8]. We investigated the anti-stress migration property of these thin films by means of our nanoindentation techniques [9]. As a result, we found that the overcoated layer is effective in preventing stress migration in layered Al thin films. We also investigated the nanostructure of the layered pure Al thin film by means of atomic force microscopy (AFM) and cross-sectional transmission electron microscopy (TEM).

2. Experiment

Two kinds of pure Al thin film [(a) and (b), thickness = 350 nm] were deposited on an LCD grade glass

* Corresponding author. Tel.: +81-462-73-3427; fax: +81-462-77-0382.
E-mail address: takatsuj@jp.ibm.com (H. Takatsuji)

PII: S0257-8972(99)00599-X

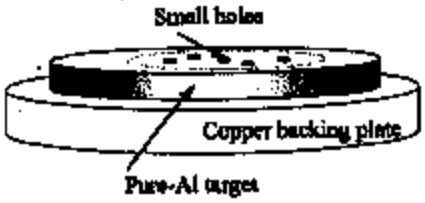

Fig. 1. Schematic diagram of a modified sputtering target for deposition of Al–In thin film.

Table 1
Sample configurations and crystallographic texture[a]

Sample ID	(111)	(200)	(220)	(311)
Pure Al (a)	3122	119	51	22
Pure Al (b)	356	138	96	96
Pure Al (c)	513	252	396	129

[a] The unit of intensity is counts per second (cps).

substrate ($300 \times 400\ mm^2$) using two types of single substrate transfer cluster type d.c. magnetron sputtering apparatus [(a) using multi-magnet type and (b) using a single bar magnet scan type] at a rate of 400 nm/min, with an argon pressure of 0.4 Pa and a substrate temperature of 120°C. Pure Al (c) and Al–In thin films (thickness = 270 nm) were deposited on LCD grade glass substrate ($125 \times 125\ mm^2$) by means of a d.c. magnetron sputtering apparatus at a rate of 36 nm/min, with an argon pressure of 0.4 Pa and a substrate temperature of 120°C. To deposit Al–In thin film, we modified the pure Al target to make indium ooze from the bonding material, as shown in Fig. 1. [Bonding material (In solder) oozed through the small hole in the target.] The indium content was measured using a CAMECA time-of-flight secondary ion mass spectrometry (TOF-SIMS) model 4 at analysis energies of 25 keV with a Ga gun, and at sputter energies of 3 keV with an Ar gun. We confirmed that the Al–In thin film contains 0.19 wt.% indium.

After deposition of the above-mentioned Al-based thin films, the substrates were exposed to the atmosphere, and a pure Al layer (with a thickness of 40 nm or 200 nm) was deposited by means of an RF sputtering apparatus at a rate of 40 nm/min, with an argon pressure of 0.6 Pa and a substrate temperature of 100°C, on Al-based thin films deposited by means of a d.c. magnetron sputtering apparatus. The resistance to stress migration was investigated by means of our nanoindentation techniques for various stress temperatures (200°C, 250°C, and 300°C). The films' crystallographic texture was measured with θ–2θ XRD using Cu Kα radiation at 50 kV/150 mA, with a scanning speed of 1°/min and a scanning range of 30–80°. Nanostructures were observed by means of AFM and cross-sectional TEM operated at 200 kV.

3. Results and discussion

3.1. Properties of Al–In and pure Al thin films deposited on glass substrate

The crystallographic textures of pure Al (a), pure Al (b), and pure Al (c) deposited on LCD grade glass substrates were investigated, with the results shown in Table 1. These indicate that pure Al (a) is a highly (111) textured film, while pure Al (b) and (c) are only slightly (111) textured (i.e. nearly random) films. The crystallographic texture of Al thin film and its anti-stress migration property are strongly correlated, and we confirmed in a previous study that the former type of Al thin film has a strong anti-stress migration property, while the

Table 2
Anti-stress migration property results obtained by nanoindentation techniques

Sample ID	200°C		250°C		300°C	
	Number of whiskers	Number of hillocks	Number of whiskers	Number of hillocks	Number of whiskers	Number of hillocks
Al–In	4	54	5	47	13	103
Pure Al (c)	0	28	3	39	6	41

Table 3
The effects of the pure Al overcoated layer in preventing hillock generation

Sample ID	No overcoated layer		40 nm thick overcoated layer		200 nm thick overcoated layer	
	200°C	300°C	200°C	300°C	200°C	300°C
Pure Al (a)	3	9	0	0	0	0
Pure Al (b)	7	67	1	0	0	0
Al–In	54	102	13	8	0	0

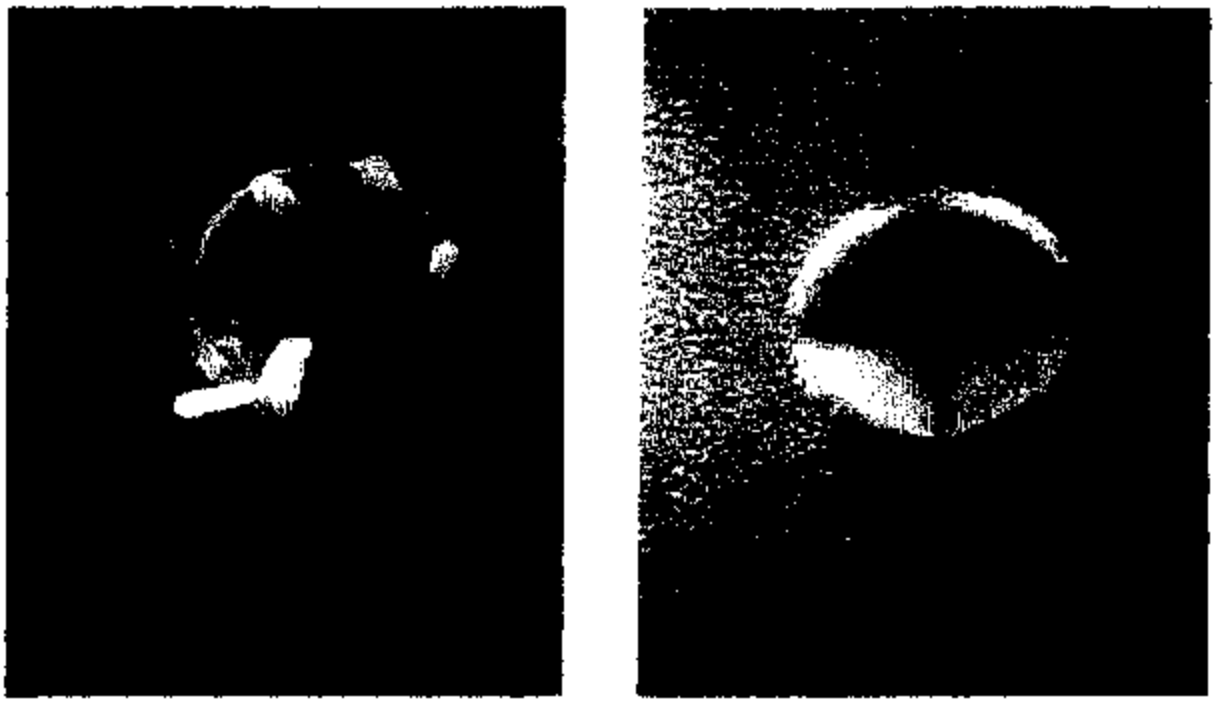

(a) non-overcoated layer (sample A) (b) layer with a 200-nm-thick overcoat (sample B)

Fig. 2. SEM images after nanoindentation techniques in the Al–In thin films corresponding to the samples: (a) non-overcoated layer (sample A); (b) layer with a 200 nm thick overcoat (sample B).

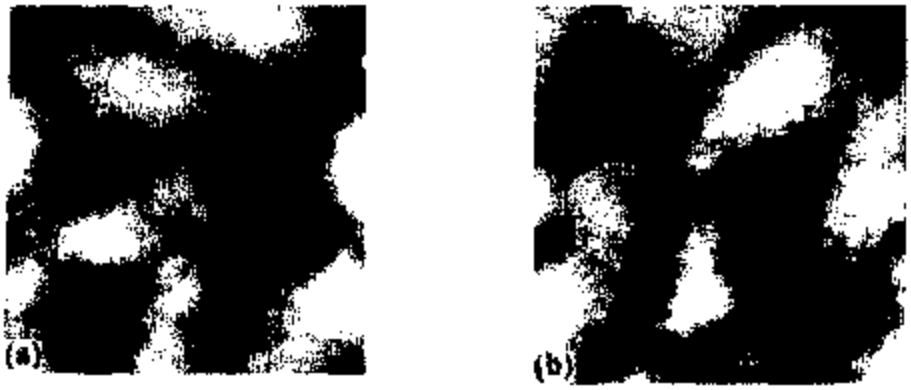

(a) before (sample 3a) annealing (b) after (sample 3b) annealing at 300°C in vacuum for 60 min

Fig. 3. AFM top views of the overcoated pure Al layer on the pure Al (b) thin films: (a) before (sample 3a); (b) after (sample 3b) annealing at 300°C in vacuum for 60 min; scale 1000 × 1000 nm².

latter type has a weak anti-stress migration property [10].

Table 2 compares the anti-stress migration properties of Al–0.19 wt.% In (Al–In) and pure Al (c) thin films deposited by the same sputtering apparatus. Whisker generation was observed in the Al–In thin-film samples at a stress temperature of 200°C, but was not observed in the pure Al (c) thin film at the same temperature. More whiskers and hillocks were generated in the Al–In thin film than in the pure Al (c) thin film at all stress temperatures. These results indicate that the use of Al–In thin film leads to the generation of whiskers and

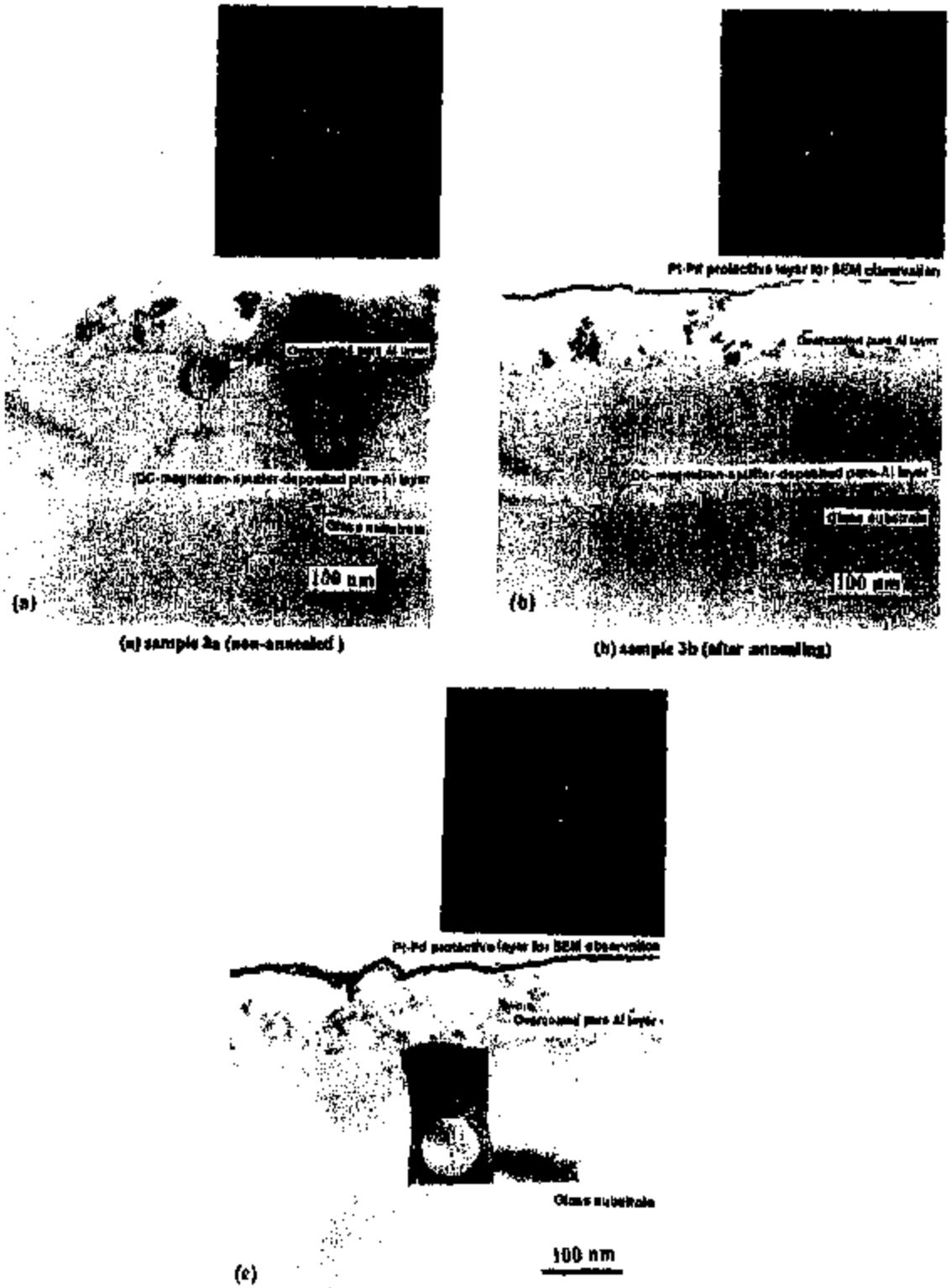

(a) sample 3a (non-annealed)

(b) sample 3b (after annealing)

(c) pure-Al (sample 3b) thin film existing under the overcoated layer

Fig. 4. Cross-sectional TEM images and analyses of the grain orientation caused by electron diffraction: (a) sample 3a (non-annealed); (b) sample 3b (after annealing); (c) pure Al (sample 3b) thin film existing under the overcoated layer.

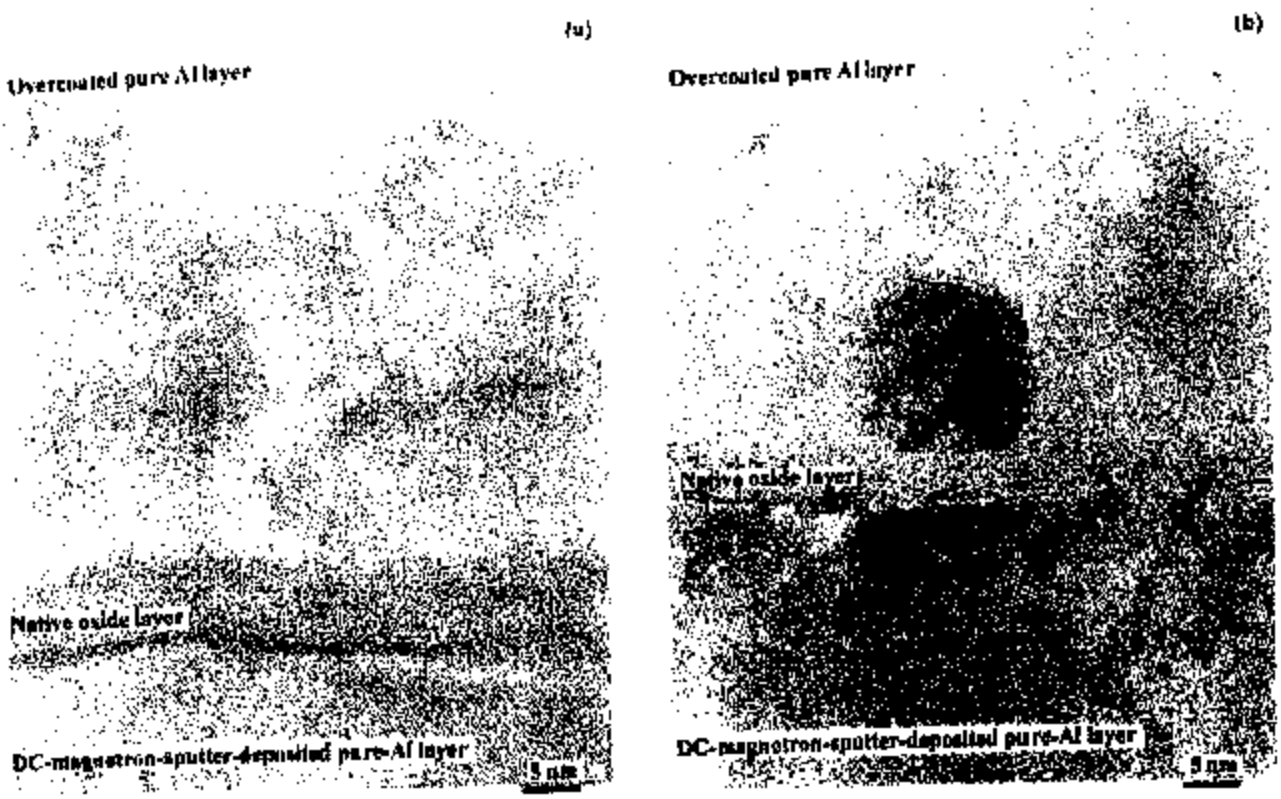

Fig. 5. Detailed nanostructure micrographs obtained by means of cross-sectional TEM corresponding to: (a) sample 3a; (b) sample 3b.

hillocks by nanoindentation techniques at lower stress temperatures than when pure Al (c) thin film is used. We conclude that the Al–In film in this study has a weaker anti-stress migration property than pure Al (c). According to the results shown in Tables 1 and 2, Al–In film has the weakest anti-stress migration property of all these samples.

3.2. Effect and properties of an overcoated pure Al thin film layer

The effect of a pure Al overcoated layer in preventing hillock generation is shown in Table 3, which indicates that the largest number of hillocks was generated in the Al–In thin film by our nanoindentation technique when no overcoated layer was used, and that both (40 nm and 200 nm thick) overcoated layers completely prevented the generation of hillocks in pure Al (a) and pure Al (b) thin films. The table also indicates that the 40 nm thick overcoated pure Al layer reduced the generation of hillocks, while the 200 nm thick layer completely prevented the generation of hillocks in the Al–In thin film, which has the weakest anti-stress migration property of the three samples. We conclude that the overcoated pure Al layer (200 nm) is very effective in preventing hillock generation, while the overcoated pure Al layer (40 nm) has an unstable effect on the Al–In thin film, since the number of hillocks generated in the Al–In thin film with the overcoated pure Al layer (40 nm) at a stress temperature of 200°C is greater than at 300°C.

Fig. 2(a) and (b) shows SEM images after nanoindentation techniques (300°C thermal stress) which correspond to the samples: Al–In thin films with a non-overcoated layer (sample A) and with a 200 nm thick overcoated layer (sample B). Whiskers and hillocks are observed on the nanoindentation marks in sample A, whereas no whiskers or hillocks are observed in sample B. A comparison of these micrographs reveals that the overcoated layer is very effective in preventing stress migration.

To investigate the characteristics of overcoated pure Al thin film, we performed AFM surface analysis and cross-sectional TEM observation. Fig. 3(a) and (b) shows AFM top views of the overcoated pure Al layer on the pure Al (b) thin films before (sample 3a) and after (sample 3b) annealing at 300°C in vacuum for 60 min. They indicate that there is no significant change in either sample, and that their grain sizes are fine.

The results of cross-sectional TEM observation of sample 3a (non-annealed) and 3b (after annealing) are shown in Fig. 4(a) and (b), which also shows the results

of electron diffraction analysis in both overcoated pure Al layers. These images reveal that the morphology of the overcoated layer is fine-grained polycrystalline, and that there is little change in the grain size after annealing, as seen in Fig. 3(a) and (b). This indicates that the overcoated layer is robust to the thermal stress. Fig. 4(c) also shows the result of electron diffraction analysis in the pure Al (sample 3b) thin film existing under the overcoated layer. It indicates that the grain is (111) oriented.

Detailed nanostructural observation was performed by means of cross-sectional TEM, as shown in Fig. 5(a) and (b), which corresponds to samples 3a and 3b. A very thin (about 3 nm thick) native oxide layer is visible between the d.c. magnetron sputter-deposited pure Al thin film and the overcoated pure Al thin film in both TEM images. We consider that this oxide layer grew in the atmosphere between the periods of d.c. magnetron sputtering and RF sputtering. Aluminum lattice patterns are sporadically observed in the overcoated layers of both samples. Judging from this result and Fig. 4(a) and (b), we conclude that the overcoated pure Al layer has a fine-grained polycrystalline structure. Fig. 5(a) and (b) also reveals that there is no significant difference between the two samples. This indicates that the morphology of the pure Al/Al_2O_3/pure-Al layered structure thin film in this study was little changed by annealing.

We consider that the Al/Al_2O_3/fine-grained polycrystalline pure Al layered structure thin film prevents stress migration from being caused by the thermal expansion mismatch between the glass substrate and itself, by absorbing the stress throughout the layered thin film. As regards application of the layered structure pure Al to interconnects in TFT arrays, since a resistivity of 3.12 Ω cm was obtained in the layered thin film by means of the four-point probe method, such a thin conductive film is suitable for low-resistivity interconnect materials in large high-resolution TFT-LCD arrays.

4. Conclusions

We confirmed that layered Al thin films with overcoated fine-grained polycrystalline pure Al thin film have a strong anti-stress migration property. With the 200 nm thick overcoated thin film, no hillocks or whiskers were generated in an Al–In thin film with a weak anti-stress migration property. By means of cross-sectional TEM analysis, we confirmed that the morphology of the layered thin film was changed little by annealing. We consider that the Al/Al_2O_3/fine-grained polycrystalline pure Al layered structure thin film prevents stress migration by absorbing the thermal stress throughout the layered thin film. Consequently, we conclude that the layered structure thin film can be used as an interconnect material in large high-resolution TFT-LCD arrays.

Acknowledgements

The authors wish to thank T. Yoshioka of JEOL Hightech Co., Ltd. for TEM observation, H. Okuhira of Hitachi Science Systems, Ltd. for TOF-SIMS analysis, S. Takeuchi and T. Hashimoto of IBM Display Business Unit for encouragement, and M. McDonald of IBM Yamato Laboratory for his comments on this article.

References

[1] O.L. Schaible, R.S. Keen, Proc. IEEE 57 (9) (1969) 1579.
[2] T. Onishi, E. Iwamura, K. Takagi, K. Yoshikawa, J. Vac. Sci. Technol. A 14 (3) (1996) 2728–2735.
[3] S. Tabuyama, N. Tanimi, Thin Solid Films 289 (1996) 289–294.
[4] E. Iwamura, T. Onishi, K. Yoshikawa, Thin Solid Films 270 (1995) 450–455.
[5] H. Takatsuji, H. Iiyori, S. Tsuji, K. Tsujimoto, K. Kuroda, H. Saka, Mater. Res. Soc. Symp. Proc. 471 (1997) 99–104.
[6] T. Tsujimura, H. Kitahara, A. Makita, P. Fryer, J. Batey, Proc. 1994 International Display Research Conference and International Workshops on AMLCD and Display Materials (1994) 424–427.
[7] T. Arai, Y. Hiromasa, S. Tsuji, Mater. Res. Soc. Symp. Proc. 424 (1997) 37–42.
[8] K. Hazama, Y. Nakamura, O. Nittono, Jpn. J. Appl. Phys. 27 (1988) 1142.
[9] H. Takatsuji, S. Tsuji, H. Kitahara, K. Tsujimoto, K. Kuroda, H. Saka, Mater. Res. Soc. Symp. Proc. 441 (1997) 415–420.
[10] H. Takatsuji, K. Tsujimoto, K. Kuroda, H. Saka, Thin Solid Films 343/344 (1999) 461–464.

ELSEVIER

Ultramicroscopy 81 (2000) 245–262

ultramicroscopy

www.elsevier.nl/locate/ultramic

Analysis of local strain in aluminium interconnects by energy filtered CBED

S. Krämer*, J. Mayer, C. Witt, A. Weickenmeier, M. Rühle

Max-Planck-Institut für Metallforschung, Seestr. 92, D-70174 Stuttgart, Germany

Received 29 July 1999; received in revised form 27 September 1999

Dedicated to Professor Harald Rose on the occasion of his 65th birthday

Abstract

Energy filtered convergent beam electron diffraction (CBED) was used to investigate localised strain in aluminium interconnects. The quantitative analysis of the experimental patterns is based on a multi-step evaluation procedure which is the main subject of the present paper. The improvements which were made to the analysis method aim at increasing both the automation and the accuracy. The detection of the higher order Laue zone (HOLZ) line positions is performed by means of the Hough transform. The required sub-pixel resolution can be achieved routinely and the achievable accuracy is only limited by the line width and the amount of noise in the patterns. The determination of the strain state is performed via a refinement algorithm which is based on varying the strain state in the sample coordinate system and simulating the patterns for the individual grains until a best fit with the experiment is obtained. For the simulation we have developed a new correction scheme in which the dynamical effects are treated separately for each individual HOLZ line. The results show that the main source of the observed strains is the difference in thermal expansion coefficients. The strain is substantially reduced underneath a hillock in the interconnect. Asymmetries in the strain distribution around the hillock show that the unidirectional diffusion during electromigration tests causes peak strains in areas next to the hillock which may be possible failure sites. © 2000 Elsevier Science B.V. All rights reserved.

Keywords: CBED; Energy filtered imaging and diffraction; Data processing/image processing; Electromigration; Finite element modelling

1. Introduction

Internal strains limit the properties and control the failure mechanisms in many materials systems composed of metals and ceramics or semiconductors. Frequently encountered sources of internal strain are the differences in thermal expansion coefficients, coherency strain developed during the growth process, or strain resulting from diffusional processes. One example of the latter is the electromigration which occurs while passing a current through a thin interconnect line. Amongst the numerous methods which have been applied to measure the internal strain, convergent beam electron diffraction [1] is undoubtedly the one with the

* Corresponding author. Tel.: +49-711-2095-225; fax: +49-711-2095-320.

E-mail address: kraemer@hrem.mpi-stuttgart.mpg.de (S. Krämer)

PII: S0304-3991(99)00191-6

highest spatial resolution. In a transmission electron microscope, probes with a diameter of a few tens of nanometers or even nanometers can easily be formed, which is well adapted to the dimensions in which the strain state may vary e.g. across interfaces. There is a growing number of studies in which the technique has successfully been applied to different materials systems (see, for example, Refs. [2–8]). However, there are a number of problems inherent to the CBED technique, e.g. thin foil relaxations, the inelastic scattering background and the dynamical scattering effects, which so far have prevented the implementation of the CBED method as a standardised technique for strain measurement.

In the present paper we want to report on a number of improvements which we have made to the method and we want to demonstrate the level of accuracy which can now be obtained for the case of Al interconnects. In terms of the instrumentation the major breakthrough was the commercial availability of energy filters for TEMs [9]. Energy filtering is very important since it helps to increase the reliability of the strain measurement using CBED. In transmission electron microscopy, it is favourable to use thick samples for the strain measurement since the effects of thin film relaxation decrease and the sharpness of the HOLZ lines increases. However, at the same time the probability of inelastic scattering (mainly plasmon losses) increases [10–12]. This not only leads to an increase in background and a broadening of the HOLZ lines, but also to a shift of the centre of the HOLZ lines. Exciting a plasmon loss of 20 eV at 100 keV is equivalent to a change of 2×10^{-4} in electron energy with a corresponding change in Bragg angle and thus in HOLZ line position. A combination of these effects can easily lead to a reduction in the accuracy of the strain analysis to about 10^{-3}. For commercial purity aluminium this strain value corresponds to the yield stress and thus a strain measurement becomes impossible.

In the analysis of the patterns, the first crucial step is finding the exact location of the HOLZ lines in the zero-order disc. The aim for any quantitative evaluation obviously is to use a computer-based, highly automated algorithm which is robust against noise in the patterns. Such an algorithm is the Hough transform [13] which in electron microscopy has become popular as an ideal tool for the analysis of Kikuchi bands in backscattering patterns obtained in a scanning electron microscope [14,15]. We have adapted the algorithm to the requirements of our CBED measurement, in particular to the fact that the line position has to be detected with sub-pixel accuracy [16]. The analysis is then carried out by comparing the measured line positions with the ones predicted from theoretical simulations for different strain states. In principle, this requires a dynamical Bloch wave simulation which, however, is much too time consuming for a thorough investigation of the parameter space being explored in the refinement algorithm. Therefore, we have developed a kinematical simulation procedure with a new dynamical correction scheme which is able to produce more reliable results than the commonly used effective high-voltage method.

In the present work, the method has been adapted to the strain measurement in thin aluminium interconnect lines on silicon substrates. Energy filtering enables one to use interconnects with dimensions which correspond to the actual geometry used in devices. Thus, no artefacts are introduced which may occur during an additional thinning step, and the measured strain state can directly be related to the failure of a line in the device. The results will be compared to the results of finite element simulations for the same specimen geometry and it will be shown that such a combined approach leads to a detailed understanding of the strain state in the system. In particular, it will be shown that local stresses exist which by many times exceed the yield stress of the bulk material. The results will be discussed and an outlook on future work will be given.

2. Instrumentation and specimen preparation

The present studies were performed on a Zeiss EM 912 Omega energy filtering TEM. The microscope was operated at a nominal high-voltage setting of 120 kV and a LaB_6 filament was used. The minimum probe size which still produces sufficient signal intensity is approximately 10 nm, however,

in most of the experiments we used probe sizes between 20 and 30 nm. In general, the experiments are best performed in a liquid-nitrogen cold stage which prevents contamination and reduces the amount of thermal diffuse scattering present in the pattern. However, this leads to an increase in the strain caused by the difference in thermal expansion coefficients and, in order to avoid this, the interconnect line was investigated at room temperature in the present work. An energy selecting slit with a width of 15 eV was inserted and centred around the zero-loss peak. The patterns were recorded by means of a GATAN 1k × 1k slow scan CCD camera.

The samples used in the present studies consisted of patterned lines on a silicon substrate. The interconnects were fabricated from a film stack on a Si substrate which consisted of 500 nm thermal oxide, 45 nm sputtered Ti, 300 nm reactively sputtered TiN, 400 nm sputtered Al and 30 nm reactively sputtered TiN. Following film deposition, the wafers were annealed for 60 min at 400°C in forming gas to allow for grain growth. Next, the metal films were patterned using UV lithography and reactive ion etching to form single lines with widths of 0.5 μm. In a second step, 5 μm long gaps in the Al were patterned leaving Al segments on the continuous TiN layer. The segment used in this experiment has a length of 50 μm. The TiN layer was kept continuous to provide electrical conductivity. The Al microstructure in the segments has an average grain size of 1.3 μm and predominantly bamboo structure [17].

Electromigration tests were performed on the 0.5 μm wide segments applying current densities of 2×10^6 A/cm^2 at a temperature of 200°C for approximately 100 h. Owing to the current-induced electromigration force, the Al atoms start to migrate in the direction of the electron flux. As a consequence the material depletes at the cathode end and hillocks form at the anode end of the segment.

For the experiments we prepared TEM specimens in which the electron beam passes through the Al segment parallel to the silicon substrate surface. The main problem of these samples is that for finite tilt angles the thick Si substrate may obscure the interconnect line. Therefore, in our case, a combination of several preparation techniques had to be applied. In the first step, a thin slice with the interconnect at the edge was cut out of the silicon wafer using a diamond wire saw. Subsequently, tripod-polishing was used to reduce the thickness of the slice to about 80 μm and to remove the edges of the substrate near the interconnect as schematically shown on the left side of Fig. 1. The remaining edge typically has a thickness of 20 μm. During the preparation the interconnect is always protected by wax. In the last step, a focused ion beam microscope (FIB) was used to remove the substrate material near the interconnect leaving a thin, 3 μm wide ridge with the interconnect on top (see Fig. 1). With the final specimens, experimental tilt angles of typically ± 15° can be obtained. In the case of the sample investigated in this paper, the 500 nm wide line was additionally thinned to a specimen thickness of about 200 nm using the FIB microscope.

The finite element program ANSYS is used to simulate the spatial distribution of the strain in the interconnect in order to get the information on the dependence of the strain on the actual geometry of the line. Purely elastic models are applied and all the parameters are adjusted to the physical parameters of the interconnect line.

3. Experimental procedures

A TEM micrograph of the area investigated is shown in Fig. 2. In the undisturbed region the nominal height of the line is 400 nm and the nominal width is 200 nm. The latter is the actual specimen thickness used in our TEM measurement. At such a thickness, the inelastic scattering background already leads to a substantial reduction in the visibility of the HOLZ lines. As mentioned above, energy filtering helps to improve the contrast, sharpen the HOLZ lines and also to make sure that they are at the Bragg position corresponding to the actual accelerating voltage.

For the analysis of the patterns an accurate value of the accelerating voltage has to be known in order to get accurate values of the strained lattice constants. For this reason, a reference material with a high crystal quality should be used, e.g. single crystalline silicon. In the following it will be shown

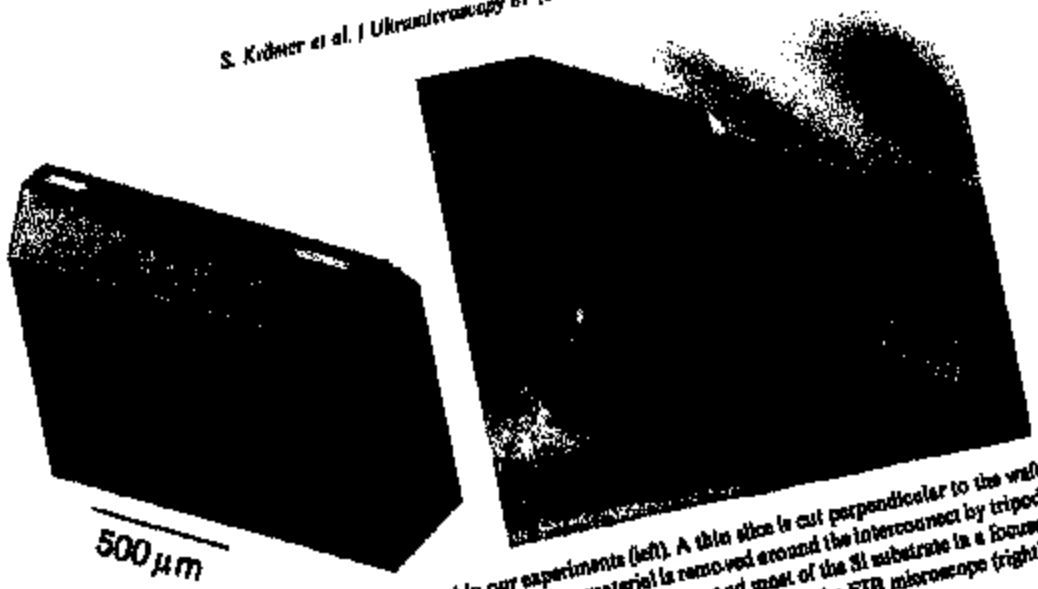

Fig. 1. Schematic drawing of the sample geometry used in our experiments (left). A thin slice is cut perpendicular to the wafer with the actual interconnect being centred on a thin face of the section. Further material is removed around the interconnect by tripod-polishing. The final electron transparent areas are obtained by removing the passivation layers and most of the Si substrate in a focused ion beam (FIB) instrument. Images of the actual electron transparent specimen area can be obtained in the FIB microscope (right).

Fig. 2. TEM micrograph of the section of the interconnect line which has been studied in our CBED experiments. In the cen a hillock is visible which has been grown in electromigration experiments before the TEM specimen was prepared.

that using careful analysis the accelerating voltage can be determined with an accuracy of about 20 V.

The actual patterns in the interconnect were acquired at a series of spots parallel and perpendicular to the line. Patterns which were acquired close to the interface at the bottom of the line and also at the top of the line close to the capping layer show a pronounced splitting of some of the HOLZ lines (Fig. 3a). This can be attributed to a bending of the lattice planes parallel to the interface which results from the inhomogeneous stress distribution close to the interfaces. This effect does not occur in patterns acquired close to the centre of the line (Fig. 3b) and therefore such patterns were used for the study of the strain distribution along the interconnect and in particular under the hillock.

In the following, the important aspects of the strain analysis using CBED are discussed including the detection of the HOLZ line positions, t ment of the dynamic effects, the correla tween the strain state and the HOLZ line and the details of the evaluation proced

3.1. HOLZ line detection

For the detection of the HOLZ line use the Hough transform [13], ginally was developed to detect p in a bubble chamber. The main the Hough transform are that it automated and that it makes us intensity distribution along a H not only, like other techniques number of traces perpendicular Therefore, the analysis can make the statistics and produces accur

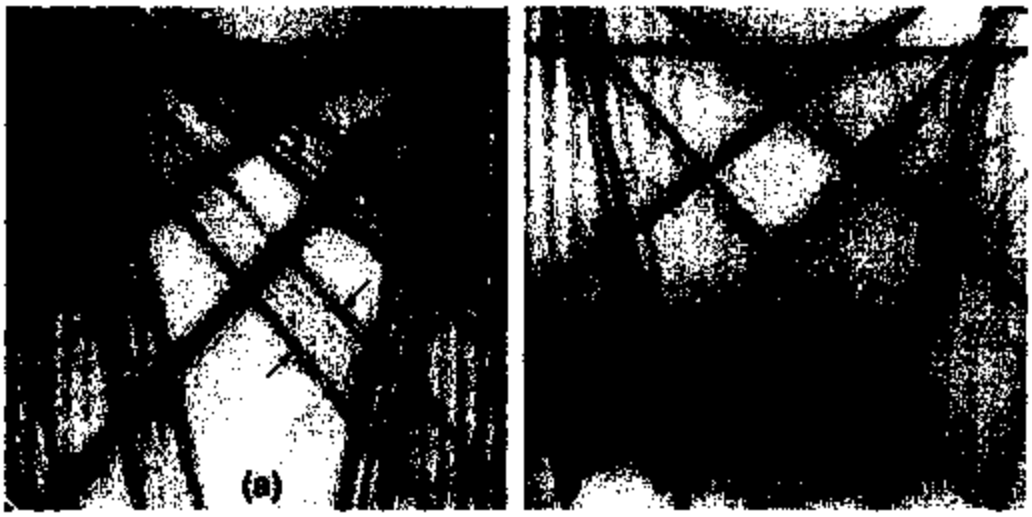

Fig. 3. (a) CBED pattern taken with the spot positioned close to the substrate interface. Some of the HOLZ lines show a pronounced splitting which is caused by a bending of the lattice planes close to the substrate. (b) From the central part of the interconnect line undisturbed patterns can be obtained.

the case of patterns which contain a large amount of noise.

The Hough transform is based on the more general Radon transform [18] which can be applied to any parametrised curve in two dimensional space:

$$R(\alpha,c) = \int_{-\infty}^{\infty}\int_{-\infty}^{\infty} f(x,y) \times \delta[y - \tan(\alpha)\cdot x - c]\,\mathrm{d}x\,\mathrm{d}y. \quad (1)$$

Here $f(x,y)$ is the intensity distribution in the two-dimensional pattern which has to be analysed, and the function in the square brackets is the parametrised version of the curve which leads to a sharp maximum in the Radon transform $R(\alpha,c)$. Mathematically, the Radon transform is defined as the integral of the intensity distribution along the curve which is defined by the parameters (α,c). In our case, the curve is a straight line with

$$y = \tan(\alpha)x + c \quad (2)$$

and $R(\alpha,c)$ is then called the Hough transform of the intensity distribution. $R(\alpha,c)$ exhibits a maximum if a straight line described by (α,c) runs along a straight maximum in the intensity distribution in (x,y)-space.

The CBED patterns are commonly recorded with a CCD camera and thus finite rectangular images with discrete pixels are obtained. In this case the integrals in Eq. (1) are replaced by summations and the details are given Ref. [16]. The main problem of the (α,c)-parameterisation of a straight line is that c diverges for $\alpha \to \pm 90°$. To overcome this divergence, the y-axis intersection c_y is only used in the angular range between $-45°$ and $+45°$, whereas the intersection c_x with the x-axis is used for slopes from $-90°$ to $-45°$ and for $+45°$ to $+90°$. Another problem is that, owing to the finite size of the pattern, the number of pixels forming a straight line decreases the closer the line segment gets to the corners of the image. This fact has to be taken into account by an appropriate biasing of the Hough intensities [16].

As an experimental example, Fig. 4a shows the central region of the zero order disc and the corresponding Hough transform of a CBED pattern acquired in ⟨1 3 3⟩ zone axis orientation from the interconnect line shown in Fig. 2. For the unstrained material, the pattern possesses mirror symmetry relative to the vertical axis. Because of the strain in the interconnect the symmetry in the arrangement of the HOLZ lines is lost which also leads to noticeable asymmetries in the arrangement of Hough peaks. The dynamical interaction of the electron waves with the crystal causes a bending and distortion of the HOLZ lines in the vicinity of

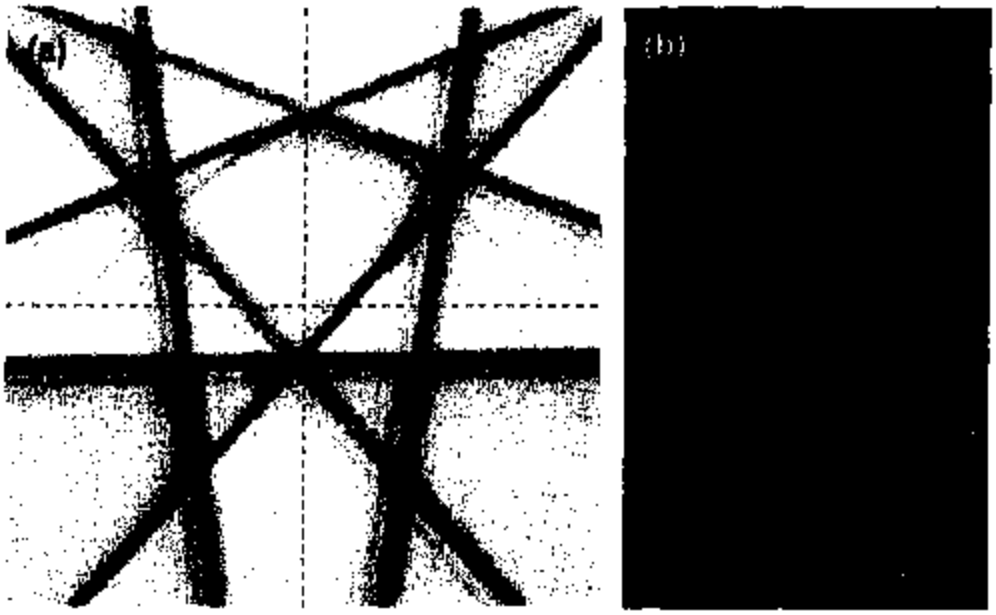

Fig. 4. (a) Central portion of a [1 3 3] CBED pattern acquired in the centre of the line and the corresponding Hough transform (b). Because of the unidirectional strain, the symmetry of the pattern is broken with respect to the vertical line.

their intersections. Therefore, the HOLZ line crossings are masked before the actual Hough transform is applied. Furthermore, in order to save computing time, areas with fairly homogeneous intensities in the patterns can also be masked. Then the Hough transform is computed with high pixel resolution and the result is shown in Fig. 4b. In order to obtain the required accuracy, the actual maximum of each Hough peak has to be determined to sub-pixel accuracy. This is achieved by fitting a two-dimensional polynomial to the intensities in the discrete pixels of the Hough peaks [16]. The maximum of the intensity in this polynomial fit can be determined with an accuracy of 0.2 pixel for the intersection c and with an angular resolution of 0.02° for the slope.

3.2. Geometry of the strain state

In a given medium, a general local strain state is defined by six components, three normal strains and three shear strains. By transforming into the eigenstate, the number reduces to three strains along the main axes. Knowing the directions of the main axes therefore drastically reduces the number of strain components which have to be detected. The directions of the main axes are mostly defined by the actual geometry of the sample, which defines the sample coordinate system.

In the general case of a thin film, two axes of the eigenstate strain lie in the film plane and the third one along the film normal. However, if a biaxial strain state within a polycrystalline film is assumed, the orientation of the two in-plane directions of the eigenstrain in a grain are not a priori known. Therefore the total in-plane strain state has to be detected, i.e. two normal strains ε_{xx}, ε_{yy} and the shear strain ε_{xy}. Together with the strain along the film normal four strain components have to be detected. Assuming a plane stress state with vanishing stresses along the film normal again reduces the number to three independent strain variables.

In our case, the geometry of the interconnect defines the directions of the sample coordinate system. The x-direction is chosen parallel to the interconnect line, the y direction perpendicular to the line and parallel to the interface and the z-direction perpendicular to the interface. Finite element

modeling (see Section 4) shows that in this geometry there mainly exists a triaxial strain state with the main axes of the eigenstrain being parallel to the x-, y- and z-direction. Therefore, in the following the aim is to measure the strain components ε_x, ε_y and ε_z in the given sample coordinate system.

In most cases the crystal unit cell axes a,b and c of the grains forming the interconnect do not coincide with the axes of the sample coordinate system. These crystal orientations thus define a separate crystal coordinate system. In the analysis, the strain state has to be transformed from the sample to the crystal coordinate system and vice versa to determine the influence of the macroscopic strain on the lattice parameters of the individual grains. In the actual measurement, a HOLZ pattern is acquired in an appropriate high-indexed zone axis orientation, which is usually selected in such a way that it is near the y-axis of the sample coordinate system. In the case of Al, a number of different zone axes can be used. In the present analysis we selected the ⟨1 3 3⟩, ⟨1 3 6⟩, ⟨1 2 5⟩ and the ⟨3 3 4⟩ zone axis patterns. In general, it is always possible to find an appropriate zone axis which is less than 15° away from the given orientation of the grains, making it possible to analyse the strain state in any given crystal.

3.3. Treatment of dynamical effects

HOLZ lines are shifted with respect to their kinematical positions due to the dynamical interaction of the beam electrons with the crystal potential. A detailed discussion of the dynamical shift has been given by Zuo and Spence [19] using the Bloch wave concept. The deviation of the actual Bragg condition of the HOLZ reflections from the kinematical case can be explained with the help of the dispersion surfaces as illustrated in Fig. 5. In a zone axis pattern, the shift of the HOLZ line positions is mainly determined by the distance of the first branch of the dispersion surface from the kinematical sphere defined by the K-vector of the incident beam [20]. The influence of the ZOLZ reflections can approximately be determined using perturbation theory [2,21]. The results show that in flat regions of the dispersion surface, the effects can approximately be simulated by using an effective high-voltage, but only for HOLZ lines in a single Laue zone. The effective high-voltage correction was first suggested by Lin et al. [21] and is widely used in literature.

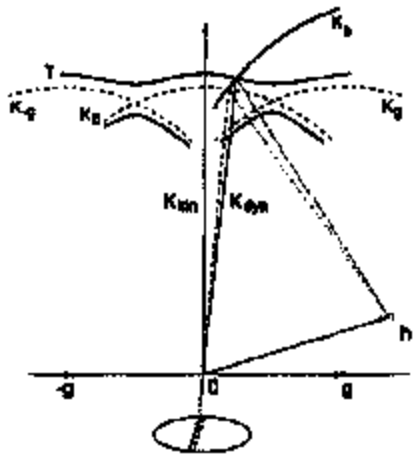

Fig. 5. Schematic drawing of the dispersion surfaces (labelled γ) which result from the strong dynamical interaction of the beam electrons with the crystal. In the crystal, the kinematical wavevectors (labelled K_g, K_0 and K_{-g}) are no longer allowed and therefore the intersection with K_h shifts from K_0 to the dispersion surface, leading to a corresponding shift of the HOLZ line in the CBED pattern.

The main drawback of the effective high-voltage approach is that it cannot describe the deviations of the dispersion surface from a spherical geometry. As shown in Fig. 5 the dynamical shift increases near the Bragg positions of low index reflections. Therefore the dynamical shift of each HOLZ line depends on the actual geometry of the surrounding Bragg positions for each incident beam direction. The most accurate method to describe the dynamical interactions is to use the fully dynamical Bloch wave formalism which accounts for all dynamical diffraction effects irrespective of thickness, material and orientation of the sample. The main problem of this method is that very time-consuming calculations are required. Our approach for increasing the accuracy of a simulation based on the kinematical algorithm is to determine a dynamical correction factor for each individual HOLZ line separately. In a first step, a highly resolved CBED pattern for the chosen zone axis is calculated for the

unstrained material using the Bloch wave formalism [3]. By comparing with the kinematical position, an effective dynamical shift for each individual HOLZ line is determined. In the following, as an example the HOLZ line arrangement near the [3 3 1] zone axis of Si will be discussed. The corresponding experimental patterns from Si are used for the high-voltage reference measurement.

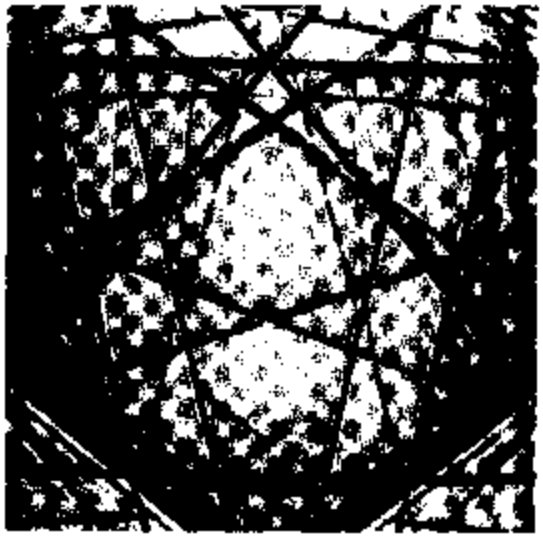

Fig. 6. Experimental pattern from the Si reference sample oriented along the [3 3 1] zone axis. The dashed lines represent the HOLZ line position detected by the Hough transform and the solid white lines represent the corresponding kinematical line positions.

Fig. 6 shows an experimental [3 3 1] zone axis pattern of silicon. Marked are both the actual line positions, as measured with the Hough transform, and the kinematical positions. With exception of the (3 3 −15) line all dynamical shifts are larger than the line width. Table 1 summarises the results of the attempts to correct for the dynamical shifts along the line normal. Two different data sets are shown with increasing sophistication in the degree of the dynamical correction. In the first set, the dynamical calculation includes the HOLZ reflections and the systematic row formed by the 2 −2 0 and −2 2 0 reflections. This corresponds to the geometrical situation depicted in Fig. 5. Even in this simplest treatment the dynamical shifts are not equal for the individual lines which is an effect of the non-spherical dispersion surface and the fact that HOLZ reflections from the 3rd and 4th Laue zone are involved. The second data set results from a calculation which includes a total of 200 reflections. The comparison shows that the dynamical shift is dominated by the reflections of the zeroth Laue zone, but including more reflections can significantly change the dynamical shift for individual

Table 1
Dynamical shift correction factors for different HOLZ lines in the Si [3 3 1] zone axis pattern. The factors were determined from a Bloch wave calculation with different numbers of excited beams. In the table, $d\alpha$ denotes the change of the slope and dr the relative shift along the line normal in reciprocal Å units (positive sign denotes a shift away from the zone centre)

	14 beams		200 beams	
	$d\alpha$ (deg)	dr (10^{-3} 1/Å)	$d\alpha$ (deg)	dr (10^{-3} 1/Å)
[3 3 −15]	0.00	1.69	0.000	−0.34
[−9 7 9]	−0.078	−1.63	−0.133	−2.08
[7 −9 9]	0.078	−1.63	0.133	2.08
[10 −4 −14]	0.029	1.45	0.244	1.37
[−4 10 −14]	−0.029	1.45	−0.244	1.37
[−12 12 4]	0.019	1.35	−0.016	1.69
[12 −12 4]	−0.019	1.35	0.016	1.69
[11 −9 −3]	−0.061	−1.29	−0.021	−2.05
[−9 11 −3]	0.061	−1.29	0.021	−2.05
[−6 2 16]	0.014	−1.51	0.034	−1.79
[2 −6 16]	−0.014	−1.51	−0.034	−1.79

Table 2
Dynamical shift correction factors for different HOLZ lines in the Al [3 3 4] zone axis pattern and different sample thicknesses. Note that the shifts are one order of magnitude lower than in the case of Si

	100 nm		300 nm	
	$d\alpha$ (deg)	dr (10^{-4} 1/Å)	$d\alpha$ (deg)	dr (10^{-4} 1/Å)
[5 5 −7]	0.00	−3.52	0.000	1.13
[−7 1 5]	0.067	1.74	−0.018	−4.47
[1 −7 5]	−0.067	1.74	0.018	−4.47
[8 −2 −4]	0.074	−0.07	−0.006	5.46
[−2 8 −4]	−0.074	−0.07	0.006	5.46
[7 −5 −1]	0.141	−3.99	0.026	2.68
[−5 7 −1]	−0.141	−3.99	−0.026	2.68

lines. In particular, the (3 3 −15) HOLZ line is strongly influenced by the neighbouring Bragg positions. Beside the shift, the slope of the lines also changes which again reflects the fact that the dispersion surface is not spherical along the lines and that the effective high-voltage correction hence would produce significant errors in the analysis.

Table 2 summarises the dynamical shifts for the HOLZ lines in the [3 3 4] zone axis of aluminium as a function of the specimen thickness. Aluminium shows weaker dynamical effects than silicon and the line shifts are in the order of the line width despite the fact that both elements have similar Z-values. This results from the fact that Al possesses smaller unit cell dimensions and fewer atoms in the cell. The thickness dependence of the line shift is caused by the anomalous absorption effect which is always in the order of the line width and increases with decreasing sample thickness [22].

3.4. Correlation between strain and HOLZ line positions

In the kinematic approximation, the HOLZ line position is given by the Bragg law

$$2\boldsymbol{K}\boldsymbol{S}_{\boldsymbol{h}} = \boldsymbol{K}^2 - (\boldsymbol{K} - \boldsymbol{h})^2 = 0, \tag{3}$$

where $\boldsymbol{K}$ is the mean wavevector inside the crystal and $\boldsymbol{h}$ is a reciprocal lattice vector. It is convenient to use zone axis orientations for the experiment since they can easily be identified by the characteristic Kikuchi line crossings. Furthermore, they often have the most dense accumulation of HOLZ lines. While this is feasible for aluminium, for crystals composed of heavier elements the dynamic effects may become too strong even in high-indexed zone axis and a random orientation avoiding any strongly scattering reflections of the ZOLZ may be preferable.

The coordinate system of the HOLZ pattern is defined by the reciprocal lattice vectors of two fundamental reflections $\boldsymbol{g}_1$ and $\boldsymbol{g}_2$ of the zero-order Laue zone of the chosen zone axis (za). This leads to the equation of the HOLZ lines

$$K_{g_2} = -\frac{h_{g_1}}{h_{g_2}} K_{g_1} + \frac{h_{za}}{h_{g_2}} K_{za} - \frac{h^2}{2h_{g_2}} \tag{4}$$

for the HOLZ reflections $\boldsymbol{h}$. In this equation, $K_{\boldsymbol{g}}$ and $h_{\boldsymbol{g}}$ denote the projections of the given vector on the basis vectors $\boldsymbol{g}_1$ and $\boldsymbol{g}_2$ or the direction of the zone axis (za), respectively.

As discussed in Section 3.2 the material is strained along certain directions, which are in most cases given by the overall sample geometry and not by the orientation of the individual crystals. The corresponding macroscopic strain has to be transformed from the sample coordinate system into the crystal coordinate system:

$$\varepsilon_{ij}^{\text{cst}} = R_{\text{is}} R_{\text{js}} \varepsilon_{\text{ss}}^{\text{sample}}, \tag{5}$$

where i, j denote the strain components along the unit cell axes a, b, c and R denotes the rotation matrix. Applying this transformed strain to the

reference lattice parameters defines the deformed unit cell which determines the g-vectors and thus the HOLZ line positions.

The sensitivity of a single HOLZ line pattern to a given strain tensor can best be understood by assuming that a zone axis za has been chosen which is parallel to the z-direction of the sample coordinate system. The HOLZ pattern is then sensitive to four strain components, the three component ε_x, ε_y and ε_{xy} in the plane normal to the zone axis and the component ε_z along the zone axis. The latter results from the fact that the g-vectors of the HOLZ lines are inclined relative to the xy-plane.

However, a line shift induced by a strain in the z-direction cannot be distinguished from an isotropic strain in the xy-plane if the HOLZ lines are from the same Laue zone. This ambiguity can easily be understood from the Ewald sphere construction in reciprocal space. Basically, a shift of one HOLZ reciprocal lattice point in the z-direction can be compensated for by a corresponding shift in the xy-direction thus leaving the position of the Ewald sphere and hence the HOLZ line unaffected. The position of the HOLZ reflections in a zone axis is defined by the intersection of the Ewald sphere with the Laue zone which is basically a circle. A strain in the z-direction shifts the whole Laue zone and as a consequence all HOLZ lines are shifted by about the same amount. It turns out that in almost all investigated HOLZ patterns in aluminium this is the case. Therefore, it is not possible to get information about the volume contraction and the ratios between the strain components at the same time. This ambiguity can only be relieved if an additional assumption is introduced or if the measurement is performed along two different directions for the same area. In the case of an interconnect it is very difficult to perform two independent measurements at each individual position. We therefore perform finite element analysis to model the dependence of the strain components on the actual geometry and the material composition.

3.5. Refinement procedure

The quantitative evaluation of the experimental HOLZ patterns is performed by simulating theoretical patterns for varying strain states and comparing them with the experimental ones searching for the best fit. For a magnification and rotation independent comparison we use normalised distances between HOLZ line intersections as suggested by Zuo [2]. In terms of the experimental patterns, the intersections are computed for the straight lines which correspond to the Hough maxima. A direct comparison of the Hough transforms of the experimental and simulated patterns is problematic because a sub-pixel deviation of the rotation or magnification of the patterns would already lead to errors.

For the comparison, we define a goodness-of-fit parameter

$$S = \frac{1}{N}\sum_i (d_i^{\exp} - c_i d_i^{\text{theory}})^2, \tag{6}$$

where N is the total number of data points, d_i the distance between two HOLZ line intersections and c_i a normalisation factor which can be interpreted as a camera length. The number of distances should be chosen in such a way that the position of each line relative to all others is taken into account. If the distances are given in pixel units a value of $S = 1.0$ means that the mean square deviation of the segment length is around one pixel.

The process of finding the best fit, i.e. the lowest S, can be performed using standard optimisation routines, like local optimisers based on Powell's method [23], or by performing a 'grid search' where all possible parameters are tested. The experiments show that a unique solution can always be obtained if the constraints for the strain components given by the volume criterion are properly taken into account.

The error in the determined strain values can be divided into four parts

$$\sigma = \sigma_I^2 + \sigma_d^2 + \sigma_{\text{mod}}^2 + 0.25\sigma_{\text{HV}}^2 \tag{7}$$

σ_I^2 is the error in the measurement of the line positions from the experimental HOLZ pattern, σ_d^2 is due to the approximations in the treatment of the dynamical interaction. Both are statistical errors with respect to the strain measurement and determine the width of the curve of the parameter S at its minimum. The sharpness of the minimum determines the statistical error in the strain

measurement. σ^2_{mod} accounts for the error introduced by a wrong model for the strain state, σ^2_{HV} is the variance in the high-voltage measurement. The two last contributions lead to a systematic over- or underestimation of the individual strain components.

3.6. Accelerating voltage reference measurement

The high-voltage of our microscope shows small long-term changes over a period of several weeks and the absolute changes lie typically in the range of 200 V. Although negligible for other applications, in the case of measuring the absolute lattice constants it is essential to know the exact value of the high-voltage during the strain measurement. We therefore routinely measure the high-voltage before and, if necessary after the strain analysis.

For the determination of a reference value of the accelerating voltage, a Si [3 3 1] zone axis pattern was acquired (Fig. 6) and the positions of the 9 HOLZ lines marked in the figure were measured using the Hough transform. 30 distances between line intersections were calculated and included in the refinement. The dynamical shifts of the second set in Table 1 and the literature value for the lattice constant $a = 0.54307$ nm of Si at room temperature are used. The refinement of the high-voltage is performed directly in the crystal coordinate system.

The value obtained for the high-voltage is 119.95 ± 0.02 kV. The differences between experimental and theoretical segment lengths are in the range of one pixel or even below, which is also reflected by the value of the goodness-of-fit parameter $S = 1.7$. A direct comparison of the experimental and fitted line parameters is possible by scaling the theoretical patterns on the experimental ones, which can be done by calculating the averaged rotation angle around the centre of the HOLZ pattern. This comparison also shows that the agreement between theory and experiment is better than one pixel.

The errors induced by measurement errors of the line positions and the approximate treatment of the dynamical interaction can be estimated from the width of the S-curve. Using the effective high-voltage approach for comparison, the value of $S = 2.9$ is obtained for the goodness-of-fit parameter which is larger than the value obtained with our new correction scheme and thus implies a larger discrepancy between model and experiment. The goodness-of-fit parameter also exhibits a shallower minimum using the effective high-voltage approach which is also indicative of a higher measurement error.

4. Finite element modelling

Finite element modelling (FEM) helps to understand the spatially varying strain and stress state of structures which have a complex geometrical shape and which are composed of different materials. The FEM model can well be adapted to the geometrical boundary conditions and parameters like the thermal expansion coefficient or the stiffness of the different materials. The finite element model applied for the investigated interconnect is composed of a sequence of layers: an infinite silicon wafer, a 500 nm thick thermal oxide, 300 nm TiN, 400 nm Al and a 30 nm TiN cap. An oxide scale at the side walls of the Al segment accounts for the surface oxidation of the metal when it is exposed to air. Elastic calculations were performed to determine the thermal strain distribution caused by the different thermal expansion coefficients of the materials. Table 3 summarises the material parameters used for the finite element simulations.

In the finite element models, three main strain components are used: ε_x along the line, ε_y parallel to the wafer surface and ε_z along the surface normal. The silicon substrate defines the thermal strain along the infinite interconnect line. Each of the different materials on top of the substrate shows a plane strain state for which ε_z is defined by the difference of the thermal expansion coefficients of

Table 3
Materials parameters used in the finite element simulations

	Si	SiO_2	TiN	Al
E (GPa)	130.4	60.0	110.0	63.2
G (GPa)	79.7	Isotropic	410.0	28.3
$\alpha(10^{-6}$ 1/K)	3.0	0.5	9.0	24.3
ν	0.279	0.18	0.34	0.362

silicon and the corresponding material. The two other components (ε_y and ε_z) are determined by a combination of the Poisson contraction, which is caused by the tensile strain in the x-direction, and of the lateral strain caused by the surrounding materials, i.e. the TiN segment, the oxide scale and the TiN capping layer.

In contrast to lines which are confined by a thick passivation layer or which adhere directly to the silicon substrate, the interconnects in the present studies are characterised by a large amount of free surfaces. In first order approximation, the Al segment exhibits a uniaxial strain state with the dominant strain along the interconnect line and Poisson contraction in the two perpendicular directions. However, the TiN layers at the top and bottom interface lead to additional tensile forces in the y-direction. Owing to the limited constraints imposed by the TiN-layers, the Al-segment can minimise the total strain energy by bending which can be recognised in Fig. 7. After a simulated cooling of 100 K, the originally rectangular mesh of the finite element model shows bending at the interfaces of the interconnect with the substrate and the cap, while in the middle straight planes remain. This strongly influences the sharpness of the HOLZ lines in the diffraction pattern. As has already shown in Fig. 3, the bend lattice planes lead to varying Bragg conditions while the electrons pass through the TEM sample which leads to a strong splitting of HOLZ lines. Although the splitting of the HOLZ lines contains additional information, flat planes are necessary for the present method of strain measurement. In the central part of the Al segment the electron beam passes straight planes which lead to sharp HOLZ lines. Therefore, only diffraction patterns acquired near the centre of the segment are analysed. The finite element model shows that at this position the y- and z-component of the strain do not change along the beam direction which is also an important condition for an accurate strain measurement.

As mentioned above, the results of the finite element calculations not only help to understand the experimental results but are also needed to relieve the ambiguity in the evaluation procedure which has been discussed above. In the refinement, we are using the predictions of the finite element model for the dependence of the volume contraction of the Al on the x-component of the strain in the interconnect. This condition fixes the relationship between the three strain components ε_x, ε_y and ε_z. The analysis shows that the volume contraction in the centre of the Al segment is almost the same as that for the simple case of a uniaxial strain state.

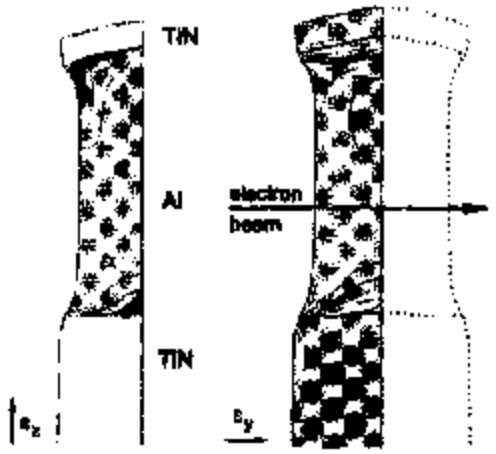

Fig. 7. Strain distribution predicted by the finite element model for the two components ε_z and ε_y. Shown is the shape of the interconnect after cooling by 100 K (the displacements are enhanced by a factor of 100 for better visibility). In the Al segment the y-component shows a transition from tensile strain at the interface to compressive strain in the central part which is a result of the bending moment of the interconnect.

5. Results of the strain analysis

In the present paper we discuss the results of strain measurements performed on an Al interconnect line which has undergone hillock formation during electromigration tests conducted at high temperatures. Both, undisturbed regions as well as areas in the vicinity of a hillock were investigated. As an example, the HOLZ patterns of two different grains of the interconnect area shown in Fig. 2 are depicted in Fig. 8. The zone axes are approximately parallel to the y-axis of the sample coordinate system. The directions of two macroscopic strain components lie in the plane of each of the CBED patterns. The white lines superimposed on the HOLZ lines in Fig. 8 represent both the measured

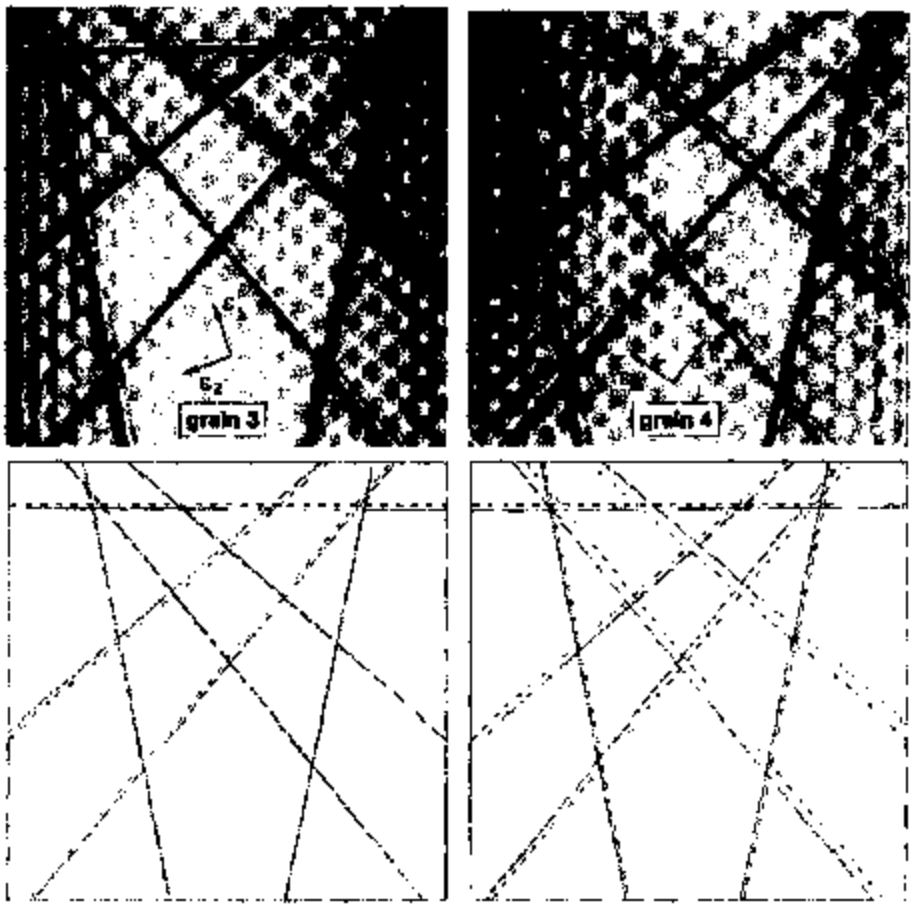

Fig. 8. CBED patterns of the third and fourth grains of the interconnect shown in Fig. 2. The uniaxial strain state clearly leads to a breaking of the symmetry in the patterns. The zone axes are approximately parallel to the y-axis of the sample coordinate system. The directions of the other two macroscopic strain components are given in each of the CBED patterns. The white lines represent both the measured and the fitted line positions which differ by less than one pixel for all HOLZ lines. The schematic patterns show a comparison between the HOLZ line positions for unstrained aluminium (dashed lines) and the actual line positions (solid lines). Grain 3, which is located underneath the hillock, is clearly less strained than grain 4.

and the fitted line positions which differ by less than one pixel for all HOLZ lines. Similar measurements were performed for the whole part of the interconnect shown in Fig. 2. Fig. 9 shows a schematic representation of the grain distribution of this part of the interconnect. Black dots mark the spots where the measurements were performed in four different grains.

Grain 3 is located directly under and grain 4 in front of the hillock with respect to the direction of the current flow. The two grains are oriented in such a way that in both cases a ⟨3 3 4⟩ zone axis could be used for the strain measurements. The distortions of the patterns depend on the orientation of the zone axis relative to the sample coordinate system. The rhombi in the middle of the patterns, for example, are in both cases elongated parallel to the x-axis, which can directly be associated with the thermal misfit strain along this direction. Simulated best-fit patterns of grains

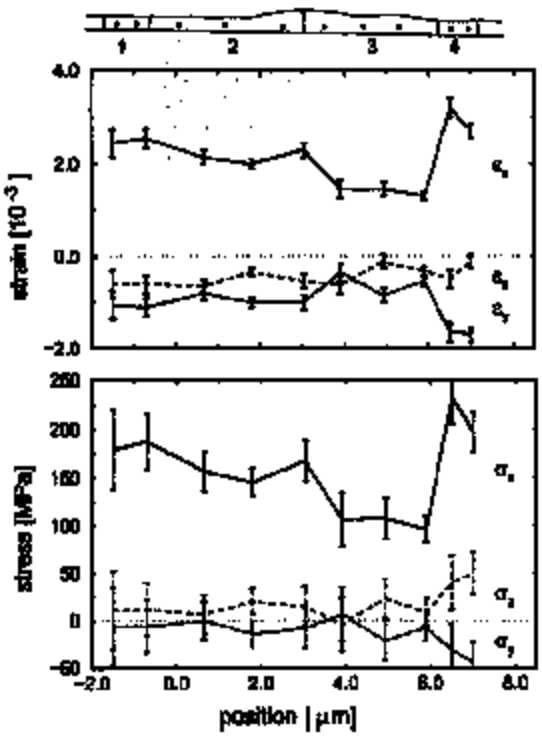

Fig. 9. Schematic drawing of the positions in which the CBED measurements were performed in the four different grains of the interconnect segment and plot of the measured strain (top) and derived stress (bottom) development along the interconnect line. A CBED pattern from grain 2 is shown in Fig. 4.

3 and 4 are also shown in Fig. 8 in comparison with the unstrained line positions. It can clearly be seen that the shifts induced by the strain are smaller in the left pattern than in the right pattern, which means that the grain under the hillock is less strained than the adjacent grain.

Fig. 9 summarises the results for the different grains. The strains were obtained by comparing the measured HOLZ line configuration with a configuration defined by the literature value of the unstrained lattice constant of pure Al at room temperature ($a = 0.40496$ nm). Also shown are the corresponding stresses along the principal axes which were derived from the measured strain values by means of the compliance matrix for pure Al.

5.1. Triaxial strain state

As expected, the strain component along the length of the interconnect, ε_x, is the largest. For a purely uniaxial strain state, one would expect ε_y and ε_z to be equal and to be related to ε_x through the Poisson contraction. However, the y- and z-component of the measured strain show different values, which reflects the inhomogeneous lateral strain caused by the surrounding materials. Two factors contribute to the inhomogeneity which is mainly caused by the small thickness of the interconnect: 1) The TiN layers at the top and bottom interfaces lead to additional tensile forces in the y-direction. As discussed in the section on FEM, this effect is only expected to be important in the Al near the TiN interface. The Al segment can minimise its total strain energy by bending and the resulting bending moment produces an additional compressive strain component in the y-direction in the middle part of the interconnect. As a result, the magnitude of ε_y becomes larger than that of ε_z. The measured strain levels in the undisturbed region correspond quite nicely to the results of finite element simulations which predict values of $\varepsilon_x = 2.10 \times 10^{-3}$, $\varepsilon_y = -0.85 \times 10^{-3}$ and $\varepsilon_z = -0.60 \times 10^{-3}$ for a temperature change of -100 K (see Fig. 7). (2) At the side walls, oxide scales form when the metal is exposed to air. Their influence increases with decreasing thickness of the interconnect line. The oxide scale prohibits the Al segment from shrinking along the z-direction which leads to a tensile contribution to the strain in the z-direction and a corresponding Poisson contraction along the y-direction.

The plot of the stress also shows that the interconnect has a dominantly uniaxial stress distribution with additional stresses building up because of the surrounding material. In the present case, the additional stresses are very small. The main contribution is given by a small tensile force building up along the z-direction which can be attributed to the oxide scale preventing the Al-segment from shrinking.

From a single HOLZ line pattern, one determines the ratios between the measured strain components in the triaxial strain state. The absolute values of the strain depend on the chosen reference

lattice constant and the assumed volume contraction. A change in the value of the volume contraction would lead to a uniform shift of the measured strain components which is three times smaller for each component than the actual change in the volume. Therefore, an uncertainty in the assumption of the volume contraction, e.g. due to uncertainties in the material parameters included in the finite element model, has only a small influence on the results. Assuming, for example, that the volume contraction is twice as large as the corresponding uniaxial value, the strain components are only raised by 5×10^{-4}.

5.2. Lateral strain distribution

The undisturbed left side of the investigated area shows almost constant tensile strain in the x-direction parallel to the interconnect, followed by a clear drop in strain level underneath the hillock and then a steep increase towards the grain on the right side. The error bars given in Fig. 9 are statistical errors which result from an analysis of the width of S-curves as a function of the strain parameters being varied. Typical S-curves for the strain measured at one position in each of the three grains are shown in Fig. 10.

The substantial drop in strain level in the region under the hillock can be understood from geometrical reasons. Because the diameter of the interconnect increases underneath the hillock, a force balance with the surrounding material is achieved at a lower strain level. This would also explain a peak in the strain level at the positions immediately adjacent to the hillock. Finite element simulations for a hillock with a comparable change in height also predict a decrease in tensile strain in the x-direction as shown in Fig. 11. A comparison with the experimental strain values given in Fig. 9 shows that both values coincide to within the error bars. However, this cannot explain the asymmetry which is evident in Fig. 9 with a strong peak only being visible in the small grain on the right side of the hillock. This asymmetry is a clear indication of electromigration-induced strain effects which in this case seem to be retained in the final TEM specimen.

The present measurements were performed ex-situ at room temperature. Despite the fact that strain inhomogeneities have clearly been identified, it is difficult to conclude on the variation of the strain during the electromigration tests. A knowledge of the actual stress state is important because it has a strong influence on both plastic and diffusional processes. With respect to the plastic behaviour, the grains do not show major differences. Table 4 summarises the geometrical data of the investigated four grains including the sample coordinate system and the zone axis which was chosen for the strain measurement. The plot of the stress in Fig. 9 shows that the interconnect exhibits approximately a uniaxial stress state. Using this assumption the Schmid factors were calculated. Listed in Table 4 are the slip systems with the largest Schmid factor. All the grains have an orientation which approximately corresponds to a 111 texture and in

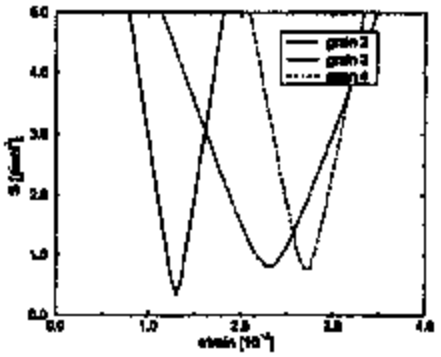

Fig. 10. Examples of the values of the goodness-of-fit parameter S as a function of the tensile strain in the x-direction for three different grains. The width of the curves is a measure of the statistical error in the measurement. As has been discussed in Fig. 8, the S-curves also show that the strain under the hillock is significantly lower than in the grain next to it.

Fig. 11. Finite element simulation of an interconnect line with a hillock. Shown is the strain component in the direction of the line. The experimentally observed drop of the strain ε_x underneath the hillock is predicted by the model.

Table 4
Geometrical data of the investigated grains: The crystal coordinate system is defined by the plane parallel to the silicon substrate surface and the direction along the interconnect line

Grain	Zone axis	Crystal coordinate (hkl) [uvw]	Schmid factor	Glide system (hkl) [uvw]
1	[1 2 5]	(8 5 −4) [6 −8 3]	0.467	(1 −1 −1) [0 1 −1]
2	[1 3 3]	(5 −7 5) [−8 −2 5]	0.483	(1 −1 −1) [1 1 0]
3	[3 3 4]	(−8 5 2) [1 4 −5]	0.459	(1 −1 1) [1 0 −1]
4	[3 3 4]	(−3 8 −5) [8 0 −6]	0.468	(1 1 −1) [1 −1 0]

each grain a slip system with a relatively high Schmid factor can be found. Therefore, none of the grains seems to be favoured with respect to plastic yielding.

The strain state measured in the present analysis is dominated by the thermal strain induced by cooling to room temperature. The reduction in the strain level underneath the hillock can mainly be attributed to the change in the geometrical thickness underneath the hillock. For the direct investigation of electromigration-induced changes we are planning to perform in-situ experiments using a special holder which has been built for that purpose.

6. Conclusions

In the present work we have shown that strain measurement with CBED increasingly becomes a standardized task which can be applied to real materials systems. The aluminium interconnects which we have treated in the present paper are a very good example for this. In this special case the specimen geometry required for the TEM experiments is not significantly different from the actual geometry of the interconnects in the semiconductor devices. From the experimental side, two major achievements have contributed to the quality of the experiments: (1) Energy filtering enables one to remove the inelastic scattering background in electron diffraction patterns and makes it possible now to obtain data of a similar quality as the competing diffraction techniques. (2) The methods for TEM specimen preparation have constantly been improved and in particular the new FIB technique is of great value for experiments in the area of structured thin films.

Based on the excellent data quality which can now be obtained experimentally we have tried to optimize the algorithms for the data evaluation. This involves a number of separate steps: (1) The identification of the HOLZ line positions, (2) a reference measurement to determine the high voltage, (3) the simulation of the HOLZ line positions for varying strain states and (4) a refinement process in which the simulation is brought into agreement with the experiment. In the present paper, we have tried to outline the complete procedure for the Al interconnects which we have chosen as an example. The contributions which we have made to the individual steps listed above will be discussed in the following.

The automated detection of the HOLZ lines in the experimental patterns so far has been one of the unresolved issues and all the techniques used previously needed manual input and frequently were limited in accuracy. Our novel approach of using the Hough transform combines both convenience and high accuracy in the detection of HOLZ line positions. The whole procedure can be highly automated and makes it possible to measure strain with an accuracy of about 10^{-4}, which is close to the physical limits of the technique. In order to achieve this high strain resolution we had to extend the whole procedure to sub-pixel accuracy. Furthermore, it is advantageous to remove any areas where strong dynamical effects occur prior to the analysis of the patterns. Therefore, we mask all the HOLZ line intersections and strong Bragg lines prior to transforming the pattern. Although this increases the effort which has to be made to evaluate the

pattern and cannot be fully automated in each case, it significantly increases the reliability of the results.

Another important question is the treatment of the dynamical effects. Although using a fully dynamical Bloch wave calculation is state of the art in the evaluation of CBED patterns, such calculations are still much too time consuming if a multi-dimensional parameter space has to be explored in a refinement of the strain state. Therefore in many investigations the effective high-voltage method has been used as a first order correction for the dynamical line shift in a kinematical simulation. In the present paper, we have shown that the effectiveness of this correction depends strongly on the shape of the dispersion surface and whether there are reflections from more than one Laue zone involved. In order to avoid these pitfalls we have developed a correction scheme which corrects for the dynamical shifts of each HOLZ line separately. In a kinematical simulation, a correction factor is assigned to each HOLZ line individually which accounts for the detailed shape of the dispersion surface in the given zone axis or crystal orientation. The validity of this correction scheme can be expanded to heavier elements, like Cu, Fe or Ni, for which the effective high-voltage method may lead to very inaccurate results.

Our present experiments have given a very detailed picture of the three-dimensional strain state in the interconnect. Interesting variations have been observed in an area where a hillock has been formed during electromigration experiments performed prior to the TEM characterisation. A detailed comparison with the results of finite element modelling revealed that most of the strain originates from the difference in thermal expansion coefficients for the materials involved. However, there are indications that diffusional processes during the electromigration tests lead to an asymmetry in the strain state and that these effects can be retained in a TEM specimen after electromigration testing. In order to resolve these issues we are planning to perform the next set of experiments in-situ using a special holder which has been built for that purpose.

In summary, our results show that even while cooling only moderately, i.e. to room temperature, strains develop in the thin interconnect which already exceed the yield stress of commercial purity bulk aluminium. While this has been known and does not lead to failure of the line, our spatially resolved experiments show that pronounced strain and thus stress maxima exist in the vicinity of hillocks which are the most probable failure sites. In future experiments we are planning to investigate the influence of the electromigration process itself on these peak stresses.

Acknowledgements

The authors would like to thank C. Volkert and R. Spolenak for many helpful discussions. Support by the Volkswagen-Stiftung is gratefully acknowledged.

References

[1] J.C.H. Spence, J.M. Zuo, Electron Microdiffraction, Plenum Press, New York, 1992.
[2] J.M. Zuo, Ultramicroscopy 41 (1991) 211–223.
[3] S.J. Rozeveld, J.M. Howe, S. Schmauder, Acta Metall. Mater. 40 (1992) S173–S193.
[4] H.J. Maier, H. Renner, H. Mughrabi, Ultramicroscopy 51 (1993) 136–145.
[5] R. Wittmann, C. Panzinger, D. Gerthsen, Ultramicroscopy 70 (1997) 145–159.
[6] D. Mukherji, R.P. Wahi, Scripta Materialia 36 (1997) 1233–1238.
[7] Y.Y. Qiu, J. Alloys Compounds 234 (1996) 157–166.
[8] M. Saito, T. Aoyama, K. Nakata, T. Suzuki, Jap. J. Appl. Phys. 34 (1995) 330–334.
[9] H. Rose, D. Krahl, in: L. Reimer (Ed.), Energy Filtering Transmission Electron Microscopy, Springer, Berlin, 1995.
[10] W.T. Pike, Ultramicroscopy 51 (1993) 136–145.
[11] C. Deininger, G. Necker, J. Mayer, Ultramicroscopy 34 (1994) 15–30.
[12] S.K. Streiffer, S. Bader, C. Deininger, J. Mayer, M. Rühle, Mat. Res. Soc. Symp. Proc. 343 (1994) 615–620.
[13] Hough, P.V.C, US Patent 3,069,654, 1962.
[14] N.C. Krieger Lassen, PhD Thesis, IMM-PHD-1994-3, Lyngby, Denmark, 1994.
[15] R.A. Schwarzer, Micron 28 (1997) 249–265.
[16] S. Krämer, J. Mayer, J. Microscopy 194 (1999) 2–11.
[17] C. Wu, C.A. Volkert, Mat. Res. Soc. Symp. Proc. 516 (1998) 33–43.
[18] S.R. Deans, IEEE Trans. Pattern. Anal., Machine Intell. 3 (1981) 185–188.

[19] J.M. Zuo, J.C.H. Spence, Ultramicroscopy 35 (1991) 185–196.
[20] E.G. Bithell, W.M. Stobbs, J. Microscopy 153 (1989) 39–49.
[21] Y.P. Lin, D.M. Bird, R. Vincent, Ultramicroscopy 27 (1989) 233–240.
[22] I. Mansfield, D. Bird, M. Saunders, Ultramicroscopy 48 (1993) 1–11.
[23] W.H. Press, B.P. Flannery, S.A. Teukolsky, W.T. Vetterling, Numerical Recipes, Cambridge University Press, Cambridge, 1989.

PERGAMON

Microelectronics Reliability 40 (2000) 947–953

MICROELECTRONICS RELIABILITY

www.elsevier.com/locate/microrel

High performance a-Si:H thin film transistors based on aluminum gate metallization

A. Nathan [a,*], R.V.R. Murthy [a], B. Park [a], S.G. Chamberlain [b]

[a] Department of Electrical and Computer Engineering, University of Waterloo, Waterloo, Ont., Canada N2L 3G1
[b] DALSA Inc., 605 McMurray Road, Waterloo, Ont., Canada N2V 2E9

Received 15 November 1999

Abstract

We present a systematic study of the sputter deposition conditions for aluminum thin films employed as gate metallization for high performance a-Si:H thin film transistors (TFTs). Here, we vary sputtering parameters such as deposition temperature, process pressure, and power, all of which have a strong bearing on the surface roughness of the film, including hillock generation induced by thermal processing. For example, at a low deposition temperature (30°C) and a low process pressure (5 mTorr), the surface roughness appeared to be significantly reduced. Transistors with gate metallization deposited under these conditions show a low leakage current (~10 fA), an ON/OFF ratio better than 10^8, and a mobility of 1.1 cm^2/Vs. In contrast, films deposited at 150°C and 10 mTorr, yield a degradation in mobility to 0.77 cm^2/V s and an increase in leakage current to 1 pA, caused by the high interface roughness of the TFT channel due to hillock formation on the Al gate.

1. Introduction

While the demand for displays and image sensor arrays with a larger area and a higher pixel integration is increasing, there remain several fundamental scaling issues associated with gate (and hence, interconnect) metallization of inverted staggered hydrogenated amorphous silicon (a-Si:H) thin film transistors (TFTs) in the active matrix. Presently, high refractory metals such as molybdenum (Mo) and chromium (Cr) are employed. Although these are stable materials, their high resistivity results in RC gate delays that impose constraints on the array size. High conductivity metals such as copper (Cu) and aluminum (Al) are highly desirable, but their use is generally constrained by process considerations. Cu typically suffers from poor adhesion to glass and reacts with silicon and other plasma-enhanced chemical vapor deposition (PECVD) films. These problems are typically overcome, although at the cost of increased process complexity, by depositing the Cu on indium tin oxide (ITO) coated glass for increased adhesion [1] or through self-passivation of the copper surface with Cr_2O_3 to avoid reactions during the PECVD process [2].

With Al, although its resistivity is higher than that of Cu, its adhesion to glass substrates is far better, and more importantly, it constitutes a mature process technology. However, Al can suffer from the problems associated with surface roughness, including possibly hillock generation, induced by subsequent process steps that are relatively high in temperature. In TFT fabrication, the gate metallization is followed by PECVD of amorphous silicon nitride (a-SiN:H) dielectric and a-Si:H active layers. A high surface roughness, as we will observe in the TFT samples considered in this article, increases the leakage current and reduces the field effect mobility. Further, Al migration can potentially lead to short circuits between TFT terminals and interconnects. Although these issues can be avoided by: passivating or capping the Al surface with a mechanically hard metal layer [3]; using a relatively low resistivity Al alloys [4–6]; anodizing the Al at room temperature prior to deposition of the PECVD films [7,8], these solutions require

* Corresponding author.
E-mail address: anathan@venus.uwaterloo.ca (A. Nathan).

0026-2714/00/$ - see front matter
PII: S0026-2714(00)00012-3

additional processing steps associated with lithography, deposition, and annealing, thus adding to process complexity and cost.

It is well known that the surface morphology depends on the film's microstructure and its thermal processing conditions. The microstructure, to a large extent, can be controlled through a careful selection of parameters associated with the sputter deposition process. In this article, the sputtering deposition conditions for the Al gate metal are varied in terms of deposition temperature, process pressure, and DC power, and the performance of corresponding TFTs are compared in terms of leakage current and field effect mobility.

2. Process description and results

To investigate surface morphology, Al films of thickness 150 nm were deposited on Corning 7059 glass substrates by DC magnetron sputtering under different deposition conditions (Table 1), and all films were subsequently annealed at 260°C for 12 h to maintain consistency with the PECVD processes pertinent to TFT fabrication.

Fig. 1 shows SEM micrographs of the Al film surface for deposition temperatures of 150°C, 100°C and 30°C. Here, the process pressure and the power were fixed at 10 mTorr and 400 W, respectively. From these SEM micrographs, the films deposited at 30°C appear to have smoother surface texture than those deposited at a higher temperature.

To further investigate the surface smoothness as a function of the deposition pressure, we deposited films at 5, 10 and 20 mTorr (Fig. 2). In this set of experiments, the deposition temperature was set to be 30°C, and power was 400 W. Here, we observe that the films deposited at 5 mTorr show very smooth texture as compared to their high pressure counterparts.

Maintaining the same process temperature, we deposited films under a different sputtering power, but at low process pressures to observe possible changes in film morphology. Fig. 3 shows SEM micrographs of Al films deposited at 200, 300 and 400 W, with the deposition temperature and the process pressure fixed at 30°C and 5 mTorr, respectively. Here, we observe that the surface of films deposited at 300 W are smooth and free from pinholes or voids, as compared to the samples deposited at 200 or 400 W.

To investigate the impact of gate surface morphology on TFT performance, we chose films with the two contrasting surfaces shown in Figs. 1(a) and 3(b). In addition, with the former, we employed a 20 nm Mo capping layer on the Al gate of the TFT to investigate the degree of roughness propagation to the active interface. What we have presented is just a qualitative assessment of the film's microstructure. Quantitative estimates of the microstructure (e.g. grain size, roughness) associated with the different deposition conditions stated above, requires X-ray diffraction (XRD), atomic force microscopy (AFM), stress, and density measurements. Work along these lines is currently in progress.

Table 1
A summary of the deposition parameters for Al used in this study

	Substrate temperature (°C)	Process pressure (mTorr)	DC Power (W)
Al	30, 100, and 150	5, 10, and 20	200, 300, and 400

3. Thin film transistor fabrication and characterization

The TFTs used in this work are based on the conventional inverted staggered structure which is widely used in a-Si:H large area displays and imaging systems. A fully wet etch process has been used in fabrication. Here, Corning 7059 glass wafers are used as the substrate material. Various Al films of 150 nm thickness are deposited on these wafers under the different conditions given in Table 2. After patterning of the Al, 250 nm of gate a-SiN_x:H, 50 nm a-Si:H layer, and 250 nm of top a-SiN_x:H are deposited in a parallel-plate electrode PECVD system within one vacuum-pump-down cycle to minimize the density of defect states at interfaces. The deposition temperature of these layers is 260°C. At source and drain regions, a highly doped microcrystalline (n^+μc-Si:H) layer is employed to reduce contact resistance with final Al metallization.

A variety of TFTs were fabricated and characterized for their current–voltage and transfer characteristics. The TFT samples were annealed at 170°C prior to DC characterization. All measurements were performed using a DC parametric test system comprising the Keithley 236 source measure units with the TFT source grounded.

Fig. 4 shows SEM cross-sections of the gate/insulator interface of TFTs fabricated at the deposition conditions as indicated. Also shown are the corresponding transfer characteristics (I_{DS} versus V_{GS}) for various V_{DS} and stability behavior ($\sqrt{I_{DS}}$ versus V_{GS}) for different time durations of electrical stress. The latter serves as a measure for the metastable shift in threshold voltage with extended bias durations.

Transistors with gate metallization deposited at 30°C/5 mTorr/300 W show a low leakage current (~10 fA at low V_{DS}), an ON/OFF current ratio better than 10^8, and a mobility of 1.1 cm^2/Vs. These values are comparable to those reported for TFTs with anodized

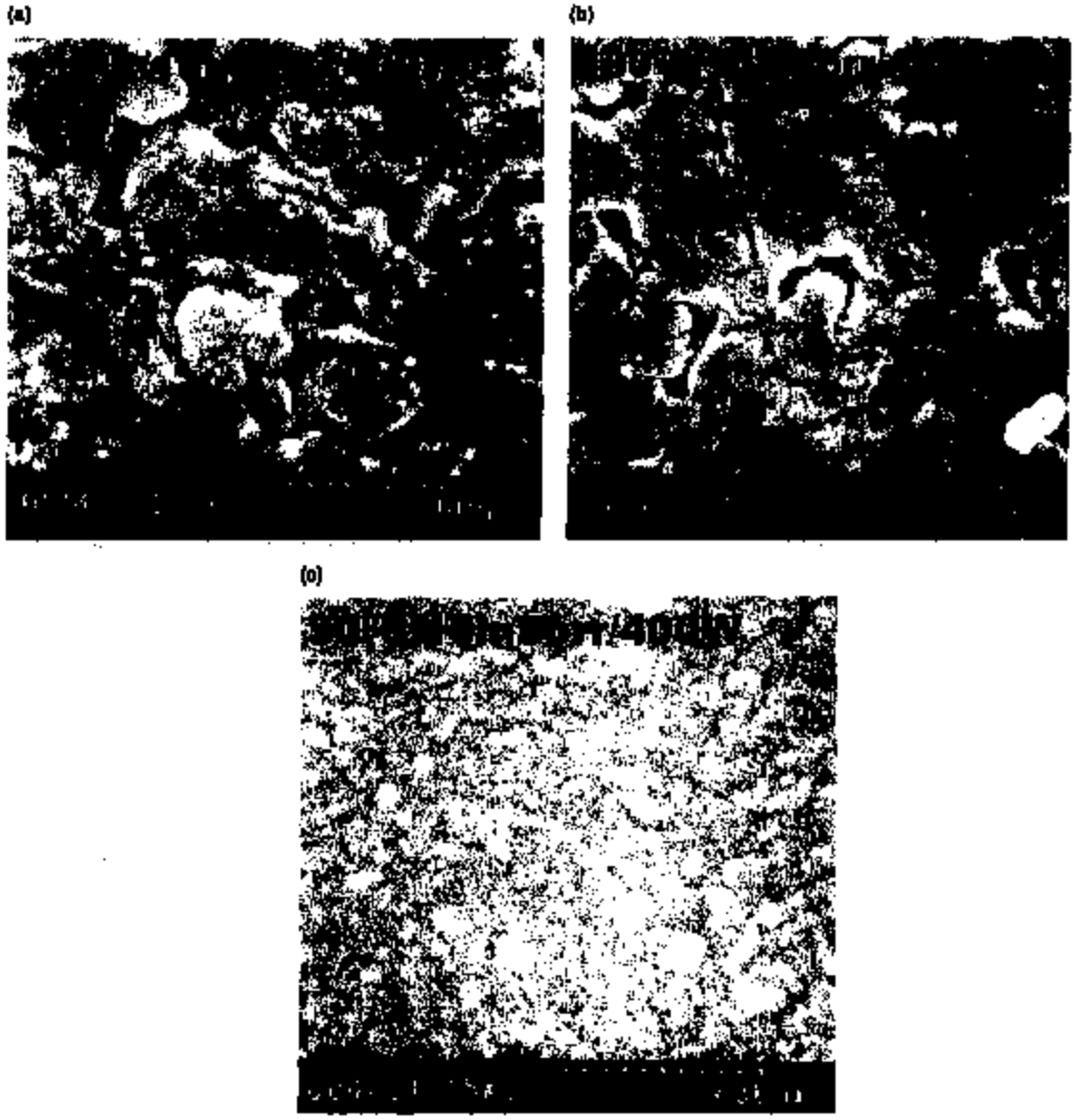

Fig. 1. SEM micrographs of the Al films deposited at (a) 150°C, (b) 100°C, and (c) 30°C, and subject to thermal annealing at 260°C for 12 h. The process pressure and power were fixed at 10 mTorr and 400 W, respectively.

Al gate [8]. In contrast, films deposited at 150°C/10 mTorr/400 W, yield a significant degradation in leakage current (~1 pA) and mobility (0.77 $cm^2/V s$). The reasons for the degradation are clear from observing the cross-section topologies shown in the figure. Here, we note a high surface roughness of the a-SiN_x:H gate insulator, and hence the TFT channel, caused by hillock formation on the Al gate. Note also that the corresponding shift in the threshold voltage is large. After 1 h bias stress of +25 V applied to the gate, the shift in threshold voltage is ΔV_T, ~5 V, as compared to the small shift of ΔV_T, ~2.3 V associated with the smoother gate. We attribute this to the metastability in the active a-Si:H layer induced by large (and perhaps even singular) localized electric fields stemming from surface non-uniformity in the channel. The same reasons hold for the leakage current. Large localized electric fields in the active region, stemming either from surface non-uniformities or

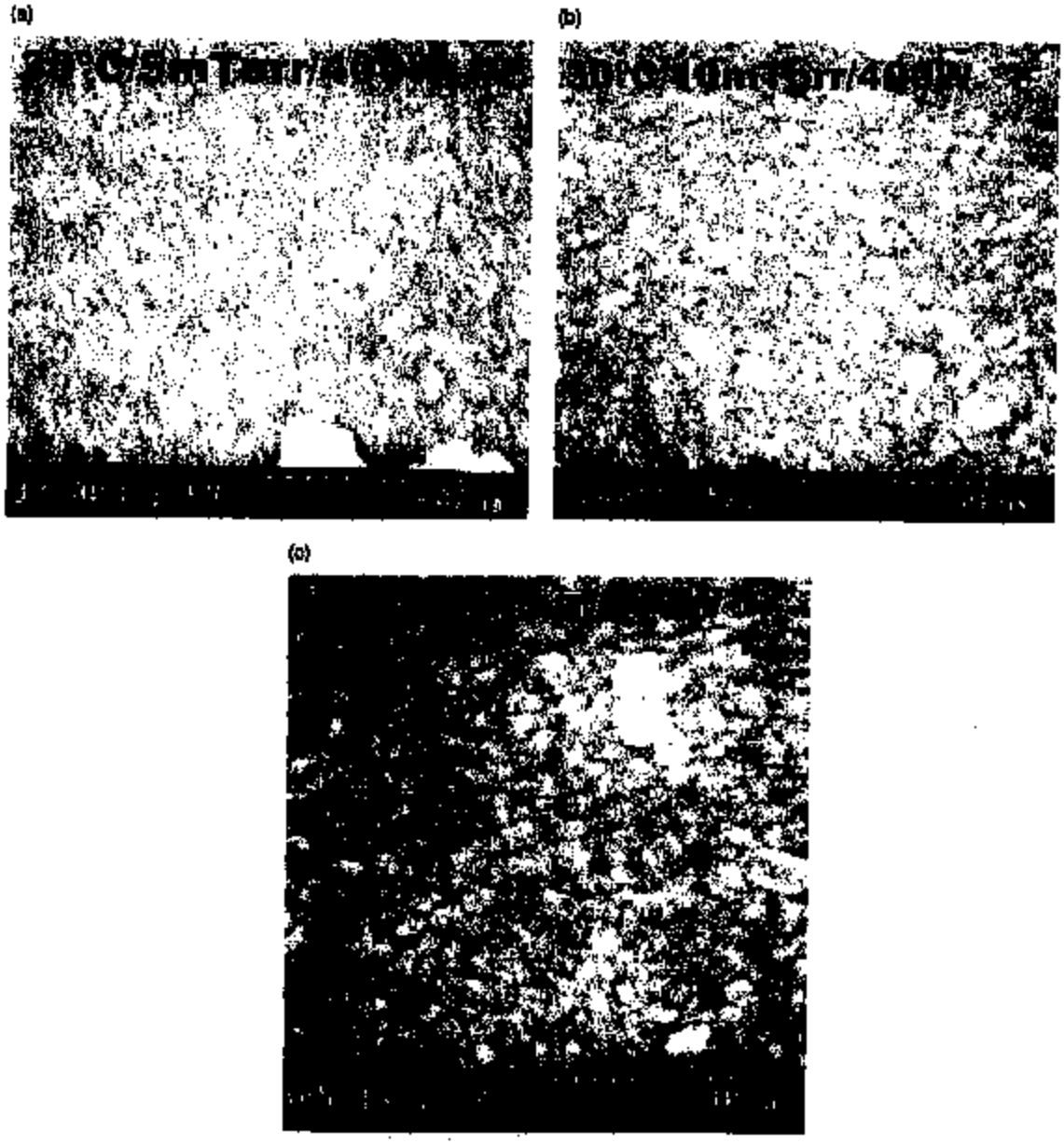

Fig. 2. SEM micrographs of the Al films deposited at (a) 5 mTorr, (b) 10 mTorr, and (c) 20 mTorr, and subject to thermal annealing at 260°C for 12 h. The deposition temperature and power were fixed at 30°C and 400 W, respectively.

applied bias (large V_{DG}), lead to an electric field dependent Frenkel–Poole type carrier generation in the active region [9]. Thus, the leakage current increases with increasing interface roughness as well as high reverse gate voltages. The field effect mobility in these transistors (Table 2), retrieved from the associated transfer characteristics, clearly shows the impact of surface roughness on mobility degradation.

For comparison, we have also included the cross-section of the TFT interface, whose Al gate is now capped with 20 nm of Mo to minimize propagation of the gate surface roughness (caused by hillock generation) to the active channel. It is clear from the cross-sectional views that the interface smoothness is as good or better, to yield improved leakage and stability characteristics.

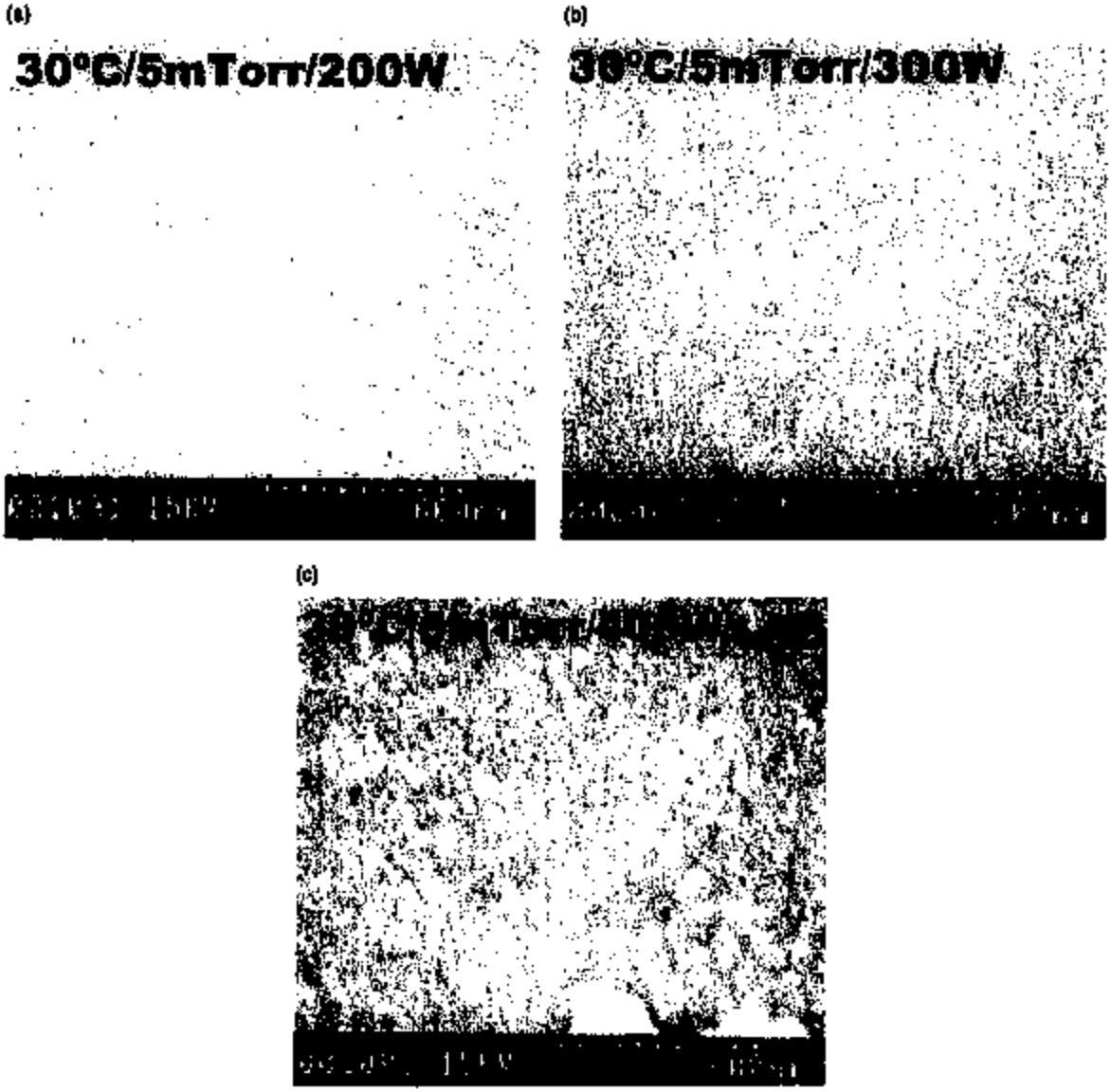

Fig. 3. SEM micrographs of the Al films deposited at (a) 200 W, (b) 300 W, and (c) 400 W, and subject to thermal annealing at 260°C for 12 h. The process pressure and temperature were fixed at 5 mTorr and 30°C, respectively.

Table 2
Values of field effect mobility retrieved from the transfer characteristics of TFTs shown in Fig. 4

Deposition conditions for Al gate	Field effect mobility (cm^2/Vs)
150°C/10 mTorr/400 W (Fig. 1(a))	0.77
30°C/5 mTorr/200 W (Fig. 3(b))	1.1

4. Conclusions

In this article, we present process considerations for Al gate metallization for a-Si:H TFTs with improved leakage current, mobility, and stability. Here, the sputter deposition conditions, i.e. deposition temperature, process pressure, and power, are varied to reduce surface roughness. A low interface roughness was achieved for TFTs with the Al gate deposited at low temperature and low pressure to yield characteristics with low leakage

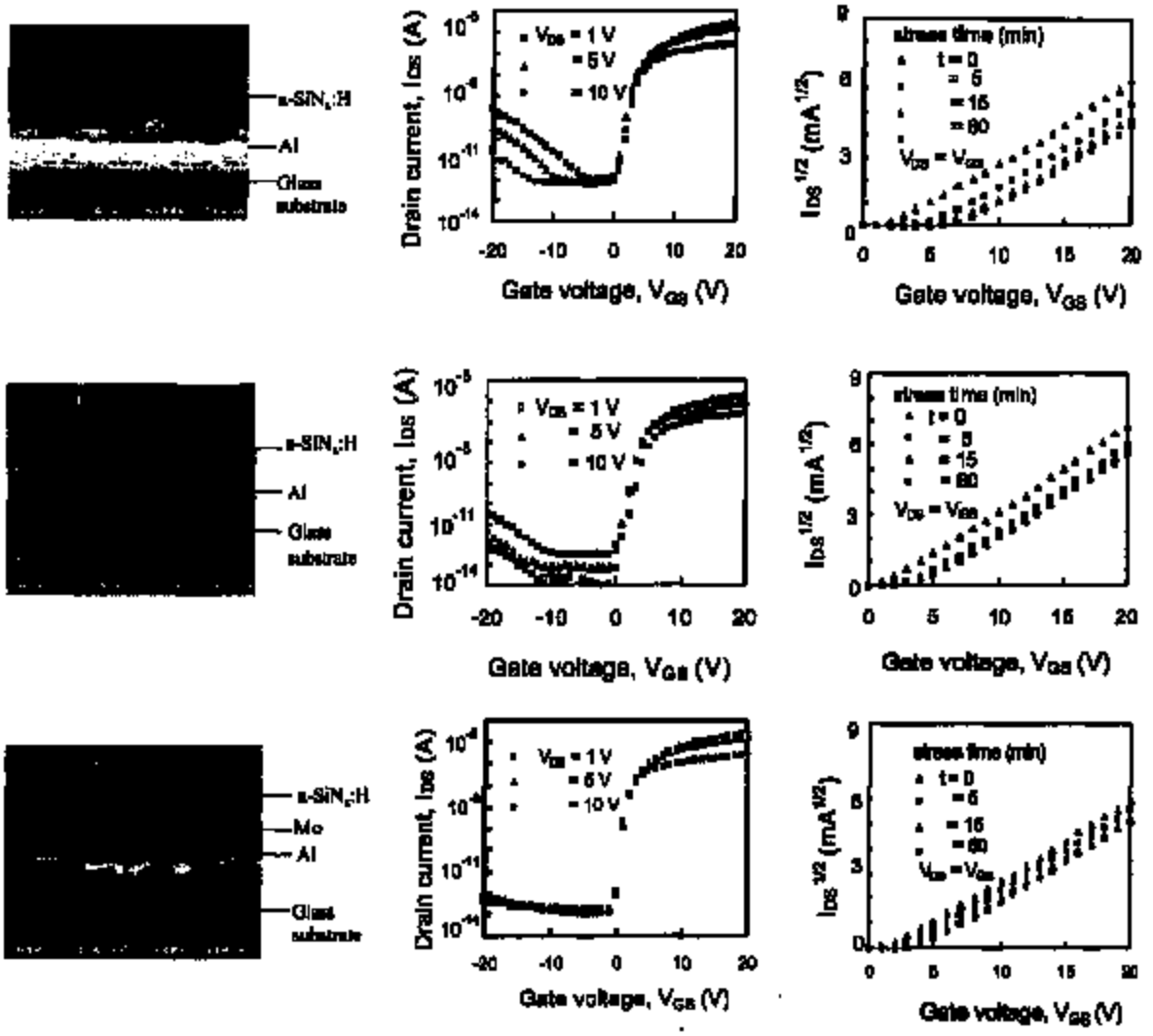

Fig. 4. Cross-sections of the gate/insulator interface and corresponding transfer characteristics (I_{DS} versus V_{GS}), at various drain source voltages (V_{DS}), and stability behavior (for $V_{GS} = V_{DS}$), when subject to electrical stress for time durations of 0, 5, 15, and 60 min. The TFTs were fabricated with the Al gate deposited under the conditions given in Table 2.

current (~10 fA), an ON/OFF ratio better than 10^8, and a high field effect mobility (1.1 cm^2/V s). These values are comparable to TFTs fabricated using anodized or Mo capped Al gates, both of which add to process complexity and cost.

Acknowledgements

This work is supported by the DALSA/NSERC Industrial Research Chair Program, Communications and Information Technology Ontario (CITO), and the Natural Science and Engineering Research Council of Canada.

References

[1] Fryer PM, Colgan EC, Galligan E, Graham W, Horton R, Hunt D, Latzko K, Nywening R, Jenkins L, John R, Koke P, Kuo Y, Libsch F, Lien A, Lovas L, Polastre R, Rothwell ME, Souk J, Wilson J, Wisnieff R, Wright S. SID Int Symp Dig Tech Papers, 1996. p. 333.

[2] Stringhaus H, Thaisa SD, Kahn A, Wagner S. IEEE Trans Electron Dev Lett 1997;18:388.
[3] Tsujimura T, Kitahara H, Makita A, Fryer P, Bailey J. Int Disp Res Conf, 1996. p. 142.
[4] Kim CW, Jeong CO, Song HS, Kim YS, Kim JH, Choi JH, Hur MK, Yang HG, Souk JH. SID Int Symp Dig Tech Papers, 1996. p. 337.
[5] Hayashi M, Inoue K, Noumi S, Sakata K, Takeguchi T, Morita T, Eguchi T. SID Int Symp Dig Tech Papers, 1997. p. 885.
[6] Takasuji H, Iiyori H, Tsuji S, Tsujimoto K, Kuroda K, Saka H. Mater Res Soc Symp Proc 1997;471:99.
[7] Arai T, Hiramasu Y, Tsuji S. Mater Res Soc Symp Proc 1997;424:37.
[8] Kim JH, Kanicki J, den Boer W. Mater Res Soc Symp Proc 1997;471:111.
[9] Nathan A, Austin M, Pereira D. Correlation between leakage current and overlap capacitance in a-Si:H TFTs. Proc IEEE Workshop Charge-Coupled Dev Adv Image Sensor, Karuizawa, Japan, 1999. p. 126–9.

Pergamon

Canadian Metallurgical Quarterly, Vol. 34, No. 3, pp. 287–292, 1995

0008-4433/95 $9.50 + 0.00

0008-4433(95)00015-1

CORRELATION BETWEEN SPECIAL GRAIN BOUNDARIES AND ELECTROMIGRATION BEHAVIOR OF ALUMINUM THIN FILMS

K. T. LEE,† J. A. SZPUNAR,† A. MORAWIEC,† D. B. KNORR‡ and K. P. RODBELL§

†Department of Mining and Metallurgical Engineering, McGill University, 3450 University Street, Montreal, Quebec, Canada, H3A 2A7
‡Materials Engineering Department, Rensselaer Polytechnic Institute, Troy, NY 12180-3590, U.S.A.
§IBM, T. J. Watson Research Center, P.O. Box 218, Yorktown Heights, NY 10598, U.S.A.

(*Received* 4 *August* 1994; *in revised form* 15 *December* 1994)

Abstract—The texture in thin films develops during processing steps such as deposition and annealing. Recent studies show that texture plays an important role in stress voiding, thermal hillock formation, grain collapse and electromigration failure. Specifically, electromigration failure depends on the grain misorientation distribution, which describes the probability of different grain boundaries and, therefore, links the grain boundary structure to the mass transport that takes place primarily along the grain boundaries. To understand the relationship between the grain misorientation and electromigration lifetime in aluminum thin films, the texture was measured on three sets of films from different manufacturing conditions. The frequency of occurrence of coincidence site lattice (CSL) grain boundaries, which represent special misorientations between grains, was obtained, and electromigration tests were done for all three conditions. Experimental results show that the lifetime of patterned films increases as the amount of {111} texture and the frequency of CSL boundaries increased.

Résumé—La texture des couches minces se développe pendant des étapes de traitement telles que le dépôt et le recuit. Des études récentes démontrent que la texture joue un rôle important dans l'annulation de la fatigue, la formation de pic thermique, la déformation des grains et la rupture par électromigration. Spécifiquement, la rupture par électromigration dépend de la distribution de mésorientation des grains laquelle décrit la probabilité de différents joints de grains et, donc, relie la structure des joints de grains au transport massif qui a lieu le long des joints de grains. Pour comprendre la relation entre la mésorientation des grains et la durée de vie de l'électromigration dans des couches minces d'aluminium, on mesure la texture de trois couches fabriquées dans des conditions différentes. Nous avons obtenu une fréquence de l'occurrence de joints de grains à réseau de coïncidence (CSL) qui représente des mésorientations spéciales entre les grains, et nous avons fait des tests sur l'électromigration dans les trois conditions. Les résultats expérimentaux démontrent que la durée de vie des couches modelées augmente quand la quantité de texture {111} et la fréquence des joints CSL augmentent.

1. INTRODUCTION

Because of the increasing sophistication in multilayer interconnect structures of silicon integrated circuit chips, thin film multilayers are becoming smaller and more complex, which induces various types of failure. One of the important mechanisms of failure in thin films is electromigration failure. Many factors influence the electromigration lifetime of thin films, including texture [1–4]. Texture in thin films develops during deposition processes such as evaporation, sputtering, chemical vapor deposition, and electrochemical deposition. In fact, it is rather difficult to deposit a sample without texture. Recent studies show that the activation energy for electromigration is texture dependent and that a strong {111} texture in aluminum thin film improves the electromigration lifetime [5, 6].

During the last few years, the research on properties of coincidence site lattice (CSL) grain boundaries has intensified, because these boundaries are linked to special physical properties of materials [7–9]. Few systematic studies have investigated the effect of CSL boundaries on electromigration failure of thin films. Fionova [10] showed that a large number of special grain boundaries (CSL boundaries) in annealed films may increase the electromigration lifetime of thin films; however, it is not clearly understood what role the CSL boundaries play in electromigration failure. The main objective of this study is to improve the understanding of the influence of

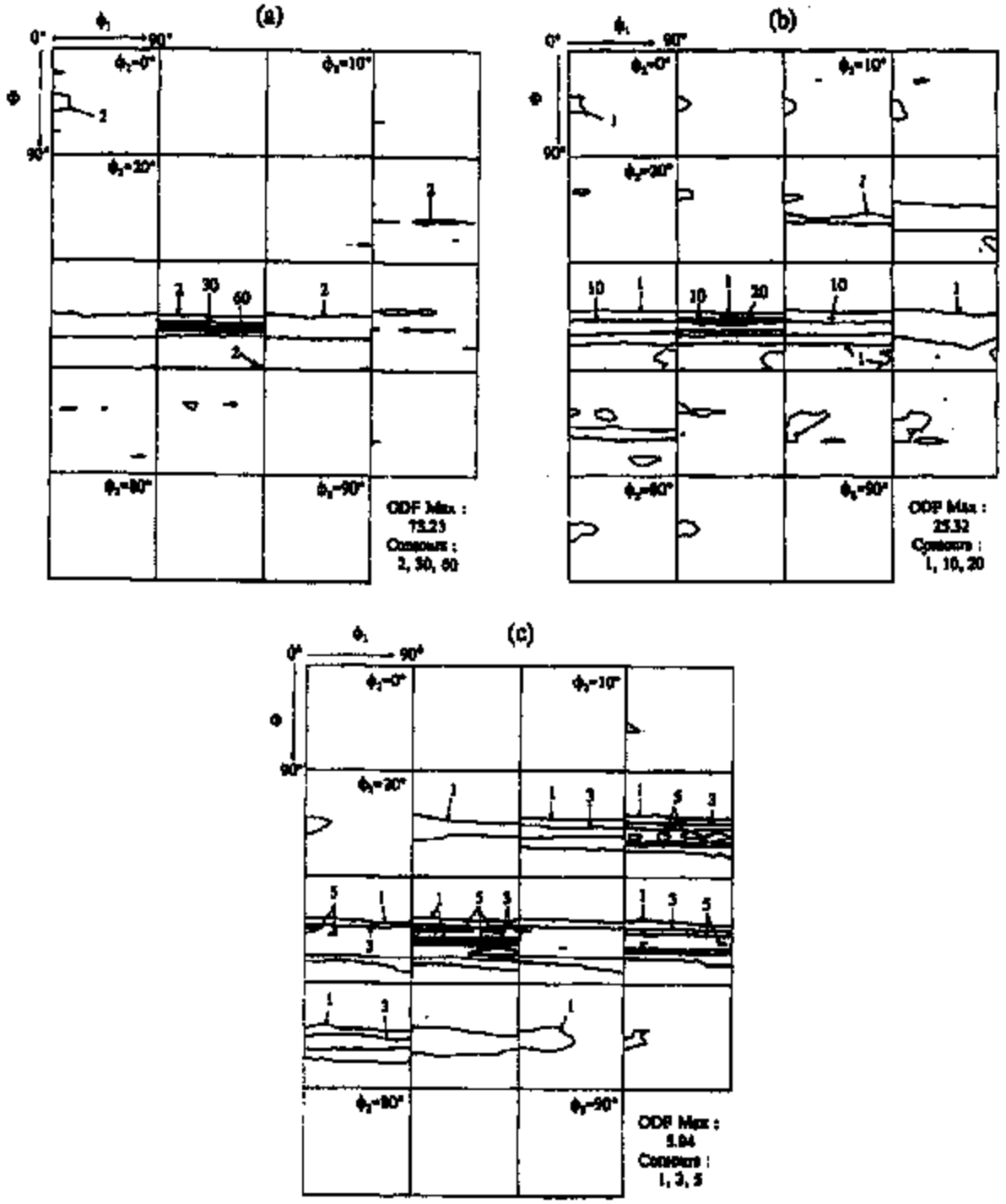

Fig. 1. Orientation distribution function (ODF) for specimens (a) PIB-2/1, (b) PIB-2/2, (c) SP-2.

CSL boundaries in electromigration failure in aluminum thin films.

2. EXPERIMENTAL PROCEDURE

Pure aluminum films were deposited on oxidized silicon by partially ionized beam (PIB) deposition [11] and by sputtering. During PIB deposition, a small fraction of evaporated aluminum atoms was ionized while a potential was applied to the substrate. Both neutral aluminum atoms and self-ions were deposited on the substrate simultaneously. The energetic ions provided enhanced surface mobility during deposition and effective in-situ cleaning. The substrate bias potential (ion energy) was fixed at 2 kV. Two specimens were deposited using the PIB technique with two different ion contents: PIB-2/1 with 1% ion content and PIB-2/2 with 2%. The substrate was held at room temperature, background pressure was 10^{-4} Pa during deposition, and deposition rate was approximately 10 Å/s. The sputtered film, SP-2, was deposited at 2 kV. The aluminum films were 1 μm thick. The samples obtained using the three different processing conditions were annealed at 400°C for an hour in forming gas (90% N_2–10% H_2).

The texture of the films was measured using a Siemens texture measuring system, consisting of a computer controlled horizontal diffractometer with an Eulerian cradle. A molybdenum x-ray source was used. Texture data were collected by step-scanning every 5 degrees over the range $0° \leqslant \alpha \leqslant 85°$ and $0° \leqslant \beta \leqslant 355°$ for the {111} pole figure. Counting time for adequate counting statistics was 2 s/step. The raw data were corrected for defocusing, background, and absorption effects, and then plotted in the form of a pole figure. The corrected data were used as input to calculate the coefficients of the orientation distribution function (ODF).

The ODF data were used to calculate the distribution of CSL boundaries. The computer program for this calculation picks two orientations with probability determined by the ODF, calculates their misorientation and checks if this misorientation is close to given sigma misorientation. The accuracy of coincidence is defined by Brandon's criterion [12], $\Delta\theta = 15° \Sigma^{-1/2}$. The calculation of the frequency of occurrence of CSL boundaries is based on the assumption that the material is spatially disordered, i.e. features such as correlation between orientation of neighbouring grains, inhomogeneities, clustering and grain size effects are not taken into account. The only fact that influences this calculation is the orientation distribution. The calculation is also carried out under the assumption that all of the grains are same size, according to which the frequency obtained represents either the numbers of grain boundaries of a certain misorientation or the total area of such boundaries. Details of this method are described in another paper [13]. Ten thousand pairs of orientations were generated from the ODF and their misorientations were classified as CSL or non-CSL boundaries. The frequency of occurrence of Σ3–Σ27 CSL boundaries was calculated.

For an electromigration analysis, thin films were patterned into test structures by standard silicon processing techniques. At least ten unpassivated lines 1.8 μm wide were tested at a current density of 1×10^6 A/cm^2 and at temperatures of 150, 175, 200, 225 and 253°C. Data for 225°C tests are used in this study.

3. RESULTS AND DISCUSSION

The results of the texture measurements for the PIB-2/1, PIB-2/2 and SP-2 are shown in Fig. 1. All three conditions have a strong {111} fibre texture as seen along the γ fibre ($\Phi = 55.4°$, $0 < \phi_1 < 90$, $f(g) = \phi_2 = 45°$). To clarify the shape of the {111} fibres, the $\phi = 45$ sections of the ODF are presented in Fig. 2 for each specimen. Figures 1 and 2 show that PIB-2/1 has the sharpest {111} fibre texture and that the maximum intensity, which is 73 times random, is located in the centre of the fibre. PIB-2/2 also has a maximum intensity of 25 in the centre, although this maximum is much weaker than that for specimen PIB-2/1. For specimen SP-2, the fibre texture is weak and spread out where the maximum intensity of 6 is located about 10° from the centre of the {111} fibre ($\Phi = 55.4°$, $\phi_2 = 45°$). This type of texture is referred to as near (111) [14].

Figure 3 illustrates the distribution of CSL boundaries up to Σ27 for all three specimens. In all specimens, the frequency of occurrence of the Σ3 and Σ7 boundaries is relatively higher than other CSL boundaries. In addition, the thin films deposited by the partially ionized beam technique (PIB-2/1, PIB-2/2) have higher frequencies of Σ3, Σ7, Σ13b, Σ19b and Σ21a boundaries than the sputtered film (SP-2). PIB-2/1 has a higher frequency of these specific CSL boundaries than PIB-2/2, especially for

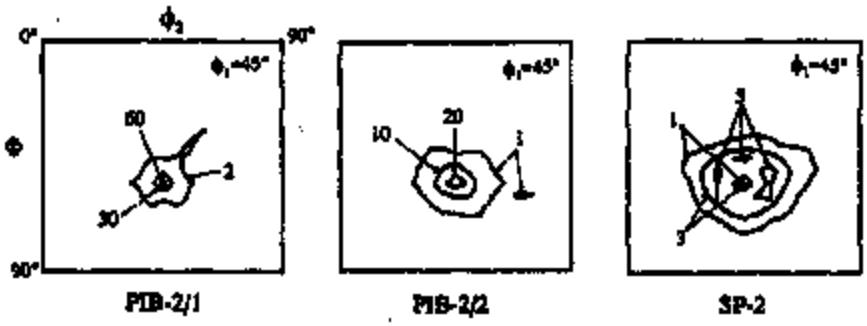

Fig. 2. $\phi_1 = 45°$ sections of the orientation distribution function (ODF) for each specimen.

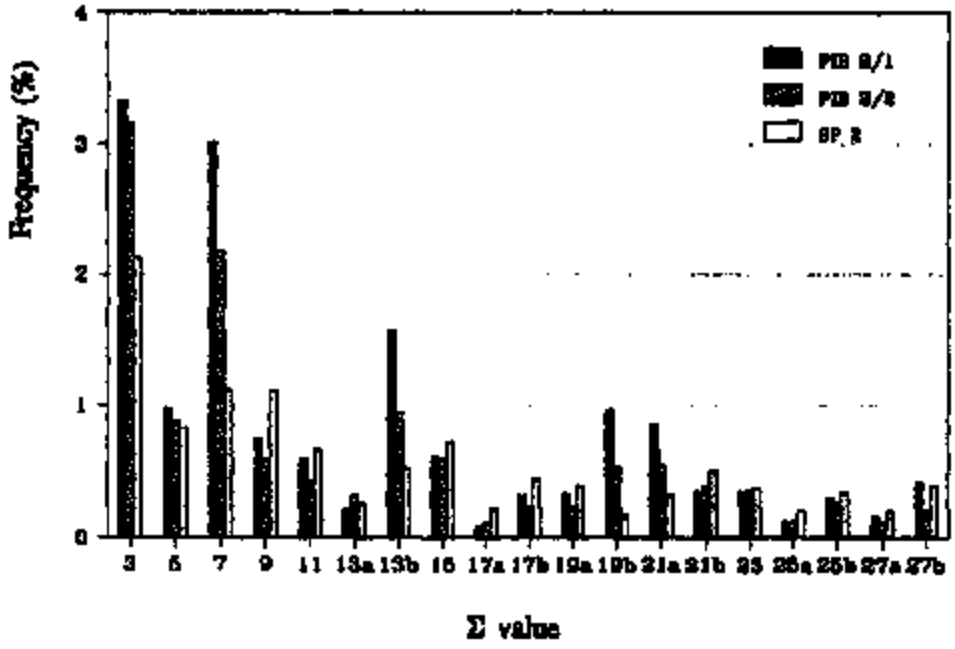

Fig. 3. Distribution of Σ3-Σ27 CSL boundaries in each specimen.

the Σ7 and Σ19b boundaries. Specimen SP-2 has a higher frequency of Σ9, Σ15, Σ17a, Σ17b and Σ21b boundaries.

Figure 4 shows the frequency of occurrence of the most prevalent CSL boundaries as a function of the maximum ODF intensity found for the {111} texture component of each specimen. Figure 4(a)–(c) shows the changes in frequency of occurrence of CSL boundaries having a common ⟨111⟩, ⟨110⟩ and ⟨100⟩ rotation axis, respectively. The frequency of the ⟨111⟩-type grain boundaries (Σ3, Σ7, Σ13b, Σ19b and Σ21a) increases as the intensity of the {111} fibre texture increases [Fig. 4(a)]. The increase of the Σ7 boundaries is the most significant. The frequency of the Σ3 boundaries in the specimen PIB-2/2 was much higher than that in specimen SP-2; however, there is only a small difference between specimens PIB-2/1 and PIB-2/2. In specimen SP-2, which has the weakest {111} texture, there is a higher amount of ⟨110⟩-type CSL boundaries, such as Σ9, Σ11, Σ19a and Σ27a boundaries [Fig. 4(b)]. In the specimen PIB-2/2, the frequency of these boundaries decreases as the maximum intensity of {111} fibre texture increases. However, it increases slightly for the specimen PIB-2/1. The frequency changes of ⟨100⟩-type CSL boundaries are shown in Fig. 4(c). As the maximum intensity of the {111} texture increases, the frequency of the Σ5 CSL boundaries increases, while the frequencies of some other boundaries decrease.

The results of the electromigration tests are shown as a cumulative failure distribution in Fig. 5 and the frequency of occurrence of prevalent CSL boundaries having ⟨111⟩, ⟨110⟩ and ⟨100⟩ rotation axis is illustrated as a function of the median time-to-failure (t_{50} value) in Fig. 6(a)–(c). The frequency change of CSL boundaries as a function of t_{50} value is very similar to the frequency change as a function of intensity of {111} texture component (Fig. 5). The results of the electromigration test are compared to the total frequency of CSL boundaries in Fig. 7. Specimen PIB-2/1 has the highest percentage of CSL boundaries, 14.9%, as well as the longest median time-to-failure, t_{50} = 736 h. Specimen PIB-2/2 has 11.9% of CSL boundaries and a t_{50} value of 235 h. Specimen SP-2 has the shortest lifetime, t_{50} = 106 h, and the lowest percentage of CSL boundaries, 10.4%. Several studies [12, 15, 16] have calculated the frequency of CSL boundaries in materials with a random grain orientation [$f(g)$ = 1]. A total of 9.2% of the boundaries were found to be Σ3-Σ27. This result indicates that the grain boundary texture in SP-2 deviates only slightly from the distribution expected in a random material. Modelling of {111} fibre textures [17] shows that the proportion of CSL boundaries continues to increase as the {111} distribution tightens beyond the levels in PIB-2/1. The trend of an increasing fraction of Σ3, Σ7, Σ13, Σ19 and Σ21 boundaries develops further. Electromigration results on very tightly textured aluminum alloy films [18] demonstrate the continuing trend of substantially longer times to failure with increasing fraction of CSL boundaries.

It is clear from this comparison that there is an association between the time-to-failure and the frequency of occurrence of CSL boundaries; a higher percentage of CSL boundaries correlates with longer lifetime in patterned lines. It is known that the diffusivity along the large-angle grain boundaries depends on the misorientation of grains [19, 20] and that the diffusivity of grain boundaries with special misorientation (CSL boundaries) is less than that for general grain boundaries by several orders of magnitude [19]. It seems that a relatively large frequency of CSL boundaries in the specimen PIB-2/1 has contributed to improvement of its electromigration lifetime. The

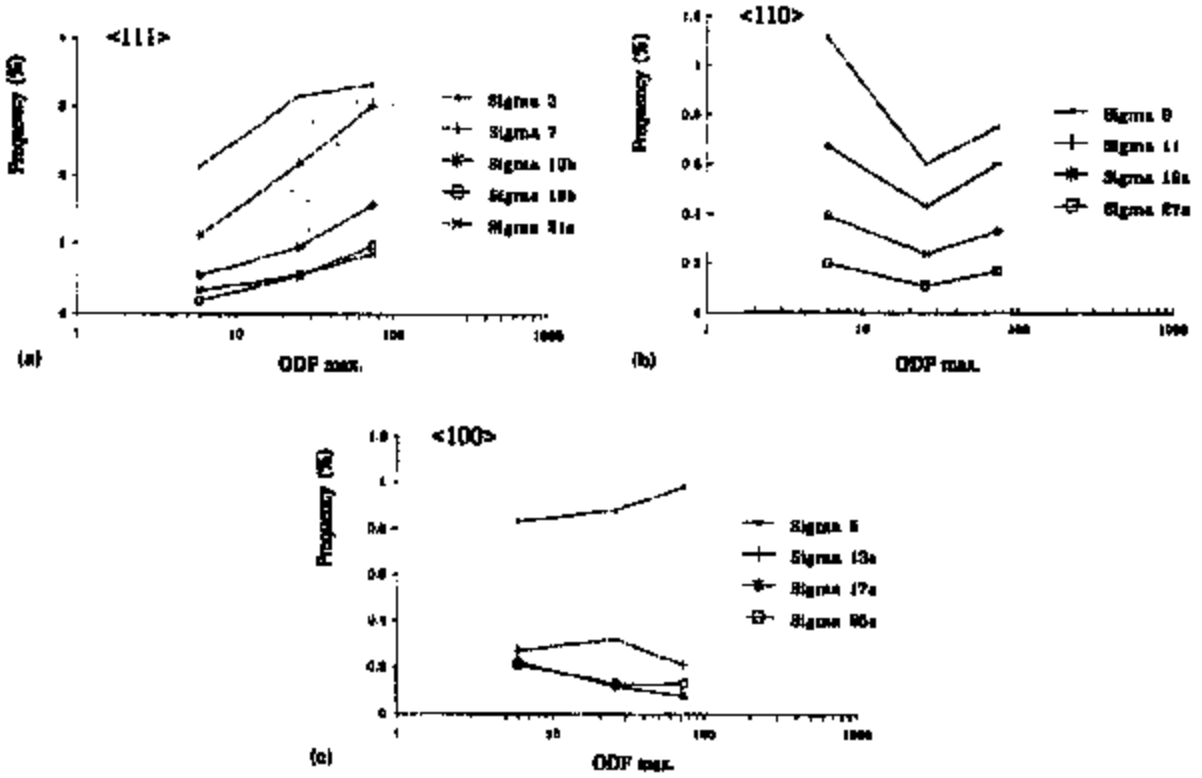

Fig. 4. Frequency of selected CSL boundaries as a function of ODF maximum for: (a) ⟨111⟩-type CSL boundaries; (b) ⟨110⟩-type CSL boundaries; (c) ⟨100⟩-type CSL boundaries.

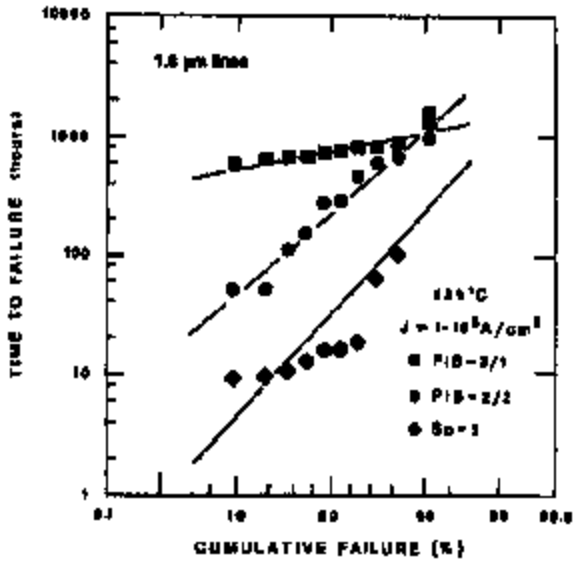

Fig. 5. Electromigration results for three specimens.

specific role of particular grain boundaries is not known. Detailed analyses of the grain orientation from many failure sites and the diffusivity along CSL boundaries are required.

4. CONCLUSIONS

The role of special grain boundaries in electromigration behaviour of aluminum thin films was investigated for three thin film specimens with different textures.

The following conclusions are drawn from this study:

1. Thin films deposited using the PIB technique have a stronger {111} fibre texture and their median time-to-failure is longer than in the thin film deposited by sputtering.
2. The frequency of occurrence of CSL boundaries for specimen PIB-2/1 is higher than that in specimen PIB-2/2, and lowest in specimen SP-2. It seems that the lifetime of thin films increases as the number of special boundaries and the strength of {111} texture increases.
3. As the intensity of the {111} texture increases, the frequency of occurrence of CSL boundaries increases. The electromigration failure in aluminum thin films is correlated with

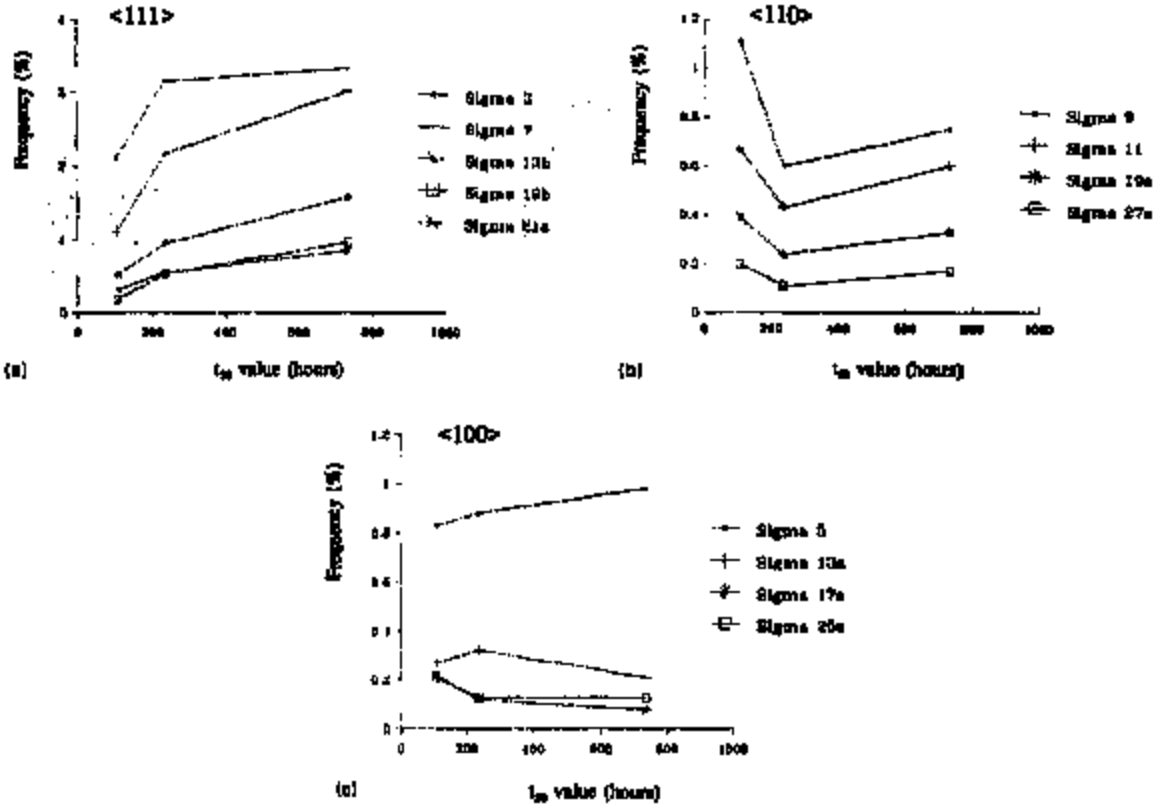

Fig. 6. Frequency of CSL boundaries as a function of median time-to-failure (t_{50} value) for: (a) ⟨111⟩-type CSL boundaries; (b) ⟨110⟩-type CSL boundaries; (c) ⟨100⟩-type CSL boundaries.

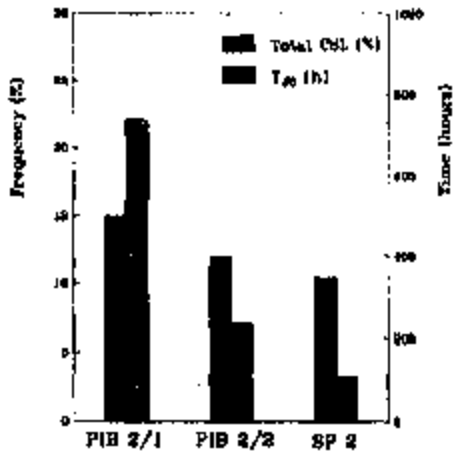

Fig. 7. Comparison of the total frequency of CSL boundaries with the t_{50} value of each specimen.

the frequency of occurrence of CSL boundaries and the strength of {111} texture.

REFERENCES

1. M. J. Attardo and R. Rosenberg, *J. Appl. Phys.* 41, 2381 (1970).
2. E. Nagasawa, H. Okabayashi, T. Nozaki and K. Nikawa, *Proceedings of The 17th Reliability Physics Symposium*, p. 64. IEEE, New York, 1979.
3. K. P. Rodbell, D. B. Knorr and D. P. Tracy, *Proc. Mat. Res. Soc. Symp.* 265, 107 (1992).
4. H. Taniguchi, T. Ushiro, Y. Okamoto, Y. Akagi and M. Kobe, *Proc. Mat. Res. Soc. Symp.* 280, 523 (1993).
5. P. Li, A. S. Yapsir, K. Rajan and T. M. Lu, *Appl. Phys. Lett.* 54, 2443 (1989).
6. D. B. Knorr and K. P. Rodbell, *Proc. Mat. Res. Soc. Symp.* 265, 113 (1992).
7. Tadao Watanabe, *Mater. Sci. Forum* 46, 25 (1989).
8. G. Palumbo, P. J. King, K. T. Aust, U. Erb and P. C. Lichtenberger, *Scripta. Metall.* 25, 177 (1991).
9. J. Harase and R. Shimizu, *Acta Metall.* 40, 1101 (1992).
10. L. K. Fionova, O. V. Kononenko and V. N. Matveev, *Thin Solid Films* 237, 54 (1993).
11. S. N. Niu and T. M. Lu, *J. Vac. Sci. Tech.* A6, 9 (1988).
12. D. G. Brandon, *Acta Metall.* 14, 1479 (1966).
13. A. Morawiec, J. A. Szpunar and D. C. Hina, *Acta Metall.* 41, 2825 (1993).
14. D. B. Knorr, *Proc. Mat. Res. Soc. Symp.* 309, 75 (1993).
15. D. H. Warrington and M. Boon, *Acta Metall.* 23, 599 (1975).
16. A. Garbacz and M. W. Grabski, *Acta Metall.* 41, 469 (1993).
17. A. Garbacz and M. W. Grabski, *Acta Metall.* 41, 475 (1993).
18. H. Toyoda, T. Kawanoue, M. Hasunuma, H. Kaneko and M. Miyauchi, *32nd Annual Proceedings Reliability Physics*, p. 178. IEEE/IRPS, NY, 1994.
19. H. Gleiter and B. Chalmers, *Progr. Mater. Sci.* 16, 142 (1972).
20. R. W. Balluffi, *Metall. Trans. A* 13, 2069 (1982).

ELSEVIER

Thin Solid Films 270 (1995) 450–455

Thin Solid Films

A study of hillock formation on Al–Ta alloy films for interconnections of TFT–LCDs

Eiji Iwamura, Takashi Ohnishi, Kazuo Yoshikawa

Electronics Research Laboratory, Kobe Steel, Ltd., 1-5-5 Takatsukadai, Nishi-ku, Kobe 651-22, Japan

Abstract

The relationship between hillock formation and microstructure was studied in Al–Ta alloy films for interconnections of thin-film transistor–liquid-crystal displays. In-situ scanning electron microscopy observation of hillock formation, transmission electron microscopy studies of microstructures of both the hillock and film, and in-situ stress measurements during isothermal annealing were carried out on Al–2at.%Ta alloy films deposited on glass substrates by d.c. magnetron sputtering. Hillock size increased with annealing temperature and time during variable temperature and isothermal annealing, respectively. Macroscopic hillock number density saturated soon after the appearance of hillocks. New hillocks were observed on the outer perimeter of old hillocks. The distance between hillocks ranged from 20 μm to 100 μm, an extremely large distance in comparison with the grain size. The relationship between hillock formation and microstructures on Al–Ta alloy films can be explained by a model in which hillock formation due to lateral diffusion, i.e. diffusion in the film plane, results in compressive stress relaxation in a large area around the hillock. The fine-grained film structure caused by the addition of Ta plays an important role in reducing hillock density.

Keywords: Aluminium; Tantalum

1. Introduction

Hillock formation in thin films during annealing has been known for many years and has been observed in several materials [1,2]. It is believed that microstructure plays an important role in hillock formation. Transmission electron microscopy (TEM) studies have revealed that hillocks form preferentially on grain boundaries or triple points due to diffusion creep [3–5]. It is also reported that grain size and crystallographic orientation affect hillock formation [6,7]. It is possible to control such microstructures by the addition of a small amount of alloying elements; some additives in Al can result in a decrease of hillock size and density [8–10]. However, the relationship between microstructure and hillock formation, or the mechanism of hillock suppression by alloying is not yet well understood.

Hillock formation, which can lead to electrical shorts during annealing, is one of the most important problems for the interconnections of liquid-crystal displays (LCDs). Aluminum and Al alloy films have recently been applied to interconnections of higher resolution and larger size LCDs with thin-film transistors (TFT). However, most Al alloy films, for instance Al–Cu alloy films which are typical interconnections of large-scale integrated circuits (LSIs), undergo higher temperature processes, and therefore form hillocks during LCD fabrication. Therefore, development of new Al alloy films with high hillock-formation resistance has been a significant important industrial problem.

Al–Ta alloy films have high hillock suppression and low electrical resistivity [11], hence Al–Ta alloy films have begun to be employed for interconnections of TFT–LCDs. In a previous paper, it was shown that atoms which comprised hillocks and whiskers were supplied from inside the film, and there is little Ta content in hillocks [12].

In this study, in-situ scanning electron microscopy (SEM) observation of hillock formation, TEM studies of microstructures of both the hillock and film, and stress measurements during isothermal annealing were carried out on Al–2at.%Ta alloy films in order to understand the effect of Ta addition upon hillock formation. The relationship between hillock formation and microstructures is also discussed.

2. Experimental procedure

Al–2at.%Ta alloy films were deposited by d.c. magnetron sputtering on $BaO–B_2O_3–SiO_2$ glass (Corning No. 7059). The substrates were water cooled during deposition. The base chamber pressure was below 1.0×10^{-6} Torr. The Ar gas pressure during deposition was 2.0×10^{-3} Torr. The sputter-

Elsevier Science S.A.

0040-6090/95/$09.50 SSDI 0040-6090(95)06812-7

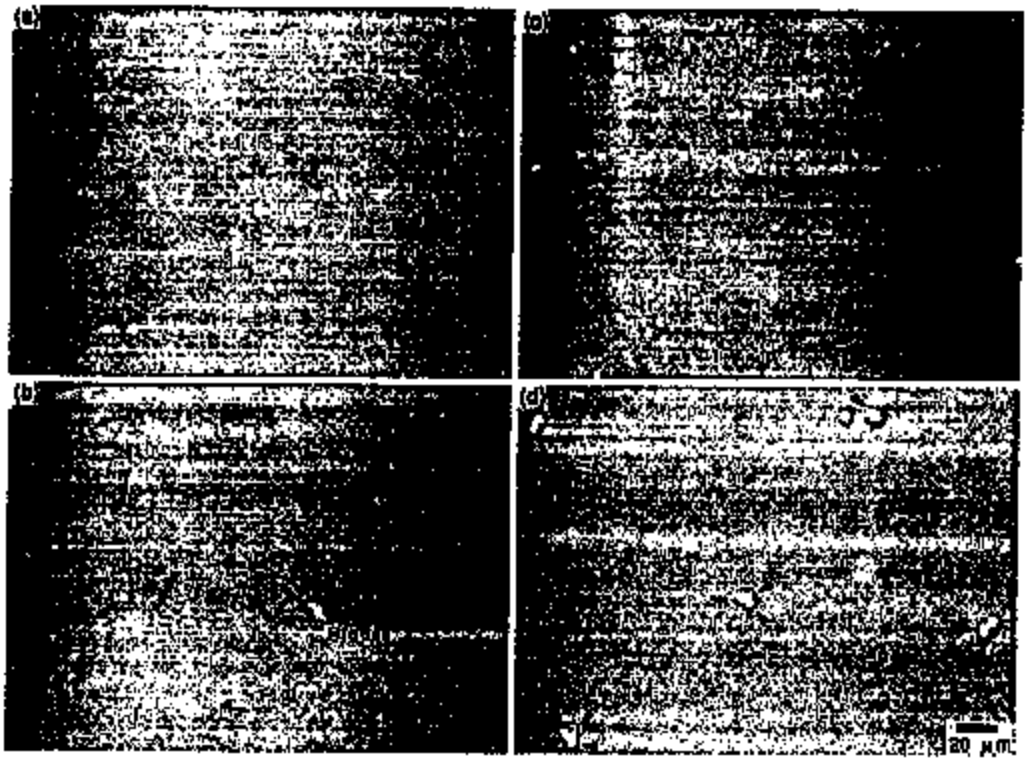

Fig. 1. SEM micrographs of the hillock formation sequence while evaluating the temperature: (a) 525 K, (b) 543 K, (c) 573 K, (d) 573 K. The heating rate was 0.067 K s^{-1}.

ing power density was 3.2 W cm^{-2}. The deposition rate was 2.5 nm s^{-1}. 1-μm-thick films were examined by SEM and TEM, while 400-nm-thick films were used for stress measurements.

Hillock formation on as-deposited films was observed in-situ in a SEM microscope while raising the temperature at a rate of 0.067 K s^{-1} and during annealing at 533 K for 10.8 ks. Samples were mounted on a stage made of stainless steel and heated with a Mo heater, and temperatures were measured by a thermocouple attached on the film side of the specimen. For isothermal annealing, the samples were heated up to 473 K at a rate of 0.17 K s^{-1} and held for 1.8 ks. The heating time from 473 K to 533 K was about 3.6 ks.

Plane-view TEM observations of an as-deposited film, films annealed at 553 K for 14.4 ks and at 673 K for 3.6 ks in a vacuum below 1×10^{-6} Torr were carried out. The cross-section microstructure of a hillock was also observed for the sample annealed at 553 K for 14.4 ks.

The film stresses as a function of isothermal annealing time were measured in-situ by using the substrate-curvature technique [13]. The isothermal annealing for 28.8 ks were carried out after heating up to the temperature 10 K higher than isothermal annealing temperature at a rate of 0.33 K s^{-1} and held for 0.6 ks. The annealing was conducted in a N_2 ambient.

3. Experimental results

3.1. Hillock formation

Fig. 1(a)–(d) show the sequence of hillock formation while elevating the temperature. No hillocks were observed on the film surface at 523 K as shown in Fig. 1(a). Hillocks began to form when the temperature was raised up to about 450 K. Fig. 1(b) was taken soon after the hillocks were identified. The hillock size increased from about 2-μm diameter at 543 K to about 4-μm diameter at 573 K as shown in Fig. 1(c). On further heating, the hillocks grew larger and new hillocks indicated with arrows in Fig. 1(d) were formed at the edges of old hillocks, i.e. hillocks which have already formed. However, no new hillocks were observed among the hillocks. Thereby, the macroscopic hillock density did not change during the annealing. The distance between hillocks ranged from about 20 μm to 100 μm. The position of each hillock also did not change.

Fig. 2(a)–(d) show the sequence of hillock formation during isothermal annealing at 533 K. The first outgrowths as shown in Fig. 2(a) were identified immediately after isothermal treatment started. The hillock number, which is thirteen in Fig. 2, was saturated within less than 0.6 ks as shown in Fig. 2(b). Fig. 2(c) and (d) show the hillock size increased as the annealing time increased. New hillocks were formed at the edge of old hillocks such that the hillock density was constant as shown in Fig. 1(d).

3.2. Microstructures of film and hillock

Fig. 3(a) shows a plan-view TEM micrograph of the as-deposited film. Average grain size of the film was 0.06 μm. Grain growth occurred after annealing as shown in Fig. 3(b) and (c). The average grain size increased to 0.1 μm and 0.21

0040-6090/95/$09.50 SSDI 0040-6090(94)06428

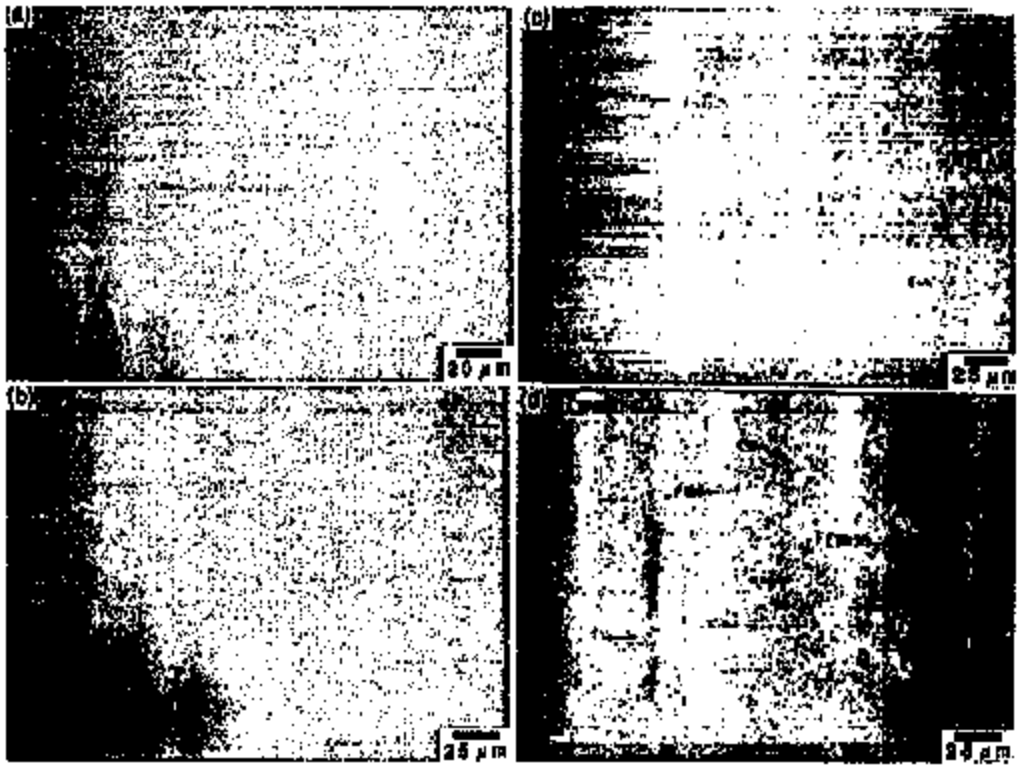

Fig. 2. SEM micrographs of the hillock sequence during isothermal annealing at 533 K: (a) 60 s, (b) 0.6 ks, (c) 2.1 ks, (d) 10.8 ks.

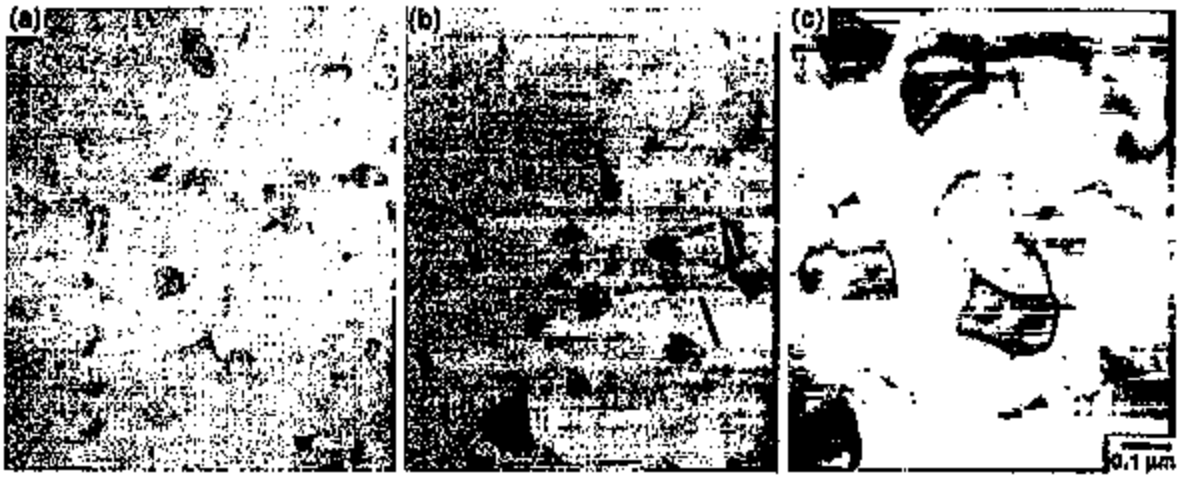

Fig. 3. Plan-view TEM micrographs of Al–2at.%Ta alloy films: (a) as-deposited, (b) annealed at 533 K for 14.4 ks, (c) annealed at 673 K for 3.6 ks.

μm after annealing at 533 K for 14.4 ks and 673 K for 3.6 ks, respectively. Precipitates which were identified as Al_3Ta by X-ray diffraction [14] were observed as shown in Fig. 3(b) and (c) with arrows.

Fig. 4(a) shows a cross-section TEM micrograph of a hillock formed by annealing at 533 for 14.4 ks and the selected-area-electron-diffraction pattern (SADP) from one of the grains in the hillock. This film corresponds to that of Fig. 3(b). The size of the hillock was about 3.4 μm in width and 1.6 μm in height. The hillock was composed of a number of crystallites. SADP indicated the crystallites were Al. The grain size in the hillock ranged from 0.1 μm to 0.8 μm. The microstructure of the hillock, i.e. grain size and shape, was different from that of the film. The film had a semi-columnar structure with small grain size. Fig. 4(b) schematically illustrates the hillock and film geometry. The original film surface (indicated with a dashed line) which should be beneath the hillock disappeared. Some grains in the hillock seemed to grow out into the film underneath the hillock. In particular, the grains in the middle of the hillock incorporate smaller grains in the film. This incorporation extended deep into the film and is indicated with a bold line.

3.3. Stress relaxation

Fig. 5 shows the change of film stress during isothermal annealing at 533 K as a function of annealing time. Com-

0040-6027/95/$09.50

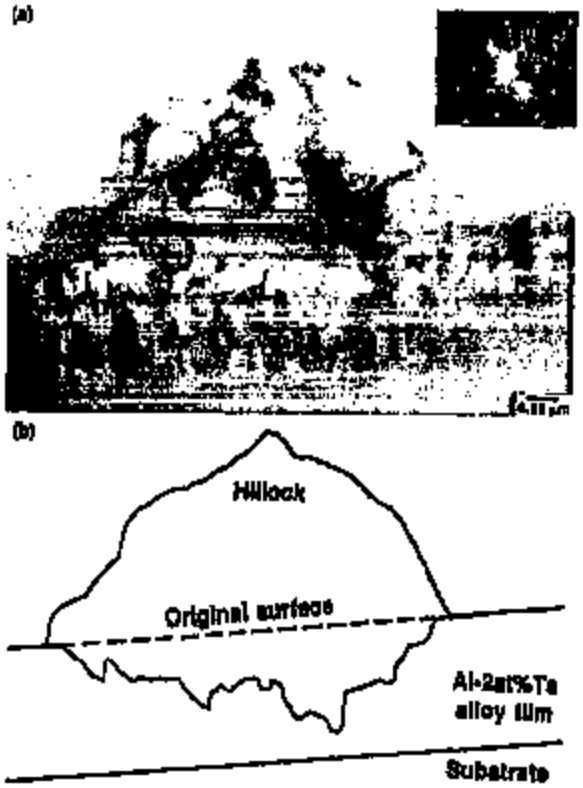

Fig. 4. (a) Cross-section TEM micrograph and (b) schematic drawing showing a hillock on a film annealed at 533 K for 14.4 ks. The inset to (a) shows the SADP of a grain in the hillock.

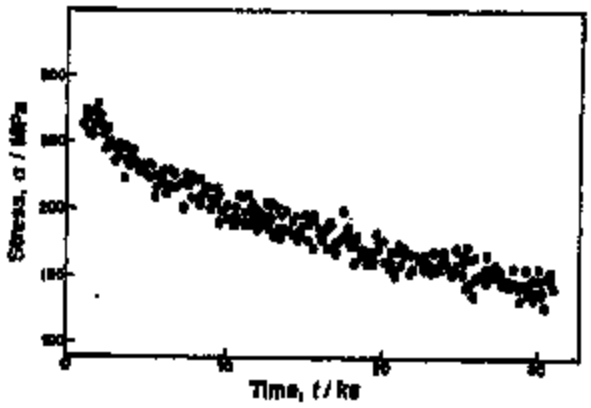

Fig. 5. Annealing-time dependence of compressive stresses for a Al–2at.%Ta alloy film held at 533 K.

pressive stress was about 720 MPa when isothermal annealing started. The stress decreased gradually as the annealing progressed. The change of film stress as a function of time can be described by the standard exponential stress decay expression.

$$\frac{\sigma-\sigma_0}{\sigma_i-\sigma_0}=\exp(-t/\tau)$$

where σ is the stress at time t, σ_0 is the remnant stress, σ_i is the initial stress and τ is the stress-relaxation time constant.

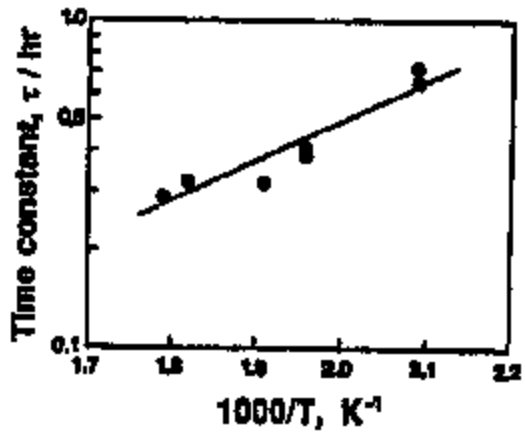

Fig. 6. Temperature dependence of the relaxation-time constant for compressive stress relaxation during isothermal annealing.

Fig. 6 shows the temperature dependence of the stress-relaxation time constant which was obtained by isothermal annealing at various temperature ranging from 473 K to 547 K. This plot gave an activation energy range from 0.3 eV to 0.4 eV. This value is smaller than that reported for the Al thin film, 0.43 eV [15].

4. Discussion

It is generally believed that hillocks form to relieve compressive stress in a film [2,16]. Grain growth [17] and precipitation [18] can also relieve compressive stress. If it is assumed that each of the hillocks which are observed in Fig. 2(d) is hemispherical with a 3.2 μm diameter, the volume ratio between hillocks and film in the area corresponds to 0.2%. The compressive stress σ_c which is relieved by the negative volume change is described by

$$\sigma_c=\frac{E\Delta V}{3(1-\nu)}$$

where $E/(1-\nu)$ is the biaxial elastic modulus of the film and ΔV is $V_{\text{Hillock}}/V_{\text{film}}$. Using the value of $E/(1-\nu)\simeq 1.143\times10^5$ Pa for Al with a (111) orientation, the negative volume change by 0.2% results in a stress of about 76 MPa. In Fig. 5, the film stress dropped from about 270 MPa to about 200 MPa during the annealing for 10.8 ks, hence about 70 MPa was relieved. Therefore, it is reasonable that hillock formation is the dominant stress-relaxation mechanism.

The distance between each hillock ranged over several ten μm, which is much larger than the grain size of the film even after grain growth took place by annealing. There are a large number of grain-boundary triple points that could serve as hillock nucleation sites, however, only a small number of hillocks were observed, and hillock density was saturated in the early stages of the appearance. New hillocks did not form among the hillocks, even though old hillocks grew to huge size with stress relaxation during the annealing.

0040-6090/95/$09.50 SSDI 0040-6090(94)06422-X

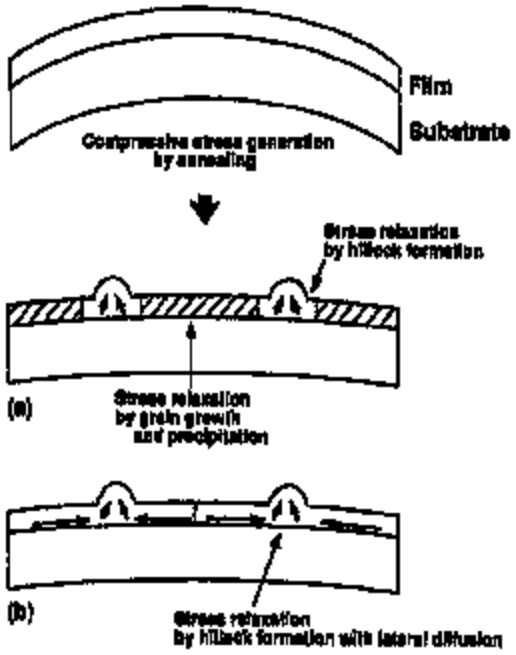

Fig. 7. Schematic drawings of two models relating to the hillock formation behavior on Al–2at.%Ta alloy films.

The question is why hillocks formed with such a low density on the film, even though there are considerable nucleation sites on the film surface.

It is reported that an natural oxide layer on a film and defects in it can influence hillock formation [19,20]. However, the oxide appears to be too pliable to suppress hillock formation [21] and reduce the hillock density. Electron spectroscopy for chemical analysis (ESCA) revealed that the thickness of the oxide layer of Al–2at.%Ta alloy films was almost the same as that of Al–2at.%Cu alloy films on which hillocks can be formed with high density.

Two stress relaxation models are possible to explain this phenomena. One is that hillocks relieve stress only locally around the hillocks, while grain growth and precipitation dominate stress relaxation elsewhere as shown schematically in Fig. 7(a). The other is that hillock formation due to lateral diffusion, i.e. diffusion within the film plane, dominates stress relaxation in a large area around the hillock as shown in Fig. 7(b).

For the former model to hold, there must be a significant difference in microstructures between the near-hillock and inter-hillock regions. However, such a distinct difference was not observed in this study. Furthermore, the hillock size observed in this study is large enough to relieve stress only in the immediate area.

Fig. 8(a)–(c) show schematic drawings of hillock formation based on the latter model comparing the film with fine grains to that with large grains. The former case, corresponding to Al–Ta alloy films in this study, is shown in Fig. 8(a). When hillocks form on the film surface, the atoms diffuse from film into hillock, which gives rise to lateral diffusion through the film around the hillock. In the film with a fine grain structure, lateral diffusion occurs easily along grain boundaries. Thus, the diffusion due to hillock formation may relieve stress in a large area around the hillocks, and hillock formation is suppressed in the neighborhood of the hillock. It is believed that the driving force of the lateral diffusion is a gradient of stress, which can be caused locally due to stress relaxation during hillock formation. It is probable that the compressive stress near hillock becomes lower than that in the neighbor, which results in a stress gradient that may induce the lateral diffusion.

The incorporation of microstructures between a hillock and the film can be responsible for new hillock formation on the outer perimeter of hold hillocks. The incorporation causes a change in the diffusion path by which atoms are supplied to hillocks along grain boundaries. Therefore, new nucleation sites may form at the edge of the old hillocks as shown in Fig. 8(b). It has been shown that underlying grains in Al films grew into the hillocks in some cases [4]. The incorporation may occur via coalescence, however this cannot be proven without clarifying the sequence of the incorporation.

The case of a film with large grain size with columnar structure is shown in Fig. 8(c). The lateral diffusion through bulk is more difficult in comparison with that along lateral grain boundary in the film with fine grains. Vertical diffusion, i.e. diffusion through the film thickness, can be enhanced by vertical grain boundaries, and brings atoms to the film surface. In this case, each grain-boundary triple point on the film

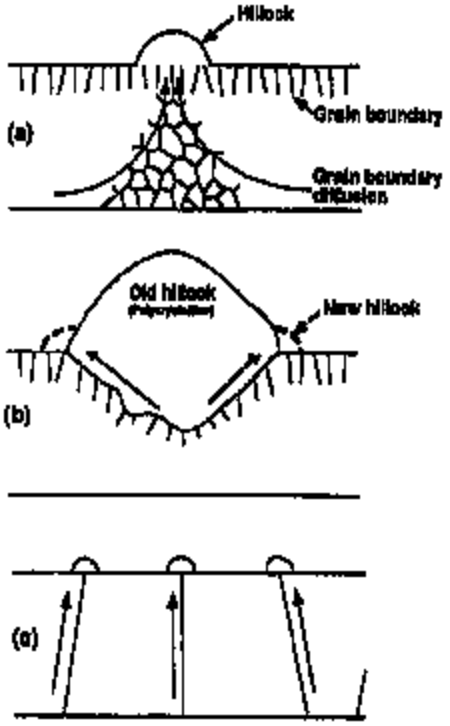

Fig. 8. Schematic drawings of hillock formation comparing a film with fine grains to a film with large grains.

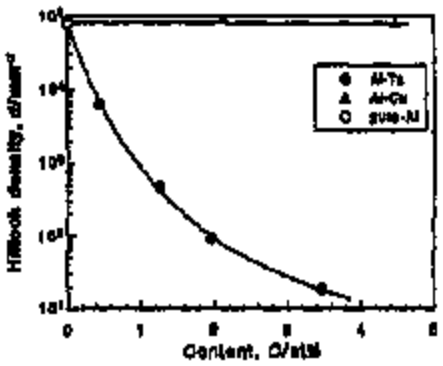

Fig. 9. Alloy-content dependence of hillock density for Al, Al–Cu, Al–Ta alloy films with 400-nm thickness annealed at 573 K for 3.6 ks [14].

surface easily results in a nucleation site of hillock formation as shown in Fig. 8(c).

On this model, larger hillocks with low density and smaller hillocks with higher density can be expected to form in films with fine grains and with large grains, respectively, when the hillocks relieve the same value of compressive stress in the films. The films with large grain size can be applied to Al or Al–Cu alloy films. The grain size of Al and Al–Cu alloy films with strong grain growth during annealing at more than about 400 K ranges from 0.5 μm to several μm, with a strongly columnar structure. Fig. 9 shows hillock density of Al, Al–Cu and Al–Ta alloy films with 400-nm-thickness annealed at 573 K for 3.6 ks as a function of alloy content. The hillock density in Al and Al–Cu is significantly higher than in Al–Ta alloy films.

5. Summary

Hillock formation, microstructures of both hillock and matrix, and compressive stress relaxation behavior during isothermal annealing were studied on Al–2at.%Ta alloy films for interconnections of TFT–LCDs. The following results were obtained.

1. Hillock size increased with increasing temperature or annealing time. Although new hillocks were observed on the outer perimeter of old hillocks, the macroscopic hillock number density reached a saturated value soon after the initial appearance of the old hillocks.
2. The distance between each hillock ranged from 20 μm to 100 μm, which is extremely large in comparison with grain size of the films, which was about 0.06 μm on an as-deposited film and about 0.2 μm even after annealing at 673 K for 3.6 ks.
3. The microstructure of hillocks was polycrystalline Al. The incorporation of microstructure was observed between a hillock and the film.
4. The time constant for compressive stress relaxation during isothermal annealing ranging from 478 K to 558 K had an activation energy of range between 0.3 eV and 0.4 eV.
5. The relationship between hillock formation and microstructure on Al–Ta alloy films can be explained by a model in which hillock formation with lateral diffusion, i.e. diffusion in the film plane, causes stress relaxation in a large area around the hillock. The film structure with fine grains due to the addition of Ta plays an important role in reducing hillock density.

Acknowledgements

The authors wish to express their gratitude to Professor Robert Sinclair at Stanford University for his help in TEM observation. Thanks are also due to Masao Kinefuchi and Yasuro Minokata and Mechanical Engineering Research Laboratory, Kobe Steel, Ltd. for their help in the in-situ SEM observation.

References

[1] P. Chaudhari, *J. Appl. Phys., 45* (1974) 4339.
[2] H.C.W. Huang, P. Chaudhari, C.J. Kircher and M. Murakami, *Philos. Mag. A, 54* (1986) 583.
[3] C.Y. Chang and R.W. Vook, *J. Mater. Res., 4* (1989) 1172.
[4] F. Ericson, N. Kristensen, J. Schweitz and U. Smith, *J. Vac. Sci. Technol., B9* (1991) 58.
[5] D. Gerth, D. Kutzer and M. Krohn, *Thin Solid Films, 208* (1992) 67.
[6] M. Ronay and C.F. Allotta, *Philos. Mag. A, 42* (1986) 181.
[7] R.A. Schwarzer and D. Gerth, *J. Electronic Mater., 22* (1993) 607.
[8] H. Onoda, B. Takahashi, S. Madokoro, H. Fukuyo and S. Sawada, *Proc. Symp. VLSI Technol.* (1990) 57.
[9] Y.K. Lee, N. Fujimura, T. Ito and N. Nishida, *J. Vac. Sci. Technol., B9* (1991) 2542.
[10] S. Ogawa and H. Nishimura, *Techn. Dig. Int. Electron Devices Meet.*, (1991) 277.
[11] S. Yamamoto, T. Ohnishi, K. Yoshikawa and Y. Koga, *Proc. 12th Int. Display Research Conf.*, (1992) 217.
[12] E. Iwamura, T. Ohnishi, K. Yoshikawa and K. Inoyama, *J. Vac. Sci. Technol. A12* (1994) 2922.
[13] P.A. Flinn, D.S. Gardner and W.D. Nix, *IEEE Trans. Electron Devices, ED-34* (1987) 689.
[14] E. Iwamura, T. Ohnishi and K. Yoshikawa, *J. Jpn. Inst. Metals*, in press (in Japanese).
[15] M. Hershkovitz, L.A. Bloch and Y. Komem, *Thin Solid Films, 130* (1985) 87.
[16] D.S. Gardner and P.A. Flinn, *IEEE Trans. Electron Devices, ED-35* (1988) 2160.
[17] P. Chaudhari, *J. Vac. Sci. Technol., 9* (1972) 520.
[18] D.S. Gardner and P.A. Flinn, *J. Appl. Phys., 67* (1990) 1831.
[19] C.Y. Chang and R.W. Vook, *Thin Solid Films, 228* (1993) 205.
[20] R.W. Vook, *Mater. Chem. Phys., 36* (1994) 199.
[21] N. Kristensen, F. Ericson and J.-A. Schweitz, *Thin Solid Films, 197* (1991) 67.

ELSEVIER

Applied Surface Science 91 (1995) 239–245

applied surface science

The effect of ion implantation on the properties of Al films

M. Zaborowski [a], A. Barcz [a], G. Gawlik [a], I.W. Rangelow [b,*]

[a] Institute of Electron Technology, Al. Lotników 32/46, 02 668 Warsaw, Poland
[b] Institute of Technical Physics, University of Kassel, Heinrich Plett-Strasse 40, 34 132 Kassel, Germany

Received 20 March 1995; accepted for publication 4 May 1995

Abstract

The influence of irradiation of Al or Al-based films on the surface morphology is studied by a number of methods. F, B, Mg, Cd, As, Sb, Cr and Ar were chosen as implanting species in order to cover a wide variety of chemical reactivities with aluminium. Implantation of boron and, to a lesser extent, of fluorine or chromium was found beneficial in suppressing population of hillocks, predominantly those of medium or larger size.

1. Introduction

Aluminium is still the most commonly used material for interconnection lines and ohmic contacts in silicon integrated circuit technology. This is mainly because of its high electrical conductivity, low resistance ohmic contact to Si, good adherence to silicon dioxide as well as the ease of deposition and etch processes. However, one of the serious disadvantages of the Al-based metallization is formation of hillocks which may lead to device failure with increasing integration scale. Hillocks are large crystallites that, upon annealing, can grow out to a height comparable to the initial layer thickness. While it is generally accepted that hillock growth is related to grain-boundary diffusion and plastic flow [1,2] a detailed understanding of the whole process is lacking [3,4].

In this paper we report on an extensive study of the influence of ion implantation on the properties of aluminium and aluminium-based alloys that are pertinent to their application as interconnecting lines in silicon IC technology with special emphasis placed on the morphology of the Al surface. It is well established that implantation of ions into metals may induce, depending on the particular ion–target system, several effects such as generation of point or extended defects, formation of solid solution or new chemical compounds, amorphization or modification of grain structure in polycrystalline materials. There are few reports in the literature concerning the effect of ion implantation on the population of hillocks [5–7]. We have chosen F, B, Mg, Cd, As, Sb, Cr and Ar as implanting species in order to cover a wide variety of chemical reactivities with aluminium. Doses and energies of implantation were such that the maximum dopant concentration of about 1 at% was located at a depth of 100–200 nm. The effect of ion implantation on the properties of Al films was investigated by means of a number of techniques including scanning electron microscopy (SEM), optical microscopy with digital image processing, stylus profiling, secondary ion mass spectrometry (SIMS), Auger electron spectroscopy (AES), transmission

* Corresponding author.

SSDI 0169-4332(95)00125-5

electron microscopy (TEM), X-ray diffraction (XRD) as well as the measurements of strain and resistivity of the metallic layers.

2. Experimental

Samples were prepared by thermal oxidation of ⟨100⟩ Si wafers to an oxide thickness of 400 nm followed by either magnetron sputter deposition of Al or Al:Si 1% alloy or by electron gun deposition of pure Al. Typical thickness of the metallic film was 1000 nm. Implantation was performed at nominally room temperature at energies 50–160 keV to doses 4×10^{15}–3.5×10^{16} cm^{-2}. Annealing was carried out at 450°C for 30 min in hydrogen or nitrogen atmosphere. For further analysis the samples were cut out so that any combinations of non-implanted, non-annealed together with implanted and annealed pieces were available for comparison from the same wafer.

Metallization topography was examined by SEM and by optical microscope equipped with a specially designed system for digital image processing enabling easy measurement of the hillock size and density distributions [8]. The system proved particularly useful in view of a large number of samples. SIMS profiling was used to establish the extent of redistribution of selected dopants. Sheet resistance of the Al films was determined by a four-point probe method. Since boron was found the most promising species in suppression of the hillock size and density some additional investigations were conducted with B^+-implanted films. TEM analysis provided information on the grain structure and, employing electron diffraction, phase identification. Tensile stress in the metallization was deduced from the contactless measurement of the radius of curvature.

3. Results

Generally, implantation into Al was found to affect either the size and population of the hillocks or their shape. An example of the modification of the shape of hillocks which resulted from the implantation of antimony ions with a fluence of 5×10^{15} cm^{-2} is shown in Fig. 1. Clearly, hillocks in the Sb-implanted layer become sharper at the top and have a whisker-like appearance. Conversely, irradia-

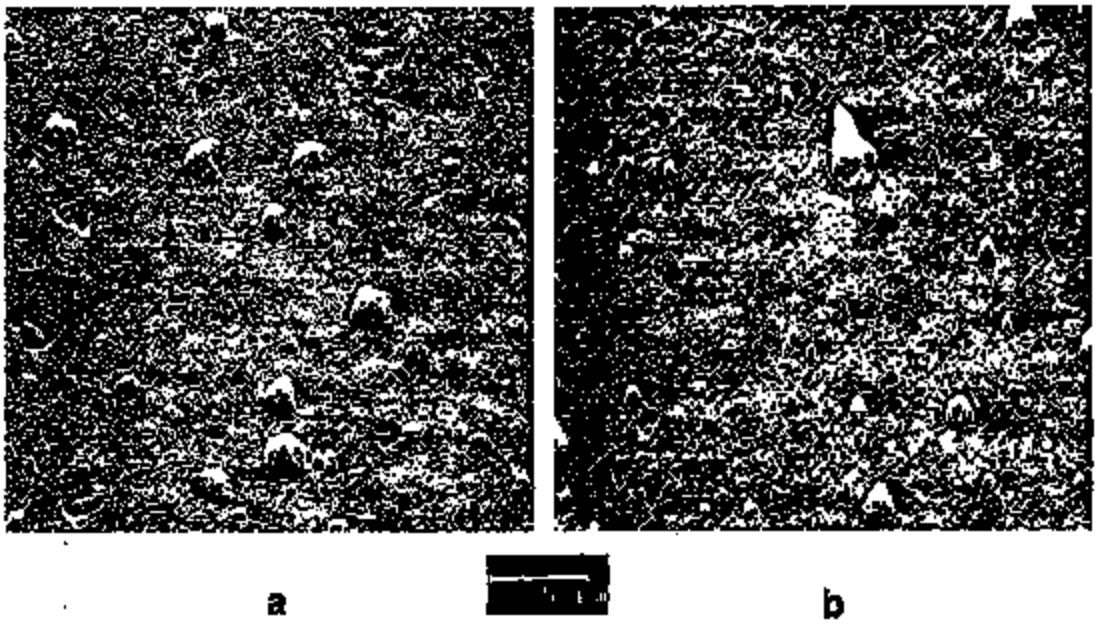

a b

Fig. 1. SEM micrograph of Al surface: (a) unimplanted; (b) implanted with 160 keV Sb^+ ions to a dose of 5×10^{15} cm^{-2}.

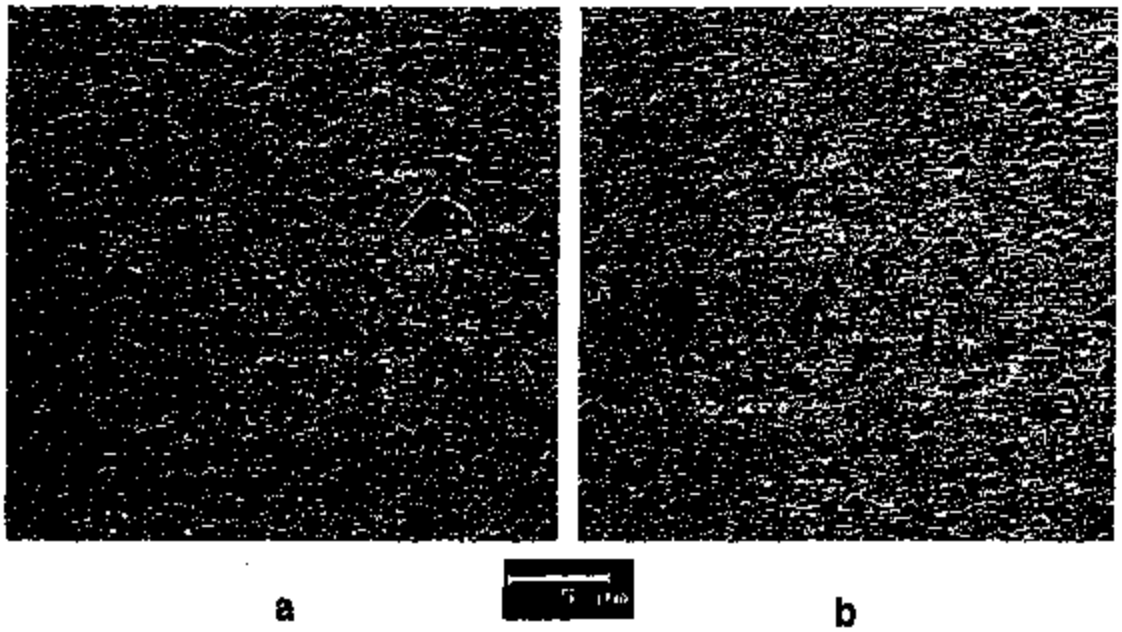

Fig. 2. SEM micrograph of Al:Si 1% surface: (a) unimplanted; (b) implanted with 130 keV Cr^+ ions to a dose of 9×10^{15} cm^{-2}, both annealed at 450°C.

tion with chromium ions leads to suppression of hillock density without noticeable change of their form (Fig. 2). In this case, the effect is observed on Al:Si alloy but not on pure Al.

Considering different species, doses and magnetron or e-gun deposited Al or Al-based alloys, the total number of samples to be analyzed exceeded one hundred. For this reason the procedure of digital image processing for hillock recognition was found as an extremely convenient tool allowing immediate statistical evaluation of the surface features. Fig. 3a shows a processed hillock image from unimplanted Al and Fig. 3b – from the surface of aluminium layer subjected to the implantation with boron ions

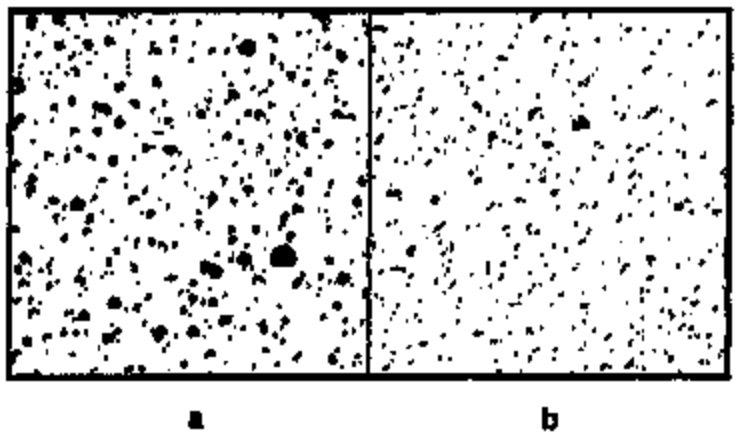

Fig. 3. Al surface examined by hillock recognition method: (a) unimplanted; (b) implanted with boron, 2.5×10^{16} cm^{-2}.

SSDI 0169-4332(94)00427-2

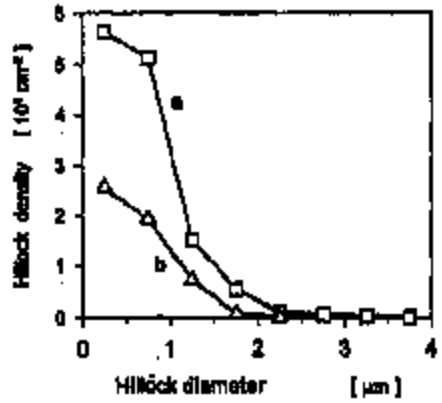

Fig. 4. Distribution of the hillock density versus hillock diameter for: (a) 1 μm Al:Si layer; (b) Al:Si layer implanted with Cr, 9×10^{15} cm^{-2}.

to a dose of 2.5×10^{16} cm^{-2}. Implantation results in substantial reduction of the hillock size. In order to quantify the influence of ion implantation on the topography of the investigated films, for all samples distribution of the hillock areal density versus their diameter was calculated on the basis of digitised images. Example of such dependence is presented in Fig. 4. It can be noticed that Cr implantation decreases the density of, predominantly, large and medium-size hillocks. Most results of this work are summarised in Table 1. Hillocks are divided into three groups: small (< 1 μm), medium (1–2.2 μm), and large (> 2.2 μm). The data represent the average number of hillocks of a given size per 10^{-3} mm^2. They concern pure aluminium deposited by magnetron sputtering and electron gun except for Cr^+ implantation where the Al:Si alloy was used. A large spread of results observed for unimplanted samples, especially as far as the smallest (< 1 μm) hillocks are concerned, does not affect the general trend because the data for 0-dose were collected from the same silicon wafer as those for implanted ones.

Out of eight implanted species, boron was found to yield the most significant and reproducible suppression of hillock growth. It is important to note that the reduction of hillock population is especially pronounced for larger objects i.e. those which are likely to cause failures in interconnection lines. This applies also to the implantation of fluorine. Irradiation with Cr^+ ions leads to hillock suppression in Al:Si and Al:Si:Cu alloys but not in pure Al. Cadmium and antimony influence the hillock shape. Magnesium, within the experimental uncertainty, does not affect either the density or the shape of hillocks while arsenic-implanted films were found to exhibit an increased number of hillocks. Results of implantation Ar^+ are not shown in the table; because due to large scatter of data from sample to sample, the effect could not be definitely established.

Although it has been demonstrated that irradiation of Al-based films with B^+, F^+ or Cr^+ ions is beneficial to the surface morphology, one has to verify whether this process does not induce other effects which would affect the performance of devices. First, it should be mentioned that in any case, implantation has no observable influence on adhesion, integrity, or continuity of the material. For boron-implanted Al, it was checked that implantation does not degrade ohmic contacts or Schottky diodes to n-Si. On the other hand, the sheet resistance of the implanted layers is higher relative to the unimplanted ones, not exceeding 5% at a dose of 10^{16} cm^{-2} with the exception of Cr. Fig. 5 shows resistivity change of B, Mg, F, As, Sb and Cr-implanted Al as a function of the ion fluence.

In an attempt to understand the mechanism of the interaction of the implanted atoms with polycrystalline Al film, leading eventually to the modification of the grain growth, we have focused on B-implanted layers on which additional experiments were per-

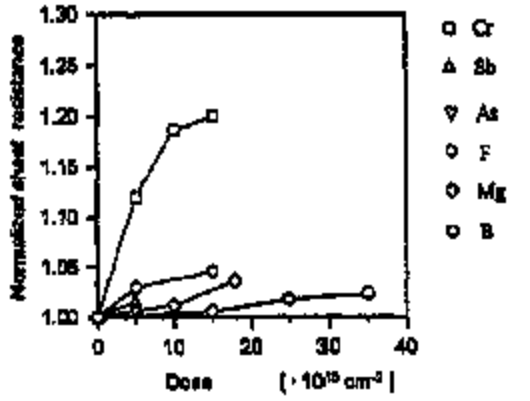

Fig. 5. Sheet resistance measurements of the implanted Al layers relative to unimplanted ones.

Table 1

Hillock density $\times 10^5$ mm^{-2}

Ion	B				F					As		Sb		Mg			Cl		Cr[a]		
Energy (keV)	60				100					60		160		100			160		130		
Dose 10^{15} (cm^{-2})	0	15	25	35	0	2	4	8	15	0	5	0	5	0	9	18	0	5	0	4	9
Sputtering																					
<1 μm	73.5	69.5	74.3	49.8	45.2	56.2	58.7	45.3		46.9	89.8	23.2	47.9	49.7	48.2	48.8	22.9	40.6	107	72.6	44.9
1–2.2 μm	29.0	99.6	5.91	6.35	11.9	15.3	7.99	5.69		14.0	22.9	13.4	12.8	14.0	12.4	11.1	10.7	13.8	21.6	9.42	8.1
>2.2 μm	3.83	0.22	0.0	0.0	0.99	1.00	0.88	0.22		1.20	0.88	1.75	1.31	1.1	0.77	0.77	2.2	2.41	0.88	0.11	0.0
Evaporation																					
<1 μm	40.5	46.9	47.9	58.9	60.7		69.4	63.5	50.2	67.9	161	73.9	81.4	76.0	99.0	108	35.3	44.3			
1–2.2 μm	20.6	15.2	4.27	1.85	16.8		12.4	7.45	8.54	15.5	25.3	24.7	10.5	28.3	21.0	16.9	16.1	12.6			
>2.2 μm	2.52	0.55	0.11	0.0	1.31		0.88	0.22	0.22	1.53	0.99	2.74	1.86	1.31	1.97	0.99	2.3	2.63			

[a] Cr implanted into Al:Si 1%.

0169-4332/95/$09.50

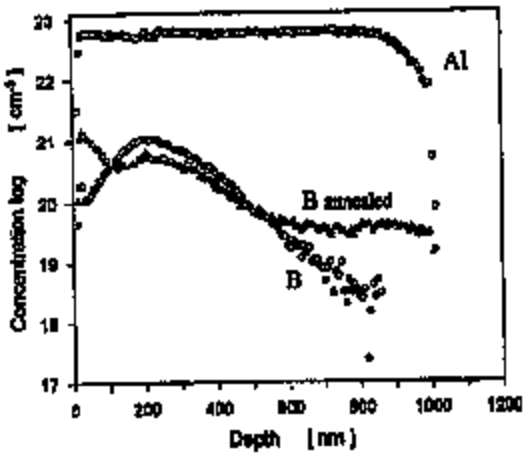

Fig. 6. SIMS depth profiles of boron in Al before and after annealing.

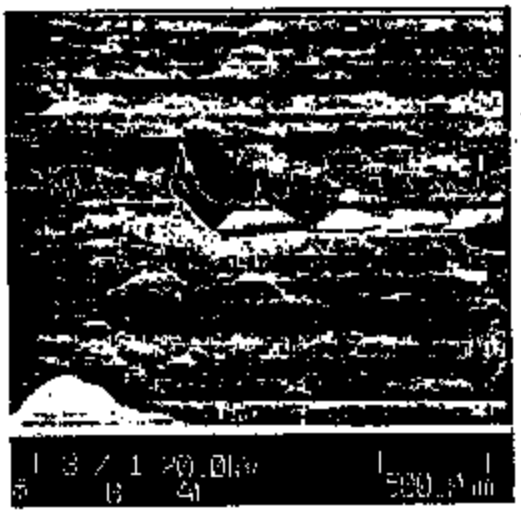

Fig. 7. Auger line-scan of boron in B^+-implanted 1 μm thick Al layer.

formed. Fig. 6 presents in-depth concentration profiles of ^{11}B before and after annealing as determined by SIMS technique. It demonstrated substantial mobility of boron atoms under this relatively low-temperature processing at 450°C. The initial Gaussian-type profile becomes flattened with a strong segregation taking place towards the Al surface and, to a lesser extent, to the Al/SiO_2 interface. Auger line-scan of boron signal gives evidence that implantation followed by annealing results in laterally non-uniform distribution of B atoms across the surface (Fig. 7).

TEM investigation provided valuable information on the precise boron location and phase identification in B-implanted layers. The polycrystalline structure visible in Fig. 8 is ⟨111⟩ textured with average grain size of 0.75 μm^2. The ⟨111⟩ texture is independently confirmed by XRD with the standard deviation being estimated to 7%–10%. Small crystallites (100 nm) located at Al grain boundaries could be classified as an AlB_{10} orthorhombic or AlB_{12} tetragonal phase as was indicated by means of electron diffraction.

Finally, tensile stress in the metallization layers which amounts to 150–200 MPa after deposition drops to 60–120 MPa as a result of boron implantation and after annealing increases to a value close to that in unimplanted layers.

Fig. 8. (a) TEM image of magnetron sputtered Al layer. (b) TEM image of B^+ implanted Al layer.

4. Concluding remarks

We have demonstrated that implantation into the Al metallization may effectively influence the surface topography. In some cases it leads to the elimination of large hillocks which grow above the initial surface of the metal in a process of relieving compressive stress that develops in the course of annealing.

Although the results of this work are not sufficient to explain, for each implanting species, a detailed mechanism of nucleation and growth of hillocks, investigations of boron-implanted provided some general guideline. Since it is well known that the material for the grain growth is supplied through the grain boundary migration rather than through lattice diffusion one obvious condition that has to be fulfilled in order to modify the growth kinetics is segregation of the incorporated atoms at the grain boundaries. This implies that best candidates to be introduced into the Al layer are those which have limited solubility in bulk aluminium. According to the Al–B phase diagram, solid solubility of boron in Al is less than 0.1 at% [9]. It is postulated that, upon sintering, the boron atoms out-diffuse from the bulk Al and then, due to their high mobility at grain boundaries, precipitate in the form of presumably AlB_{10} compound. Indeed, as supported by SIMS profiling, at a temperature of 450°C boron spreads throughout the layer and such a fast transport could not be attained by bulk diffusion. AlB_{10} precipitates located at aluminum grain boundaries are believed to be the main cause of strengthening the polycrystalline structure and preventing the grains from excessive vertical growth.

Fluorine, chromium and, particularly, boron implanted to aluminium seem promising in the reliability improvement of multilevel metallization systems. Additional advantage of applying B or F ions is that these elements are easily accessible in typical high-current implanters used in silicon technology.

Acknowledgements

The authors wish to acknowledge Professor W. Rosiński, Dr. J. Kozubowski and J. Adamczewska for performing some of the measurements and valuable discussions. This work was supported by the State Committee for Scientific Research, Poland, under Grant No. BS50102605.

References

[1] F.M. d'Heurle, Int. Mater. Rev. 34 (1989) 53.
[2] K.N. Tu, J.W. Mayer and L.C. Feldman, Electronic Thin Film Science (Macmillan, New York, 1992) p. 373.
[3] F. Ericson, N. Kristensen, J. Schweitz and U. Smith, J. Vac. Sci. Technol. B 9 (1991) 58.
[4] R.A. Schwarzer and D. Gerth, J. Electron. Mater. 22 (1993) 607.
[5] O.W. Holland and J.R. Alvis, J. Electrochem. Soc. 134 (1987) 2017.
[6] N. Peacock, Thin Solid Films 156 (1988) 173.
[7] K.P. Mac Williams, L.B. Lowry, M. Isaac, D. Colbert and T.C. Zielow, 1990 Symposium on VLSI Technology, June 4-7, Honolulu.
[8] M. Zaborowski, M. Adamiec and A. Barcz, 1990 Symposium on VLSI Technology, June 4-7, Honolulu.
[9] C.J. Smithells, Metals Reference Book, Vol. II (Butterworths, London 1967) p. 390.

ELSEVIER

Thin Solid Films 348 (1999) 222–226

Thin Solid Films

Enhanced optical performance of aluminum films by copper inclusion

C. Kylner[a,1,*], L. Mattsson[b]

[a]Department of Physics II - Optics, Royal Institute of Technology, SE-100 44 Stockholm, Sweden
[b]Surface Emmission Laboratory, Institute of Optical Research, SE-100 44 Stockholm, Sweden

Received 25 July 1998; accepted 4 September 1998

Abstract

The aluminum film is a standard coating material for optics. It yields a high reflectance over a broad wavelength region, and films can be made sufficiently smooth for high quality optical applications. However, it suffers from a high sensitivity to hillock formation and severe degradation of its low light scattering properties, already at temperatures of 70–80°C. In order to raise the temperature for onset of hillock formation we have co-evaporated a slight amount (3 at.%) of Cu into the Al film. The anti-hillocking performance was indeed confirmed by raising this temperature to ~130°C. But, we also greatly reduced the surface roughness of the as-deposited 3600 Å films to the outstanding values of 1-3 Å rms as measured by the ASTM F 1048-87 total integrated scattering (TIS) method. This yields very low light scattering films despite their thickness. Also, the specular reflectance was coming out just as high as for a pure Al film over a wide wavelength range. The enhanced optical performance is attributed to less light scattering of the co-evaporated film and to the strengthening effect in the film. © 1999 Elsevier Science S.A. All rights reserved.

Keywords: Aluminum; Light scattering; Optical properties; Surface roughness

1. Introduction

Aluminum films have been used for a long time as broad band front reflecting surfaces on high quality optics like mirrors and gratings [1]. For low light scattering optics special care has to be taken in depositing these films, but evaporated under good conditions very high quality films can be obtained with a roughness of a few Å rms. Normally, the thicker the film the rougher the surface will be [2]. Typical roughness values obtained by the ASTM F 1048-87 approved total integrated scattering (TIS) technique [3] for high quality films evaporated in ultra high vacuum are 2 Å for about 800 Å thick films and 4–5 Å for about 2300 Å thick films. However, one drawback of the Al film is its sensitivity to hillocking at temperatures higher than about 75°C [4]. This is particularly cumbersome when dielectric top coatings requiring elevated temperatures, well above 100°C, for good densification are to be deposited as protective layers. The hillocking phenomenon that is due to the thermal mismatch between the film and the substrate causes surface protrusions in the Al film that raises the light scattering level by orders of magnitude. Thus, by being subject to heating at moderate temperatures, a super polished high quality mirror may easily turn into a low performance reflector. As the hillocking is an irreversible deterioration of the film surface there are no other means than stripping and recoating the mirror blank to regain its former low light scattering properties. In earlier investigations we have shown that the formation of the first hillocks is associated with a compressive stress maximum in the film which is subject to a constant heating rate [5]. This is followed by an overall relaxation in the film while simultaneously a great number of hillocks are being formed. One way to reduce the number of hillocks is to use a low heating rate [6], but that is not a cost efficient way for a manufacturing process. The ideal way would be to strengthen the Al film to withstand a higher stress before hillocking occurs, and thereby also withstand higher temperatures.

In this paper we present a technique that shows great promise of achieving that goal without sacrificing the optical quality of the Al film. Rather, it reduces the surface roughness and yields very low light scattering surfaces even for films of thickness in the range of 3000–4000 Å. The key to the improved quality is the introduction of a few per cent copper as an alloying element in the Al film. The reason for adding Cu is that it has shown improving effects on hillocking of very thick Al films (11.2 μm) [7]. Also, the

* Corresponding author. Tel.: + 1-650-723-6144; fax: + 1-650-725-4034.
E-mail address: ckylner@leland.stanford.edu (C. Kylner)
[1] Present address: Department of Material Science and Engineering, Stanford University, Stanford, CA, USA.

PII: S0040-6090(98)01398-4

discovery of the beneficial effect of Cu additions on the lifetime of Al metalization layers subject to electromigration [8] was a major breakthrough for the microelectronics development. Since then lots of work have been done in the microelectronics field. On the contrary, we found only two papers refering to dilute Cu alloying in high optical quality Al films in the literature [9,10]. The early paper by Beaglehole and Wihl [9] reports on a thorough experimental investigation and analysis of bulk electronic structure of Al films co-evaporated with Cu. In the letter by Rieck et al. [10] they report the reflectance of a magnetron sputtered 600 Å thick Al-4% Cu film to be better than for the pure Al film. This observation was made at 780 nm wavelength only and no analysis or attempt of explanation for the enhanced reflectance was given. Other works reporting on reflectance properties have been made at substrate temperatures far too high to yield low light scattering high quality films [7,11].

In an initial work for improving the optical quality of Al films we used an interface layer of Cu and found that the temperature for onset of hillock formation was raised by approximately 20°C [12]. The present work presents the advantage of co-evaporating Cu and Al and its effect on the optical quality. After the experimental presentations, results are given that show the improved hillocking suppression, the low light scattering and the generally better optical performance over a wide wavelength range. A short discussion is given on the analysis of the films.

2. Experimental

2.1. Sample preparation

Two batches of samples were used in this investigation. One batch of pure Al films was evaporated onto one set of silicon wafers, and an other batch of Al-Cu films was co-evaporated onto a second set of silicon wafers. In both cases the wafers were sitting close to the periphery of a rotary mount spinning at approximately 60 rev/min at a distance of 40 cm above the evaporation sources. The Al that was evaporated by an e-beam gun had a purity of 99.999% (Balzers) and the Cu had a similar purity. The ultra high vacuum (UHV) system used for the evaporation has one electron beam gun and one thermal source. The Al was evaporated from the e-beam gun and the Cu from the thermal source. Prior to the evaporation thickness calibration was made by checking the actual film thickness with our Talystep surface profilometer and adjusting the quartz crystal balance to be showing the correct deposition rate. After deposition of the samples the final film thickness was measured by the Talystep, confirming the final film thickness to be about 3400 Å for the Al films and 3600 Å for the Al-Cu films. The films were deposited onto the polished side of 0.5 mm thick, 3" (100) oriented silicon wafers (Virginia semiconductors). The wafers, coming straight out of wafer boxes and having a native oxide, were kept at room temperature during the film deposition. The background pressure in the vacuum chamber was $< 10^{-6}$ Pa. During the deposition the pressure rose by one order of magnitude. The deposition rate was approximately 20 Å/s for the Al batch and 18 Å/s for the Al-Cu batch. The deposition rate between the Al and the Cu in the co-evaporation was balanced so that the final Al-Cu film should contain about 3 at.% (6 wt.%) of Cu. The composition of Al relative to Cu was checked by energy dispersive X-ray (EDX) technique installed in a scanning electron microscope (SEM). It was found that the Al-Cu composition of the samples did not differ significantly from each other.

2.2. Characterisation

The as-deposited samples were analyzed by several methods. The light scattering and surface roughness of the films were characterized by total integrated scattering (TIS) [4,13]. TIS is an ASTM F 1048-87 approved [3] non-contact, non-destructive method for measuring the effective surface roughness of optical components. It is extremely sensitive to microtopography having surface spatial frequency components in the range of 0.07–1.5 μm^{-1}, i.e. the frequencies that mainly determine the light scattering losses of optical components. The measured surface roughness thus depends on the surface spatial frequencies that can be detected by the TIS instrument, but averaged from several measurement spots (each 1 mm^2) on the surface. The TIS value is defined as the ratio between the scattered light and the total reflected light, expressed in reflectance ratio as R_d/R_0

$$\mathrm{TIS} = \frac{R_d}{R_0} \approx \left(\frac{4\pi\delta\cos\theta_i}{\lambda}\right)^2 \quad (1)$$

The scalar scattering theory relates the measured TIS value to the root mean square (rms) surface roughness δ, the incident wavelength λ (633 nm) and the angle of incidence of light θ_i on the surface [14]. The TIS measured rms roughness according to ASTM F 1048-87 can not be directly compared with the roughness obtained by e.g. an atomic force microscope, as the instrumental footprints of these two techniques are indeed different. (The AFM measures much higher spatial frequencies and is limited to areas of only 0.01 mm^2.) For the assessment of the optical performance the TIS roughness is therefore preferred and used in the results section. Nevertheless, for a better understanding of the results the microtopography was examined by a Dimension 3000 atomic force microscope (APM) operated in tapping mode both with and without the "phase contrast" image enhancement. A direct measurement of the specular reflectance ratio of the two batches of films was made in a Lambda 9 spectrophotometer after the first heat treatment, in order to confirm the overall optical properties over a wide wavelength range.

The onset of hillock formation was revealed in real time by the vacuum compatible partial integrated scattering and

Table 1
Summary of the total integrated scattering (TIS) investigation

Sample #	Initial total integrated scattering	Initial root mean square (rms) roughness (Å)
1 (Pure Al)	$3.3–4.4 \times 10^{-4}$	9.2–10.6
2 (Pure Al)	$3.5–4.4 \times 10^{-4}$	9.4–10.6
3 (Pure Al)	$3.2–4.3 \times 10^{-4}$	9.0–10.4
4 (Al-Cu)	$0.8–2.0 \times 10^{-5}$	1.4–2.2
5 (Al-Cu)	$0.7–3.3 \times 10^{-5}$	1.3–2.9
6 (Al-Cu)	$0.7–2.6 \times 10^{-5}$	1.3–2.6
7 (Si-wafer)	$2.4–4.7 \times 10^{-6}$	0.8–1.1

deflection (VaCPISD) instrument [15] yielding a light scattering profile of the surface vs. time and temperature while the samples were radiotively heated in air using a temperature ramp of 3°C/s up to a temperature well exceeding the temperature for onset of hillock formation. Our thermal treatments were done within the two-phase Al_2Cu-Al region in the phase diagram of Al-Cu, i.e. well below the solvus temperature, and were expected to cause Al_2Cu (θ) phase precipitates at aluminum grain boundaries to grow and precipitates within aluminum grains to diminish [16,17].

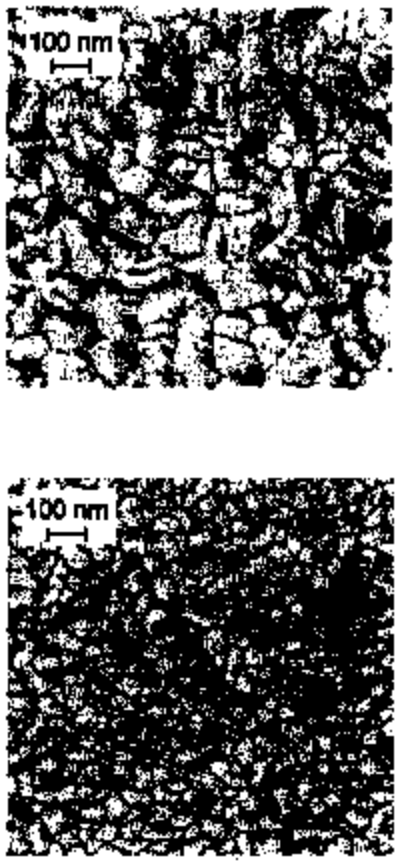

Fig. 1. 1×1 μm² AFM images of: (a) the pure Al film and (b) the Al-3 at.% Cu film obtained in the phase sensitive tapping mode.

3. Results and discussion

3.1. Light scattering, surface roughness and grain size

Table 1 shows the TIS values (= diffuse reflectance divided by total reflectance) and the corresponding TIS measured surface roughness δ for the Al and Al-Cu film batches after the deposition, but before any thermal treatment. For comparison a typical Si wafer used for the film deposition is also included in the same table. We can see that all the pure 3400 Å thick Al films have TIS values less than 5×10^{-4} and the 3600 Å thick Al-Cu films have TIS values less than 4×10^{-5}. These TIS values correspond to surface roughness of <11 Å rms and <3 Å rms, respectively, over the TIS sensitive surface wavelength range of 0.7–15 μm. From previous experience the 9–11 Å rms roughness is in the high end of where we expect such a thick Al film to be. Typical roughness would have been 7–8 Å rms. However, the 1–3 Å rms for the Al-Cu film is by far better than we have ever seen for any Al films with a thickness of 3600 Å. The surface quality is thus considerably improved by the inclusion of the Cu atoms.

Within each batch only small variations in TIS values were observed. This confirms that the sample position in the rotary mount was not critical for the final surface quality of the films, i.e. they had almost identical as-deposited surface roughness. The main contribution to the roughness comes from the film, since the roughness of the silicon wafers was in the 1 Å range. Earlier studies have shown that the as-deposited surface roughness of the films depends on both the film thickness and the deposition conditions such as background pressure and deposition pressures [1]. Since surface roughness increases with film thickness as a result of increasing grain size [18,19], the Al-Cu films were purposely chosen to be slightly thicker (3600 Å) than the Al films (3400 Å) to exclude this thickness effect. Already at this point of our investigation, with the low TIS values and surface roughness numbers, we can make a guess that the grain size is considerably smaller in the Al-Cu film.

Other parameters known to be influencing the grain size are deposition rate and substrate temperature. A higher deposition rate and a lower substrate temperature will create smaller grains. As both substrate temperature and deposition rate were about the same for the two batches, we conclude that the Cu atoms played an important role in the grain development, making the grains smaller. The final proof of that was obtained by AFM investigations that revealed the mean grain size of the Al-Cu film to be about 50 nm, only half of the grain size of the Al film. This is shown in the 1×1 μm² AFM "phase contrast" images of Fig. 1. Knowledge from the literature combined with our present results thus confirm that alloying has the effect of producing small-

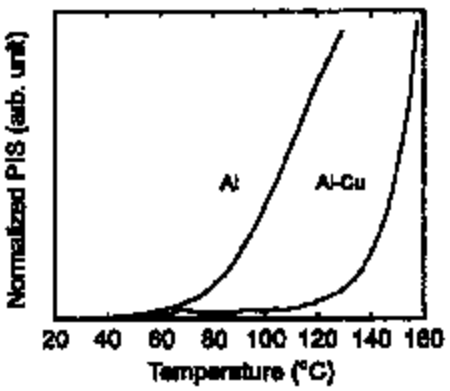

Fig. 2. Real-time partial integrated scattering (PIS) obtained at 633 nm wavelength from the pure Al film and the Al-Cu film versus sample temperature when subject to a temperature ramp of 3°C/s. Note that the low PIS curve for Al-Cu is magnified by 100× in the vertical direction to be comparable with the PIS curve for the pure Al film.

ler grain sizes and thereby a surface that scatters a lot less light than the pure Al film surface. But, will it also increase the yield strength of the film [20] and thereby make it more resistant to hillocking?

3.2. Strengthening effect

In order to answer that question the samples were positioned one at a time in the VaCPISD instrument [15] and were subject to identical thermal treatments, a continuous temperature ramp of 3°C/s, starting from room temperature.

During the heating process there is a build up of compressive stress due to the expansion of the film relative to the much less expanding silicon wafer and therefore no voids were expected to be formed. Only a few growth hillocks were observed on the samples prior to the heat treatment.

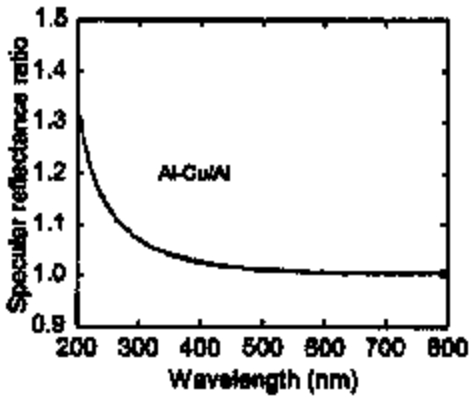

Fig. 3. Specular reflectance ratio (Al-Cu film/pure Al film) versus wavelength for samples that have been heated to 130°C (Al) and 180°C (Al-3 at.% Cu). The enhanced reflectance of the Al-Cu film at the shorter wavelengths is attributed to less light scattering losses from hillocks.

The experimental results from this investigation appear as partial integrated scattering (PIS) versus the sample temperature, where the PIS is a relative measure of the number and size of hillocks apparent within the approximately 1 mm^2 area irradiated by the laser beam in the instrument. Two representative PIS curves (averages from each batch) are shown in Fig. 2, one for the pure Al film and one for the Al-Cu film. They have been set to the same initial scattering level and magnified for a more easy visualization of the differences. It is obvious that the Al-Cu film withstands hillock formation up to a much higher temperature ~130°C as compared to ~75°C for the pure Al film. Analogously with the discussion of film thickness and grain size, the film strength is known to increase when the film is getting thinner. As the pure Al film is thinner this can not be the explanation for the higher strength and hillocking resistance for the Al-Cu film. Again, the strength of the Al-Cu film must be an effect of the Cu atoms. So far we have achieved a three times smoother film with much improved anti-hillocking performance up to about 130°C, by adding 3 at.% Cu into the Al film. But what about its optical performance as a reflector material? Has the copper content reduced the reflectance in the blue region as could be expected from the fact that copper has a lower reflectance than aluminum at wavelengths shorter than about 650 nm [1] and as indicated in early optical studies of the electronic structure of Al-Cu alloys [9].

3.3. Reflectance

To get the answer to that question a direct measurement of the specular reflectance ratio of Al-Cu film/Al film was made in the Lambda 9 spectrophotometer, using the pure Al film as the reference surface. The measurement was performed in the wavelength region 200–800 nm. The result of such a measurement after the samples had been subject to a thermal treatment is shown in Fig. 3. In this graph the specular reflectance ratio of Al-Cu film/Al film is plotted versus the wavelength. Again we see that the Al-Cu film has a better performance over the entire spectrum. In particular it shows a better performance for short wavelengths. This can be explained by the higher light scattering losses in the rougher Al film having a considerable larger number of hillocks on its surface after the heat treatment. The smaller grain size of the Al-Cu film also reduces the surface roughness and thereby the light scattering losses, but not to the amount that it is revealed in the specular reflectance ratio. Absolute reflectance was also measured at 633 nm, using a laser power meter. Within a 0.5% error limit, both films had a reflectance of 90%.

Our reflectance results seem to contradict the early work of Beaglehole and Wihl [9], who found the reflectance to drop by 1–3% for a 3000 Å thick Al-1.4 at.% Cu alloy at wavelengths shorter than ~750 nm. However, there is a reasonable explanation for this difference. As we have ramped our films up to temperatures of ~180°C for the Al

0040-6090 29435

Cu film and ~130°C for the Al film before making the reflectance measurements, we get a much higher number of hillocks in the pure Al film for reasons given above. We therefore attribute the enhanced specular reflectivity at shorter wavelengths for our alloy samples to the fact that they have less number of scattering sites than the pure Al film. Other differences that also might influence a comparison are the effect of residual gases in the vacuum camber. Our system operated at residual gas pressures roughly two orders lower than that of the system used by Beglehole and Whil, and our absolute reflectance results agree better at 633 nm with the in situ data of Bennett [21] than the original data of Beglehole and Whil.

4. Conclusions

Al-Cu films with approximately 3 at.% Cu content were co-evaporated onto silicon wafers. The optical performance of the films was superior to pure Al films of similar thickness. The Cu content had reduced the grain size and thereby reduced the surface roughness to 1–3 Å rms as measured by total integrated scattering. The light scattering was strongly reduced and was exceedingly low despite a film thickness of 3600 Å. The Cu content had also strengthened the films so that hillock formation on heating was prevented up to about 130°C as compared to 75°C for a pure Al film. Although 3 at.% Cu was incorporated in the film the specular reflectance property was as good as or better than the pure Al film after it had been heated. This investigation has shown that the optical and mechanical performance of metal film reflectors can be considerably improved by using alloying elements in the film growth.

Acknowledgements

Laurent Krummenacher at the Surface Evaluation Laboratory, Institute of Optical Research, is greatly acknowledged for the deposition of the samples and for performing the AFM and spectrophotometer measurements. The authors would like to thank Anders Möller at the Division of Fusion Plasma Physics, Alfvén laboratory, Royal Institute of Technology for performing the EDX analysis. This work has been supported by the Swedish Research Council for Engineering Sciences (TFR) and the Göran Gustafsson Foundation.

References

[1] G. Hass, E. Ritter, J. Vac. Sci. Technol. 4 (2) (1967) 71.
[2] L. Mattsson, Workshop on Optical Fabrication and Testing Technical Digest 1987, 19, Optical Society of America, Washington, DC, 1987, pp. 85–89.
[3] Standard test method for measuring the effective surface roughness of optical components by total integrated scattering, American Society for Testing and Materials, Standard F 1048-87, 1987.
[4] L. Mattsson, Y.H. Le Page, F. Ericsson, Thin Solid Films 198 (1991) 149.
[5] C. Kyhner, L. Mattsson, J. Mater. Res. 13 (6) (1998) 1666.
[6] C. Kyhner, L. Mattsson, Thin Solid Films 307 (1997) 169.
[7] G.J. Hale, Thin Solid Films 63 (1979) 95.
[8] I. Ames, F.M. d'Heurle, R.E. Horstmann, IBM J. Res. Dev. 14 (1970) 461.
[9] D. Beaglehole, M. Wihl, J. Phys. F: Metal Phys. 2 (1972) 43.
[10] U. Rieck, C.A. Sweeny, K.H. Norian, Thin Solid Films 167 (1988) L35.
[11] S. Dietrich, M. Schmeißer, M. Menke, K. Saarwer, Thin Solid Films 275 (1996) 159.
[12] L. Mattsson, in: G. Akos, T. Lippényi, G. Lupkovics, A. Polmanikoky (Eds.), Optics as a Key to High Technology, Proc. SPIE 1963 - The International Society for Optical Engineering, Washington, 1993, p. 964.
[13] L. Mattsson, in: J.R. Jacobsson (Ed.), Thin Film Technologies, Proc. SPIE 652 - The International Society for Optical Engineering, Washington, 1986, p. 264.
[14] J.M. Elson, H.E. Bennett, J.M. Bennett, in: R.R. Shannon, J.C. Wyant (Eds.), Applied Optics and Optical Engineering, Academic Press, New York, 1979, p. 191.
[15] C. Kyhner, L. Mattsson, Rev. Sci. Instrum. 68 (1) (1997) 143.
[16] D.R. Frear, J.E. Sanchez, A.D. Romig, J.W. Morris Jr., Metall. Trans. A 21A (1990) 2449.
[17] T.B. Massalski (Ed.), Binary Alloy Phase Diagrams American Society, Metmerials Park, OH, 1993.
[18] A.K. Sinha, T.T. Sheng, Thin Solid Films 48 (1978) 117.
[19] G. Hass, N.W. Seidl, J. Opt. Soc. Am. 39 (1949) 179.
[20] E. Philofsky, K. Ravi, E. Hall, J. Black, In: 9th Int. Annual Reliability Physics Symp. IEEE, New York, 1971, pp. 120–128.
[21] H.E. Bennett, M. Silver, E.J. Ashley, J. Opt. Soc. Am. 53 (1963) 1089.

Up to 2wt% Si is used to prevent "contact spiking". This is caused by pipe diffusion of Al causing shorts between conductors in the silicon device (Fanger and Tonneman, p. 97).

The difference between hillocks and electromigration is that the latter has a current induced diffusive flux in one direction that causes pileup of material further down the conductor that can cause voiding and the conductor to fail. Hillocks are caused by preferential growth of certain grains to relieve stresses caused by growth or temperature.

Hillocks can cause interlayer shorts (Fanger and Tonneman, p.97).

David Fanger and Roger Tonneman, "Aluminum and Copper-Based Conductors" in *Characterization in Silicon Processing*", Yale Strausser, ed. (Boston": Butterworth-Heinemann, 1993) p97.

1-2% Nd reduces hillock formation by a factor of 1000 or more, but as annealing temperatures increase from 300°C to 400°C, hillock density increases. At 350°C 1%Nd lowers density by a factor of 10, and at 400°C 2%Nd has only a slight effect (perhaps a factor of 2). (Arai et al. 2001, p 288.)w

Toshiaki Arai, et al., "Mo-capped Al-Nd alloy for both gate and data bus lines of liquid crystal displays," *Thin Solid Films* 383(2001)287-291.

Hillock formation dramatically reduced adding 0.5wt% Cu to Al or Al-1wt%Si alloy.
Michal Zaborowski and Piotr Dumania, "Kinetics of hillock growth in Al and Al-alloys", *Microelectronic Engineering* 50(200)301-309.

FIB cross sections show different stages in production of hillocks. The first stages is delamination and blistering of film with nucleation of randomly oriented grains nucleating between the film and substrate. Columnar grains in film remain intact. Further lifting of the blister-like film eventually causes cracks and a large random grain caps the hillock, filling the crack. Further growth of the hillock may consume much of the skin of the blister, producing large random grains that go completely through the film, and may become whiskers. Pure 1μm thick films grown at room temperature onto 0.2μm LPCVD SiO_2 on Si, thenpassivated with TiW layer which was removed by plasma etching.
Deok-kee Kim, B. Heiland, W.D. Nix, E. Arzt, M.D. Deal, and J.D. Plummer, "Microstructure of thermal hillocks on blanket Al thin films," *Thin Solid Films* 371(2000)278-282.

WEB SEARCH
Wisker vs. Hillock growth in thin films. Precipitation at grain boundaries can suppress grain boundary sliding, which suppresses hillock growth. When grain boundaries are pinned, whishker growth appears as a means of relieving stress.

R.S. Bailey, "Effects of Target Microstructure on Aluminum Alloy Sputtered Thin Film Properties," Presented at the 38th Annual Symposium of the American Vaccum Society
Seattle, Washington
November 1991

4.L. Succo, J. Esposito, Monty Cleeves, S. Whitney, R.B. Lionetti, and C.E. Wickersham, Jr., Journal of
Vacuum Science and Technology, A7, 814 (1989).

UofM
45. G. S. Was, D. J. Srolovitz, Z. Ma and L. Dong, "Microstructure Control for Hillock Suppression in Thin Film Metallization," Society for Information Display Conference, September 22-23. 1997.

D.J. Srolovitz, et al. "Controlling Textture during the Deposition of Thin Metal Films" MURI review, May 17, 1999. University of Michigan

Effects of Target Microstructure on Aluminum Alloy Sputtered Thin Film Properties

By: R. S. Bailey Tosoh SMD, Inc.

TOSOH SMD Technical Note TKN 2.001A

Abstract

Target microstructure influences the properties of sputter deposited films. In this paper, we report the effect of target microstructure on aluminum alloy sputtering from conical targets. We have controlled the fabrication of Al-Si and Al-Si-Cu targets to produce differing amounts of Al_2Cu and Si second phase precipitates and grain sizes. Films, 1 µm thick, were sputter deposited onto oxidized silicon wafers at several different substrate temperatures. The characterization of these films is presented both as sputtered, and after annealing. The thin film properties studied include: resistivity, resistance ratio, reflectivity, and silicon nodule formation. The amount of second phase in a target was found to impact film properties, while target grain size had no effect on the film properties examined.

Presented at the 38th Annual Symposium of the American Vaccum Society
Seattle, Washington
November 1991.

I. Introduction

Aluminum metallization is used extensively in the integrated circuit industry. Typically, aluminum is alloyed with other elements to improve its performance for certain applications. As an example, silicon is often added to aluminum to satisfy its solubility at its maximum processing temperature, to prevent the so-called "spiking" phenomenon[1]. Another common reason for alloying is to reduce electromigration related failures in aluminum interconnects. Copper is often added to aluminum for this purpose[2].

Sputter deposition is the most popular method for producing metal films for integrated circuits. The properties of the target material influence the sputter deposited film microstructure. For aluminum alloy sputter deposition, the major target properties to consider are: grain size, alloy content, the amount and distribution of second phase precipitates, and crystallographic texture.

The effect of target crystallographic orientation has been studied[3]. It was found that sputtered atoms tend to leave the surface of the target along preferred crystallographic directions. The uniformity of the deposited film is strongly affected by the texture of the polycrystalline target.

The amount of second phase precipitates in a target has been found to influence the growth of "whiskers" in aluminum-silicon-copper sputter deposited films[4]. Whisker growth, which relieves stress at temperatures greater than 400°C, was

found to be more pronounced in films deposited from heavily precipitated targets. Compressive stress in an aluminum film is usually relieved by grain boundary sliding which forms hillocks. The emission of molecules (dimers and trimers) from regions of second phase in the target is proposed to create nucleation sites for precipitation in the film. The increase in precipitation in a film is thought to suppress hillock growth by "pinning" the grain boundaries. This suppression causes film stress to increase, and a second mode of stress relief, whisker growth, to occur.

The work described here is an investigation of the effects of target microstructure on sputtered thin film properties. Aluminum alloy targets were produced under controlled conditions to create a range of precipitation levels and grain sizes. Measurements made on the films deposited from these targets are presented. The results show a significant influence of target precipitate level on film properties. This effect is explained by the theory of molecular emission from second phase material in the target. No significant effects were found for grain size variations in the target.

II. Experimental

A. Sample Preparation

Aluminum alloy targets were fabricated with different microstructures. The targets used in this study were seven inch diameter conical magnetron sputtering targets, for use in the Varian 3180® sputtering source. In some cases, heat treatments after forging were used to create targets with either a heavily precipitated microstructure, or a single phase structure. In other cases, ingots cast under various conditions were used to create targets with different grain sizes. The alloys studied in this experiment were limited to Al-1%Si, Al-1%Cu, Al-1%Si-1%Cu, and Al-1%Si-.5%Cu (all compositions are in weight percent). These targets were used to deposit films on oxidized silicon substrates in a Varian 3260® DC magnetron sputtering system. Silicon wafers were oxidized in steam at 1100°C to a thickness of ~0.12μm. Metal films were sputter deposited at 9.6kW with 0.8 Pa Ar pressure to a thickness of 1 μm. The substrate temperature was varied from room temperature up to 450°C. Some films, after deposition, were annealed in N_2 at 420°C for 30 minutes in a quartz furnace tube.

B. Film Measurements

A variety of measurement techniques were used to compare the properties of the films. Most of the data was obtained using routine methods such as sheet resistance, resistance ratio, and reflectivity measurements. This section briefly describes the various techniques used.

Sheet resistance measurements were made with a Magnetron® 4-point probe system. Comparisons of resistivity between films requires measuring both the sheet resistance and film thickness. Since the latter is often less precisely known, sheet resistance is generally inadequate for comparing subtle differences between films. To eliminate the need for accurately determining film thickness, resistance ratio measurements[3] are preferred. Wafer level sheet resistance measurements were made using the Van der Pauw technique[4] with a 4-terminal μΩ-meter (Cambridge model 510A). The sheet resistance, R_s, is measured in this fashion at room

temperature and in liquid nitrogen. The resistance ratio, RR, is calculated by $RR=R_s(TR_{295^oK})/R_s(T_{77^oK})$.

Film thickness uniformity was determined using an optical densitometer with thin films (60-80nm) deposited on glass plates. Measurements were made at 1 cm intervals across a 100 mm wafer diameter. The variation in film thickness was calculated by %Var=(max-min)/(max+min)x100%.

Reflectivity measurements were made using a Varian Cary 3® spectrophotometer over the wavelength range from 200 to 900 nm. Both specular and diffuse reflectivity were measured. For the diffuse reflectance measurements, an integrating sphere is used to collect all light scattered in the non-specular directions.

The precipitation levels in the films were determined after annealing. Wafers were placed in an acid bath (H_3PO_4:HNO_3:H_2O 16:1:2 at 60°C) to dissolve away the aluminum and leave the Si precipitates on the surface of the wafer. Optical microscopy was used to characterize the amount and distribution of second phase material.

III. Results

A. Effects of Target Precipitation Level

The effects of target precipitation level on the reflectivity of Al-1%Si-1%Cu films deposited at different substrate temperatures are seen in Figure 1(a-f). For the intermediate temperature ranges, films deposited from the precipitated target have higher reflectivity than films from the single phase target. At higher deposition temperatures the reflectivity of the films become similar. At lower deposition temperatures the film reflectivity differences due to the target type are less pronounced, with an exception observed in Figure 1-a in the short wavelength range. The difference in the spectra of Fig. 1-a is thought to be due to process fluctuations, not target differences, as will be described in Section IV.

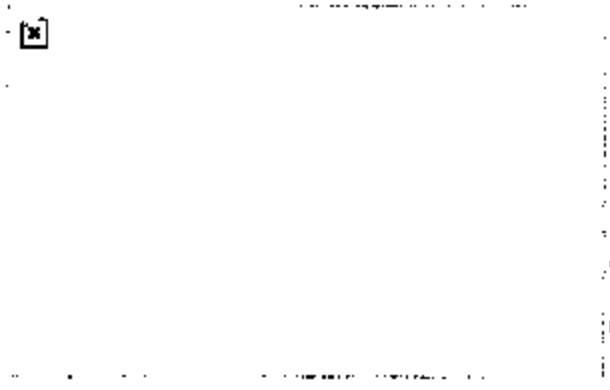

Figure 1: Specular reflectance from Al-1%Si-1%Cu films, as deposited at different temperatures.

Resistance ratio, RR, measurements were made on the same Al-1%Si-1%Cu films deposited from the single phase and precipitated targets. Figure 2 shows the results from these measurements. The films from the precipitated target have higher RR values for the intermediate deposition temperatures.

The films sputtered from the two types of Al-1%Si-1%Cu targets were annealed at 420°C in N_2 for 30 minutes. Film measurements were repeated to see if any differences due to the target type remained.

Figure 3 shows the differences in precipitate size and distribution formed in the films after the anneal. Films from the precipitated target show larger precipitates at a lower density compared to films from the single phase target. This difference is very pronounced for the films deposited at lower temperatures, and becomes more subtle at higher deposition temperatures.

The resistance ratio was measured for these Al-1%Si-1%Cu films after the anneal. All the films were found to have a RR of about 4.7. The variations in the as-deposited solute levels of the films, as inferred from the initial RR measurements (Figure 2), have been reduced by the anneal treatment. The data also suggests there was no significant grain size differences in these films after the anneal. However, grain size measurements were not completed for these films.

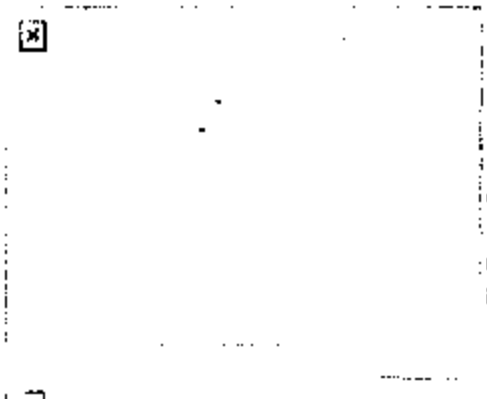

Figure 2: Resistance ratio measured from Al-1%Si-1%Cu films, as deposited from targets of different precipitate levels, as a function of temperature.

Figure 3: Precipitate distribution in Al-1%Si-1%Cu films after annealing at 420°C for 30 minutes, for targets of different precipitate levels, and different deposition temperature.

Figure 4(a-f) shows the reflectivity measurements made on the Al-1%Si-1%Cu films after annealing. For the films deposited at lower temperatures, a significant difference is seen between the two target types. This is in contrast to the as-deposited reflectivity curves, of Figure 1, where the more pronounced differences were seen at intermediate temperatures. The exaggerated reflectivity differences at lower deposition temperatures, as seen in the spectra of Figure 4(a,b), coincides with the greatest film precipitation differences observed in Figure 3. Probable causes for these reflectivity differences are discussed in Section IV.

B. Effects of Target Grain Size

Targets were fabricated with different grain sizes, as described in Section II. Figure 5 shows the results of reflectivity measurements made on Al-1%Si-.5%Cu films deposited from 3 targets with average grain sizes of 230, 750, and 1600 µm, respectively. In these spectra, there is very little difference due to target grain size. The differences in the spectra at short wavelengths, for the low temperature deposited films, are not due to target differences, as explained in Section IV. Targets of Al-1%Si and Al-1%Cu were also fabricated with similar variations in grain size. Reflectivity measurements on films deposited from these targets, showed no affect of target grain size. Resistance ratio measurements on these films are shown in Figure 6. The target grain size does not have a significant influence on the resistance ratio for these films. The film uniformity measured for all of these targets was 3% or better. No obvious relationships to grain size were detected. This was not unexpected since these targets were all fabricated to have similar crystallographic textures, which is known to have the major impact on film uniformity.

Figure 4: Specular reflections from Al-1%Si-1%Cu films, after annealing at 420°C for 30 minutes, deposited at different substrate temperatures.

IV. Discussion

A. Precipitation Effects

The effects of target precipitation level on film properties can be explained by the theory of molecular emission from the target. The precipitated target sputters more molecules of Si or Al_2Cu by dimer or trimer emission from areas of second phase. These molecules act as nucleation sites causing more second phase to precipitate in the film deposited from the precipitated target. At low deposition temperatures there is little precipitation in the film due to the low diffusion rates of Si and Cu, so differences in the number of nucleation sites coming from the target have little impact on film properties. At intermediate temperatures diffusion rates are higher and a greater amount of solute can precipitate out at the nucleation sites. At higher temperatures the solubility has increased to the point were many of the nucleation sites coming from the target are dissolved. The films deposited at intermediate temperatures from the precipitated target have less silicon or copper in solid solution, and exhibit a higher resistance ratio. Part of the reflectance differences seen between the films from the single phase and precipitated targets is explained by conductivity differences due to these precipitation effects.

Figure 5: Specular reflections from Al-1%Si-.5Cu films, as deposited at different substrate temperatures, from different grain size targets.

The precipitate distribution in annealed films is influenced by the precipitation level of the target. Films deposited from the single phase target have small precipitates, at a higher density. At first thought, this result seems to contradict the theory, discussed previously, on the sputtering differences between single phase and precipitated targets. However, it is still believed that films deposited from the precipitated target have more nucleation sites. The precipitates formed in the as-deposited film from the precipitated target, though numerous, are very small. While films sputtered from the single phase target have fewer precipitates, these precipitates grow larger. The annealing process causes the smaller precipitates to dissolve in favor of larger ones, due to the variation in free energy with particle size[7]. A distribution of very fine precipitates at high density is lost into solution during the anneal, and results in a distribution of large particles at low density. The very pronounced difference between the two target types, as seen in Figure 3, for the lower temperature deposited films supports this explanation.

Figure 6: Effect of target grain size on resistance ratio of films as a function of deposition temperatures, for three different alloys.

B. Reflectivity measurements

Film reflectivity is very sensitive to the deposition conditions, and such measurements are valuable in comparing subtle differences caused by target microstructure. Examples of different reflectance spectra measured from films sputtered under different conditions are shown in Figures 1, 4, and 5. It is worthwhile to consider the film morphology differences that might cause the changes seen in these spectra. The resistivity of the films can influence reflectivity. Figure 7-a shows the calculated reflectivity as a function of film resistivity. These calculations were done by including the film conductivity effect on the damping frequency term in the Lorentz-Drude model[8]. While the resistivity of the film is seen to effect reflectivity, the changes are not great enough to explain the differences in the measured spectra. The effect of surface roughness on light scattering can be modeled by a simple scalar scattering theory[9]. According to this theory, the relationship between the RMS surface roughness (δ), the specular reflectance (R_s), the diffuse reflectance (R_d), and wavelength (λ), is given by $R_s/(R_s+R_d)=\exp(-(4\pi\delta/\lambda)^2)$, for

normal incidence. This model has been found to be accurate when the surfar roughness is small compared to the wavelength, and when the lateral dimensions are comparable to or greater than the wavelength. Figure 7-b shows the reflectivity calculated for aluminum films including the effects of surface roughness. By including a RMS surface roughness in this simple model we are able to approximate the measured spectra from the films studied in this work. The dip in reflectivity at 820 nm seen in the spectra of Figures 4 and 5, is due to a well-known interband transition of conduction electrons in aluminum[9].

Some of these spectra exhibit sharp reflectivity dips in the 200-400nm range which do not fit the scalar scattering theory. In Figure 1(a,b) the films deposited at "room temperature" and at 100°C show a sharper reflectance fall off at shorter wavelengths. This drop in reflectance is not associated with an increase in light scattering from the film's surface. Diffuse reflectance measurements for these same films do not show an increase in this wavelength range. The sharp reflectance drops in Figure 1(a,b) can not be explained by the reflection and scattering theories discussed earlier. Jebarl et al11 have reported on a similar anomalous absorption, in the wavelength range from 240-300 nm, for pure aluminum films deposited at cold temperatures (T=140-250°K). They attribute this phenomenon to surface plasmon resonant absorption occurring in small voids or pores in the film. The lower temperature deposited films are likely to be more porous, consisting of smaller grains separated by open grain boundaries. The temperature range for which this anomalous absorption is observed is higher in this work, where an alloy is being deposited. The alloy impurities have increased the temperature required for grain boundary diffusion.

Figure 7: Calculated reflectivity spectra using Lorentz-Drude model with scalar scattering theory, a) effect of film resistivity, b) effect of RMS surface roughness.

The shape and position of the reflectivity minima observed in the 200-300nm range, for the colder deposited films, are inconsistent between wafers deposited under identical conditions. The morphology of films deposited at these temperatures is very sensitive to small fluctuations in deposition conditions. At lower temperatures the grain size in the films is relatively small, limited by the separation of the initial nucleation islands during film growth. At higher temperatures these islands coalesce and grain size begins to approach the film thickness. The films deposited at "r.t." to 100°C are in the temperature range where grain coalescing begins to occur during film deposition. TEM micrographs of films deposited in this range show a wider distribution of grain sizes. The volume fraction of open grain boundaries, and perhaps the width of these crevices are very sensitive to deposition temperature fluctuations. Variations in reflectivity in this critical area cannot be attributed to target

differences without greater data sampling.

The spectra in Figure 4 from the precipitated target show a more pronounced dip around 200-300 nm which may be associated with open grain boundaries. With these films, deposited from the precipitated target, the loss of nucleation sites during annealing may have resulted in increased grain boundary precipitation. Increased film stress coupled with reduced grain boundary diffusion could have caused the grain boundaries to open up during the anneal. Further work is needed to test this speculation.

V. Conclusions

The microstructure of aluminum alloy targets was found to influence the properties of sputtered thin films. Of the target effects studied in this work, second phase precipitates and grain size, only the amount of second phase precipitates was found to affect film properties. The results can be explained by increased molecular emission from areas of second phase in the target. These second phase molecules are incorporated into the film and act as nucleation sites for precipitation. The degree of the target second phase effect depends on substrate temperature during sputtering. Post deposition film annealing was found to be effective in enhancing film reflectivity differences due to target precipitation level. Target grain size was not found to influence the film properties examined.

References

1. D. Pramanik, and A.N. Saxena, Solid State Technology, 26, (1983).
2. G.A. Walker, and C.C. Goldsmith, Journal of Applied Physics, 44, 2452 (1973).
3. C.E. Wickersham, Jr., Journal of Vacuum Science and Technology, A7, 2355 (1989).
4. L. Sucoo, J. Esposito, Monty Cleeves, S. Whitney, R.E. Lionetti, and C.E. Wickersham, Jr., Journal of Vacuum Science and Technology, A7, 614 (1989).
5. W. Baerg, K. Wu, P. Davies, Giang Dao, and D. Fraser, IEEE Proceedings of Reliability Physics, 28, 119 (1990).
6. L.J. Van der Pauw, Philips Research Reports, 13(1), 1 (1958).
7. see for example: R.E. Reed-Hill, "Physical Metallurgy Principles", 2nd edition, PWS Publishers, Boston MA, p.372 (1973).
8. M.I. Markovic, and A.D. Rakic, Applied Optics, 29(24), 3479 (1990).
9. J.M. Elson, and J.M. Bennett, Optical Engineering, 18(2), 116 (1979).
10. N.W. Ashcroft, and K. Sturm, Physical Review B, 3(6), 1898 (1971).
11. M. Jabari, Y. Borenszteln, and G. Vuye, Physica A, 167, 371 (1989).

PERGAMON

Microelectronics Reliability 39 (1999) 1631–1645

MICROELECTRONICS RELIABILITY

www.elsevier.com/locate/microrel

Electromigration induced aluminum atom migration retarding by grain boundary structure stabilization and copper doping

M. Hasunuma*, H. Toyoda, H. Kaneko

ULSI Process Engineering Laboratory, Microelectronics Engineering Laboratory, Toshiba Corp., Semiconductor Company, 8 Shinsugita-cho, Isogo-ku, Yokohama 235-8522, Japan

Received 18 February 1999

Abstract

In order to clarify the relationship between Al line reliability and film microstructure, most notably grain boundary structure, we have tested three kinds of highly textured Al lines, namely a single-crystal Al line, a quasi single-crystal Al line and a hyper-textured Al line. Consequently, it has been shown that these kinds of lines have excellent endurance against electromigration (EM), compared with conventional Al lines deposited on TiN/Ti and SiO_2. The improvement of Al line reliability is attributable to the following factors; firstly, homogeneous microstructure and high activation energy, 1.28 eV, of the single-crystal Al line ($\omega = 0.18°$); secondly, subgrain boundaries, consisting of dislocation arrays found in the quasi single-crystal Al line ($\omega = 0.26°$), have turned out to be no more effective mass transport paths because dislocation lines are perpendicular to the direction of electron wind; finally, the decrease of the (1 1 1) full width at half maximum (FWHM) value promotes the formation of subgrain boundaries and low-angle boundaries, which have small grain boundary diffusivity, as revealed by the detailed orientation analysis of individual grains in the hyper-textured line (FWHM = 0.5°) formed by using an amorphous Ta–Al underlayer (Toyoda H, Kawanoue T, Hasunuma M, Kaneko H, Miyauchi M. Proc. 32nd Ann. Int. Reliab. Phys. Symp., IEEE, 1994;178). Moreover, the diffusivity reduction and the uniformity of atomic flux result in the suppression of void/hillock pair in the Al lines. It has been clarified that a FWHM value is a useful criterion of reliability for an interconnection. Also, the Cu doping effect against EM endurance by using Cu implantation of the single-crystal Al lines has been examined. It has been clarified that EM lifetime is lengthened by about one order of magnitude for the Cu concentration of 0.1 at% in spite of almost the same diffusion coefficients. Moreover, the incubation time for a void nucleation has been observed even in the case of a pure-Al line. Thus, in accordance with the stress evolution model, it is concluded that the mechanism of lifetime improvement by Cu doping is such that critical stress for EM void nucleation is increased by the Cu doping. These results have confirmed that control of texture and/or grain boundary structure so as to suppress EM induced metal atom migration is a promising approach for the development of Al lines and Cu lines capable of withstanding the higher current densities required in future ULSIs.

1. Introduction

Open circuit failure of Al line induced by EM and/or thermal stress has become a more serious reliability

* Corresponding author.
E-mail address: hasunuma@sanc.toshiba.co.jp (M. Hasunuma).

0026-2714/99/$ - see front matter
PII: S0026-2714(99)00167-5

problem due to current density increase and line width shrinkage in accordance with the progressive miniaturization of ULSIs. To improve the endurance of metal lines against EM, many efforts have been focused on seeking new alloying elements, such as Al–Si–Ti [2], Al–Cu–Ti [3], Al–Pd–Si [4] and Al–Sc [5] alloys, or on employing a layered-structure with TiW and TiN/Ti underlying barrier metals [6,7]. From the viewpoint of Al film microstructure, efforts to facilitate bamboo alternation by abnormal grain growth [8] or rapid thermal annealing [9] and (1 1 1) texture improvement have stimulated basic research to elucidate the role of grain boundaries. Although recent research has revealed that (1 1 1) texture improvement lengthens EM lifetime [1,10,11], the mechanism of the improvement has not been completely understood.

Stress induced open failure has also become a serious concern. Although this failure had appeared to be settled by utilizing refractory metal barrier layer, it has been clarified that stress induced voids degrade the EM lifetime [12,13]. Originally, stress induced failure is due to high tensile stress induced in metal lines because of the thermal expansion mismatch between Al and SiO_2, and is well predicted by the power-law creep model [14]. However, these results do not indicate how to improve the endurance, because the creep only takes into account the macroscopic physical properties. Therefore, a microscopic understanding of void growth and open failures is essential.

Transmission electron microscopy (TEM) and scanning electron microscopy (SEM) observations of realtime and/or in-situ voiding phenomena have already revealed the relationship between the surfaces surrounding voids and the specific crystal planes, such as {1 1 1}, {1 0 0} [13,15]. Moreover, according to the thermodynamic analysis of the nucleation and growth of void formation in bamboo-like structure lines, the critical free energy change for void nucleation is a function of the grain boundary energy and its energy change is small for high energy grain boundary, i.e., random grain boundary [16]. This analysis strongly suggests that in order to achieve reliable Al lines, it is necessary to remove the specific grain boundary that leads to slit-like open failure where {1 1 1} planes of adjoining grains contact almost face to face [17,18]. It has also been pointed out that grain boundary energy decrease prevents a nucleation of void, and a single-crystal metal line is an ultimate product since it does not include any fast diffusion paths for void growth [18,19]. Therefore, the control of grain boundary structure is indispensable in order to obtain a guiding principle for realizing reliable metal lines.

On the other hand, in the case of polycrystalline lines, Cu doping has been found to markedly improve EM and SM endurance [20–22]. An Al(Cu) alloy system is known to be a precipitate hardening system in bulk materials. However, the role of Cu respecting thin film has not been clarified, i.e., the grain boundary diffusion suppression by $CuAl_2$ precipitates [20] or solute drag effects on dislocations by Cu solute [21].

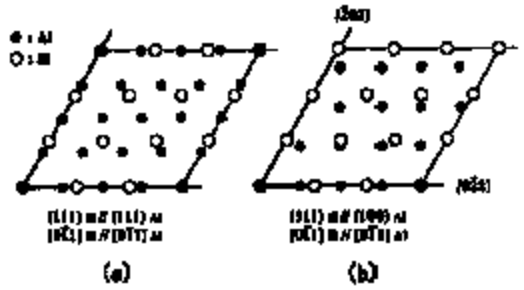

Fig. 1. (a) Schematic diagram showing the superlattice for the Al(1 1 1)/Si(1 1 1) interface. In this model, four Al lattice spacings match three Si lattice spacings; (b) one of the superlattices for the Al(1 0 0)/Si(1 1 1) interface. Only [0 −1 1] direction matches. Open circles and solid circles indicate the position of Si lattice and Al lattice, respectively.

This paper aims to clarify the relationship between EM reliability and microstructure for three kinds of films and the effect of Cu doping of a single-crystal Al film: firstly, a single-crystal Al (further denoted as s-Al) film deposited directly onto the Si(1 1 1) substrate by the CVD technique [23]; secondly, a quasi single-crystal Al (further denoted as qs-Al) film deposited directly onto Si(1 1 1) substrate [24,25], and containing subgrain boundaries with the lowest grain boundary energy; thirdly, a hyper-textured Al (further denoted as ht-Al) film developed using an amorphous Ta–Al underlayer [1]; and finally, a Cu doped single-crystal Al (further denoted as s-Al(Cu)) in which case the s-Al film was prepared prior to Cu ion implantation. The FWHM values of the (1 1 1) rocking curve were 0.18° for an s-Al film, 0.26° for a qs-Al film, and 0.5° for an ht-Al film. The amount of doped Cu was 0.1 at%, within solid solubility. In the ht-Al film, many subgrain boundaries with a homogeneous and low grain boundary energy were found. The mutual orientation of adjacent grains has been determined by TEM analysis. In the case of the ht-Al film it is possible to analyze the grain boundary structure by such a simple method, because the grain boundary structure is simplified by eliminating the twist angle component.

Furthermore, hyper-textured Cu (further denoted as ht-Cu) films, the most promising interconnection for future metallization, have been achieved by means of the same concept as the ht-Al films with several kinds of amorphous underlayers.

Fig. 2. Cross-sectional lattice image of Al(1 1 1)/Si(1 1 1) interface. An aluminum film deposited by GTC-CVD technique. Incident electron beam is parallel to Si [1 1 0] direction.

2. Film preparation

2.1. Single-crystal Al film (s-Al film)

An s-Al film was directly deposited onto clean Si(1 1 1) substrate by the gas-temperature-controlled chemical vapor deposition technique (GTC-CVD) [23]. Fig. 1(a) shows a schematic diagram of the common superlattice for the Al(1 1 1)/Si(1 1 1) interface. In this model, four Al lattice spacings are matched to three Si lattice spacings along the [1 1 0] direction, because the lattice constant mismatch between Al(1 1 1) (d = 2.338 Å) and Si(1 1 1) (d = 3.135 Å) is approximately 25%. The closed circles and open circles represent the positions of Al and Si atom, respectively. A cross-sectional lattice image is shown in Fig. 2. The arrows indicate possible atom matching points, which have a periodicity of every three Si lattice spacings, which is the same as the relationship shown in the schematic diagram of Fig. 1(a). From the electron diffraction analysis, the epitaxial relation between Al and Si was Al(1 1 1) // Si(1 1 1) and Al [1−1 0] // Si [1−1 0] [24,25], as shown in Fig. 1(a).

The degree of the crystallinity was evaluated by the FWHM value of the rocking curve for the Al(1 1 1) peak. The rocking curve was measured by 4-crystal collimated x-ray diffraction using the CuK_α radiation by scanning an incident angle θ, while the diffraction angle 2θ was fixed for the Al(1 1 1) peak. The FWHM value of 400 nm thick s-Al film was 0.18°.

2.2. Quasi single-crystal Al film (qs-Al film)

Al films were deposited onto Si(1 1 1) substrate by RF–DC coupled magnetron sputtering system at ambient temperature. It has been found that the Al film growth by sputtering consists of three stages of different texture. The Al film textures were examined by reflection high-energy electron diffraction (RHEED) in the chamber without breaking vacuum.

Fig. 3 shows the change in the epitaxial structure during the deposition by RHEED. In the initial stage, when the film thickness is no more than 10 nm, Al layer consists of three types of (1 0 0)-oriented domains that were rotated approximately 30° with respect to each other in accordance with the following relations: Al(1 0 0) // Si(1 1 1), Al[0 1 1] // Si[−2 1 1]: Al(1 0 0) // Si(1 1 1), Al[0 1 1] // Si[−1 1 0] (as shown in Fig. 1(b)): Al(1 0 0) // Si(1 1 1), Al[0 1 1] // Si[−1 2 −1] [24]. No pattern of (1 1 1) texture has been observed in the initial stage. In the second stage, the film thickness ranges from 10 to 100 nm, and the Al (1 1 1) domain which includes twins was observed in addition to the three kinds of Al(1 0 0) domains. This

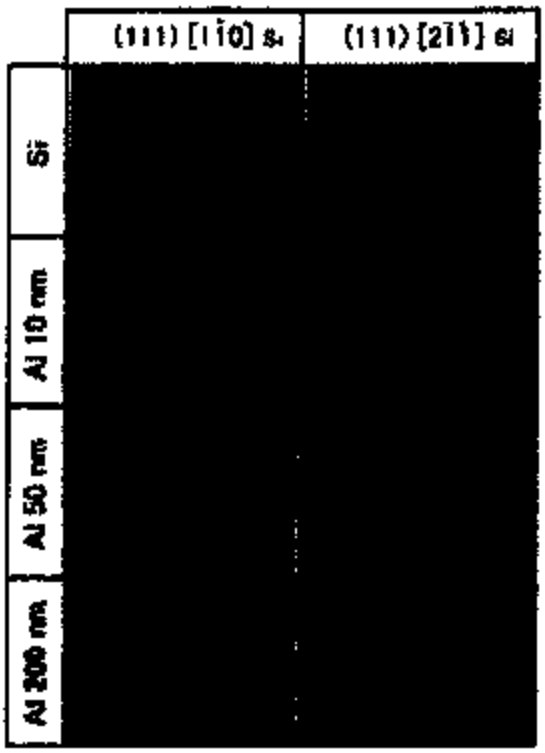

Fig. 3. In situ observation of Al epitaxial growth on Si(1 1 1) substrate by sputtering. In initial stage, three kinds of Al(1 0 0) domains were observed. Subsequently, the Al(1 1 1) domains grow by reorientation of the Al(1 0 0) domains. Finally, only the Al(1 1 1) structure remained.

Al(1 1 1) domain would be formed by the coalescence of the three kinds of Al(1 0 0) domains or recrystallization triggered at the Al / Si interface. A lot of Al(1 0 0) domains remained in the film. In the final stage, when the film thickness exceeds a few hundreds of nm, Al(1 1 1) // Si(1 1 1), Al[0 1 1] // Si[0 1 1] relation was completed. This dynamic structural change caused the subgrain boundaries in the qs-Al film. The FWHM value of 400 nm qs-Al film was 0.26°. This value is slightly larger than that of s-Al film. Fig. 4 shows the bright-field image and the diffraction pattern. The arc-like diffuse scattering near the [1 1 0] spots in the diffraction pattern indicates that there exists angular misorientation. In the TEM bright-field image, subgrain boundaries with periodic arrays of strain-field contrasts are observed. These subgrain boundaries are parallel to the {1 1 0} plane. Assuming that these dislocations are pure tilt type subgrain boundaries, the rotation angle between the two adjacent grains would be less than a few degrees.

Fig. 4. A bright-field image and a selective area diffraction pattern of the 400 nm thick qs-Al film deposited by sputtering. Many dislocation arrays were observed.

2.3. Cu-doped single-crystal Al film (s-Al(Cu) film)

An s-Al(Cu) film was prepared by Cu ion implantation into an s-Al film deposited by the GTC–CVD technique. Cu ion implantation was carried out with the acceleration voltages of 370 keV and 2.4×10^{15} ions/cm^2. The concentration of 400 nm thick s-Al(Cu) film is 0.1 at%Cu, which was near the solid solubility in Al matrix at 250°C [26]. Thus, at the EM acceleration test temperature which includes the Joule heating

Fig. 5. A bright-field image and selective area diffraction patterns of the 400 nm thick s-Al(Cu) film deposited by GTC-CVD technique and subsequently implanted with Cu. In SAD on grain boundary, some streaks attributed to GP-zone were observed at ambient temperature.

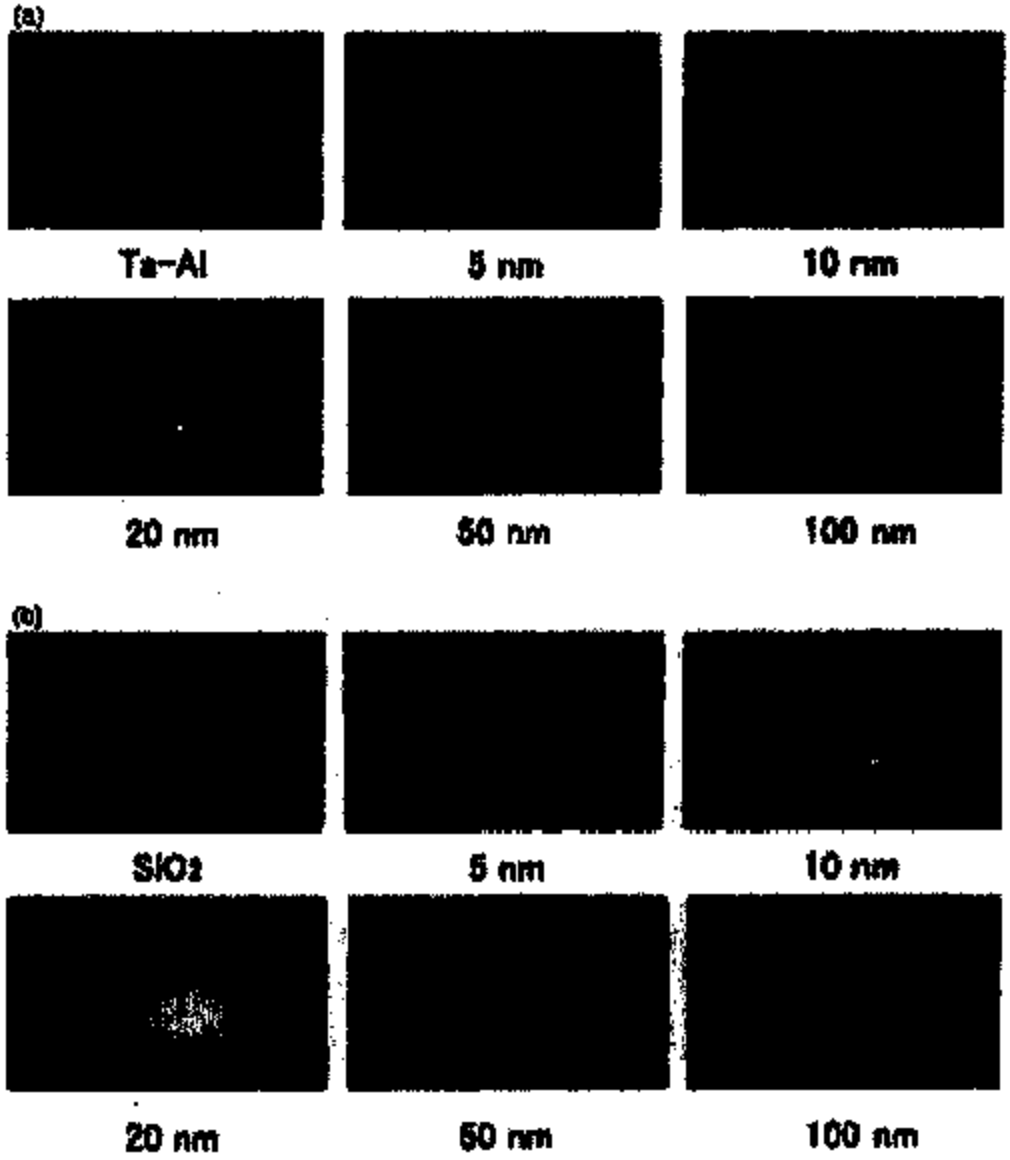

Fig. 6. (a) In situ RHEED observation results of growth of Al deposited on the amorphous Ta–Al underlayer; (b) In situ RHEED observation results of growth of Al deposited on SiO_2.

factor, the Cu elements almost dissolve into the Al matrix. A post thermal treatment of 30 min at 400°C was carried out in order to remove lattice defects introduced by ion implantation process and to homogenize Cu distribution.

Fig. 5 shows the top-view image and a selective area diffraction patterns (SADs) of s-Al(Cu). A subgrain boundary was also observed in this film. This dislocation array might be produced by recovery of various lattice defects introduced by ion implantation process. In the SAD, some streaks attributable to GP-zone were observed only near the subgrain boundary area at room temperature and precipitated during cooling process after the acceleration test. It shows that Cu strongly interacts with lattice defects in Al films. From the results of the x-ray analysis using $\sin^2\Psi$ method, the compressive stress of the Cu implanted film was 30 MPa. Consequently, the tensile stress varied to approximately 150 MPa after thermal treatment.

Therefore, the s-Al(Cu) film microstructure is almost

the same as that of the s-Al film except for containing small amounts of subgrain boundaries.

2.4. Hyper-textured Al films (ht-Al films)

An ht-Al film was developed using an amorphous underlayer [1]. An Al–0.1 at%Cu film deposited on Ta–Al amorphous underlayer indicated an FWHM value of 0.5°. This ht-Al line made it possible to estimate the effect of the texture on the EM lifetime in regions ranging from a conventional polycrystal to a single-crystal.

At the early stage of the film growth, Al islands are formed on a substrate, and they coalesce and become a continuous film as in the case of a qs-Al film on Si(1 1 1). According to the classical theory, the shape of the island is determined by Young's equation. The relation is expressed as

$$\cos\theta = \frac{\sigma_s - \sigma_i}{\sigma_f} \quad (1)$$

where θ is the wetting angle of the island, σ_s and σ_f are the surface energies of the substrate and the island, respectively, and σ_i is the interfacial energy between the island and the substrate. When $\sigma_s - \sigma_i > \sigma_f$, it is considered that the film grows two-dimensionally (layer-growth). By this layer-growth mode, it is expected that two-dimensional (2D) island with stable (1 1 1) surface would be formed. An amorphous substrate will enhance this tendency, because there is no specific crystal lattice matching restriction between a film and a substrate that obstructs the stable (1 1 1) 2D-island formation. Assuming that the (1 1 1) texture of the film is improved by approaching the layer-growth mode, high σ_s and low σ_i are preferable for realizing a small wetting angle according to Eq. (1). The effect of the surface energy on the texture of the Al film for amorphous underlayers was investigated, because the origin of σ_i on an amorphous substrate still remains unknown. The surface energy of an amorphous alloy was assumed to be the sum of the fractional surface energies of individual elements.

Various kinds of amorphous and polycrystalline 100 nm thick underlayers were deposited on thermally oxidized Si substrates. Al films were deposited and examined using the same methods as for qs-Al film.

Fig. 6 shows the RHEED patterns for the Al films on the amorphous 75 at%Ta–25 at%Al alloy (Fig. 6(a)) and SiO_2 (Fig. 6(b)), which are observed for various kinds of Al film thickness. The patterns on both amorphous underlayers exhibited a (1 1 1) texture even for 5 nm thickness film and the pattern on Ta–Al was sharper than that on SiO_2, and this tendency was the same for the thicker films. Furthermore, the texture of Al films improved with increasing thickness, and by post annealing. Thus, it has been proved that the texture improvement will be accompanied with grain growth. Al–0.1 at%Cu films showed a better texture than pure Al films probably because σ_f in Eq. (1) decreases by Cu addition. A sintered 400 nm Al(Cu) film on Ta–Al indicated an FWHM value of 0.5°. The FWHM values of 20 nm thick Al films on various underlayers are plotted against the surface energy of the underlayers in Fig. 7. No clear relation was found between the FWHM value and the surface energy on polycrystalline underlayer. This scattering of the texture might be due to both lattice mismatch and the difference in the underlayer texture. On the other

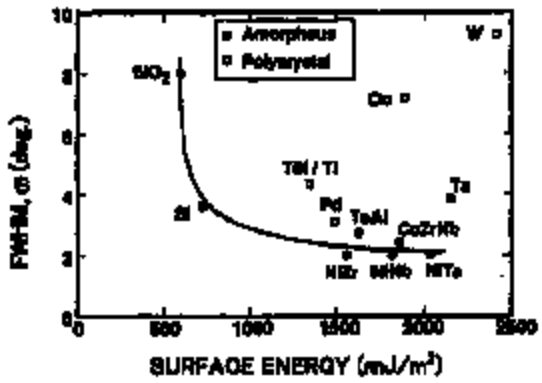

Fig. 7. The relationship between surface energy of underlayer and the FWHM values of 20 nm thick Al films deposited on the underlayers. The open squares and closed circles indicate polycrystalline underlayers and amorphous underlayers, respectively.

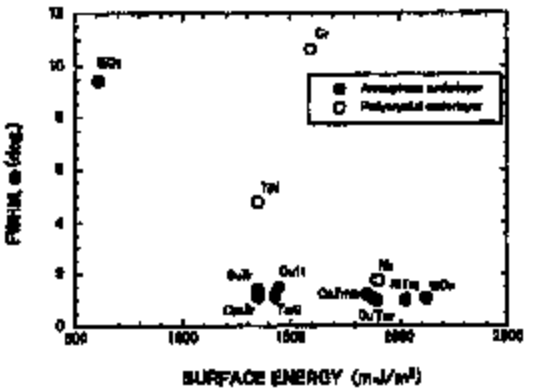

Fig. 8. The relationship between surface energy of underlayer and the FWHM values of 100 nm thick Cu films deposited on the underlayers. The open circles and closed circles indicate polycrystalline underlayers and amorphous underlayers, respectively.

Fig. 9. SEM photographs of the s-Al line after EM accelerated test for 19 h.

hand, the FWHM value for the Al film decreased with an increase in the surface energy for amorphous underlayers. These results confirmed that both a high surface energy and an amorphous state are necessary for improving the texture. It is also considered that the interfacial energy σ_i is uniform and might be small for amorphous underlayers.

2.5. Hyper-textured Cu films (Hyper-textured Cu films)

Ht-Cu films were also developed using amorphous underlayers. The concept of ht-Cu film development is the same as that of ht-Al films. Fig. 8 shows the relation between the (1 1 1) FWHM value for the Cu 100 nm thick film and the surface energy of the amorphous underlayer. The (1 1 1) FWHM values for Cu films deposited onto polycrystalline underlayers, i.e., Cr, TiN, and amorphous underlayer which has low surface energy were all above 4°, and Cu (2 0 0) peak was observed by the θ–2θ X-ray diffraction method in these lower textured films. On the other hand, the (1 1 1) FWHM values for Cu films deposited onto the metallic amorphous underlayers that have relatively high surface energy were approximately 1° and no other peaks were detected. With respect to the Nb underlayer, Nakasaki et al. calculated the interfacial energy as a sum of interatomic potential energies [27]. The Cu (1 1 1) and Nb (1 1 0) were expected to show the epitaxial relationship with a Nishiyama–Wassermann (NW) relationship with fcc [1−1 0] // bcc [0 0 1] [27], and the Cu film deposited onto (1 1 0) oriented polycrystalline Nb underlayer resulted in hyper-textured film. In the case of Cu crystal, an average surface energy is higher and the difference between surface energy of (1 1 1) and (2 0 0) is smaller than in the case of Al [28]. As a result, (2 0 0) compared with Al, Cu grains might be more easily grown during deposition of films. Thus, the lower textured Cu films and even the hyper-textured Cu film deposited onto the Nb underlayer had the mixed orientation with (1 1 1) and (2 0 0) grains. However, in the case of metallic amorphous underlayers, only hyper-textured (1 1 1) crystal grains were grown, even though the surface energy (σ_s) was nearly equal to the surface energy (σ_f) of Cu. It is considered that the interfacial energy (σ_i) between the metallic amorphous underlayer and Cu (1 1 1) might be very small.

3. Accelerated electromigration test procedure

The test lines were about 1.5 μm wide, 0.4 μm thick, and 50 μm long. The positive and the negative ends of the line were terminated with each 50 μm wide square pad without a taper and lines were unpassivated. The EM accelerated testing was carried out in a vacuum at pressures below 2×10^{-6} Torr. The acceleration conditions of films with high endurance to EM, i.e., s-Al and s-Al(Cu) lines, was 35 MA/cm^2 at 150°C ambient temperature. Under these severe conditions, conventional polycrystalline Al lines failed within a few seconds. The qs-Al and ht-Al were tested under the condition of 15 MA/cm^2 at 200°C and 5 MA/cm^2 at 200°C, respectively.

The EM induced damage, such as voids and hillocks, was examined after the accelerated test using SEM and TEM.

4. Results and discussion

4.1. Reliability of s-Al lines

The line operated at the electrical current density of

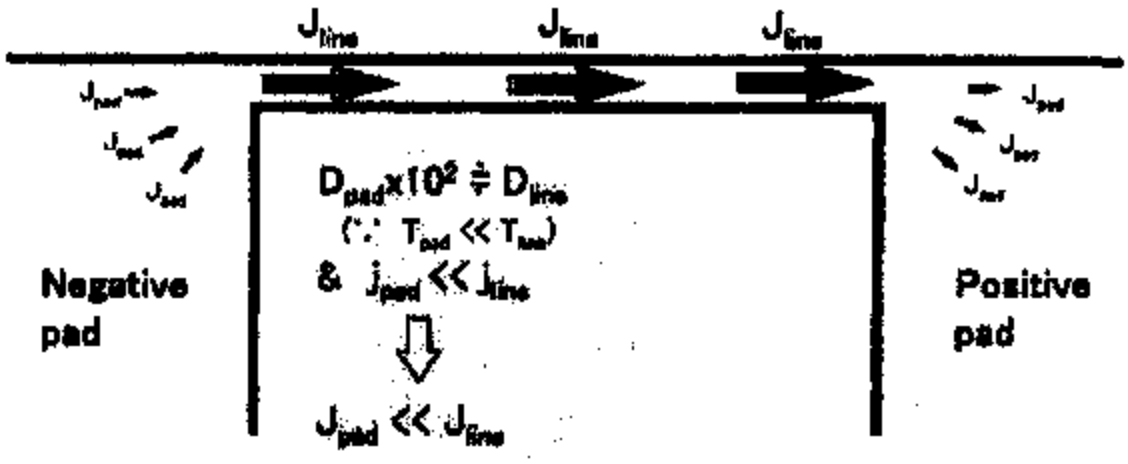

Fig. 10. Schematic diagram of highly accelerated EM test condition.

1 MA/cm^2 did not show any apparent EM damage at 150°C for 3000 h [17]. In order to obtain further acceleration, the lines were operated at a high current density of 35 MA/cm^2 in order to generate a steep temperature gradient at the junction between the line and the pad by Joule heating [29].

SEM photographs of an s-Al line after EM accelerated test for 19 h are shown in Fig. 9. Hillocks were formed mostly at the junction between the line and the positive pad and partly in the positive pad. Some hillocks were like a whisker and others were like a flat extrusion. On the other hand, voids were mostly accumulated in the negative pad and small voids were observed in the line near the negative pad. It is obvious from the void shape that the void is surrounded by {1 1 1} planes with the lowest surface energy in an fcc lattice. However, no voids were observed in the middle part of the line. These are the damage characteristics expected in the case that the temperature difference between the line and the pad is actualized by Joule heating. Actually, the average line temperatures monitored by the line electrical resistance range from 200 to 260°C. And the local temperature distribution generated by Joule heating was obtained by self-consistent finite element calculation [29]. In a typical case, the average temperature, line temperature and pad temperature were 240, 259 and 165°C, respectively.

Fig. 10 shows a schematic diagram of highly accelerated EM test condition. The temperature (T_{line}) of the line was about 100°C higher than that (T_{pad}) of the pad. It followed that the diffusion coefficient (D_{line}) of the line was more than two orders of magnitude higher than that (D_{pad}) of pad. Furthermore, the Al atoms in the line at higher current density (j_{line}) are subjected to a much higher stress (electron wind) than those at lower current density (j_{pad}) in the pad because of a shape factor. The migration in the line away from the line–pad junctions is much faster than that in the pad. The atomic flux of negative line–pad junction and that of positive line–pad junction produced atom depletion and atom accumulation, respectively. Thus, in spite of single-layered structure line, the principle of the atomic flux divergence is similar to that of W stud multiple layered line structure.

Fig. 11 shows the relationship between normalized electrical resistance change and elapsed time. The resistance initially decreased, next increased gradually.

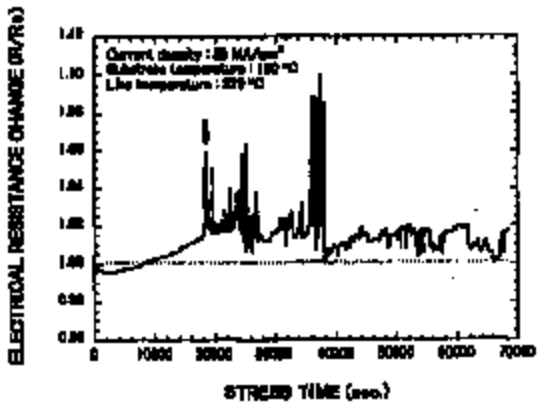

Fig. 11. Electrical resistance change for an s-Al line during EM accelerated testing with current density of 35 MA/cm^2.

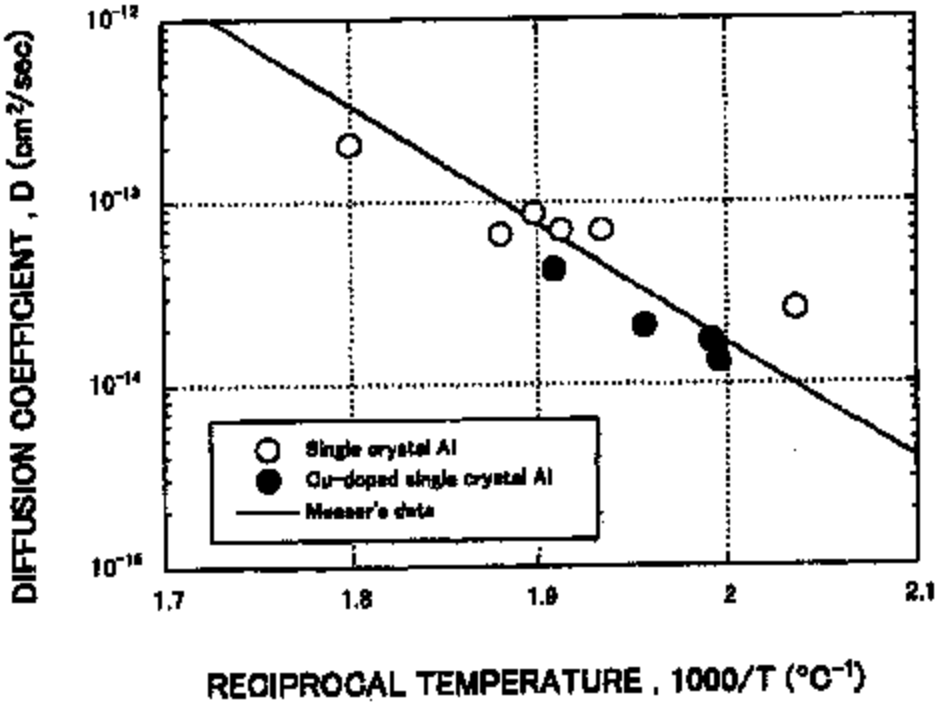

Fig. 12. Arrhenius plot of the Al diffusion coefficients obtained from void growth rate. The open circles and the closed circles indicate s-Al and s-Al(Cu), respectively, and solid line presents Messer's data.

and finally oscillated violently. To clarify the behavior of initial resistance decrease, no current loading test was carried out. After keeping some EM test lines at 150°C for 15 h, the resistance decreased from 1.5 to 2.3% at ambient temperature, which might be caused by recovery of various kinds of lattice defects introduced by thermal cycle and/or Si precipitation. From in situ SEM observation, a void appearance and voids movement corresponded with the resistance increase and the resistance oscillation, respectively. In particular, the violent oscillation of electrical resistance might be caused by a serious void shape change and occasional jumping [30]. The initial decrease, the subsequent increase and final violent oscillation were considered to be due to the recovery and/or Si precipitation, voids growth near the negative pad and voids migration, respectively. Therefore, the beginning of violent oscillation is defined as the guideline of lifetime for s-Al, as shown by an arrow in Fig. 11.

Fig. 12 shows the Arrhenius plot of the obtained diffusion coefficients calculated from the void growth rate [9]. The EM-induced void volume was obtained from the sum of the volumes of individual voids based on the assumption that the voids completely penetrated the Si substrate surface. The Al atom flux divergence, $\mathrm{div}(J)$, which contributes to the void growth near the line–pad junction, is expressed as

$$\mathrm{div}(J) = \{J(T_{\mathrm{line}}) - J(T_{\mathrm{pad}})\}/\Delta x \tag{2}$$

where $J(T_{\mathrm{line}})$ and $J(T_{\mathrm{pad}})$ are the Al atom flux at line temperature (T_{line}) and at the line–pad junction temperature (T_{pad}), respectively, and Δx is the length of the temperature changing region, 10 μm, obtained by the finite element calculation. The experimentally obtained void growth rate dV/dt could be connected to Eq. (2) as

$$(dV/dt)N/S/\Delta x = \mathrm{div}(J) \tag{3}$$

where N is the atomic density of Al, and S is the cross-sectional area of line. An ideal Al atom flux induced by EM is also expressed by the Nernst–Einstein's relationship [31]. The flux is expressed as

$$J = DNZ^*e\rho j/kT \tag{4}$$

where D is the diffusion coefficient for Al, k the Boltzmann constant, T the absolute temperature, Z^* the effective charge number, e the elementary charge, ρ

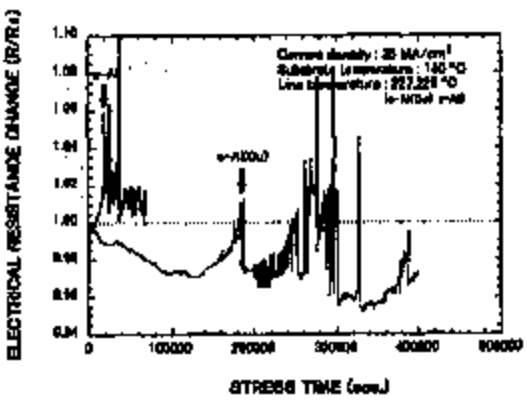

Fig. 13. Electrical resistance change for s-Al and s-Al(Cu) lines during EM accelerated testing with current density of 35 MA/cm^2.

the resistivity of Al and j the current density, respectively. The diffusion coefficients of Al were calculated from Eqs. (2)–(4). Open circles indicate the s-Al results. The straight line in this plot is the Al lattice diffusion coefficients with an activation energy of 1.28 eV and pre-exponential factor of 0.137 cm^2/s. A fairly good agreement was observed [32]. Consequently, it has been confirmed that the void growth in a s-Al line was by lattice diffusion control.

However, it is noteworthy that a fairly large amount of grown voids accumulated in the negative pads. The maximum Al atom flux divergence was generated near the negative pad where the steep temperature gradient existed. It is natural to expect that the EM-induced voids nucleate and grow in this area. However, the voids fully grown in the line near the negative pad moved into the negative pad and accumulated. This movement of the voids in s-Al lines is ascribed to their homogeneity, i.e., this film is free from trapping and/or flux divergent sites, such as grain boundaries. An s-Al line has excellent endurance against EM because of its homogeneous microstructure [17,25,29]. Consequently, the s-Al line survives an open circuit failure, and, in fact, no sample failed in the present experiment.

4.3. Reliability of s-Al(Cu) lines

The line resistance change behavior, the initial decrease, gradual increase and final violent oscillation, and the observed surface morphology of the s-Al(Cu) line after EM accelerated test were similar to the s-Al line (see Fig. 13), except for the following points;

1. The lifetime observed for the s-Al(Cu) line was approximately one order of magnitude longer than that for the s-Al.
2. The maximum resistance decrease for the s-Al(Cu) line was 3%, whereas the s-Al line resistance decrease was only 0.5%.
3. The resistance increase and decrease speeds for the s-Al(Cu) line were slower than those for the s-Al line.

It is noteworthy that the Cu doping is effective for prolonging the Al EM lifetime even though there are no grain boundaries. This result indicates that the EM lifetime improvement frequently observed in the case of Cu doped polycrystalline Al lines is not due to the diffusivity retardation by the $CuAl_2$ precipitation in the grain boundary [20]. Moreover, the Al diffusion coefficients both for the s-Al and the s-Al(Cu) lines, calculated by the void volume by using Eqs. (2)–(4) plotted in Fig. 12, differed slightly. Therefore, the Al lattice diffusion retardation by the Cu doping is not the dominant mechanism for the EM lifetime improvement. On the other hand, it is also interesting to note that the initial 3% resistance decrease observed for the s-Al(Cu) line was well explained by the Cu depletion, because the 0.1 at%Cu solution increases the Al line resistivity by almost the same amount (0.75 μΩ cm/at%Cu [33]). This hypothesis is consistent with the view of the Cu depletion proposed by Hu et al. [34]. However, it should be emphasized that the s-Al line had the incubation time for the void nucleation even though it was pure-Al and was not included in Hu's model.

Therefore, the tensile stress evolution near the negative end of line due to the absence of atom supply [35,36] should be taken into account in order to explain the incubation time for pure-Al line and to understand the effect of Cu doping. There is a critical stress that enables the void nucleation, and the incubation time is defined as the time for generating large enough tensile stress to permit nucleation. Since the present test lines were unpassivated, the tensile stresses contained in the s-Al and s-Al(Cu) line were small, approximately 150 Mpa. Therefore, the longer incubation time is necessary compared with the passivated Al line which has sufficiently large stress to nucleate a void before the EM current loading. Since the Al diffusivities both for the s-Al and the s-Al(Cu) line are almost the same, as shown in Fig. 12, the identical critical stress for the void nucleation should possess the same incubation time. Therefore, the longer incubation time for s-Al(Cu) is probably due to the critical stress increase. Similar Cu doping effect has been reported, namely only 0.1 wt%Cu doping was sufficient to improve the SM lifetime [22]. The decrease in the Al surface energy by Cu doping [28] also supports this hypothesis, because the lower surface energy increases the

Fig. 14. Bright-field image and selected area diffraction pattern of qs-Al line after EM acceleration test.

critical energy for the void nucleation. However, the large resistance decrease indicates that the Cu depletion did occur during EM testing, and the Cu depletion and/or the preferential Cu migration induced by EM always reduce the impact on the critical stress increase.

4.3. Reliability of qs-Al lines

Fig. 14 shows the microstructure of qs-Al line after EM accelerated test with the current density of 15 MA/cm^2 for 150 min and the line temperature of 200°C. Many subgrain boundaries consisting of dislocation arrays were observed, as described above. Fig. 15 shows SEM photographs after the EM accelerated test and (1 1 1) pole figure that is adjusted to the direction of the test line. In spite of this severe test condition, no voids and hillocks appeared in the middle of the line, though voids and many whisker-like hillocks formed in the negative pad and the positive pad, respectively. The voids formed in the negative pad were also surrounded by {1 1 1} planes. Thus, the endurance against EM of qs-Al line is essentially the same as that of s-Al line. In other words, subgrain boundaries do not behave as fast diffusing paths because the dislocation line of the subgrain boundary exists perpendicular to the electron wind. Moreover, the voids produced in the line near the negative pad were not immobilized by subgrain boundaries that possess lowest grain boundary energy.

4.4. Hypertextured Al lines (ht-Al line)

The measured electrical resistance changes of the lines during the tests are shown in Fig. 16. The initial increase in the resistance was due to Joule heating by current loading. The resistance of the sintered Al(Cu) line on Ta–Al increased less than 10% after 10 h. SEM photographs of the lines after 10% resistance increase are shown in Fig. 16, and for the sintered Al(Cu) line, a photograph of the line after 10 h accelerated testing is shown. Fewer defects were observed inside the Al(Cu) line, whereas many void-hillock pairs are found along the grain boundaries for the other lines. The grain size was smaller than the line width and grain-networks existed along the line direction. This means that the flux divergence at a triple point of grain boundaries is very small. It is known that grain boundary diffusivity depends on the boundary structure [37]. Al films that show no or broad texture have random grain boundaries, and the individual diffusivities of grain boundaries are quite different, and so the flux divergence occurred at a triple point and resulted in a void-hillock pair formation.

After 250 h current loading test, the resistivity change of the sintered Al(Cu) line increased to 7.5%. Most of the voids were formed inside the negative pad, which enables the vacancy flux estimation from the void volume. The obtained vacancy flux is 8.9×10^{17} m^{-2} s^{-1} and this value is the same order of magnitude as that in an s-Al line, 2.5×10^{17} m^{-2} s^{-1} [9]. Therefore, grain boundaries formed in ht-Al film are no more effective than these of conventional broad textured film as fast diffusion paths for mass-transport phenomenon by EM.

Furthermore, a detailed analysis of grain boundary structure was carried out by TEM. Fig. 17 shows the plan view of the Al(Cu) film and many subgrain boundaries were also observed in this film. The average grain size is 280 nm, but large scattering was observed in grain size. This fact suggests that the large grains have coarsened and unified because of the fairly good

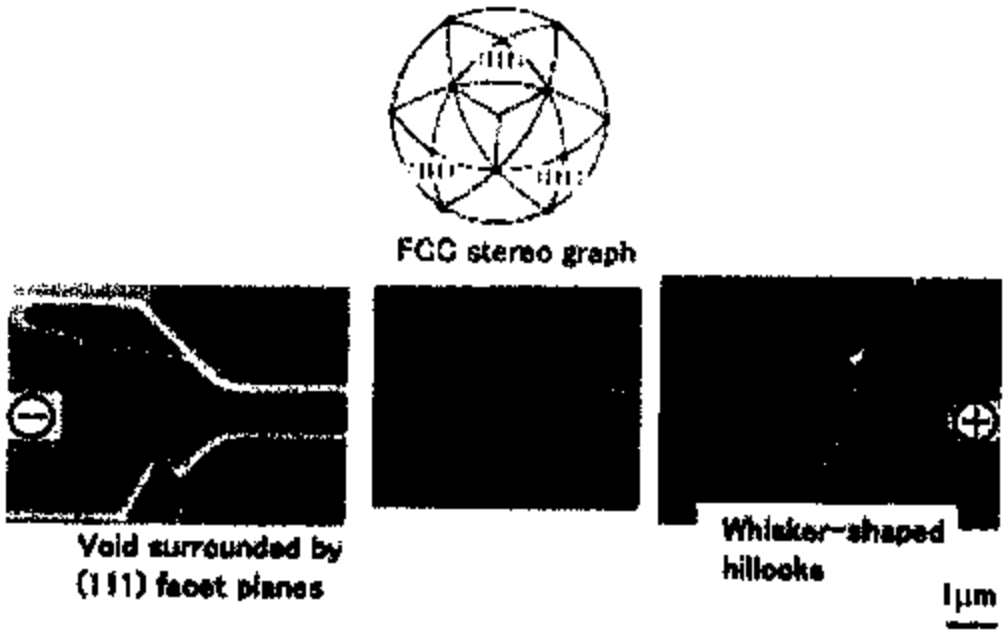

Fig. 15. SEM photograph of qs-Al line after EM acceleration test.

orientation matching among the neighbor grains. The SADs of the individual grains are shown in Fig. 17 and it proves that all the grains have (1 1 1) orientation. Assuming that the grain boundaries are perpendicular to the substrate, the most stable plane is {1 1 0} for fcc structure. The angles between a grain boundary and the {1 1 0} planes of grains on both sides are measured to investigate the property of the grain boundary structure. The angles are defined to be positive when the deviation is counterclockwise and are restricted within 30° because of the crystallographic symmetry. Fifty-one grain boundaries are plotted in Fig. 18, and 18 boundaries are subgrain boundaries (35%) indicated by closed circles. The grain boundary on the line $\theta 1 = \theta 2$ is considered to be formed by the two grains which have the same orientation, and so

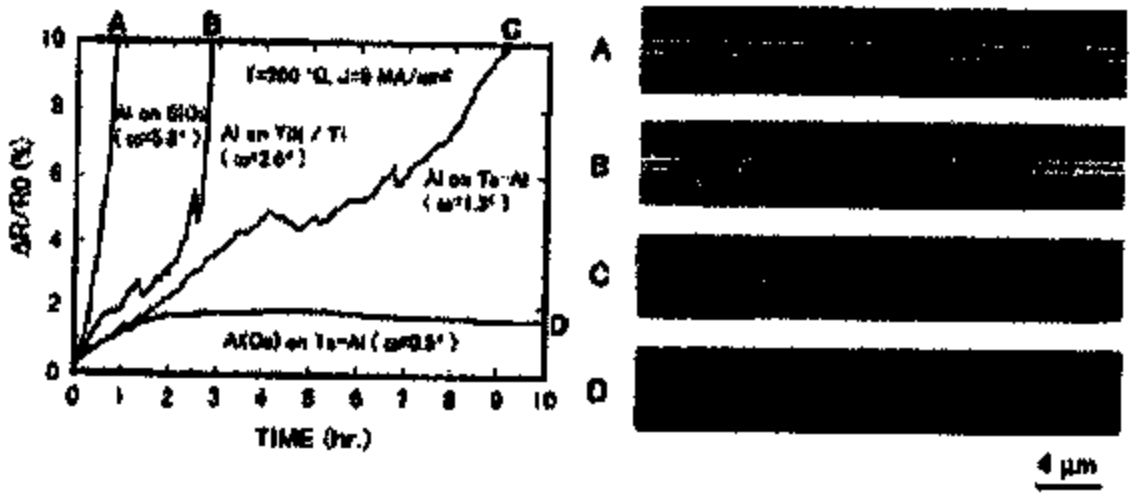

Fig. 16. Electrical resistance change for Al lines of various degree of (1 1 1) texture during EM acceleration test and morphology change after EM acceleration test.

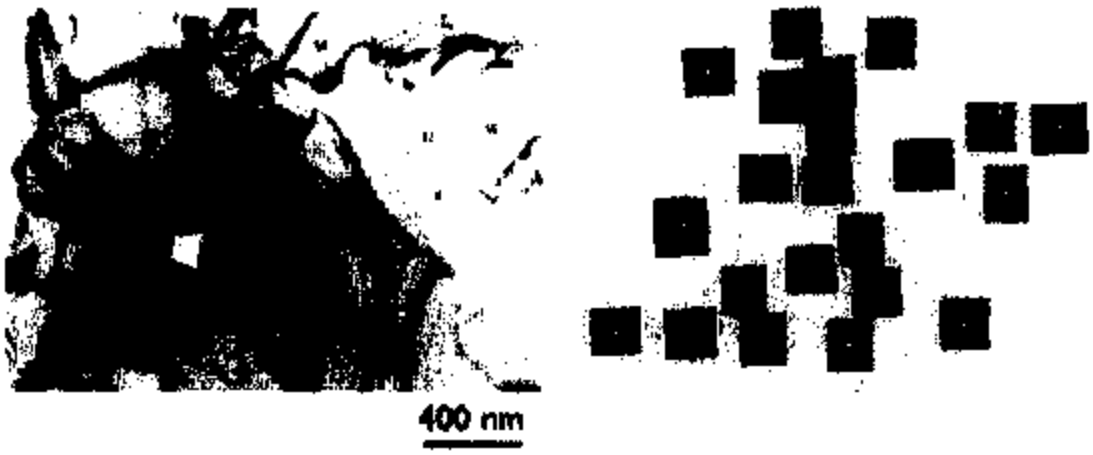

Fig. 17. Bright-field image and diffraction pattern of individual grains of ht-Al film deposited on Ta–Al underlayer.

the energy of the boundary is the lowest. On the other hand, the grain boundary on the dotted line $\theta 1 = -\theta 2$ is considered to form the symmetrical tilt-grain boundary. The grain boundary energy among ⟨1 1 1⟩ symmetrical tilt grain-boundary for fcc metal is reported by Wolf [38]. According to this simulation, the energy increases with tilt angle up to 10° (i.e., $\theta 1 = -5°$, $\theta 2 = 5°$) and the cusp exists at 50° (i.e., $\theta 1 = -30°$, $\theta 2 = 30°$). The former area corresponds to the hatched area and the latter point corresponds to the upper-left on the dotted line. As a result, the grain-boundary energy in the hatched area and on the upper-left point is relatively low compared with the random boundary, and almost half of the grain boundaries are included in this area for ht-Al film. These facts show that a hyper-texture not only eliminated the twist component of grain boundaries, but also changed the grain boundary to the low-angle boundary structure and reduced grain boundary energy. This grain boundary energy reduction would suppress the grain boundary diffusivities and the void's nucleation at a triple point in the ht-Al line. The EM lifetime of Al lines with different degree of texture ($\alpha = 0.5–7°$) are plotted in Fig. 19. The obtained dependence of the lifetime τ on the FWHM value ω is [1]

$$\tau \propto \omega^{-2} \tag{5}$$

This empirical relation has revealed that the EM lifetime of the Al line is improved with a decrease in the FWHM value. From the detailed grain boundary analysis, it has been clarified that the grain boundaries found in ht-Al film were, on average, lower-grain boundaries than those of low textured films. This average tilt (misorientation) angle decrease would reduce the mass transportation along the boundaries and sup-

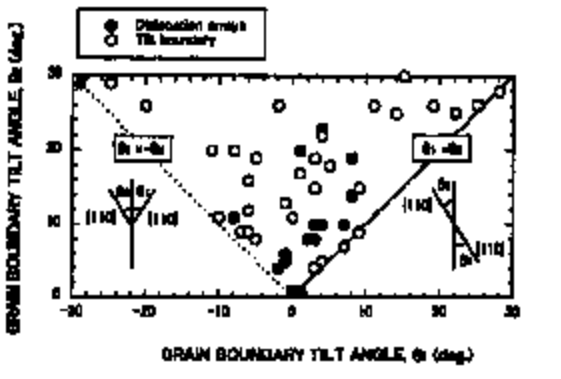

Fig. 18. Misorientation angle between the grains on both sides at grain boundary closed circle : dislocation array; open circle : tilt boundary.

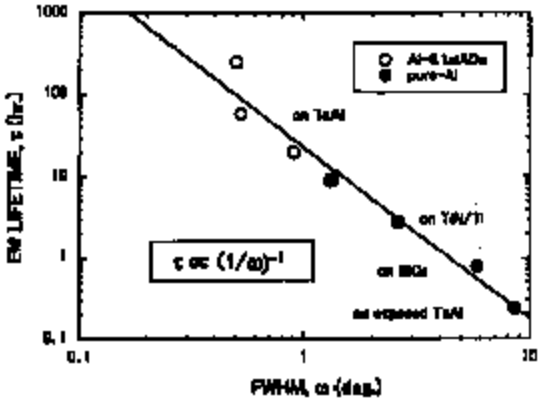

Fig. 19. Dependence of EM lifetime(τ) on the FWHM value (ω) of Al (1 1 1) rocking curve.

press the void and hillock formation at the triple points. The inverse proportionality of EM lifetime τ to the FWHM value α suggests that the decrease in the average twist angle α leads to the decrease in the average misorientation angle.

5. Conclusion

High reliability of single-crystal Al line ($\omega = 0.18°$) was ascribed to its homogeneous microstructure and the lattice diffusion controlled mass transport with the high activation energy of 1.28 eV. The quasi single-crystal Al line ($\omega = 0.26°$) essentially had the same endurance against EM as the single-crystal Al line, because subgrain boundaries found in this line never behaved as effective mass transport paths. The void movement was never disturbed by these subgrain boundaries, because of their lower boundary energy, i.e., a very small amount of defects along the boundary. It has been clarified that the grain boundaries found in hyper-textured Al film ($\omega = 0.5°$) were low-angle grain boundaries though this film still contained random boundaries. It has also been clarified that the texture improvement promoted the low-angle grain boundary formation. The atom and/or vacancy transportation along these boundaries has been found to be the same order of magnitude as that of the lattice diffusion. This reduction of atomic mass transport reduced the flux divergence at the triple points, i.e., void and hillock formation, and resulted in longer lifetime.

On the other hand, it has been concluded that the doping effect of Cu in Al matrix within solid solubility is due to the critical stress increase for the EM induced void nucleation, which markedly prolonged the incubation time of α-Al(Cu).

Finally, hyper-textured Cu films have been achieved by using several kinds of amorphous underlayers. The presence of the hyper-textured Cu film will guarantee the highly reliable metallization for the future ULSI.

Acknowledgements

The authors would like to thank Mrs. Ito, Mrs. Kohunawa, Mr. Kawanoue and Dr. Komatsu for help and discussion throughout this work. They are also grateful to Mr. Miyauchi, Dr. Iizuka, Dr. Hayasaka and Dr. Okumura for their encouragement.

References

[1] Toyoda H, Kawanoue T, Hasunuma M, Kaneko H, Miyauchi M. In: Proc. 32nd Ann. Int. Reliab. Phys. Symp., IEEE. 1994. p. 178.
[2] Towner JM, Darka AG, Tien T. In: Proc. 24th Ann. Int. Reliab. Phys. Symp., IEEE. 1986. p. 7.
[3] Hosoda T, Yagi H, Tsuchikawa T. In: Proc. 27th Ann. Int. Reliab. Phys. Symp., IEEE. 1989. p. 202.
[4] Onuki J, Koibuchi Y, Fukada S, Suwa M, Misawa Y, Isagaki T. IEDM Tech. Dig., IEEE, 1988, p. 454.
[5] Ogawa S, Nishimura H. IEDM Tech. Dig., IEEE, 1991. p. 277.
[6] Lin T, Ahn KY, Harper JME, Chaloux PN. In: IEEE VMIC Conf. 1998. p. 76.
[7] Hinode K, Homma Y. In: Proc. 28th Ann. Int. Reliab. Phys. Symp., IEEE. 1990. p. 25.
[8] Ho PS, Howard JK, White JF. J Appl Phys 1978;49:4083.
[9] Kawanoue T, Kaneko H, Hasunuma M, Miyauchi M. J Appl Phys 1993;74(7):4423.
[10] Vaidya S, Sinclair AK. Thin Solid Films 1981;75:253.
[11] Knorr DB, Lu TM. Appl Phys Lett 1989;54:2210.
[12] Lytle SA, Oates AS. J Appl Phys 1992;71(1):174.
[13] Marieb TN, Abrakowski E, Bravman JC, Madden M, Flinn P. In: Ho PS, Li CY, Totta P, editors, AIP Conf. Proc. No. 305, 1994, p. 1.
[14] Yue JT, Fussen WF, Taylar RV. In: Proc. 23th Ann. Int. Reliab. Phys. Symp., IEEE. 1985. p. 1.
[15] Tanikawa, Ohsabuyashi H, Mori H, Fujita H. Proc. 28th Ann. Int. Reliab. Phys. Symp., IEEE, 1990. p. 209.
[16] Kaneko H, Hasunuma M, Sawabe A, Kawanoue T, Kohunawa Y, Komatsu S, Miyauchi M. In: Proc. 28th Ann. Int. Reliab. Phys. Symp., IEEE. 1990. p. 194.
[17] Hasunuma M, Kaneko H, Sawabe A, Kawanoue T, Kohunawa Y, Komatsu S, Miyauchi M. IEDM Tech. Dig., IEEE, 1989. p. 677.
[18] Hinode K, Owada N, Nishida T, Mukai K. J Vac Sci Technol 1987;B5:518.
[19] Gangulee A, d'Heurle FM. Thin Solid Films 1973;16:227.
[20] d'Heurle FM. Met Trans 1971;2:683.
[21] Spolenak R, Kraft O, Arzt E. Microelectron Reliab 1998;38:1015.
[22] Miyauni S, Umemoto T, Shishino M, Murajima H, Ueda S, Inoue M. In: Proc. 25th Ann. Int. Reliab. Phys. Symp., IEEE. 1987. p. 15.
[23] Kobayashi T, Sekiguchi A, Akiyama N, Honokawa N, Asamaki T. J Vac Sci Technol 1992;A10:525.
[24] Yamada I, Inokawa H, Takagi T. J Appl Phys 1984;56:2746.
[25] d'Heurle F, Berenbaum L, Rosenberg R. Trans of AIME 1968;242:502.
[26] Murray JL. Int Met Rev 1985;30(5):211.
[27] Nakasaki Y, Minamihaba G, Sugano K. J Appl Phys 1995;77:3454.
[28] Murr LE. Interfacial phenomena in metals and alloys. Reading: Addison-Wesley, 1975.
[29] Kaneko H, Kawanoue T, Hasunuma M, Miyauchi M. In: Ho PS, Li CY, Totta P, editors, AIP Conf. Proc. No. 305, 1994. p. 179.
[30] Shingubara S, Kaneko H, Saitoh M. In: Extended Abstracts of the 21st Conference on Solid State Devices and Materials. Tokyo. 1989. p. 33.

[31] Huntington HB, Grone AR. J Phys Chem Solids 1961;20:76.
[32] Meixner R, Dais S, Wolf D. In: Proc. 18th Ampere Congress (Nottingham, England). 1974.
[33] Bradley MJ, Slinger JJ. Phys F 1974;4:839.
[34] Ho CK, Rosenberg R, Tu KN. In: Ho PS, Li CY, Totta P, editors. AIP Conf. Proc. No. 305. 1994, p. 195.
[35] Bleck IA, Herring C. Appl Phys Lett 1976;29:131.
[36] Korhonen MA, Bergman P, Tu KN, Li CY. J Appl Phys 1993;73(8):3790.
[37] Balluffi RW. Met Trans 1982;13B:527.
[38] Wolf D. J Mater Res 1990;5:1708.

Theoretical Study of the Validity of the Born-Oppenheimer Approximation in the Cl + H_2 → HCl + H Reaction

Millard H. Alexander,[1]* Gabriella Capecchi,[2] Hans-Joachim Werner[2]*

Reactivity of the excited spin-orbit state of Cl with H^2 to yield ground-state HCl products is forbidden by the Born-Oppenheimer (BO) approximation. We used new *ab initio* potential energy surfaces and exact quantum scattering calculations to explore the extent of electronic nonadiabaticity in this reaction. In direct contrast to recent experiments, we predict that the BO-allowed reaction of the ground spin-orbit state will be much more efficient than the BO-forbidden reaction of the excited spin-orbit state. Also, Coriolis coupling opens up an electronically nonadiabatic inelastic channel, which competes substantially with reaction.

The kinetics of the Cl + H_2 reaction has been the object of study for more than a century (*1*, *2*). The reaction has played an important role in the development of transition state theory, has provided verification of the kinetic isotope effect, and is the paradigm for the reaction of Cl with hydrocarbons, which is of importance in many atmospheric environments. Recently, molecular beam techniques have been used to yield information on this reaction at well-defined collision energies (*2*–*6*). Quasi-classical trajectory and precise quantum scattering investigations have been reported (*7*–*16*) on several potential energy surfaces (PESs) (*17*, *18*). All previous theoretical work has been based on the approximation that only a single PES governs the reaction and that the open-shell character of the Cl atom plays no role in the dynamics.

The approach of molecular hydrogen to an atom in a ^2P electronic state splits the degeneracy of this state, giving rise to three PESs (*18*–*21*). Of these only the lowest, which corresponds to the lower state of A' symmetry in C_s geometry (Σ symmetry in collinear geometry), correlates with the electronic ground state of the products [H + HCl($X^1\Sigma^+$)]. The PESs of the two other states (the higher state of A' symmetry and the unique state of A'' symmetry) correlate with HCl products in the $a^3\Pi$ electronic state, which is considerably higher in energy (*22*) (Fig. 1).

The excited spin-orbit (SO) state of the Cl atom ($^2P_{1/2}$), which lies 880 cm^{-1} (2.52 kcal/mol) above the ground SO state (*23*), does not correlate adiabatically with the electronic ground state of the reaction products. Thus, if the reaction were to proceed adiabatically on a single PES, as would be predicted by the Born-Oppenheimer (BO) approximation, then the excited SO state would not react (*24*, *25*). For the chemically similar F + H_2 reaction, both theory (*21*) and experiment (*26*, *27*) agree that the reactivity of the excited SO state is, at most, 10% of that of the ground state. The Cl + H_2 reaction differs in two respects: (i) the spin-orbit splitting is more than a factor of 2 greater (*23*) and (ii) the barrier height is much higher. The larger SO splitting suggests that the breakdown in the BO approximation would be less important in the Cl + H_2 reaction. However, because the internal SO energy might help to overcome the higher barrier, nonadiabaticity might be more important in Cl + H_2.

In recent molecular beam experiments, Liu and co-workers (*4*–*6*) used two different Cl atom sources to characterize the reactivity of the two SO states of the Cl atom. Except at the lowest collision energies, they conclude that the excited SO state has a substantially larger reactive cross section. This result is surprising, because the body of prior experimental work indicates that BO-allowed (adiabatically allowed) pathways always dominate (*25*, *28*).

This breakdown in the BO approximation inferred by Liu and co-workers (*4*–*6*) demands further theoretical investigation. Two questions must be answered: (i) How large is the reactivity of the adiabatically forbidden channel [Cl($^2P_{1/2}$) + H_2], and (ii) how well can the reactivity of the adiabatically allowed channel [Cl($^2P_{3/2}$) + H_2] be predicted by standard scattering calculations (*7*–*16*), based on a single PES in which nonadiabatic effects are of necessity neglected. We used exact quantum scattering calculations to answer these questions.

We first need accurate PESs for the three electronic states mentioned above. For the subsequent scattering calculations, it is necessary to transform the two states of A' symmetry into an electronically diabatic basis, in which the orientation of the missing 3*p* electron on the Cl atom remains unchanged in the body frame (*21*). Capecchi and Werner (*29*) have carried out internally contracted, multireference, configuration-interaction calculations (*30*, *31*) of these PESs and the SO coupling matrix elements. Transformation into the diabatic basis results in four PESs. Capecchi and Werner subsequently developed multiparameter global fits (*29*) to these

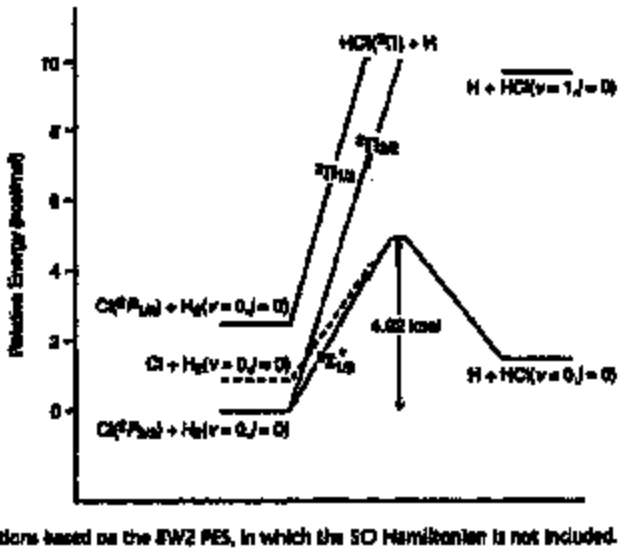

Fig. 1. Schematic plot of the energetics of the Cl + H_2 reaction. The relative reactant energies, the position of the barrier, and the position of the indicated HCl product channels are drawn to scale. All energies include zero-point corrections; those for the barrier were determined from the constants published by Stark and Werner [table 8 of (*18*)]. Linear-molecule Σ and Π state labels are used, which is appropriate for a collinear transition state. The dashed line indicates the schematic reaction profile for single-surface calculations based on the BW2 PES, in which the SO Hamiltonian is not included.

[1]Department of Chemistry and Biochemistry and Institute for Physical Sciences and Technology, University of Maryland, College Park, MD 20742-2021, USA. [2]Institut für Theoretische Chemie, Universität Stuttgart, D-70569 Stuttgart, Germany.

*To whom correspondence should be addressed. E-mail: mha@umd.edu (M.H.A.); werner@theochem.uni-stuttgart.de (H.-J.W.)

PESs and to the two SO coupling functions (*21*). Their calculations extend the earlier work of Bian and Werner (*18*), which was limited to the lowest electronically adiabatic ClH_2 PES.

In the Cl + H_2 arrangement, there are six electronic states. These correspond to the three spatial orientations of the 3*p* hole on the Cl atom and the two possible spin-projection quantum numbers. In each H + HCl product arrangement, we neglect the high-lying Π states of HCl (*22*). In general, outside the reactant arrangement, the description of the Cl + H_2 system is unchanged from the original BW1 fit (*18*), which was limited to the lowest electronically adiabatic PES.

If the sum of the electronic interaction Hamiltonian plus the SO coupling in the 6 × 6 electronic basis is diagonalized at each value of the coordinates, the lowest root will define what we will call the fully (electronic + SO) adiabatic Capecchi-Werner (CWad) PES and corresponds to the reactive PES illustrated schematically in Fig. 1. This PES differs from the BW2 PES (*18*), which is obtained by diagonalizing only the electrostatic Hamiltonian, without inclusion of the SO Hamiltonian.

The SO Hamiltonian couples the reactive PES ($^2\Sigma_{1/2}$ in linear geometry) with the two repulsive PESs ($^2\Pi_{3/2}$ and $^2\Pi_{1/2}$ in linear geometry). Because the latter are so much higher in energy at the barrier, inclusion of the SO coupling has a negligible effect at the barrier. However, inclusion of the SO coupling in the asymptotic reactant region lowers the lowest adiabatic PES by ≈1/3 the SO splitting of the Cl atom. Thus, when compared to the BW2 PES, the barrier to reaction on the CWad PES is ≈0.84 kcal/mol higher (*18*, *21*, *32*–*34*).

In addition to the electrostatic and SO Hamiltonians, it is also necessary to determine matrix elements of the orbital angular momentum of the triatomic system $L^2 = (J - l - s - j)^2$, where *J* is the total angular momentum, *j* is the rotational angular momentum of the diatomic moiety, and *l* and *s* are the electronic orbital and spin angular momenta (*21*).

With the required ClH_2 PESs in the diabatic basis, it is possible to carry out complete quantum scattering calculations. We drew from the formalism presented by Schatz on the Cl + HCl exchange reaction (*32*) and use the algorithms and computer program developed over the past decade by Manolopoulos and co-workers (*35*, *36*), extended, as we have described previously (*21*), to treat abstraction reactions involving an atom in a ^2P electronic state. The choice of integration parameters was identical to those adopted in the single-state studies of the Cl + H_2 reaction (*18*).

We obtain, at each value of the total angular momentum *J*, probabilities for transition from a given initial state to any particular final state of either the reactants (an inelastic collision) or products (a reactive collision). By summing the latter over all accessible product states and averaging over the rotational $(2j + 1)$ and electronic $(2j_a + 1)$ degeneracy of the initial state (j_a = 3/2 or 1/2), one extracts a total probability.

In Fig. 2 we compare, at the low... of the total angular momentum (J = 0.5), the calculated total probabilities for reaction of H_2 in $v = 0$, $j = 0$ (the lowest rotational level of para-H_2). The multistate results, determined with the full set of diabatic PESs, are compared in Fig. 2 with the $J = 0$ transition probabilities, as predicted by single-state calculations on the CWad PES. In the latter calculation, both the SO and electronic-orbital angular momenta of the Cl atom were neglected, as in any standard single-state treatment of a triatomic reaction (*13*, *14*, *35*, *36*). The reaction probabilities are plotted as a function of collision energy, which is the fundamental dynamical variable in a molecular beam experiment. Thermal rate constants could then be obtained by integration over a Maxwellian distribution of collision velocities, although an equally valid expression involves integration over the total (collision + internal) energy of the "cumulative reaction probability" (*37*).

In the multistate treatment, four states correlate with the ground-state reactants $Cl(^2P_{3/2})$ + H_2; namely, as seen in Fig. 1, $\Sigma_{\pm 1/2}$ and $\Pi_{\pm 3/2}$. Of these, the Π states are repulsive, within the BO approximation, so that, to zeroth order, only 50% of the reactants will approach on a PES that leads to reaction. However, in the single-state calculations, one assumes that all (100%) of the reactants will approach on the reactive PES. To take into account this fundamental difference, previous investigators (*21*, *37*) have divided the single-state results by a factor of 2 to compare with the cross sections and probabilities for reaction out of the j_a = 3/2 level of a ^2P atom obtained from multistate calculations.

The probability for (adiabatically forbidden) reaction out of the excited (j_a = 1/2) SO state of Cl is much smaller than the probability for the adiabatically allowed reaction of the ground SO state. Only at collision energies below the zero-point corrected barrier to reaction [E_{coll} < 9.93 kcal/mol (Fig. 1)] does the adiabatically forbidden channel start to dominate, because the threshold for reaction of the excited SO state is 2.52 kcal/mol lower.

We also observe that the reaction probabilities predicted by single-state calculations on the fully adiabatic CWad PES agree very well with the multistate probabilities for the adiabatically allowed channel. As discussed above, the single-state probabilities have been divided by 2. Because the excited Π states are very high in energy in the region of the barrier, the topology of the barrier, which controls the flux from reactants to products, is virtually identical in the multistate and single-state calculations.

The pronounced staircase-like structure in the reaction probability out of the lower (adi-

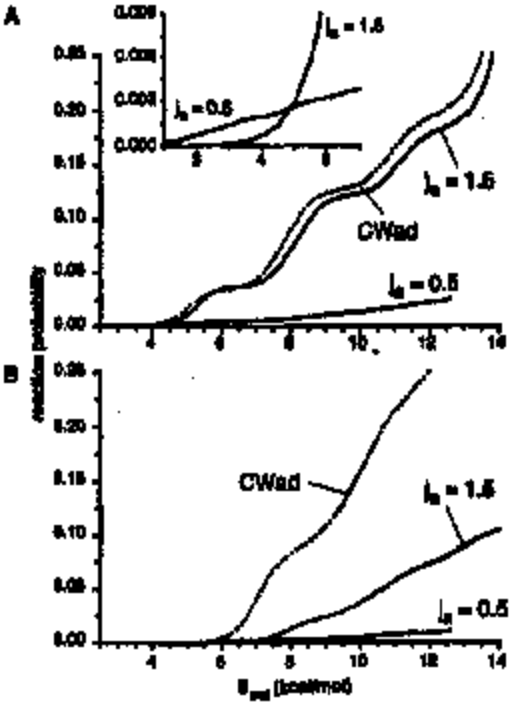

Fig. 2. (A) Probabilities for reaction of Cl in the j_a = 3/2 ($^2P_{3/2}$) and j_a = 1/2 ($^2P_{1/2}$) SO states with H_2 ($v = j = 0$) for J = 0.5. The abscissa is the collision energy. Also shown are reaction probabilities determined from single-state calculations based on the fully adiabatic (CWad) PESs for J = 0 but divided by a factor of 2. (Inset) The low-energy behavior of the multistate probabilities. (B) Similar reaction probabilities, but for J = 17.5.

physically allowed) SO state corresponds to the successive opening of additional vibrational states at the barrier.

The lower panel of Fig. 2 displays similar reactive transition probabilities, but for J = 17.5. Again, the CWad probabilities have been divided by 2. At this higher angular momentum, the centrifugal barrier has increased. Consequently, the threshold for reaction occurs at a higher collision energy. At J = 17.5, the multistate reactions are now substantially smaller than those predicted by the single-state CWad calculations, even after division by 2. Similar comparisons at other values of J reveal that as J increases, the multistate reaction probabilities become increasingly smaller than the comparable single-state probabilities. Because the discrepancy grows roughly linearly with J, Coriolis coupling would seem to be responsible.

In the single-state calculations, only three outcomes of a collision are possible: (i) elastic scattering, (ii) inelastic scattering on the reactive PES, or (iii) reactive scattering. In the multistate calculations, additional inelastic channels are present for collisions of Cl in its ground SO state with H_2, namely (Fig. 1) (iv) elastic and inelastic scattering on the repulsive $^2\Pi_{1/2}$) PES; (v) inelastic scattering from the $^2\Sigma_{1/2}$) PES to the $^2\Pi_{3/2}$) PES, which will be accompanied by SO excitation of the Cl atom without reaction; and (vi) inelastic scattering from the reactive ($^2\Sigma_{1/2}$) PES back to the $^2\Pi_{1/2}$ PES. The last process will yield Cl in its ground SO state, accompanied by rotational and/or vibrational excitation of the H_2. At low J, these additional inelastic channels do not seem to deplete the reactive scattering, because the single- and multistate reaction probabilities shown in Fig. 2A are virtually identical. However, a difference between the single-state and multistate probabilities for reaction of Cl($^2P_{3/2}$) does emerge as J increases (Fig. 2B). It is the inelastic channels that are responsible for this difference.

We find that the sum of the reactive and inelastic transition probabilities as predicted by the multistate calculations at J = 0.5 and 17.5 agrees very closely with a similar sum, but divided by a factor of 2, of the inelastic and reactive probabilities predicted by the single-state CWad calculations at J = 0 and 17. Because this agreement is obtained by dividing the single-state results by a factor of 2, we conclude that incoming flux on the repulsive $^2\Pi_{1/2}$ PES (Fig. 1) has an insignificant probability of either reaction (as discussed above) or inelastic scattering.

Because at higher J the summed (inelastic + reactive) probabilities agree whereas the reactive probabilities are significantly lower for the multistate (as compared to the single-state) calculations (Fig. 2), we conclude that, at higher J, the multistate inelastic probabilities must exceed those predicted by the single-state calculations. This is indeed the case, as illustrated in Fig. 3.

At low energy, below the barrier to reaction, the multistate calculations at J = 17.5 reveal a pronounced oscillatory structure. This structure is the manifestation of quantum interference between trajectories that undergo an inelastic transition from the less repulsive $^2\Sigma_{1/2}$ PES to the more repulsive $^2\Pi_{1/2}$ PES when the system passes through the zone of strong nonadiabatic coupling as the atoms approach and then again as they recede, having bounced off the barrier to reaction (*38*).

As the collision energy rises above the barrier, the inelastic probabilities predicted by the CWad single-state calculations remain relatively independent of J. However, the multistate inelastic transition probabilities show a pronounced increase. This is a consequence of the presence of an additional electronic channel(s), not present in the single-state calculations.

In a linear molecule, the non-BO coupling between $^2\Sigma_{1/2}$ and $^2\Pi_{1/2}$ states is due to "J-uncoupling" (*39*), which arises from the J_+ term in expansion of the L^2 operator. Further investigation shows that the J-dependent enhancement of the inelastic probabilities in the multistate calculations can be attributed predominately to rovibrational excitation of the H_2 molecule without excitation of the Cl atom and hence corresponds (Fig. 1) to transitions from the $^2\Sigma_{1/2}$ to the $^2\Pi_{3/2}$ PESs.

Integral cross sections are proportional to the sum over J of the transition probabilities weighted by $(2J + 1)$ (*21*). In general, as the collision energy increases, successively greater values of J contribute. Because the multistate reaction probabilities are increasingly depressed at higher J (compared to the single-state probabilities), we expect that the increase of the multistate reactive cross sections with increasing collision energy will be smaller than the prediction from single-state calculations on the CWad PES. This is indeed the case, as shown in Fig. 4.

In the experiments of Liu and co-workers (*4–6*), only the lowest three (j = 0, 1, and 2) rotational levels of H_2 are present in the beam. By weighting the cross sections out of each j level by the experimental populations of these levels, we can obtain reactive cross sections appropriate to the experiments with p-H_2 or n-H_2 (Fig. 5).

We observe, similarly to the transition probabilities, that the cross section for the adiabatically forbidden reaction of Cl in its excited SO state is small in comparison with that for reaction of the ground SO state, which is adiabatically allowed. Only at very low collision energy, where the adiabatically allowed reaction is throttled off by the large barrier, does the adiabatically forbidden reaction begin to dominate. This is a consequence of the greater internal energy of the excited SO state, which does, albeit inefficiently, allow the barrier to be surmounted. Figure 5 is qualitatively similar to our earlier predictions of the relative reactivity of the two SO states of the F atom (*21*).

Because the statistical degeneracy of the ground SO state of Cl is twice as large as that of the excited state, which is not taken into ac-

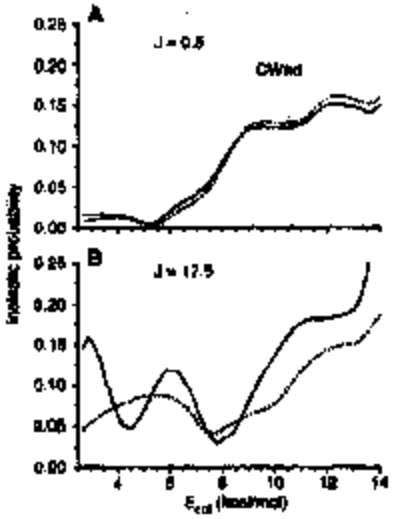

Fig. 3. (A) Solid curve indicates the inelastic transition probabilities for $Cl(^2P_{3/2}) + H_2(v = j = 0)$ for J = 0.5, summed over all energetically accessible final states. The abscissa is the collision energy. Dashed curve indicates a similar sum, but divided by 2, of inelastic transition probabilities from single-state calculations on the CWad PES for J = 0. The abscissa is the collision energy. (B) Similar plot of the inelastic transition probabilities but for J = 17.5 (J = 17 for the CWad calculations).

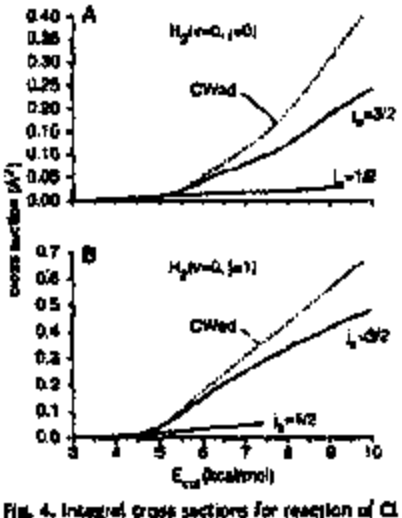

Fig. 4. Integral cross sections for reaction of Cl with $H_2(v = 0, j = 0)$ (A) and with $H_2(v = 0, j = 1)$ (B). Also shown are the predictions of single-state calculations based on the fully adiabatic (CWad) PES, divided by a factor of 2.

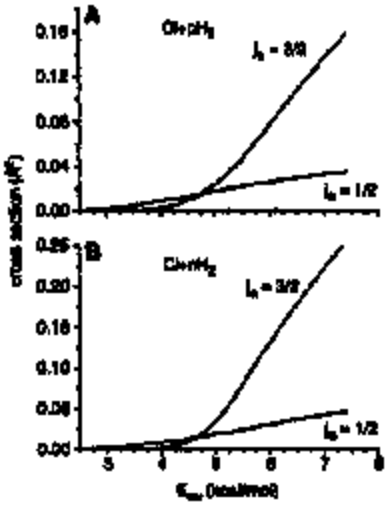

Fig. 5. (A) Integral cross sections for reaction of Cl [in its ground (j_a = 3/2) and excited (j_a = 1/2) SO state with p-H_2. (B) Similar integral cross sections for reaction with n-H_2. The relative rotational state populations of the j = 0, 1 and 2 H_2 rotational levels were taken from (4–6).

count in Fig. 5, the observed reactivity of the excited SO state will be a factor of 2 less than predicted by Fig. 5.

We predict, fully in agreement with the body of available experimental evidence on other reactions (23, 25), that the adiabatically allowed [$Cl(^2P_{3/2}) + H_2$] reaction will dominate the adiabatically forbidden reaction [$Cl(^2P_{1/2}) + H_2$], except for collision energies below 5 kcal/mol. This prediction is in direct contrast with the recent work of Liu and coworkers (4–6). This disagreement is one of the major currently unsolved problems in the dynamics of elementary chemical reactions.

Although we predict the reactivity of the adiabatically forbidden channel to be small, we conclude that the breakdown in the BO approximation nevertheless plays an important role in the Cl + H_2 reaction. The coupling between the electronic-orbital angular momentum and the overall orbital motion of the reactants opens up a inelastic channel that competes with reaction. The predicted reactive cross sections are smaller than those calculated from more traditional treatments, in which these nonadiabatic inelastic processes are not taken into account.

We have shown that nonadiabatic processes influence the Cl + H_2 reaction dynamics in subtle and as yet not fully understood ways. In the ab initio calculations of Capecchi and Werner, the nonreactive Π states were characterized only in the reactant arrangement, where these states lie relatively close in energy to the reactive Σ state. It may be that additional electronic couplings at (or inside) the reaction barrier underlie the discrepancy with Liu's experiments. The need for further studies, both theoretical and experimental, is clear.

References and Notes

1. T. C. Allison *et al.*, in *Gas-Phase Reaction Systems: Experiments and Models 100 Years after Max Bodenstein*, H.-R. V. J. Wolfrum, R. Rannacher, J. Warnatz, Eds. (Springer, Heidelberg, Germany, 1996), pp. 111–124.
2. P. Casavecchia, *Rep. Prog. Phys.* **63**, 355 (2000).
3. M. Alagia *et al.*, *Science* **289**, 1519 (1998).
4. S.-H. Lee, L.-H. Lai, K. Liu, H. Chang, *J. Chem. Phys.* **110**, 8229 (1999).
5. S.-H. Lee, K. Liu, *J. Chem. Phys.* **111**, 6253 (1999).
6. F. Dong, S.-H. Lee, K. Liu, *J. Chem. Phys.* **113**, 1197 (2000).
7. F. J. Aoiz, L. Bañares, *J. Phys. Chem.* **100**, 18108 (1996).
8. S. C. Hsiao, T. C. Allison, D. G. Truhlar, D. W. Schwenke, *J. Phys. Chem.* **100**, 13580 (1996).
9. H. Wang, W. H. Thompson, W. H. Miller, *J. Chem. Phys.* **107**, 7194 (1997).
10. D. Skouteris *et al.*, *Science* **286**, 1713 (1999).
11. U. Manthe, W. Bian, H.-J. Werner, *Chem. Phys. Lett.* **313**, 647 (1999).
12. N. Balucani *et al.*, *Chem. Phys. Lett.* **328**, 90 (2000).
13. S.-H. Yang, H.-T. Cao, K.-L. Han, J. Z. H. Zhang, *J. Chem. Phys.* **113**, 1434 (2000).
14. D. Skouteris *et al.*, *J. Chem. Phys.* **114**, 10662 (2001).
15. F. J. Aoiz *et al.*, *J. Chem. Phys.* **113**, 2074 (2001).
16. C. Shen, T. Wu, G. Ju, W. Bian, *Chem. Phys.* **272**, 61 (2001).
17. T. C. Allison, G. C. Lynch, D. G. Truhlar, M. S. Gordon, *J. Phys. Chem.* **100**, 13575 (1996).
18. W. Bian, H.-J. Werner, *J. Chem. Phys.* **112**, 220 (2000).
19. F. Bobamovic, W. A. Lester Jr., *J. Chem. Phys.* **58**, 3737 (1973).
20. V. Aquilanti, S. Cavalli, D. De Fazio, A. Volpi, *J. Chem. Phys.* **109**, 3805 (1998).
21. M. H. Alexander, D. E. Manolopoulos, H. J. Werner, *J. Chem. Phys.* **113**, 11084 (2000).
22. M. H. Alexander, B. Pouilly, T. Duhoo, *J. Chem. Phys.* **99**, 1752 (1993).
23. C. E. Moore, *Atomic Energy Levels*, NSRDS-NBS 35 (U. S. Government Printing Office, Washington, DC, 1971).
24. K. L. Shuler, *J. Chem. Phys.* **21**, 624 (1953).
25. R. J. Donovan, D. Husain, *Chem. Rev.* **70**, 489 (1970).
26. D. M. Neumark, A. M. Wodtke, G. N. Robinson, C. C. Hayden, Y. T. Lee, *J. Chem. Phys.* **82**, 3045 (1985).
27. M. Faubel *et al.*, *J. Chem. Phys.* **101**, 2108 (1994).
28. P. J. Dagdigian, M. L. Campbell, *Chem. Rev.* **87**, 1 (1987).
29. G. Capecchi, H.-J. Werner, in preparation.
30. H.-J. Werner, P. J. Knowles, *J. Chem. Phys.* **89**, 5803 (1988).
31. P. J. Knowles, H.-J. Werner, *Chem. Phys. Lett.* **145**, 514 (1988).
32. G. C. Schatz, *J. Phys. Chem.* **89**, 2192 (1985).
33. K. Stark, H.-J. Werner, *J. Chem. Phys.* **104**, 6515 (1996).
34. B. Hartke, H.-J. Werner, *Chem. Phys. Lett.* **200**, 430 (1992).
35. J. F. Castillo, D. E. Manolopoulos, K. Stark, H.-J. Werner, *J. Chem. Phys.* **104**, 6531 (1996).
36. D. Skouteris, J. F. Castillo, D. E. Manolopoulos, *Comput. Phys. Commun.* **133**, 128 (2000).
37. F. J. Aoiz, L. Bañares, J. F. Castillo, *J. Chem. Phys.* **111**, 4013 (1999).
38. B. Pouilly, T. Orlikowski, M. H. Alexander, *J. Phys. B* **28**, 1953 (1995).
39. H. Lefebvre-Brion, R. W. Field, *Perturbations in the Spectra of Diatomic Molecules* (Academic Press, New York, 1986), pp. 116–121.
40. M.H.A. is grateful to NSF for support under grant CHE-9975810. H.J.W. was supported by the Deutsche Forschungsgemeinschaft and the Fonds der Chemischen Industrie. G.C. was supported by a fellowship as a participant in the European Union-Training and Mobility of Researchers network 'Reaction Dynamics,' contract no. HPRN-CT-1999-00007. Finally, the authors are grateful to K. Liu and D. Manolopoulos for their encouragement and for many productive discussions.

1 February 2002; accepted 19 March 2002

Dynamic Aggregation of Chiral Spinners

Bartosz A. Grzybowski* and George M. Whitesides*

An object spinning at the surface of a liquid creates a chiral vortex. If the spinning object is itself chiral, its shape modifies the characteristics of the vortex interactions between that vortex and other vortices than depend on the chirality of the objects that produce them. This paper describes the aggregation of millimeter-sized, chiral magnetized plates floating at a liquid-air interface and rotating under the influence of a rotating external magnetic field. This external field confines all the plates at densities that cause the vortices they generate to interact strongly. For one set of plates investigated, plates of one chirality attract one another, and plates of the other chirality repel other plates of both chiralities.

The properties and interactions of chiral molecules are a central concern in chemistry, with applications in chromatographic separations, asymmetric catalysis, and medicinal chemistry (*1*, *2*). Chiral interactions between molecules are conceptually well understood (*3*, *4*). Interactions between chiral objects larger than molecules are, however, less well explored or exploited. Here, we describe a study of the interactions between millimeter-scale vortices generated in a fluid by the rotation of chiral objects floating at the surface of that fluid. This system has the characteristics that it is dynamic (*5*–*10*)—that is, the interacting objects (the vortices) exist only when there is a flux of energy into the system—and that both the vortices and the objects that generate them are macroscopic. The system consists of magnetically doped

Department of Chemistry and Chemical Biology, Harvard University, 12 Oxford Street, Cambridge, MA 02138, USA.

*To whom correspondence should be addressed. E-mail: bgrzybowski@gmwgroup.harvard.edu (B.A.G.); gwhitesides@gmwgroup.harvard.edu (G.M.W.)

intel.

SCR Latch-Up Model — Preventing Latch-Up in Intel® Transceivers

Application Note

January 2001

Order Number: 249160-001

As of January 15, 2001, this document replaces the Level One document known as *AP048*.

Application Note

EA82-027 29467

Contents

1.0 Introduction 5

1.1 SCR Latch-Up Description 5
1.2 Design Guidelines 6

Figures

1 SCR Latch-Up Model 5
2 Applications of Redundancy 7

1.0 Introduction

The purpose of this application note is to familiarize designers in the use of Intel CMOS transceivers. Intel devices are designed to meet, but not to exceed the absolute maximum specifications for Silicon Controlled Rectifier (SCR) latch-up. SCR latch-up in CMOS devices is a condition that can cause maximum specifications to be exceeded. This application note provides the necessary design considerations to avoid SCR latch-up.

Following these design guidelines will:

- Avoid exceeding maximum transceiver ratings
- Simplify application maintenance
- Reduce SCR latch-up related downtime in systems
- Improve system reliability

Figure 1. SCR Latch-Up Model

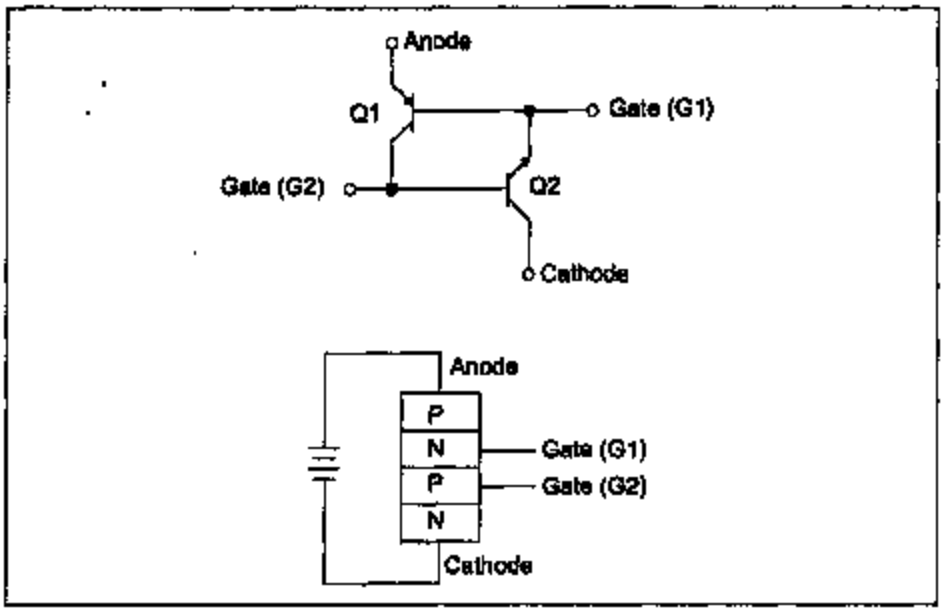

1.1 SCR Latch-Up Description

Once triggered, an SCR latch-up condition turns on a parasitic SCR internal to CMOS circuits that creates a low resistance path from Vcc to ground. The resulting internal high currents can damage the devices.

Modeled as a cross coupled transistor, the SCR has two basic trigger mechanisms: one forces current into its gate and the other places a large voltage between the anode and cathode. When forward biasing a diode, current injected into the base of Q2 turns this transistor on and the collector current (beta times its base current) flows into the base of Q1. This causes Q1 to be

amplified by beta and fed back into the base of Q2, where the current is again amplified. If the beta of both transistors is greater than 1, the current gain continues until the transistors saturate and the SCR is triggered. Once the regenerative condition occurs, a large anode current flows. The SCR remains on after the gate current is removed, if enough anode current flows to sustain latch-up.

In the case of large voltages on its anode and cathode, a trigger condition can occur even if no current is applied to the gate. In the forward blocking state, a small leakage current is present but will not trigger the SCR. If the voltage is increased to allow a significant leakage current, then a SCR could trigger. The beta of the NPN and PNP must be greater than one for the latch condition to occur.

There are a number of scenarios that can cause a SCR trigger to occur at inputs and outputs (latch condition) including insertion and removal of a circuit card from a powered system. To be effectively controlled (either when integrated or at the system level) designers must have a clear understanding of the causes of SCR latch-up.

1.2 Design Guidelines

1. If the circuit card design includes "hot-swapping" capability, insure that power reaches the devices (transceivers, PALs, etc.) before applying any voltages to the input or output pins (i.e., power and ground pins make contact before input and output pins). Refer to the "Short-haul FAQ" (question 4.3) for recommended methods of protecting the line driver, receiver and power supply pins. The Short-haul FAQ is located our web site under: short-haul, products, LXT30X.
2. When multiple power supplies feed the same device, arrange the pins so the supplies connect in ascending order. Thus, if a circuit card requires +5 V, +12 V, and -12 V, the +5 V pins should connect first, the +12 V pins next and finally the -12 V pins. In any event, before any voltage pins make contact, the ground should connect first to insure that the positive supplies do not pull the negative supplies or vise versa.
3. When devices drive other devices on separate boards, be aware that large amounts of local decoupling can cause power supply ramps to be slower on some boards than others.
4. Insure that the voltages to the input/output pins do not exceed the supply voltage. Clamping circuits are needed to reduce the input voltage.
5. Insure that the input current does not exceed the absolute maximum rating of 100 mA. If this is expected, current limiting may be necessary to prevent the SCR latching condition. Consult Intel applications engineering for other options.
6. Never allow the output driver to drive another output driver in applications of redundancy. See Figure 2. This can be accomplished only if a break before make connection of the two drivers is observed. These high current drivers are capable of exceeding the trigger currents necessary for a SCR latch condition. Note that some transceivers (such as the LXT305A) have the ability to tri-state.

Figure 2. Applications of Redundancy

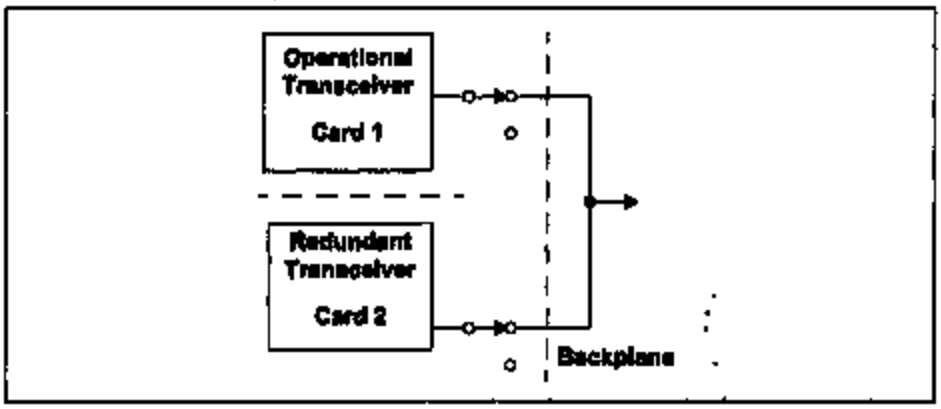

ELSEVIER

Microelectronic Engineering 50 (2000) 301–309

MICROELECTRONIC ENGINEERING

www.elsevier.nl/locate/mee

Kinetics of hillock growth in Al and Al-alloys

Michal Zaborowski*, Piotr Dumania

Institute of Electron Technology, Al. Lotników 32/46, 02 668 Warsaw, Poland

Abstract

Hillock growth kinetics and size distribution were investigated in Al, Al:Si 1% and Al:Si1%:Cu 0.5% layers. Metallization surface was examined by optical, SEM and TEM microscopy, stylus profiling and an automatic method of hillock recognition from a microscope image. The method allowed for counting hillocks in a desired range of their diameter d. Surface density of hillocks was measured as a function of time of furnace annealing at 400°C and as a function of temperature of RTP annealing. A maximum hillock size was found to increase linearly with metallization layer thickness and with logarithm of annealing time. A total area occupied by hillocks was evaluated. Hillock density decreased versus $1/T$ with an activation energy of 0.28 eV for Al and 0.31 eV for Al:Si. It was found, that a normalized hillock density N may be expressed by a formula $N = N_0 \exp(-cd)$. Values for N_0 and c are given together with a short discussion. © 2000 Elsevier Science B.V. All rights reserved.

Keywords: Metallization; Aluminum thin film; Polycrystalline layer morphology; Hillock growth

1. Introduction

Aluminum-based metallization still remains the most commonly used material for interconnecting lines in silicon ICs and electro-mechanical microsystems. Polycrystalline Al layers alter their surface morphology as a consequence of heat treatment and other processes performed at elevated temperature (250–500°C). Large crystallites, so-called hillocks, can outgrow above the initial metal surface [1,2]. The driving force of hillock growth is a compressive stress caused by large mismatch of thermal expansion coefficients between Al and Si or SiO_2 substrate [3,4]. Hillocks are particularly undesirable in multilevel metal systems.

The aim of this work was to investigate both the growth kinetics and the size distribution of the hillocks.

2. Experimental

Samples were prepared by thermal oxidation of (100) oriented Si wafers to an oxide thickness of

*Corresponding author. Fax: +48-22-716-5951.
E-mail address: mzab@ine.waw.pl (M. Zaborowski)

0167-9317/00/$ – see front matter
PII: S0167-9317(99)00296-8

0.4 μm followed by magnetron sputter deposition of the metallization. The vacuum was better than 1×10^{-4} Pa and Ar pressure was equal to 0.5 Pa. We used pure Al 5 N, Al:Si 1% alloy or Al: Si 1%:Cu 0.5% alloy as a target material. Metal layer thickness ranged from 0.5 to 2.5 μm. Substrates were heated up to approximately 180°C before sputtering. The Al reference layers were produced by means of e-gun evaporation under the same temperature conditions. All samples were annealed in a furnace or RTP reactor. Nitrogen, hydrogen or argon were used as an annealing ambient. Metallization surface was examined by a number of methods: optical, SEM and TEM microscopy, stylus profiling and an automatic method of hillock recognition from a microscope image. The last method consists of the processing of surface images acquired by a monochromatic TV camera and allows hillock-like objects to be visualized separately and measured [5].

3. Results and discussion

All manufactured metallization layers were polycrystalline, with grain dimensions dependent on the layer thickness and annealing conditions. A ⟨111⟩ preferred orientation was found from XRD measurements. SEM micrographs revealed numerous hillocks protruded into the metal layer surface (Fig. 1). Shapes and sizes of hillocks involved in Al:Si:Cu alloy by a 30 min annealing at a temperature of 450°C differ significantly from those in Al and Al:Si metallization. No influence of annealing atmosphere (nitrogen, hydrogen or argon) on the surface morphology was noted. The stylus

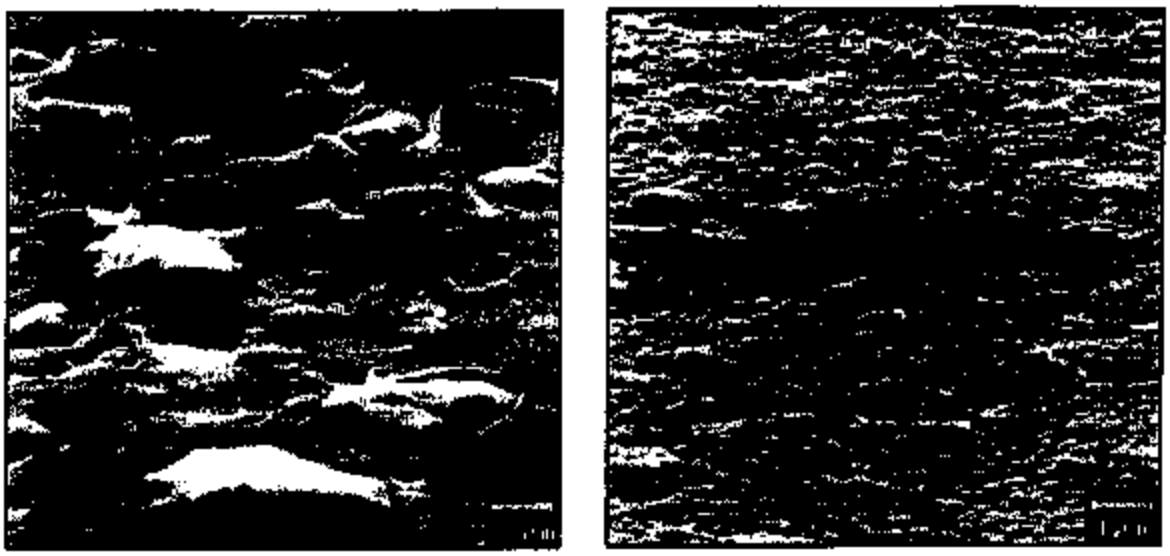

a b

Fig. 1. Metallization surface examined by SEM after annealing (450°C, 30 min): (a) magnetron sputtered Al layer 1 μm thick; (b) similar layer of Al:Si:Cu alloy.

profiling method was useless in the case of Al:Si:Cu because of the relatively large radius of the tip (2.5 μm). This technique applied for Al and Al:Si metallization gave results comparable to the results of hillock recognition method. Nevertheless, this last method was extensively used in present investigations for reason of better hillock surface area estimation.

Hillocks start to grow up almost immediately at the beginning of annealing. Two-minute annealing of a 0.7 μm thick Al layer at the relatively low temperature of 400°C is sufficient for creation of small hillocks. Fig. 2 presents surface density of these objects as a function of the time of furnace annealing in flowing nitrogen. Hillocks are collected in 0.4 μm groups with regard to their average diameters, lower measurement limit is equal to 0.33 μm. Longer annealing does not change the population of hillocks inside each group noticeably, but induces greater hillocks. Smaller hillocks seem to be a source of larger ones, therefore it is evident that the hillock number is here in a kind of dynamic equilibrium. A maximum hillock size, defined as a diameter of 1% of the whole hillock population exhibiting largest dimensions in the examined surface, is presented in Fig. 3. The maximum hillock size depends nearly linearly on the logarithm of annealing time. Each curve represents a different wafer and a different metal deposition process. Generally, the values for an Al:Si alloy are close to those for pure aluminum. Maximum hillocks in Al:Si:Cu are several times smaller than in Al, after the same time of annealing.

Samples were divided into four parts and covered with an Al of different thickness in order to estimate the dependence of the maximum hillock size on the layer thickness. Fig. 4 shows the results of furnace annealing at a temperature of 400°C for 8 min in N_2. Maximum hillock size increases linearly with metallization layer thickness ranging from 0.5 to 2 μm, with some scatter from one sample to another. Changing the annealing conditions to 450°C and 5 min (wafer no. 4) does not influence the maximum hillock sizes.

The method of hillock recognition allows for summing the areas of all detected hillocks. A fraction of the sample surface occupied by hillocks increases during annealing (Fig. 5). The total hillock area

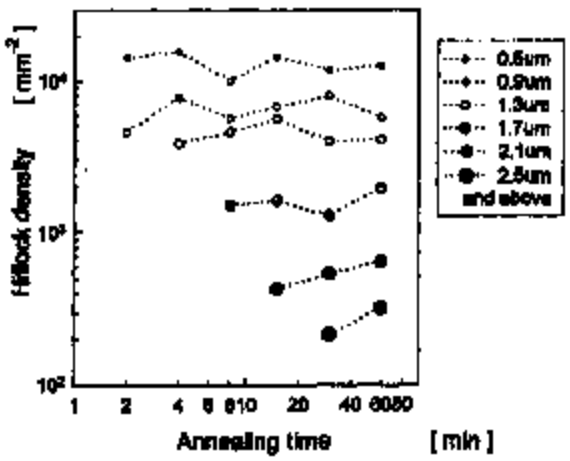

Fig. 2. Surface density of hillocks as a function of annealing time at a temperature of 400°C in N_2 for sputter-deposited Al layer of 0.7 μm thickness.

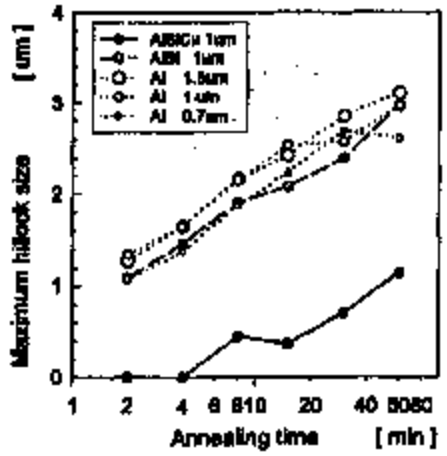

Fig. 3. Maximum hillock size as a function of annealing time at the temperature of 400°C in N_2, for Al:Si:Cu layer, Al:Si layer and three Al layers of different thickness.

does not exceed 3.5% in the aluminum layer. There is roughly two times less hillocks in the Al:Si layer than in pure Al after these rather low-temperature (400°C) annealings. Analogous ratio for the Al:Si:Cu metallization reaches 100.

The total hillock area varies with a metal layer thickness and annealing conditions. Fig. 6 presents results of hillock measurements after a 'moderate' annealing, performed at 400°C for 8 min, and a 'standard' annealing, at 450°C for 30 min. An influence of time and temperature product is predominant; however, both curves demonstrate similar features. The total hillock area decreases to zero for thin Al layers and saturates for the layers thicker than approximately 1.5 μm. Linear dependence of the area on the layer thickness can be easily explained because an average hillock size

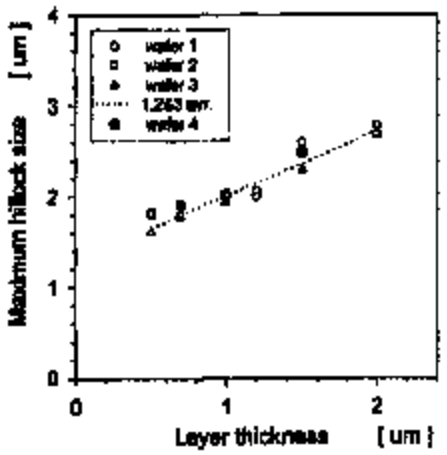

Fig. 4. Maximum hillock size versus Al layer thickness after furnace annealing at a temperature of 400°C for 8 min in N_2 (samples 1, 2 and 3). Sample no. 4 was annealed at 450°C for 5 min.

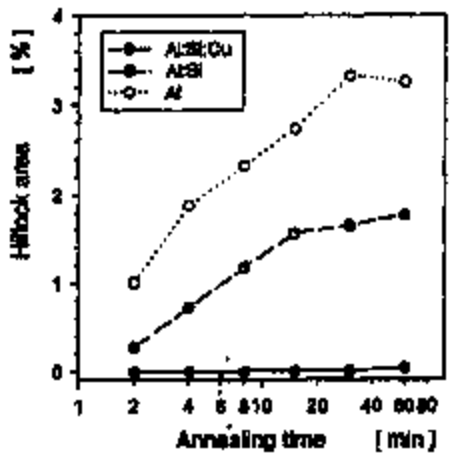

Fig. 5. Total area of hillocks normalized to the sample area as a function of annealing time at a temperature of 400°C in N_2 atmosphere for 1 μm thick Al and Al-based metallization layers.

is also proportional to the thickness of the Al layer in that range. Saturation of the plot, on the contrary, is less obvious. We may suppose that the reason for this phenomenon is a change of mechanism of hillock growth. Grains of the investigated 1 μm thick Al films were found to be columnar from TEM measurements, and the mean grain area was equal to 1.2 μm^2. The authors suppose that the shape of grains may be different in thicker films, but the problem was not studied in detail.

Surface density of hillocks rises with increase of the temperature of annealing. A series of isochronal annealings was performed using an RTP method and an argon atmosphere. A typical Arrhenius dependence was found versus $1/T$. Activation energies of total hillock density were

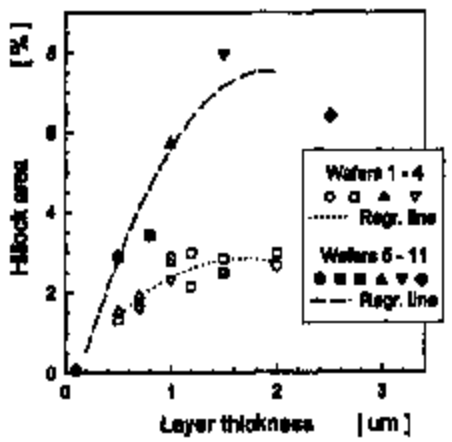

Fig. 6. Total area of hillocks normalized to the sample area versus Al layer thickness. Samples 1–4 were annealed at a temperature of 400°C for 8 min; samples 5–11 at 'standard' conditions (450°C, 30 min).

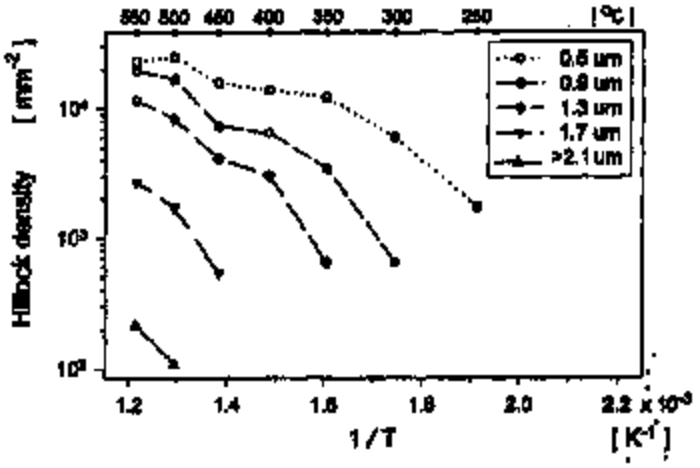

Fig. 7. Distribution of density of aluminum hillocks grouped with regard to their average diameters, as a function of reciprocal of temperature of 5 min isochronal annealings in an RTP reactor in an argon atmosphere.

calculated for the temperature range of 350–550°C, annealing time of 5 min, as 0.28 and 0.31 eV, for 1-μm thick Al and Al:Si layers, respectively.

Hillock size statistics depends also on the temperature of annealing. Fig. 7 displays the density of hillocks in an Al layer with a thickness of 1 μm as a function of $1/T$, with the average hillock diameter as a parameter. One can see that the slope of the density curves becomes higher for larger hillocks. An Arrhenius plot of the maximum hillock size represents a near straight line with an activation energy equal to 0.15 eV for Al and 0.17 eV for Al:Si.

A conclusion can be drawn from the above-presented plots that the surface hillock density, in general, decreases with the hillock diameter. A comparison of the hillock population was done for Al layers of different thickness, subjected to furnace heat treatment at a temperature of 400°C for 8 min in flowing N_2. Fig. 8 shows results for the layers of 0.7 and 1 μm. The hillock density versus hillock size curves do not fall monotonously after such moderate annealing, but its derivative with respect to hillock diameter shows a maximum for 1–1.5 μm hillock size values. This is close to a mean grain size which was established as 1.23 μm for a 1-μm thick Al layer. This suggests that the most probable mechanism of hillock growth during first few minutes of annealing is pushing out a whole grain of the film.

The above-mentioned phenomena have been investigated employing a short time and relatively low temperature of annealing. Such an approach allows for precise analysis of hillock growth kinetics. Nevertheless, the longer annealings have a more practical meaning. In order to effectively compare the morphology of the layers we have introduced a normalized hillock density N, defined as hillock number divided by the examined area of the sample and by the width of the range of diameters of hillocks taken into account. A unit of the normalized hillock density is $mm^{-2}\ mm^{-1}$ ($= mm^{-3}$). Normalized hillock density versus hillock size data for Al and Al-based metallization annealed at a temperature of 450°C for 30 min are gathered in Fig. 9. Data represent mean values from several samples, each layer thickness is equal to 1 μm. The previously mentioned increase of the density of hillocks with dimensions above 1 μm (in the case of a short annealing) is hardly visible here. The

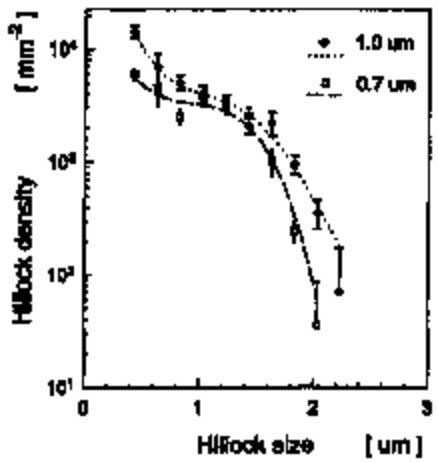

Fig. 8. Distribution of the hillock density versus hillock diameter for aluminum layers of different thickness. Vertical bars represent standard deviations of the measured values.

points for each kind of metallization are scattered near by a straight line in a logarithmic scale given by the formula:

$$N = N_0 \exp(-cd)$$

where d is hillock diameter, N_0 is the density of hillocks of diameter close to zero, and c is the curve slope. Layers made of e-gun-evaporated Al, sputter-deposited Al and Al:Si produce hillocks of similar density (dashed line in Fig. 9). An Al:Si:Cu alloy gives smaller density of hillocks, particularly those of larger size. Values of N_0 and c together with a standard deviation σ_d are gathered in Table 1. Some remarks related to presented parameters can be made. The grain density can be calculated from mean

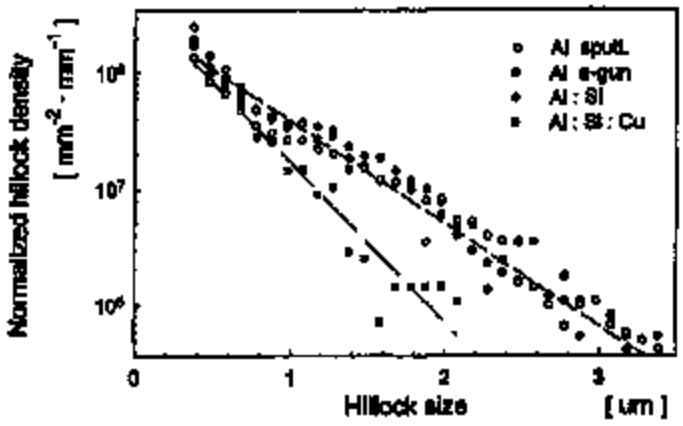

Fig. 9. Normalized density of hillocks versus hillock average diameter for often used metallization materials. Each point represent a mean value, calculated from a number of samples, annealed at a temperature of 450°C for 30 min. Dashed lines, approximate values for both Al together with Al:Si, and for Al:Si:Cu, respectively.

Table 1
Values of N_0, c and σ_n

Layer	c (μm^{-1})	N_0 (mm^{-2})	σ_n
Al, sputtering	1.85	2.07×10^{5}	0.25
Al, e-gun	2.09	3.33×10^{5}	0.33
Al:Si alloy	2.14	3.29×10^{5}	0.60
Al:Si:Cu alloy	3.18	4.05×10^{4}	0.45

grain size (1.23 μm) for aluminum layer. The value of N_0 does not exceed the mean grain density in the sputter-deposited Al layer, which is physically reasonable. It means that there are less potential hillocks than grains in Al metallization. A similar consideration for the Al:Si alloy (mean grain size of 1.95 μm) provides a conclusion, that each grain of the layer is accompanied by roughly two nuclei of hillocks. This gives evidence of the importance of Si-precipitations for hillock growth in this alloy.

4. Conclusion

In this paper new details of hillock behavior are described. The size distribution of the hillocks confirms that phenomena responsible for their growth have a statistical character. The increased population of the hillocks of diameter close to the mean grain size of the metal layer was reported for the first time, to our knowledge. A decrease of the density of the smallest hillocks reported by other authors [3,4] may be explained by a sensitivity limitation of the measuring technique (e.g., stylus profiling). We believe that the automatic optical hillock recognition method is more accurate, enabling a minimum hillock size limit of 0.33 μm (laterally). The high sensitivity of the used method calls for definition of the small hillocks. In our measurements we defined hillocks as protruded objects, surrounded by sharp edges. Therefore, an absence of these edges is particularly important in any approach for hillock suppression in metallization technology.

Acknowledgements

Authors wish to acknowledge Professor A. Barcz for productive discussion. The work was partially supported by the State Committee for Scientific Research in Poland under Grant No. 8T 11C0114.

References

[1] K.N. Tu, J.W. Mayer, L.C. Feldman, in: Electronic Thin Film Science, Macmillan, New York, 1992.
[2] F.M. d'Heurle, Metallurgical topics in silicon device interconnections: thin film stresses, Int. Mater. Rev. 34 (2) (1989) 53.
[3] B. Baccommier et al., A study of heating rate and texture influences on annealing hillocks by a statistical characterization of Al thin-film topography, J. Appl. Phys. 64 (11) (1988) 6483.

[4] S. Accto, C.Y. Chang, R.W. Vook. Hillock growth on aluminum and aluminum alloy films, Thin Solids Films 219 (1992) 80.
[5] M. Zaborowski, M. Adamiec, A. Barcz. Hillock recognition by digital image processing, Appl. Surf. Sci. 91 (1995) 246.

AN-600

Fairchild Semiconductor
Application Note
January 1989
Revised April 1998

FAIRCHILD SEMICONDUCTOR™

Understanding Latch-Up in Advanced CMOS Logic

Latch-up has long been a bane to CMOS IC applications; its occurrence and theory have been the subjects of numerous studies and articles. The applications engineer and systems designer, however, are not so much concerned with the theory and modeling of latch-up as they are with the consequences of latch-up and what has been done by the device designer and process engineer to render ICs resistant to latch-up.

Of equal interest are those precautions, if any, which must be observed to limit the liability of designs to latch-up.

WHAT IS LATCH-UP?

Latch-up is a failure mechanism of CMOS integrated circuits characterized by excessive current drain coupled with functional failure, parametric failure and/or device destruction. It may be a temporary condition that terminates upon removal of the exciting stimulus, a catastrophic condition that requires the shutdown of the system to clear or a fatal condition that requires replacement of damaged parts. Regardless of the severity of the condition, latch-up is an undesirable but controllable phenomenon. In many cases, latch-up is avoidable.

The cause of the latch-up exists in all junction-isolated or bulk CMOS processes: parasitic PNPN paths. Figure 1, a basic N-substrate CMOS cross section, shows the parasitic NPN and PNP bipolar transistors which most frequently participate in latch-up. The P+ sources and drains of the P-channel MOS devices act as the emitters (and sometimes collectors) of lateral PNP devices; the N-substrate is the base of this device and collector of a vertical NPN device. The P-well acts as the collector of the PNP and the base of the NPN. Finally, the N+ sources and drains of the N-channel MOS devices serve as the emitter of the NPN. The substrate is normally connected to V_{CC}, the most positive circuit voltage, via an N+ diffusion tap while the P-well is terminated at GND, the most negative circuit voltage, through a P+ diffusion. These power supply connections involve bulk or spreading resistance to all points of the substrate and P-well.

Similarly, Figure 2, a basic P-substrate CMOS cross section, shows the parasitic PNP and NPN bipolar transistors which most frequently participate in latch-up. The N+ sources and drains of the N-channel MOS devices act as the emitters (and sometimes collectors) of lateral NPN devices; the P-substrate is the base of this device and collector of a vertical PNP device. The N-well acts as the collector of the NPN and the base of the PNP. Finally, the N+ sources and drains of the P-channel MOS devices serve as the emitter of the PNP. The N-well is normally connected to V_{CC}, the most positive circuit voltage, via an N+ diffusion tap while the substrate is terminated at GND, the most negative circuit voltage, through a P+ diffusion. These power supply connections involve bulk or spreading resistance to all points of the substrate and N-well.

Although the rest of this application note will refer to the N-substrate model, the same discussion is true for the P-substrate model, as illustrated by Figure 1, Figure 2.

Normally, only a small leakage current flows between the substrate and P-well causing only a minute bias to be built up across the bulk due to the resistivity of the material. In this case the depletion layer formed around the reverse-biased PN junction between P-well and the substrate supports the majority of the V_{CC}-GND voltage drop. As long as the MOS source and drain junctions remain reverse-biased, CMOS is well behaved. In the presence of intense ionizing radiation, thermal or over-voltage stress, however, current can be injected into the PNP emitter-base junction, forward-biasing it and causing current to flow through the substrate and into the P-well. At this point, the NPN device turns on, increasing the base drive to the PNP. The circuit now enters a regenerative phase and begins to draw significant current from the external network thus causing most of the undesirable consequences of latch-up. Once established, a latch-up site, through the fields generated by the currents being conducted, may trigger similar action in both elements of the IC.

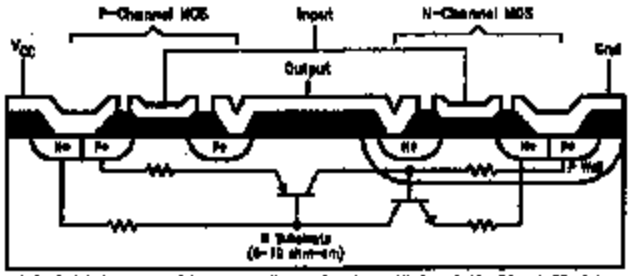

FIGURE 1. Basic CMOS Inverter Cross Section with Latch-Up Circuit Model

FACT™ is a trademark of Fairchild Semiconductor Corporation

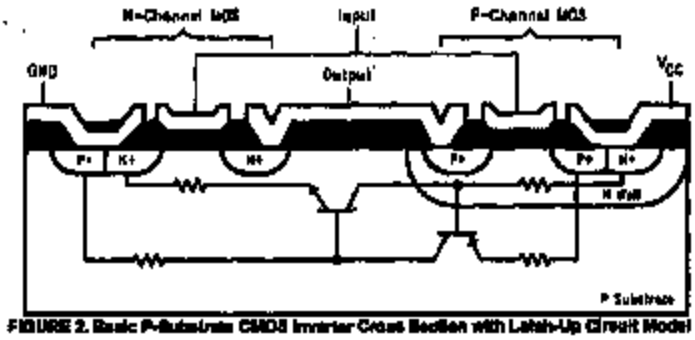

FIGURE 2. Basic P-Substrate CMOS Inverter Cross Section with Latch-Up Circuit Model

WHAT TO DO

As might be expected, latch-up is highly dependent on the characteristics of the bipolar devices involved in the latch-up loop. Device current gains, emitter efficiencies, minority carrier life times and the degree of NPN-PNP circuit coupling are all important factors relating to both the sensitivity of the particular latch-up device and to the severity of the failure once it has been excited. Layout geometry and process both contribute significantly to these parameters: CMOS, like other technologies, has been shrunk to provide more function per unit area, increasing susceptibility to latch-up. All major CMOS vendors have upgraded their processes and/or design rules to compensate for this increased susceptibility, some with more success than others. The lateral PNP is typically the weak link in the latch-up loop. As such, various devices can be applied toward reducing the effectiveness of the PNP to participate in latch-up. Guard banding, device placement, the installation of pseudo-collectors between the P-channel devices and the P-well, and the use of a low resistivity substrate under an epitaxial layer are a few of the IC design tactics now being practiced to reduce the current gain or to control the action of the lateral PNP structures in state-of-the-art CMOS devices.

Vendors of CMOS ICs have always been aware of the latch-up phenomenon and have considerably improved their designs and processes to reduce the danger of latch-up occurring under normal usage. Abnormal applications and misuse of CMOS ICs may still pose problems that the CMOS vendor has little control over. Hence, CMOS users must be aware of what they are doing and those measures which must be taken to reduce the susceptibility to latch-up. The use of CMOS at or beyond its rated maximum voltage range and the presence of inductive transients are applications-related situations which can trigger latch-up. Environment, including thermal stress, poorly regulated or noisy supplies and radiation incidence can also contribute to or cause latch-up. The system engineer must consider these situations when using CMOS in designs.

While latch-up is generally recognized as resulting from regenerative switching along a PNPN path, many designers incorrectly assume that this regenerative action places the device in a state that can only be recovered from if the system is powered down. The fact is that there is probably an equal, if not greater, chance that the regenerative switching, when encountered, will be non-sustaining (the condition, more accurately referred to as current amplification, will disappear when the triggering stimulus is removed); over-voltage applied to properly designed input protection networks is one example of controlled current amplification. For sustained latch-up to occur, the regeneration loop must have sufficient gain and the power source must be able to supply a minimum current. From this we can see that current-limited power supplies might be used to recover from or reduce the effects of latch-up. Another method uses current-limiting series resistors in the power connections of offending ICs in conjunction with storage capacitors shunting the devices. Normal switching current will be drawn from the capacitors while DC current will be limited by the resistors.

In the loop of positive current feedback formed by the parasitic PNP and NPN transistors of the latch-up structures, regenerative switching may result if sufficient loop gain is available. One must remember, though, that three conditions are necessary for latch-up to occur.

1. both parasitic bipolars must be biased into the active state;
2. the product of the parasitic bipolar transistor current gains (β_{npn}·β_{pnp}) must be sufficient to allow regeneration, i.e., greater than or equal to one;
3. the terminal network must be capable of supplying a current greater than the holding current required by the PNPN path. In processes utilizing an epitaxial silicon, this current is usually in excess of 1A.

If any of these conditions is not met both during the initiation and in the steady state, then the latch-up condition is either non-sustaining or cannot be initiated. If the current to the latched structure is not limited, permanent damage may result. Again, any means to prevent any of these conditions from being satisfied will protect the circuit from exhibiting sustained latch-up.

The prevention of biasing the bipolars into the active region and the limiting of the current which may be supplied by the network are the two factors which system designers have under their control. Many of the protective measures long exercised in discrete and TTL designs may also be applied to CMOS designs to reduce susceptibility and prevent damage to these systems. Diode clamping of inductive loads, signal and supply level regulation, and steering of large DC loads by several devices with suitable series limiting resistors to distribute thermal stress over a larger area or multiple ICs are all positive-preventive measures to apply.

While we have been considering the CMOS device in a generic manner, there are two primary structures used in all CMOS ICs which have latch-up paths associated with them; these are the inverter or gate and the transmission

switch. Both structures may be susceptible under the right conditions. While the CMOS inverter can exhibit latch-up independent of circuit configuration, the transmission switch usually has lower holding current, and thus, a lower threshold for latch-up, but is dependent on its external connections for latch-up to occur. Figure 3 shows the lumped equivalent circuit of the N-substrate inverter. Figure 4 shows the same lumped equivalent circuit of the P-substrate inverter. Notice the shunting resistors across the base-emitter junctions of the bipolar transistors: these resistors divert base drive from the bipolars and as a result increase both the trigger current and holding current levels required for the structures to participate in latch-up. A further increase in these current levels can be achieved by further decreasing the shunt resistance. Diffusing all active components into an epitaxial silicon, under which would be a substrate of substantially less resistivity, will have a dramatic effect on decreasing the shunt resistance, therefore increasing the trigger current and holding current levels required for latch-up.

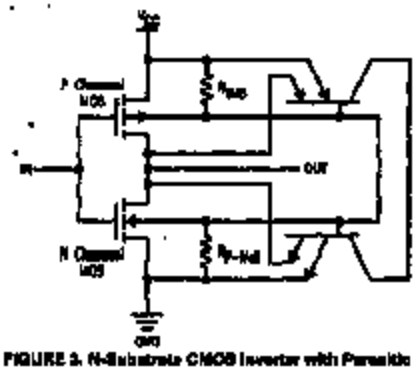

FIGURE 3. N-Substrate CMOS Inverter with Parasitic Bipolars

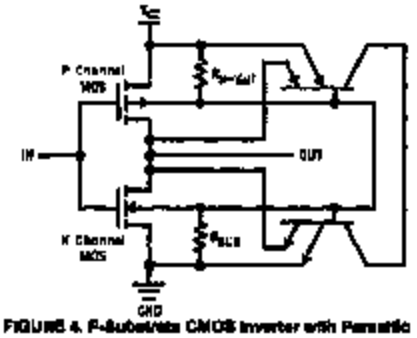

FIGURE 4. P-Substrate CMOS Inverter with Parasitic Bipolars

THE CIRCUIT CONNECTION

As we have seen above, the external circuit connections are regular participants in the latch-up process. The current for latch-up comes from these connections and often the triggering mechanism is external to the latching device. All three classes of external connections (power, input and output) are important in latch-up. We will now look at how these connections relate to this process.

Current injection through the power terminals when the power supply voltage is beyond the maximum need for the CMOS device can directly cause latch-up through base collector leakage or breakdown mechanisms. One aspect of high power supply voltages that is not often recognized is the effect of field-aiding lateral currents under the emitters of the PNP devices. This can effect a significant increase in the beta of these devices, making internally triggered latch-up much more prevalent. Again, the warning to the system designer is to avoid using CMOS at maximum rated supply voltages unless precautions are taken to insure latch-up is unlikely or is at least acceptable and recoverable. Switching transients coupled onto power lines has become a problem now that CMOS has become a high-speed logic technology. Attention to power supply decoupling is now a necessity when designing with high-speed CMOS. Of course, CMOS processes incorporating an epitaxial silicon over a substrate of very low resistivity is less prone to latch-up under these conditions. These recommended precautions should be taken just the same.

Latch-up involving input terminals, next to gate oxide rupture, used to be one of the most common failure mechanisms of CMOS. Transients exceeding the power supply routinely caused either or both of these effects to occur. Fortunately, CMOS vendors have learned to make better input protection networks and have learned that proper placement of these components with respect to the rest of the chip circuitry is necessary to reduce susceptibility to latch-up. The system designer should review foreign input signals to CMOS systems and take precautions necessary to limit the severity of overshoot/undershoot from these sources. Measures which could be used to reduce the possibility of latch-up induced by input signals are: proper termination of transmission lines driving CMOS, series current limiting resistors, AC coupling with DC restoration to the CMOS supplies, and the addition of Schottky diode clamps to the CMOS power rails. As an additional measure there are several CMOS circuits which have input protection networks that can handle over voltage in one direction or the other and which are specifically designed to act as interface circuits between other logic families and CMOS. Judicious application of these will also aid in suppressing any tendencies of CMOS systems to latch-up.

Finally, attention to CMOS outputs, their loading and the stresses applied to them will also enable the designer to generate latch-up free systems. Historically, output terminals of CMOS have been least likely to cause latch-up though they can participate in latch-up once it is initiated. The normal mode of failure in this respect is, again, the application of voltages beyond the CMOS supplies or the maximum limit for the devices through excessive current has also been linked to latch-up failure at elevated temperatures. Inductive surges and transmission line reflections are the most likely sources of output latch-up in CMOS and should be attended to in the most applicable method, i.e., by clamping, termination or through dissipative measures.

WHAT WE HAVE DONE

Fairchild Semiconductor, as an important supplier of advanced CMOS to all segments of the industry, has made a commitment to provide IC designs which make use of state-of-the-art latch-up suppression techniques in an effort to support its customers before they need support. The three most important actions which we have taken to guard our customers from latch-up are in the areas of layout, power distribution and process design. These techniques,

along with recognized good design practice, yield a product line that lives up to the intent of an advanced CMOS family. In brief review, Fairchild Semiconductor's attack on latch-up is summarized in the following.

Latch-Up Protection Geometries

Every FACT™, VHC, and LCX IC employs special geometries to isolate every input protection device and every output from active areas on the chip. In this way, structures which would normally participate in latch-up loops are decoupled and are thus less troublesome. All devices are scrutinized for potential latch-up sites and are protected by similar geometries where any risk is significant.

Power Distribution

Careful attention to on-chip power distribution and enhanced termination of P-wells or N-wells and substrate is used by Fairchild Semiconductor to improve latch-up resistance. Our metal process affords the advantage in maintaining low impedance distribution of power and ground potentials over the entire chip; the potential gradient-caused fields which often induce or enhance latch-up are thus minimized while functional performance is enhanced by cleaner on-chip power supplies.

Process Design

By design, the FACT, VHC, and LCX processes are better both in low latch-up susceptibility and in enhanced device performance. The most significant advancement of these processes has been the incorporation of an epitaxial silicon layer. Figure 5 illustrates a modified version of Figure 1, utilizing an epitaxial layer of silicon to contain all of the active components of the CMOS circuit. This epitaxial layer allows the use of a separate layer of substrate silicon, of a resistivity some three orders of magnitude lower than the epitaxial layer. The effect is also modeled in Figure 6.

As illustrated, the resistivity of the epitaxial silicon, R_1, is on the order of 8 ohm-cm to 10 ohm-cm. The underlying substrate resistivity, R_2, is as low as 0.008 ohm-cm to 0.025 ohm-cm. The result is a parallel combination of resistivities. R_1 and R_2, that is equivalent to R_2. What has now happened is that the gain of the parasitic PNP-NPN circuit has been dramatically slashed. Under the same latch-up conditions described earlier, the introduction of the low resistivity substrate now means that at least 10 times more current is needed to trigger the parasitic PNP-NPN combination.

The active components within the epitaxial layer maintain the same performance characteristics as those of the active area illustrated in the non-epitaxial CMOS circuit of Figure 1. Therefore the introduction of the epitaxial layer to the FACT,VHC, and LCX processes does not reduce any AC, DC, functional or ESD performance. However, what we have are advanced CMOS logic families that are now virtually latch-up immune.

Thus, through innovative and careful layout, attention to eliminating circuit situations which could be latch-up prone and by careful selection and maintenance of our advanced CMOS process, FACT, VHC, and LCX set the standard for latch-up resistance.

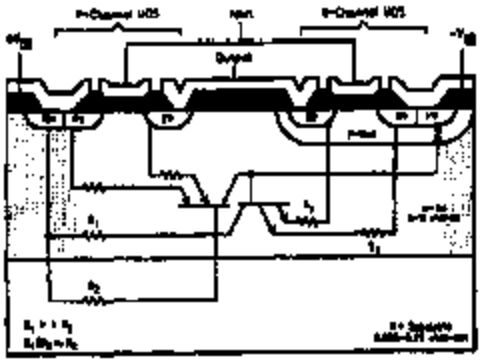

FIGURE 6.

ELSEVIER

Thin Solid Films 307 (1997) 169–177

thin solid films

Initial development of the lateral hillock distribution in optical quality Al thin films studied in real time

C. Kylner [a,*], L. Mattsson [b]

[a] Department of Physics II (Optics), Royal Institute of Technology, Stockholm S-100 44, Sweden
[b] Surface Evaluation Laboratory, Institute of Optical Research, Stockholm S-100 44, Sweden

Received 24 March 1997; accepted 21 May 1997

Abstract

Our previous investigations using real-time total integrated scattering (TIS) have shown a very distinct onset of hillock formation in optical quality Al films on Si wafers at temperatures well below 100°C. This paper extends those investigations by studying in real time the *initial* development of the lateral hillock distribution. After the first hillocks appeared the number of hillocks accelerated rapidly with increased temperature, in particular for higher heating rates. The lateral hillock distributions were further statistically analyzed by the Quadrate counts method to get more objective results. This analysis indicates that hillocks tend to be clustered over larger areas. The nearest neighbor distance between hillocks was also calculated. The hillocks had a tendency of lining up in distorted ring shaped patterns. This is interpreted as an effect of inhomogeneous stress distributions at the local grain level. The observations were made possible by using an imaging partial integrated scattering (PIS) system comprising of a dark field microscope objective and a charge coupled device (CCD) camera with an image processor and a data acquisition system. ©1997 Elsevier Science S.A.

Keywords: Aluminum; Optical coatings; Heat treatment; Light scattering

1. Introduction

Aluminum (Al) is the interconnection material most commonly found in integrated circuits. Thermal cycling during fabrication and high current densities in the operation of the integrated circuits generate large stresses, which may result in short circuits caused by hillocks or open circuits caused by voids and cracks. Similar problems with hillock and void formations are also known in the optical device industry. For example, the surface of an Al coated mirror is often exposed to harsh treatment and chemicals. To withstand these treatments a transparent protective layer is necessary. When silica is used as a protective layer it needs to be deposited at a temperature well above 100°C. Heated to that temperature hillocks will start to form in the evaporated Al films [1]. As high quality mirrors are degraded even by very small changes in the surface microtopography, the formation of hillocks is very detrimental to the optical quality of the film. A deeper understanding of mechanical stress in thin films is thus crucial for further miniaturization and higher device densities of very large scale integrated (VLSI) circuits, as well as for producing metal coated mirrors of high optical quality.

For a metal film that adhere well to a relatively thick or a sufficiently stiff (high modulus) substrate, the lateral film dimensions are controlled by the substrate. During a thermal cycling of such a sandwiched structure, volume changes caused by the thermal expansion mismatch between the film and the substrate will result in a build-up of mechanical stress in the film. This stress will bend the substrate to the shape of a spherical shell. If the biaxial elastic modulus is isotropic in the plane of the substrate, as it is for e.g. (100) silicon substrates [2]. If the stress in the film exceeds the elastic limit it will relax by various mechanisms of plasticity and creep [3]. Dislocation glide and grain boundary diffusion are generally accepted to play an important role in the hillock growth [4–8], but a detailed understanding of the mechanisms is still lacking.

Stress relaxation in thin films is affected by several parameters such as the substrate temperature during deposition [9,10], the film thickness [11,12], the grain size [6,8], the grain orientation [5–7], the alloying elements [13], and the surface oxides [14,15]. In addition, it also depends on

* Corresponding author. E-mail: carina@optics.kth.se

PII S0040-6090(97)00315-5

the thermal treatment which several authors have studied during isothermal treatments at various elevated temperatures [9,16]. Some investigations have also been made concerning the influence of the heating rate, see for example Baconnier et al. [17]. Gerth and Schwarzer [5,6] and Gerth et al. [8] have in several studies compared stepwise heating with isothermal heating.

The most common way to quantify hillock formation has been to express it in terms of hillock size, hillock density [9,10,17], or distance between hillocks [15]. By tradition hillocks have been extensively studied using scanning electron microscopy (SEM) [9,10,15,18], transmission electron microscopy (TEM) [5,15], and optical microscopy [16]. Investigations have also been made using stylus profilometers and atomic force microscopy (AFM) [19].

However, when studying the formation of the first hillocks it is crucial that the analysis technique does not influence the development of the hillocks, as easily can happen with electron beams when using SEM and TEM. Therefore, we have previously been using very sensitive non-contacting optical techniques such as total integrated scattering (TIS) [1], and the Vacuum Compatible Partial Integrated Scattering and Deflection (VaCPISD) technique [19,20]. Based on the fact that the integrated scattering methods are exceedingly sensitive real-time techniques for investigating minute topographical changes in a heated film, we have now developed the technique to also be imaging. With the developed imaging partial integrated scattering (PIS) system we are able to simultaneously acquire the scattered intensity as well as the absolute positions of the discrete scatter sites (hillocks) in the film. Using this technique, hillock formations can be revealed at an earlier stage and over larger areas than by using conventional SEM and TEM. The purpose of the present study is to make use of the imaging PIS technique to quantitatively and in real time examine how the thermal treatment influences the time before the first hillocks show up, the speed at which discrete hillocks are being formed, and how they are laterally distributed on the film surface. To our knowledge there has been no thorough study in real time of the initial development of the lateral hillock distribution. This paper also presents the experimental and statistical tools used for evaluating the lateral hillock distribution on heated optical quality Al films, and it is followed by a discussion of the observed findings in terms of inhomogeneous distribution of stress tolerance in the film.

2. Experimental

2.1. Sample preparation

Al films were evaporated in an ultra high vacuum system by an e-beam gun from 99.999% pure Al (Balzers) onto the polished side of 0.5 mm thick, 3-in. silicon (100) wafers (Virginia semiconductors). The wafers, coming straight out of the wafer box and having a native oxide, were kept at room temperature during the film deposition. The deposition rate was approximately 2.1 nm/s and the pressure at the film deposition was 7.7×10^{-6} Pa. The background pressure before the deposition was 8.8×10^{-7} Pa. The samples were rotated at a distance of about 40 cm from the Al source to achieve uniform optical quality films. The achieved film thickness was 0.2 μm as measured by a Talystep surface profilometer [21] and the lateral grain size of the films was about 100 nm as determined by atomic force microscopy (AFM). TIS investigations have shown that the hillock formation process is very repetitive for samples evaporated in the same batch. Therefore, all samples used in this study were taken from the same deposition batch.

2.2. Heater and thermal treatments

The experimental setup consists of a microscope stage equipped with a specially designed nichrome resistive heater and sample holder. A view of the sample compartment is shown in Fig. 1. The sample holder clamps the silicon wafer at the edge, and the temperature sensing Pt-100 element is attached to the thin film side of the sample. A heat shield with a circular hole is placed between the heater and the optical system consisting of a dark field microscope objective. The shield prevents damage to the optical parts and reduces the effect of thermal turbulence in the imaging path. The size of the hole is adapted so that most of the scattered light from the hillocks in the film is received by the microscope objective. A ceramic plate and an Al sheet thermally insulate the heater from the microscope stage.

The samples were heated from room temperature with different power levels for 10 min. The final temperatures were 144°C for treatment A, 132°C for treatment B and 124°C for treatment C, yielding average heating rates of 11.7°C/min (A), 10.5°C/min (B) and 8.8°C/min (C). The initial heating rates for the first minutes were 19.5°C/min (A), 15.8°C/min (B) and 13.6°C/min (C). The temperature vs. heating time diagram for the three different thermal treatments is shown in Fig. 2.

2.3. Imaging PIS

Total integrated scattering is a non-contact light measurement technique capable of sensing surface roughness at sub-ångström roughness levels [22]. In its standard setup it collects the scattered light from a surface by means of an almost hemispherical mirror, and focus this radiation onto a detector. Due to the large spherical aberration of the mirror the technique is not suitable for direct imaging of single hillocks. Thanks to the wide angular scattering distribution from small surface features such as hillocks, we can get a decent scattering signal by using a somewhat reduced solid angle of the light collecting system. An

Fig. 1. Close-up on the sample compartment.

example of such a system is the VaCPISD instrument with its partial integrated scattering detector unit [19,20]. Another example is the conventional reflection mode dark field microscope objective, that has the advantage of being corrected for good imaging properties. In this study we used a Zeiss objective mounted on a Zeiss Axiophot microscope, for obtaining the light collection with simultaneous high quality imaging of the scatter sites. Provided with a Hamamatsu charge coupled device (CCD) camera C3077, a Hamamatsu Argus 50 image processor and image acquisition system, we obtain a complete imaging PIS system, capable of detecting the overall scattered intensity and the position of local scatter sites while the sample is being heated. A great advantage with the system is that with the selected objective it can also be operated in the differential interference contrast (DIC) mode, giving the possibility of focusing onto supersmooth Al film surfaces. Before starting the thermal treatment and image acquisition, the microscope is switched over to the dark field mode and a dark field image is acquired of the untreated film. This image, which is normally black, is later subtracted from the acquired series of images of hillocks obtained in the heating process. For the high optical quality Al films used in this study, practically no growth hillocks (or voids) were observed in the initial dark field image prior to heating. During heating the films develop to compressive stress so no voids are expected to be formed. Substrate bending caused by the compressive film stress can be compensated for by manual refocusing. The first hillock in the field of view of the imaging PIS system will show up as a bright spot after an incubation time of some minutes and then, as the overall compressive stress gets too high, hillocks are popping up everywhere as bright stars. Video recordings of the course of the events are indeed very illustrative of the local relaxation in the film. An image (512 × 511 pixels) corresponds to a physical area of 7.56×10^{-4} cm^2 and is integrated from 128 video frames. Such an image is stored every 6.1 s throughout the measurement series. The images have a dynamic range of 256 gray levels, where the background typically corresponds to the ten darkest levels in the images. In the images to follow, we have for the sake of printing reproduction, inverted the images so that the scatter sites appear as black spots on a white background rather than bright spots on a dark background.

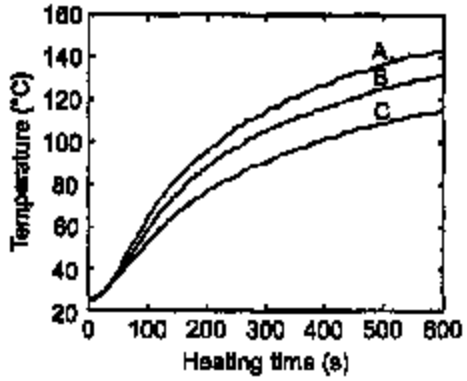

Fig. 2. Thermal treatments plotted as sample temperature vs. heating time.

The sum of scattered light from individual hillocks is proportional to the number of hillocks illuminated on the surface, at least as long as the hillocks are small and well separated. When they get close enough, less than about 5

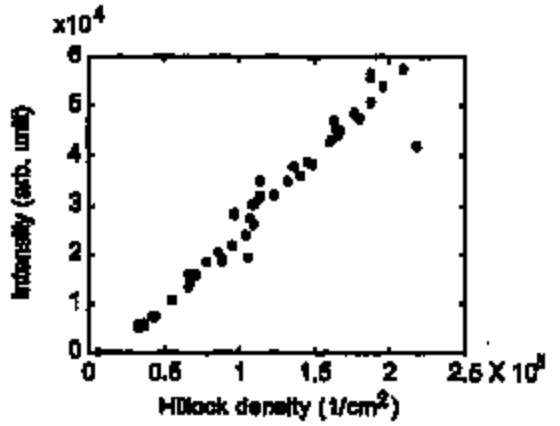

Fig. 3. Average intensity of CCD camera image vs. number of hillocks/cm^2 present for the images acquired in thermal treatment C. The average intensity is a number related to that obtained by total integrated scattering.

wavelengths of the incident light, multiple scattering will come into effect and a proportionality will no longer exist. The wavelength limit is rather fuzzy but this is the distance where the density of surface features has been shown to influence the polarization properties of the light [23]. In the initial heating cycle studied in this investigation, the hillocks are well separated. Hence, we get a good correlation (see Fig. 3) between the acquired average intensity (the equivalent of the TIS signal) and the number of hillocks present in the field of view of the imaging PIS.

2.4. Total integrated scattering measurements

For comparison and confirmation of the imaging PIS data we also measured the samples before and after the thermal treatments by means of the standard TIS equipment [22]. Before heating, the samples had the same TIS value (= diffuse reflectance divided by total reflectance), of 9.1×10^{-5}, confirming their identical as-deposited surface roughness, δ. Earlier studies have confirmed that the as-deposited surface roughness of the films depends on both the film thickness and the deposition conditions such as background and deposition pressures [24,25]. By using ultra high vacuum deposition at room temperature we achieved smooth, low scatter Al films with low surface roughness values. After the different thermal treatments, the TIS values were 1.1×10^{-3} for A, 6.5×10^{-4} for B and 4.1×10^{-4} for C. As we have seen before, the higher temperatures used during the heating the higher the TIS value became. A summary of the TIS investigation is given in Table 1.

Table 1
Summary of the total integrated scattering (TIS) investigation

Treatment	Initial		Final		
	Total integrated scattering	Root mean square (rms) roughness (Å)	Temperature (°C)	Total integrated scattering	Equivalent root mean square (rms) roughness (Å)
A	9.1×10^{-5}	4.80	144	1.1×10^{-3}	16.7
B	9.1×10^{-5}	4.80	132	6.5×10^{-4}	12.8
C	9.1×10^{-5}	4.80	115	4.1×10^{-4}	10.2

3. Analysis methods of lateral hillock distribution

The (x,y) position of a hillock center was calculated with ARGUS-50/CA code from Hamamatsu and we refer to this center as a scatter site. Data in the form of a set of points, irregularly distributed within an area arise in many different contexts. A common question is whether the points appear completely random, regularly spaced or clustered. The study of spatial point patterns has a long history in ecology and forestry. In the first analysis of the lateral hillock distribution we apply the Quadrate counts method [26]. The basics of the method are briefly described below.

The study region, A, is partitioned into m sub-blocks or quadrates each with an area B. The data to be analyzed comprises independent counts $n_1, n_2, \ldots, n_m$ in these m quadrates. To test the hypothesis that n_i are an independent random sample from a Poisson distribution the Quadrate counts method is applied. Under Complete Spatial Randomness (CSR), the number of counts $N(B)$ in a quadrate follows a Poisson distribution with the mean λB, where λ is the number of counts per area B. The probability distribution of $N(B)$ is given by

$$p_n(B) = \exp(-\lambda B)\frac{\lambda B^n}{n!}, n = 0,1,2\ldots \quad (1)$$

The dominating test statistic for the Quadrate counts method is the index of dispersion, I,

$$I = \frac{s^2}{s^2_{\text{rand}}} \quad (2)$$

also referred to as variance ratio, formation number and relative variance. The numerator,

$$s^2 = \frac{1}{m-1}\sum_{i=1}^{m}(n_i - \bar{n})^2 \quad (3)$$

estimates the variance of $N(B)$ when no distributional assumptions are made, whilst the denominator, s^2_{rand}, estimates the variance when CSR holds and is equal to the mean $\bar{n}$.

Values of I greater than one indicate that the scatter sites are clustered. On the other hand, if I is less than one then this indicates a tendency for regular spacing. With

this method, it is possible to focus on small-scale or large-scale phenomena depending on the choice of quadrate size, B.

In the second analysis of the lateral hillock distribution, the nearest neighbor distance between hillocks was calculated. This calculation is effected by the edges of the images, and we solved this problem by the so called free zone method, i.e. the distance to a hillock is not accounted for if the hillock is closer to an edge than to its nearest neighbor.

4. Results and discussion

From previous measurements using the TIS technique we know that Al films evaporated in the same batch shows a repeatable TIS response for identical heat treatments. The samples used in this study were from the same batch. We are therefore confident that the observed differences between the samples can mainly be attributed to the different thermal treatments.

4.1. Development of the hillock formation

The imaging TIS study yielded a large library of images for each of the samples, showing the progressive development of the hillocks. Fig. 4 shows some examples of the inverted binary dark-field images obtained at different heating times and temperatures during the thermal treatments. In the left column of this figure the first scatter sites are seen and the right column shows the scatter sites when the hillock density was about 2.5×10^5 cm^{-2}. One interesting result from this comparison is that the lowest heating rate (8.8°C/min) on average produces fewer hillocks per cm^2 at a given temperature, than the higher heating rates do. This implies that one possible way of reducing the number of hillocks in an Al film is to have a gentle rather than a forced heating treatment. From these images it is possible to see that the hillocks were inhomogeneously distributed over the examined sample area. See for example the thermal treatment A as compared to treatment B and C, indicating different stress tolerance in different regions of the film.

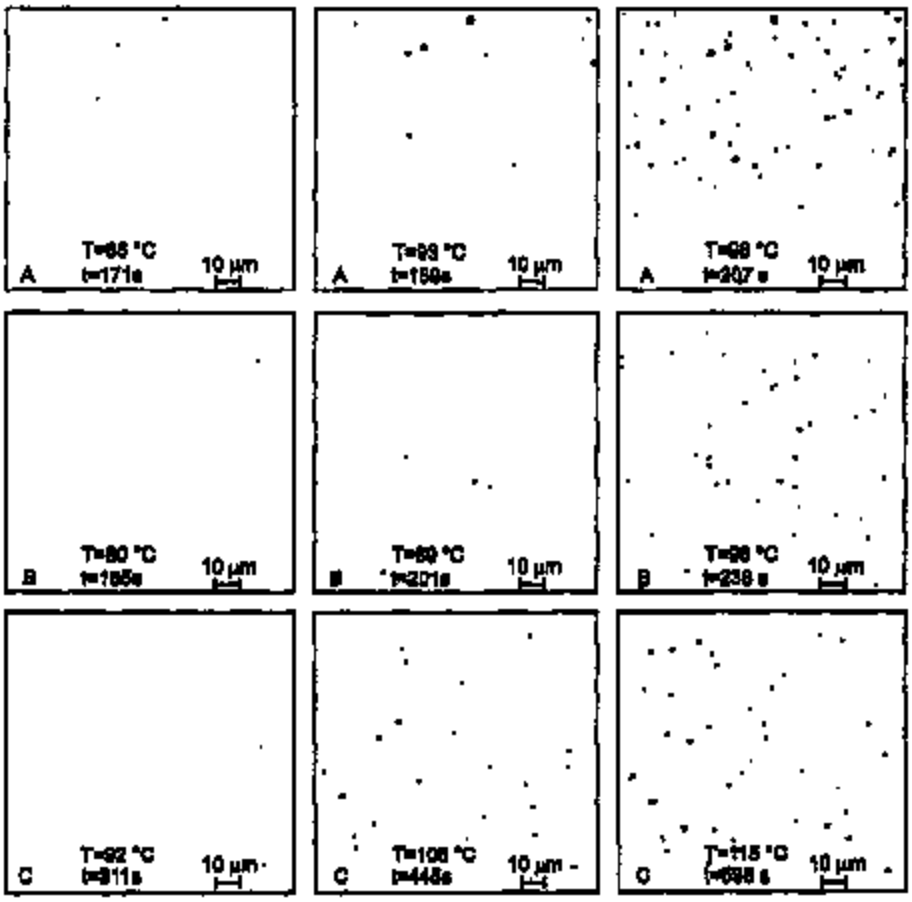

Fig. 4. The inverted binary dark-field images for the thermal treatments (A, B and C) when the hillock density was about the lowest detectable (left column), about 50% of 2.5×10^5 cm^{-2} (middle column) and at about 2.5×10^6 cm^{-2} (right column). In order for the scatter sites to be clearly visible we only show about 20% of the acquired image.

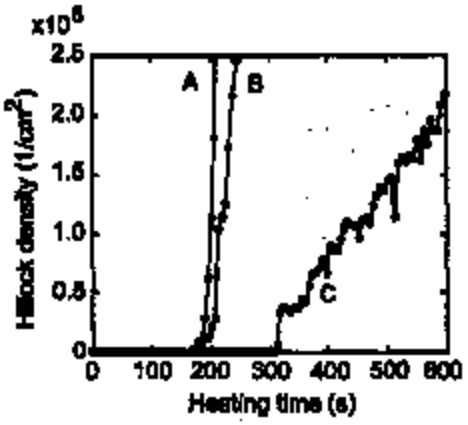

Fig. 5. Hillock density plotted vs. heating time.

4.2. Hillock density

The increase in the number of hillocks per cm^2 as detected in the field of view of the imaging PIS system from the first hillock up to a density of about 2.5×10^5 cm^2 is shown in Fig. 5. From this figure it is seen that the incubation time, i.e., the time before the hillocks starts to form, was almost the same for treatment A and B (about 3 min), but was considerably longer for treatment C (about 5 min). The temperature corresponding to the observation of the first hillock was $T = 88$°C (A), $T = 80$°C (B) and $T = 92$°C (C). Thus, the onset of hillock growth occurred within a confined temperature range apparently independent of the heating rate. After the incubation time the number of hillocks started to increase, first slowly, then more rapidly. The average increase in number of hillocks for a hillock density up to about 2.5×10^5/cm^2 was 4.2×10^3/(s cm^2) for treatment A, 2.7×10^3/(s cm^2) for B and 7.5×10^2/(s cm^2) for C. With the corresponding average heating rates of 11.7°C/min, 10.5°C/min and 8.8°C/min for treatment A, B and C respectively it is worth noticing that a 33% increase in heating rate yielded an increase of hillocks formation by an almost six times higher rate. The density of hillocks was also found to be higher for higher heating rate at a given temperature. This is another indication that a slower heating is to be preferred for obtaining a reduced number of hillocks.

It is known that when the stress in the film exceeds the yield strength of the film material plastic deformation occurs. The temperature and the heating rate during thermal treatments influence the dominating deformation mechanisms in the film [8,27,28]. In the case of low temperature and relatively high heating rate, which was valid for our experiments, the thermally induced stress is relaxed mainly by dislocation glide so the flow stress of that temperature. The significant difference in increase in number of hillocks for the samples may indicate that a higher heating rate caused more grain deformation by dislocation glide.

4.3. Ring shaped patterns of hillocks

The large library of images revealed the interesting result that many hillocks were preferentially lined up along distorted ring shaped patterns, at least as interpreted by the human eye. In Fig. 6 we show an example of an image where some patterns of this kind can be seen. To our knowledge such ring patterns have not previously been reported. We try to explain these patterns by starting from existing deformation mechanism descriptions and finally making a qualified guess.

As is well-known dislocation glide occurs preferentially on planes of high atomic density along close-packed directions and, as for all fcc metals, deformation is caused by slip on {111} planes in ⟨110⟩ directions. The shear stress per strain on the slip systems ⟨110⟩ is higher, up to about two times, for grains deviating from ⟨111⟩ texture [7]. In polycrystalline films, the grains may be gathered in what Flinova and Artemyev [29] call colonies. Such colonies are grain groups with close orientation. Therefore, the yield strength may be reached at different stress levels in different regions of polycrystalline films. In some regions yielding is not exceeded, in others it is exceeded resulting in an inhomogeneous deformation, which makes the stress even more inhomogeneous. However, yield strength is not well defined for polycrystalline materials, due to the inhomogeneous deformation, and it depends on the heating rate and the temperature. This implies that grains deviating from ⟨111⟩ texture will be the first to deform plastically with associated hillock formation. The reason for the hillocks to line up along distorted ring shaped patterns is still an unresolved question. A qualified guess is that the grain orientations in the 100 nm large grains of the Al

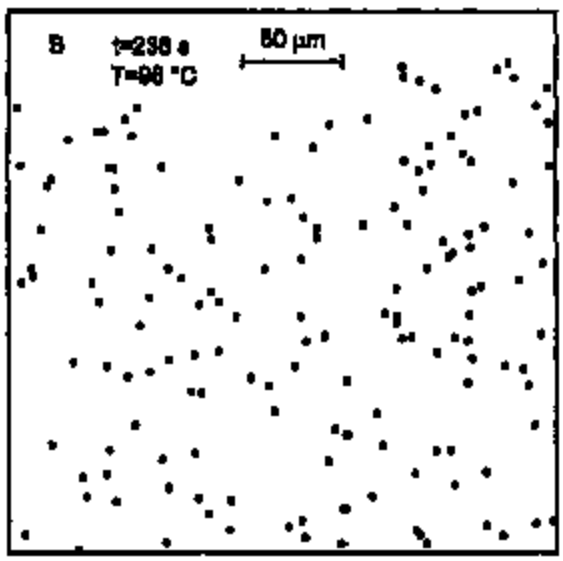

Fig. 6. The hillocks often tended to line up along distorted ring shaped patterns. The arrow sizes have been enlarged for easier observation.

films were influenced by the substrate microstructure, and that the lines of hillocks revealed this structure. One reason for making such a guess is that we have observed similar ring shaped zones on bare silicon wafers of both ⟨100⟩ and ⟨111⟩ type using contrast enhanced reflection microscopy. In those cases the patterns appear as 20–50 μm large 'grains' with just barely discernible reflection differences. If the boundary between those large 'grains' influences the nucleation of the Al film we can expect an influence on the stress tolerance in the film according to the discussion above.

The observed distorted ring shaped patterns are not easily expressed in geometrical terms. Therefore, to get a more objective description of the lateral hillock distributions, the acquired images were further analyzed by two statistical methods.

4.4. Test of randomness in the lateral hillock distributions

As we have not found any literature reference on lateral hillock distribution analysis in terms of randomness we introduce a technique picked up from forestry investigations [26]. In the first analysis, a statistical description of the lateral hillock distribution was obtained by applying the Quadrate counts method described in Section 3. This method tests the Complete Spatial Randomness (CSR) using the index of dispersion, I, to classify the pattern as regular ($I < 1$), random ($I = 1$) or clustered ($I > 1$). The index of dispersion corresponds in our case to the ratio between the variance of the measured number of hillocks in the quadrates and the variance of the number of hillocks following a Poisson distribution. The results from this analysis for the different thermal treatments are shown in Fig. 7. The index of dispersion is plotted vs. heating time for the same sample area with three different quadrate grids (2 × 2, 4 × 4 and 8 × 8 grid of quadrates). The index of dispersion increased during the thermal treatment for all samples independent of the grid refinement. Further, the index of dispersion was larger for coarser grid, which implies that the lateral hillock distributions over large areas (1.89×10^{-4} cm^2) appear more clustered than over small areas (1.18×10^{-5} cm^2). The clustered distributions thus confirm the result of inhomogeneous deformation.

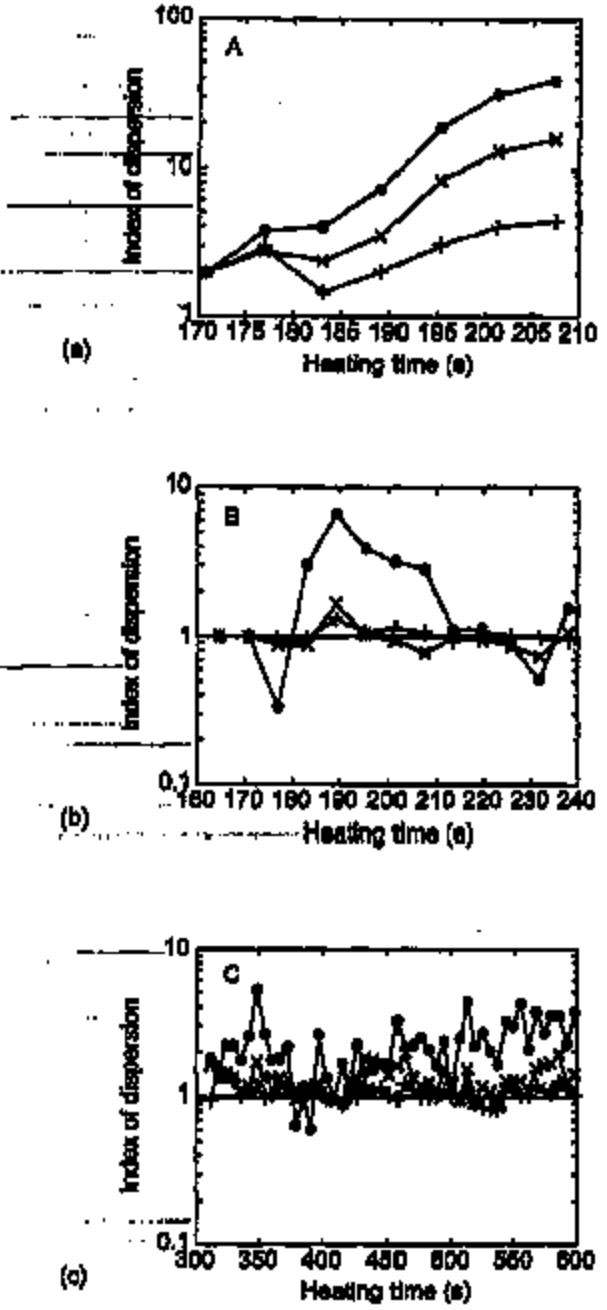

Fig. 7. Test of randomness in the lateral hillock distributions. Index of dispersion, I, for thermal treatment (a) A, (b) B and (c) C, and three quadrate sizes ((●) 2×2, (×) 4×4 and (+) 8×8 grid of quadrates). Distribution is regular for $I < 1$, random for $I = 1$ and clustered for $I > 1$.

4.5. Nearest neighbor distance between hillocks

In the second analysis of the lateral hillock distribution, we calculated the nearest neighbor distance between hillocks. The mean value of the nearest neighbor distance and its standard deviation were calculated for each image for all samples up to a hillock density of about 2.5×10^5 cm^2. The result is presented in Fig. 8. As expected a general tendency for all treatments was that the mean distance decreased with heating time, and at the temperatures obtained here it approached about 10 μm. This is 100 times larger than the typical grain size of the evaporated Al films, which was measured to be about 0.1 μm using atomic force microscopy. Another general behavior was that the standard deviation of the nearest neighbor distance between hillocks also decreased with heating time.

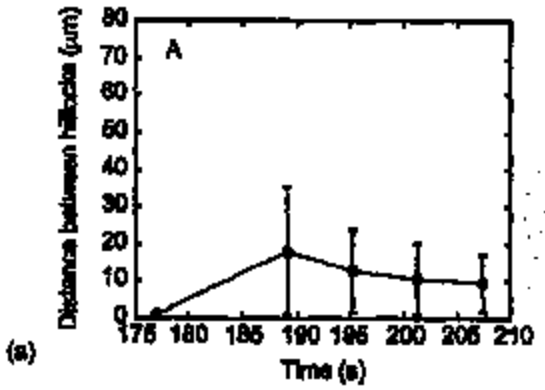

(a)

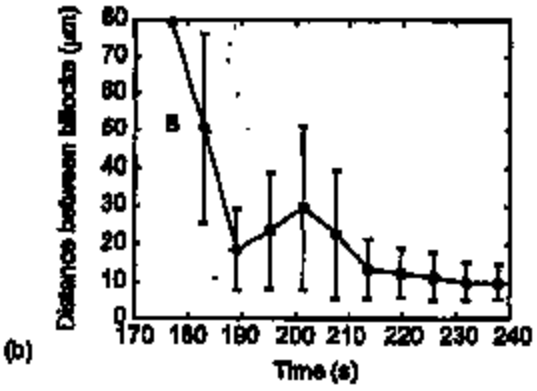

(b)

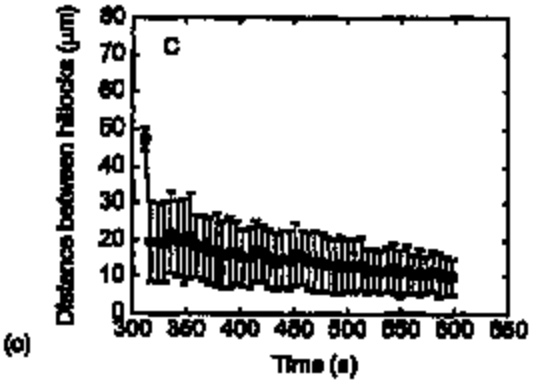

(c)

Fig. 8. The nearest neighbor distance between hillocks as a function of heating time for thermal treatment A (a), B (b) and C (c). The standard deviation is given by the bars.

Although the mean distance approached 10 μm, hillocks along the distorted ring shaped patterns (e.g., Figs. 4 and 6) can be considerably more closely spaced. Our result can be compared with the distance between hillocks reported in Ref. [15] ranging from about 20 μm to 100 μm for sputter deposited Al − 2 at.% alloy films with grain size, which was about 0.2 μm after heating at 400°C.

5. Conclusions

Real-time imaging partial integrated scattering technique, applied on optical quality Al films on Si wafers, has shown the initial development of the lateral hillock distribution in the films for different heating rates. The formation of the first hillocks was found to appear within a confined temperature interval, independent of the heating rate. After the onset of hillocks, the density of hillocks increased considerably faster for the higher heating rates than for the lower. We therefore conclude that a low heating rate is to be preferred if the number of hillocks should be minimized at a particular temperature. We also found by visual observation and statistical analysis that the hillocks tend to be clustered, and line up in distorted ring shaped patterns at this initial stage of hillock formation. We suggest that these patterns are caused by inhomogeneous stress distribution at the local grain level of the film, and that the inhomogeneous stress can be derived from substrate influence causing different grain orientations.

Acknowledgements

The authors are very grateful to L. Kjellberg and S. Bolin for the electronic and mechanical workshop assistance and L. Krummenacher for thin film deposition, AFM and Talystep measurements. The research and development was financially supported by the Swedish Research Council for Engineering Sciences (TFR) and the Göran Gustafsson Association.

References

[1] L. Mattsson, Y.-H. Le Page, F. Ericsson, Thin Solid Films 198 (1991) 149.
[2] W.D. Nix, Metall. Trans. 20A (1989) 2217.
[3] V.M. Kolesnika, V.F. Ballikly, L.V. Kiryushin, Thin Solid Films 142 (1986) 199.
[4] M.S. Jackson, C.-Y. Li, Acta Metall. 30 (1982) 1993.
[5] D. Gerth, R.A. Schwarzer, Mater. Sci. Forum 119-121 (1993) 621.
[6] D. Gerth, R.A. Schwarzer, Mater. Sci. Forum 119-121 (1993) 619.
[7] R.A. Schwarzer, D. Gerth, J. Electron Mater. 22 (6) (1993) 607.
[8] D. Gerth, D. Katzer, M. Krohn, Thin Solid Films 208 (1992) 67.
[9] S. Asano, C.Y. Chang, R.W. Vook, Thin Solid Films 219 (1992) 80.
[10] C.J. Sunseri, J. Electrochem. Soc. 116 (1969) 361.
[11] R. Venkatraman, J.C. Bravman, J. Mater. Res. 7 (8) (1992) 2040.
[12] M.F. Doerner, D.S. Gardner, W.D. Nix, J. Mater. Res. 1 (6) (1986) 845.
[13] D.S. Gardner, P.A. Flinn, Mater. Res. Soc. Symp. Proc. 130 (1989) 69.
[14] C.Y. Chang, R.W. Vook, Thin Solid Films 228 (1993) 205.
[15] E. Iwamura, T. Ohnishi, K. Yoshikawa, Thin Solid Films 270 (1995) 450.
[16] C.A. Volkert, C.F. Aloft, J.R. Liefting, J. Mater. Res. 9 (9) (1994) 1147.
[17] B. Baroncini, G. Lormand, M. Papapietro, M. Aubard, A.-M. Papon, J. Appl. Phys. 64 (11) (1988) 6483.
[18] S.K. Lahiri, D.C. Walls, Appl. Phys. Lett. 15 (1969) 234.

[19] C. Kylner, L. Mattsson, Mater. Res. Soc. Symp. Proc. 436 (1996) 297.
[20] C. Kylner, L. Mattsson, Rev. Sci. Instrum. 68 (1) (1997) 145.
[21] J.M. Bennett, J.H. Dancy, Appl. Opt. 20 (10) (1981) 1785.
[22] L. Mattsson, Proc. SPIE 652 (1986) 264.
[23] E.O. Laowen, M. Nevière, D. Maystre, J. Opt. Soc. Am. 68 (4) (1977) 495.
[24] L. Mattsson, Workshop on Optical Fabrication and Testing Technical Digest 1987, Optical Society of America, Washington, 1987, pp. 85–89.
[25] F.M. Reinits, P.B. Barna, Acta Phys. Acad. Sci. Hung. 49 (1-3) (1980) 237.
[26] N.A.C. Cressie, Statistics for Spatial Data, Wiley, New York, 1993.
[27] M.D. Theodoss, Annu. Rev. Mater. Sci. 25 (1995) 69.
[28] M.F. Doerner, W.D. Nix, Crit. Rev. Solid State Mater. Sci. 14 (3) (1988) 225.
[29] L.S. Palatnik, A.V. Ankinovich, Grain Boundaries in Metals and Semiconductors, Les éditions de Physique, Les Ulis Cedex, France, 1993.

Up to 2wt% Si is used to prevent "contact spiking". This is caused by pipe diffusion of Al causing shorts between conductors in the silicon device (Fanger and Tonneman, p. 97).

The difference between hillocks and electromigration is that the latter has a current induced diffusive flux in one direction that causes pileup of material further down the conductor that can cause voiding and the conductor to fail. Hillocks are caused by preferential growth of certain grains to relieve stresses caused by growth or temperature.

Hillocks can cause interlayer shorts (Fanger and Tonneman, p.97).

David Fanger and Roger Tonneman, "Aluminum and Copper-Based Conductors" in *Characterization in Silicon Processing*", Yale Strausser, ed. (Boston": Butterworth-Heinemann, 1993) p97.

1-2% Nd reduces hillock formation by a factor of 1000 or more, but as annealing temperatures increase from 300°C to 400°C, hillock density increases. At 350°C 1%Nd lowers density by a factor of 10, and at 400°C 2%Nd has only a slight effect (perhaps a factor of 2). (Arai et al. 2001, p 288.)w

Toshiaki Arai, et al., "Mo-capped Al-Nd alloy for both gate and data bus lines of liquid crystal displays," *Thin Solid Films* 383(2001)287-291.

Hillock formation dramatically reduced adding 0.5wt% Cu to Al or Al-1wt%Si alloy.
Michal Zaborowski and Piotr Dumania, "Kinetics of hillock growth in Al and Al-alloys", *Microelectronic Engineering* 50(200)301-309.

FIB cross sections show different stages in production of hillocks. The first stages is delamination and blistering of film with nucleation of randomly oriented grains nucleating between the film and substrate. Columnar grains in film remain intact. Further lifting of the blister-like film eventually causes cracks and a large random grain caps the hillock, filling the crack. Further growth of the hillock may consume much of the skin of the blister, producing large random grains that go completely through the film, and may become whiskers. Pure 1μm thick films grown at room temperature onto 0.2μm LPCVD SiO_2 on Si, thenpassivated with TiW layer which was removed by plasma etching.
Deok-kee Kim, B. Heiland, W.D. Nix, E. Arzt, M.D. Deal, and J.D. Plummer, "Microstructure of thermal hillocks on blanket Al thin films," *Thin Solid Films* 371(2000)278-282.

WEB SEARCH
Wisker vs. Hillock growth in thin films. Precipitation at grain boundaries can suppress grain boundary sliding, which suppresses hillock growth. When grain boundaries are pinned, whishker growth appears as a means of relieving stress.

R.S. Bailey, "Effects of Target Microstructure on Aluminum Alloy Sputtered Thin Film Properties," Presented at the 38th Annual Symposium of the American Vacuum Society
Seattle, Washington
November 1991

4.L. Succo, J. Esposito, Monty Cleeves, S. Whitney, R.E. Lionetti, and C.E. Wickersham, Jr., Journal of
Vacuum Science and Technology, A7, 814 (1989).

UofM
45. G. S. Was, D. J. Srolovitz, Z. Ma and L. Dong, "Microstructure Control for Hillock Suppression in Thin Film Metallization," Society for Information Display Conference, September 22-23. 1997.

D.J. Srolovitz, et al. "Controlling Texture during the Deposition of Thin Metal Films" MURI review, May 17, 1999. University of Michigan

Research Topic task started on Tue Mar 26, 2002 at 7:11 PM

5 Research Topic candidates were identified in CAPLUS.
using the phrase "hillock in aluminum thin films"

Selected 2 of 5 candidate topics.
1 reference was found containing "hillock in aluminum thin films" as entered.
45 references were found containing the two concepts "hillock" and "aluminum thin films" closely associated with one another.

Copyrights:

CAPATENTFAMILY: Copyright 2001 ACS
CAPLUS: Copyright 2001 ACS
REGISTRY: Copyright 2001 ACS (some records contain information from GenBank (R) which is a registered trademark of the U.S. Department of Health and Human Services for the Genetic Sequence Data Bank.)
CASREACT: Copyright 2001 ACS (some records from 1974 to 1991 are derived from the ZIC/VINITI data file and provided by InfoChem)
CHEMCATS: Copyright 2001 ACS
MEDLINE: Copyright 2001 NLM
CHEMLIST: Copyright 2001 ACS

Bibliographic Information

Hillock formation in aluminum thin films during thermal cycling. Kim, Deok-Kee. Stanford Univ., Stanford, CA, USA. Avail. UMI, Order No. DA3002008. (2001), 139 pp. From: Diss. Abstr. Int., B 2001, 62(1), 473. Dissertation written in English. CAN 136:138041 AN 2001:898168 CAPLUS

Bibliographic Information

Thin film transistor without hillocks due to gates and simplified method of manufacturing the same. Lyu, Ki-Hyun; Hwang, Kwang-Jo. (S. Korea). U.S. Pat. Appl. Publ. (2001), 11 pp. CODEN: USXXCO US 20010048107 A1 20011206 Patent written in English. Application: US 97-979843 19971126. Priority: KR 96-9662231 19961206. CAN 136:14221 AN 2001:886737 CAPLUS

Patent Family Information

Abstract

A thin film transistor is disclosed, including an insulating substrate, a semiconductor layer formed on the insulating substrate, the semiconductor layer having an active region and an impurity region, a gate insulating layer formed on the active region of the semiconductor layer, a 1st gate metal layer formed on a predetd. portion of the active region of the semiconductor layer to define a channel region, and a 2nd gate metal layer formed on the 1st gate metal layer. The 1st and 2nd gate metal layers have different compns., such that the 2nd gate metal layer etches faster than the 1st gate metal layer, thereby preventing formation of a hillock. A 1st protective layer is formed over the structure, then a light shielding layer, and then a 2nd protective layer is formed over the light shielding layer.

Bibliographic Information

Application of anodization technology to liquid crystal displays. Mizutani, Fumikazu; Ue, Makoto. Tsukuba Research Center, Mitubishi Chemical Corporation, Ami-Imashiki, Ibaraki, Japan. Hyomen Kagaku (2001), 22(6), 376-381. CODEN: HYKAET ISSN: 0388-5321. Journal; General Review written in Japanese. CAN 135:160025 AN 2001:607129 CAPLUS

Abstract

Anodization technol. used in LCDs (Liq. Crystal Displays) is reviewed.(41 refs.). The wet anodization process has an advantage over other dry processes to produce thin oxide films with very smooth surface and less pinholes Aluminum or its alloy gate lines used in some TFT (Thin Film Transistor)-LCDs are covered with anodic oxide thin film to prevent their hillock formation and corrosion. On the other hand, anodic oxide films of tantalum or its alloys are also used as an insulator of non linear switching elements in TFD (Thin Film Diode)-LCDs. Anodization is carried out in aq. or nonaq. electrolyte solns. However, only limited electrolyte solns. have been used for manufg. TFT-LCDs. Here, we introduce our recent results on the anodization of sputtered Al-Nd alloy films in ethylene glycol-based nonaq. electrolyte solns.

Bibliographic Information

Study of the effect of grain boundary migration on hillock formation in Al thin films. Kim, Deok-kee; Nix, William D.; Vinci, Richard P.; Deal, Michael D.; Plummer, James D. Center for Integrated Systems, Stanford University, Stanford, CA, USA. Journal of Applied Physics (2001), 90(2), 781-788. CODEN: JAPIAU ISSN: 0021-8979. Journal written in English. CAN 135:230201 AN 2001:478290 CAPLUS

Abstract

The authors have studied the effect of grain boundary migration on hillock formation in unpassivated Al thin films during thermal cycling. Hillocking occurs more frequently in Al films that experience grain growth during thermal cycling than in films with stabilized grain structures. The hillocking frequency is at least four times greater in the films that experience grain growth, as judged by the no. of hillocks obsd. per initial grain boundary triple junction. This latter measure takes account of the smaller initial grain size in the film that experiences grain growth and shows that grain boundary migration itself must enhance the hillocking frequency.

Bibliographic Information

Aluminum alloy thin film electrodes in semiconductor devices and sputtering targets for deposition of thin films thereof. Takagi, Katsuji; Ondahi, Takashi. (Kobe Steel, Ltd., Japan). Jpn. Kokai Tokkyo Koho (2001), 15 pp. CODEN: JKXXAF JP 2001028348 A2 20010130 Patent written in Japanese. Application: JP 99-201650 19990715. CAN 134:140349 AN 2001:68293 CAPLUS

Patent Family Information

Abstract

The Al alloy thin film compn. contains CY ≥0.3, CIVa ≥0.2, and (0.3CY+3CIVa) ≤2 at.%, wherein CY and CIVa denote at.% for Y and Group IVA metal. Group IVA metal may be Ti, Zr, and/of Hf. The sputtering targets fulfilling the compn. of the thin film electrodes gives the electrodes low resistance, high hillock prevention, high void prevention, and high corrosion resistance against basic solns. The Al thin film electrodes may be useful for high precision LCDs.

Bibliographic Information

Suppression of hillock formation in thin aluminum films on semiconductor devices using multilayers. Raina, Kanwal K.; Zhang, Tianhong; McTeer, Allen. (Micron Technology, Inc., USA). U.S. (2000), 9 pp. CODEN: USXXAM US 6140701 A 20001031 Patent written in English. Application: US 99-387133 19990831. CAN 133:316504 AN 2000:769137 CAPLUS

Patent Family Information

Abstract

A multilayer structure is provided which suppresses hillock formation due to post-heat treatment steps in thin Al films deposited on other substrates by sandwiching the Al film between thin layers of Al Ti nitride. The 1st Al Ti nitride layer acts as a compatibilizing layer to provide a better match between the coeffs. of thermal expansion of the substrate and Al metal layer. The 2nd Al Ti nitride layer acts as a cap layer to suppress hillock formation.

Bibliographic Information

Diffusional hillock formation in Al thin films controlled by creep. Kim, Deok-Kee; Nix, William D.; Arzt, Eduard; Deal, Michael D.; Plummer, James D. Center for Integrated Systems, Stanford University, Stanford, CA, USA. Mater. Res. Soc. Symp. Proc. (2000), 594(Thin Films--Stresses and Mechanical Properties VIII), 129-134. CODEN: MRSPDH ISSN: 0272-9172. Journal written in English. CAN 133:353450 AN 2000:722740 CAPLUS

Abstract

Thermal hillocks in sputter-deposited Al films have been studied. Trace amts. of the impurities Ti, W, and O were incorporated into the films during deposition and caused them to be much stronger than most sputter-deposited Al films. Stress measurement during thermal cycling, using the wafer curvature method, showed that these Al films are high strength and was corroborated by hardness measurements. Microstructural studies using TEM and FIB showed that the hillocks start to form at the Al/SiO2 interface and grow under the original Al film having a columnar grain structure. In some cases, the film fails as hillocks grow completely through the original film. The Al film on top of the hillocks appears to inhibit hillock growth by creating a back pressure assocd. with power-law creep of the film. Hillock formation was modeled by modifying the boundary conditions in Chaudhari's hillock model (1974). The new model describes the hillock formation by diffusion of Al atoms from the surrounding area into isolated hillocks, assuming that the original Al film on top of hillocks deforms according to power-law creep. The model can be applied to many different situations by using different creep laws for the top Al film.

Bibliographic Information

Creep-controlled diffusional hillock formation in blanket aluminum thin films as a mechanism of stress relaxation. Kim, Deok-Kee; Nix, William D.; Deal, Michael D.; Plummer, James D. Center for Integrated Systems, Stanford University, Stanford, CA, USA. Journal of Materials Research (2000), 15(8), 1709-1718. CODEN: JMREEE ISSN: 0884-2914. Journal written in English. CAN 133:166994 AN 2000:557676 CAPLUS

Abstract

Hillock formation, a stress-induced diffusional relaxation process, was studied in sputter-deposited Al films. The grain sizes in these films were small compared to those in other sputter-deposited Al films, and impurities (O, Ti, W) were incorporated during the prepn. of the films. Stress and hardness measurements both indicate that the Al films were strengthened by the small grain size and incorporated impurities. We obsd. a new type of hillock in these Al thin films after annealing for 2 h at 450°C in a forming gas ambient. The hillocks were composed of large Al grains created between the substrate and the original Al film with its columnar grain structure, apparently by diffusion from the surrounding area. By modifying the boundary conditions of Chaudhari's hillock formation model, we have created a new model that can describe the expti. obsd. hillocks. Our model seems to explain the expti. obsd. abnormal hillock formation and may be applied to other types of hillock formation using different creep laws.

Bibliographic Information

Fabrication of a thin film transistor with a doped aluminum anodizing layer. Kim, Jung-hyun. (Lg Electronics Co., Ltd., S. Korea). Repub. Korea (1997), No pp. given. CODEN: KRXXFC KR

9706256 B1 19970425 Patent written in Korean. Application: KR 94-9408116 19940418. CAN 133:128547 AN 2000:546153 CAPLUS

Patent Family Information

Abstract

On a semitransparent substrate, a doped Al layer and an anode oxide film are sequentially formed. A Si oxide film is formed on the anode oxide film. An hydrogenated amorphous Si layer and a doped amorphous Si layer are formed on the Si oxide film. A nitride treatment film is interposed between the Si oxide film and the hydrogenated amorphous Si layer. Using the doped Al layer as the anodizing material, it is possible to prevent the generation of hillock. Also, using the anode oxide instead of a Si nitride, the reliability of the transistor is increased.

Bibliographic Information

Kinetics of hillock growth in Al and Al-alloys. Zaborowski, M. x.; Dumania, P. Institute of Electron Technology, Warsaw, Pol. Microelectron. Eng. (2000), 50(1-4), 301-309. CODEN: MIENEF ISSN: 0167-9317. Journal written in English. CAN 132:201514 AN 2000:10242 CAPLUS

Abstract

Hillock growth kinetics and size distribution were studied in Al, Al-Si 1% and Al-Si 1-Cu 0.5% layers. Metalization surface was examd. by optical, SEM and TEM microscopy, stylus profiling and an automatic method of hillock recognition from a microscope image. The method allowed for counting hillocks in a desired range of their diam. d. Surface d. of hillocks was measured as a function of time of furnace annealing at 400° and as a function of temp. of RTP annealing. A max. hillock size increases linearly with metalization layer thickness and with logarithm of annealing time. A total area occupied by hillocks was evaluated. Hillock d. decreased vs. 1/T with an activation energy of 0.28 eV for Al and 0.31 eV for Al-Si. A normalized hillock d. N may be expressed by N = N0 exp(-cd), where d is hillock diam., N0 is the d. of hillocks of diam. close to 0, and c is the curve slope. Values for N0 and c are given together with a short discussion.

Bibliographic Information

Formation of aluminum thin film. Arai, Makoto; Ishibashi, Akira; Kiyota, Junya; Sugiura, Isao; Hayashi, Yukiaki; Nakamura, Hajime; Hori, Takahide; Ohta, Yoshifumi. (ULVC Japan, Ltd., Japan). Jpn. Kokai Tokkyo Koho (1999), 7 pp. CODEN: JKXXAF JP 11354469 A2 19991224 Heisei. Patent written in Japanese. Application: JP 98-163227 19980611. CAN 132:57892 AN 1999:814116 CAPLUS

Patent Family Information

Abstract

The thin film is formed on a substrate by sputtering an Al-contg. target with a sputtering gas in vacuum after applying weak high-frequency elec. power to the target. The process removes oxidising gases from the sputtering target and substrate by plasma cleaning and prevents formation of hillocks on Al (alloy) thin-film wiring for semiconductor devices, display devices, etc.

Bibliographic Information

Aluminum gates including ion implanted composite layers for a thin film transistor. Hong, Mun-pyo. (Samsung Electronics Co., Ltd., S. Korea). U.S. (1999), 11 pp. CODEN: USXXAM US 5969386 A 19991019 Patent written in English. Application: US 97-940066 19970929. Priority: KR 96-9644015 19961004. CAN 131:280270 AN 1999:671055 CAPLUS

Patent Family Information

Abstract

An aluminum gate for a thin film transistor is fabricating by implanting ions into the exposed surface of the aluminum gate. The ions are preferably selected from the group consisting of nitrogen, carbon, oxygen and boron ions. A composite layer of aluminum and the implanted ions thereby formed at the exposed surface of the aluminum layer. Gates for thin film transistors, including an aluminum layer and a composite layer of aluminum and another element at the surface thereof can suppress hillocks in the aluminum gate which may be caused by compressive stresses during subsequent fabrication steps. The composite layer can have a low resistance and can allow a direct contact with an indium tin oxide conductive layer.

Bibliographic Information

Texture and grain boundary structure dependence of hillock formation in thin metal films. Novell, Matthew M.; Field, David P. TexSEM Laboratories, Draper, UT, USA. Mater. Res. Soc. Symp. Proc. (1998), 516(Materials Reliability in Microelectronics VIII), 115-120. CODEN: MRSPDH ISSN: 0272-9172. Journal written in English. CAN 130:74321 AN 1998:779137 CAPLUS

Abstract

The development of hillocks on metal films during annealing is detrimental to downstream processing of integrated circuit structures. This work focuses upon the local character of texture and grain boundary structure near hillocks in metal films. It is apparent from the results that local grain boundary structure and texture strength are important parameters in identifying locations in the films that are preferentially susceptible to failure under given conditions. Results in aluminum and platinum films indicate that non-(111) oriented grains preferentially contain hillocks. In addn., (111) oriented grains with boundaries characterized by high angle rotations about random axes are prone to hillock formation.

Bibliographic Information

Hillock behavior on aluminum thin films deposited on polyimide film. Kang, Young-Seok. Center for Materials Science and Engineering, The University of Texas at Austin, Austin, TX, USA. Han'guk Chaelyo Hakhoechi (1998), 8(9), 802-806. CODEN: HCHAEU ISSN: 1225-0562. Journal written in English. CAN 130:74286 AN 1998:704210 CAPLUS

Abstract

Behavior of hillocks on Al films deposited on polyimide-coated SiO2 wafers was studied using an at. force microscopy with variation of the film thickness and annealing treatment. Growth hillocks were obsd. on as-received films and hillock d. was decreased while hillocks grew in size with the film thickness. After annealing, av. hillock size was increased but d. was decreased. The reduced hillock d. in these films is in contrast with the results from the films deposited directly on a rigid substrate. This is attributed to the presence of soft polyimide layer which relaxes the stress and thereby locks the stress-induced grain boundary diffusion in Al films. Probably in this situation, no addnl. hillocks emerge and small hillocks are consumed by growing large hillocks.

Bibliographic Information

Structure engineering for hillock-free pure aluminum sputter deposition for gate and source line fabrication in active-matrix liquid crystal displays. Voutsas, Apostolos T.; Hibino, Yoshi; Pethe, Rajiv; Demaray, Ernest. Corporate Strategic Engineering Center, Sharp Microelectronics Technology, Incorporated, Camas, WA, USA. J. Vac. Sci. Technol., A (1998), 16(4), 2668-2677. CODEN: JVTAD6 ISSN: 0734-2101. Journal written in English. CAN 129:154634 AN 1998:437587 CAPLUS

Abstract

In this article we present the results of a study aimed at developing hillock-free, pure-Al thin-film material suitable for the fabrication of gate and source lines in thin film transistor active-matrix liq. crystal displays. Strong Al(111) texture was shown to be a key attribute for achieving good resistance to hillock formation. To obtain this strong Al(111) texture, we explored the incorporation of a thin metal layer, under the Al film, and we showed that Ti could be an appropriate candidate for further optimization. Key variables affecting the quality of Al were found to be the roughness of the glass substrate, the thickness of the titanium, the background vacuum quality, and the sputtering temp. By optimizing the deposition process for both Al and Ti layers, we showed that aluminum films with very strong (111) texture (rocking curve full width at half max. 0.86°), very smooth surface (root mean square surface roughness 1.8 nm), and a uniform, columnar grain size (0.3-0.5 μm) could be deposited by dc magnetron sputtering. In addn. to improving the aluminum microstructure, optimization of the gate dielec. process was also performed with the aim of reducing hillock formation. Combined optimization of the sputtering and gate dielec. deposition processes yielded an overall redn. in hillock d. of 3.5-4 orders of magnitude, without the need for anodic oxida. or other means of capping the aluminum film. By combining Al/Ti dc sputtering, dry-etching technol. for one-step patterning of the composite Al/Ti film, and gate insulator deposition at 300 °C we demonstrated, for the first time, gate metalization technol. based on pure Al with excellent step coverage and ultralow hillock d. (<103 cm-2).

Bibliographic Information

Effect of Ti content on properties of Al-Ti alloy film for address lines of TFT-LCDs. Wu, Lijun; Xia, Hui; Liu, Ansheng; Han, Xue; Lu, Biao. General Res. Inst. Non-Ferrous Metals, Beijing, Peop. Rep. China. Rare Met. (Beijing) (1998), 17(2), 94-97. CODEN: RARME8 ISSN: 1001-0521. Journal written in English. CAN 129:102486 AN 1998:425740 CAPLUS

Abstract

Employing pure aluminum for address lines of TFT-LCDs (thin film transistor-liq. crystal display) has a severe problem of hillock formation at elevated temp. However, in the case of large TFT-LCDs more than 254 mm, it is impossible to use refractory metals for address lines because of their high resistivity. The Al-Ti alloy films for address lines of TFT-LCDs were studied and it was found that Al-Ti alloy film has excellent resistance of Al-Ti alloy to hillocks. The effect of Ti content on properties of Al-Ti alloy film was investigated.

Bibliographic Information

Nanostructural investigation of whiskers and hillocks of aluminum-based metallization in thin-film transistor liquid-crystal displays. Tsujimoto, Katsuhiro; Tenji, Satoshi; Takatsuji, Hiroshi; Kuroda, Kotaro; Saka, Hiroyasu; Suzuki, Yukinobu. Display Technology, IBM Japan, Yamato, Japan. AIP Conf. Proc. (1998), 418(Stress Induced Phenomena in Metallization), 395-400. CODEN: APCPCS ISSN: 0094-243X. Journal written in English. CAN 128:224348 AN 1998:152114 CAPLUS

Abstract

The nanostructure of whiskers and hillocks in various aluminum-based thin films for thin-film transistor (TFT) on glass substrates has been investigated. The authors developed a novel technique to fabricate whiskers and hillocks artificially, using nanoindentation technique and annealing in a vacuum furnace. During the annealing, some Al whiskers and hillocks are formed, particularly on the edges of indentation marks. The high degree of whisker formation in this technique correlated to the weak hillock formation resistance in actual TFT arrays. Nanostructure of these thin films was investigated by cross-sectional TEM microscopy. The surface morphol. of as-deposited films was also investigated by at. force microscopy.

Bibliographic Information

Whisker growth on aluminum thin films during heat treatment. Hinode, Kenji; Homma, Yoshio; Sasaki, Yasushi. Central Research Laboratory, Hitachi, Ltd., Tokyo, Japan. AIP Conf. Proc. (1998), 418(Stress Induced Phenomena in Metallization), 359-370. CODEN: APCPCS ISSN: 0094-243X. Journal written in English. CAN 128:211024 AN 1998:152108 CAPLUS

Abstract

The authors studied whisker formation on Al films on Si substrates during heat treatments. Although both whiskers and hillocks are formed by the stress caused by thermal expansion mismatches, three addnl. conditions help induce whisker growth: (1) Contamination of films by O, N, or other contaminants from the residual sputtering atm. suppresses Al film grain growth during heat treatment, which causes highly localized film stress relief, resulting in whisker formation. (2) A nonoxidizing atm., either a vacuum or inert gas, is required during the heat treatment. (3) Keeping the sample within a narrow temp. range (in the present case, 230-300°).

Bibliographic Information

Initial development of the lateral hillock distribution in optical quality Al thin films studied in real time. Kylner, C.; Mattsson, L. Department of Physics II (Optics), Royal Institute of Technology, Stockholm S-100 44, Swed. Thin Solid Films (1997), 307(1,2), 169-177. CODEN: THSFAP ISSN: 0040-6090. Journal written in English. CAN 128:94699 AN 1997:780979 CAPLUS

Abstract

The authors' previous studies using real-time total integrated scattering (TIS) showed a very distinct onset of hillock formation in optical quality Al films on Si wafers at temps. well <100°. This paper extends those studies by studying in real time the initial development of the lateral hillock distribution. After the 1st hillocks appeared the no. of hillocks accelerated rapidly with increased temp., in particular for higher heating rates. The lateral hillock distributions were further statistically analyzed by the Quadrate counts method to get more objective results. This anal. indicates that hillocks tend to be clustered over larger areas. The nearest neighbor distance between hillocks was also calcd. The hillocks had a tendency of lining up in distorted ring shaped patterns. This is interpreted as an effect of inhomogeneous stress distributions at the local grain level. The observations were made possible by using an imaging partial integrated scattering (PIS) system comprising of a dark field microscope objective and a charge coupled device (CCD) camera with an image processor and a data acquisition system.

Bibliographic Information

Nanocharacterization of texture and hillock formation in thin Al and Al-0.2%Cu films for thin-film transistors. Takatsuji, H.; Tsuji, S.; Kitahara, H.; Tsujimoto, K.; Kuroda, K.; Saka, H. IBM Japan Ltd., Display Technology, Shiga, Japan. Mater. Res. Soc. Symp. Proc. (1997), 441(Thin Films--Structure and Morphology), 415-420. CODEN: MRSPDH ISSN: 0272-9172. Journal written in English. CAN 127:255880 AN 1997:555299 CAPLUS

Abstract

The relation between the nanostructure of pure Al and Al-0.2 wt.% Cu thin films on glass substrates and anti-stress migration properties were investigated. These films were deposited on liq.-crystal display (LCD) grade glass substrate (550 × 650 mm) by means of two types of dc magnetron multi-chamber sputtering app. We developed the nanoindentation techniques to accelerate the characterization time for stress migration test. By AFM and cross-sectional TEM observations, we found an unusual three-layer structure in a Al-Cu thin film with strong anti-stress migration property.

Bibliographic Information

Microstructure control for thin film metallization. Was, G. S.; Srolovitz, D. J.; Ma, Z.; Liang, D. Nuclear Engineering and Radiological Sciences, University of Michigan, Ann Arbor, MI, USA. Mater. Res. Soc. Symp. Proc. (1997), 441(Thin Films--Structure and Morphology), 311-322. CODEN: MRSPDH ISSN: 0272-9172. Journal written in English. CAN 127:270899 AN 1997:555283 CAPLUS

Abstract

A strategy was developed for controlling hillock formation in thin metal films by controlling the fiber texture to be of a relatively weak orientation. Two-dimensional mol. dynamics (MD) simulations were performed to det. the parameter dependencies of texturing under ion beam assisted deposition. Simulations showed that even for film orientations that have a lower no. of nearest neighbor surface bonds, the redn. in sputtering rate by ion channeling will favor the growth of the grains aligned with their channeling direction in the direction of the ion beam. Higher energies should result in greater sputtering and a higher surface roughness. Confirmatory expts. were performed by growing Al films using ion beam assisted depositions in which the Ne ion beam was normal to the substrate surface. For all energies above 0 eV/atom, the fiber texture contained a (220) component and, at high normalized energies, the fiber texture was heavily (220) dominated. Subsequent annealing at 450° for 30 min resulted in hillock formation in the PVD (phys. vapor deposition) condition, a redn. in the hillock d. by two orders of magnitude in the 120 eV/atom condition and complete elimination of hillocking at >800 eV/atom. Although the surface roughness increased with ion beam energy as modeled by MD, the surface became smoother during annealing. The fiber texture can be controlled in a thin metal film in such a way as to eliminate hillock formation, mol. dynamics simulation is a valuable predictive tool for guiding expts. in the development of thin film microstructures and ion beam assisted deposition is an effective, practical tool for controlling microstructures of thin metal films.

Bibliographic Information

Effects of Nd content in Al thin films on hillock formation. Onishi, Takashi; Iwamura, Eiji; Takagi, Katsutoshi; Watanabe, Takashi. Electronics Research Laboratory, Kobe Steel, Ltd., Kobe, Japan. J. Vac. Sci. Technol., A (1997), 15(4), 2339-2348. CODEN: JVTAD6 ISSN: 0734-2101. Journal written in English. CAN 127:193804 AN 1997:482441 CAPLUS

Abstract

The effect of Nd content in Al films on hillock formation was investigated for applications of interconnections for thin film transistor crystal displays. It was found that the hillock d. of Al-Nd alloy films was strongly dependent on the Nd content, and the hillocks were completely suppressed in Al-2.0-6.0 at. % Nd alloy films. X-ray diffractometry, x-ray absorption fine-structure spectroscopy, and TEM indicated that the microstructures of Al-Nd alloy films strongly depend on the Nd content, and Al-2.0-6.0 at. % Nd alloy films form a stable solid soln. with a polycryst. α-Al-like structure. The results obtained from microstructural anal. were largely in agreement with hillock formation behavior. In this study, the excellent hillock resistance of Al-2.0-6.0 at. % Nd alloy films originates from solid-soln. hardening by the strongly distorted α-Al-like structure.

Bibliographic Information

Test structures for hillock growth, via filling and for measuring the quality of thin films. Bennett, D. J.; O'Hara, A.; Underwood, I.; Waltson, A. J. Dep. Electrical Eng., Univ. Edinburgh, Edinburgh, UK. IEEE Int. Conf. Microelectron. Test Struct. Proc. (1997), 11-15. Publisher: Institute of Electrical and Electronics Engineers, New York, N. Y CODEN: 64KWAG Conference written in English. CAN 127:88752 AN 1997:362925 CAPLUS

Abstract

A test structure for assessing the quality of thin aluminum films is described. An anal. of the relationship between grain structure and hillock growth in small exposed areas of thin films during high temp.

processing shows that there is a relationship between hillock growth, grain size and grain boundary structure. The test structure consists of arrays of via holes of various sizes etched in a thin layer of SiO2 deposited at low temp. onto the metal surface. After furnace annealing, the no. of vias of each size which contain hillocks can be interpreted to obtain information on film quality.

Bibliographic Information

Relationship between the void and hillock formation and the grain growth in thin aluminum films. Kononenko, O. V.; Matveev, V. N. Institute Microelectronics Technology High Purity Materials, Russian Academy Sciences, Moscow, Russia. Mater. Res. Soc. Symp. Proc. (1997), 436(Thin Films: Stresses and Mechanical Properties VI), 423-428. CODEN: MRSPDH ISSN: 0272-9172. Journal written in English. CAN 126:285926 AN 1997:149846 CAPLUS

Abstract

Void and hillock formation during annealing was studied depending on the deposition conditions. Aluminum films were deposited onto oxidized silicon substrates by the self-ion assisted technique. The bias 0 or 6 kV was applied to the substrate during deposition. The films were then annealed in vacuum for 1 h in the temp. range from 150° to 550°C. The structure of the films was investigated by transmission electron microscopy. The void and hillock formation was studied with optical and scanning electron microscopes. It was found that recrystn. and void and hillock formation in the films depend on the bias during deposition. Normal grain growth occurred in the films deposited without bias. Abnormal grain growth was obsd. in the 6 kV-films. It was also found that the mechanism of stress relaxation during thermal cycling depends on the self-ion bombardment. In the films prepd. without bias, stress relaxation proceeds by diffusion creep. In the films deposited at the 6 kV bias, stress relaxation proceeds by plastic deformation.

Bibliographic Information

Relationship between the void and hillock formation and the grain growth in thin aluminum films. Kononenko, O. V.; Matveev, V. N. Inst. Microelectron Tech., Russian Acad. Sci., Chernogolovka, Russia. Mater. Res. Soc. Symp. Proc. (1996), 428(Materials Reliability in Microelectronics VI), 493-498. CODEN: MRSPDH ISSN: 0272-9172. Journal written in English. CAN 126:53759 AN 1996:741167 CAPLUS

Abstract

Void and hillock formation during annealing was studied depending on the deposition conditions. Al films were deposited onto oxidized Si substrates by the self-ion assisted technique. The bias 0 or 6 kV was applied to the substrate during deposition. The films were then annealed in vacuum for 1 h at 150-550°. The structure of the films was studied by TEM. The void and hillock formation was studied with optical and scanning electron microscopes. Recrystn. and void and hillock formation in the films depend on the bias during deposition. Normal grain growth occurred in the films deposited without bias. Abnormal grain growth was obsd. in the 6 kV-films. Also the mechanism of stress relaxation during thermal cycling depends on the self-ion bombardment. In the films prepd. without bias, stress relaxation proceeds by diffusion creep. In the films deposited at the 6 kV bias, stress relaxation proceeds by plastic deformation.

Bibliographic Information

Patterning of circuit associated with prevention of hillock formation on semiconductor device. Ogawa, Takashi. (Mitsumi Electric Co, Japan). Jpn. Kokai Tokkyo Koho (1996), 4 pp. CODEN: JKXXAF JP 08236531 A2 19960913 Heisei. Patent written in Japanese. Application: JP 95-65091 19950228. CAN 125:290830 AN 1996:664154 CAPLUS

Patent Family Information

Abstract

In formation of circuit by a process including following successive steps; (1) forming a metal layer on an oxide film on a semiconductor substrates, (2) forming a resist pattern as an etching mask, (3) forming a circuit pattern on the metal layer by removing the resist and the metal, and (4) forming a protecting film or interlayer insulating film, a thin film of the same substance as the protecting film or interlayer insulating film is formed on the metal layer, i.e., between step (1) and (2), which is supposed to be etching mask of the metal layer. Formation of hillock in sintering the metal layer is prevented and coverage of the protecting film or interlayer insulating film is improved in the process.

Bibliographic Information

Influence of adding transition metal elements to an aluminum target on electrical resistivity and hillock resistance in sputter-deposited aluminum alloy thin films. Onishi, Takashi; Iwamura, Eiji; Takagi, Katsutoshi; Yoshikawa, Kazuo. Electronics Research Laboratory, Kobe Steel, Ltd., Kobe, Japan. J. Vac. Sci. Technol., A (1996), 14(5), 2728-2735. CODEN: JVTAD6 ISSN: 0734-2101. Journal written in English. CAN 125:235280 AN 1996:594127 CAPLUS

Abstract

Effects of adding Group VIII transition metals (Fe, Co, and Ni) to an Al target on elec. resistivity and hillock suppression of sputter-deposit Al alloy films were studied. The group VIII transition metals and Al formed a complete series of metastable solid solns. in the as-deposited state. The solid solns. were decompd. into intermetallic compds., and the microstructures of the Al alloy films changed during annealing up to 300°. The elec. resistance of Al-Fe, Al-Co, and Al-Ni alloy films changed corresponding to the change in their microstructures, and markedly decreased to 5.0 μΩ cm at the pptn. points. The film stresses also changed corresponding to the change in the microstructure of the Al alloy films, and were abruptly relieved by pptn. of intermetallic compds. and grain growth. Since Al-Fe, Al-Co, and Al-Ni alloy films did not yield, they are highly resistant to hillock formation. The low elec. resistivity and the excellent resistance to hillock formation of Al-group VIII transition metal alloy films were explained from microstructural changes before and after annealing.

Bibliographic Information

Experimental study to validate a model of hillock formation in aluminum thin films. Genin, F. Y.; Slekhaus, W. J. Chemistry and Materials Science, Lawrence Livermore National Laboratory, Livermore, CA, USA. J. Appl. Phys. (1996), 79(7), 3560-6. CODEN: JAPIAU ISSN: 0021-8979. Journal written in English. CAN 124:275297 AN 1996:183255 CAPLUS

Abstract

The growth of holes and hillocks in thin films has been reported extensively and for a multitude of film-substrate systems. A recently developed model which analyzes the formation of a ridge at a traveling grain boundary due to stress and capillarity driving forces provides a quant. description of the growth of the hillocks. In order to test the model, the surface morphol. of aluminum thin films deposited on oxidized silicon substrates and annealed at 450° in argon is investigated; the profiles of thermal hillocks were measured by at. force microscopy. The comparison shows excellent agreement between modeled and exptl. profiles.

Bibliographic Information

Hillock-free multilayer metallic wires for high-performance thin-film printed circuits. (Xerox Corp., USA). Jpn. Kokai Tokkyo Koho (1995), 6 pp. CODEN: JKXXAF JP 07302792 A2 19951114 Heisei. Patent written in Japanese. Application: JP 95-95231 19950420. Priority: US 94-234897 19940428. CAN 124:73861 AN 1996:30041 CAPLUS

Patent Family Information

Abstract

The circuits have an alternately laminated base-metal/barrier-metal multilayer formed on a substrate, wherein the thickness of the base metal layers is thinner than that of the barrier metal layers. The arrangement prevents hillock formation without decreasing the metal layer sp. resistance.

Bibliographic Information

Use of fractals and kinetic equations to model thermally induced hillock formation and growth in thin metal films. Chaiken, J.; Goodisman, J. Dep. Chem., Syracuse Univ., Syracuse, NY, USA. Thin Solid Films (1995), 260(2), 243-51. CODEN: THSFAP ISSN: 0040-6090. Journal written in English. CAN 123:63069 AN 1995:640114 CAPLUS

Abstract

We investigated the applicability of a model based on fractals and the M.V. Smoluchowski (1916) kinetic equations to describe hillock formation in thin metal films. We have previously used this model to analyze cluster and ultrafine particle prodn. We show how to ext. two parameters from measured hillock size distributions which may reveal the scaling of the mobility of clusters and vacancies in films with varying hillock size. On the basis of our application of this model to certain data taken from the literature, the model shows considerable potential for being able to provide an internally consistent quant. basis for monitoring thermally driven mass redistribution processes in metal films.

Bibliographic Information

Substrate for thin film transistor array for liquid crystal display. Kubo, Akira. (Tokyo Shibaura Electric Co, Japan). Jpn. Kokai Tokkyo Koho (1994), 4 pp. CODEN: JKXXAF JP 06301054 A2 19941028 Heisei. Patent written in Japanese. Application: JP 93-87160 19930414. CAN 122:174674 AN 1995:428843 CAPLUS

Patent Family Information

Abstract

In manufg. the title substrate for a thin film transistor array for a liq. crystal display by (1) forming a scanning line jointly serving as a gate electrode on an insulator substrate, (2) forming a semiconductor layer on the above gate electrode via an insulator layer, (3) forming on the semiconductor layer a signal line jointly serving as drain electrode and a drain electrode connected to the display electrode, the above scanning line serving as gate electrode is obtained by laminating a high-melting metal layer on an Al-base metal layer, alloying the metal layer surface with the above high-melting metal layer while simultaneously oxidizing the high-melting metal layer to form an oxide layer, and removing the oxide layer from the above insulator substrate. Al hillock formation is suppressed to prevent short-circuiting.

Bibliographic Information

Hillock formation during electromigration in Cu and Al thin films: three-dimensional grain growth. Gladkikh, A.; Lereah, Y.; Glickman, E.; Karpovski, M.; Palevski, A.; Schubert, J. Dep. Electronic Devices Materials, Tel Aviv Univ., Ramat Aviv, Israel. Appl. Phys. Lett. (1995), 66(10), 1214-15. CODEN: APPLAB ISSN: 0003-6951. Journal written in English. CAN 122:167232 AN 1995:408196 CAPLUS

Abstract

The evolution of microstructure in Al and Cu thin film lines during electromigration has been studied using

a transmission electron microscopy. Grain boundary migration was found to be critically involved in the electromigration induced hillock formation that can be described as a three-dimensional growth of a single grain.

Bibliographic Information

Formation of aluminum thin-films. Tsuda, Yoshiaki; Yasui, Hideaki. (Matsushita Electric Ind Co Ltd, Japan). Jpn. Kokai Tokkyo Koho (1994), 4 pp. CODEN: JKXXAF JP 06145962 A2 19940527 Heisei. Patent written in Japanese. Application: JP 92-296833 19921106. CAN 122:44090 AN 1995:283167 CAPLUS

Patent Family Information

Abstract

Title formation involves depositing an Al-Si alloy thin film on a substrate followed by an Al thin-film on the alloy film, wherein the thickness of the Al film is 50-70 nm. The double layer Al conductor film prevents abnormal growth of Al crystals for prepn. of smooth Al film surface without hillocks.

Bibliographic Information

Thin-film transistor having aluminum-containing gate electrode. Itoida, Satoshi. (Nippon Electric Co, Japan). Jpn. Kokai Tokkyo Koho (1993), 4 pp. CODEN: JKXXAF JP 05299655 A2 19931112 Heisei. Patent written in Japanese. Application: JP 92-86812 19920408. CAN 120:122735 AN 1994:122735 CAPLUS

Patent Family Information

Abstract

In the transistor consisting of a gate electrode, an elec. insulating film, a semiconductor layer, and a source-drain electrode, the gate electrode comprises a bilayer contg. Al and an Al-base alloy and optionally a part of the insulating film comprises an anodized film of Al and Al alloy. The transistor showed good hillock and stress-migration resistance.

Bibliographic Information

Correlation between grain growth and hillock growth in thin thermally annealed aluminum-1% silicon films on silicon substrates. Gerth, D.; Katzer, D.; Schwarzer, R. Inst. Festkoerperphys. Elektronenmikrosk., Halle, Germany. Mater. Sci. Forum (1992), 94-96(Grain Growth Polycryst. Mater., Pt. 2), 557-62. CODEN: MSFOEP ISSN: 0255-5476. Journal written in English. CAN 118:64544 AN 1993:64544 CAPLUS

Abstract

The mutual relation between grain and hillock growth in Al-1%Si films on oxidized Si substrates was studied by electron microscopy. The grain specific textures of the Al alloy films were detd. by evaluation of Kikuchi patterns. The orientations of hillocks and adjacent grains were compared with the texture of the film. The shapes of the hillocks were revealed by electron microscopy. An example is given of the correlation between hillock growth and grain growth during the in situ investigation. The thermally-induced stresses, vertical strains, strain energies and shear stresses on the glide planes in the glide directions of the dislocations of differently oriented grains and hillocks were calcd. The relationship between these locally varying quantities in the polycryst. film and the expti. results of grain growth and hillock growth is discussed considering the possible micromechanisms of stress relaxation. It is assumed that the location and height of hillocks is detd. by stress gradients. Local stress is relaxed by dislocation movement and diffusional mass transport on grain boundaries.

Bibliographic Information

Thin-film transistor having double-layered electrode. Naito, Hideo. (Casio Computer Co., Ltd., Japan). Jpn. Kokai Tokkyo Koho (1992), 8 pp. CODEN: JKXXAF JP 04188770 A2 19920707 Heisei. Patent written in Japanese. Application: JP 90-315774 19901122. CAN 117:162356 AN 1992:562356 CAPLUS

Patent Family Information

Abstract

In the transistor consisting of a glass substrate coated with a gate electrode, a gate insulating film, a semiconductor layer, and a source-drain electrode, the lower electrode of the gate electrode and the source-drain electrode consists of a hard metal lower film and a Ti-contg. Al upper film. The transistor had low hillocks and low decrease of insulation breakage voltage.

Bibliographic Information

Manufacture of aluminum thin film by sputtering. Kakiuchi, Koji. (Seiko Instruments and Electronics, Ltd., Japan). Jpn. Kokai Tokkyo Koho (1991), 3 pp. CODEN: JKXXAF JP 03166722 A2 19910718 Heisei. Patent written in Japanese. Application: JP 89-308415 19891127. CAN 115:196191 AN 1991:596191 CAPLUS

Patent Family Information

Abstract

The Al (contg. ≤1% impurity) film is manufd. by sputtering with cooling a substrate. A MOS device showed no hillock on the Al thin film surface.

Bibliographic Information

Characterization of the early stages of electromigration at grain boundary triple junctions. Gemut, M.; Li, Z.; Bauer, C. L.; Mahajan, S.; Tang, P. F.; Milnes, A. G. Dep. Metall. Eng. Mater. Sci., Carnegie Mellon Univ., Pittsburgh, PA, USA. Appl. Phys. Lett. (1991), 58(21), 2354-6. CODEN: APPLAB ISSN: 0003-6951. Journal written in English. CAN 115:19551 AN 1991:419551 CAPLUS

Abstract

The formation and growth of holes and hillocks at grain boundary triple junctions in thin-film conductors of gold on gallium arsenide and thin-film conductors of aluminum-1 wt.% silicon on (oxidized) silicon during the early stages of electromigration have been investigated through measurement of fractional change of elec. resistance ΔR/R and microstructural characterization by SEM and TEM. Each grain boundary triple junction is characterized by a unique structure factor ΔY, which defines the degree of cumulative flux divergence and, consequently, the degree of susceptibility to formation and growth of holes or hillocks. Resultant holes are characterized by a shape factor f, which defines the degree of noncircularity and, consequently, relates fractional change of hole area to ΔR/R. Ests. of the upper limit for ΔY and the av. value of f are in good agreement with measured values of ΔR/R and consistent with obsd. microstructure.

Bibliographic Information

A transmission electron microscopy study of hillocks in thin aluminum films. Ericson, Fredric; Kristensen, Nils; Schweitz, Jan Aake; Smith, Ulf. Mater. Sci. Div., Uppsala Univ., Uppsala, Swed. J. Vac. Sci. Technol., B (1991), 9(1), 58-63. CODEN: JVTBD9 ISSN: 0734-211X. Journal written in

English. CAN 114:130016 AN 1991:130016 CAPLUS

Abstract

Hillocks, small outgrowths on a film surface, form when compressional stresses in an Al film are relaxed at ≥90°, for instance during the phase of rising temp. in an annealing cycle. This paper reports a study of hillock formation in Al films of thicknesses in the interval 0.25-2.2 μm which have been deposited by electron beam evapn. Hillock sizes, shapes, no. and formation temps. were detd., the latter on a heating stage in situ in a SEM. The internal structure of the hillocks was studied by cross-sectional TEM technique. These studies provided strong support for the idea that hillocks are formed by migration of material along grain boundaries, presumably at triple junctions, up to the surface where it is deposited in a growing hillock. Initially, the hillocks are sepd. from the original film surface by a grain boundary-like interface, but prolonged annealing will cause underlaying grains to grow into the hillocks, until they become integrated in the film.

Bibliographic Information

Influence of heat-treatment temperature and aluminum thickness on hillock formation in thin aluminum films. Zlatanovic, D.; Davinic, G. Elektron. Ind., RO "El-Mikroelektronika", Nis, Yugoslavia. Vacuum (1990), 40(1-2), 157-9. CODEN: VACUAV ISSN: 0042-207X. Journal written in English. CAN 112:221478 AN 1990:221478 CAPLUS

Abstract

The effect of heat-treatment temp. and thickness on hillock formation in Al-0.5 Si thin films vacuum deposited by sputtering onto Si and SiO2 surfaces was studied. Surface roughness was measured by using stylus-surface profilometry. The hillock d. and size were measured by using optical microscopy and SEM, resp. Hillock growth is affected both by heat-treatment temp. and film thickness.

Bibliographic Information

A study of heating rate and texture influences on annealing hillocks by a statistical characterization of aluminum thin-film topography. Baconnier, B.; Lormand, G.; Papapietro, M.; Achard, M.; Papon, A. M. CEA, IRDI, Grenoble, Fr. J. Appl. Phys. (1988), 64(11), 6483-9. CODEN: JAPIAU ISSN: 0021-8979. Journal written in English. CAN 110:86381 AN 1989:86381 CAPLUS

Abstract

In order to study the quant. influence of thin-film elaboration conditions on annealing hillock characteristics, an original statistical anal. of profilometer recording was performed. It allows, with suitable hypothesis on hillock shape, a detn. of the true hillock vol. per unit area. On various annealed Al-Si-Ti films this vol. decreases when the degree of preferred orientation increases. On both Al and Al-Si-Ti films an increase of heating rate induces a decrease of hillock vol. A stress relaxation model was developed where relative relaxing mechanism contributions are computed vs. grain size and heating rate. Exptl. results integrated through this model confirm the preponderance of grain boundary diffusion mechanisms in mass transport during hillock growth. The correlation between preferred orientation and hillock vol. in Al-Si-Ti films was related to both grain boundary diffusivity and grain size. The absence of small hillocks on high-temp. deposited Al-Si-Ti films is discussed.

Bibliographic Information

Ion beam suppression of hillock growth in aluminum thin films. Peacock, N. Br. Telecom Res. Lab., Ipswich, UK. Thin Solid Films (1988), 156(1), 173-80. CODEN: THSFAP ISSN: 0040-6090. Journal written in English. CAN 108:119557 AN 1988:119557 CAPLUS

Abstract

Ion irradn. as a method of hillock suppression in Al thin films was investigated. Implants of Ar, As, B and Si at doses between 1.6 × 1013 and 1.6 × 1016 ions/cm2 and at energies between 30 and 180 keV were used. A mechanism for the effects of different doses and species on hillock growth is proposed. Ar ion implantation at 120 keV to a dose of 5 × 1014 ions/cm2, or at 30 keV to a dose of 1.6 × 1015 ions/cm2, offers a practical method of hillock suppression on first level metal in silicon device wafers.

Bibliographic Information

Hillock growth in thin aluminum films. Mashita, Masao. Tokyo Shibaura Electr. Ltd., Kawasaki, Japan. Shinku (1972), 15(6), 196-204. CODEN: SHINAM Journal; General Review written in Japanese. CAN 77:117217 AN 1972:517217 CAPLUS

Abstract

A review, is given on formation, growth, and inhibition of hillocks of thin Al films for integrated circuits. 29 refs.

Bibliographic Information

Morphology of void-hillock formation at transverse scratches in aluminum thin film. Howard, J. K.; Ross, Rupert Foster. Components Div., IBM, Hopewell Junction, N. Y., USA. J. Appl. Phys. (1971), 42(7), 2996-8. CODEN: JAPIAU Journal written in English. CAN 75:55201 AN 1971:455201 CAPLUS

Abstract

Photoprocessed Al films subjected to elec. stresses showed shallow surface scratches with hillocks agglomerated on the cathode side of the scratch, and voids clustering on the anode side. The shallow scratches formed prior or during the photoprocessing. The polarity of the void-hillock structures is caused to grain-boundary diffusion. The asymmetry in the void-hillock sc. d. is due to a temp. gradient and elec.-field effect.

Bibliographic Information

Hillock-free aluminum thin films for electronic devices. Sato, Kikuji; Oi, Tetsu; Matsumaru, Haruo; Okubo, Toshio; Nishimura, Takeo. Cent. Res. Lab., Hitachi Ltd., Tokyo, Japan. Met. Trans. (1971), 2(3), 691-7. CODEN: MTGTBF Journal written in English. CAN 74:132028 AN 1971:132028 CAPLUS

Abstract

The addn. of an alloying element was proposed to suppress hillocks which grow on the surface of deposited Al conductors after they were subjected to thermal cycling (200° to room temp.) or high-temp. heat treatment (400°). The alloying element, Sn, which has a small diffusion coeff., a large binding energy with a lattice vacancy, and a large at. diam., and Mn, which has a relatively small solid soly. in Al, were evaluated since they also have proper values of vapor pressure for ease of evapn. with Al. Alloy compn. was detd. to be just above the solid soly. of the element in Al at deposition temp. of 350°. It was proved exptl. that Al-0.06 wt.% Sn and Al-0.1 wt.% Mn, which had been selected for the above-mentioned reason, had a marked effect in suppressing the growth of hillocks.

ELSEVIER

Thin Solid Films 307 (1997) 169–177

Thin Solid Films

Initial development of the lateral hillock distribution in optical quality Al thin films studied in real time

C. Kylner [a,*], L. Mattsson [b]

[a] Department of Physics II (Optics), Royal Institute of Technology, Stockholm S-100 44, Sweden
[b] Surface Evaluation Laboratory, Institute of Optical Research, Stockholm S-100 44, Sweden

Received 24 March 1997; accepted 21 May 1997

Abstract

Our previous investigations using real-time total integrated scattering (TIS) have shown a very distinct onset of hillock formation in optical quality Al films on Si wafers at temperatures well below 100°C. This paper extends those investigations by studying in real time the *initial* development of the lateral hillock distribution. After the first hillocks appeared the number of hillocks accelerated rapidly with increased temperature, in particular for higher heating rates. The lateral hillock distributions were further statistically analyzed by the Quadrate counts method to get more objective results. This analysis indicates that hillocks tend to be clustered over larger areas. The nearest neighbor distance between hillocks was also calculated. The hillocks had a tendency of lining up in distorted ring shaped patterns. This is interpreted as an effect of inhomogeneous stress distributions at the local grain level. The observations were made possible by using an imaging partial integrated scattering (PIS) system comprising of a dark field microscope objective and a charge coupled device (CCD) camera with an image processor and a data acquisition system. © 1997 Elsevier Science S.A.

Keywords: Aluminum; Optical coatings; Heat treatment; Light scattering

1. Introduction

Aluminum (Al) is the interconnection material most commonly found in integrated circuits. Thermal cycling during fabrication and high current densities in the operation of the integrated circuits generate large stresses, which may result in short circuits caused by hillocks or open circuits caused by voids and cracks. Similar problems with hillock and void formations are also known in the optical device industry. For example, the surface of an Al coated mirror is often exposed to harsh treatment and chemicals. To withstand these treatments a transparent protective layer is necessary. When silica is used as a protective layer it needs to be deposited at a temperature well above 100°C. Heated to that temperature hillocks will start to form in the evaporated Al films [1]. As high quality mirrors are degraded even by very small changes in the surface microtopography, the formation of hillocks is very detrimental to the optical quality of the film. A deeper understanding of mechanical stress in thin films is thus crucial for further miniaturization and higher device densities of very large scale integrated (VLSI) circuits, as well as for producing metal coated mirrors of high optical quality.

For a metal film that adhere well to a relatively thick or a sufficiently stiff (high modulus) substrate, the lateral film dimensions are controlled by the substrate. During a thermal cycling of such a sandwiched structure, volume changes caused by the thermal expansion mismatch between the film and the substrate will result in a build-up of mechanical stress in the film. This stress will bend the substrate to the shape of a spherical shell, if the biaxial elastic modulus is isotropic in the plane of the substrate, as it is for e.g. (100) silicon substrates [2]. If the stress in the film exceeds the elastic limit it will relax by various mechanisms of plasticity and creep [3]. Dislocation glide and grain boundary diffusion are generally accepted to play an important role in the hillock growth [4–8], but a detailed understanding of the mechanisms is still lacking.

Stress relaxation in thin films is affected by several parameters such as the substrate temperature during deposition [9,10], the film thickness [11,12], the grain size [6,8], the grain orientation [5–7], the alloying elements [13], and the surface oxides [14,15]. In addition, it also depends on

* Corresponding author. E-mail: carina@optics.kth.se

PII S0040-6090(97)00315-5

the thermal treatment which several authors have studied during isothermal treatments at various elevated temperatures [9,16]. Some investigations have also been made concerning the influence of the heating rate, see for example Baccommier et al. [17]. Gerth and Schwarzer [5,6] and Gerth et al. [8] have in several studies compared stepwise heating with isothermal heating.

The most common way to quantify hillock formation has been to express it in terms of hillock size, hillock density [9,10,17], or distance between hillocks [15]. By tradition hillocks have been extensively studied using scanning electron microscopy (SEM) [9,10,15,18], transmission electron microscopy (TEM) [5,15], and optical microscopy [16]. Investigations have also been made using stylus profilometers and atomic force microscopy (AFM) [19].

However, when studying the formation of the first hillocks it is crucial that the analysis technique does not influence the development of the hillocks, as easily can happen with electron beams when using SEM and TEM. Therefore, we have previously been using very sensitive non-contacting optical techniques such as total integrated scattering (TIS) [1], and the Vacuum Compatible Partial Integrated Scattering and Deflection (VaCPISD) technique [19,20]. Based on the fact that the integrated scattering methods are exceedingly sensitive real-time techniques for investigating minute topographical changes in a heated film, we have now developed the technique to also be imaging. With the developed imaging partial integrated scattering (PIS) system we are able to simultaneously acquire the scattered intensity as well as the absolute positions of the discrete scatter sites (hillocks) in the film. Using this technique, hillock formations can be revealed at an earlier stage and over larger areas than by using conventional SEM and TEM. The purpose of the present study is to make use of the imaging PIS technique to quantitatively and in real time examine how the thermal treatment influences the time before the first hillocks show up, the speed at which discrete hillocks are being formed, and how they are laterally distributed on the film surface. To our knowledge there has been no thorough study in real time of the initial development of the lateral hillock distribution. This paper also presents the experimental and statistical tools used for evaluating the lateral hillock distribution on heated optical quality Al films, and it is followed by a discussion of the observed findings in terms of inhomogeneous distribution of stress tolerance in the film.

2. Experimental

2.1. Sample preparation

Al films were evaporated in an ultra high vacuum system by an e-beam gun from 99.999% pure Al (Balzers) onto the polished side of 0.5 mm thick, 3-in. silicon (100) wafers (Virginia semiconductors). The wafers, coming straight out of the wafer box and having a native oxide, were kept at room temperature during the film deposition. The deposition rate was approximately 2.1 nm/s and the pressure at the film deposition was 7.7×10^{-4} Pa. The background pressure before the deposition was 8.8×10^{-7} Pa. The samples were rotated at a distance of about 40 cm from the Al source to achieve uniform optical quality films. The achieved film thickness was 0.2 μm as measured by a Talystep surface profilometer [21] and the lateral grain size of the films was about 100 nm as determined by atomic force microscopy (AFM). TIS investigations have shown that the hillock formation process is very repetitive for samples evaporated in the same batch. Therefore, all samples used in this study were taken from the same deposition batch.

2.2. Heater and thermal treatments

The experimental setup consists of a microscope stage equipped with a specially designed nichrome resistive heater and sample holder. A view of the sample compartment is shown in Fig. 1. The sample holder clamps the silicon wafer at the edge, and the temperature sensing Pt-100 element is attached to the thin film side of the sample. A heat shield with a circular hole is placed between the heater and the optical system consisting of a dark field microscope objective. The shield prevents damage to the optical parts and reduces the effect of thermal turbulence in the imaging path. The size of the hole is adapted so that most of the scattered light from the hillocks in the film is received by the microscope objective. A ceramic plate and an Al sheet thermally insulate the heater from the microscope stage.

The samples were heated from room temperature with different power levels for 10 min. The final temperatures were 144°C for treatment A, 132°C for treatment B and 124°C for treatment C, yielding average heating rates of 11.7°C/min (A), 10.5°C/min (B) and 8.8°C/min (C). The initial heating rates for the first minutes were 19.5°C/min (A), 15.8°C/min (B) and 13.6°C/min (C). The temperature vs. heating time diagram for the three different thermal treatments is shown in Fig. 2.

2.3. Imaging PIS

Total integrated scattering is a non-contact light measurement technique capable of sensing surface roughness at subångström roughness levels [22]. In its standard setup it collects the scattered light from a surface by means of an almost hemispherical mirror, and focus this radiation onto a detector. Due to the large spherical aberration of the mirror the technique is not suitable for direct imaging of single hillocks. Thanks to the wide angular scattering distribution from small surface features such as hillocks, we can get a decent scattering signal by using a somewhat reduced solid angle of the light collecting system. An

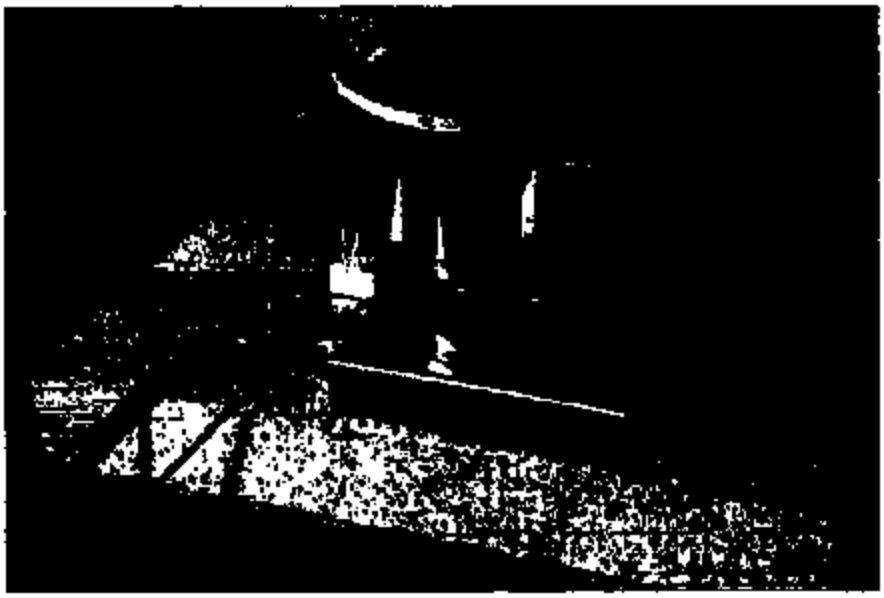

Fig. 1. Close-up on the sample compartment.

example of such a system is the VaCPISD instrument with its partial integrated scattering detector unit [19,20]. Another example is the conventional reflection mode dark field microscope objective, that has the advantage of being corrected for good imaging properties. In this study we used a Zeiss objective mounted on a Zeiss Axiophot microscope, for obtaining the light collection with simultaneous high quality imaging of the scatter sites. Provided with a Hamamatsu charge coupled device (CCD) camera C3077, a Hamamatsu Argus 50 image processor and image acquisition system, we obtain a complete imaging PIS system, capable of detecting the overall scattered intensity and the position of local scatter sites while the sample is being heated. A great advantage with the system is that with the selected objective it can also be operated in the differential interference contrast (DIC) mode, giving the possibility of focusing onto supersmooth Al film surfaces. Before starting the thermal treatment and image acquisition, the microscope is switched over to the dark field mode and a dark field image is acquired of the untreated film. This image, which is normally black, is later subtracted from the acquired series of images of hillocks obtained in the heating process. For the high optical quality Al films used in this study, practically no growth hillocks (or voids) were observed in the initial dark field image prior to heating. During heating the films develop to compressive stress so no voids are expected to be formed. Substrate bending caused by the compressive film stress can be compensated for by manual refocusing. The first hillock in the field of view of the imaging PIS system will show up as a bright spot after an incubation time of some minutes and then, as the overall compressive stress gets too high, hillocks are popping up everywhere as bright stars. Video recordings of the course of the events are indeed very illustrative of the local relaxation in the film. An image (512 × 511 pixels) corresponds to a physical area of 7.56×10^{-4} cm^2 and is integrated from 128 video frames. Such an image is stored every 6.1 s throughout the measurement series. The images have a dynamic range of 256 gray levels, where the background typically corresponds to the ten darkest levels in the images. In the images to follow, we have for the sake of printing reproduction, inverted the images so that the scatter sites appear as black spots on a white background rather than bright spots on a dark background.

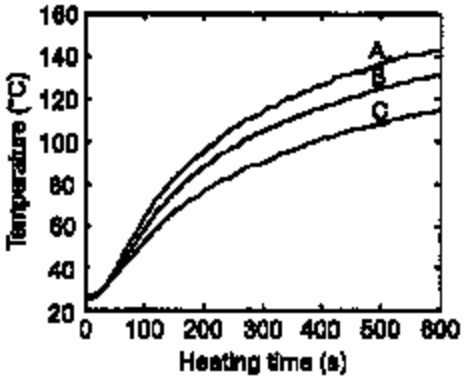

Fig. 2. Thermal treatments plotted as sample temperature vs. heating time.

The sum of scattered light from individual hillocks is proportional to the number of hillocks illuminated on the surface, at least as long as the hillocks are small and well separated. When they get close enough, less than about 5

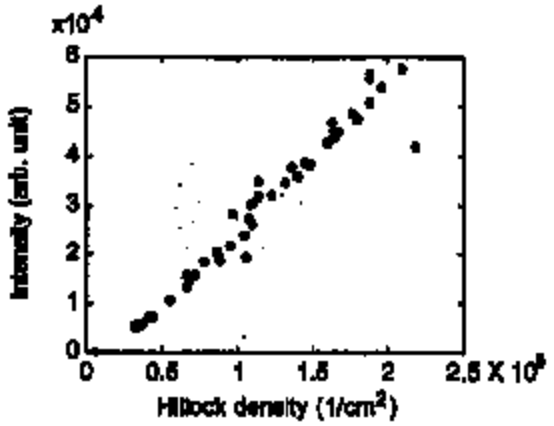

Fig. 3. Average intensity of CCD camera image vs. number of hillocks/cm^2 protrusions for the images acquired in thermal treatment C. The average intensity is intended related to data obtained by total integrated scattering.

wavelengths of the incident light, multiple scattering will come into effect and a proportionality will no longer exist. The wavelength limit is rather fuzzy but this is the distance where the density of surface features has been shown to influence the polarization properties of the light [23]. In the initial heating cycle studied in this investigation, the hillocks are well separated. Hence, we get a good correlation (see Fig. 3) between the acquired average intensity (the equivalent of the TIS signal) and the number of hillocks present in the field of view of the imaging PIS.

2.4. Total integrated scattering measurements

For comparison and confirmation of the imaging PIS data we also measured the samples before and after the thermal treatments by means of the standard TIS equipment [22]. Before heating, the samples had the same TIS value (= diffuse reflectance divided by total reflectance), of 9.1×10^{-3}, confirming their identical as-deposited surface roughness, δ. Earlier studies have confirmed that the as-deposited surface roughness of the films depends on both the film thickness and the deposition conditions such as background and deposition pressures [24,25]. By using ultra high vacuum deposition at room temperature we achieved smooth, low scatter Al films with low surface roughness values. After the different thermal treatments, the TIS values were 1.1×10^{-3} for A, 6.5×10^{-4} for B and 4.1×10^{-4} for C. As we have seen before, the higher temperatures used during the heating the higher the TIS value became. A summary of the TIS investigation is given in Table 1.

Table 1
Summary of the total integrated scattering (TIS) investigation

Treatment	Initial		Final		
	Total integrated scattering	Root mean square (rms) roughness (Å)	Temperature (°C)	Total integrated scattering	Equivalent root mean square (rms) roughness (Å)
A	9.1×10^{-3}	4.80	144	1.1×10^{-3}	16.7
B	9.1×10^{-3}	4.80	132	6.5×10^{-4}	12.8
C	9.1×10^{-3}	4.80	115	4.1×10^{-4}	10.2

3. Analysis methods of lateral hillock distribution

The (x, y) position of a hillock center was calculated with ARGUS-50/CA code from Hamamatsu and we refer to this center as a scatter site. Data in the form of a set of points, irregularly distributed within an area arise in many different contexts. A common question is whether the points appear completely random, regularly spaced or clustered. The study of spatial point patterns has a long history in ecology and forestry. In the first analysis of the lateral hillock distribution we apply the Quadrate counts method [26]. The basics of the method are briefly described below.

The study region, A, is partitioned into m sub-blocks or quadrates each with an area B. The data to be analyzed comprises independent counts $n_1, n_2, \ldots, n_m$ in these m quadrates. To test the hypothesis that n_i are an independent random sample from a Poisson distribution the Quadrate counts method is applied. Under Complete Spatial Randomness (CSR), the number of counts $N(B)$ in a quadrate follows a Poisson distribution with the mean λB, where λ is the number of counts per area B. The probability distribution of $N(B)$ is given by

$$P_n(B) = \exp(-\lambda B)\frac{\lambda B^n}{n!}, n = 0,1,2,\ldots \quad (1)$$

The dominating test statistic for the Quadrate counts method is the index of dispersion, I,

$$I = \frac{s^2}{s^2_{rand}} \quad (2)$$

also referred to as variance ratio, formation number and relative variance. The numerator,

$$s^2 = \frac{1}{m-1}\sum_{i=1}^{m}(n_i - \bar{n})^2 \quad (3)$$

estimates the variance of $N(B)$ when no distributional assumptions are made, whilst the denominator, s^2_{rand}, estimates the variance when CSR holds and is equal to the mean $\bar{n}$.

Values of I greater than one indicate that the scatter sites are clustered. On the other hand, if I is less than one then this indicates a tendency for regular spacing. With

this method, it is possible to focus on small-scale or large-scale phenomena depending on the choice of quadrate size, R.

In the second analysis of the lateral hillock distribution, the nearest neighbor distance between hillocks was calculated. This calculation is affected by the edges of the images, and we solved this problem by the so called free zone method, i.e. the distance to a hillock is not accounted for if the hillock is closer to an edge than to its nearest neighbor.

4. Results and discussion

From previous measurements using the TIS technique we know that Al films evaporated in the same batch shows a repeatable TIS response for identical heat treatments. The samples used in this study were from the same batch. We are therefore confident that the observed differences between the samples can mainly be attributed to the different thermal treatments.

4.1. Development of the hillock formation

The imaging TIS study yielded a large library of images for each of the samples, showing the progressive development of the hillocks. Fig. 4 shows some examples of the inverted binary dark-field images obtained at different heating times and temperatures during the thermal treatments. In the left column of this figure the first scatter sites are seen and the right column shows the scatter sites when the hillock density was about 2.5×10^4 cm^{-2}. One interesting result from this comparison is that the lowest heating rate (8.8°C/min) on average produces fewer hillocks per cm^2 at a given temperature, than the higher heating rates do. This implies that one possible way of reducing the number of hillocks in an Al film is to have a gentle rather than a forced heating treatment. From these images it is possible to see that the hillocks were inhomogeneously distributed over the examined sample area. See for example the thermal treatment A as compared to treatment B and C, indicating different stress tolerance in different regions of the film.

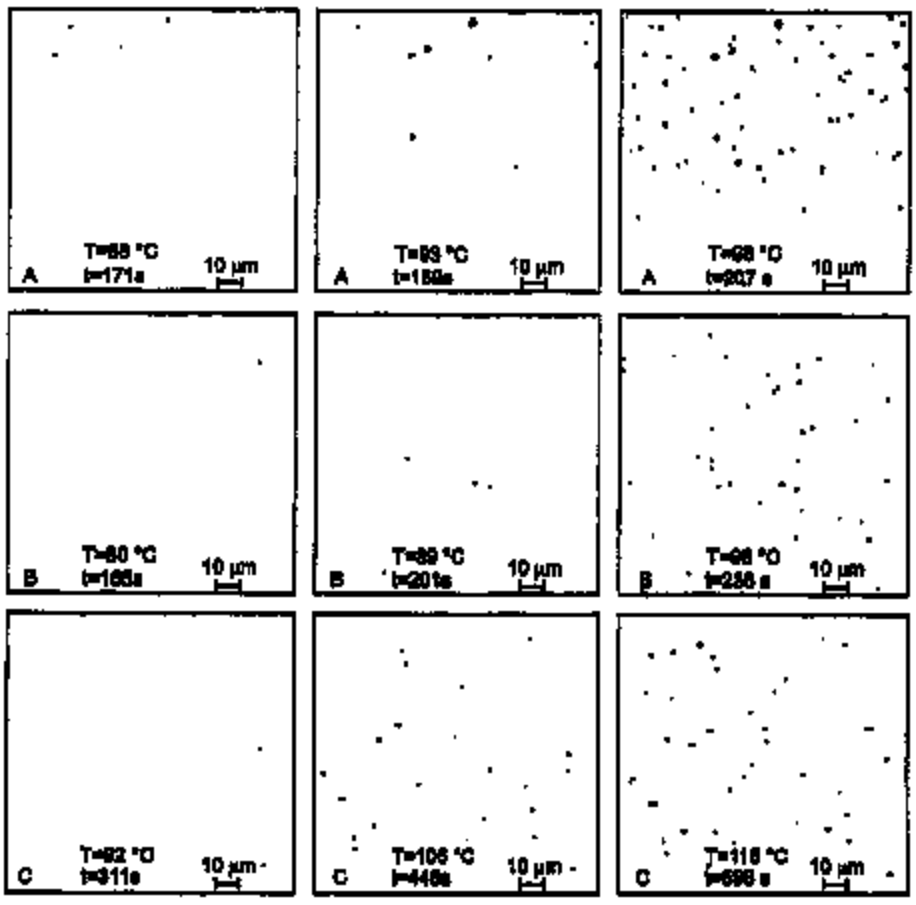

Fig. 4. The inverted binary dark-field images for the thermal treatments (A, B and C) when the hillock density was about the lowest detectable (left column), about 50% of 2.5×10^3 cm^{-2} (middle column) and at about 2.5×10^4 cm^{-2} (right column). In order for the scatter sites to be clearly visible we only show about 20% of the acquired image.

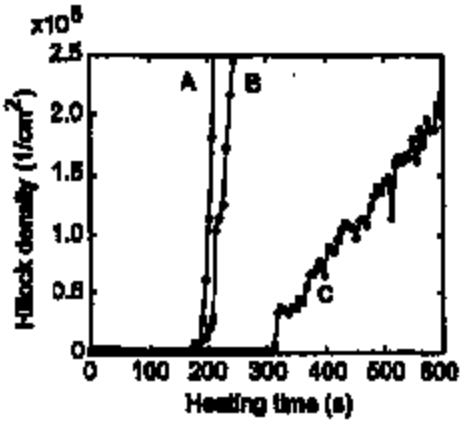

Fig. 5. Hillock density plotted vs. heating time.

4.2. Hillock density

The increase in the number of hillocks per cm^2 as detected in the field of view of the imaging FIS system from the first hillock up to a density of about 2.5×10^3 cm^2 is shown in Fig. 5. From this figure it is seen that the incubation time, i.e., the time before the hillocks start to form, was almost the same for treatment A and B (about 3 min), but was considerably longer for treatment C (about 5 min). The temperature corresponding to the observation of the first hillock was $T = 88°C$ (A), $T = 80°C$ (B) and $T = 92°C$ (C). Thus, the onset of hillock growth occurred within a confined temperature range apparently independent of the heating rate. After the incubation time the number of hillocks started to increase, first slowly, then more rapidly. The average increase in number of hillocks for a hillock density up to about $2.5 \times 10^3/cm^2$ was $4.2 \times 10^5/(s\ cm^2)$ for treatment A, $2.7 \times 10^5/(s\ cm^2)$ for B and $7.5 \times 10^4/(s\ cm^2)$ for C. With the corresponding average heating rates of 11.7°C/min, 10.5°C/min and 8.8°C/min for treatment A, B and C respectively it is worth noticing that a 33% increase in heating rate yielded an increase of hillocks formation by an almost six times higher rate. The density of hillocks was also found to be higher for higher heating rate at a given temperature. This is another indication that a slower heating is to be preferred for obtaining a reduced number of hillocks.

It is known that when the stress in the film exceeds the yield strength of the film material plastic deformation occurs. The temperature and the heating rate during thermal treatments influence the dominating deformation mechanisms in the film [8,27,28]. In the case of low temperature and relatively high heating rate, which was valid for our experiments, the thermally induced stress is relaxed mainly by dislocation glide to the flow stress of that temperature. The significant difference in increase in number of hillocks for the samples may indicate that a higher heating rate caused more grain deformation by dislocation glide.

4.3. Ring shaped patterns of hillocks

The large library of images revealed the interesting result that many hillocks were preferentially lined up along distorted ring shaped patterns, at least as interpreted by the human eye. In Fig. 6 we show an example of an image where some patterns of this kind can be seen. To our knowledge such ring patterns have not previously been reported. We try to explain these patterns by starting from existing deformation mechanism descriptions and finally making a qualified guess.

As is well-known dislocation glide occurs preferentially on planes of high atomic density along close-packed directions and, as for all fcc metals, deformation is caused by slip on {111} planes in ⟨110⟩ directions. The shear stress per strain on the slip systems ⟨110⟩ is higher, up to about two times, for grains deviating from ⟨111⟩ texture [7]. In polycrystalline films, the grains may be gathered in what Planova and Artemyev [29] call colonies. Such colonies are grain groups with close orientation. Therefore, the yield strength may be reached at different stress levels in different regions of polycrystalline films. In some regions yielding is not exceeded, in others it is exceeded resulting in an inhomogeneous deformation, which makes the stress even more inhomogeneous. However, yield strength is not well defined for polycrystalline materials, due to the inhomogeneous deformation, and it depends on the heating rate and the temperature. This implies that grains deviating from ⟨111⟩ texture will be the first to deform plastically with associated hillock formation. The reason for the hillocks to line up along distorted ring shaped patterns is still an unresolved question. A qualified guess is that the grain orientations in the 100 nm large grains of the Al

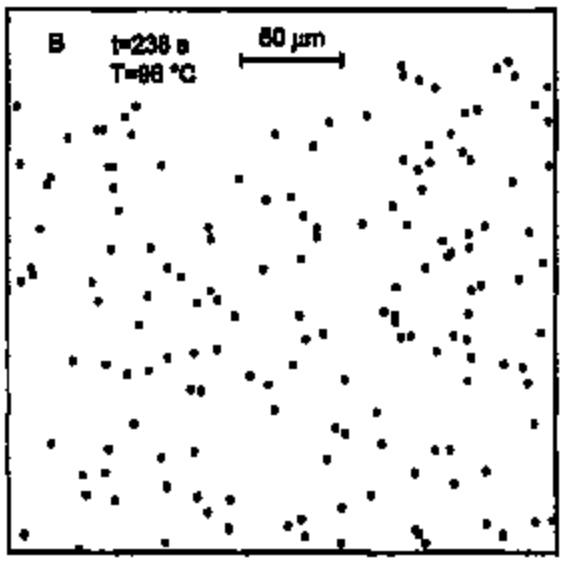

Fig. 6. The hillocks often tended to line up along distorted ring shaped patterns. The center dots have been enlarged for easier observation.

0042-6027 29618

films were influenced by the substrate microstructure, and that the lines of hillocks revealed this structure. One reason for making such a guess is that we have observed similar ring shaped zones on bare silicon wafers of both ⟨100⟩ and ⟨111⟩ type using contrast enhanced reflection microscopy. In those cases the patterns appear as 20–50 μm large 'grains' with just barely discernible reflection differences. If the boundary between those large 'grains' influences the nucleation of the Al film we can expect an influence on the stress tolerance in the film according to the discussion above.

The observed distorted ring shaped patterns are not easily expressed in geometrical terms. Therefore, to get a more objective description of the lateral hillock distributions, the acquired images were further analyzed by two statistical methods.

4.4. Test of randomness in the lateral hillock distributions

As we have not found any literature reference on lateral hillock distribution analysis in terms of randomness we introduce a technique picked up from forestry investigations [26]. In the first analysis, a statistical description of the lateral hillock distribution was obtained by applying the Quadrate counts method described in Section 3. This method tests the Complete Spatial Randomness (CSR) using the index of dispersion, I, to classify the pattern as regular ($I < 1$), random ($I = 1$) or clustered ($I > 1$). The index of dispersion corresponds in our case to the ratio between the variance of the measured number of hillocks in the quadrates and the variance of the number of hillocks following a Poisson distribution. The results from this analysis for the different thermal treatments are shown in Fig. 7. The index of dispersion is plotted vs. heating time for the same sample area with three different quadrate grids (2 × 2, 4 × 4 and 8 × 8 grid of quadrates). The index of dispersion fluctuated during the thermal treatment for all samples independent of the grid refinement. Further, the index of dispersion was larger for coarser grid, which implies that the lateral hillock distributions over large areas (1.89×10^{-4} cm^2) appear more clustered than over small areas (1.18×10^{-5} cm^2). The clustered distributions thus confirm the result of inhomogeneous deformation.

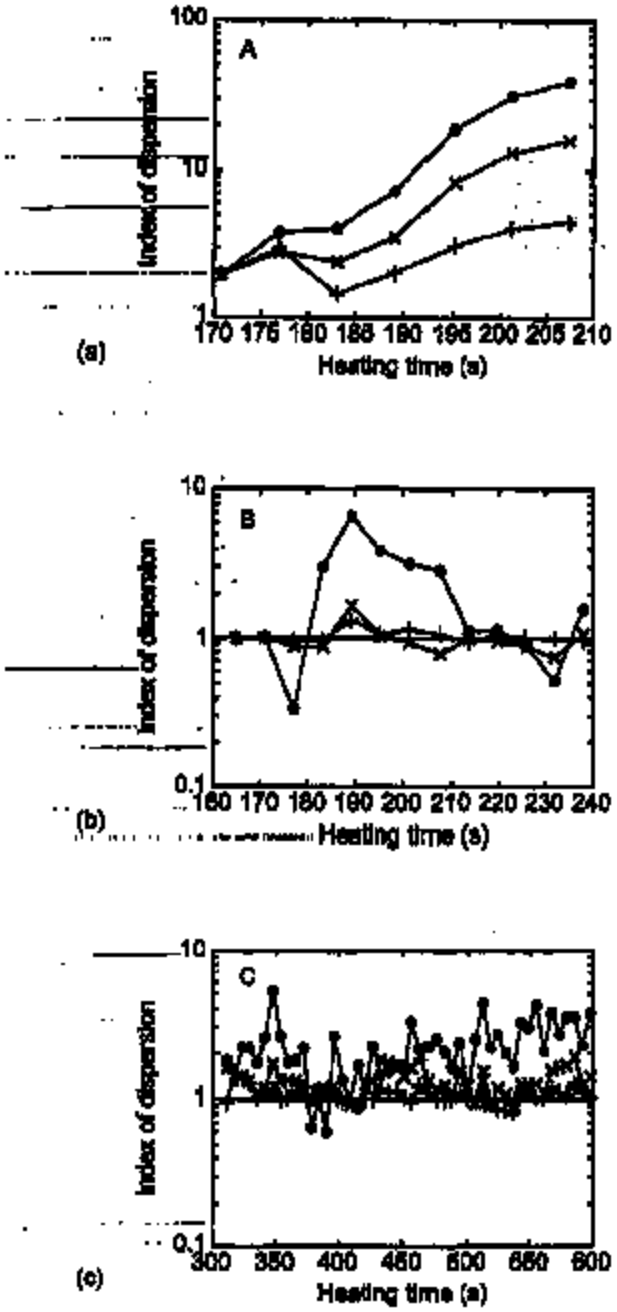

Fig. 7. Test of randomness in the lateral hillock distributions. Index of dispersion, I, for thermal treatment (a) A, (b) B and (c) C, and three quadrate sizes ((●) 2 × 2, (×) 4 × 4 and (+) 8 × 8 grid of quadrates). Distribution is regular for $I < 1$, random for $I = 1$ and clustered for $I > 1$.

4.5. Nearest neighbor distance between hillocks

In the second analysis of the lateral hillock distribution, we calculated the nearest neighbor distance between hillocks. The mean value of the nearest neighbor distance and its standard deviation were calculated for each image for all samples up to a hillock density of about 2.5×10^5 cm^{-2}. The result is presented in Fig. 8. As expected a general tendency for all treatments was that the mean distance decreased with heating time, and at the temperatures obtained here it approached about 10 μm. This is 100 times larger than the typical grain size of the evaporated Al films, which was measured to be about 0.1 μm using atomic force microscopy. Another general behavior was that the standard deviation of the nearest neighbor distance between hillocks also decreased with heating time.

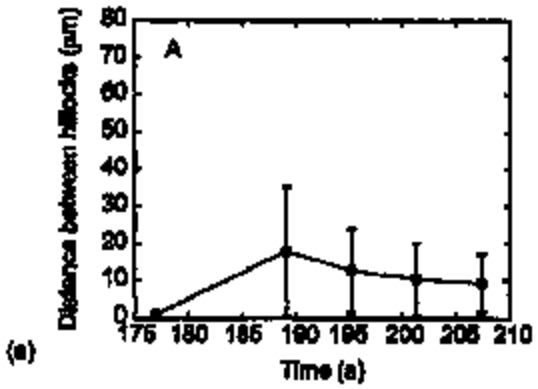

(a)

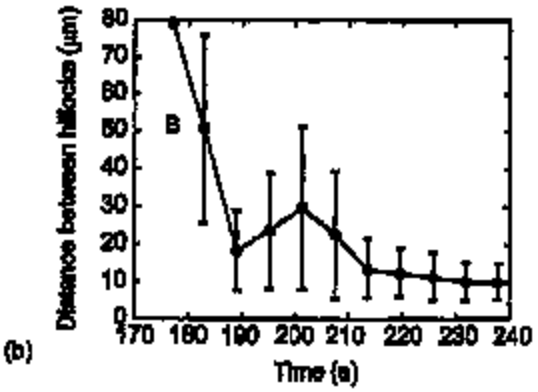

(b)

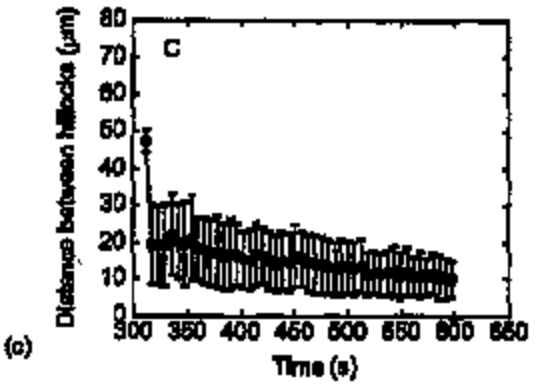

(c)

Fig. 8. The nearest neighbor distance between hillocks as a function of heating time for thermal treatment A (a), B (b) and C (c). The standard deviation is given by the bars.

Although the mean distance approached 10 μm, hillocks along the distorted ring shaped patterns (e.g., Figs. 4 and 6) can be considerably more closely spaced. Our result can be compared with the distance between hillocks reported in Ref. [15] ranging from about 20 μm to 100 μm for sputter deposited Al – 2 at.% alloy films with grain size, which was about 0.2 μm after heating at 400°C.

5. Conclusions

Real-time imaging partial integrated scattering technique, applied on optical quality Al films on Si wafers, has shown the initial development of the lateral hillock distribution in the films for different heating rates. The formation of the first hillocks was found to appear within a confined temperature interval, independent of the heating rate. After the onset of hillocks, the density of hillocks increased considerably faster for the higher heating rates than for the lower. We therefore conclude that a low heating rate is to be preferred if the number of hillocks should be minimized at a particular temperature. We also found by visual observation and statistical analysis that the hillocks tend to be clustered, and line up in distorted ring shaped patterns at this initial stage of hillock formation. We suggest that these patterns are caused by inhomogeneous stress distribution at the local grain level of the film, and that the inhomogeneous stress can be derived from substrate influence causing different grain orientations.

Acknowledgements

The authors are very grateful to L. Kjellberg and S. Bolin for the electronic and mechanical workshop assistance and L. Krummenacher for thin film deposition, AFM and Talystep measurements. The research and development was financially supported by the Swedish Research Council for Engineering Sciences (TFR) and the Göran Gustafsson Association.

References

[1] L. Mattsson, Y.-H. Le Page, P. Ericsson, Thin Solid Films 198 (1991) 149.
[2] W.D. Nix, Metall. Trans. 20A (1989) 2217.
[3] V.M. Kolotilin, V.F. Belitsky, I.V. Klyuyshin, Thin Solid Films 142 (1986) 199.
[4] M.S. Jackson, C.-Y. Li, Acta Metall. 30 (1982) 1993.
[5] D. Gerth, R.A. Schwarzer, Mater. Sci. Forum 119-115 (1993) 615.
[6] D. Gerth, R.A. Schwarzer, Mater. Sci. Forum 119-115 (1993) 619.
[7] R.A. Schwarzer, D. Gerth, J. Electron Mater. 22 (6) (1993) 607.
[8] D. Gerth, D. Kaiser, M. Krohn, Thin Solid Films 209 (1992) 67.
[9] S. Ameo, C.Y. Chang, R.W. Vook, Thin Solid Films 219 (1992) 80.
[10] C.J. Sasson, J. Electrochem. Soc. 116 (1969) 361.
[11] R. Venkatraman, J.C. Bravman, J. Mater. Res. 7 (8) (1992) 2040.
[12] M.F. Doerner, D.S. Gardner, W.D. Nix, J. Mater. Res. 1 (6) (1986) 845.
[13] D.S. Gardner, P.A. Flinn, Mater. Res. Soc. Symp. Proc. 130 (1989) 69.
[14] C.Y. Chang, R.W. Vook, Thin Solid Films 228 (1993) 205.
[15] E. Iwamura, T. Choldd, K. Yoshikawa, Thin Solid Films 270 (1995) 450.
[16] C.A. Volkert, C.F. Alofs, J.R. Liefting, J. Mater. Res. 9 (2) (1994) 1147.
[17] B. Baccanaler, G. Lormand, M. Papapietro, M. Achard, A.-M. Papon, J. Appl. Phys. 64 (11) (1988) 6483.
[18] S.K. Lahiri, G.C. Wells, Appl. Phys. Lett. 15 (1969) 234.

[19] C. Kylner, L. Mattsson, Mater. Res. Soc. Symp. Proc. 436 (1996) 297.
[20] C. Kylner, L. Mattsson, Rev. Sci. Instrum. 68 (1) (1997) 143.
[21] J.M. Bennett, J.H. Dancy, Appl. Opt. 20 (10) (1981) 1785.
[22] L. Mattsson, Proc. SPIE 652 (1986) 264.
[23] E.G. Loewen, M. Nevière, D. Maystre, J. Opt. Soc. Am. 67 (4) (1977) 496.
[24] L. Mattsson, Workshop on Optical Fabrication and Testing Technical Digest 1987, Optical Society of America, Washington, 1987, pp. 85–88.
[25] F.M. Reicha, P.B. Barna, Acta Phys. Acad. Sci. Hung. 49 (1-3) (1980) 237.
[26] N.A.C. Cressie, Statistics for Spatial Data, Wiley, New York, 1993.
[27] M.D. Tiwaloss, Annu. Rev. Mater. Sci. 25 (1995) 69.
[28] M.F. Doerner, W.D. Nix, Crit. Rev. Solid State Mater. Sci. 14 (3) (1988) 225.
[29] L.E. Pinsova, A.V. Anisimov, Optic Examination in Metals and Semiconductors, Les éditions de Physique, Les Ulis Cedex, France, 1995.

ELSEVIER

Thin Solid Films 371 (2000) 278–282

Thin Solid Films

www.elsevier.com/locate/tsf

Microstructure of thermal hillocks on blanket Al thin films

Deok-kee Kim[a,*], Birgit Heiland[c], William D. Nix[b], Eduard Arzt[c], Michael D. Deal[a], James D. Plummer[a]

[a] *Center for Integrated Systems, Stanford University, Stanford, CA 94305, USA*
[b] *Department of Materials Science and Engineering, Stanford University, Stanford, CA, USA*
[c] *Max-Planck-Institut für Metallforschung, Stuttgart, Germany*

Received 9 October 1999; received in revised form 11 February 2000; accepted 11 April 2000

Abstract

The microstructure of thermal hillocks on blanket Al thin films has been studied for the first time by several techniques, including sectioning and imaging in a focused ion beam system. It is found that the new material in the hillock area lifts the original film up and in some cases penetrates it. The micrographs also reveal the grain structures and give valuable insight into the mechanisms of hillock growth. © 2000 Elsevier Science S.A. All rights reserved.

Keywords: Aluminum; Hillock formation; Microstructure; Focused ion beam; Creep deformation; Stress relaxation

1. Introduction

Thin metallic films are widely used as components in microdevices. Because of their potential limitations on device reliability, mechanical stresses in such thin-film systems have been studied extensively [1]. It is generally found that thin films support much higher stresses than bulk materials of similar composition; this observation has been attributed to constraints on lattice defects due to the fine microstructures and the influence of the substrate. Consequently, stress relaxation, which requires the movement of dislocations is more difficult than in large-scale materials and is, despite recent modeling attempts, not fully understood.

An important source of mechanical stress in thin films is the thermal mismatch between the film and the substrate material. Depending on the sign of the mismatch and of the temperature change, tensile or compressive stresses can develop in the film. One mechanism of compressive stress relaxation which is specific to thin films is the formation of hillocks, i.e. extrusions of material out of the plane of the film. Such hillocking, which results in considerable roughening of the film surface, has frequently been reported in the literature [2–6]. However, the structure of the hillocks has not been investigated in detail. Also the exact mechanism of hillock growth, apart from some suggestions involving condensation of atoms along dislocation lines, remains unclear.

The purpose of this paper is to report the microstructure of thermal hillocks on Al films. The micrographs were obtained by several methods, i.e. side-view scanning electron microscopy (SEM) and cross-sectional transmission electron microscopy (TEM). The most detailed insight resulted from sectioning and viewing selected hillocks with a focused ion beam (FIB). Based on the microstructural information, a possible

* Corresponding author. Tel.: +1-650-725-0417; fax: +1-650-723-4659.
E-mail address: deokkee@leland.stanford.edu (D. Kim).

0040-6090/00/$ - see front matter
PII: S0040-6090(00)00971-8

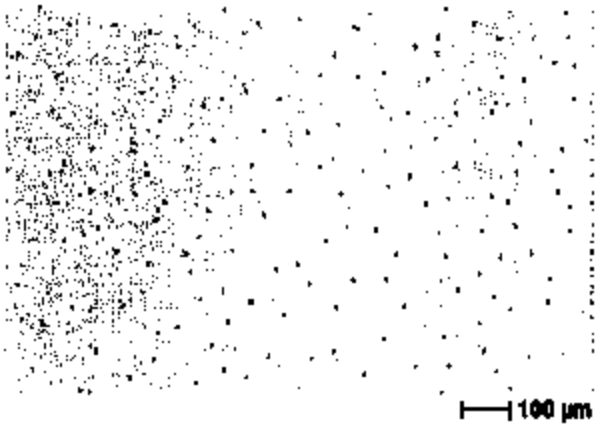

Fig. 1. Optical micrograph of a film after annealing in plan view.

mechanism for the growth of these hillocks is suggested. A more thorough quantitative analysis which includes a mathematical modeling will be published elsewhere [7].

2. Experimental

Pure Al films of 1 μm thickness were magnetron sputter-deposited at room temperature onto Si (100) wafers coated with 0.2 μm LPCVD SiO_2. The Al films were first passivated with a 0.3-μm thick TiW layer, which was subsequently removed by plasma etching. The purpose of the TiW films was to suppress hillock formation in the experiment that we originally planned (not described here). The films were annealed for 2 h at 450°C in forming gas which is composed of 5% H_2 and 95% N_2. Because of the higher coefficient of thermal expansion of the film relative to the substrate, this anneal produced a compressive stress in the film which amounted to several hundred MPa (Fig. 6). Following the anneal, the films were cooled in air. Stress measurement was made by measuring wafer curvature during thermal cycling; thermal cycle includes a 2 h hold at 450°C.

The microstructure of the films was examined by plan view optical and side view scanning electron microscopy using a Hitachi S-800. For closer inspection of individual hillocks, TEM cross-section specimens were prepared in the following way [8]: the Si wafers, containing Al films, were cut and glued together. The glued specimen was cut into thin slices using a diamond saw and 3-mm-diameter disks were cut from the slice. The disks were thinned on a grinding wheel, dimpled, and ion milled to electron transparency. TEM micrographs were taken with a Philips CM20 at an accelerating voltage of 200 kV and typical magnifications of 13 000–17 500.

The additional use of a focused ion beam (FIB) system offers the advantage of sectioning selected hillocks with high precision. The cross-section can then be imaged by collecting the secondary electrons; because the ions are subjected to a strong channeling effect, the resulting micrographs exhibit clear grain orientation contrast and hence allow thorough analysis of the grain structures. In this study, an FEI FIB 200 workstation with 30 kV accelerating voltage was used; sectioning was performed with an ion current of 1 nA, followed by cleaning at 150 pA and imaging at 70 pA.

3. Results and discussion

Whereas the as-deposited films were planar, the annealing resulted in extensive hillocking as can be seen by optical and scanning electron microscopy (Figs. 1 and 2). The hillocks are homogeneously distributed and have a typical spacing of approximately 70 μm. Typical dimensions of a hillock are 4 μm in width and in height. Cross-sectional TEM reveals the microstructure of the film between the hillocks and of an individual hillock (Fig. 3). Note that the film consists of columnar grains (Fig. 3b), which have grown during the anneal from an initial size of approximately 69 nm to a final size of 90 nm. These values are unusually small in comparison to other studies where grain sizes of the order of the film thickness are commonly found [3,6,9]. This can be attributed to the room-temperature sputtering process and subsequent grain boundary pinning during the annealing by sizeable contents of O, Ti and W impurities which were found to be present by EDS measurements. Small amounts of Ti and W seem to have been incorporated into the Al film, due to the TiW layer which has been removed before the anneal. At the site of the hillock, new material has been deposited between the film and the substrate, displacing the original film upward (Fig. 3a).

While the exact location of the cross-section with respect to the hillock cannot be inferred in the TEM micrograph, some hillocks were sectioned along their central axis by FIB (Fig. 4). Fig. 4a is an example of a hillock in which the original film has been lifted in a similar way to Fig. 3a; it is remarkable that the hillock has an almost perfectly conical shape and that the original film appears to be largely intact. A more extreme case is illustrated in Fig. 4b where the newly deposited material has penetrated the original film and formed a nearly spherical cap. Of particular interest is the grain structure of the new material: Fig. 4 reveal that the grains in this region are not all columnar and their size greatly exceeds that in the original film. Note also that the grain size increases from the film/substrate interface to the top of the hillock; in Fig. 4b new grains even seem to have nucleated in the 'cap' region.

The unexpected microstructures of the hillocks visible in Figs. 3 and 4 have not been reported in the literature before. They provide insight into possible

Fig. 2. Scanning electron micrographs of (a) a single hillock, (b) an unusually big hillock.

mechanisms of hillock growth. We propose the following sequence of events (Fig. 5):

1. Preferred nucleation sites for thermal hillocks are locations at the weakly bonded film/substrate interface, where delamination occurs due to very high compressive stresses in these films. This allows the interface to act initially as a sink for atoms. The regularity of the arrangement of hillocks may be associated with the stress relaxation zones surrounding each hillock.
2. Hillock growth occurs by diffusion of atoms, under the action of the compressive stress, from the vicinity of a nucleation site to the site of the hillock.

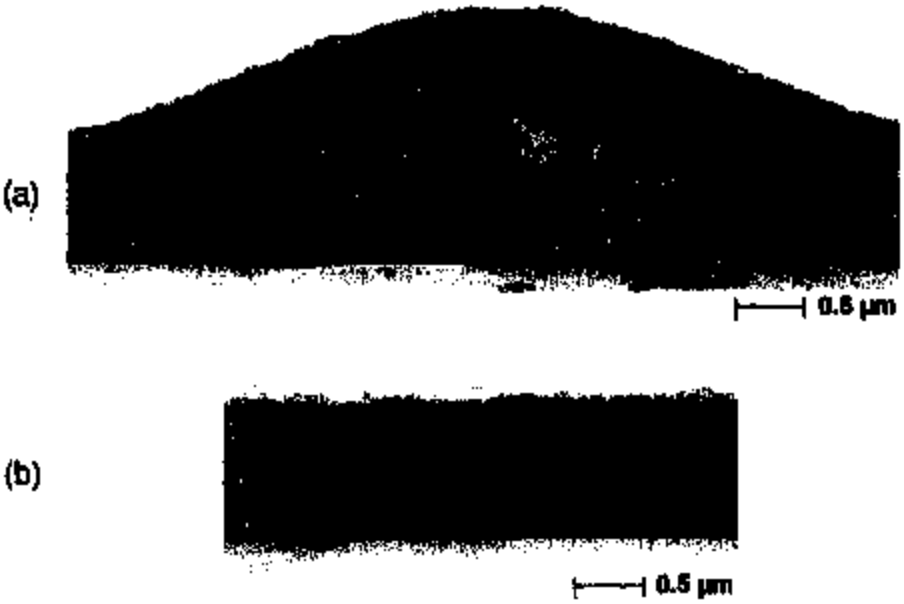

Fig. 3. Cross-sectional TEM images of (a) a hillock, (b) the film remote from a hillock.

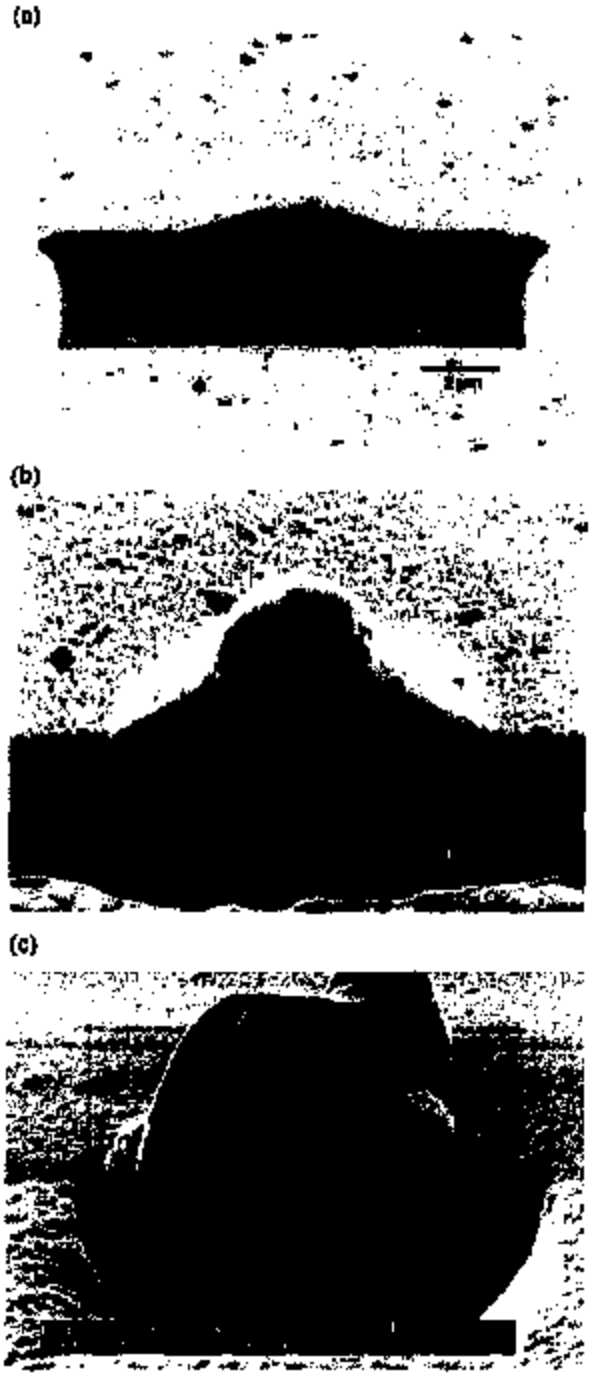

Fig. 4. Focused ion beam (FIB) images of hillock cross-sections: (a) cone-shaped hillock, (b) hillock with spherical 'cap', (c) hillock which has completely penetrated through the original Al film.

The most likely atom sources are the columnar grain boundaries of the original film, where the chemical potential for atoms is raised due to the compressive stress. The diffusion path is, depending on the temperature, the grain boundary, the film/substrate interface or the lattice. The first-arriving atoms are deposited at the film/substrate interface where new grains are nucleated. Subsequently-arriving atoms are deposited at the interface between the original film and the hillock material. In this way the grain size can increase in the direction normal to the film surface. Alternatively, the arriving atoms may have been plated at the film/substrate interface and grain growth may have occurred in-situ to adjust the grain size to the new film thickness.

3. During deposition of the atoms, the original film is displaced upward and stays intact at first. It is likely that the bending of the film is controlled by creep deformation and exerts a back stress on the material beneath. Once the film deformation exceeds a critical value, it fractures and new material penetrates to the top. To minimize the surface area, it forms a spherical cap.

One of the most striking observations is the grain structure in the hillock region which differs substantially from that of the original film. The large grains are believed to result from the combination of two factors: first, growth of these regions occurs at an elevated temperature of 450°C at which atom mobility is high; and, second, the material there is much purer than the original film because the diffusion process has left behind the impurities present in the film. It is not clear how the new grains in the cap region of Fig. 4b have nucleated.

Finally, we attempt to estimate the amount of stress relief caused by the formation of the hillocks in these films. The stress relief can be approximated by

$$\Delta\sigma = M\frac{\Delta V/A}{2t_f} = M\frac{(A_{base}\times h)/A}{2t_f} \quad (1)$$

where M is the biaxial modulus and t_f the thickness of the film, ΔV the excess volume of a hillock assumed to be cylinder-shaped with base area A_{base} and height h. A is the film area per hillock, which is assumed to be $70^2 = 4900\ \mu m^2$ using the average hillock spacing 70 μm (Fig. 1). Using a value of 100 GPa for the biaxial modulus, we obtain a theoretical stress relief of approximately 510 MPa. This value is reasonable in view of the total stress relief (approx. 700 MPa), inferred from the stress measurements during thermal cycling, as shown in Fig. 6. The dominant stress relief mechanism in the Al film under study appears to be hillock formation.

Fig. 5. Schematic of the likely mechanism of hillock growth.

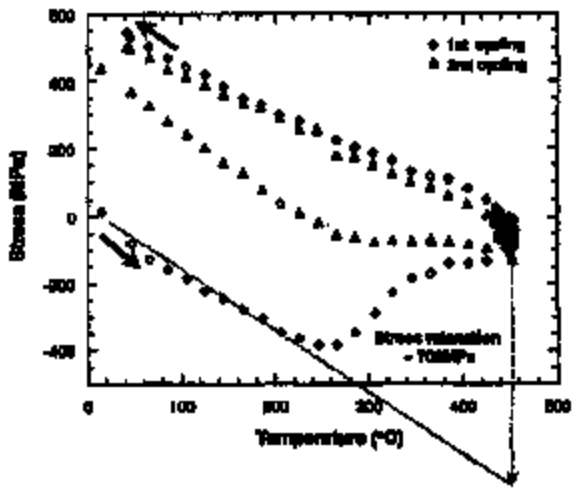

Fig. 6. Stresses vs. temperature during the first and the second thermal cycling of the Al film.

4. Conclusion

We have characterized the microstructure of thermal hillocks in Al films which had been annealed at 450°C. At the sites of the hillocks, the original films are found to be displaced by material inserted under them to give hillocks with a conical shape. The micrographs also reveal the grain structures and give valuable new insight into mechanisms of hillock growth. Based on the microstructural observations, we propose that the hillocks grow by diffusion of atoms from the vicinity to the interface between the original film and the newly-deposited material. The stress relief due to hillock growth is estimated from the size and spacing of the hillocks and found to amount to reasonable values. Hillock formation appears to be the dominant stress relief mechanism in the Al film under study. The proposed hillock model may not be applicable to all kinds of hillocks, but seems to describe the experimentally observed hillock formation in these small-grained films.

Acknowledgements

This work was funded by Sematech, SIA, and DARPA under the MARCO Interconnect Focus Center Program.

References

[1] W.D. Nix, Metall. Trans. A 20 (1989) 2217.
[2] F. Chaudhari, J. Appl. Phys. 45 (1974) 4339.
[3] C.Y. Chang, R.W. Vook, Thin Solid films 228 (1993) 205.
[4] D. Gerth, D. Katzer, R. Schwarzer, Mater. Sci. Forum 94–96 (1992) 537.
[5] E. Iwamura, T. Ohnishi, K. Yoshikawa, Thin Solid Films 270 (1995) 450.
[6] B. Racoosin, G. Lormand, M. Papapietro, M. Achard, A.-M. Papon, J. Appl. Phys. 64 (1988) 5483.
[7] D.-K. Kim, W.D. Nix, M.D. Deal, J.D. Plummer, Creep-controlled diffusional hillock formation in blanket aluminum thin films as a mechanism of stress relaxation (to be published in J. Mater. Res.).
[8] J. Brennan, R. Sladek, J. Electron Microsc. Tech. 1 (1984) 53.
[9] R. Venkatraman, S. Chen, J.C. Bravman, J. Vac. Sci. Technol. A 9 (1991) 2536.

Research Topic task started on Tue Mar 26, 2002 at 7:11 PM

5 Research Topic candidates were identified in CAPLUS.
using the phrase "hillock in aluminum thin films"

Selected 2 of 5 candidate topics.
1 reference was found containing "hillock in aluminum thin films" as entered.
45 references were found containing the two concepts "hillock" and "aluminum thin films" closely associated with one another.

Bibliographic Information

Hillock formation in aluminum thin films during thermal cycling. Kim, Deok-Kee. Stanford Univ., Stanford, CA, USA. Avail. UMI, Order No. DA3002008. (2001), 139 pp. From: Diss. Abstr. Int., B 2001, 62(1), 473. Dissertation written in English. CAN 136:138041 AN 2001:898168 CAPLUS

Bibliographic Information

Thin film transistor without hillocks due to gates and simplified method of manufacturing the same. Lyu, Ki-Hyun; Hwang, Kwang-Jo. (S. Korea). U.S. Pat. Appl. Publ. (2001), 11 pp. CODEN: USXXCO US 20010048107 A1 20011206 Patent written in English. Application: US 97-979843 19971126. Priority: KR 96-9662231 19961206. CAN 136:14221 AN 2001:886737 CAPLUS

Patent Family Information

Abstract

A thin film transistor is disclosed, including an insulating substrate, a semiconductor layer formed on the insulating substrate, the semiconductor layer having an active region and an impurity region, a gate insulating layer formed on the active region of the semiconductor layer, a 1st gate metal layer formed on a predetd. portion of the active region of the semiconductor layer to define a channel region, and a 2nd gate metal layer formed on the 1st gate metal layer. The 1st and 2nd gate metal layers have different compns., such that the 2nd gate metal layer etches faster than the 1st gate metal layer, thereby preventing formation of a hillock. A 1st protective layer is formed over the structure, then a light shielding layer, and then a 2nd protective layer is formed over the light shielding layer.

Bibliographic Information

Application of anodization technology to liquid crystal displays. Mizutani, Fumikazu; Ue, Makoto. Tsukuba Research Center, Mitubishi Chemical Corporation, Ami-Inashiki, Ibaraki, Japan. Hyomen Kagaku (2001), 22(6), 376-381. CODEN: HYKAET ISSN: 0388-5321. Journal; General Review written in Japanese. CAN 135:160025 AN 2001:607129 CAPLUS

Abstract

Anodization technol. used in LCDs (Liq. Crystal Displays) is reviewed.(41 refs.). The wet anodization process has an advantage over other dry processes to produce thin oxide films with very smooth surface and less pinholes Aluminum or its alloy gate lines used in some TFT (Thin Film Transistor)-LCDs are covered with anodic oxide thin film to prevent their hillock formation and corrosion. On the other hand, anodic oxide films of tantalum or its alloys are also used as an insulator of non linear switching elements in TFD (Thin Film Diode)-LCDs. Anodization is carried out in aq. or nonaq. electrolyte solns. However, only limited electrolyte solns. have been used for manufg. TFT-LCDs. Here, we introduce our recent results on the anodization of sputtered Al-Nd alloy films in ethylene glycol-based nonaq. electrolyte solns.

Bibliographic Information

Study of the effect of grain boundary migration on hillock formation in Al thin films. Kim, Deok-kee; Nix, William D.; Vinci, Richard P.; Deal, Michael D.; Plummer, James D. Center for Integrated Systems, Stanford University, Stanford, CA, USA. Journal of Applied Physics (2001), 90(2), 781-788. CODEN: JAPIAU ISSN: 0021-8979. Journal written in English. CAN 135:230201 AN 2001:478290 CAPLUS

Abstract

The authors have studied the effect of grain boundary migration on hillock formation in unpassivated Al thin films during thermal cycling. Hillocking occurs more frequently in Al films that experience grain growth during thermal cycling than in films with stabilized grain structures. The hillocking frequency is at least four times greater in the films that experience grain growth, as judged by the no. of hillocks obsd. per initial grain boundary triple junction. This latter measure takes account of the smaller initial grain size in the film that experiences grain growth and shows that grain boundary migration itself must enhance the hillocking frequency.

Bibliographic Information

Aluminum alloy thin film electrodes in semiconductor devices and sputtering targets for deposition of thin films thereof. Takagi, Katsuji; Oniahi, Takashi. (Kobe Steel, Ltd., Japan). Jpn. Kokai Tokkyo Koho (2001), 15 pp. CODEN: JKXXAF JP 2001028348 A2 20010130 Patent written in Japanese. Application: JP 99-201650 19990715. CAN 134:140349 AN 2001:68293 CAPLUS

Patent Family Information

Abstract

The Al alloy thin film compn. contains CY ≥0.3, CIVa ≥0.2, and (0.3CY+3CIVa) ≤2 at.%, wherein CY and CIVa denote at.% for Y and Group IVA metal. Group IVA metal may be Ti, Zr, and/or Hf. The sputtering targets fulfilling the compn. of the thin film electrodes gives the electrodes low resistance, high hillock prevention, high void prevention, and high corrosion resistance against basic solns. The Al thin film electrodes may be useful for high precision LCDs.

Bibliographic Information

Suppression of hillock formation in thin aluminum films on semiconductor devices using multilayers. Raina, Kanwal K.; Zhang, Tianhong; McTeer, Allen. (Micron Technology, Inc., USA). U.S. (2000), 9 pp. CODEN: USXXAM US 6140701 A 20001031 Patent written in English. Application: US 99-387133 19990831. CAN 133:316504 AN 2000:769137 CAPLUS

Patent Family Information

Abstract

A multilayer structure is provided which suppresses hillock formation due to post-heat treatment steps in thin Al films deposited on other substrates by sandwiching the Al film between thin layers of Al Ti nitride. The 1st Al Ti nitride layer acts as a compatibilizing layer to provide a better match between the coeffs. of thermal expansion of the substrate and Al metal layer. The 2nd Al Ti nitride layer acts as a cap layer to suppress hillock formation.

Bibliographic Information

Diffusional hillock formation in Al thin films controlled by creep. Kim, Deok-Kee; Nix, William D.; Arzt, Eduard; Deal, Michael D.; Plummer, James D. Center for Integrated Systems, Stanford University, Stanford, CA, USA. Mater. Res. Soc. Symp. Proc. (2000), 594(Thin Films--Stresses and Mechanical Properties VIII), 129-134. CODEN: MRSPDH ISSN: 0272-9172. Journal written in English. CAN 133:353450 AN 2000:722740 CAPLUS

Abstract

Thermal hillocks in sputter-deposited Al films have been studied. Trace amts. of the impurities Ti, W, and O were incorporated into the films during deposition and caused them to be much stronger than most sputter-deposited Al films. Stress measurement during thermal cycling, using the wafer curvature method, showed that these Al films are high strength and was corroborated by hardness measurements. Microstructural studies using TEM and FIB showed that the hillocks start to form at the Al/SiO2 interface and grow under the original Al film having a columnar grain structure. In some cases, the film fails as hillocks grow completely through the original film. The Al film on top of the hillocks appears to inhibit hillock growth by creating a back pressure assocd. with power-law creep of the film. Hillock formation was modeled by modifying the boundary conditions in Chaudhari's hillock model (1974). The new model describes the hillock formation by diffusion of Al atoms from the surrounding area into isolated hillocks, assuming that the original Al film on top of hillocks deforms according to power-law creep. The model can be applied to many different situations by using different creep laws for the top Al film.

Bibliographic Information

Creep-controlled diffusional hillock formation in blanket aluminum thin films as a mechanism of stress relaxation. Kim, Deok-Kee; Nix, William D.; Deal, Michael D.; Plummer, James D. Center for Integrated Systems, Stanford University, Stanford, CA, USA. Journal of Materials Research (2000), 15(8), 1709-1718. CODEN: JMREEE ISSN: 0884-2914. Journal written in English. CAN 133:166994 AN 2000:557676 CAPLUS

Abstract

Hillock formation, a stress-induced diffusional relaxation process, was studied in sputter-deposited Al films. The grain sizes in these films were small compared to those in other sputter-deposited Al films, and impurities (O, Ti, W) were incorporated during the prepn. of the films. Stress and hardness measurements both indicate that the Al films were strengthened by the small grain size and incorporated impurities. We obsd. a new type of hillock in these Al thin films after annealing for 2 h at 450°C in a forming gas ambient. The hillocks were composed of large Al grains created between the substrate and the original Al film with its columnar grain structure, apparently by diffusion from the surrounding area. By modifying the boundary conditions of Chaudhari's hillock formation model, we have created a new model that can describe the exptl. obsd. hillocks. Our model seems to explain the exptl. obsd. abnormal hillock formation and may be applied to other types of hillock formation using different creep laws.

Bibliographic Information

Fabrication of a thin film transistor with a doped aluminum anodizing layer. Kim, Jung-hyun. (Lg Electronics Co., Ltd., S. Korea). Repub. Korea (1997), No pp. given. CODEN: KRXXFC KR

9706256 B1 19970425 Patent written in Korean. Application: KR 94-9408116 19940418. CAN 133:128547 AN 2000:546153 CAPLUS

Patent Family Information

Abstract

On a semitransparent substrate, a doped Al layer and an anode oxide film are sequentially formed. A Si oxide film is formed on the anode oxide film. An hydrogenated amorphous Si layer and a doped amorphous Si layer are formed on the Si oxide film. A nitride treatment film is interposed between the Si oxide film and the hydrogenated amorphous Si layer. Using the doped Al layer as the anodizing material, it is possible to prevent the generation of hillock. Also, using the anode oxide instead of a Si nitride, the reliability of the transistor is increased.

Bibliographic Information

Kinetics of hillock growth in Al and Al-alloys. Zaburowski, M. x.; Dumania, P. Institute of Electron Technology, Warsaw, Pol. Microelectron. Eng. (2000), 50(1-4), 301-309. CODEN: MIENEF ISSN: 0167-9317. Journal written in English. CAN 132:201514 AN 2000:10242 CAPLUS

Abstract

Hillock growth kinetics and size distribution were studied in Al, Al-Si 1% and Al-Si 1-Cu 0.5% layers. Metalization surface was examd. by optical, SEM and TEM microscopy, stylus profiling and an automatic method of hillock recognition from a microscope image. The method allowed for counting hillocks in a desired range of their diam. d. Surface d. of hillocks was measured as a function of time of furnace annealing at 400° and as a function of temp. of RTP annealing. A max. hillock size increases linearly with metalization layer thickness and with logarithm of annealing time. A total area occupied by hillocks was evaluated. Hillock d. decreased vs. 1/T with an activation energy of 0.28 eV for Al and 0.31 eV for Al-Si. A normalized hillock d. N may be expressed by N ≈ N0 exp(-cd), where d is hillock diam., N0 is the d. of hillocks of diam. close to 0, and c is the curve slope. Values for N0 and c are given together with a short discussion.

Bibliographic Information

Formation of aluminum thin film. Arai, Makoto; Ishibashi, Akira; Kiyota, Junya; Sughra, Isao; Hayashi, Yukiaki; Nakamura, Hajime; Hori, Takahide; Ohta, Yoshifumi. (ULVC Japan, Ltd., Japan). Jpn. Kokai Tokkyo Kobo (1999), 7 pp. CODEN: JKXXAF JP 11354469 A2 19991224 Heisei. Patent written in Japanese. Application: JP 98-163227 19980611. CAN 132:57892 AN 1999:814116 CAPLUS

Patent Family Information

Abstract

The thin film is formed on a substrate by sputtering an Al-contg. target with a sputtering gas in vacuum after applying weak high-frequency elec. power to the target. The process removes oxidizing gases from the sputtering target and substrate by plasma cleaning and prevents formation of hillocks on Al (alloy) thin-film wiring for semiconductor devices, display devices, etc.

Bibliographic Information

Aluminum gates including ion implanted composite layers for a thin film transistor. Hong, Mun-pyo. (Samsung Electronics Co., Ltd., S. Korea). U.S. (1999), 11 pp. CODEN: USXXAM US 5969386 A 19991019 Patent written in English. Application: US 97-940066 19970929. Priority: KR 96-9644015 19961004. CAN 131:280270 AN 1999:671055 CAPLUS

Patent Family Information

Abstract

An aluminum gate for a thin film transistor is fabricating by implanting ions into the exposed surface of the aluminum gate. The ions are preferably selected from the group consisting of nitrogen, carbon, oxygen and boron ions. A composite layer of aluminum and the implanted ions thereby formed at the exposed surface of the aluminum layer. Gates for thin film transistors, including an aluminum layer and a composite layer of aluminum and another element at the surface thereof can suppress hillocks in the aluminum gate which may be caused by compressive stresses during subsequent fabrication steps. The composite layer can have a low resistance and can allow a direct contact with an indium tin oxide conductive layer.

Bibliographic Information

Texture and grain boundary structure dependence of hillock formation in thin metal films. Nowell, Matthew M.; Field, David P. TexSEM Laboratories, Draper, UT, USA. Mater. Res. Soc. Symp. Proc. (1998), 516(Materials Reliability in Microelectronics VIII), 115-120. CODEN: MRSPDH ISSN: 0272-9172. Journal written in English. CAN 130:74321 AN 1998:779137 CAPLUS

Abstract

The development of hillocks on metal films during annealing is detrimental to downstream processing of integrated circuit structures. This work focuses upon the local character of texture and grain boundary structure near hillocks in metal films. It is apparent from the results that local grain boundary structure and texture strength are important parameters in identifying locations in the films that are preferentially susceptible to failure under given conditions. Results in aluminum and platinum films indicate that non-(111) oriented grains preferentially contain hillocks. In addn., (111) oriented grains with boundaries characterized by high angle rotations about random axes are prone to hillock formation.

Bibliographic Information

Hillock behavior on aluminum thin films deposited on polyimide film. Kang, Young-Seok. Center for Materials Science and Engineering, The University of Texas at Austin, Austin, TX, USA. Han'guk Chaolyo Hakhoechi (1998), 8(9), 802-806. CODEN: HCHAEU ISSN: 1225-0562. Journal written in English. CAN 130:74286 AN 1998:704210 CAPLUS

Abstract

Behavior of hillocks on Al films deposited on polyimide-coated SiO2 wafers was studied using an at. force microscopy with variation of the film thickness and annealing treatment. Growth hillocks were obsd. on as-received films and hillock d. was decreased while hillocks grew in size with the film thickness. After annealing, av. hillock size was increased but d. was decreased. The reduced hillock d. in these films is in contrast with the results from the films deposited directly on a rigid substrate. This is attributed to the presence of soft polyimide layer which relaxes the stress and thereby lacks the stress-induced grain boundary diffusion in Al films. Probably in this situation, no addnl. hillocks emerge and small hillocks are consumed by growing large hillocks.

Bibliographic Information

Structure engineering for hillock-free pure aluminum sputter deposition for gate and source line fabrication in active-matrix liquid crystal displays. Voutsas, Apostolos T.; Hibino, Yoshi; Pathe, Rajiv; Demaray, Ernest. Corporate Strategic Engineering Center, Sharp Microelectronics Technology, Incorporated, Camas, WA, USA. J. Vac. Sci. Technol., A (1998), 16(4), 2668-2677. CODEN: JVTAD6 ISSN: 0734-2101. Journal written in English. CAN 129:154634 AN 1998:437587 CAPLUS

Abstract

In this article we present the results of a study aimed at developing hillock-free, pure-Al thin-film material suitable for the fabrication of gate and source lines in thin film transistor active-matrix liq. crystal displays. Strong Al(111) texture was shown to be a key attribute for achieving good resistance to hillock formation. To obtain this strong Al(111) texture, we explored the incorporation of a thin metal layer, under the Al film, and we showed that Ti could be an appropriate candidate for further optimization. Key variables affecting the quality of Al were found to be the roughness of the glass substrate, the thickness of the titanium, the background vacuum quality, and the sputtering temp. By optimizing the deposition process for both Al and Ti layers, we showed that aluminum films with very strong (111) texture (rocking curve full width at half max. 0.86°), very smooth surface (root mean square surface roughness 1.8 nm), and a uniform, columnar grain size (0.3–0.5 μm) could be deposited by dc magnetron sputtering. In addn. to improving the aluminum microstructure, optimization of the gate dielec. process was also performed with the aim of reducing hillock formation. Combined optimization of the sputtering and gate dielec. deposition processes yielded an overall redn. in hillock d. of 3.5–4 orders of magnitude, without the need for anodic oxidn. or other means of capping the aluminum film. By combining Al/Ti dc sputtering, dry-etching technol. for one-step patterning of the composite Al/Ti film, and gate insulator deposition at 300 °C we demonstrated, for the first time, gate metalization technol. based on pure Al with excellent step coverage and ultralow hillock d. (<103 cm-2).

Bibliographic Information

Effect of Ti content on properties of Al-Ti alloy film for address lines of TFT-LCDs. Wu, Lijun; Xia, Hui; Liu, Anzheng; Han, Xue; Lu, Biao. General Res. Inst. Non-Ferrous Metals, Beijing, Peop. Rep. China. Rare Met. (Beijing) (1998), 17(2), 94-97. CODEN: RARME8 ISSN: 1001-0521. Journal written in English. CAN 129:102486 AN 1998:425740 CAPLUS

Abstract

Employing pure aluminum for address lines of TFT-LCDs (thin film transistor-liq. crystal display) has a severe problem of hillock formation at elevated temp. However, in the case of large TFT-LCDs more than 254 mm, it is impossible to use refractory metals for address lines because of their high resistivity. The Al-Ti alloy films for address lines of TFT-LCDs were studied and it was found that Al-Ti alloy film has excellent resistance of Al-Ti alloy to hillocks. The effect of Ti content on properties of Al-Ti alloy film was investigated.

Bibliographic Information

Nanostructural investigation of whiskers and hillocks of aluminum-based metallization in thin-film transistor liquid-crystal displays. Tsujimoto, Katsuhiro; Tsuji, Satoshi; Takatsuji, Hiroshi; Kuroda, Kotaro; Saka, Hiroyasu; Suzuki, Yukinobu. Display Technology, IBM Japan, Yamato, Japan. AIP Conf. Proc. (1998), 418(Stress Induced Phenomena in Metallization), 395-400. CODEN: APCPCS ISSN: 0094-243X. Journal written in English. CAN 128:224348 AN 1998:152114 CAPLUS

Abstract

The nanostructure of whiskers and hillocks in various aluminum-based thin films for thin-film transistor (TFT) on glass substrates has been investigated. The authors developed a novel technique to fabricate whiskers and hillocks artificially, using nanoindentation technique and annealing in a vacuum furnace. During the annealing, some Al whiskers and hillocks are formed, particularly on the edges of indentation marks. The high degree of whisker formation in this technique correlated to the weak hillock formation resistance in actual TFT arrays. Nanostructure of these thin films was investigated by cross-sectional TEM microscopy. The surface morphol. of as-deposited films was also investigated by at. force microscopy.

Bibliographic Information

Whisker growth on aluminum thin films during heat treatment. Hinode, Kenji; Homma, Yoshio; Sasaki, Yasushi. Central Research Laboratory, Hitachi, Ltd., Tokyo, Japan. AIP Conf. Proc. (1998), 418(Stress Induced Phenomena in Metallization), 359-370. CODEN: APCPCS ISSN: 0094-243X. Journal written in English. CAN 128:211024 AN 1998:152108 CAPLUS

Abstract

The authors studied whisker formation on Al films on Si substrates during heat treatments. Although both whiskers and hillocks are formed by the stress caused by thermal expansion mismatches, three addnl. conditions help induce whisker growth: (1) Contamination of films by O, N, or other contaminants from the residual sputtering atm. suppresses Al film grain growth during heat treatment, which causes highly localized film stress relief, resulting in whisker formation. (2) A nonoxidising atm., either a vacuum or inert gas, is required during the heat treatment. (3) Keeping the sample within a narrow temp. range (in the present case, 230-300°).

Bibliographic Information

Initial development of the lateral hillock distribution in optical quality Al thin films studied in real time. Kylner, C.; Mattsson, L. Department of Physics II (Optics), Royal Institute of Technology, Stockholm S-100 44, Swed. Thin Solid Films (1997), 307(1,2), 169-177. CODEN: THSFAP ISSN: 0040-6090. Journal written in English. CAN 128:94699 AN 1997:780979 CAPLUS

Abstract

The authors' previous studies using real-time total integrated scattering (TIS) showed a very distinct onset of hillock formation in optical quality Al films on Si wafers at temps. well <100°. This paper extends those studies by studying in real time the initial development of the lateral hillock distribution. After the 1st hillocks appeared the no. of hillocks accelerated rapidly with increased temp., in particular for higher heating rates. The lateral hillock distributions were further statistically analyzed by the Quadrate counts method to get more objective results. This anal. indicates that hillocks tend to be clustered over larger areas. The nearest neighbor distance between hillocks was also calcd. The hillocks had a tendency of lining up in distorted ring shaped patterns. This is interpreted as an effect of inhomogeneous stress distributions at the local grain level. The observations were made possible by using an imaging partial integrated scattering (PIS) system comprising of a dark field microscope objective and a charge coupled device (CCD) camera with an image processor and a data acquisition system.

Bibliographic Information

Nanocharacterization of texture and hillock formation in thin Al and Al-0.2%Cu films for thin-film transistors. Takatsuji, H.; Tsuji, S.; Kitahara, H.; Tsujimoto, K.; Kuroda, K.; Sake, H. IBM Japan Ltd., Display Technology, Shiga, Japan. Mater. Res. Soc. Symp. Proc. (1997), 441(Thin Films--Structure and Morphology), 415-420. CODEN: MRSPDH ISSN: 0272-9172. Journal written in English. CAN 127:255880 AN 1997:555299 CAPLUS

Abstract

The relation between the nanostructure of pure Al and Al-0.2 wt.% Cu thin films on glass substrates and anti-stress migration properties were investigated. These films were deposited on liq.-crystal display (LCD) grade glass substrate (550 × 650 mm) by means of two types of dc magnetron multi-chamber sputtering app. We developed the nanoindentation techniques to accelerate the characterization time for stress migration test. By AFM and cross-sectional TEM observations, we found an unusual three-layer structure in a Al-Cu thin film with strong anti-stress migration property.

Bibliographic Information

Microstructure control for thin film metallization. Was, G. S.; Srolovitz, D. J.; Ma, Z.; Liang, D. Nuclear Engineering and Radiological Sciences, University of Michigan, Ann Arbor, MI, USA. Mater. Res. Soc. Symp. Proc. (1997), 441(Thin Films--Structure and Morphology), 311-322. CODEN: MRSPDH ISSN: 0272-9172. Journal written in English. CAN 127:270899 AN 1997:555283 CAPLUS

Abstract

A strategy was developed for controlling hillock formation in thin metal films by controlling the fiber texture to be of a relatively weak orientation. Two-dimensional mol. dynamics (MD) simulations were performed to det. the parameter dependencies of texturing under ion beam assisted deposition. Simulations showed that even for film orientations that have a lower no. of nearest neighbor surface bonds, the redn. in sputtering rate by ion channeling will favor the growth of the grains aligned with their channeling direction in the direction of the ion beam. Higher energies should result in greater sputtering and a higher surface roughness. Confirmatory expts. were performed by growing Al films using ion beam assisted deposition in which the Ne ion beam was normal to the substrate surface. For all energies above 0 eV/atom, the fiber texture contained a (220) component and, at high normalized energies, the fiber texture was heavily (220) dominated. Subsequent annealing at 450° for 30 min resulted in hillock formation in the PVD (phys. vapor deposition) condition, a redn. in the hillock d. by two orders of magnitude in the 120 eV/atom condition and complete elimination of hillocking at >600 eV/atom. Although the surface roughness increased with ion beam energy as modeled by MD, the surface became smoother during annealing. The fiber texture can be controlled in a thin metal film in such a way as to eliminate hillock formation, mol. dynamics simulation is a valuable predictive tool for guiding expts. in the development of thin film microstructures and ion beam assisted deposition is an effective, practical tool for controlling microstructures of thin metal films.

Bibliographic Information

Effects of Nd content in Al thin films on hillock formation. Onishi, Takashi; Iwamura, Eiji; Takagi, Katsutoshi; Watanabe, Takashi. Electronics Research Laboratory, Kobe Steel, Ltd., Kobe, Japan. J. Vac. Sci. Technol., A (1997), 15(4), 2339-2348. CODEN: JVTAD6 ISSN: 0734-2101. Journal written in English. CAN 127:193804 AN 1997:482441 CAPLUS

Abstract

The effect of Nd content in Al films on hillock formation was investigated for applications of interconnections for thin film transistor crystal displays. It was found that the hillock d. of Al-Nd alloy films was strongly dependent on the Nd content, and the hillocks were completely suppressed in Al-2.0-6.0 at. % Nd alloy films. X-ray diffractometry, x-ray absorption fine-structure spectroscopy, and TEM indicated that the microstructures of Al-Nd alloy films strongly depend on the Nd content, and Al-2.0-6.0 at. % Nd alloy films form a stable solid soln. with a polycryst. α-Al-like structure. The results obtained from microstructural anal. were largely in agreement with hillock formation behavior. In this study, the excellent hillock resistance of Al-2.0-6.0 at. % Nd alloy films originates from solid-soln. hardening by the strongly distorted α-Al-like structure.

Bibliographic Information

Test structures for hillock growth, via filling and for measuring the quality of thin films. Bennett, D. J.; O'Hara, A.; Underwood, I.; Watson, A. J. Dep. Electrical Eng., Univ. Edinburgh, Edinburgh, UK. IEEE Int. Conf. Microelectron. Test Struct. Proc. (1997), 11-15. Publisher: Institute of Electrical and Electronics Engineers, New York, N. Y CODEN: 64KWAG Conference written in English. CAN 127:88752 AN 1997:362925 CAPLUS

Abstract

A test structure for assessing the quality of thin aluminum films is described. An anal. of the relationship between grain structure and hillock growth in small exposed areas of thin films during high temp.

processing shows that there is a relationship between hillock growth, grain size and grain boundary structure. The test structure consists of arrays of via holes of various sizes etched in a thin layer of SiO2 deposited at low temp. onto the metal surface. After furnace annealing, the no. of vias of each size which contain hillocks can be interpreted to obtain information on film quality.

Bibliographic Information

Relationship between the void and hillock formation and the grain growth in thin aluminum films. Konoenko, O. V.; Matveev, V. N. Institute Microelectronics Technology High Purity Materials, Russian Academy Sciences, Moscow, Russia. Mater. Res. Soc. Symp. Proc. (1997), 436(Thin Films: Stresses and Mechanical Properties VI), 423-428. CODEN: MRSPDH ISSN: 0272-9172. Journal written in English. CAN 126:285926 AN 1997:149846 CAPLUS

Abstract

Void and hillock formation during annealing was studied depending on the deposition conditions. Aluminum films were deposited onto oxidized silicon substrates by the self-ion assisted technique. The bias 0 or 6 kV was applied to the substrate during deposition. The films were then annealed in vacuum for 1 h in the temp. range from 150° to 550°C. The structure of the films was investigated by transmission electron microscopy. The void and hillock formation was studied with optical and scanning electron microscopes. It was found that recrystn. and void and hillock formation in the films depend on the bias during deposition. Normal grain growth occurred in the films deposited without bias. Abnormal grain growth was obsd. in the 6 kV-films. It was also found that the mechanism of stress relaxation during thermal cycling depends on the self-ion bombardment. In the films prepd. without bias, stress relaxation proceeds by diffusion creep. In the films deposited at the 6 kV bias, stress relaxation proceeds by plastic deformation.

Bibliographic Information

Relationship between the void and hillock formation and the grain growth in thin aluminum films. Konoenko, O. V.; Matveev, V. N. Inst. Microelectron Tech., Russian Acad. Sci., Chernogolovka, Russia. Mater. Res. Soc. Symp. Proc. (1996), 428(Materials Reliability in Microelectronics VI), 493-498. CODEN: MRSPDH ISSN: 0272-9172. Journal written in English. CAN 126:53759 AN 1996:741167 CAPLUS

Abstract

Void and hillock formation during annealing was studied depending on the deposition conditions. Al films were deposited onto oxidized Si substrates by the self-ion assisted technique. The bias 0 or 6 kV was applied to the substrate during deposition. The films were then annealed in vacuum for 1 h at 150-550°. The structure of the films was studied by TEM. The void and hillock formation was studied with optical and scanning electron microscopes. Recrystn. and void and hillock formation in the films depend on the bias during deposition. Normal grain growth occurred in the films deposited without bias. Abnormal grain growth was obsd. in the 6 kV-films. Also the mechanism of stress relaxation during thermal cycling depends on the self-ion bombardment. In the films prepd. without bias, stress relaxation proceeds by diffusion creep. In the films deposited at the 6 kV bias, stress relaxation proceeds by plastic deformation.

Bibliographic Information

Patterning of circuit associated with prevention of hillock formation on semiconductor device. Ogawa, Takashi. (Mitsumi Electric Co, Japan). Jpn. Kokai Tokkyo Koho (1996), 4 pp. CODEN: JKXXAF JP 08236531 A2 19960913 Heisei. Patent written in Japanese. Application: JP 95-65091 19950228. CAN 125:290830 AN 1996:664154 CAPLUS

Patent Family Information

Abstract

In formation of circuit by a process including following successive steps; (1) forming a metal layer on an oxide film on a semiconductor substrates, (2) forming a resist pattern as an etching mask, (3) forming a circuit pattern on the metal layer by removing the resist and the metal, and (4) forming a protecting film or interlayer insulating film, a thin film of the same substance as the protecting film or interlayer insulating film is formed on the metal layer, i.e., between step (1) and (2), which is supposed to be etching mask of the metal layer. Formation of hillock in sintering the metal layer is prevented and coverage of the protecting film or interlayer insulating film is improved in the process.

Bibliographic Information

Influence of adding transition metal elements to an aluminum target on electrical resistivity and hillock resistance in sputter-deposited aluminum alloy thin films. Onishi, Takashi; Iwamura, Eiji; Takagi, Kazutoshi; Yoshikawa, Kazuo. Electronics Research Laboratory, Kobe Steel, Ltd., Kobe, Japan. J. Vac. Sci. Technol., A (1996), 14(5), 2728-2735. CODEN: JVTAD6 ISSN: 0734-2101. Journal written in English. CAN 125:235280 AN 1996:594127 CAPLUS

Abstract

Effects of adding Group VIII transition metals (Fe, Co, and Ni) to an Al target on elec. resistivity and hillock suppression of sputter-deposit Al alloy films were studied. The group VIII transition metals and Al formed a complete series of metastable solid solns. in the as-deposited state. The solid solns. were decompd. into intermetallic compds., and the microstructures of the Al alloy films changed during annealing up to 300°. The elec. resistance of Al-Fe, Al-Co, and Al-Ni alloy films changed corresponding to the change in their microstructures, and markedly decreased to 5.0 μΩ cm at the pptn. points. The film stresses also changed corresponding to the change in the microstructure of the Al alloy films, and were abruptly relieved by pptn. of intermetallic compds. and grain growth. Since Al-Fe, Al-Co, and Al-Ni alloy films did not yield, they are highly resistant to hillock formation. The low elec. resistivity and the excellent resistance to hillock formation of Al-group VIII transition metal alloy films were explained from microstructural changes before and after annealing.

Bibliographic Information

Experimental study to validate a model of hillock formation in aluminum thin films. Genin, F. Y.; Slekhaus, W. J. Chemistry and Materials Science, Lawrence Livermore National Laboratory, Livermore, CA, USA. J. Appl. Phys. (1996), 79(7), 3560-6. CODEN: JAPIAU ISSN: 0021-8979. Journal written in English. CAN 124:275297 AN 1996:183255 CAPLUS

Abstract

The growth of holes and hillocks in thin films has been reported extensively and for a multitude of film-substrate systems. A recently developed model which analyzes the formation of a ridge at a traveling grain boundary due to stress and capillarity driving forces provides a quant. description of the growth of the hillocks. In order to test the model, the surface morphol. of aluminum thin films deposited on oxidized silicon substrates and annealed at 450° in argon is investigated; the profiles of thermal hillocks were measured by at. force microscopy. The comparison shows excellent agreement between modeled and exptl. profiles.

Bibliographic Information

Hillock-free multilayer metallic wires for high-performance thin-film printed circuits. (Xerox Corp., USA). Jpn. Kokai Tokkyo Koho (1995), 6 pp. CODEN: JKXXAF JP 07302792 A2 19951114 Heisei. Patent written in Japanese. Application: JP 95-95231 19950420. Priority: US 94-234897 19940428. CAN 124:73861 AN 1996:30041 CAPLUS

Patent Family Information

Abstract

The circuits have an alternately laminated base-metal/barrier-metal multilayer formed on a substrate, wherein the thickness of the base metal layers is thinner than that of the barrier metal layers. The arrangement prevents hillock formation without decreasing the metal layer sp. resistance.

Bibliographic Information

Use of fractals and kinetic equations to model thermally induced hillock formation and growth in thin metal films. Chaiken, J.; Goodisman, J. Dep. Chem., Syracuse Univ., Syracuse, NY, USA. Thin Solid Films (1995), 260(2), 243-51. CODEN: THSFAP ISSN: 0040-6090. Journal written in English. CAN 123:63069 AN 1995:640114 CAPLUS

Abstract

We investigated the applicability of a model based on fractals and the M.V. Smoluchowski (1916) kinetic equations to describe hillock formation in thin metal films. We have previously used this model to analyze cluster and ultrafine particle prodn. We show how to ext. two parameters from measured hillock size distributions which may reveal the scaling of the mobility of clusters and vacancies in films with varying hillock size. On the basis of our application of this model to certain data taken from the literature, the model shows considerable potential for being able to provide an internally consistent quant. basis for monitoring thermally driven mass redistribution processes in metal films.

Bibliographic Information

Substrate for thin film transistor array for liquid crystal display. Kubo, Akira. (Tokyo Shibaura Electric Co, Japan). Jpn. Kokai Tokkyo Koho (1994), 4 pp. CODEN: JKXXAF JP 06301054 A2 19941028 Heisei. Patent written in Japanese. Application: JP 93-87160 19930414. CAN 122:174674 AN 1995:428843 CAPLUS

Patent Family Information

Abstract

In manufg. the title substrate for a thin film transistor array for a liq. crystal display by (1) forming a scanning line jointly serving as a gate electrode on an insulator substrate, (2) forming a semiconductor layer on the above gate electrode via an insulator layer, (3) forming on the semiconductor layer a signal line jointly serving as drain electrode and a drain electrode connected to the display electrode, the above scanning line serving as gate electrode is obtained by laminating a high-melting metal layer on an Al-base metal layer, alloying the metal layer surface with the above high-melting metal layer while simultaneously oxidizing the high-melting metal layer to form an oxide layer, and removing the oxide layer from the above insulator substrate. Al hillock formation is suppressed to prevent short-circuiting.

Bibliographic Information

Hillock formation during electromigration in Cu and Al thin films: three-dimensional grain growth. Gladkikh, A.; Lereah, Y.; Glickman, E.; Karpovski, M.; Palevski, A.; Schubert, J. Dep. Electronic Devices Materials, Tel Aviv Univ., Ramat Aviv, Israel. Appl. Phys. Lett. (1995), 66(10), 1214-15. CODEN: APPLAB ISSN: 0003-6951. Journal written in English. CAN 122:167232 AN 1995:408196 CAPLUS

Abstract

The evolution of microstructure in Al and Cu thin film lines during electromigration has been studied using

a transmission electron microscopy. Grain boundary migration was found to be critically involved in the electromigration induced hillock formation that can be described as a three-dimensional growth of a single grain.

Bibliographic Information

Formation of aluminum thin-films. Tsuda, Yoshiki; Yasui, Hideaki. (Matsushita Electric Ind Co Ltd, Japan). Jpn. Kokai Tokkyo Koho (1994), 4 pp. CODEN: JKXXAF JP 06145962 A2 19940527 Heisei. Patent written in Japanese. Application: JP 92-296833 19921106. CAN 122:44090 AN 1995:283167 CAPLUS

Patent Family Information

Abstract

Title formation involves depositing an Al-Si alloy thin film on a substrate followed by an Al thin-film on the alloy film, wherein the thickness of the Al film is 50-70 nm. The double layer Al conductor film prevents abnormal growth of Al crystals for prepn. of smooth Al film surface without hillocks.

Bibliographic Information

Thin-film transistor having aluminum-containing gate electrode. Itoida, Satoshi. (Nippon Electric Co, Japan). Jpn. Kokai Tokkyo Koho (1993), 4 pp. CODEN: JKXXAF JP 05299655 A2 19931112 Heisei. Patent written in Japanese. Application: JP 92-86812 19920408. CAN 120:122735 AN 1994:122735 CAPLUS

Patent Family Information

Abstract

In the transistor consisting of a gate electrode, an elec. insulating film, a semiconductor layer, and a source-drain electrode, the gate electrode comprises a bilayer contg. Al and an Al-base alloy and optionally a part of the insulating film comprises an anodized film of Al and Al alloy. The transistor showed good hillock and stress-migration resistance.

Bibliographic Information

Correlation between grain growth and hillock growth in thin thermally annealed aluminum-1% silicon films on silicon substrates. Gerth, D.; Kaiser, D.; Schwarzer, R. Inst. Festkoerperphys. Elektronenmikrosk., Halle, Germany. Mater. Sci. Forum (1992), 94-96(Grain Growth Polycryst. Mater., Pt. 2), 557-62. CODEN: MSFOEP ISSN: 0255-5476. Journal written in English. CAN 118:64544 AN 1993:64544 CAPLUS

Abstract

The mutual relation between grain and hillock growth in Al-1%Si films on oxidized Si substrates was studied by electron microscopy. The grain specific textures of the Al alloy films were detd. by evaluation of Kikuchi patterns. The orientations of hillocks and adjacent grains were compared with the texture of the film. The shapes of the hillocks were revealed by electron microscopy. An example is given of the correlation between hillock growth and grain growth during the in situ investigation. The thermally-induced stresses, vertical strains, strain energies and shear stresses on the glide planes in the glide directions of the dislocations of differently oriented grains and hillocks were calcd. The relationship between these locally varying quantities in the polycryst. film and the exptl. results of grain growth and hillock growth is discussed considering the possible micromechanisms of stress relaxation. It is assumed that the location and height of hillocks is detd. by stress gradients. Local stress is relaxed by dislocation movement and diffusional mass transport on grain boundaries.

Bibliographic Information

Thin-film transistor having double-layered electrode. Naito, Hideo. (Casio Computer Co., Ltd., Japan). *Jpn. Kokai Tokkyo Koho* (1992), 8 pp. CODEN: JKXXAF JP 04188770 A2 19920707 Heisei. Patent written in Japanese. Application: JP 90-315774 19901122. CAN 117:162356 AN 1992:562356 CAPLUS

Patent Family Information

Abstract

In the transistor consisting of a glass substrate coated with a gate electrode, a gate insulating film, a semiconductor layer, and a source-drain electrode, the lower electrode of the gate electrode and the source-drain electrode consists of a hard metal lower film and a Ti-contg. Al upper film. The transistor had low hillocks and low decrease of insulation breakage voltage.

Bibliographic Information

Manufacture of aluminum thin film by sputtering. Kakiuchi, Koji. (Seiko Instruments and Electronics, Ltd., Japan). *Jpn. Kokai Tokkyo Koho* (1991), 3 pp. CODEN: JKXXAF JP 03166722 A2 19910718 Heisei. Patent written in Japanese. Application: JP 89-306415 19891127. CAN 115:196191 AN 1991:596191 CAPLUS

Patent Family Information

Abstract

The Al (contg. ≤1% impurity) film is manufd. by sputtering with cooling a substrate. A MOS device showed no hillock on the Al thin film surface.

Bibliographic Information

Characterization of the early stages of electromigration at grain boundary triple junctions. Genut, M.; Li, Z.; Bauer, C. L.; Mahajan, S.; Tang, P. F.; Milnes, A. G. Dep. Metall. Eng. Mater. Sci., Carnegie Mellon Univ., Pittsburgh, PA, USA. *Appl. Phys. Lett.* (1991), 58(21), 2354-6. CODEN: APPLAB ISSN: 0003-6951. Journal written in English. CAN 115:19551 AN 1991:419551 CAPLUS

Abstract

The formation and growth of holes and hillocks at grain boundary triple junctions in thin-film conductors of gold on gallium arsenide and thin-film conductors of aluminum-1 wt.% silicon on (oxidized) silicon during the early stages of electromigration have been investigated through measurement of fractional change of elec. resistance ΔR/R and microstructural characterization by SEM and TEM. Each grain boundary triple junction is characterized by a unique structure factor ΔY, which defines the degree of cumulative flux divergence and, consequently, the degree of susceptibility to formation and growth of holes or hillocks. Resultant holes are characterized by a shape factor f, which defines the degree of noncircularity and, consequently, relates fractional change of hole area to ΔR/R. Ests. of the upper limit for ΔY and the av. value of f are in good agreement with measured values of ΔR/R and consistent with obsd. microstructure.

Bibliographic Information

A transmission electron microscopy study of hillocks in thin aluminum films. Ericson, Fredric; Kristensen, Nils; Schweitz, Jan Aake; Smith, Ulf. Mater. Sci. Div., Uppsala Univ., Uppsala, Swed. *J. Vac. Sci. Technol., B* (1991), 9(1), 58-63. CODEN: JVTBD9 ISSN: 0734-211X. Journal written in

English. CAN 114:130016 AN 1991:130016 CAPLUS

Abstract

Hillocks, small outgrowths on a film surface, form when compressional stresses in an Al film are relaxed at ≥90°, for instance during the phase of rising temp. in an annealing cycle. This paper reports a study of hillock formation in Al films of thicknesses in the interval 0.25-2.2 μm which have been deposited by electron beam evapn. Hillock sizes, shapes, no. and formation temps. were detd., the latter on a heating stage in situ in a SEM. The internal structure of the hillocks was studied by cross-sectional TEM technique. These studies provided strong support for the idea that hillocks are formed by migration of material along grain boundaries, presumably at triple junctions, up to the surface where it is deposited in a growing hillock. Initially, the hillocks are sepd. from the original film surface by a grain boundary-like interface, but prolonged annealing will cause underlaying grains to grow into the hillocks, until they become integrated in the film.

Bibliographic Information

Influence of heat-treatment temperature and aluminum thickness on hillocks formation in thin aluminum films. Zletanovic, D.; Davinic, G. Elektron. Ind., RO "El-Mikroelektronika", Nis, Yugoslavia. Vacuum (1990), 40(1-2), 157-9. CODEN: VACUAV ISSN: 0042-207X. Journal written in English. CAN 112:221478 AN 1990:221478 CAPLUS

Abstract

The effect of heat-treatment temp. and thickness on hillock formation in Al-0.5 Si thin films vacuum deposited by sputtering onto Si and SiO2 surfaces was studied. Surface roughness was measured by using stylus-surface profilometry. The hillock d. and size were measured by using optical microscopy and SEM, resp. Hillock growth is affected both by heat-treatment temp. and film thickness.

Bibliographic Information

A study of heating rate and texture influences on annealing hillocks by a statistical characterization of aluminum thin-film topography. Baccouche, B.; Lormand, G.; Papapietro, M.; Achard, M.; Papon, A. M. CEA, IRDI, Grenoble, Fr. J. Appl. Phys. (1988), 64(11), 6483-9. CODEN: JAPIAU ISSN: 0021-8979. Journal written in English. CAN 110:86381 AN 1989:86381 CAPLUS

Abstract

In order to study the quant. influence of thin-film elaboration conditions on annealing hillock characteristics, an original statistical anal. of profilometer recording was performed. It allows, with suitable hypothesis on hillock shape, a detn. of the true hillock vol. per unit area. On various annealed Al-Si-Ti films this vol. decreases when the degree of preferred orientation increases. On both Al and Al-Si-Ti films an increase of heating rate induces a decrease of hillock vol. A stress relaxation model was developed where relative relaxing mechanism contributions are computed vs. grain size and heating rate. Exptl. results integrated through this model confirm the preponderance of grain boundary diffusion mechanisms in mass transport during hillock growth. The correlation between preferred orientation and hillock vol. in Al-Si-Ti films was related to both grain boundary diffusivity and grain size. The absence of small hillocks on high-temp. deposited Al-Si-Ti films is discussed.

Bibliographic Information

Ion beam suppression of hillock growth in aluminum thin films. Peacock, N. Br. Telecom Res. Lab., Ipswich, UK. Thin Solid Films (1988), 156(1), 173-80. CODEN: THSFAP ISSN: 0040-6090. Journal written in English. CAN 108:119557 AN 1988:119557 CAPLUS

Abstract

Ion irradn. as a method of hillock suppression in Al thin films was investigated. Implants of Ar, As, B and Si at doses between 1.6 × 1013 and 1.6 × 1016 ions/cm2 and at energies between 30 and 180 keV were used. A mechanism for the effects of different doses and species on hillock growth is proposed. Ar ion implantation at 120 keV to a dose of 5 × 1014 ions/cm2, or at 30 keV to a dose of 1.6 × 1015 ions/cm2, offers a practical method of hillock suppression on first level metal in silicon device wafers.

Bibliographic Information

Hillock growth in thin aluminum films. Mashita, Masao. Tokyo Shibaura Electr. Ltd., Kawasaki, Japan. Shinku (1972), 15(6), 196-204. CODEN: SHINAM Journal; General Review written in Japanese. CAN 77:117217 AN 1972:517217 CAPLUS

Abstract

A review, is given on formation, growth, and inhibition of hillocks of thin Al films for integrated circuits. 29 refs.

Bibliographic Information

Morphology of void-hillock formation at transverse scratches in aluminum thin film. Howard, J. K.; Rosa, Rupert Foster. Components Div., IBM, Hopewell Junction, N. Y., USA. J. Appl. Phys. (1971), 42(7), 2996-8. CODEN: JAPIAU Journal written in English. CAN 75:55201 AN 1971:455201 CAPLUS

Abstract

Photoprocessed Al films subjected to elec. stresses showed shallow surface scratches with hillocks agglomerated on the cathode side of the scratch, and voids clustering on the anode side. The shallow scratches formed prior or during the photoprocessing. The polarity of the void-hillock structures is caused to grain-boundary diffusion. The asymmetry in the void-hillock no. d. is due to a temp. gradient and elec.-field effect.

Bibliographic Information

Hillock-free aluminum thin films for electronic devices. Sato, Kikuji; Oi, Tetsu; Matsumura, Haruo; Okubo, Toshio; Nishimura, Takeo. Cent. Res. Lab., Hitachi Ltd., Tokyo, Japan. Met. Trans. (1971), 2(3), 691-7. CODEN: MTGTBF Journal written in English. CAN 74:132028 AN 1971:132028 CAPLUS

Abstract

The addn. of an alloying element was proposed to suppress hillocks which grow on the surface of deposited Al conductors after they were subjected to thermal cycling (200° to room temp.) or high-temp. heat treatment (400°). The alloying element, Sn, which has a small diffusion coeff., a large binding energy with a lattice vacancy, and a large at. diam., and Mn, which has a relatively small solid soly. in Al, were evaluated since they also have proper values of vapor pressure for ease of evapn. with Al. Alloy compn. was detd. to be just above the solid soly. of the element in Al at deposition temp. of 350°. It was proved expti. that Al-0.05 wt.% Sn and Al-0.1 wt.% Mn, which had been selected for the above-mentioned reason, had a marked effect in suppressing the growth of hillocks.

PERGAMON

Microelectronics Reliability 39 (1999) 1631–1645

MICROELECTRONICS RELIABILITY

www.elsevier.com/locate/microrel

Electromigration induced aluminum atom migration retarding by grain boundary structure stabilization and copper doping

M. Hasunuma*, H. Toyoda, H. Kaneko

ULSI Process Engineering Laboratory, Microelectronics Engineering Laboratory, Toshiba Corp., Semiconductor Company, 8 Shinsugita-cho, Isogo-ku, Yokohama 235-8522, Japan

Received 18 February 1999

Abstract

In order to clarify the relationship between Al line reliability and film microstructure, most notably grain boundary structure, we have tested three kinds of highly textured Al lines, namely a single-crystal Al line, a quasi single-crystal Al line and a hyper-textured Al line. Consequently, it has been shown that these kinds of lines have excellent endurance against electromigration (EM), compared with conventional Al lines deposited on TiN/Ti and SiO_2. The improvement of Al line reliability is attributable to the following factors; firstly, homogeneous microstructure and high activation energy, 1.28 eV, of the single-crystal Al line ($\omega = 0.18°$); secondly, subgrain boundaries, consisting of dislocation arrays found in the quasi single-crystal Al line ($\omega = 0.26°$), have turned out to be no more effective mass transport paths because dislocation lines are perpendicular to the direction of electron wind; finally, the decrease of the (1 1 1) full width at half maximum (FWHM) value promotes the formation of subgrain boundaries and low-angle boundaries, which have small grain boundary diffusivity, as revealed by the detailed orientation analysis of individual grains in the hyper-textured line (FWHM=0.5°) formed by using an amorphous Ta–Al underlayer (Toyoda H, Kawanoue T, Hasunuma M, Kaneko H, Miyauchi M. Proc. 32nd Ann. Int. Reliab. Phys. Symp., IEEE, 1994;178). Moreover, the diffusivity reduction and the uniformity of atomic flux result in the suppression of void/hillock pair in the Al lines. It has been clarified that a FWHM value is a useful criterion of reliability for an interconnection. Also, the Cu doping effect against EM endurance by using Cu implantation of the single-crystal Al lines has been examined. It has been clarified that EM lifetime is lengthened by about one order of magnitude for the Cu concentration of 0.1 at% in spite of almost the same diffusion coefficients. Moreover, the incubation time for a void nucleation has been observed even in the case of a pure-Al line. Thus, in accordance with the stress evolution model, it is concluded that the mechanism of lifetime improvement by Cu doping is such that critical stress for EM void nucleation is increased by the Cu doping. These results have confirmed that control of texture and/or grain boundary structure so as to suppress EM induced metal atom migration is a promising approach for the development of Al lines and Cu lines capable of withstanding the higher current densities required in future ULSIs.

1. Introduction

Open circuit failure of Al line induced by EM and/or thermal stress has become a more serious reliability

* Corresponding author.
E-mail address: hasunuma@amc.toshiba.co.jp (M. Hasunuma).

0026-2714/99/$ - see front matter
PII: S0026-2714(99)00167-5

problem due to current density increase and line width shrinkage in accordance with the progressive miniaturization of ULSIs. To improve the endurance of metal lines against EM, many efforts have been focused on seeking new alloying elements, such as Al–Si–Ti [2], Al–Cu–Ti [3], Al–Pd–Si [4] and Al–Sc [5] alloys, or on employing a layered-structure with TiW and TiN/Ti underlying barrier metals [6,7]. From the viewpoint of Al film microstructure, efforts to facilitate bamboo alternation by abnormal grain growth [8] or rapid thermal annealing [9] and (1 1 1) texture improvement have stimulated basic research to elucidate the role of grain boundaries. Although recent research has revealed that (1 1 1) texture improvement lengthens EM lifetime [1,10,11], the mechanism of the improvement has not been completely understood.

Stress induced open failure has also become a serious concern. Although this failure had appeared to be settled by utilizing refractory metal barrier layer, it has been clarified that stress induced voids degrade the EM lifetime [12,13]. Originally, stress induced failure is due to high tensile stress induced in metal lines because of the thermal expansion mismatch between Al and SiO_2, and is well predicted by the power-law creep model [14]. However, these results do not indicate how to improve the endurance, because the creep only takes into account the macroscopic physical properties. Therefore, a microscopic understanding of void growth and open failures is essential.

Transmission electron microscopy (TEM) and scanning electron microscopy (SEM) observations of real-time and/or in-situ voiding phenomena have already revealed the relationship between the surfaces surrounding voids and the specific crystal planes, such as (1 1 1), (1 0 0) [13,15]. Moreover, according to the thermodynamic analysis of the nucleation and growth of void formation in bamboo-like structure lines, the critical free energy change for void nucleation is a function of the grain boundary energy and its energy change is small for high energy grain boundary, i.e., random grain boundary [16]. This analysis strongly suggests that in order to achieve reliable Al lines, it is necessary to remove the specific grain boundary that leads to slit-like open failure where (1 1 1) planes of adjoining grains contact almost face to face [17,18]. It has also been pointed out that grain boundary energy decrease prevents a nucleation of void, and a single-crystal metal line is an ultimate product since it does not include any fast diffusion paths for void growth [18,19]. Therefore, the control of grain boundary structure is indispensable in order to obtain a guiding principle for realizing reliable metal lines.

On the other hand, in the case of polycrystalline lines, Cu doping has been found to markedly improve EM and SM endurance [20–22]. An Al(Cu) alloy system is known to be a precipitate hardening system in bulk materials. However, the role of Cu respecting this film has not been clarified, i.e., the grain boundary diffusion suppression by $CuAl_2$ precipitates [20] or solute drag effects on dislocations by Cu solute [21].

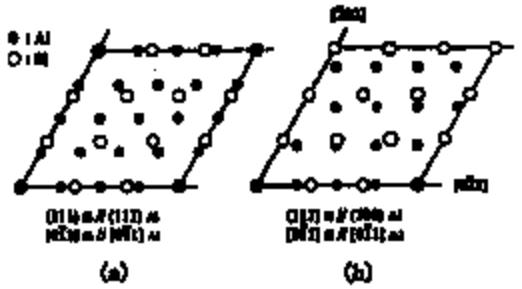

Fig. 1. (a) Schematic diagram showing the superlattice for the Al(1 1 1)/Si(1 1 1) interface. In this model, four Al lattice spacings match three Si lattice spacings; (b) one of the superlattices for the Al(1 0 0)/Si(1 1 1) interface. Only [0 −1 1] direction matches. Open circles and solid circles indicate the position of Si lattice and Al lattice, respectively.

This paper aims to clarify the relationship between EM reliability and microstructure for three kinds of films and the effect of Cu doping of a single-crystal Al film: firstly, a single-crystal Al (further denoted as s-Al) film deposited directly onto the Si(1 1 1) substrate by the CVD technique [23]; secondly, a quasi single-crystal Al (further denoted as qs-Al) film deposited directly onto Si(1 1 1) substrate [24,25], and containing subgrain boundaries with the lowest grain boundary energy; thirdly, a hyper-textured Al (further denoted as ht-Al) film developed using an amorphous Ta–Al underlayer [1]; and finally, a Cu doped single-crystal Al (further denoted as s-Al(Cu)) in which case the s-Al film was prepared prior to Cu ion implantation. The FWHM values of the (1 1 1) rocking curve were 0.18° for an s-Al film, 0.26° for a qs-Al film, and 0.5° for an ht-Al film. The amount of doped Cu was 0.1 at%, within solid solubility. In the ht-Al film, many subgrain boundaries with a homogeneous and low grain boundary energy were found. The mutual orientation of adjacent grains has been determined by TEM analysis. In the case of the ht-Al film it is possible to analyze the grain boundary structure by such a simple method, because the grain boundary structure is simplified by eliminating the twist angle component.

Furthermore, hyper-textured Cu (further denoted as ht-Cu) films, the most promising interconnection for future metallization, have been achieved by means of the same concept as the ht-Al films with several kinds of amorphous underlayers.

Fig. 2. Cross-sectional lattice image of Al(1 1 1)/Si(1 1 1) interface. An aluminum film deposited by GTC-CVD technique. Incident electron beam is parallel to Si [1 1 0] direction.

2. Film preparation

2.1. Single-crystal Al film (s-Al film)

An s-Al film was directly deposited onto clean Si(1 1 1) substrate by the gas-temperature-controlled chemical vapor deposition technique (GTC-CVD) [23]. Fig. 1(a) shows a schematic diagram of the common superlattice for the Al(1 1 1)/Si(1 1 1) interface. In this model, four Al lattice spacings are matched to three Si lattice spacings along the [1 1 0] direction, because the lattice constant mismatch between Al(1 1 1) (d = 2.338 Å) and Si(1 1 1) (d = 3.135 Å) is approximately 25%. The closed circles and open circles represent the positions of Al and Si atom, respectively. A cross-sectional lattice image is shown in Fig. 2. The arrows indicate possible atom matching points, which have a periodicity of every three Si lattice spacings, which is the same as the relationship shown in the schematic diagram of Fig. 1(a). From the electron diffraction analysis, the epitaxial relation between Al and Si was Al(1 1 1) // Si(1 1 1) and Al [1−1 0] // Si [1−1 0] [24,25], as shown in Fig. 1(a).

The degree of the crystallinity was evaluated by the FWHM value of the rocking curve for the Al(1 1 1) peak. The rocking curve was measured by 4-crystal collimated x-ray diffraction using the CuK_α radiation by scanning an incident angle θ, while the diffraction angle 2θ was fixed for the Al(1 1 1) peak. The FWHM value of 400 nm thick s-Al film was 0.18°.

2.2. Quasi single-crystal Al film (qs-Al film)

Al films were deposited onto Si(1 1 1) substrate by RF–DC coupled magnetron sputtering system at ambient temperature. It has been found that the Al film growth by sputtering consists of three stages of different texture. The Al film textures were examined by reflection high-energy electron diffraction (RHEED) in the chamber without breaking vacuum.

Fig. 3 shows the change in the epitaxial structure during the deposition by RHEED. In the initial stage, when the film thickness is no more than 10 nm, Al layer consists of three types of (1 0 0)-oriented domains that were rotated approximately 30° with respect to each other in accordance with the following relations: Al(1 0 0) // Si(1 1 1), Al[0 1 1] // Si[−2 1 1]: Al(1 0 0) // Si(1 1 1), Al[0 1 1] // Si[−1 1 0] (as shown in Fig. 1(b)): Al(1 0 0) // Si(1 1 1), Al[0 1 1] // Si[−1 2 −1] [24]. No pattern of (1 1 1) texture has been observed in the initial stage. In the second stage, the film thickness ranges from 10 to 100 nm, and the Al (1 1 1) domain which includes twins was observed in addition to the three kinds of Al(1 0 0) domains. This

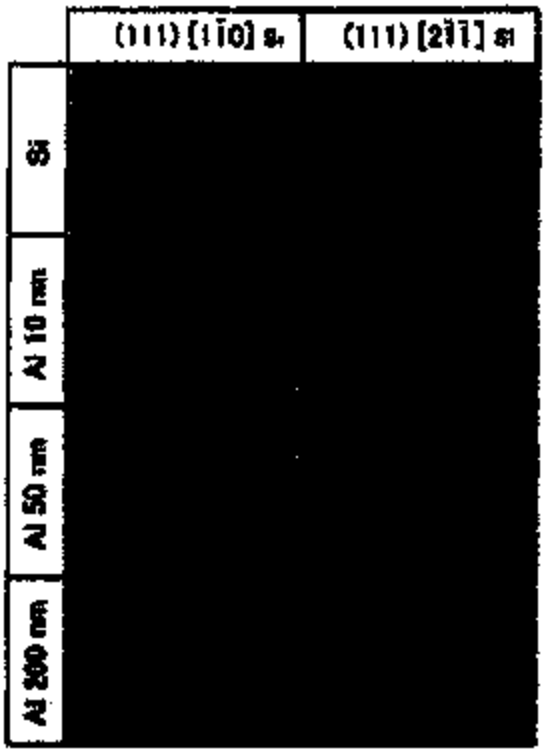

Fig. 3. In situ observation of Al epitaxial growth on Si(1 1 1) substrate by sputtering. In initial stage, three kinds of Al(1 0 0) domains were observed. Subsequently, the Al(1 1 1) domains grew by reorientation of the Al(1 0 0) domains. Finally, only the Al(1 1 1) structure remained.

Al(1 1 1) domain would be formed by the coalescence of the three kinds of Al(1 0 0) domains or recrystallization triggered at the Al / Si interface. A lot of Al(1 0 0) domains remained in the film. In the final stage, when the film thickness exceeds a few hundreds of nm, Al(1 1 1) // Si(1 1 1), Al[0 1 1] // Si[0 1 1] relation was completed. This dynamic structural change caused the subgrain boundaries in the qs-Al film. The FWHM value of 400 nm qs-Al film was 0.26°. This value is slightly larger than that of s-Al film. Fig. 4 shows the bright-field image and the diffraction pattern. The arc-like diffuse scattering near the [1 1 0] spots in the diffraction pattern indicates that there exists angular misorientation. In the TEM bright-field image, subgrain boundaries with periodic arrays of strain-field contrasts are observed. These subgrain boundaries are parallel to the {1 1 0} plane. Assuming that these dislocations are pure tilt type subgrain boundaries, the rotation angle between the two adjacent grains would be less than a few degrees.

Fig. 4. A bright-field image and a selective area diffraction pattern of the 400 nm thick qs-Al film deposited by sputtering. Many dislocation arrays were observed.

2.3. Cu-doped single-crystal Al film (s-Al(Cu) film)

An s-Al(Cu) film was prepared by Cu ion implantation into an s-Al film deposited by the GTC–CVD technique. Cu ion implantation was carried out with the acceleration voltages of 370 keV and 2.4×10^{15} ions/cm^2. The concentration of 400 nm thick s-Al(Cu) film is 0.1 at%Cu, which was near the solid solubility in Al matrix at 250°C [26]. Thus, at the EM acceleration test temperature which includes the Joule heating

Fig. 5. A bright-field image and selective area diffraction patterns of the 400 nm thick s-Al(Cu) film deposited by GTC–CVD technique and subsequently implanted with Cu. In SAD on grain boundary, some streaks attributed to GP-zone were observed at ambient temperature.

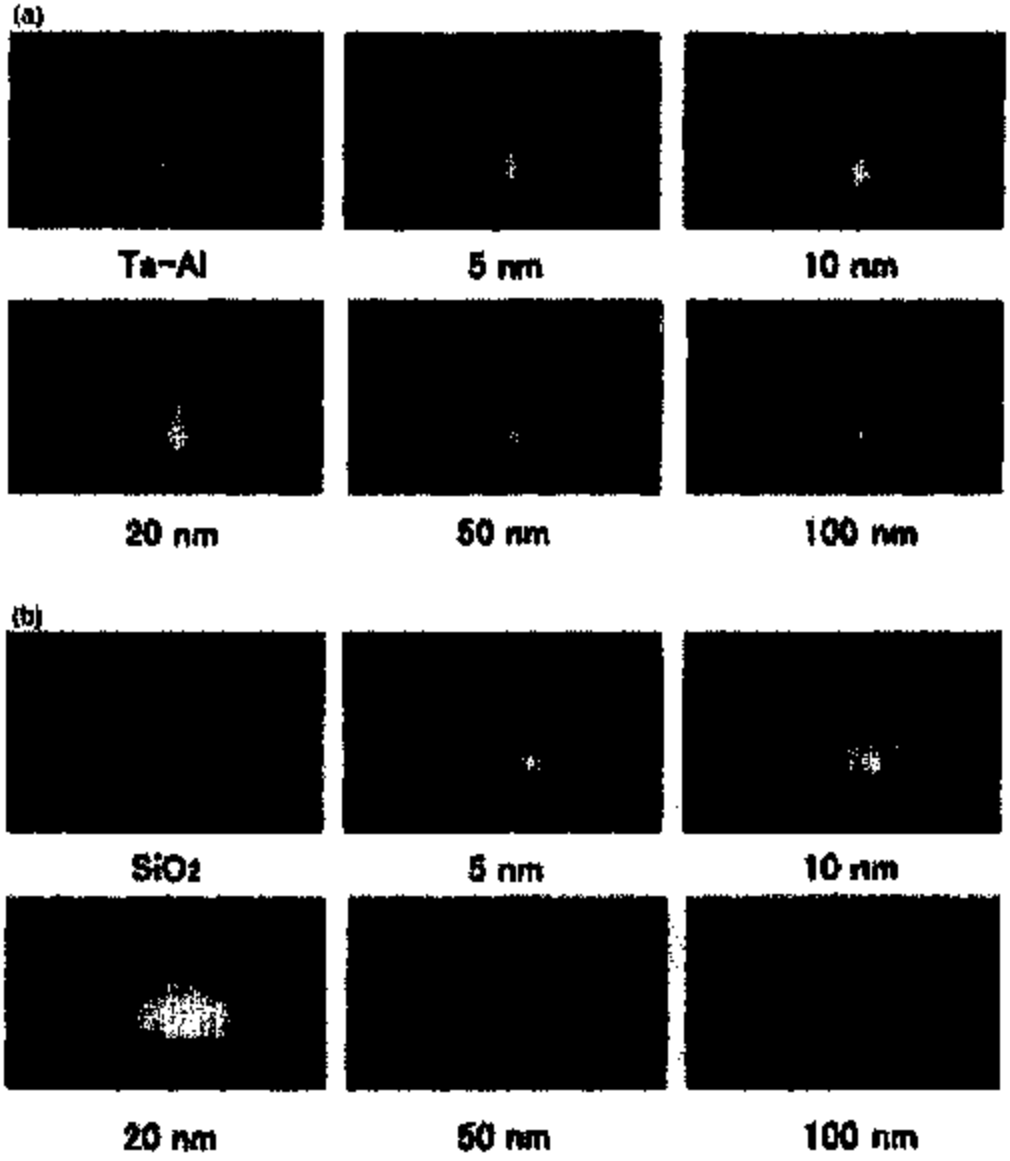

Fig. 6. (a) In situ RHEED observation results of growth of Al deposited on the amorphous Ta–Al underlayer; (b) In situ RHEED observation results of growth of Al deposited on SiO_2.

factor, the Cu elements almost dissolve into the Al matrix. A post thermal treatment of 30 min at 400°C was carried out in order to remove lattice defects introduced by ion implantation process and to homogenize Cu distribution.

Fig. 5 shows the top-view image and a selective area diffraction patterns (SADs) of s-Al(Cu). A subgrain boundary was also observed in this film. This dislocation array might be produced by recovery of various lattice defects introduced by ion implantation process. In the SAD, some streaks attributable to GP-zone were observed only near the subgrain boundary area at room temperature and precipitated during cooling process after the acceleration test. It shows that Cu strongly interacts with lattice defects in Al films. From the results of the x-ray analysis using $\sin^2\Psi$ method, the compressive stress of the Cu implanted film was 30 MPa. Consequently, the tensile stress varied to approximately 150 MPa after thermal treatment.

Therefore, the s-Al(Cu) film microstructure is almost

the same as that of the c-Al film except for containing small amounts of subgrain boundaries.

2.4. Hyper-textured Al films (ht-Al films)

An ht-Al film was developed using an amorphous underlayer [1]. An Al–0.1 at%Cu film deposited on Ta–Al amorphous underlayer indicated an FWHM value of 0.5°. This ht-Al line made it possible to estimate the effect of the texture on the EM lifetime in regions ranging from a conventional polycrystal to a single-crystal.

At the early stage of the film growth, Al islands are formed on a substrate, and they coalesce and become a continuous film as in the case of a cp-Al film on Si(1 1 1). According to the classical theory, the shape of the island is determined by Young's equation. The relation is expressed as

$$\cos\theta = \frac{\sigma_s - \sigma_i}{\sigma_f} \qquad (1)$$

where θ is the wetting angle of the island, σ_s and σ_f are the surface energies of the substrate and the island, respectively, and σ_i is the interfacial energy between the island and the substrate. When $\sigma_s - \sigma_i > \sigma_f$, it is considered that the film grows two-dimensionally (layer-growth). By this layer-growth mode, it is expected that two-dimensional (2D) island with stable (1 1 1) surface would be formed. An amorphous substrate will enhance this tendency, because there is no specific crystal lattice matching restriction between a film and a substrate that obstructs the stable (1 1 1) 2D-island formation. Assuming that the (1 1 1) texture of the film is improved by approaching the layer-growth mode, high σ_s and low σ_i are preferable for realizing a small wetting angle according to Eq. (1). The effect of the surface energy on the texture of the Al film for amorphous underlayers was investigated, because the origin of σ_i on an amorphous substrate still remains unknown. The surface energy of an amorphous alloy was assumed to be the sum of the fractional surface energies of individual elements.

Various kinds of amorphous and polycrystalline 100 nm thick underlayers were deposited on thermally oxidized Si substrates. Al films were deposited and examined using the same methods as for cp-Al film.

Fig. 6 shows the RHEED patterns for the Al films on the amorphous 75 at%Ta–25 at%Al alloy (Fig. 6(a)) and SiO_2 (Fig. 6(b)), which are observed for various kinds of Al film thickness. The patterns on both amorphous underlayers exhibited a (1 1 1) texture even for 5 nm thickness film and the pattern on Ta–Al was sharper than that on SiO_2, and this tendency was the same for the thicker films. Furthermore, the texture of Al films improved with increasing thickness, and by post annealing. Thus, it has been proved that the texture improvement will be accompanied with grain growth. Al–0.1 at%Cu films showed a better texture than pure Al films probably because σ_f in Eq. (1) decreases by Cu addition. A sintered 400 nm Al(Cu) film on Ta–Al indicated an FWHM value of 0.5°. The FWHM values of 20 nm thick Al films on various underlayers are plotted against the surface energy of the underlayers in Fig. 7. No clear relation was found between the FWHM value and the surface energy on polycrystalline underlayer. This scattering of the texture might be due to both lattice mismatch and the difference in the underlayer texture. On the other

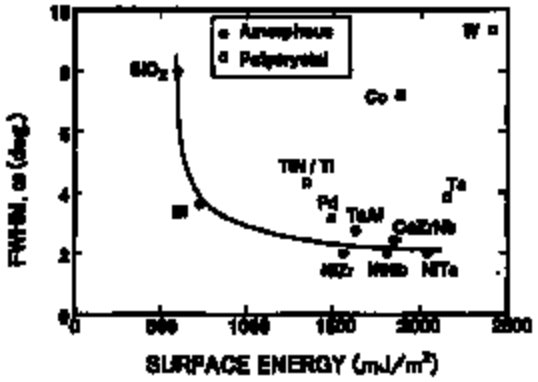

Fig. 7. The relationship between surface energy of underlayer and the FWHM values of 20 nm thick Al films deposited on the underlayers. The open squares and closed circles indicate polycrystalline underlayers and amorphous underlayers, respectively.

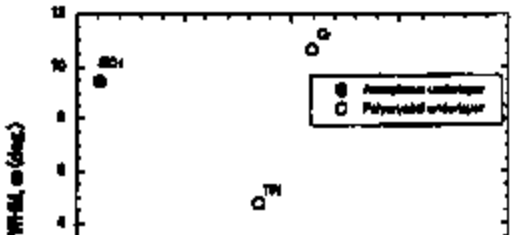

Fig. 8. The relationship between surface energy of underlayer and the FWHM values of 100 nm thick Cu films deposited on the underlayers. The open circles and closed circles indicate polycrystalline underlayers and amorphous underlayers, respectively.

Fig. 9. SEM photographs of the s-Al line after EM accelerated test for 19 h.

hand, the FWHM value for the Al film decreased with an increase in the surface energy for amorphous underlayers. These results confirmed that both a high surface energy and an amorphous state are necessary for improving the texture. It is also considered that the interfacial energy σ_i is uniform and might be small for amorphous underlayers.

2.5. Hyper-textured Cu films (Hyper-textured Cu films)

Ht-Cu films were also developed using amorphous underlayers. The concept of ht-Cu film development is the same as that of ht-Al films. Fig. 8 shows the relation between the (1 1 1) FWHM value for the Cu 100 nm thick film and the surface energy of the amorphous underlayer. The (1 1 1) FWHM values for Cu films deposited onto polycrystalline underlayers, i.e., Cr, TiN, and amorphous underlayer which has low surface energy were all above 4°, and Cu (2 0 0) peak was observed by the θ–2θ X-ray diffraction method in these lower textured films. On the other hand, the (1 1 1) FWHM values for Cu films deposited onto the metallic amorphous underlayers that have relatively high surface energy were approximately 1° and no other peaks were detected. With respect to the Nb underlayer, Nakasaki et al. calculated the interfacial energy as a sum of interatomic potential energies [27]. The Cu (1 1 1) and Nb (1 1 0) were expected to show the epitaxial relationship with a Nishiyama–Wassermann (NW) relationship with fcc [1−1 0] // bcc [0 0 1] [27], and the Cu film deposited onto (1 1 0) oriented polycrystalline Nb underlayer resulted in hyper-textured film. In the case of Cu crystal, an average surface energy is higher and the difference between surface energy of (1 1 1) and (2 0 0) is smaller than in the case of Al [28]. As a result, (2 0 0) compared with Al, Cu grains might be more easily grown during deposition of films. Thus, the lower textured Cu films and even the hyper-textured Cu film deposited onto the Nb underlayer had the mixed orientation with (1 1 1) and (2 0 0) grains. However, in the case of metallic amorphous underlayers, only hyper-textured (1 1 1) crystal grains were grown, even though the surface energy (σ_s) was nearly equal to the surface energy (σ_f) of Cu. It is considered that the interfacial energy (σ_i) between the metallic amorphous underlayer and Cu (1 1 1) might be very small.

3. Accelerated electromigration test procedure

The test lines were about 1.5 μm wide, 0.4 μm thick, and 50 μm long. The positive and the negative ends of the line were terminated with each 50 μm wide square pad without a taper and lines were unpassivated. The EM accelerated testing was carried out in a vacuum at pressures below 2×10^{-6} Torr. The acceleration conditions of films with high endurance to EM, i.e., s-Al and s-Al(Cu) lines, was 35 MA/cm^2 at 150°C ambient temperature. Under these severe conditions, conventional polycrystalline Al lines failed within a few seconds. The qs-Al and ht-Al were tested under the condition of 15 MA/cm^2 at 200°C and 5 MA/cm^2 at 200°C, respectively.

The EM induced damage, such as voids and hillocks, was examined after the accelerated test using SEM and TEM.

4. Results and discussion

4.1. Reliability of s-Al lines

The line operated at the electrical current density of

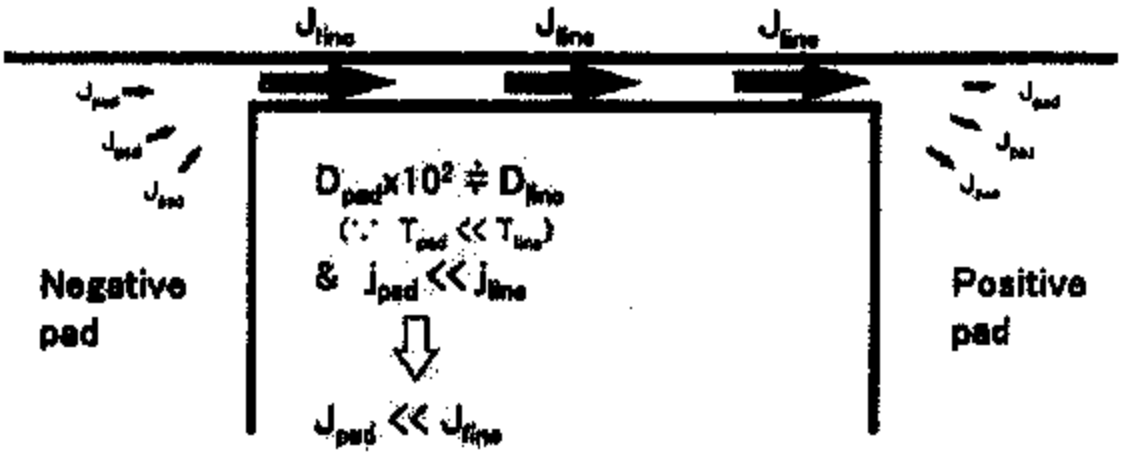

Fig. 10. Schematic diagram of highly accelerated EM test condition.

1 MA/cm^2 did not show any apparent EM damage at 150°C for 3000 h [17]. In order to obtain further acceleration, the lines were operated at a high current density of 35 MA/cm^2 in order to generate a steep temperature gradient at the junction between the line and the pad by Joule heating [29].

SEM photographs of an a-Al line after EM accelerated test for 19 h are shown in Fig. 9. Hillocks were formed mostly at the junction between the line and the positive pad and partly in the positive pad. Some hillocks were like a whisker and others were like a flat extrusion. On the other hand, voids were mostly accumulated in the negative pad and small voids were observed in the line near the negative pad. It is obvious from the void shape that the void is surrounded by {1 1 1} planes with the lowest surface energy in an fcc lattice. However, no voids were observed in the middle part of the line. These are the damage characteristics expected in the case that the temperature difference between the line and the pad is actualized by Joule heating. Actually, the average line temperatures monitored by the line electrical resistance range from 200 to 260°C. And the local temperature distribution generated by Joule heating was obtained by self-consistent finite element calculation [29]. In a typical case, the average temperature, line temperature and pad temperature were 240, 259 and 165°C, respectively.

Fig. 10 shows a schematic diagram of highly accelerated EM test condition. The temperature (T_{line}) of the line was about 100°C higher than that (T_{pad}) of the pad. It followed that the diffusion coefficient (D_{line}) of the line was more than two orders of magnitude higher than that (D_{pad}) of pad. Furthermore, the Al atoms in the line at higher current density (j_{line}) are subjected to a much higher stress (electron wind) than those at lower current density (j_{pad}) in the pad because of a shape factor. The migration in the line away from the line–pad junctions is much faster than that in the pad. The atomic flux of negative line–pad junction and that of positive line–pad junction produced atom depletion and atom accumulation, respectively. Thus, in spite of single-layered structure line, the principle of the atomic flux divergence is similar to that of W stud multiple layered line structure.

Fig. 11 shows the relationship between normalized electrical resistance change and elapsed time. The resistance initially decreased, next increased gradually,

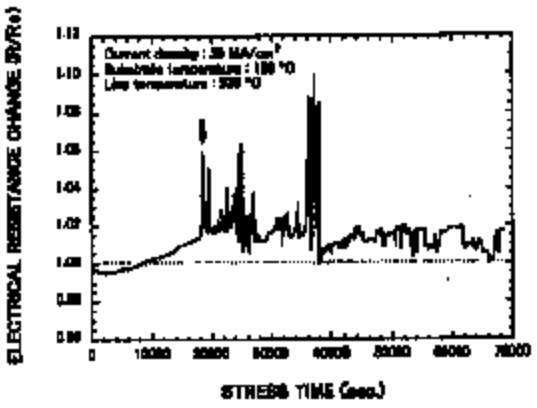

Fig. 11. Electrical resistance change for an a-Al line during EM accelerated testing with current density of 35 MA/cm^2.

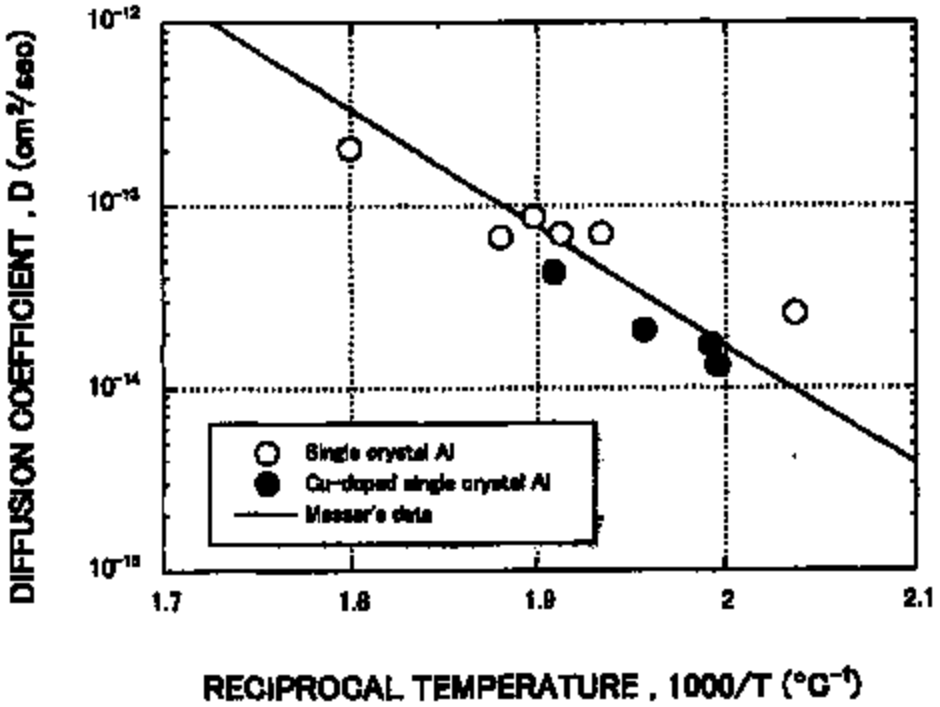

Fig. 12. Arrhenius plot of the Al diffusion coefficients obtained from void growth rate. The open circles and the closed circles indicate s-Al and s-Al(Cu), respectively, and solid line presents Mosser's data.

and finally oscillated violently. To clarify the behavior of initial resistance decrease, no current loading test was carried out. After keeping some EM test lines at 150°C for 15 h, the resistance decreased from 1.5 to 2.3% at ambient temperature, which might be caused by recovery of various kinds of lattice defects introduced by thermal cycle and/or Si precipitation. From in situ SEM observation, a void appearance and voids movement corresponded with the resistance increase and the resistance oscillation, respectively. In particular, the violent oscillation of electrical resistance might be caused by a serious void shape change and occasional jumping [30]. The initial decrease, the subsequent increase and final violent oscillation were considered to be due to the recovery and/or Si precipitation, voids growth near the negative pad and voids migration, respectively. Therefore, the beginning of violent oscillation is defined as the guideline of lifetime for s-Al, as shown by an arrow in Fig. 11.

Fig. 12 shows the Arrhenius plot of the obtained diffusion coefficients calculated from the void growth rate [9]. The EM-induced void volume was obtained from the sum of the volumes of individual voids based on the assumption that the voids completely penetrated the Si substrate surface. The Al atom flux divergence, div(J), which contributes to the void growth near the line–pad junction, is expressed as

$$\mathrm{div}(J) = (J(T_{\mathrm{line}}) - J(T_{\mathrm{pad}}))/\Delta x \tag{2}$$

where $J(T_{\mathrm{line}})$ and $J(T_{\mathrm{pad}})$ are the Al atom flux at line temperature (T_{line}) and at the line–pad junction temperature (T_{pad}), respectively, and Δx is the length of the temperature changing region, 10 μm, obtained by the finite element calculation. The experimentally obtained void growth rate dV/dt could be connected to Eq. (2) as

$$(dV/dt)N/S/\Delta x = \mathrm{div}(J) \tag{3}$$

where N is the atomic density of Al, and S is the cross-sectional area of line. An ideal Al atom flux induced by EM is also expressed by the Nernst–Einstein's relationship [31]. The flux is expressed as

$$J = DNZ^*e\rho j/kT \tag{4}$$

where D is the diffusion coefficient for Al, k the Boltzmann constant, T the absolute temperature, Z^* the effective charge number, e the elementary charge, ρ

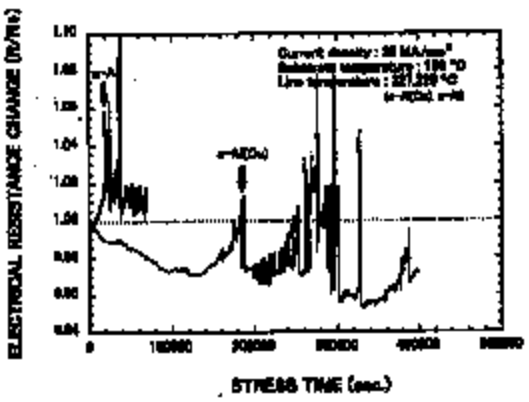

Fig. 13. Electrical resistance change for s-Al and s-Al(Cu) lines during EM accelerated testing with current density of 35 MA/cm^2.

the resistivity of Al and j the current density, respectively. The diffusion coefficients of Al were calculated from Eqs. (2)–(4). Open circles indicate the s-Al results. The straight line in this plot is the Al lattice diffusion coefficients with an activation energy of 1.28 eV and pre-exponential factor of 0.137 cm^2/s. A fairly good agreement was observed [32]. Consequently, it has been confirmed that the void growth in a s-Al line was by lattice diffusion control.

However, it is noteworthy that a fairly large amount of grown voids accumulated in the negative pads. The maximum Al atom flux divergence was generated near the negative pad where the steep temperature gradient existed. It is natural to expect that the EM-induced voids nucleate and grow in this area. However, the voids fully grown in the line near the negative pad moved into the negative pad and accumulated. This movement of the voids in s-Al lines is ascribed to their homogeneity, i.e., this film is free from trapping and/or flux divergent sites, such as grain boundaries. An s-Al line has excellent endurance against EM because of its homogeneous microstructure [17,25,29]. Consequently, the s-Al line survives an open circuit failure, and, in fact, no sample failed in the present experiment.

4.2. Reliability of s-Al(Cu) lines

The line resistance change behavior, the initial decrease, gradual increase and final violent oscillation, and the observed surface morphology of the s-Al(Cu) line after EM accelerated test were similar to the s-Al line (see Fig. 13), except for the following points:

1. The lifetime observed for the s-Al(Cu) line was approximately one order of magnitude longer than that for the s-Al.
2. The maximum resistance decrease for the s-Al(Cu) line was 3%, whereas the s-Al line resistance decrease was only 0.5%.
3. The resistance increase and decrease speeds for the s-Al(Cu) line were slower than those for the s-Al line.

It is noteworthy that the Cu doping is effective for prolonging the Al EM lifetime even though there are no grain boundaries. This result indicates that the EM lifetime improvement frequently observed in the case of Cu doped polycrystalline Al lines is not due to the diffusivity retardation by the $CuAl_2$ precipitation in the grain boundary [20]. Moreover, the Al diffusion coefficients both for the s-Al and the s-Al(Cu) lines, calculated by the void volume by using Eqs. (2)–(4) plotted in Fig. 12, differed slightly. Therefore, the Al lattice diffusion retardation by the Cu doping is not the dominant mechanism for the EM lifetime improvement. On the other hand, it is also interesting to note that the initial 3% resistance decrease observed for the s-Al(Cu) line was well explained by the Cu depletion, because the 0.1 at%Cu solution increases the Al line resistivity by almost the same amount (0.75 μΩ cm/at%Cu [33]). This hypothesis is consistent with the view of the Cu depletion proposed by Hu et al. [34]. However, it should be emphasized that the s-Al line had the incubation time for the void nucleation even though it was pure-Al and was not included in Hu's model.

Therefore, the tensile stress evolution near the negative end of line due to the absence of atom supply [35,36] should be taken into account in order to explain the incubation time for pure-Al line and to understand the effect of Cu doping. There is a critical stress that enables the void nucleation, and the incubation time is defined as the time for generating large enough tensile stress to permit nucleation. Since the present test lines were unpassivated, the tensile stresses contained in the s-Al and s-Al(Cu) line were small, approximately 150 Mpa. Therefore, the longer incubation time is necessary compared with the passivated Al line which has sufficiently large stress to nucleate a void before the EM current loading. Since the Al diffusivities both for the s-Al and the s-Al(Cu) line are almost the same, as shown in Fig. 12, the identical critical stress for the void nucleation should possess the same incubation time. Therefore, the longer incubation time for s-Al(Cu) is probably due to the critical stress increase. Similar Cu doping effect has been reported, namely only 0.1 wt%Cu doping was sufficient to improve the SM lifetime [22]. The decrease in the Al surface energy by Cu doping [28] also supports this hypothesis, because the lower surface energy increases the

Fig. 14. Bright-field image and selected area diffraction pattern of qs-Al line after EM acceleration test.

critical energy for the void nucleation. However, the large resistance decrease indicates that the Cu depletion did occur during EM testing, and the Cu depletion and/or the preferential Cu migration induced by EM always reduce the impact on the critical stress increase.

4.3. Reliability of qs-Al lines

Fig. 14 shows the microstructure of qs-Al line after EM accelerated test with the current density of 15 MA/cm^2 for 150 min and the line temperature of 200°C. Many subgrain boundaries consisting of dislocation arrays were observed, as described above. Fig. 15 shows SEM photographs after the EM accelerated test and (1 1 1) pole figure that is adjusted to the direction of the test line. In spite of this severe test condition, no voids and hillocks appeared in the middle of the line, though voids and many whisker-like hillocks formed in the negative pad and the positive pad, respectively. The voids formed in the negative pad were also surrounded by (1 1 1) planes. Thus, the endurance against EM of qs-Al line is essentially the same as that of s-Al line. In other words, subgrain boundaries do not behave as fast diffusing paths because the dislocation line of the subgrain boundary exists perpendicular to the electron wind. Moreover, the voids produced in the line near the negative pad were not immobilized by subgrain boundaries that possess lowest grain boundary energy.

4.4. Hypertextured Al lines (ht-Al line)

The measured electrical resistance changes of the lines during the tests are shown in Fig. 16. The initial increase in the resistance was due to Joule heating by current loading. The resistance of the sintered Al(Cu) line on Ta–Al increased less than 10% after 10 h. SEM photographs of the lines after 10% resistance increase are shown in Fig. 16, and for the sintered Al(Cu) line, a photograph of the line after 10 h accelerated testing is shown. Fewer defects were observed inside the Al(Cu) line, whereas many void-hillock pairs are found along the grain boundaries for the other lines. The grain size was smaller than the line width and grain-networks existed along the line direction. This means that the flux divergence at a triple point of grain boundaries is very small. It is known that grain boundary diffusivity depends on the boundary structure [37]. Al films that show no or broad texture have random grain boundaries, and the individual diffusivities of grain boundaries are quite different, and so the flux divergence occurred at a triple point and resulted in a void-hillock pair formation.

After 250 h current loading test, the resistivity change of the sintered Al(Cu) line increased to 7.5%. Most of the voids were formed inside the negative pad, which enables the vacancy flux estimation from the void volume. The obtained vacancy flux is 8.9×10^{17} m^{-2} s^{-1} and this value is the same order of magnitude as that in an s-Al line, 2.5×10^{17} m^{-2} s^{-1} [9]. Therefore, grain boundaries formed in ht-Al film are no more effective than those of conventional broad textured film as fast diffusion paths for mass-transport phenomenon by EM.

Furthermore, a detailed analysis of grain boundary structure was carried out by TEM. Fig. 17 shows the plan view of the Al(Cu) film and many subgrain boundaries were also observed in this film. The average grain size is 280 nm, but large scattering was observed in grain size. This fact suggests that the large grains have coarsened and unified because of the fairly good

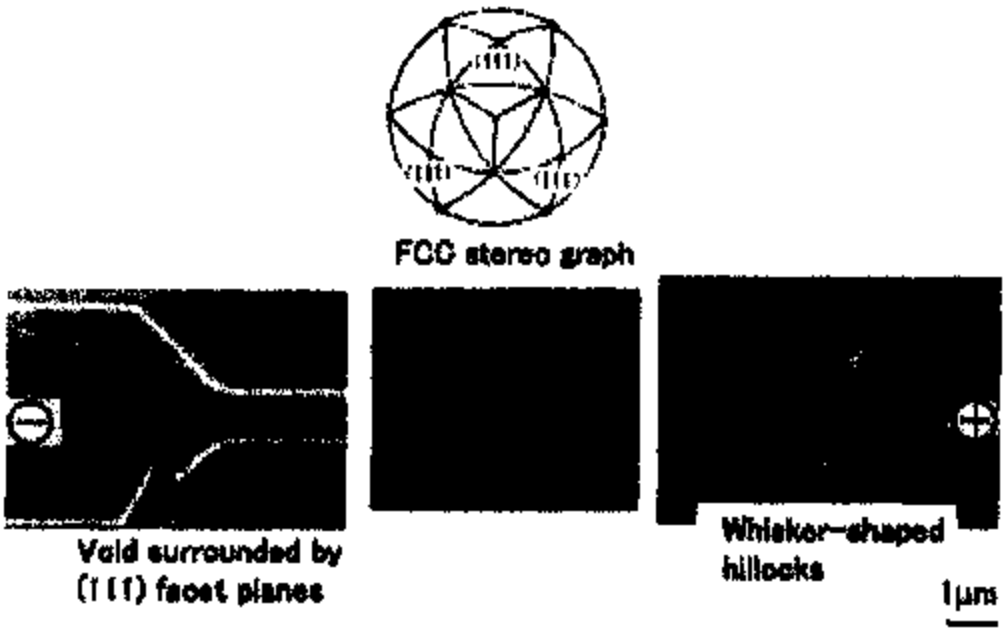

Fig. 15. SEM photograph of α-Al line after EM acceleration test.

orientation matching among the neighbor grains. The SADs of the individual grains are shown in Fig. 17 and it proves that all the grains have (1 1 1) orientation. Assuming that the grain boundaries are perpendicular to the substrate, the most stable plane is {1 1 0} for fcc structure. The angles between a grain boundary and the {1 1 0} planes of grains on both sides are measured to investigate the property of the grain boundary structure. The angles are defined to be positive when the deviation is counterclockwise and are restricted within 30° because of the crystallographic symmetry. Fifty-one grain boundaries are plotted in Fig. 18, and 18 boundaries are subgrain boundaries (35%) indicated by closed circles. The grain boundary on the line $\theta 1 = \theta 2$ is considered to be formed by the two grains which have the same orientation, and so

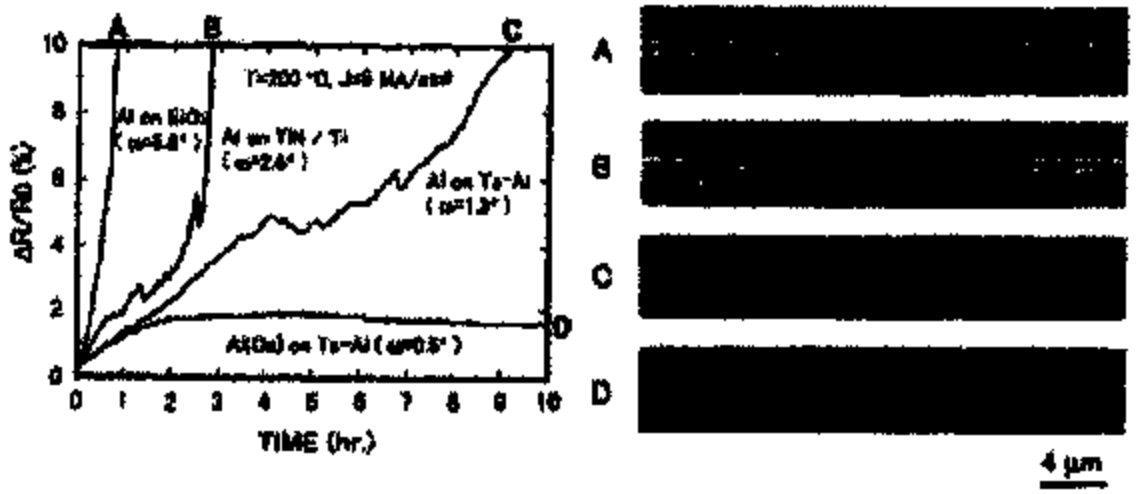

Fig. 16. Electrical resistance change for Al lines of various degree of (1 1 1) texture during EM acceleration test and morphology change after EM acceleration test.

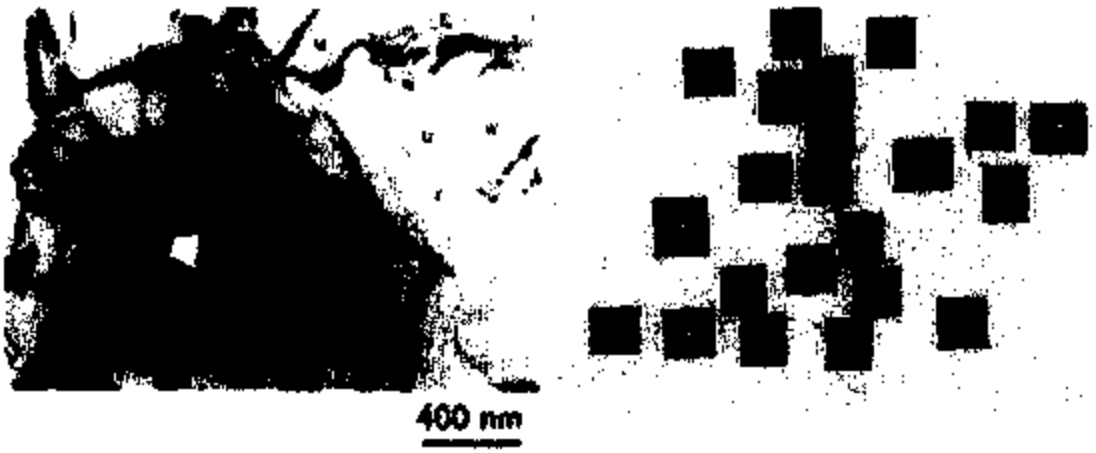

Fig. 17. Bright-field image and diffraction pattern of individual grains of ht-Al film deposited on Ta–Al underlayer.

the energy of the boundary is the lowest. On the other hand, the grain boundary on the dotted line $\theta 1 = -\theta 2$ is considered to form the symmetrical tilt-grain boundary. The grain boundary energy among (1 1 1) symmetrical tilt grain-boundary for fcc metal is reported by Wolf [38]. According to this simulation, the energy increases with tilt angle up to 10° (i.e., $\theta 1 = -5°$, $\theta 2 = 5°$) and the cusp exists at 60° (i.e., $\theta 1 = -30°$, $\theta 2 = 30°$). The former area corresponds to the hatched area and the latter point corresponds to the upper-left on the dotted line. As a result, the grain-boundary energy in the hatched area and on the upper-left point is relatively low compared with the random boundary, and almost half of the grain boundaries are included in this area for ht-Al film. These facts show that a hyper-texture not only eliminated the twist component of grain boundaries, but also changed the grain boundary to the low-angle boundary structure and reduced grain boundary energy. This grain boundary energy reduction would suppress the grain boundary diffusivities and the void's nucleation at a triple point in the ht-Al line. The EM lifetime of Al lines with different degree of texture ($\omega = 0.5$–7°) are plotted in Fig. 19. The obtained dependence of the lifetime τ on the FWHM value ω is [1]

$$\tau \propto \omega^{-2} \tag{3}$$

This empirical relation has revealed that the EM lifetime of the Al line is improved with a decrease in the FWHM value. From the detailed grain boundary analysis, it has been clarified that the grain boundaries found in ht-Al film were, on average, lower-grain boundaries than those of low textured films. This average tilt (misorientation) angle decrease would reduce the mass transportation along the boundaries and sup-

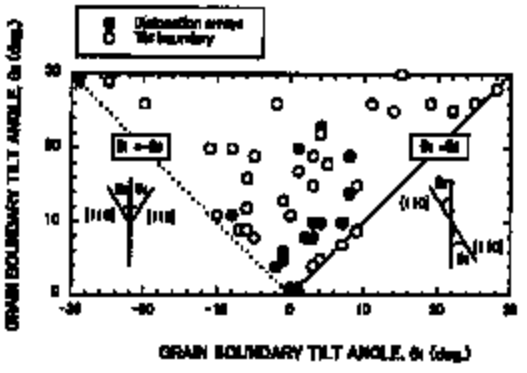

Fig. 18. Misorientation angle between the grains on both sides at grain boundary closed circle : dislocation array; open circle : tilt boundary.

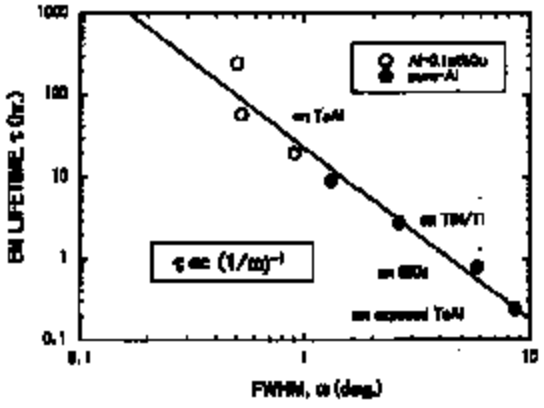

Fig. 19. Dependence of EM lifetime(τ) on the FWHM value (ω) of Al (1 1 1) rocking curve.

press the void and hillock formation at the triple points. The inverse proportionality of EM lifetime τ to the FWHM value ω suggests that the decrease in the average twist angle ω leads to the decrease in the average misorientation angle.

5. Conclusion

High reliability of single-crystal Al line ($\omega = 0.18°$) was ascribed to its homogeneous microstructure and the lattice diffusion controlled mass transport with the high activation energy of 1.28 eV. The quasi single-crystal Al line ($\omega = 0.26°$) essentially had the same endurance against EM as the single-crystal Al line, because subgrain boundaries found in this line never behaved as effective mass transport paths. The void movement was never disturbed by these subgrain boundaries, because of their lower boundary energy, i.e., a very small amount of defects along the boundary. It has been clarified that the grain boundaries found in hyper-textured Al film ($\omega = 0.5°$) were low-angle grain boundaries though this film still contained random boundaries. It has also been clarified that the texture improvement promoted the low-angle grain boundary formation. The atom and/or vacancy transportation along these boundaries has been found to be the same order of magnitude as that of the lattice diffusion. This reduction of atomic mass transport reduced the flux divergence at the triple points, i.e., void and hillock formation, and resulted in longer lifetime.

On the other hand, it has been concluded that the doping effect of Cu in Al matrix within solid solubility is due to the critical stress increase for the EM induced void nucleation, which markedly prolonged the incubation time of α-Al(Cu).

Finally, hyper-textured Cu films have been achieved by using several kinds of amorphous underlayers. The presence of the hyper-textured Cu film will guarantee the highly reliable metallization for the future ULSI.

Acknowledgements

The authors would like to thank Mrs. Ito, Mrs. Kohanawa, Mr. Kawanoue and Dr. Kometsu for help and discussion throughout this work. They are also grateful to Mr. Miyauchi, Dr. Iizuka, Dr. Hayasaka and Dr. Okumura for their encouragement.

References

[1] Toyoda H, Kawanoue T, Hasunuma M, Kaneko H, Miyauchi M. In: Proc. 32nd Ann. Int. Reliab. Phys. Symp., IEEE. 1994. p. 178.
[2] Towner JM, Darbo AG, Tien T. In: Proc. 24th Ann. Int. Reliab. Phys. Symp., IEEE. 1986. p. 7.
[3] Hosoda T, Yagi H, Tsuchikawa T. In: Proc. 27th Ann. Int. Reliab. Phys. Symp., IEEE. 1989. p. 202.
[4] Ozaki J, Koibuchi Y, Fukuda S, Sawa M, Minawa Y, Itagaki T. IEDM Tech. Dig., IEEE, 1988, p. 454.
[5] Ogawa S, Nishimura H. IEDM Tech. Dig., IEEE, 1991, p. 277.
[6] Lin T, Aha KY, Harper JME, Cheloux FN. In: IEEE VMIC Conf. 1990. p. 76.
[7] Hisode K, Hosoya Y. In: Proc. 28th Ann. Int. Reliab. Phys. Symp., IEEE. 1990. p. 25.
[8] Ho PS, Howard JK, White JF. J Appl Phys 1978;49:4083.
[9] Kawanoue T, Kaneko H, Hasunuma M, Miyauchi M. J Appl Phys 1993;74(7):4423.
[10] Vaidya S, Sinha AK. Thin Solid Films 1981;75:253.
[11] Knorr DB, Lu TM. Appl Phys Lett 1989;54:2210.
[12] Lyde SA, Oates AS. J Appl Phys 1992;71(1):174.
[13] Marieb TN, Abratowski E, Bravman JC, Maddux M, Filas P. In: Ho PS, Li CY, Totta P, editors, AIP Conf. Proc. No. 305, 1994, p. 1.
[14] Yue JT, Funston WP, Taylor RV. In: Proc. 23th Ann. Int. Reliab. Phys. Symp., IEEE. 1985. p. 1.
[15] Tanikawa, Okabayashi H, Mori H, Fujita H. Proc. 28th Ann. Int. Reliab. Phys. Symp., IEEE, 1990, p. 209.
[16] Kaneko H, Hasunuma M, Sawabe A, Kawanoue T, Kobanawa Y, Komatsu S, Miyauchi M. In: Proc. 28th Ann. Int. Reliab. Phys. Symp., IEEE. 1990. p. 194.
[17] Hasunuma M, Kaneko H, Sawabe A, Kawanoue T, Kobanawa Y, Komatsu S, Miyauchi M. IEDM Tech. Dig., IEEE, 1989, p. 677.
[18] Hisode K, Owada N, Nishida T, Mukai K. J Vac Sci Technol 1987;B5:518.
[19] Ganguler A, d'Heurle FM. Thin Solid Films 1973;16:227.
[20] d'Heurle FM. Met Trans 1971;2:683.
[21] Spolenak R, Kraft O, Arzt E. Microelectron Reliab 1998;38:1015.
[22] Mayumi S, Umemoto T, Shishiku M, Nanatsue H, Ueda S, Inoue M. In: Proc. 25th Ann. Int. Reliab. Phys. Symp., IEEE. 1987. p. 15.
[23] Kobayashi T, Saiguchi A, Akiyama N, Honokawa N, Asanuki T. J Vac Sci Technol 1992;A10:525.
[24] Yamada I, Inokawa H, Takagi T. J Appl Phys 1984;56:2746.
[25] d'Heurle F, Berenbaum L, Rosenberg R. Trans of AIME 1968;242:582.
[26] Murray JL. Int Met Rev 1985;30(5):211.
[27] Nakasaki Y, Minamikata G, Sagara K. J Appl Phys 1995;77:2454.
[28] Murr LE. Interfacial phenomena in metals and alloys. Reading: Addison-Wesley, 1975.
[29] Kaneko H, Kawanoue T, Hasunuma M, Miyauchi M. In: Ho PS, Li CY, Totta P, editors, AIP Conf. Proc. No. 305, 1994, p. 179.
[30] Shingubara S, Kaneko H, Saitoh M. In: Extended Abstracts of the 21st Conference on Solid State Devices and Materials, Tokyo. 1989. p. 33.

[31] Huntington HB, Grone AR. J Phys Chem Solids 1961;20:76.
[32] Meaner R, Dais S, Wolf D. In: Proc. 16th Ampere Congress (Nottingham, England). 1974.
[33] Bradley MJ, Slinger JI. Phys F 1974;4:839.
[34] Ho CK, Rosenberg R, Ts EN. In: Ho PS, Li CY, Tsui P, editors, AIP Conf. Proc. No. 305, 1994, p. 195.
[35] Blech IA, Herring C. Appl Phys Lett 1976;29:131.
[36] Korhonen MA, Borgesen P, Ts EN, Li CY. J Appl Phys 1993;73(8):3790.
[37] Balluffi RW. Met Trans 1982;13B:527.
[38] Wolf D. J Mater Res 1990;5:1708.

PERGAMON

Microelectronics Reliability 39 (1999) 1631–1645

MICROELECTRONICS RELIABILITY

www.elsevier.com/locate/microrel

Electromigration induced aluminum atom migration retarding by grain boundary structure stabilization and copper doping

M. Hasunuma*, H. Toyoda, H. Kaneko

ULSI Process Engineering Laboratory, Microelectronics Engineering Laboratory, Toshiba Corp., Semiconductor Company, 8 Shinsugita-cho, Isogo-ku, Yokohama 235-8522, Japan

Received 18 February 1999

Abstract

In order to clarify the relationship between Al line reliability and film microstructure, most notably grain boundary structure, we have tested three kinds of highly textured Al lines, namely a single-crystal Al line, a quasi single-crystal Al line and a hyper-textured Al line. Consequently, it has been shown that these kinds of lines have excellent endurance against electromigration (EM), compared with conventional Al lines deposited on TiN/Ti and SiO_2. The improvement of Al line reliability is attributable to the following factors; firstly, homogeneous microstructure and high activation energy, 1.2ff eV, of the single-crystal Al line ($\omega = 0.18°$); secondly, subgrain boundaries, consisting of dislocation arrays found in the quasi single-crystal Al line ($\omega = 0.26°$), have turned out to be no more effective mass transport paths because dislocation lines are perpendicular to the direction of electron wind; finally, the decrease of the (1 1 1) full width at half maximum (FWHM) value promotes the formation of subgrain boundaries and low-angle boundaries, which have small grain boundary diffusivity, as revealed by the detailed orientation analysis of individual grains in the hyper-textured line (FWHM = 0.5°) formed by using an amorphous Ta–Al underlayer (Toyoda H, Kawanoue T, Hasunuma M, Kaneko H, Miyauchi M. Proc. 32nd Ann. Int. Reliab. Phys. Symp., IEEE, 1994;178). Moreover, the diffusivity reduction and the uniformity of atomic flux result in the suppression of void/hillock pair in the Al lines. It has been clarified that a FWHM value is a useful criterion of reliability for an interconnection. Also, the Cu doping effect against EM endurance by using Cu implantation of the single-crystal Al lines has been examined. It has been clarified that EM lifetime is lengthened by about one order of magnitude for the Cu concentration of 0.1 at% in spite of almost the same diffusion coefficients. Moreover, the incubation time for a void nucleation has been observed even in the case of a pure-Al line. Thus, in accordance with the stress evolution model, it is concluded that the mechanism of lifetime improvement by Cu doping is such that critical stress for EM void nucleation is increased by the Cu doping. These results have confirmed that control of texture and/or grain boundary structure so as to suppress EM induced metal atom migration is a promising approach for the development of Al lines and Cu lines capable of withstanding the higher current densities required in future ULSIs.

1. Introduction

Open circuit failure of Al line induced by EM and/or thermal stress has become a more serious reliability

* Corresponding author.
E-mail address: hasunuma@sme.toshiba.co.jp (M. Hasunuma).

0026-2714/99/$ - see front matter
PII: S0026-2714(99)00167-5

problem due to current density increase and line width shrinkage in accordance with the progressive miniaturization of ULSIs. To improve the endurance of metal lines against EM, many efforts have been focused on seeking new alloying elements, such as Al–Si–Ti [2], Al–Cu–Ti [3], Al–Pd–Si [4] and Al–Sc [5] alloys, or on employing a layered-structure with TiW and TiN/Ti underlying barrier metals [6,7]. From the viewpoint of Al film microstructure, efforts to facilitate bamboo alternation by abnormal grain growth [8] or rapid thermal annealing [9] and (1 1 1) texture improvement have stimulated basic research to elucidate the role of grain boundaries. Although recent research has revealed that (1 1 1) texture improvement lengthens EM lifetime [1,10,11], the mechanism of the improvement has not been completely understood.

Stress induced open failure has also become a serious concern. Although this failure had appeared to be settled by utilizing refractory metal barrier layer, it has been clarified that stress induced voids degrade the EM lifetime [12,13]. Originally, stress induced failure is due to high tensile stress induced in metal lines because of the thermal expansion mismatch between Al and SiO_2, and is well predicted by the power-law creep model [14]. However, these results do not indicate how to improve the endurance, because the creep only takes into account the macroscopic physical properties. Therefore, a microscopic understanding of void growth and open failures is essential.

Transmission electron microscopy (TEM) and scanning electron microscopy (SEM) observations of real-time and/or in-situ voiding phenomena have already revealed the relationship between the surfaces surrounding voids and the specific crystal planes, such as {1 1 1}, {1 0 0} [13,15]. Moreover, according to the thermodynamic analysis of the nucleation and growth of void formation in bamboo-like structure lines, the critical free energy change for void nucleation is a function of the grain boundary energy and its energy change is small for high energy grain boundary, i.e., random grain boundary [16]. This analysis strongly suggests that in order to achieve reliable Al lines, it is necessary to remove the specific grain boundary that leads to slit-like open failure where {1 1 1} planes of adjoining grains contact almost face to face [17,18]. It has also been pointed out that grain boundary energy decrease prevents a nucleation of void, and a single-crystal metal line is an ultimate product since it does not include any fast diffusion paths for void growth [18,19]. Therefore, the control of grain boundary structure is indispensable in order to obtain a guiding principle for realizing reliable metal lines.

On the other hand, in the case of polycrystalline lines, Cu doping has been found to markedly improve EM and SM endurance [20–22]. An Al(Cu) alloy system is known to be a precipitate hardening system in bulk materials. However, the role of Cu respecting thin film has not been clarified, i.e., the grain boundary diffusion suppression by $CuAl_2$ precipitates [20] or solute drag effects on dislocations by Cu solute [21].

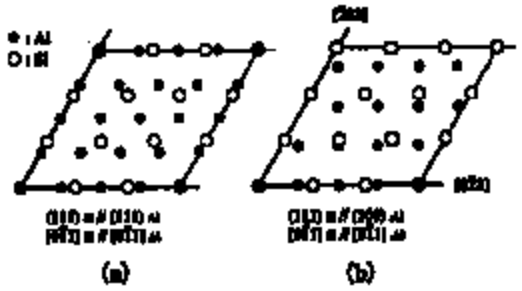

Fig. 1. (a) Schematic diagram showing the superlattice for the Al(1 1 1)/Si(1 1 1) interface. In this model, four Al lattice spacings match three Si lattice spacings; (b) one of the superlattices for the Al(1 0 0)/Si(1 1 1) interface. Only [0 −1 1] direction matches. Open circles and solid circles indicate the position of Si lattice and Al lattice, respectively.

This paper aims to clarify the relationship between EM reliability and microstructure for three kinds of films and the effect of Cu doping of a single-crystal Al film: firstly, a single-crystal Al (further denoted as s-Al) film deposited directly onto the Si(1 1 1) substrate by the CVD technique [23]; secondly, a quasi single-crystal Al (further denoted as qs-Al) film deposited directly onto Si(1 1 1) substrate [24,25], and containing subgrain boundaries with the lowest grain boundary energy; thirdly, a hyper-textured Al (further denoted as ht-Al) film developed using an amorphous Ta–Al underlayer [1]; and finally, a Cu doped single-crystal Al (further denoted as s-Al(Cu)) in which case the s-Al film was prepared prior to Cu ion implantation. The FWHM values of the (1 1 1) rocking curve were 0.18° for an s-Al film, 0.26° for a qs-Al film, and 0.5° for an ht-Al film. The amount of doped Cu was 0.1 at%, within solid solubility. In the ht-Al film, many subgrain boundaries with a homogeneous and low grain boundary energy were found. The mutual orientation of adjacent grains has been determined by TEM analysis. In the case of the ht-Al film it is possible to analyze the grain boundary structure by such a simple method, because the grain boundary structure is simplified by eliminating the twist angle component.

Furthermore, hyper-textured Cu (further denoted as ht-Cu) films, the most promising interconnection for future metallization, have been achieved by means of the same concept as the ht-Al films with several kinds of amorphous underlayers.

Fig. 2. Cross-sectional lattice image of Al(1 1 1)/Si(1 1 1) interface. An aluminum film deposited by GTC-CVD technique. Incident electron beam is parallel to Si [1 1 0] direction.

2. Film preparation

2.1. Single-crystal Al film (s-Al film)

An s-Al film was directly deposited onto clean Si(1 1 1) substrate by the gas-temperature-controlled chemical vapor deposition technique (GTC-CVD) [23]. Fig. 1(a) shows a schematic diagram of the common superlattice for the Al(1 1 1)/Si(1 1 1) interface. In this model, four Al lattice spacings are matched to three Si lattice spacings along the [1 1 0] direction, because the lattice constant mismatch between Al(1 1 1) (d = 2.338 Å) and Si(1 1 1) (d = 3.135 Å) is approximately 25%. The closed circles and open circles represent the positions of Al and Si atom, respectively. A cross-sectional lattice image is shown in Fig. 2. The arrows indicate possible atom matching points, which have a periodicity of every three Si lattice spacings, which is the same as the relationship shown in the schematic diagram of Fig. 1(a). From the electron diffraction analysis, the epitaxial relation between Al and Si was Al(1 1 1) // Si(1 1 1) and Al [1−1 0] // Si [1−1 0] [24,25], as shown in Fig. 1(a).

The degree of the crystallinity was evaluated by the FWHM value of the rocking curve for the Al(1 1 1) peak. The rocking curve was measured by 4-crystal collimated x-ray diffraction using the CuK_α radiation by scanning an incident angle θ, while the diffraction angle 2θ was fixed for the Al(1 1 1) peak. The FWHM value of 400 nm thick s-Al film was 0.18°.

2.2. Quasi single-crystal Al film (qs-Al film)

Al films were deposited onto Si(1 1 1) substrate by RF–DC coupled magnetron sputtering system at ambient temperature. It has been found that the Al film growth by sputtering consists of three stages of different texture. The Al film textures were examined by reflection high-energy electron diffraction (RHEED) in the chamber without breaking vacuum.

Fig. 3 shows the change in the epitaxial structure during the deposition by RHEED. In the initial stage, when the film thickness is no more than 10 nm, Al layer consists of three types of (1 0 0)-oriented domains that were rotated approximately 30° with respect to each other in accordance with the following relations: Al(1 0 0) // Si(1 1 1), Al[0 1 1] // Si[−2 1 1]; Al(1 0 0) // Si(1 1 1), Al[0 1 1] // Si[−1 1 0] (as shown in Fig. 1(b)): Al(1 0 0) // Si(1 1 1), Al[0 1 1] // Si[−1 2 −1] [24]. No pattern of (1 1 1) texture has been observed in the initial stage. In the second stage, the film thickness ranges from 10 to 100 nm, and the Al (1 1 1) domain which includes twins was observed in addition to the three kinds of Al(1 0 0) domains. This

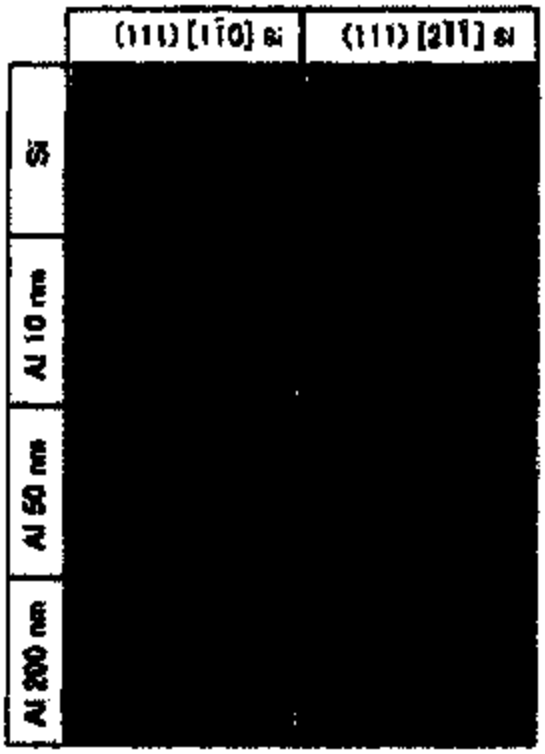

Fig. 3. In situ observation of Al epitaxial growth on Si(1 1 1) substrate by sputtering. In initial stage, three kinds of Al(1 0 0) domains were observed. Subsequently, the Al(1 1 1) domains grew by reorientation of the Al(1 0 0) domains. Finally, only the Al(1 1 1) structure remained.

Al(1 1 1) domain would be formed by the coalescence of the three kinds of Al(1 0 0) domains or recrystallization triggered at the Al / Si interface. A lot of Al(1 0 0) domains remained in the film. In the final stage, when the film thickness exceeds a few hundreds of nm, Al(1 1 1) // Si(1 1 1), Al[0 1 1] // Si[0 1 1] relation was completed. This dynamic structural change caused the subgrain boundaries in the qs-Al film. The FWHM value of 400 nm qs-Al film was 0.26°. This value is slightly larger than that of s-Al film. Fig. 4 shows the bright-field image and the diffraction pattern. The arc-like diffuse scattering near the [1 1 0] spots in the diffraction pattern indicates that there exists angular misorientation. In the TEM bright-field image, subgrain boundaries with periodic arrays of strain-field contrasts are observed. These subgrain boundaries are parallel to the {1 1 0} plane. Assuming that these dislocations are pure tilt type subgrain boundaries, the rotation angle between the two adjacent grains would be less than a few degrees.

Fig. 4. A bright-field image and a selective area diffraction pattern of the 400 nm thick qs-Al film deposited by sputtering. Many dislocation arrays were observed.

2.3. Cu-doped single-crystal Al film (s-Al(Cu) film)

An s-Al(Cu) film was prepared by Cu ion implantation into an s-Al film deposited by the GTC–CVD technique. Cu ion implantation was carried out with the acceleration voltages of 370 keV and 2.4×10^{15} ions/cm^2. The concentration of 400 nm thick s-Al(Cu) film is 0.1 at%Cu, which was near the solid solubility in Al matrix at 250°C [26]. Thus, at the EM acceleration test temperature which includes the Joule heating

Fig. 5. A bright-field image and selective area diffraction patterns of the 400 nm thick s-Al(Cu) film deposited by GTC–CVD technique and subsequently implanted with Cu. In SAD on grain boundary, some streaks attributed to GP-zone were observed at ambient temperature.

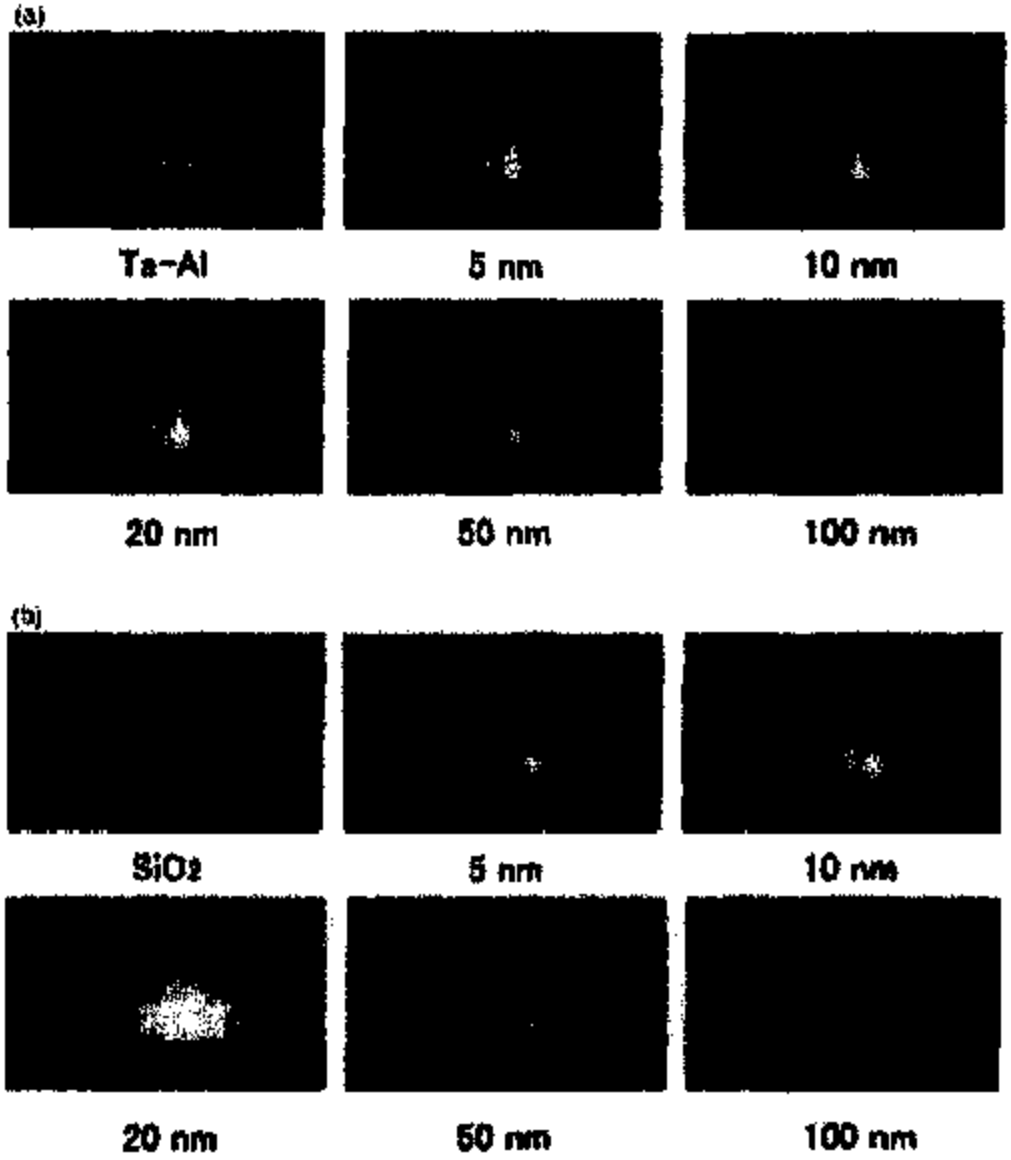

Fig. 6. (a) In situ RHEED observation results of growth of Al deposited on the amorphous Ta–Al underlayer; (b) In situ RHEED observation results of growth of Al deposited on SiO_2.

factor, the Cu elements almost dissolve into the Al matrix. A post thermal treatment of 30 min at 400°C was carried out in order to remove lattice defects introduced by ion implantation process and to homogenize Cu distribution.

Fig. 5 shows the top-view image and a selective area diffraction patterns (SADs) of s-Al(Cu). A subgrain boundary was also observed in this film. This dislocation array might be produced by recovery of various lattice defects introduced by ion implantation process. In the SAD, some streaks attributable to GP-zone were observed only near the subgrain boundary area at room temperature and precipitated during cooling process after the acceleration test. It shows that Cu strongly interacts with lattice defects in Al films. From the results of the x-ray analysis using $\sin^2\Psi$ method, the compressive stress of the Cu implanted film was 30 MPa. Consequently, the tensile stress varied to approximately 150 MPa after thermal treatment.

Therefore, the s-Al(Cu) film microstructure is almost

the same as that of the s-Al film except for containing small amounts of subgrain boundaries.

2.4. Hyper-textured Al films (ht-Al films)

An ht-Al film was developed using an amorphous underlayer [1]. An Al–0.1 at%Cu film deposited on Ta–Al amorphous underlayer indicated an FWHM value of 0.5°. This ht-Al line made it possible to estimate the effect of the texture on the EM lifetime in regions ranging from a conventional polycrystal to a single-crystal.

At the early stage of the film growth, Al islands are formed on a substrate, and they coalesce and become a continuous film as in the case of a qs-Al film on Si(1 1 1). According to the classical theory, the shape of the island is determined by Young's equation. The relation is expressed as

$$\cos\theta = \frac{\sigma_s - \sigma_i}{\sigma_f} \quad (1)$$

where θ is the wetting angle of the island, σ_s and σ_f are the surface energies of the substrate and the island, respectively, and σ_i is the interfacial energy between the island and the substrate. When $\sigma_s - \sigma_i > \sigma_f$, it is considered that the film grows two-dimensionally (layer-growth). By this layer-growth mode, it is expected that two-dimensional (2D) island with stable (1 1 1) surface would be formed. An amorphous substrate will enhance this tendency, because there is no specific crystal lattice matching restriction between a film and a substrate that obstructs the stable (1 1 1) 2D-island formation. Assuming that the (1 1 1) texture of the film is improved by approaching the layer-growth mode, high σ_s and low σ_i are preferable for realising a small wetting angle according to Eq. (1). The effect of the surface energy on the texture of the Al film for amorphous underlayers was investigated, because the origin of σ_i on an amorphous substrate still remains unknown. The surface energy of an amorphous alloy was assumed to be the sum of the fractional surface energies of individual elements.

Various kinds of amorphous and polycrystalline 100 nm thick underlayers were deposited on thermally oxidized Si substrates. Al films were deposited and examined using the same methods as for qs-Al film.

Fig. 6 shows the RHEED patterns for the Al films on the amorphous 75 at%Ta–25 at%Al alloy (Fig. 6(a)) and SiO_2 (Fig. 6(b)), which are observed for various kinds of Al film thickness. The patterns on both amorphous underlayers exhibited a (1 1 1) texture even for 5 nm thickness film and the pattern on Ta–Al was sharper than that on SiO_2, and this tendency was the same for the thicker films. Furthermore, the texture of Al films improved with increasing thickness, and by

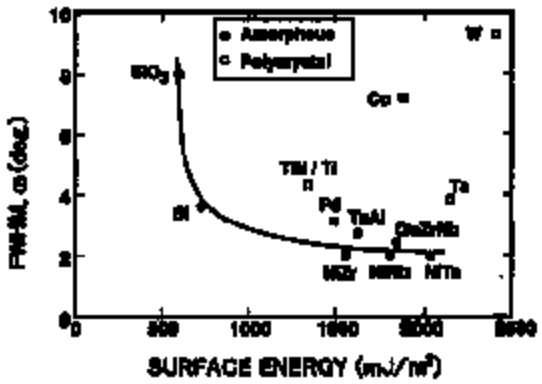

Fig. 7. The relationship between surface energy of underlayer and the FWHM values of 20 nm thick Al films deposited on the underlayers. The open squares and closed circles indicate polycrystalline underlayers and amorphous underlayers, respectively.

port annealing. Thus, it has been proved that the texture improvement will be accompanied with grain growth. Al–0.1 at%Cu films showed a better texture than pure Al films probably because σ_f in Eq. (1) decreases by Cu addition. A sintered 400 nm Al(Cu) film on Ta–Al indicated an FWHM value of 0.5°. The FWHM values of 20 nm thick Al films on various underlayers are plotted against the surface energy of the underlayers in Fig. 7. No clear relation was found between the FWHM value and the surface energy on polycrystalline underlayer. This scattering of the texture might be due to both lattice mismatch and the difference in the underlayer texture. On the other

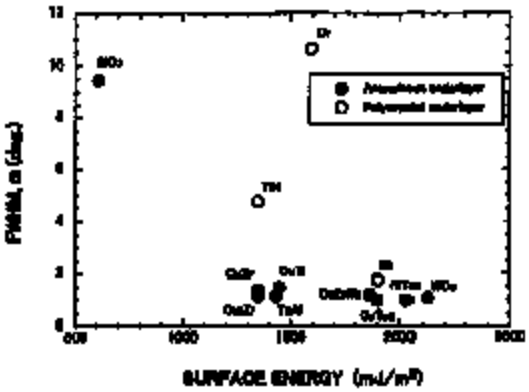

Fig. 8. The relationship between surface energy of underlayer and the FWHM values of 100 nm thick Cu films deposited on the underlayers. The open circles and closed circles indicate polycrystalline underlayers and amorphous underlayers, respectively.

Fig. 9. SEM photographs of the s-Al line after EM accelerated test for 19 h.

hand, the FWHM value for the Al film decreased with an increase in the surface energy for amorphous underlayers. These results confirmed that both a high surface energy and an amorphous state are necessary for improving the texture. It is also considered that the interfacial energy σ_i is uniform and might be small for amorphous underlayers.

2.5. Hyper-textured Cu films (Hyper-textured Cu films)

Ht-Cu films were also developed using amorphous underlayers. The concept of ht-Cu film development is the same as that of ht-Al films. Fig. 8 shows the relation between the (1 1 1) FWHM value for the Cu 100 nm thick film and the surface energy of the amorphous underlayer. The (1 1 1) FWHM values for Cu films deposited onto polycrystalline underlayers, i.e., Cr, TiN, and amorphous underlayer which has low surface energy were all above 4°, and Cu (2 0 0) peak was observed by the θ–2θ X-ray diffraction method in these lower textured films. On the other hand, the (1 1 1) FWHM values for Cu films deposited onto the metallic amorphous underlayers that have relatively high surface energy were approximately 1° and no other peaks were detected. With respect to the Nb underlayer, Nakasaki et al. calculated the interfacial energy as a sum of interatomic potential energies [27]. The Cu (1 1 1) and Nb (1 1 0) were expected to show the epitaxial relationship with a Nishiyama–Wassermann (NW) relationship with fcc [1–1 0] // bcc [0 0 1] [27], and the Cu film deposited onto (1 1 0) oriented polycrystalline Nb underlayer resulted in hyper-textured film. In the case of Cu crystal, an average surface energy is higher and the difference between surface energy of (1 1 1) and (2 0 0) is smaller than in the case of Al [28]. As a result, (2 0 0) compared with Al, Cu grains might be more easily grown during deposition of films. Thus, the lower textured Cu films and even the hyper-textured Cu film deposited onto the Nb underlayer had the mixed orientation with (1 1 1) and (2 0 0) grains. However, in the case of metallic amorphous underlayers, only hyper-textured (1 1 1) crystal grains were grown, even though the surface energy (σ_s) was nearly equal to the surface energy (σ_f) of Cu. It is considered that the interfacial energy (σ_i) between the metallic amorphous underlayer and Cu (1 1 1) might be very small.

3. Accelerated electromigration test procedure

The test lines were about 1.5 μm wide, 0.4 μm thick, and 50 μm long. The positive and the negative ends of the line were terminated with each 50 μm wide square pad without a taper and lines were unpassivated. The EM accelerated testing was carried out in a vacuum at pressures below 2×10^{-6} Torr. The acceleration conditions of films with high endurance to EM, i.e., s-Al and s-Al(Cu) lines, was 35 MA/cm^2 at 150°C ambient temperature. Under these severe conditions, conventional polycrystalline Al lines failed within a few seconds. The qs-Al and ht-Al were tested under the condition of 15 MA/cm^2 at 200°C and 5 MA/cm^2 at 200°C, respectively.

The EM induced damage, such as voids and hillocks, was examined after the accelerated test using SEM and TEM.

4. Results and discussion

4.1. Reliability of s-Al lines

The line operated at the electrical current density of

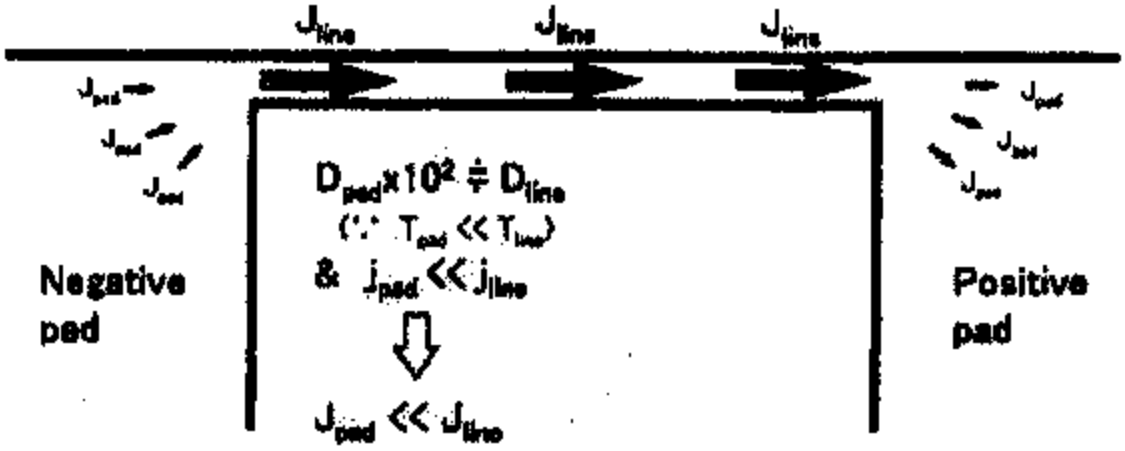

Fig. 10. Schematic diagram of highly accelerated EM test condition.

1 MA/cm^2 did not show any apparent EM damage at 150°C for 3000 h [17]. In order to obtain further acceleration, the lines were operated at a high current density of 35 MA/cm^2 in order to generate a steep temperature gradient at the junction between the line and the pad by Joule heating [29].

SEM photographs of an s-Al line after EM accelerated test for 19 h are shown in Fig. 9. Hillocks were formed mostly at the junction between the line and the positive pad and partly in the positive pad. Some hillocks were like a whisker and others were like a flat extrusion. On the other hand, voids were mostly accumulated in the negative pad and small voids were observed in the line near the negative pad. It is obvious from the void shape that the void is surrounded by {1 1 1} planes with the lowest surface energy in an fcc lattice. However, no voids were observed in the middle part of the line. These are the damage characteristics expected in the case that the temperature difference between the line and the pad is actualized by Joule heating. Actually, the average line temperatures monitored by the line electrical resistance range from 200 to 260°C. And the local temperature distribution generated by Joule heating was obtained by self-consistent finite element calculation [29]. In a typical case, the average temperature, line temperature and pad temperature were 240, 259 and 165°C, respectively.

Fig. 10 shows a schematic diagram of highly accelerated EM test condition. The temperature (T_{line}) of the line was about 100°C higher than that (T_{pad}) of the pad. It followed that the diffusion coefficient (D_{line}) of the line was more than two orders of magnitude higher than that (D_{pad}) of pad. Furthermore, the Al atoms in the line at higher current density (j_{line}) are subjected to a much higher stress (electron wind) than those at lower current density (j_{pad}) in the pad because of a shape factor. The migration in the line away from the line–pad junctions is much faster than that in the pad. The atomic flux of negative line–pad junction and that of positive line–pad junction produced atom depletion and atom accumulation, respectively. Thus, in spite of single-layered structure line, the principle of the atomic flux divergence is similar to that of W stud multiple layered line structure.

Fig. 11 shows the relationship between normalized electrical resistance change and elapsed time. The resistance initially decreased, next increased gradually,

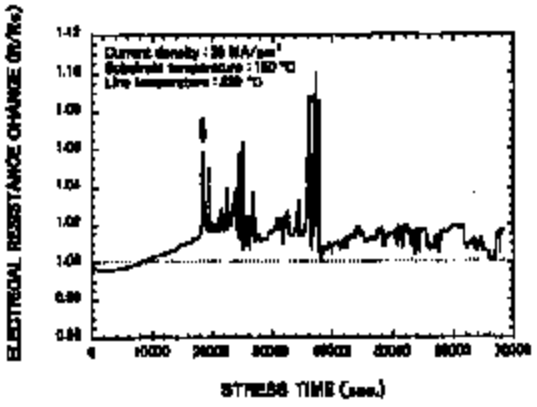

Fig. 11. Electrical resistance change for an s-Al line during EM accelerated testing with current density of 35 MA/cm^2.

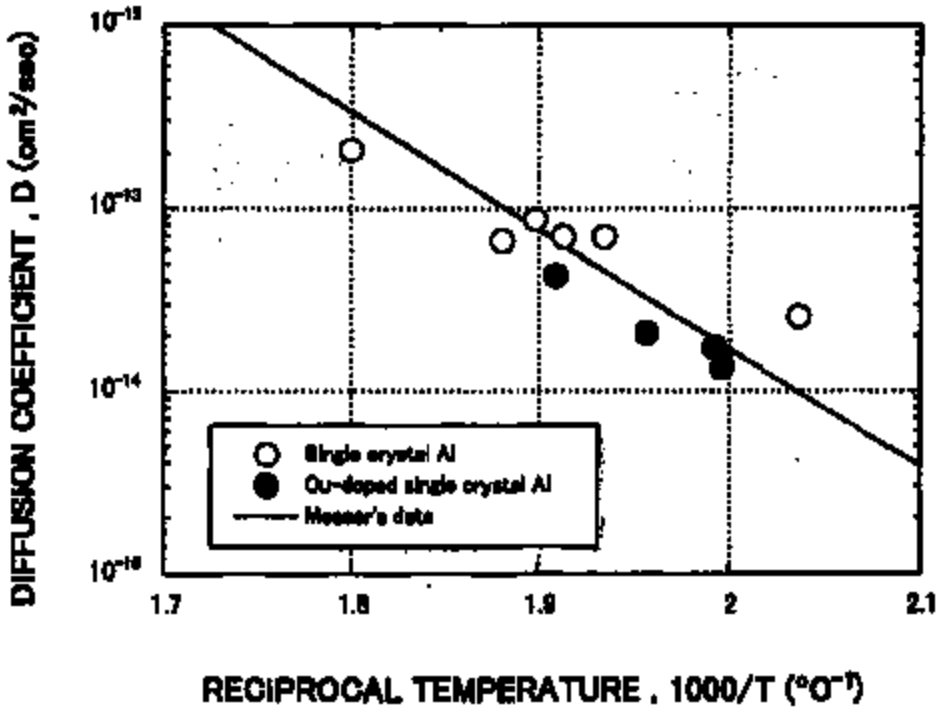

Fig. 12. Arrhenius plot of the Al diffusion coefficients obtained from void growth rate. The open circles and the closed circles indicate s-Al and s-Al(Cu), respectively, and solid line presents Messer's data.

and finally oscillated violently. To clarify the behavior of initial resistance decrease, no current loading test was carried out. After keeping some EM test lines at 150°C for 15 h, the resistance decreased from 1.5 to 2.3% at ambient temperature, which might be caused by recovery of various kinds of lattice defects introduced by thermal cycle and/or Si precipitation. From in situ SEM observation, a void appearance and voids movement corresponded with the resistance increase and the resistance oscillation, respectively. In particular, the violent oscillation of electrical resistance might be caused by a serious void shape change and occasional jumping [30]. The initial decrease, the subsequent increase and final violent oscillation were considered to be due to the recovery and/or Si precipitation, voids growth near the negative pad and voids migration, respectively. Therefore, the beginning of violent oscillation is defined as the guideline of lifetime for s-Al, as shown by an arrow in Fig. 11.

Fig. 12 shows the Arrhenius plot of the obtained diffusion coefficients calculated from the void growth rate [9]. The EM-induced void volume was obtained from the sum of the volumes of individual voids based on the assumption that the voids completely penetrated the Si substrate surface. The Al atom flux divergence, $\mathrm{div}(J)$, which contributes to the void growth near the line–pad junction, is expressed as

$$\mathrm{div}(J) = (J(T_{\mathrm{line}}) - J(T_{\mathrm{pad}}))/\Delta x \quad (2)$$

where $J(T_{\mathrm{line}})$ and $J(T_{\mathrm{pad}})$ are the Al atom flux at line temperature (T_{line}) and at the line–pad junction temperature (T_{pad}), respectively, and Δx is the length of the temperature changing region, 10 μm, obtained by the finite element calculation. The experimentally obtained void growth rate dV/dt could be connected to Eq. (2) as

$$(dV/dt)N/S/\Delta x = \mathrm{div}(J) \quad (3)$$

where N is the atomic density of Al, and S is the cross-sectional area of line. An ideal Al atom flux induced by EM is also expressed by the Nernst–Einstein's relationship [31]. The flux is expressed as

$$J = DNZ^*e\rho j/kT \quad (4)$$

where D is the diffusion coefficient for Al, k the Boltzmann constant, T the absolute temperature, Z^* the effective charge number, e the elementary charge, ρ

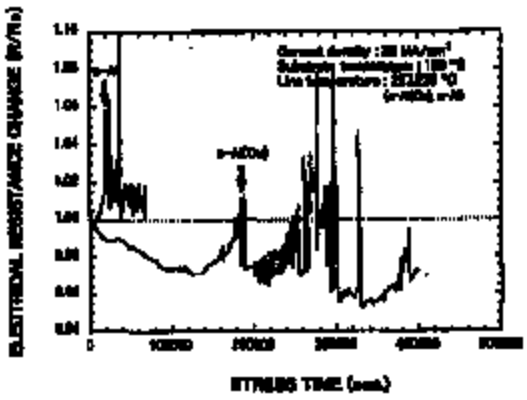

Fig. 13. Electrical resistance change for s-Al and s-Al(Cu) lines during EM accelerated testing with current density of 35 MA/cm^2.

the resistivity of Al and j the current density, respectively. The diffusion coefficients of Al were calculated from Eqs. (2)–(4). Open circles indicate the s-Al results. The straight line in this plot is the Al lattice diffusion coefficients with an activation energy of 1.28 eV and pre-exponential factor of 0.137 cm^2/s. A fairly good agreement was observed [32]. Consequently, it has been confirmed that the void growth in a s-Al line was by lattice diffusion control.

However, it is noteworthy that a fairly large amount of grown voids accumulated in the negative pads. The maximum Al atom flux divergence was generated near the negative pad where the steep temperature gradient existed. It is natural to expect that the EM-induced voids nucleate and grow in this area. However, the voids fully grown in the line near the negative pad moved into the negative pad and accumulated. This movement of the voids in s-Al lines is ascribed to their homogeneity, i.e., this film is free from trapping and/or flux divergent sites, such as grain boundaries. An s-Al line has excellent endurance against EM because of its homogeneous microstructure [17,25,29]. Consequently, the s-Al line survives an open circuit failure, and, in fact, no sample failed in the present experiment.

4.2. Reliability of s-Al(Cu) lines

The line resistance change behavior, the initial decrease, gradual increase and final violent oscillation, and the observed surface morphology of the s-Al(Cu) line after EM accelerated test were similar to the s-Al line (see Fig. 13), except for the following points:

1. The lifetime observed for the s-Al(Cu) line was approximately one order of magnitude longer than that for the s-Al.
2. The maximum resistance decrease for the s-Al(Cu) line was 3%, whereas the s-Al line resistance decrease was only 0.5%.
3. The resistance increase and decrease speeds for the s-Al(Cu) line were slower than those for the s-Al line.

It is noteworthy that the Cu doping is effective for prolonging the Al EM lifetime even though there are no grain boundaries. This result indicates that the EM lifetime improvement frequently observed in the case of Cu doped polycrystalline Al lines is not due to the diffusivity retardation by the $CuAl_2$ precipitation in the grain boundary [20]. Moreover, the Al diffusion coefficients both for the s-Al and the s-Al(Cu) lines, calculated by the void volume by using Eqs. (2)–(4) plotted in Fig. 12, differed slightly. Therefore, the Al lattice diffusion retardation by the Cu doping is not the dominant mechanism for the EM lifetime improvement. On the other hand, it is also interesting to note that the initial 3% resistance decrease observed for the s-Al(Cu) line was well explained by the Cu depletion, because the 0.1 at%Cu solution increases the Al line resistivity by almost the same amount (0.75 μΩ cm/at%Cu [33]). This hypothesis is consistent with the view of the Cu depletion proposed by Hu et al. [34]. However, it should be emphasized that the s-Al line had the incubation time for the void nucleation even though it was pure-Al and was not included in Hu's model.

Therefore, the tensile stress evolution near the negative end of line due to the absence of atom supply [35,36] should be taken into account in order to explain the incubation time for pure-Al line and to understand the effect of Cu doping. There is a critical stress that enables the void nucleation, and the incubation time is defined as the time for generating large enough tensile stress to permit nucleation. Since the present test lines were unpassivated, the tensile stresses contained in the s-Al and s-Al(Cu) line were small, approximately 150 Mpa. Therefore, the longer incubation time is necessary compared with the passivated Al line which has sufficiently large stress to nucleate a void before the EM current loading. Since the Al diffusivities both for the s-Al and the s-Al(Cu) line are almost the same, as shown in Fig. 12, the identical critical stress for the void nucleation should possess the same incubation time. Therefore, the longer incubation time for s-Al(Cu) is probably due to the critical stress increase. Similar Cu doping effect has been reported, namely only 0.1 wt%Cu doping was sufficient to improve the SM lifetime [22]. The decrease in the Al surface energy by Cu doping [28] also supports this hypothesis, because the lower surface energy increases the

Fig. 14. Bright-field image and selected area diffraction pattern of qs-Al line after EM acceleration test.

critical energy for the void nucleation. However, the large resistance decrease indicates that the Cu depletion did occur during EM testing, and the Cu depletion and/or the preferential Cu migration induced by EM always reduce the impact on the critical stress increase.

4.3. Reliability of qs-Al lines

Fig. 14 shows the microstructure of qs-Al line after EM accelerated test with the current density of 15 MA/cm^2 for 150 min and the line temperature of 200°C. Many subgrain boundaries consisting of dislocation arrays were observed, as described above. Fig. 15 shows SEM photographs after the EM accelerated test and {1 1 1} pole figure that is adjusted to the direction of the test line. In spite of this severe test condition, no voids and hillocks appeared in the middle of the line, though voids and many whisker-like hillocks formed in the negative pad and the positive pad, respectively. The voids formed in the negative pad were also surrounded by {1 1 1} planes. Thus, the endurance against EM of qs-Al line is essentially the same as that of s-Al line. In other words, subgrain boundaries do not behave as fast diffusing paths because the dislocation line of the subgrain boundary exists perpendicular to the electron wind. Moreover, the voids produced in the line near the negative pad were not immobilized by subgrain boundaries that possess lowest grain boundary energy.

4.4. Hypertextured Al lines (ht-Al line)

The measured electrical resistance changes of the lines during the tests are shown in Fig. 16. The initial increase in the resistance was due to Joule heating by current loading. The resistance of the sintered Al(Cu) line on Ta–Al increased less than 10% after 10 h. SEM photographs of the lines after 10% resistance increase are shown in Fig. 16, and for the sintered Al(Cu) line, a photograph of the line after 10 h accelerated testing is shown. Fewer defects were observed inside the Al(Cu) line, whereas many void-hillock pairs are found along the grain boundaries for the other lines. The grain size was smaller than the line width and grain-networks existed along the line direction. This means that the flux divergence at a triple point of grain boundaries is very small. It is known that grain boundary diffusivity depends on the boundary structure [37]. Al films that show no or broad texture have random grain boundaries, and the individual diffusivities of grain boundaries are quite different, and so the flux divergence occurred at a triple point and resulted in a void-hillock pair formation.

After 250 h current loading test, the resistivity change of the sintered Al(Cu) line increased to 7.5%. Most of the voids were formed inside the negative pad, which enables the vacancy flux estimation from the void volume. The obtained vacancy flux is 8.9×10^{17} m^{-2} s^{-1} and this value is the same order of magnitude as that in an s-Al line, 2.5×10^{17} m^{-2} s^{-1} [9]. Therefore, grain boundaries formed in ht-Al film are no more effective than those of conventional broad textured film as fast diffusion paths for mass-transport phenomenon by EM.

Furthermore, a detailed analysis of grain boundary structure was carried out by TEM. Fig. 17 shows the plan view of the Al(Cu) film and many subgrain boundaries were also observed in this film. The average grain size is 280 nm, but large scattering was observed in grain size. This fact suggests that the large grains have coarsened and unified because of the fairly good

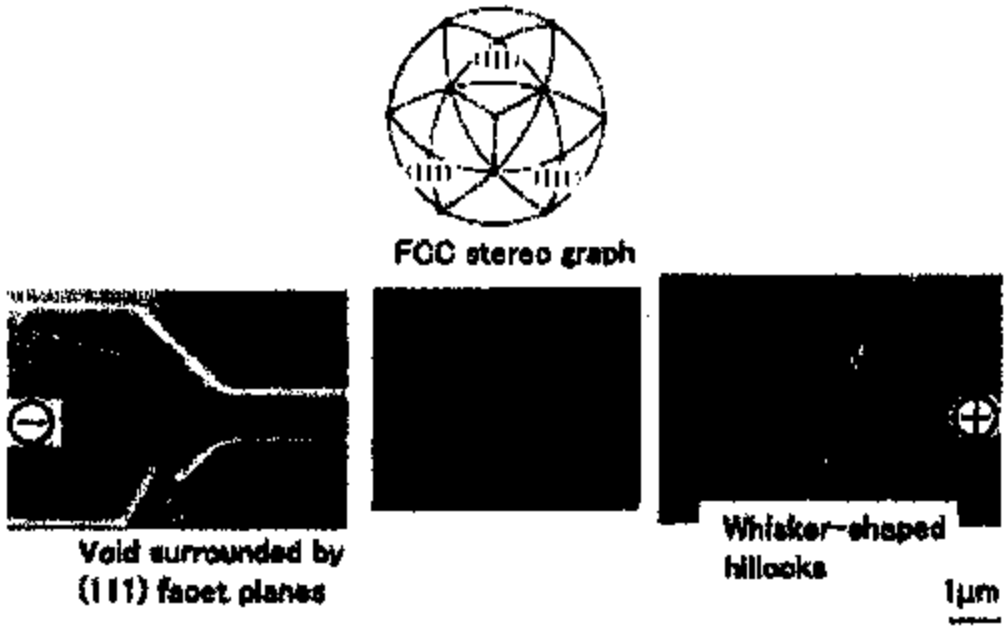

Fig. 15. SEM photograph of qs-Al line after EM acceleration test.

orientation matching among the neighbor grains. The SADs of the individual grains are shown in Fig. 17 and it proves that all the grains have (1 1 1) orientation. Assuming that the grain boundaries are perpendicular to the substrate, the most stable plane is {1 1 0} for fcc structure. The angles between a grain boundary and the {1 1 0} planes of grains on both sides are measured to investigate the property of the grain boundary structure. The angles are defined to be positive when the deviation is counterclockwise and are restricted within 30° because of the crystallographic symmetry. Fifty-one grain boundaries are plotted in Fig. 18, and 18 boundaries are subgrain boundaries (35%) indicated by closed circles. The grain boundary on the line $\theta 1 = \theta 2$ is considered to be formed by the two grains which have the same orientation, and so

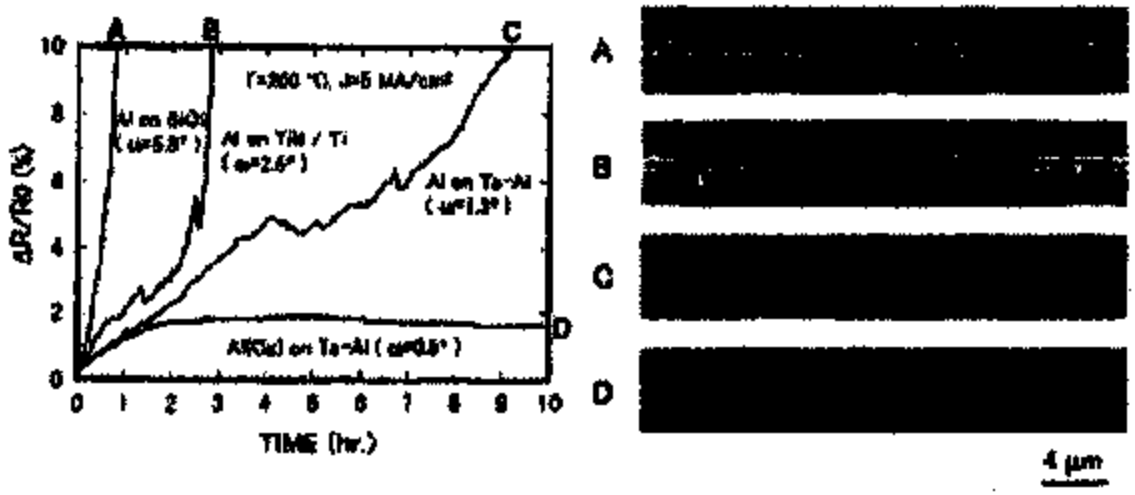

Fig. 16. Electrical resistance change for Al lines of various degree of (1 1 1) texture during EM acceleration test and morphology change after EM acceleration test.

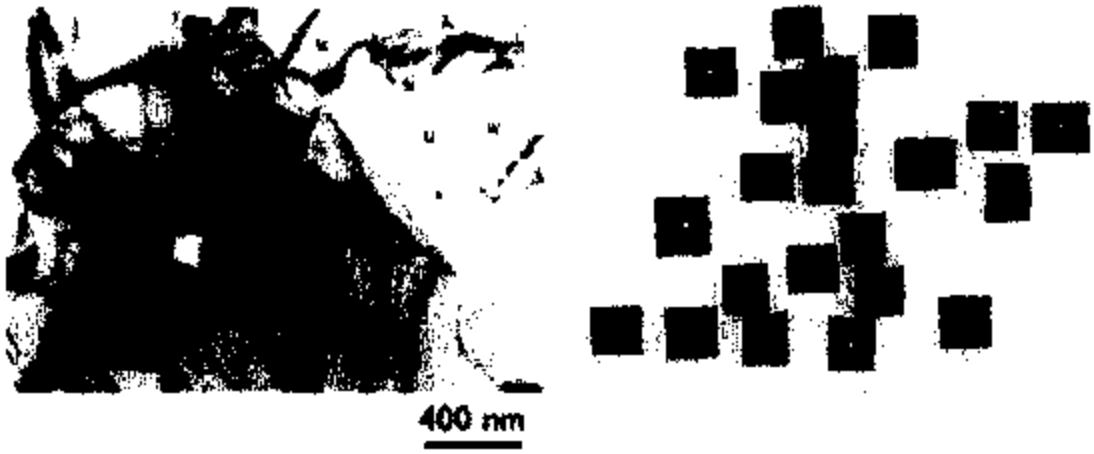

Fig. 17. Bright-field image and diffraction pattern of individual grains of ht-Al film deposited on Ta–Al underlayer.

the energy of the boundary is the lowest. On the other hand, the grain boundary on the dotted line $\theta 1 = -\theta 2$ is considered to form the symmetrical tilt-grain boundary. The grain boundary energy among (1 1 1) symmetrical tilt grain-boundary for fcc metal is reported by Wolf [38]. According to this simulation, the energy increases with tilt angle up to 10° (i.e., $\theta 1 = -5°$, $\theta 2 = 5°$) and the cusp exists at 60° (i.e., $\theta 1 = -30°$, $\theta 2 = 30°$). The former area corresponds to the hatched area and the latter point corresponds to the upper-left on the dotted line. As a result, the grain-boundary energy in the hatched area and on the upper-left point is relatively low compared with the random boundary, and almost half of the grain boundaries are included in this area for ht-Al film. These facts show that a hyper-texture not only eliminated the twist component of grain boundaries, but also changed the grain boundary to the low-angle boundary structure and reduced grain boundary energy. This grain boundary energy reduction would suppress the grain boundary diffusivities and the void's nucleation at a triple point in the ht-Al line. The EM lifetime of Al lines with different degree of texture ($\omega = 0.5$–$7°$) are plotted in Fig. 19. The obtained dependence of the lifetime τ on the FWHM value ω is [1]

$$\tau \propto \omega^{-2} \tag{3}$$

This empirical relation has revealed that the EM lifetime of the Al line is improved with a decrease in the FWHM value. From the detailed grain boundary analysis, it has been clarified that the grain boundaries found in ht-Al film were, on average, lower-grain boundaries than those of low textured films. This average tilt (misorientation) angle decrease would reduce the mass transportation along the boundaries and sup-

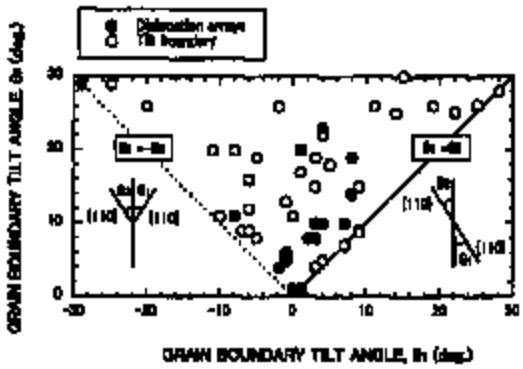

Fig. 18. Misorientation angle between the grains on both sides of grain boundary closed circle : dislocation array; open circle : tilt boundary.

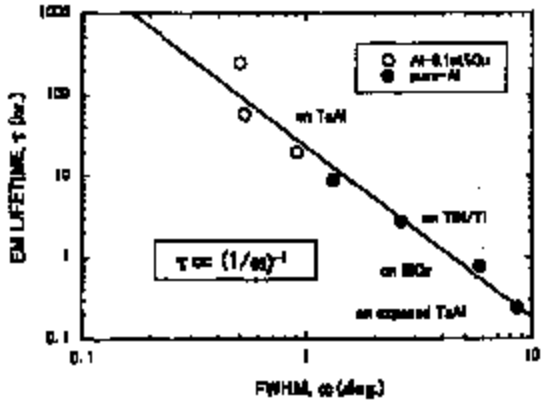

Fig. 19. Dependence of EM lifetime(τ) on the FWHM value (ω) of Al (1 1 1) rocking curve.

press the void and hillock formation at the triple points. The inverse proportionality of EM lifetime τ to the FWHM value ω suggests that the decrease in the average twist angle ω leads to the decrease in the average misorientation angle.

5. Conclusion

High reliability of single-crystal Al line ($\omega = 0.18°$) was ascribed to its homogeneous microstructure and the lattice diffusion controlled mass transport with the high activation energy of 1.28 eV. The quasi single-crystal Al line ($\omega = 0.26°$) essentially had the same endurance against EM as the single-crystal Al line, because subgrain boundaries found in this line never behaved as effective mass transport paths. The void movement was never disturbed by these subgrain boundaries, because of their lower boundary energy, i.e., a very small amount of defects along the boundary. It has been clarified that the grain boundaries found in hyper-textured Al film ($\omega = 0.5°$) were low-angle grain boundaries though this film still contained random boundaries. It has also been clarified that the texture improvement promoted the low-angle grain boundary formation. The atom and/or vacancy transportation along these boundaries has been found to be the same order of magnitude as that of the lattice diffusion. This reduction of atomic mass transport reduced the flux divergence at the triple points, i.e., void and hillock formation, and resulted in longer lifetime.

On the other hand, it has been concluded that the doping effect of Cu in Al matrix within solid solubility is due to the critical stress increase for the EM induced void nucleation, which markedly prolonged the incubation time of α-Al(Cu).

Finally, hyper-textured Cu films have been achieved by using several kinds of amorphous underlayers. The presence of the hyper-textured Cu film will guarantee the highly reliable metallization for the future ULSI.

Acknowledgements

The authors would like to thank Mrs. Ito, Mrs. Kohanawa, Mr. Kawanoue and Dr. Komatsu for help and discussion throughout this work. They are also grateful to Mr. Miyauchi, Dr. Iizuka, Dr. Hayasaka and Dr. Okumura for their encouragement.

References

[1] Toyoda H, Kawanoue T, Hasunuma M, Kaneko H, Miyauchi M. In: Proc. 32nd Ann. Int. Reliab. Phys. Symp., IEEE. 1994. p. 178.
[2] Towner JM, Darks AG, Tien T. In: Proc. 24th Ann. Int. Reliab. Phys. Symp., IEEE. 1986. p. 7.
[3] Hosoda T, Yagi H, Tetsuchikawa T. In: Proc. 27th Ann. Int. Reliab. Phys. Symp., IEEE. 1989. p. 202.
[4] Ozaki J, Koibuchi Y, Fukuda S, Suzuo M, Mizawa Y, Ingaki T. IEDM Tech. Dig., IEEE, 1988, p. 454.
[5] Ogawa S, Nakamura H. IEDM Tech. Dig., IEEE, 1991, p. 277.
[6] Lin T, Ahn KY, Harper JME, Chaiem PN. In: IEEE VMIC Conf. 1998. p. 76.
[7] Hisode K, Honma Y. In: Proc. 28th Ann. Int. Reliab. Phys. Symp., IEEE. 1990. p. 25.
[8] Ho PS, Howard JK, White JF. J Appl Phys 1978;49:4083.
[9] Kawanoue T, Kaneko H, Hasunuma M, Miyauchi M. J Appl Phys 1993;74(7):4423.
[10] Vaidya S, Shinha AK. Thin Solid Films 1981;75:253.
[11] Knorr DB, Lu TM. Appl Phys Lett 1989;54:2210.
[12] Lytle SA, Oates AS. J Appl Phys 1992;71(1):174.
[13] Marieb TN, Abratowski E, Bravman JC, Madden M, Flinn P. In: Ho PS, Li CY, Totta P. editors, AIP Conf. Proc. No. 305, 1994, p. 1.
[14] Yue JT, Funston WP, Taylor RV. In: Proc. 23th Ann. Int. Reliab. Phys. Symp., IEEE. 1985. p. 1.
[15] Tanikawa, Okabayashi H, Mori H, Fujita H. Proc. 28th Ann. Int. Reliab. Phys. Symp., IEEE, 1990, p. 209.
[16] Kaneko H, Hasunuma M, Sawabe A, Kawanoue T, Kohanawa Y, Komatsu S, Miyauchi M. In: Proc. 28th Ann. Int. Reliab. Phys. Symp., IEEE. 1990. p. 194.
[17] Hasunuma M, Kaneko H, Sawabe A, Kawanoue T, Kohanawa Y, Komatsu S, Miyauchi M. IEDM Tech. Dig., IEEE, 1989, p. 677.
[18] Hisode K, Owada N, Nishida T, Mukai K. J Vac Sci Technol 1987;B5:518.
[19] Cinqunies A, d'Heurle FM. Thin Solid Films 1973;16:227.
[20] d'Heurle FM. Met Trans 1971;2:683.
[21] Spolenak R, Kraft O, Arzt E. Microelectron Reliab 1998;38:1015.
[22] Mayumi S, Umemoto T, Shishino M, Nanatsue H, Ueda S, Inoue M. In: Proc. 25th Ann. Int. Reliab. Phys. Symp., IEEE. 1987. p. 15.
[23] Kobayashi T, Saitiguchi A, Akiyama N, Hosokawa N, Amemiki T. J Vac Sci Technol 1992;A10:525.
[24] Yamada I, Inokawa H, Takagi T. J Appl Phys 1984;56:2746.
[25] d'Heurle F, Berenbaum L, Rosenberg R. Trns of AIME 1968;242:502.
[26] Murray JL. Int Met Rev 1985;30(5):211.
[27] Nakasaki Y, Mirasolhaba G, Suguro K. J Appl Phys 1995;77:2454.
[28] Murr LE. Interfacial phenomena in metals and alloys. Reading: Addison-Wesley, 1975.
[29] Kaneko H, Kawanoue T, Hasunuma M, Miyauchi M. In: Ho PS, Li CY, Totta P. editors, AIP Conf. Proc. No. 305, 1994, p. 179.
[30] Shingubara S, Kaneko H, Saitoh M. In: Extended Abstracts of the 21st Conference on Solid State Devices and Materials, Tokyo. 1989. p. 33.

[31] Huntington HB, Grone AR. J Phys Chem Solids 1961;20:76.
[32] Messer R, Dais S, Wolf D. In: Proc. 18th Ampere Congress (Nottingham, England). 1974.
[33] Bradley MJ, Singer JJ. Phys F 1974;4:839.
[34] Ho CK, Rosenberg R, Tu KN. In: Ho PS, Li CY, Totta P, editors, AIP Conf. Proc. No. 305, 1994, p. 195.
[35] Black IA, Herring C. Appl Phys Lett 1976;29:131.
[36] Korhonen MA, Borgesen P, Tu KN, Li CY. J Appl Phys 1993;73(8):3790.
[37] Balluffi RW. Met Trans 1982;13B:527.
[38] Wolf D. J Mater Res 1990;5:1708.

ELSEVIER

Surface and Coatings Technology 125 (2000) 167–172

www.elsevier.nl/locate/surfcoat

Pure Al thin film protective layer to prevent stress migration in Al wiring for thin-film transistors

H. Takatsuji [a,*], K. Haruta [b], S. Tsuji [a], K. Kuroda [b], H. Saka [b]

[a] Display Technology, IBM Japan, Ltd., Shimotsuruma, Yamato-shi, Kanagawa 242, Japan
[b] Department of Quantum Engineering, Nagoya University, Nagoya 464-01, Japan

Accepted 28 June 1999

Abstract

The anti-stress migration property of layered structure aluminum (Al) thin films overcoated with pure Al was investigated for application of such films as interconnect materials in large arrays of high-resolution thin-film transistor liquid crystal displays (TFT-LCDs). It was found that no hillock or whisker generation occurred in a pure Al thin film with a sputter-deposited fine-grained polycrystalline pure Al layer after exposure to mechanical and 300°C thermal stresses. Atomic force microscopy (AFM) and cross-sectional transmission electron microscopy (TEM) analyses revealed the morphology of the layered structure thin film and the mechanism for the prevention of stress migration in the film. © 2000 Elsevier Science S.A. All rights reserved.

Keywords: Nanoindentation techniques; Overcoated pure aluminum thin film; Sputtering; Stress migration; Thin-film transistor liquid crystal displays

1. Introduction

The performance of thin-film transistor liquid crystal displays (TFT-LCDs) has improved over the past several years with a change in standard display size from 10.4 to 12.1 or 13.3 inches, and the resolution has also improved with the transition from VGA to SVGA, XGA, and SXGA. Consequently, pure aluminum (Al) and Al alloys have attracted much attention for their potential use as interconnect materials in high-performance TFT-LCD arrays formed on glass substrates, because of their low resistivity and good patterning ability [1]. However, stress migration due to the thermal expansion mismatch between Al films and the glass substrate, which leads to phenomena such as the growth of hillocks (including whiskers), is a major concern, because it affects the yield loss during TFT device fabrication. There are several ways to protect against stress migration, of which one using Al alloys with rare earth or transition metals has been the subject of many reports [2–5]. However, two shortcomings of such alloys for TFT-LCD applications are their higher electrical resistivity and the higher cost of the sputtering target than in the case of pure Al. Other methods coat clad or capped thin-film layers with transition metals (Ti, Mo, etc.) on Al interconnects, or form anodized Al_2O_3 layers on Al interconnects [6,7]. The shortcoming of these techniques is that they need an additional photolithographic or special anodizing process step, which increases the manufacturing cost. Accordingly, to reduce the thermal expansion stress, we focus on Al interconnects with a layered structure using only pure Al.

In this work, we demonstrate the anti-stress migration property of overcoated pure Al thin film (thickness = 40–200 nm) sputter-deposited on several kinds of pure Al thin film (thickness = 350 nm) and Al–indium (Al–In) thin film (thickness = 270 nm) with a weak anti-stress migration property, formed on LCD grade large glass substrates [8]. We investigated the anti-stress migration property of these thin films by means of our nanoindentation techniques [9]. As a result, we found that the overcoated layer is effective in preventing stress migration in layered Al thin films. We also investigated the nanostructure of the layered pure Al thin film by means of atomic force microscopy (AFM) and cross-sectional transmission electron microscopy (TEM).

2. Experiment

Two kinds of pure Al thin film [(a) and (b), thickness = 350 nm] were deposited on an LCD grade glass

* Corresponding author. Tel.: +81-462-73-2427; fax: +81-462-77-0382.
E-mail address: takatsuj@jp.ibm.com (H. Takatsuji)

PII: S0257-8972(99)00599-X

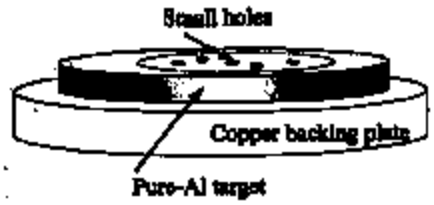

Fig. 1. Schematic diagram of a modified sputtering target for deposition of Al–In thin film.

Table 1
Sample configurations and crystallographic texture[a]

Sample ID	(111)	(200)	(220)	(311)
Pure Al (a)	3122	119	51	22
Pure Al (b)	356	158	96	96
Pure Al (c)	513	252	396	128

[a] The unit of intensity is counts per second (cps).

substrate ($300 \times 400\ mm^2$) using two types of single substrate transfer cluster type d.c. magnetron sputtering apparatus [(a) using multi-magnet type and (b) using a single bar magnet scan type] at a rate of 400 nm/min, with an argon pressure of 0.4 Pa and a substrate temperature of 120°C. Pure Al (c) and Al–In thin films (thickness = 270 nm) were deposited on LCD grade glass substrate ($125 \times 125\ mm^2$) by means of a d.c. magnetron sputtering apparatus at a rate of 36 nm/min, with an argon pressure of 0.4 Pa and a substrate temperature of 120°C. To deposit Al–In thin film, we modified the pure Al target to make indium ooze from the bonding material, as shown in Fig. 1. [Bonding material (In solder) oozed through the small hole in the target.] The indium content was measured using a CAMECA time-of-flight secondary ion mass spectrometry (TOF-SIMS) model 4 at analysis energies of 25 keV with a Ga gun, and at sputter energies of 3 keV with an Ar gun. We confirmed that the Al–In thin film contains 0.19 wt.% indium.

After deposition of the above-mentioned Al-based thin films, the substrates were exposed to the atmosphere, and a pure Al layer (with a thickness of 40 nm or 200 nm) was deposited by means of an RF sputtering apparatus at a rate of 40 nm/min, with an argon pressure of 0.6 Pa and a substrate temperature of 100°C, on Al-based thin films deposited by means of a d.c. magnetron sputtering apparatus. The resistance to stress migration was investigated by means of our nanoindentation techniques for various stress temperatures (200°C, 250°C, and 300°C). The films' crystallographic texture was measured with θ–2θ XRD using Cu Kα radiation at 50 kV/150 mA, with a scanning speed of 1°/min and a scanning range of 30–80°. Nanostructures were observed by means of AFM and cross-sectional TEM operated at 200 kV.

3. Results and discussion

3.1. Properties of Al–In and pure Al thin films deposited on glass substrate

The crystallographic textures of pure Al (a), pure Al (b), and pure Al (c) deposited on LCD grade glass substrates were investigated, with the results shown in Table 1. These indicate that pure Al (a) is a highly (111) textured film, while pure Al (b) and (c) are only slightly (111) textured (i.e. nearly random) films. The crystallographic texture of Al thin film and its anti-stress migration property are strongly correlated, and we confirmed in a previous study that the former type of Al thin film has a strong anti-stress migration property, while the

Table 2
Anti-stress migration property results obtained by nanoindentation techniques

Sample ID	200°C		250°C		300°C	
	Number of whiskers	Number of hillocks	Number of whiskers	Number of hillocks	Number of whiskers	Number of hillocks
Al–In	4	54	5	47	13	103
Pure Al (c)	0	28	3	39	6	41

Table 3
The effects of the pure Al overcoated layer in preventing hillock generation

Sample ID	No overcoated layer		40 nm thick overcoated layer		200 nm thick overcoated layer	
	200°C	300°C	200°C	300°C	200°C	300°C
Pure Al (a)	3	9	0	0	0	0
Pure Al (b)	7	67	1	0	0	0
Al–In	54	102	13	8	0	0

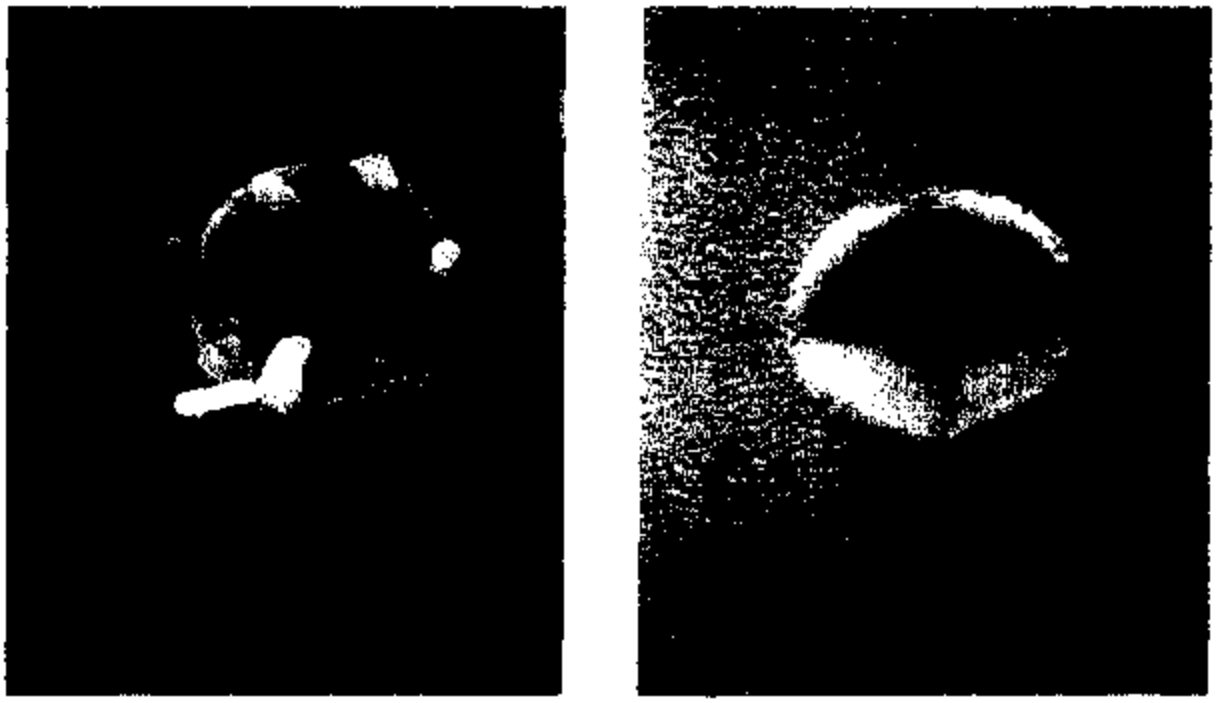

(a) non-overcoated layer (sample A) (b) layer with a 200-nm-thick overcoat (sample B)

Fig. 2. SEM images after nanoindentation technique in the Al–In thin films corresponding to the samples: (a) non-overcoated layer (sample A); (b) layer with a 200 nm thick overcoat (sample B).

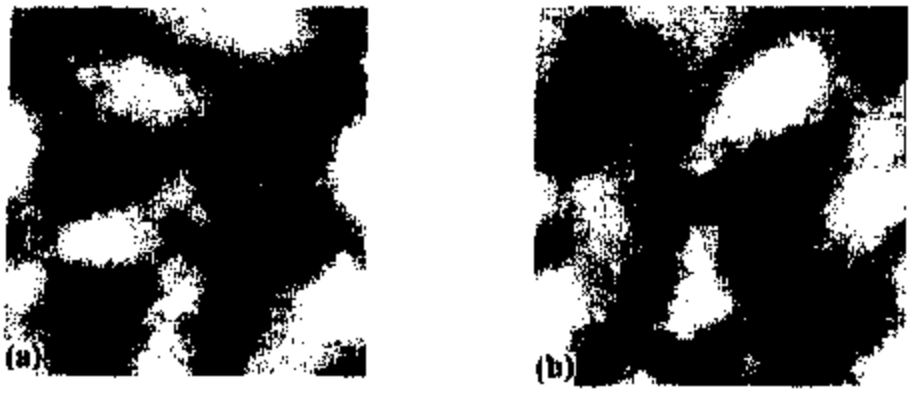

(a) before (sample 3a) annealing (b) after (sample 3b) annealing at 300°C in vacuum for 60 min

Fig. 3. AFM top views of the overcoated pure Al layer on the pure Al (b) thin films: (a) before (sample 3a); (b) after (sample 3b) annealing at 300°C in vacuum for 60 min; scale 1000 × 1000 nm².

latter type has a weak anti-stress migration property [10].

Table 2 compares the anti-stress migration properties of Al–0.19 wt% In (Al–In) and pure Al (c) thin films deposited by the same sputtering apparatus. Whisker generation was observed in the Al–In thin-film samples at a stress temperature of 200°C, but was not observed in the pure Al (c) thin film at the same temperature. More whiskers and hillocks were generated in the Al–In thin film than in the pure Al (c) thin film at all stress temperatures. These results indicate that the use of Al–In thin film leads to the generation of whiskers and

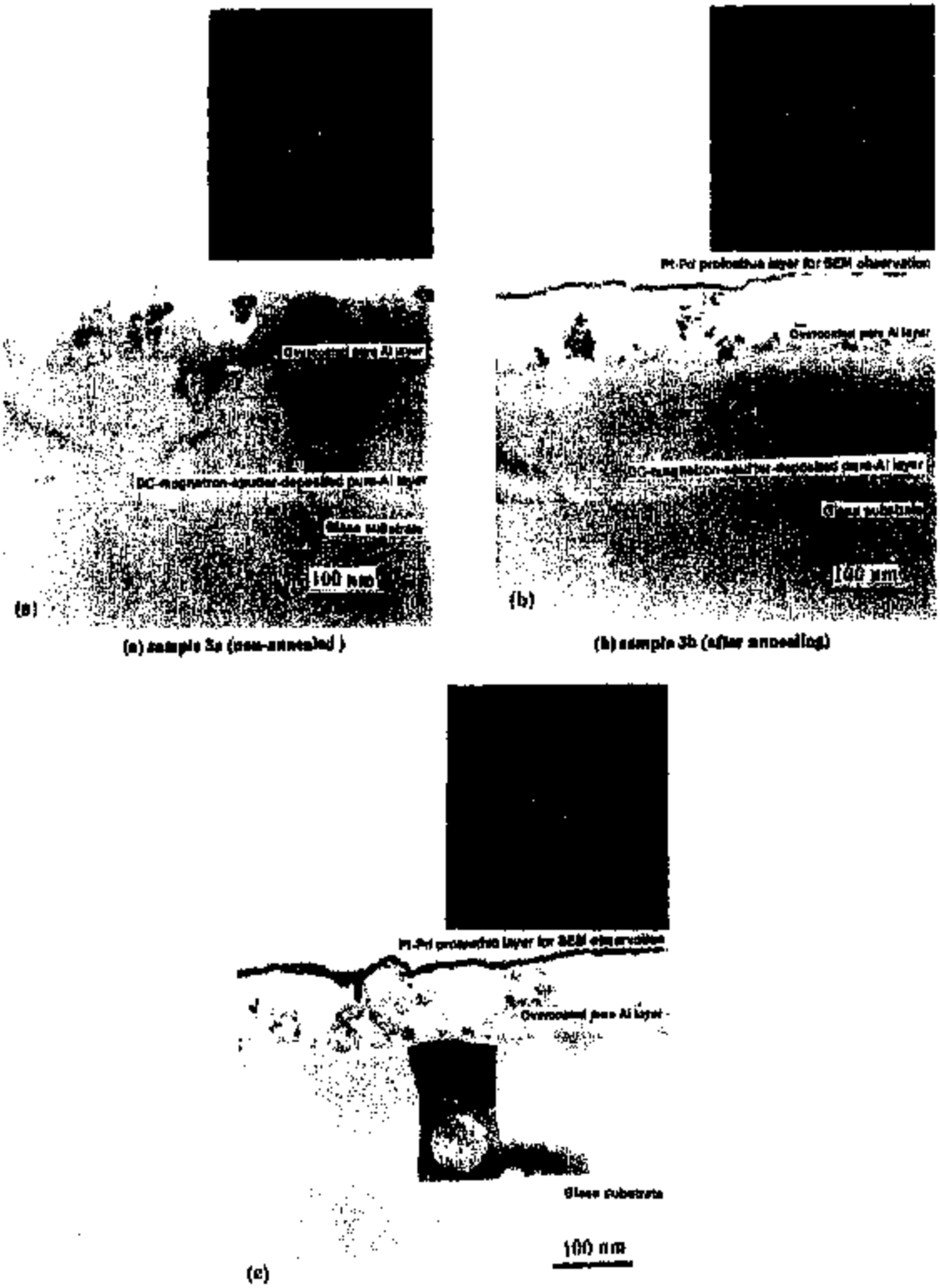

(a) sample 3a (non-annealed)

(b) sample 3b (after annealing)

(c) pure-Al (sample 3b) thin film existing under the overcoated layer

Fig. 4. Cross-sectional TEM images and analyses of the grain orientation caused by electron diffraction: (a) sample 3a (non-annealed); (b) sample 3b (after annealing); (c) pure Al (sample 3b) thin film existing under the overcoated layer.

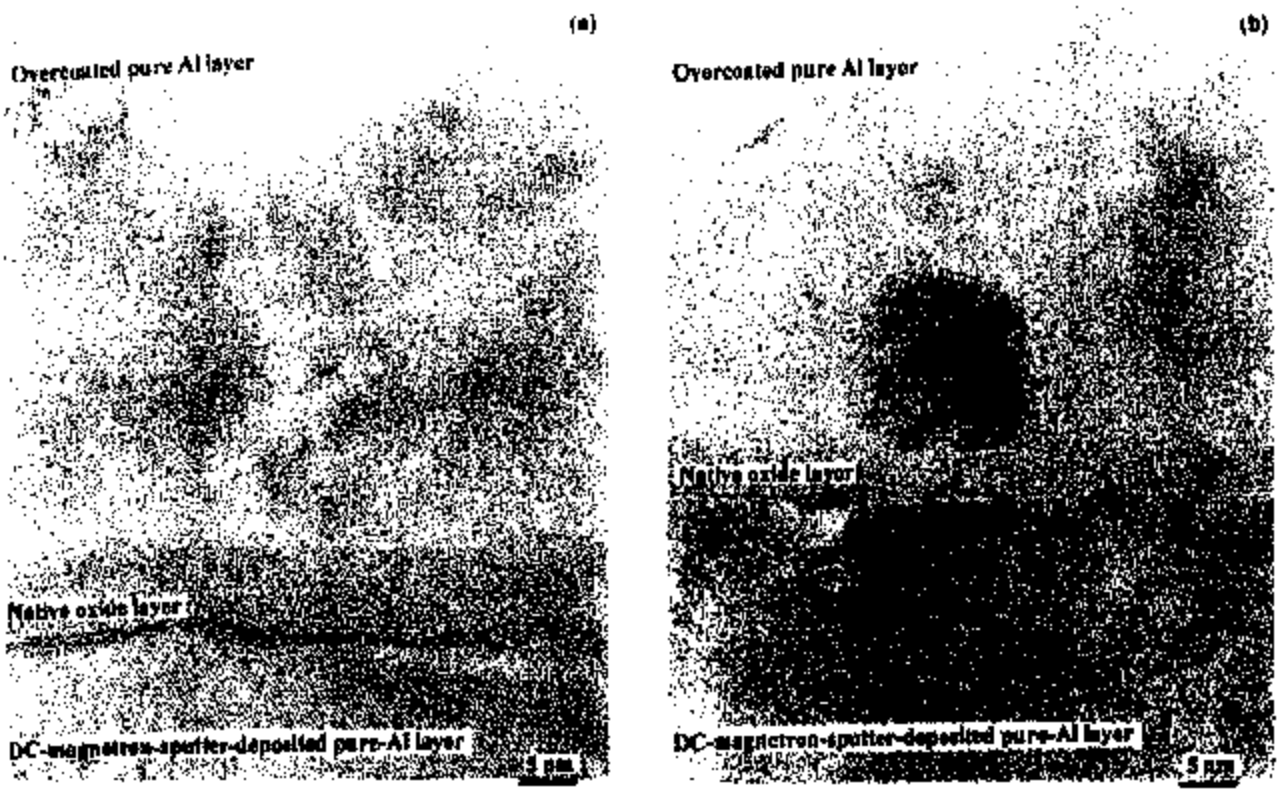

Fig. 3. Detailed nanostructure micrographs obtained by means of cross-sectional TEM corresponding to: (a) sample 3a; (b) sample 3b.

hillocks by nanoindentation techniques at lower stress temperatures than when pure Al (c) thin film is used. We conclude that the Al–In film in this study has a weaker anti-stress migration property than pure Al (c). According to the results shown in Tables 1 and 2, Al–In film has the weakest anti-stress migration property of all these samples.

3.2. Effect and properties of an overcoated pure Al thin film layer

The effect of a pure Al overcoated layer in preventing hillock generation is shown in Table 3, which indicates that the largest number of hillocks was generated in the Al–In thin film by our nanoindentation technique when no overcoated layer was used, and that both (40 nm and 200 nm thick) overcoated layers completely prevented the generation of hillocks in pure Al (a) and pure Al (b) thin films. The table also indicates that the 40 nm thick overcoated pure Al layer reduced the generation of hillocks, while the 200 nm thick layer completely prevented the generation of hillocks in the Al–In thin film, which has the weakest anti-stress migration property of the three samples. We conclude that the overcoated pure Al layer (200 nm) is very effective in preventing hillock generation, while the overcoated pure Al layer (40 nm) has an unstable effect on the Al–In thin film, since the number of hillocks generated in the Al–In thin film with the overcoated pure Al layer (40 nm) at a stress temperature of 200°C is greater than at 300°C.

Fig. 2(a) and (b) shows SEM images after nanoindentation techniques (300°C thermal stress) which correspond to the samples: Al–In thin films with a non-overcoated layer (sample A) and with a 200 nm thick overcoated layer (sample B). Whiskers and hillocks are observed on the nanoindentation marks in sample A, whereas no whiskers or hillocks are observed in sample B. A comparison of these micrographs reveals that the overcoated layer is very effective in preventing stress migration.

To investigate the characteristics of overcoated pure Al thin film, we performed AFM surface analysis and cross-sectional TEM observation. Fig. 3(a) and (b) shows AFM top views of the overcoated pure Al layer on the pure Al (b) thin films before (sample 3a) and after (sample 3b) annealing at 300°C in vacuum for 60 min. They indicate that there is no significant change in either sample, and that their grain sizes are fine.

The results of cross-sectional TEM observation of sample 3a (non-annealed) and 3b (after annealing) are shown in Fig. 4(a) and (b), which also shows the results

of electron diffraction analysis in both overcoated pure Al layers. These images reveal that the morphology of the overcoated layer is fine-grained polycrystalline, and that there is little change in the grain size after annealing, as seen in Fig. 3(a) and (b). This indicates that the overcoated layer is robust to the thermal stress. Fig. 4(c) also shows the result of electron diffraction analysis in the pure Al (sample 3b) thin film existing under the overcoated layer. It indicates that the grain is (111) oriented.

Detailed nanostructural observation was performed by means of cross-sectional TEM, as shown in Fig. 5(a) and (b), which corresponds to samples 3a and 3b. A very thin (about 3 nm thick) native oxide layer is visible between the d.c. magnetron sputter-deposited pure Al thin film and the overcoated pure Al thin film in both TEM images. We consider that this oxide layer grew in the atmosphere between the periods of d.c. magnetron sputtering and RF sputtering. Aluminum lattice patterns are sporadically observed in the overcoated layers of both samples. Judging from this result and Fig. 4(a) and (b), we conclude that the overcoated pure Al layer has a fine-grained polycrystalline structure. Fig. 5(a) and (b) also reveals that there is no significant difference between the two samples. This indicates that the morphology of the pure Al/Al_2O_3/pure Al layered structure thin film in this study was little changed by annealing.

We consider that the Al/Al_2O_3/fine-grained polycrystalline pure Al layered structure thin film prevents stress migration from being caused by the thermal expansion mismatch between the glass substrate and itself, by absorbing the stress throughout the layered thin film. As regards application of the layered structure pure Al to interconnects in TFT arrays, since a resistivity of 3.12 Ω cm was obtained in the layered thin film by means of the four-point probe method, such a thin conductive film is suitable for low-resistivity interconnect materials in large high-resolution TFT-LCD arrays.

4. Conclusions

We confirmed that layered Al thin films with overcoated fine-grained polycrystalline pure Al thin film have a strong anti-stress migration property. With the 200 nm thick overcoated thin film, no hillocks or whiskers were generated in an Al–In thin film with a weak anti-stress migration property. By means of cross-sectional TEM analysis, we confirmed that the morphology of the layered thin film was changed little by annealing. We consider that the Al/Al_2O_3/fine-grained polycrystalline pure Al layered structure thin film prevents stress migration by absorbing the thermal stress throughout the layered thin film. Consequently, we conclude that the layered structure thin film can be used as an interconnect material in large high-resolution TFT-LCD arrays.

Acknowledgements

The authors wish to thank T. Yoshioka of JEOL Hightech Co., Ltd. for TEM observation, H. Okuhira of Hitachi Science Systems, Ltd. for TOF-SIMS analysis, S. Takeuchi and T. Hashimoto of IBM Display Business Unit for encouragement, and M. McDonald of IBM Yamato Laboratory for his comments on this article.

References

[1] G.L. Schnable, R.S. Keen, Proc. IEEE 57 (9) (1969) 1570.
[2] T. Oshibi, E. Iwamura, K. Takagi, K. Yoshikawa, J. Vac. Sci. Technol. A 14 (5) (1996) 2728–2733.
[3] S. Takayama, N. Tsunoi, Thin Solid Films 289 (1996) 289–294.
[4] E. Iwamura, T. Oshibi, K. Yoshikawa, Thin Solid Films 270 (1995) 450–455.
[5] H. Takatsuji, H. Ilyori, S. Tsuji, K. Tsujimoto, K. Kuroda, H. Saka, Mater. Res. Soc. Symp. Proc. 471 (1997) 99–104.
[6] T. Tsujimura, H. Kitahara, A. Mukita, P. Pryor, J. Batey, Proc. 1994 International Display Research Conference and International Workshops on AMLCD and Display Materials (1994) 424–427.
[7] T. Arai, Y. Hironaga, S. Tsuji, Mater. Res. Soc. Symp. Proc. 434 (1997) 37–42.
[8] K. Hamana, Y. Nakamura, O. Nittono, Jpn. J. Appl. Phys. 27 (1988) 1142.
[9] H. Takatsuji, S. Tsuji, H. Kitahara, K. Tsujimoto, K. Kuroda, H. Saka, Mater. Res. Soc. Symp. Proc. 441 (1997) 415–420.
[10] H. Takatsuji, K. Tsujimoto, K. Kuroda, H. Saka, Thin Solid Films 343/344 (1999) 461–464.

PERGAMON

Microelectronics Reliability 40 (2000) 947–953

MICROELECTRONICS RELIABILITY

www.elsevier.com/locate/microrel

High performance a-Si:H thin film transistors based on aluminum gate metallization

A. Nathan [a,*], R.V.R. Murthy [a], B. Park [a], S.G. Chamberlain [b]

[a] Department of Electrical and Computer Engineering, University of Waterloo, Waterloo, Ont., Canada N2L 3G1
[b] DALSA Inc., 605 McMurray Road, Waterloo, Ont., Canada N2V 2E9

Received 15 November 1999

Abstract

We present a systematic study of the sputter deposition conditions for aluminum thin films employed as gate metallization for high performance a-Si:H thin film transistors (TFTs). Here, we vary sputtering parameters such as deposition temperature, process pressure, and power, all of which have a strong bearing on the surface roughness of the film, including hillock generation induced by thermal processing. For example, at a low deposition temperature (30°C) and a low process pressure (5 mTorr), the surface roughness appeared to be significantly reduced. Transistors with gate metallization deposited under these conditions show a low leakage current (~10 fA), an ON/OFF ratio better than 10^8, and a mobility of 1.1 cm^2/Vs. In contrast, films deposited at 150°C and 10 mTorr, yield a degradation in mobility to 0.77 cm^2/Vs and an increase in leakage current to 1 pA, caused by the high interface roughness of the TFT channel due to hillock formation on the Al gate. © 2000 Elsevier Science Ltd. All rights reserved.

1. Introduction

While the demand for displays and image sensor arrays with a larger area and a higher pixel integration is increasing, there remain several fundamental scaling issues associated with gate (and hence, interconnect) metallization of inverted staggered hydrogenated amorphous silicon (a-Si:H) thin film transistors (TFTs) in the active matrix. Presently, high refractory metals such as molybdenum (Mo) and chromium (Cr) are employed. Although these are stable materials, their high resistivity results in RC gate delays that impose constraints on the array size. High conductivity metals such as copper (Cu) and aluminum (Al) are highly desirable, but their use is generally constrained by process considerations. Cu typically suffers from poor adhesion to glass and reacts with silicon and other plasma-enhanced chemical vapor deposition (PECVD) films. These problems are typically overcome, although at the cost of increased process complexity, by depositing the Cu on indium tin oxide (ITO) coated glass for increased adhesion [1] or through self-passivation of the copper surface with Cr_2O_3 to avoid reactions during the PECVD process [2].

With Al, although its resistivity is higher than that of Cu, its adhesion to glass substrates is far better, and more importantly, it constitutes a mature process technology. However, Al can suffer from the problems associated with surface roughness, including possibly hillock generation, induced by subsequent process steps that are relatively high in temperature. In TFT fabrication, the gate metallization is followed by PECVD of amorphous silicon nitride (a-SiN:H) dielectric and a-Si:H active layers. A high surface roughness, as we will observe in the TFT samples considered in this article, increases the leakage current and reduce the field effect mobility. Further, Al migration can potentially lead to short circuits between TFT terminals and interconnects. Although these issues can be avoided by: passivating or capping the Al surface with a mechanically hard metal layer [3]; using a relatively low resistivity Al alloys [4–6]; anodizing the Al at room temperature prior to deposition of the PECVD films [7,8], these solutions require

* Corresponding author.
E-mail address: anathan@vems.uwaterloo.ca (A. Nathan).

PII: S0026-2714(00)00012-3

additional processing steps associated with lithography, deposition, and annealing, thus adding to process complexity and cost.

It is well known that the surface morphology depends on the film's microstructure and its thermal processing conditions. The microstructure, to a large extent, can be controlled through a careful selection of parameters associated with the sputter deposition process. In this article, the sputtering deposition conditions for the Al gate metal are varied in terms of deposition temperature, process pressure, and DC power, and the performance of corresponding TFTs are compared in terms of leakage current and field effect mobility.

2. Process description and results

To investigate surface morphology, Al films of thickness 150 nm were deposited on Corning 7059 glass substrates by DC magnetron sputtering under different deposition conditions (Table 1), and all films were subsequently annealed at 260°C for 12 h to maintain consistency with the PECVD processes pertinent to TFT fabrication.

Fig. 1 shows SEM micrographs of the Al film surface for deposition temperatures of 150°C, 100°C and 30°C. Here, the process pressure and the power were fixed at 10 mTorr and 400 W, respectively. From these SEM micrographs, the films deposited at 30°C appear to have smoother surface texture than those deposited at a higher temperature.

To further investigate the surface smoothness as a function of the deposition pressure, we deposited films at 5, 10 and 20 mTorr (Fig. 2). In this set of experiments, the deposition temperature was set to be 30°C, and power was 400 W. Here, we observe that the films deposited at 5 mTorr show very smooth texture as compared to their high pressure counterparts.

Maintaining the same process temperature, we deposited films under a different sputtering power, but at low process pressures to observe possible changes in film morphology. Fig. 3 shows SEM micrographs of Al films deposited at 200, 300 and 400 W, with the deposition temperature and the process pressure fixed at 30°C and 5 mTorr, respectively. Here, we observe that the surface of films deposited at 300 W are smooth and free from pinholes or voids, as compared to the samples deposited at 200 or 400 W.

To investigate the impact of gate surface morphology on TFT performance, we chose films with the two contrasting surfaces shown in Figs. 1(a) and 3(b). In addition, with the former, we employed a 20 nm Mo capping layer on the Al gate of the TFT to investigate the degree of roughness propagation to the active interface. What we have presented is just a qualitative assessment of the film's microstructure. Quantitative estimates of the microstructure (e.g. grain size, roughness) associated with the different deposition conditions stated above, requires X-ray diffraction (XRD), atomic force microscopy (AFM), stress, and density measurements. Work along these lines is currently in progress.

Table 1
A summary of the deposition parameters for Al used in this study

	Substrate temperature (°C)	Process pressure (mTorr)	DC Power (W)
Al	30, 100, and 150	5, 10, and 20	200, 300, and 400

3. Thin film transistor fabrication and characterization

The TFTs used in this work are based on the conventional inverted staggered structure which is widely used in a-Si:H large area displays and imaging systems. A fully wet etch process has been used in fabrication. Here, Corning 7059 glass wafers are used as the substrate material. Various Al films of 150 nm thickness are deposited on these wafers under the different conditions given in Table 2. After patterning of the Al, 250 nm of gate a-SiN_x:H, 50 nm a-Si:H layer, and 250 nm of top a-SiN_x:H are deposited in a parallel-plate electrode PECVD system within one vacuum-pump-down cycle to minimize the density of defect states at interfaces. The deposition temperature of these layers is 260°C. At source and drain regions, a highly doped microcrystalline ($n^+\mu c$-Si:H) layer is employed to reduce contact resistance with final Al metallization.

A variety of TFTs were fabricated and characterized for their current–voltage and transfer characteristics. The TFT samples were annealed at 170°C prior to DC characterization. All measurements were performed using a DC parametric test system comprising the Keithley 236 source measure units with the TFT source grounded.

Fig. 4 shows SEM cross-sections of the gate/insulator interface of TFTs fabricated at the deposition conditions as indicated. Also shown are the corresponding transfer characteristics (I_{DS} versus V_{GS}) for various V_{DS} and stability behavior ($\sqrt{I_{DS}}$ versus V_{GS}) for different time durations of electrical stress. The latter serves as a measure for the metastable shift in threshold voltage with extended bias durations.

Transistors with gate metallization deposited at 30°C/5 mTorr/300 W show a low leakage current (~10 fA at low V_{DS}), an ON/OFF current ratio better than 10^8, and a mobility of 1.1 cm^2/Vs. These values are comparable to those reported for TFTs with anodized

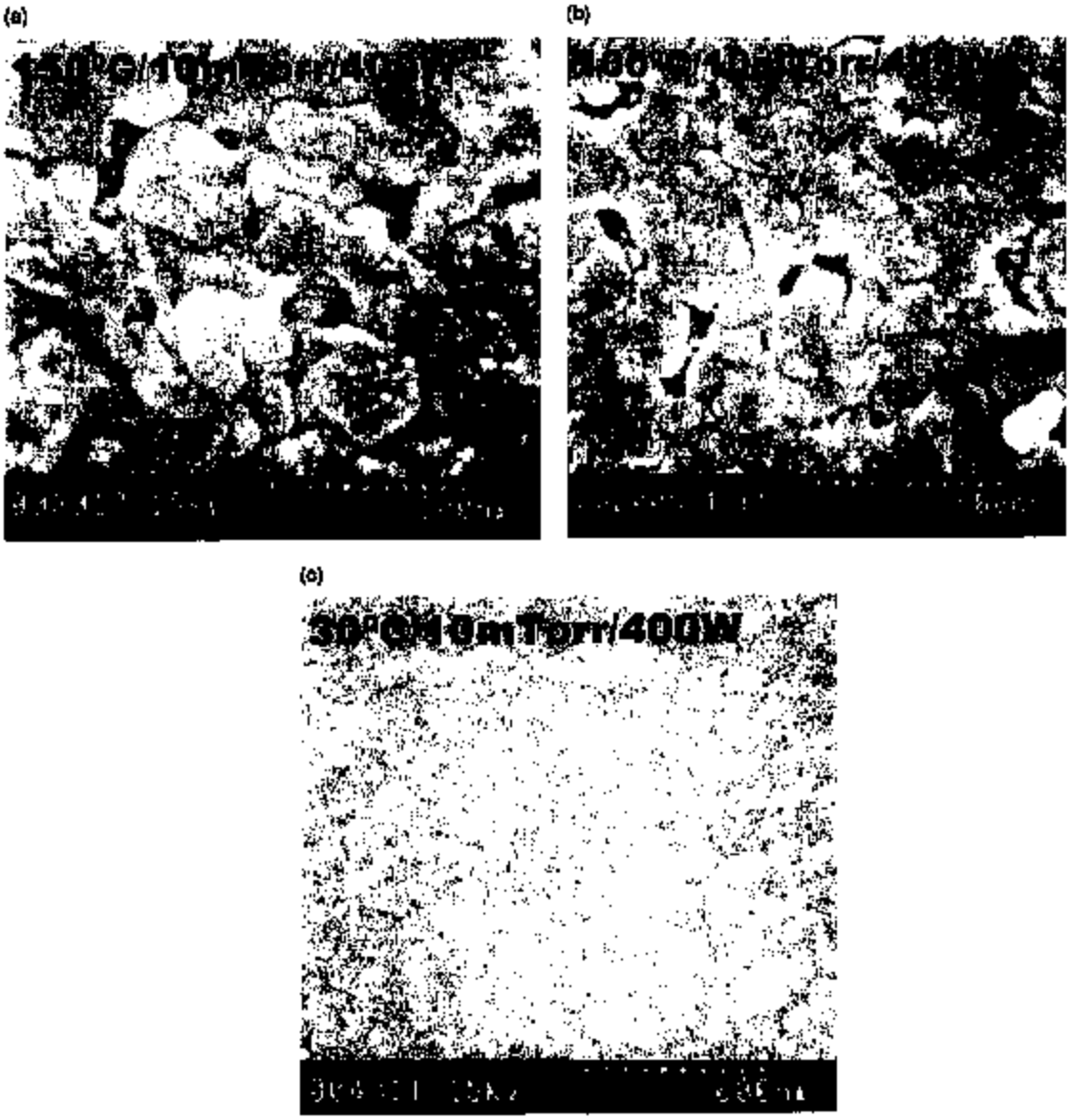

Fig. 1. SEM micrographs of the Al films deposited at (a) 150°C, (b) 100°C, and (c) 30°C, and subject to thermal annealing at 260°C for 12 h. The process pressure and power were fixed at 10 mTorr and 400 W, respectively.

Al gate [8]. In contrast, films deposited at 150°C/10 mTorr/400 W, yield a significant degradation in leakage current (~1 pA) and mobility (0.77 cm^2/V s). The reasons for the degradation are clear from observing the cross-section topologies shown in the figure. Here, we note a high surface roughness of the a-SiN_x:H gate insulator, and hence the TFT channel, caused by hillock formation on the Al gate. Note also that the corresponding shift in the threshold voltage is large. After 1 h bias stress of +25 V applied to the gate, the shift in threshold voltage is ΔV_T, ~5 V, as compared to the small shift of ΔV_T, ~2.3 V associated with the smoother gate. We attribute this to the metastability in the active a-Si:H layer induced by large (and perhaps even singular) localized electric fields stemming from surface non-uniformity in the channel. The same reasons hold for the leakage current. Large localized electric fields in the active region, stemming either from surface non-uniformities or

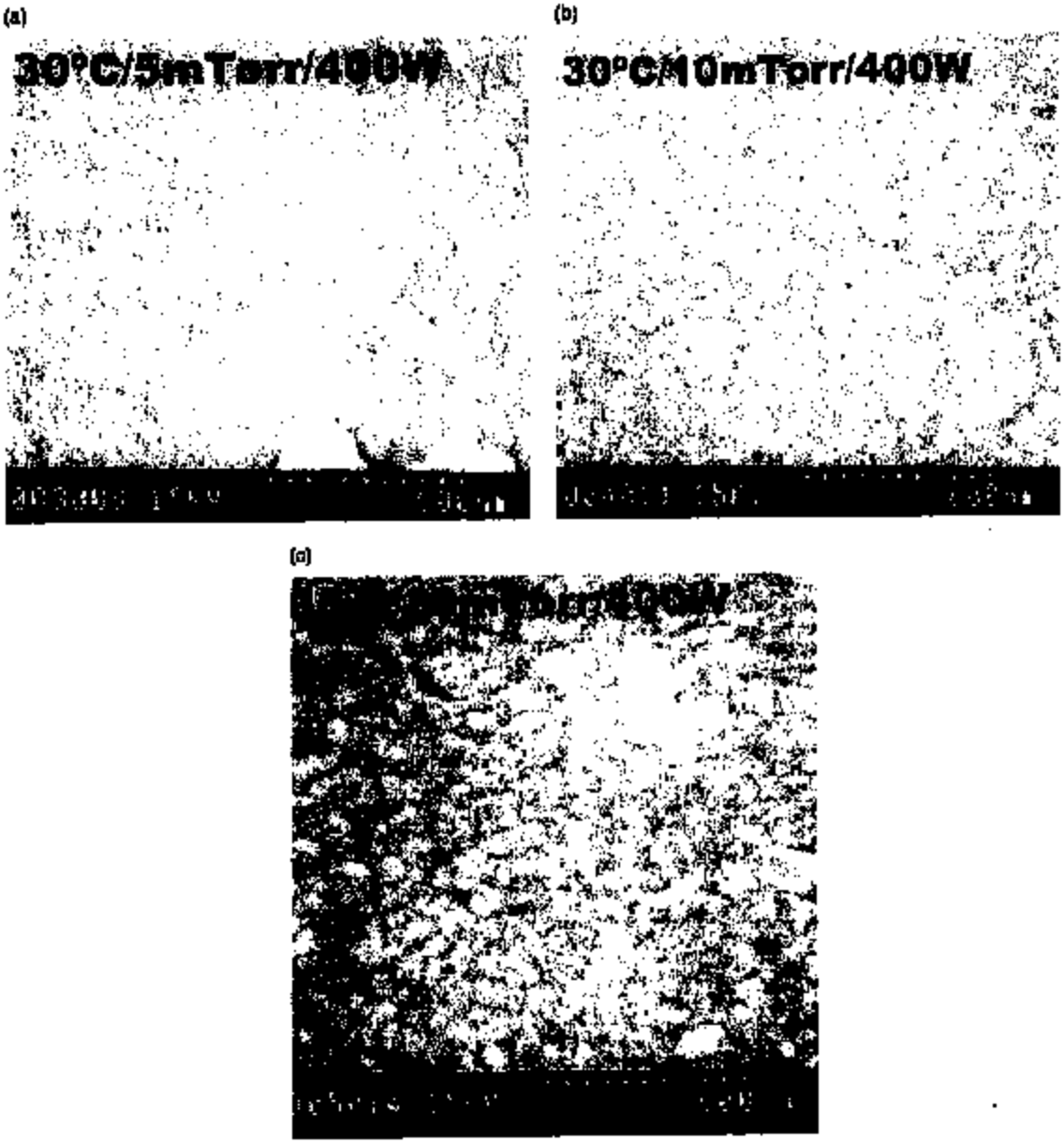

Fig. 2. SEM micrographs of the Al films deposited at (a) 5 mTorr, (b) 10 mTorr, and (c) 20 mTorr, and subject to thermal annealing at 260°C for 12 h. The deposition temperature and power were fixed at 30°C and 400 W, respectively.

applied bias (large V_{DG}), lead to an electric field dependent Frenkel–Poole type carrier generation in the active region [9]. Thus, the leakage current increases with increasing interface roughness as well as high reverse gate voltages. The field effect mobility in these transistors (Table 2), retrieved from the associated transfer characteristics, clearly shows the impact of surface roughness on mobility degradation.

For comparison, we have also included the cross-section of the TFT interface, whose Al gate is now capped with 20 nm of Mo to minimize propagation of the gate surface roughness (caused by hillock generation) to the active channel. It is clear from the cross-sectional views that the interface smoothness is as good or better, to yield improved leakage and stability characteristics.

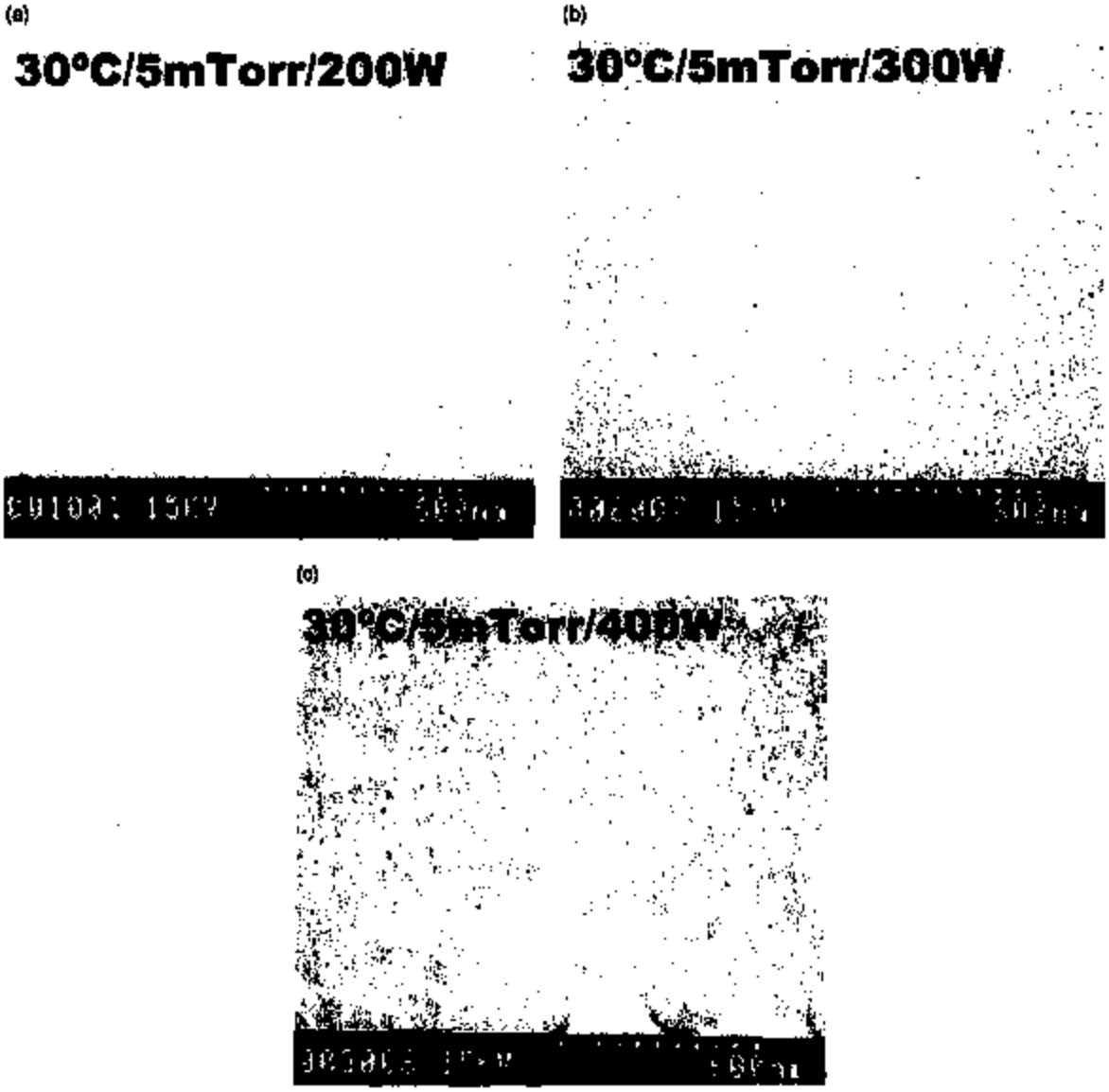

Fig. 3. SEM micrographs of the Al films deposited at (a) 200 W, (b) 300 W, and (c) 400 W, and subject to thermal annealing at 260°C for 12 h. The process pressure and temperature were fixed at 5 mTorr and 30°C, respectively.

Table 2
Values of field effect mobility retrieved from the transfer characteristics of TFTs shown in Fig. 4

Deposition conditions for Al gate	Field effect mobility (cm^2/Vs)
150°C/10 mTorr/400 W (Fig. 1(a))	0.77
30°C/5 mTorr/200 W (Fig. 3(b))	1.1

4. Conclusions

In this article, we present process considerations for Al gate metallization for a-Si:H TFTs with improved leakage current, mobility, and stability. Here, the sputter deposition conditions, i.e. deposition temperature, process pressure, and power, are varied to reduce surface roughness. A low interface roughness was achieved for TFTs with the Al gate deposited at low temperature and low pressure to yield characteristics with low leakage

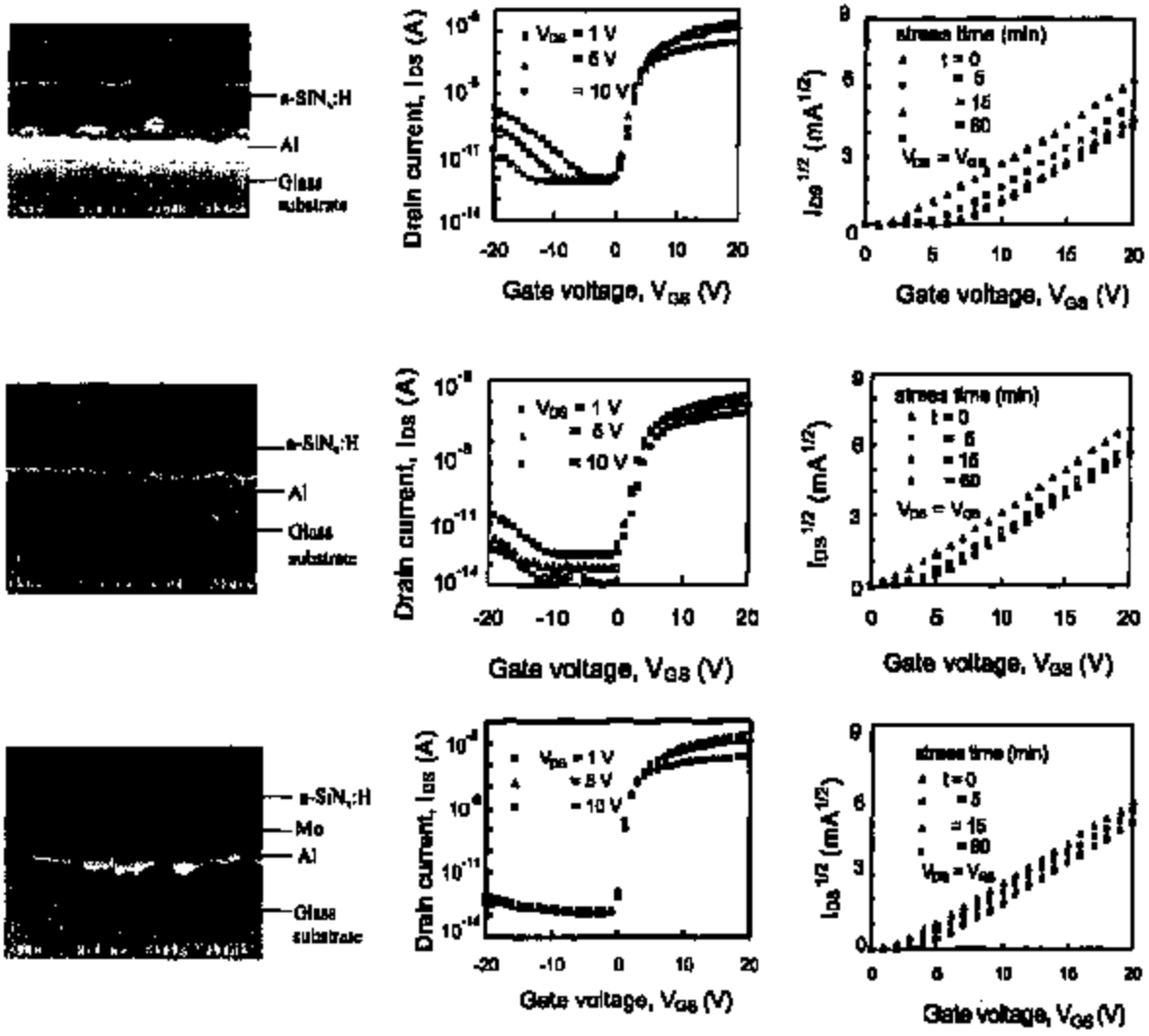

Fig. 4. Cross-sections of the gate/insulator interface and corresponding transfer characteristics (I_{DS} versus V_{GS}), at various drain source voltages (V_{DS}), and stability behavior (for $V_{GS} = V_{DS}$), when subject to electrical stress for time durations of 0, 5, 15, and 60 min. The TFTs were fabricated with the Al gate deposited under the conditions given in Table 2.

current (~10 fA), an ON/OFF ratio better than 10^8, and a high field effect mobility (1.1 cm^2/V s). These values are comparable to TFTs fabricated using anodized or Mo capped Al gates, both of which add to process complexity and cost.

Acknowledgements

This work is supported by the DALSA/NSERC Industrial Research Chair Program, Communications and Information Technology Ontario (CITO), and the Natural Science and Engineering Research Council of Canada.

References

[1] Fryer PM, Colgan EC, Galligan E, Graham W, Horton R, Hunt D, Latzko K, Nywening R, Jenkins L, John R, Koka P, Kuo Y, Libsch F, Lien A, Lovas J, Polastre R, Rothwell ME, Souk J, Wilson J, Wisnieff R, Wright S. SID Int Symp Dig Tech Papers, 1996. p. 333.

[2] Stringfellow H, Theiss SD, Kahn A, Wagner S. IEEE Trans Electron Dev Lett 1997;18:388.
[3] Tsujimura T, Kitahara H, Makita A, Fryer F, Batey J. Int Displ Res Conf, 1996, p. 142.
[4] Kim CW, Jeong CO, Song HS, Kim YE, Kim JH, Choi JH, Har MK, Yang HG, Souk JH. SID Int Symp Dig Tech Papers, 1996. p. 337.
[5] Hayashi M, Inoue K, Nozmi S, Sakata K, Takeguchi T, Morita T, Eguchi T. SID Int Symp Dig Tech Papers, 1997. p. 885.
[6] Takatsuji H, Ihori H, Tsuji S, Tsujimoto K, Kuroda K, Saka H. Mater Res Soc Symp Proc 1997;471:99.
[7] Arai T, Hiromasu Y, Tsuji S. Mater Res Soc Symp Proc 1997;424:37.
[8] Kim JH, Kanicki J, den Boer W. Mater Res Soc Symp Proc 1997;471:111.
[9] Nathan A, Austin M, Pereira D. Correlation between leakage current and overlap capacitance in a-Si:H TFTs. Proc IEEE Workshop Charge-Coupled Dev Adv Image Sensor, Karuizawa, Japan, 1999. p. 126–9.

Pergamon

Acta mater. Vol. 47, No. 1, pp. 89–98, 1998

Printed in Great Britain
PII: S1359-6454(98)00346-2
1359-6454/99 $19.00 + 0.00

INTERCONNECT DAMAGE BY ELECTROMIGRATION: EXPERIMENT AND NUMERICAL SIMULATION

J.-M. HUANG, W. YANG† and Z.-J. ZHAO
Department of Engineering Mechanics, Tsinghua University, Beijing 100084, P.R. China

(Received 5 August 1998; accepted 22 September 1998)

Abstract—Electromigration is a severe reliability issue for polycrystalline aluminum-based interconnects. The phenomenon is amplified by taking exposed interconnects at an elevated temperature. The intense electric currents they carry would drive atoms to diffuse, and leave hillocks or sinks along the interconnects. Experimental observations revealed that the hillocks grow against the surrounding grains in four stages: the incubation, the jump start, the deceleration, and the final stabilization. An analytical model is proposed to address features such as fluctuating mass flows into grains, particles of mass flown through the surface and the defect layers, stresses induced by the mass flow, and resistance against the grain boundary sliding. The incubation time and the protruding height are determined. The incubation time is proportional, while the protruding height is roughly inversely proportional, to the square of the grain size. Numerical simulations are exploited to quantify the experimental phenomenon. To design against the electromigration, one needs to raise the incubation time of an interconnect beyond its service life. To comply with this criterion, a polycrystal line with large and uniform grains (if not a bamboo line or even a single crystal line) with small variation in grain boundary diffusivities should be pursued. © *1998 Acta Metallurgica Inc. Published by Elsevier Science Ltd. All rights reserved.*

1. INTRODUCTION

Aluminum-based interconnects consist of more than 90% of the metal lines used in integrated circuits. The low resistance and good processing capability give aluminum an advantage with respect to RC delay and allow for higher performance circuit design. In the integrated circuits, the interconnects have small cross-sections (less than 1 μm wide and about 0.5 μm thick), carry intense electric current (above 10^{10} A/m^2), and may operate at a temperature of nearly half of the melting point (933 K) of aluminum. The flowing electrons exert a force (the electron wind force) on aluminum atoms, which drives aluminum atoms to diffuse. Mass diffusion under electric current, known as electromigration, raises the reliability concerns. The situation is further accentuated by the continuing trend toward miniaturization in integrated circuits, especially in the VLSI and power semiconductor devices.

Experimental observations revealed that single crystal interconnects can sustain a very long life [1, 2], for they have perfect microstructures and homogeneous material properties. The damage by voiding can nucleate only along the interfaces between the interconnect and its passivation [3]. The migration of a void is controlled by the mass flow along the void surface [4]. Subjected to electromigration, a void basically moves by surface diffusion, and may break away from a grain boundary [5–8]. For a bamboo line, electromigration may cause damage nucleation and failure by the unbalanced atomic flux into the triple junctions, creating either a void [9] or a transgranular slit [10–14]. These studies indicated that the failure by electromigration is manifested by the growth, shape change, and migration of voids or hillocks, and an interconnect evolves like a dynamical system that has multiple thermodynamic forces and undergoes dissipative processes.

Electromigration becomes a severe reliability issue for polycrystalline lines [8, 15], especially for the exposed lines. The mass flows along the side surfaces, the top surface, the grain boundaries, the surface grooves, and the defects like dislocations. They provide fast diffusion paths under electromigration, and the mass flow through them might be non-uniform [16, 17]. Surface damage is nucleated by the mass flow instability and intensified by the subsequent morphological evolution [15].

We begin with the electromigration experiment on polycrystalline aluminum lines. At ambient and elevated temperatures, hillocks and sinks are observed along the exposed surfaces of the interconnects, as reported in Section 2. The experiments revealed that hillocks and sinks grow against the surrounding grains in four stages: the incubation, the jump start, the deceleration, and the final stabilization. Section 3 presents an analytical model featuring the mass flow fluctuation and the grain boundary resistance. A scheme for the morphological evolution under electromigration is exploited in

†To whom all correspondence should be addressed.

Table 1. Failure times in various tests

Specimen number	Testing temperature (K)	Current density (10^{10} A/m^2)	Line width (μm)	Lifetime (h)
100-03	300	3.56	7.5	1171
100-09	300	3.67	1.5	275
100-10	300	3.14	3.5	506
200-01	300	6.16	1.5	65
200-02	300	2.64	3.5	3408
200-06	300	2.50	11.5	3040
400-09	300	3.67	1.5	489
600-09	300	3.67	1.5	893

Section 4, where numerical simulations are carried out to quantify the experimental phenomena.

2. ELECTROMIGRATION EXPERIMENT

2.1. *Damage of aluminum-based interconnects*

The authors conducted a series of electromigration tests of unpassivated polycrystalline interconnects. Only room temperature testing is described here. The metallizations consisted of films of Al/Si (mass fraction 99% Al and 1% Si) alloy of 1 μm thickness, which were sputter deposited at a rate of 0.03 μm/min on silicon substrates covered by a SiO_2 film of 0.4 μm. The film/substrate assembly was then annealed at 723 K for about 30 min. The processing followed the conventional technique in China to manufacture micron-width interconnects, and was carried out in the Institute of Microelectronics, Tsinghua University. The thin films were then etched to testing lines of 100 μm length and various widths (from 1.5 to 11.5 μm). The failure times of various tests are listed in Table 1. They are substantially lower than the testing data reported in the literature. The specimens were observed under a field-emission scanning electron microscope (Hitachi S-4200) at the Institute of Physics, Chinese Academy of Science. The intercon-

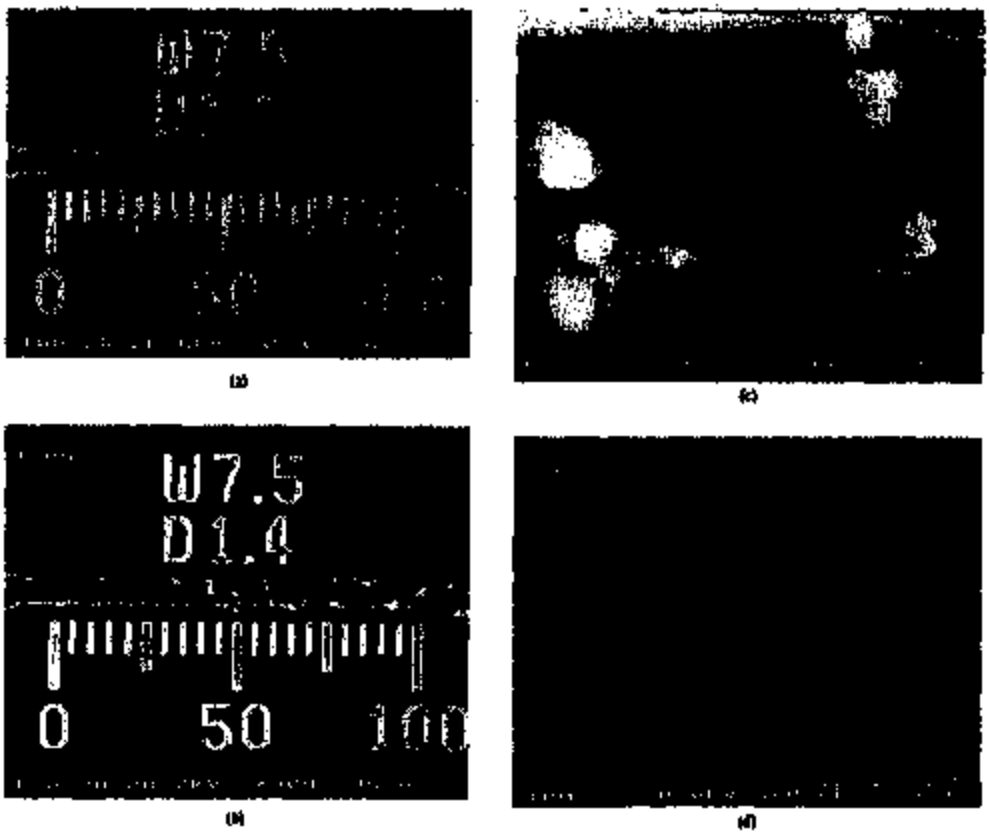

(a) (c) (b) (d)

Fig. 1(a, b, c and d).

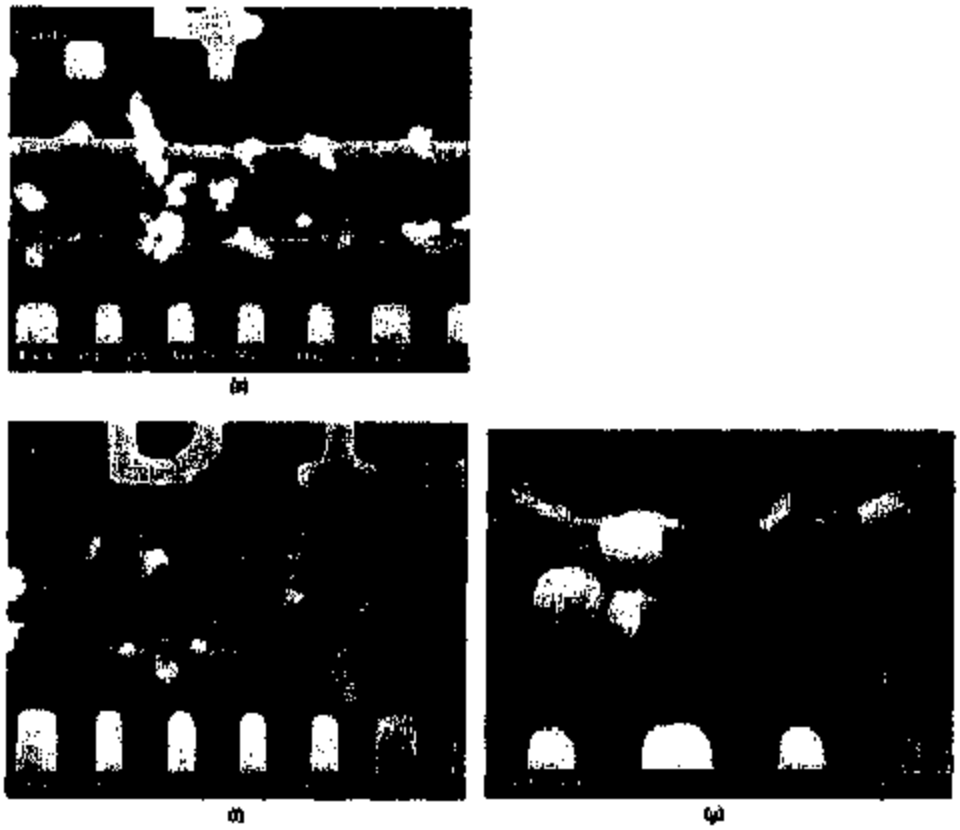

Fig. 1. SEM micrographs following a time sequence showing the damage of an interconnect under electromigration: (a) initial configuration; (b)–(d) 520 h; (e) 904 h; (f), (g) 1171 h.

necks are featured by the tiny columnar grain microstructures. The grains are about 0.115 μm in diameter and 1 μm in height, with possible lateral defects.

2.2. *Four stages of protrusion*

Figures 1(a)–(g) show a typical sequence of the morphological evolution of an interconnect tested at room temperature (300 K) under a current density of 3.56×10^{10} A/m^2 and a line width of 7.5 μm. These microscopic photographs were taken by interrupting the test after 0, 520, 904, and 1171 h of testing. In all graphs, the direction of the electron flow is from right to left. The exposed surfaces are initially flat, and surface damage is not detected, as shown in Fig. 1(a). The surface damage sets in when the electric current is switched on, but needs an incubation period for the hillocks to appear. As the time increases, the unbalanced mass flux accumulated in local areas becomes unstable. Suddenly many tiny hillocks and sinks burst from the interconnect, as shown in Fig. 1(b) at 520 h. An amplified view for a hillock protruding from the surrounding grains is shown in the lower-left corner of Fig. 1(c). The hillock is about 1.5 μm long and 2 μm in diameter. The detailed structure of a connected sink is shown in Fig. 1(d). The protruding motion of hillocks continues after their formation, see Fig. 1(e) at 904 h. The aspect ratio of the hillock becomes slender. The protruding motion decelerates. Gradually the matured hillocks become stabilized, but the new ones are still growing rapidly. The growing kinetics renders the picture shown in Fig. 1(f) at 1171 h. The longest protrusion in the figure has a length of about 4 μm, which imposes a severe threat of short-circuit failure. On the other hand, the local sinking becomes deeper and deeper, and finally cuts the line at 1171 h, see Fig. 1(g). Many sinks can be observed in the broken-down section. These results agree quantitatively with those of other experiments [6–9].

Grain boundaries play an important role in the electromigration of polycrystalline interconnects. They not only provide a fast path for electromigration, but also shape the evolution of the hillocks and sinks. We attribute the above-mentioned experimental phenomena to the fluctuation in the grain boundary configurations and the variation of the grain boundary diffusivities. These diversities provoke the unbalance of mass flows in the intercon-

Table 2. Evolution of hillocks during the test #108-86

Testing hours	Number of hillocks	Ave. height (μm)	Max. height (μm)
0	0	0	0
65	6	0.4	0.5
112	12	0.5	0.6
242	18	0.6	0.8
336	23	0.7	1.1
528	40	0.75	1.5
744	60	0.8	1.9
984	100	0.85	2.9
1171	150	0.87	4.0

next. In the area of mass flux surplus, the mass injection into a defect causes compressive stress which pushes the upper grain to protrude, against the sliding resistance by the surrounding grains. In the area of mass flux loss, the mass leakage leads to the formation of sinks which eventually sever the interconnect.

Quantitative counts on the micrographs provide the results listed in Table 2. The number of hillocks assumes an upturn curve with respect to the testing hours. The growth of the average hillock height is much slower than the growth of the maximum hillock height. Several nearby hillocks also have the tendency to merge into a wider hillock, then the growth of its height accelerates.

3. ANALYTICAL MODEL

The experimental observations indicate that the interconnects are composed of tiny columnar grains, whose cross-section can be simplified as the hexagon assembly shown in Fig. 2.

3.1. Mass flow under electromigration

Consider the configuration of a thin film interconnect shown in Fig. 2. Attention is focused on the mass flowing along the grain boundaries. Let J be the atomic flux, namely the number of atoms per unit length per unit time, due to the action of electromigration and the influence of back stress. It is given by [3]

$$J = -\frac{D\delta}{K_B T}\left(\frac{Z^* e E_t}{\Omega} + \frac{\delta \sigma_n}{\partial l}\right) \qquad (1)$$

where D and δ denote the diffusivity and the thickness of the grain boundary, K_B the Boltzmann constant, T the absolute temperature, Ω the atomic volume of the migrating species, Z^* the effective valence of the migrating ions, e the electron charge, E_t the tangential electric field along the grain boundary, σ_n the back stress normal to the grain boundary, and l the tangential coordinate measured along the grain boundary. Equation (1) is rigorous only if the grain boundary is flat.

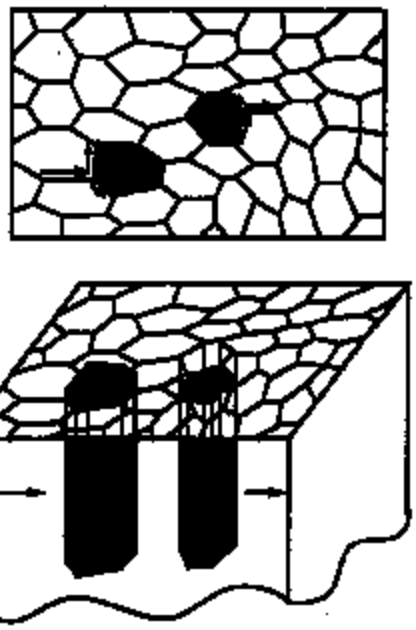

Fig. 2. Sketch on the emergence of a hillock or a sink along the grain boundaries under electromigration.

Since our tests were carried out for unpassivated and exposed lines, the constraining stress is small, and most of the mass flow will be absorbed by the stress-free morphological evolution. A substantial stress gradient like that analysed by Thouless *et al.* [3] cannot be built up. Thus, the back stress term is neglected in the subsequent analysis, and equation (1) is reduced to

$$J = -\frac{D\delta}{\Omega K_B T} Z^* e E_t. \qquad (2)$$

The rate of accumulation of material at a point in the grain boundary, $\dot{u}_n$, relates to the atomic flux, J, by mass conservation

$$\dot{u}_n = -\Omega \frac{\partial J}{\partial l}. \qquad (3)$$

3.2. Mass flux into a grain

Under electromigration, the mass flown into (or out of) a particular grain by the six grain boundaries it connects, as shown in Fig. 3. Let us introduce a global coordinate system OXY for the grain, with the X-axis aligned with the electric field vector $\mathbf{E}$. The angle between the ith connected grain boundary and the X-axis is denoted by θ_i ($i = 1,2,\ldots,6$). Without loss of generality, we regard that each grain boundary has the same thickness δ but different diffusion constants D_i

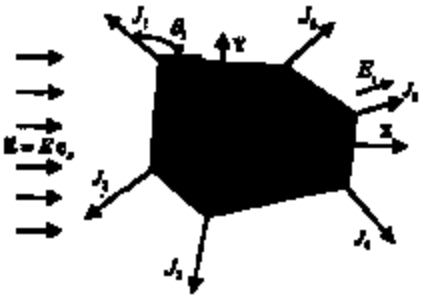

Fig. 3. Calculation of mass fluxes into a grain by electromigration.

$(i = 1,2,\ldots,6)$. From equation (2), the atomic flux into the grain (termed the grain flux J_g) is given by

$$J_g = -\frac{Z^* eE\delta}{\Omega K_B T}\sum_{i=1}^{6} D_i \cos\theta_i. \tag{4}$$

First consider the case of regular hexagon grains, as shown in Fig. 7(a). The diffusivities of various grain boundaries are assumed to obey a normal distribution, $N(\bar{D},s_D^2)$, with the expected diffusivity D and the standard deviation s_D. It can be shown that the grain flux, J_g, also obeys a normal distribution. The expectation of the grain flux is zero, and the standard deviation of the grain flux is $\sqrt{3}(Z^* eE\delta/\Omega K_B T)s_D$.

Now consider the case of general hexagon grains, as shown in Fig. 8(a), where the grain size and the grain shape only have mild fluctuations. The diffusivities of the grain boundaries obey a normal distribution $N(D,s_D^2)$. Through considerable algebra, the expectation of the grain flux is obtained by

$$J_g = \frac{Z^* eE\delta}{\Omega K_B T} D\left[\cos\left(\frac{\pi}{3}-\theta+\varphi_1\right)+\cos\left(\frac{\pi}{3}+\varphi_2\right)+\cos\left(\frac{\pi}{3}+\theta+\varphi_3\right)-\cos\left(\frac{\pi}{3}-\theta+\varphi_4\right)-\cos(\theta+\varphi_5)-\cos\left(\frac{\pi}{3}+\theta+\varphi_6\right)\right] \tag{5}$$

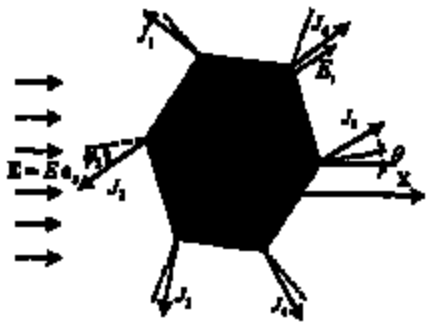

Fig. 4. Configuration of a general hexagon grain assembly.

where θ denotes the angle between the X-axis and the 5th grain boundary of a hypothetical regular hexagon, and φ_i the angle deviations from the regular hexagon, as depicted in Fig. 4. To fix the value of θ, we require that the sum of φ_i $(i = 1,2,\ldots,6)$ vanishes. The standard deviation of the grain flux is given by

$$s(J_g) = \frac{Z^* eE\delta}{\Omega K_B T} s_D \left[3+\cos^2\left(\frac{\pi}{3}-\theta+\varphi_1\right)+\cos^2\left(\frac{\pi}{3}+\varphi_2\right)+\cos^2\left(\frac{\pi}{3}+\theta+\varphi_3\right)+\cos^2\left(\frac{\pi}{3}-\theta+\varphi_4\right)+\cos^2(\theta+\varphi_5)+\cos^2\left(\frac{\pi}{3}+\theta+\varphi_6\right)\right]^{1/2}. \tag{6}$$

We further assume that the deviation angles, φ_i $(i = 1,2,\ldots,6)$, obey a normal distribution of $N(0,s_\varphi^2)$. Then the grain flux, J_g, also obeys a normal distribution. The expectation of the grain flux is zero, and its standard deviation is calculated by

$$s(J_g) = \sqrt{3}\frac{Z^* eE\delta}{\Omega K_B T} s_D \sqrt{2-\exp(-s_\varphi^2)}. \tag{7}$$

3.3. *Partition of mass flow*

The lateral defects which might cut through the tiny columnar grains provide channels to accommodate the fluctuation of the mass flow. As shown in Fig. 5, let h represent the distance of the initial defect from the original top surface, W the protruding height of the grain, and H the thickness of the injected mass measured over the cross-section. The unbalanced mass flow is accommodated through two layers: the surface layer and the defect layer. The surface layer covers the region from the top surface to a depth of H_0, where the mass flow is predominantly through surface migration, regardless of the location of the defect. The defect layer covers a range of characteristic sizes H_D^* above and below the current defect height. Accordingly, the evolution law for the height of the injected mass, H, can be phrased by

$$H(t) = \begin{cases} \dfrac{2\Omega J_g}{\pi R^2}\displaystyle\int_0^t H_D^*(t)\,dt & t<t_0 \\ H_0+\dfrac{2\Omega J_g}{\pi R^2}\displaystyle\int_{t_0}^t H_D^*(t)\,dt & t\geq t_0 \end{cases} \tag{8}$$

where t is the time and t_0 the incubation time for a hillock or a sink to appear, and H_0 denotes the critical thickness of mass injection or the value of H at t_0. The size of the influence region of the defect layer, H_D^*, relies on the defect location, $h+(H/2)-W$, from the original top surface. We adopt the following piece-wise linear relation of H_D^* with respect to the defect location

$$H_D^* = \begin{cases} 0, & h+\frac{1}{2}H-W<H_S \\ h+\frac{1}{2}H-W-H_S, & H_S\le h+\frac{1}{2}H-W<H_S+H_D \\ \frac{H_D}{H_S+H_D}\left(h+\frac{1}{2}H-W\right), & h+\frac{1}{2}H-W\ge H_S+H_D \end{cases} \tag{9}$$

where H_D is a characteristic size of the defect layer. The mass injection into the defect will terminate if

$$h+\frac{1}{2}H(t)-W(t)=H_S. \tag{10}$$

The two length parameters H_S and H_D dictate the partition of mass flow.

3.4. Stress due to mass flow

The injection (or leakage) of masses into (or from) those defects would induce local confining stresses normal to the film plane. Though they have little effect on the mass transport along the grain boundaries that are normal to the film plane, they do cause the protruding motion of hillocks. Take the example of mass injection into a defect. The confining stress is compressive and should be balanced by the shear resistance along the grain boundaries around the upper half grain which intends to protrude. If the compressive stress multiplied by the cross-section of the columnar grain reaches the maximum value of the slip resistance offered by the surrounding grains, the hillock will emerge from the grain.

A simple model is adopted to calculate the compressive stress of the grain. We approximate a columnar hexagon grain by a cylindrical grain of the same height and the same cross-section. This approximation enables an axi-symmetric modeling of a prismatic dislocation loop, as shown in Fig. 6. In the figure, C is a planar circular loop of the prismatic dislocation with radius R in the XOY plane, whose normal directs along the Z-axis. The vector r marks the projection of a generic point P on the dislocation plane, while a point on the loop is marked by r'. The vector r forms an angle θ with the positive X-direction. By the Peach–Koehler formula [18], the stress field, σ, due to the dislocation loop is given by

$$\sigma = \frac{\mu}{4\pi}\left\{\oint_C (\mathbf{b}\times\nabla')\frac{1}{|\mathbf{r}-\mathbf{r}'|}\otimes d\mathbf{r}' + \oint_C d\mathbf{r}'\otimes(\mathbf{b}\times\nabla')\frac{1}{|\mathbf{r}-\mathbf{r}'|} - \frac{1}{1-\nu}\oint_C [(\nabla\otimes\nabla-1\nabla^2)\mathbf{r} - \mathbf{r}'[\nabla'\cdot(\mathbf{b}\times d\mathbf{r}')]\right\} \tag{11}$$

where μ denotes the shear modulus, ν the Poisson ratio, and $\mathbf{b}$ the Burgers vector (which relates to the mass injection thickness H). The gradient symbols ∇ and ∇' are operated on the field and on the planar dislocation loop, respectively. Through lengthy algebra, the compressive stress normal to the plane of the dislocation loop can be calculated as

$$\sigma_z = -\frac{\mu H}{4\pi(1-\nu)}\int_0^{2\pi}\frac{d\phi}{\sqrt{r^2+R^2-2rR\cos(\theta-\phi)}} \tag{12}$$

where ϕ is the integration angle around the dislocation loop. The overall compressive force on the upper columnar grain is

$$P_z = -2\pi\int_0^R r\sigma_z\,dr = \frac{2\mu}{1-\nu}RH \tag{13}$$

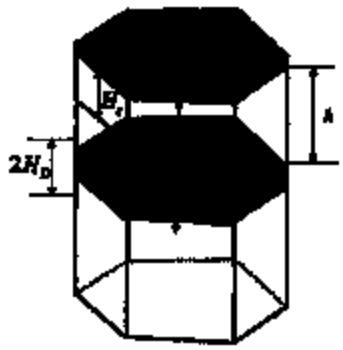

Fig. 5. Geometry and various characteristic lengths for the protruding motion of a grain.

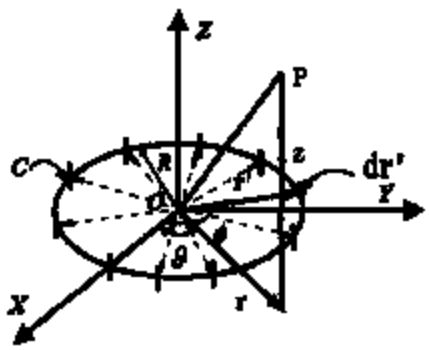

Fig. 6. Compressive stress field by a prismatic dislocation loop induced by the injected mass.

where P_a provides the driving force for a grain to protrude.

3.5. Sliding condition and incubation time

The slip resistance against the grain with mass injection, prior to any movement of the defect, is composed of shear stresses along the vertical surfaces surrounding the grain

$$P_\tau = 2\pi R h \tau_s \tag{14}$$

where τ_s denotes the shear strength of the grain boundary.

The onset of protrusion instability is dictated by the condition of $P_a = P_\tau$. Combining equations (13) and (14), one obtains the critical thickness of the mass injection

$$H_c = \pi(1-\nu)\frac{\tau_s}{\mu}h. \tag{15}$$

Substituting equation (15) into equations (8) and (9), one arrives at the incubation time for the appearance of a hillock

$$t_c = \frac{\pi R^2}{\Omega J_g}\frac{H_S + H_D}{H_D}\ln\left(1 + \frac{\pi(1-\nu)\tau_s}{2\mu}\right) \tag{16}$$

provided that $h + \frac{1}{2}H_c \geq H_S + H_D$. The incubation time is proportional to the square of the grain size. The hillocks will not form in an interconnect during its service life if the grain size is sufficiently large.

We next introduce the concept of the minimum incubation time. For a normal distribution, the unbalanced material fluxes mostly lie in a region of $\pm 3s(J_g)$. Therefore, the minimum incubation time for a protrusion can be derived by

$$t_{c,\min} = \frac{\pi R^2}{3\Omega s(J_g)}\frac{H_S + H_D}{H_D}\ln\left(1 + \frac{\pi(1-\nu)\tau_s}{2\mu}\right) \tag{17}$$

where $s(J_g)$ is equal to $\sqrt{3}(Z^* e\bar{\delta}\delta/\Omega k_B T)\mu_D$ for the case of *regular* hexagon grains, and is given by equation (7) for the case of general hexagon grains.

3.6. Protruding height and sinking depth

Consider the subsequent evolution of a hillock or a sink. As shown in Fig. 5, the slip resistance caused by the surrounding grains against the subsequent evolution is

$$P_\tau = 2\pi R\left(h + \frac{H}{2} - W\right)\tau_s \tag{18}$$

where it is tacitly assumed that the injected masses are evenly distributed to the top and the bottom grain matrices. The compressive force due to the mass flux into the defect is

$$P_c = \frac{2\mu}{1-\nu}R(H - W). \tag{19}$$

The balance of two forces provides an expression for the amount of grain slide. When a hillock is caused by the mass injection, or a sink caused by the mass leakage, the amount of grain slide, W, is obtained by

$$W(t) = -\frac{\pi(1-\nu)\tau_s}{\mu - \pi(1-\nu)\tau_s}h + \frac{2\mu - \pi(1-\nu)\tau_s}{2\mu - 2\pi(1-\nu)\tau_s}H(t), \quad t \geq t_c. \tag{20}$$

Accordingly, the protruding height is roughly proportional to R^{-2}.

4. NUMERICAL SCHEME AND DAMAGE SIMULATION

We now devise a numerical scheme to simulate the protruding and sinking motions. Two simplified polycrystalline configurations are generated by computer for the aluminum interconnect shown in Fig. 2. The first one is an array of regular hexagon grains. As mentioned before, the 5th grain boundary connected to the grain forms an angle θ with the X-axis. The connection angles of other grain boundaries, denoted by $\bar{\theta}_i$ $(i = 1,2,3,4,6)$, differs from $\bar{\theta}_5 = \theta$ by multiples of $\pi/3$. The second configuration deviates from the first by fluctuating the connection angles according to $\theta_i = \bar{\theta}_i + \varphi_i$ $(i = 1,\ldots,6)$, with φ_i being described by a normal distribution of $N(0,s_\varphi^2)$. The diffusivities of different grain boundary segments are assigned by a normal distribution of $N(D,s_D^2)$. Prior to the switching on of the electric current, the interconnect assumes a perfectly flat top surface and no mass injects in any grain defects. After the switching on of the electric current at $t = 0$, the material fluxes into each grain can be calculated through equation (4). For a particular grain, a protruding or sinking process commences at the critical time determined by equation (16). The subsequent evolution is governed by equations (8), (9) and (20). It consists of a set of integral equations, and can be solved by the explicit Euler iteration. During the simulation, the interconnect is composed of 3445 grains, with 6892 triple junctions and 10 336 grain boundary segments.

The physical constants for aluminum-based interconnects are listed in Table 3. The electric field is calculated from the measured current density and the conductivity of aluminum (3.55×10^7 A/V m). The average grain size $\bar{R} = 0.115$ μm is obtained by counting the grain number in a fixed observation area. The assignments of the mean diffusivity $D\delta$, and the effective valence Z^* are worth of explanation. A wide range of the diffusivity data for aluminum exist. For example, Wang *et al.* [14] quoted the surface diffusion data from Wohlbier [19] which gives $Z^* = 20$, $D = 10^{-4} \times \exp[-0.7(\text{eV})/k_B T]\ \text{m}^2/\text{s}$, and $\delta = 0.286$ nm. They lead to a small value of $D\delta = 5.1 \times 10^{-37}\ \text{m}^3/\text{s}$ at 300 K. On the other hand, Borgesen *et al.* [20] adopted the value of $Z^* = 10$ and quoted the grain boundary diffusion data by Kaur *et al.* [21], which gives a

Table 3. Physical constants for aluminum interconnects

μ (GPa)	κ (GPa)	ν	K_B (J/K)	T (K)	ϵ (C)	E (V/m)	R (μm)	$D\delta$ (m^3/s)	Z^*
24.5	1.54	0.348	1.38×10^{-23}	300	1.6×10^{-19}	1003	0.115	1.02×10^{-29}	20

much larger $D\delta$ value of 6.4×10^{-23} m^3/s. In the present simulation, we adopt the value of $Z^* = 20$ and take an intermediate value of $\tilde{D}\delta = 1.02 \times 10^{-29}$ m^3/s.

We assume that the location of defect, h, obeys a normal distribution $N(\bar{h}, s_h^2)$. Since the defects appear mostly in the lower-bottom of the film, we take the expected location as $\bar{h} = 6\bar{R}$, and the standard deviation as $s_h = 0.5\bar{R}$. The other standard deviations are taken as $s_D = 0.1\bar{D}$ and $s_\phi = \pi/4$ in the calculation. Under this s_ϕ value, the polycrystal configuration, as shown in Fig. 8(a), resembles the statistical feature of the actual microstructure. The thickness for the surface layer H_S and that for the defect layer H_D are taken as $\bar{R}$ and $0.5\bar{R}$, respectively. The latter is less than the former since the attraction for the incoming masses is stronger near the surface layer than that near the defect layer. The evolution is measured by the normalized time

$$\tilde{t} = \frac{\tilde{D}\delta}{K_B T \bar{R}^3} Z^* e E t.$$

The simulation indicates that the mass flows in the interconnect indeed have four stages: the incubation stage, the rapid growing stage, the

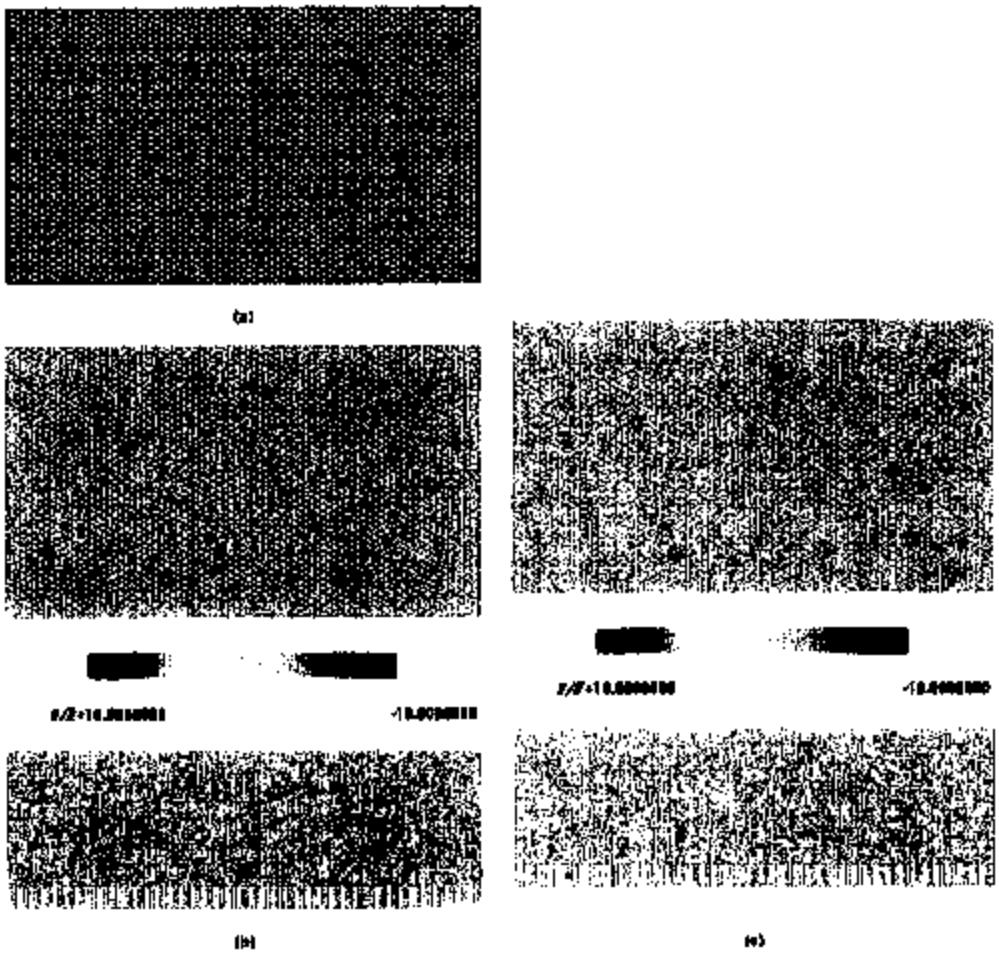

Fig. 7. Morphological evolution for regular hexagonal grains: (a) the initial configuration; (b) at $\tilde{t} = 5$; (c) at $\tilde{t} = 10$. [W denotes the protruding height (> 0) or the sink depth (< 0) and $\bar{R}$ the average grain radius].

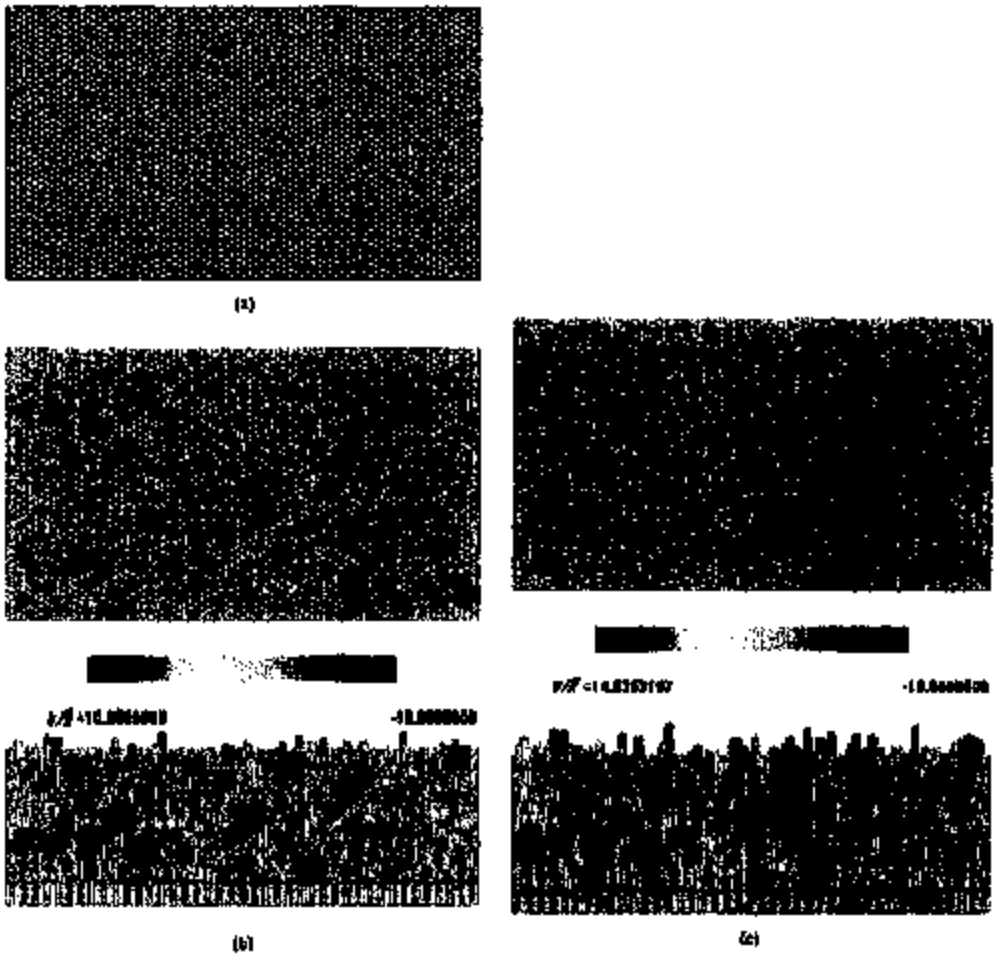

Fig. 8. Morphological evolution for general hexagonal grains: (a) the initial configuration; (b) at $\bar{t} = 5$; (c) at $\bar{t} = 10$.

deceleration stage, and the final stabilization. We now describe the two cases of calculation in detail.

The initial configuration for the case of regular hexagon grains is shown in Fig. 7(a). Figures 7(b) and (c) show two snapshots of the interconnect at $\bar{t} = 5$ and 10, which depict the damage evolution of the grains. The regularity of the configuration suppresses the fluctuation in the grain fluxes. The interconnect will have a relatively long life. The case of general hexagon grains in Fig. 8(a) bears more resemblance to the actual configuration. Figures 8(b) and (c) illustrate two snapshots of the damage evolutions in the interconnect at the instant $\bar{t} = 5$ and 10. In the same time intervals, the hillocks and sinks are more severe, and the number and the average height of the hillocks are greater than the interconnect of regular hexagons. The variations of the protruding height and the sinking depth are shown in Fig. 9 vs the normalized drag. The grain flux J_g is taken to be $2.34s(J_g)$ in the calculation. The protruding motion jumps to a fast growing stage after an incubation time, then gradually slows down to approach a stabilized height, in good agreement with our experiments.

The predictions on the morphological fluctuations due to the regular grain assembly and the general grain assembly are very different. Figure 10 plots the curves of $s_W/\bar{R}$ vs $\bar{t}$, where s_W represents the standard deviation of the surface morphology W. The general grain assembly can cause a more severe morphological instability than the regular one. The effect due to the angular deviation s_ϕ is two-fold. First, the angular deviation leads to larger standard deviation in mass flow, as quantified by equation (7). Second, it also results in the fluctuation of the grain sizes from their average value $\bar{R}$, and that causes further morphological fluctuation

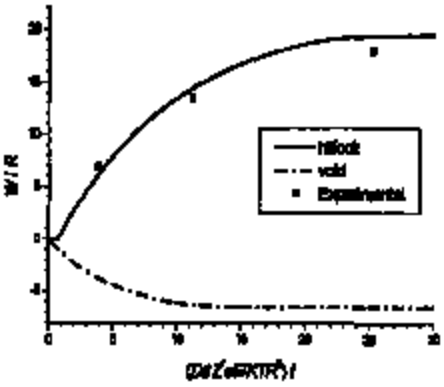

Fig. 9. Protruding height and the sinking depth vs the normalized time, $\bar{t} = 2.34\kappa(t)$.

of the microstructure since the inverse square dependence of the hillock height with respect to R.

To address the importance of grain size on morphological evolution under electromigration, we include a further example of general hexagon array in Fig. 11(a), featuring a much larger average grain size of $3R$. The interconnect is composed of 481 grains, with 964 triple junctions and 1444 grain boundary segments. Other parameters are the same as the previous case. Since the incubation time for the case in Fig. 8 is about $\bar{t} = 1$, its square dependence on the grain size would lead to an average incubation time of $\bar{t} = 9$ for the present case (for the sake of comparison, the previous R value is used to get the normalized time). The simulation confirms this prediction. At $\bar{t} = 5$, there are hardly any morphological changes. At $\bar{t} = 10$, the damage evolution just starts, as shown in Fig. 11(b). It is much subdued when compared with Fig. 8(c).

To design against the electromigration, one needs to raise the incubation time of an interconnect beyond its service life. To comply with this criterion, a polycrystal line with large and uniform grains (if not a bamboo line or even a single crystal line) with small variation in grain boundary diffusivities is desirable.

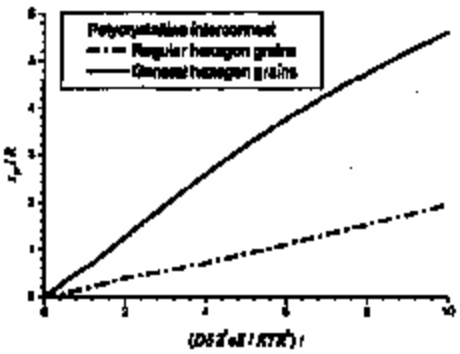

Fig. 10. Development of morphological fluctuation (in terms of the standard deviation of W) with respect to the normalized time.

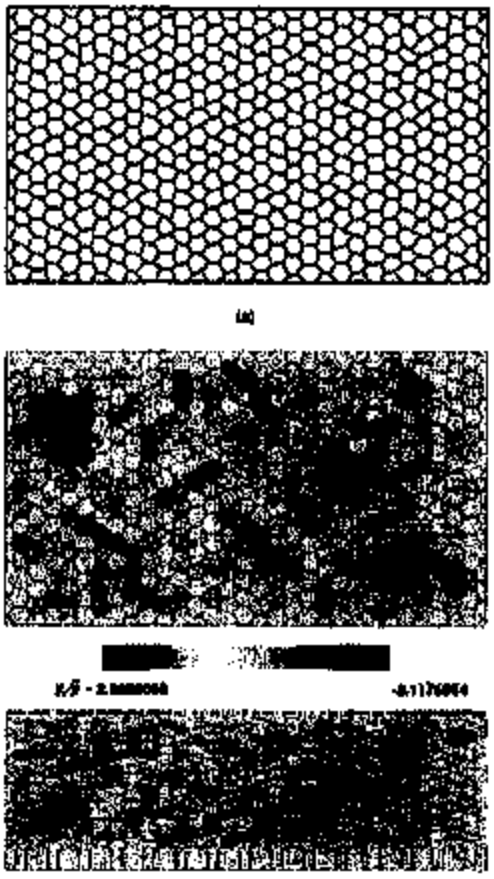

(a)

(b)

Fig. 11. Morphological evolution for a general hexagonal array of much larger grain size of 0.343 μm: (a) the initial configuration; (b) at $\bar{t} = 10$.

To conclude this paper, we mention that the failures of the polycrystalline interconnects often result from a combination of different mechanisms, such as stress migration, grain boundary diffusion, and thermal migration. A coupled analysis is worthwhile in the future.

Acknowledgements—The authors appreciate the support by the National Natural Science Foundation of China.

REFERENCES

1. D'Heurle, F. M. and Ames, I., *Appl. Phys. Lett.*, 1970, 16, 80.
2. D'Heurle, F. M., *Proc. IEEE*, 1971, 59, 1409.
3. Thouless, M. D., Yu, H., Zhao, Z. and Yang, W., *J. Mech. Phys. Solids*, 1996, 44, 371.
4. Yang, W., Wang, W. and Sun, Z., *J. Mech. Phys. Solids*, 1994, 42, 897.

5. Li, C.-Y., Bergman, P. and Korhonen, M. A., *Appl. Phys. Lett.*, 1992, 61, 411.
6. Besser, P. R., Madden, M. C. and Flinn, P. A., *J. appl. Phys.*, 1992, 72, 3792.
7. Kraft, O., Bader, S., Sanchez, J. E. and Arzt, E., *Mater. Res. Symp. Proc.*, 1993, 309, 199.
8. Marieb, T., Flinn, P., Bravman, J. C., Gardner, D. and Madden, M., *J. appl. Phys.*, 1994, 76, 1026.
9. Arzt, E., Kraft, O., Nix, W. D. and Sanchez, J. E., *J. appl. Phys.*, 1994, 76, 1563.
10. Sanchez, J. E. and Arzt, E., *Scripta metall. mater.*, 1992, 27, 285.
11. Sanchez, J. E., McKelly, L. T. and Morris, J. W., *J. appl. Phys.*, 1992, 72, 3201.
12. Rose, J. H., *Appl. Phys. Lett.*, 1992, 61, 2170.
13. Sun, Z., Wang, W. and Yang, M., *Appl. Phys. Lett.*, 1994, 64, 1944.
14. Wang, W., Sun, Z. and Hao, T.-H., *J. appl. Phys.*, 1986, 59, 2394.
15. Zhao, Z. and Yang, W., *Tsinghua Sci. Technol.*, 1997, 2, 274.
16. Thompson, C. V. and Kahn, H., *J. Electron. Mater.*, 1993, 22, 581.
17. Sun, Z., *Acta metall. mater.*, 1994, 42, 3581.
18. Pesch, M. O. and Kottler, J. S., *Phys. Rev.*, 1950, 80, 436.
19. Weichler, F. H., *Diffusion and Defect Data—Solid State Data*, Vol. 47. Trans. Tech. Publications, Switzerland, 1986, p. 4.
20. Bergman, P., Korhonen, M. A., Stillman, T. D., Brown, D. D. and Li, C.-Y., in *Thin Films: Stress and Mechanical Properties III, MRS Symposium Proceedings*, Vol. 239, ed. W. D. Nix, J. C. Bravman, E. Arzt and L. B. Freund, 1992, p. 483.
21. Kaur, I., Gust, W. and Bravman, L., *Handbook of Grain and Interphase Boundary Diffusion Data*. Ziegler Press, Stuttgart, 1989.

ELSEVIER

Ultramicroscopy 81 (2000) 245–262

ultramicroscopy

www.elsevier.nl/locate/ultramic

Analysis of local strain in aluminium interconnects by energy filtered CBED

S. Krämer*, J. Mayer, C. Witt, A. Weickenmeier, M. Rühle

Max-Planck-Institut für Metallforschung, Seestr. 92, D-70174 Stuttgart, Germany

Received 29 July 1999; received in revised form 27 September 1999

Dedicated to Professor Harald Rose on the occasion of his 65th birthday

Abstract

Energy filtered convergent beam electron diffraction (CBED) was used to investigate localised strain in aluminium interconnects. The quantitative analysis of the experimental patterns is based on a multi-step evaluation procedure which is the main subject of the present paper. The improvements which were made to the analysis method aim at increasing both the automation and the accuracy. The detection of the higher order Laue zone (HOLZ) line positions is performed by means of the Hough transform. The required sub-pixel resolution can be achieved routinely and the achievable accuracy is only limited by the line width and the amount of noise in the patterns. The determination of the strain state is performed via a refinement algorithm which is based on varying the strain state in the sample coordinate system and simulating the patterns for the individual grains until a best fit with the experiment is obtained. For the simulation we have developed a new correction scheme in which the dynamical effects are treated separately for each individual HOLZ line. The results show that the main source of the observed strains is the difference in thermal expansion coefficients. The strain is substantially reduced underneath a hillock in the interconnect. Asymmetries in the strain distribution around the hillock show that the unidirectional diffusion during electromigration tests causes peak strains in areas next to the hillock which may be possible failure sites.

Keywords: CBED; Energy filtered imaging and diffraction; Data processing/image processing; Electromigration; Finite element modelling

1. Introduction

Internal strains limit the properties and control the failure mechanisms in many materials systems composed of metals and ceramics or semiconductors. Frequently encountered sources of internal strain are the differences in thermal expansion coefficients, coherency strain developed during the growth process, or strain resulting from diffusional processes. One example of the latter is the electromigration which occurs while passing a current through a thin interconnect line. Amongst the numerous methods which have been applied to measure the internal strain, convergent beam electron diffraction [1] is undoubtedly the one with the

* Corresponding author. Tel.: +49-711-2095-225; fax: +49-711-2095-320.

E-mail address: kraemer@hrem.mpi-stuttgart.mpg.de (S. Krämer)

0304-3991/00/$ - see front matter
PII: S0304-3991(99)00191-6

highest spatial resolution. In a transmission electron microscope, probes with a diameter of a few tens of nanometers or even nanometers can easily be formed, which is well adapted to the dimensions in which the strain state may vary e.g. across interfaces. There is a growing number of studies in which the technique has successfully been applied to different materials systems (see, for example, Refs. [2–8]). However, there are a number of problems inherent to the CBED technique, e.g. thin foil relaxations, the inelastic scattering background and the dynamical scattering effects, which so far have prevented the implementation of the CBED method as a standardised technique for strain measurement.

In the present paper we want to report on a number of improvements which we have made to the method and we want to demonstrate the level of accuracy which can now be obtained for the case of Al interconnects. In terms of the instrumentation the major breakthrough was the commercial availability of energy filters for TEMs [9]. Energy filtering is very important since it helps to increase the reliability of the strain measurement using CBED. In transmission electron microscopy, it is favourable to use thick samples for the strain measurement since the effects of thin film relaxation decrease and the sharpness of the HOLZ lines increases. However, at the same time the probability of inelastic scattering (mainly plasmon losses) increases [10–12]. This not only leads to an increase in background and a broadening of the HOLZ lines, but also to a shift of the centre of the HOLZ lines. Exciting a plasmon loss of 20 eV at 100 keV is equivalent to a change of 2×10^{-4} in electron energy with a corresponding change in Bragg angle and thus in HOLZ line position. A combination of these effects can easily lead to a reduction in the accuracy of the strain analysis to about 10^{-3}. For commercial purity aluminium this strain value corresponds to the yield stress and thus a strain measurement becomes impossible.

In the analysis of the patterns, the first crucial step is finding the exact location of the HOLZ lines in the zero-order disc. The aim for any quantitative evaluation obviously is to use a computer-based, highly automated algorithm which is robust against noise in the patterns. Such an algorithm is the Hough transform [13] which in electron microscopy has become popular as an ideal tool for the analysis of Kikuchi bands in backscattering patterns obtained in a scanning electron microscope [14,15]. We have adapted the algorithm to the requirements of our CBED measurement, in particular to the fact that the line position has to be detected with sub-pixel accuracy [16]. The analysis is then carried out by comparing the measured line positions with the ones predicted from theoretical simulations for different strain states. In principle, this requires a dynamical Bloch wave simulation which, however, is much too time consuming for a thorough investigation of the parameter space being explored in the refinement algorithm. Therefore, we have developed a kinematical simulation procedure with a new dynamical correction scheme which is able to produce more reliable results than the commonly used effective high-voltage method.

In the present work, the method has been adapted to the strain measurement in thin aluminium interconnect lines on silicon substrates. Energy filtering enables one to use interconnects with dimensions which correspond to the actual geometry used in devices. Thus, no artefacts are introduced which may occur during an additional thinning step, and the measured strain state can directly be related to the failure of a line in the device. The results will be compared to the results of finite element simulations for the same specimen geometry and it will be shown that such a combined approach leads to a detailed understanding of the strain state in the system. In particular, it will be shown that local stresses exist which by many times exceed the yield stress of the bulk material. The results will be discussed and an outlook on future work will be given.

2. Instrumentation and specimen preparation

The present studies were performed on a Zeiss EM 912 Omega energy filtering TEM. The microscope was operated at a nominal high-voltage setting of 120 kV and a LaB_6 filament was used. The minimum probe size which still produces sufficient signal intensity is approximately 10 nm, however,

in most of the experiments we used probe sizes between 20 and 30 nm. In general, the experiments are best performed in a liquid-nitrogen cold stage which prevents contamination and reduces the amount of thermal diffuse scattering present in the pattern. However, this leads to an increase in the strain caused by the difference in thermal expansion coefficients and, in order to avoid this, the interconnect line was investigated at room temperature in the present work. An energy selecting slit with a width of 15 eV was inserted and centred around the zero-loss peak. The patterns were recorded by means of a GATAN 1k × 1k slow scan CCD camera.

The samples used in the present studies consisted of patterned lines on a silicon substrate. The interconnects were fabricated from a film stack on a Si substrate which consisted of 500 nm thermal oxide, 45 nm sputtered Ti, 300 nm reactively sputtered TiN, 400 nm sputtered Al and 30 nm reactively sputtered TiN. Following film deposition, the wafers were annealed for 60 min at 400°C in forming gas to allow for grain growth. Next, the metal films were patterned using UV lithography and reactive ion etching to form single lines with widths of 0.5 μm. In a second step, 5 μm long gaps in the Al were patterned leaving Al segments on the continuous TiN layer. The segment used in this experiment has a length of 50 μm. The TiN layer was kept continuous to provide electrical conductivity. The Al microstructure in the segments has an average grain size of 1.3 μm and predominantly bamboo structure [17].

Electromigration tests were performed on the 0.5 μm wide segments applying current densities of 2×10^6 A/cm^2 at a temperature of 200°C for approximately 100 h. Owing to the current-induced electromigration force, the Al atoms start to migrate in the direction of the electron flux. As a consequence the material depletes at the cathode end and hillocks form at the anode end of the segment.

For the experiments we prepared TEM specimens in which the electron beam passes through the Al segment parallel to the silicon substrate surface. The main problem of these samples is that for finite tilt angles the thick Si substrate may obscure the interconnect line. Therefore, in our case, a combination of several preparation techniques had to be applied. In the first step, a thin slice with the interconnect at the edge was cut out of the silicon wafer using a diamond wire saw. Subsequently, tripod-polishing was used to reduce the thickness of the slice to about 80 μm and to remove the edges of the substrate near the interconnect as schematically shown on the left side of Fig. 1. The remaining edge typically has a thickness of 20 μm. During the preparation the interconnect is always protected by wax. In the last step, a focused ion beam microscope (FIB) was used to remove the substrate material near the interconnect leaving a thin, 3 μm wide ridge with the interconnect on top (see Fig. 1). With the final specimens, experimental tilt angles of typically ± 15° can be obtained. In the case of the sample investigated in this paper, the 500 nm wide line was additionally thinned to a specimen thickness of about 200 nm using the FIB microscope.

The finite element program ANSYS is used to simulate the spatial distribution of the strain in the interconnect in order to get the information on the dependence of the strain on the actual geometry of the line. Purely elastic models are applied and all the parameters are adjusted to the physical parameters of the interconnect line.

3. Experimental procedures

A TEM micrograph of the area investigated is shown in Fig. 2. In the undisturbed region the nominal height of the line is 400 nm and the nominal width is 200 nm. The latter is the actual specimen thickness used in our TEM measurement. At such a thickness, the inelastic scattering background already leads to a substantial reduction in the visibility of the HOLZ lines. As mentioned above, energy filtering helps to improve the contrast, sharpen the HOLZ lines and also to make sure that they are at the Bragg position corresponding to the actual accelerating voltage.

For the analysis of the patterns an accurate value of the accelerating voltage has to be known in order to get accurate values of the strained lattice constants. For this reason, a reference material with a high crystal quality should be used, e.g. single crystalline silicon. In the following it will be shown

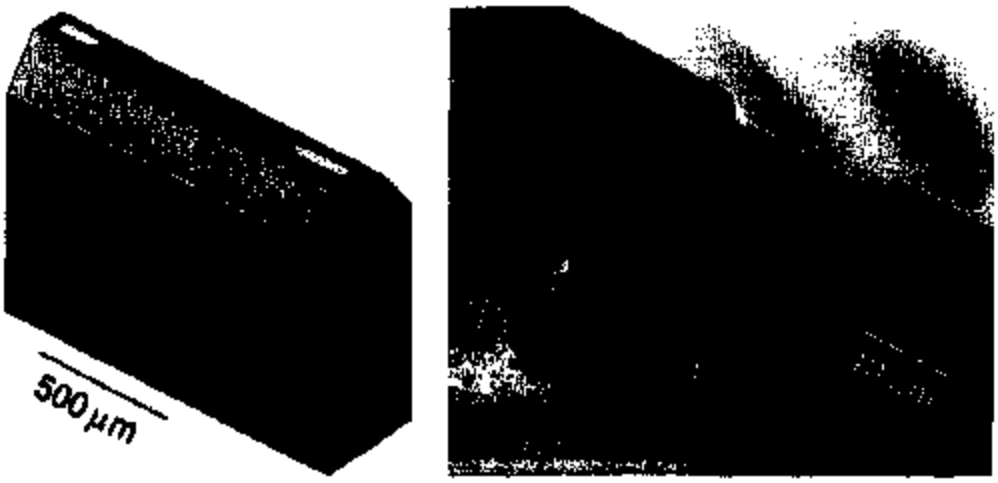

Fig. 1. Schematic drawing of the sample geometry used in our experiments (left). A thin slice is cut perpendicular to the wafer with the actual interconnect being centred on a thin face of the section. Further material is removed around the interconnect by tripod-polishing. The final electron transparent areas are obtained by removing the passivation layers and most of the Si substrate in a focused ion beam (FIB) instrument. Images of the actual electron transparent specimen area can be obtained in the FIB microscope (right).

Fig. 2. TEM micrograph of the section of the interconnect line which has been studied in our CBED experiments. In the central part a hillock is visible which has been grown in electromigration experiments before the TEM specimen was prepared.

that using careful analysis the accelerating voltage can be determined with an accuracy of about 20 V.

The actual patterns in the interconnect were acquired at a series of spots parallel and perpendicular to the line. Patterns which were acquired close to the interface at the bottom of the line and also at the top of the line close to the capping layer show a pronounced splitting of some of the HOLZ lines (Fig. 3a). This can be attributed to a bending of the lattice planes parallel to the interface which results from the inhomogeneous stress distribution close to the interfaces. This effect does not occur in patterns acquired close to the centre of the line (Fig. 3b) and therefore such patterns were used for the study of the strain distribution along the interconnect and in particular under the hillock.

In the following, the important aspects of the strain analysis using CBED are discussed including the detection of the HOLZ line positions, the treatment of the dynamic effects, the correlation between the strain state and the HOLZ line positions and the details of the evaluation procedure.

3.1. HOLZ line detection

For the detection of the HOLZ line positions we use the Hough transform [13], which originally was developed to detect particle traces in a bubble chamber. The main advantages of the Hough transform are that it can easily be automated and that it makes use of the whole intensity distribution along a HOLZ line and not only, like other techniques, in a limited number of traces perpendicular to a HOLZ line. Therefore, the analysis can make much better use of the statistics and produces accurate results even in

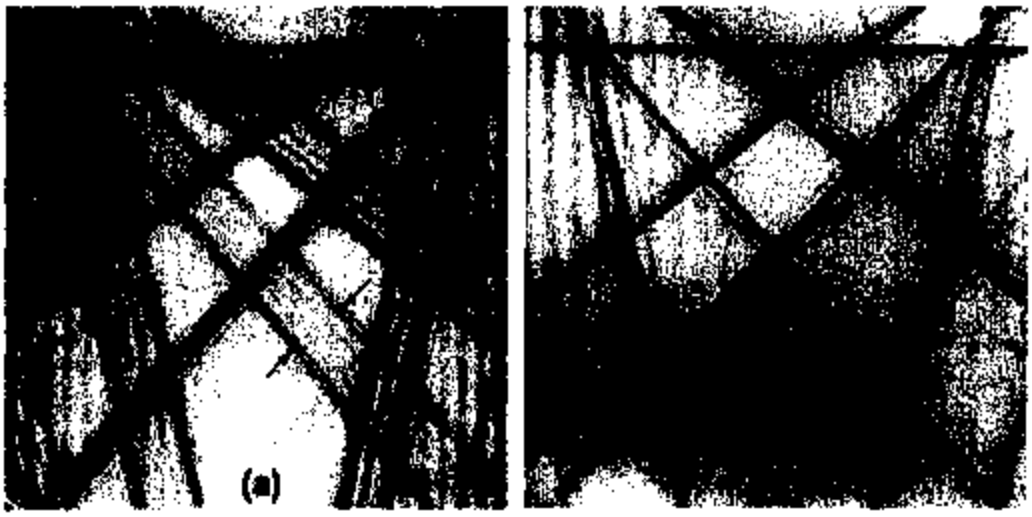

Fig. 3. (a) CBED pattern taken with the spot positioned close to the substrate interface. Some of the HOLZ lines show a pronounced splitting which is caused by a bending of the lattice planes close to the substrate. (b) From the central part of the interconnect line undisturbed patterns can be obtained.

the case of patterns which contain a large amount of noise.

The Hough transform is based on the more general Radon transform [18] which can be applied to any parametrised curve in two dimensional space:

$$R(\alpha,c)=\int_{-\infty}^{\infty}\int_{-\infty}^{\infty} f(x,y) \times \delta[y-\tan(\alpha)\cdot x-c]\,\mathrm{d}x\,\mathrm{d}y. \quad (1)$$

Here $f(x,y)$ is the intensity distribution in the two-dimensional pattern which has to be analysed, and the function in the square brackets is the parametrised version of the curve which leads to a sharp maximum in the Radon transform $R(\alpha,c)$. Mathematically, the Radon transform is defined as the integral of the intensity distribution along the curve which is defined by the parameters (α,c). In our case, the curve is a straight line with

$$y=\tan(\alpha)x+c \quad (2)$$

and $R(\alpha,c)$ is then called the Hough transform of the intensity distribution. $R(\alpha,c)$ exhibits a maximum if a straight line described by (α,c) runs along a straight maximum in the intensity distribution in (x,y)-space.

The CBED patterns are commonly recorded with a CCD camera and thus finite rectangular images with discrete pixels are obtained. In this case the integrals in Eq. (1) are replaced by summations and the details are given Ref. [16]. The main problem of the (α,c)-parameterisation of a straight line is that c diverges for $\alpha\to\pm 90°$. To overcome this divergence, the y-axis intersection c_y is only used in the angular range between $-45°$ and $+45°$, whereas the intersection c_x with the x-axis is used for slopes from $-90°$ to $-45°$ and for $+45°$ to $+90°$. Another problem is that, owing to the finite size of the pattern, the number of pixels forming a straight line decreases the closer the line segment gets to the corners of the image. This fact has to be taken into account by an appropriate biasing of the Hough intensities [16].

As an experimental example, Fig. 4a shows the central region of the zero order disc and the corresponding Hough transform of a CBED pattern acquired in ⟨1 3 3⟩ zone axis orientation from the interconnect line shown in Fig. 2. For the unstrained material, the pattern possesses mirror symmetry relative to the vertical axis. Because of the strain in the interconnect the symmetry in the arrangement of the HOLZ lines is lost which also leads to noticeable asymmetries in the arrangement of Hough peaks. The dynamical interaction of the electron waves with the crystal causes a bending and distortion of the HOLZ lines in the vicinity of

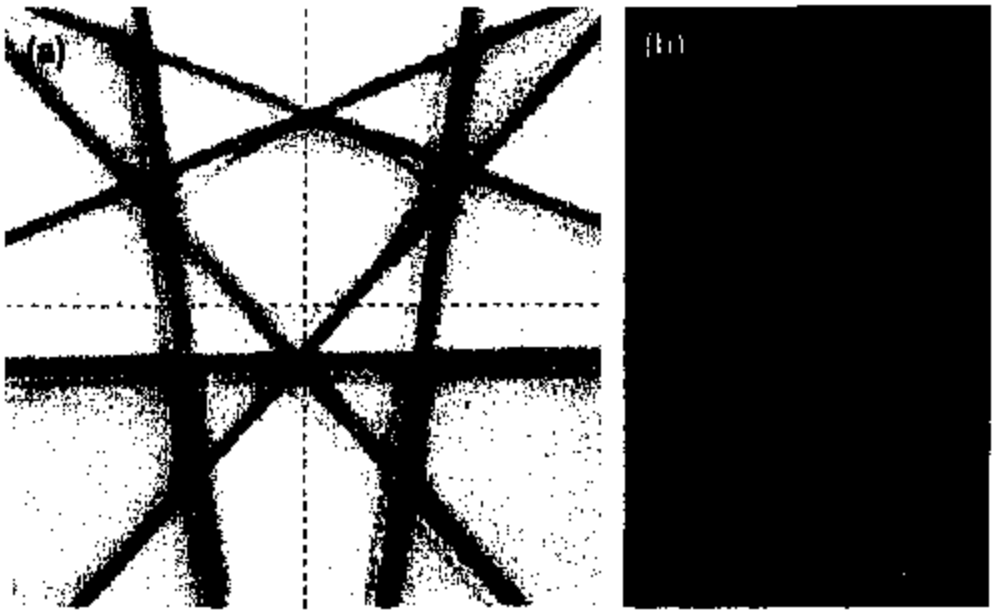

Fig. 4. (a) Central portion of a [1 3 3] CBED pattern acquired in the centre of the line and the corresponding Hough transform (b). Because of the unidirectional strain, the symmetry of the pattern is broken with respect to the vertical line.

their intersections. Therefore, the HOLZ line crossings are masked before the actual Hough transform is applied. Furthermore, in order to save computing time, areas with fairly homogeneous intensities in the patterns can also be masked. Then the Hough transform is computed with high pixel resolution and the result is shown in Fig. 4b. In order to obtain the required accuracy, the actual maximum of each Hough peak has to be determined to sub-pixel accuracy. This is achieved by fitting a two-dimensional polynomial to the intensities in the discrete pixels of the Hough peaks [16]. The maximum of the intensity in this polynomial fit can be determined with an accuracy of 0.2 pixel for the intersection c and with an angular resolution of 0.02° for the slope.

3.2. Geometry of the strain state

In a given medium, a general local strain state is defined by six components, three normal strains and three shear strains. By transforming into the eigenstate, the number reduces to three strains along the main axes. Knowing the directions of the main axes therefore drastically reduces the number of strain components which have to be detected. The directions of the main axes are mostly defined by the actual geometry of the sample, which defines the sample coordinate system.

In the general case of a thin film, two axes of the eigenstate strain lie in the film plane and the third one along the film normal. However, if a biaxial strain state within a polycrystalline film is assumed, the orientation of the two in-plane directions of the eigenstrain in a grain are not a priori known. Therefore the total in-plane strain state has to be detected, i.e. two normal strains ε_x, ε_y and the shear strain ε_{xy}. Together with the strain along the film normal four strain components have to be detected. Assuming a plane stress state with vanishing stresses along the film normal again reduces the number to three independent strain variables.

In our case, the geometry of the interconnect defines the directions of the sample coordinate system. The x-direction is chosen parallel to the interconnect line, the y direction perpendicular to the line and parallel to the interface and the z-direction perpendicular to the interface. Finite element

modeling (see Section 4) shows that in this geometry there mainly exists a triaxial strain state with the main axes of the eigenstrain being parallel to the x-, y- and z-direction. Therefore, in the following the aim is to measure the strain components ε_x, ε_y and ε_z in the given sample coordinate system.

In most cases the crystal unit cell axes a,b and c of the grains forming the interconnect do not coincide with the axes of the sample coordinate system. These crystal orientations thus define a separate crystal coordinate system. In the analysis, the strain state has to be transformed from the sample to the crystal coordinate system and vice versa to determine the influence of the macroscopic strain on the lattice parameters of the individual grains. In the actual measurement, a HOLZ pattern is acquired in an appropriate high-indexed zone axis orientation, which is usually selected in such a way that it is near the y-axis of the sample coordinate system. In the case of Al, a number of different zone axes can be used. In the present analysis we selected the $\langle 1\,3\,3\rangle$, $\langle 1\,3\,6\rangle$, $\langle 1\,2\,5\rangle$ and the $\langle 3\,3\,4\rangle$ zone axis patterns. In general, it is always possible to find an appropriate zone axis which is less than 15° away from the given orientation of the grains, making it possible to analyse the strain state in any given crystal.

3.3. Treatment of dynamical effects

HOLZ lines are shifted with respect to their kinematical positions due to the dynamical interaction of the beam electrons with the crystal potential. A detailed discussion of the dynamical shift has been given by Zuo and Spence [19] using the Bloch wave concept. The deviation of the actual Bragg condition of the HOLZ reflections from the kinematical case can be explained with the help of the dispersion surfaces as illustrated in Fig. 5. In a zone axis pattern, the shift of the HOLZ line positions is mainly determined by the distance of the first branch of the dispersion surface from the kinematical sphere defined by the K-vector of the incident beam [20]. The influence of the ZOLZ reflections can approximately be determined using perturbation theory [2,21]. The results show that in flat regions of the dispersion surface, the effects can approximately be simulated by using an effective high-voltage, but only for HOLZ lines in a single Laue zone. The effective high-voltage correction was first suggested by Lin et al. [21] and is widely used in literature.

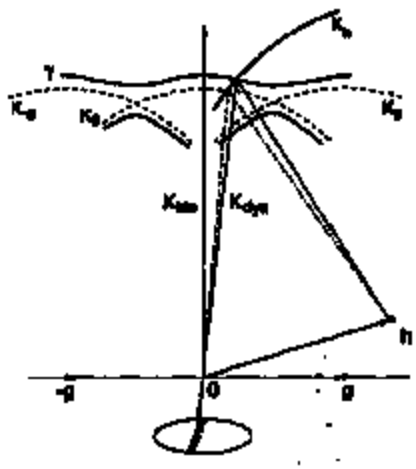

Fig. 5. Schematic drawing of the dispersion surfaces (labelled γ) which result from the strong dynamical interactions of the beam electrons with the crystal. In the crystal, the kinematical wavevectors (labelled K_0, K_g and K_{-g}) are no longer allowed and therefore the intersection with K_0 shifts from K_0 to the dispersion surface, leading to a corresponding shift of the HOLZ line in the CBED pattern.

The main drawback of the effective high-voltage approach is that it cannot describe the deviations of the dispersion surface from a spherical geometry. As shown in Fig. 5 the dynamical shift increases near the Bragg positions of low index reflections. Therefore the dynamical shift of each HOLZ line depends on the actual geometry of the surrounding Bragg positions for each incident beam direction. The most accurate method to describe the dynamical interactions is to use the fully dynamical Bloch wave formalism which accounts for all dynamical diffraction effects irrespective of thickness, material and orientation of the sample. The main problem of this method is that very time-consuming calculations are required. Our approach for increasing the accuracy of a simulation based on the kinematical algorithm is to determine a dynamical correction factor for each individual HOLZ line separately. In a first step, a highly resolved CBED pattern for the chosen zone axis is calculated for the

unstrained material using the Bloch wave formalism [1]. By comparing with the kinematical position, an effective dynamical shift for each individual HOLZ line is determined. In the following, as an example the HOLZ line arrangement near the [3 3 1] zone axis of Si will be discussed. The corresponding experimental patterns from Si are used for the high-voltage reference measurement.

Fig. 6. Experimental pattern from the Si reference sample oriented along the [3 3 1] zone axis. The dashed lines represent the HOLZ line position detected by the Hough transform and the solid white lines represent the corresponding kinematical line positions.

Fig. 6 shows an experimental [3 3 1] zone axis pattern of silicon. Marked are both the actual line positions, as measured with the Hough transform, and the kinematical positions. With exception of the (3 3 −15) line all dynamical shifts are larger than the line width. Table 1 summarises the results of the attempts to correct for the dynamical shifts along the line normal. Two different data sets are shown with increasing sophistication in the degree of the dynamical correction. In the first set, the dynamical calculation includes the HOLZ reflections and the systematic row formed by the 2 −2 0 and −2 2 0 reflections. This corresponds to the geometrical situation depicted in Fig. 5. Even in this simplest treatment the dynamical shifts are not equal for the individual lines which is an effect of the non-spherical dispersion surface and the fact that HOLZ reflections from the 3rd and 4th Laue zone are involved. The second data set results from a calculation which includes a total of 200 reflections. The comparison shows that the dynamical shift is dominated by the reflections of the zeroth Laue zone, but including more reflections can significantly change the dynamical shift for individual

Table 1
Dynamical shift correction factors for different HOLZ lines in the Si [3 3 1] zone axis pattern. The factors were determined from a Bloch wave calculation with different numbers of excited beams. In the table, $d\alpha$ denotes the change of the slope and dr the relative shift along the line normal in reciprocal Å units (positive sign denotes a shift away from the zone centre)

	14 beams		200 beams	
	$d\alpha$ (deg)	dr (10^{-3} 1/Å)	$d\alpha$ (deg)	dr (10^{-3} 1/Å)
[3 3 −15]	0.06	1.69	0.000	−0.34
[−9 7 9]	−0.078	−1.63	−0.133	−2.08
[7 −9 9]	0.078	−1.63	0.133	2.08
[10 −4 −14]	0.029	1.45	0.244	1.37
[−4 10 −14]	−0.029	1.45	−0.244	1.37
[−12 12 4]	0.019	1.35	−0.016	1.69
[12 −12 4]	−0.019	1.35	0.016	1.69
[11 −9 −3]	−0.081	−1.29	−0.021	−2.05
[−9 11 −3]	0.081	−1.29	0.021	−2.05
[−6 2 16]	0.014	−1.51	0.034	−1.79
[2 −6 16]	−0.014	−1.51	−0.034	−1.79

Table 2
Dynamical shift correction factors for different HOLZ lines in the Al [3 3 4] zone axis pattern and different sample thicknesses. Note that the shifts are one order of magnitude lower than in the case of Si

	100 nm		300 nm	
	$d\alpha$ (deg)	dr (10^{-4} 1/Å)	$d\alpha$ (deg)	dr (10^{-4} 1/Å)
[5 5 −7]	0.00	−3.53	0.000	1.13
[−7 1 5]	0.067	1.74	−0.018	−4.47
[1 −7 5]	−0.067	1.74	0.018	−4.47
[8 −2 −4]	0.074	−0.97	−0.006	5.46
[−2 8 −4]	−0.074	−0.97	0.006	5.46
[7 −5 −1]	0.141	−3.99	0.026	2.68
[−5 7 −1]	−0.141	−3.99	−0.026	2.68

lines. In particular, the (3 3 −15) HOLZ line is strongly influenced by the neighbouring Bragg positions. Beside the shift, the slope of the lines also changes which again reflects the fact that the dispersion surface is not spherical along the lines and that the effective high-voltage correction hence would produce significant errors in the analysis.

Table 2 summarises the dynamical shifts for the HOLZ lines in the [3 3 4] zone axis of aluminium as a function of the specimen thickness. Aluminium shows weaker dynamical effects than silicon and the line shifts are in the order of the line width despite the fact that both elements have similar Z-values. This results from the fact that Al possesses smaller unit cell dimensions and fewer atoms in the cell. The thickness dependence of the line shift is caused by the anomalous absorption effect which is always in the order of the line width and increases with decreasing sample thickness [22].

3.4. Correlation between strain and HOLZ line positions

In the kinematic approximation, the HOLZ line position is given by the Bragg law

$$2KS_h = K^2 - (K - h)^2 = 0, \tag{3}$$

where K is the mean wavevector inside the crystal and h is a reciprocal lattice vector. It is convenient to use zone axis orientations for the experiment since they can easily be identified by the characteristic Kikuchi line crossings. Furthermore, they often have the most dense accumulation of HOLZ lines. While this is feasible for aluminium, for crystals composed of heavier elements the dynamic effects may become too strong even in high-indexed zone axis and a random orientation avoiding any strongly scattering reflections of the ZOLZ may be preferable.

The coordinate system of the HOLZ pattern is defined by the reciprocal lattice vectors of two fundamental reflections g_1 and g_2 of the zero-order Laue zone of the chosen zone axis (za). This leads to the equation of the HOLZ lines

$$K_{g_z} = -\frac{h_{g_1}}{h_{g_z}}K_{g_1} + \frac{h_{za}}{h_{g_z}}K_{za} - \frac{h^2}{2h_{g_z}} \tag{4}$$

for the HOLZ reflections h. In this equation, K_g and h_g denote the projections of the given vector on the basis vectors g_1 and g_2 or the direction of the zone axis (za), respectively.

As discussed in Section 3.2 the material is strained along certain directions, which are in most cases given by the overall sample geometry and not by the orientation of the individual crystals. The corresponding macroscopic strain has to be transformed from the sample coordinate system into the crystal coordinate system:

$$\varepsilon_{ij}^{\text{cryst}} = R_{ik}R_{jl}\varepsilon_{kl}^{\text{sample}}, \tag{5}$$

where i, j denote the strain components along the unit cell axes a, b, c and R denotes the rotation matrix. Applying this transformed strain to the

reference lattice parameters defines the deformed unit cell which determines the g-vectors and thus the HOLZ line positions.

The sensitivity of a single HOLZ line pattern to a given strain tensor can best be understood by assuming that a zone axis za has been chosen which is parallel to the z-direction of the sample coordinate system. The HOLZ pattern is then sensitive to four strain components, the three component ε_x, ε_y and ε_{xy} in the plane normal to the zone axis and the component ε_z along the zone axis. The latter results from the fact that the g-vectors of the HOLZ lines are inclined relative to the xy-plane.

However, a line shift induced by a strain in the z-direction cannot be distinguished from an isotropic strain in the xy-plane if the HOLZ lines are from the same Laue zone. This ambiguity can easily be understood from the Ewald sphere construction in reciprocal space. Basically, a shift of one HOLZ reciprocal lattice point in the z-direction can be compensated for by a corresponding shift in the xy-direction thus leaving the position of the Ewald sphere and hence the HOLZ line unaffected. The position of the HOLZ reflections in a zone axis is defined by the intersection of the Ewald sphere with the Laue zone which is basically a circle. A strain in the z-direction shifts the whole Laue zone and as a consequence all HOLZ lines are shifted by about the same amount. It turns out that in almost all investigated HOLZ patterns in aluminium this is the case. Therefore, it is not possible to get information about the volume contraction and the ratios between the strain components at the same time. This ambiguity can only be relieved if an additional assumption is introduced or if the measurement is performed along two different directions for the same area. In the case of an interconnect it is very difficult to perform two independant measurements at each individual position. We therefore perform finite element analysis to model the dependence of the strain components on the actual geometry and the material composition.

3.5. Refinement procedure

The quantitative evaluation of the experimental HOLZ patterns is performed by simulating theoretical patterns for varying strain states and comparing them with the experimental ones searching for the best fit. For a magnification and rotation independent comparison we use normalised distances between HOLZ line intersections as suggested by Zuo [2]. In terms of the experimental patterns, the intersections are computed for the straight lines which correspond to the Hough maxima. A direct comparison of the Hough transforms of the experimental and simulated patterns is problematic because a sub-pixel deviation of the rotation or magnification of the patterns would already lead to errors.

For the comparison, we define a goodness-of-fit parameter

$$S = \frac{1}{N}\sum_i (d_i^{exp} - c_l d_i^{theory})^2, \tag{6}$$

where N is the total number of data points, d_i the distance between two HOLZ line intersections and c_l a normalisation factor which can be interpreted as a camera length. The number of distances should be chosen in such a way that the position of each line relative to all others is taken into account. If the distances are given in pixel units a value of $S = 1.0$ means that the mean square deviation of the segment length is around one pixel.

The process of finding the best fit, i.e. the lowest S, can be performed using standard optimisation routines, like local optimisers based on Powell's method [23], or by performing a 'grid search' where all possible parameters are tested. The experiments show that a unique solution can always be obtained if the constraints for the strain components given by the volume criterion are properly taken into account.

The error in the determined strain values can be divided into four parts

$$\sigma = \sigma_I^2 + \sigma_A^2 + \sigma_{mat}^2 + 0.25\sigma_{HV}^2 \tag{7}$$

σ_I^2 is the error in the measurement of the line positions from the experimental HOLZ pattern, σ_A^2 is due to the approximations in the treatment of the dynamical interaction. Both are statistical errors with respect to the strain measurement and determine the width of the curve of the parameter S at its minimum. The sharpness of the minimum determines the statistical error in the strain

measurement. σ^2_{mod} accounts for the error introduced by a wrong model for the strain state, σ^2_{HV} is the variance in the high-voltage measurement. The two last contributions lead to a systematic over- or underestimation of the individual strain components.

3.6. Accelerating voltage reference measurement

The high-voltage of our microscope shows small long-term changes over a period of several weeks and the absolute changes lie typically in the range of 200 V. Although negligible for other applications, in the case of measuring the absolute lattice constants it is essential to know the exact value of the high-voltage during the strain measurement. We therefore routinely measure the high-voltage before and, if necessary after the strain analysis.

For the determination of a reference value of the accelerating voltage, a Si [3 3 1] zone axis pattern was acquired (Fig. 6) and the positions of the 9 HOLZ lines marked in the figure were measured using the Hough transform. 30 distances between line intersections were calculated and included in the refinement. The dynamical shifts of the second set in Table 1 and the literature value for the lattice constant $a = 0.54307$ nm of Si at room temperature are used. The refinement of the high-voltage is performed directly in the crystal coordinate system.

The value obtained for the high-voltage is 119.95 ± 0.02 kV. The differences between experimental and theoretical segment lengths are in the range of one pixel or even below, which is also reflected by the value of the goodness-of-fit parameter $S = 1.7$. A direct comparison of the experimental and fitted line parameters is possible by scaling the theoretical patterns on the experimental ones, which can be done by calculating the averaged rotation angle around the centre of the HOLZ pattern. This comparison also shows that the agreement between theory and experiment is better than one pixel.

The errors induced by measurement errors of the line positions and the approximate treatment of the dynamical interaction can be estimated from the width of the S-curve. Using the effective high-voltage approach for comparison, the value of $S = 2.9$ is obtained for the goodness-of-fit parameter which is larger than the value obtained with our new correction scheme and thus implies a larger discrepancy between model and experiment. The goodness-of-fit parameter also exhibits a shallower minimum using the effective high-voltage approach which is also indicative of a higher measurement error.

4. Finite element modelling

Finite element modelling (FEM) helps to understand the spatially varying strain and stress state of structures which have a complex geometrical shape and which are composed of different materials. The FEM model can well be adapted to the geometrical boundary conditions and parameters like the thermal expansion coefficient or the stiffness of the different materials. The finite element model applied for the investigated interconnect is composed of a sequence of layers: an infinite silicon wafer, a 500 nm thick thermal oxide, 300 nm TiN, 400 nm Al and a 30 nm TiN cap. An oxide scale at the side walls of the Al segment accounts for the surface oxidation of the metal when it is exposed to air. Elastic calculations were performed to determine the thermal strain distribution caused by the different thermal expansion coefficients of the materials. Table 3 summarizes the material parameters used for the finite element simulations.

In the finite element models, three main strain components are used: ε_x along the line, ε_y parallel to the wafer surface and ε_z along the surface normal. The silicon substrate defines the thermal strain along the infinite interconnect line. Each of the different materials on top of the substrate shows a plane strain state for which ε_z is defined by the difference of the thermal expansion coefficients of

Table 3
Materials parameters used in the finite element simulations

	Si	SiO_2	TiN	Al
E (GPa)	130.4	60.0	110.0	63.2
G (GPa)	79.7	Isotropic	410.0	28.3
$\alpha(10^{-6}$ 1/K)	3.0	0.5	9.0	24.3
ν	0.279	0.18	0.34	0.362

silicon and the corresponding material. The two other components (ε_y and ε_z) are determined by a combination of the Poisson contraction, which is caused by the tensile strain in the x-direction, and of the lateral strain caused by the surrounding materials, i.e. the TiN segment, the oxide scale and the TiN capping layer.

In contrast to lines which are confined by a thick passivation layer or which adhere directly to the silicon substrate, the interconnects in the present studies are characterised by a large amount of free surfaces. In first order approximation, the Al segment exhibits a uniaxial strain state with the dominant strain along the interconnect line and Poisson contraction in the two perpendicular directions. However, the TiN layers at the top and bottom interface lead to additional tensile forces in the y-direction. Owing to the limited constraints imposed by the TiN-layers, the Al-segment can minimise the total strain energy by bending which can be recognised in Fig. 7. After a simulated cooling of 100 K, the originally rectangular mesh of the finite element model shows bending at the interfaces of the interconnect with the substrate and the cap, while in the middle straight planes remain. This strongly influences the sharpness of the HOLZ lines in the diffraction pattern. As has already shown in Fig. 3, the bend lattice planes lead to varying Bragg conditions while the electrons pass through the TEM sample which leads to a strong splitting of HOLZ lines. Although the splitting of the HOLZ lines contains additional information, flat planes are necessary for the present method of strain measurement. In the central part of the Al segment the electron beam passes straight planes which lead to sharp HOLZ lines. Therefore, only diffraction patterns acquired near the centre of the segment are analysed. The finite element model shows that at this position the y- and z-component of the strain do not change along the beam direction which is also an important condition for an accurate strain measurement.

As mentioned above, the results of the finite element calculations not only help to understand the experimental results but are also needed to relieve the ambiguity in the evaluation procedure which has been discussed above. In the refinement, we are using the predictions of the finite element

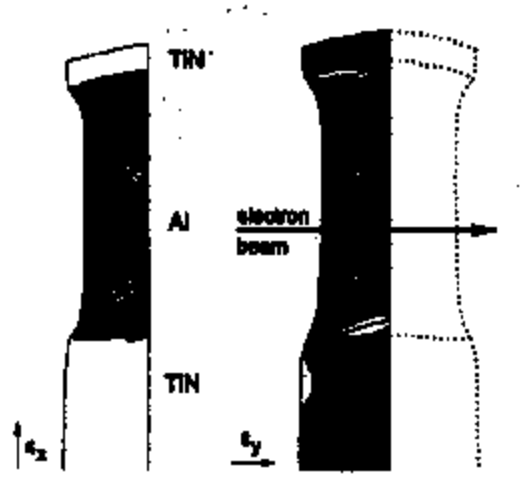

Fig. 7. Strain distribution predicted by the finite element model for the two components ε_z and ε_y. Shown is the shape of the interconnect after cooling by 100 K (the displacements are enhanced by a factor of 100 for better visibility). In the Al segment the y-component shows a transition from tensile strain at the interface to compressive strain in the central part which is a result of the bending moment of the interconnect.

model for the dependence of the volume contraction of the Al on the x-component of the strain in the interconnect. This condition fixes the relationship between the three strain components ε_x, ε_y and ε_z. The analysis shows that the volume contraction in the centre of the Al segment is almost the same as that for the simple case of a uniaxial strain state.

5. Results of the strain analysis

In the present paper we discuss the results of strain measurements performed on an Al interconnect line which has undergone hillock formation during electromigration tests conducted at high temperatures. Both, undisturbed regions as well as areas in the vicinity of a hillock were investigated. As an example, the HOLZ patterns of two different grains of the interconnect area shown in Fig. 2 are depicted in Fig. 8. The zone axes are approximately parallel to the y-axis of the sample coordinate system. The directions of two macroscopic strain components lie in the plane of each of the CBED patterns. The white lines superimposed on the HOLZ lines in Fig. 8 represent both the measured

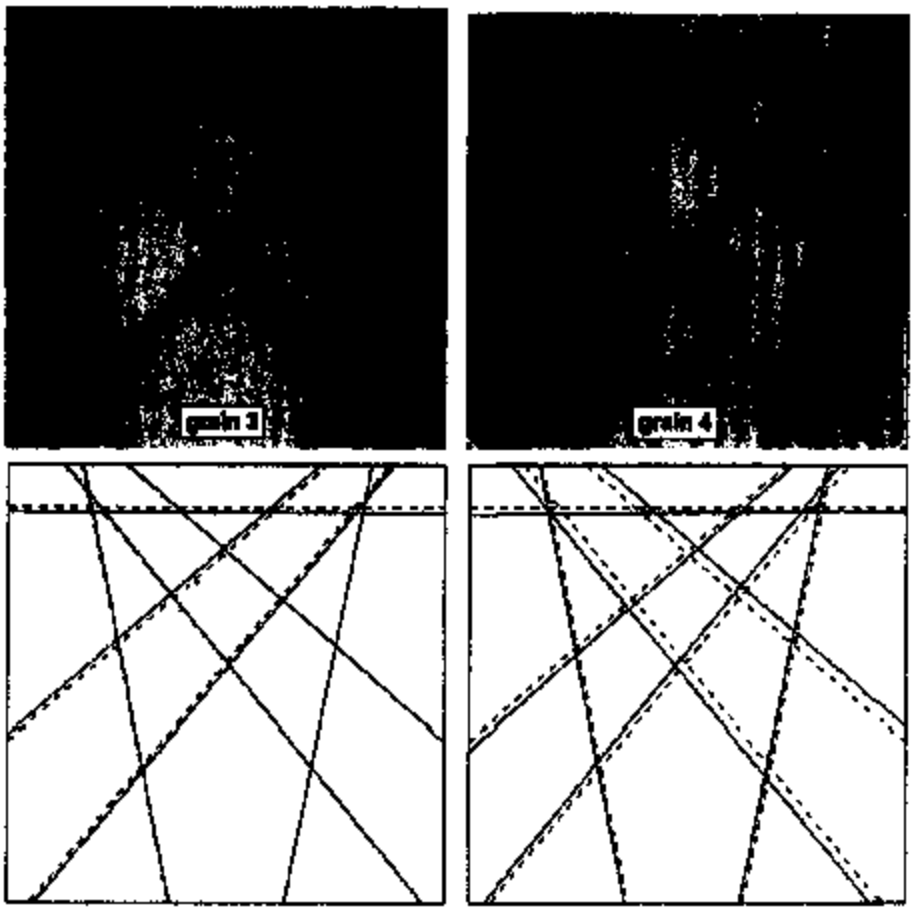

Fig. 8. CBED patterns of the third and fourth grains of the interconnect shown in Fig. 2. The uniaxial strain state clearly leads to a breaking of the symmetry in the patterns. The zone axes are approximately parallel to the y-axis of the sample coordinate system. The directions of the other two macroscopic strain components are given in each of the CBED patterns. The white lines represent both the measured and the fitted line positions which differ by less than one pixel for all HOLZ lines. The schematic patterns show a comparison between the HOLZ line positions for unstrained aluminium (dashed lines) and the actual line positions (solid lines). Grain 3, which is located underneath the hillock, is clearly less strained than grain 4.

and the fitted line positions which differ by less than one pixel for all HOLZ lines. Similar measurements were performed for the whole part of the interconnect shown in Fig. 2. Fig. 9 shows a schematic representation of the grain distribution of this part of the interconnect. Black dots mark the spots where the measurements were performed in four different grains.

Grain 3 is located directly under and grain 4 in front of the hillock with respect to the direction of the current flow. The two grains are oriented in such a way that in both cases a ⟨3 3 4⟩ zone axis could be used for the strain measurements. The distortions of the patterns depend on the orientation of the zone axis relative to the sample coordinate system. The rhombi in the middle of the patterns, for example, are in both cases elongated parallel to the x-axis, which can directly be associated with the thermal misfit strain along this direction. Simulated best-fit patterns of grains

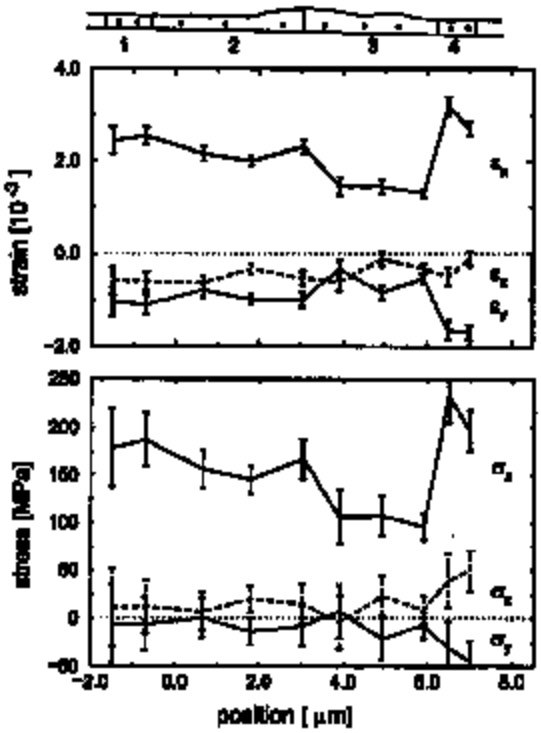

Fig. 9. Schematic drawing of the positions in which the CBED measurements were performed in the four different grains of the interconnect segment and plot of the measured strain (top) and derived stress (bottom) development along the interconnect line. A CBED pattern from grain 2 is shown in Fig. 4.

3 and 4 are also shown in Fig. 8 in comparison with the unstrained line positions. It can clearly be seen that the shifts induced by the strain are smaller in the left pattern than in the right pattern, which means that the grain under the hillock is less strained than the adjacent grain.

Fig. 9 summarises the results for the different grains. The strains were obtained by comparing the measured HOLZ line configuration with a configuration defined by the literature value of the unstrained lattice constant of pure Al at room temperature ($a = 0.40496$ nm). Also shown are the corresponding stresses along the principal axes which were derived from the measured strain values by means of the compliance matrix for pure Al.

5.1. Triaxial strain state

As expected, the strain component along the length of the interconnect, ε_z, is the largest. For a purely uniaxial strain state, one would expect ε_y and ε_x to be equal and to be related to ε_z through the Poisson contraction. However, the y- and x-component of the measured strain show different values, which reflects the inhomogeneous lateral strain caused by the surrounding materials. Two factors contribute to the inhomogeneity which is mainly caused by the small thickness of the interconnect: 1) The TiN layers at the top and bottom interfaces lead to additional tensile forces in the y-direction. As discussed in the section on FEM, this effect is only expected to be important in the Al near the TiN interface. The Al segment can minimise its total strain energy by bending and the resulting bending moment produces an additional compressive strain component in the y-direction in the middle part of the interconnect. As a result, the magnitude of ε_y becomes larger than that of ε_x. The measured strain levels in the undisturbed region correspond quite nicely to the results of finite element simulations which predict values of $\varepsilon_x = 2.10\times10^{-3}$, $\varepsilon_y = -0.85\times10^{-3}$ and $\varepsilon_z = -0.60\times10^{-3}$ for a temperature change of -100 K (see Fig. 7). (2) At the side walls, oxide scales form when the metal is exposed to air. Their influence increases with decreasing thickness of the interconnect line. The oxide scale prohibits the Al segment from shrinking along the x-direction which leads to a tensile contribution to the strain in the x-direction and a corresponding Poisson contraction along the y-direction.

The plot of the stress also shows that the interconnect has a dominantly uniaxial stress distribution with additional stresses building up because of the surrounding material. In the present case, the additional stresses are very small. The main contribution is given by a small tensile force building up along the z-direction which can be attributed to the oxide scale preventing the Al-segment from shrinking.

From a single HOLZ line pattern, one determines the ratios between the measured strain components in the triaxial strain state. The absolute values of the strain depend on the chosen reference

lattice constant and the assumed volume contraction. A change in the value of the volume contraction would lead to a uniform shift of the measured strain components which is three times smaller for each component than the actual change in the volume. Therefore, an uncertainty in the assumption of the volume contraction, e.g. due to uncertainties in the material parameters included in the finite element model, has only a small influence on the results. Assuming, for example, that the volume contraction is twice as large as the corresponding uniaxial value, the strain components are only raised by 5×10^{-4}.

5.2. Lateral strain distribution

The undisturbed left side of the investigated area shows almost constant tensile strain in the x-direction parallel to the interconnect, followed by a clear drop in strain level underneath the hillock and then a steep increase towards the grain on the right side. The error bars given in Fig. 9 are statistical errors which result from an analysis of the width of S-curves as a function of the strain parameters being varied. Typical S-curves for the strain measured at one position in each of the three grains are shown in Fig. 10.

The substantial drop in strain level in the region under the hillock can be understood from geometrical reasons. Because the diameter of the interconnect increases underneath the hillock, a force balance with the surrounding material is achieved at a lower strain level. This would also explain a peak in the strain level at the positions immediately adjacent to the hillock. Finite element simulations for a hillock with a comparable change in height also predict a decrease in tensile strain in the x-direction as shown in Fig. 11. A comparison with the experimental strain values given in Fig. 9 shows that both values coincide to within the error bars. However, this cannot explain the asymmetry which is evident in Fig. 9 with a strong peak only being visible in the small grain on the right side of the hillock. This asymmetry is a clear indication of electromigration-induced strain effects which in this case seem to be retained in the final TEM specimen.

The present measurements were performed ex-situ at room temperature. Despite the fact that strain inhomogeneities have clearly been identified, it is difficult to conclude on the variation of the strain during the electromigration tests. A knowledge of the actual stress state is important because it has a strong influence on both plastic and diffusional processes. With respect to the plastic behaviour, the grains do not show major differences. Table 4 summarizes the geometrical data of the investigated four grains including the sample coordinate system and the zone axis which was chosen for the strain measurement. The plot of the stress in Fig. 9 shows that the interconnect exhibits approximately a uniaxial stress state. Using this assumption the Schmid factors were calculated. Listed in Table 4 are the slip systems with the largest Schmid factor. All the grains have an orientation which approximately corresponds to a 111 texture and in

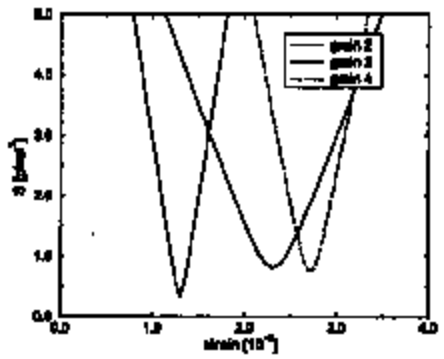

Fig. 10. Examples of the values of the goodness-of-fit parameter S as a function of the tensile strain in the x-direction for three different grains. The width of the curves is a measure of the statistical error in the measurement. As has been discussed in Fig. 8, the S-curves also show that the strain under the hillock is significantly lower than in the grain next to it.

Fig. 11. Finite element simulation of an interconnect line with a hillock. Shown is the strain component in the direction of the line. The experimentally observed drop of the strain ε_x underneath the hillock is predicted by the model.

Table 4
Geometrical data of the investigated grains: The crystal coordinate system is defined by the plane parallel to the silicon substrate surface and the direction along the interconnect line

Grain	Zone axis	Crystal coordinate (hkl) [uvw]	Schmid factor	Glide system (hkl) [uvw]
1	[1 2 5]	(8 5 −4) [6 −8 2]	0.467	(1 −1 −1) [0 1 −1]
2	[1 3 3]	(5 −7 5) [−8 −2 5]	0.483	(1 −1 −1) [1 1 0]
3	[3 3 4]	(−8 5 2) [1 4 −5]	0.439	(1 −1 1) [1 0 −1]
4	[3 3 4]	(−3 8 −5) [8 0 −6]	0.468	(1 1 −1) [1 −1 0]

each grain a slip system with a relatively high Schmid factor can be found. Therefore, none of the grains seems to be favoured with respect to plastic yielding.

The strain state measured in the present analysis is dominated by the thermal strain induced by cooling to room temperature. The reduction in the strain level underneath the hillock can mainly be attributed to the change in the geometrical thickness underneath the hillock. For the direct investigation of electromigration-induced changes we are planning to perform in-situ experiments using a special holder which has been built for that purpose.

6. Conclusions

In the present work we have shown that strain measurement with CBED increasingly becomes a standardised task which can be applied to real materials systems. The aluminium interconnects which we have treated in the present paper are a very good example for this. In this special case the specimen geometry required for the TEM experiments is not significantly different from the actual geometry of the interconnects in the semiconductor devices. From the experimental side, two major achievements have contributed to the quality of the experiments: (1) Energy filtering enables one to remove the inelastic scattering background in electron diffraction patterns and makes it possible now to obtain data of a similar quality as the competing diffraction techniques. (2) The methods for TEM specimen preparation have constantly been improved and in particular the new FIB technique is of great value for experiments in the area of structured thin films.

Based on the excellent data quality which can now be obtained experimentally we have tried to optimise the algorithms for the data evaluation. This involves a number of separate steps: (1) The identification of the HOLZ line positions, (2) a reference measurement to determine the high voltage, (3) the simulation of the HOLZ line positions for varying strain states and (4) a refinement process in which the simulation is brought into agreement with the experiment. In the present paper, we have tried to outline the complete procedure for the Al interconnects which we have chosen as an example. The contributions which we have made to the individual steps listed above will be discussed in the following.

The automated detection of the HOLZ lines in the experimental patterns so far has been one of the unresolved issues and all the techniques used previously needed manual input and frequently were limited in accuracy. Our novel approach of using the Hough transform combines both convenience and high accuracy in the detection of HOLZ line positions. The whole procedure can be highly automated and makes it possible to measure strain with an accuracy of about 10^{-4}, which is close to the physical limits of the technique. In order to achieve this high strain resolution we had to extend the whole procedure to sub-pixel accuracy. Furthermore, it is advantageous to remove any areas where strong dynamical effects occur prior to the analysis of the patterns. Therefore, we mask all the HOLZ line intersections and strong Bragg lines prior to transforming the pattern. Although this increases the effort which has to be made to evaluate the

pattern and cannot be fully automated in each case, it significantly increases the reliability of the results.

Another important question is the treatment of the dynamical effects. Although using a fully dynamical Bloch wave calculation is state of the art in the evaluation of CBED patterns, such calculations are still much too time consuming if a multi-dimensional parameter space has to be explored in a refinement of the strain state. Therefore in many investigations the effective high-voltage method has been used as a first order correction for the dynamical line shift in a kinematical simulation. In the present paper, we have shown that the effectiveness of this correction depends strongly on the shape of the dispersion surface and whether there are reflections from more than one Laue zone involved. In order to avoid these pitfalls we have developed a correction scheme which corrects for the dynamical shifts of each HOLZ line separately. In a kinematical simulation, a correction factor is assigned to each HOLZ line individually which accounts for the detailed shape of the dispersion surface in the given zone axis or crystal orientation. The validity of this correction scheme can be expanded to heavier elements, like Cu, Fe or Ni, for which the effective high-voltage method may lead to very inaccurate results.

Our present experiments have given a very detailed picture of the three-dimensional strain state in the interconnect. Interesting variations have been observed in an area where a hillock has been formed during electromigration experiments performed prior to the TEM characterisation. A detailed comparison with the results of finite element modelling revealed that most of the strain originates from the difference in thermal expansion coefficients for the materials involved. However, there are indications that diffusional processes during the electromigration tests lead to an asymmetry in the strain state and that these effects can be retained in a TEM specimen after electromigration testing. In order to resolve these issues we are planning to perform the next set of experiments in-situ using a special holder which has been built for that purpose.

In summary, our results show that even while cooling only moderately, i.e. to room temperature, strains develop in the thin interconnect which already exceed the yield stress of commercial purity bulk aluminium. While this has been known and does not lead to failure of the line, our spatially resolved experiments show that pronounced strain and thus stress maxima exist in the vicinity of hillocks which are the most probable failure sites. In future experiments we are planning to investigate the influence of the electromigration process itself on these peak stresses.

Acknowledgements

The authors would like to thank C. Volkert and R. Spolenak for many helpful discussions. Support by the Volkswagen-Stiftung is gratefully acknowledged.

References

[1] J.C.H. Spence, J.M. Zuo, Electron Microdiffraction, Plenum Press, New York, 1992.
[2] J.M. Zuo, Ultramicroscopy 41 (1991) 211–223.
[3] S.J. Rozeveld, J.M. Howe, S. Schmauder, Acta Metall. Mater. 40 (1992) S173–S193.
[4] H.J. Maier, H. Renner, H. Mughrabi, Ultramicroscopy 51 (1993) 136–145.
[5] R. Wittmann, C. Panzinger, D. Gerthsen, Ultramicroscopy 70 (1997) 145–159.
[6] D. Mukherji, R.P. Wahi, Scripta Materialia 36 (1997) 1233–1238.
[7] Y.Y. Qiu, J. Alloys Compounds 234 (1996) 157–166.
[8] M. Saka, T. Aoyama, K. Nakata, T. Suzuki, Jap. J. Appl. Phys. 34 (1995) 350–354.
[9] H. Ross, D. Krahl, in: L. Reimer (Ed.), Energy Filtering Transmission Electron Microscopy, Springer, Berlin, 1995.
[10] W.T. Pike, Ultramicroscopy 51 (1993) 136–145.
[11] C. Deininger, G. Necker, J. Mayer, Ultramicroscopy 54 (1994) 15–30.
[12] S.K. Streiffer, S. Basu, C. Deininger, J. Mayer, M. Rühle, Mat. Res. Soc. Symp. Proc. 343 (1994) 615–620.
[13] Hough, P.V.C, US Patent 3,069,654, 1962.
[14] N.C. Krieger Lassen, PhD Thesis, IMM-PHD-1994-3, Lyngby, Denmark, 1994.
[15] R.A. Schwarzer, Micron 28 (1997) 249–265.
[16] S. Kräusser, J. Mayer, J. Microscopy 194 (1999) 2–11.
[17] C. Witt, C.A. Volkert, Mat. Res. Soc. Symp. Proc. 516 (1998) 33–43.
[18] S.R. Deans, IEEE Trans. Pattern. Anal. Machine Intell. 3 (1981) 185–188.

[19] J.M. Zuo, J.C.H. Spence, Ultramicroscopy 35 (1991) 185–196.
[20] E.G. Bithell, W.M. Stobbs, J. Microscopy 153 (1989) 39–49.
[21] Y.P. Lin, D.M. Bird, R. Vincent, Ultramicroscopy 27 (1989) 233–240.
[22] J. Mansfield, D. Bird, M. Saunders, Ultramicroscopy 48 (1993) 1–11.
[23] W.H. Press, B.P. Flannery, S.A. Teukolsky, W.T. Vetterling, Numerical Recipes, Cambridge University Press, Cambridge, 1989.

0982-827 29613

ELSEVIER

Thin Solid Films 282 (1997) 103–117

Thin Solid Films

Transmission electron microscopy of Al–Cu interconnects during in-situ electromigration testing

W.C. Shih, A.L. Greer

Department of Materials Science and Metallurgy, University of Cambridge, Pembroke Street, Cambridge CB2 3QZ, UK

Received 15 February 1996; accepted 16 May 1996

Abstract

Transmission electron microscopy of 2.1 μm wide Al–4 wt.% Cu interconnects during in-situ electromigration stressing shows microstructural evolution and the development of damage, including failure. Voids which develop early stop growing and are not fatal. Hillocking is associated with Al–Cu precipitates; voiding which leads to failure is associated with copper depletion. Void initiation is at the upstream end of inclined grain boundaries crossing the lines, which have a near-bamboo microstructure. Healing events occur as damage develops, arising from further voiding or from stress build-up. Open-circuit failure can occur when the proximity of grain boundaries impairs the stress-driven healing. A schematic model for open-circuit failure in bamboo lines is proposed. The relative advantages of in-situ and conventional testing are discussed.

Keywords: Transmission electron microscopy; Aluminium; Copper; Electromigration

1. Introduction

As interconnect line-widths decrease, the study of how electromigration damage limits the metallization reliability remains important. New atomic transport paths and damage mechanisms can become dominant, rendering earlier studies invalid. In particular, the damage mechanisms and failure modes can be strongly related to the alloy microstructure in the lines [1]; earlier work concentrated on polycrystalline lines, whereas interest is now in bamboo lines (where all grain boundaries are approximately normal to the line length and there are no grain-boundary junctions), or near-bamboo lines (consisting of bamboo segments with some polygranular segments) [1]. It is possible to derive some links between microstructure and electromigration damage and failure using surface-sensitive techniques such as scanning electron microscopy (SEM) (see, for example, Ref. [2]), and focused ion-beam microscopy (FIB) [3]. Clearly, however, transmission electron microscopy (TEM) is more powerful for characterising microstructure, and has the greatest potential for elucidating the related mechanisms of damage and failure. This is particularly so if electromigration testing can be performed in-situ in the microscope. TEM has the disadvantage that specimen preparation is much more difficult, the semiconductor substrate needing to be thinned or removed locally to permit electron transparency. A more fundamental concern is that since heat conduction into the substrate is so important in testing, the removal of this heat sink from the area being examined greatly changes the testing conditions, notably leading to high temperature gradients (discussed further in Section 2.2). With limitations on instrument time, in-situ testing in the TEM is also often much accelerated in comparison with conventional accelerated testing. Together with the necessary lack of passivation, these factors lead to uncertainty about whether the mechanisms observed in in-situ testing can apply in the interpretation of conventional testing or of failures in service (discussed in Section 4.1).

Pioneering work on in-situ testing in TEM was carried out by Blech and Meieran [4]. They observed thinning and formation of voids and hillocks in polycrystalline lines (i.e. with grain size < line-width) of nominally pure aluminium. Void formation was associated with grain boundaries. Further work by these authors and others [5–7] on similar specimens related the stages in damage development in-situ to resistance changes and to failure, and showed that the orientation of grain boundaries could be important. Addition of copper to aluminium greatly improves interconnect lifetime [8], and alloys of this kind (with 6 wt.% Cu [9] and 7 wt.% Cu [10], greater than in the present work and much greater than what is now common) have been studied by in-situ testing in TEM. The early work confirmed the slower damage rate [9]. The

PII S0040-6090(96)08944-4

later work found Al_2Cu precipitates, and showed that under electromigration stressing the copper is transported (in the same direction as the electrons) faster than the aluminium, thereby becoming depleted. The depletion was seen in the dissolution of precipitates and, in confirmation of earlier suggestions (see, for example, Ref. [8]), it was in depleted areas that voids formed [10].

The in-situ testing of Al–Cu was again on wide polycrystalline lines. There has been little or no such work on near-bamboo lines. Vaure and Lobotka [11] studied near-bamboo, wide lines of pure aluminium (average grain size 15 μm, in 10 μm line-width). To obtain the large grain size, the metallization was relatively thick (6 μm) and then thinned for TEM observation. Both voids and hillocks were formed in the in-situ testing. In these samples, voids formed inside grains and migrated in an elongated shape along the lines.

In the present study, the lines are 2.1 μm wide, Al–4 wt.% Cu, with near-bamboo microstructure. In contrast to earlier in-situ work, the lines have been the subject of a wider study and have not been patterned specially for the in-situ work. The wider study has included damage morphology and precipitate distribution [2], life-testing [12,13], quantitative monitoring of damage development (by SEM) [12–16], the structure of the Al–Cu precipitates [17] and electrical measurements [15,18]. The SEM shows that there are precipitates in the lines and that these precipitates evolve during electromigration stressing. As is generally known, and confirmed by the electrical resistance measurements in the present project [15], there are in the later stages of line lifetime not only sharp increases but also sharp decreases in resistance. That is, there are healing events, and these form an important part of the overall behaviour under electromigration stressing.

In a number of the above cases of in-situ testing, the current was reversed after some damage had developed. It was found that damage could be at least partially reversed, voids refilling [4,6,10] and precipitates reappearing [10]. There has been study of a.c. stressing [19]. However there appears to have been no study of healing while current stressing in the same direction was continuing. Nor has there been a detailed study of how damage leads to failure. Healing and failure processes are the focus of the present study.

2. Experimental details

2.1. Methods

Samples were supplied by GEC–Plessey Semiconductors Ltd. The metallization was Al–4 wt.% Cu, 1 μm thick, with a nominal sheet resistance of 32.5 mΩ/□. Deposition was by sputtering; the silicon substrate, with 0.5 μm SiO_2 on top was held at 150 °C. The metallization was patterned by standard techniques and then annealed under nitrogen gas for 30 min at 435 °C. The lines are 1.4 mm long, with nominal widths of 1.4, 1.8 and 2.4 μm; only the widest are used in this work. After an etching undercut of 0.3 μm was estimated from the variation of resistance with width, the actual width of the lines in this study was found to be 2.1 μm. Each line has two 4.5 μm wide parallel guard rails of the same metallization, designed for detecting short-circuiting due to hillocking. These guard rails are not subjected to any current. In the present study the unchanging microstructure of the guard rails provides useful reference points for changes in the central, stressed line. No passivation was applied.

To prepare the samples for TEM examination, dice were cut ultrasonically, ground from the back side, and jet-polished from that side to produce a dimple. The polishing solution was $HF–HNO_3–CH_3COOH$ (3:5:3) [20]. The specimens were further etched from the back side using a solution of $HF–HNO_3$ (1:4) until an area transparent to light appeared. The etching solution removed Si substrate and reached the SiO_2 separating the etching solution from the Al–Cu test lines. The degree of etching was then controlled with care until the transparent area grew to include a substantial area of the desired test line. Each die was fixed to a carrier using silver dag. The lines to be tested were Al-wire bonded to the carrier contacts. The carrier contacts were then electrically connected to the holder contacts by soldering a Cu wire. An example of a specimen which has gone through these processing steps is shown in Fig. 1.

TEM examination was performed in a JEOL 2000FX microscope operating at 200 kV. A cold-stage specimen holder was used, with an Oxford Instruments ITC4 temperature controller. After loading the carrier into the holder, electrical connections were made to the holder by soldering

Fig. 1. SEM image of a processed specimen showing the region over which the silicon has been removed and its oxide thinned to leave electron-transparent segments of line. In this case the test line is 10 μm wide, with a length of 3 × 1.4 mm. This sample was used for estimating Joule heating effects. (Montage of two micrographs)

copper wires to the bonding pads. Apart from initial tests, the base temperature of the holder during electromigration stressing was held at 123 K.

For each line tested, the electromigration experiment was completed within one specimen loading, and the line was tested to failure. Initial stressing was at a current density of 0.5×10^{10} A m^{-2} (abbreviated here as 0.5 j) for 30 min. This did not induce damage but did allow the die temperature to increase, reducing thermal transients during the main stressing. The main stressing was at 0.7 and 0.8 j at which damage proceeded rapidly, but from time to time the current density was reduced to 0.5 j to slow down the damage development for the convenience of imaging.

2.2. Temperature profile

In in-situ testing, the central, electron-transparent segment of the line heats up markedly because of the lack of heat-sinking into a massive silicon substrate. In the present work it was not feasible to measure the temperature profiles along the lines under test. However, the heating effects were estimated from the onset of melting in 10 μm lines and the parameters thus determined were used in the calculation of temperature profiles in the 2.1 μm lines used for in-situ testing. The temperature profile in the electron-transparent segment of line was calculated according to the analysis thoroughly discussed in earlier work [6,10]. It is assumed that the only significant heat flow out of this segment of line is conduction along the line itself and the temperature profile $T(x)$ for the segment is then given by

$$T=T_0+\frac{1}{\alpha}\left(\frac{\cos b\,(d-x)}{\cos b\,d}-1\right)\quad 0<x<2d \qquad (1)$$

where T_0 is the temperature of the ends of the segment and d is the half-length of the segment. The parameter b is given by

$$b^2=\frac{\alpha\rho_0}{\kappa}j^2 \qquad (2)$$

where α and ρ_0 are the temperature coefficient of resistivity and the resistivity of the metallization at T_0, κ is its thermal conductivity and j is the current density in the line. Tabulated data [21] were used to estimate the resistivity ρ of Al–4 wt.% Cu to be $(53+1.27T)\times10^{-10}$ Ω m, where T is the absolute temperature, and this expression was used to derive ρ_0 and α. The thermal conductivity was taken to be 160 W m^{-1} K^{-1} [10]. Lines of 10 μm width (of the kind in Fig. 1) were stressed at current densities in the range $(0.2–0.4)\times10^{10}$ A m^{-2} (0.2–0.4 j), and it was found that the melting behaviour could not be fitted if it was assumed that T_0 remained equal to the sample holder temperature T_h in the TEM (203 K in these tests). The Joule heating was assumed to give a temperature rise in the die such that

$$T_0=T_h+c\,w\,j^2 \qquad (3)$$

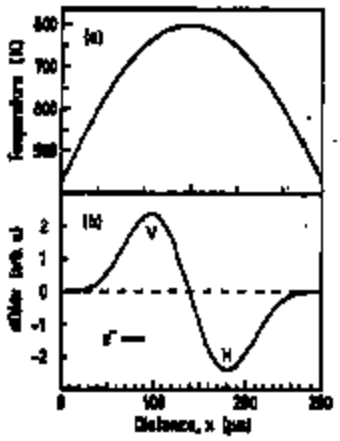

Fig. 2. (a) Calculated temperature profile for an electron-transparent segment of Al–4 wt.% Cu line during electromigration testing in the TEM. The segment is 280 μm long, 2.1 μm wide and 1 μm thick, stressed at 0.8×10^{10} A m^{-2}. In this most severe stressing used in the present study, the maximum temperature approaches the Al–Cu eutectic at 821 K. (b) The spatial derivative of diffusivity (activation energy 0.86 eV atom^{-1}) corresponding to the temperature profile in (a). For electron flow in the positive direction, the maximum in $\partial D/\partial x$ gives faster voiding (V) and the minimum fastest hillocking (H). The distance between these regions matches that observed (Fig. 5(b)).

where w is the total width of lines under test (i.e. 30 μm in Fig. 1). The constant c was treated as adjustable, and by matching whether lines melted or not, a value of 2.3×10^{-12} K m^3 A^{-2} was estimated.

Calculations based on these parameters were performed for the 2.1 μm lines under current densities of $(0.5–0.8)\times10^{10}$ A m^{-2}. An example of a calculated temperature profile is shown in Fig. 2(a); this is for a line with an electron-transparent segment 280 μm long ($d=140$ μm), tested under the most extreme condition, 0.8 j. It can be seen that there is a marked temperature variation in the observable segment of the line and that the maximum temperature approaches the eutectic (821 K) of Al–Cu. In view of the uncertainties in the analysis and in the estimation of the relevant parameters, calculated profiles of this kind can be taken only as rough guides to the temperature; even so, they are useful in interpreting the damage pattern in the tested lines.

Electromigration damage in general arises from a divergence in the atomic flux. If it is assumed that the divergence is caused only by the spatial variation of atomic diffusivity D (i.e. local microstructural effects are ignored), then initial damage would be concentrated at the places of maximum $\partial D/\partial x$. The spatial derivative of diffusivity, $\partial D/\partial x$ corresponding to the temperature profile in Fig. 2(a) is shown in Fig. 2(b). In the calculation of $\partial D/\partial x$ it is assumed that the diffusivity has the same activation energy as the mean time to failure of the same lines; this has been determined to be 0.86 eV atom^{-1} [12,13]. For the case in Fig. 2, it is therefore predicted that the initial voiding and hillocking should occur 40 μm on either side of the centre of the line. This conclusion is not dependent on the specific diffusion being considered (whether of the aluminium or of the copper).

3. Results

3.1. Overall damage development

The effects of temperature profiles such as that in Fig. 2(a) are evident when the overall distribution of damage is examined. Fig. 3(a) is a low magnification SEM image of a 2.1 μm wide line (and associated guard rails) before electromigration stressing, showing an overview of the electron-transparent area. The segment of line in the electron-transparent area shows no difference in microstructure from the rest of the line. After electromigration stressing to failure, the overall pattern of damage can be seen in Fig. 3(b) which is a low-resolution backscattered electron image of the electron-transparent line segment. In the figure, electron flow is from left to right. Almost all of the voids are just to the left of the centre, and the hillocks to the right of the centre. Also, between the voiding and hillocking regions there is an essentially total depletion of the copper-rich precipitates (which appear bright in the backscattered electron image). These features can be seen in greater detail in the enlarged image in Fig. 3(c); this clearly shows that the copper from the central zone has migrated to the hillocking region. All of these phenomena are consistent with the temperature profile suggested in Section 2.2 and with aluminium and copper migration in the direction of the electron flow, the copper being faster. In the left-hand segment of the line the temperature is increasing in the direction of electron and atom flow; at the point of maximum atomic flux divergence (near the point of maximum temperature gradient), voids form. In the right-hand side, with temperature decreasing, correspondingly hillocks form. In the hottest, central area of the line dissolution of the copper-rich precipitates is favoured and the copper migration is fastest, resulting in depletion. The hillocks form in the region where copper is accumulating and mostly consist of copper-rich precipitates. It appears that almost all of the voids (except the early developed voids) do not develop until there is local depletion of copper, reflected in the disappearance of the precipitates. The regions of maximum voiding and hillocking are 30–40 μm on either side of the line centre, in excellent agreement with the positions suggested in Fig. 2(b). Open-circuit failure occurs at the position of maximum voiding in a total test time which is roughly one order of magnitude less than the failure time predicted by extrapolating mean times to failure in conventional testing [12,13] to the temperature at the place of the voiding.

The distribution of damage along the line illustrates the importance of the temperature profile in testing of electron-transparent, poorly heat-sunk, lines. The temperature profile and damage distribution are markedly different from those found in conventional accelerated testing or in service. However, the advantage for in-situ studies is that the damage is concentrated in the electron-transparent portion, and that different types of damage are available for study. Despite the steep temperature gradients, it is assumed that the damage processes reflect electromigration without any significant contribution from thermomigration, which is a small effect in aluminium [22]. That failure is more rapid than expected from extrapolation of conventional test data presumably reflects the influence of temperature gradients on the electromigration flux. The following sections describe more detailed work on particular phenomena within the overall development of damage and failure.

3.2. Microstructural development and hillocking

Fig. 4 shows a short length of a 2.1 μm wide line with its two 4.5 μm wide guard rails. As can be seen, the 200 kV

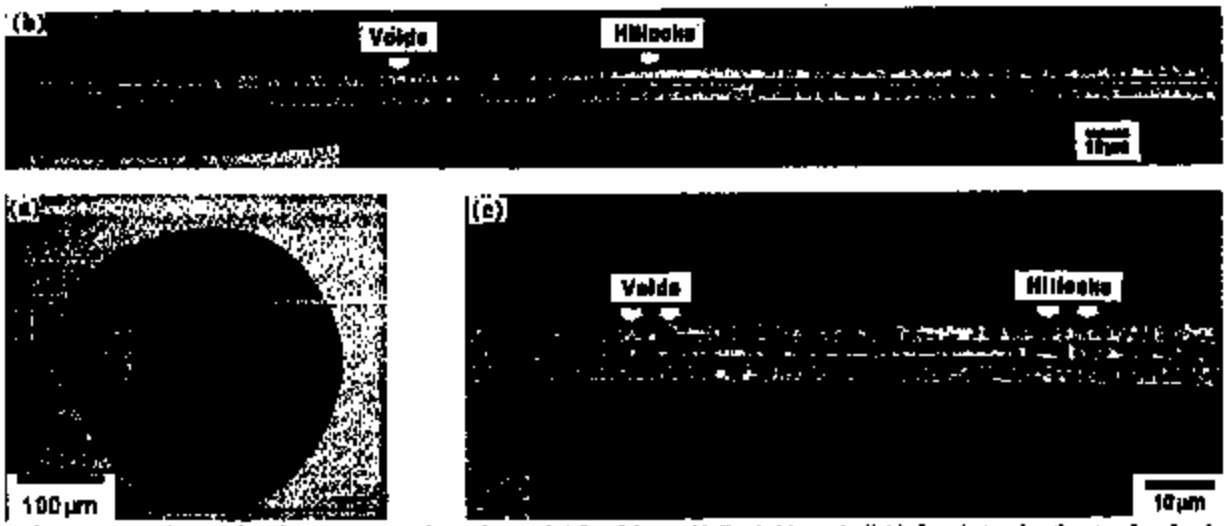

Fig. 3. (a) Low magnification SEM image (montage of two micrographs) for a 2.1 μm wide line (with guard rails) before electromigration stressing, showing the electron-transparent area. (b) and (c) Backscattered electron images in SEM for the electron-transparent segment after failure, showing voids and hillocks in distinct regions on either side of the centre of the transparent segment, with the depletion of the Al–Cu precipitates between these regions. (c) A close-up of (b).

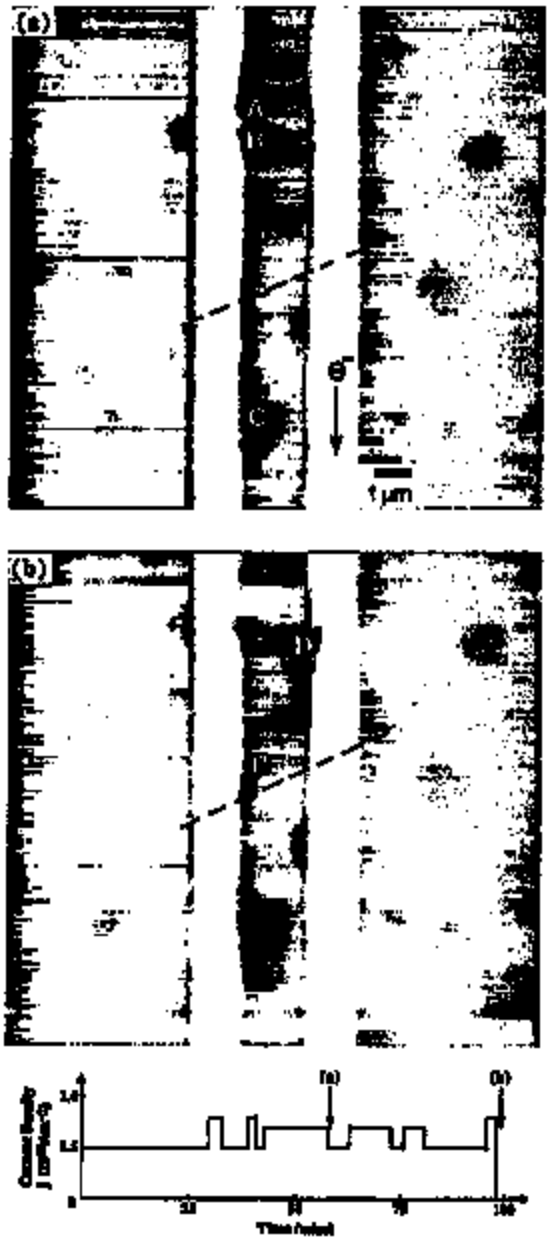

Fig. 4. TEM images for a segment of test line, (a) after 58 min and (b) after a further 40 min of in-situ electromigration testing (profile shown at bottom of figure). Comparison of (a) and (b) shows the formation of an Al–Cu hillock at D, the dissolution of an Al–Cu precipitate at C, and the migration of a precipitate at B—all consistent with the migration of copper parallel to the electron flow (top to bottom).

accelerating voltage used provides sufficient transparency for imaging of the metallization microstructure although the lines are 1 μm thick on a 0.5 μm oxide. There is, however, some degradation of image quality due to charging effects on the non-conducting SiO_2 film. In the microstructure the distribution of Al–Cu precipitates (dark particles) can readily be seen. In some areas individual aluminium grains can also be distinguished. In the narrow test lines generally, and there is evidence for this in Fig. 4, there is a clear tendency for the precipitates to be at the line edges at the end of grain boundaries crossing the line in the "bamboo" configuration.

Fig. 4(a) shows the specimen after current ramping from 0.5 J to 0.8 J over 58 min. As observed during this period, an aluminium hillock has developed at A and two precipitate hillocks at B and C. (The precipitate hillocks can be distinguished because of their darker appearance due to greater absorption.) Given that the electron flow is from top to bottom in Fig. 4, the aluminium hillock can be attributed to the blocking of the line cross-section by precipitates. Evidence for this has been seen also in SEM studies [2]. Fig. 4(b) shows the same line after a further 40 min of stressing. In comparing Fig. 4(a) and 4(b), precipitates in the unstressed guard rails are useful as reference points; the dashed lines linking these points do not always appear in the same orientation because of changing specimen tilt. During the further stressing, an Al–Cu hillock has formed at D and it appears to be a single grain. Also, the precipitates in the centre line have evolved. The changes clearly confirm that the copper migration is parallel to the electron flow; for example, the precipitate C is spreading along the direction of the electron flow (compare in Fig. 4(a) and Fig. 4(b)). The precipitate B has, in effect, migrated 0.7 μm in the direction of electron flow. This appears to occur by erosion of the upstream surface and deposition at the downstream surface, giving a somewhat changing shape. These observations of precipitate evolution provide confirmation of the behaviour in the same type of tracks inferred from intermittent SEM observations [15].

3.3. Early voids and void initiation

Electromigration failure is predominantly associated with voiding, and consequently much electromigration work has focused on the mechanisms of void initiation and growth. In the present work, it is found that voids always initiate at the edge of the lines beneath the aluminium oxide skin, as is shown in Figs. 5 and 6(a) as well as in Figs. 7(a), 8(a) and

Fig. 5. TEM image showing the initiation of voids at the end of the electron-transparent segment of line. The voids developed early, at the edge of the line and beneath the oxide skin. Electron flow: top to bottom.

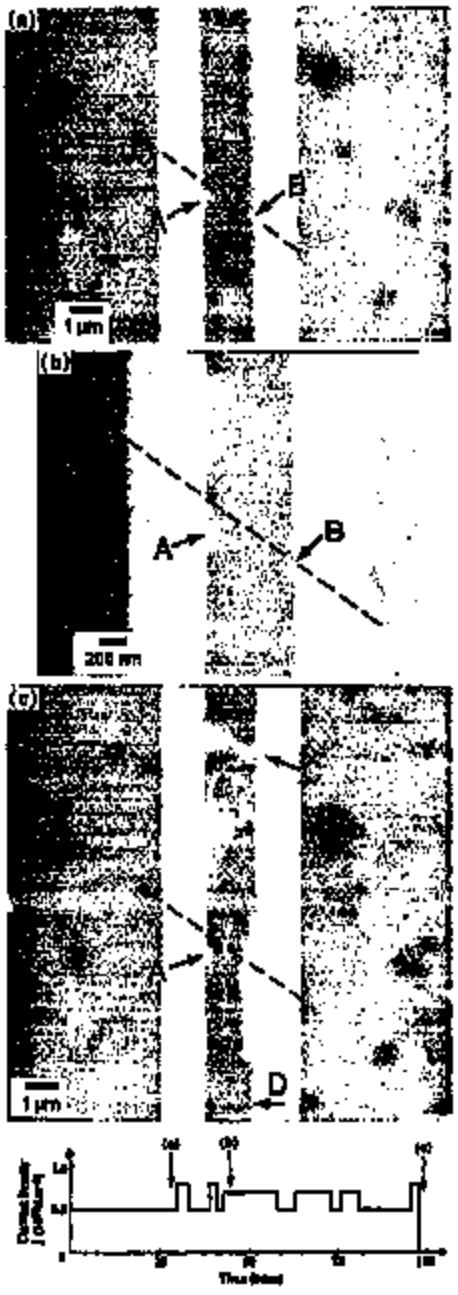

Fig. 6. TEM images of a line segment, showing that voids which develop early may grow even in the region of maximum atomic flux divergence giving the maximum voiding under electromigration testing. In (a) there are two early voids at A and B with precipitates nearby. After another 13 min of electromigration testing, the slightly higher magnification image (b) shows the depletion of Al–Cu precipitates has coalesced voids at A and B. In (c), the line has failed at C, but despite the heavy damage site in this region of high $\partial D/\partial x$ (Fig. 2(b)), the early void at A has still not grown further. The timing and current density at which each micrograph was taken are presented in the diagram at the bottom of the figure. Electron flow: top to bottom.

9(a). Subsequent growth of the voids can take different forms. In particular, the voids which develop early, such as in Figs. 5 and 6, behave differently from those shown in Figs. 7–9. Whether these early voids would lead to failure has been an issue for discussion [15,23]. Here more direct evidence provides further insight. Figs. 5 and 6(a) were obtained at the end of the first 30 min stressing at 0.5 j. The small voids shown in these two figures have three features which make them significantly different from the others. Firstly, these voids appear before the local depletion of Cu atoms, in contrast to those discussed in Section 3.1; as can be seen in Fig. 5, there are precipitates very close to the voids. Secondly, the position of these voids seems to be not affected by the long-range temperature profile discussed in Section 2.2 and Section 3.1; at about the same time, voids of this type develop at the end of the transparent line segment which experiences a relatively low temperature increase (Fig. 5), and in the hot region with the maximum divergence in atomic flux (Fig. 6). The third feature is that these voids do not grow much during further electromigration stressing, as is shown in Fig. 6 (where, as in Fig. 4, a dashed line based on precipitates in the guard rails is used as a reference to identify the same position in the test line). After Fig. 6(a), Fig. 6(b) was taken after another two cycles of electromigration stressing between 0.5 and 0.8 J (another 13 min). In this slightly higher magnification image, it can be seen that both voids A and B did not grow much while the precipitates nearby are disappearing. After the test line failed with a lifetime of 98 min, Fig. 6(c) was obtained. In the lifetime of this line, these two voids did not grow further, although they are in the most heavily voided region in the vicinity of failure site (labelled C). In Fig. 6(c), void A still retains its initial morphology as in Fig. 6(a); void B also retained its morphology until in this case it was incorporated into another void growing from position D after the local depletion of Al–Cu precipitates (see Fig. 7). These three features of the early voids suggest that they have different mechanism for void development and they are unlikely to be fatal. All the voids discussed in the following sections appeared after the local depletion of copper (Al–Cu precipitates).

3.4. Void development

The most attractive feature of the in-situ work is the ability to follow the development of voids. Fig. 7(a)–7(j) show the evolution of a void under stressing between 0.5 J and 0.8 J. Initial stressing at 0.5 j for 30 min did not produce any detectable damage. In stressing for 3 min at 0.8 J a void appeared at the edge of the line and grew fast. The current density was reduced to 0.5 j to obtain the image in Fig. 7(a). After a further 2 min stressing at 0.8 J and reduction again to 0.5 J, the void evolved into the shape in Fig. 7(b). Subsequent stressing was at 0.7 j, again with periodic interruptions at 0.5 j. Over 30 min, the evolution followed the pattern seen in Fig. 7(c)–7(g). After initial growth across the line the void grew rapidly upstream along the edge. When it encountered

a boundary across the line (Fig. 7(e)–7(g)), sharp growth occurred along the boundary. (Presumably this is a grain boundary, though this was not verified using electron diffraction.) After Fig. 7(g), the current density was reduced to 0.5 j to avert failure. Almost immediately, the new slit-like growth front of the void was filled. After 3 min at 0.5 j, the current density was again raised to 0.7 j for 5 min and the development of the void now followed a different course; as shown in Fig. 7(h) and 7(i), its growth direction changed and it broke through the boundary, continuing its growth along the edge of the line. After a further 15 min at 0.5 j, the void had evolved into the shape shown in Fig. 7(j).

When the void at D (Fig. 7(a)) grew along the edge of the line, the growth front encountered other grain boundaries (judging from the varying contrast level) before it reached the similarly inclined grain boundary at B (Fig. 7(e)). Thus it seems that void growth along the edge of the line does not change into void growth along a grain boundary unless the growth front reaches the upstream end of an inclined grain boundary.

The sequence of images in Fig. 7, when compared using the reference line, shows that the growth of the void is predominantly upstream, with the earlier parts being filled in with aluminium migrating downstream. Such filling in, and the change between Fig. 7(g) and 7(h), can be regarded as healing events. Similar events were then subjected to further study.

3.5. Healing

Fig. 8 shows a sequence of micrographs from a different segment of line. For the specimen tilt used, the predominant contrast is from thickness variations. Again, no damage was evident after 30 min at the initial electromigration stress of 0.5×10^{10} A m^{-2} (0.5 j). After a further 33 min in which

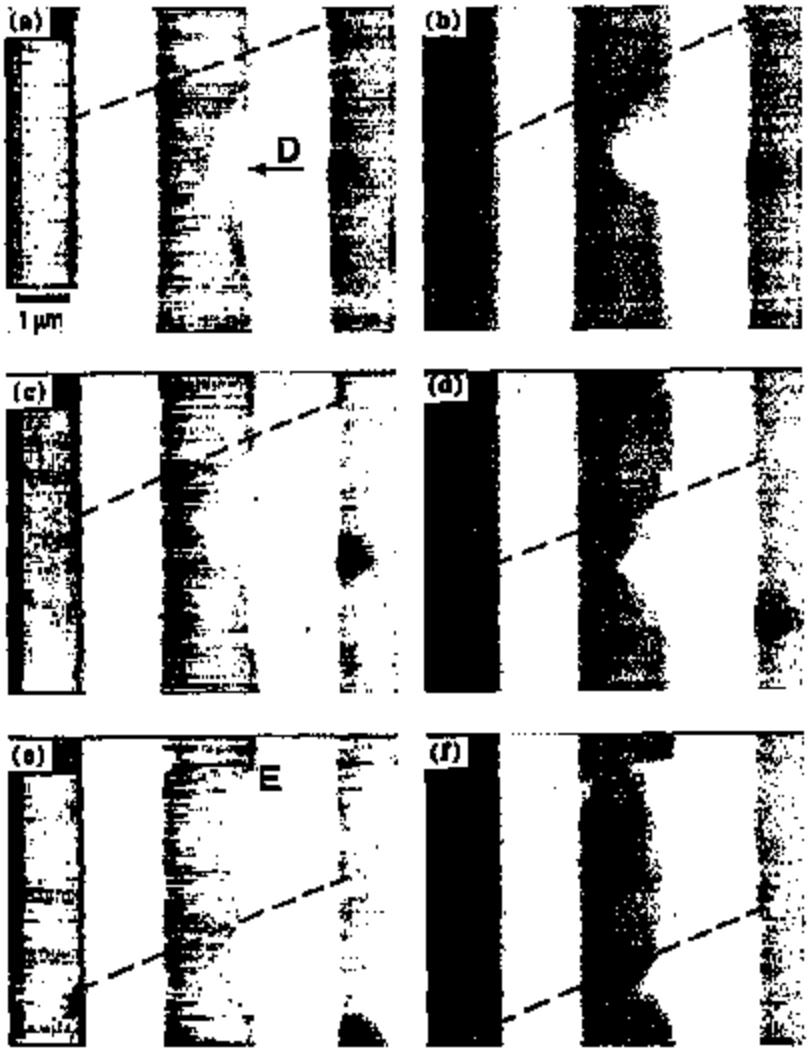

Fig. 7. (continued)

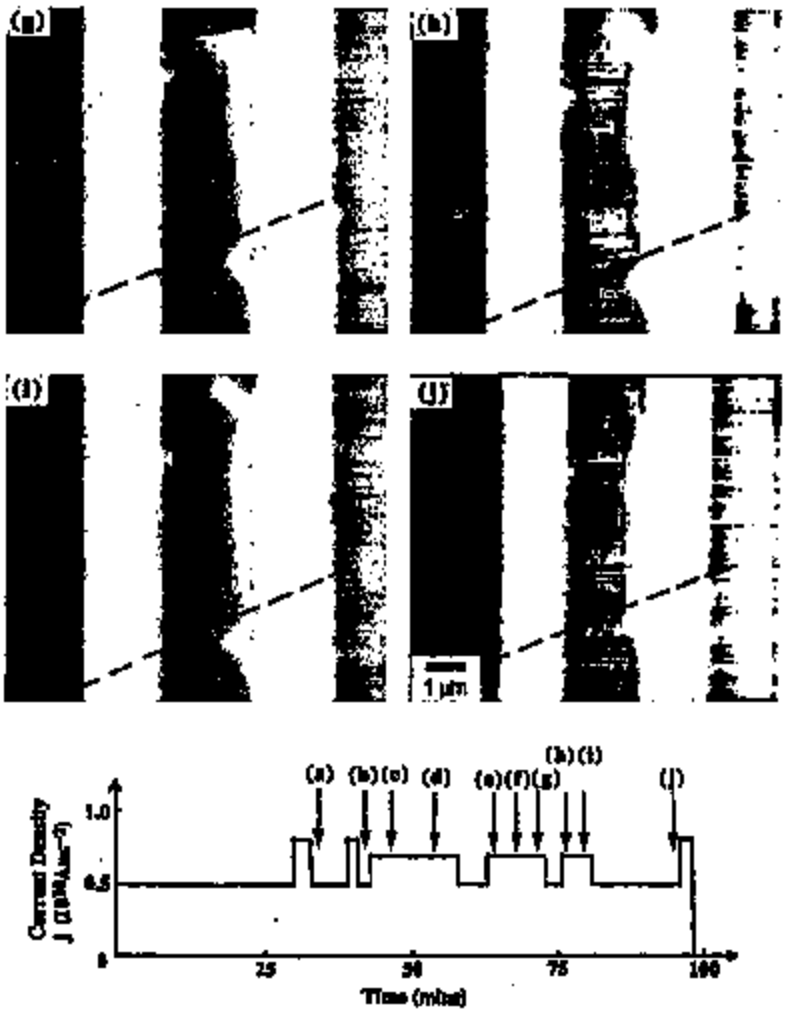

Fig. 7. Sequential TEM images (a)–(j) for a segment of line under in-situ electromigration testing, showing the evolution (initiation, growth along the line, partial refilling, growth across grain boundaries and growth along a grain boundary) of a void stressed with a current density ranging between 0.5×10^{10} A m^{-2} and 0.8×10^{10} A m^{-2}. The timing and current density at which each micrograph was taken are presented in the diagram at the bottom of the figure. Electron flow: top to bottom.

there were three cycles of current density between 0.5 j and 0.8 j, still no damage was evident. A void formed at the edge of the line after further stressing at 0.7 j. Fig. 8(a) shows it after 10 min, and Fig. 8(b) after a further 5 min in which it has crossed the entire width of the line, though not the entire thickness. Observations of line thinning of this kind have often been reported (see, for example, Ref. [24]) and taken as evidence for surface or interface transport. As in Fig. 7, the effective void migration can be seen to be against the electron flow (which is again from top to bottom in the micrographs). Comparing the images, the small void just above the reference line in Fig. 8(a) becomes part of the main void in Fig. 8(b), while the partly thinned lower part of the void in Fig. 8(a) becomes separated from the main body of the void by refilling of aluminium at A. As a result the void appears to migrate about 0.5 μm against the electron flow.

For imaging in Fig. 8(a) and 8(b) the current density was reduced to 0.5 j. After Fig. 8(b), when the current density was held at 0.5 j, it was found that the line structure continued to evolve. The changes in the following 15 min are shown in Fig. 8(c)–8(e). The effect is that the line is healed, apparently by aluminium migrating against the electron flow. When the current density was then increased to 0.8 j, damage recommenced but in a different form, as is shown in Fig. 8(f). In comparison with other observations, the evolution of line structure at 0.5 j was unusual. This observed large-scale healing was close to the centre of the transparent line segment, where higher temperature may contribute to the healing event, as discussed further in Section 4.3.

3.6. Open-circuit failure

Fig. 9 illustrates the development of a void to failure. Initial stressing for 30 min at 0.5 j again produced no detectable

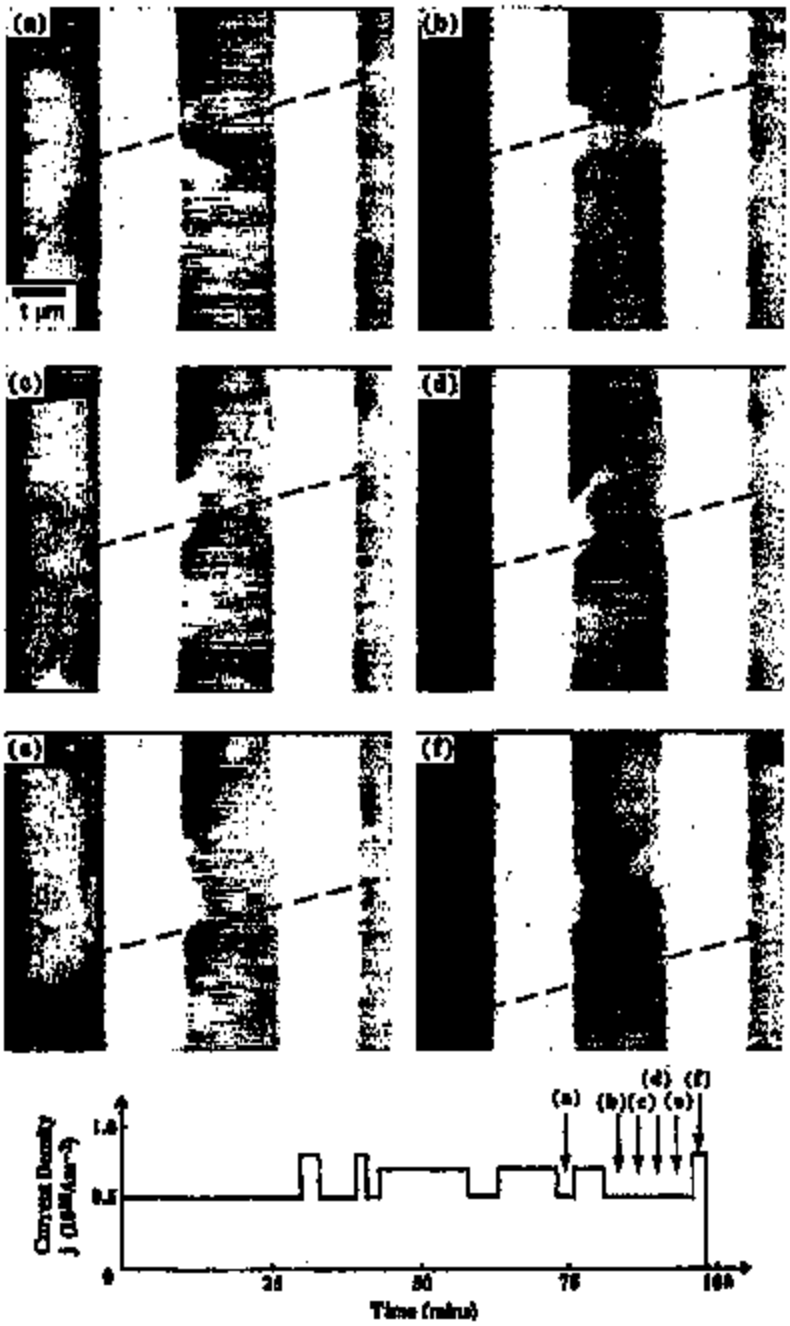

Fig. 8. Sequential TEM images (a)–(f) for a segment of line under in-situ electromigration testing, showing the growing and healing of a void. The timing and current density at which each micrograph was taken are presented in the diagram at the bottom of the figure. Electrons flow top to bottom.

damage. After 3 min at 0.8 j a void had developed as shown in Fig. 9(a), and at higher magnification in Fig. 9(b). Consistent with the observations in Fig. 7 (particularly Fig. 7(g)), it appears that sharp growth across the line occurs when the void meets an inclined plane acting as a barrier.

There is evidence that line failure can be strongly associated with slit-like voids, and that such slits are transgranular [3]. It was therefore of interest to assess whether the sharp void seen in Fig. 9(b), for example, was of this kind. In particular it is important to know whether the plane along which the void is developing has a particular crystallographic orientation within one grain, or whether it is a grain boundary. During a further 6 min at 0.5 j (in which there was no significant damage development), the test line in Fig. 9 was

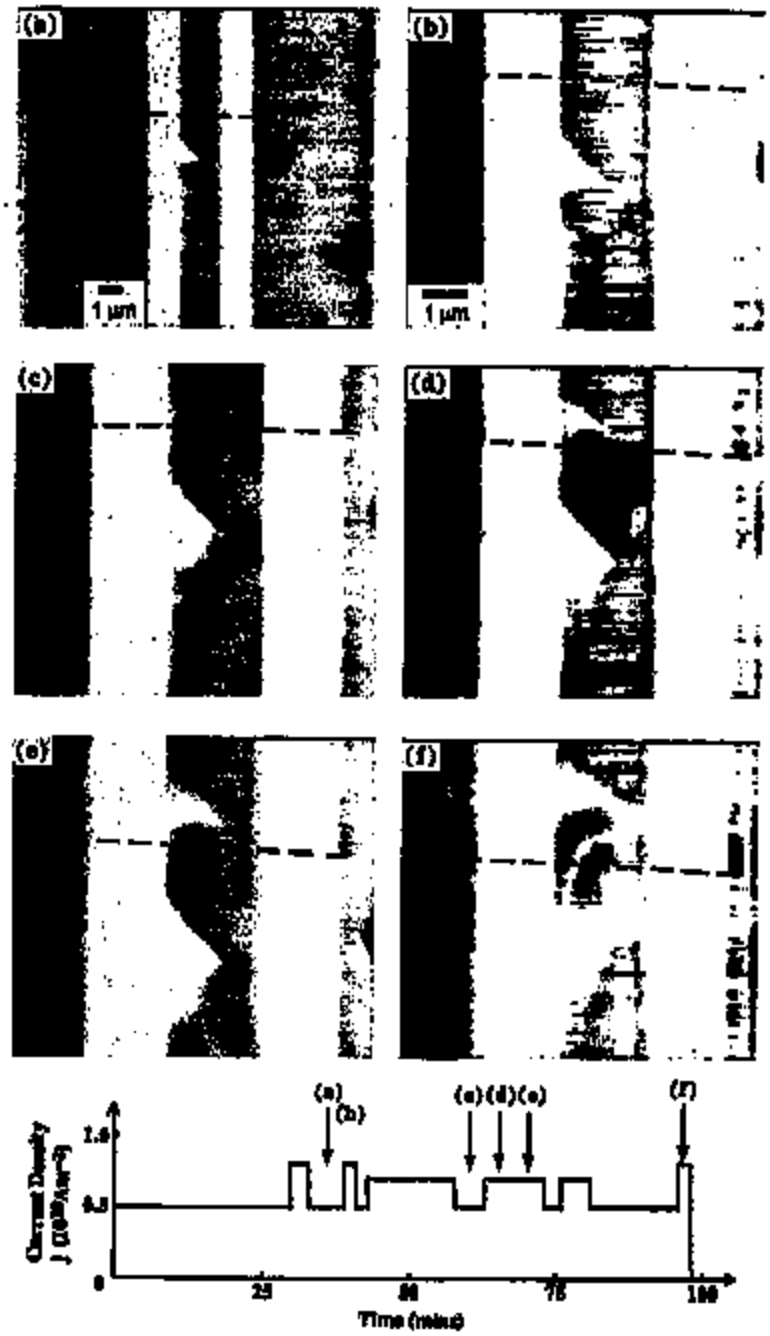

Fig. 9. Sequential TEM images (a)–(f) for a segment of line under in-situ electromigration testing, showing the development of voids to failure. The development suggests that for wormhole voids, the compressive stress built up at the downstream end of the grain boundaries can be relieved by plastic flow towards large voids nearby and that there can thus be failure. The timing and current density at which each micrograph was taken are presented in the diagram at the bottom of the figure. Electron flow: top to bottom.

tilted to a near diffracting condition, imaged and tilted back to the original orientation. As shown in Fig. 10, the plane in this case is confirmed to be a grain boundary across the line; the diffraction pattern in Fig. 10(b) for the grain above the boundary is clearly different from that in Fig. 10(c) for the grain below the boundary.

Resuming the main study of the line, stressing at 0.6 j for 2 min and 0.5 j for 2 min did not give any noticeable change in the void. After a further 15 min at 0.7 j (and return to 0.5 j) Fig. 9(c) was obtained; the void growth has broken through the boundary shown in Fig. 10 and started growing downstream along the left-hand edge of the line. In a further

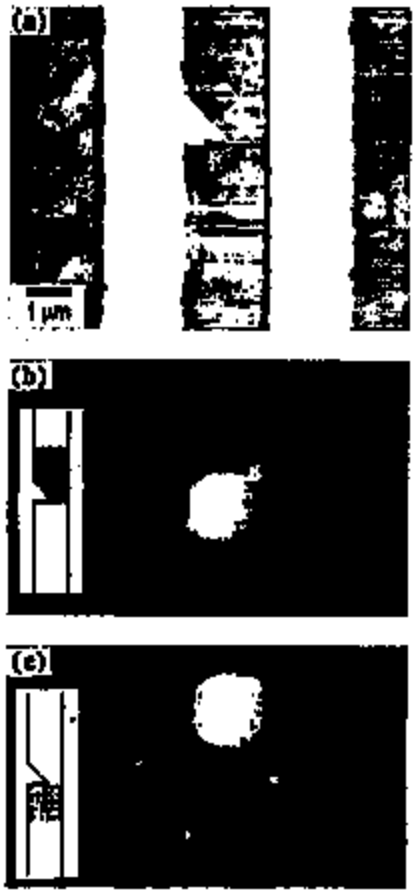

Fig. 10. TEM image for the line segment shown in Fig. 9(b) but in diffract ion conditions, confirming that the planar feature is a grain boundary across the width of the test line. The diffraction patterns in (b) and (c) for the grains above and below the boundary demonstrate that they are two different grains.

10 min at 0.7 j, Fig. 9(d) and 9(e) were obtained. A second void develops upstream from the first and grows sharply across the line. The line was subjected to further stressing of 3 min at 0.5 j, 5 min at 0.7 j and 15 min at 0.5 j without much apparent change. The line finally failed in 2 min after increase of the current density to 0.8 j. The failure site is shown in Fig. 9(f).

After 15 min the failure site showed no significant change. However, TEM examination of the failed line four days later (Fig. 11) showed a much wider open-circuit gap. As the thermal expansion coefficient of aluminium is greater than that of silicon (or SiO_2), it can be expected that the differential contraction on cooling would put the aluminium lines into tension (even when relatively unsupported as in the electron transparent regions). Creep to relieve this tension could explain the widening gap. The diffraction patterns in Fig. 11(b) and 11(c), from above and below the failure site respectively, are consistent with different grains with no particular crystallographic orientation relationship. An examination was also made of the other damage sites on this line; four days of ageing at room temperature did not produce any change in their morphology.

4. Discussion

4.1. Relevance of in-situ testing

Given the distinctive temperature profile and distribution of damage in lines which are subjected to in-situ electromigration stressing, it is important to consider whether the mechanisms of damage and failure can be the same as in conventional accelerated testing or in service. For the lines in this study it is fortunately possible to make a direct comparison with the observations of microstructural change and damage development in conventional testing of the same lines (also unpassivated). The phenomena observed in the two cases appear to be the same. In particular, conventional testing also shows the migration of copper and Al–Cu precipitates in the direction of the electron flow [15], the occurrence of hillocks associated with precipitates [2,14], and the initiation of voids at line edges [15]. Electrical measurements in con-

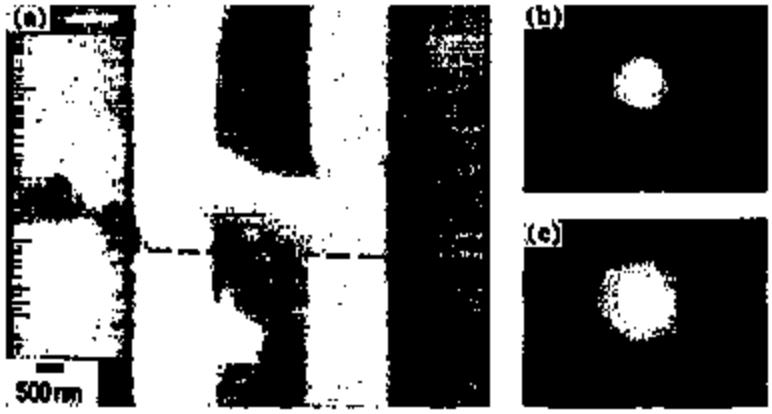

Fig. 11. TEM image of the failure site shown in Fig. 9(f) but taken 4 days after it failed, showing a wider open-circuit gap than in Fig. 9(f). The diffraction patterns in (b) and (c) for the Al line above and below the failure site respectively, do not show any particular relationship in crystallographic orientation.

ventional testing of the same lines show healing events such as could be associated with the changes seen in the in-situ testing [15]. Higher temperatures are likely to be encountered in the in-situ testing, and it has been suggested that at higher temperatures, transport paths other than grain boundaries could become relatively more important [13,25]. However, as the discussion in Section 4.2 will show, grain boundary transport remains of first importance in the development of damage in in-situ testing.

The electromigration phenomena observed here also appear qualitatively the same as those in passivated lines which can be observed through the passivation using high-voltage SEM [23,26,27]. In the passivated lines it is observed that: voids always initiate at the edge of the line; there are voids which do not move during testing; migrating voids do so in the direction opposite to the electron flow; the migrating voids can move across grain boundaries; early voids which grow little do not lead to failure; coalescence of electromigration voids happens in the later stages of the lifetime; final failure is dominated by fast growing and moving voids appearing late in the test; there is healing (refilling) of voids; healing at one place can sometimes be correlated with voiding nearby. Since all these are observed in the unpassivated lines in the present study and/or in earlier studies [2,6,15,28,29], we conclude that the native oxide on our lines can act as a weak passivation. Under applied passivation there will be a higher hydrostatic tensile stress component (e.g. an increase of 0.2% in interplanar spacings of (422) planes of Al–0.5% Cu metallization [30]), suppressing hillocking and promoting voiding, but the basic mechanisms controlling electromigration behaviour are unaltered.

Overall then, it seems that the phenomena observed in the present in-situ testing are similar to those in conventional accelerated lifetesting of the same lines. Undoubtedly the processes are greatly accelerated in in-situ testing, both by increased temperature and by increased atomic flux divergence arising from temperature gradients. In different regions of the lines tested in-situ, the divergences lead to void or hillock formation. Though these divergences are larger than may be usual in conventional testing, divergences of both kinds can still arise in conventional testing through microstructural variations. Since voids are the damage type mostly associated with failure, their formation and development will be considered most closely.

4.2. *Void formation and growth*

In the present work there is no evidence for the elongated voids apparently within grains reported by Vaynman and Lobotka [11] in their near-bamboo lines. This may be because the line-width is less in the present work, because of the different preparation of the metallization (in Ref. [11] the lines were electrochemically thinned), or because of the lack of copper in the metallization in Ref. [11].

In previous work [15] it was observed that, in interrupted testing, voids which developed early did not grow. Since it is known that interruptions or reductions in stressing current can change the pattern of damage development, the behaviour of the early voids could be attributed to the interruptions. However, the present work shows (Fig. 6) that even in periods with a steady current the early voids do not grow. There has been discussion of the distinction between stress-induced and electromigration-induced voids, the former developing early and not growing much during current stressing [27]. In the present work the early voids presumably correspond to the "stress-induced" category. It is found that they appear during electromigration testing, but in the very early stages and at lower values of current than for the development of full electromigration damage. Thus it appears that they may indeed be associated mainly with mechanical stresses present in the lines before electromigration testing.

A classification of voids has recently been proposed [31,32], as shown in Fig. 12. Voids with a basic triangular shape in single crystals are classified as "critical" or "uncritical" on the basis of their orientation relative to the electron flow in the test line. For critical voids the migration along the inclined surface leads to sharp growth of the void across the line, while for uncritical voids the migration along the inclined surface leads to the growth along the edge of the line. It is found in the present work that even for a line with grain boundaries across its width, this classification of void behaviour is still generally valid. For voids with the critical shape, grain boundaries facilitate growth across the line; for voids with the uncritical shape, the electromigration flux along grain boundaries is somewhat balanced by the stress built up at the downstream end of the grain boundaries. This stress-driven back flux would prevent the void from growing further along the grain boundaries. Fig. 7(e)–7(g) show two linked voids associated with grain boundaries across the width of the line. The downstream void is uncritical in orientation, the upstream one critical, and their subsequent development matches the simple model. Also, in Fig. 8(a) and 8(b) the void is critical and does grow to cross the line. For uncritical voids, the compressive stress built up at the

Fig. 12. Schematic diagram of critical and uncritical void geometries as proposed by Arzt et al. [32]. The predominant atomic transport is along the internal free surface of the metallization as shown by the small arrows.

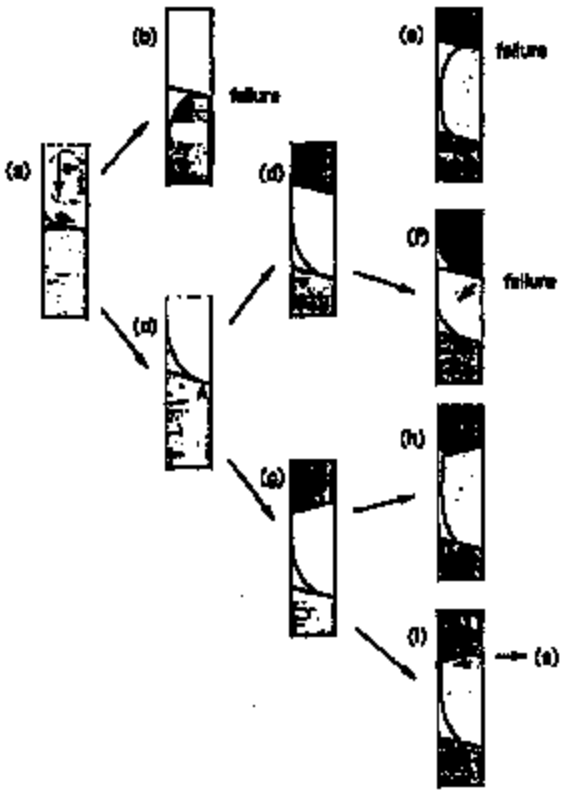

Fig. 13. A schematic model for electromigration-induced open-circuit failure in bamboo lines with inclined grain boundaries, showing possible alternative sequences of events. The shading indicates distinct grains. The unshaded areas are voids forming under the original oxide skin of the line. Damage is concentrated at boundaries which are inclined to the current. Precipitates are not considered in this model as copper depletion (and consequent precipitate dissolution) usually precedes damage.

downstream end of the grain boundaries could be relaxed by plastic flow towards large voids nearby, and there could then be failure. An example of this is shown in Fig. 9(d)–9(f) (no interruption of current), where two incritical voids at the ends of inclined grain boundaries across the line combine to produce a open-circuit failure site along one of the grain boundaries.

From Figs. 7–9 it is striking that void initiation and development is strongly associated with the upstream end of inclined grain boundaries crossing the lines (shown schematically in Fig. 13(a)). This is exactly as would be expected if grain boundary transport is significant, as this (in the direction shown by the arrow in Fig. 13(a)) would transport atoms away from the void initiation site. The effect of such boundaries on mean time to failure has been studied in detail for controlled boundaries [33]. In a bamboo line, such as illustrated schematically in Fig. 13, the linked development of damage along the line requires atomic transport by paths other than just grain boundaries. Transport at the interface between the metallization and its oxide, or the underlying oxide, seems more likely than bulk diffusion. It appears from the rapid void growth which can occur upstream along line edges (e.g. in Fig. 7(d)–7(g)), that especially significant transport can occur on free surfaces, when these are created under the oxide skin by voiding.

4.3. Healing

In Figs. 7 and 9 there is evidence for successive void formation, later voids forming upstream of earlier ones. As the later voids grow, the material from them is transported downstream to give partial refilling of the earlier voids. In Section 4.4, a model for damage development and failure is developed from these observations. The void refilling can be regarded as a healing event. Subsequent void regrowth at the original site is initially prevented by the supply of atoms from growing upstream voids. Later, when the upstream voids are further away, damage may recur at the original site, but may be in a different form because of changed grain boundary configurations.

A less expected form of healing is shown in Fig. 8. The void refilling may be aided by atomic transport from upstream voids. However, the observation that it occurs at a lowered current density strongly suggests a significant contribution from stresses in the line. It is evident that electromigration can lead to the build-up of stresses through atomic flux divergence [34]. The stress gradients give mechanodiffusion fluxes which act in opposition to the electromigration fluxes. Such effects are responsible for the observation that electromigration damage and failure rates are proportional to the square of the current density used in testing [35]. Stresses can also give rise to plastic flow, such as is associated with hillocking. When the current density is reduced, as is the case before the sequence Fig. 8(c)–8(e), the electromigration force on the atoms is reduced but the stress gradient remains and can now dominate to drive the atoms against the electron flow. If there is local heating due to the reduced line cross-section, this may also act to promote healing by facilitating plastic flow (also in the direction against the electron flow) under the stress. When the current density is returned to a higher value, the damage may not resume in the same way as before, because the stress distribution is now different (partially relaxed) and the grain boundary configurations may have changed. If plastic flow has occurred, the material in the healed zone may also be work-hardened.

The healing event in Fig. 8 seems clearly to be promoted by the reduction in current density, and this effect can be understood. It seems from other observations in the present work that the pattern of damage development can often be altered after a brief reduction in current density, presumably because of small-scale healing processes. On the one hand, this suggests that the nature of the current density (constant, varied or intermittent) applied in a lifetest could have significant consequences. On the other hand, it raises the question of whether the present results are valid in interpreting non-stop conventional lifetests at constant applied current density, and whether the results from non-stop conventional lifetests at constant current density are valid in interpreting the device

performance in service (experiencing switching on and off). It should be noted, however, that even in the non-stop conventional test, the line microstructure and its evolution and the development of damage will lead to local fluctuations in both current density and temperature. These fluctuations could equally promote healing events.

Berenbaum [7] showed that the reversal of damage (in particular, refilling of voids) by reversal of current could not be obtained if the sample was oxidized (by exposure to air for several days) before the reversed current was applied. Oxidation effects are not believed to operate in the present work in which the lines were tested over short periods in the TEM vacuum and with the original oxide skin of the lines still in place.

4.4. A model for failure of bamboo lines

The observations in Figs. 7 and 9 suggest a pattern for void initiation, growth, and healing or failure. This pattern is the basis for a simple model proposed in Fig. 13 for the failure of bamboo and near-bamboo lines. The overall atomic transport down the line (i.e. in the direction of electron flow, from top to bottom in Fig. 13) will be deflected sideways at inclined grain boundaries, resulting in the void initiation at the upstream end of the boundary as shown in Fig. 13(a). Voids can develop into the critical shape (Fig. 13(b)), or the uncritical shape (Fig. 13(c)). In Fig. 13(b), the main growth direction of the critical void (across the line-width) coincides with the grain boundary and growth is thus facilitated leading to open-circuit failure. For uncritical voids (Fig. 13(c)) where the main growth direction would be along the line edge, the grain boundary transport will lead to a compressive stress build up at A (the downstream end of the inclined grain boundary). The resulting stress gradient along the grain boundary path will lead to a mechanodiffusion back-flux, eventually halting the grain boundary transport. The reduced line cross-section near A can lead to local heating which promotes plastic flow. This plastic flow is against the electromigration flux and thus provides some local healing. In this way, there are "restoring forces" to inhibit open circuit failure arising at a single boundary. The restoring forces can also be thought of in terms of a vacancy concentration gradient; the links between the stress and vacancy concentration descriptions are discussed in Ref. [35].

However, these uncritical voids can still lead to failure in two ways. An uncritical void can grow along the edge of the line until it reaches another grain boundary inclined similarly to the first (Fig. 13(d)); then rapid transport along the free surface between the two grain boundaries could give rapid void growth at the upstream boundary leading to failure, accompanied by some refilling (healing) of the original void (Fig. 13(e)). A direct example of this can be seen in Fig. 7(g). If the first void stabilizes and the second boundary which follows the pattern seen in Fig. 13(a) and 13(c) is nearby (Fig. 13(f)), the stress at the downstream end of the second boundary can be relieved by plastic flow in a direction (shown by the arrow) not otherwise available—into the original void. In this case the restoring forces inhibiting continued void growth along the boundary are greatly reduced, and catastrophic failure ensues. A direct example of this is shown in Fig. 9(f).

When an uncritical void growing along the line edge encounters an oppositely inclined boundary (i.e. the downstream end of an inclined grain boundary as is shown in Fig. 13(g)), it may cross the grain boundary (Fig. 13(h)), as seen in Fig. 7; it may also induce the growth of a void at the upstream end of the second grain boundary (Fig. 13(i)). The new void in Fig. 13(i), is similar to that Fig. 13(a) (giving a possible repetition of events), but the possible restoring forces inhibiting void growth along the boundary are greatly reduced.

According to this simple model, damage development and failure in bamboo lines are promoted by similarly inclined boundaries such as are shown in Fig. 13(d).

4.5. Post-mortem observations

The evolution of microstructure and the development of damage which occur during electromigration stressing can be examined either in-situ or by interrupted testing; in the latter, the specimen is periodically removed from stressing for examination, usually at room temperature. Each technique has its advantages and disadvantages. The present observations suggest some advantages of the in-situ technique. Firstly, it seems possible that the interruptions themselves would affect the progress of the test; both the change in current density, and the thermal mismatch stresses arising from the thermal cycling may affect the development of damage. Secondly, as the observations in Fig. 11 show, the mismatch stresses on cooling the sample for observation may change the line structure so that the observations do not accurately reflect the configuration at the test temperature.

5. Conclusions

It is demonstrated that lines patterned for conventional lifetesting can be prepared for in-situ stressing in TEM. The microstructural evolution and damage development in the in-situ testing show the same phenomena as in conventional testing of analogous lines. Despite the very different thermal conditions in the two types of test, the in-situ observations can be relevant for the analysis of failure in conventional lifetesting, or in service. The phenomena also appear to be the same as those observed in passivated lines, suggesting that the different stresses with and without passivation do not change the basic electromigration mechanisms.

The present work confirms a number of earlier observations. Copper migrates faster than aluminium and voiding in the lines occurs mainly in regions of copper depletion. The lines contain precipitates and these are often associated with hillocking. Dissolution of copper at the upstream side of the

precipitates and reprecipitation on the downstream side can lead to their effective downstream (i.e. in the same direction as the electron flow) migration. Conversely, voids migrate upstream.

Voids can develop early, before the depletion of copper. Such voids show very limited growth, and are unlikely to lead to failure.

The lines in this study have a near-bamboo microstructure. In this microstructure, void initiation is at the upstream end of inclined grain boundaries, indicating the importance of grain boundary transport. Rapid atomic transport on free surfaces leads to the upstream spreading of voiding. When boundaries are sufficiently far apart, this leads to a succession of voiding and healing events. When the boundaries are close, open-circuit failure can result, particularly for similarly inclined boundaries.

Healing (void refilling) is a natural process in lines under continuous test and leads to changes in the pattern of damage development. It can occur by surface transport of material from a growing upstream void or by the action of stresses. In the latter case it is promoted by reductions in current density or increases in temperature.

It is concluded that line reliability will be improved if the grain boundaries are more normal to the current flow, if they are further apart and if the copper content of the metallization is higher.

Acknowledgements

This work forms part of projects supported by the Engineering and Physical Sciences Research Council (formerly the SERC) and the Department of Trade and Industry. Interactions with partners and others associated with the project are gratefully acknowledged: GEC Plessey Semiconductors Ltd, who provided the samples for this work; BNR (Europe) Ltd; GEC Marconi Materials Research Ltd; and the Universities of Lancaster, Kent, Newcastle and York. Thanks are due to Dr P. Augustus for advice on specimen preparation.

References

[1] J. Cho and C.V. Thompson, *Appl. Phys. Lett.*, *54* (1989) 2577.
[2] A.L. Greer and W.C. Shih, *Mater. Res. Soc. Symp. Proc.*, *265* (1992) 83.
[3] J. Sanchez and E. Arzt, *Mater. Res. Soc. Symp. Proc.*, *265* (1992) 1511.
[4] I.A. Blech and E.S. Meieran, *Appl. Phys. Lett.*, *11* (1967) 263.
[5] R. Rosenberg and L. Berenbaum, *Appl. Phys. Lett.*, *12* (1968) 201.
[6] I.A. Blech and E.S. Meieran, *J. Appl. Phys.*, *40* (1969) 485.
[7] L. Berenbaum, *J. Appl. Phys.*, *42* (1971) 880.
[8] F.M. D'Heurle, *Metall. Trans.*, *2* (1971) 683.
[9] S.J. Horowitz and I.A. Blech, *Mater. Sci. Eng.*, *10* (1972) 169.
[10] I. Vavra, P. Lobotka, F. Zachar and J. Cernik, *Phys. Status Solidi (a)*, *63* (1981) 363.
[11] I. Vavra and P. Lobotka, *Phys. Status Solidi (a)*, *65* (1981) K107.
[12] W.C. Shih, T.C. Denton and A.L. Greer, *Mater. Res. Soc. Symp. Proc.*, *265* (1992) 101.
[13] W.C. Shih, T.C. Denton and A.L. Greer, to be published.
[14] W.C. Shih and A.L. Greer, *EMRS'92 Proc.*, (1992) 347.
[15] W.C. Shih, A.L. Greer, Z. Xu and B.K. Jones, *Mater. Res. Soc. Symp. Proc.*, *309* (1993) 369.
[16] W.C. Shih and A.L. Greer, *Mater. Res. Soc. Symp. Proc.*, *391* (1995) 391.
[17] W.C. Shih and A.L. Greer, *J. Electron. Mater.*, *23* (1994) 1315.
[18] B.K. Jones and Y.Z. Xu, *Microelectron. Reliab.*, *33* (1993) 1629.
[19] P. Lobotka and I. Vavra, *Phys. Status Solidi (a)*, *63* (1981) 655.
[20] C.Y. Chang and R.W. Vook, *J. Mater. Res.*, *4* (1989) 1172.
[21] *Landolt-Börnstein Tables*, New Series, Springer, Berlin, 1993.
[22] R.A. McKee and J.P. Stark, *Acta Metall.*, *23* (1975) 1145.
[23] P.R. Besser, M.C. Madden and P.A. Flinn, *J. Appl. Phys.*, *73* (1992) 3792.
[24] J.R. Black, *IEEE Trans. Elec. Dev., ED-16* (1969) 338.
[25] C.Y. Chang and R.W. Vook, *Mater. Res. Soc. Symp. Proc.*, *225* (1991) 125.
[26] M.C. Madden, B.V. Abramowski, T. Marieb and P.A. Flinn, *Mater. Res. Soc. Proc.*, *265* (1992) 33.
[27] T. Marieb, J.C. Bravman, P. Flinn, D.B. Gardner and M. Madden, *Appl. Phys. Lett.*, *64* (1994) 2424.
[28] R.W. Thomas and D.W. Calabrese, *21st Proc. of IEEE IRPS*, IEEE, New York, 1983, p. 1.
[29] E. Castano, J. Metz, P. Flinn and M. Madden, *Appl. Phys. Lett.*, *59* (1991) 139.
[30] B. Greenebaum, A.I. Sauer, P.A. Flinn and W.D. Nix, *Appl. Phys. Lett.*, *58* (1991) 1645.
[31] O. Kraft, S. Bader, J.R. Sanchez, Jr., and E. Arzt, *Mater. Res. Soc. Proc.*, *309* (1991) 199.
[32] E. Arzt, O. Kraft, W.D. Nix, and J.E. Sanchez, Jr., *J. Appl. Phys.*, *76* (1994) 1563.
[33] H.P. Longworth and C.V. Thompson, *Appl. Phys. Lett.*, *60* (1992) 2219.
[34] C.A. Ross and J.E. Evetts, *Scr. Metall.*, *21* (1987) 1077.
[35] M.A. Korhonen, P. Borgesen, K.N. Tu and C.Y. Li, *J. Appl. Phys.*, *73* (1993) 3790.

ELSEVIER

Thin Solid Films 343–344 (1999) 465–468

Thin Solid Films

The influence of cooling water flowing in the sputtering target on aluminum based thin film nanostructure deposited on glass substrates

Hiroshi Takatsuji[a,*], Satoshi Tsuji[a], K. Kuroda[b], H. Saka[b]

[a]Display Technology, IBM Japan, Ltd., Shinoumura, Yamato-shi, Kanagawa 242, Japan
[b]Department of Quantum Engineering, Nagoya University, Nagoya 464-01, Japan

Abstract

The influence of the cooling efficiency of the sputtering cathode on the nanostructure of an aluminum based (Al-based) thin film sputter-deposited on a large glass substrate (550 × 650 mm) was investigated. With high cooling efficiency, a highly (111)-textured pure-Al film was formed. On the other hand, low cooling efficiency contributes to the formation of a three-layer structure Al-Cu thin film that showed strong resistance to hillock and whisker generation.

Keywords: Large glass substrate; Hillock; Whisker; Sputtering; Aluminum; Thin film

1. Introduction

Over the past several years, there has been strong pressure to achieve high productivity in the manufacturing process of thin-film-transistor (TFT) arrays [1,2]. One approach to meeting this requirement has been to use large glass substrates with a consequent reduction in the process time of each array. Accordingly, a high deposition rate is required in the sputtering process for the large glass substrates (550 × 650 mm). Cooling of the sputtering target material is a major concern in high power sputtering processes for TFT arrays, because of the problem of peeling between the target material and the backing plate. However, there has been few reports on the nanostructure of the sputtered film and target cooling. This paper investigates the relation between the nanostructure of Al-based alloy thin films deposited on glass substrate by means of a dc magnet-scan-type sputtering apparatus and the rate of which the cooling water flows in the sputtering target. We find that the flow rate of the cooling water in the sputtering target has a strong influence on nanostructure of the aluminum (Al) film. In the case of a pure-Al thin film, the degradation of the flow rate has an undesirable influence on the film's crystallographic texture. However, an Al-0.2 wt.% Cu alloy thin film deposited at a low cooling water flow rate contained a layered nanostructure that showed strong resistance to hillock and whisker generation. The nanostructure of the thin film was analyzed by atomic force microscopy (AFM), X-ray diffraction (XRD), and cross-sectional transmission electron microscopy (TEM), while the resistance to hillock and whisker generation was investigated by means of our nano-indentation techniques [3]. We demonstrated the mechanism of the layered thin film growth by these nanostructure analysis methods for sputter-deposited thin film and by thermal conductivity analysis for the cooling of the sputtering cathode.

2. Experiment

Fig. 1 shows a cross-sectional schematic diagram of a sputtering chamber for 550 × 650 mm glass substrate, which was used with a dc magnetron multi-chamber sputtering apparatus in this study. A bar magnet behind a target controlled the plasma density by moving the magnet. Cooling water flowed within a backing plate. To investigate the effect of the cooling water flow rate on the nanostructure of a sputter-deposited thin film, two flow rates (20 and 60 l/min) were used in this study.

Pure-aluminum and Al-0.2 wt.% Cu thin films were deposited on large LCD-grade glass substrates (550 × 650 mm) with pure-Al (5N purity) and Al-alloy (0.2 wt.% Cu content) targets. The films were deposited at a power of 44 kW with 10 two-way magnet scans, an argon pressure of 0.7 Pa, and a substrate temperature of 120°C.

The film's crystallographic textures were measured by θ–2θ XRD using Cu K_α radiation at 50 kV/150 mA, with a scan speed of 1°/min, and a scan range of 30–80°. Their

* Corresponding author. Tel.: +81-462-73-2427; fax: +81-462-73-4537.
E-mail address: takatsuj@jp.ibm.com (H. Takatsuji)

0040-6090/99/$ - see front matter
PII: S0040-6090(98)01677-0

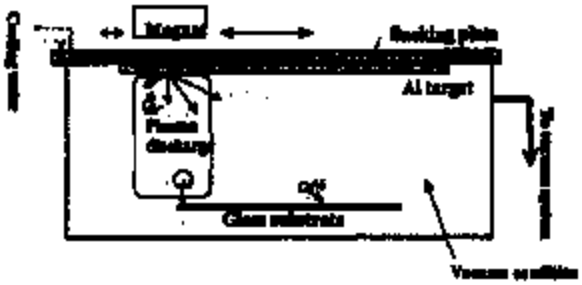

Fig. 1. Cross-sectional schematic diagram of the sputtering chamber.

nanostructures were observed by using an AFM and TEM operated at 400 kV. The resistance to stress migration was investigated by means of our nano-indentation techniques.

3. Results and discussion

3.1. Thermal conductivity analysis for cooling of the sputtering cathode

The cooling efficiency of the sputtering cathode C_w was calculated from the equation

$$C_w = F \times 60 \times \Delta T_w / Q \quad (1)$$

where F is the cooling water flow, ΔT_w is the difference in temperature of the cooling water at input and output, and Q is the sputtering power.

C_w in both conditions was estimated at 33.3% (20 l/min.) and 47.6% (60 l/min.), respectively. It was found that the sputtering chamber heated up more at a low cooling water flow (20 l/min.) than at a high flow rate (60 l/min.) during sputtering. We consider that low cooling efficiency causes transformation of parts in the sputtering chamber and outgassing from the chamber wall because of heat accumulation. We also confirmed by quadrupole mass spectrometer (Q-mass) analysis that out-gassing of nitrogen and oxygen elements arises toward the end of the sputtering time.

To investigate the effect of the cooling efficiency on the sputtering target, because no direct temperature measurement is possible during sputtering, we calculated the temperature of the target surface during sputtering T_i by using the following equation based on Fourier's law

$$T_i = \bar{T} + \frac{C_w Q}{A_m h} + \frac{C_w Q x_1}{A_m \lambda_{Cu}} + \frac{C_t Q x_2}{A_m \lambda_{Al}} \quad (2)$$

where $\bar{T}$ is the average temperature of the cooling water, C_w is the cooling efficiency of the sputtering cathode, Q is the sputtering power, x_1 is the distance between the bonding surface and the cooling water tube, x_2 is the thickness of the target, A_m is the surface area of the magnet, λ_{Cu} is the thermal transmittance coefficient of copper, λ_{Al} is the thermal transmittance coefficient of aluminum, and h is the thermal conductivity of cooling water given by Colburn's equation [4]

$$h = 0.023 \frac{\lambda}{D} (Re)^{0.8} (Pr)^{1/3} \quad (3)$$

where λ is the thermal transmittance coefficient, Re is the Reynolds number, Pr is the Prandtl number, and D is the diameter of the cooling water tube. The estimated temperature of the target surface was at 61.1°C at a flow rate of 20 l/min. And 43.1°C at a flow rate of 60 l/min. We conclude that the properties of the sputtering target do not change within this temperature range.

3.2. Effect on sputter-deposited thin films

The crystallographic texture of pure-Al films obtained at a low cooling water flow rate (20 l/min.) and a high flow rate (60 l/min.), were investigated, with the results shown in Table 1. The results indicate that deposition at a high flow rate (sample B) produced a highly (111)-textured film, whereas deposition at a low flow rate (sample A) produced a low (111)-textured (i.e., nearly random) film. In the case of a pure-Al thin film, we conclude that the degradation of the flow rate has an undesirable influence on the film's crystallographic texture. On the other hand, there was no significant difference between Al-0.2 wt.% Cu thin films sputter-deposited at a low cooling water flow rate (sample C) and a high flow rate (sample D), as shown in Table 1. However, there is a significant difference between sample C and sample D in the anti-stress migration property obtained by using nano-indentation techniques, as shown in Table 1. No whisker or hillock generation was observed in sample C. The AFM images in Fig. 2a,b show that the grain size of sample C is finer and more uniform than that of sample D. Cross-sectional TEM observation of samples C and D revealed a three-layer structure in the sample C, but no

Table 1
Sample configuration, film texture, and the results of nano-indentation techniques[a]

Sample ID	(111)	(200)	(220)	(311)	Number of hillocks	Number of whiskers
A	415 (63.4)	86 (13.1)	106 (16.2)	47 (7.2)	39	3
B	1764 (6.1)	125 (4.5)	93 (4.5)	52 (3.6)	27	2
C	722 (14.8)	164 (14.5)	161 (14.5)	62 (5.6)	0	0
D	666 (61.0)	116 (22.3)	344 (22.3)	66 (6.0)	15	0

[a] A: Pure-Al (20 l/min), B: Pure-Al (60 l/min), C: Al-0.2 wt.% Cu (20 l/min), D: Al-0.2 wt.% Cu (60 l/min). The unit of intensity is in counts per second (cps). Numbers in parenthesis denote the intensity fraction of each texture.

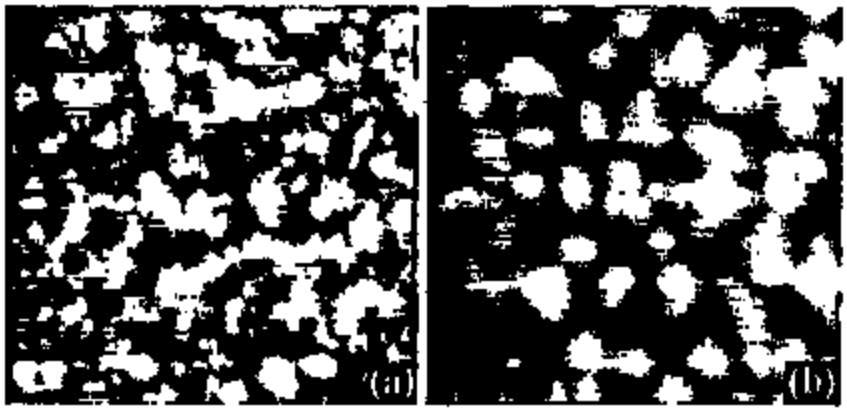

Fig. 2. Two-dimensional AFM images of Al-0.2 wt.% Cu films corresponding to the samples in Table 1: (a) Sample C (20 l/min.), (b) Sample D (60 l/min.). Scale: 2000×2000 nm.

significant structure was revealed in sample D, as shown in Fig. 3a,b. In the case of pure-Al, as in samples A and B, no three-layer structure of the Al-Cu thin film like that in sample C was observed. Sample C showed particularly unusual properties, since the structure of the top layer looked like an amorphous film and appeared to be dense, and the wet etching rate was one-eighth that of sample D. To investigate these characteristics of sample C, we performed depth profile electron spectroscopy for chemical analysis (ESCA), as shown in Fig. 4. The results indicated that aluminum oxide (Al-O) constitutes about 50% of the material in the top layer from the film surface to a depth of about 30 nm. They also indicate that the quantity of the aluminum element increases as the Al-O, oxygen, and nitrogen elements are decreased at around 32 nm. These data suggest that the top layers contain very large amounts of oxygen and nitrogen, while the middle layer contains none, and that the thickness of the top layer of sample C is about 30 nm. The

Fig. 3. Cross-sectional TEM micrographs of Al-0.2 wt.% Cu film corresponding to the samples in Fig. 2: (a) Sample C, (b) Sample D.

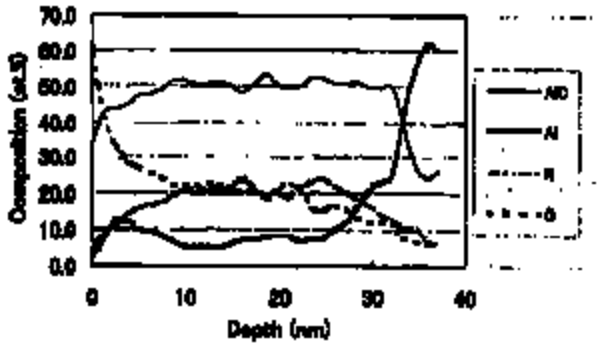

Fig. 4. Depth profile of ESCA spectra of the top amorphous layer of sample C.

thickness can also be estimated at about 30 nm from Fig. 3a. On the basis of TEM, ESCA, Q-mass, and thermal conductivity analysis for cooling of the sputtering cathode, we conclude that the oxygen and nitrogen in the top layer originate in the sputtering chamber wall and the top layer formed during the last magnet scan. We consider this to be the reason that the layered structure formed only with Al-Cu material, which reacts more readily with oxygen and nitrogen during sputter-deposition than pure-Al [5,6].

4. Conclusions

The cooling efficiency of the sputtering cathode influences the nanostructure of the sputter-deposited film. High cooling efficiency contributes to the formation of highly (111)-textured film in pure-Al, while low cooling efficiency causes out-gassing from the sputtering chamber wall during sputtering. However, a three-layer structure Al-Cu thin film that showed strong resistance to the formation of hillocks (including whiskers) when the cooling efficiency was low. We conclude that the mechanism for the formation of the three layer-structure of the Al-Cu thin film was as follows: the top amorphous layer was formed by reaction with the materials (i.e., nitrogen and oxygen) outgassed from the chamber wall, which had been heated up by sputtering energy, and the bottom layer was formed by reaction with small quantities of residual out-gassed materials (i.e. N_2 and O_2) in the sputtering chamber.

Acknowledgements

We wish to thank K. Tsujimoto of IBM Display Technology for TEM observation, M. Sakauchi of IBM Fujisawa plant for ESCA analysis, and M. McDonald of IBM Yamato for his comments on this article.

References

[1] W.E. Howard, J. SID 3/3 (1995) 127.
[2] W.C. O'Mara, Solid State Technol. (July) (1996) 76.
[3] H. Takasaki, S. Tsuji, H. Kimbara, K. Tsujimoto, K. Kuroda, H. Sato, M.R.S. Symp. Proc. 441 (1997) 415.
[4] Tz. Colbun, AIChE 29 (1933) 174.
[5] W.W.Y. Lee, D. Oblas, J. Appl. Phys. 46 (1975) 1728.
[6] H.F. Winters, E. Kay, J. Appl. Phys. 43 (1972) 794.

ELSEVIER

Thin Solid Films 289 (1996) 289–294

Thin Solid Films

Al–Sm and Al–Dy alloy thin films with low resistivity and high thermal stability for microelectronic conductor lines

Shinji Takayama [a,*], Naganori Tsutsui [b]

[a] Hosei University, Department of Electrical Engineering, 3-7-2 Kajino-cho, Koganei, Tokyo 184, Japan
[b] ITEC Co, Ltd, 800 Ishiwatashi, Yuzu-cho, Yuzu-gun, Shiga 520-23, Japan

Received 14 November 1995; accepted 9 April 1996

Abstract

The addition of either Sm or Dy rare earth metal elements to Al thin films decreases markedly the grain size of the Al matrix and largely suppresses the growth of hillock and whisker thermal defects at high temperatures (350–450 °C). A large number of particles of fine metallic compounds of Al_3RE (RE = Sm or Dy) were segregated in an Al matrix, mostly at grain boundaries, after annealing at 350 °C. The resistivities of the films after annealing at the above temperatures show very low values of less than about 30 nΩ m, without salient formation of hillocks or whiskers on the film surfaces.

Keywords: Aluminium; Conductivity; Heat treatment; Resistivity

1. Introduction

There has recently been a strong need for the development of lower cost, larger size, and higher resolution TFT-LCDs (thin film transistor liquid-crystal displays), to increase the range of their applications. However, the larger the TFT-LCD panel is, the more serious the gate-line pulse delay problem becomes. Moreover, to achieve higher resolution, the gate-line width is being made narrower; thus, the microstructure of thin film conductors is of vital importance as regards their reliability. For these reasons, Al alloy thin films with low resistivity have recently received much attention [1–7]. It was reported by the present authors that Al–rare-earth alloy systems in particular showed very low resistivities without the formation of hillocks and whiskers, even after annealing at high temperatures (350–450 °C) [4–6].

In this report, we study in more detail the effects of adding Sm or Dy to Al thin films on the structure and conductivity after isochronal or isothermal annealing.

2. Experimental details

Al–rare-earth alloy films about 400–600 nm thick were deposited onto 7059 glass substrate using a d.c. magnetron sputtering apparatus at an Ar pressure of 0.7 Pa. The composition of the films was varied by using a composite target consisting of 100 mm Al disks (99.99% purity) and $5 \times 5 \times 1$ mm^3 rare earth metal element chips (99.9% purity). The film composition was determined by inductively coupled plasma (ICP) spectroscopy. The electrical resistance of the film was measured using a conventional four-point probe at room temperature. The film structures were examined using an X-ray diffractometer operated at 50 kV and 200 mA, and a transmission electron microscope (TEM) operated at 400 kV.

3. Results

Fig. 1 shows the change in resistivity in as-made Al–RE (RE = Sm or Dy) alloy thin film samples as a function of the content of the elements added to Al. The resistivities after annealing at 450 °C are also included in the figure for reference. The resistivity increases almost linearly within the composition range of the present study. The slope of the curve for as-made Al–Sm alloy films is steeper than that for as-made Al–Dy alloy films. Note that the resistivities of the samples decrease markedly and lie almost on the same straight line after annealing at 450 °C, regardless of the type of element added, as is discussed later. X-ray diffraction measurements showed that in all the alloy systems studied here, the growth of a highly oriented Al(111) plane was strongly suppressed by adding only a small amount of the

* Corresponding author. IBM Research, Tokyo Research Laboratory, Shimotsuruma, Yamato-shi, Kanagawa 242, Japan.

0040-6090/96/$15.00 © 1996 Published by Elsevier Science S.A.
PII S0040-6090(96)08882-7

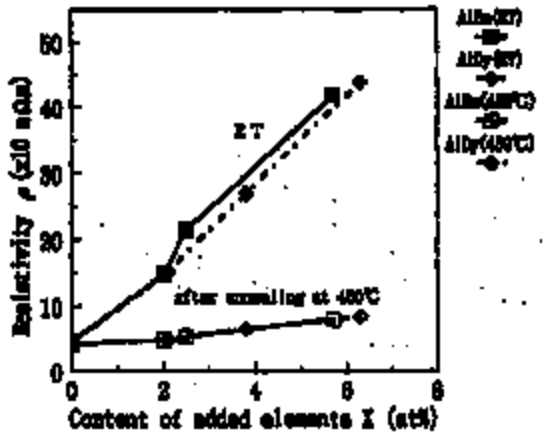

Fig. 1. Change in resistivity ρ with composition in as-made and annealed (at 450 °C) $Al_{100-x}RE_x$ alloy thin films (RE = Sm and Dy).

rare earth metal elements to pure Al, but that the diffraction intensity and width of the peaks continued to increase with a further addition of elements. This is shown representatively in Fig. 2. In the figure, the values shown on the right in atomic per cent indicate the amounts of elements added to Al. The above findings indicate that the thin films tend to lose their initial highly oriented crystal structure and to acquire a more randomly oriented polycrystalline structure with the addition of small amounts of foreign atoms to Al. The increase in the diffraction intensity with further addition of foreign rare earth elements is due most probably to some segregation of metallic compounds, though this is not clear from the X-ray results shown in Fig. 2. Although the solid solubility of the rare earth metal elements is very low (less than 0.01 at.%), the noticeable diffraction peaks associated with Al alloy metallic compounds are barely observable, as the figures show. TEM observation revealed that these as-made Al–light-rare-earth alloy films (containing about 3 at.% added element) have very fine grains less than 100 nm in diameter (see Fig. 3(a) and (b)). Note that these alloy films, like other Al–rare-earth alloy thin films (Al–RE, RE = Y or Gd) reported in [4,5], do not show a clear grain boundary image. Judging from the appearance of the bright field images in Fig. 3, the structure of the alloys may be considered as a metastable phase. Selective area diffraction analysis of the samples in Fig. 3 shows that there is a shift in the position of the diffraction rings with respect to the rings for pure Al, without showing the clear diffraction rings associated with a segregated metallic compound. This indicates that the film structures consist mainly of highly supersaturated solid solutions of the Al phase. The corresponding energy-dispersive X-ray analysis (EDX) of TEM samples in Fig. 3, reveals that the added Sm and Dy elements are distributed almost homogeneously in the Al matrix compared with those in the annealed samples. This is shown representatively in Fig. 4 for the as-made $Al_{97.5}Sm_{2.5}$ thin film sample shown in Fig. 3(a). The left (a) and right (b) images in Fig. 4 show a scanning transmission electron micrograph (STEM) image and the distribution of Sm in the Al matrix, observed by EDX analysis, respectively. Note that the added Sm seems to be distributed not only inside grains,

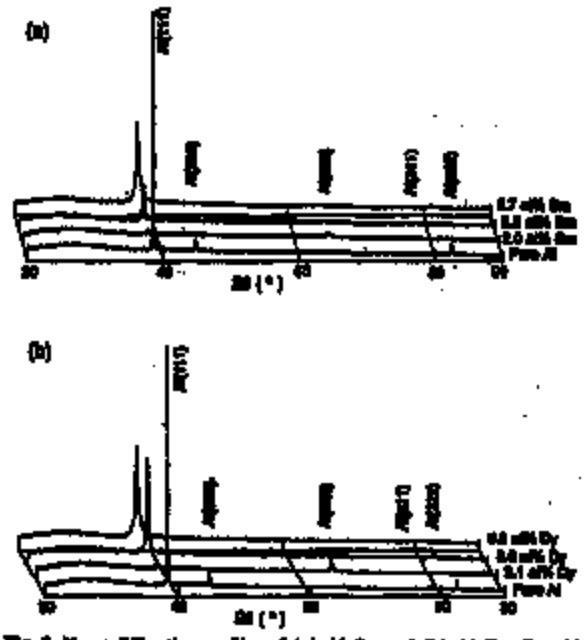

Fig. 2. X-ray diffraction profiles of (a) Al–Sm and (b) Al–Dy alloy thin films as a function of the content of the element added to Al.

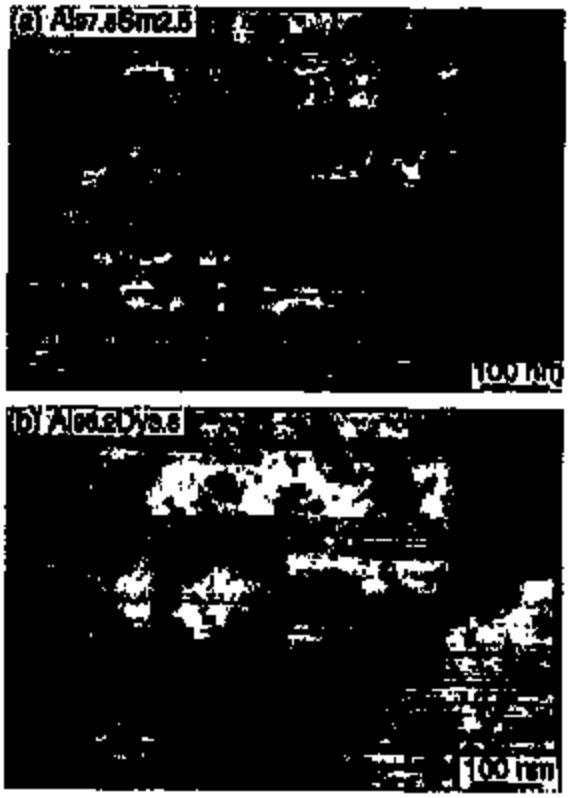

Fig. 3. Bright field images and diffraction patterns of as-deposited (a) $Al_{97.5}Sm_{2.5}$ and (b) $Al_{96.2}Dy_{3.8}$ alloy thin films.

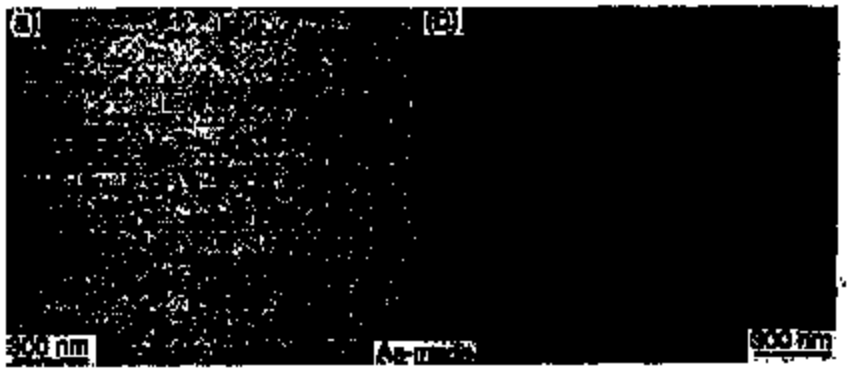

Fig. 4. (a) STEM image of the as-deposited $Al_{97.5}Sm_{2.5}$ alloy film sample in Fig. 3(a), and (b) the distribution of Sm measured by EDX in the same area as (a).

but also along grain boundaries. However, the Sm is distributed relatively homogeneously in the as-made Al matrix compared with the annealed samples, as described below (see Fig. 11).

All the as-made Al–rare-earth alloy film samples in Fig. 1 were annealed isochronally in a vacuum (less than 10^{-4} Pa) at various temperatures for 30 min. The changes in their resistivities are shown in Fig. 5 as functions of both the annealing temperature and the composition of each added element. The results for pure Al films are also included in the figure, for comparison. The solid lines and dotted lines represent the curves obtained for the Al–Dy and Al–Sm alloy systems respectively. The values in atomic per cent shown on the right of the figure indicate the amounts of the elements added to Al. Note that the general features of the change in resistivity in each alloy system are similar, regardless of the composition of added elements. The resistivity starts to decrease sharply at 250 °C and 300 °C for the Al–Dy and Al–Sm alloy systems respectively, and then saturates when it approaches the value for pure Al above 350 °C. Note here that the change in resistivity in pure Al thin films on isochronal annealing is negligibly small (see the bottom part of Fig. 5). This fact probably implies that the changes in resistivity due to grain growth, internal stress relief, and annihilation of point or line defects are small in the present sputtered Al films within the accuracy of the present measurement.

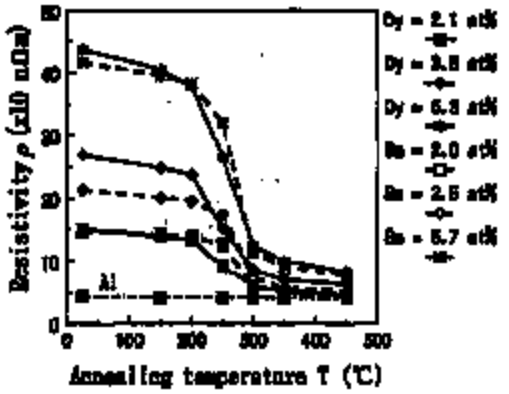

Fig. 5. Change in resistivity ρ of Al–RE alloy films (RE = Sm and Dy) as a function of the isochronal annealing temperature (for 30 min) and composition.

Representative X-ray diffraction profiles of the annealed $Al_{97.5}Sm_{2.5}$ and $Al_{96.2}Dy_{3.8}$ samples in Fig. 5 are shown in Fig. 6(a) and (b) respectively. Visible diffraction peaks associated with the segregation of metallic compounds started to appear after annealing above 250 °C and 300 °C for the Al–Dy and Al–Sm samples respectively. Most of the diffraction peaks that appeared after annealing were indexed, using available data, as belonging to an Al_3RE metallic compound (RE = Sm or Dy), as shown in the figure. It should be noticed here that the appearance of diffraction peaks associated with the segregation of metallic compounds coincides closely with the large drop in resistivity shown in Fig. 5.

Fig. 7 shows the changes in the resistivities of the $Al_{97.5}Sm_{2.5}$ and $Al_{96.2}Dy_{3.8}$ samples when they were annealed

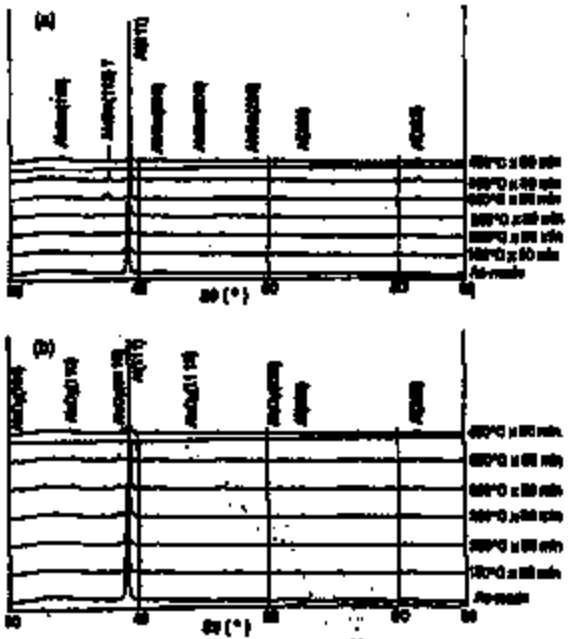

Fig. 6. X-ray diffraction profiles of (a) $Al_{97.5}Sm_{2.5}$ and (b) $Al_{96.2}Dy_{3.8}$ alloy thin films of Fig. 4, annealed isochronally up to 450 °C.

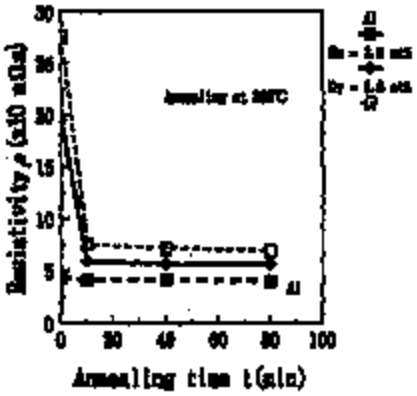

Fig. 7. Change in resistivity ρ of $Al_{97.5}Sm_{2.5}$ and $Al_{94.2}Dy_{5.8}$ alloy thin films after isothermal annealing at 350 °C.

isothermally in a vacuum at 350 °C. In the figure, the results for pure Al films are also included for comparison. The resistivities decreased steeply to low values of less than 80 nΩ m within a very short annealing time, and almost saturated on further annealing. X-ray diffraction profiles corresponding to the annealed $Al_{97.5}Sm_{2.5}$ and $Al_{94.2}Dy_{5.8}$ samples in Fig. 6 are shown in Fig. 8(a) and (b) respectively. These measured profiles, again, clearly demonstrate that segregation of the metallic compounds Al_2RE (RE = Sm and Dy), corresponding to the large drop in resistivity shown in Fig. 7, takes place within 10 min of annealing at 350 °C. The diffraction peaks at $2\theta \approx 35°$ are not clear, but are most probably related to Al_2Sm metallic compounds for the Al–Sm sample and Al_2Dy compounds for the Al–Dy sample, as shown in the figures. It is worth noticing that the growth of hillocks was barely observed on the surface of the above Al–Sm and Al–Dy alloy samples in Figs. 5 and 7. Fig. 9 shows optical micrographs of (a) $Al_{97.5}Sm_{2.5}$ and (b) $Al_{94.2}Dy_{5.8}$ film surfaces annealed at 350 °C for 80 min. The observed features of an $Al_{99}Zr_1$ alloy film annealed under the same heat treatment conditions are also included for comparison, where dark spots (needles) in the photographs indicate hillocks (or whiskers). The figure clearly reveals that hillocks or whiskers are barely observable in the present Al–rare-earth alloy films, whereas relatively

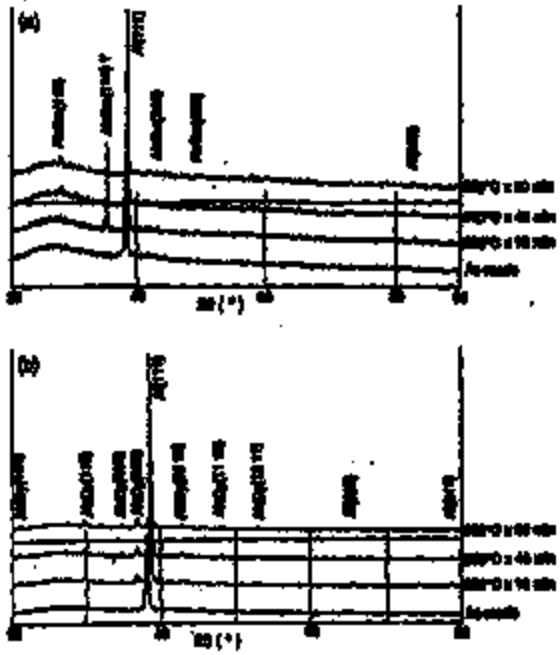

Fig. 8. X-ray diffraction profiles of (a) $Al_{97.5}Sm_{2.5}$ and (b) $Al_{94.2}Dy_{5.8}$ alloy thin films annealed isothermally at 350 °C.

large thermal defects are formed on the annealed Al–Zr film surfaces. This tendency for the growth of thermal defects to be largely suppressed is similar to that reported previously for other Al–rare-earth alloy films [4,5].

TEM observations of samples annealed at 350 °C for 80 min are shown in Fig. 10(a) and (b) for $Al_{97.5}Sm_{2.5}$ and $Al_{94.2}Dy_{5.8}$ alloy thin films respectively. Both selective area diffraction and EDX analyses indicated that most of the relatively small and dark image grains in these photos can be considered to be Al_2RE (RE = Sm or Dy) metallic compounds, while large and bright grey image grains correspond to the pure Al matrix. The photographs clearly reveal that small particles (less than 100 nm in diameter) of metallic compounds are segregated in the Al matrix, mostly at the grain boundaries of the Al matrix. Furthermore, the mean

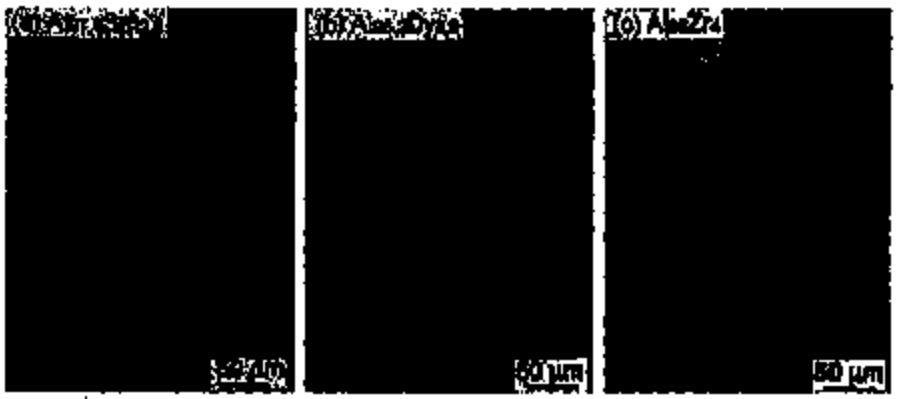

Fig. 9. Polarized optical micrographs of Al alloy thin film surfaces annealed at 350 °C for 80 min: (a) $Al_{97.5}Sm_{2.5}$, (b) $Al_{94.2}Dy_{5.8}$, and (c) $Al_{99}Zr_1$.

Fig. 10. Bright field images and diffraction patterns of (a) $Al_{97.8}Sm_{2.2}$ and (b) $Al_{96.2}Dy_{3.8}$ alloy thin films annealed at 350 °C for 60 min.

grain size of the Al matrix is relatively small (less than 200 nm) in comparison with that of pure Al thin films (more than 300 nm) annealed under the same heat treatment conditions. Fig. 11 shows the STEM image and the corresponding distribution of Sm in the Al matrix for the annealed $Al_{97.8}Sm_{2.2}$ thin film sample shown in Fig. 10(a). It is worth noting that the added Sm is clearly segregated in the Al matrix after annealing at 350 °C.

4. Discussion

In view of the lack of a salient change in resistivity on isochronal annealing of the sputtered Al films shown in Fig. 5, we can conclude that the large resistivity change in the Al alloy films studied here results mainly from (1) removal of impurities from the Al matrix and (2) segregation of metallic compounds. A detailed discussion of these subjects can be found in Ref. [5]. Thus, since the structure of as-made samples in Fig. 1 consists mainly of a supersaturated solid solution of the Al phase, as previously described, the main cause of the electron scattering resistance of the present as-made samples is most probably the presence of added impurities in the Al matrix. Accordingly, the resistivity is expected to increase in proportion to the amount of impurities, as shown in Fig. 1 (see also Refs. [5] and [6]).

The resistivities started to decrease markedly at 250 °C and 300 °C for Al–Dy and Al–Sm alloy films respectively, as shown in Fig. 5. It is interesting that, on the whole, the annealing temperature at the beginning of the large drop in resistivity was also independent of the amount of added element within the composition range studied. Taking account of the results of both TEM observation and X-ray diffraction analysis of the annealed samples in Figs. 6–8 and Fig. 10, it can be concluded that the sharp drops in resistivity at 250 °C in Fig. 5 result mainly from the segregation of metallic compounds, together with the removal of impurities from the Al matrix, as explained above. Note that metallic compounds Al_3RE (RE = Sm and Dy) appear at Al-rich compositions in the phase diagrams of Al–Sm and Al–Dy alloy systems respectively [7].

The removal of added elements from the Al matrix was confirmed by EDX chemical element mapping analysis, as demonstrated in Fig. 11. Furthermore, the measured mean distance between segregated metallic compounds in Fig. 10 was more than 100 nm, which is much larger than the estimated electron mean free path in pure Al (about 10 nm) [5]. This implies qualitatively that segregated metallic compounds do not significantly obstruct conduction electrons in

Fig. 11. (a) STEM image of the $Al_{97.8}Sm_{2.2}$ alloy film sample annealed at 350 °C for 60 min in Fig. 10(a), and (b) the distribution of Sm measured by EDX in the same area as (a).

the annealed structure of Al–light-rare-earth alloy films, even though they become scattering centers for conduction electrons. In addition, the resistivities of metallic compounds formed in the present alloy systems are expected to be low, as in the well known AuCu alloy systems [5]. This may be one reason why the change in resistivity with composition after annealing at 450 °C follows nearly the same curve, regardless of the type of light rare earth element, as shown in the bottom part of Fig. 1. The increase in resistivity with composition after annealing at 450 °C occurs most probably mainly as a result of the increase in the number of segregated metallic compounds, though we need further study to verify this.

Most segregation of metallic compounds in the present alloy thin films takes place at the grain boundaries of the Al matrix, as can be clearly seen in the TEM results shown in Fig. 10. This segregation at grain boundaries at relatively low annealing temperatures may play a large role in preventing grain boundary diffusion, resulting in strong suppression of the growth of hillocks and whiskers on the film surfaces.

5. Summary

The changes in the resistivity and structure of Al–RE alloy films (RE = Sm and Dy) on annealing were studied as functions of the composition of added elements, in order to assess the potential use of the films as microelectronic gate-electrode line materials. The results may be summarized as follows.

1. Al–RE alloy films (RE = Sm and Dy) showed very low resistivities of less than 50 nΩ m (depending on the content of added elements) after annealing above 350 °C. They also showed, on the whole, high thermal stabilities without the growth of hillocks or whiskers on the film surfaces at high temperatures.
2. It was concluded from TEM observation and X-ray diffraction analysis that the large resistivity change on annealing resulted from the segregation of metallic compounds, such as Al_3RE (RE = Sm and Dy), together with the removal of added elements from the Al matrix.

Acknowledgements

The authors are grateful to Mr Michael McDonald for kindly reviewing this paper. Most of this work was performed at IBM Research, Tokyo Research Laboratory, IBM Japan, Ltd. (Shimotsuruma, Yamato-shi, Kanagawa, Japan).

References

[1] K. Yoshikawa, S. Nishi, H. Matsuzaki, T. Onishi and Y. Koga, *Materia Japan*, *33* (8) (1993) 932 (in Japanese).
[2] M. Yamamoto, I. Kobayashi, T. Hirose, S.M. Bhatt, N. Tsuboi, Y. Mino, M. Ohshiji and T. Tamura, *1994 SID International Display Research Conference, Monterey, CA, USA, Digest, 1994*, p. 142.
[3] Y.K. Lee, N. Fujiwara and T. Ito, *J. Vac. Sci. Technol. B*, *9* (1991) 3542.
[4] S. Tokuyama and N. Tsunoi, *Extended Abstracts of the 1995 Int. Conf. on Solid State Devices and Materials (SSDM '95), Osaka, 1995*, pp. 314, 350.
[5] S. Tokuyama and N. Tsunoi, *J. Vac. Sci. Soc., Technol. A 14(4)* (1996) 2499.
[6] S. Tokuyama and N. Tsunoi, *J. Vac. Sci. Technol. B*, in press 1996.
[7] W.G. Moffatt, *The Handbook of Binary Phase Diagrams*, Genium, New York, 1987.
[8] N.F. Mott and H. Jones, *The Theory of the Properties of Metals and Alloys*, Dover, New York, 1958, pp. 240–302.

ELSEVIER

Thin Solid Films 300 (1997) 25–29

Thin Solid Films

Electromigration in layered Al lines studied by in-situ ultra-high voltage electron microscopy

H. Mori [a,*], H. Okabayashi [b], M. Komatsu [a]

[a] Research Center for Ultra-High Voltage Electron Microscopy, Osaka University, Yamadaoka, Suita, Osaka 565 Japan
[b] Research and Development Group, NEC Corporation, 34 Miyukigaoka, Tsukuba 305 Japan

Received 9 May 1996; accepted 7 November 1996

Abstract

In-situ side-view transmission electron microscopy (TEM) observations of electromigration in Al-on-TiN lines with a drift velocity measurement structure have been carried out using an ultrahigh voltage (2 MV) electron microscope. Thick chips as-diced from silicon substrates served as TEM samples. The observations revealed the dynamic behavior of electromigration-induced voids and hillocks during forward and reverse current feeding through the Al lines. The results include vertical growth of voids bounded by facated Al, refilling of voids, void growth in a hillock upon current reversal, and whisker growth. © 1997 Elsevier Science S.A.

Keywords: Aluminium; Electromigration; Electron diffraction; Electron microscopy

1. Introduction

In-situ observations of electromigration (EM) in Al lines for integrated circuits have employed various microscopy techniques, such as scanning electron microscopy (SEM) [1] and transmission electron microscopy (TEM) (see, for example, Refs. [2–5] and references cited therein). So far, TEM observations have been conducted solely in the plan-view mode, and such aspects as the preferential void evolution at the three-fold node of grain boundaries have been revealed [2]. However, in plan-view observations, it is difficult to obtain the vertically-resolved (in the depth direction) information on the microstructure in Al lines. Such depth-resolved information is indispensable for analyzing electromigration in the layered lines which are currently used in advanced LSIs, because the interlayer interfaces may play an essential role in these lines. Furthermore, in plan-view TEM samples, the Si substrate has to be locally thinned to a thickness of electron transparency. In such samples a non-uniform stress distribution due to both the local thinning and the local joule heating along Al lines is often induced, which eventually leads to bending of the samples.

To overcome these drawbacks, we have developed a side-view TEM technique, in which an Al line on a thick substrate is observed with a high voltage electron microscope (HVEM) with the incident beam parallel to the substrate surface and perpendicular to the Al line [6,7]. This technique utilizes the ability of HVEM to observe relatively thick samples. Additionally, since the substrate does not need to be thinned, difficulties encountered in the preparation and observation of conventional plan-view TEM samples can be avoided. With the use of this technique, the detailed behavior of EM-induced gaps which are formed between the cathode and the anode in Al-on-TiN lines has been studied [6]. Also, the growth process of voids at the cathode in Al–0.5 wt.%Cu-on-TiN lines has been examined [7].

In the present work, successive stages of EM-induced void formation at the cathode and of EM-induced hillock formation at the anode in Al-on-TiN lines have been investigated by the side-view TEM technique.

2. Experimental procedures

An Al-on-Ti/TiN line with a drift-velocity measurement structure, which provides information on electromigration in a line without reservoirs, was fabricated on an oxidized Si wafer [6]. This structure consisted of an Al overlayer lying on the central part of a Ti/TiN underlayer

* Corresponding author. Tel: +81 6 873 0828; fax: +81 6 873 0449; e-mail: ad2217a@sutlac.osaka-u.ac.jp

PII S0040-6090(96)09517-X

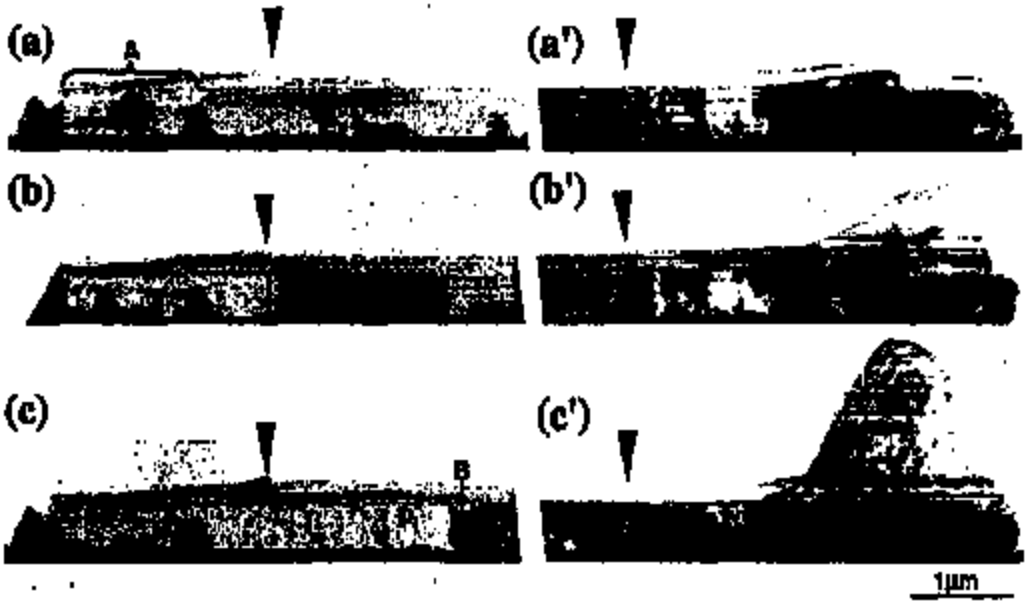

Fig. 1. Successive stages of electromigration in an Al-on-TiN line observed by side-view TEM. Damage evolution at the cathode and the anode of the line during current feeding in the forward direction are depicted in (a)–(c) and (a')–(c'), respectively. Current feeding time t for each figure is as follows: (a) t = 720 s, (b) t = 2.8 ks, (c) t = 7.4 ks, (a') t = 1.6 ks, (b') t = 2.9 ks, and (c') t = 7.6 ks.

conductor [6]. Both the Ti and TiN layers were 0.2 μm thick. The length of the Ti/TiN portion between the bonding pad and the Al was 120 μm. The Al was 0.7 μm wide, 0.5 μm thick, and 100 μm long. The samples used in these experiments varied in width of Ti/TiN underlayer. Sample 1 had a pure Al line on top of a 2 μm wide Ti/TiN underlayer and Sample 2 also had a pure Al line, but the Ti/TiN underlayer was 0.7 μm wide.

The Al lines were not passivated, but a thin photoresist layer remained on the surface after washing in an oxygen

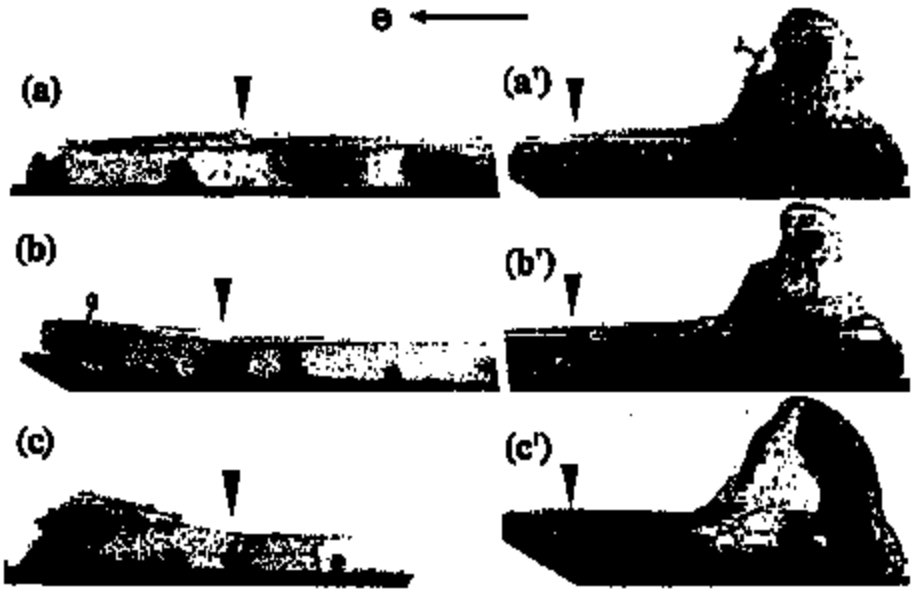

Fig. 2. Electromigration-induced damage at the (new) anode and the (new) cathode of the line during current feeding in the reverse direction are depicted in (a)–(c) and (a')–(c'), respectively. Current feeding time t_r (after the reversal) is as follows. (a) t_r = 1.1 ks, (b) t_r = 11.9 ks, (c) t_r = 15.9 ks, (a') t_r = 2.5 ks, (b') t_r = 2.8 ks, and (c') t_r = 15.7 ks. The black triangle-shaped arrows in Fig. 1(a)–1(c)/Fig. 2(a)–2(c) indicate a fixed position of the sample, and those in Fig. 1(a')–1(c')/Fig. 2(a')–2(c') another fixed position. The width of the Ti/TiN layer in this sample was 2 μm.

atmosphere. The fabricated wafers were annealed in nitrogen gas at 723 K for 1.8 ks. The Al line exhibited a near-bamboo structure. A chip, ~0.5 mm × ~6 mm in size and 0.45 mm thickness, was then diced from the wafer and served as the side-view HVEM sample. Neither the Al lines nor the silicon substrates were thinned prior to observation.

The Al lines were directly observed from the side with an HVEM operating at an accelerating voltage of 2 MV. The sample was heated during observation by the Joule heating predominantly at the Ti/TiN portions without overlayer Al. The temperature of the Al was not measured, but a comparison of the drift velocities obtained by in-situ HVEM experiments with those from standard accelerated measurements suggested that the average temperature of the Al may have been between 573 and ~623 K.

The results of the experiment using Sample 1 are shown in Fig. 1. A current of 50 mA (current density $j = \sim 13$ MA cm^{-2}) was first fed for ~14 s. This stressing time was limited by the melting of the solder which bonded the current feeding wires to the electrodes of the HVEM sample holder. After the solder bonds were repaired, the in-situ observation was resumed at a current of ~26 mA ($j = \sim 6.5$ MA cm^{-2}). After feeding for 7.8 ks, the current direction was reversed and the observations were continued for 16.2 ks; these results are shown in Fig. 2. (In the text and the caption referring to Figs. 1 and 2, the feeding times of a 26 mA current before and after the current reversal are designated as t and t_r, respectively).

The results of the experiment using Sample 2 are shown in Figs. 3 and 4. Current was fed only in one direction in this case.

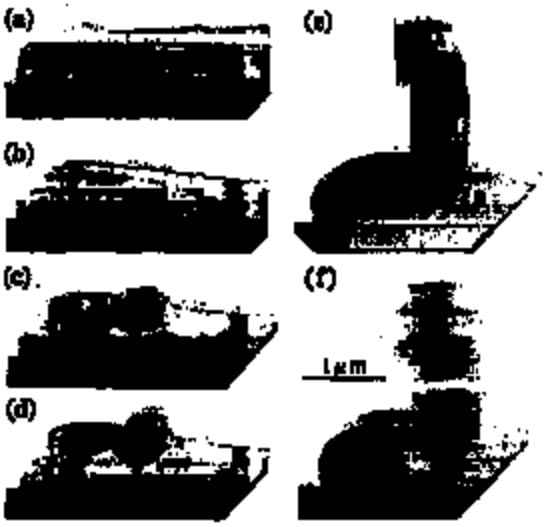

Fig. 3. Successive stages of whisker growth at the anode of an Al-on-TiN line. In this experiment, a 19 mA current was first fed for 5.5 ks and then the current was increased to 23 mA. Current feeding time t is as follows: (a) $t = 0$ s, (b) $t = 4.08$ ks, (c) $t = 5.70$ ks, (d) $t = 6.18$ ks, (e) $t = 9.78$ ks, and (f) $t = 13.48$ ks. Electrons flowed from right to left. The width of the Ti/TiN layer in this sample was 0.7 μm.

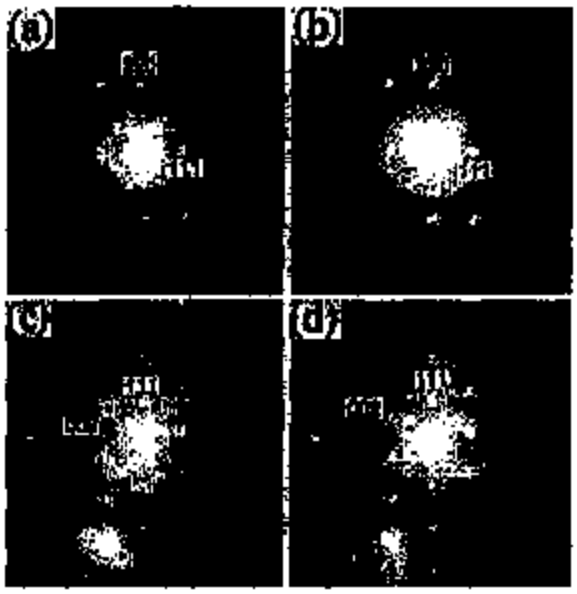

Fig. 4. Selected area electron diffraction (SAED) patterns taken from the whisker and the Al line shown in Fig. 3(e). (a) and (b) are taken from positions A and B in Fig. 3(a) respectively, while (c) and (d) are from positions C and D respectively.

3. Results and discussion

3.1. EM-induced damage at the cathode and the anode in forward current feeding

Fig. 1(a) is a bright-field (BF) image of the cathode of an Al-on-TiN line after feeding of the 26 mA current for 720 s (i.e. $t = 720$ s). A locally depleted region (A) was formed adjacent to the cathode edge. The same area after feeding for 2.8 ks (i.e. $t = 2.8$ ks) is presented in Fig. 1(b), where it is shown that the depleted region extended ~2.5 μm towards the anode from the cathode edge. Fig. 1(c) shows the same area at $t = 7.4$ ks. At this stage, the depleted region extended over ~4.4 μm from the cathode edge.

Two points are noteworthy in Fig. 1(c). (1) One of the characteristic depletion modes verified by side-view TEM appears at B in front of the large depleted region in the figure. Void growth proceeds towards the substrate within a single grain; the top surface of the remaining material at B is (111) faceted. In some cases, this type of voiding proceeded grain by grain sequentially from the cathode end [7]. (2) Small Al islands are formed on the inner surface of the natural oxide film covering the depleted region. Similar islands on the inner surface of the top and bottom natural oxide films were observed in Ref. [4].

Islands close to the front of the growing depleted region were smaller than those further away. For example, the diameter of island D, located near the front, was about 10 nm, whereas that of island C, further from the front, was about 100 nm. This suggests that islands grow by the diffusion and coalescence of Al atoms left on the inner surface of the oxide film [4]. Larger islands further from the front simply reflect the extra time for diffusion and coalescence. The presence of well-defined facets associated with voids in front of the large depleted region, such as a facet seen at B in Fig. 1(c), shows that Al does not melt there and that melting of Al is not a cause of the island formation.

Fig. 1(a′) is a BF image of the anode of the same line after feeding of the 26 mA current for 1.6 ks ($t = 1.6$ ks), where a small hillock is noticed to be formed at the anode. In Fig. 1(b′), which was taken from the same area at $t = 2.9$ ks, it is shown that the hillock grew to a height of approximately 0.9 μm. As seen in this figure, some grains within this hillock exhibited brightness completely different from those of the grains composing the original line, while other grains showed diffraction contrast reminiscent of the epitaxy of the corresponding grains in the line. This fact suggests that hillocking took place not only via an epitaxial growth process but via a nucleation and growth process and differently oriented grains were formed on the top surface of the anode. The microstructure at the interface between the original bamboo grains and the hillock, which might shed light on the mechanism behind the hillocking, is unfortunately not well resolved in this micrograph. The same area after feeding current for 7.6 ks is shown in Fig. 1(c′). At this stage, the height of the hillock reached approximately 1.7 μm. In one of grains composing the hillock, there appears a series of equal thickness fringes, as seen at B in Fig. 1(c′). From the intervals between the neighboring fringes, it is possible to obtain information on the three-dimensional shape of the hillock. In the present case, a hillock in the shape of a dome was deduced from such an analysis, and the shape was in agreement with the result by an independent SEM observation.

3.2. EM-induced damage at the cathode and the anode in reverse current feeding

The cathode before the current-direction reversal served as the anode after the reversal; thus, healing of the depletion damage was expected to occur there. Fig. 2(a) is a BF image of the anode after the current-direction reversal, which was taken at $t_r = 1.1$ ks. This area is the same as that shown in Fig. 1(a)–(c). It is evident from a comparison of Fig. 1(c) with Fig. 2(a) that the preferentially-voided portion B in Fig. 1(c) had already been annihilated at this stage, and aluminum began to fill the depleted region (grain F in Fig. 2(a)). Fig. 2(b) shows the same area at $t_r = 11.9$ ks. The depleted region was now completely filled with aluminum and even a small hillock was formed at the anode (G in Fig. 2(b)). In the grain associated with the hillock, a high density of dislocations was observed (H in Fig. 2(b)). This fact suggests that hillocking of this type took place under somewhat stressed conditions. Possible origins of the stress field are: (1) bending of the grain due to a bulge of underlying grain(s) (I in Fig. 2(b)); and (2) compression due to the mass accumulation. More experiments are necessary to clarify the nature of the stress field. In Fig. 2(c), which shows the same area at $t_r = 15.9$ ks, it is seen that the hillock grew to a height of approximately 0.5 μm in this final stage.

The anode before the current-direction reversal served as the cathode after the reversal; thus, depletion was expected to occur there. Fig. 2(a′) is a BF image of the cathode after the current-direction reversal that was taken at $t_r = 2.5$ ks. This area is the same as that shown in Fig. 1(a′)–1(c′). Voiding did not occur at the Al/TiN interface at the cathode where a high current density is expected, rather it took place halfway up the hillock (J in Fig. 2(a′)). The current density at site J is supposed to be quite low. In high magnification images of the hillock before current reversal (not shown here), a thin line appeared which intersected the surface at a position almost identical with site J in Fig. 2(a′). The thin line might correspond to a grain boundary, a dislocation line, or a slip trace of dislocations. This observation suggests that the void might have nucleated preferentially at a surface defect site. With continued current feeding, this void grew (Fig. 2(b′) at $t_r = 2.8$ ks), and eventually the interior of the hillock was almost completely depleted, leaving only the natural oxide film and the photoresist residue which had covered the hillock (Fig. 2(c′) at $t_r = 15.7$ ks).

3.3. Whisker growth at the anode

Fig. 3 shows an example of whisker growth at the anode, which was observed in another pure Al sample. In this experiment, a 19 mA current ($j = \sim 5$ MA cm^{-2}) was first fed for 5.5 ks and then the current was increased to 25 mA ($j = \sim 6.5$ MA cm^{-2}). Fig. 3(a) is a BF image of the anode before current feeding. Fig. 3(b) shows the same area after feeding 19 mA for 4.08 ks, where it is seen that a small hillock formed on the anode. The same area after feeding 19 mA for 5.46 ks and 25 mA for 240 s is shown in Fig. 3(c). At this stage, a small, faceted whisker appeared on the hillock. With continued current feeding, the whisker grew (Fig. 3(d) and 3(e)), and eventually the height of the whisker reached to approximately 1.6 μm (Fig. 3(f)). Fig. 4 shows a series of selected area electron diffraction (SAED) patterns taken from the whisker and the Al line: the SAED patterns in Fig. 4(a) and 4(b) were taken respectively from positions A and B of the whisker in Fig. 3(e), while those in Fig. 4(c) and 4(d) were taken respectively from positions C and D of the line in Fig. 3(a). The former two patterns are identical to each other

and they can be indexed as the ~[112] aluminum diffraction pattern. The long axis of the whisker is almost parallel to the [110] direction. The latter two patterns can be indexed as the ~[110] aluminum pattern. The normal to the original top surface of the Al line (i.e. the normal to the Si substrate) is nearly parallel to the [111] direction. It is concluded from Fig. 4 that the whisker had a different orientation from the grain on which it nucleated and grew.

4. Summary and conclusions

We have observed the dynamic behavior of electromigration voids and hillocks in Al-on-TiN lines by in-situ side-view TEM using an HVEM. Such side-view observations reveal information not obtainable by conventional plan-view TEM.

It was revealed that, frequently, voids were bounded by faceted Al planes and grew preferentially in the vertical direction on the anode side of grain boundaries. After reversing the current direction, voiding occurred in the hillock at the former anode, not at the Al-underlayer interface, where current crowding was expected.

Polycrystalline hillocks grew partly in epitaxy to the grains in the line. A whisker, however, was found to have a crystallographic orientation different from the grains in the line.

Acknowledgements

We would like to thank Professor H. Nishihara and Dr H. Watanabe for their encouragement. We would also like to thank Dr D. Grosjean for reading the manuscript.

References

[1] See for example, the following papers and references cited therein: R.W. Thomas and D.W. Calderwood, *Proc. 1983 IEEE Int. Reliability Phys. Symp.*, The Institute of Electrical and Electronics Engineers, Inc., New York, 1983, p. 1; T.N. Marieb, E. Arzt-Gerold, J. Bravman, M. Madden and P. Flinn, in P.S. Ho, C.-Y. Li and F. Tung (eds.), *Stress-Induced Phenomena in Metallization*, AIP Conference Proc. 305, AIP, New York, 1994, p. 1.
[2] L. Berenbaum, *J. Appl. Phys.*, *42* (1971) 880.
[3] A. Takeuchi, N. Okaya and K. Ura, *Microsc. Microanal. Microstruct.* *4* (1993) 239.
[4] C.Y. Chang and R.W. Vook, *Thin Solid Films*, *235* (1993)23.
[5] S.P. Riege, A.W. Bhat and J.A. Prybyla, in A.S. Oates, W.F. Filter, R. Rosenberg, A.L. Greer and E. Gadepally (eds.), Materials Reliability in Microelectronics V, *Mater. Res. Soc. Symp. Proc.*, Vol. 391, Mater. Res. Soc., Pittsburgh, PA, 1995, p. 249.
[6] H. Okabayashi, H. Kitamura, M. Komatsu and H. Mori, *Appl. Phys. Lett.*, *68* (1996)1666.
[7] H. Okabayashi, M. Komatsu and H. Mori, *Jpn. J. Appl. Phys., Part 1*, *35* (2B) (1996)1102.

ELSEVIER

Applied Surface Science 91 (1995) 239–245

applied surface science

The effect of ion implantation on the properties of Al films

M. Zaborowski [a], A. Barcz [a], G. Gawlik [a], I.W. Rangelow [b,*]

[a] Institute of Electron Technology, Al. Lotników 32 / 46, 02 668 Warsaw, Poland
[b] Institute of Technical Physics, University of Kassel, Heinrich Plett-Strasse 40, 34 132 Kassel, Germany

Received 20 March 1995; accepted for publication 4 May 1995

Abstract

The influence of irradiation of Al or Al-based films on the surface morphology is studied by a number of methods. F, B, Mg, Cd, As, Sb, Cr and Ar were chosen as implanting species in order to cover a wide variety of chemical reactivities with aluminium. Implantation of boron and, to a lesser extent, of fluorine or chromium was found beneficial in suppressing population of hillocks, predominantly those of medium or larger size.

1. Introduction

Aluminium is still the most commonly used material for interconnection lines and ohmic contacts in silicon integrated circuit technology. This is mainly because of its high electrical conductivity, low resistance ohmic contact to Si, good adherence to silicon dioxide as well as the ease of deposition and etch processes. However, one of the serious disadvantages of the Al-based metallization is formation of hillocks which may lead to device failure with increasing integration scale. Hillocks are large crystallites that, upon annealing, can grow out to a height comparable to the initial layer thickness. While it is generally accepted that hillock growth is related to grain-boundary diffusion and plastic flow [1,2] a detailed understanding of the whole process is lacking [3,4].

In this paper we report on an extensive study of the influence of ion implantation on the properties of aluminium and aluminium-based alloys that are pertinent to their application as interconnecting lines in silicon IC technology with special emphasis placed on the morphology of the Al surface. It is well established that implantation of ions into metals may induce, depending on the particular ion–target system, several effects such as generation of point or extended defects, formation of solid solution or new chemical compounds, amorphization or modification of grain structure in polycrystalline materials. There are few reports in the literature concerning the effect of ion implantation on the population of hillocks [5–7]. We have chosen F, B, Mg, Cd, As, Sb, Cr and Ar as implanting species in order to cover a wide variety of chemical reactivities with aluminium. Doses and energies of implantation were such that the maximum dopant concentration of about 1 at% was located at a depth of 100–200 nm. The effect of ion implantation on the properties of Al films was investigated by means of a number of techniques including scanning electron microscopy (SEM), optical microscopy with digital image processing, stylus profiling, secondary ion mass spectrometry (SIMS), Auger electron spectroscopy (AES), transmission

* Corresponding author.

SSDI 0169-4332(95)00125-5

electron microscopy (TEM), X-ray diffraction (XRD) as well as the measurements of strain and resistivity of the metallic layers.

2. Experimental

Samples were prepared by thermal oxidation of ⟨100⟩ Si wafers to an oxide thickness of 400 nm followed by either magnetron sputter deposition of Al or Al:Si 1% alloy or by electron gun deposition of pure Al. Typical thickness of the metallic film was 1000 nm. Implantation was performed at nominally room temperature at energies 50–160 keV to doses 4×10^{15}–3.5×10^{16} cm^{-2}. Annealing was carried out at 450°C for 30 min in hydrogen or nitrogen atmosphere. For further analysis the samples were cut out so that any combinations of non-implanted, non-annealed together with implanted and annealed pieces were available for comparison from the same wafer.

Metallization topography was examined by SEM and by optical microscope equipped with a specially designed system for digital image processing enabling easy measurement of the hillock size and density distributions [8]. The system proved particularly useful in view of a large number of samples. SIMS profiling was used to establish the extent of redistribution of selected dopants. Sheet resistance of the Al films was determined by a four-point probe method. Since boron was found the most promising species in suppression of the hillock size and density some additional investigations were conducted with B^+-implanted films. TEM analysis provided information on the grain structure and, employing electron diffraction, phase identification. Tensile stress in the metallization was deduced from the contactless measurement of the radius of curvature.

3. Results

Generally, implantation into Al was found to affect either the size and population of the hillocks or their shape. An example of the modification of the shape of hillocks which resulted from the implantation of antimony ions with a fluence of 5×10^{15} cm^{-2} is shown in Fig. 1. Clearly, hillocks in the Sb-implanted layer become sharper at the top and have a whisker-like appearance. Conversely, irradia-

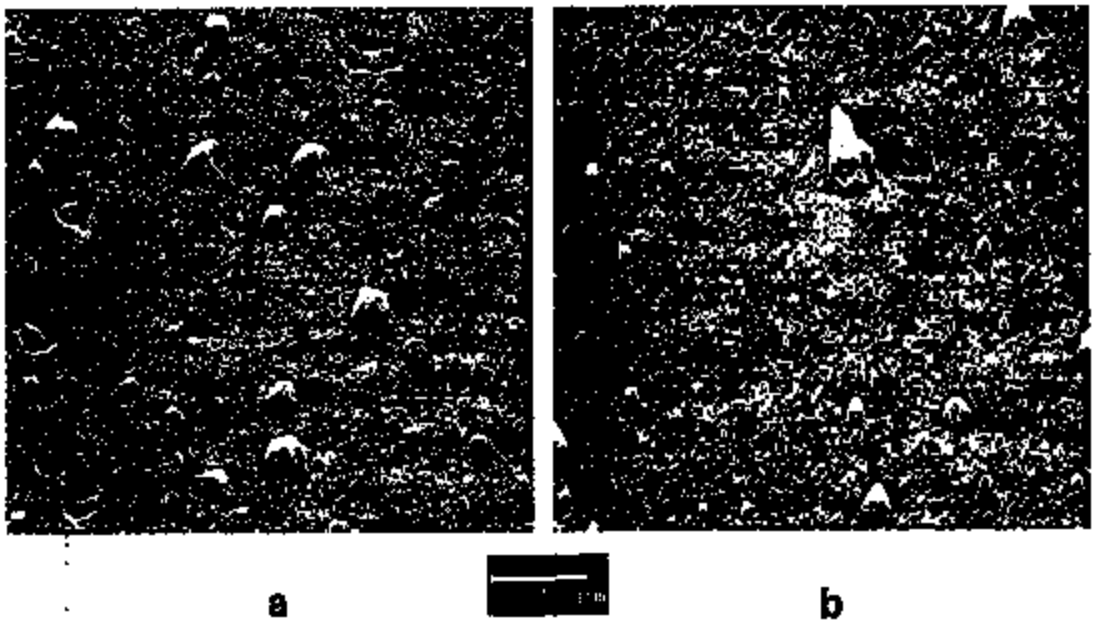

a b

Fig. 1. SEM micrograph of Al surface: (a) unimplanted; (b) implanted with 160 keV Sb^+ ions to a dose of 5×10^{15} cm^{-2}.

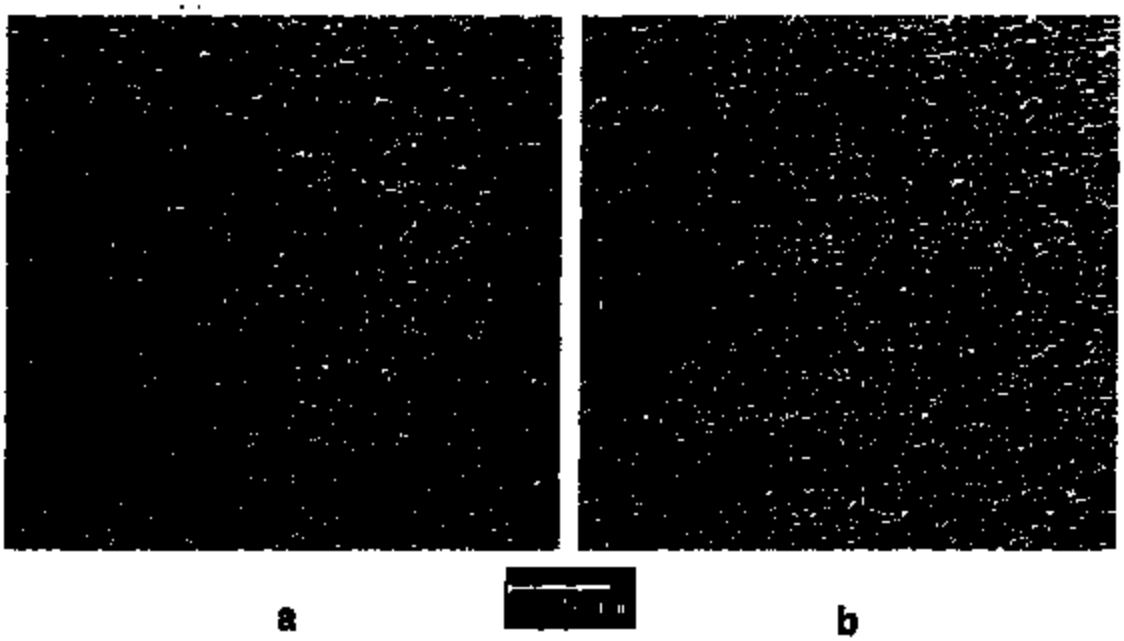

Fig. 2. SEM micrograph of Al:Si 1% surface: (a) unimplanted; (b) implanted with 150 keV Cr^+ ions to a dose of 9×10^{15} cm^{-2}, both annealed at 450°C.

tion with chromium ions leads to suppression of hillock density without noticeable change of their form (Fig. 2). In this case, the effect is observed on Al:Si alloy but not on pure Al.

Considering different species, doses and magnetron or e-gun deposited Al or Al-based alloys, the total number of samples to be analyzed exceeded one hundred. For this reason the procedure of digital image processing for hillock recognition was found as an extremely convenient tool allowing immediate statistical evaluation of the surface features. Fig. 3a shows a processed hillock image from unimplanted Al and Fig. 3b – from the surface of aluminium layer subjected to the implantation with boron ions

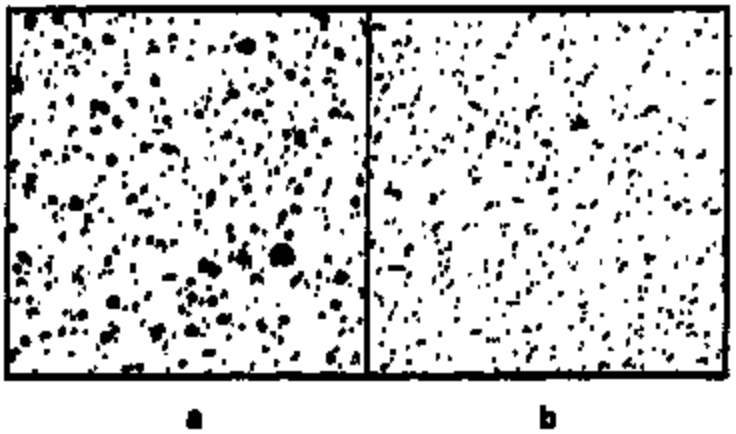

Fig. 3. Al surface examined by hillock recognition method: (a) unimplanted; (b) implanted with boron, 2.5×10^{16} cm^{-2}.

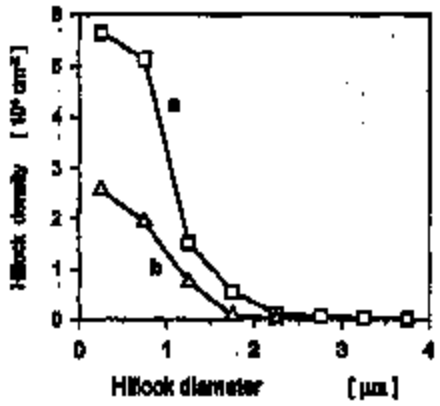

Fig. 4. Distribution of the hillock density versus hillock diameter for: (a) 1 μm Al:Si layer; (b) Al:Si layer implanted with Cr, 9×10^{13} cm^{-2}.

to a dose of 2.5×10^{16} cm^{-2}. Implantation results in substantial reduction of the hillock size. In order to quantify the influence of ion implantation on the topography of the investigated films, for all samples distribution of the hillock areal density versus their diameter was calculated on the basis of digitised images. Example of such dependence is presented in Fig. 4. It can be noticed that Cr implantation decreases the density of, predominantly, large and medium-size hillocks. Most results of this work are summarised in Table 1. Hillocks are divided into three groups: small (< 1 μm), medium (1–2.2 μm), and large (> 2.2 μm). The data represent the average number of hillocks of a given size per 10^{-3} mm^2. They concern pure aluminium deposited by magnetron sputtering and electron gun except for Cr^+ implantation where the Al:Si alloy was used. A large spread of results observed for unimplanted samples, especially as far as the smallest (< 1 μm) hillocks are concerned, does not affect the general trend because the data for 0-dose were collected from the same silicon wafer as those for implanted ones.

Out of eight implanted species, boron was found to yield the most significant and reproducible suppression of hillock growth. It is important to note that the reduction of hillock population is especially pronounced for larger objects i.e. those which are likely to cause failures in interconnection lines. This applies also to the implantation of fluorine. Irradiation with Cr^+ ions leads to hillock suppression in Al:Si and Al:Si:Cu alloys but not in pure Al. Cadmium and antimony influence the hillock shape. Magnesium, within the experimental uncertainty, does not affect either the density or the shape of hillocks while arsenic-implanted films were found to exhibit an increased number of hillocks. Results of implantation Ar^+ are not shown in the table; because due to large scatter of data from sample to sample, the effect could not be definitely established.

Although it has been demonstrated that irradiation of Al-based films with B^+, F^+ or Cr^+ ions is beneficial to the surface morphology, one has to verify whether this process does not induce other effects which would affect the performance of devices. First, it should be mentioned that in any case, implantation has no observable influence on adhesion, integrity, or continuity of the material. For boron-implanted Al, it was checked that implantation does not degrade ohmic contacts or Schottky diodes to n-Si. On the other hand, the sheet resistance of the implanted layers is higher relative to the unimplanted ones, not exceeding 5% at a dose of 10^{16} cm^{-2} with the exception of Cr. Fig. 5 shows resistivity change of B, Mg, F, As, Sb and Cr-implanted Al as a function of the ion fluence.

In an attempt to understand the mechanism of the interaction of the implanted atoms with polycrystalline Al film, leading eventually to the modification of the grain growth, we have focused on B-implanted layers on which additional experiments were per-

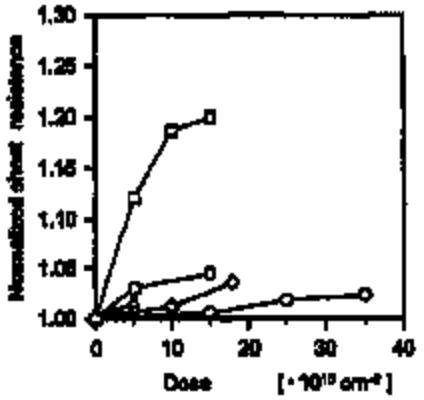

Fig. 5. Sheet resistance measurements of the implanted Al layers relative to unimplanted ones.

Table 1

Hillock density $\times 10^3$ mm^{-2}

Ion	B				F					As		Sb		Mg			Cl		Cr[a]		
Energy (keV)	60				100					60		160		100			160		130		
Dose 10^{15} (cm^{-2})	0	15	25	55	0	2	4	8	15	0	5	0	5	0	9	18	0	5	0	4	9
Sputtering																					
<1 μm	73.5	69.5	74.3	49.8	45.2	56.2	58.7	45.3		46.9	89.8	23.2	47.9	49.7	48.2	48.8	22.9	40.6	307	72.6	44.9
1–2.2 μm	29.0	59.6	5.91	6.35	11.9	15.3	7.99	5.69		34.0	22.9	13.4	12.8	14.0	12.4	11.1	10.7	13.8	21.6	9.42	8.1
>2.2 μm	3.89	0.22	0.0	0.0	0.99	1.00	0.88	0.22		1.20	0.88	1.75	1.31	1.1	0.77	0.77	2.2	2.41	0.88	0.11	0.0
Evaporation																					
<1 μm	40.5	46.9	47.9	58.9	60.7		69.4	63.5	50.2	67.9	161	73.9	81.4	76.0	99.0	108	35.3	44.3			
1–2.2 μm	20.6	15.2	4.27	1.86	16.8		12.4	7.45	8.54	15.3	25.3	24.7	10.3	28.3	21.0	16.9	16.1	12.6			
>2.2 μm	2.52	0.55	0.11	0.0	1.31		0.88	0.22	0.22	1.53	0.99	2.74	1.86	1.31	1.97	0.99	2.3	2.63			

[a] Cr implanted into Al:Si 1%.

0169-4332/95/$09.50

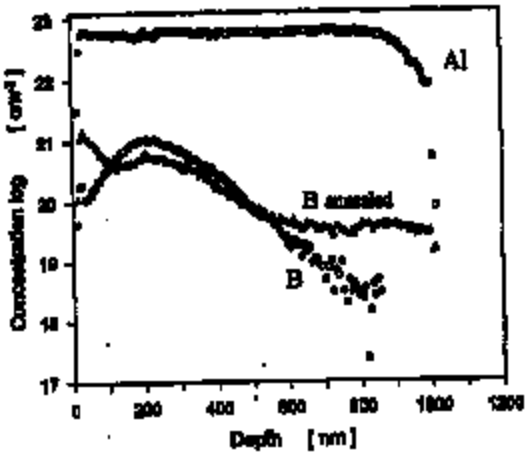

Fig. 6. SIMS depth profiles of boron in Al before and after annealing.

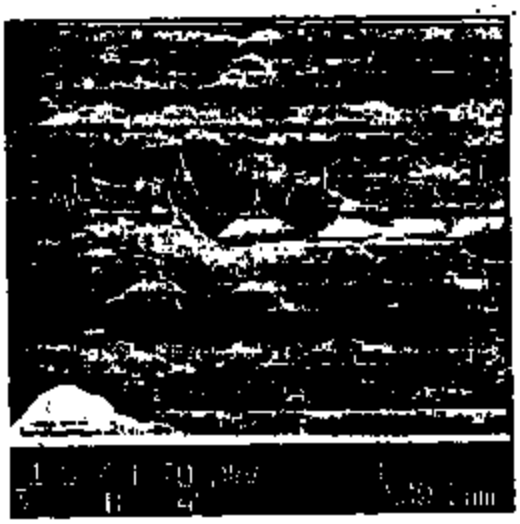

Fig. 7. Auger line-scan of boron in B^+-implanted 1 μm thick Al layer.

formed. Fig. 6 presents in-depth concentration profiles of ^{11}B before and after annealing as determined by SIMS technique. It demonstrated substantial mobility of boron atoms under this relatively low-temperature processing at 450°C. The initial Gaussian-type profile becomes flattened with a strong segregation taking place towards the Al surface and, to a lesser extent, to the Al/SiO_2 interface. Auger line-scan of boron signal gives evidence that implantation followed by annealing results in laterally non-uniform distribution of B atoms across the surface (Fig. 7).

TEM investigation provided valuable information on the precise boron location and phase identification in B-implanted layers. The polycrystalline structure visible in Fig. 8 is ⟨111⟩ textured with average grain size of 0.75 μm^2. The ⟨111⟩ texture is independently confirmed by XRD with the standard deviation being estimated to 7%–10%. Small crystallites (100 nm) located at Al grain boundaries could be classified as an AlB_{10} orthorhombic or AlB_{12} tetragonal phase as was indicated by means of electron diffraction.

Finally, tensile stress in the metallization layers which amounts to 150–200 MPa after deposition drops to 60–120 MPa as a result of boron implantation and after annealing increases to a value close to that in unimplanted layers.

Fig. 8. (a) TEM image of magnetron sputtered Al layer. (b) TEM image of B^+ implanted Al layer.

4. Concluding remarks

We have demonstrated that implantation into the Al metallization may effectively influence the surface topography. In some cases it leads to the elimination of large hillocks which grow above the initial surface of the metal in a process of relieving compressive stress that develops in the course of annealing.

Although the results of this work are not sufficient to explain, for each implanting species, a detailed mechanism of nucleation and growth of hillocks, investigations of boron-implanted provided some general guideline. Since it is well known that the material for the grain growth is supplied through the grain boundary migration rather than through lattice diffusion one obvious condition that has to be fulfilled in order to modify the growth kinetics is segregation of the incorporated atoms at the grain boundaries. This implies that best candidates to be introduced into the Al layer are those which have limited solubility in bulk aluminium. According to the Al–B phase diagram, solid solubility of boron in Al is less than 0.1 at% [9]. It is postulated that, upon sintering, the boron atoms out-diffuse from the bulk Al and then, due to their high mobility at grain boundaries, precipitate in the form of presumably AlB_{10} compound. Indeed, as supported by SIMS profiling, at a temperature of 450°C boron spreads throughout the layer and such a fast transport could not be attained by bulk diffusion. AlB_{10} precipitates located at aluminum grain boundaries are believed to be the main cause of strengthening the polycrystalline structure and preventing the grains from excessive vertical growth.

Fluorine, chromium and, particularly, boron implanted to aluminium seem promising in the reliability improvement of multilevel metallization systems. Additional advantage of applying B or F ions is that these elements are easily accessible in typical high-current implanters used in silicon technology.

Acknowledgements

The authors wish to acknowledge Professor W. Rozbiski, Dr. J. Kozubowski and I. Adamczewska for performing some of the measurements and valuable discussions. This work was supported by the State Committee for Scientific Research, Poland, under Grant No. 8S501026O5.

References

[1] F.M. d'Heurle, Int. Metar. Rev. 34 (1989) 53.
[2] K.N. Tu, J.W. Mayer and L.C. Feldman, Electronic Thin Film Science (Macmillan, New York, 1992) p. 378.
[3] F. Bidaux, N. Kobayasi, J. Schwartz and U. Smith, J. Vac. Sci. Technol. B 9 (1991) 58.
[4] R.A. Schwarzer and D. Gerth, J. Electron. Mater. 22 (1993) 607.
[5] O.W. Holland and J.R. Alvis, J. Electrochem. Soc. 134 (1987) 2017.
[6] N. Peacock, Thin Solid Films 155 (1948) 173.
[7] K.F. Mac Williams, L.B. Lowry, M. Isaac, D. Cohart and T.C. Zielow, 1990 Symposium on VLSI Technology, June 4-7, Honolulu.
[8] M. Zaborowski, M. Adamiec and A. Barcz, 1990 Symposium on VLSI Technology, June 4-7, Honolulu.
[9] C.J. Smithells, Metals Reference Book, Vol. II (Butterworths, London 1967) p. 390.